

CAMBRIDGE
AEROSPACE
SERIES



AIRCRAFT DESIGN

AJOY KUMAR KUNDU

CAMBRIDGE

www.cambridge.org/9780521885164

This page intentionally left blank

AIRCRAFT DESIGN

Aircraft Design explores the conceptual phase of a fixed-wing aircraft design project. Designing an aircraft is a complex, multifaceted process that embraces many technical challenges in a multidisciplinary environment. By definition, the topic requires intelligent use of aerodynamic knowledge to configure aircraft geometry suited specifically to a customer's demands. It involves configuring aircraft shape, estimating its weight and drag, and computing the available thrust from the matched engine. The methodology includes formal sizing of the aircraft, engine matching, and substantiating performance to comply with a customer's demands and government regulatory standards. Associated topics include safety issues; environmental issues; material choice; structural layout; and understanding the flight deck, avionics, and systems (for both civil and military aircraft). Cost estimation and manufacturing considerations also are discussed. The chapters are arranged to optimize understanding of industrial approaches to aircraft-design methodology. Example exercises based on the author's industrial experience with typical aircraft design are included. Additional sections specific to military aircraft highlighted with an asterisk are available on the Web at www.cambridge.org/Kundu

Ajoy Kumar Kundu was educated in India (Jadavpur University), the United Kingdom (Cranfield University and Queen's University Belfast), and the United States (University of Michigan and Stanford University). His experience spans nearly thirty years in the aircraft industry and fifteen years in academia. In India, he was Professor at the Indian Institute of Technology, Kharagpur; and Chief Aircraft Designer at Hindustan Aeronautics Ltd., Bangalore. In North America, he was Research Engineer for the Boeing Aircraft Company, Renton, and Intermediate Engineer for Canadair Ltd., Montreal. He began his aeronautical career in the United Kingdom with Short Brothers and Harland Ltd., retiring from Bombardier Aerospace-Shorts, Belfast, as Chief Assistant Aerodynamicist. He is currently associated with Queen's University Belfast. He held British, Indian, and Canadian private pilot licenses. He is a Fellow of the Royal Aeronautical Society and the Institute of Mechanical Engineers and an Associate Fellow of the American Institute of Aeronautics and Astronautics.

Cambridge Aerospace Series

Editors Wei Shyy and Michael J. Rycroft

1. J. M. Rolfe and K. J. Staples (eds.): *Flight Simulation*
2. P. Berlin: *The Geostationary Applications Satellite*
3. M. J. T. Smith: *Aircraft Noise*
4. N. X. Vinh: *Flight Mechanics of High-Performance Aircraft*
5. W. A. Mair and D. L. Birdsall: *Aircraft Performance*
6. M. J. Abzug and E. E. Larrabee: *Airplane Stability and Control*
7. M. J. Sidi: *Spacecraft Dynamics and Control*
8. J. D. Anderson: *A History of Aerodynamics*
9. A. M. Cruise, J. A. Bowles, C. V. Goodall, and T. J. Patrick: *Principles of Space Instrument Design*
10. G. A. Khoury and J. D. Gillett (eds.): *Airship Technology*
11. J. Fielding: *Introduction to Aircraft Design*
12. J. G. Leishman: *Principles of Helicopter Aerodynamics, 2nd Edition*
13. J. Katz and A. Plotkin: *Low Speed Aerodynamics, 2nd Edition*
14. M. J. Abzug and E. E. Larrabee: *Airplane Stability and Control: A History of the Technologies that Made Aviation Possible, 2nd Edition*
15. D. H. Hodges and G. A. Pierce: *Introduction to Structural Dynamics and Aeroelasticity*
16. W. Fehse: *Automatic Rendezvous and Docking of Spacecraft*
17. R. D. Flack: *Fundamentals of Jet Propulsion with Applications*
18. E. A. Baskharone: *Principles of Turbomachinery in Air-Breathing Engines*
19. D. D. Knight: *Numerical Methods for High-Speed Flows*
20. C. Wagner, T. Hüttl, and P. Sagaut: *Large-Eddy Simulation for Acoustics*
21. D. Joseph, T. Funada, and J. Wang: *Potential Flows of Viscous and Viscoelastic Fluids*
22. W. Shyy, Y. Lian, H. Liu, J. Tang, and D. Viieru: *Aerodynamics of Low Reynolds Number Flyers*
23. J. H. Saleh: *Analyses for Durability and System Design Lifetime*
24. B. K. Donaldson: *Analysis of Aircraft Structures, Second Edition*
25. C. Segal: *The Scramjet Engine: Processes and Characteristics*
26. J. Doyle: *Guided Explorations of the Mechanics of Solids and Structures*
27. A. Kundu: *Aircraft Design*
28. M. Friswell, J. Penny, S. Garvey, and A. Lees: *Fundamentals of Rotor Dynamics*
29. B. Conway (ed): *Spacecraft Trajectory Optimization*

Aircraft Design

Ajoy Kumar Kundu
Queen's University Belfast



CAMBRIDGE UNIVERSITY PRESS
Cambridge, New York, Melbourne, Madrid, Cape Town, Singapore,
São Paulo, Delhi, Dubai, Tokyo

Cambridge University Press
The Edinburgh Building, Cambridge CB2 8RU, UK

Published in the United States of America by Cambridge University Press, New York

www.cambridge.org

Information on this title: www.cambridge.org/9780521885164

© Ajoy Kundu 2010

This publication is in copyright. Subject to statutory exception and to the provision of relevant collective licensing agreements, no reproduction of any part may take place without the written permission of Cambridge University Press.

First published in print format 2010

ISBN-13 978-0-511-67785-4 eBook (NetLibrary)

ISBN-13 978-0-521-88516-4 Hardback

Cambridge University Press has no responsibility for the persistence or accuracy of urls for external or third-party internet websites referred to in this publication, and does not guarantee that any content on such websites is, or will remain, accurate or appropriate.

Contents

<i>List of Symbols and Abbreviations</i>	<i>page</i> xxi
<i>Preface</i>	xxxix
<i>Road Map of the Book</i>	xxxv
The Arrangement	xxxv
Suggested Route for the Coursework	xxxix
Suggestions for the Class	xli
Use of Semi-empirical Relations	xlii
1 Introduction	1
1.1 Overview	1
1.1.1 What Is to Be Learned?	1
1.1.2 Coursework Content	1
1.2 Brief Historical Background	2
1.3 Current Aircraft Design Status	7
1.3.1 Forces and Drivers	8
1.3.2 Current Civil Aircraft Design Trends	9
1.3.3 Current Military Aircraft Design Trends*	11
1.4 Future Trends	11
1.4.1 Civil Aircraft Design: Future Trends	12
1.4.2 Military Aircraft Design: Future Trends*	14
1.5 Learning Process	15
1.6 Units and Dimensions	17
1.7 Cost Implications	17
2 Methodology to Aircraft Design, Market Survey, and Airworthiness	19
2.1 Overview	19
2.1.1 What Is to Be Learned?	20
2.1.2 Coursework Content	20
2.2 Introduction	20
2.3 Typical Design Process	21

* These sections are found on the Cambridge University Web site at www.cambridge.org/Kundu

2.3.1	Four Phases of Aircraft Design	23
2.3.2	Typical Resources Deployment	25
2.3.3	Typical Cost Frame	26
2.3.4	Typical Time Frame	26
2.4	Typical Task Breakdown in Each Phase	26
2.4.1	Functional Tasks during the Conceptual Study (Phase 1: Civil Aircraft)	28
2.4.2	Project Activities for Small Aircraft Design	29
2.5	Aircraft Familiarization	31
2.5.1	Civil Aircraft and Its Component Configurations	31
2.5.2	Military Aircraft and Its Component Configurations*	33
2.6	Market Survey	33
2.7	Civil Aircraft Market	35
2.7.1	Aircraft Specifications and Requirements for Three Civil Aircraft Case Studies	36
2.8	Military Market*	39
2.8.1	Aircraft Specifications/Requirements for Military Aircraft Case Studies*	39
2.9	Comparison between Civil and Military Aircraft Design Requirements	40
2.10	Airworthiness Requirements	41
2.11	Coursework Procedures	42
3	Aerodynamic Considerations	43
3.1	Overview	43
3.1.1	What Is to Be Learned?	43
3.1.2	Coursework Content	44
3.2	Introduction	44
3.3	Atmosphere	46
3.4	Fundamental Equations	48
3.5	Airflow Behavior: Laminar and Turbulent	50
3.5.1	Flow Past Aerofoil	55
3.6	Aircraft Motion and Forces	56
3.6.1	Motion	56
3.6.2	Forces	57
3.7	Aerofoil	58
3.7.1	Groupings of Aerofoils and Their Properties	59
3.8	Definitions of Aerodynamic Parameters	62
3.9	Generation of Lift	63
3.10	Types of Stall	65
3.10.1	Gradual Stall	66
3.10.2	Abrupt Stall	66
3.11	Comparison of Three NACA Aerofoils	66
3.12	High-Lift Devices	67
3.13	Transonic Effects – Area Rule	68

* These sections are found on the Cambridge University Web site at www.cambridge.org/Kundu

3.14	Wing Aerodynamics	70
3.14.1	Induced Drag and Total Aircraft Drag	73
3.15	Aspect Ratio Correction of 2D Aerofoil Characteristics for 3D Finite Wing	73
3.16	Wing Definitions	76
3.16.1	Planform Area, S_W	76
3.16.2	Wing Aspect Ratio	77
3.16.3	Wing Sweep Angle, Λ	77
3.16.4	Wing Root (c_{root}) and Tip (c_{tip}) Chord	77
3.16.5	Wing Taper Ratio, λ	77
3.16.6	Wing Twist	78
3.16.7	High/Low Wing	78
3.16.8	Dihedral/Anhedral Angles	79
3.17	Mean Aerodynamic Chord	79
3.18	Compressibility Effect: Wing Sweep	80
3.19	Wing Stall Pattern and Wing Twist	82
3.20	Influence of Wing Area and Span on Aerodynamics	83
3.20.1	The Square-Cube Law	84
3.20.2	Aircraft Wetted Area (A_W) versus Wing Planform Area (S_w)	85
3.20.3	Additional Vortex Lift	87
3.20.4	Additional Surfaces on Wing	87
3.21	Finalizing Wing Design Parameters	89
3.22	Empennage	90
3.22.1	H-Tail	90
3.22.2	V-Tail	91
3.22.3	Tail Volume Coefficients	91
3.23	Fuselage	93
3.23.1	Fuselage Axis/Zero-Reference Plane	93
3.23.2	Fuselage Length, L_{fus}	94
3.23.3	Fineness Ratio, FR	94
3.23.4	Fuselage Upsweep Angle	94
3.23.5	Fuselage Closure Angle	94
3.23.6	Front Fuselage Closure Length, L_f	94
3.23.7	Aft Fuselage Closure Length, L_a	95
3.23.8	Midfuselage Constant Cross-Section Length, L_m	95
3.23.9	Fuselage Height, H	95
3.23.10	Fuselage Width, W	95
3.23.11	Average Diameter, D_{ave}	95
3.23.12	Cabin Height, H_{cab}	96
3.23.13	Cabin Width, W_{cab}	96
3.23.14	Pilot Cockpit/Flight Deck	96
3.24	Undercarriage	96
3.25	Nacelle and Intake	96
3.26	Speed Brakes and Dive Brakes	96

4 Aircraft Classification, Statistics, and Choices for Configuration	98
4.1 Overview	98
4.1.1 What Is to Be Learned?	99
4.1.2 Coursework Content	99
4.2 Introduction	99
4.3 Aircraft Evolution	100
4.3.1 Aircraft Classification and Their Operational Environment	101
4.4 Civil Aircraft Mission (Payload-Range)	104
4.5 Civil Subsonic Jet Aircraft Statistics (Sizing Parameters and Regression Analysis)	105
4.5.1 Maximum Takeoff Mass versus Number of Passengers	106
4.5.2 Maximum Takeoff Mass versus Operational Empty Mass	107
4.5.3 Maximum Takeoff Mass versus Fuel Load	108
4.5.4 Maximum Takeoff Mass versus Wing Area	109
4.5.5 Maximum Takeoff Mass versus Engine Power	111
4.5.6 Empennage Area versus Wing Area	112
4.5.7 Wing Loading versus Aircraft Span	113
4.6 Civil Aircraft Component Geometries	113
4.7 Fuselage Group	114
4.7.1 Fuselage Width	114
4.7.2 Fuselage Length	117
4.7.3 Front (Nose Cone) and Aft-End Closure	117
4.7.4 Flight Crew (Flight Deck) Compartment Layout	121
4.7.5 Cabin Crew and Passenger Facilities	121
4.7.6 Seat Arrangement, Pitch, and Posture (95th Percentile) Facilities	122
4.7.7 Passenger Facilities	123
4.7.8 Cargo Container Sizes	124
4.7.9 Doors – Emergency Exits	125
4.8 Wing Group	126
4.9 Empennage Group (Civil Aircraft)	128
4.10 Nacelle Group	130
4.11 Summary of Civil Aircraft Design Choices	133
4.12 Military Aircraft: Detailed Classification, Evolutionary Pattern, and Mission Profile*	134
4.13 Military Aircraft Mission*	134
4.14 Military Aircraft Statistics (Sizing Parameters – Regression Analysis)*	135
4.14.1 Military Aircraft Maximum Take-off Mass (MTOM) versus Payload*	135
4.14.2 Military MTOM versus OEM*	135
4.14.3 Military MTOM versus Fuel Load M_f^*	135
4.14.4 MTOM versus Wing Area (Military)*	135

* These sections are found on the Cambridge University Web site at www.cambridge.org/Kundu

4.14.5	MTOM versus Engine Thrust (Military)*	135
4.14.6	Empennage Area versus Wing Area (Military)*	136
4.14.7	Aircraft Wetted Area versus Wing Area (Military)*	136
4.15	Military Aircraft Component Geometries*	136
4.16	Fuselage Group (Military)*	136
4.17	Wing Group (Military)*	136
4.17.1	Generic Wing Planform Shapes*	136
4.18	Empennage Group (Military)*	136
4.19	Intake/Nacelle Group (Military)*	137
4.20	Undercarriage Group*	137
4.21	Miscellaneous Comments*	137
4.22	Summary of Military Aircraft Design Choices*	137
5	Aircraft Load	138
5.1	Overview	138
5.1.1	What Is to Be Learned?	138
5.1.2	Coursework Content	139
5.2	Introduction	139
5.2.1	Buffet	140
5.2.2	Flutter	140
5.3	Flight Maneuvers	140
5.3.1	Pitch Plane (X-Z) Maneuver (Elevator/Canard-Induced)	140
5.3.2	Roll Plane (Y-Z) Maneuver (Aileron-Induced)	141
5.3.3	Yaw Plane (Z-X) Maneuver (Rudder-Induced)	141
5.4	Aircraft Loads	141
5.4.1	On the Ground	141
5.4.2	In Flight	141
5.5	Theory and Definitions	141
5.5.1	Load Factor, n	142
5.6	Limits – Load and Speeds	143
5.6.1	Maximum Limit of Load Factor	144
5.6.2	Speed Limits	144
5.7	V - n Diagram	145
5.7.1	Low-Speed Limit	145
5.7.2	High-Speed Limit	146
5.7.3	Extreme Points of a V - n Diagram	146
5.8	Gust Envelope	147
6	Configuring Aircraft	149
6.1	Overview	149
6.1.1	What Is to Be Learned?	150
6.1.2	Coursework Content	150
6.2	Introduction	150
6.3	Shaping and Layout of a Civil Aircraft Configuration	152
6.3.1	Considerations in Configuring the Fuselage	154

* These sections are found on the Cambridge University Web site at www.cambridge.org/Kundu

6.3.2	Considerations in Configuring the Wing	157
6.3.3	Considerations in Configuring the Empennage	158
6.3.4	Considerations in Configuring the Nacelle	159
6.4	Civil Aircraft Fuselage: Typical Shaping and Layout	160
6.4.1	Narrow-Body, Single-Aisle Aircraft	163
6.4.2	Wide-Body, Double-Aisle Aircraft	167
6.4.3	Worked-Out Example: Civil Aircraft Fuselage Layout	171
6.5	Configuring a Civil Aircraft Wing: Positioning and Layout	174
6.5.1	Aerofoil Selection	174
6.5.2	Wing Design	175
6.5.3	Wing-Mounted Control-Surface Layout	176
6.5.4	Positioning of the Wing Relative to the Fuselage	177
6.5.5	Worked-Out Example: Configuring the Wing in Civil Aircraft	177
6.6	Configuring a Civil Aircraft Empennage: Positioning and Layout	180
6.6.1	Horizontal Tail	181
6.6.2	Vertical Tail	181
6.6.3	Worked-Out Example: Configuring the Empennage in Civil Aircraft	182
6.7	Configuring a Civil Aircraft Nacelle: Positioning and Layout of an Engine	184
6.7.1	Worked-Out Example: Configuring and Positioning the Engine and Nacelle in Civil Aircraft	185
6.8	Undercarriage Positioning	187
6.9	Worked-Out Example: Finalizing the Preliminary Civil Aircraft Configuration	187
6.10	Miscellaneous Considerations in Civil Aircraft	189
6.11	Configuring Military Aircraft – Shaping and Laying Out*	189
6.12	Worked-Out Example – Configuring Military Advanced Jet Trainer*	189
6.12.1	Use of Statistics in the Class of Military Trainer Aircraft*	190
6.12.2	Worked-Out Example – Advanced Jet Trainer Aircraft (AJT) – Fuselage*	190
6.12.3	Miscellaneous Considerations – Military Design*	190
6.13	Variant CAS Design*	190
6.13.1	Summary of the Worked-Out Military Aircraft Preliminary Details*	190
7	Undercarriage	191
7.1	Overview	191
7.1.1	What Is to Be Learned?	192
7.1.2	Coursework Content	192
7.2	Introduction	193
7.3	Types of Undercarriage	194
7.4	Undercarriage Layout, Nomenclature, and Definitions	195

* These sections are found on the Cambridge University Web site at www.cambridge.org/Kundu

7.5	Undercarriage Retraction and Stowage	197
7.5.1	Stowage Space Clearances	199
7.6	Undercarriage Design Drivers and Considerations	199
7.7	Turning of an Aircraft	201
7.8	Wheels	202
7.9	Loads on Wheels and Shock Absorbers	202
7.9.1	Load on Wheels	203
7.9.2	Energy Absorbed	205
7.9.3	Deflection under Load	206
7.10	Runway Pavement Classification	206
7.10.1	Load Classification Number Method	207
7.10.2	Aircraft Classification Number and Pavement Classification Number Method	208
7.11	Tires	209
7.12	Tire Friction with Ground: Rolling and Braking Friction Coefficient	212
7.13	Undercarriage Layout Methodology	213
7.14	Worked-Out Examples	215
7.14.1	Civil Aircraft: Bizjet	215
7.14.2	Military Aircraft: AJT	219
7.15	Miscellaneous Considerations	221
7.16	Undercarriage and Tire Data	222
8	Aircraft Weight and Center of Gravity Estimation	223
8.1	Overview	223
8.1.1	What Is to Be Learned?	224
8.1.2	Coursework Content	224
8.2	Introduction	225
8.3	The Weight Drivers	227
8.4	Aircraft Mass (Weight) Breakdown	228
8.5	Desirable CG Position	228
8.6	Aircraft Component Groups	230
8.6.1	Civil Aircraft	231
8.6.2	Military Aircraft (Combat Category)*	232
8.7	Aircraft Component Mass Estimation	233
8.8	Rapid Mass Estimation Method: Civil Aircraft	234
8.9	Graphical Method for Predicting Aircraft Component Weight: Civil Aircraft	234
8.10	Semi-empirical Equation Method (Statistical)	238
8.10.1	Fuselage Group – Civil Aircraft	238
8.10.2	Wing Group – Civil Aircraft	241
8.10.3	Empennage Group – Civil Aircraft	242
8.10.4	Nacelle Group – Civil Aircraft	243
8.10.5	Undercarriage Group – Civil Aircraft	243
8.10.6	Miscellaneous Group – Civil Aircraft	244

* This subsection is found on the Cambridge University Web site at www.cambridge.org/Kundu

8.10.7	Power Plant Group – Civil Aircraft	244
8.10.8	Systems Group – Civil Aircraft	246
8.10.9	Furnishing Group – Civil Aircraft	246
8.10.10	Contingency and Miscellaneous – Civil Aircraft	246
8.10.11	Crew – Civil Aircraft	246
8.10.12	Payload – Civil Aircraft	246
8.10.13	Fuel – Civil Aircraft	247
8.11	Worked-Out Example – Civil Aircraft	247
8.11.1	Fuselage Group Mass	247
8.11.2	Wing Group Mass	249
8.11.3	Empennage Group Mass	250
8.11.4	Nacelle Group Mass	250
8.11.5	Undercarriage Group Mass	250
8.11.6	Miscellaneous Group Mass	250
8.11.7	Power Plant Group Mass	250
8.11.8	Systems Group Mass	251
8.11.9	Furnishing Group Mass	251
8.11.10	Contingency Group Mass	251
8.11.11	Crew Mass	251
8.11.12	Payload Mass	251
8.11.13	Fuel Mass	251
8.11.14	Weight Summary	251
8.12	Center of Gravity Determination	252
8.12.1	Bizjet Aircraft CG Location Example	253
8.12.2	First Iteration to Fine Tune CG Position Relative to Aircraft and Components	254
8.13	Rapid Mass Estimation Method – Military Aircraft*	254
8.14	Graphical Method to Predict Aircraft Component Weight – Military Aircraft*	255
8.15	Semi-empirical Equation Methods (Statistical) – Military Aircraft*	255
8.15.1	Military Aircraft Fuselage Group (SI System)*	255
8.15.2	Military Aircraft Wing Mass (SI System)*	255
8.15.3	Military Aircraft Empennage*	255
8.15.4	Nacelle Mass Example – Military Aircraft*	255
8.15.5	Power Plant Group Mass Example – Military Aircraft*	255
8.15.6	Undercarriage Mass Example – Military Aircraft*	255
8.15.7	System Mass – Military Aircraft*	255
8.15.8	Aircraft Furnishing – Military Aircraft*	255
8.15.9	Miscellaneous Group (M_{MISC}) – Military Aircraft*	255
8.15.10	Contingency (M_{CONT}) – Military Aircraft*	255
8.15.11	Crew Mass*	255
8.15.12	Fuel (M_{FUEL})*	256
8.15.13	Payload (M_{PL})*	256

* These sections are found on the Cambridge University Web site at www.cambridge.org/Kundu

8.16 Classroom Example of Military AJT/CAS Aircraft Weight Estimation*	256
8.16.1 AJT Fuselage Example (Based on CAS Variant)*	256
8.16.2 AJT Wing Example (Based on CAS Variant)*	256
8.16.3 AJT Empennage Example (Based on CAS Variant)*	256
8.16.4 AJT Nacelle Mass Example (Based on CAS Variant)*	256
8.16.5 AJT Power Plant Group Mass Example (Based on AJT Variant)*	256
8.16.6 AJT Undercarriage Mass Example (Based on CAS Variant)*	256
8.16.7 AJT Systems Group Mass Example (Based on AJT Variant)*	256
8.16.8 AJT Furnishing Group Mass Example (Based on AJT Variant)*	256
8.16.9 AJT Contingency Group Mass Example*	256
8.16.10 AJT Crew Mass Example*	256
8.16.11 Fuel (M_{FUEL})*	256
8.16.12 Payload (M_{PL})*	256
8.16.13 Weights Summary – Military Aircraft*	256
8.17 CG Position Determination – Military Aircraft*	256
8.17.1 Classroom Worked-Out Military AJT CG Location Example*	257
8.17.2 First Iteration to Fine Tune CG Position and Components Masses*	257
9 Aircraft Drag	258
9.1 Overview	258
9.1.1 What Is to Be Learned?	259
9.1.2 Coursework Content	259
9.2 Introduction	259
9.3 Parasite Drag Definition	261
9.4 Aircraft Drag Breakdown (Subsonic)	262
9.5 Aircraft Drag Formulation	263
9.6 Aircraft Drag Estimation Methodology (Subsonic)	265
9.7 Minimum Parasite Drag Estimation Methodology	265
9.7.1 Geometric Parameters, Reynolds Number, and Basic C_F Determination	266
9.7.2 Computation of Wetted Areas	267
9.7.3 Stepwise Approach to Compute Minimum Parasite Drag	268
9.8 Semi-empirical Relations to Estimate Aircraft Component Parasite Drag	268
9.8.1 Fuselage	268
9.8.2 Wing, Empennage, Pylons, and Winglets	271
9.8.3 Nacelle Drag	273
9.8.4 Excrescence Drag	277

* These sections are found on the Cambridge University Web site at www.cambridge.org/Kundu

9.8.5	Miscellaneous Parasite Drags	278
9.9	Notes on Excrescence Drag Resulting from Surface Imperfections	279
9.10	Minimum Parasite Drag	280
9.11	ΔC_{Dp} Estimation	280
9.12	Subsonic Wave Drag	281
9.13	Total Aircraft Drag	282
9.14	Low-Speed Aircraft Drag at Takeoff and Landing	282
9.14.1	High-Lift Device Drag	282
9.14.2	Dive Brakes and Spoilers Drag	286
9.14.3	Undercarriage Drag	286
9.14.4	One-Engine Inoperative Drag	288
9.15	Propeller-Driven Aircraft Drag	288
9.16	Military Aircraft Drag	289
9.17	Supersonic Drag	290
9.18	Coursework Example: Civil Bizjet Aircraft	292
9.18.1	Geometric and Performance Data	292
9.18.2	Computation of Wetted Areas, Re , and Basic C_F	293
9.18.3	Computation of 3D and Other Effects to Estimate Component C_{Dpmin}	295
9.18.4	Summary of Parasite Drag	299
9.18.5	ΔC_{Dp} Estimation	299
9.18.6	Induced Drag	299
9.18.7	Total Aircraft Drag at LRC	299
9.19	Coursework Example: Subsonic Military Aircraft	299
9.19.1	Geometric and Performance Data of a Vigilante RA-C5 Aircraft	300
9.19.2	Computation of Wetted Areas, Re , and Basic C_F	302
9.19.3	Computation of 3D and Other Effects to Estimate Component C_{Dpmin}	303
9.19.4	Summary of Parasite Drag	305
9.19.5	ΔC_{Dp} Estimation	306
9.19.6	Induced Drag	306
9.19.7	Supersonic Drag Estimation	306
9.19.8	Total Aircraft Drag	310
9.20	Concluding Remarks	310
10	Aircraft Power Plant and Integration	314
10.1	Overview	314
10.1.1	What Is to Be Learned?	314
10.1.2	Coursework Content	315
10.2	Background	315
10.3	Definitions	319
10.4	Introduction: Air-Breathing Aircraft Engine Types	320
10.4.1	Simple Straight-Through Turbojet	320
10.4.2	Turbofan: Bypass Engine	321
10.4.3	Afterburner Engine	322

10.4.4	Turboprop Engine	323
10.4.5	Piston Engine	323
10.5	Simplified Representation of the Gas Turbine Cycle	324
10.6	Formulation and Theory: Isentropic Case	325
10.6.1	Simple Straight-Through Turbojet Engine: Formulation	325
10.6.2	Bypass Turbofan Engine: Formulation	327
10.6.3	Afterburner Engine: Formulation	329
10.6.4	Turboprop Engine: Formulation	330
10.7	Engine Integration with an Aircraft: Installation Effects	331
10.7.1	Subsonic Civil Aircraft Nacelle and Engine Installation	332
10.7.2	Turboprop Integration to Aircraft	335
10.7.3	Combat Aircraft Engine Installation	336
10.8	Intake and Nozzle Design	338
10.8.1	Civil Aircraft Intake Design: Inlet Sizing	338
10.8.2	Military Aircraft Intake Design*	341
10.9	Exhaust Nozzle and Thrust Reverser	341
10.9.1	Civil Aircraft Thrust Reverser Application	342
10.9.2	Civil Aircraft Exhaust Nozzles	343
10.9.3	Coursework Example of Civil Aircraft Nacelle Design	344
10.9.4	Military Aircraft Thrust Reverser Application and Exhaust Nozzles*	345
10.10	Propeller	345
10.10.1	Propeller-Related Definitions	348
10.10.2	Propeller Theory	349
10.10.3	Propeller Performance: Practical Engineering Applications	355
10.10.4	Propeller Performance: Blade Numbers $3 \leq N \leq 4$	357
10.10.5	Propeller Performance at STD Day: Worked-Out Example	358
10.11	Engine-Performance Data	359
10.11.1	Piston Engine	361
10.11.2	Turboprop Engine (Up to 100 Passengers Class)	363
10.11.3	Turbofan Engine: Civil Aircraft	365
10.11.4	Turbofan Engine: Military Aircraft*	370
11	Aircraft Sizing, Engine Matching, and Variant Derivative	371
11.1	Overview	371
11.1.1	What Is to Be Learned?	371
11.1.2	Coursework Content	372
11.2	Introduction	372
11.3	Theory	373
11.3.1	Sizing for Takeoff Field Length	374
11.3.2	Sizing for the Initial Rate of Climb	377
11.3.3	Sizing to Meet Initial Cruise	378
11.3.4	Sizing for Landing Distance	378

* These sections are found on the Cambridge University Web site at www.cambridge.org/Kundu

11.4	Coursework Exercises: Civil Aircraft Design (Bizjet)	379
11.4.1	Takeoff	379
11.4.2	Initial Climb	380
11.4.3	Cruise	380
11.4.4	Landing	381
11.5	Coursework Exercises: Military Aircraft Design (AJT)*	381
11.5.1	Takeoff – Military Aircraft*	381
11.5.2	Initial Climb – Military Aircraft*	381
11.5.3	Cruise – Military Aircraft*	381
11.5.4	Landing – Military Aircraft*	381
11.6	Sizing Analysis: Civil Aircraft (Bizjet)	381
11.6.1	Variants in the Family of Aircraft Design	382
11.6.2	Example: Civil Aircraft	383
11.7	Sizing Analysis: Military Aircraft*	384
11.7.1	Single-Seat Variant in the Family of Aircraft Design*	384
11.8	Sensitivity Study	384
11.9	Future Growth Potential	385
12	Stability Considerations Affecting Aircraft Configuration	387
12.1	Overview	387
12.1.1	What Is to Be Learned?	388
12.1.2	Coursework Content	388
12.2	Introduction	388
12.3	Static and Dynamic Stability	389
12.3.1	Longitudinal Stability: Pitch Plane (Pitch Moment, M)	392
12.3.2	Directional Stability: Yaw Plane (Yaw Moment, N)	393
12.3.3	Lateral Stability: Roll Plane (Roll Moment, L)	393
12.3.4	Summary of Forces, Moments, and Their Sign Conventions	396
12.4	Theory	396
12.4.1	Pitch Plane	396
12.4.2	Yaw Plane	400
12.4.3	Roll Plane	401
12.5	Current Statistical Trends for H- and V-Tail Coefficients	402
12.6	Inherent Aircraft Motions as Characteristics of Design	403
12.6.1	Short-Period Oscillation and Phugoid Motion	404
12.6.2	Directional and Lateral Modes of Motion	406
12.7	Spinning	408
12.8	Design Considerations for Stability: Civil Aircraft	409
12.9	Military Aircraft: Nonlinear Effects*	413
12.10	Active Control Technology: Fly-by-Wire	413
13	Aircraft Performance	417
13.1	Overview	417
13.1.1	What Is to Be Learned?	417
13.1.2	Coursework Content	418

* These sections are found on the Cambridge University Web site at www.cambridge.org/Kundu

13.2	Introduction	418
13.2.1	Aircraft Speed	419
13.3	Establish Engine Performance Data	420
13.3.1	Turbofan Engine (BPR < 4)	420
13.3.2	Turbofan Engine (BPR > 4)	422
13.3.3	Military Turbofan (Advanced Jet Trainer/CAS Role – Very Low BPR) – STD Day*	422
13.3.4	Turboprop Engine Performance	423
13.4	Derivation of Pertinent Aircraft Performance Equations	425
13.4.1	Takeoff	425
13.4.2	Landing Performance	429
13.4.3	Climb and Descent Performance	430
13.4.4	Initial Maximum Cruise Speed	435
13.4.5	Payload Range Capability	435
13.5	Aircraft Performance Substantiation: Worked-Out Examples (Bizjet)	437
13.5.1	Takeoff Field Length (Bizjet)	437
13.5.2	Landing Field Length (Bizjet)	442
13.5.3	Climb Performance Requirements (Bizjet)	443
13.5.4	Integrated Climb Performance (Bizjet)	444
13.5.5	Initial High-Speed Cruise (Bizjet)	446
13.5.6	Specific Range (Bizjet)	446
13.5.7	Descent Performance (Bizjet)	447
13.5.8	Payload Range Capability	448
13.6	Aircraft Performance Substantiation: Military Aircraft (AJT)	451
13.6.1	Mission Profile	451
13.6.2	Takeoff Field Length (AJT)	452
13.6.3	Landing Field Length (AJT)	456
13.6.4	Climb Performance Requirements (AJT)	457
13.6.5	Maximum Speed Requirements (AJT)	458
13.6.6	Fuel Requirements (AJT)	458
13.7	Summary	459
13.7.1	The Bizjet	461
13.7.2	The AJT	462
14	Computational Fluid Dynamics	464
14.1	Overview	464
14.1.1	What Is to Be Learned?	465
14.1.2	Coursework Content	465
14.2	Introduction	465
14.3	Current Status	466
14.4	Approach to CFD Analyses	468
14.4.1	In the Preprocessor (Menu-Driven)	470
14.4.2	In the Flow Solver (Menu-Driven)	470
14.4.3	In the Postprocessor (Menu-Driven)	470
14.5	Case Studies	471

* This subsection is found on the Cambridge University Web site at www.cambridge.org/Kundu

14.6	Hierarchy of CFD Simulation Methods	472
14.6.1	DNS Simulation Technique	473
14.6.2	Large Eddy Simulation (LES) Technique	473
14.6.3	Detached Eddy Simulation (DES) Technique	473
14.6.4	RANS Equation Technique	473
14.6.5	Euler Method Technique	473
14.6.6	Full-Potential Flow Equations	474
14.6.7	Panel Method	474
14.7	Summary	475
15	Miscellaneous Design Considerations	476
15.1	Overview	476
15.1.1	What Is to Be Learned?	477
15.1.2	Coursework Content	477
15.2	Introduction	477
15.2.1	Environmental Issues	478
15.2.2	Materials and Structures	478
15.2.3	Safety Issues	478
15.2.4	Human Interface	478
15.2.5	Systems Architecture	478
15.2.6	Military Aircraft Survivability Issues	479
15.2.7	Emerging Scenarios	479
15.3	Noise Emissions	479
15.3.1	Summary	485
15.4	Engine Exhaust Emissions	487
15.5	Aircraft Materials	487
15.5.1	Material Properties	489
15.5.2	Material Selection	491
15.5.3	Coursework Overview	493
15.6	Aircraft Structural Considerations	494
15.7	Doors: Emergency Egress	495
15.8	Aircraft Flight Deck (Cockpit) Layout	497
15.8.1	Multifunctional Display and Electronic Flight Information System	498
15.8.2	Combat Aircraft Flight Deck	499
15.8.3	Civil Aircraft Flight Deck	500
15.8.4	Head-Up Display	500
15.8.5	Helmet-Mounted Display	501
15.8.6	Hands-On Throttle and Stick	502
15.8.7	Voice-Operated Control	502
15.9	Aircraft Systems	502
15.9.1	Aircraft Control Subsystem	503
15.9.2	Engine and Fuel Control Subsystems	505
15.9.3	Emergency Power Supply	508
15.9.4	Avionics Subsystems	509
15.9.5	Electrical Subsystem	510
15.9.6	Hydraulic Subsystem	511
15.9.7	Pneumatic System	513

15.9.8	Utility Subsystem	517
15.9.9	End-of-Life Disposal	518
15.10	Military Aircraft Survivability*	521
15.10.1	Military Emergency Escape*	521
15.10.2	Military Aircraft Stealth Consideration*	521
15.10.3	Low Observable (LO) Aircraft Configuration*	521
15.11	Emerging Scenarios	522
16	Aircraft Cost Considerations	523
16.1	Overview	523
16.1.1	What Is to Be Learned?	526
16.1.2	Coursework Content	526
16.2	Introduction	526
16.3	Aircraft Cost and Operational Cost	528
16.4	Aircraft Costing Methodology: Rapid-Cost Model	531
16.4.1	Nacelle Cost Drivers	533
16.4.2	Nose Cowl Parts and Subassemblies	536
16.4.3	Methodology (Nose Cowl Only)	536
16.4.4	Cost Formulas and Results	540
16.5	Aircraft Direct Operating Cost	544
16.5.1	Formulation to Estimate DOC	546
16.5.2	Worked-Out Example of DOC: Bizjet	548
17	Aircraft Manufacturing Considerations	551
17.1	Overview	551
17.1.1	What Is to Be Learned?	553
17.1.2	Coursework Content	553
17.2	Introduction	553
17.3	Design for Manufacture and Assembly	554
17.4	Manufacturing Practices	555
17.5	Six Sigma Concept	557
17.6	Tolerance Relaxation at the Wetted Surface	559
17.6.1	Sources of Aircraft Surface Degeneration	560
17.6.2	Cost-versus-Tolerance Relationship	560
17.7	Reliability and Maintainability	561
17.8	Design Considerations	562
17.8.1	Category I: Technology-Driven Design Considerations	563
17.8.2	Category II: Manufacture-Driven Design Considerations	564
17.8.3	Category III: Management-Driven Design Considerations	564
17.8.4	Category IV: Operator-Driven Design Considerations	565
17.9	“Design for Customer”	565
17.9.1	Index for “Design for Customer”	566
17.9.2	Worked-Out Example	567

* These sections are found on the Cambridge University Web site at www.cambridge.org/Kundu

17.10	Digital Manufacturing Process Management	568
17.10.1	Product, Process, and Resource Hub	570
17.10.2	Integration of CAD/CAM, Manufacturing, Operations, and In-Service Domains	571
17.10.3	Shop-Floor Interface	572
17.10.4	Design for Maintainability and 3D-Based Technical Publication Generation	573
Appendix A	Conversion	575
Appendix B	International Standard Atmosphere	577
Appendix C	Aerofoils*	579
Appendix D	Case Studies	580
Appendix E	Tire Data*	590
	<i>References</i>	591
	<i>Index</i>	600

* These appendixes are on the Cambridge University Press Web site at www.cambridge.org/Kundu

Symbols and Abbreviations

Symbols

A	area
A_1	intake highlight area
A_{th}	throat area
APR	augmented power rating
AR	aspect ratio
A_w	wetted area
a	speed of sound; acceleration
\bar{a}	average acceleration at $0.7 V_2$
ac	aerodynamic center
B	breadth, width
b	span
C_R, C_B	root chord
C_D	drag coefficient
C_{Di}	induced drag coefficient
C_{Dp}	parasitic drag coefficient
C_{Dpmin}	minimum parasitic drag coefficient
C_{Dw}	wave drag coefficient
C_v	specific heat at constant volume
C_F	overall skin friction coefficient; force coefficient
C_f	local skin friction coefficient; coefficient of friction
C_L	lift coefficient
C_l	sectional lift coefficient; rolling moment coefficient
C_{Li}	integrated design lift coefficient
$C_{L\alpha}$	lift curve slope
$C_{L\beta}$	sideslip curve slope
C_m	pitching-moment coefficient
C_n	yawing-moment coefficient
C_p	pressure coefficient; power coefficient; specific heat at constant pressure
C_T	thrust coefficient
C_{HT}	horizontal tail volume coefficient

C_{VT}	vertical tail volume coefficient
C_{xxxx}	cost, with subscript identifying parts assembly
C'_{xxxx}	cost, heading for the type
CC	combustion chamber
CG	center of gravity
c	chord
c_{root}	root chord
c_{tip}	tip chord
cp	center of pressure
D	drag; diameter
D_{skin}	skin friction drag
D_{press}	pressure drag
d	diameter
E	modulus of elasticity
e	Oswald's factor
F	force
f	flat-plate equivalent of drag; wing span
f_c	ratio of speed of sound (altitude to sea level)
F_{ca}	aft-fuselage closure angle
F_{cf}	front-fuselage closure angle
F_B	body axis
F_I	inertia axis
F_W	wind axis
F_{xxx}	component mass fraction; subscript identifies the item (see Section 8.8)
F/m_a	specific thrust
FR	fineness ratio
g	acceleration due to gravity
H	height
h	vertical distance; height
J	advance ratio
k	constant (sometimes with subscript for each application)
L	length; lift
L_{FB}	nacelle forebody length
L_{HT}	horizontal tail arm
L_N	nacelle length
L_{VT}	vertical tail arm
L	length
M	mass; moment
M_f	fuel mass
M_i	component group mass; subscript identifies the item (see Section 8.6)
M_{xxx}	component item mass; subscript identifies the item (see Section 8.6)
\dot{m}_a	airmass flow rate
\dot{m}_f	fuel mass flow rate

\dot{m}_p	primary (hot) airmass flow rate (turbofan)
\dot{m}_s	secondary (cold) airmass flow rate (turbofan)
N	revolutions per minute; number of blades; normal force
N_e	number of engines
n	load factor
ng	load factor \times acceleration due to gravity
P, p	static pressure; angular velocity about <i>X</i> -axis
p_e	exit plane static pressure
p_∞	atmospheric (ambient) pressure
P_t, p_t	total pressure
Q	heat energy of the system
q	dynamic head; heat energy per unit mass; angular velocity about <i>Y</i> -axis
R	gas constant; reaction
Re	Reynolds number
Re_{crit}	critical Reynolds number
r	radius; angular velocity about <i>X</i> -axis
S	area (usually with the subscript identifying the component)
S_H	horizontal tail reference area
S_n	maximum cross-sectional area
S_W	wing reference area
S_V	vertical tail reference area
sfc	specific fuel consumption
T	temperature; thrust; time
T_C	nondimensional thrust
T_F	nondimensional force (for torque)
T_{SLs}	sea-level static thrust at takeoff rating
T/W	thrust loading
t/c	thickness-to-chord ratio
tf	turbofan
U_g	vertical gust velocity
U_∞	freestream velocity
u	local velocity along <i>X</i> -axis
V	freestream velocity
V_A	aircraft stall speed at limit load
V_B	aircraft speed at upward gust
V_C	aircraft maximum design speed
V_D	aircraft maximum dive speed
V_S	aircraft stall speed
V_e	exit plane velocity (turbofan)
V_{ep}	primary (hot) exit plane velocity (turbofan)
V_{es}	secondary (cold) exit plane velocity (turbofan)
W	weight; width
W_A	useful work done on aircraft
W_E	mechanical work produced by engine
W/S_w	wing; loading

X	distance along X-axis
y	distance along Y-axis
z	vertical distance

Greek Symbols

α	angle of attack
β	CG angle with vertical at main wheel; blade pitch angle; sideslip angle
Γ	dihedral angle; circulation
γ	ratio of specific heat; fuselage clearance angle
Δ	increment measure
δ	deflection
ε	downwash angle
η_t	thermal efficiency
η_p	propulsive efficiency
η_o	overall efficiency
θ	angle
Λ	wing sweep (subscript indicates the chord line)
λ	taper ratio
μ	friction coefficient; wing mass
Σ	summation
ρ	density
θ	fuselage upsweep angle
π	pi
σ	atmospheric density ratio
τ	thickness parameter
ω	angular velocity

Subscripts (In many cases, subscripts are spelled out and are not listed here.)

a	aft
ave	average
ep	primary exit plane
es	secondary exit plane
f	front; fuselage
f_b	blockage factor for drag
f_h	drag factor for nacelle profile drag (propeller-driven)
fus	fuselage
HT	horizontal tail
M	middle
N, nac	nacelle
o	freestream condition
p	primary (hot) flow
s	stall; secondary (cold) flow
t, tot	total

w	wing
VT	vertical tail
∞	freestream condition

Abbreviations

AB	afterburning
ACAS	advanced close air support
ACN	aircraft classification number
ACT	active control technology
AEA	Association of European Airlines
AEW	airborne early warning
AF	activity factor
AGARD	Advisory Group for Aerospace Research and Department
AGS	aircraft general supply
AIAA	American Institute for Aeronautics and Astronautics
AIP	Aeronautical Information Publication
AJT	advanced jet trainer
AMPR	Aeronautical Manufacturer's Planning Report
APR	augmented power rating
APU	auxiliary power unit
AST	Air Staff Target
ATA	Aircraft Transport Association
ATC	air traffic control
ATF	advanced tactical support
AVGAS	aviation gasoline (petrol)
AVTUR	aviation turbine fuel
BAS	Bombardier Aerospace–Shorts
BFL	balanced field length
BOM	bill of material
BPR	bypass ratio
BRM	brake release mass
BVR	beyond visual range
BWB	blended wing body
CAA	Civil Aviation Authority
CAD	computer-aided design
CAE	computer-aided engineering
CAM	computer-aided manufacture
CAPP	computer-aided process planning
CAS	close air support; control augmentation system; calibrated air speed
CAT	clear air turbulence
CBR	California bearing ratio
CCV	control configured vehicle
CFD	computational fluid dynamics
CFL	critical field length

CG	center of gravity
CRT	cathode ray tube
CV	control volume
DBT	design-build team
DCPR	Design Controller's Planning Report
DES	detached eddy simulation
DFFS	Design for Six Sigma
DFM/A	design for manufacture and assembly
DNS	direct numerical simulation
DOC	direct operating cost
DTLCC	design to life cycle cost
EAS	equivalent air speed
EASA	European Aviation Safety Agency
EBU	engine-build unit
ECS	environment control system
EDP	engine-driven pump
EFIS	electronic flight information system
EGT	exhaust gas temperature
EI	emission index
EPA	U.S. Environmental Protection Agency
EPNL	effective perceived noise level
EPR	exhaust–pressure ratio
ESDU	Engineering Sciences Data Unit
ESHP	equivalent SHP
ESWL	equivalent single wheel load
ETOPS	extended twin operations
EW	electronic warfare
FAA	Federal Aviation Administration
FADEC	full authority digital electronic control
FAR	Federal Aviation Regulations (U.S.)
FBW	fly-by-wire
FEM	finite element method
FPS	foot, pound, second
FS	factor of safety
GAW	Global Atmosphere Watch
HAL	Hindustan Aeronautics Ltd.
HMD	helmet-mounted display
HOTAS	hands-on throttle and stick
HP	horse power; high pressure
HSC	high-speed cruise
HST	hypersonic transport
H-tail	horizontal tail
HUD	head-up display
IAS	indicated air speed
IATA	International Air Transport Association
ICAO	International Civil Aviation Organization
IIT	Indian Institute of Technology

IMC	instrument meteorological conditions
INCOSE	International Council of Systems Engineering
IOC	indirect operational cost
IPPD	Integrated Product and Process Development
ISA	International Standard Atmosphere
ISRO	Indian Space Research Organization
JAA	Joint Aviation Authority
JAR	Joint Airworthiness Regulation
JPT	jet pipe temperature
JUCAS	Joint Unmanned Combat Air System
KE	kinetic energy
KEAS	knots equivalent air speed
km	kilometer
LA	light aircraft
LAM	lean and agile manufacturing
LCA	light combat aircraft
LCC	life cycle cost
LCD	liquid crystal display
LCG	load classification group
LCN	load classification number
LCR	lip contraction ratio
LD, L/D	lift-to-drag (ratio)
LE	leading edge
LES	large eddy simulation
LF	load factor
LFL	landing field length
LOH	liquid hydrogen
LP	low pressure
LPO	long-period oscillation
LRC	long-range cruise
LRU	line replacement unit
MAC	mean aerodynamic chord
MDA	multidisciplinary analysis
MDO	multidisciplinary optimization
MEM (W)	manufacturer's empty mass (weight)
MFD	multifunctional display
MFR	mass flow rate
MoD	Ministry of Defense
MOGAS	motor gasoline (petrol)
MP	minor parts
mph	miles per hour
MPM	manufacturing process management
MRM	maximum ramp mass
m/s	meters per second
MTM	maximum taxi mass
MTOM (W)	maximum take off mass (weight)
NACA	National Advisory Committee for Aeronautics

NASA	National Aeronautics and Space Administration
NBAA	National Business Aircraft Association
NC	numerically controlled
NHA	negative high angle of attack
NIA	negative intermediate angle of attack
NLA	negative low angle of attack
nm	nautical miles
NP	neutral point
NRC	non-recurring cost
NTC	normal training configuration
OC	operational cost
OEM (W)	operator's empty mass (weight)
OEMF	operational empty mass fraction
OEFW	operational empty weight fraction
PAX	passenger
PCN	pavement classification number
PCU	power control unit
PE	potential energy
PFD	primary flight display
PHA	positive high angle of attack
PIA	positive intermediate angle of attack
PLA	positive low angle of attack
PLM	product life cycle management
PNdB	perceived noise decibel
PNL	perceived noise level
PPR	product, process, and resource
PRSOV	pressure-reducing shutoff valve
psfc	power-specific fuel consumption
psi	pounds per square inch
PTU	power transfer unit
QFD	quality function deployment
QUB	The Queen's University Belfast
RAE	Royal Aircraft Establishment
RAeS	Royal Aeronautical Society
RANS	Reynolds Average Navier–Stokes
RAT	ram air turbine
RC	rate of climb, recurring cost
RCS	radar cross-section signature
RD&D	research, design, and development
RDDMC	research, design, development, manufacture, and cost
RDD&T	research, design, development, and test
RFP	Request for Proposal
RJ	regional jet
R&M	reliability and maintainability
rpm	revolutions per minute; revenue passenger mile
rps	revolutions per second
RPV	remotely piloted vehicle

SAS	stability augmentation system
SATS	Small Aircraft Transportation System
SAWE	Society of Allied Weights Engineers
SEP	specific excess power
sfc	specific fuel consumption
SHP	shaft horsepower
SI	system international
SOV	shutoff valve
SPL	sound pressure level
SPO	short-period oscillation
SST	supersonic transport
STOL	short takeoff and landing
STR	structures
TAF	total activity factor
TAS	true air speed
TBO	time between overhauls
t/c	thickness to chord
TET	turbine entry temperature
TGT	turbine guide vane temperature
TOC	total operating cost
TOFL	takeoff field length
TP	thrust power
TQM	Total Quality Management
TR	thrust reverser
TTOM	typical takeoff mass (military)
T&E	training and evaluation
UAV	unmanned air vehicle
UCA	unmanned combat aircraft
UHBPR	ultra-high BPR
UHC	unburned hydrocarbons
ULD	unit load device
USDOT	U.S. Department of Transportation
VOC	voice-operated control
VPI	Virginia Polytechnic Institute
V-tail	vertical tail
VTOL	vertical takeoff and landing
ZFM (W)	zero fuel mass (weight)

Preface

This book is about the conceptual phase of a fixed-winged aircraft design project. It is primarily concerned with commercial aircraft design, although it does not ignore military aircraft design considerations. The level of sophistication of the latter is such that were I to discuss advanced military aircraft design, I would quickly deviate from the objective of this book, which is for introductory but extensive coursework and which provides a text for those in the industry who wish to broaden their knowledge. The practicing aircraft design engineer also will find the book helpful. However, this book is primarily meant for intensive undergraduate and introductory postgraduate coursework.

A hundred years after the first controlled flight of a manned, heavier-than-air vehicle, we can look back with admiration at the phenomenal progress that has been made in aerospace science and technology. In terms of hardware, it is second to none; furthermore, integration with software has made possible almost anything imaginable. Orville and Wilbur Wright and their contemporaries would certainly be proud of their progenies. Hidden in every mind is the excitement of participating in such feats, whether as operator (pilot) or creator (designer): I have enjoyed both no less than the Wright brothers.

The advancement of aerospace science and technology has contributed most powerfully to the shaping of society, regardless to which part of the world one refers. Sadly, of course, World War II was a catalyst for much of what has been achieved in the past six decades. My career spans the 1960s to the beginning of the twenty-first century, possibly the “golden age” of aeronautics! In that period, investment in the aerospace sector by both government and private organizations led to rapid changes in the acquisition, application, and management of resources. Aerospace design and manufacturing practices were transformed into their present manifestation.

The continuous changes in aircraft design and manufacturing procedures and methodologies have resulted in leaner aerospace infrastructure (sometimes to an “anorexic” level). New graduate-level engineers are expected to contribute to the system almost immediately, with minimal supervision, and to “do it right the first time.” The route to the design office through apprentice training is not open to as many as it once was. Life is now more stressful for both employers and employees than it was the day I started my career: Organizational survivability and consequent loyalty are not what they used to be. The singular aim of this book is to

prepare readers as much as possible for industry-standard engineering practices. The methodology adopted herein is in line with what is practiced in industry; the simplifications adopted for classroom use are supported by explanations so that an appreciation of industry expectations will not be lost. Aircraft conceptual design necessarily entails an iterative process. In the classroom, one or two iterations should prove sufficient as a time-efficient procedure to refine component sizes and to freeze aircraft configurations.

My student days were almost devoid of any aircraft design book. Wood [1] and Corning [2] were the early books that brought aircraft design into textbook form, followed by an excellent text written by Nicolai [3]. In 1982, Torenbeek [4] covered substantial ground with contemporary treatises in his book. Roskam's compilation [5] furthered the cause. I have benefited greatly from the works of these five authors. Gradually, more aircraft design books have appeared in the literature [6–18], each with its own strength. There is still considerable scope to advance the subject, specifically by preparing new engineers to cope with the demand for a high level of proficiency in the industry. (I recommend that readers review the Virginia Tech Web site of aircraft design bibliographies [18]. It is a comprehensive compilation of aircraft design information sources.)

One-third of my career has been spent in academia and two-thirds in aircraft design. I can see a clear gap between academic pursuits and what industry expects from new graduates as finished university “products.” The United States and the United Kingdom are aware of this problem [19–24], and both make periodic recommendations. However, the problem is acute in the developing world, where tasks among scientists with advanced degrees and engineers are not as clearly defined as they are in the West. (If I may digress slightly, I have found from personal experience that a major hindrance to progress in some of the developing world comes from the inability to administrate technological goals even when there is no dearth of technical manpower – those who perform better when working in the advanced world. People know about political asylum. However, professional asylum, also known as the “brain drain,” is a real issue. Although design is not accomplished via the democratic process, the design culture should encourage the free sharing of knowledge and liberal distribution of due recognition to subordinates. Lack of accountability in higher offices is a root cause of the failure to exploit the full potential of natural and human resources.) In time, things are changing but unfortunately slower than its potential because higher management still maintains older attitudes that masquerade behind seemingly modern views. Technology can be purchased, but progress has to be earned. I hope to prepare the readers to contribute to the progress.

The roles of scientists and engineers are well defined. According to Von Karman, “A scientist discovers what already exists. An engineer creates what never was” [25]. Converting ideas into reality for customer use proves more difficult than adding any number of publications to a list (except those papers that break new ground or advance a cause that is being adapted to enrich a generation). Perhaps the measure by which to judge scientists should be like that of engineers – namely, how much wealth has the work generated (where wealth is defined in broad terms as all that encompasses the commonweal). It should be clearly understood that scientists and engineers have to work together and not in a fallacious hierarchy in which advanced degrees stand above significant experience. Consider engineers such as

Johnson, Mitchell, and Dassault – these are the people to whom I refer. Today’s engineers must have strong analytical and applied abilities to convert ideas into profitable products. I hope that this book serves this cause by combining analytical methods and engineering practices and adapting them to aircraft design. Prerequisites are second-year (U.K.) or junior-level (U.S.) mathematics and aerodynamics. It is not difficult to acquire these prerequisites – simply a semester of effort in a class found in any university syllabus. Of course, by including “experience,” this book offers more than just analysis; aircraft design must be practiced.

Engineering design is a process, and today’s practices have so matured that they demonstrate systematic patterns despite the differences that exist between companies or countries, whether military or civil. The laws that govern the behavior of nature are universal. The differences are in the governing rules and practices of resource acquisition and management. The resulting products within the course still remain in close competition and may even show similarities in presentation and performance, not necessarily dependent on any 007 work!

I thank my teachers, supervisors, colleagues, students, shop-floor workers, and all those who taught and supported me during my career. I remember (in no particular order) the late Professor Holt Ashley of Stanford University; Professor Arthur Messiter of the University of Michigan; James Palmer of Cranfield University; Professor Shankar Lal of the Indian Institute of Technology, where I was Professor; Kenneth Hoefs of the new airplane project group of the Boeing Company, who taught me aircraft sizing and drag estimation; James Fletcher of Short Brothers and Harland, who baptized me into the aircraft industry; Tom Johnston, Director and Chief Engineer of Bombardier Aerospace–Shorts (BAS) who provided considerable help in bringing out this book; the late Dr. Vikram Sarabhai, who gave me the opportunity to be associated with the Indian Space Research Organisation; and Wing Commander Baljit Kapur, Chairman of Hindustan Aeronautics Limited (HAL [26]), where I served as the Chief Aircraft Designer. My special thanks to Dr. Tom Cummings of BAS; Noel Weir of Canadair Ltd; Stephen Snyder, formerly of the Boeing Company and now an independent consultant; and B. C. Chamundaiah and the shop-floor workers of HAL, who stood by me during difficult days. I derive tremendous pleasure from teaching and have valued interaction with students in India, Iraq, the United Kingdom, and the United States. They came to me as a bouquet of flowers. I aver that they have taught me no less than I have taught them. This book reflects the universal demands of students. In their company, I was able to remember my youth.

I am thankful to my former colleagues Colin Elliott, Director of Engineering; David Riordan, Chief Engineer; and James Tweedie, Senior Engineer, BAS, who have helped me bring out an industry-standard book on aircraft design. David’s review work is thankfully acknowledged. The contribution of BAS is gratefully acknowledged. I started my aeronautical career with BAS (then Short Brothers and Harland Ltd.) and, after a long break, rejoined and then retired from the company, the first aerospace company to celebrate its centenary.

The aim of this book is to enable new graduates to seamlessly join the industry in order to become productive as soon as possible. The book also could be used in the industry for training purposes. In today’s world, engineers may need to be retrained in broader disciplines to offer support in areas beyond their main area of specialization. To ensure continuity and overcome any current deficiencies in a second

edition, I will be grateful for readers' suggestions and criticisms. Please contact the publisher or email the author at a.kundu@qub.ac.uk with any relevant information.

I am indebted to *Jane's All the World Aircraft Manual* [27], NASA, Airbus, Saweed, BAE Systems, Hamilton Standard Propellers, Europa Aircraft Company, Dr. John McMasters (Boeing Aircraft Company), Professor Michael Niu, Professor Jan Roskam (DARcorp), Professor Egbert Torenbeek, Dr. Bill Gunston, and the late Dr. L. Pazmany. There are many excellent Web sites in the public domain. I am thankful to Richard.Ferriere.free.fr/3vues, Aerosite, and Virtual Aircraft Museum for permitting me to use some of their diagrams. I gratefully acknowledge the help of many other Web sites. The wisdom of these organizations and people will take the next generation forward with confidence as they substantiate what is learned in classrooms. To familiarize readers with many types of aircraft, I provide diagrams of various types (some are not operational). I apologize if I have inadvertently infringed on any proprietary diagrams for educational purposes. For a few of the many diagrams I have collected over the years, the sources have gotten lost. Please forgive me for the error. Any infringement on proprietary information was not deliberate and I hope may be overlooked for the sake of preparing the next generation. If brought to my notice, I will acknowledge sources and make any necessary corrections in the next edition of this book.

I am indebted to many people at The Queen's University Belfast (QUB) for suggestions on how to improve the quality of this book. They include my present and former colleagues and former students. (I must have done a good job – it is a pleasure to learn from them.) In no particular order, they are Dr. John Watterson, Dr. Mark Price, Dr. Adrian Murphy, Dr. Simon Hall, Dr. Neil Forsythe, Dr. Rachel Moore, Dr. Brendan Sloan, Damien Quinn, and David Lisk. I typed the entire manuscript and therefore am responsible for any loss of quality in the text due to typographical and grammatical errors. I am grateful to QUB for providing all of the facilities necessary to complete this book.

Peter Gordon, Senior Editor of the respected Cambridge University Press, offered me the finest support throughout the writing of this book. The hard, tireless work of Eleanor Umali of Aptara gave this book its shape. I offer my personal and heartfelt thanks to both of them and their organizations.

I owe thanks to my grandfather, the late Dr. Kunja Behari Kundu; my father, the late Dr. Kamakhya Prosad Kundu; and my cousin-brother, the late Dr. Gora Chand Kundu. They inspired and motivated me to remain studious. I cannot conclude without thanking my wife, Gouri. I did not give her much choice, but it was not a problem. She kept me nourished and maintained all domestic systems. When I sometimes pushed to the maximum permissible speed limits – her patience was remarkable.

I was educated in the United Kingdom (Cranfield University and QUB) and in the United States (University of Michigan and Stanford University); I also worked in the United Kingdom (BAS) and in North America (Boeing and Canadair). I have found that nature is the same on both sides of the Atlantic, as is the language. Any differences are trivial. In today's world of cooperative ventures among countries, especially in the defense sector, the methodologies adopted in this book should apply.

I dedicate this book to both sides of the Atlantic to where I immigrated, and to those who gave me their best education, their best jobs, and their fine homes. I left only to return and take this opportunity to write.

Road Map of the Book

The Arrangement

In a step-by-step manner, I have developed an approach to aircraft design methodology at the conceptual stage that can be followed in the classroom, from the initial stages of finding a market to the final stages of freezing the aircraft configuration. In the aircraft industry, after the “go-ahead” is obtained, the development program moves to the next phase (i.e., the Project [or Product] Definition Phase), which is not within the scope of this book. The book covers two semesters of work: the first, from Chapters 1 through 13, encompasses the conceptual design; and the second, from Chapters 14 through 17, deals with a more detailed exposition of the first semester’s work, advancing the concept through more analysis. Some of the second-semester work on cost and manufacturing considerations may require outside, aeronautical-school assistance. The recommended two-semester curriculum is outlined at the end of this road map.

The chapters are arranged linearly; there is not much choice in tailoring a course. I attempt to keep the treatise interesting by citing historical cases. The main driver for readers is the motivation to learn. Except for Chapter 1, the book is written in the third person. (Actual coursework starts in Chapter 6 after a brief mock market survey by the students, as discussed in Chapter 2.)

I omit discussions of vertical takeoff and landing/short takeoff and landing (VTOL/STOL), as well as helicopters in their entirety – these subjects require their own extensive treatment.

Aircraft design is a rigorous discipline with a conservative approach – it is not schoolday fantasies of exotic *Star Wars* shapes. It is essential to learn the basics through conventional designs and then move on to innovations after mastering these basics. Coursework methodology should be in harmony with industrial practices; otherwise, the gap between academia and industry (mentioned previously) would interfere. Using computational fluid dynamics (CFD) during conceptual study is now a routine industrial practice to establish a baseline configuration and must be introduced to students so that they may appreciate the capabilities of CFD. I am aware that the introduction to CFD comes late in undergraduate study and, therefore, its use is postponed until the second semester or, even better, until post-graduate project work, assuming that students will be familiar with CFD by then.

I recommend the use of computer-aided drawing (CAD) in generating configurations, which facilitates any subsequent CFD work. These aspects of the classroom learning process are discussed in further detail in Section 1.5.

What, specifically, does this book offer? The road map of the book is described as follows. Chapter 1 is purely introductory – no coursework is embedded in it. It serves as a “starter course,” intended for easy reading written in the first person. To a newcomer, some statements may appear unsubstantiated, but rest assured that they have been well tested by my colleagues in various countries and companies – the facts will be revealed as progress is made. Chapter 1 begins with a brief historical outline intended to inspire readers’ interest in our aerospace heritage (one of the few areas in which reality can be more interesting than fiction). The fascinating stories of human achievement are motivational, and I urge students to read books and peruse Internet Web sites that are dedicated to aerospace history. They cover the full range of human emotions: from disappointment due to failures and fatalities to the joy of successes; from light-hearted circus flying to flying in spectacular display that defies imagination. Chapter 1 continues with a description of typical current designs and associated market drivers. Next, I look into the future, ending the chapter with units and dimensions used in design practice.

Marketing and airworthiness are the two most important requirements that shape a product. Chapter 2 describes typical project phases as generic procedures for aircraft design: from the conceptual stage to the finished product. It continues with a discussion of the importance of market information. Students are encouraged to conduct a short mock market study to generate a specification for which experienced guidance is required. For commercial aircraft, the specification is primarily the mission profile for the payload range capability. The differences between military and civil aircraft specifications and the associated financial outlay are significant. Military specifications are substantially more complex, depending on the specific combat role: They vary widely, and complexity spirals when multirole capabilities are required. Substantiation of airworthiness regulations is mandatory in the industry and also is discussed in Chapter 2. The U.S. Federal Aviation Regulations (FAR) are now in wide use, and I adhere to them. The recently established European Aviation Safety Agency (EASA) standards are similar to FAR and therefore are not discussed here.

Aerodynamic considerations are central to shaping a streamlined aircraft configuration. Therefore, aerodynamic considerations are introduced in Chapter 3 to expose students to what is needed for the aircraft design course. Extensive treatment of aerodynamics is provided separately in all aeronautical schools; here, only the necessary aerodynamic information has been compiled for reference as the aircraft design coursework progresses. Crucial aerofoil aerodynamics information is provided in Chapter 3 and characteristics are found in Appendix C. Chapter 3 does not provide sequential coursework to start with, but students are required to know the facts and to refer to and apply them when required.

Following the history of achievements are the statistics, covered in Chapter 4. As mentioned previously, products from different origins show similarities that indicate a strong statistical pattern that provides an idea of what is to be expected in a new design. A new design, with commercial considerations, must be a cautious progression, advancing through the introduction of the latest proven technologies.

It is not surprising, therefore, to observe a strong statistical correlation with the past. Military aircraft designs necessarily must be bolder and make bigger leaps to stay decisively ahead of potential adversaries, regardless of the cost. Eventually, older, declassified military technology trickles down to commercial use. One example is fly-by-wire (FBW) technology. Chapter 4 also discusses various possible aircraft component configurations currently in use to assist in rational selection. *Jane's All the World's Aircraft Manual* (published annually) is an indispensable source for vital aircraft statistics and has served many generations of aeronautical engineers around the world for more than half a century. Chapter 4 is intended to be a data source for aircraft design, and students will refer to it as coursework progresses. This information is provided early in the book so that expectations for new designs can benefit from the experiences of past designs. Chapter 5 addresses the aircraft speed envelope (i.e., the $V-n$ diagram).

Formal, conceptual aircraft design work starts in Chapter 6, following the release of a market specification as discussed in Chapter 2. Civil and military aircraft configurations are discussed separately because they are so different in approach. Students must retrieve information from previous chapters to configure their aircraft. Chapter 6 addresses the fuselage, the shape of the wing, the empennage, the engine positions, and so forth and provides candidate aircraft configurations with definite geometric dimensions that meet market requirements. The aircraft conceptual design must consider offering a family of variants to cover a wider market at low cost by retaining significant component commonalities. This point is emphasized throughout the book. Considering families of variants must begin at the initial stage to make products right the first time (i.e., the Six Sigma approach).

Chapter 7 sizes and locates the undercarriage for the configurations arrived at in Chapter 6. Next in the sequence, Chapter 8 discusses component and aircraft mass (i.e., weight) estimations and location of the center of gravity (CG) and its movement with payload variation. (Chapter 12 discusses the role of the CG position in aircraft static stability.) As demonstrated, weight estimation must be an iterative process because fine tuning the design from past designs presented in Chapters 4 and 6 is otherwise merely a guess. Chapter 9 addresses the difficult aspect of drag estimation for both military and civil aircraft. Successful understanding of these topics is of paramount importance for students. Another emphasis throughout this book is presenting the industry-standard approach to estimate aircraft and the breakdown of component drag.

Relevant information on aircraft power plants is integral to aircraft design. Although this book does not focus on aircraft engine design, aircraft designers should thoroughly understand the propulsion system as the “heart” of the aircraft. Chapter 10 discusses in detail gas turbine and piston engine performance, as well as related topics concerning engine and aircraft integration. This information is necessary for shaping nacelles and estimating their installed drag.

When the configuration is finalized, the aircraft mass estimated, the CG located, and the drag polar becomes available, the freezing of configuration by sizing the aircraft for the family concept and finding matched engines to meet customer specifications is described in Chapter 11. This phase closely conforms to industry practices. The procedure offers a “satisfying” solution for the most important sizing parameters, complying with constraints imposed by market specifications. These

parameters lead to candidate aircraft configurations. Parametric sensitivity studies are required, which eventually prove to be the key to success through balancing comfort with cost in a fiercely competitive market. Safety is never compromised.

Chapter 12 discusses aircraft static stability, which can affect the overall configuration in an effort to find a mass distribution that satisfactorily locates the CG. Tail sizing establishes the CG envelope, and iterations typically are required to refine the result. The iteration process should progress quickly by using spreadsheets for repetitive calculations. Fortunately, aircraft dynamic behavior and control responses are not addressed in the conceptual phase – they are considered after the configuration is finalized. If required later, the control geometries are tailored or adjusted, possibly requiring another iteration to update the configuration. To save time in the classroom, the iterations of control surface tailoring are avoided. The design configuration is now complete but still requires fine tuning of the aircraft mass and CG location.

Chapter 13 covers aircraft performance: the proof of the product that demonstrates compliance with the customer's requirements as listed in the specifications. Another iteration may be required if performance falls short of its goal. The derivation of aircraft performance equations is kept to a minimum because many excellent books on the subject are available.

As previously stated, the first thirteen chapters of this book constitute the curriculum for a one-semester preliminary design exercise. However, aircraft design must also consider environmental and safety issues, systems requirements, typical structural layout, manufacturing and assembly (DFM/A) methodology, design, and, most important, cost implications – topics that are addressed in Chapters 15 through 17. These considerations constitute the conceptual design study phase, which undergoes management review for the go-ahead of a project. A second semester could include Chapters 14 through 17, with the discussion of CFD being a significant part of the coursework.

Chapter 14 provides an overview of how CFD is involved during the conceptual-design study phase. This book is not about CFD, which is an exhaustive subject itself to which scientists and engineers can devote their entire careers. Today, almost all undergraduate aeronautical engineering courses introduce CFD in the final year so that students can gain proficiency in application software. If the first semester's work on aircraft configuration is done using a 3D CAD model, at least time required for aircraft geometry generation can be saved. Undergraduate work is best suited to conventional subsonic jet transport aircraft with simple shapes.

Each chapter of the book starts with an overview, a summary of what is to be learned, and the coursework content. There are no exercises at the end of the chapters; each continues the project progression of students.

Many categories of aircraft have been designed; this book covers a wide range for coursework exercises and provides adequate exposure to important categories. After students become proficient, they could then undertake less conventional aircraft designs. Associated examples in the book are the turbofan-powered Learjet 45 class of aircraft for civil applications and a turbofan-powered military, advanced jet trainer aircraft of the Royal Air Force (RAF) Hawk class. Case studies are indispensable to the coursework and classroom exercises must be close to actual aircraft that have been modified to maintain “commercial in confidence.” Additional

examples in Appendix D are based on actual designs worked out by the author. The results are not from the industry but have been compared with available performance data. The industry is not liable for what is presented herein.

The three aircraft cases are (1) a turbofan-powered Learjet 45 class Bizjet; (2) a high-subsonic jet in the Boeing 737/Airbus 320 aircraft class; and (3) a military advanced jet trainer (AJT) in the B.Ae Hawk class, which has a close support-role variant. Designing an F22 class of aircraft is beyond the scope of this book – I question whether any textbook can be used for undergraduate coursework without first offering an exercise on simpler designs. Nevertheless, advanced work on military designs is possible only when the basics have been mastered – the aim of this book. Developing a configuration within a family concept so that variants can be designed at low cost and cover a wider market area is emphasized. One might even say, “Design one and get the second at half the development cost.” The jet transport aircraft is recommended as the most suitable for coursework projects. Chapter 2 lists a few projects of interest to students. Other projects could be extracted from the competitions held by R.Ae.S in the United Kingdom and organizations such as NASA, the FAA, and AIAA in the United States.

For classroom practice, using manual computation is recommended, with spreadsheets developed by students because the repetitive aspect is part of the learning process. It is essential for students to develop a sense for numbers and to understand the labor content of design (it is expensive to make midcourse changes). It is common nowadays to provide CDs with companion software. However, I do not follow this practice because the software for handling repetitive tasks constrains students from interacting more with the governing equations and is part of the learning experience.

If students elect to use off-the-shelf software, then it must be reputable. For U.S. readers, well-circulated NASA programs are available. However, these are more meaningful after the subject of aircraft design is well understood – that is, after completing the coursework using manual computations. This leads to an appreciation of how realistic the computer output is, as well as how changes in input to improve results are made. It is better to postpone using conceptual design software until entering the industry or doing postgraduate work. In academia, students can use CFD and finite element method (FEM) analyses to complement the aircraft design learning process.

Flying radio-controlled model aircraft may be interesting to students, but I do not think it is relevant because it is not an industrial practice unless the project concerns radio-controlled aircraft such as remotely piloted vehicles (RPVs) and unmanned air vehicles (UAVs). Some combat aircraft have an unpowered, accurately scaled, radio-controlled model dropped from the mother aircraft to test stability behavior. However, if there is interest, students can take up model-aircraft flying as a hobby.

Suggested Route for the Coursework

The author suggests the following path for the two-semester coursework. Each semester entails 36 hours of lecture and coursework: specifically, 12 to 14 hours of lectures by the instructor followed by computational work in class. Any unguided

work may be left for routine computation to complete the assignment of the chapter. The final week of coursework is reserved for report writing. An outline of the final-report requirements may be given to students at the beginning of the course. Students are required to submit brief preliminary reports at the completion of each chapter so that the instructor can offer improvement guidelines. This reduces student workload at the end of the semester and enables them to complete their report without loss of quality. The coursework progresses sequentially following the chapters of this book.

First Semester

	<i>Lecture hours (14)</i>
1. Establish the project specification with a mock market study as described in Chapter 2 (e.g., a 10-passenger, 2,000-nm Bizjet in the Learjet 45 class, the example used throughout this book).	1
2. Configure the aircraft (Chapter 6 with input from Chapters 3 and 4).	2
3. Select aerofoil and establish wing characteristics.	2
4. Complete undercarriage layout and tire sizing (Chapter 7).	1
5. Estimate component and aircraft weight and determine the CG location (Chapter 8, first iteration).	1
6. Estimate aircraft drag (Chapter 9).	1
7. Establish engine data (Chapter 10).	1
8. Size the aircraft and find a matched engine (Chapter 11).	1
9. Determine the family of variant design (Chapter 11).	1
10. Evaluate stability considerations. This requires a second iteration to fine tune aircraft weight and accurately locate the CG position (Chapter 12).	1
11. Conduct a performance evaluation to check whether the market specification is met (Chapter 13). If it is not, then fine tune the configuration and engine size, and reiterate the computational process until the performance meets specifications.	2

Classroom work hours with the instructor: 22 hours total

Classroom management and requirements for submission of work in report form is determined by the instructor.

Second Semester

The second semester continues the work done in the first semester, progressing as follows:

	<i>Lecture hours (11)</i>
1. Discuss material and structural considerations and preliminary layout (Chapter 15).	2
2. Discuss safety and environmental issues (Chapter 15).	1

3. Establish system and instrument requirements (e.g., electrical, mechanical, control, communication navigation) (Chapter 15).	2
4. Review of first-semester work in conjunction with information gained so far in the second semester. If required, refine weights and configuration.	1
5. Review total airworthiness requirements.	1
6. Discuss manufacturing considerations.	1
7. Discuss cost estimates (e.g., aircraft unit and direct operating costs [DOCs]).	2
8. Discuss flight and ground test plans.	1
Classroom work hours with the instructor:	22 hours total

Classroom management and requirements for submission of work in report form are determined by the instructor. (CFD [Chapter 14] and FEM analyses are separate tasks and are beyond the scope of this book.)

Suggestions for the Class

Coursework starts with a mock market survey to get a sense of how an aircraft design is conceived (its importance is highlighted in Section 2.3). Inexperienced students depend on instruction; therefore, a teacher's role is important at the beginning. Here, I offer some of my experiences in the hope that they may be helpful.

The teacher divides the class into groups of four, which then work as teams. After introducing the course content and expectations, the teacher assigns (with student participation) the type of aircraft to be undertaken in the coursework (the example of the Learjet 45 class of aircraft is used in this book). The teacher gives the students the payload and range for the aircraft and asks them to list what they think are the requirements from the operator's (customer's) perspective and directs them to produce a scaled three-view sketch. I recommend that students consult *Aerospace America* [23] to study similar designs and tabulate the statistical data to arrive at their proposition. (Relevant Web sites also provide substantial information.) Understandably, in most cases, the specifications and concept configuration designs may not be realistic; however, some students could arrive at surprisingly advanced concepts.

It is unrealistic to assume full understanding by students at the start of the design exercise, but I have found that comprehension of task obligations improves rapidly. The teacher explains the merits and demerits of each team's proposition, retaining only the best cases. Finally, the teacher selects one configuration (after pooling ideas from the groups) but allows the students to retain configuration differences (e.g., high or low wing, or tail position) that have been tailored to a realistic shape and will be systematically fine tuned as the class progresses to the final design. When specifications have been standardized and the configurations decided, the class assumes a smooth routine. I recommend that the teacher encourage differences among configurations to compare the designs at the end of the semester. The comparison of the final design with their initial propositions, as the evidence of the learning process, will provide students with satisfaction.

This type of project work does not have closed-book final examination – grades are based on project documents submitted by students. Grading is at the discretion of the teacher, as it should be, but peer review contributes. Working in teams requires honest feedback among students because the teacher cannot track individuals working on their own. Leadership qualities of individual students should be recognized but should not overshadow a quieter student’s performance. The students will soon be competing in the reality of the industry, and a spirit of teamwork must be experienced in the classroom. This spirit is not only about cooperation with others; it also is about being an effective contributing member working in harmony within a team. By this time, the teacher would have adequate feedback on individual work quality and capability.

A note of caution: What is accomplished in 36 hours of classroom lectures takes approximately 36 weeks in industry, not including the work put in by the experienced engineers engaged in the work. The undergraduate coursework must stay on schedule to conclude on time. Therefore, to maintain the schedule, the teacher must remain in close contact with students.

Use of Semi-empirical Relations

DATCOM (U.S.) and RAE data sheets (U.K., recently replaced by ESDU) have served many generations of engineers for more than a half century and are still in use. Over time, as technology has advanced, new tools using computer-aided engineering (CAE) have somewhat replaced earlier methods.

Semi-empirical relations and graphs cannot guarantee exact results; at best, error-free results are coincidental. A user of semi-empirical relations and graphs must be aware of the extent of error that can be incurred. Even when providers of semi-empirical relations and graphs give the extent of error range, it is difficult to substantiate any errors in a particular application. Other methods could provide better results.

If test results are available, they should be used instead of semi-empirical relations and graphs. Tests (e.g., aerodynamics, structures, and systems) are expensive to conduct, but they are indispensable to the process. Certifying agencies impose mandatory requirements on manufacturers to substantiate their designs with test results. These test results are archived as a databank to ensure that in-house semi-empirical relations are kept “commercial in confidence” as proprietary information. CFD and FEM are the priority, before semi-empirical relations and graphs. The consistency of CFD in predicting drag (see Chapter 14) has to be proven conclusively when semi-empirical relations and graphs are used extensively. This also is true for weight prediction.

This book does not include many of the DATCOM/ESDU semi-empirical relations and graphs. Inclusion will prove meaningless unless their use is shown in worked-out examples. Typically, their use during conceptual studies can be postponed until the next phase of study (see Chapter 2), which is beyond the scope of this book. It is important for instructors to compile as many test data as possible in their library of resources.

1 Introduction

1.1 Overview

This book begins with a brief historical introduction in which our aeronautical legacy is surveyed. The historical background illustrates the human quest to conquer the sky and is manifested in a system shaping society as it stands today: in commerce, travel, and defense. Its academic outcome is to prepare the next generation for the advancement of this cause.

Some of the discussion in this chapter is based on personal experience and is shared by many of my colleagues in several countries; I do not contest any differences of opinion. Aerospace is not only multidisciplinary but also multidimensional – it may look different from varying points of view. Only this chapter is written in the first person to retain personal comments as well as for easy reading.

Current trends indicate maturing technology of the classical aeronautical sciences with diminishing returns on investment, making the industry cost-conscious. To sustain the industry, newer avenues are being searched through better manufacturing philosophies. Future trends indicate “globalization,” with multinational efforts to advance technology to be better, faster, and less expensive beyond existing limits.

1.1.1 What Is to Be Learned?

This chapter covers the following topics:

- Section 1.2: A brief historical background
- Section 1.3: Current design trends for civil and military aircraft
- Section 1.4: Future design trends for civil and military aircraft
- Section 1.5: The classroom learning process
- Section 1.6: Units and dimensions
- Section 1.7: The importance of cost for aircraft designers

1.1.2 Coursework Content

There is no classroom work in this chapter, but I recommend reading it to motivate readers to learn about our inheritance. Classwork begins in [Chapter 6](#) (except for the mock market survey in [Chapter 2](#)).

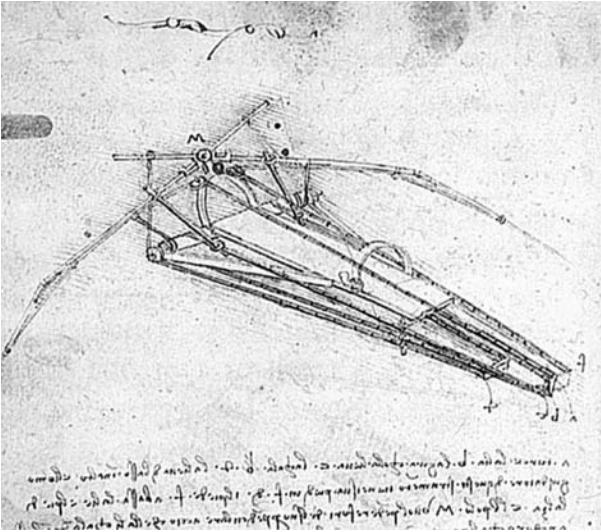


Figure 1.1. Da Vinci's flying machine

1.2 Brief Historical Background

This section provides a compressed tour of history, which I hope will motivate individuals to explore human aerial achievements in more detail. Many books cover the broad sweep of aeronautical history and many others depict particular cases such as famous people and their achievements in aeronautics ([1] is a good place to start). Innumerable Web sites on these topics exist; simply enter keywords such as *Airbus*, *Boeing*, or anything that piques your curiosity.

The desire to become airborne is ancient and it is reflected in our imagination and dreams. In the West, Daedalus and Icarus of Greek mythology were the first aviators; in the East, there are even more ancient myths – with no crashes. In Indian mythology, Pakshiraj is a white stallion with wings; the Greeks had a flying horse called Pegasus; and the Swedes also have flying horses. Garuda of Indonesia – half man and half bird – is another example from the Ramayana epic. Middle Eastern and South Asiatic “flying carpets” are seen in many Western cartoons and films. These contraptions are fully aerobatic with the ability to follow terrain; there are no seat belts and they can land inside rooms as well as on rooftops. Recreational possibilities and military applications abound!

Unfortunately, history is somewhat more “down to earth” than mythology, with early pioneers leaping from towers and cliffs, only to leave the Earth in a different but predictable manner because they underestimated the laws of nature. Our dreams and imagination became reality only about 100 years ago on December 17, 1903, with the first heavier-than-air flight by the Wright brothers. Yet, man first landed on the Moon about three decades ago, less than 70 years after the first powered flight.

The first scientific attempts to design a mechanism for aerial navigation were by Leonardo da Vinci (1452–1519) – he was the true grandfather of modern aviation, even if none of his machines ever defied gravity (Figure 1.1). He sketched many contraptions in his attempt to make a mechanical bird. However, birds possess such refined design features that the human path into the skies could not take that route; da Vinci's ideas contradicted the laws of nature.

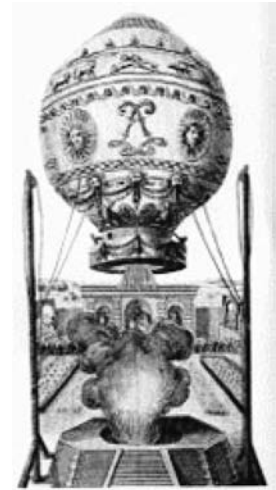


Figure 1.2. Montgolfier balloon

After da Vinci, and after an apparent lull for more than a century, the next prominent name is that of Sir Isaac Newton (1642–1727). Perhaps we lack the documentary evidence for I am convinced that human fascination with and endeavor for flight did not abate. Newton developed a theory of lift that although erroneous for low-speed flows, actually has some hypersonic application (although, of course, this was beyond his seventeenth-century understanding of fluid mechanics). Flight is essentially a practical matter, so real progress paralleled other industrial developments (e.g., isolating gas for buoyancy).

In 1783, de Rozier and d'Arlandes were the first to effectively defy gravity, using a Montgolfier (France) balloon (Figure 1.2). For the first time, it was possible to sustain and somewhat control altitude above the ground at will. However, these pioneers were subject to the prevailing wind direction and therefore were limited in their navigational options. To become airborne was an important landmark in human endeavor. The fact that the balloonists did not have wings does not diminish the importance of their achievement. The Montgolfier brothers (Joseph and Etienne) should be considered among the fathers of aviation. In 1784, Blanchard (France) added a hand-powered propeller to a balloon and was the first to make an aerial crossing of the English Channel on July 15, 1785. Jules Verne's fictional trip around the world in eighty days in a balloon became a reality when Steve Fossett circumnavigated the globe in fewer than fifteen days in 2002 – approximately three centuries after the first balloon circumnavigation.

In 1855, Joseph Pline was the first to use the word *aeroplane* in a paper he wrote proposing a gas-filled dirigible glider with a propeller.

Tethered kites flew in the Far East for a long time – in China, 600 B.C. However, in 1804, Englishman Sir George Cayley constructed and flew a kite-like glider (Figure 1.3) with movable control surfaces – the first record of a successful heavier-than-air controllable machine to stay freely airborne. In 1842, English engineer Samuel Henson secured a patent on an aircraft design that was driven by a steam engine.

With his brother Gustav, Otto Lilienthal was successfully flying gliders (Figure 1.4) in Berlin more than a decade (ca. 1890) before the Wright brothers' first

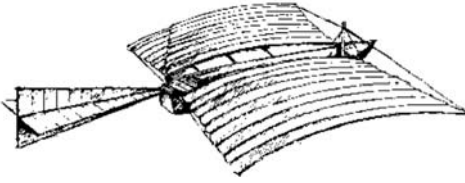


Figure 1.3. Cayley's kite glider

experiments. His flights were controlled but not sustained. The overestimation of the power requirement for sustained flight (based on work by Sir Isaac Newton, among others) may have discouraged the attempts of the best enginemakers of the time in Germany to build an aircraft engine – it would have been too heavy. Sadly, Lilienthal's aerial developments ended abruptly and his experience was lost when he died in a flying accident in 1896.

The question of who was the first to succeed naturally attracts a partisan spirit. The Wright Brothers (United States) are recognized as the first to achieve sustained, controlled flight of a heavier-than-air manned flying machine. Before discussing their achievement, however, some “also-rans” deserve mention (see various related Web sites). It is unfair not to credit John Stringfellow with the first powered flight of an unmanned heavier-than-air machine, made in 1848 in England. The Frenchman Ader also made a successful flight in his “Eole.” Gustav Weisskopf (Whitehead), a Bavarian who immigrated to the United States, claimed to have made a sustained, powered flight [2] on August 14, 1901, in Bridgeport, Connecticut. Karl Jatho of Germany made a 200-ft hop (longer than the Wright Brothers first flight) with a powered (10-HP Buchet engine) flight on August 18, 1903. At what distance a “hop” becomes a “flight” could be debated. Perhaps most significant are the efforts of Samuel P. Langley, who made three attempts to get his designs airborne with a pilot at the controls (Figure 1.5). His designs were aerodynamically superior to the Wright flyer, but the strategy to ensure pilot safety resulted in structural failure while catapulting from a ramp toward water. (A replica of Langley's aircraft was successfully flown from a conventional takeoff.) His model aircraft were flying successfully since 1902. The breaking of the aircraft also broke Professor Langley – a short time afterward, he died of a heart attack. The Wright Brothers were mere bicycle mechanics without any external funding, whereas Professor Langley was a highly qualified scientist whose project had substantial government funding.

The discussion inevitably turns to the Wright Brothers. Their aircraft (Figure 1.6) was inherently unstable but – good bicycle manufacturers that they were – they understood that stability could be sacrificed if sufficient control authority was maintained. They employed a foreplane for pitch control, which also served as a stall-prevention device – as today's Rutan-designed aircraft have demonstrated.

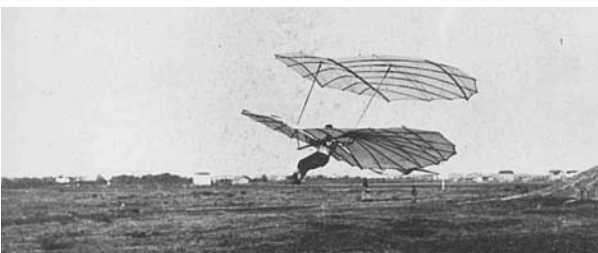
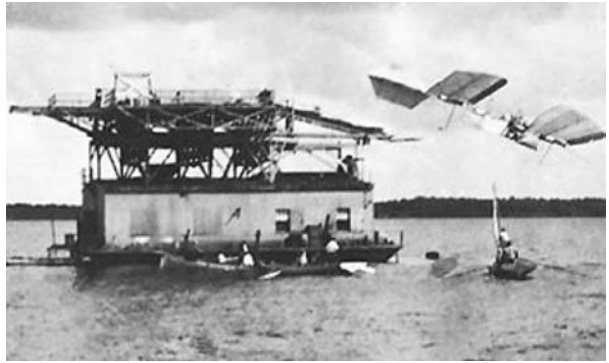


Figure 1.4. One of Lilienthal's gliders

Figure 1.5. Langley's catapult launch

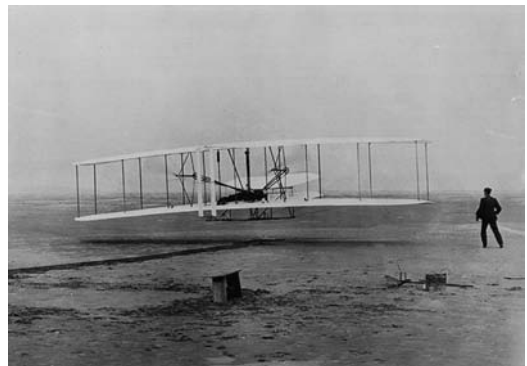


Exactly a century later, a flying replica model of the Wright flyer failed to lift off on its first flight. The success of the Wright Brothers was attributed to a freak gust of wind to assist the liftoff. A full-scale nonflying replica of the Wright flyer is on display at the Smithsonian Museum in Washington, DC, and the exhibit and others are well worth a trip.

Strangely, the Wright Brothers did not exploit their invention; however, having been shown that sustained and controlled flight was possible, a new generation of aerial entrepreneurs quickly arose. Newer inventions followed in succession by pioneering names such as Santos Dumas, Bleriot, and Curtis, and the list grew rapidly. Each inventor presented a new contraption, some of which demonstrated genuine design improvements. Fame, adventure, and "*Gefühl*" (feelings) were the drivers; the first few years barely demonstrated any financial gain except through "joy rides" and air shows – spectacles never seen before then and still just as appealing to the public now. It is interesting to observe the involvement of brothers from the eighteenth to the twentieth century – the Montgolfiers, du Temples, Lilienthas, and Wrights – perhaps they saw the future potential and wanted to keep progress confidential, and who can be better trusted than a brother?

It did not take long to demonstrate the advantages of aircraft, such as in mail delivery and military applications. At approximately 100 miles per hour (mph), on average, aircraft were traveling three times faster than any surface vehicle – and in straight lines. Mail was delivered in less than half the time. The potential for military applications was dramatic and well demonstrated during World War I. About a decade after the first flight in 1903, aircraft manufacturing had become a lucrative business. I am privileged to have started my own aeronautical engineering career

Figure 1.6. The Wright flyer



with Short Brothers and Harland (now part of the Bombardier Aerospace group), a company that started aircraft manufacturing by contracting to fabricate the Wright designs. The company is now the oldest surviving aircraft manufacturer still in operation. In 2008, it celebrated its centenary, the first aircraft company ever to do so.

The post-World War I aircraft industry geared up in defense applications and in civil aviation, with financial gain as the clear driver. The free-market economy of the West contributed much to aviation progress; its downside, possibly reflecting greed, was under-regulation. The proliferation showed signs of compromise with safety issues, and national regulatory agencies quickly stepped in, legislating for mandatory compliance with airworthiness requirements. Today, every nation has its own regulatory agency. The FAA in the United States and the Joint Aviation Authority (JAA) in Europe (recently renamed EASA) are the most recognized.

Early aircraft design was centered on available engines, and the size of the aircraft depended on the use of multiple engines. The predominant material used was wood. The combination of engines, materials, and aerodynamic technology enabled aircraft speeds of approximately 200 mph; altitude was limited by human physiology. Junker demonstrated the structural benefit of thick wing sections and metal construction. In the 1930s, Durener Metallwerke of Germany introduced *duralumin*, with higher strength-to-weight ratios of isotropic material properties, and dramatic increases in speed and altitude resulted. The introduction of metal brought a new dimension to manufacturing technology. Structure, aerodynamics, and engine development paved the way for substantial gains in speed, altitude, and maneuvering capabilities. These improvements were seen preeminently in World War II designs such as the Supermarine Spitfire, the North American P-51, the Focke Wolfe 190, and the Mitsubishi Jeero-Sen. Multiengine aircraft also grew to sizes never before seen.

The invention of the jet engine (independently by Whittle of the United Kingdom and von Ohain of Germany) realized the potential for unheard-of leaps in speed and altitude, resulting in parallel improvements in aerodynamics, materials, structures, and systems engineering. A better understanding of supersonic flow and a suitable rocket engine made it possible for Chuck Yeager to break the sound barrier in a Bell X1 in 1949. (The record-making aircraft is on exhibit at the Smithsonian Air and Space Museum in Washington, DC.)

Less glamorous multiengine heavy-lifters were slower in progress but with no less success. Tens of thousands of the Douglas C-47 Dakota and Boeing B17 Flying Fortress were produced. Postwar, the De Havilland Comet was the first commercial jet aircraft in service; however, plagued by several tragic crashes, it failed to become the financial success it promised. (The first Comet crash occurred at Dum Dum, near Calcutta, in 1952, in a monsoon storm. At that time, I lived about 12 miles from the crash site.)

The 1960s and 1970s saw rapid progress with many new commercial and military aircraft designs boasting ever-increasing speed, altitude, and payload capabilities. Scientists made considerable gains in understanding the relevant branches of nature: in aerodynamic [3] issues concerning high lift and transonic drag; in materials and metallurgy, improving the structural integrity; and in significant discoveries in solid-state physics. Engineers made good use of the new understanding. Some of the outstanding designs of those decades emerged from the Lockheed

Company, including the F104 Starfighter, the U2 high-altitude reconnaissance aircraft, and the SR71 Blackbird. These three aircraft, each holding a world record of some type, were designed in Lockheed's Skunk Works, located at the Los Angeles airport, under the supervision of Clarence (Kelly) Johnson, who graduated from the University of Michigan (my alma mater). I recommend that readers study the design of the nearly 40-year-old SR71, which still holds the speed–altitude record for aircraft powered by air-breathing engines.

During the late 1960s, the modular approach to gas turbine technology gave aircraft designers the opportunity to match aircraft requirements (i.e., mission specifications and economic considerations) with “rubberized” engines. This was an important departure from the 1920s and 1930s, when aircraft sizing was based around multiples of fixed-size engines. The core high-pressure gas turbine module could now be integrated with an appropriate low-pressure compressor, and turbine modules could offer designs with more than 50% thrust variation from the largest to the smallest in a family of derivatives. This advancement resulted in the development of families of aircraft design. Plugging the fuselage and, if necessary, allowing wing growth covered a wider market area at a lower development cost because considerable component commonality could be retained in a family: a cost-reduction design strategy – that is, “design one and get the other at half price.”

Rocket-powered aircraft first appeared during World War II. The advent and success of the Rutan-designed Space Ship One in 2004 (see [Figure 1.14](#)) to the fringes of the atmosphere will certainly bring about the large market potential of rocket-powered airplanes. Rocketry first entered the Western European experience when Tippu Sultan used rockets against the British-led Indian army at the Battle of Srirangapatnum in 1792. The propellants were based on a Chinese formula nearly a thousand years old. Many people are unaware that the experience of Tippu's rockets led the British to develop missiles at the Royal Laboratory of Woolwich Arsenal, under the supervision of Sir William Congreve, in the late eighteenth century. Von Braun [4] mentions that he took the idea from Tippu's success for his V2 rocket, paving the way for today's achievement in space flight as an expanded envelope beyond winged flight vehicles.

There was a time when designers could make sketches to generate candidate configurations, sometimes stretching to exotic “star-wars” shapes; gradually, however, creating ideas with a pencil has diminished. Capitalistic objectives render designers quite conservative, forcing them to devote considerably more time to analysis. The next section discusses why commercial aircraft designs are similar, with the exception of a few one-off, special-purpose vehicles. Military designs emerge from more extensive analysis – for example, the strange-looking Northrop F117 is configured using stealth features to minimize radar signature. Now, more matured stealth designs look conventional; however, some aircraft are still exotic (e.g., the Lockheed F22).

1.3 Current Aircraft Design Status

This section discusses the current status of forces and drivers that control design activities. It is followed by a review of civil and military aircraft design status. Readers are advised to search various Web sites on this topic.

1.3.1 Forces and Drivers

The current aircraft design strategy is linked to industrial growth, which in turn depends on national infrastructure, governmental policies, workforce capabilities, and natural resources; these are generally related to global economic–political circumstances. More than any other industry, the aerospace sector is linked to global trends. A survey of any newspaper provides examples of how civil aviation is affected by recession, fuel price increases, spread of infectious diseases, and international terrorism. In addition to its importance for national security, the military aircraft sector is a key element in several of the world’s largest economies. Indeed, aerospace activities must consider the national infrastructure as an entire system. A skilled labor force is an insufficient condition for success if there is no harmonization of activity with national policies; the elements of the system must progress in tandem. Because large companies affect regional health, they must share socio-economic responsibility for the region in which they are located. In the next two subsections, civil and military aircraft design status are discussed separately.

The current status stems from the 1980s when returns on investment in classical aeronautical technologies such as aerodynamics, propulsion, and structures began to diminish. Around this time, however, advances in microprocessors enabled the miniaturization of control systems and the development of microprocessor-based automatic controls (e.g., FBW), which also had an additional weight-saving benefit. Dramatic but less ostensive radical changes in aircraft management began to be embedded in design. At the same time, global political issues raised new concerns as economic inflation drove man-hour rates to a point at which cost-cutting measures became paramount. In the last three decades of the twentieth century, man-hour rates in the West rose four to six times (depending on the country), resulting in aircraft price hikes (e.g., typically by about six times for the Boeing 737) – accompanied, of course, by improvements in design and operational capabilities. Lack of economic viability resulted in the collapse or merger/takeover of many well-known aircraft manufacturers. The number of aircraft companies in Europe and North America shrunk by nearly three quarters; currently, only two aircraft companies (i.e., Boeing and Airbus in the West) are producing large commercial transport aircraft. Bombardier Aerospace has risen rapidly to the third largest in the West and recently entered the large-aircraft market with an aircraft capacity of more than 100 passengers. Embraer of Brazil has also entered in the market.

Over time, aircraft operating-cost terminologies have evolved and currently, the following are used in this book (Section 16.5 gives details).

IOC – Indirect Operating Cost: Consists of costs not directly involved with the sortie (trip)

COC – Cash Operating Cost: Consists of the trip (sortie) cost elements

FOC – Fixed Operating Cost: Consists of cost elements even when not flying

DOC – Direct Operating Cost: = COC + FOC

TOC – Total Operating Cost: = IOC + DOC

Because there are variances in definitions, this book uses these standardized definitions.

With rising fuel prices, air travelers have become cost-sensitive. In commercial aircraft operations, the DOC depends more on the acquisition cost (i.e., unit price) than on the fuel cost (2000 prices) consumed for the mission profile. Today, for the majority of mission profiles, fuel consumption constitutes between 15% and 25% of the DOC, whereas the aircraft unit price contributes between three and four times as much, depending on the payload range [5]. For this reason, manufacturing considerations that can lower the cost of aircraft production should receive as much attention as the aerodynamic saving of drag counts. The situation would change if the cost of fuel exceeds the current airfare sustainability limit (see [Section 1.7](#) and [Chapter 16](#)). The price of fuel in 2008 was approaching the limit when drag-reduction efforts were regaining ground.

A major concern that emerged in the commercial aircraft industry from the market trend and forecast analysis of the early 1990s was the effect of inflation on aircraft manufacturing costs. Airline operators conveyed to aircraft manufacturers that unless the acquisition cost was lowered by a substantial margin, growth in air-traffic volume would prove difficult. In addition to this stringent demand, there was fierce competition among aircraft manufacturers and their subcontractors. Since the mid-1990s, all major manufacturers have implemented cost-cutting measures, as have the subcontracting industries. It became clear that a customer-driven design strategy is the best approach for survival in a fiercely competitive marketplace. The paradigm of “better, farther, and cheaper to market” replaced, in a way, the old mantra of “higher, faster, and farther” [6]. Manufacturing considerations came to the forefront of design at the conceptual stage and new methodologies were developed, such as DFM/A and Six Sigma.

The importance of environmental issues emerged, forcing regulatory authorities to impose limits on noise and engine emission levels. Recent terrorist activities are forcing the industry and operators to consider preventive design features.

The conceptual phase of aircraft design is now conducted using a multidisciplinary approach (i.e., concurrent engineering), which must include manufacturing engineering and an appreciation for the cost implications of early decisions; the “buzzword” is integrated product and process development (IPPD). [Chapter 2](#) describes typical project phases as they are practiced currently. A chief designer’s role has changed from *telling* to *listening*; he or she synthesizes information and takes full command if and when differences of opinion arise. Margins of error have shrunk to the so-called zero tolerance so that tasks are done right the first time; the Six Sigma approach is one management tool used to achieve this end.

1.3.2 Current Civil Aircraft Design Trends

Current commercial transport aircraft in the 100- to 300-passenger classes all have a single slender fuselage, backward-swept low-mounted wings, two underslung wing-mounted engines, and a conventional *empennage* (i.e., a horizontal tail and a vertical tail); this conservative approach is revealed in the similarity of configuration. The similarity in larger aircraft is the two additional engines; there have been three-engine designs but they were rendered redundant by variant engine sizes that cover the in-between sizes and extended twin operations (ETOPS).



Figure 1.7. Boeing Sonic Cruiser

Boeing tried to break the pattern with a “Sonic Cruiser” (Figure 1.7) that proved, at best, to be a premature concept. Boeing returned with the Boeing 787 Dreamliner (Figure 1.8) as a replacement for its successful Boeing 767 and 777 series, aiming at competitive economic performance; however, the configuration remains conventional.

The last three decades witnessed a 5 to 6% average annual growth in air travel, exceeding 2×10^9 revenue passenger miles (rpms) per year. Publications by the International Civil Aviation Organization (ICAO), National Business Aviation Association (NBAA), and other journals provide overviews of civil aviation economics and management. The potential market for commercial aircraft sales is on the order of billions of dollars per year. However, the demand for air travel is cyclical and – given that it takes about 4 years from the introduction of a new aircraft design to market – operators must be cautious in their approach to new acquisitions: They do not want new aircraft to join their fleet during a downturn in the air-travel market. Needless to say, market analysis is important in planning new purchases. Chapter 2 briefly addresses market studies.

Deregulation of airfares has made airlines compete more fiercely in their quest for survival. The growth of budget airlines compared to the decline of established airlines is another challenge for operators. However, the reputation of an aircraft manufacturer significantly influences aircraft sales. When Boeing introduced its 737 twinjet aircraft (derived from the three-engine B727, the best seller at the time), the dominant-selling two-engine commercial transport aircraft were the Douglas DC-9 and BAe 111. I was employed at Boeing then and remember the efforts by engineers to improve the aircraft. The Boeing 737 series, spanning nearly four decades of production to this day, has become the best seller in the history of the commercial-aircraft market. Of course, in that time, considerable technological advancements



Figure 1.8. Boeing 787 Dreamliner

Figure 1.9. Airbus 380



have been incorporated, improving the B737's economic performance by about 50%.

The largest commercial jet transport aircraft, the Airbus 380 (Figure 1.9) made its first flight on April 27, 2005, and is currently in service. The heretofore unchallenged and successful Boeing 747, the largest commercial transport aircraft in operation today, now has a competitor.

The gas turbine turboprop offers better fuel economy than to current turbofan engines. However, because of propeller limitations, the turboprop-powered aircraft's cruise speed is limited to about two thirds of the high-speed subsonic turbofan-powered aircraft. For lower operational ranges (e.g., less than 1,000 nautical miles [nm]), the difference in sortie time would be on the order of less than a half hour, yet there is an approximate 20% saving in fuel cost. If a long-range time delay can be tolerated (e.g., for cargo or military heavy-lift logistics), then large turboprop aircraft operating over longer ranges become meaningful. Figure 1.10 shows an Antonov A70 turboprop aircraft.

1.3.3 Current Military Aircraft Design Trends

This extended section of the book can be found on the Web at www.cambridge.org/Kundu and gives a brief overview of today's military aircraft design trends, covering typical cost frame, operational roles, and design challenges. Figure 1.10 shows the Antonov A70. Figure 1.11 shows (a) F117 Nighthawk, (b) F22 Raptor, and B2 Bomber.

Figure 1.10. Antonov A70

Figure 1.11. Current combat aircraft

1.4 Future Trends

One does not have to be a prophet to predict near-future trends in the next two to three decades – the same time-frame during which younger readers will begin their career and prepare for the challenges required. It is clear that the vehicle-capability boundaries will be pushed to the extent permitted by economic and defense factors and infrastructure requirements (e.g., navigation, ground handling, and support, etc.). It is no exception from past trends that speed, altitude, and payload will be expanded in both civil and military capabilities. Reference [7] provides coverage on the aircraft-design process in the next few decades. In technology, smart



Figure 1.12. Supersonic transport aircraft

material (e.g., adaptive structure) will gain ground, microprocessor-based systems will advance to reduce weight and improve functionality, and manufacturing methodology will become digital. However, unless the price of fuel increases beyond affordability, investment in aerodynamic improvement will be next in priority.

Readers are advised to search various Web sites for information on this topic.

1.4.1 Civil Aircraft Design: Future Trends

The speed–altitude extension will progress initially through supersonic transport (SST) and then hypersonic transport (HST) vehicles. The SST technology is well proven by three decades of the Anglo-French–designed Concorde, which operated above Mach 2 at a 50,000-ft altitude carrying 128 passengers.

The next-generation SST will have about the same speed–altitude capability (possibly less in speed capability, around Mach 1.8), but the size will vary from as few as 10 business passengers to approximately 300 passengers to cover at least transatlantic and transcontinental operations. Transcontinental operations (Figure 1.12) would demand sonic-shock-strength reduction through aerodynamic gains rather than speed reduction; anything less than Mach 1.6 has less to offer in terms of time savings. The real challenge would be to have HST (Figure 1.13) operating at approximately Mach 6 that would require operational altitudes above 100,000 ft. Speed above Mach 6 offers diminishing returns in time saved because the longest distance necessary is only 12,000 nm (i.e., ≈ 3 hours of flight time). Military applications for HST vehicles are likely to precede civil applications.

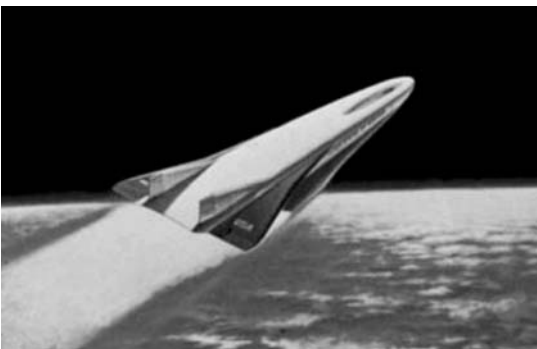


Figure 1.13. Hypersonic aircraft

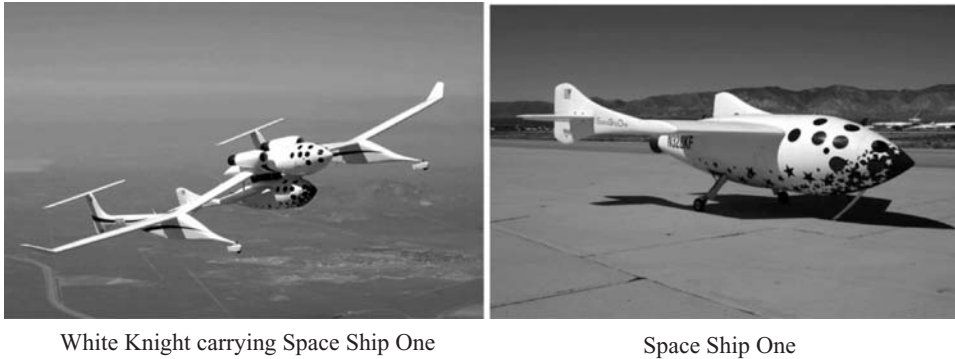


Figure 1.14. Rocket-powered aircraft

Considerable development in power plant technology is required to make either SST or HST commercially viable. Small-scale HST has been flown recently.

A new type of speed–altitude capability will come from suborbital space flight using rocket-powered aircraft, as demonstrated by Rutan’s Space Ship One that hitchhiked with the White Knight to altitude (Figure 1.14), from where it made the ascent. Interest in this aircraft has continued to grow – the prize of \$10 million offered could be compared with that of a transatlantic prize followed by commercial success. A larger Space Ship Two is currently being developed.

Any extension of payload capability will remain subsonic for the foreseeable future and will lie in the wake of gains made by higher-speed operational success. High-capacity operations will remain around the size of the Airbus 380. Further size increases will use the benefits of a blended wing body (BWB) because the wing-root thickness would be sufficient to permit merging (Figure 1.15) with the fuselage, thereby benefiting from the fuselage’s contribution to lift (see Section 3.20 for BWB configurational advantages). Another alternative would be that of the joined-wing concept (Figure 1.16). Studies of twin-fuselage, large transport aircraft also have shown potential.

Both operators and manufacturers will be alarmed if the price of fuel continues to rise to a point where the air transportation business finds it difficult to sustain operations. The industry would demand that power plants use alternative fuels such as biofuel, liquid hydrogen (LOH), and possibly nuclear power for large transport aircraft covering long ranges. Aircraft fueled by LOH have been used in experimental flying for some time, and fossil fuel mixed with biofuel is currently being flight-tested.

A new type of vehicle known as a ground-effect vehicle is a strong candidate for carrying a large payload (e.g., twice that of the Boeing 747) and flying close to the

Figure 1.15. Blended wing body aircraft (Airbus)





Figure 1.16. Joined-wing aircraft (Airbus)

surface, almost exclusively over water (Figure 1.17). (A ground-effect vehicle is not really new: The Russians built a similar vehicle called the “Ekranoplan,” but it did not appear in the free market economy.)

Smaller Bizjets and regional jets will morph, and unfamiliar shapes may appear on the horizon, but small aircraft in personal ownership used for utility and pleasure flying are likely to revolutionize the concept of flying through their popularity, similar to how the automobile sector grew. The revolution will occur in short-field capabilities, as well as vertical takeoffs, and safety issues in both design and operation. Smaller aircraft used for business purposes will see more private ownership to stay independent of the more cumbersome airline operations. There is a good potential for airparks to grow. The NASA, the U.S. Department of Transportation (USDOT), FAA, industry stakeholders, and academia have joined forces to pursue a National General Aviation Roadmap leading to a Small Aircraft Transportation System (SATS). This strategic undertaking has a 25-year goal to bring the next generation of technologies to and improve travel between remote communities and transportation centers in urban areas by utilizing the nation’s 5,400 public-use general-aviation airports (United States). The density of these airfields in Europe is much higher. The major changes would be in system architecture through miniaturization, automation, and safety issues for all types of aircraft.

1.4.2 Military Aircraft Design: Future Trends

This extended section of the book can be found on the Web at www.cambridge.org/Kundu and gives a brief overview of near-future military-aircraft design trends, covering typical, new, and emerging operational roles (e.g., UAVs and design challenges). Figures 1.18 and 1.19 are associated with the section.

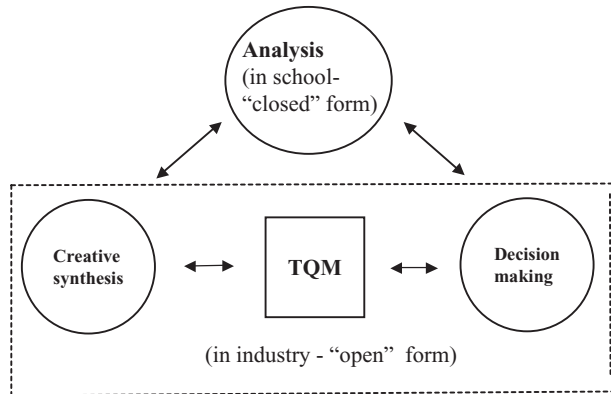
Figure 1.18. JUCAS prototypes (X47B)

Figure 1.19. Future design type



Figure 1.17. Pelican (Boeing)

Figure 1.20. Associative features of “closed-” and “open-” form education



1.5 Learning Process

To meet the objectives of offering close-to-industrial practice in this book, it is appropriate to reiterate and expand on remarks made in the preface about the recognized gap between academia and the industry. It is impertinent to explain the aircraft-design process before outlining the intended classroom learning process. The methodology suggested herein is the same as what I experienced in industry.

It is clear that unless an engineer has sufficient analytical ability, it will be impossible for him or her to convert creative ideas to a profitable product. Today’s innovators who have no analytical and practical skills must depend on engineers to accomplish routine tasks under professional investigation and analysis and to make necessary decisions to develop a marketable product.

Traditionally, universities develop analytical abilities by offering the fundamentals of engineering science. Courses are structured with all the material available in textbooks or notes; problem assignments are straightforward with unique answers. This may be termed a “closed-form” education. Closed-form problems are easy to grade and a teacher’s knowledge is not challenged (relatively). Conversely, industry requires the tackling of “open-form” problems for which there is no single answer. The best solution is the result of interdisciplinary interaction of concurrent engineering within design built teams (DBTs), in which Total Quality Management (TQM) is needed to introduce “customer-driven” products at the best value. Offering open-ended courses in design education that cover industrial requirements is more difficult and will challenge a teacher, especially when industrial experience is lacking. The associative features of closed- and open-form education are shown in Figure 1.20 ([9] and [10]).

To meet industry’s needs, newly graduated engineers need a brief transition before they can become productive, in line with the specialized tasks assigned to them. They must have a good grasp of the mathematics and engineering sciences necessary for analysis and sufficient experience for decision making. They must be capable of working under minimal supervision with the creative synthesis that comes from experience that academia cannot offer. The industrial environment will require new recruits to work in a team, with an appreciation of time, cost, and quality under TQM – which is quite different from classroom experience.

The purpose of my book is to provide in the coursework close-to-industry standard computations and engineering approaches sciences necessary for analysis and



Figure 1.21. Typical CAD drawing of Airbus A400

enough experience to work on a team. The level of mathematics in this book is not advanced but contains much technological information.

Here, I compare what can be achieved in about 36 hours of classroom lectures plus 60 hours by each of about 30 inexperienced students to what is accomplished by 20 experienced engineers each contributing 800 hours (≈ 6 months). Once the task was clearly defined shadowing industrial procedures, leaving out multiple iterations, I found that a reduced workload is possible in a classroom environment. It cuts down manhour content, especially when iterations are minimized to an acceptable level. My goal is to offer inexperienced students a powerful analytical capability without underestimating the importance of innovation and decision making.

For this reason, I emphasize that introductory classwork projects should be familiar to students so that they can relate to the examples and subsequently substantiate their work with an existing type. Working on an unfamiliar nonexistent design does not enhance the learning process at the introductory level.

Although it is not essential for the classwork, I highly recommend that modern conceptual aircraft designers be conversant with 3D modeling in CAD (Figure 1.21 is a CAD drawing example) (most recent graduates are). The 3D modeling provides fuller, more accurate shapes that are easy to modify, and it facilitates maintenance of sequential configurations – benefits that become evident as one starts to configure.

There are considerably more benefits from CAD (3D) solid modeling: It can be uploaded directly into CFD analysis to continue with aerodynamic estimations, as one of the first tasks is to estimate loading (CFD) for structural analysis using the FEM. The solid model offers accurate surface constraints for generating internal structural parts. CAD drawings can be uploaded directly to computer-aided manufacture (CAM) operations, ultimately leading to paperless design and manufacture offices (see Chapter 17). Today's conceptual aircraft designers must master many trades and specialize in at least one, not ignoring the state-of-the-art “rules of thumb” gained from past experience; there is no substitute. They need to be good “number-crunchers” with relatively good analytical ability. They also need assistance from an equally good support team to encompass wider areas. Vastly

increased computer power has reached the desktop with parallel processing. CAE (e.g., CAD, CAM, CFD, FEM, and systems analyses) is the accepted practice in the industry. Those who can afford supercomputers will have the capability to conduct research in areas hitherto not explored or facing limitations (e.g., high-end CFD, FEM, and multidisciplinary optimization [MDO]). This book is not about CAE; rather, it provides readers with the basics of aircraft design that are in practice in the industry and that would prepare them to use CAD/CAE.

Finally, I recommend that aircraft designers have some flying experience, which is most helpful in understanding the flying qualities of aircraft they are trying to design. Obtaining a license requires effort and financial resources, but even a few hours of planned flight experience would be instructive. One may plan and discuss with the flight instructor what needs to be demonstrated – that is, aircraft characteristics in response to control input, stalling, “g” force in steep maneuvers, stick forces, and so forth. Some universities offer a few hours of flight tests as an integral part of aeronautical engineering courses; however, I suggest even more: hands-on experience under the supervision of a flight instructor. A driver with a good knowledge of the design features has more appreciation for the automobile.

1.6 Units and Dimensions

The postwar dominance of British and American aeronautics has kept the use of the foot–pound–second (FPS) system current, despite the use of nondecimal fractions and the ambiguity of the word *pound* in referring to both mass and weight. The benefits of the system international (SI) are undeniable: a decimal system and a distinction between mass and weight. However, there being “nowt so queer as folk,” I am presented with an interesting situation in which both FPS and SI systems are used. Operational users prefer FPS (i.e., altitudes are “measured” in feet); however, scientists and engineers find SI more convenient. This is not a problem if one can become accustomed to the conversion factors. Appendix A provides an exhaustive conversion table that adequately covers the information in this book. However, readers will be relieved to know that in most cases, the text follows current international standards in notation units and the atmospheric table.

Aircraft performance is conducted at the International Standard Atmosphere (ISA) (see [Section 3.3](#)). References are given when design considerations must cater to performance degradation in a nonstandard day.

1.7 Cost Implications

Aircraft design strategy is constantly changing. Initially driven by the classical subjects of aerodynamics, structures, and propulsion, the industry is now customer-driven and design strategies consider the problems for manufacture and assembly that lead the way in reducing manufacturing costs. [Chapter 16](#) addressed cost considerations in detail. In summary, an aircraft designer must be cost-conscious now and even more so in future projects.

It is therefore important that a basic exercise on cost estimation (i.e., second-semester classwork) be included in the curriculum. A word of caution: Academic pursuit on cost analysis to find newer tools is still not amenable to industrial

use – manufacturers must rely on their own costing methodologies, which are not likely to appear in the public domain. How industry determines cost is sensitive information used to stay ahead in free-market competition.

I emphasize here that there is a significant difference between civil and military programs in predicting costs related to aircraft unit-price costing. The civil aircraft design has an international market with cash flowing back from revenues earned from fare-paying customers (i.e., passengers and freight) – a regenerative process that returns funds for growth and sustainability to enhance the national economy. Conversely, military aircraft design originates from a single customer demand for national defense and cannot depend on export potential – it does not have cash flowing back and it strains the national economy out of necessity. Civil aircraft designs share common support equipment and facilities, which appear as indirect operational costs (IOCs) and do not significantly load aircraft pricing. The driving cost parameter for civil aircraft design is the DOC, omitting the IOC component. Therefore, using a generic term of life cycle cost ($LCC = (DOC + IOC)$) in civil applications, it may be appropriate in context but would prove to be off the track for aircraft design engineers. Military design and operations incorporating discreet advances in technology necessarily have exclusive special support systems, equipment, and facilities. The vehicles must be maintained for operation-readiness around the clock. Part of the supply costs and support costs for aircraft maintenance must be borne by manufacturers that know best and are in a position to keep confidential the high-tech defense equipment. The role of a manufacturer is defined in the contractual agreement to support its product “from cradle to grave” – that is, the entire life cycle of the aircraft. Here, LCC is meaningful for aircraft designers in minimizing costs for the support system integral to the specific aircraft design. Commercial transports would have nearly five times more operating hours than military vehicles in peacetime (i.e., hope for the life of the aircraft). Military aircraft have relatively high operating costs even when they sit idle on the ground. Academic literature has not been able to address clearly the LCC issues in order to arrive at an applicable standardized costing methodology.

Aircraft design and manufacture are not driven by cost estimators and accountants; they are still driven by engineers. Unlike classical engineering sciences, costing is not based on natural laws; it is derived to some extent from manmade policies, which are rather volatile, being influenced by both national and international origins. The academic pursuit to arrest costing in knowledge-based algorithms may not prove readily amenable to industrial applications. However, the industry could benefit from the academic research to improve in-house tools based on actual data. I am pleased to present in this book a relevant, basic cost-modeling methodology [11] from an engineer’s perspective reflecting the industrial perspective so engineers may be aware of the labor content to minimize cost without sacrificing design integrity. The sooner that engineers include costing as an integral part of design, the better will be the competitive edge.

2 Methodology to Aircraft Design, Market Survey, and Airworthiness

2.1 Overview

This chapter is concerned with how aircraft design projects are managed in a company. It is recommended that newly initiated readers read through this chapter because it tackles an important part of the work – that is, to generate customer specifications so that an aircraft configuration has the potential to succeed. A small part of the coursework starts in this chapter. The road to success has a formal step-by-step approach through phases of activities and must be managed.

The go-ahead for a program comes after careful assessment of the design with a finalized aircraft configuration having evolved during the conceptual study (i.e., Phase 1). The prediction accuracy at the end of Phase 1 must be within at least $\pm 5\%$. In Phase 2 of the project, when more financing is available after obtaining the go-ahead, the aircraft design is fine-tuned through testing and more refined analysis. This is a time- and cost-consuming effort, with prediction accuracy now at less than ± 2 to $\pm 3\%$, offering guarantees to potential buyers. This book does not address project-definition activities (i.e., Phase 2); these are in-depth studies conducted by specialists and offered in specialized courses such as CFD, FEM, Simulink, and CAM.

This book is concerned with the task involved in the conceptual design phase but without rigorous optimization. Civil aircraft design lies within a verified design space; that is, it is a study within an achievable level of proven but leading-edge technology involving routine development efforts. Conversely, military aircraft design lies within an aspirational design space; that is, it is a study of unproven advanced technology requiring extensive development efforts. Obviously, the latter is technologically more complex, challenging, and difficult. Generally, the go-ahead for a project is preceded by a demonstration of the technology to prove the concept.

Jane's All the World's Aircraft Manual [1] is an indispensable source of aircraft statistics vital for any aircraft-design work. The following three magazines are also highly recommended resources:

- *Flight International* [2]. A weekly publication from the United Kingdom. It is a newsletter-type journal, providing the latest brief coverage of aerospace activities around the world.

- *Aviation Week and Space Technology* [3]. A weekly publication from the United States that provides more in-depth analysis of aerospace developments and thoroughly covers the U.S. scenario as well as worldwide coverage.
- *Interavia* [4]. A bimonthly publication that covers aerospace news, specializing in topics of interest in an essay format. The commercial airline business is well covered.

2.1.1 What Is to Be Learned?

This chapter covers the following topics:

- Section 2.2: Chapter introduction
- Section 2.3: Management concept of aircraft design process in the industry; describes project phases and systems approach to design, including management in phases, a typical work schedule, resource deployment, and the time frame involved
- Section 2.4: Task breakdown in each phase and functional activities, highlighting the conceptual study phase
- Section 2.5: Aircraft familiarization (civil and military); indispensable information about various aircraft components
- Section 2.6: Market survey (civil and military); coursework begins with a mock market survey to generate customer specifications (i.e., requirements)
- Section 2.7: Typical civil aircraft design specifications
- Section 2.8: Typical military aircraft design specifications
- Section 2.9: Comparison between civil and military designs
- Section 2.10: Airworthiness requirements, mandatory requirements for aircraft design and configuration
- Section 2.11: Coursework procedures

2.1.2 Coursework Content

With guidance from the instructor, students conduct a mock market survey. Students generate a bar chart (i.e., Gantt) to monitor progress during the semester. The remainder of the chapter is recommended easy reading. The coursework activity begins in Section 2.6 with a mock market survey to generate aircraft specifications and requirements and helps students understand its importance in the success or failure of a product.

2.2 Introduction

Existing aircraft indicate how the market is served and should indicate what is needed for the future. Various aircraft have been designed, and new designs should perform better than any existing designs. Designers are obligated to search for proven advanced technologies that emerge. There could be more than one option so the design team must conduct trade-off studies to arrive at a “satisfying” design that will satisfy the customer. Economy and safety are possibly the strongest drivers

in commercial transport. Aircraft design drivers for combat are performance capability and survivability (i.e., safety).

Despite organizational differences that exist among countries, one thing is common to all: namely, the constraint that the product must be “fit for the purpose.” It is interesting to observe that organizational structures in the East and the West are beginning to converge in their approach to aircraft design. The West is replacing its vertically integrated setup with a major investor master company in the integrating role along with risk-sharing partners. Since the fall of communism in Eastern Europe, the socialist bloc is also moving away from specialist activities to an integrated environment with risk-sharing partners. Stringent accountability has led the West to move away from vertical integration – in which the design and manufacture of every component were done under one roof – to outsourcing design packages to specialist companies. The change was inevitable – and it has resulted in better products and profitability, despite increased logistical activities.

The aircraft design process is now set in rigorous methodology, and there is considerable caution in the approach due to the high level of investment required. The process is substantially front-loaded, even before the project go-ahead is given. In this chapter, generic and typical aircraft design phases are described as practiced in the industry, which includes market surveys and airworthiness requirements. A product must comply with regulatory requirements, whether in civil or military applications. New designers must realize from the beginning the importance of meeting mandatory design requirements imposed by the certifying authorities.

Exceeding budgetary provisions is not uncommon. Military aircraft projects undergo significant technical challenges to meet time and cost frames; in addition, there could be other constraints. (The “gestation” period of the Eurofighter project has taken nearly two decades. An even more extreme example is the Indian Light Combat Aircraft, which spanned nearly three decades and is yet to be operational; the original specifications already may be obsolete.) Some fighter aircraft projects have been canceled after the prototype aircraft was built (e.g., the Northrop F20 Tigershark and the BAC TSR2). A good design organization must have the courage to abandon concepts that are outdated and mediocre. The design of combat aircraft cannot be compromised because of national pride; rather, a nation can learn from mistakes and then progress step-by-step to a better future.

2.3 Typical Design Process

The typical aircraft design process follows the classical systems approach pattern. The official definition of *system*, adopted by the International Council of Systems Engineering (INCOSE) [5] is: “A system is an interacting combination of elements, viewed in relation to function.” The design system has an input (i.e., a specification or requirement) that undergoes a process (i.e., phases of design) to obtain an output (i.e., certified design through substantiated aircraft performance), as shown in Figure 2.1.

As subsystems, the components of an aircraft are interdependent in a multidisciplinary environment, even if they have the ability to function on their own (e.g., wing-flap deployment on the ground is inert whereas in flight, it affects vehicle motion). Individual components such as the wings, nacelle, undercarriage, fuel

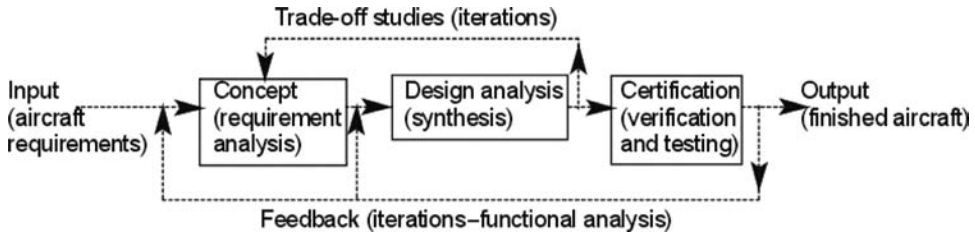


Figure 2.1. Aircraft design process (see Chart 2.1)

system, and air-conditioning also can be viewed as subsystems. Components are supplied for structural and system testing in conformance with airworthiness requirements in practice. Close contact is maintained with the planning engineering department to ensure that production costs are minimized, the schedule is maintained, and build tolerances are consistent with design requirements.

Chart 2.1 suggests a generalized functional envelope of aircraft design architecture, which is in line with the Aircraft Transport Association (ATA) index [6] for commercial transport aircraft. Further descriptions of subsystems are provided in subsequent chapters.

Extensive wind-tunnel, structure, and systems testing is required early in the design cycle to ensure that safe flight tests result in airworthiness certification approval. The multidisciplinary systems approach to aircraft design is carried out within the context of IPPD. Four phases comprise the generic methodology (discussed in the next section) for a new aircraft to be conceived, designed, built, and certified.

Civil aircraft projects usually proceed to preproduction aircraft that will be flight-tested and sold, whereas military aircraft projects proceed with technical demonstrations of prototypes before the go-ahead is given. The prototypes are typically scaled-down aircraft meant to substantiate cutting-edge technologies and are not sold for operational use.

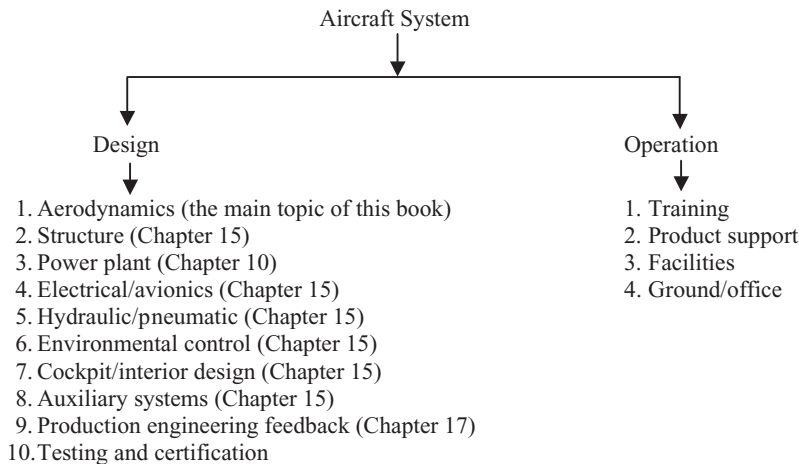


Chart 2.1. Aircraft system

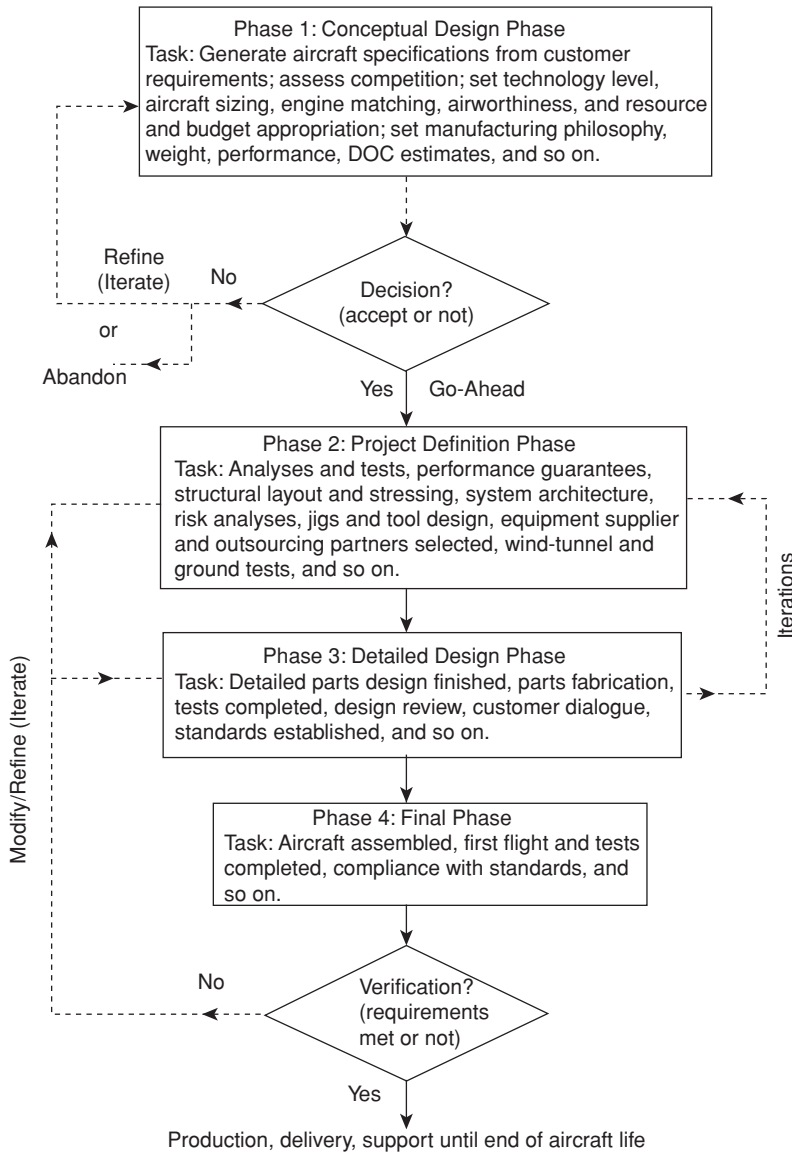


Chart 2.2. Four phases of aircraft design and development process

2.3.1 Four Phases of Aircraft Design

Aircraft manufacturers conduct year-round exploratory work on research, design, and technology development as well as market analysis to search for a product. A new project is formally initiated in the four phases shown in Chart 2.2, which is applicable for both civil and military projects. (A new employee should be able to sense the pulse of organizational strategies as soon joining a company.)

Among organizations, the terminology of the phases varies. Chart 2.2 offers a typical, generic pattern prevailing in the industry. The differences among terminologies are trivial because the task breakdown covered in various phases is

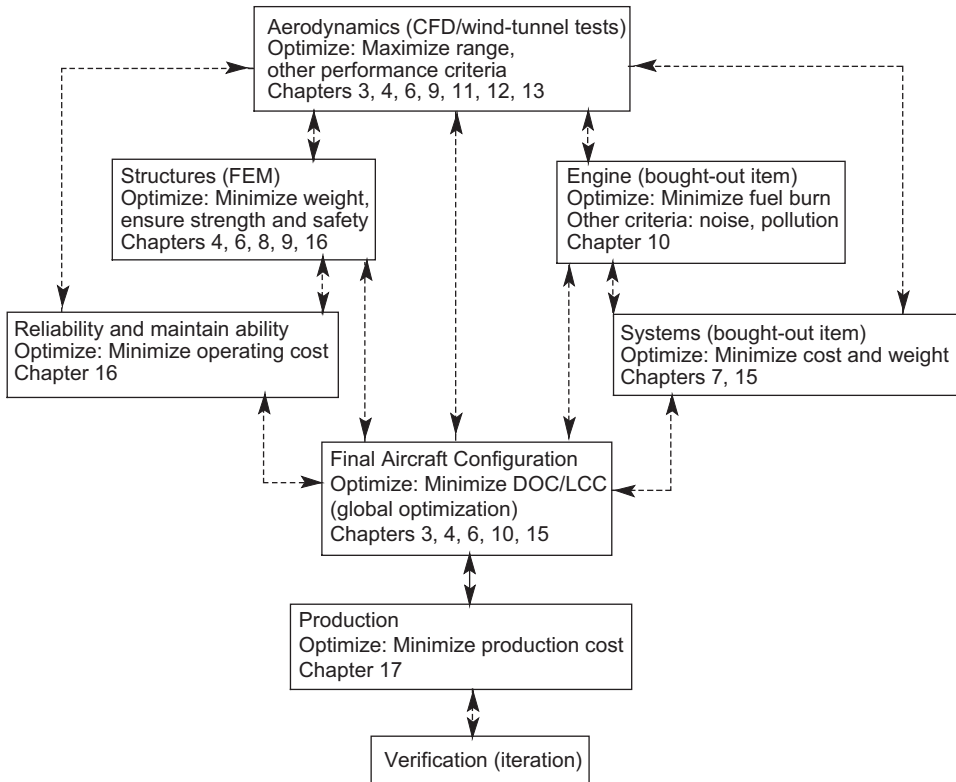


Chart 2.3. MDA and MDO flowchart

approximately the same. For example, some may call the market study and specifications and requirements Phase 1, with the conceptual study as Phase 2; others may define the project definition phase (Phase 2) and detailed design phase (Phase 3) as the preliminary design and full-scale development phases, respectively. Some prefer to invest early in the risk analysis in Phase 1; however, it could be accomplished in Phase 2 when the design is better defined, thereby saving the Phase 1 budgetary provisions in case the project fails to obtain the go-ahead. A military program may require early risk analysis because it would be incorporating technologies not yet proven in operation. Some may define disposal of aircraft at the end as a design phase of a project. Some companies may delay the go-ahead until more information is available, and some Phase 2 tasks (e.g., risk analysis) may be carried out as a Phase 1 task to obtain the go-ahead.

Company management establishes a DBT to meet at regular intervals to conduct design reviews and make decisions on the best compromises through multidisciplinary analysis (MDA) and MDO, as shown in [Chart 2.3](#); this is what is meant by an IPPD (i.e., concurrent engineering) environment.

Specialist areas may optimize design goals, but in an IPPD environment, compromise must be sought. It is emphasized frequently that optimization of individual goals through separate design considerations may prove counterproductive and usually prevents the overall (i.e., global) optimization of ownership cost. MDO offers

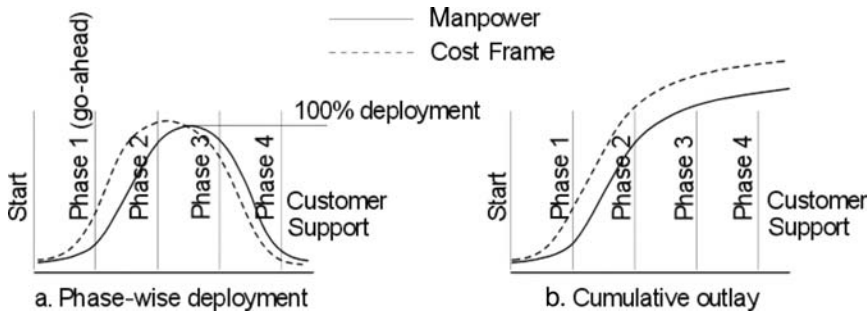


Figure 2.2. Resource deployments (manpower and finance)

good potential but it is not easy to obtain global optimization; it is still evolving. In a way, global MDO involving many variables is still an academic pursuit. Industries are in a position to use sophisticated algorithms in some proven areas. An example is reducing manufacturing costs by reshaping component geometry as a compromise – such as minimizing complex component curvature. The compromises are evident in offering a family of variant aircraft because none of the individuals in the family is optimized, whereas together, they offer the best value.

When an aircraft has been delivered to the operators (i.e., customers), a manufacturer is not free from obligation. Manufacturers continue to provide support with maintenance, design improvements, and attention to operational queries until the end of an aircraft's life. Modern designs are expected to last for three to four decades of operation. Manufacturers may even face litigation if customers find cause to sue. Compensation payments have crippled some well-known general aviation companies. Fortunately, the 1990s saw a relaxation of litigation laws in general aviation – for a certain period after a design is established, a manufacturer's liabilities are reduced – which resulted in a revitalization of the general aviation market. Military programs involve support from “cradle to grave” (see Section 1.7.)

This emphasizes that the product must be done right the first time. Midcourse changes add unnecessary costs that could be detrimental to a project – a major change may not prove sustainable. Procedural methodologies such as the Six Sigma approach have been devised to ensure that changes are minimized.

2.3.2 Typical Resources Deployment

All phases do not work under uniform manpower-loading; naturally, Phase 1 starts with light manpower during the conceptual study and reaches peak manpower (100%) at Phase 3; it decreases again when flight testing starts, by which stage the design work is virtually done and support work continues. Figure 2.2a is a typical distribution of cost and manpower loading (an average percentage is shown); the manpower-loading forecast must be finalized during the Phase 1 study. Figure 2.2b shows the cumulative deployment. At the end of a project, it is expected that the actual figure should be close to the projected figure. Project costs consist primarily of salaries (most of the cost), bought-out items, and relatively smaller miscellaneous amounts (e.g., advertising, travel, and logistics). Chain lines in Figure 2.2 illustrate the cost-frame outlay.

Table 2.1. *Development costs up to certification included*

Aircraft class (turbofan)	Development cost (US\$*)	Unit cost (US\$*)
6-passenger general aviation aircraft	6 to 10 million	≈1 to 2 million
10-passenger business aircraft	20 to 40 million	5 to 8 million
50-passenger regional aircraft	50 to 100 million	20 to 30 million
150-passenger midsized aircraft	200 to 500 million	40 to 50 million
500+ –passenger large aircraft	2 to 10 billion?	140 to 200 million
Military combat aircraft (high end)	5 to 15 billion?	100+ million?

*Does not include production launch cost. Typical cost at 2000 level.

2.3.3 Typical Cost Frame

A crude development cost up to certification (in year 2000 U.S. Dollars) is shown in Table 2.1. Typical unit aircraft costs by class are also given (there is variation among companies). A substantial part of the budget is committed to Phase 1.

2.3.4 Typical Time Frame

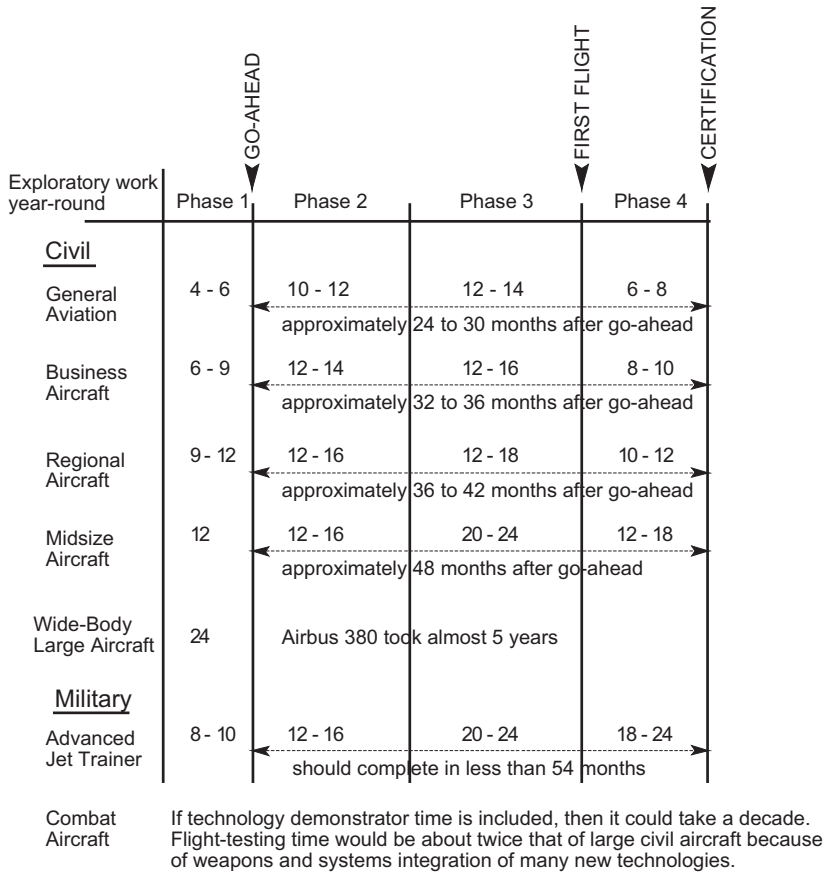
Typical time frames for the phases of different types of projects are shown in Chart 2.4. All figures are the approximate number of months. Exploratory work continues year-round to examine the viability of incorporating new technologies and to push the boundaries of company capabilities – which is implied rather than explicit in Chart 2.4.

2.4 Typical Task Breakdown in Each Phase

Typical task obligations in each phase of civil aircraft design are defined in this section. Military aircraft designs follow the same pattern but more rigorously. Military aircraft must deal with new technologies, which could still require operational proving; therefore, there is uncertainty involved in military aircraft projects.

Phase 1: Conceptual Study Phase (Feasibility Study)

Much of the work in the conceptual study phase can be streamlined through a good market study to identify a product line within a company’s capabilities. In this phase, findings of the market study are developed with candidate configurations; the technology to be adopted is firmed up and the economic viability is finalized. This is accomplished through aircraft sizing, engine matching, preliminary weight estimation, and evolution of a family of aircraft with payload and range combinations (i.e., aircraft performance) for all configurations. Planning portfolios with budgetary provisions, manpower requirements, progress milestones, potential subcontract/risk-sharing partners’ inputs, and so forth are included as the starting point of the design process. In general, at the end of this phase, management decision for a go-ahead is expected with a final configuration selected from the candidate configurations offered. Continuous interaction with potential customers (i.e., operators and subcontractors) occurs during this phase, with the objective of arriving at a family of aircraft as the most “satisfying” design with compromises rather than an



Military aircraft projects have large variations.

Chart 2.4. Typical project time frame

“optimum” solution. Management may request a level of detail (e.g., risk analysis) that could extend the study phase or flow into the next phase, thereby delaying the go-ahead decision to the early part of Phase 2. This is likely if the candidate aircraft configurations are short-listed instead of finalized. For those designers who have planned ahead, Phase 1 should finish early – especially if they are well versed in the product type and have other successful designs in their experience.

Phase 2: Project Definition Phase (Preliminary Design)

This phase begins after the go-ahead has been given to a project, and a “point of no-return” is reached during this phase. Project definition sometimes may overlap with the detailed design phase (i.e., Phase 3). During the advanced design phase, the project moves toward a finer definition, with a guarantee that the aircraft capabilities will meet if not exceed the specifications. Some iteration invariably takes place to fine-tune the product. Details of the technology level to be used and manufacturing planning are essential, and partnership outsourcing is initiated in this phase. Procurement cost reviews and updates also are ongoing to ensure that project viability is maintained. Many fine aircraft projects have been stalled for lack of proper

planning and financial risk management. (Readers may study recent case histories of products such as the Swearingen SJ30 [now certified and under production] and the Fairchild–Dornier 928.) The beginning of metal cutting and parts fabrication as well as deliveries of bought-out items (e.g., engine and avionics) must be completed in Phase 2. In this phase, extensive wind-tunnel testing, CFD analysis, detailed weights estimation, detailed structural layout and FEM analysis, system definitions, production planning, and so forth are carried out.

Phase 3: Detailed Design Phase (Full-Scale Product Development)

In this phase, manufacturers push toward completion – when peak manpower is deployed for the project. Normally, projects cannot sustain delay – time is money. All aspects of detailed design and systems architecture testing are completed in this phase. (The test rig is called an “iron bird” – it simulates full-scale control and system performance.) At the end of Phase 3, the aircraft assembly should near, if not achieve, completion.

Phase 4: Final Phase (Certification)

Phase 4 must start with the rapid completion of the aircraft assembly for ground-testing of installed systems and other mandatory structural strength-testing to prepare for flight-testing. In general, two to four aircraft are needed to complete nearly 200 to 800 flight-testing sorties (depending on the type of aircraft) toward substantiation for certification of the airworthiness standard. At this stage, there should be no major setbacks because the engineers have learned and practiced aircraft design well with minimal errors.

Each project has a characteristic timeline; – this book uses a 4-year project time. Remember, however, that some projects have taken more or less time. Section 2.4.2 is a detailed breakdown of a small aircraft project for a small or medium company. The author recommends that similar detailed milestone charts be drawn for course-work projects to give an idea of the manpower requirements.

2.4.1 Functional Tasks during the Conceptual Study (Phase 1: Civil Aircraft)

Because this book is concerned only with Phase 1, it is important to delineate functional task obligations assigned to individual designers – also known as top-level definition. Market specifications should first be delineated to develop task content, as shown in [Chart 2.5](#) for the mission profile. Payload determines the fuselage size and shape and leads into undercarriage design, depending on wing and engine positioning. Wing design largely determines the range, operational envelope, and field-performance objectives. Considering all requirements together, the aircraft configuration evolves: There can be more than one candidate configuration (e.g., high or low wing, nacelle location, and empennage arrangement).

Aircraft configuration starts with the fuselage layout followed by the steps worked out in this book. The military aircraft design approach is not significantly different except that the payload is armament, which is generally underslung or kept inside the fuselage bay.

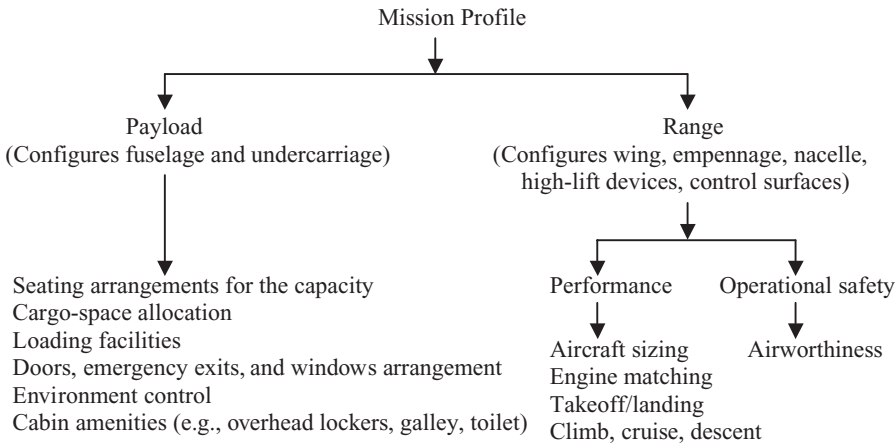


Chart 2.5. Top-level definition (Phase 1, Conceptual Study)

Chart 2.5 can be divided into functional work group activity to focus attention on specific areas – necessarily in IPPD environment for MDA. Other chapters of this book address specific work group activity.

2.4.2 Project Activities for Small Aircraft Design

Typical work content and milestones for a small aircraft project are given here in blocks of time; readers need to expand this in bar chart form (the coursework involved in drawing the Gantt chart may alter the contents of the table, as required). Larger-aircraft design follows similar activities in an expanded scale suited to task obligations.

Phase 1: Conceptual Design (6 Months)

1. Perform the market survey to establish aircraft specifications from customer requirements; information is extracted from year-round exploratory work.
2. Lay out candidate aircraft configurations starting with fuselage, followed by wing, undercarriage, power plant, and so forth.
3. Establish wing parameters because they will acquire prime importance in synthesizing aircraft design; the parameters include the wing reference area, aspect ratio, wing sweep, taper ratio, aerofoil thickness-to-chord ratio, wing twist, spar location, flap area, flight control, and wing location with respect to fuselage.
4. Initiate CAD 3D surface modeling.
5. Conduct preliminary CFD analysis to establish pressure distribution and loads on aircraft.
6. Conduct preliminary wind-tunnel tests.
7. Determine preliminary weights and CG estimates.
8. Determine aircraft preliminary drag estimate.
9. Size aircraft and match engine.
10. Establish engine data.
11. Conduct preliminary aircraft and engine performance tests.

12. Freeze the configuration to one aircraft.
13. Lay out internal structures and arrange fuselage interior.
14. Complete mock-up drawings, construction, and initial evaluation.
15. Complete the control system concept layout in CAD.
16. Complete the electrical/avionics systems concept layout in CAD.
17. Complete the mechanical systems concept layout in CAD.
18. Complete the power plant installation concept in CAD.
19. Create a database for materials and parts.
20. Establish a plan for bought-out items and delivery schedule.
21. Plan for outsourcing, if applicable.
22. Provide the preliminary cost projection.
23. Obtain management's go-ahead.

Phase 2: Project Definition (9 Months)

1. Create integrated and component drawings in CAD.
2. Complete FEM stress analysis of all components (e.g., wing and fuselage).
3. Complete mock-up and final assessment.
4. Complete advanced CFD analysis.
5. Conduct wind-tunnel model testing and CFD substantiation.
6. Conduct flutter analysis.
7. Conduct extensive and final aircraft and engine performance tests.
8. Create detailed part design and issue manufacturing/production drawings in CAD. This follows stress analyses of parts.
9. Perform aircraft stability and control analysis and control-surface sizing.
10. Finalize control system design in CAD.
11. Finalize electrical/avionics system design in CAD.
12. Finalize mechanical system design in CAD.
13. Finalize power plant installation design in CAD.
14. Produce jigs and tool design.
15. Plan for subcontracting, if applicable.
16. Place order for bought-out items and start receiving items.
17. Complete cost analysis.
18. Complete design review.
19. Continue customer dialogue and updating (no change in specifications).

Phase 3: Detailed Design (Product Development) (12 Months)

1. Complete detailed component design in CAD.
2. Complete stress analysis.
3. Complete CFD analysis.
4. Revise to final weights analysis.
5. Complete and issue all production drawings in CAD/CAM.
6. Complete production jigs and tools.
7. Complete parts manufacture and begin aircraft component subassembly.
8. Finish receiving all bought-out items.
9. Complete standards, schedules, and checklists.

10. Finalize ground/flight test schedules.
11. Complete prototype shop status schedules.
12. Revise cost analysis.
13. Begin ground tests.
14. Complete design review.
15. Continue customer dialogue and updating (no change in specifications).

Phase 4: Testing and Certification (9 Months)

1. Complete final assembly and prototype equipping.
2. Complete ground and flight tests and analysis.
3. Review analysis and modify design, if required.
4. Complete overall design review.
5. Review cost estimate.
6. Complete customer dialogue and sales arrangement.
7. Continue design review and support.

Production launch costs are typically kept separate from design and development costs. Total time to complete a project is 3 years (i.e., 2.5 years from the go-ahead), which is tight but feasible.

2.5 Aircraft Familiarization

This section introduces generic civil and military aircraft. Geometric definitions relevant to aerodynamic considerations are addressed in [Chapter 3](#) and detailed descriptions of various types of aircraft and their classification are provided in [Chapter 4](#). A diagram of aircraft with major subassemblies as components is provided herein. Indeed, aircraft design has become highly modular in the interests of the “family” concept, which facilitates low development cost by maintaining a high degree of parts commonality.

Aircraft span, length, and height are currently restricted by the ICAO to 80 m, 80 m, and 80 ft, respectively, for ground handling and storage considerations. The height is in feet but the span and length are in meters; this restriction may change. Section 1.6 highlighted the mix of SI and FPS units in aerospace engineering. In the future, only SI units will be used.

2.5.1 Civil Aircraft and Its Component Configurations

In general, the civil aircraft category includes five types: (1) small club trainers, (2) utility aircraft, (3) business aircraft, (4) narrow-body commercial transporters (regional aircraft to midsize), and (5) wide-body large transporters. The various types of available configuration options are described in [Chapter 4](#). The aircraft components shown in [Figure 2.3](#) are some of the obvious ones (e.g., wing, fuselage, nacelle, and empennage); others (e.g., winglets, strakes, and auxiliary control surfaces) are less obvious but play vital roles – otherwise, they would not be included. Because there are many options, components are associated in groups for convenience, as described in the following subsections (refer to [Figure 2.3](#)).

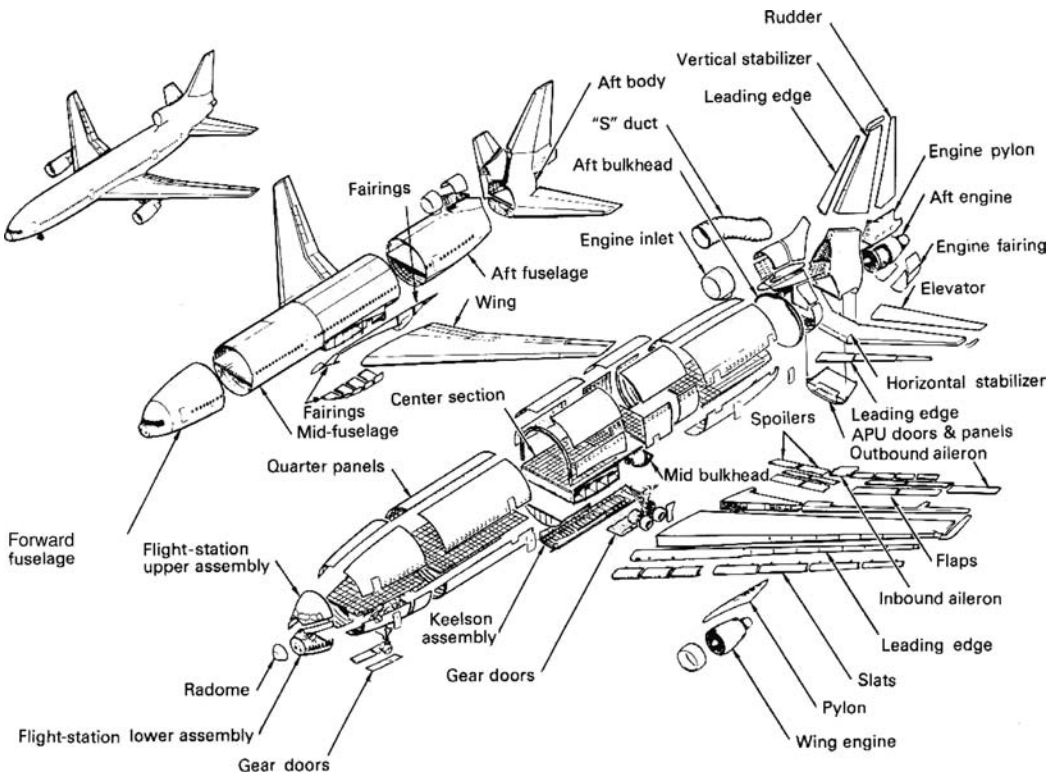


Figure 2.3. Lockheed 1011 diagram (courtesy of Michael Niu [10])

Fuselage Group

This group includes the nose cone, the constant midsection fuselage, the tapered aft fuselage, and the tail cone. The fuselage belly fairing (shown in Figure 2.3 as several subassembly components below the fuselage) may be used to house equipment at the wing–fuselage junction, such as the undercarriage wheels.

Wing Group

This group consists of the main wing, high-lift devices, spoilers, control surfaces, tip devices, and structural wing box that passes through the fuselage. High-lift devices include leading-edge slats or trailing-edge flaps. In Figure 2.3, the leading-edge slats are shown attached to the main wing and the trailing-edge flaps and spoilers are shown detached from the port wing. Spoilers are used to decelerate aircraft on descent; as the name suggests, they “spoil” lift over the wing and are useful as “lift dumpers” on touchdown. This allows the undercarriage to more rapidly absorb the aircraft’s weight, enabling a more effective application of the brakes. In some aircraft, a small differential deflection of spoilers with or without the use of ailerons is used to stabilize an aircraft’s rolling tendencies during disturbances. In Figure 2.3, the wing is shown with winglets at the tip; winglets are one of a set of tip treatments that can reduce the induced drag of an aircraft.

Empennage Group

The empennage is the set of stability and control surfaces at the back of an aircraft. In Figure 2.3, it is shown as a vertical tail split into a fin in the front and a rudder at

the back, with an end cap on the top. The horizontal tail, shown as a T-tail set at the top of the vertical tail, consists of the stabilizer and the elevator. Canard configuration has ‘tail’ in front.

Nacelle Group

Podded nacelles are slung under the wings and one is mounted on the aft fuselage; pylons affect the attachment. Engines can be mounted on each side of the fuselage. The nacelle design is discussed in detail in [Chapter 10](#). Turbofans are preferred for higher subsonic speed.

Undercarriage Group

The undercarriage, or landing gear, usually consists of a nose-wheel assembly and two sets of main wheels that form a tricycle configuration. Tail-dragging, bicycle, and even quad configurations are possible, depending on the application of an aircraft. Wheels are usually retracted in flight, and the retraction mechanism and stowage bay comprise part of the undercarriage group. Undercarriage design is discussed in [Chapter 7](#).

Not shown in [Figure 2.3](#) are the trimming surfaces used to reduce control forces experienced by the pilot. During the conceptual phase, these surfaces generally are shown schematically, with size based on past experience. The sizing of trim surfaces is more appropriate once the aircraft configuration is frozen (i.e., a Phase 2 activity). Trim-surface sizing is accomplished by using semi-empirical relations and is fine-tuned by tailoring the surfaces and areas or adjusting the mechanism during flight trials. In this book, trim surfaces are treated schematically – the main task is to size the aircraft and finalize the configuration in Phase 1. On larger aircraft, powered controls are used; pitch trimmings in conjunction with moving tail planes. A propeller-driven aircraft is preferred for cruise speeds below Mach 0.5.

2.5.2 Military Aircraft and Its Component Configurations

This extended section of the book can be found on the Web at www.cambridge.org/Kundu and depicts typical military aircraft components, with [Figure 2.4](#) depicting an exploded view of an F16-type aircraft configuration.

Figure 2.4. Military aircraft configuration

Figure 2.5. A diagram of the General Dynamics (now Boeing) F16

2.6 Market Survey

In a free market economy, an industry cannot survive unless it grows; in a civil-market economy, governmental sustenance is only a temporary relief. The starting point to initiate a new aircraft design project is to establish the key drivers – that is, the requirements and objectives based on market, technical, certification, and organizational requirements. These key drivers are systematically analyzed and then documented by aircraft manufacturers ([Chart 2.6](#)).

In several volumes, documents that describe details of the next tier of design specifications (i.e., requirements) are issued to those organizations involved with

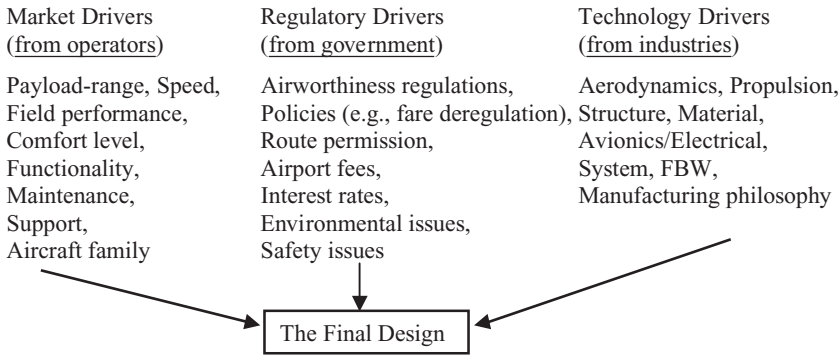


Chart 2.6. The design drivers (in a free market economy, it faces competition)

a project. A market survey is one way to determine customer requirements – that is, user feedback guides the product. In parallel, the manufacturers incorporate the latest but proven technologies to improve design and stay ahead of the competition, always restricted by the financial viability of what the market can afford. Continual dialogue among manufacturers and operators results in the best design.

Military aircraft product development has a similar approach but requires modifications to Chart 2.6. Here, government is both the single customer and the regulatory body; therefore, competition is only among the bidding manufacturers. The market is replaced by the operational requirements arising from perceived threats from potential adversaries. Column 1 of Chart 2.6 becomes “operational drivers” that includes weapons management, counterintelligence, and so on. Hence, this section on the market survey is divided into civilian and military customers, as shown in Chart 2.7. *Customer* is a broad term that is defined in this book as given in the chart.

In the U.K. military, the Ministry of Defense (MoD), as the single customer, searches for a product and circulates a Request for Proposal (RFP) to the national infrastructure, where most manufacturing is run privately. It is similar in the United States using different terminology. The product search is a complex process – the MoD must know a potential adversary’s existing and future capabilities and administrate national research, design, and development (RD&D) infrastructures to be ready with discoveries and innovations to supersede an adversary’s capabilities.

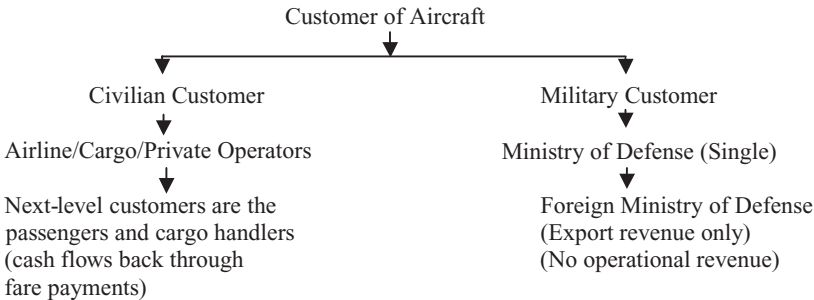


Chart 2.7. Customers of aircraft manufacturer

The Air Staff Target (AST) is an elaborate aircraft specification as a customer requirement. A military project is of national interest and, in today's practice, capable companies are invited to first produce a technology demonstrator as proof of concept. The loser in the competition is paid by the government for the demonstrator and learns about advanced technology for the next RFP or civilian design. Therefore, in a sense, there is no loser, and the nation hones its technical manpower.

Although it is used, the author does not think an RFP is appropriate terminology in civilian applications: Who is making the request? It is important for aircraft manufacturers to know the requirements of many operators and supply a product that meets the market's demands in performance, cost, and time frame. Airline, cargo, and private operators are direct customers of aircraft manufacturers, which do not have direct contact with the next level of customers (i.e., passengers and cargo handlers) (see [Chart 2.7](#)). Airlines do their market surveys of passenger and freight requirements and relay the information to manufacturers. The surveys often are established by extensive studies of target-city pairs, current market coverage, growth trends, and passenger input. Inherent in the feedback are diverse requirements that must be coalesced into a marketable product. A major order from a single operator could start a project, but manufacturers must cater to many operators to enlarge and stabilize their market share. The civilian market is searched through a multitude of queries to various operators (i.e., airlines), both nationally and internationally. In civil aviation, the development of the national infrastructure must be coordinated with aircraft manufacturers and operators to ensure national growth. Airlines generate revenue by carrying passengers and freight, which provide the cash flow that supports the maintenance and development of the civil aviation infrastructure. Cargo generates important revenues for airlines and airports, and the market for it should not be underestimated – even if it means modifying older airplanes. Manufacturers and operators are in continual contact to develop product lines with new and/or modified aircraft. Aircraft manufacturers must harmonize the diversity in requirements such that management decides to undertake a conceptual study to obtain the go-ahead. There is nothing comparable to the process taken by the MoD to initiate an RFP with a single customer demand.

The private or executive aircraft market is driven by operators that are closely connected to business interests and cover a wide spectrum of types, varying from four passengers to specially modified midsized jets.

Military aircraft utilization in peacetime is approximately 7,500 hours, about one-tenth that of commercial transport aircraft (i.e., $\approx 75,000$ hours) in its lifespan. Annual peacetime military aircraft utilization is low (i.e., ≈ 600 hours) compared to annual civil aircraft utilization, which can exceed 3,000 hours.

2.7 Civil Aircraft Market

Following up on the review in [Chapter 1](#), about the current status of the civil aircraft market, this section describes how to generate aircraft specifications that will help to sell the product and generate a profit. The coursework starts here with a mock (i.e., representative) market survey leading to what must be designed – that is, the conception of the aircraft, the Phase 1 obligations.

Input from operators to manufacturers is significant and varied. The manufacturer needs to group the requirements intelligently in a family of aircraft sizes and capabilities. It is necessary to cover as much ground as the market demands yet maintain component commonalities in order to lower development costs of the derivative aircraft in the family. This book lists only those market parameters that affect aircraft aerodynamic design, the most important being the payload-range capability of the aircraft, which has the greatest influence in shaping the aircraft. Details of other requirements (e.g., systems requirements, maintenance, and passenger services) are not discussed here but are briefly introduced.

For the mock market studies, students may be asked to table aircraft requirements as if they are representing the airlines' interest. It is understandable that due to inexperience, they may list requirements that are not practicable. It is therefore the instructor's responsibility to provide reasons for discarding each impracticable point and then coalesce the remainder into a starting point. Section 2.7.1 suggests interesting cases for coursework experience. There is a wide variety of civil aircraft in operation; following are requirements for the three classes addressed in the scope of this book.

2.7.1 Aircraft Specifications and Requirements for Three Civil Aircraft Case Studies

It is recommended that the introductory coursework exercise use one of the three specifications provided as a starting point. Accordingly, the initial follow-up activity is limited to work on the Learjet 45 class aircraft (see the second design specification).

Design Specifications of a Four-Seater Piston Engine Aircraft as Baseline (FAR 23)

Payload:	4 passengers (including pilot) + baggage (e.g., 2 golf bags) = 4×85 (averaged) + 60 = 400 kg
Range:	800 miles + reserve
Maximum Cruise Speed:	Above 200 mph
Cruise Altitude:	Unpressurized cabin; approximately 10,000 ft (ceiling could be higher)
Takeoff Distance:	500 m @ sea level to 35 ft
Landing Distance:	500 m (at takeoff weight) @ sea level from 50 ft
Initial Rate of Climb:	8 meters per second (m/s)
Undercarriage:	Retractable
Cabin Comfort:	Cabin heating, side-by-side seating, cabin interior width = 50 in.
Technology Level:	Conventional
Power Plant:	Piston engine

DERIVATIVE VERSION AS A LIGHTER TWO-SEATER LIGHT CLUB TRAINER/USAGE AIRCRAFT (FAR 23). (Derivatives are more difficult to develop for smaller aircraft because there is less room with which to work. Fuselage unplugging is difficult unless

the baseline design made provision for it. There are considerable savings in certification cost.)

Payload:	2 passengers plus light baggage = 200 kg
Range:	400 miles + reserve
Maximum Cruise Speed:	140 mph
Takeoff Distance:	300 m @ sea level to 35 ft
Landing Distance:	300 m (at takeoff weight) @ sea level from 50 ft
Initial Rate of Climb:	5 m/s
Undercarriage:	Fixed
Cabin Comfort:	Cabin heating, side-by-side seating, cabin interior width = 46 in.

(The other specifications are the same as in the baseline four-seater design.)

Derivative versions are achieved by shortening the wing root and empennage tips, unplugging the fuselage section (which is difficult if it is not a continuous section but is possible if the design of the baseline four-passenger aircraft considers this in advance), lightening the structural members, re-engining to lower the power, and so forth.

Design Specifications of a Baseline Eight- to Ten-Passenger (Learjet 45 Class) Aircraft (FAR 25)

Payload:	8 to 10 passengers and 2 pilots + baggage
High Comfort Level:	8×100 (averaged) + 300 = 1,100 kg
Medium Comfort Level:	10×80 (averaged) + 300 = 1,100 kg
Range:	2,000 miles + reserve
Maximum Cruise Speed:	Mach 0.7
Cruise Altitude:	Above 40,000 ft (ceiling over 50,000 ft)
Takeoff Distance:	1,000 m @ sea level to 15 m
Landing Distance:	1,000 m (at takeoff weight) @ sea level from 15 m
Initial Rate of Climb:	16 m/s
Undercarriage:	Retractable
Cabin Comfort:	Pressurized cabin with air-conditioning and oxygen supply, cabin interior width = 58 in.
Technology Level:	Advanced
Power Plant:	Turbofan engine

SHORTENED DERIVATIVE VERSION: FOUR TO SIX PASSENGERS IN A BASELINE AIRCRAFT FAMILY (FAR 25). (This derivative works by unplugging continuous-section fuselage barrel on both sides of the wing.)

Payload:	4 to 6 passengers and 2 pilots + baggage
High Comfort Level:	4×100 (averaged) + 200 = 600 kg
Medium Comfort Level:	6×80 (averaged) + 120 = 600 kg
Range:	2,000 miles + reserve
Maximum Cruise Speed:	Mach 0.7
Cruise Altitude:	Above 40,000 ft (ceiling over 50,000 ft)
Takeoff Distance:	800 m @ sea level to 15 m
Landing Distance:	800 m (at takeoff weight) @ sea level from 15 m

(The other specifications are the same as in the baseline design.)

LENGTHENED DERIVATIVE VERSION: TWELVE TO FOURTEEN PASSENGERS IN THE BASELINE AIRCRAFT FAMILY (FAR 25). (The longer derivative works in the same way by inserting continuous-section fuselage plugs on both sides of the wing.)

Payload:	12 to 14 passengers and 2 pilots + baggage
High Comfort Level:	12×100 (averaged) + 300 = 1,500 kg
Medium Comfort Level:	14×80 (averaged) + 380 = 1,500 kg
Range:	2,000 miles + reserve
Takeoff Distance:	1,200 m @ sea level to 15 m
Landing Distance:	1,200 m (at takeoff weight) @ sea level from 15 m

(The other specifications are the same as in the baseline design.)

Design Specifications of a Baseline 150-Passenger (Airbus 320 Class) Aircraft (FAR 25)

Payload:	150 passengers = $90 \times 150 = 14,500$ kg
Range:	2,800 nm (nautical miles) + reserve
Crew:	2 pilots + 5 attendants
Maximum Cruise Speed:	0.75 Mach
Cruise Altitude:	Above 30,000 ft (ceiling over 40,000 ft)
Takeoff Distance:	2,000 m @ sea level to 15 m
Landing Distance:	2,000 m (at 95% takeoff weight) @ sea level from 15 m
Initial Rate of Climb:	14 m/s
Undercarriage:	Retractable
Cabin Comfort:	Pressurized cabin with air conditioning and oxygen supply, cabin interior diameter = 144 in.
Technology Level:	Advanced
Power Plant:	Turbofan engine

DERIVATIVE VERSION IN THE AIRCRAFT FAMILY (TYPICALLY AIRBUS 319 AND AIRBUS 321 CLASS ON BOTH SIDES OF THE BASELINE AIRBUS 320 AIRCRAFT). This is accomplished by plugging and unplugging the fuselage as in a Bizjet design. Readers are referred to *Jane's All the World's Aircraft* for derivative details and Appendix D for an example. Wide-body aircraft design follows the methodology.

(Note: The author encourages readers to explore market surveys for other classes of aircraft. To diversify, following are brief specifications for two interesting examples [7]).

A. Agriculture Applications Aircraft

1. Airframe must be highly corrosion resistant.
2. Airframe must be easily cleaned (i.e., removable side panels).
3. Airframe must be flushed with water after last flight.
4. Airframe must be easily inspected.
5. Airframe must be easily repaired.
6. Airframe must be highly damage tolerant.
7. Dry and wet chemicals must be loaded easily and quickly.
8. Cockpit must have excellent pilot crash protection.
9. Pilot must have excellent visibility (i.e., flagman, ground crew, and obstacles).

10. The stall speed must be 60 knots or less.
11. The service ceiling is 15,000 ft.
12. Takeoff performance: 20,000-ft field length (rough field) with 50-ft obstacles.
13. Hopper capacity: 400 U.S. gallons/3,200 lbs.

It is suggested that the design be approached through use of FAR Parts 137, 135, and 123. Readers may review current designs from *Jane's All the World's Aircraft*. Key considerations include choice of materials, configuration and structural layout, and systems design. In every other respect, the design should follow the standard approach described herein.

B. Airport Adaptive Regional Transport with Secondary Role to Support U.S. Homeland Security (Abridged from [7])

Payload:	49 passengers + flight and cabin crew
Range:	1,500 miles with reserve
Takeoff and Landing	2,500 ft
Field Length:	
Maximum Speed:	400 knots
Mission Profile:	Multiple takeoffs and landings without refueling

For the airport adaptive role, the aircraft can simultaneously approach a major airport in noninterfering adverse weather and takeoff and land from shorter, largely unused runways, subrunways, and taxiways. The aircraft will be evaluated for an automatic spiral-descending, decelerating approach in instrument meteorological conditions (IMC) (Category 3C) conditions and be able to continue with one engine inoperative. The aircraft also has the following secondary roles:

- Serve the civil reserve fleet and be available during a homeland-security crisis
- Serve as an ambulance
- Serve as transport firefighters to remote wilderness areas
- Serve as an emergency response vehicle for urban terrorism or a natural disaster by changing passenger-accommodation fitment

The aircraft will have half of the payload and a 750-mile range into makeshift landing zones of at least 1,000 ft.

More information is required for the specifications, but the level of technology is not within the scope of this book.

Other than drag estimation and certification regulations (e.g., noise), the SST design is similar to subsonic transport, aircraft design methodology. Supersonic drag estimation is addressed in [Chapter 9](#).

2.8 Military Market

This extended section of the book can be found on the Web at www.cambridge.org/Kundu and describes the typical military aircraft aviation market, starting with compliance with national defense requirements (MoD).

2.8.1 Aircraft Specifications/Requirements for Military Aircraft Case Studies

This extended section of the book can be found on the Web at www.cambridge.org/Kundu and outlines specifications for introductory classroom work on military aircraft design (e.g., the Advanced Jet Trainer).

Table 2.2. *Comparison between civil and military aircraft design requirements*

Issue	Civil aircraft	Military aircraft
Design space	Verified	Aspirational
Certification standards	Civil (FAR – U.S.)	Military (Milspecs – U.S.)
Operational environment	Friendly	Hostile
safety issues	Uncompromised, no ejection	Survivability requires ejection
Mission profile	Routine and monitored by air traffic control (ATC)	As situation demands and could be unmonitored
Flight performance	Near-steady-state operation and scheduled; gentle maneuvers	Large variation in speed and altitudes; pilot is free to change briefing schedule; extreme maneuvers
Flight speed	Subsonic and scheduled (not addressing SST here)	Have supersonic segments; in combat, unscheduled
Engine performance	Set throttle dependency, no afterburner (subsonic)	Varied throttle usage, with afterburner
Field performance	Mostly metal runways, generous in length, with ATC support	Different surfaces with restricted lengths; marginal ATC
Systems architecture	Moderately complex, high redundancies, no threat analysis	Very complex, lower redundancies, threat acquisition
Environmental issues	Strictly regulated; legal minimum standards	Relaxed; peacetime operation in restricted zones
Maintainability	High reliability with low maintenance cost	High reliability but at a considerably higher cost
Ground handling	Extensive ground-handling support with standard equipment	Specialized and complex ground-support equipment
Economics	Minimize DOC; cash flow back through revenue earned	Minimize LCC; no cash flow back
Training	Routine	Specialized and more complex

2.9 Comparison between Civil and Military Aircraft Design Requirements

This section compares the civil and military aircraft design classes, as shown in [Table 2.2](#).

Once the configuration is finalized, the governing equations for sizing, engine matching, and performance analysis are the same for all categories (although drag estimation presents some difficulty for complex configurations, especially supersonic designs). The crux of a military aircraft design is systems integration for survivability, maneuver control (i.e., FBW), target acquisition, weapons management, navigation (i.e., unknown terrain), and communication strategies (e.g., identification of friend or foe). Military aircraft design is very different compared to civil aircraft design. A major aspect of combat aircraft design is the systems architecture for threat analysis and survivability – without these in the combat aircraft design of the Eurofighter Typhoon or the F22 Raptor class, any coursework exercise is meaningless. Military certification standards are more elaborate and time consuming. These crucial issues are not within the scope of this book – only a few specialist books are available that address systems architecture for threat analysis and survivability – and

Table 2.3. FAR categories of airworthiness standards

Aircraft types	General	Normal	Transport
Aircraft	FAR Part 23	FAR Part 23	FAR Part 25
Engine	FAR Part 33	FAR Part 33	FAR Part 33
Propeller	FAR Part 35	FAR Part 35	FAR Part 35
Noise	FAR Part 36	FAR Part 36	FAR Part 36
General operations	FAR Part 91	FAR Part 91	FAR Part 91
Agriculture	FAR Part 137		
Large commercial transport	Not applicable	Not applicable	FAR Part 121

some of those are obviously confidential. However, seminars on these topics are offered to those who are well versed in aircraft design.

The simpler case of an AJT in subsonic operation provides an idea of military aircraft design, although the author would not apply the certification regulations as extensively as in the civil aircraft examples for reasons discussed previously. It is possible that the CAS version of the AJT could become supersonic in a shallow dive.

2.10 Airworthiness Requirements

From the days of barnstorming and stunt-flying in the 1910s, it became obvious that commercial interests had the potential to short-circuit safety considerations. Government agencies quickly stepped in to safeguard people's security and safety without deliberately harming commercial interests. Safety standards were developed through multilateral discussions, which continue even today. Western countries developed and published thorough and systematic rules – these are in the public domain (see relevant Web sites). In civil applications, they are FAR for the United States [8] and CS (EASA) for Europe. They are quite similar and may eventually merge into one agency. The author's preference is to work with the established FAR; pertinent FARs are cited when used in the text and examples. FAR documentation for certification has branched out into many specialist categories, as shown in Table 2.3.

Table 2.4 provides definitions for general, normal, and transport categories of aviation.

Table 2.4. Aircraft categories

Aircraft types	General	Normal	Transport
MTOW (lbs)	Less than 12,500	Less than 12,500	More than 12,500
No. of engines	0 or more	More than 1	More than 1
Type of engine	All types	Propeller only	All types
Flight crew	1	2	2
Cabin crew	None	None up to 19 PAX	None up to 19 PAX
Maximum no. of occupants	10	23	Unrestricted
Maximum operating altitude	25,000 ft	25,000 ft	Unrestricted

Note:

MTOW = maximum takeoff weight

PAX = passengers

In military applications, the standards are Milspecs (U.S.) and Defense Standard 970 (previously AvP 970) (U.K.); they are different in some places.

Since 2004, in the United States, new sets of airworthiness requirements came into force for light-aircraft (LA) designs and have eased certification procedures and litigation laws, rejuvenating the industry in the sector. Europe also has a similar approach but its regulations differ to an extent. Small/light aircraft and microlight types have different certification standards not discussed in this book.

2.11 Coursework Procedures

The coursework task is to conduct a mock market study. The instructor divides the class into groups of four or five students who will work as a team (see the Road Map of the Book, which gives the typical allotted time). However, how the class is conducted is at the instructor's discretion.

- Step 1: The instructor decides which class of aircraft will be used for the design project. Students will have input but the instructor ultimately explains why a certain aircraft is chosen. Designing a conventional civil or a military trainer aircraft is appropriate for undergraduate introductory work. In this book, a Bizjet and an AJT aircraft design are used.
- Step 2: The instructor discusses each suggestion, discarding the impractical and coalescing the feasible. The instructor will add anything that is missing, with explanations.
- Step 3: Each team must submit a scaled, three-view sketch of the proposed design. There will be differences in the various configurations. CAD is recommended.
- Step 4: The instructor discusses each configuration, tailoring the shape, with explanation, to a workable shape. Each team works on its revised configuration; preferably, the class will work with just one design.

3 Aerodynamic Considerations

3.1 Overview

This chapter is concerned with the aerodynamic information required at the conceptual design stage of a new aircraft design project. It provides details that influence shaping and other design considerations and defines the various parameters integral to configuring aircraft mould lines. Any object moving through air interacts with the medium at each point of the wetted (i.e., exposed) surface, creating a pressure field around the aircraft body. An important part of aircraft design is to exploit this pressure field by shaping its geometry to arrive at the desired performance of the vehicle, including shaping to generate lifting surfaces, to accommodate payload, to house a suitable engine in the nacelle, and to tailor control surfaces. Making an aircraft streamlined also makes it look elegant.

Aeronautical engineering schools offer a series of aerodynamic courses, starting with the fundamentals and progressing toward the cutting edge. It is assumed that readers of this book have been exposed to aerodynamic fundamentals; if so, then readers may browse through this chapter for review and then move on to the next chapter. Presented herein is a brief compilation of applied aerodynamics without detailed theory beyond what is necessary. Many excellent textbooks are available in the public domain for reference. Because the subject is so mature, some nearly half-century-old introductory aerodynamics books still serve the purpose of this course; however, more recent books relate better to current examples.

3.1.1 What Is to Be Learned?

This chapter covers the following topics:

- Section 3.2: Introduction to aerodynamics
- Section 3.3: Atmosphere through which aircraft flies
- Section 3.4: Useful equations
- Section 3.5: Airflow behavior past a body; viscosity and boundary layer concepts introduced to explain drag
- Section 3.6: Aircraft motion and the forces acting on it
- Section 3.7: Aerofoil definition and classification
- Section 3.8: Definition of relevant aerodynamic coefficients (e.g., C_L , C_D)

- Section 3.9: Lift generation, aerodynamic center, and center of pressure
- Section 3.10: Types of stall
- Section 3.11: Comparison of aerofoils and selection of appropriate choice
- Section 3.12: Introduction to high-lift devices
- Section 3.13: Transonic effects (area rule)
- Section 3.14: Wing aerodynamics (3D geometry)
- Section 3.15: Aspect ratio correction (2D to 3D)
- Section 3.16: Wing planform reference area definition, dihedral angle
- Section 3.17: Mean aerodynamic chord
- Section 3.18: Compressibility effect
- Section 3.19: Wing stall and twist
- Section 3.20: Influence of wing area and span on aerodynamics
- Section 3.21: Finalizing wing design parameters
- Section 3.22: Empennage, tail volume definition, canard
- Section 3.23: Fuselage
- Section 3.24: Undercarriage (see [Chapter 7](#))
- Section 3.25: Nacelle and intake
- Section 3.26: Speed and dive brakes

3.1.2 Coursework Content

The information in this chapter is essential for designers. Coursework is postponed until [Chapter 6](#) (except for the mock market survey in [Chapter 2](#)). Readers should return to [Chapters 2](#) through [5](#) to extract information necessary to configure the aircraft in [Chapter 6](#).

3.2 Introduction

Aircraft conceptual design starts with shaping an aircraft, finalizing geometric details through aerodynamic considerations in a multidisciplinary manner (see [Section 2.3](#)) to arrive at the technology level to be adopted. In the early days, aerodynamic considerations dictated aircraft design; gradually, other branches of science and engineering gained equal importance.

All fluids have some form of viscosity (see [Section 3.5](#)). Air has a relatively low viscosity, but it is sufficiently high to account for its effects. Mathematical modeling of viscosity is considerably more difficult than if the flow is idealized to have no viscosity (i.e., inviscid); then, simplification can obtain rapid results for important information. For scientific and technological convenience, all matter can be classified as shown in [Chart 3.1](#).

This book is concerned with air (gas) flow. Air is compressible and its effect is realized when it is flowing. Aircraft design requires an understanding of both incompressible and compressible fluids. Nature is conservative (other than nuclear physics) in which mass, momentum, and energy are conserved.

Aerodynamic forces of lift and drag (see [Section 3.9](#)) are the resultant components of the pressure field around an aircraft. Aircraft designers seek to obtain the maximum possible lift-to-drag ratio (i.e., a measure of minimum fuel burn) for an efficient design (this simple statement is complex enough to configure, as will be

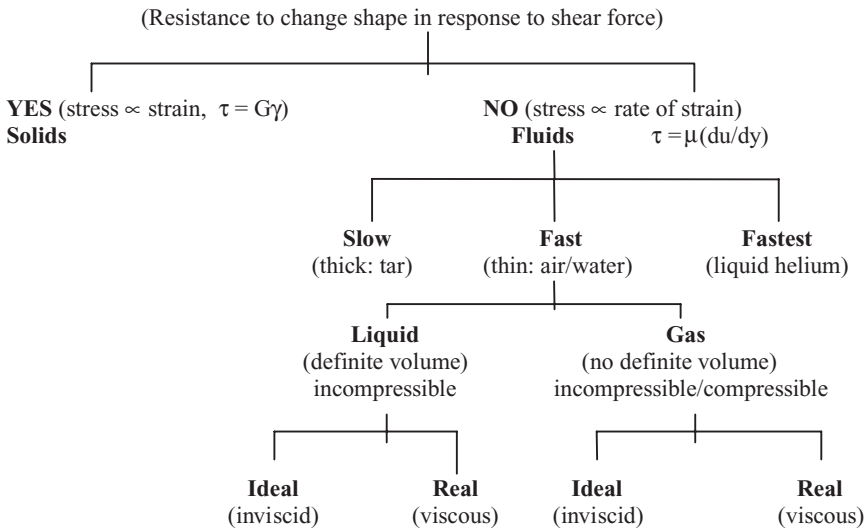


Chart 3.1. All matter

observed throughout the coursework). Aircraft stability and control are the result of harnessing these aerodynamic forces. Aircraft control is applied through the use of aerodynamic forces modulated by the control surfaces (e.g., elevator, rudder, and aileron). In fact, the sizing of all aerodynamic surfaces should lead to meeting the requirements for the full flight envelope without sacrificing safety.

To continue with sustained flight, an aircraft requires a lifting surface in the form of a plane – hence, *aeroplane* (the term *aircraft* is used synonymously in this book). The secret of lift generation is in the sectional characteristics (i.e., *aerofoil*) of the lifting surface that serve as wings, similar to birds. This chapter explains how the differential pressure between the upper and lower surfaces of the wing is the lift that sustains the aircraft weight. Details of aerofoil characteristics and the role of empennage that comprises the lifting surfaces are explained as well. The stability and control of an aircraft are aerodynamic-dependent and discussed in [Chapter 12](#).

Minimizing the drag of an aircraft is one of the main obligations of aerodynamicists. Viscosity contributes to approximately two-thirds of the total subsonic aircraft drag. The effect of viscosity is apparent in the wake of an aircraft as disturbed airflow behind the body. Its thickness and intensity are indications of the extent of drag and can be measured. One way to reduce aircraft drag is to shape the body such that it will result in a thinner wake. The general approach is to make the body in a teardrop shape with the aft end closing gradually, as compared to the blunter front-end shape for subsonic flow. (Behavior in a supersonic flow is different but it is still preferable for the aft end to close gradually.) The smooth contouring of teardrop shaping is called *streamlining*, which follows the natural airflow lines around the aircraft body – it is for this reason that aircraft have attractive smooth contour lines. Streamlining is synonymous with speed and its aerodynamic influence in shaping is revealed in any object in a relative moving airflow (e.g., boats and automobiles).

New aircraft designers need to know about the interacting media – that is, the air (i.e., atmosphere). The following sections address atmosphere and the behavior of air interacting with a moving body.

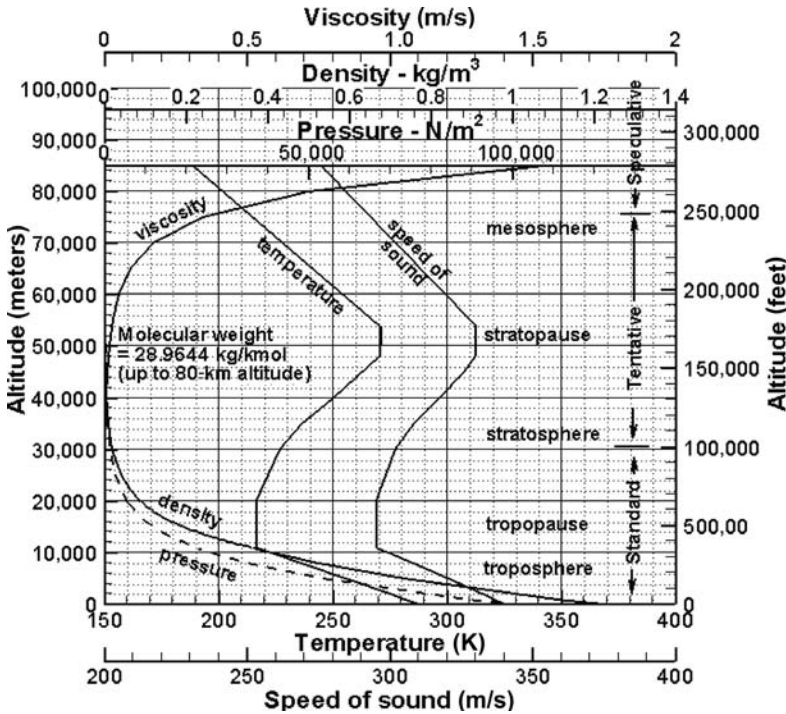


Figure 3.1. Atmosphere (see Appendix B for accurate values)

3.3 Atmosphere

Knowledge of the atmosphere is an integral part of design – the design of an aircraft is a result of interaction with the surrounding air. The atmosphere, in the classical definition up to 40-kilometer (km) altitude, is dense (continuum): Its homogeneous constituent gases are nitrogen (78%), oxygen (21%), and others (1%). After substantial data generation, a consensus was reached to obtain the ISA [1], which is in static condition and follows hydrostatic relations. Appendix B includes an ISA table with up to 20-km altitudes, which is sufficient for this book because all aircraft (except rocket-powered special-purpose aircraft – e.g., space plane) described would be flying below 20 km. Linear interpolation of properties may be carried out between low altitudes. At sea level, the standard condition gives the following properties:

$$\begin{aligned} \text{pressure} &= 101,325 \text{ N/m}^2 \text{ (14.7 lb/in}^2\text{)} \\ \text{temperature} &= 288.16^\circ \text{K (518.69}^\circ \text{R)} \\ \text{viscosity} &= 1.789 \times 10^{-5} \text{ m/s (5.872} \times 10^{-5} \text{ ft/s)} \\ \text{acceleration due to gravity} &= 9.81 \text{ m/s}^2 \text{ (32.2 ft/s}^2\text{)} \end{aligned}$$

In reality, an ISA day is difficult to find; nevertheless, it is used to standardize aircraft performance to a reference condition for assessment and comparison. With altitude gain, the pressure decreases, which can be expressed through the use of hydrostatic equations. However, temperature behaves strangely: It decreases linearly up to 11 km at a lapse rate of 6.5°K/km , then holds constant at 216.66°K until it reaches 20 km, at which it starts increasing linearly at a rate of 4.7°K/km up to

47 km. The 11-km altitude is called the *tropopause*; below the tropopause is the *troposphere* and above it is the *stratosphere*, extending up to 47 km. Figure 3.1 shows the typical variation of atmospheric properties with altitude. The ISA is up to 100,000-ft altitude. From 100,000- to 250,000-ft altitude, the atmospheric data are currently considered tentative. Above a 250,000-ft altitude, variations in atmospheric data are speculative.

Typical atmospheric stratification (based primarily on temperature variation) is as follows (the applications in this book do not exceed 100,000 ft [≈ 30.5 km]):

Troposphere:	up to 11 km (36,089 ft)
Tropopause:	11 km (36,089 ft)
Stratosphere:	from 20 to 47 km (65,600 to 154,300 ft)
Stratopause:	47 km (154,300 ft)
Mesosphere:	from 54 to 90 km
Mesopause:	90 km
Thermosphere:	from 100 to 550 km (can extend and overlap with ionosphere)
Ionosphere:	from 550 to 10,000 km
Exosphere:	above 10,000 km

In the absence of the ISA table, the following hydrostatics equations give the related properties for the given altitude, h , in meters. Pressure decreases with altitude increase, obeying hydrostatic law; however, atmospheric temperature variation with altitude is influenced by natural phenomenon.

Temperature, T , in $^{\circ}\text{K} = 288.15 - (0.0065 \times h)$ up to 11,000 m altitude (in the troposphere) and thereafter constant at 216.66°K until it reaches 25,000 m.

Above 25,000 m, use T in $^{\circ}\text{K} = 216.66 + (0.0047 \times h)$ up to 47,000 m altitude (in the stratosphere).

$$\begin{aligned} \text{Pressure, } p \text{ in kg/m}^2 &= 101,325 \times (T/288.16)^{(g/0.0065R)} && \text{in the troposphere} \\ p \text{ in N/m}^2 &= 101,325 \times e^{(gh/RT)} && \text{in the stratosphere} \\ \text{Density, } \rho \text{ in kg/m}^3 &= 1.225 \times (T/288.16)^{(g/0.0065R)-1} && \text{in the troposphere} \\ \rho \text{ in kg/m}^3 &= 1.225 \times e^{-(gh/RT)} && \text{in the stratosphere} \end{aligned}$$

Kinematic viscosity

$$v \text{ in m}^2/\text{s} = 1.46 \times 10^{-5} \times e^{(gh/RT)} \quad (3.1)$$

Acceleration due to gravity is inversely proportional to the square of the radius (average radius $r_0 = 6,360$ km) from the center of the Earth. If r is the altitude of an aircraft from the Earth's surface, then it is at a distance ($r_0 + r$) from the center of the Earth. Figure 3.2 shows schematically the aircraft distance from the center of the Earth.

Then, acceleration due to gravity, g , at height r is expressed as:

$$g = g_0 \left(\frac{r_0}{r_0 + r} \right)^2, \quad (3.2)$$

where g_0 is the acceleration due to gravity at sea level (i.e., surface).

For terrestrial flights, r is much less than r_0 ; there is less than a 1% change in g up to 30 km; hence, g is kept invariant at the sea level value of 9.81 m/s^2 for aircraft

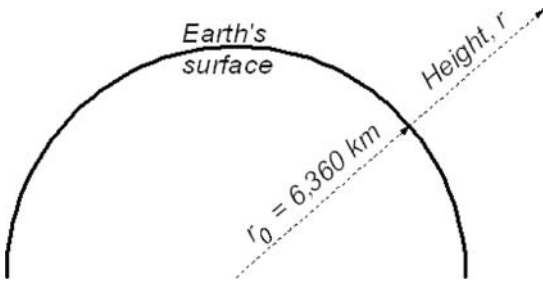


Figure 3.2. Aircraft distance from the center of the Earth

applications. The small error arising from keeping g constant results in geopotential altitude that is slightly lower than the geometric altitude. This book uses the geometric altitude from the ISA table.

As mentioned previously, an aircraft rarely encounters the ISA. Wind circulation over the globe is always occurring. Surface wind current such as *doldrums* (i.e., slow winds in equatorial regions), *trade winds* (i.e., predictable wind currents blowing from subtropical to tropical zones), *westerlies* (i.e., winds blowing in the temperate zone), and *polar easterlies* (i.e., year-round cold winds blowing in the polar regions) are well known. In addition, there are characteristic winds in typical zones – for example, *monsoon* storms; wind-tunneling effects of strong winds blowing in valleys and ravines in mountainous and hilly regions; steady up and down drafts at hill slopes; and daily coastal breezes. At higher altitudes, these winds have an effect. Storms, twisters, and cyclones are hazardous winds that must be avoided. There are more complex wind phenomena such as wind-shear, high-altitude jet streams, and vertical gusts. Some of the disturbances are not easily detectable, such as clear air turbulence (CAT). Humidity in the atmosphere is also a factor to be considered. The air-route safety standards have been improved systematically through round-the-clock surveillance and reporting. In addition, modern aircraft are fitted with weather radars to avoid flight paths through disturbed areas. Flight has never been safer apart from manmade hazards. This book addresses only an ISA day, with the exception of *gust load*, which is addressed in [Chapter 5](#) for structural integrity affecting aircraft weights.

Aircraft design must also consider specific nonstandard conditions. On a hot day, the density of air decreases and aircraft performance degradation will take place as a result of lowered engine power. Certification authorities (i.e., FAA and CAA) require that aircraft demonstrate the ability to perform as predicted in hot and cold weather and in gusty wind. The certification process also includes checks on the ability of the environmental control system (ECS) (e.g., anti-icing/de-icing, and air-conditioning) to cope with extreme temperatures. In this book, performance degradation on a non-ISA day is not addressed. The procedure to address nonstandard atmospheres is identical with the computation using the ISA conditions, except that the atmospheric data are different.

3.4 Fundamental Equations*

Some elementary yet important equations are listed herein. Readers must be able to derive them and appreciate the physics of each term for intelligent application

* See Symbols and Abbreviations, this volume, pp. xix–xxvii.

to aircraft design. The equations are not derived herein – readers may refer to any introductory aerodynamic textbook for their derivation.

In a flowing fluid, an identifiable physical boundary defined as control volume (CV) (see Figure 10.11) can be chosen to describe mathematically the flow characteristics. A CV can be of any shape but the suitable CVs confine several streamlines like well-arranged “spaghetti in a box” in which the ends continue along the streamline, crossing both cover ends but not the four sides. The conservative laws within the CV for steady flow (independent of time, t) that are valid for both inviscid incompressible and compressible flow are provided herein. These can be equated between two stations (e.g., Stations 1 and 2) of a streamline. Inviscid (i.e., ideal) flow undergoing a process without any heat transfer is called the *isentropic process*. During the conceptual study phase, all external flow processes related to aircraft aerodynamics are considered isentropic, making the mathematics simpler. (Combustion in engines is an internal process.)

Newton’s law: *applied force, $F = \text{mass} \times \text{acceleration} = \text{rate of change of momentum}$*

From kinetics, *force = pressure \times area*

and *work = force \times distance*

Therefore, energy (i.e., rate of work) for the unit mass flow rate \dot{m} is as follows:

energy = force \times (distance/time) = pressure \times area \times velocity = pAV

$$\text{mass conservation: mass flow rate } \dot{m} = \rho AV = \text{constant} \quad (3.3)$$

$$\text{Momentum conservation: } dp = -\rho V dV \text{ (known as Euler’s equation)} \quad (3.4)$$

With viscous terms, it becomes the Navier–Stokes equation. However, friction forces offered by the aircraft body can be accounted for in the inviscid-flow equation as a separate term:

$$\text{energy conservation: } C_p T + \frac{1}{2} V^2 = \text{constant} \quad (3.5)$$

When velocity is stagnated to zero (e.g., in the hole of a Pitot tube), then the following equations can be derived for the isentropic process. The subscript t represents the stagnation property, which is also known as the “total” condition. The equations represent point properties – that is, valid at any point of a streamline (γ stands for the ratio of specific heats and M for the Mach number):

$$\frac{T_t}{T} = \left(1 + \frac{\gamma - 1}{2} M^2 \right) \quad (3.6)$$

$$\frac{\rho_t}{\rho} = \left(1 + \frac{\gamma - 1}{2} M^2 \right)^{\frac{1}{\gamma - 1}} \quad (3.7)$$

$$\frac{p_t}{p} = \left(1 + \frac{\gamma - 1}{2} M^2 \right)^{\frac{\gamma}{\gamma - 1}} \quad (3.8)$$

$$\left(\frac{p_t}{p} \right) = \left(\frac{\rho_t}{\rho} \right)^\gamma = \left(\frac{T_t}{T} \right)^{\frac{\gamma}{\gamma - 1}} \quad (3.9)$$

The conservation equations yield many other significant equations. In any streamline of a flow process, the conservation laws exchange pressure energy with the

kinetic energy. In other words, if the velocity at a point is increased, then the pressure at that point falls and vice versa (i.e., Bernoulli's and Euler's equations). Following are a few more important equations. At stagnation, the total pressure, p_t , is given.

Bernoulli's equation: For incompressible isentropic flow,

$$p/\rho + V^2/2 = \text{constant} = p_t \quad (3.10)$$

Clearly, at any point, if the velocity is increased, then the pressure will fall to maintain conservation. This is the crux of lift generation: The upper surface has lower pressure than the lower surface.

Euler's equation: For compressible isentropic flow,

$$\left[\frac{(p_t - p)}{p} + 1 \right]^{\frac{\gamma-1}{\gamma}} - 1 = \frac{(\gamma - 1)V^2}{2a^2} \quad (3.11)$$

There are other important relations using thermodynamic properties, as follows.

From the gas laws (combining Charles's law and Boyle's law), the equation for the state of gas for the unit mass is $p\nu = RT$, where for air:

$$R = 287 \text{ J/kgK} \quad (3.12)$$

$$C_p - C_v = R \text{ and } \gamma = C_p/C_v \quad (3.13)$$

From the energy equation, total temperature:

$$T_t = T + \frac{T(\gamma - 1)V^2}{2RT\gamma} = T + \frac{V^2}{2C_p} \quad (3.14)$$

Mach number = V/a , where a = speed of sound and

$$a^2 = \gamma RT = (dp/d\rho)_{\text{isentropic}} \quad (3.15)$$

3.5 Airflow Behavior: Laminar and Turbulent

Understanding the role of the viscosity of air is important to aircraft designers. The simplification of considering air as inviscid may simplify mathematics, but it does not represent the reality of design. Inviscid fluid does not exist, yet it provides much useful information rather quickly. Subsequently, the inviscid results are improvised. To incorporate the real effects of viscosity, designs must be tested to substantiate theoretical results.

The fact that airflow can offer resistance due to viscosity has been understood for a long time. Navier in France and Stokes in England independently arrived at the same mathematical formulation; their equation for momentum conservation embedding the viscous effect is known as the Navier–Stokes equation. It is a non-linear partial differential equation still unsolved analytically except for some simple body shapes. In 1904, Ludwig Prandtl presented a flow model that made the solution of viscous-flow problems easier [2]. He demonstrated by experiment that the viscous effect of flow is realized only within a small thickness layer over the contact surface boundary; the rest of the flow remains unaffected. This small thickness layer is called the boundary layer (Figure 3.3). Today, numerical methods (i.e., CFD) can address viscous problems to a great extent.

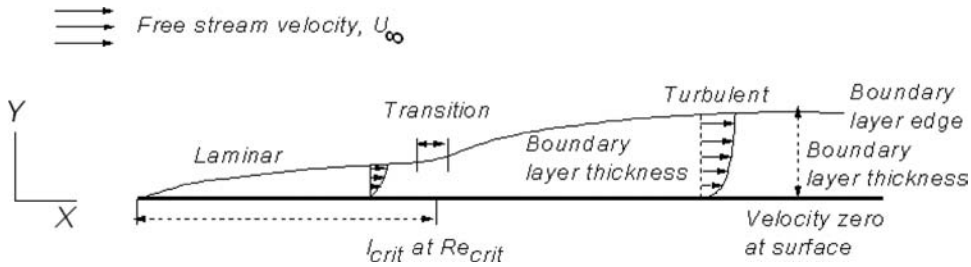


Figure 3.3. Boundary layer over a flat plate

The best way to model a continuum (i.e., densely packed) airflow is to consider the medium to be composed of very fine spheres of molecular scale (i.e., diameter 3×10^{-8} cm and intermolecular space 3×10^{-6} cm). Like sand, these spheres flow one over another, offering friction in between while colliding with one another. Air flowing over a rigid surface (i.e., acting as a flow boundary) will adhere to it, losing velocity; that is, there is a depletion of kinetic energy of the air molecules as they are trapped on the surface, regardless of how polished it may be. On a molecular scale, the surface looks like the crevices shown in Figure 3.4, with air molecules trapped within to stagnation. The contact air layer with the surface adheres and it is known as the “no-slip” condition. The next layer above the stagnated no-slip layer slips over it – and, of course, as it moves away from the surface, it will gradually reach the airflow velocity. The pattern within the boundary layer flow depends on how fast it is flowing.

Here is a good place to define the parameter called the *Reynolds Number* (Re). Re is a useful and powerful parameter – it provides information on the flow status with the interacting body involved:

$$\begin{aligned}
 Re &= (\rho_{\infty} U_{\infty} l) / \mu_{\infty} & (3.16) \\
 &= (\text{density} \times \text{velocity} \times \text{length}) / \text{coefficient of viscosity} \\
 &= (\text{inertia force}) / (\text{viscous force})
 \end{aligned}$$

where μ_{∞} = coefficient of viscosity.

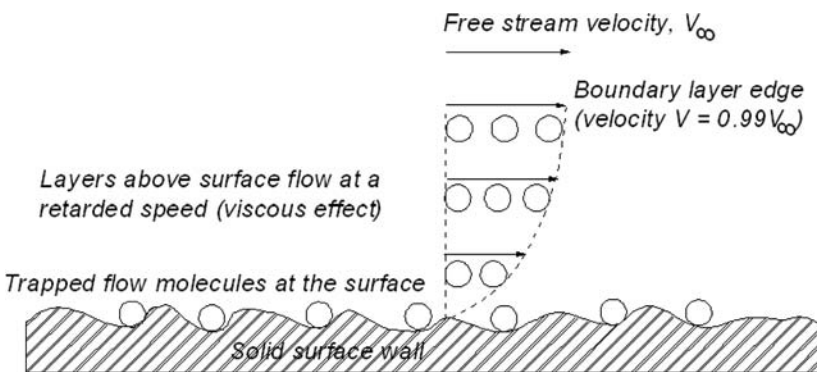


Figure 3.4. Magnified view of airflow over a rigid surface (boundary)

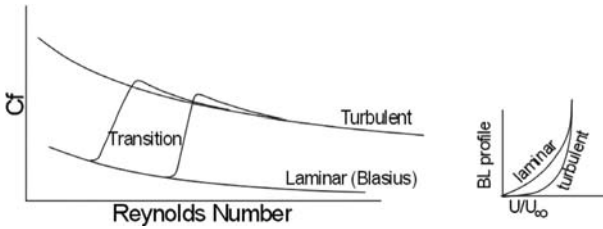


Figure 3.5. Viscous effect of air on a flat plate

It represents the degree of skin friction depending on the property of the fluid. The subscript infinity, ∞ , indicates the condition (i.e., undisturbed infinite distance ahead of the object). Re is a grouped parameter, which reflects the effect of each constituent variable, whether they vary alone or together. Therefore, for a given flow, characteristic length, l , is the only variable in Re . Re increases along the length. In an ideal flow (i.e., inviscid approximation), Re becomes infinity – not much information is conveyed beyond that. However, in real flow with viscosity, it provides vital information: for example, on the nature of flow (turbulent or laminar), on separation, and on many other characteristics.

Figure 3.3 describes a boundary layer of airflow over a flat surface (i.e., plate) aligned to the flow direction (i.e., X axis). Initially, when the flow encounters the flat plate at the leading edge (LE), it develops a boundary layer that keeps growing thicker until it arrives at a critical length, when flow characteristics then make a transition and the profile thickness suddenly increases. The friction effect starts at the LE and flows downstream in an orderly manner, maintaining the velocity increments of each layer as it moves away from the surface – much like a sliding deck of cards (in lamina). This type of flow is called a *laminar flow*. Surface skin-friction depletes the flow energy transmitted through the layers until at a certain distance (i.e., critical point) from the LE, flow can no longer hold an orderly pattern in lamina, breaking down and creating turbulence. The boundary layer thickness is shown as δ at a height where 99% of the free streamflow velocity is attained.

The region where the transition occurs is called the *critical point*. It occurs at a predictable distance from the LE l_{crit} , having a critical Re of Re_{crit} at that point. At this distance along the plate, the nature of the flow makes the transition from laminar to *turbulent flow*, when eddies of the fluid mass randomly cross the layers. Through mixing between the layers, the higher energy of the upper layers energizes the lower layers. The physics of turbulence that can be exploited to improve performance (e.g., dents on a golf ball forces a laminar flow to a turbulent flow) is explained later.

With turbulent mixing, the boundary layer profile changes to a steeper velocity gradient and there is a sudden increase in thickness, as shown in Figure 3.5. For each kind of flow situation, there is a Re_{crit} . As it progresses downstream of l_{crit} , the turbulent flow in the boundary layer is steadily losing its kinetic energy to overcome resistance offered by the sticky surface. If the plate is long enough, then a point may be reached where further loss of flow energy would fail to negotiate the surface constraint and would leave the surface as a *separated flow* (Figure 3.6 shows separation on an aerofoil). Separation also can occur early in the laminar flow.

The extent of velocity gradient, du/dy , at the boundary surface indicates the tangential nature of the frictional force; hence, it is shear force. At the surface where

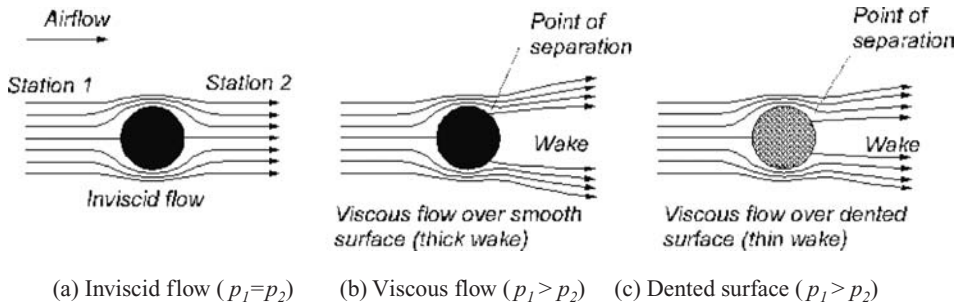


Figure 3.6. Airflow past aerofoil

$u = 0$, du/dy is the velocity gradient of the flow at that point. If F is the shear force on the surface area, A , is due to friction in fluid, then shear stress is expressed as follows:

$$F/A = \tau = \mu(du/dy), \quad (3.17)$$

where μ is the coefficient of viscosity = $1.789 \times 10^{-5} \text{ kg/ms}$ or Ns/m^2 ($1 \text{ g/ms} = 1 \text{ poise}$) for air at sea level ISA. Kinematic viscosity, $\nu = \mu/\rho \text{ m}^2/\text{s}$ ($1 \text{ m}^2/\text{s} = 10^4 \text{ stokes}$), where ρ is density of fluid. The measure of the frictional shear stress is expressed as a *coefficient of friction*, C_f , at the point:

$$\text{coefficient of friction, } C_f = \tau/q_\infty, \quad (3.18)$$

where $q_\infty = \frac{1}{2}\rho V_\infty^2 =$ dynamic head at the point.

The difference of du/dy between laminar and turbulent flow is shown in Figure 3.6a; the latter has a steeper gradient – hence, it has a higher C_f as shown in Figure 3.6b. The up arrow indicates increase and vice versa for incompressible flow, $\text{temp} \uparrow \mu \downarrow$, which reads as viscosity decreases with a rise in temperature, and for compressible flow, $\text{temp} \uparrow \mu \uparrow$.

The pressure gradient along the flat plate gives $dp/dx = 0$. Airflow over the curved surfaces (i.e., 3D surface) accelerates or decelerates depending on which side of the curve the flow is negotiating. It results in a pressure field variation inverse to the velocity variation ($dp/dx \neq 0$).

Extensive experimental investigations on the local skin friction coefficient, C_f , on a 2D flat plate are available for a wide range of Re_s (the typical trend is shown in Figure 3.5). The overall coefficient of skin friction over a 3D surface is expressed as C_F and is higher than the 2D flat plate. C_f increases from laminar to turbulent flow, as can be seen from the increased boundary layer thickness. In general, C_F is computed semi-empirically from the flat plate C_f (see Chapter 9).

To explain the physics of drag, the classical example of flow past a sphere is shown in Figure 3.6. A sphere in inviscid flow will have no drag (Figure 3.6a) because it has no skin friction and there is no pressure difference between the front and aft ends, there is nothing to prevent the flow from negotiating the surface curvature. Diametrically opposite to the front stagnation point is a rear stagnation point, equating forces on the opposite sides. This ideal situation does not exist in nature but can provide important information.

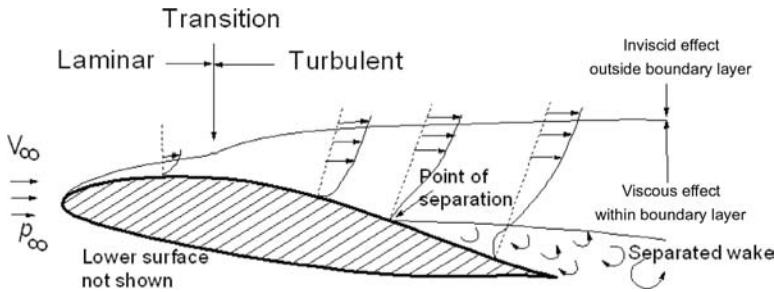


Figure 3.7. Flow past a sphere

In the case of a real fluid with viscosity, the physics changes nature of offering drag as a combination of skin friction and the pressure difference between fore and aft of the sphere. At low Re , the low-energy laminar flow near the surface of the smooth sphere (Figure 3.6b) separates early, creating a large wake in which the static pressure cannot recover to its initial value at the front of the sphere. The pressure at the front is now higher at the stagnation area, resulting in a pressure difference that appears as pressure drag. It would be beneficial if the flow was made turbulent by denting the sphere surface (Figure 3.6c). In this case, high-energy flow from the upper layers mixes randomly with flow near the surface, reenergizing it. This enables the flow to overcome the spheres curvature and adhere to a greater extent, thereby reducing the wake. Therefore, a reduction of pressure drag compensates for the increase in skin-friction drag (i.e., C_f increases from laminar to turbulent flow). This concept is applied to golf-ball design (i.e., low Re velocity and small physical dimension). The dented golf ball would go farther than an equivalent smooth golf ball due to reduced drag. Therefore:

$$\text{drag} = \text{skin friction drag} + \text{pressure drag} \quad (3.19)$$

The situation changes drastically for a body at high Re (i.e., high velocity and/or large physical dimension; e.g., an aircraft wing or even a golf ball hit at a very high speed that would require more than any human effort) when flow is turbulent almost from the LE. A streamlined aerofoil shape does not have the highly steep surface curvature of a golf ball; therefore, separation occurs very late, resulting in a thin wake. Therefore, pressure drag is low. The dominant contribution to drag comes from skin friction, which can be reduced if the flow retains laminarization over more surface area (although it is not applicable to a golf ball). Laminar aerofoils have been developed to retain laminar-flow characteristics over a relatively large part of the aerofoil. These aerofoils are more suitable for low-speed operation (i.e., Re higher than the golf-ball application) such as gliders and have the added benefit of a very smooth surface made of composite materials.

Clearly, the drag of a body depends on its profile – that is, how much wake it creates. The blunter the body, the greater the wake size will be; it is for this reason that aircraft components are streamlined. This type of drag is purely viscous-dependent and is termed *profile drag*. In general, in aircraft applications, it is also called *parasite drag*, as explained in Chapter 9.

Scientists have been able to model the random pattern of turbulent flow using statistical methods. However, at the edges of the boundary layer, the physics is

unpredictable. This makes accurate statistical modeling difficult, with eddy patterns at the edge extremely unsteady and the flow pattern varying significantly. It is clear why the subject needs extensive treatment (see [2]).

3.5.1 Flow Past Aerofoil

A typical airflow past an aerofoil is shown in Figure 3.6; it is an extension of the diagram of flow over a flat plate (see Figure 3.4). In Figure 3.7, the front curvature of the aerofoil causes the flow to accelerate, with the associated drop in pressure, until it reaches the point of inflection on the upper surface of the aerofoil. This is known as a region of favorable pressure gradient because the lower pressure downstream favors airflow. Past the inflection point, airflow starts to decelerate, recovering the pressure (i.e., flow in an adverse pressure gradient) that was lost while accelerating. For inviscid flow, it would reach the trailing edge, regaining the original free streamflow velocity and pressure condition. In reality, the viscous effect depletes flow energy, preventing it from regaining the original level of pressure. Along the aerofoil surface, airflow is depleting its energy due to friction (i.e., the viscous effect) of the aerofoil surface.

The result of a loss of energy while flowing past the aerofoil surface is apparent in adverse pressure gradient – it is like climbing uphill. A point may be reached where there is not enough flow energy left to encounter the adverse nature of the downstream pressure rise – the flow then leaves the surface to adjust to what nature allows. Where the flow leaves the surface is called the *point of separation*, and it is critical information for aircraft design. When separation happens over a large part of the aerofoil, it is said that the aerofoil has *stalled* because it has lost the intended pressure field. Generally, it happens on the upper surface; in a stalled condition, there is a loss of low-pressure distribution and, therefore, a loss of lift, as described in Section 3.6. This is an undesirable situation for an aircraft in flight. There is a minimum speed below which stalling will occur in every winged aircraft. The speed at which an aircraft stalls is known as the *stalling speed*, V_{stall} . At stall, an aircraft cannot maintain altitude and can even become dangerous to fly; obviously, stalling should be avoided.

For a typical surface finish, the magnitude of skin-friction drag depends on the nature of the airflow. Below Re_{crit} , laminar flow has a lower skin friction coefficient, C_f , and, therefore, a lower friction (i.e., lower drag). The aerofoil LE starts with a low Re and rapidly reaches Re_{crit} to become turbulent. Aerofoil designers must shape the aerofoil LE to maintain laminar flow as much as possible.

Aircraft surface contamination is an inescapable operational problem that degrades surface smoothness, making it more difficult to maintain laminar flow. As a result, Re_{crit} advances closer to the LE. For high-subsonic flight speed (high Re), the laminar flow region is so small that flow is considered fully turbulent.

This section points out that designers should maintain laminar flow as much as possible over the wetted surface, especially at the wing LE. As mentioned previously, gliders – which operate at a lower Re – offer a better possibility to deploy an aerofoil with laminar-flow characteristics. The low annual utilization in private usage favors the use of composite material, which provides the finest surface finish. However, although the commercial transport wing may show the promise of partial

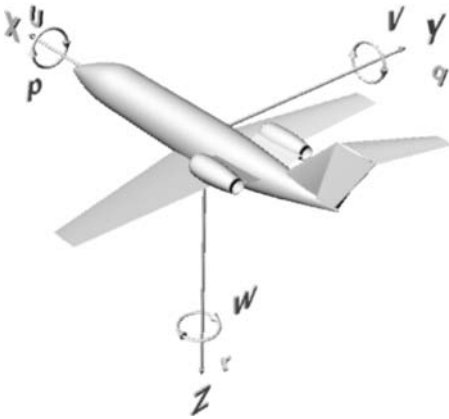


Figure 3.8. Six degrees of freedom in body axes F_B

laminar flow at the LE, the reality of an operational environment at high utilization does not guarantee adherence to the laminar flow. For safety reasons, it would be appropriate for the governmental certifying agencies to examine conservatively the benefits of partial laminar flow. This book considers the fully turbulent flow to start from the LE of any surface of a high-subsonic aircraft.

3.6 Aircraft Motion and Forces

An aircraft is a vehicle in motion; in fact, it must maintain a minimum speed above the stall speed. The resultant pressure field around the aircraft body (i.e., wetted surface) is conveniently decomposed into a usable form for designers and analysts. The pressure field alters with changes in speed, altitude, and orientation (i.e., attitude). This book primarily addresses a steady level flight pressure field; the unsteady situation is considered transient in maneuvers. [Chapter 5](#) addresses certain unsteady cases (e.g., gusty winds) and references are made to these design considerations when circumstances demands it. This section provides information on the parameters concerning motion (i.e., kinematics) and force (i.e., kinetics) used in this book.

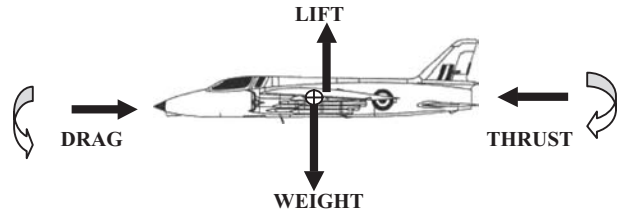
3.6.1 Motion

Unlike an automobile, which is constrained by the road surface, an aircraft is the least restricted vehicle, having all six degrees of freedom ([Figure 3.8](#)): three linear and three rotational motions along and about the three axes. These can be represented in any coordinate system; however, in this book, the righthanded Cartesian coordinate system is used. Controlling motion in six degrees of freedom is a complex matter. Careful aerodynamic shaping of all components of an aircraft is paramount, but the wing takes top priority. Aircraft attitude is measured using Eulerian angles – ψ (azimuth), θ (elevation), and ϕ (bank) – and are in demand for aircraft control; however, this is beyond the scope of this book.

In classical flight mechanics, many types of Cartesian coordinate systems are in use. The three most important are as follows:

1. *Body-fixed axes, F_B* , is a system with the origin at the aircraft CG and the X-axis pointing forward (in the plane of symmetry), the Y-axis going over the right wing, and the Z-axis pointing downward.

Figure 3.9. Equilibrium flight (CG at \oplus). (Folland Gnat: the 1960s, United Kingdom – world’s smallest fighter aircraft. Fuselage length = 9.68 m, span = 7.32 m, height = 2.93 m)



2. *Wind-axes system, F_W* , also has the origin (gimballed) at the CG and the X-axis aligned with the relative direction of airflow to the aircraft and points forward. The Y- and Z-axes follow the righthanded system. Wind axes vary, corresponding to the airflow velocity vector relative to the aircraft.
3. *Inertial axes, F_I* , fixed on the Earth. For speed and altitudes below Mach 3 and 100,000 ft, respectively, the Earth can be considered flat and not rotating, with little error, so the origin of the inertial axes is pegged to the ground. Conveniently, the X-axis points north and the Y-axis east, making the Z-axis point vertically downward in a righthanded system.

In a body-fixed coordinate system, F_B , the components are as follows:

Linear velocities:	U along X-axis (+ve forward)
	V along Y-axis (+ve right)
	W about Z-axis (+ve down)
Angular velocities:	p about X-axis, known as roll (+ve)
	q about Y-axis, known as pitch (+ve nose up)
	r about Z-axis, known as yaw (+ve)
Angular acceleration:	\dot{p} about X-axis, known as roll rate (+ve)
	\dot{q} about Y-axis, known as pitch rate (+ve nose up)
	\dot{r} about Z-axis, known as yaw rate (+ve)

In a wind-axes system, F_W , the components are as follows:

Linear velocities:	V along X-axis (+ve forward)
Linear accelerations:	\dot{V} along X-axis (+ve forward)

and so on.

If the parameters of one coordinate system are known, then the parameters in another coordinate system can be found through the transformation relationship.

3.6.2 Forces

In a steady-state level flight, an aircraft is in equilibrium under the applied forces (i.e., lift, weight, thrust, and drag) as shown in Figure 3.9. Lift is measured perpendicular to aircraft velocity (i.e., free streamflow) and drag is opposite to the direction of aircraft velocity (naturally, the wind axes, F_W , are suited to analyze these parameters). In a steady level flight, lift and weight are opposite one another; opposite forces may not be collinear. In steady level flight (equilibrium),

$$\sum \text{Force} = 0;$$

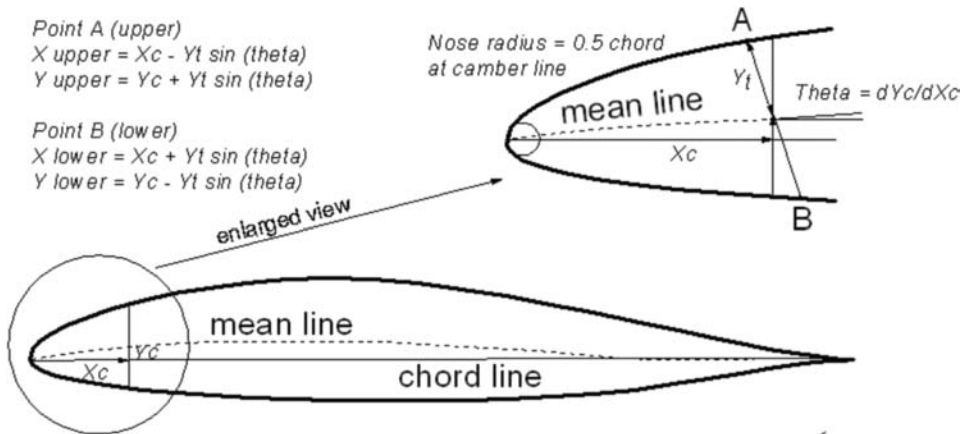


Figure 3.10. Aerofoil section and definitions – NACA family

that is, in the vertical direction, lift = weight, and in the horizontal direction, thrust = drag.

The aircraft weight is exactly balanced by the lift produced by the wing (the fuselage and other bodies could share a part of the lift – discussed later). Thrust provided by the engine is required to overcome drag.

Moments arising from various aircraft components are summed to zero to maintain a straight flight (i.e., in steady level flight, $\sum \text{Moment} = 0$).

Any force/moment imbalance would show up in the aircraft flight profile. This is how an aircraft is maneuvered – through force and/or moment imbalance – even for the simple actions of climb and descent.

3.7 Aerofoil

The cross-sectional shape of a wing (i.e., the bread-slice-like sections of a wing comprising the aerofoil) is the crux of aerodynamic considerations. The wing is a 3D surface (i.e., span, chord, and thickness). An aerofoil represents 2D geometry (i.e., chord and thickness). Aerofoil characteristics are over the unit span at midwing to eliminate effects of the finite 3D wing tip effects. The 3D effects of a wing are discussed in Section 3.11. To standardize aerofoil geometry, Figure 3.10 provides the universally accepted definitions that should be well understood [4].

Chord length is the maximum straight-line distance from the LE to the trailing edge. The *mean line* represents the midlocus between the upper and lower surfaces; the *camber* represents the aerofoil expressed as the percent deviation of the mean line from the chord line. The mean line is also known as the camber line. Coordinates of the upper and lower surfaces are denoted by Y_U and Y_L for the distance X measured from the LE. The *thickness* (t) of an aerofoil is the distance between the upper and the lower contour lines at the distance along the chord, measured perpendicular to the mean line and expressed in percentage of the full chord length. Conventionally, it is expressed as the *thickness to chord* (t/c) ratio in percentage. A small radius at the LE is necessary to smooth out the aerofoil contour. It is convenient to present aerofoil data with the chord length nondimensionalized to unity so that the data can be applied to any size aerofoil by multiplying its chord length.

Aerofoil pressure distribution is measured in a wind tunnel to establish its characteristics, as shown in [4]. Wind-tunnel tests are conducted at midspan of the wing model so that results are as close as possible to 2D characteristics. These tests are conducted at several Re. Higher Re indicates higher velocity; that is, it has more kinetic energy to overcome the skin friction on the surface, thereby increasing the pressure difference between the upper and lower surfaces and, hence, more lift.

In earlier days, drawing the full-scale aerofoils of a large wing and their manufacture was not easy and great effort was required to maintain accuracy to an acceptable level; their manufacture was not easy. Today, CAD/CAM and microprocessor-based numerically controlled lofters have made things simple and very accurate. In December 1996, NASA published a report outlining the theory behind the U.S. National Advisory Committee for Aeronautics (NACA) (predecessor of the present-day NASA) airfoil sections and computer programs to generate NACA aerofoils.

3.7.1 Groupings of Aerofoils and Their Properties

From the early days, European countries and the United States undertook intensive research to generate better aerofoils to advance aircraft performance. By the 1920s, a wide variety of aerofoils appeared and consolidation was needed. Since the 1930s, NACA generated families of aerofoils benefiting from what was available in the market and beyond. It presented the aerofoil geometries and test results in a systematic manner, grouping them into family series. The generic pattern of the NACA aerofoil family is listed in [4] with well-calibrated wind-tunnel results. The book was published in 1949 and has served aircraft designers (civil and military) for more than a half-century and is still useful. Since its publication, research to generate better aerofoils for specific purposes continued, but they are made in the industry and are “commercial in confidence.”

Designations of the NACA series of aerofoils are as follows: the four-digit, the five-digit, and the six-digit, given herein. These suffice for the purposes of this book – many fine aircraft have used the NACA series of aerofoils. However, brief comments on other types of aerofoils are also included. The NACA four- and five-digit aerofoils were created by superimposing a simple camber-line shape with a thickness distribution that was obtained by fitting with the following polynomial [4]:

$$y = \pm (t/0.2) \times (0.2969 \times x^{0.5} - 0.126 \times x - 0.3537 \times x^2 + 0.2843 \times x^3 - 0.1015 \times x^4) \quad (3.20)$$

NACA Four-Digit Aerofoil

Each of the four digits of the nomenclature represents a geometrical property, as explained here using the example of the NACA 2315 aerofoil:

2	3	15
Maximum camber position in % chord	Maximum thickness of maximum camber in 1/10 of chord	The last two digits are maximum t/c ratio in % of chord

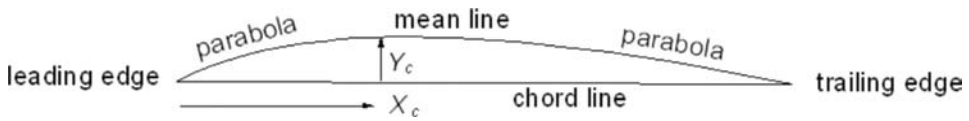


Figure 3.11. Camber line distribution

The camber line of four-digit aerofoil sections is defined by a parabola from the LE to the position of maximum camber followed by another parabola to the trailing edge (Figure 3.11). This constraint did not allow the aerofoil design to be adaptive. For example, it prevented the generation of an aerofoil with more curvature toward the LE in order to provide better pressure distribution.

NACA Five-Digit Aerofoil

After the four-digit sections came the five-digit sections. The first two and the last two digits represent the same definitions as in the four-digit NACA aerofoil. The middle digit represents the aft position of the mean line, resulting in the change in the defining camber line curvature. The middle digit has only two options: 0 for a straight and 1 for an inverted cube. The NACA five-digit aerofoil has more curvature toward the LE. Following are the examples of the NACA 23015 and NACA 23115:

2	3	0 or 1	15
Maximum camber position in % chord	Maximum thickness of maximum camber in 1/10 of chord	0: straight, 1: inverted cube	the last two digits are maximum t/c ratio in % of chord

NACA Six-Digit Aerofoil

The five-digit family was an improvement over the four-digit NACA series aerofoil; however, researchers subsequently found better geometric definitions to represent a new family of a six-digit aerofoil. The state-of-the-art for a good aerofoil often follows reverse engineering – that is, it attempts to fit a cross-sectional shape to a given pressure distribution. The NACA six-digit series aerofoil came much later (it was first used for the P51 Mustang design in the late 1930s) from the need to generate a desired pressure distribution instead of being restricted to what the relatively simplistic four- and five-digit series could offer. The six-digit series aerofoils were generated from a more or less prescribed pressure distribution and were designed to achieve some laminar flow. This was achieved by placing the maximum thickness far back from the LE. Their low-speed characteristics behave like the four- and five-digit series but show much better high-speed characteristics. However, the drag bucket seen in wind-tunnel test results may not show up in actual flight. Some of the six-digit aerofoils are more tolerant to production variation as compared to typical five-digit aerofoils.

The definition for the NACA six-digit aerofoil example 63₂-212 is as follows:

6	3	Subscript 2	2	12
Six series	Location of minimum C_p in 1/10 chord	Half width of low drag bucket in 1/10 of C_l	Ideal C_l in tenths (design)	Maximum thickness in % of chord

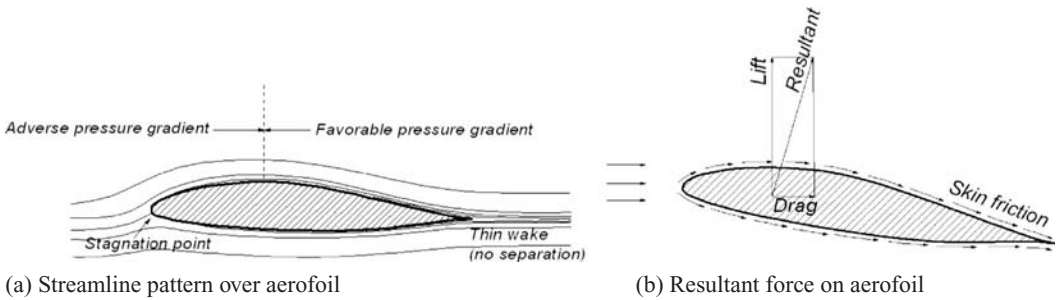


Figure 3.12. Flow field around aerofoil

An example of the NACA 65₃-421 is a six-series airfoil for which the minimum pressure's position is in tenths of a chord, indicated by the second digit (at the 50% chord location). The subscript 3 indicates that the drag coefficient is near its minimum value over a range of lift coefficients of 0.3 above and below the design lift coefficient. The next digit indicates the design lift coefficient of 0.4, and the last two digits indicate the maximum thickness in percent chord of 21% [4].

Other Types of Aerofoils

After the six-series sections, aerofoil design became more specialized with aerofoils designed for their particular application. In the mid-1960s, Whitcomb's "supercritical" aerofoil allowed flight with high critical Mach numbers (operating with compressibility effects, producing in wave drag) in the transonic region. The NACA seven and eight series were designed to improve some aerodynamic characteristics. In addition to the NACA aerofoil series, there are many other types of aerofoils in use.

To remain competitive, the major industrial companies generate their own aerofoils. One example is the peaky-section aerofoils that were popular during the 1960s and 1970s for the high-subsonic flight regime. Aerofoil designers generate their own purpose-built aerofoils with good transonic performance, good maximum lift capability, thick sections, low drag, and so on – some are in the public domain but most are held commercial in confidence for strategic reasons of the organizations. Subsequently, more transonic supercritical aerofoils were developed, by both research organizations and academic institutions. One such baseline design in the United Kingdom is the RAE 2822 aerofoil section, whereas the CAST 7 evolved in Germany. It is suggested that readers examine various aerofoil designs.

The NASA General Aviation Wing (GAW) series evolved later for low-speed applications and use by general aviation. Although the series showed better lift-to-drag characteristics, their performance with flaps deployment, tolerance to production variation, and other issues are still in question. As a result, the GAW aerofoil has yet to compete with some of the older NACA aerofoil designs. However, a modified GAW aerofoil has appeared with improved characteristics. Appendix D provides an example of the GAW series aerofoil.

Often, a wing design has several aerofoil sections varying along the wing span (Figure 3.12). Appendix D provides six types of aerofoil [4] for use in this book. Readers should note that the 2D aerofoil wind-tunnel test is conducted in restricted conditions and will need corrections for use in real aircraft (see Section 3.12).

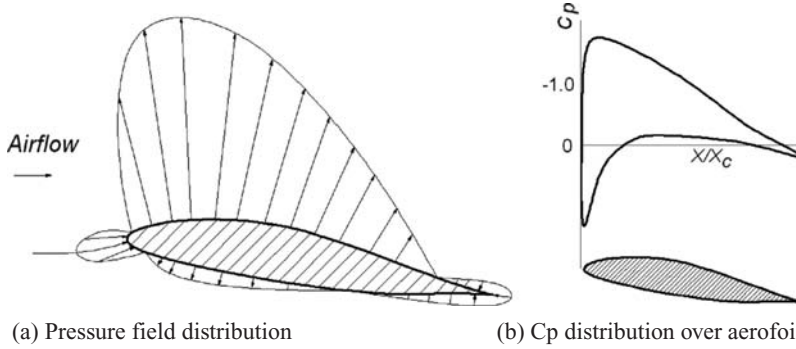


Figure 3.13. Pressure field representations around aerofoil

3.8 Definitions of Aerodynamic Parameters

Section 3.4 defines Re and describes the physics of the laminar/turbulent boundary layer. This section provides other useful nondimensional coefficients and derived parameters frequently used in this book. The most common nomenclature – without any conflicts on either side of the Atlantic – are listed here; it is internationally understood.

$$\text{Let } q_{\infty} = 1/2\rho V_{\infty}^2 = \text{dynamic head} \quad (3.21)$$

(The subscript ∞ represents the free streamflow condition and is sometimes omitted.) ‘ q ’ is a parameter extensively used to nondimensionalize grouped parameters.

The coefficients of the 2D aerofoil and the 3D wing differ, as shown here (the lowercase subscripts represent the 2D aerofoil and the uppercase letters are for the 3D wing).

2-D aerofoil section (subscripts with lowercase letters):

$$\begin{aligned} C_l &= \text{sectional aerofoil-lift coefficient} = \text{section lift}/qc \\ C_d &= \text{sectional aerofoil-drag coefficient} = \text{section drag}/qc \\ C_m &= \text{aerofoil pitching-moment coefficient} \\ &= \text{section pitching moment}/qc^2(+ \text{ nose up}) \end{aligned} \quad (3.22)$$

3D wing (subscripts with uppercase letters), replace chord, c by wing area, S_W :

$$\begin{aligned} C_L &= \text{lift coefficient} = \text{lift}/qS_W \\ C_D &= \text{drag coefficient} = \text{drag}/qS_W \\ C_M &= \text{pitching-moment coefficient} = \text{lift}/qS_W^2(+ \text{ nose up}) \end{aligned} \quad (3.23)$$

Section 3.14 discusses 3D wings, where correction to the 2D results is necessary to arrive at 3D values. Figure 3.13 shows the pressure distribution at any point over the surface in terms of the pressure coefficient, C_p , which is defined as follows:

$$C_p = (p_{local} - p_{\infty})/q \quad (3.24)$$

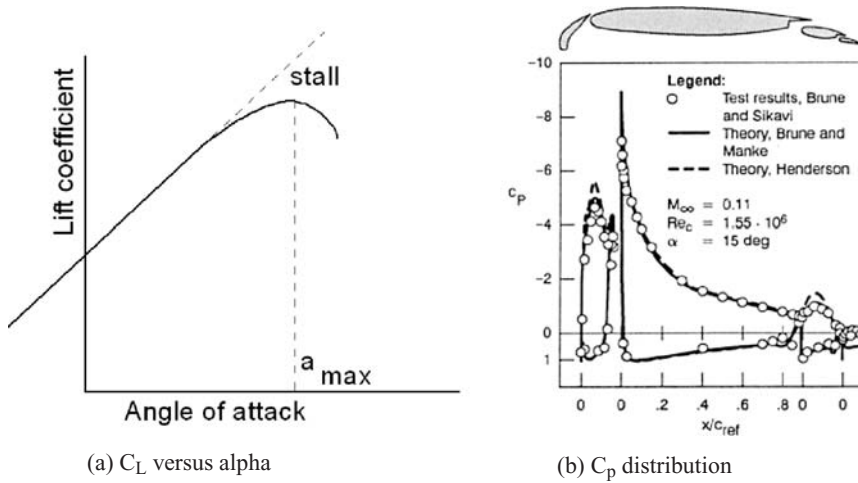


Figure 3.14. Aerofoil characteristics

3.9 Generation of Lift

Figure 3.12 is a qualitative description of the flow field and its resultant forces on the aerofoil. The result of skin friction is the drag force, shown in Figure 3.12b. The lift is normal to the flow.

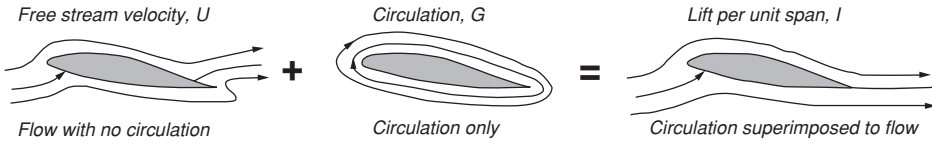
Section 3.5 explains that a typical aerofoil has an upper surface more curved than the lower surface, which is represented by the camber of the aerofoil. Even for a symmetrical aerofoil, the increase in the angle of attack increases the velocity at the upper surface and the aerofoil approaches stall, a phenomenon described in Section 3.10.

Figure 3.13a shows the pressure field around the aerofoil. The pressure at every point is given as the pressure coefficient distribution, as shown in Figure 3.13b. The upper surface has lower pressure, which can be seen as a negative distribution. In addition, cambered aerofoils have moments that are not shown in the figure.

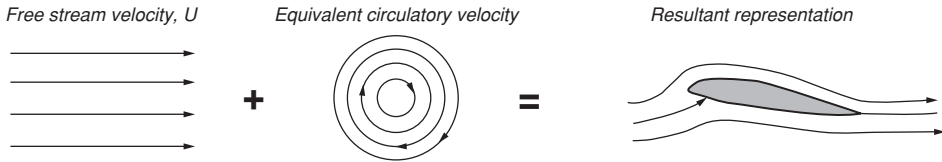
Figure 3.14a shows the typical test results of an aerofoil as plotted against a variation of the angle of attack, α . Initially, the variation is linear; then, at about 10 deg α , it starts to deviate and reaches maximum C_l (C_{lmax} at α_{max}). Past α_{max} , the C_l drops rapidly – if not drastically – when stall is reached. Stalling starts at reaching α_{max} . These graphs show aerofoil characteristics. Figure 3.14b depicts the corresponding distribution of the pressure coefficient C_p at an angle of attack of 15 deg.

Deflection of either the control surface or a change in the angle of attack will alter the pressure distribution. The positive Y-direction has negative pressure on the upper surface. The area between the graphs of the upper and lower surface C_p distribution is the lift generated for the unit span of this aerofoil.

Figure 3.15 shows flow physics around the aerofoil. At the LE, the streamlines move apart: One side negotiates the higher camber of the upper surface and the other side negotiates the lower surface. The higher curvature at the upper surface generates a faster flow than the lower surface. They have different velocities when they meet at the trailing edge, creating a vortex sheet along the span. The phenomenon can be decomposed into a set of straight streamlines representing the



(a) Inviscid flow representation of flow around airfoil



(b) Mathematical representation by superimposing free vortex flow over parallel flow

Figure 3.15. Lift generation on airfoil

free streamflow condition and a set of circulatory streamlines of a strength that matches the flow around the airfoil. The circulatory flow is known as the *circulation* of the airfoil. The concept of *circulation* provides a useful mathematical formulation to represent lift. Circular flow is generated by the effect of the airfoil camber, which gives higher velocity over the upper wing surface. The directions of the circles show the increase in velocity at the top and the decrease at the bottom, simulating velocity distribution over the airfoil.

The flow over an airfoil develops a lift per unit span of $L = \rho U \Gamma$ (see other textbooks for the derivation). Computation of circulation Γ is not easy. This book uses accurate experimental results to obtain the lift.

The center of pressure, *cp*, is the point through which the resultant force of the pressure field around the body acts. For an airfoil, it moves forward as the angle of attack is increased until stall occurs as a degenerate case (Figure 3.16).

The aerodynamic center, *ac*, is concerned with moments about a point, typically on the chord line (Figures 3.17). The relationship between the moment and the angle of attack depends on the approximate point at which the moment is taken. However, at the quarter-chord point (there could be minor variations among airfoils but they

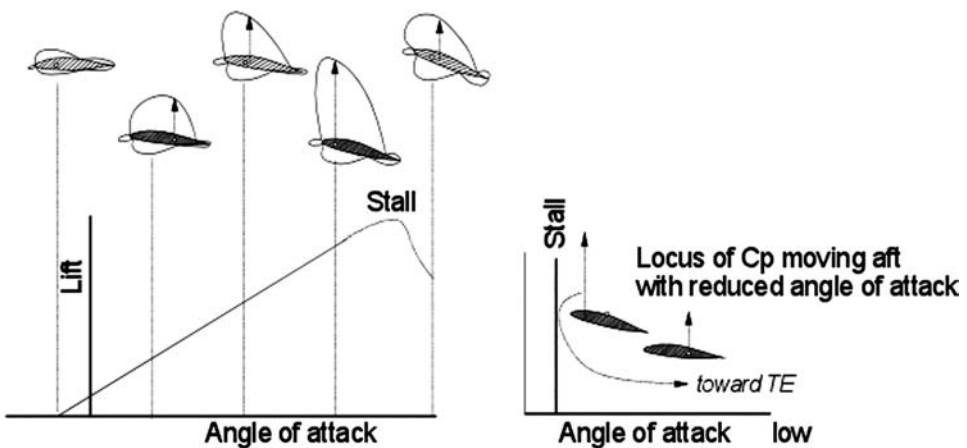
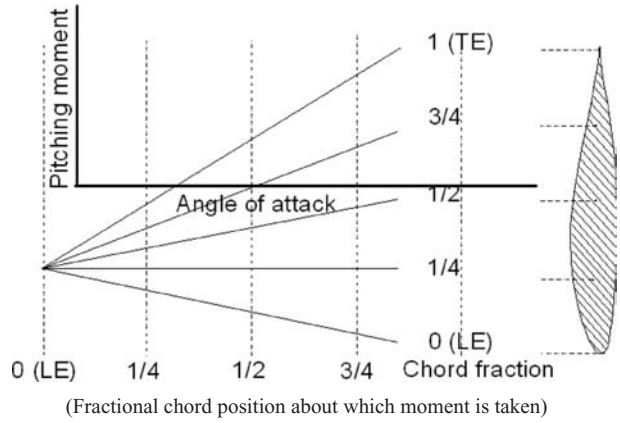


Figure 3.16. Movement of center of pressure with change in lift

Figure 3.17. Aerodynamic center – invariant near quarter-chord



are ignored in this book), it is noticed that the moment is invariant to the angle of attack until stall occurs. This point at the quarter chord is called the ac, which is a natural reference point through which all forces and moments are defined to act. The ac offers much useful information that is discussed later.

The higher the positive camber, the more lift is generated for a given angle of attack; however, this leads to a greater nose-down moment. To counter this nose-down moment, conventional aircraft have a horizontal tail with the negative camber supported by an elevator. For tailless aircraft (e.g., delta wing designs in which the horizontal tail merges with the wing), the trailing edge is given a negative camber as a “reflex.” This balancing is known as *trimming* and it is associated with the type of drag known as *trim drag*. Aerofoil selection is then a compromise between having good lift characteristics and a low moment.

3.10 Types of Stall

Section 3.3 describes the physics of stall phenomena over an aerofoil. It is essential that designers understand stalling characteristics because wing stall is an undesirable state for an aircraft to enter. Figure 3.18 shows the general types of stall that

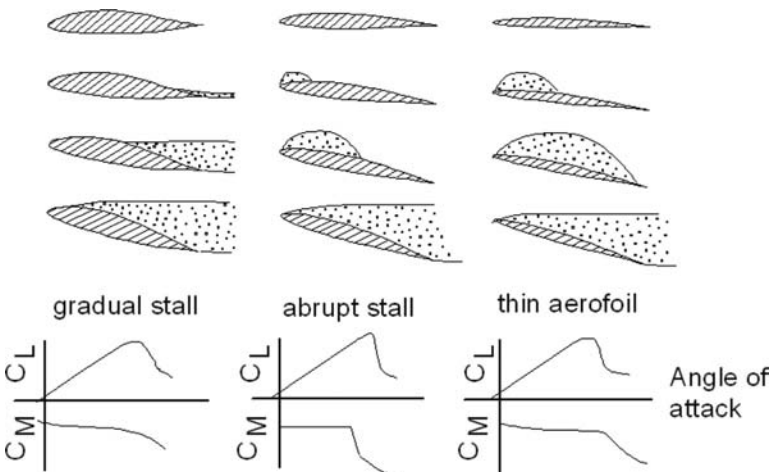


Figure 3.18. Stall patterns

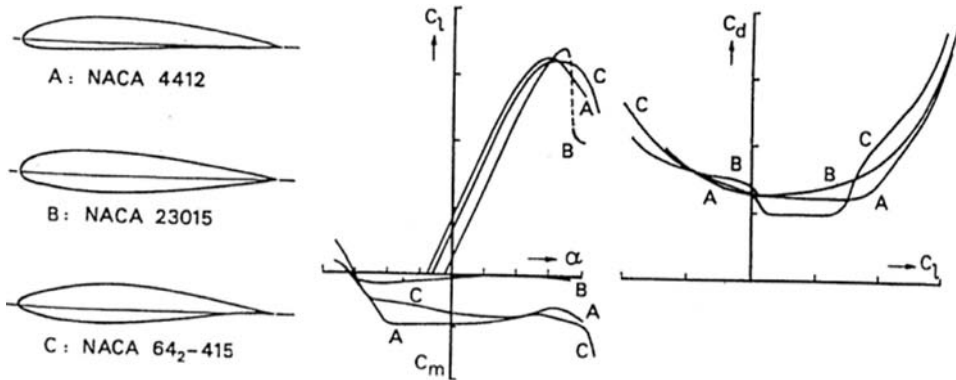


Figure 3.19. Comparison of three NACA aerofoils

can occur. This section describes how these different types of stall affect aircraft design.

3.10.1 Gradual Stall

This is a desirable pattern and occurs when separation is initiated at the trailing edge of the aerofoil; the remainder maintains the pressure differential. As the separation moves slowly toward the LE, the aircraft approaches stall gradually, giving the pilot enough time to take corrective action. The forgiving and gentle nature of this stall is ideal for an ab initio trainee pilot. The type of aerofoil that experiences this type of stall has a generously rounded LE, providing smooth flow negotiation but not necessarily other desirable performance characteristics.

3.10.2 Abrupt Stall

This type of stall invariably starts with separation at the LE, initially as a small bubble. Then, the bubble either progresses downstream or bursts quickly and catastrophically (i.e., abruptly). Aerofoils with a sharper LE, such as those found on higher-performance aircraft, tend to exhibit this type of behavior.

Aircraft stall is affected by wing stall, which depends on aerofoil characteristics. [Section 3.19](#) addresses wing stall (see [Figure 3.40](#)).

3.11 Comparison of Three NACA Aerofoils

The NACA 4412, NACA 23015, and NACA 642-415 are three commonly used aerofoils – there are many different types of aircraft that use one of these aerofoils. [Figure 3.19](#) shows their characteristics for comparison purposes.

The NACA 23015 has sharp stalling characteristics; however, it can give a higher sectional lift, C_l , and lower sectional moment, C_m , than others. Drag-wise, the NACA 642-415 has a bucket to give the lowest sectional drag. The NACA 4412 is the oldest and, for its time, was the favorite. Of these three examples, the NACA 642-415 is the best for gentle stall characteristics and low sectional drag, offsetting the small amount of trim drag due to the relatively higher moment coefficient. Designers

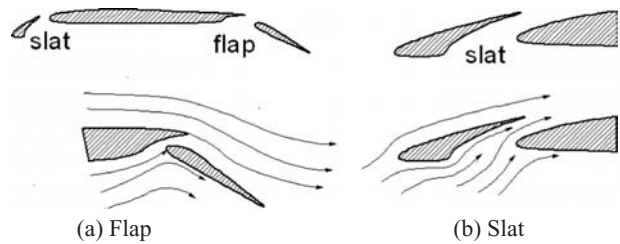


Figure 3.20. Flap and slat flow field (see Figure 3.43 for slat and flap effects)

must choose from a wide variety of aerofoils or generate one suitable for their purposes.

Designers look for the following qualities in the characteristics of a 2D aerofoil:

1. The lift should be as high as possible; this is assessed by the C_{Lmax} of the test results.
2. The stalling characteristics should be gradual; the aerofoil should be able to maintain some lift past C_{Lmax} . Stall characteristics need to be assessed for the application. For example, for ab initio training, it is better to have aircraft with forgiving, gentle stalling characteristics. For aircraft that will be flown by experienced pilots, designers could compromise with gentle stalling characteristics and better performance.
3. There should be a rapid rise in lift; that is, a better lift–curve slope given by $dC_L/d\alpha$.
4. There should be low drag using a drag bucket, retaining flow laminarization as much as possible at the design C_L (i.e., angle of incidence).
5. C_m characteristics should give nose-down moments for a positively cambered aerofoil. It is preferable to have low C_m to minimize trim drag.

An aerofoil designer must produce a suitable aerofoil that encompasses the best of all five qualities – a difficult compromise to make. Flaps are also an integral part of the design. Flap deflection effectively increases the aerofoil camber to generate more lift. Therefore, a designer also must examine all five qualities at all possible flap and slat deflections.

From this brief discussion, it is apparent that aerofoil design itself is state of the art and is therefore not addressed in this book. However, experimental data on suitable aerofoils are provided in Appendix C.

3.12 High-Lift Devices

High-lift devices are small aerofoil-like elements that are fitted at the trailing edge of the wing as a *flap* and/or at the LE as a *slat* (Figures 3.20a and b). In typical cruise conditions, the flaps and slats are retracted within the contour of the aerofoil. Flaps and slats can be used independently or in combination. At low speed, they are deflected about a hinge line, rendering the aerofoil more curved as if it had more camber. A typical flow field around the flaps and slats is shown in Figure 3.20. The entrainment effect through the gap between the wing and the flap allows flow to remain attached in order to provide the best possible lift.




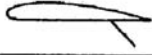
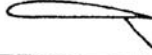
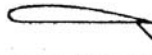
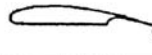

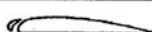

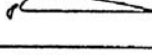
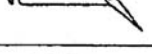
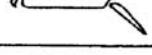
Designation	Diagram	$C_{L_{max}}$	α at $C_{L_{max}}$ (degrees)	L/D at $C_{L_{max}}$	$C_{m_{ac}}$	Reference NACA
Basic aerofoil Clark Y		1.29	15	7.5	-.085	TN 459
.30c Plain flap deflected 45°		1.95	12	4.0	-	TR 427
.30c Slotted flap deflected 45°		1.98	12	4.0	-	TR 427
.30c Split flap deflected 45°		2.16	14	4.3	-0.250	TN 422
.30c hinged at .80c Split flap (Zap) deflected 45°		2.26	13	4.43	-0.300	TN 422
.30c hinged at .90c Split flap (Zap) deflected 45°		2.32	12.5	4.45	-0.385	TN 422
.30c Fowler flap deflected 40°		2.82	13	4.55	-0.660	TR 534
.40c Fowler flap deflected 40°		3.09	14	4.1	-0.860	TR 534
Fixed slot		1.77	24	5.35	-	TR 427
Handley Page automatic slot		1.84	28	4.1	-	TN 459
Fixed slot and .30c plain flap deflected 45°		2.18	19	3.7	-	TR 427
Fixed slot and .30c slotted flap deflected 45°		2.26	18	3.77	-	TR 427
Handley Page slot and .40c Fowler flap deflected 40°		3.36	16	3.7	-0.740	TN 459

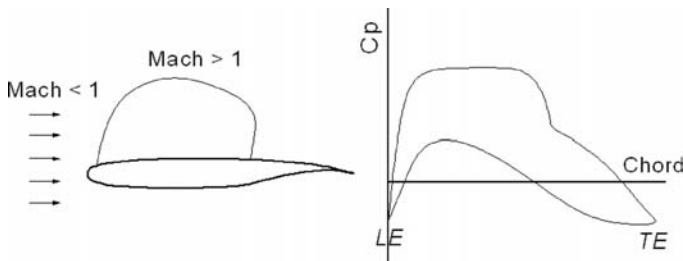
Figure 3.21. High-lift devices

Considerable lift enhancement can be obtained by incorporating high-lift devices at the expense of additional drag and weight. Figure 3.21 lists the experimental values of the incremental lift coefficients of the Clark Y aerofoil. These values are representative of other types of NACA aerofoils and may be used if actual data are not available.

Higher-performance, high-lift devices are complex in construction and therefore heavier and more expensive. Selection of the type is based on cost-versus-performance trade-off studies – in practice, past experience is helpful in making selections.

3.13 Transonic Effects – Area Rule

At high subsonic speeds, the local velocity along a curved surface (e.g., on an aerofoil surface) can exceed the speed of sound, whereas flow over the rest of the surface



Typical flat upper surface with aft camber for rear loading

Figure 3.22. Transonic flow (supercritical Whitcomb aerofoil)

remains subsonic. In this case, the aerofoil is said to be in *transonic flow*. At higher angles of attack, transonic effects can appear at lower flight speeds. Aerofoil-thickness distribution along the chord length is the parameter that affects the induction of transonic flow. Transonic characteristics exhibit an increase in wave drag (i.e., the compressibility effect; refer to aerodynamic textbooks). These effects are undesirable but unavoidable; however, aircraft designers keep the transonic effect to a minimum. Special attention is necessary in generating the aerofoil section design, which shows a flatter upper surface. Figure 3.22 depicts a typical transonic aerofoil (i.e., the Whitcomb section) and its characteristics.

The Whitcomb section, which appeared later, advanced the flight speed by minimizing wave drag (i.e., the critical Mach-number effects); therefore, it is called the *supercritical aerofoil section*. The geometrical characteristics exhibit a round LE, followed by a flat upper surface and rear-loading with camber; the lower surface at the trailing edge shows the cusp. All modern high-subsonic aircraft have the supercritical aerofoil section characteristics. Manufacturers develop their own section or use any data available to them.

For an aircraft configuration, it has been shown that the cross-sectional area distribution along the body axis affects the wave drag associated with transonic flow. The bulk of this area distribution along the aircraft axis comes from the fuselage and the wing. The best cross-sectional area distribution that minimizes wave drag is a cigar-like smooth distribution (i.e., uniform contour curvature; lowest wave drag) known as the *Sears-Haack ideal body* (Figure 3.23). The fuselage shape approximates it; however, when the wing is attached, there is a sudden jump in volume distribution (Figure 3.23). In the late 1950s, Whitcomb demonstrated through experiments that “waisting” of the fuselage in a “coke-bottle” shape could accommodate wing volume, as shown in the last of Figure 3.23. This type of procedure for wing–body shaping is known as the *area rule*. A smoother distribution of the cross-sectional area reduces wave drag.

Whitcomb’s finding was deployed on F102 Delta Dragger fighter aircraft (see Figure 3.23). The modified version with area ruling showed considerably reduced transonic drag (see Figure 4.29). For current designs with wing–body blending, it is less visible, but designers still study the volume distribution to make it as smooth as possible. Even the hump of a Boeing 747 flying close to transonic speed helps with the area ruling. The following subsection considers wing (i.e., 3D body) aerodynamics.

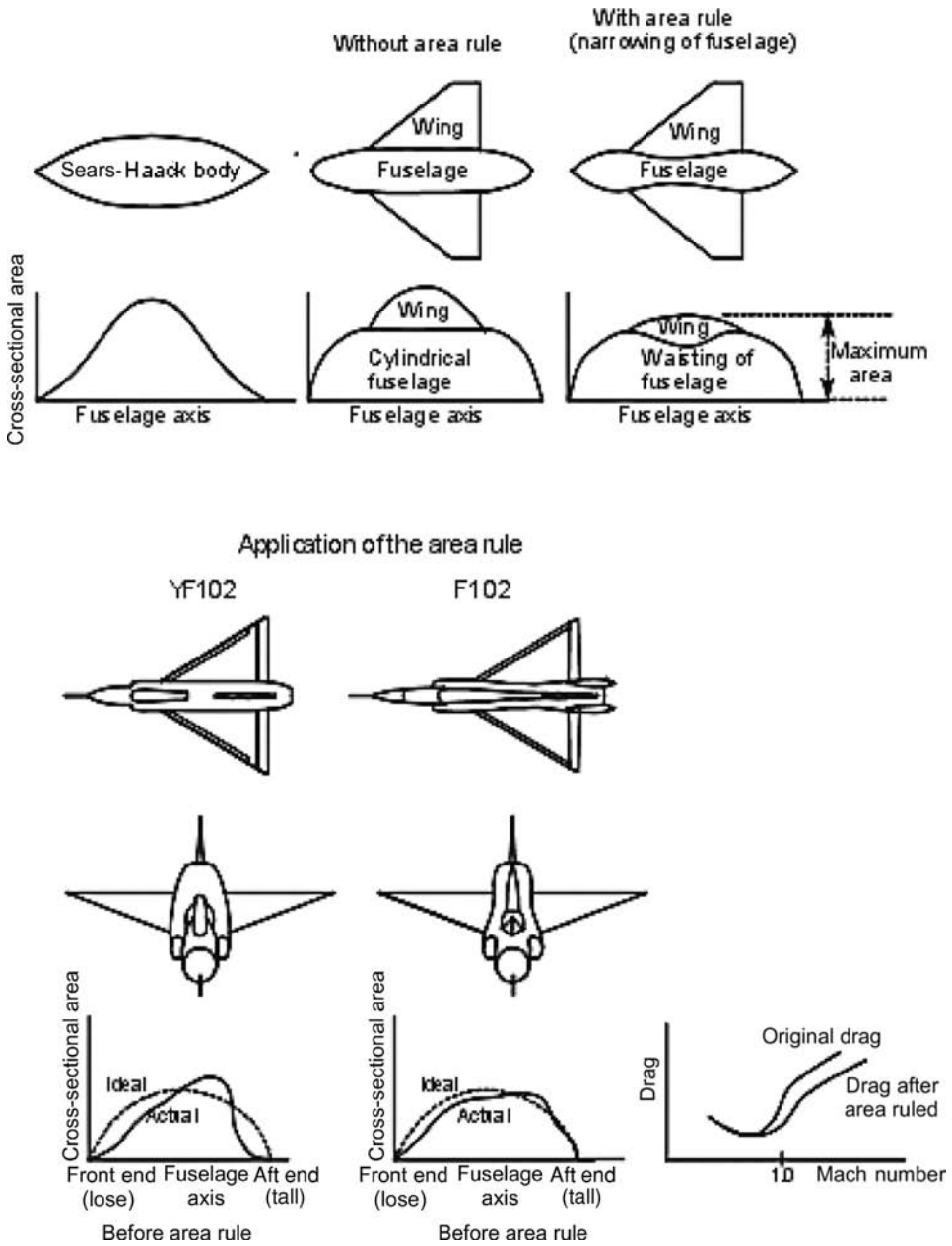


Figure 3.23. Area rule

3.14 Wing Aerodynamics

Similar to a bird's wing, an aircraft's wing is the lifting surface with the chosen aerofoil section, which can vary spanwise. The lift generated by the wing sustains the weight of the aircraft to make flight possible. Proper wing planform shape and size are crucial to improving aircraft efficiency and performance; however, aerofoil parameters are often compromised with the cost involved.

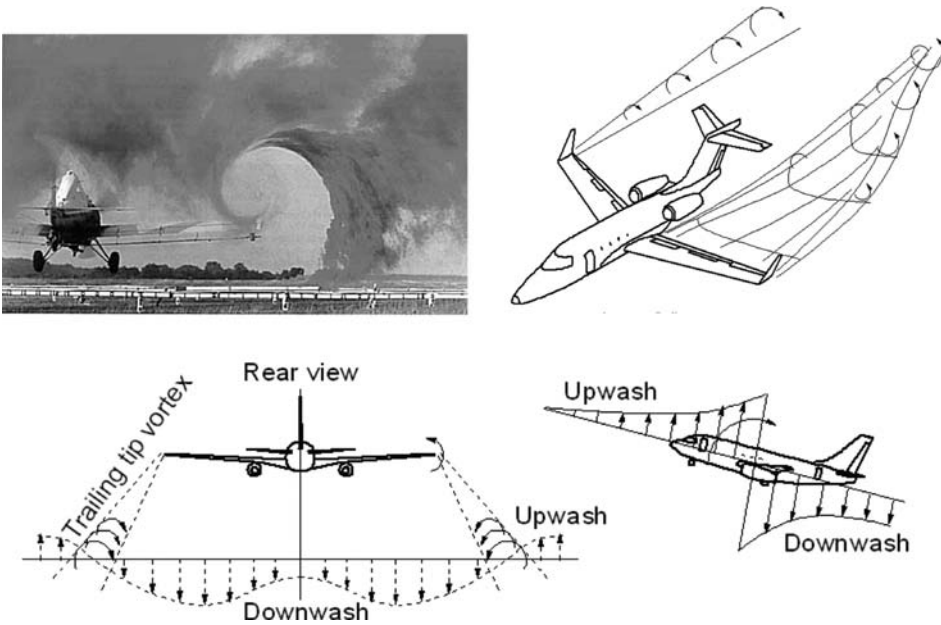


Figure 3.24. Wing tip vortex

A 3D finite wing produces vortex flow as a result of tip effects, as shown in Figure 3.24 and explained in Figure 3.25. The high pressure from the lower surface rolls up at the free end of the finite wing, creating the tip vortex.

The direction of vortex flow is such that it generates downwash, which is distributed spanwise at varying strengths. A reaction force of this downwash is the lift generated by the wing. Energy consumed by the downwash appears as lift-dependent induced drag, D_i , and its minimization is a goal of aircraft designers.

The physics explained thus far is represented in geometrical definitions, as shown in Figure 3.26. This is used in formulations, as discussed herein. An elliptical wing planform (e.g., the Spitfire fighter of World War II) creates a uniform spanwise

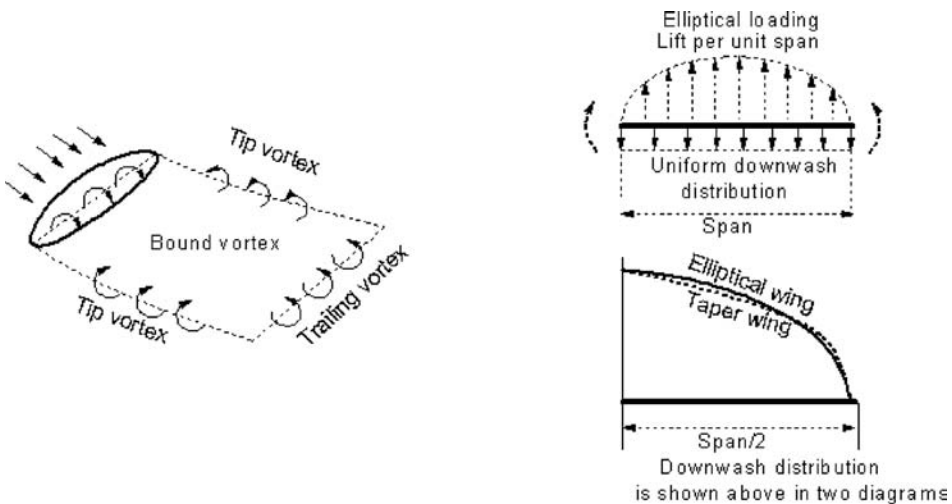


Figure 3.25. Pressure, flow pattern, and downwash effect of finite 3D wing

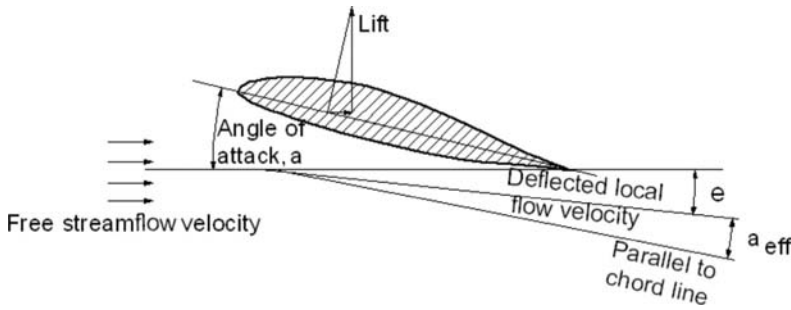


Figure 3.26. Downwash angle and its distribution on elliptical wing planform

downwash at its lowest magnitude and leads to minimum induced drag. Figure 3.26 shows that the downwash effect of a 3D wing deflects free streamflow, V_∞ , by an angle, ϵ , to V_{local} . It can be interpreted as if the section of 3D wing behaves as a 2D infinite wing with:

$$\text{effective angle of incidence, } \alpha_{eff} = (\alpha - \epsilon), \quad (3.25)$$

where α is the angle of attack at the aerofoil section, by V_∞ .

Aerodynamics textbooks may be consulted to derive theoretically the downwash angle:

$$\epsilon = C_L / \mu AR \text{ (in radians)} = 57.3 C_L / \mu AR \text{ (in deg)} \quad (3.26)$$

For a nonelliptical wing planform, the downwash will be higher and a semi-empirical correction factor, e , called *Oswald's efficiency factor* (always ≤ 1) is applied, as follows:

$$\text{average downwash angle, } \epsilon = C_L / e \mu AR \text{ (in radians)} = 57.3 C_L / e \mu AR \text{ (in deg)} \quad (3.27)$$

The extent of downwash is lift-dependent; that is, it increases with an increase in C_L . Strictly speaking, Oswald's efficiency factor, e , varies with wing incidence; however, the values used are considered an average of those found in the cruise segment and remain constant. In that case, for a particular aircraft design, the average downwash angle, ϵ , is treated as a constant taken at the midcruise condition. Advanced wings of commercial transport aircraft can be designed in such a way that at the design point, $e \approx 1.0$.

Equations 3.26 and 3.27 show that the downwash decreases with an increase in the aspect ratio, AR . When the aspect ratio reaches infinity, there is no downwash and the wing becomes a 2D infinite wing (i.e., no tip effects) and its sectional characteristics are represented by aerofoil characteristics. The downwash angle, ϵ , is small – in general, less than 5 deg for aircraft with a small aspect ratio. The aerofoil section of the 3D wing apparently would produce less lift than the equivalent 2D aerofoil. Therefore, 2D aerofoil test results would require correction for a 3D wing application, as explained in the following section.

Local lift, L_{local} , produced by a 3D wing, is resolved into components perpendicular and parallel to free streamflow, V_∞ . In coefficient form, the integral of these

forces over the span gives the following:

$$C_L = L \cos \varepsilon / q S_W \text{ and } C_{Di} = L \sin \varepsilon / q S_W \text{ (the induced-drag coefficient)}$$

For small angles, ε , it reduces to:

$$C_L = L / q S_W \quad \text{and} \quad C_{Di} = L \varepsilon / q S_W = C_L \varepsilon \quad (3.28)$$

C_{Di} is the drag generated from the downwash angle, ε , and is lift-dependent (i.e., induced); hence, it is called the *induced-drag coefficient*. For a wing planform, Equations 3.27 and 3.28 become:

$$C_{Di} = C_L \varepsilon = C_L \times C_L / e \mu AR = C_L^2 / e \mu AR \quad (3.29)$$

Induced drag is lowest for an elliptical wing planform, when $e = 1$; however, it is costly to manufacture. In general, the industry uses a trapezoidal planform with a taper ratio, $\lambda \approx 0.4$ to 0.5 , resulting in an e value ranging from 0.85 to 0.98 (an optimal design approaches 1.0). A rectangular wing has a ratio of $\lambda = 1.0$ and a delta wing has a ratio of $\lambda = 0$, which result in an average e below 0.8 . A rectangular wing with its constant chord is the least expensive planform to manufacture for having the same-sized ribs along the span.

3.14.1 Induced Drag and Total Aircraft Drag

Equation 3.19 gives the basic definition of drag, which is viscous-dependent. The previous section showed that the tip effects of a 3D wing generate additional drag for an aircraft that appears as induced drag, D_i . Therefore, the total aircraft drag in incompressible flow would be as follows:

$$\begin{aligned} \text{aircraft drag} &= \text{skin-friction drag} + \text{pressure drag} + \text{induced drag} \\ &= \text{parasite drag} + \text{induced drag} \end{aligned} \quad (3.30)$$

Most of the first two terms does not contribute to the lift and is considered parasitic in nature; hence, it is called the *parasite drag*. In coefficient form, it is referred to as C_{DP} . It changes slightly with lift and therefore has a minimum value. In coefficient form, it is called the *minimum parasite drag coefficient*, C_{DPmin} , or C_{D0} . The induced drag is associated with the generation of lift and must be tolerated. Incorporating this new definition, Equation 3.30 can be written in coefficient form as follows:

$$C_D = C_{DP} + C_{Di} \quad (3.31)$$

Chapter 9 addresses aircraft drag in more detail and the contribution to drag due to the compressibility effect also is presented.

3.15 Aspect Ratio Correction of 2D Aerofoil Characteristics for 3D Finite Wing

To incorporate the tip effects of a 3D wing, 2D test data need to be corrected for Re and span. This section describes an example of the methodology.

Equation 3.25 indicates that a 3D wing will produce α_{eff} at an attitude when the aerofoil is at the angle of attack, α . Because α_{eff} is always less than α , the wing produces less C_L corresponding to aerofoil C_l (see Figure 3.28). This section describes

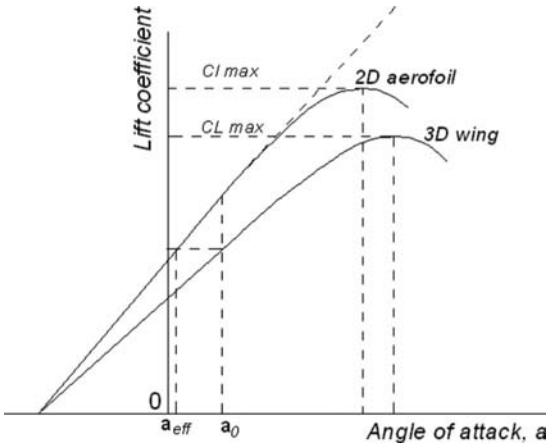


Figure 3.27. Lift-curve-slope correction for aspect ratio

how to correct the 2D aerofoil data to obtain the 3D wing lift coefficient, C_L , versus the angle of attack, α , relationship. Within the linear variation, $dC_L/d\alpha$ needs to be evaluated at low angles (e.g., from -2 to 8 deg).

$$\text{The 2D aerofoil lift-curve slope } a_0 = (dC_L/d\alpha), \quad (3.32)$$

where α = angle of attack (incidence).

The 2D aerofoil will generate the same lift at a lower α of α_{eff} (see Equation 3.25) than what the wing will generate at α ($\alpha_{3D} > \alpha_{2D}$). Therefore, using the 2D aerofoil data, the wing lift coefficient C_L can be worked at the angle of attack, α , as shown here (all angles are in degrees). The wing lift at an angle of attack, α , is as follows:

$$C_L = a_0 \times \alpha_{\text{eff}} + \text{constant} = a_0 \times (\alpha - \varepsilon) + \text{constant} \quad (3.33)$$

or

$$C_L = a_0 \times (\alpha - 57.3C_L/e\mu/AR) + \text{constant}$$

or

$$C_L + (57.3 C_L \times a_0/e\mu AR) = a_0 \times \alpha + \text{constant}$$

or

$$C_L = (a_0 \times \alpha)/[1 + (57.3 \times a_0/e\mu AR)] + \text{constant}/[1 + (57.3 \times a_0/e\mu AR)] \quad (3.34)$$

Differentiating with respect to α , it becomes:

$$dC_L/d\alpha = a_0/[1 + (57.3/e\mu AR)] = a = \text{lift - curve slope of the wing} \quad (3.35)$$

The wing tip effect delays the stall by a few degrees because the outer-wing flow distortion reduces the local angle of attack; it is shown as $\Delta\alpha_{\text{max}}$. Note that $\Delta\alpha_{\text{max}}$ is the shift of $C_{L\text{max}}$; this value $\Delta\alpha_{\text{max}}$ is determined experimentally. In this book, the empirical relationship of $\Delta\alpha_{\text{max}} = 2$ deg, for $AR > 5$ to 12 , $\Delta\alpha_{\text{max}} = 1$ deg, for $AR > 12$ to 20 , and $\Delta\alpha_{\text{max}} = 0$ deg, for $AR > 20$.

Evidently, the wing-lift-curve slope, $dC_L/d\alpha = a$, is less than the 2D aerofoil-lift-curve slope, a_0 . Figure 3.27 shows the degradation of the wing-lift-curve slope, $dC_L/d\alpha$, from its 2D aerofoil value.

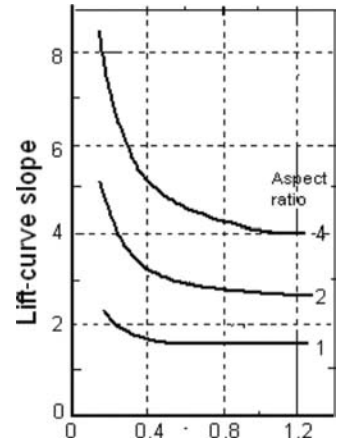


Figure 3.28. Effect of t/c on $dC_L/d\alpha$

The 2D test data offer the advantage of representing any 3D wing when corrected for its aspect ratio. The effect of the wing sweep and aspect ratio on $dC_L/d\alpha$ is shown in Figures 3.28 and 3.29 (taken from NASA).

If the flight Re is different from the experimental Re , then the correction for C_{Lmax} must be made using linear interpolation. In general, experimental data provide C_{Lmax} for several Re s to facilitate interpolation and extrapolation.

Example: Given the NACA 2412 aerofoil data (see test data in Appendix D), construct wing C_L versus α graph for a rectangular wing planform of aspect ratio 7 having an Oswald’s efficiency factor, $e = 0.75$, at a flight $Re = 1.5 \times 10^6$.

From the 2D aerofoil test data at $Re = 6 \times 10^6$, find $dC_l/d\alpha = a_0 = 0.095$ per degree (evaluate within the linear range: -2 to 8 deg). C_{lmax} is at $\alpha = 16$ deg.

Use Equation 3.26 to obtain the 3D wing-lift-curve slope:

$$dC_L/d\alpha = a = a_0/[1 + (57.3/e\mu AR)] = 0.095/[1 + (57.3/0.75 \times 3.14 \times 7)] = 0.095/1.348 = 0.067$$

From the 2D test data, C_{lmax} for three Re s for smooth aerofoils and one for a rough surface, interpolation results in a wing $C_{lmax} = 1.25$ at flight

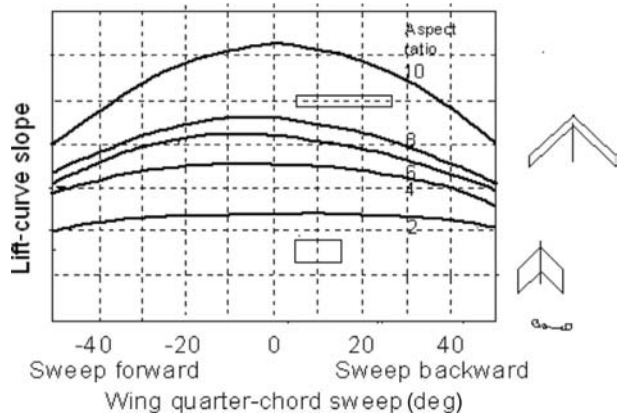


Figure 3.29. Effect of sweep on $dC_L/d\alpha$

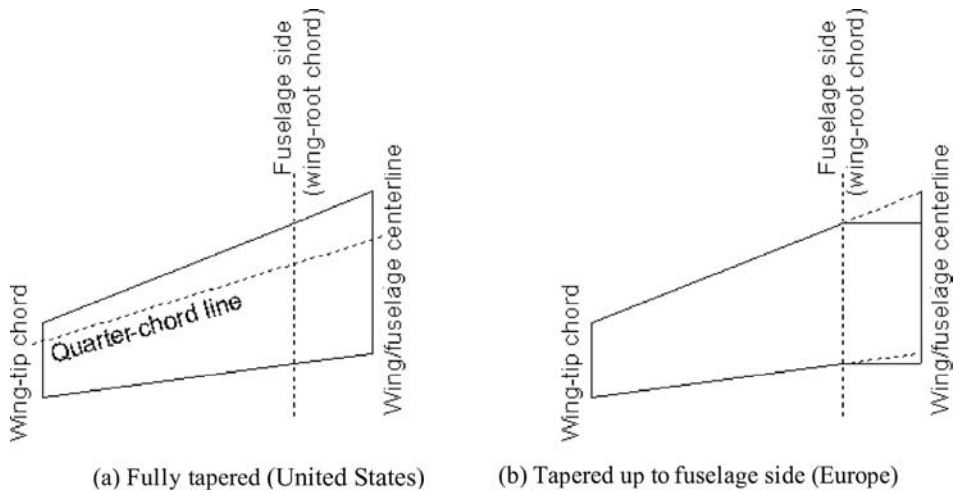


Figure 3.30. Wing planform definition (half wing shown)

$Re = 1.5 \times 10^6$. Finally, for $AR = 7$, the $\Delta\alpha_{\max}$ increment is 1 deg, which means that the wing is stalling at $(16 + 1) = 17$ deg.

The wing has lost some lift-curve slope (i.e., less lift for the same angle of attack) and stalls at a slightly higher angle of attack compared to the 2D test data. Draw a vertical line from the 2D stall $\alpha_{\max} + 1$ deg (the point where the wing maximum lift is reached). Then, draw a horizontal line with $C_{L_{\max}} = 1.25$. Finally, translate the 2D stalling characteristic of $\Delta\alpha$ to the 3D wing-lift-curve slope joining the portion to the $C_{L_{\max}}$ point following the test-data pattern.

This demonstrates that the wing C_L versus the angle of attack, α , can be constructed (see Figure 3.27).

3.16 Wing Definitions

This section defines the parameters used in wing design and explains their role. The parameters are the wing planform area (also known as the wing reference area, S_W); wing-sweep angle, Λ ; and wing taper ratio, λ (dihedral and twist angles are given after the reference area is established). Also, the reference area generally does not include any extension area at the leading and trailing edges. Reference areas are concerned with the projected rectangular/trapezoidal area of the wing.

3.16.1 Planform Area, S_W

The wing planform area acts as a reference area for computational purposes. The wing planform reference area is the projected area, including the area buried in the fuselage shown as a dashed line in Figure 3.30. However, the definition of the wing planform area differs among manufacturers. In commercial transport aircraft design, there are primarily two types of definitions practiced (in general) on either side of the Atlantic. The difference in planform area definition is irrelevant as long as the type is known and adhered to. This book uses the first type (Figure 3.30a), which is prevalent in the United States and has straight edges extending to the fuselage centerline. Some European definitions show the part buried inside the fuselage

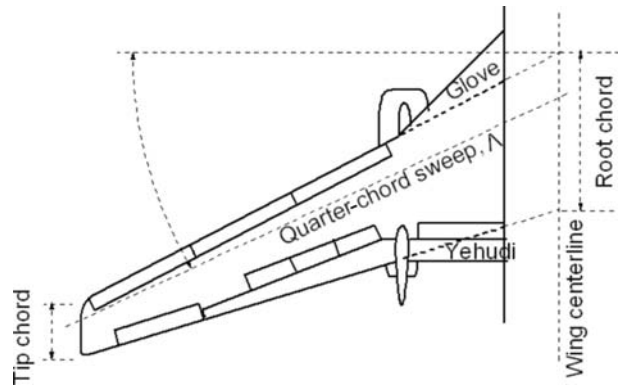


Figure 3.31. Wing geometry definition (Boeing 737 half wing)

as a rectangle (Figure 3.30b); that is, the edges are not straight up to centerline unless it is a rectangular wing normal to the centerline. Section 4.8 describes the various options available from which to choose a wing planform.

A typical subsonic commercial transport-type wing is shown in Figure 3.31. An extension at the LE of the wing root is called a *glove* and an extension at the trailing edge is called a *yehudi* (this is Boeing terminology). The yehudi's low-sweep trailing edge offers better flap characteristics. These extensions can originate in the baseline design or on the existing platform to accommodate a larger wing area. A glove and/or a yehudi can be added later as modifications; however, this is not easy because the aerofoil geometry would be affected.

3.16.2 Wing Aspect Ratio

In the simplest rectangular wing planform area, the aspect ratio is defined as aspect ratio, $AR = (\text{span}, b)/(\text{chord}, c)$. For a generalized trapezoidal wing planform area:

$$\text{aspect ratio, } AR = (b \times b)/(b \times c) = (b^2)/(S_w) \quad (3.36)$$

3.16.3 Wing Sweep Angle, Λ

The wing quarter-chord line is the locus of one fourth of the chord of the reference wing planform area measured from the LE, as shown in Figure 3.31. The wing sweep is measured by the angle of the quarter-chord line extended from the line perpendicular to the centerline.

3.16.4 Wing Root (c_{root}) and Tip (c_{tip}) Chord

These are the aerofoil chords parallel to the aircraft at the centerline and the tip, respectively, of the trapezoidal reference area.

3.16.5 Wing Taper Ratio, λ

This is defined as the ratio of the wing tip chord to the wing root chord ($c_{\text{tip}}/c_{\text{root}}$). The best taper ratio is in the range from 0.3 to 0.6. The taper ratio improves the wing efficiency by giving a higher Oswald's efficiency factor (see Section 3.10).

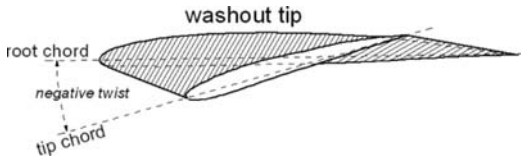


Figure 3.32. Wing twist

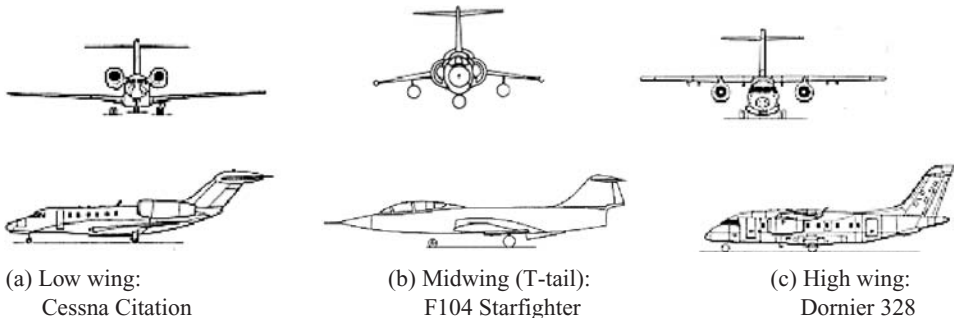
3.16.6 Wing Twist

The wing can be twisted by making the wing tip nose down (i.e., washout) relative to the wing root (Figure 3.32), which causes the wing root to stall earlier (i.e., retain aileron effectiveness). Typically, a 1- to 2-deg washout twist is sufficient. Twisting the wing tip upward is known as *washin*.

3.16.7 High/Low Wing

Depending on the design drivers, an aircraft configuration can place the wing anywhere from the top (i.e., high wing) to the bottom (i.e., low wing) of the fuselage or in between (i.e., midwing), as shown in Figure 3.33. Structural considerations of the wing attachment to the fuselage comprise a strong design driver, although in the civil aircraft market, the choice could be dictated by customer preference. The wing center section should not interfere with the cabin passage-height clearance – especially critical for smaller aircraft. A fairing is shown for low-wing aircraft (Figure 3.33a, Cessna Citation) or high-wing aircraft (Figure 3.33c, Dornier 328), where the wing passes under or over the fuselage, respectively. Both cases have a generous fairing that conceals the fuselage mould-line kink (i.e., drag-reduction measure), which would otherwise be visible. Midwing (or near-midwing) designs are more appropriate to larger aircraft with a passenger cabin floorboard high enough to allow the wing box positioned underneath it.

Aircraft with a high wing allow better ground clearance (see Figures 3.33c and 3.49) and the fuselage to be closer to the ground, which makes cargo-loading easier – especially with a rear-fuselage cargo door. Turboprops favor a high-wing configuration to allow sufficient ground clearance for the propeller. The main undercarriage is mounted on the fuselage sides with the bulbous fairing causing some additional drag. However, this configuration provides better aerodynamics (e.g., the BAe RJ100 and Dornier 328 are successful high-wing designs). The dominant configuration for civil transport aircraft has been a low wing, which provides a wider



(a) Low wing:
Cessna Citation

(b) Midwing (T-tail):
F104 Starfighter

(c) High wing:
Dornier 328

Figure 3.33. Positioning of wing with respect to fuselage (all T-tail configurations)

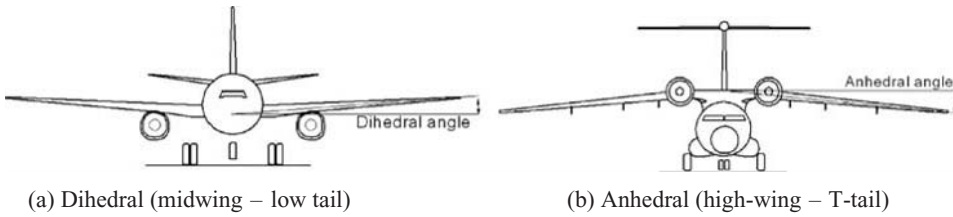


Figure 3.34. Wing dihedral and anhedral angles

main-undercarriage wheel track (see Chapter 7), allowing better ground maneuvering. A low wing also offers a better crashworthy safety feature in the extremely rare emergency situation of a belly landing. However, the author believes more high-winged, large commercial transport aircraft could be developed. Design trends shows that military transport aircraft have predominantly high wings with large rear-mounted cargo doors.

3.16.8 Dihedral/Anhedral Angles

Aircraft in a yaw/roll motion have a cross-flow over the wing affecting the aircraft roll stability (see Chapter 12). The *dihedral angle* (i.e., the wing tip chord raised above the wing root chord) assists roll stability. A typical dihedral angle is between 2 and 3 deg and rarely exceeds 5 deg. Figure 3.34a shows that the dihedral angle with a low-wing configuration also permits more ground clearance for the wing tip. The opposite of a dihedral angle is an *anhedral angle*, which lowers the wing tip with respect to the wing root and is typically associated with high-wing aircraft (Figure 3.34b). The dihedral or anhedral angle also can be applied to the horizontal tail.

3.17 Mean Aerodynamic Chord

Various wing reference geometries and parameters are used in aerodynamic computations. A most important parameter is the mean aerodynamic chord (MAC), which is the chord-weighted average chord length of the wing, defined as follows:

$$MAC = \frac{2}{S_W} \int_0^{b/2} c^2 dy, \tag{3.37}$$

where c is the local wing chord and S_W is the wing reference area:

trapezoidal wing reference area, S_W (with sweep) (Figure 3.35)
 half wing area = rectangle – two triangles

$$\begin{aligned} &= A \times B - \frac{1}{2}(A - C_R) \times B - \frac{1}{2}(A - C_T) \times B \\ &= A \times B - \frac{1}{2}(A \times B) + \frac{1}{2}(B \times C_R) - \frac{1}{2}(A \times B) + \frac{1}{2}(B \times C_T) \\ &= \frac{1}{2}(C_R + C_T) \times B \end{aligned}$$

For the full wing when the span $b = 2B$:

$$\text{wing area, } S_W = \frac{1}{2} (C_R + C_T) \times b$$

Evaluating Equation 3.20 for the linear trapezoidal wing results in:

$$c = C_{root} - 2(C_{root} - C_{tip})y/b$$

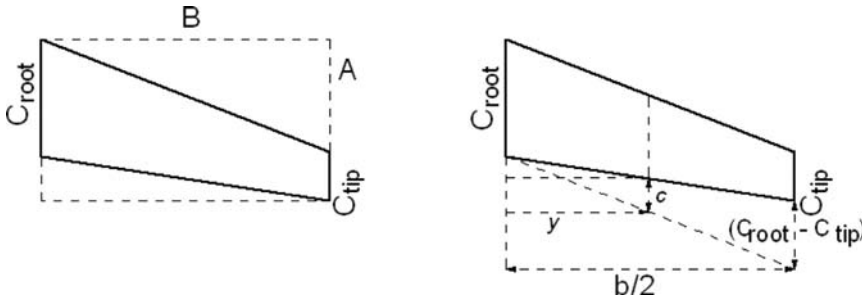


Figure 3.35. Trapezoidal wing planform – MAC

When substituting the integral, Equation 3.37 becomes:

$$\begin{aligned} \text{MAC} &= \frac{2}{S_W} \left[(C_R^2)_0^{b/2} - \left\{ \frac{4C_R}{b}(C_R - C_T) \right\}_0^{b/2} - \left\{ 4(C_R - C_T)^2 \frac{y^3}{3b^2} \right\}_0^{b/2} \right] \\ &= (2/S_W)[bC_r^2/2 - bC_R(C_R - C_T)/2 - b(C_R - C_T)^2/6] \end{aligned}$$

When substituting for the S_W :

$$\begin{aligned} \text{MAC} &= [2/(C_R + C_T)][C_r^2 - C_T^2 + C_r C_T + C_r^{2/3} + C_T^2/3 - 2C_r C_T/3] \\ &= [2/(C_R + C_T)][C_r^2/3 + C_T^2/3 - C_r C_T/3] \\ &= \frac{2}{3} \left[\frac{(C_R + C_T)^2}{(C_R + C_T)} - \frac{C_R C_T}{(C_R + C_T)} \right] \end{aligned}$$

For a linearly tapered (trapezoidal) wing, this integral is equal to:

$$\text{MAC} = 2/3[C_{\text{root}} + C_{\text{tip}} - C_{\text{root}}C_{\text{tip}}/(C_{\text{root}} + C_{\text{tip}})] \quad (3.38)$$

For wings with a glove/yehudi, the MAC may be computed by evaluating each linearly tapered portion and then taking an average, weighted by the area of each portion. In many cases, however, the MAC of the reference trapezoidal wing is used. The MAC is often used in the nondimensionalization of pitching moments as well as to compute the reference length for calculating the Re as part of the wing drag estimation. The MAC is preferred for computation over the simpler mean geometric chord for aerodynamic quantities whose values are weighted more by the local chord, which are reflected by their contribution to the area.

3.18 Compressibility Effect: Wing Sweep

Section 3.7.1 explains the transonic effect resulting from the thickness distribution along an aircraft body. On the wing, the same phenomenon can occur, most importantly along the wing chord but altered due to the 3D wing tip influence. A local shock interacting with the boundary layer can trigger early separation, resulting in unsteady vibration and – in extreme cases – even causing the wing to stall. A typical consequence is a rapid drag increase due to the compressibility effect resulting from the transonic-flow regime. Military aircraft in hard maneuver can enter into such an undesirable situation even at a lower speed. As much as possible, designers try to

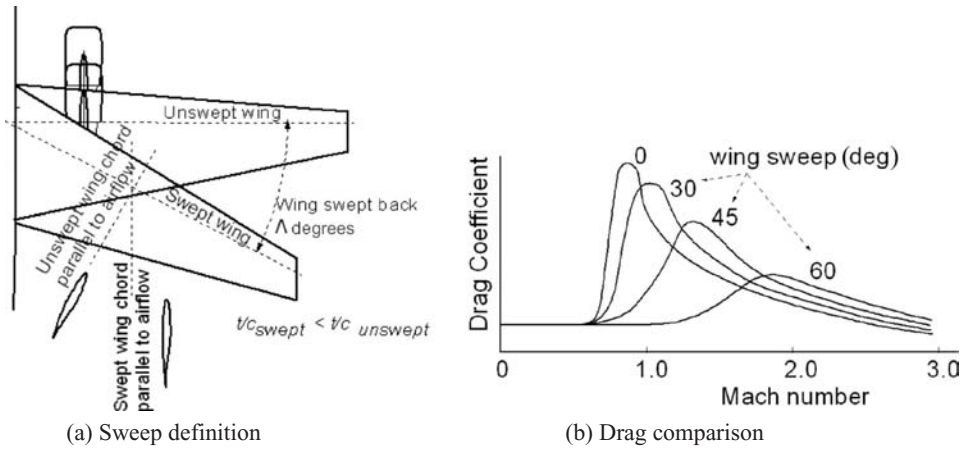


Figure 3.36. Sweep of wing

avoid, delay, or minimize the onset of flow separation over the wing due to local shocks.

Drag divergence is a sudden increase in drag. A 20-count drag rise ($C_D = 0.002$) at the Mach number is known as the *drag divergence mach* (M_{DD}), shown in Figure 3.36b. The critical Mach (M_{crit}) is the onset of the transonic-flow field and is lower than the M_{DD} . Some texts use M_{crit} with a 20-count drag increase.

Structural engineers prefer aerofoil sections to be as thick as possible, which favors structural integrity at lower weights and allows the storage of more fuel onboard. However, aerodynamicists prefer the aerofoil to be as thin as possible to minimize the transonic-flow regime in order to keep the wave drag rise lower. One way to delay the M_{crit} is to sweep the wing (Figure 3.36a) either backward (see Figure 3.31, Boeing 737) or forward (see Figure 4.37e, SU47 [at www.cambridge.org/Kundu]), which thins the aerofoil t/c ratio and delays the sudden drag rise (Figure 3.36b). The former is by far more prevalent because of structural considerations. Wing slide (i.e., in which the chord length remains the same) is different from wing sweep, in which the chord length is longer by the secant of the sweep angle.

Shown here is the relationship between the sweep angle and wing geometries. The chord length of a swept wing increases, resulting in a decrease in the t/c ratio:

$$\text{chord}_{\text{swept}} = (\text{chord}_{\text{unswept}}) / \text{Cos} \Delta \tag{3.39}$$

This results in:

$$(\text{thickness} / \text{chord}_{\text{swept}}) < (\text{thickness} / \text{chord}_{\text{unswept}}) \tag{3.40}$$

This directly benefits the drag divergence Mach number, divided by the cosine of the sweep angle:

$$\Lambda_{1/4}; \text{ that is, } \text{Mach}_{\text{div_swept}} = \text{Mach}_{\text{div_unswept}} / \text{Cos} \Lambda_{1/4} \tag{3.41}$$

The sweep also degrades the C_{Lmax} by the cosine of the sweep angle, $\Lambda_{1/4}$; that is:

$$C_{Lmax_swept} = C_{Lmax_unswept} \times \text{Cos} \Lambda_{1/4} \tag{3.42}$$

If the trailing edge can remain unswept, then flap effectiveness is less degraded due to a quarter-chord sweep.

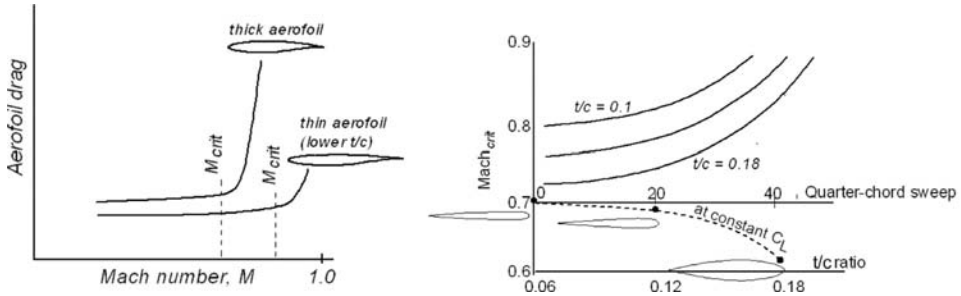


Figure 3.37. Wing sweep versus aerofoil t/c ratio

Qualitative characteristics between the wing sweep and the t/c ratio variation are shown in Figure 3.37.

Figure 3.38 shows typical values used in various aircraft. Another effect of speed gain is a change in C_{Lmax} , as shown in Figure 3.39. For a particular wing, the ratio of $C_{Lmax.compressible}/C_{Lmax.incompressible}$ decreases to approximately 0.7, as shown in Figure 3.39.

Designers require this body of information for the aerofoil selection. The choice decides the extent of wing sweep required to lower the t/c ratio to achieve the desired result (i.e., to minimize the compressible drag increase for the cruise Mach number) while also satisfying the structural requirements. To standardize drag-rise characteristics, the flow behavior is considered to be nearly incompressible up to M_{crit} and can tolerate up to M_{DD} , allowing a 20-count drag increase ($\Delta C_D = 0.002$).

3.19 Wing Stall Pattern and Wing Twist

The lower the speed at landing, the safer is the aircraft in case of any inadvertent mishap. An aircraft landing occurs near the wing stall condition when the aileron effectiveness should be retained to avoid a wing tip hitting the ground. In other words, when approaching the stall condition, its gradual development should start from the wing root, which allows the aileron at the wing tip to retain its ability to maintain level flight. Figure 3.40 (see also Figure 3.18) shows typical wing stall propagation patterns on various types of wing planforms.

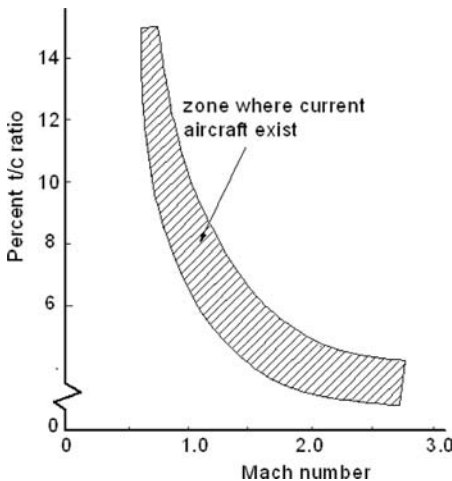


Figure 3.38. Thickness-to-chord ratio for various aircraft

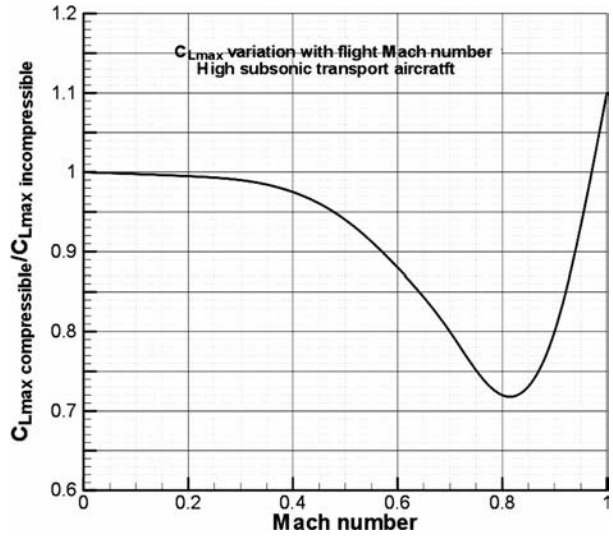


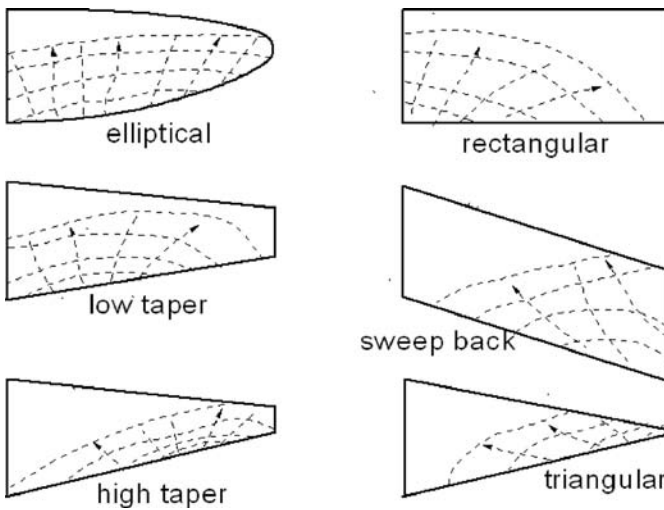
Figure 3.39. Mach number effect

Because a swept-back wing tends to stall at the tip first, twisting of the wing tip downward (i.e., washout) is necessary to force the root section to stall first, thereby retaining roll control during the landing.

A good way to ensure the delay of the wing tip stall is to twist the wing about the Y-axis so that the tip LE is lower than the wing root LE (see Figure 3.32). Typical twist-angle values are 1 to 2 deg and rarely exceed 3 deg.

3.20 Influence of Wing Area and Span on Aerodynamics

For a given wing loading (i.e., the wing area and maximum takeoff mass [MTOM] invariant), aerodynamicists prefer a large wingspan to improve the aspect ratio in order to reduce induced drag at the cost of a large wing root bending moment. Structural engineers prefer to see a lower span resulting in a lower aspect ratio.



Stall progressing from trailing edge as angle of attack is increased

Figure 3.40. Wing stall patterns

The BWB (see Figure 1.15) design for larger aircraft has proven merits over conventional designs but awaits technological and market readiness. Interesting deductions are made in the following sections.

3.20.1 The Square-Cube Law

For an example, increase the linear dimensions of a solid cube from 1 to 2 units. From the following example, it can be seen that the increase in weight is faster than the increase in area (the subscript 1 represents the small cube and the subscript 2 represents the larger cube):

$$\begin{aligned} \text{area}_2 &= \text{area}_1 \times (\text{length}_2/\text{length}_1)^2, \text{ a 4-fold increase from 6 to 24 square units} \\ \text{volume}_2 &= \text{volume}_1 \times (\text{length}_2/\text{length}_1)^3, \text{ an 8-fold increase from 1 to 8 cube units} \end{aligned}$$

Applying this concept to a wing, increasing its span (i.e., linear dimension, b – maintaining geometric similarity) would increase its volume faster than the increase in surface area, although not at the same rate as for a cube. Volume increase is associated with weight increase, which in turn would require stiffening of the structure, thereby further increasing the weight in a cyclical manner. This is known as the *square-cube law* in aircraft design terminology. This logic was presented a half-century ago by those who could not envisage very large aircraft.

$$\text{weight, } W \propto \text{span}^3 \quad \text{wing planform area, } S_w \propto \text{span}^2 \quad (3.43)$$

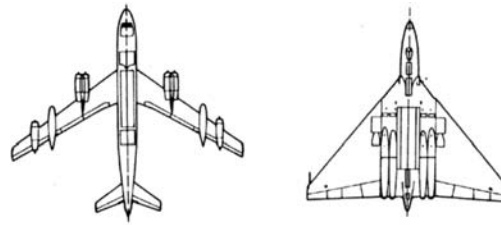
Then,

$$\text{wing-loading, } W/S_w \propto b$$

This indicates that for the given material used, because of excessive weight growth, there should be a size limit beyond which aircraft design may not be feasible. If the fuselage is considered, then it would be even worse with the additional weight.

Yet, aircraft size keeps growing – the size of the Airbus A380 would have been inconceivable to earlier designers. In fact, a bigger aircraft provides better structural efficiency, as shown in Figure 4.6, for operating empty weight fraction (OEWf) reduction with maximum takeoff weight (MTOW) gain. Researchers have found that advancing technology with newer materials – with considerably better strength-to-weight ratio, weight reduction by the miniaturization of systems, better high-lift devices to accommodate higher wing-loadings, better fuel economy, and so forth – has defied the square-cube law. Strictly speaking, there is no apparent limit for further growth (up to a point) using the current technology.

The author believes that the square-cube law needs better analysis to define it as a law. Currently, it indicates a trend and is more applicable to weight growth with an increase in aspect ratio. What happens if the aspect ratio does not change? The following section provides an excellent example of how a low aspect ratio can compete with a high aspect-ratio design.



	B-47	Vulcan
Gross wing area (sq. ft.)	1,430	3,446
Total wetted area (sq. ft.)	11,300	9,500
Span (ft)	116	99
Max. wing-loading (W/S _w)	140	43.5
Max. span-loading (W/b)	1,750	1,520
Aspect ratio	9.43	2.84
CD ₀	0.0198	0.0069
L/D _{max} /C _{Lopt}	17.25/0.682	17.0/0.235
C _{Lmax} at maximum cruise	0.48	0.167

Figure 3.41. Torenbeek's comparison between a B-47 and a Vulcan

3.20.2 Aircraft Wetted Area (A_W) versus Wing Planform Area (S_W)

The previous section raised an interesting point on aircraft size, especially related to wing geometry. This section discusses another consideration on how the aircraft wing planform area and the entire aircraft wetted surface areas can be related. Again, the wing planform area, S_W , serves as the reference area and does not account for other wing parameters (e.g., dihedral and twist).

The conflicting interests between aerodynamicists and stress engineers on the wing aspect ratio presents a challenge for aircraft designers engaged in conceptual design studies (this is an example of the need for concurrent engineering). Both seek to give the aircraft the highest possible *lift-to-drag* (L/D) ratio as a measure of efficient design. Using Equations 3.23 and 3.31, the following can be shown (i.e., incompressible flow):

$$\text{drag, } D = q S_W C_D = q S_W (C_{DP} + C_{Di})$$

or

$$CD = (C_{DP} + C_{Di}) \quad (3.44)$$

Clearly, $C_{DP} \propto$ wetted area, A_W and C_{Di} is $\propto (1/AR) = S_W/b^2$ (from Equation 3.43).

Define the wetted-area aspect ratio as follows:

$$AR_{wet} = b^2/A_W = AR/(A_W/S_W) \quad (3.45)$$

This is an informative parameter to show how close the configuration is to the wing-body configuration. Section 4.5 provides statistical data for various designs.

Torenbeek [5] made a fine comparison to reveal the relationship between the aircraft wetted area, A_W , and the wing planform area, S_w . Later, Roskam [6] presented his findings to reinforce Torenbeek's point, whose result is shown in Figure 3.41.

Table 3.1. *Wing span, aspect ratio, and reference area analyses*

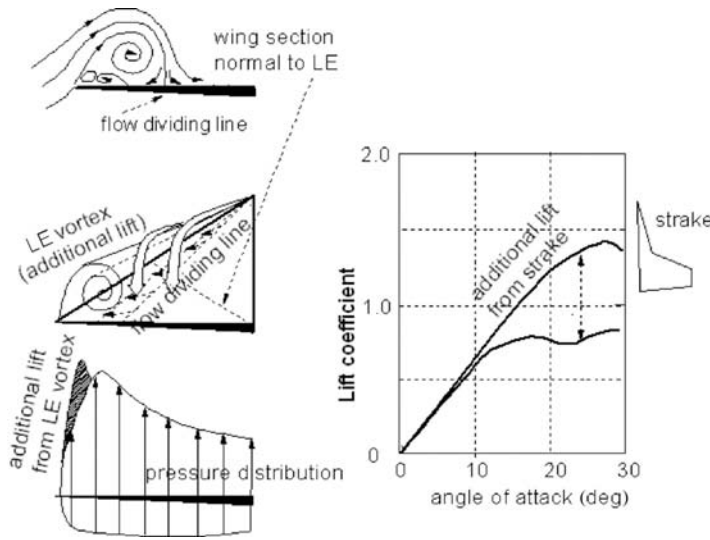
Type	AR	$b - ft$	$S_W - ft^2$	A_W/S_W	b^2/A_W	$(L/D)_{max}$
<i>Small aircraft</i>						
Fixed wheel: Piper Cherokee				3.5 to 4.5	1.2 to 1.8	10 to 15
	6.2	32.5	175	3.72	1.62	13.5
Retractable wheel: Learjet 45				4 to 5.5	1.4 to 2	12 to 16
	7.5	49.2	323	5.05	1.48	15.8
<i>Transport aircraft</i>						
Large/medium jets: A320				6 to 7	1.2 to 1.6	16 to 18
	9.37	111.2	1,320	6.2	1.52	16.5
Regional jets: F28				5.5 to 7	1.1 to 1.3	15 to 17
	7.3	77.4	822	5.7	1.29	15.5
Turboprop: SD330				5 to 7	1.1 to 1.8	14 to 17
	12.3	75	453	6.73	1.8	15
Three-surface (with canard): Piaggio Avanti				4.5 to 6	0.5 to 1.0	10 to 12
	12.3	46	172.2			high
<i>Military aircraft</i>						
Single-surface (delta wing): Vulcan				2.5 to 3	0.5 to 0.8	8 to 10
	2.84	99	3,448	2.8	1.1	17
Two-surface (with H-tail): Vigilante				4 to 5.5	0.4 to 1.2	9 to 12
	3.75	53.14	700	4.63	0.87	12.2
AJT				5.2	1.02	13
Conventional bomber: B47				6 to 8	1.2 to 2	15 to 18
	9.43	116	1,430	7.6	1.2	17.2
<i>All-wing aircraft</i>						
B49				2.2 to 3	0.6 to 1.2	17 to 18
				2.22		

Toreenbeck compared an all-wing aircraft (i.e., the Avro Vulcan bomber) to a conventional design (i.e., Boeing B47B bomber) with a similar weight of approximately 90,000 kg and a similar wing span of about 35 m. It was shown that these designs can have a similar L/D ratio despite the fact that the all-wing design has an aspect ratio less than one third of the former. This was possible because the all-wing aircraft precludes the need for a separate fuselage, which adds extra surface area and thereby generates more skin-friction drag. Lowering the skin-friction drag by having a reduced wetted area of the all-wing aircraft compensates for the increase in induced drag for having the lower aspect ratio.

All-wing aircraft provide the potential to counterbalance the low aspect ratio by having a lower wetted area. Again, the concept of BWB gains credence.

Table 3.1 provides statistical information to demonstrate that a BWB is a good design concept to satisfy both aerodynamicists and stress engineers with a good L/D ratio and a low-aspect-ratio wing, respectively. In the table, a new parameter – wetted aspect ratio, $b^2/A_W = AR/(A_W/S_W)$ – is introduced.

The table provides the relationship among the aspect ratio, wing area, and wetted area and how it affects the aircraft aerodynamic efficiency in terms of the ratio. Within the same class of wing planform shape, the trend shows that a higher aspect ratio provides a better L/D ratio. However, all-wing aircraft (e.g., BWB) provide an interesting perspective, as discussed in this section.



(a) Additional vortex lift (half wing shown) (b) Additional lift by strake

Figure 3.42. Additional vortex lift

3.20.3 Additional Vortex Lift

Stalling of conventional wings, such as those configured for high-subsonic civil aircraft, occurs around the angle of attack, α , anywhere from 14 to 18 deg. Difficult maneuvering demanded by military aircraft requires a much higher stall angle (i.e., 30 to 40 deg). This can be achieved by having a carefully placed additional low-aspect-ratio lifting surface – for example, having a LE strake (e.g., F16 and F18) or a canard (e.g., Eurofighter and Su37). BWB configurations also can benefit from this phenomenon.

At high angles of attack, the LE of these surfaces produces a strong vortex tube, as shown in Figure 3.42, which influences the flow phenomenon over the main wing. Vortex flow has low pressure at its core, where the velocity is high (refer to aerodynamic textbooks for more information).

The vortex flow sweeping past the main wing reenergizes the streamlines, delaying flow separation at a higher angle of attack. At airshows during the early 1990s, MIG-29s demonstrated flying at very high angles of attack (i.e., above 60 deg); their transient “cobra” movement had never before been seen by the public.

3.20.4 Additional Surfaces on Wing

Flaps and slats on a 2D aerofoil are described in Section 3.10. This section describes their installation (Figure 3.43a) on a 3D wing.

Flaps comprise about two thirds of an inboard wing at the trailing edge and are hinged on the rear spar (positioned at 60 to 66%; the remaining third by the aileron) of the wing chord, which acts as a support. Slats run nearly the full length of the LE. The deployment mechanism of these high-lift devices can be quite complex. The associated lift-characteristic variation with incidence is shown in Figure 3.43b. Slat deployment extends the wing maximum lift, whereas flap deployment offers incremental lift increase at the same incidence.

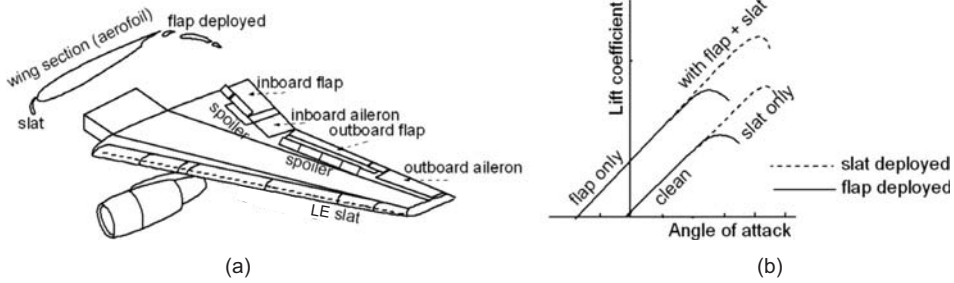


Figure 3.43. High-lift devices

The aileron acts as the roll-control device and is installed at the extremities of the wing for about a third of the span at the trailing edge, extending beyond the flap. The aileron can be deflected on both sides of the wing to initiate roll on the desired side. In addition, ailerons can have trim surfaces to alleviate pilot loads. A variety of other devices are associated with the wing (e.g., spoiler, vortex generator, and wing fence).

Spoilers (or *lift dumpers*) (Figure 3.44) are flat plates that can be deployed nearly perpendicular to the airflow over the wing. They are positioned close to the CG (i.e., X-axis) at the MAC to minimize the pitching moment, and they also act as air brakes to decrease the aircraft speed. They can be deployed after touchdown on landing, when they would “spoil” the flow on the upper wing surface, which destroys the lift generated (the U.S. terminology is *lift dumper*). This increases the ground reaction for more effective use of wheel brakes.

Many types of wing tip devices reduce induced drag by reducing the intensity of the wing tip vortex. Figure 3.44 shows the prevalent type of *winglets*, which modify the tip vortex to reduce induced drag. At low speed, the extent of drag reduction is minimal and many aircraft do not have a winglet. At higher speeds, it is now recognized that there is some drag reduction no matter how small, and it has begun to appear in many aircraft – even as a styling trademark on some. The Blended

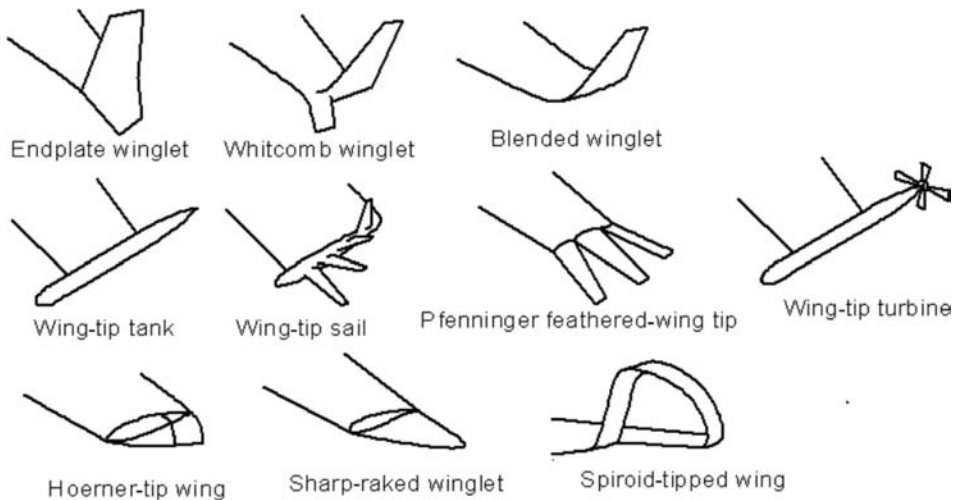


Figure 3.44. Types of winglets (from NASA)

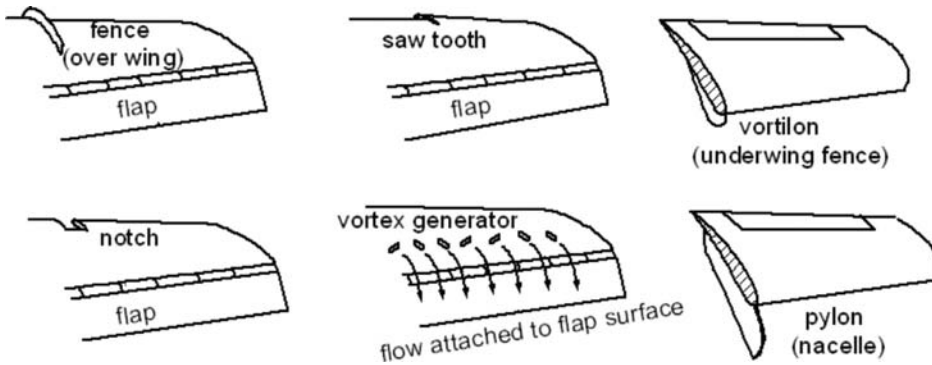


Figure 3.45. Wing flow modifier and vortex generators

winglet and Whitcomb types are seen in high-subsonic aircraft. The Hoerner type and sharp-raked winglet are used in lower-speed aircraft.

The Whitcomb-type wing tip and its variants without the lower extension are popular with high-subsonic turbofan aircraft. Extensive analyses and tests indicate that approximately 1% of induced-drag reduction may be possible with a carefully designed winglet. Until the 1970s and 1980s, the winglet was not prominent in aircraft. In this book, no credit is taken for the use of the winglet. Coursework can incorporate the winglet in project work.

Wing flow modifier devices (Figure 3.45) are intended to improve the flow quality over the wing. In the figure, a *fence* is positioned at about half the distance of the wingspan. The devices are carefully aligned to prevent airflow that tends to move spanwise (i.e., outward) on swept wings.

Figure 3.45 also shows examples of *vortex generators*, which are stub wings carefully placed in a row to generate vortex tubes that energize flow at the aft wing. This enables the flow to remain attached; however, additional drag increase due to vortex generators must be tolerated to gain this benefit.

Vortex generators and/or a fence also can be installed on a nacelle to prevent separation.

3.21 Finalizing Wing Design Parameters

Sections 3.11 through 3.20 cover a wide range of wing design features. This section describes the considerations necessary to finalize the wing design. Selection of the aerofoil is the most important initial task. The wing aerofoil t/c ratio is established for the maximum cruise speed by the choice of aerofoil and sweep. It can vary along the span, with the root demanding the thickest section to withstand the bending moment. Once the aerofoil is selected, six parameters must be established for wing design: (1) wing planform area, (2) wing aspect ratio, (3) wing span, (4) wing sweep, (5) wing dihedral, and (6) wing twist.

1. Establish the wing reference area (see Chapter 11).
2. Establish the wing planform geometry (i.e., the maximum aspect ratio permitted by the structural technology). The statistics provided previously are a good guide. A new design should have higher aspect ratios compared to current designs.

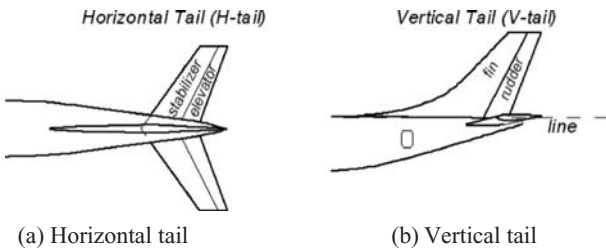


Figure 3.46. Horizontal tail and vertical tail

3. Establish the wing sweep for the Mach number of operations.
4. Establish the wing span from the previous three steps. For commercial transport aircraft, the wing span is currently restricted to a maximum of 80 m.
5. Establish the wing dihedral and anhedral angles; it is generally within 1 to 5 deg for the dihedral.
6. Establish the wing twist; it is usually within 1 to 2 deg (generally downwash).

At the conceptual stage, the twist, dihedral, and anhedral are taken from experience. Subsequently, CFD analyses can fine-tune all related parameters for the best compromise. Ultimately, wind-tunnel tests are required to substantiate the design.

3.22 Empennage

Typically, the empennage consists of horizontal and vertical tails for aircraft stability and control. Various types of empennage configurations are described in [Chapter 4](#). The dominant type has a vertical tail (V-tail; U.K. terms are *fin* and *rudder*) in the plane of symmetry with a symmetrical aerofoil. A horizontal tail (H-tail; U.K. terms are *stabilizer* and *elevator*) is like a small wing at the tail (i.e., the aft end of the fuselage). The last two decades have seen the return of aerodynamic surfaces placed in front of the wing (see [Figure 3.48](#)); these are called *canards* and are discussed in subsequent chapters. This section addresses the definitions associated with the empennage and canard as well as the tail volume coefficients (see [Chapter 12](#)).

The V-tail of a single-engine, propeller-driven aircraft may have an offset of 1 to 2 deg to counter the effects of rotating propeller slipstream.

3.22.1 H-Tail

The H-tail consists of the stabilizer (fixed or moving) and the elevator (moving) for handling the pitch degree of freedom ([Figure 3.46a](#)). The H-tail can be positioned low through the fuselage, in the middle cutting through the V-tail, or at the top of the V-tail to form a T-tail (see [Figure 3.33](#)).

Military aircraft can have all moving H-tails with emergency splitting in case there is failure, and there are several choices for positioning it (see [Chapter 4](#)). [Figure 3.46a](#) shows the geometrical definition of conventional-type H-tail surfaces. Like the wing planform definition, the H-tail reference area, S_H , is the planform area including the portion buried inside the fuselage or V-tail for a low- or mid-tail location, respectively. The T-tail position at the top has a fully exposed planform.

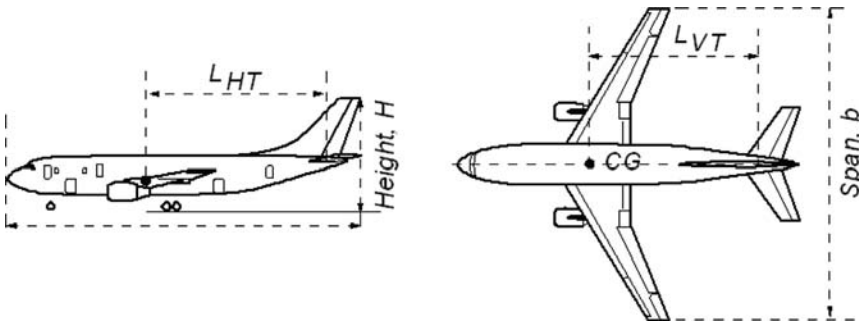


Figure 3.47. Geometric parameters for the tail volume coefficients

3.22.2 V-Tail

The V-tail consists of a fin (fixed) and a rudder (moving) to control the roll and yaw degrees of freedom (see Figure 3.46). The figure shows the geometrical definition of a conventional-type V-tail surface reference area, S_V . The projected trapezoidal/rectangular area of the V-tail up to this line is considered the reference area, S_V . Depending on the closure angle of the aft fuselage, the root end of the V-tail is fixed arbitrarily through a line drawn parallel to the fuselage centerline, passing through the point where the midchord of the V-tail intersects the line.

3.22.3 Tail Volume Coefficients

Tail volume coefficients are used to determine the empennage reference areas, S_H and S_V . The definition of the tail volume coefficients is derived from the aircraft stability equations provided herein. The CG position (see Chapter 8) is shown in Figure 3.47. The distances from the CG to the aerodynamic center at the MAC of the V-tail and H-tail (i.e., MAC_{VT} and MAC_{HT}) are designated L_{HT} and L_{VT} , respectively, as shown in Figure 3.47. The ac is taken at the quarter-chord of the MAC.

H-Tail Volume Coefficient, C_{HT}

From the pitching-moment equation (see Chapter 12) for steady-state (i.e., equilibrium) level flight, the H-tail volume coefficient is given as the H-tail plane reference area:

$$S_{HT} = (C_{HT})(S_W \times MAC)/L_{HT}, \quad (3.46)$$

where C_{HT} is the H-tail volume coefficient, $0.5 < C_{HT} < 1.2$; a good value is 0.8. L_{HT} is the H-tail arm = distance between the aircraft CG to the ac of MAC_{HT} . In general, the area ratio $S_{HT}/S_W \approx 0.25$ to 0.35 .

V-Tail Volume Coefficient, C_{VT}

From the yawing-moment equation (see Chapter 12) for steady-state (i.e., equilibrium) level flight, the V-tail volume coefficient is given as the V-tail plane reference area:

$$S_{VT} = (C_{VT})(S_W \times \text{wing span})/L_{VT}, \quad (3.47)$$

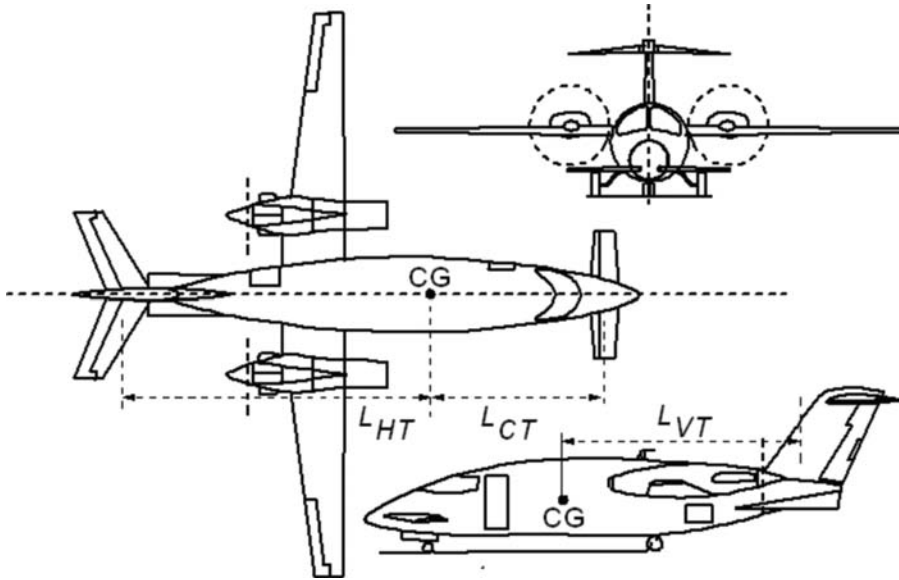


Figure 3.48. Three-surface canard configuration (Piaggio P180 Avanti)

where C_{VT} is the V-tail volume coefficient, $0.05 < C_{VT} < 0.1$; a good value is 0.07. L_{VT} is the H-tail arm = distance between the aircraft CG to the ac of MAC_{VT} . In general, the area ratio $S_{VT}/S_W \approx 0.15$ to 0.25.

Chapter 6 describes how to estimate the empennage areas; a number of design iterations are necessary. Figures 12.15 and 12.16 give statistical values of tail volume coefficients.

Canard Configuration

Canard is French for “goose,” which in flight stretches out its long neck with its bulbous head in front. When a horizontal surface is placed in front of the aircraft, it presents a similar configuration; hence, this surface is sometimes called a canard.

The Wright Brothers’ Flyer had a control surface at the front (with a destabilizing effect), which resulted in a sensitive control surface. Military aircraft use a canard to enhance pitch control. However, the use of a canard in civil aircraft applications serves a different purpose (Figure 3.48).

In general, the inherent nose-down moment (unless a reflex trailing edge is employed) of a wing requires a downward force by the H-tail to maintain level flight. This is known as *trimming force*, which contributes to trim drag. For an extreme CG shift (which can happen as fuel is consumed), high trim drag can exist in a large portion of the cruise sector. The incorporation of a canard surface can reduce trim drag as well as the H-tail area, S_H . However, it adds to the manufacturing cost and, until recently, the benefit from the canard application in large transport aircraft has not been marketable.

Many small civil aircraft have a canard design (e.g., Rutan designs). A successful Bizjet design is the Piaggio P180 Avanti shown in Figure 3.48. It has achieved a very high speed for its class of aircraft through careful design considerations embracing not only superior aerodynamics but also the use of composite materials to reduce weight.

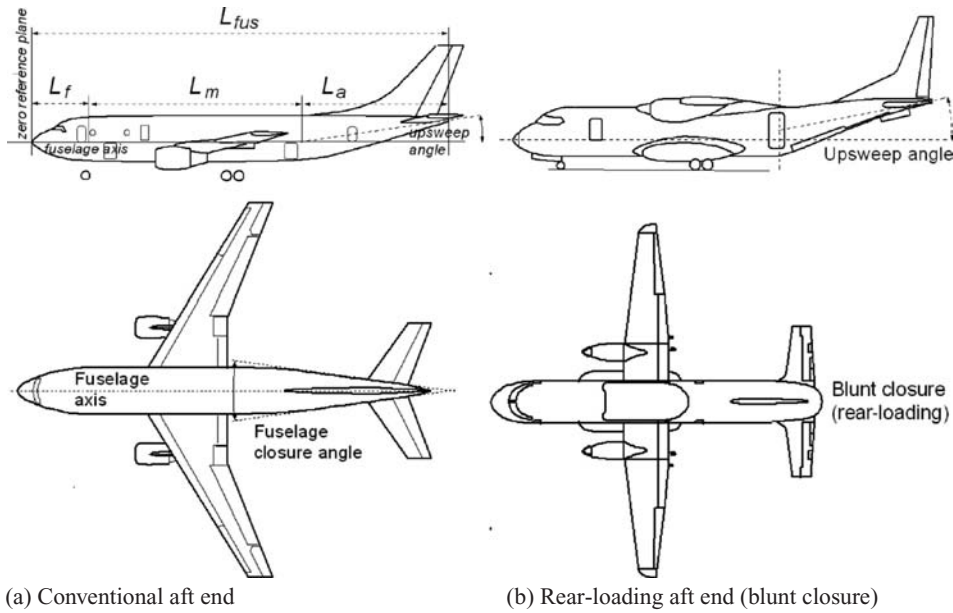


Figure 3.49. Fuselage geometrical parameters: lengths associated with the fuselage

Canard Volume Coefficient, C_{CT}

This also is derived from the pitching-moment equation for steady-state (i.e., equilibrium) level flight. The canard reference area, S_C , has the same logic for its definition as that of the H-tail. Its tail arm is L_{CT} . The canard reference area is given as:

$$S_{CT} = (C_{CT})(S_W \times MAC)/L_{CT}, \quad (3.48)$$

where C_{CT} is the H-tail volume coefficient, $0.5 < C_{HT} < 1.2$; a good value is 0.6 to 0.9, depending on whether it is a conventional H-tail. The L_{CT} is the H-tail arm = distance between the aircraft CG to the ac of MAC_{CT} . In general, $S_{CT}/S_W \approx 0.2$ to 0.3 .

3.23 Fuselage

A civil aircraft fuselage is designed to carry revenue-generating payloads, primarily passengers but the cargo version can also carry containers or suitably packaged cargo. It is symmetrical to a vertical plane and maintains a constant cross-section with front and aft-end closures in a streamlined shape. The aft fuselage is subjected to adverse pressure gradients and therefore is prone to separation. This requires a shallow closure of the aft end so that the low-energy boundary layer adheres to the fuselage, minimizing pressure drag (see Section 3.3). The fuselage also can produce a small amount of lift, but this is typically neglected in the conceptual stages of a configuration study. The following definitions are associated with the fuselage geometry (Figure 3.49).

3.23.1 Fuselage Axis/Zero-Reference Plane

Fuselage axis is a line parallel to the centerline of the constant cross-section part of the fuselage barrel. It typically passes through the farthest point of the nose cone,

facilitating the start of reference planes normal to it. The fuselage axis may or may not be parallel to the ground. The principal inertia axis of the aircraft can be close to the fuselage axis. In general, the zero-reference plane is at the nose cone, but designers can choose any station for their convenience, within or outside of the fuselage. This book considers the fuselage zero-reference plane to be at the nose cone, as shown in [Figure 3.49](#).

3.23.2 Fuselage Length, L_{fus}

This is along the fuselage axis, measuring the length of the fuselage from the tip of the nose cone to the tip of the tail cone (which is unlikely to be on the axis). This is not the same as the aircraft length, L , shown in [Figure 3.49a](#).

3.23.3 Fineness Ratio, FR

This is the ratio of fuselage length to average diameter, $FR = L/D_{ave}$. A good value for commercial transport aircraft design is from 8 to 10.

3.23.4 Fuselage Upsweep Angle

In general, the fuselage aft end incorporates an upsweep ([Figure 3.49b](#)) for ground clearance at rotation on takeoff. The upsweep angle is measured from the fuselage axis to the mean line of aft fuselage height. It may not be a straight line if the upsweep is curved like a banana; in that case, it is segmented to smaller straight lines. The rotation clearance angle is kept to 12 to 16 deg; however, the slope of the bottom mould line depends on the undercarriage position and height. Rear-loading aircraft have a high wing with the undercarriage located close to the fuselage belly. Therefore, the upsweep angle for this type of design is high. The upsweep angle can be seen in the elevation plane of a three-view drawing. There is significant variation in the upsweep angle among designs. A higher upsweep angle leads to more separation and, hence, more drag.

3.23.5 Fuselage Closure Angle

The closure angle is the aft fuselage closure seen in a plan view of the three-view drawing and it varies among designs. The higher the closure angle, the greater the pressure drag component offered by the fuselage. In rear-loading aircraft, the fuselage closes at a blunt angle; combined with a large upsweep, this leads to a high degree of separation and, hence, increased pressure drag.

3.23.6 Front Fuselage Closure Length, L_f

This is the length of the front fuselage from the tip of the nose cone to the start of the constant cross-section barrel of the mid-fuselage ([Figure 3.49a](#)). It encloses the pilot cockpit/flight deck and the windscreen – most of which is associated with a kink in the mould lines to allow for a better vision polar (see [Section 4.7.4](#)) and to enable the use of flat windscreens to reduce cost. In general, it includes the front door and passenger amenities, and may have a row or two of passenger seating.

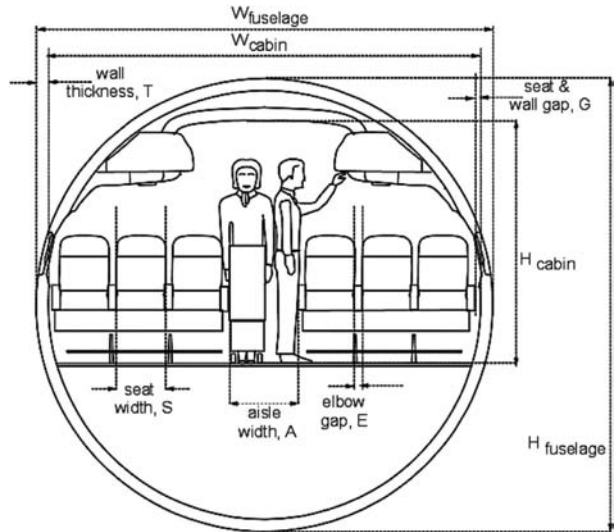


Figure 3.50. Fuselage cross-section geometrical parameters

3.23.7 Aft Fuselage Closure Length, L_a

This starts from the end of the constant cross-section barrel of the mid-fuselage up to the tip of the tail cone (Figure 3.49a). It encloses the last few rows of passenger seating, rear exit door, toilet, and – for a pressurized cabin – the aft pressure bulkhead, which is an important component from a structural design perspective ($L_a > L_f$).

3.23.8 Midfuselage Constant Cross-Section Length, L_m

This is the constant cross-section midbarrel of the fuselage, where passenger seating and other facilities are accommodated (including windows and emergency exit doors, if required).

3.23.9 Fuselage Height, H

This is the maximum distance of the fuselage from its underside (not from the ground) to the top in the vertical plane (Figure 3.50).

3.23.10 Fuselage Width, W

This is the widest part of the fuselage in the horizontal plane. For a circular cross-section, it is the diameter shown in Figure 3.50.

3.23.11 Average Diameter, D_{ave}

For a noncircular cross-section, this is the average of the fuselage height and width at the constant cross-section barrel part ($D_{ave} = (H + W)/2$). Sometimes this is defined as $D_{effective} = \sqrt{(H \cdot W)}$; another suitable definition is $D_{equivalent} = \text{perimeter}/2\pi$. This book uses the first definition.

3.23.12 Cabin Height, H_{cab}

This is the internal cabin height from the floor, as shown in [Figure 3.50](#).

3.23.13 Cabin Width, W_{cab}

This is a the internal cabin width, as shown in [Figure 3.50](#).

3.23.14 Pilot Cockpit/Flight Deck

This is a term used for the enclosed space for the flight crew in the front fuselage. [Chapter 15](#) describes the flight deck in more detail.

A military aircraft fuselage is very different because it does not have passengers to carry and is more densely packed. Various types of fuselage cross-sections are shown in [Figure 4.7](#) (see [Web site](#)). Their associated fineness ratios and other statistical data on fuselage parameters are provided in [Section 4.7](#).

3.24 Undercarriage

[Chapter 7](#) is devoted entirely to a discussion of undercarriage design.

3.25 Nacelle and Intake

A *nacelle* is the structural housing for an aircraft engine. In civil aircraft, nacelles are invariably externally pod-mounted, either slung under or mounted over the wing or attached to the fuselage (see [Figure 4.28](#)). The front part of the nacelle is the intake and the aft end is the nozzle. Military aircraft engines are invariably buried in the fuselage; the front is called the *intake* in the absence of a nacelle. [Chapter 10](#) discusses the nacelle in detail.

In addition to housing the engine, the main purpose of the nacelle is to facilitate the internal airflow reaching the engine face (or the fan of gas turbines) with minimum distortion over a wide range of aircraft speeds and attitudes. For subsonic turbofans, the intake acts as a diffuser with an acoustic lining to abate noise generation. The inhaled air-mass flow demanded by an engine varies considerably: At idle, just enough is required to sustain combustion, whereas at maximum thrust, the demand is many times higher. A rigid intake must be sized such that during critical operations (i.e., takeoff, climb, and cruise), the engine does not suffer and generates adequate thrust. Supersonic intakes are even more complex and are designed to minimize loss resulting from shock waves.

3.26 Speed Brakes and Dive Brakes

Speed brakes and *dive brakes* have the same definition. They are mounted specifically on the fuselage for military aircraft and as spoilers on the wings for civil aircraft ([Figure 3.51](#)). However, there are civil aircraft that use this type of device mounted on the fuselage.

Speed brakes are specifically designed to reduce speed rapidly, typically on approach and in military combat maneuvers.

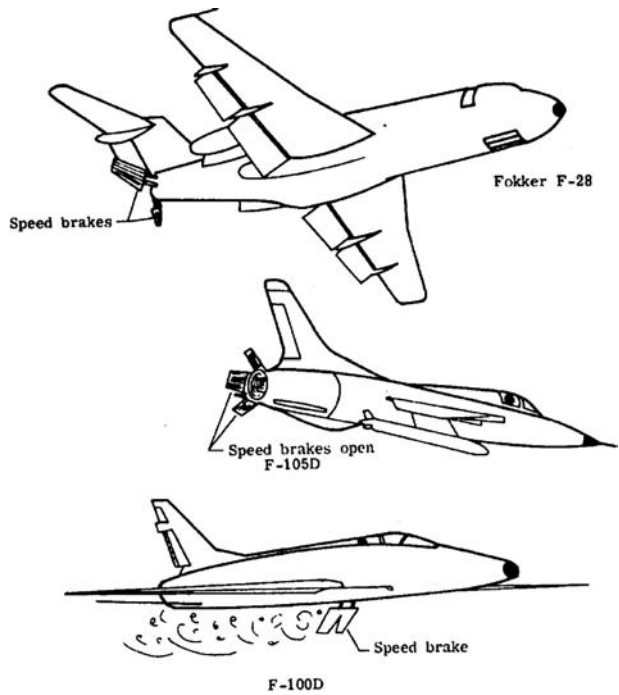


Figure 3.51. Speed brakes and dive brakes

Speed and dive brakes are primarily drag-producing devices positioned in those areas that will create the smallest change in moments (i.e., kept symmetrical to the aircraft axis with the least moment arm from the CG). Figure 3.51 shows fuselage-mounted devices.

The Boeing F22 does not have a separate dive brake. It uses the two rudders of the canted V-tail deflected in opposite directions along with spoilers and flaps deflected upward and downward, respectively.

4

Aircraft Classification, Statistics, and Choices for Configuration

4.1 Overview

This chapter presents important information on aircraft configuration that is required in [Chapter 6](#) coursework. The current design and configuration parameters from aircraft production and operations serve as a template for identifying considerations that could influence new designs with improvements.

During the last century, many aircraft configurations have appeared; today, most of those are not relevant to current practice. Older designs, no matter how good they were, cannot compete with today's designs. This book addresses only those well-established designs as shown in the recent *Jane's All the World's Aircraft Manual*; however, references are made to interesting and unique older aircraft configurations. The chapter starts by examining growth patterns in the aircraft operational envelope (e.g., speed-altitude capabilities). It continues with a classification of generic aircraft types that show distinct patterns within the class in order to narrow down the wide variety of choices available. Statistics is a powerful tool for establishing design trends, and some pertinent statistical parameters are provided herein.

This chapter compiles the available choices for aircraft-component configurations, including types of wing planform, fuselage shape, intake shapes and positioning, and empennage arrangements. These are the “building blocks” for shaping an aircraft, and as many configurations as possible are described. Artistic aesthetics are considered as long as they do not unduly penalize cost and performance – everyone appreciates the attractive streamline aircraft shapes. The new Boeing 787 Dreamliner (see [Figure 1.8](#)) shape is a good example of the company's latest subsonic commercial transport aircraft. It is interesting that the Dreamliner configuration transitioned to the new B787 with more conventional aeroshaping. The B787's advances in technology were not as radical an aerodynamic venture compared to Boeing's earlier Sonic Cruiser proposal (see [Figure 1.7](#)), which was shelved. These decisions were made by one of the world's biggest and best companies; the Sonic Cruiser was not a fantasy – it simply was not timed with market demand. It signifies the importance of conducting a market study, as emphasized in [Chapter 2](#).

Civil and military aircraft design are discussed separately because of the differences in their mission roles (see [Table 2.2](#)).

4.1.1 What Is to Be Learned?

This chapter covers the following topics:

- Section 4.2: Chapter introduction
- Section 4.3: Evolutionary patterns in current aircraft design trends and their classification into distinct categories
- Section 4.4: Civil aircraft mission (domain served, role of economics)
- Section 4.5: Civil aircraft statistics (template for new design)
- Section 4.6: Civil aircraft component geometries (possible options)
- Section 4.7: Fuselage group (e.g., statistics, options)
- Section 4.8: Wing group (e.g., statistics, options)
- Section 4.9: Empennage group (e.g., statistics, options)
- Section 4.10: Nacelle group (e.g., statistics, options)
- Section 4.11: Summary of civil aircraft design choices
- Section 4.12: Military aircraft detailed classification
- Section 4.13: Military aircraft mission (domain served)
- Section 4.14: Military aircraft statistics (template for new design)
- Section 4.15: Military aircraft component geometries (possible options)
- Section 4.16: Fuselage group (e.g., statistics, options)
- Section 4.17: Wing group (e.g., statistics, options)
- Section 4.18: Empennage group (e.g., statistics, options)
- Section 4.19: Nacelle group (e.g., statistics, options)
- Section 4.20: Undercarriage
- Section 4.21: Miscellaneous
- Section 4.22: Summary of military aircraft design choices

4.1.2 Coursework Content

The author recommends that readers browse through this chapter even though there is no coursework involved yet. This information is essential for designers, and this chapter will be better understood after reading [Chapter 11](#) on aircraft sizing and engine matching to finalize the design. Readers will use the information provided in this chapter in [Chapter 6](#).

4.2 Introduction

Previous designs have a strong influence on future designs – real-life experience has no substitute and is dependable. It is therefore important that past information be properly synthesized by studying statistical trends and examining all aspects of any influencing parameters in shaping a new aircraft – this is one of the goals of this book. Many types of aircraft are in production serving different sector requirements – the civil and military missions differ substantially. It is important to classify aircraft categories in order to identify strong trends existing within each class.

Existing patterns of correlation (through regression analysis) within a class of aircraft indicate what may be expected from a new design. There are no surprise elements until new research establishes a radical change in technology or designers

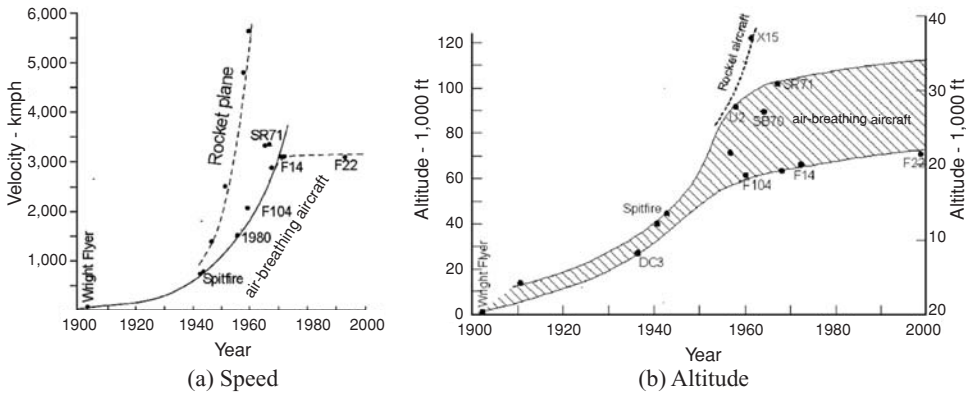


Figure 4.1. Aircraft operational envelope

introduce a new class of aircraft (e.g., Airbus 380). In civil aircraft design, a 10 to 15% improvement in the operating economics of current designs within the class is considered good; a 20% improvement is excellent. Of course, economic improvements must be supported by gains in safety, reliability, and maintainability, which in turn add to the cost.

Readers are encouraged to examine the potential emerging design trends within an aircraft class. In general, new commercial aircraft designs are extensions of existing designs that conservatively incorporate newer, proven technologies (some result from declassified military applications). Currently, the dominant aerodynamic design trends show diminishing returns on investment. Structure technologies seek suitable new materials (e.g., composites, metal alloys, and smart adaptive materials) if they can reduce cost, weight, or provide aerodynamic gains. Engine design still needs aerodynamic improvements to save on fuel consumption and/or weight. [Chapter 1](#) highlights that the current challenge lies in manufacturing philosophy, better maintainability, and reliability incorporating vastly improved and miniaturized systems (including microprocessor-based avionics for control, navigation, communication, and monitoring). This book briefly addresses these topics, particularly from the weight-saving perspective. It also describes conventional aerodynamic and structural considerations and available types of power plants.

4.3 Aircraft Evolution

[Figure 4.1](#) shows the history of progress in speed and altitude capabilities. The impressive growth in one century is astounding – leaving the Earth’s surface in a heavier-than-air vehicle and returning from the Moon in fewer than 66 years!

It is interesting that for air-breathing engine powered aircraft, the speed–altitude record is still held by the more than 40-year-old design, the SR71 (Blackbird; see [Figure 1.11](#)), capable of operating at around Mach 3.0 and a 100,000-ft altitude. Aluminum-alloy properties would allow a flight speed up to Mach 2.5. Above Mach 2.5, a change in material and/or cooling would be required because the stagnation temperature would approach 600°K, exceeding the strength limit of aluminum alloys. Aircraft speed–altitude capabilities have remained stagnant since the 1960s. A recent breakthrough was the success of “Spaceship One” which took aircraft to

the atmosphere edge to 100 km altitude. In civil aviation, the SST aircraft “Concorde” was designed nearly four decades ago and has not yet been supplanted. The Concorde’s speed–altitude capability is Mach 2.2 at around 60,000 ft.

In military aircraft scenarios, gone (almost) are the days of “dogfights” that demanded a high-speed chase to bring an adversary within machine-gun firing range (i.e., low projectile speed, low impact energy, and no homing); if the target was missed, the hunter became the hunted. In the post–World War II period, around the late 1960s, air-superiority combat required fast acceleration and speed (e.g., the Lockheed F104 Starfighter) to engage with infrared homing missiles firing at a relatively short distance from the target. As missile capabilities advanced, the current combat aircraft design trend showed a decrease in speed capabilities. Instead, high turning rates and acceleration, integrated with superior missile capabilities (i.e., guided, high speed, and high impact even when detonated in proximity of the target), comprise the current trend. Target acquisition beyond visual range (BVR) – using an advance warning system from a separate platform – and rapid aiming comprise the combat rules for mission accomplishment and survivability. Current military aircraft operate below Mach 2.5; hypersonic aircraft are in the offing.

4.3.1 Aircraft Classification and Their Operational Environment

An aircraft can be classified based on its role, use, mission, power plants, and so forth, as shown in [Chart 4.1](#). Here, the first level of classification is based on operational role (i.e., civil or military discussion on military aircraft is given on [Web site](#)) – and this chapter is divided into these two classes. In the second level, the classification is based on the generic mission role, which also would indicate size. The third level proceeds with classification based on the type of power plant used and so on. The examples worked out in this book are the types that cover a wide range of aircraft design, which provides an adequate selection for an aircraft design course.

[Figure 4.2](#) indicates the speed–altitude regimes for the type of power plant used. Currently, low-speed–low-altitude aircraft are small and invariably powered by piston engines of no more than 500 horsepower (HP) per engine (turboprop engines start to compete with piston engines above 400 HP). World War II had the Spitfire aircraft powered by Rolls Royce Merlin piston engines (later by Griffon piston engines) that exceeded 1,000 HP; these are nearly extinct, surviving only in museum collections. Moreover, aviation gasoline (AVGAS) for piston engines is expensive and in short supply.

The next level in speed–altitude is by turboprops operating at shorter ranges (i.e., civil aircraft application) and not critical to time due to a slower speed (i.e., propeller limitation). Turboprop fuel economy is best in the gas turbine family of engines. Subsonic cargo aircraft and military transport aircraft may be more economical to run using turboprops because the question of time is less critical, unlike passenger operations that is more time critical with regard to reaching their destinations.

The next level is turbofans operating at higher subsonic speeds. Turbofans (i.e., bypass turbojets) begin to compete with turboprops at ranges of more than 1,000 nm due to time saved as a consequence of higher flight speed. Fuel is not the only factor contributing to cost – time is also money. A combat aircraft power plant

Chart 4.1 Aircraft Classification

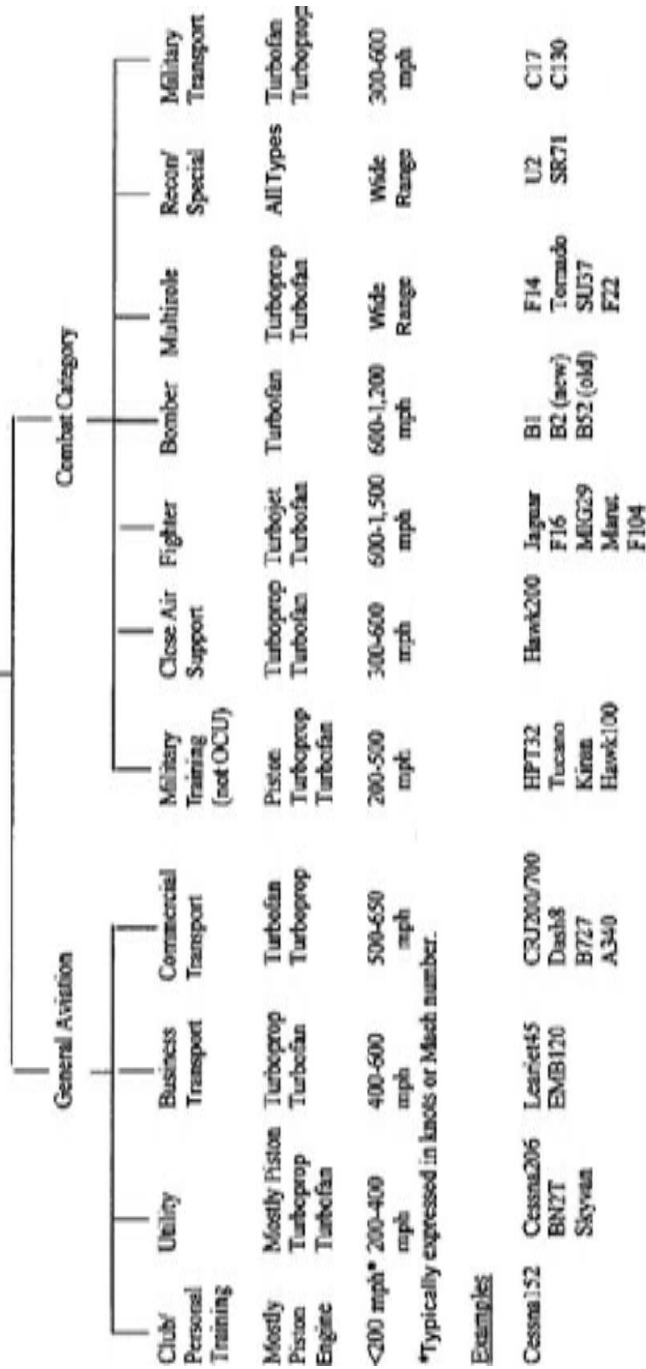
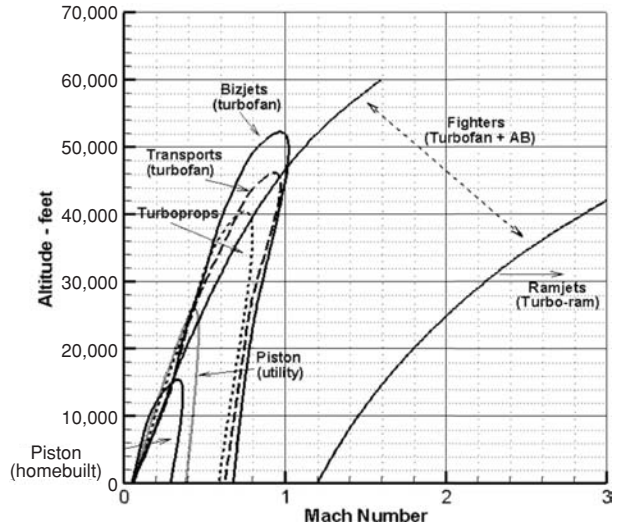


Chart 4.1. Aircraft classification

Figure 4.2. Engine selections for speed–altitude capabilities

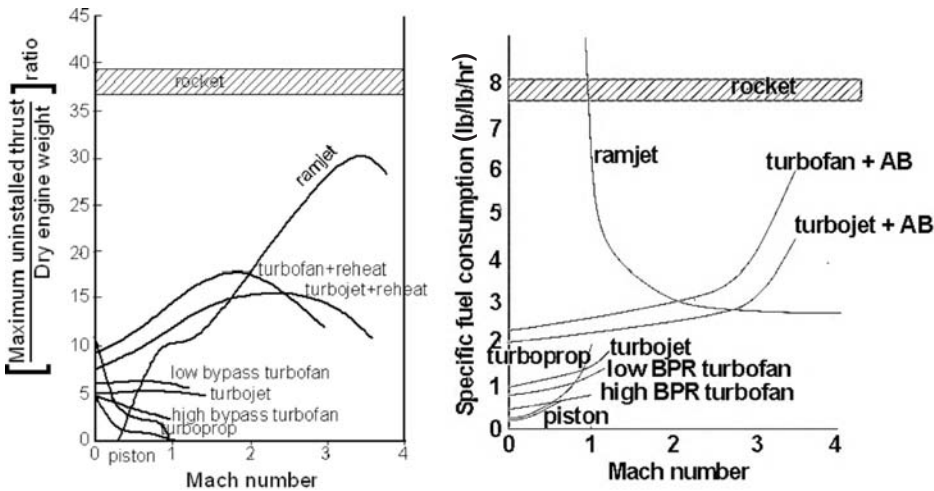


uses lower bypass turbofans; in earlier days, there were straight-through (i.e., no bypass) turbojets. Engines are discussed in more detail in [Chapter 10](#).

Figure 4.3a illustrates the thrust-to-weight ratio of various types of engines. Figure 4.3b illustrates the specific fuel consumption (*sfc*) at sea-level static takeoff thrust (T_{SLS}) rating in an ISA day for various classes of current engines. At cruise speed, the *sfc* would be higher.

Design lessons learned so far on the current trend are summarized as follows:

- *Civil aircraft design:* For the foreseeable future, aircraft will remain subsonic and operating below 60,000 ft (large subsonic jets <45,000 ft). However, aircraft size could grow even larger if the ground infrastructure can handle the volume



(a) Thrust-to-weight ratio
Figure 4.3. Engine performance

(b) Specific fuel consumption (*sfc*)

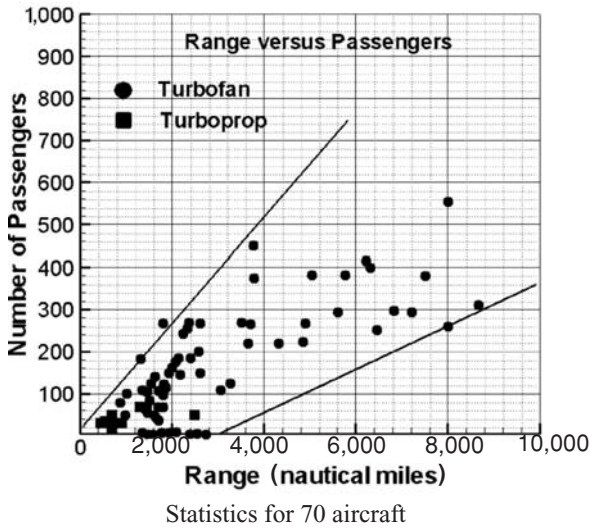


Figure 4.4. Range versus passengers

of passenger movement. Lower acquisition costs, lower operational costs, and improved safety and environmental issues would act as design drivers. The SST would attempt an entry and HST operations still could be several decades away.

- *Military aircraft design:* Very agile aircraft incorporating extensive micro-processor-based control and systems management operating below Mach 2.5, high altitude (> 60,000 ft), and BVR capabilities would be the performance demand. The issue of survivability is paramount – if required, aircraft could be operated unmanned. The military version of hypersonic combat aircraft could arrive sooner, paving the way to advance civil aircraft operations. Armament- and missile-development activities would continue at a high level and would act as one of the drivers for vehicle design.

4.4 Civil Aircraft Mission (Payload-Range)

The payload-range capability constitutes the two most important parameters to represent commercial transport aircraft. It is the basic aircraft specification and requirement as a result of market studies for new aircraft designs.

Figure 4.4 shows the payload-range capabilities for several subsonic-transport aircraft (i.e., turbofans and turboprops). The figure captures more than fifty different types of current designs. The trend shows that the range increases with payload increases, reflecting the market demand for the ability to fly longer distances. Long-range aircraft will have fewer sorties and will need to carry more passengers at one time. The classic debate on the A380 versus the B787 passenger capacity is captured within the envelope shown between the two straight lines in Figure 4.4. It is interesting that there are almost no products carrying a high passenger load for shorter ranges (i.e., < 2,000 nm). At the other extreme, the high-subsonic, long-distance executive jets, the Bombardier Global Express and Gulfstream V, are already on the market (not shown in Figure 4.4) carrying executives and a small number of passengers very long ranges (> 6,500 nm) at a considerably higher cost per passenger. It is obvious that because of considerably lower speeds, turboprop-powered

aircraft cater to the shorter-range market sector – they provide better fuel economy than turboprops. The author considers that the future may show potential markets in the less affluent areas. Major countries with substantial population centers could fly more passengers within their borders, such as in China, India, Indonesia, Russia, and the United States.

The points in Figure 4.4 include the following aircraft: Lear 31A, Lear 45, Lear 60, Cessna 525A, Cess 650, Cess 500, Cess 550, Cess 560, Cess 560XL, ERJ 135ER, ERJ 140, ERJ 145ER, CRJ 100, CRJ 700, ERJ 170, DC-9-10, CRJ 900, ERJ 190, 737-100, 717-200, A318-100, A319-100, A320-100, Tu204, A321-100, 757-200, A310-200, 767-200, A330-200, L1011, A340-200, A300-600, A300-100, DC-10-10, MD11, 777-200, 747-100, A380, Short 330 and 360, ATR 42 and 72, Jetstream 31, Saab 340A, Dash 7 and 8, Jetstream 41, EMB 120, EMB 120ER, Dornier 328-100, and Q400.

Commercial aircraft operation is singularly dependent on revenue earned from fare-paying passengers and cargo. In the operating sector, *load factor* is defined as the ratio of occupied seats to available seats. Typically, for aircraft of medium sizes and larger, operational costs break even at approximately one-third full capacity (this varies among airlines; fuel costs at 2000 level with regular fares) – that is, a load factor of about 0.33. Of course, the empty seats could be filled with reduced fares, thereby contributing to the revenue earned.

It is appropriate here to introduce the definition of the dictating parameter, *seat-mile cost*, which represents the unit of the aircraft DOC that determines airfare to meet operational costs and sustain profits. DOC is the total cost of operation for the mission sector (operational economics are discussed in detail in Chapter 16). The U.S. dollar is the international standard for aircraft cost estimation.

$$\text{seat-mile cost} = \frac{DOC}{\text{number of passengers} \times \text{range in nm}} = (\text{cents/seat/nm}) \quad (4.1)$$

The higher the denominator in Equation 4.1, the lower is the seat-mile cost (i.e., DOC). The seat-mile cost is the aircraft operating cost per passenger per nm of the mission sector. Therefore, the longer an aircraft flies and/or the more it carries, the lower the seat-mile cost becomes. Until the 1960s, passenger fares were fixed under government regulation. Since the 1970s, the fare structure has been deregulated – an airline can determine its own airfare and vary as the market demands.

A careful market study could fine-tune an already overcrowded marketplace for a mission profile that offers economic gains with better designs. Section 2.6 addresses the market study so that readers understand its importance.

4.5 Civil Subsonic Jet Aircraft Statistics (Sizing Parameters and Regression Analysis)

This section examines the statistics of current aircraft geometry and weight to identify aircraft sizing parameters. Regression analyses are carried out to demonstrate a pattern as proof of expectations. With available statistics, aircraft can be roughly sized to meet specifications. This is the starting point; Chapter 11 discusses formal sizing to finalizing aircraft configuration.

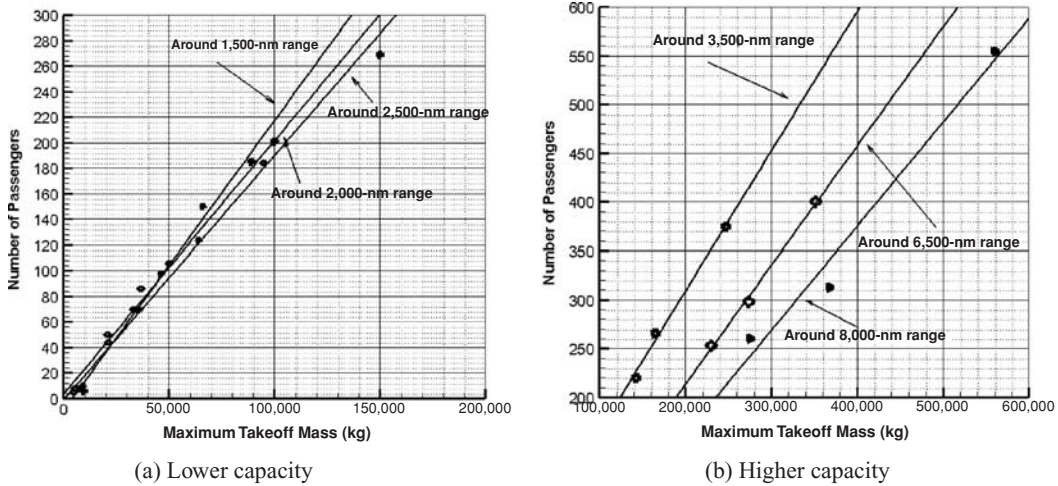


Figure 4.5. Number of passengers versus MTOM

Definitions of various types of aircraft mass (i.e., weight) are provided in [Chapter 8](#); some are required in this section, as follows (payload could be passengers and/or cargo):

- MEM: manufacturer's empty mass – the finished aircraft mass rolls out from the factory line
- OEM: operator's empty mass = MEM + crew + consumable – it is now ready for operation
- MTOM: maximum takeoff mass = OEM + payload + fuel – loaded to maximum design mass

MEM is the design outcome from catering to the MTOM, in which fuel load and payload are traded. The trade-off between payload (i.e., passenger) and fuel is at the operator's discretion, who has the choice to trade between them (see [Chapter 13](#)). Keeping the MTOM invariant, the operator can offload some passengers to increase the fuel load to the extent that the tankage capacity would allow a farther flying distance. Conversely, fuel could be offloaded to a shorter range, allowing an increase in passengers to the extent the aircraft can accommodate. Mass per passenger is revised to 100 kg (220 lb) from the earlier value of 90 kg (200 lb), which includes baggage allowance; there could be additional cargo load.

4.5.1 Maximum Takeoff Mass versus Number of Passengers

[Figure 4.5](#) describes the relationship between passenger capacity and MTOM, which also depends on the mission range for carrying more fuel for longer ranges. In conjunction with [Figure 4.4](#), it shows that lower-capacity aircraft generally have lower ranges ([Figure 4.5a](#)) and higher-capacity aircraft are intended for higher ranges ([Figure 4.5b](#)). Understandably, at lower ranges, the effect of fuel mass on MTOM is not shown as strongly as for longer ranges that require large amounts of fuel. There is no evidence of the square-cube law, as discussed in [Section 3.20.1](#). It is possible for the aircraft size to grow, provided the supporting infrastructure is sufficient.

Table 4.1. Maximum takeoff mass per passenger versus range

Range (nm)	MTOM/passenger (kg/PAX)
1,500	400
3,500	600
6,500	900
8,000	1,050

Figure 4.5 shows an excellent regression of the statistical data. It is unlikely that this trend will be much different in the near future. Considerable scientific breakthroughs will be required to move from the existing pattern to better values. Light but economically viable material, superior engine fuel economy, and miniaturization of systems architecture are some of the areas in which substantial weight reduction is possible.

In conjunction with Figure 4.4, it can be seen that longer-range aircraft generally have higher MTOM; estimates of MTOM per passenger are provided herein (Table 4.1). At the start of a conceptual study, the MTOM must be guessed – these statistics provide a reasonable estimate. Below 2,500 nm, the accuracy degenerates; the weight for in-between ranges is interpolated.

EXAMPLE: For a mission profile with 300 passengers and a 5,000-nm range, the MTOM is estimated at $750 \times 300 = 225,000$ kg (comparable to the Airbus 300–300).

4.5.2 Maximum Takeoff Mass versus Operational Empty Mass

Figure 4.6 provides crucial information to establish the relationship between the MTOM and the OEM. The important ratio of OEM to MTOM, known as the *operational empty mass fraction (OEMF)*, is obtained by this graph.

Figure 4.6a shows the regression analysis of the MTOM versus the OEM for twenty-six turbofan aircraft, indicating a predictable OEM growth with MTOM almost linearly. At the lower end, aircraft with fewer than 70 passengers (i.e., Bizjet, utility, and regional jet class) have a higher OEMF (around 0.6 – sharply

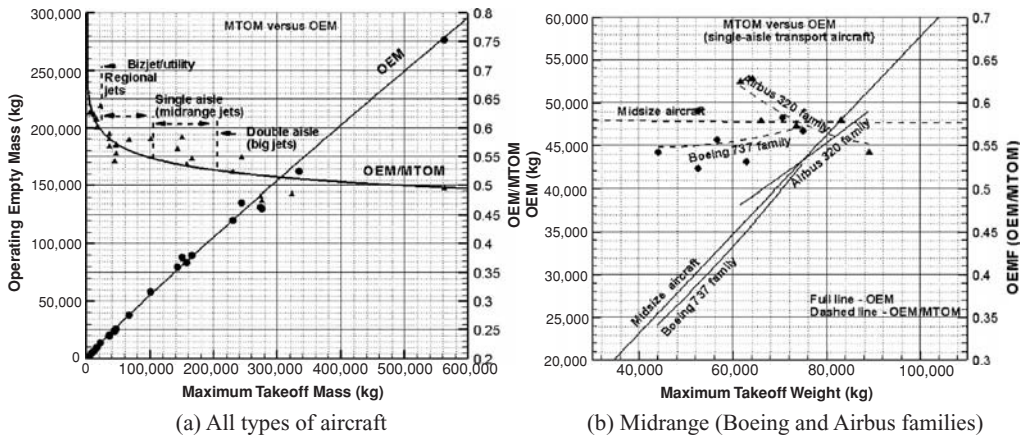


Figure 4.6. OEM versus MTOM

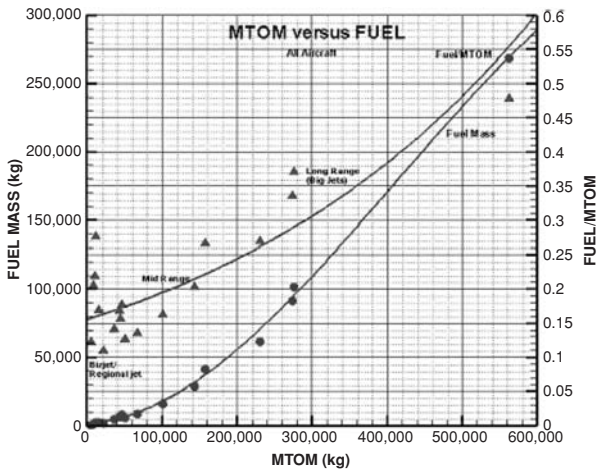


Figure 4.7. MTOM versus fuel load

decreasing). In the midrange (i.e., 70- to 200-passenger class – single-aisle, narrow-body), the OEMF is around 0.56. At the higher end (i.e., more than 200 passengers – double-aisle, wide-body), it is leveling out at around 0.483; the MTOM is slightly more than twice the OEM. The decreasing trend of the weight fraction is due to better structural efficiencies achieved with larger geometries, the use of lighter material, and the more accurate design and manufacturing methods of more recent designs.

The OEM is a function of aircraft load experienced on both the ground and in the air, which depends on the MTOM. The load in the air is a result of aircraft speed–altitude capabilities, the maneuverability limit, and wind. A higher speed capability would increase the OEMF to retain structural integrity; however, the OEM would reflect the range capability for the design payload at the MTOM (see Figure 4.5). Payload and fuel load can be exchanged to reach the MTOM from the OEM.

Figure 4.6a is represented in higher resolution when it is plotted separately, as shown in Figure 4.6b for midrange-size aircraft. It also provides insight to the statistical relationship between the derivative aircraft of the Boeing 737 and Airbus 320 families. The approaches of the two companies are different. Boeing, which pioneered the idea, had to learn the approach to the family concept of design. The Boeing 737–100 was the baseline design, the smallest in the family. Its growth required corresponding growth in other aerostructures yet maintaining component commonality as much as possible. Conversely, Airbus learned from the Boeing experience: Their baseline aircraft was the A320, in the middle of the family. The elongated version became the A321 by plugging in constant cross-section fuselage sections in the front and aft of the wing, while retaining all other aerostructures. In the shortened versions, the A319 came before the even shorter A318, maintaining the philosophy of retaining component commonalities. The variants were not the optimized size, but they were substantially less costly, decreasing the DOC and providing a competitive edge.

4.5.3 Maximum Takeoff Mass versus Fuel Load

Figure 4.7 shows the relationship between fuel load, M_f , and the MTOM for twenty turbofan aircraft; this graph provides the fuel fraction, $M_f/MTOM$. It may be

examined in conjunction with Figures 4.4, 4.5, and 4.6, which show the range increase with the MTOM increase.

Fuel mass increases with aircraft size, reflecting today's market demand for longer ranges. The long-range aircraft fuel load, including reserves, is less than half the MTOM. For the same passenger capacity, there is statistical dispersion at the low end. This indicates that for aircraft with a wider selection of comfort levels and choice of aerodynamic devices, the fuel content is determined by the varied market demand: from short ranges of around 1,400 nm to cross-country ranges of around 2,500 nm. At the higher end, the selection narrows, showing a linear trend. Figure 4.6 indicates that larger aircraft have better structural efficiency, offering a better OEMF; Figure 4.7 indicates that they also have a higher fuel fraction for longer ranges.

4.5.4 Maximum Takeoff Mass versus Wing Area

Whereas the fuselage size is determined from the specified passenger capacity, the wing must be sized to meet performance constraints through a matched engine (see Chapter 11). Figure 4.8 shows the relationships between the wing planform reference area, S_w , and the wing-loading versus the MTOM. These graphs are useful for obtaining a starting value (i.e., preliminary sizing) for a new aircraft design that would be refined through the sizing analysis.

Wing-loading, W/S_w , is defined as the ratio of the MTOM to the wing planform reference area. ($W/S_w = \text{MTOM}/\text{wing area}$, kg/m^2 , if expressed in terms of weight; then, the unit becomes N/m^2 or lb/ft^2 .) This is a significant sizing parameter and has an important role in aircraft design.

The influence of wing-loading is illustrated in the graphs in Figure 4.8. The tendency is to have lower wing-loading for smaller aircraft and higher wing-loading for larger aircraft operating at high-subsonic speed. High wing-loading requires the assistance of better high-lift devices to operate at low speed; better high-lift devices are heavier and more expensive.

The growth of the wing area with aircraft mass is necessary to sustain flight. A large wing planform area is required for better low-speed field performance, which exceeds the cruise requirement. Therefore, wing-sizing (see Chapter 11) provides the minimum wing planform area to satisfy simultaneously both the takeoff and the cruise requirements. Determination of wing-loading is a result of the wing-sizing exercise.

Smaller aircraft operate in smaller airfields and, to keep the weight and cost down, simpler types of high-lift devices are used. This results in lower wing-loading (i.e., 200 to 500 kg/m^2), as shown in Figure 4.8a. Aircraft with a range of more than 3,000 nm need more efficient high-lift devices. It was shown previously that aircraft size increases with increases in range, resulting in wing-loading increases (i.e., from 400 to 700 kg/m^2 for midrange aircraft) when better high-lift devices are considered.

Here, the trends for variants in the family of aircraft design can be examined. The Airbus 320 baseline aircraft is in the middle of the family. The A320 family retains the wing to maintain component commonality, which substantially reduces manufacturing cost because not many new modifications are necessary for the variants. This resulted in large changes in wing-loading: The smallest in the family

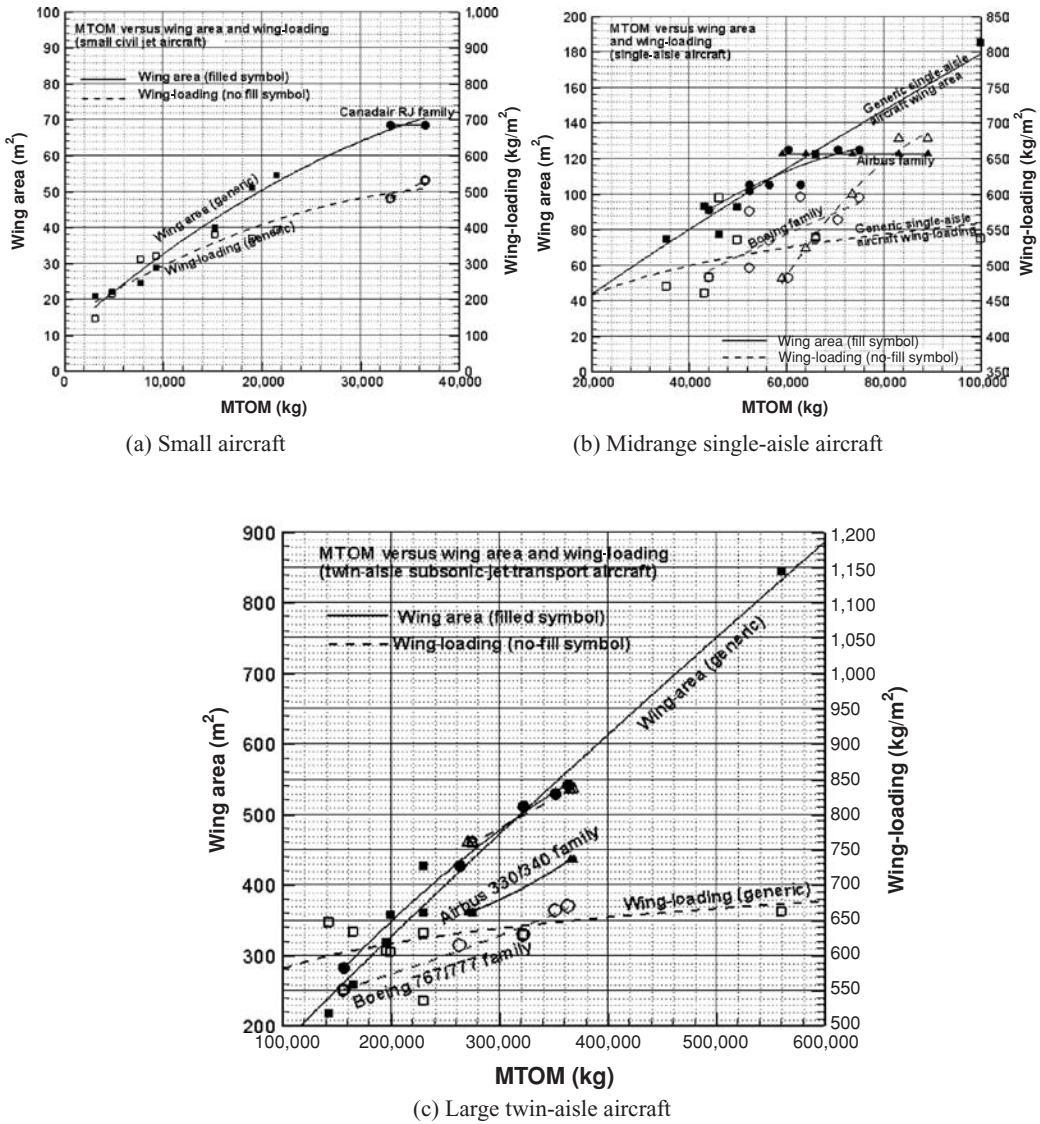


Figure 4.8. Wing area, S_w , versus MTOM

(A318) has low wing-loading with excellent field performance, and the largest in the family (A321) has high wing-loading that requires higher thrust-loading to keep field performance from degrading below the requirements. Conversely, the Boeing 737 baseline aircraft started with the smallest in the family and was forced into wing growth with increases in weight and cost; this keeps changes in wing-loading at a moderate level.

Larger aircraft have longer ranges; therefore, wing-loading is higher to keep the wing area low, thereby decreasing drag. For large twin-aisle, subsonic jet aircraft (see Figure 4.8c), the picture is similar to the midrange-sized, single-aisle aircraft but with higher wing-loadings (i.e., 500 to 900 kg/m²) to keep wing size relatively small (which counters the square-cube law discussed in Section 3.20.1). Large aircraft require advanced high-lift devices and longer runways.

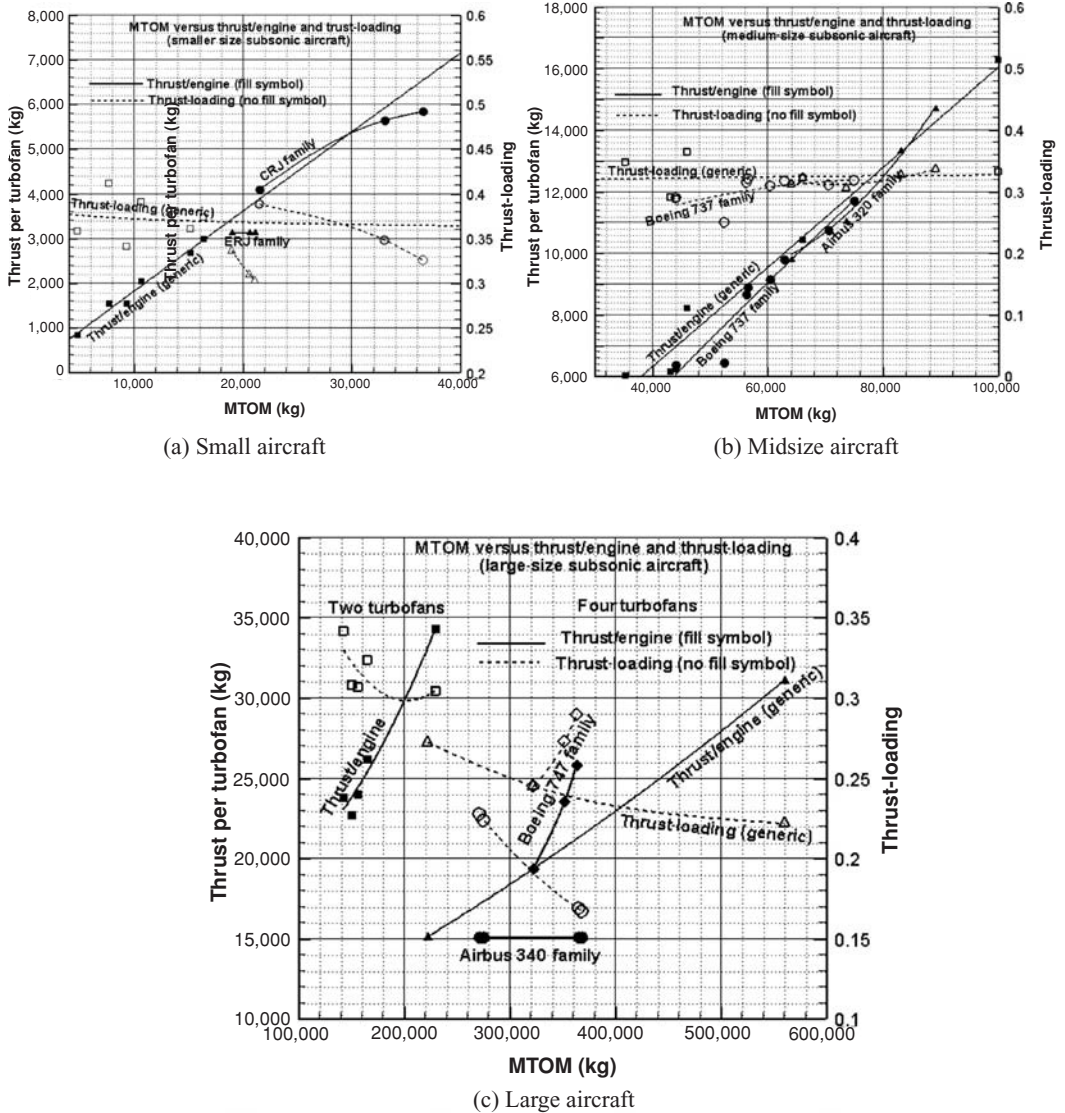


Figure 4.9. Total sea-level static thrust versus MTOM

4.5.5 Maximum Takeoff Mass versus Engine Power

The relationships between engine sizes and the MTOM are shown in Figure 4.9. Turbofan engine size is expressed as sea-level static thrust (T_{SLs}) in the ISA day at takeoff ratings, when the engine produces maximum thrust (see Chapter 10). These graphs can be used only for preliminary sizing; formal sizing and engine matching are described in Chapter 11.

Thrust-loading (T/W), is defined as the ratio of total thrust ($T_{SLs,tot}$) of all engines to the weight of the aircraft. Again, a clear relationship can be established through regression analysis. Mandatory airworthiness regulations require that multiengine aircraft should be able to climb in a specified gradient (see FAA requirements in Chapter 13) with one engine inoperative. For a twin-engine aircraft,

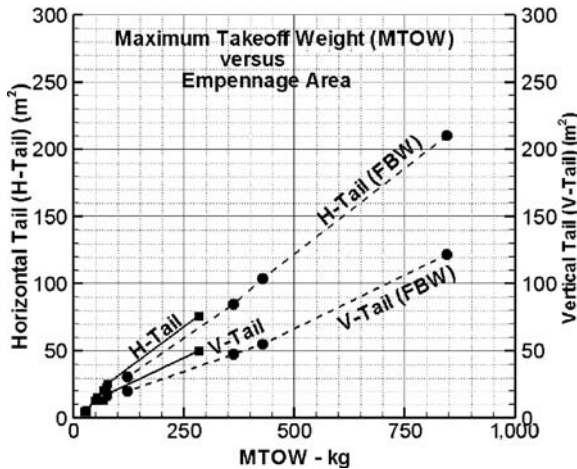


Figure 4.10. Empennage area versus wing area

failure of an engine amounts to a 50% loss of power, whereas for a four-engine aircraft, it amounts to a 25% loss of power. Therefore, the T/W for a two-engine aircraft would be higher than for a four-engine aircraft.

The constraints for engine matching are that it should simultaneously satisfy sufficient takeoff thrust to meet the (1) field length specifications, (2) initial climb requirements, and (3) initial high-speed cruise requirements from market specifications. An increase in engine thrust with aircraft mass is obvious for meeting takeoff performance. Engine matching depends on wing size, number of engines, and type of high-lift device used. Propeller-driven aircraft are rated in power P in kw (hp or shp), which in turn provides the thrust. Turboprops are rated in power loading, P/W , instead of T/W .

Smaller aircraft operate in smaller airfields and are generally configured with two engines and simpler flap types to keep costs down. Figure 4.9a shows thrust growth with size for small aircraft. Here, thrust-loading is from 0.35 to 0.45. Figure 4.9b shows midrange statistics, mostly for two-engine aircraft. Midrange aircraft operate in better and longer airfields than smaller aircraft; hence, the thrust-loading range is at a lower value, between 0.3 and 0.37. Figure 4.9c shows long-range statistics, with some two- and four-engine aircraft – the three-engine configuration is not currently in use. Long-range aircraft with superior high-lift devices and long runways ensure that thrust-loading can be maintained between 0.22 and 0.33; the lower values are for four-engine aircraft. Trends in family variants in each of the three classes are also shown in Figure 4.9.

4.5.6 Empennage Area versus Wing Area

Once the wing area is established along with fuselage length and matched engine size, the empennage areas (i.e., H-tail, S_H , and V-tail, S_V) can be estimated from the static stability requirements. Section 3.22 discusses the empennage tail-volume coefficients to determine empennage areas.

Figure 4.10 shows growth for H-tail and V-tail surface areas with the MTOM. The variants in the families do not show change in empennage areas to maintain component commonality.

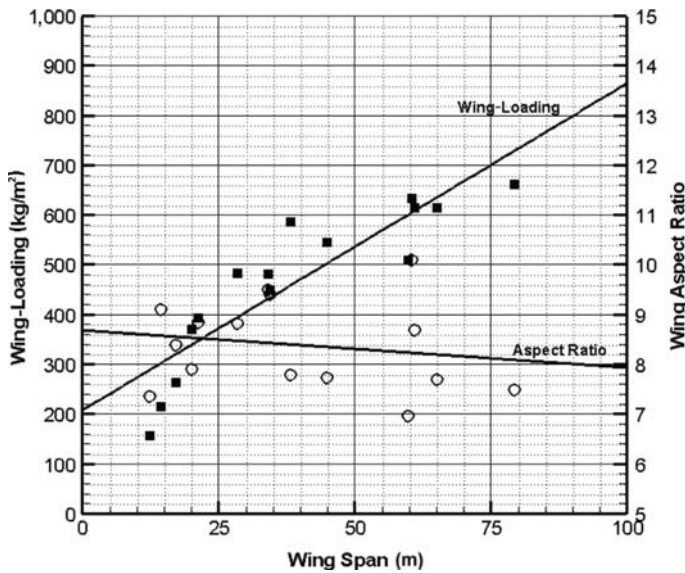


Figure 4.11. Wing span versus wing-loading and aspect ratio

4.5.7 Wing Loading versus Aircraft Span

Figure 4.11 substantiates Equation 3.43 in Section 3.20.1, which states that the growth of the wing span is associated with the growth in wing loading.

With steady improvements in new-material properties, miniaturization of equipment, and better fuel economy, wing span is increasing with the introduction of bigger aircraft (e.g., Airbus 380). Growth in size results in a wing root thickness large enough to encompass the fuselage depth when a BWB configuration becomes an attractive proposition for large-capacity aircraft. Although technically feasible, it awaits market readiness, especially from the ground-handling perspective at airports.

The aspect ratio shows a scattering trend. In the same wing-span class, the aspect ratio could be increased with advanced technology but it is restricted by the increase in wing load. Current technology provides for an aspect ratio from 8 to 14.

4.6 Civil Aircraft Component Geometries

Previous sections discussed statistical relationships of weight and geometries for a complete aircraft. Section 2.4.1 provides familiarization with typical civil aircraft and its components. The next level of information pertains to the aircraft component geometries available, as building blocks, to shape a new aircraft. There is a wide range of options available from which to choose. The choices are not arbitrary – definite reasons are associated with the choices made (see Chapter 6). This section provides pertinent information on the fuselage, wing, empennage, and nacelle groups, which are required to configure civil aircraft designs.

1. *Fuselage Group*. This is concerned with shaping and sizing of the fuselage, from where the civil aircraft configuration exercise begins. Related information ascertains seating arrangement, comfort level, and cabin width to accommodate

passenger loading so that the longest in an aircraft family does not exceed the fineness ratio on the order of 13. The appropriate front and aft-end closure choices are then made. When the fuselage shell is established, the next task is to configure the interior for passenger and crew requirements. The flight-crew space in the forward closure (i.e., cockpit) and the pilot vision polar are then established. Inside the cabin, the crew and passenger requirements are approached simultaneously as integral requirements (e.g., seating, toilets, and galleys).

2. *Wing Group*. This is the most important component of the aircraft. The plan-form shape must be established and then sized for operational-field and flight-performance requirements. Options for high-lift devices are described in Section 3.12. Other smaller components (e.g., winglets) also are considered (see Section 3.21) but not all aircraft incorporate winglets.
3. *Empennage Group*. Choice, size, and placement result from the aircraft's CG position and wing size. This book adheres to the conventional H-tail and V-tail configuration.
4. *Nacelle Group*. This topic is addressed in [Chapter 10](#); only an outline for the shaping choice is provided herein.

These four groups of aircraft components provide the preliminary shaping of candidate aircraft configurations. After the wing-sizing and engine-matching exercises, the choice must be narrowed to one final configuration that offers the best compromise for the family variants to cover a wide market. The undercarriage is addressed separately in [Chapter 7](#).

Iterations are required to position the empennage and undercarriage with respect to the wing because the CG position initially is not known. Weights are estimated from a provisional positioning and then the positions are fine tuned through iterations. (In a classroom exercise, one iteration is sufficient.)

4.7 Fuselage Group

Fuselage geometry is determined from the designed passenger capacity (see [Chapter 6](#)). There are two parameters to size (i.e., fuselage width [W] and fuselage length [L_f]), which determine the constant-section fuselage-barrel length. In turn, this depends on the seat pitch and width for the desired passenger comfort level. [Table 4.2](#) lists the statistics for existing designs – a new design would be similar. The width and length of the fuselage must be determined simultaneously, bearing in mind that the maximum growth potential in the family of variants cannot be too long or too short and keeping the fineness ratio from 7 to 14 (a good value is around 10). Boeing 757–300 records the highest fineness ratio of 14.7. A seating arrangement with two aisles results in more than six abreast (average diameter, $D_{ave} = [H + W]/2$; see [Figure 4.14](#)).

4.7.1 Fuselage Width

The first parameter to determine for the fuselage average diameter is the number of abreast seating for passenger capacity. There is an overlap on choice for

Table 4.2. *Number of passengers versus number of abreast seating and fineness ratio*

Baseline aircraft	Passenger capacity	Abreast seating	Fuselage Dia _{ave} -m	Length m	Fineness ratio	Cross-section
Learjet45	6 (4 to 8)	2	1.75	17.20	≈10.00	circular
Dornier 228	18	2			≈	rectangular
Dornier 328	24	3	2.20	20.92	≈	circular
ERJ135	37	3	2.28	24.39	≈10.70	circular
ERJ145	50	3	2.28	27.93	≈12.25	stretched version
Canadair CL600	19	4	2.69	18.77	≈7.00	short fuselage
Canadair RJ200	50	4	2.69	24.38	≈9.06	circular
Canadair RJ900	86	4	2.69	36.16	≈13.44	stretched version
Boeing 717–200	117	5	3.34	34.34	≈10.28	noncircular
BAe145 (RJ100)	100	5	3.56	30.00	≈8.43	
Airbus 318	107	6	3.96	30.50	≈7.70	circular
Airbus 321	185	6	3.96	44.00	≈11.10	circular
Boeing 737–100	200	6	3.66	28.00	≈7.65	noncircular
Boeing 737–900	200	6	3.66	42.11	≈11.50	family variant
Boeing 757–300	230	6	3.66	54.00	≈14.70	highest ratio
Boeing 767–300	260	7	5.03	53.67	≈10.70	circular
Airbus 330–300	250	8	5.64	63.00	≈11.20	circular
Airbus 340–600	380	8	5.64	75.30	≈13.35	circular
Boeing 777–300	400	9	6.20	73.86	≈11.90	circular
Boeing 747–400*	500	10	≈6.50	68.63	≈10.55	partial double deck
Airbus 380*	600	10	≈6.70	72.75	≈10.80	full double deck

* More than 450-passenger capacity, the fuselage cross-section becomes a double-deck arrangement due to current restrictions of fuselage length to 80 m (262.5 ft). In the future, this restriction could be relaxed.

the midrange capacity in the family of design; for example, an A330 with 240 to 280 passengers has seven-abreast seating whereas the same passenger capacity in a B767 has eight-abreast seating. When seating number is increased to more than six abreast, the number of aisles is increased to two to alleviate congestion in passenger movement. Because of the current fuselage-length limitation of 80 m, larger-capacity aircraft have a double-deck arrangement (e.g., the B747 and the A380). It would be interesting to try a two-aisle arrangement with six-abreast seating that would eliminate a middle seat. A three-aisle arrangement with ten-abreast seating would eliminate the cluster of four seats together. A BWB would have more than two aisles; there is no reason to not consider a triple-deck arrangement.

Although a circular cross-section is the most desirable relative to stress (minimize weight) and manufacture (minimize cost), the market requirements for the below-cabin floorspace arrangement could result in a cross-section elongated to an oval or elliptical shape. The Boeing 747 with a more narrow upper-deck width is a unique oval shape in the partial length that it extends. This partial length of the upper deck helps cross-sectional area distribution (see Section 3.23) and area ruling.

Figures 4.12 and 4.13 show various options for aircraft fuselage cross-sections to accommodate different seating arrangements. All fuselage cross-sections are symmetrical to the vertical plane. In general, aircraft with four-abreast seating and more have space below the cabin floor for baggage and cargo.

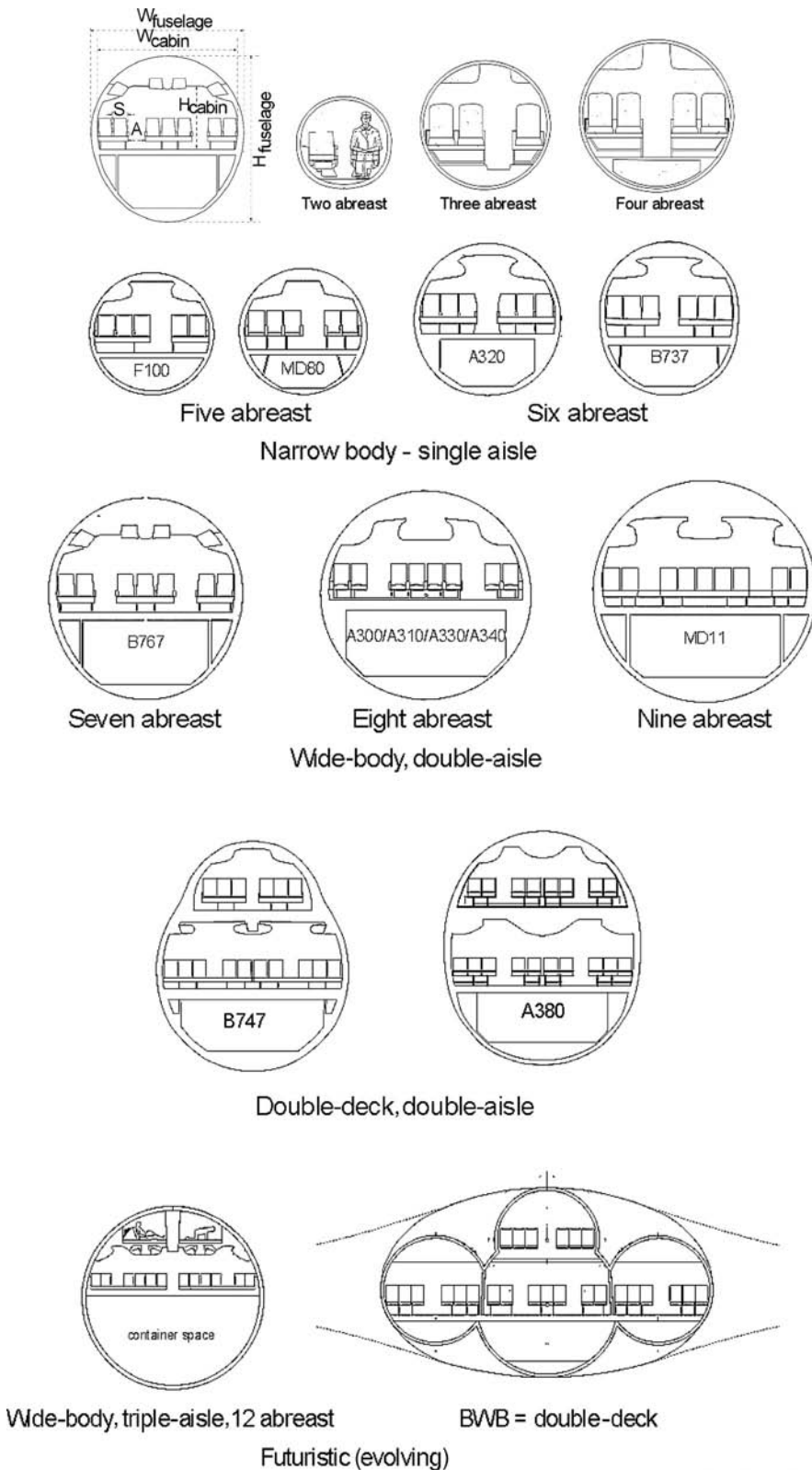


Figure 4.12. Typical commercial transport aircraft fuselage cross-section (not to scale)

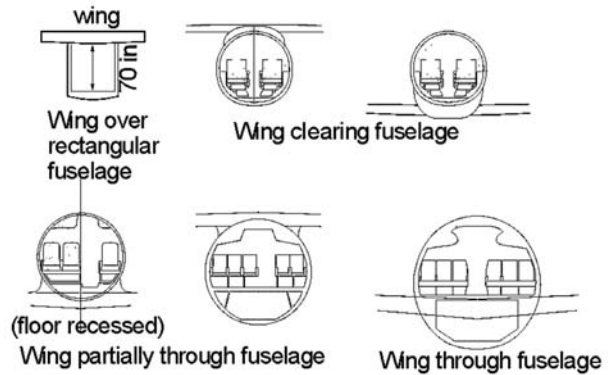


Figure 4.13. Typical choices for the wing-fuselage position

Unpressurized propeller-driven aircraft operating at lower altitudes can have rectangular cross-sections to reduce manufacturing costs, as well as offer more space (e.g., Shorts 360 aircraft). A pressurized fuselage cross-section would invariably be circular or nearly circular to minimize weight from the point of hoop-stress considerations. A two-abreast circular cross-section would have cramped legroom; a better option is a slightly widened lower lobe (e.g., Learjet 45) to accommodate legroom. In general, with a three-passenger capacity and more, the midsection fuselage has a constant cross-section with front and aft ends tailored to suit the requirements. The wing box arrangement for smaller aircraft should pass over (e.g., high-wing DO328) (Figure 4.13) or under (e.g., Learjet 45) the fuselage.

4.7.2 Fuselage Length

The overall fuselage length, L (see Figure 3.49) consists of the (1) nose cone, (2) constant cross-section midsection barrel, and (3) aft-end closure. The constant cross-section mid-fuselage length is established from the passenger seating arrangement and combined with the class arrangement (i.e., first class, business class, and economy/tourist class). Section 4.7.6 provides seat dimensions for the two main classes (i.e., business and economy).

Aircraft length may not be equal to fuselage length if any other part of the aircraft extends beyond the fuselage extremities (e.g., the tail sweep may go beyond the tail cone of the fuselage; see Figure 6.8). Figure 4.14 shows the fuselage geometry relationship to the number of passengers. The fuselage width increases in increments with the number of passenger-abreast seating, one seat width at a time. Because of passenger comfort, a designer selects options from the sensitivity study (i.e., drag and cost variations); the continuous line in Figure 4.14 represents a typical average value. The actual width is determined in Chapter 6.

4.7.3 Front (Nose Cone) and Aft-End Closure

The tear-drop-shaped streamlined closure of the fuselage at both ends of the constant midsection keeps the nose cone blunter than the gradually tapered aft cone, as shown in Figure 4.15.

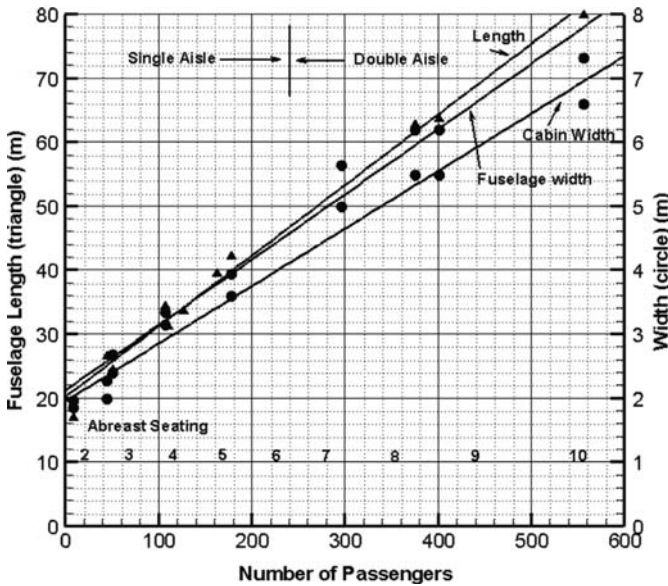


Figure 4.14. Passenger number versus fuselage length (courtesy of MacMasters)

Figure 4.15 illustrates the front fuselage closure (i.e., nose cone) length, L_f , enclosing the flight deck (i.e., pilot cockpit), followed by the constant-section payload (passengers, in this case) shell. Being in a favorable pressure gradient of the flow, it is blunter than the aft closure. The aft-fuselage closure (tail cone) length, L_a , encloses the rear pressure bulkhead with a gradual closure in an adverse pressure gradient and has some degree of upsweep. In the center, the rotated cross-sectional view of the fuselage is shown.

$$\begin{aligned} \text{average diameter, } D_{ave} &= (H + W)/2 \\ \text{front-fuselage closure ratio, } F_{cf} &= L_f/D_{ave} \text{ (also known as the } & (4.2) \\ & \text{nose fineness ratio)} \\ \text{aft-fuselage closure ratio, } F_{ca} &= L_a/D_{ave} \end{aligned}$$

Figure 4.16 shows several examples of current types of commercial transport aircraft designs. Statistical values for the front- and aft-fuselage closure are summarized in Table 4.3.

The front-end closure of bigger aircraft appears to be blunter than on smaller aircraft because the nose cone is sufficiently spacious to accommodate pilot positioning and instrumentation. A kink appears in the windscreen mould lines of the

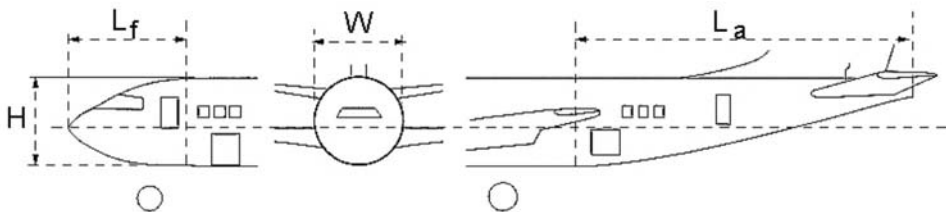


Figure 4.15. Front (nose cone) and aft-end closure

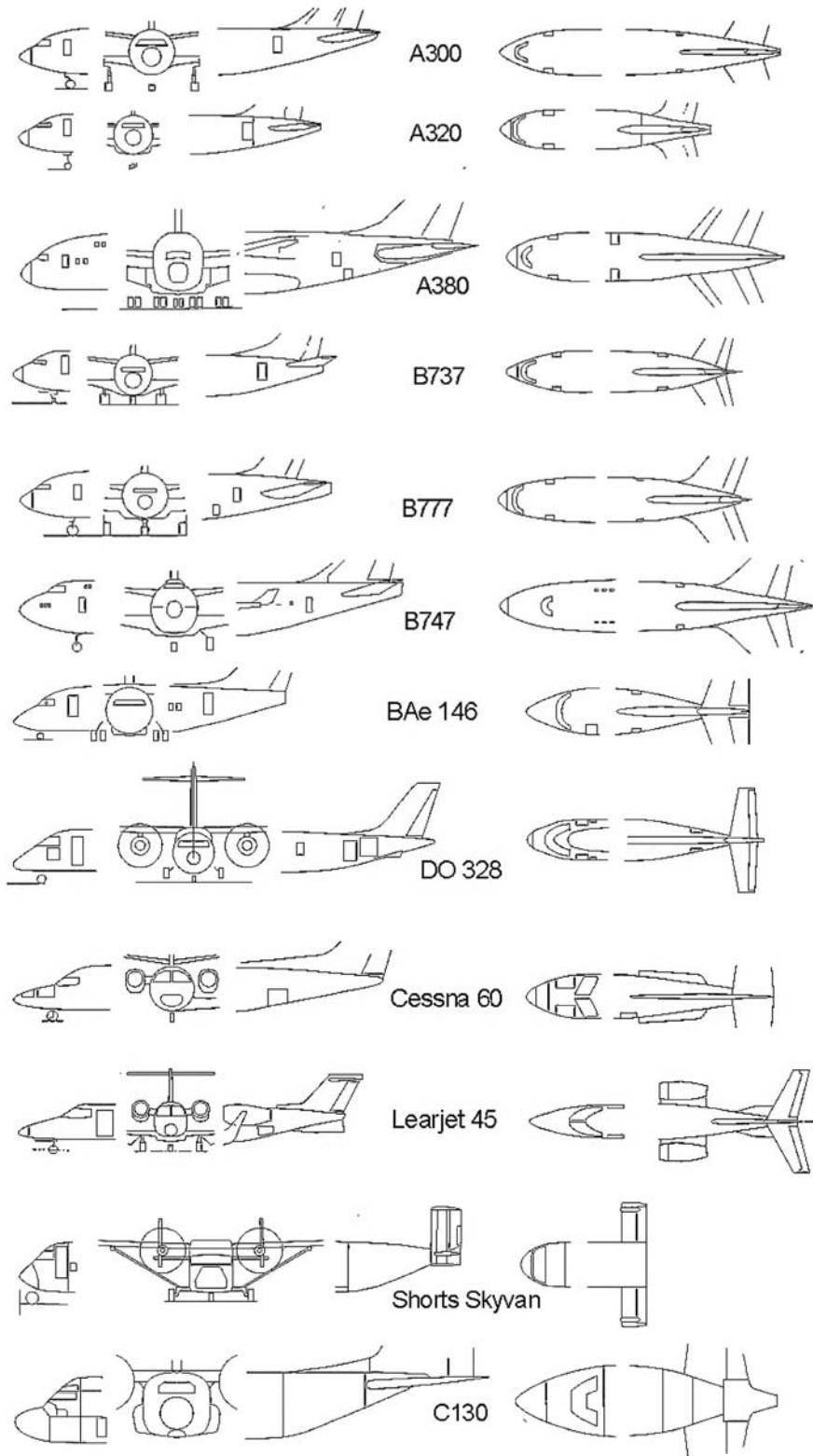


Figure 4.16. Examples of several front and aft-end closure options (scale differs for each aircraft)

Table 4.3. *Fuselage closure parameters*

Aircraft	L (m)	D (m)	H – (m)	W – (m)	H/W	L _f /D	L _a /D	UA	CA
A300–600 (TA, TF, LW)	53.62	5.64	5.64	5.64	1	2.60	3.103	5	9
A310–300 (TA, TF, LW)	46.66	5.64	5.64	5.64	1	1.60	3.40	5	11
A320–200 (TA, TF, LW)	37.57	3.96	3.96	3.96	1	1.50	3.40	4	8
A330–300 (TA, TF, LW)	59.00	5.64	5.64	5.64	1	1.82	3.64	8	11
A340–600 (TA, TF, LW)	59.39	5.64	5.64	5.64	1	1.60	3.32	8	9
A380 (TA, TF, LW)	70.40	7.78	8.41	7.14		1.50	3.91	5	11
Boeing 737 (TA, TF, LW)	31.28	3.95	4.11	3.79		1.10	2.80	7	15
Boeing 747 (TA, TF, LW)	68.63	7.30	8.10	6.50		1.31	3.31	5	11
Boeing 757 (TA, TF, LW)	46.96	4.05	4.00	4.10		1.64	2.91	6	13
Boeing 767 (TA, TF, LW)	47.24	5.03	5.03	5.03	1	1.17	2.67	7	15
Boeing 777 (TA, TF, LW)	63.73	6.20	6.20	6.20	1	1.23	2.85	7	13
MD11 (TA, TF, LW)	58.65	6.02	6.02	6.02	1	1.45	2.82	5	13
Tupolev 204 (TA, TF, LW)	46.10	3.95	3.80	4.10		1.46	2.96	5	9
Fokker 100 (TA, TF, LW)	32.50	3.30	3.05	3.49		1.42	3.42	2	10
Dornier 728 (TA, TF, LW)	27.03	2.56	2.05	3.25		1.34	2.60	5	13
Dornier 328 (RA, TF, LW)	20.92	2.42	2.425	2.415		1.27	2.64	5	10
Dash8 Q400 (RA, TP, HW)	25.68	2.07	2.03	2.11		1.71	3.22	4	9
Bae RJ85 (RA, TP, HW)	28.55	3.56	3.56	3.56	1	1.46	2.62	4	12
Skyvan (RA, TP, HW)	12.22	square	2.20	2.20		0.95	2.00	9	0
Cessna 560 (BJ, TF, LW)	15.79	5.64	5.64	5.64	1	2.05	2.91	2	8
Learjet 31A (BJ, TF, LW)	x	5.64	1.63	1.63		2.17	3.64	2	5
Cessna 750 (BJ, TF, LW)	21.00	1.80	1.80	1.80	1	2.00	3.00	7	15
Cessna 525 (BJ, TF, LW)	14.00	1.60	1.60	1.60	1	2.00	2.56	7	13
Learjet 45 (BJ, TF, LW)		5.64	1.75	1.72		1.91	2.86	8	4
Learjet 60 (BJ, TF, LW)	17.02	3.96	1.96	1.96	1	1.91	2.82	2	5
CRJ 700 (RA, TF, LW)		2.69	2.69	2.69	1	1.60	3.15	5	12
ERJ 140 (RA, TF, LW)	26.58					2.00	2.89	3	14
ERJ 170 (RA, TF, LW)	29.90	3.15	3.35	2.95		1.56	2.67	3	13
C17 (MT, TF, HW)	49.50	6.85	6.85	6.85	1	0.85	3.41	10	12
C130 (MT, TF, HW)	34.37	4.33	4.34	4.32		0.95	2.56	9	12

Notes:

TA – Transport aircraft	LW – Low wing	H – Fuselage height
RA – Regional aircraft	HW – High wing	W – Fuselage width
BJ – Business jet	L – Fuselage length	L _f – Front-closure length
MT – Military transport	D – Fuselage diameter	L _a – Aft-closure length
TF – Turbofan		UA – Upsweep angle, deg
TP – Turboprop		CA – Closure angle, deg

fuselage to fit flat glasses on a curved fuselage body; flat surfaces permit wiper installation and are less costly to manufacture. Some small aircraft have curved windcreens that permit smooth fuselage mould lines.

The aft-end closure is shallower to minimize airflow separation when the boundary layer becomes thicker. All fuselages have some upsweep for aircraft rotational clearances at takeoff. The difference in shaping is minor and is a result of the designer's choice. Designers must configure a satisfactory geometry with attention to all operation and structural requirements (e.g., pilot vision polar [see Section 4.7.4], pressure bulkhead positions, and various doors). Table 4.4 lists typical guidelines for the fuselage front- and aft-end closure ratios; the range represents current statistical values.

Table 4.4. Fuselage front- and aft-closure ratios (no rear door)

Seating abreast	Front-fuselage closure ratio, F_{cf}	Aft-fuselage closure ratio, F_{ca}	Aft-closure angle (deg)
≤ 3	≈ 1.7 to 2	≈ 2.6 to 3.5	≈ 5 to 10
4 to 6	≈ 1.5 to 1.75	≈ 2.5 to 3.75	≈ 8 to 14
≥ 7	≈ 1.5	≈ 2.5 to 3.75	≈ 10 to 15

A finer aft-closure angle is desired; however, for larger aircraft, the angle increases to keep the length (L_f) to an acceptable level to reduce weight and cost.

There are special designs that may not fall in this generalized table. Designers may exercise their own judgment in making a suitable streamline shape to allow for an upsweep to clear for aircraft rotation at takeoff.

4.7.4 Flight Crew (Flight Deck) Compartment Layout

The pilot cockpit, of course, is at the front-closure end of the fuselage to provide forward vision. The maximum accommodation is two side-by-side, generously spaced seats; an additional crew member for larger aircraft is seated behind the two pilots (Figure 4.17). In the past, there were two flight crews to assist two pilots; today, with improved and reliable systems, two flight crews have become redundant. There could be provision for one.

The pilot's seat is standardized as shown in Figure 4.18, with generous elbow-room to reduce physical stress. The windscreen size must allow adequate vision (see Figure 4.17), especially looking downward at high altitudes, during landing, and during ground maneuvers.

4.7.5 Cabin Crew and Passenger Facilities

A vital fuselage design consideration is offering passenger services – the more passengers, the more complex the design. This book does not cover details of interior design, a specialized state-of-the-art feature that is more than the mere functionality of safety, comfort, and efficient servicing. The aesthetics also offer an appealing

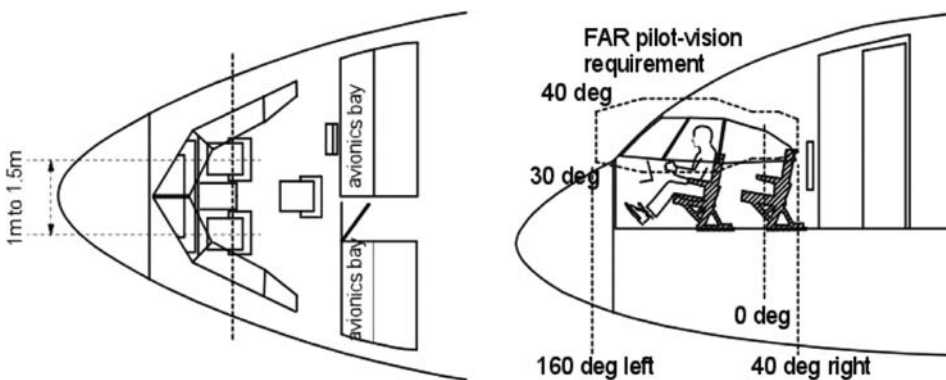


Figure 4.17. Pilot cockpit

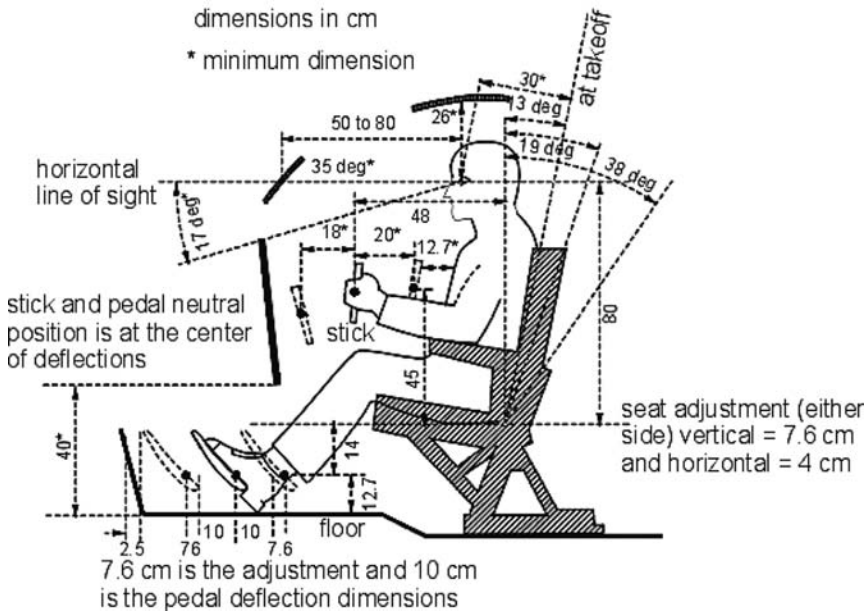


Figure 4.18. Pilot-seat dimensions

and welcoming friendly environment to passengers. Physiological and psychological issues such as thrombosis, claustrophobia, and fear of flying can be minimized through careful design of the seat-pitch arrangement, window locations, environmental controls (i.e., pressurization and air-conditioning), and first-aid facilities. Discussed herein are typical seat pitch, toilet, and service-galley arrangements in fuselage-space management that contribute to fuselage length.

The minimum number of seats abreast is one row, which is not a practical design – one would have to crawl into the cabin space. There must be at least two-abreast seating (e.g., Beech 200 and Learjet 45); the most to date is ten-abreast seating with two aisles in the Boeing 747 and Airbus 380. The two-aisle arrangement is convenient for more than six-abreast seating. As passenger capacity exceeds six hundred (if not in a double-deck arrangement), the fuselage depth allows an attractive design with BWB when more than two aisles are possible. A BWB military combat aircraft has been successfully designed but its high-capacity civil aircraft version awaits development, delayed primarily by the technology-development and airport-infrastructure limitations; the market has yet to evolve as well.

The minimum number of cabin crew is subject to government regulations. For fewer than nineteen passengers, no cabin crew is required but can be provided if an operator desires. For 19 to 29 passengers, at least 1 cabin crew is required. For 30 or more passengers, more than 1 cabin crew is required. The number of cabin crew increases correspondingly with the number of passengers.

4.7.6 Seat Arrangement, Pitch, and Posture (95th Percentile) Facilities

Figure 4.19 illustrates a typical passenger seating-arrangement design, which can be more generous depending on the facilities offered by the operator. *Pitch* is the

Table 4.5. *Seat and aisle pitch and width*

	Seat pitch cm (inches)	Seat width cm (inches)	Aisle width cm (inches)
Economy Class	71–81 (28–32)	46–51 (18–20)	43–61 (17–24)
Business Class	84–91.5 (33–36)	53–56 (21–22)	56–63.5 (22–25)

distance between two seats and varies from 28 (tight) to 36 inches (good comfort). Seat and aisle width are shown in the next figure. Typically, seat widths vary from 17 (tight) to 22 inches (good comfort). Seats are designed to meet the 16-g government impact regulations.

Table 4.5 lists currently typical seat pitch and width and aisle width (there are variations in dimensions among operators). Flexibility is built into the design to convert the seating arrangement as the market demands.

Smaller aircraft with fewer passengers (i.e., up to four abreast – the lower range) can have a narrower aisle because there is less aisle traffic and service. For larger aircraft, the minimum aisle width should be at least 22 inches.

Recently, some operators have offered sleeping accommodations in larger aircraft for long-range flights. This is typically accomplished by rearranging cabin space – the interior securing structure is designed with flexibility to accommodate changes.

4.7.7 Passenger Facilities

The typical layout of passenger facilities is shown in Figure 4.20 and includes toilets, service galleys, luggage compartments, and wardrobes. Cabin crew are provided with folding seats.

The type of service depends on the operator and ranges from almost no service for low-cost operations to the luxury of first-class service. Figure 4.21 illustrates a typical galley arrangement for a midrange passenger-carrying aircraft; other types of server trolleys are also shown. Figure 4.19 shows a trolley in the aisle being pushed by cabin crew.

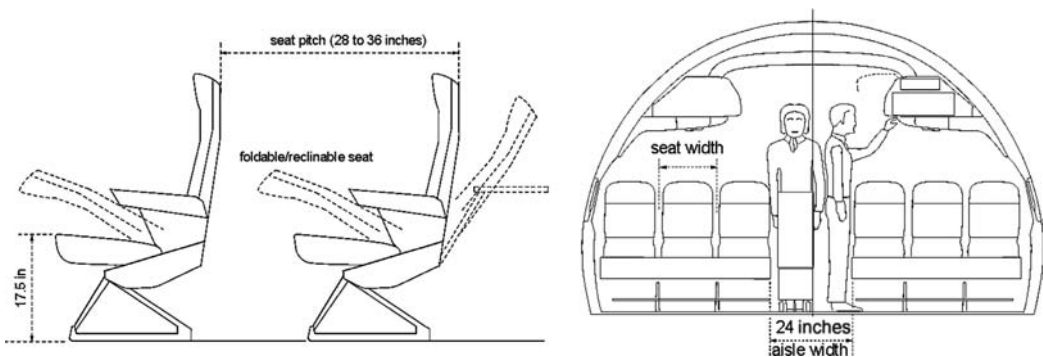


Figure 4.19. Seat pitch and width

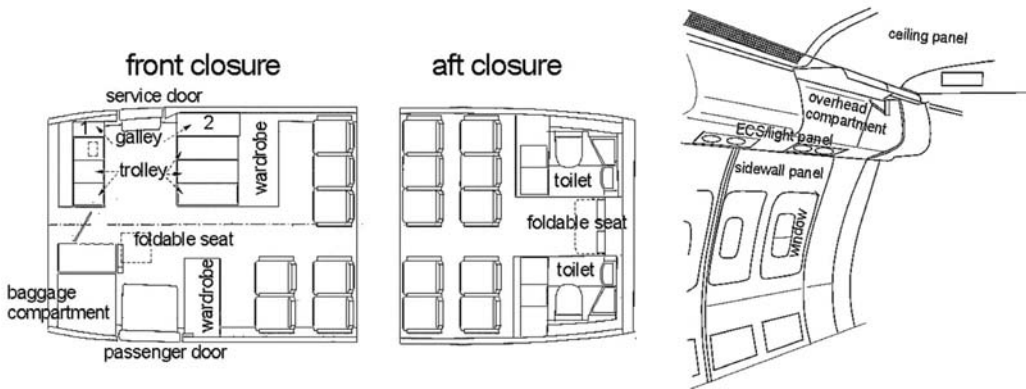


Figure 4.20. Cabin layout showing passenger facilities

Galleys are located in the passenger cabin to provide convenient and rapid service. Generally, they are installed in the cabin adjacent to the forward- and aft-galley service doors. Equipment in the galley units consists of the following:

- high-speed ovens
- hot-beverage containers
- hot-cup receptacles
- refrigeration
- main storage compartments

The electrical control-panel switches and circuit breakers for this equipment are conveniently located. Storage space, miscellaneous drawers, and waste containers are also integrated into each galley unit.

For a small Bizjet, the toilet can be minimized unless there is a demand for a luxury facility. Figure 4.21 shows a typical toilet arrangement for larger passenger-carrying aircraft.

4.7.8 Cargo Container Sizes

As the fuselage diameter increases with passenger load, the under-floorboard space can be used for cargo and baggage transportation. With operating costs becoming

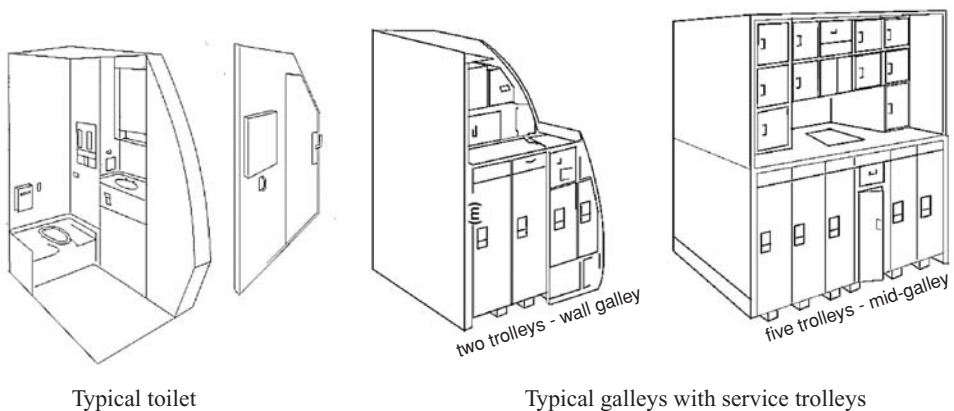


Figure 4.21. Typical aircraft galley types

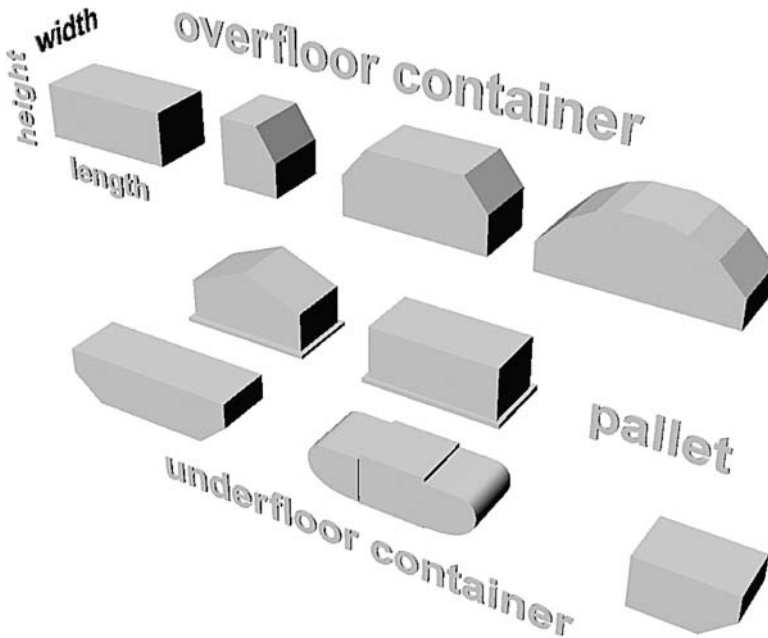


Figure 4.22. Typical container shapes

more competitive, the demand for cargo shipment is increasing, to the extent that variant aircraft are being designed as cargo aircraft (e.g., no windows and a lower level of cabin pressurization). An attractive variant is the “combi” design, which can convert the cabin layout according to the sector payload, in which the passenger load is smaller and the cargo load is higher. The combi layout can quickly reconfigure the cabin interior for passengers in the forward part and cargo in the rear, which facilitates passenger loading and unloading through the front door.

Cargo and baggage could be handled more efficiently by keeping items in containers (Figure 4.22) and having both destination and interior-space management. At the destination, the entire container is unloaded quickly so the aircraft is free for quick turnaround utilization. Container sizes are now standardized to fit in the fuselage and are internationally interchangeable.

The term *unit load device (ULD)* is commonly used when referring to containers, pallets, and pallet nets. The purpose of the ULD is to enable individual pieces of cargo to be assembled into standardized units to ease the rapid loading and unloading of airplanes and to facilitate the transfer of cargo between airplanes with compatible handling and restraint systems.

Those containers intended for below-floorboard placement (designated LD) need to have the base smaller than the top to accommodate fuselage curvature. Those containers have rectangular cross-sections and are designated “M.” Figure 4.22 shows typical container shapes; Table 4.6 lists standard container sizes, capacities (there are minor variations in dimensions), and designations.

4.7.9 Doors – Emergency Exits

Readers are referred to Section 15.7.

Table 4.6. *Standard container sizes and capacity (dimensions in cm; IATA designation not given)*

Type	Length	Width	Height	Base length	Capacity (kg)	Volume (m ³)
LD1	228.0	145.0	162.6	147.0	1,588	4.80
LD2	156.2	153.4	162.6	119.2	1,225	3.40
LD3	200.7	153.4	162.6	156.2	1,588	4.80
LD4	244.0	153.4	162.6	244.0	2,450	6.10
LD6	406.4	153.4	162.6	317.5	3,175	8.80
LD7	317.5	223.5	162.5	317.5	4,627	9.91
LD8	317.5	153.4	162.5	243.8	2,449	6.94
LD11	307.0	145.0	162.5	307.0	3,176	7.00
LD 26	400.0	214.0	162.5	307.0	6,033	12.00
M1	318.0	224.0	224.0	318.0	6,804	17.58
PGA Pallet	608.0	244.0	244.0	608.0	11,340	36.20

Note:

IATA = International Air Transport Association

4.8 Wing Group

Whereas the fuselage size is determined from the operator's specified capacity, the wing size depends on many factors and requires a rigorous sizing exercise (see [Chapter 11](#)) to determine the planform reference area. The wing contributes to lift generation and the characteristics are based on the chosen aerofoil section in use. A given priority of wing design is selecting the aerofoil(s) that fits the purpose with the aim to improve existing designs. The aerofoil section is selected using the considerations described in Section 3.11; high-lift devices are described in Section 3.12. This section describes typical options for available wing planform shapes (generic options are listed in Section 4.17.1).

After obtaining the wing planform area, other geometrical details must be determined (e.g., aspect ratio, sweep, taper ratio, dihedral, and twist). The wing span is the result of the values of the aspect ratio, sweep, and taper ratio. Equation 3.18 defines the aerodynamic MAC parameter. The three-view diagrams in [Figure 4.23](#) illustrate the fundamental planform-shape choices; each shape is discussed separately herein. For speeds exceeding Mach 0.5, sweeping the wing backward ([Figure 4.23e](#)) or forward (see [Figure 4.40b](#)) is necessary to delay the compressibility effects on the wing, as explained in Section 3.18.

1. *Rectangular planform.* This rectangular planform is used for low-speed (i.e., incompressible flow) aircraft below Mach 0.4. It is the most elementary shape with constant rib sections along the wingspan. Therefore, the cost to manufacture is lower because only one set of tooling for ribs is needed for the entire wing. However, this planform has the least efficient spanwise loading. This type of planform is well suited to small aircraft, typically for private ownership and homebuilt types. There are larger aircraft that have the rectangular wing (e.g., Shorts SD360 series and BN Islander).
2. *Tapered (trapezoidal) planform.* This is the most common planform shape in use because it offers good aerodynamic loading with a good spanwise load distribution. The taper ratio can vary – the delta-wing planform has an extreme value

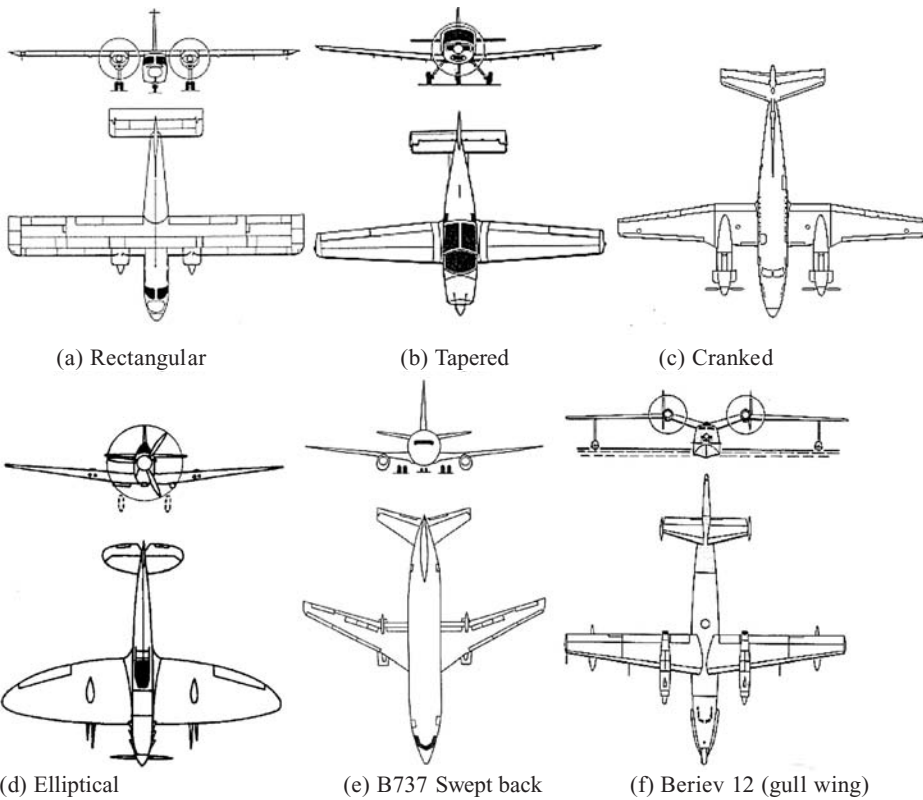


Figure 4.23. Aircraft wing planform shapes

of zero. In [Figure 4.23b](#), the LE has a small backward sweep; other designs have a straight LE, and the Saab Safir has a forward sweep, which provides pilot visibility in a high-wing aircraft. With almost no sweep, this type of wing can be designed for a maximum speed of Mach 0.5. If it must go faster, then more wing sweep is required. The production costs of a tapered wing are higher than for a rectangular wing because the ribs are different spanwise. However, the tapered wing maintains straight lines at the leading and trailing edges, which provides some ease in jig and fixture designs.

3. *Cranked-wing planform.* The Beech 200 shown in [Figure 4.23c](#) is a good example of combining the available options. In this case, the center section is rectangular and the outboard wings are tapered. Other combinations are possible. A tapered wing can be modified with a crank incorporated (i.e., two tapered wings blended into one). The glove and yehudi can be used to extend areas at leading and trailing edges, respectively.
4. *Elliptical planform.* The Spitfire aircraft shown in [Figure 4.23d](#) is a fine example of an elliptical wing, which offers the best aerodynamic efficiency for having the best spanwise load distribution. However, it is the most expensive to manufacture and designers should avoid the elliptical planform because a good tapered planform approximates the elliptical load distribution, yet its manufacture is substantially less costly. Curved-wing leading and trailing edges would require relatively more expensive tooling. The Spitfire aircraft reached very high speeds for the time.

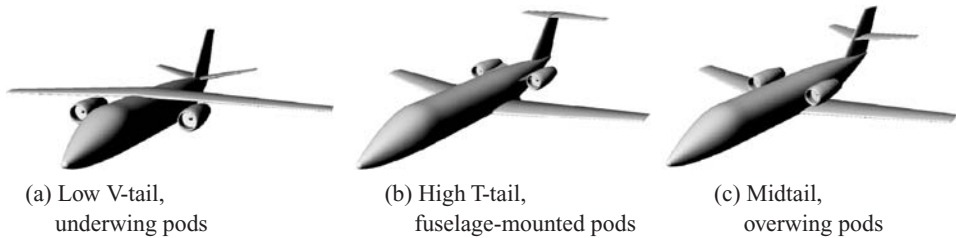


Figure 4.24. Dominant empennage design options (This figure can be used to illustrate the wing and nacelle position options.)

The Beriev 12 shown in Figure 4.23f has a gull-wing shape and the Junkers Stuka has the dihedral the other way for specific reasons. At the conceptual stage, the dihedral and the twist are taken from past experience and statistical data. Other wing parameters (e.g., aspect ratio and tapered ratio) are also available. Eventually, the wing design is fine-tuned with CFD analysis followed by wind-tunnel tests.

4.9 Empennage Group (Civil Aircraft)

Geometrical definitions and sizing of the empennage group (i.e., H-tail and V-tail) are provided in Section 3.22. These are the lifting surfaces that stabilize and control an aircraft. Because they are lifting surfaces, they follow the same rule of wing shaping. Chart 4.2 systematically tabulates the types of empennage configuration options available. Other types of empennage configuration are possible. An aircraft with pitch stability and control surface in the front is known as the canard configuration. The canard surface can share some lift (in civil aircraft designs) with the wing. The H-tail can have either a dihedral or anhedral angle. The twin V-tail can be straight or inclined either way.

Most civil aircraft designs have two surfaces almost orthogonal to each other like the V-tail and H-tail. The V-tail is always symmetrical to the aircraft centerline (there are exceptions). The H-tail can have either a dihedral or anhedral angle. The H-tail can be positioned low at the fuselage (with dihedral), at the top as a tail (with anhedral), or anywhere in between as a midtail configuration (Figure 4.24). Any combination of the scheme is feasible, but it ultimately is decided from the

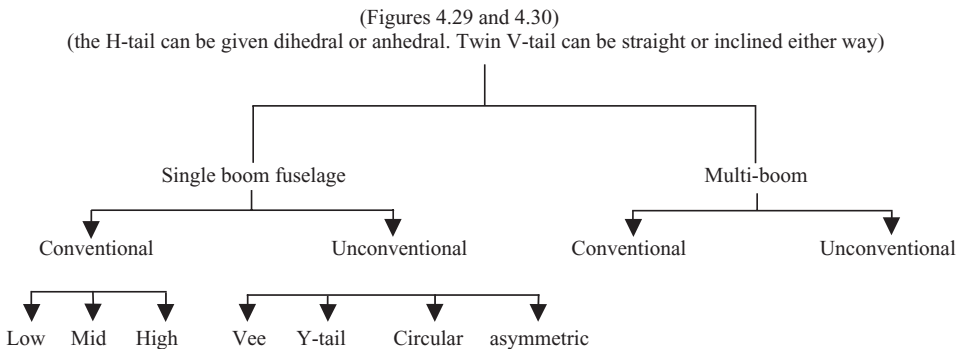


Chart 4.2. Types of Empennage Configurations

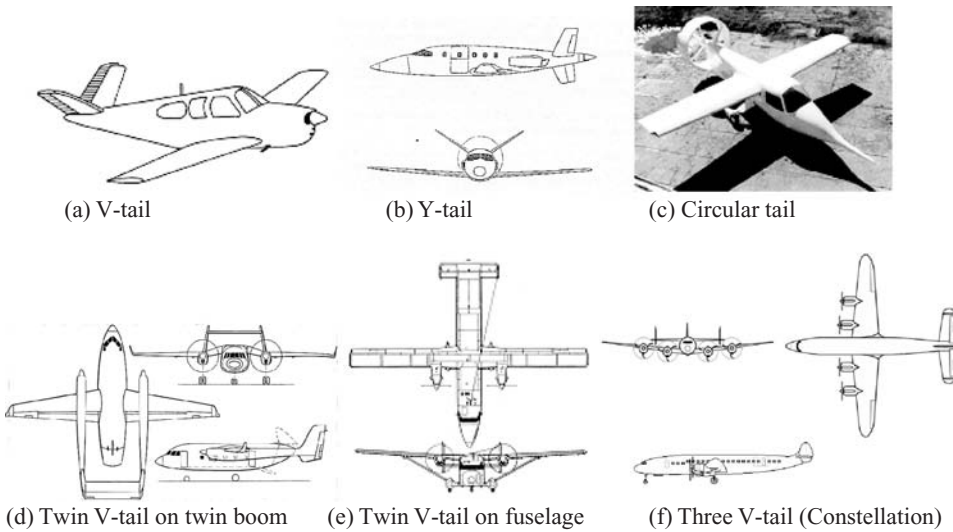


Figure 4.25. Other types of civil aircraft empennage design options

various aerodynamic, stability, and control considerations, which are discussed in Chapters 3, 4, 6, and 11.

The civil aircraft empennage layout is relatively simpler; however, there are also unconventional types. Some interesting empennage arrangements are shown in Figure 4.30. The Beechcraft Bonanza 35 has a V-shaped tail (Figure 4.25a); in some designs, it can be inverted to a V-tail. One of the early Lear designs had a Y-shaped empennage (Figure 4.25b) – that is, a V-tail with a vertical fin extending below the fuselage. In the past, a circular-duct empennage has appeared (Figure 4.25c). The merits of the unconventional empennage are its applicability, but most designs have horizontal and vertical surfaces. V-tail, Y-tail, and circular-tail designs are more complex but follow the same routine as conventional designs – that is, resolving the forces on the surface into vertical and horizontal directions. This book discusses only the conventional designs.

If the V-tail size is large due to a short tail arm, the area could be split into two or three V-tails (Figure 4.25d, e, and f) from the structural and aerodynamic considerations. The twin V-tail can be straight or inclined either way.

The H-tail position relative to the V-tail is a significant consideration; the options available are shown in Figure 4.26. It can be from the lowest position through the fuselage to the other extreme, on the top as a T-tail. Any position in between is considered the midtail position.

Designers must ensure that the H-tail does not shield the V-tail. The wake (i.e., dashed lines in Figure 4.26) from the H-tail should not cover more than 50% of the V-tail surface and should also have more than 50% of the rudder area free from its wake to maintain control effectiveness, especially during spin and stall recoveries. Shifting the V-tail aft with the rudder extending below the fuselage will bring the fin and rudder adequately outside the wake. A dorsal and ventral fin can bring out more fin surface outside the wake, but the rudder must be larger to retain effectiveness. Lowering the H-tail would move the wake aft; however, if it is too low, it may hit the ground at rotation – especially if the aircraft experienced a sudden bank due to wind

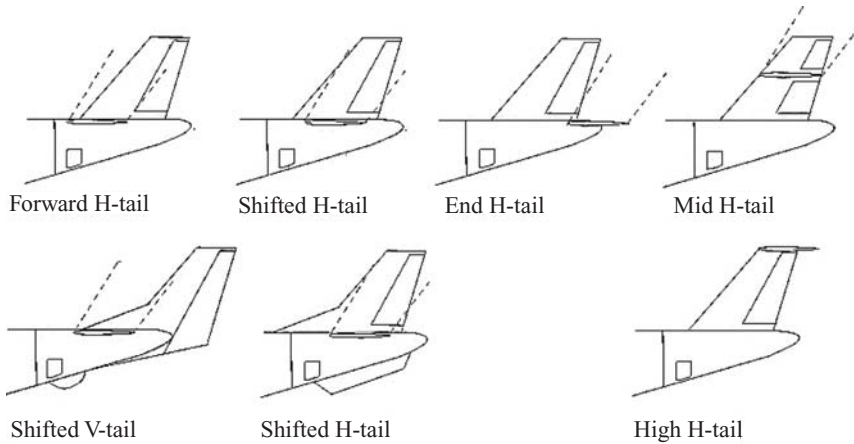


Figure 4.26. Positioning of the horizontal tail

gusts. [Chapter 6](#) discusses the H-tail position relative to the wing; that is, at a high angle of attack, the wing wake should avoid the H-tail in the near-stall condition so that the pitch control remains adequate.

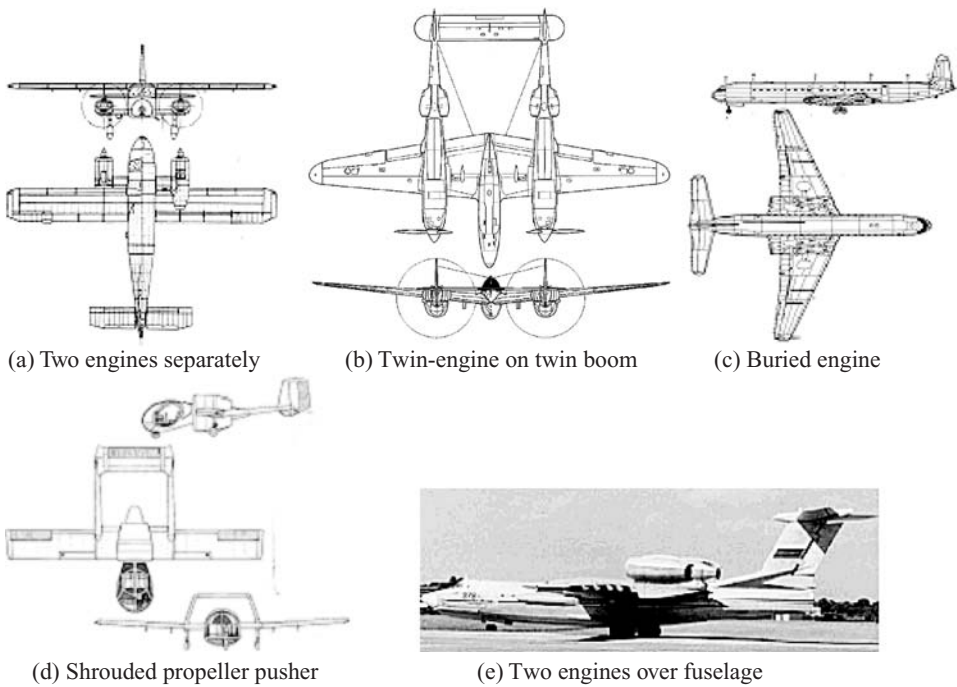
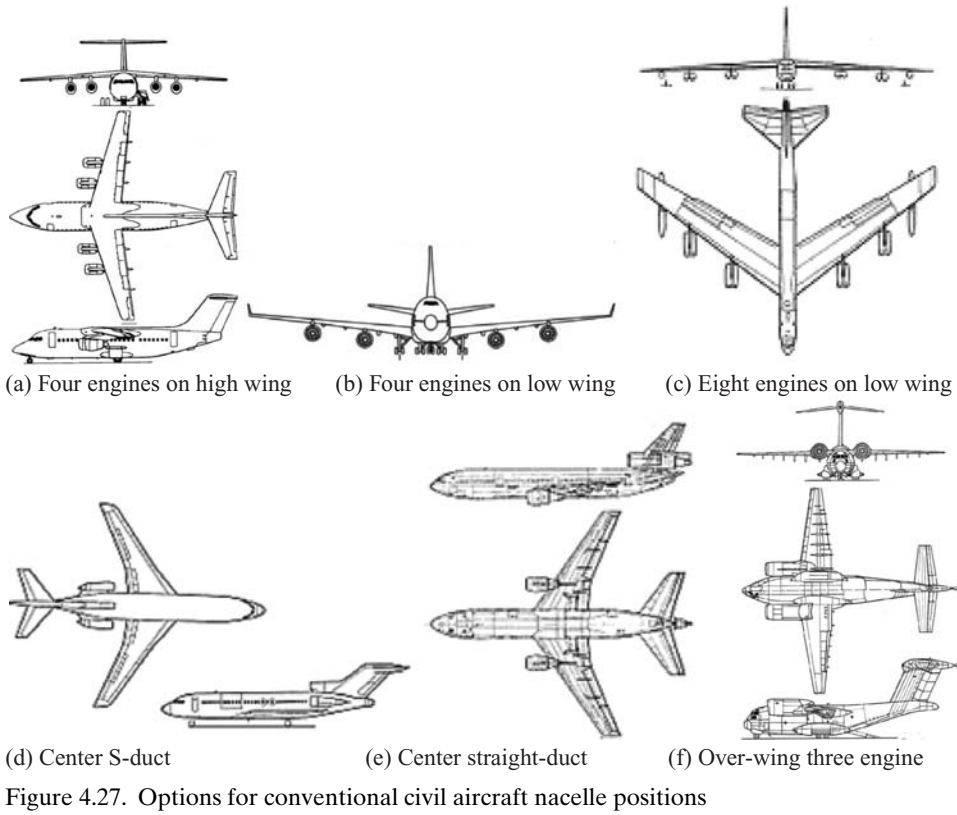
Care must be taken so that the H-tail is not within the entrainment effects of the jet exhaust situated at the aft end, which is typical for aft-mounted or within-fuselage jet engines. A military aircraft engine is inside the fuselage, which may require a pen-nib-type extension to shield the jet-efflux effect on the H-tail. In that case, the H-tail is moved up to either the midlevel or the T-tail.

4.10 Nacelle Group

In a civil aircraft design with more than one engine (i.e., turboprop or turbofan), the engines are invariably pod-mounted on the wing or the aft fuselage. The predominant options in civil aircraft design are shown in [Figures 4.25](#) and [4.27](#). Here, some military designs are shown because they can be applied to civil aircraft design as well.

Larger aircraft have nacelle pods mounted under the wing ([Figure 4.24a](#)), but low-wing small aircraft have fuselage-mounted ([Figure 4.24b](#)) nacelle pods because there is insufficient ground clearance. An overwing nacelle pod ([Figure 4.24c](#)) on a smaller low-wing aircraft is gaining credence. Four-engine underwing nacelles are shown in [Figures 4.27a](#) and [4.27b](#) (i.e., high and low wings, respectively). Introductory coursework may use any combination of these configurations.

Other options for engine positions are shown in [Figures 4.28](#) and [4.29](#). The first commercial jet transport aircraft, the de Havilland Comet, had engines buried in the wing root ([Figure 4.28c](#)). These were not efficiently designed and are not pursued any longer in civil aircraft designs. For an odd number of engines, the odd one is placed in the centerline (e.g., Douglas DC10); if it is buried in the fuselage, then its intake may require an S-duct-type intake (e.g., Boeing 727) (see [Figure 4.27d](#)). In the 1970s, the proposed Heinkel 211 (not shown) had two S-ducted engines with the two surfaces of its V-tail. The overwing slipper-nacelle design



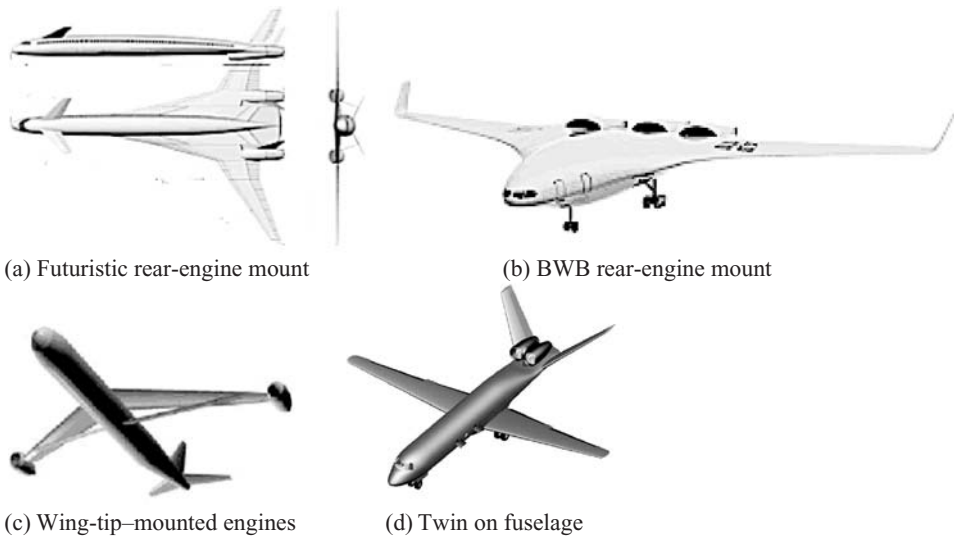


Figure 4.29. Futuristic options for the nacelle positions

has been flown by both Boeing (see [Figure 4.27f](#)) and Douglas for STOL performance. The engines on single-engine aircraft are at the centerline (except on special-purpose aircraft), mostly buried into the fuselage. The Boeing B52 bomber has eight engines in four pods slung under the wing. If propeller-driven, an engine can either be a tractor (i.e., most designs) or a pusher-propeller mounted at the rear.

Some unconventional single- and twin-engine positions are shown in [Figure 4.28](#); futuristic nacelle design options are shown in [Figure 4.29](#) and have yet to be built. [Figure 4.29a](#) shows a Boeing Super Cruiser and [Figure 4.29b](#) is the Silent aircraft BWB proposed by MIT and Cambridge University.

Some helicopter designs have rotor-tip-mounted thruster engines and some VTOL aircraft have wing-tip-mounted tilt engines; all are special-purpose designs. Virginia Polytechnic Institute (VPI) conducted studies on interesting aircraft configurations with potential. Through their MDO studies of high-subsonic aircraft with engines at the tip of a strutted wing ([Figure 4.29c](#)), they found better weight and drag characteristics than in conventional cantilevered designs [7]. Although the studies have merit and they have considered the critical issues, more detailed analysis is required using better resolution. The structural weight gain due to a truss-supported wing and the aerodynamic gain due to induced-drag reduction of the wing-tip engines are not coupled even when the former offers structural support for the latter. A major concern will be to satisfy the mandatory requirement of a one-engine inoperative case. This will result in a considerably larger tail, possibly divided in half, depleting some weight benefits. Cost is another factor that the studies did not consider. The proposed aircraft will be more expensive, which may erode the DOC gains. The new aircraft certification will further add to the cost. Until more details are available, the author does not recommend the wing-tip-mounted engine installation, especially during an introductory course. Engines should be kept close to the aircraft centerline but away from any wake effects. The nose-wheel spray may require the nacelle to be at least 30 deg, away from the nose wheel (see [Chapter 10](#)). Detailed sensitivity studies are required for comparative

analyses of this novel configuration when a simple winglet provides induced-drag reduction. However, VPI's study of twin side-by-side engines between the V-tail (Figure 4.29d) concluded that it would be better with a winglet.

4.11 Summary of Civil Aircraft Design Choices

This section summarizes some of the information discussed in Sections 4.5 through 4.10. Readers will have a better appreciation after completing the sizing exercise in Chapter 11. The seven graphs shown in Figures 4.5 through 4.11 capture all the actual aircraft data from the *Jane's All the World's Aircraft Manual* and other sources (acknowledged in the preface of this book). These statistical data (with some dispersion) prove informative at the conceptual design stage for an idea of the options that can be incorporated in a new design to stay ahead of the competition with a superior product. It is amazing that with these seven graphs, the reader can determine what to expect from a basic customer (i.e., operator) specification for the payload range. Readers may have to wait until their project is completed to compare how close it is to the statistical data, but it will not be surprising if the coursework result falls within the statistical envelope. Civil aircraft layout methodology is summarized as follows:

1. Size the fuselage for the passenger capacity and the amenities required from the customer's specification. Next, "guesstimate" the MTOM from Figure 4.6 (i.e., statistics) for the payload range.
2. Select the wing planform area from Figure 4.9 for the MTOM. Establish the wing sweep, taper ratio, and t/c for the high-speed Mach-number capability.
3. Decide whether the aircraft will be high wing, midwing, or low wing using the customer's requirements. Decide the wing dihedral or anhedral angle based on wing position relative to the fuselage. Decide the twist.
4. Guesstimate the engine size for the MTOM from Figure 4.10. Decide the number of engines required. For smaller aircraft (i.e., baseline aircraft for fewer than 70 passengers), configure the engines aft-mounted; otherwise, use a wing-mounted podded nacelle.
5. Estimate H-tail and V-tail sizes for the wing area from Section 4.5.6.

The industry expends enormous effort to make reality align with predictions – it has achieved performance predictions within $\pm 3\%$ and within $\pm 1.5\%$ for the big aircraft. The generic methods adopted in this book are in line with the industry – the difference is that the industry makes use of more detailed and investigative analyses to improve accuracy in order to remain competitive. Industry could take 10 to 20 man-years (very experienced) to perform a conceptual study of mid-sized commercial aircraft using conventional technology. In a classroom, a team effort could take at most 1 man-year (very inexperienced) to conduct a concise conceptual study. There may be a lower level of accuracy in coursework, yet learning to design aircraft this way is close to industrial practices.

It is interesting that no two aircraft or two engines of the same design behave identically in operation. This is primarily due to production variances within the

manufacturing tolerance allocations. The difference is minor: The maximum deviation is on the order of less than $\pm 0.2\%$. An older aircraft would degrade in performance: During operation, the aircraft surface would become deformed, dented, warped, and/or contaminated, increasing viscous drag, and so forth. Manufacturers consider actual problems of operational use by maintaining a record of performance of all aircraft produced. Manufacturers' comments cover average aircraft degradation only up to a point. In other words, like any product, a brand new aircraft generally would perform slightly better than what is indicated in the pilot's manual – and this margin serves the operators well.

If a new design fails to reach the predicted value, who is at fault: Is the shortcoming originating in the aircraft or the engine design or from both? Is it a bad aircraft or a bad engine (if a new engine design is incorporated)? Over time, the aerospace industry has successfully approached these issues. As mentioned previously, some aerospace stories could be more exciting than fiction; readers may examine some old design cases. Today, engine and aircraft designers work cooperatively to identify the nature of and then repair shortfalls. In general, it is convenient for the shaping of external nacelle mould lines to be the responsibility of airframe designers and the internal shaping (i.e., intake duct and exhaust duct) to be that of engine designers.

The compressibility effect of the airflow influences the shaping of an aircraft. Airflow below Mach 0.3 is nearly incompressible – in a regime, all aircraft are propeller-driven (i.e., piston engine). From Mach 0.3 to Mach 0.6, the compressibility effect gradually builds up; however, turboprops are still effective up to Mach 0.5. Above Mach 0.6, the aircraft component geometry caters to compressibility effects. Jet propulsion with reactionary thrust becomes more suitable above Mach 0.6. Therefore, the aircraft component configuration is divided into two classes: one for flying below Mach 0.5 and one for flying above Mach 0.6. A carefully designed turbo-prop can operate at up to Mach 0.6, with the latest technology pushing toward Mach 0.7. Lifting-surface geometries are those that are affected by compressibility. The fuselage being cylindrical (i.e., axi-symmetric) makes it easier to address the compressibility effect.

4.12 Military Aircraft: Detailed Classification, Evolutionary Pattern, and Mission Profile

This extended section of the book can be found on the Web at www.cambridge.org/Kundu and gives introductory comments on typical military aircraft classification; military aircraft role, statistics, and design considerations; and some relatively newer requirements (evolutionary patterns), and so forth. Figure 4.30 shows (a) Lockheed F104, Starfighter; (b) McDonnell F4, Phantom; (c) Grumman F14, Tomcat; (d) Northrop F117; and (e) Lockheed F22.

Figure 4.30. Chronology of fighter aircraft design evolution (USA)

4.13 Military Aircraft Mission

This extended section of the book can be found on the Web at www.cambridge.org/Kundu and describes military aircraft multiroles, indicating that the same class

of military aircraft can have a wide variety of payload ranges. Figure 4.31 shows weapon configurations for (a) air interdiction, (b) close air support, (c) air defense, and (d) maritime attack.

Figure 4.31. Typical multirole missions

4.14 Military Aircraft Statistics (Sizing Parameters – Regression Analysis)

This extended section of the book can be found on the Web at www.cambridge.org/Kundu and gives the statistics of military aircraft as discussed in the following subsections.

4.14.1 Military Aircraft Maximum Take-off Mass (MTOM) versus Payload

In this subsection, at www.cambridge.org/Kundu, Figure 4.32 shows typical statistics of military aircraft payload – range.

Figure 4.32. Military aircraft payload – range (no drop tank or refueling)

4.14.2 Military MTOM versus OEM

In this subsection, at www.cambridge.org/Kundu, Figure 4.33 gives the relation between MTOM and OEM, as well as the operational empty mass fraction (ratio of OEM to MTOM).

Figure 4.33. MTOM versus OEM

4.14.3 Military MTOM versus Fuel Load M_f

In this subsection, at www.cambridge.org/Kundu, Figure 4.34 gives the relationship between internal fuel load and fuel fraction versus MTOM.

Figure 4.34. MTOM versus fuel load

4.14.4 MTOM versus Wing Area (Military)

In this subsection, at www.cambridge.org/Kundu, Figure 3.35 shows wing area, S_w , and wing-loading $MTOM/S_w$ versus MTOM.

Figure 4.35. MTOM versus wing area

4.14.5 MTOM versus Engine Thrust (Military)

In this subsection, at www.cambridge.org/Kundu, Figure 4.36 presents the relationship between total TSLs and the two types of aircraft mass (e.g., MTOM and TTOM).

Figure 4.36. Aircraft weight versus total take-off thrust

4.14.6 Empennage Area versus Wing Area (Military)

This subsection, at www.cambridge.org/Kundu, gives a brief comment on military aircraft empennage area.

4.14.7 Aircraft Wetted Area versus Wing Area (Military)

This brief subsection, at www.cambridge.org/Kundu, is on military aircraft wetted and wing areas.

4.15 Military Aircraft Component Geometries

This extended section of the book can be found on the Web at www.cambridge.org/Kundu and describes military aircraft component geometries (e.g., fuselage group, wing group, empennage group, and Nacelle group/intake).

4.16 Fuselage Group (Military)

This extended section of the book can be found on the Web at www.cambridge.org/Kundu and describes military aircraft fuselage group.

4.17 Wing Group (Military)

This extended section of the book can be found on the Web at www.cambridge.org/Kundu and describes the military aircraft wing group with Figure 4.37. Military trainer-aircraft wing group is illustrated in Figure 4.38.

Figure 4.37. Fighter aircraft configurations

One surface configuration: (Figure 4.37a - Mirage 2000 and SAAB Draken).

Two surface configuration: (Figure 4.37b - MIG 21 and Mirage F1).

(Figure 4.37c - Eurofighter and SAAB Viggen)

(Figure 4.37d - F16 and F18)

Three surface configuration: (Figure 4.37e - SU 37 and SU 47).

Figure 4.38. Advanced jet trainer aircraft capable of close support combat

4.17.1 Generic Wing Planform Shapes

This extended subsection, at www.cambridge.org/Kundu, describes how military aircraft wing planforms can be presented in a unified manner and includes civil designs (i.e., from delta to rectangular shapes) as shown in Figure 4.39.

Figure 4.39. Wing planform shape

4.18 Empennage Group (Military)

This extended section of the book can be found on the Web at www.cambridge.org/Kundu and describes various aspects of military aircraft empennage

configurations and available options using several figures (listed above) and Figure 4.40 (YF12, F29 and B2).

Figure 4.40. Empennage options

4.19 Intake/Nacelle Group (Military)

This extended section of the book can be found on the Web at www.cambridge.org/Kundu and gives a broad classification of military fighter aircraft engine-intake configuration, as given in Chart 4.3. Some older design engine positions are shown in Figure 4.41 (P38, B & V141, Heinkel 162, F107, Corsair, and a Tupolev design).

Chart 4.3. Types of empennage configurations

Figure 4.41. Options for engine positions of some older designs

4.20 Undercarriage Group

This extended section of the book can be found on the Web at www.cambridge.org/Kundu and refers to Chapter 7.

4.21 Miscellaneous Comments

This extended section of the book can be found on the Web at www.cambridge.org/Kundu and gives some pertinent comments on miscellaneous aspects of military aircraft design.

4.22 Summary of Military Aircraft Design Choices

This extended section of the book can be found on the Web at www.cambridge.org/Kundu and summarizes military aircraft design choices and various approaches to it.

5 Aircraft Load

5.1 Overview

Aircraft structures must withstand the imposed load during operations; the extent depends on what is expected from the intended mission role. The bulkiness of the aircraft depends on its structural integrity to withstand the design load level. The heavier the load, the heavier is the structure; hence, the MTOW affecting aircraft performance. Aircraft designers must comply with mandatory certification regulations to meet the minimum safety standards.

This book does not address load estimation in detail but rather continues with design information on load experienced by aircraft. Although the information provided herein is not directly used in configuring aircraft, the knowledge and data are essential for understanding design considerations that affect aircraft mass (i.e., weight). Only the loads and associated V - n diagram in symmetrical flight are discussed herein. It is assumed that designers are supplied with aircraft V - n diagrams by the aerodynamics and structures groups. Estimation of load is a specialized subject covered in focused courses and textbooks. However, this chapter does outline the key elements of aircraft loads. Aircraft shaping dictates the pattern of pressure distribution over the wetted surface that directly affects load distribution. Therefore, aircraft loads must be known early enough to make a design “right the first time.”

5.1.1 What Is to Be Learned?

This chapter covers the following topics:

- Section 5.2: Introduction to aircraft load, buffet, and flutter
- Section 5.3: Flight maneuvers
- Section 5.4: Aircraft load
- Section 5.5: Theory and definitions (limit and ultimate load)
- Section 5.6: Limits (load limit and speed limit)
- Section 5.7: V - n diagram (the safe flight envelope)
- Section 5.8: Gust envelope

5.1.2 Coursework Content

This chapter provides the basic information required to generate conceptual aircraft configurations. To continue, it is recommended that readers peruse this chapter even though there is no coursework involved yet. The chapter can be skipped if the subject has been learned in other coursework. However, readers should be able to draw schematically a representative V - n diagram of their aircraft (explained in [Section 5.8](#)).

5.2 Introduction

Loads are the external forces applied to an aircraft – whether static or dynamic, in flight or on the ground. In-flight loads are due to symmetrical flight, unsymmetrical flight, or atmospheric gusts from any direction; on-ground loads result from ground handling and field performance (e.g., takeoff and landing). Aircraft designers must be aware of aircraft loads given that configurations must be capable of withstanding them. During the design study phase, aerodynamicists compute in-flight aerodynamic loads and relate the information to stress engineers, who ensure structural integrity. Computation of aerodynamic load is involved, currently undertaken using computers. The subject matter concerns interaction between aerodynamics and structural dynamics (i.e., deformation occurring under load), a subject that is classified as *aeroelasticity*. Even the simplified assumption of an aircraft as an elastic body requires study beyond the scope of this book. Generally, conceptual design addresses rigid aircraft.

User specifications define the maneuver types and speeds that influence aircraft weight (i.e., MTOM), which then dictates aircraft-lifting and control surface design. In addition, enough margin must be allocated to cover inadvertent excessive load encountered through pilot induced maneuvers (i.e., inadvertent internal input in excess of the specifications), or sudden severe atmospheric disturbances (i.e., external input), or a combination of the two scenarios. The limits of these inadvertent situations are derived from historical statistical data and pilots must avoid exceeding the margins. To ensure safety, governmental regulatory agencies have intervened with mandatory requirements for structural integrity. *Load factor* (not to be confused with the passenger load factor, as described in [Section 4.4.1](#)) is a term that expresses structural-strength requirements. The structural regulatory requirements are associated with V - n diagrams, which are explained in [Section 5.7](#). Limits of the margins are set by the regulatory agencies. In fact, they not only stipulate the load limits, they also require mandatory strength tests to determine ultimate loads. The ultimate load tests must be completed before the first flight, with the exceptions of homebuilt and experimental categories of aircraft.

Civil aircraft designs have conservative limits; there are special considerations for the aerobatic category aircraft. Military aircraft have higher limits for hard maneuvers, and there is no guarantee that under threat, a pilot would be able to adhere to the regulations. Survivability requires widening the design limits and strict maintenance routines to ensure structural integrity. Typical human limits are currently taken at 9 g in sustained maneuvers and can reach 12 g for instantaneous loading. Continuous monitoring of the statistical database retrieved from

aircraft-mounted “black boxes” provides feedback to the next generation of aircraft design or at midlife modifications. A g -meter in the flight deck records the g -force and a second needle remains at the maximum g reached in the sortie. If the prescribed limit is exceeded, then the aircraft must be grounded for a major inspection and repaired, if required.

An important aspect of design is to know what could happen at the extreme points of the flight envelope (i.e., the V - n diagram). In the following sections, buffet and flutter are introduced.

5.2.1 Buffet

At the initial development phase of stall (or during extreme maneuvers), airflow over the wing becomes unsteady; the separation line over the wing (or over any other lifting surface) keeps fluctuating. This causes the aircraft to shudder and is a warning to the pilot. The aircraft structure is not affected and is not necessarily at its maximum loading.

5.2.2 Flutter

This is the vibration of the structure – primarily the wing but also any other component depending on its stiffness. At transonic speed, the load on the aircraft is high while the shock–boundary layer interaction could result in an unsteady flow causing vibration over the wing, for example. The interaction between aerodynamic forces and structural stiffness is the source of flutter. A weak structure enters into flutter; in fact, if it is too weak, flutter could happen at any speed because the deformation would initiate the unsteady flow. If it is in resonance, then it could be catastrophic – such failures have occurred. Flutter is an aeroelastic phenomenon.

5.3 Flight Maneuvers

Although throttle-dependent linear acceleration would generate flight load in the direction of the flight path, pilot-induced control maneuvers could generate the extreme flight loads that may be aggravated by inadvertent atmospheric conditions. Aircraft weight is primarily determined by the air load generated by maneuvers in the pitch plane. Therefore, the associated V - n diagram described in [Section 5.7](#) is useful information for proposing candidate aircraft configurations. Section 3.6 describes the six deg of freedom for aircraft motions – three linear and three angular. Given herein are the three Cartesian coordinate planes of interest.

5.3.1 Pitch Plane (X-Z) Maneuver (Elevator/Canard-Induced)

The pitch plane is the symmetrical vertical plane (i.e., X-Z plane) in which the elevator/canard-induced motion occurs with angular velocity, q , about the Y -axis, in addition to linear velocities in the X-Z plane. Changes in the pitch angle due to angular velocity q results in changes in C_L . The most severe aerodynamic loading occurs in this plane.

5.3.2 Roll Plane (Y-Z) Maneuver (Aileron-Induced)

The aileron-induced motion generates the roll maneuver with angular velocity, p , about the X -axis, in addition to velocities in the Y - Z plane. Aircraft structures designed to the pitch-plane loading are the most critical; therefore, roll-plane loading is not discussed herein.

5.3.3 Yaw Plane (Z-X) Maneuver (Rudder-Induced)

The rudder-induced motion generates the yaw (coupled with the roll) maneuver with angular velocity, r , about the Z -axis, in addition to linear velocities in the Z - X plane. Aerodynamic loading of an aircraft due to yaw is also necessary for structural design.

5.4 Aircraft Loads

An aircraft is subject to load at any time. The simplest case is an aircraft stationary on the ground experiencing its own weight. Under heavy landing, an aircraft can experience severe loading, and there have been cases of structural collapse. Most of these accidents showed failure of the undercarriage, but breaking of the fuselage also has occurred. In flight, aircraft loading varies with maneuvers and/or when gusts are encountered. Early designs resulted in many structural failures in flight.

5.4.1 On the Ground

Loads on the ground are taken up by the undercarriage and then transmitted to the aircraft main structure. Landing-gear loads depend on the specification of V_{stall} , the maximum allowable sink speed rate at landing, and the MTOM. This is addressed in greater detail in [Chapter 7](#), which discusses undercarriage layout for conceptual study.

5.4.2 In Flight

In-flight loading in the pitch plane is the main issue considered in this chapter. The aircraft structure must be strong enough at every point to withstand the pressure field around the aircraft, along with the inertial loads generated by flight maneuvers. The V - n diagram is the standard way to represent the most severe flight loads that occur in the pitch plane (i.e., X - Z plane), which is explained in detail in [Section 5.7](#). The load in other planes is not discussed herein.

5.5 Theory and Definitions

In steady-level flight, an aircraft is in equilibrium; that is, the lift, L , equals the aircraft weight, W , and the thrust, T , equals drag, D . During conceptual design, when generating the preliminary aircraft configuration, it is understood that the wing produces all the lift with a spanwise distribution (see [Section 3.14](#)).

In equation form, for steady-level flight:

$$L = W \quad \text{and} \quad T = D \quad (5.1)$$

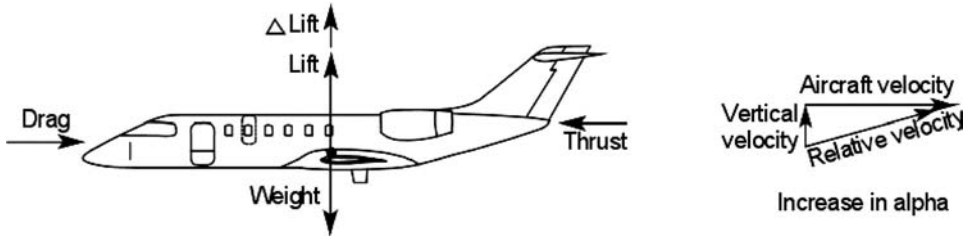


Figure 5.1. Equilibrium flight

5.5.1 Load Factor, n

Newton's law states that change from an equilibrium state requires an additional applied force; this is associated with some form of acceleration, a . When applied in the pitch plane, the force appears as an increment in lift, ΔL , and it would overcome the weight, W , to an increased altitude initiated by rotation of the aircraft (Figure 5.1).

From Newton's law:

$$\Delta L = \text{centrifugal acceleration} \times \text{mass} = a \times W/g \quad (5.2)$$

The resultant force equilibrium gives:

$$L + \Delta L = W + a \times W/g = W(1 + a/g) \quad (5.3)$$

where L is the steady-state lift equaling weight, W load factor, n , is defined as:

$$n = (1 + a/g) = L/W + \Delta L/W = 1 + \Delta L/W \quad (5.4)$$

The load factor, n , indicates the increase in force contributed by the centrifugal acceleration, a . The load factor, $n = 2$, indicates a twofold increase in weight; that is, a 90-kg person would experience a 180-kg weight. The load factor, n , is loosely termed as the g -load; in this example, it is the 2- g -load.

A high g -load damages the human body, with the human limits of the instantaneous g -load higher than for continuous g -loads. For a fighter pilot, the limit (i.e., continuous) is taken as 9 g ; for the civil aerobatic category, it is 6 g . Negative g -loads are taken as half of the positive g -loads. Fighter pilots use pressure suits to control blood flow (i.e., delay blood starvation) to the brain to prevent "blackouts." A more inclined pilot seating position reduces the height of the carotid arteries to the brain, providing an additional margin on the g -load that causes a blackout.

Because they are associated with pitch-plane maneuvers, pitch changes are related to changes in the angle of attack, α , and the velocity, V . Hence, there is variation in C_L , up to its limit of $C_{L\max}$, in both the positive and negative sides of the wing incidence to airflow. The relationship is represented in a V - n diagram, as shown in Figure 5.2. Atmospheric disturbances are natural causes that appear as a gust load from any direction. Aircraft must be designed to withstand this unavoidable situation up to a statistically determined point that would encompass almost all-weather flights except extremely stormy conditions. Based on the sudden excess in loading that can occur, margins are built in, as explained in the next section.

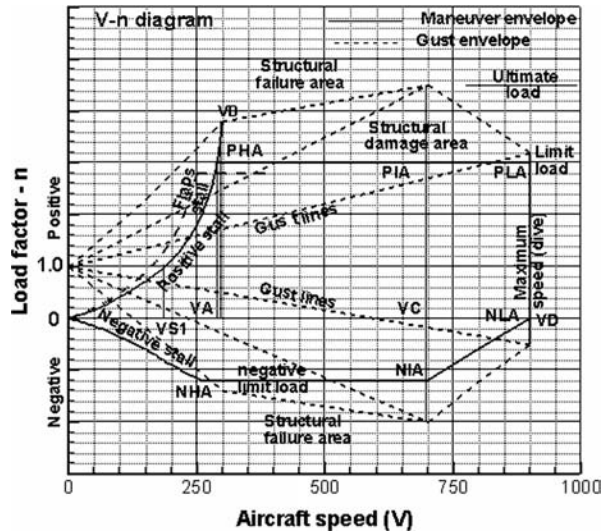


Figure 5.2. Typical V - n diagram showing load and speed limits

5.6 Limits – Load and Speeds

Limit load is defined as the maximum load that an aircraft can be subjected to in its life cycle. Under the limit load, any deformation recovers to its original shape and would not affect structural integrity. Structural performance is defined in terms of stiffness and strength. Stiffness is related to flexibility and deformations and has implications for aeroelasticity and flutter. Strength concerns the loads that an aircraft structure is capable of carrying and is addressed within the context of the V - n diagram.

To ensure safety, a margin (factor) of 50% increase (civil aviation) is enforced through regulations as a factor of safety to extend the limit load to the ultimate load. A flight load exceeding the limit load but within the ultimate load should not cause structural failure but could affect integrity with permanent deformation. Aircraft are equipped with g -meters to monitor the load factor – the n for each sortie – and, if exceeded, the airframe must be inspected at prescribed areas and maintained by prescribed schedules that may require replacement of structural components. For example, an aerobatic aircraft with a 6- g -limit load will have an ultimate load of 9 g . If an in-flight load exceeds 6 g (but is below 9 g), the aircraft may experience permanent deformation but should not experience structural failure. Above 9 g , the aircraft would most likely experience structural failure.

The factor of safety also covers inconsistencies in material properties and manufacturing deviations. However, aerodynamicists and stress engineers should calculate for load and component dimensions such that their errors do not erode the factor of safety. Geometric margins, for example, should be defined such that they add positively to the factor of safety.

$$\text{ultimate load} = \text{factor of safety} \times \text{limit load}$$

For civil aircraft applications, the factor of safety equals 1.5 (FAR 23 and FAR 25, Vol. 3).

Table 5.1. *Typical permissible g-load for civil aircraft*

Type	Ultimate positive n	Ultimate negative n
FAR 25		
Transport aircraft less than 50,000 lb	3.75	-1 to -2
Transport aircraft more than 50,000 lb	$[2.1 + 24,000/(W + 10,000)]$ Should not exceed 3.8	-1 to -2
FAR 23		
Aerobatic category (FAR 23 only)	6	-3

5.6.1 Maximum Limit of Load Factor

This is the required maneuver load factor at all speeds up to V_C . (The next section defines speed limits.) Maximum elevator deflection at V_A and pitch rates from V_A to V_D also must be considered. Table 5.1 gives the g -limit of various aircraft classes.

For military aircraft applications, in general, the factor of safety equals 1.5 but can be modified through negotiation (see Military Specifications MIL-A-8860, MIL-A-8861, and MIL-A-8870).

Typical g -levels for various types of aircraft are shown in Table 5.2. These limits are based on typical human capabilities.

5.6.2 Speed Limits

The V - n diagram (see Figure 5.2) described in Section 5.7 uses various speed limits, defined as follows:

- V_S : Stalling speed at normal level flight.
- V_A : Stalling speed at limit load. In a pitch maneuver, an aircraft stalls at a higher speed than the V_S . In an accelerated maneuver of pitching up, the angle of attack, α , decreases and therefore stalls at higher speeds. The tighter the maneuver, the higher is the stalling speed until it reaches V_A .
- V_B : Stalling speed at maximum gust velocity. It is the design speed for maximum gust intensity V_B and is higher than V_A .
- V_C : Maximum level speed.
- V_D : Maximum permissible speed (occurs in a dive; also called the *placard speed*).

An aircraft can fly below the stall speed if it is in a maneuver that compensates loss of lift or if the aircraft attitude is below the maximum angle of attack, α_{\max} , for stalling.

Table 5.2. *Typical g-load for classes of aircraft*

Club flying	Sports aerobatic	Transport	Fighter	Bomber
+4 to -2	+6 to -3	3.8 to -2	+9 to -4.5	+3 to -1.5

5.7 V-n Diagram

To introduce the V - n diagram, the relationship between load factor, n , and lift coefficient, C_L , must be understood. Pitch-plane maneuvers result in the full spectrum of angles of attack at all speeds within the prescribed boundaries of limit loads. Depending on the direction of pitch-control input, at any given aircraft speed, positive or negative angles of attack may result. The control input would reach either the $C_{L\max}$ or the maximum load factor n , whichever is the lower of the two. The higher the speed, the greater is the load factor, n . Compressibility has an effect on the V - n diagram. In principle, it may be necessary to construct several V - n diagrams representing different altitudes. This chapter explains only the role of the V - n diagram in aircraft design.

Figure 5.2 represents a typical V - n diagram showing varying speeds within the specified structural load limits. The figure illustrates the variation in load factor with airspeed for maneuvers. Some points in a V - n diagram are of minor interest to configuration studies – for example, at the point $V = 0$ and $n = 0$ (e.g., at the top of the vertical ascent just before the tail slide can occur). The points of interest are explained in the remainder of this section.

Inadvertent situations may take aircraft from within the limit-load boundaries to conditions of ultimate-load boundaries (see Figure 5.2).

5.7.1 Low-Speed Limit

At low speeds, the maximum load factor is constrained by the aircraft maximum C_L . The low-speed limit in a V - n diagram is established at the velocity at which the aircraft stalls in an acceleration flight load of n until it reaches the limit-load factor. At higher speeds, the maneuver-load factor may be restricted to the limit-load factor, as specified by the regulatory agencies.

Let V_{S1} be the stalling speed at 1 g . Then:

$$V_{S1}^2 = \left(\frac{1}{0.5\rho C_{L\max}} \right) \left(\frac{W}{S} \right) \quad \text{or} \quad L = W = (0.5\rho V_{S1}^2 S) C_{L\max}$$

Let V_{Sn} be the stalling speed at ng , where n is a number. Then:

$$nW = (0.5\rho V_{Sn}^2 S) C_{L\max}$$

Using Equations 5.1 and 5.2,

$$n \times (0.5\rho V_{S1}^2 S) C_{L\max} = (0.5\rho V_{Sn}^2 S) C_{L\max}$$

or

$$n = V_{Sn}^2 / V_{S1}^2 = \frac{(0.5\rho C_{L\max}) V_{Sn}^2}{(W/S)} \quad \text{until } n \text{ reaches the limit-load factor} \quad (5.5)$$

V_A is the speed at which the positive-stall and maximum-load factor limits are simultaneously satisfied (i.e., $V_A = V_{S1}\sqrt{n_{\text{limit}}}$).

The negative side of the boundary can be estimated similarly.

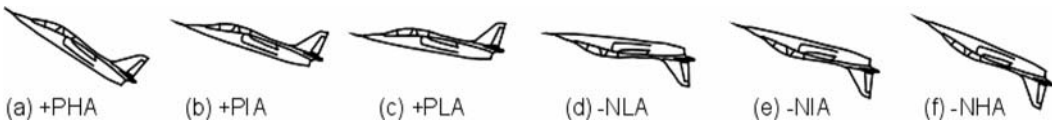


Figure 5.3. Aircraft angles of attack in pitch-plane maneuvers

5.7.2 High-Speed Limit

V_D is equal to the maximum design speed. It is limited by the maximum dynamic pressure that an airframe can withstand. At high altitude, V_D may be limited by the onset of high-speed flutter.

5.7.3 Extreme Points of a V - n Diagram

The corner points of the flight envelope (see Figure 5.2) is of interest for stress engineers. Enhancing structures would establish aircraft weight that must be predicted at the conceptual design phase.

Figure 5.3 shows various attitudes in pitch-plane maneuvers associated with the V - n diagram, each of which is explained herein. The maneuver is a transient situation, and the various positions shown in Figure 5.3 can occur under more than one scenario. Only the attitudes associated with the predominant cases in pitch-plane maneuvers are addressed below. Negative g is when the maneuver force is directed in the opposite direction toward the pilot's head, irrespective of his or her orientation relative to the Earth.

Positive Loads

This is when an aircraft (and its occupants) experiences a force more than its normal weight. An aircraft stalls at a maneuver reaching α_{\max} ; following are the various scenarios. In level flight at $1g$, the aircraft angle of attack, α , increases with slowing down of speed and reaches its maximum value, α_{\max} , at which the aircraft would stall at a speed V_S .

1. *Positive High Angle of Attack (+PHA)*. This occurs during a pull-up maneuver that raises the aircraft nose in a high pulling g -force, reaching the limit. The aircraft could stall if it is pulled harder. At the limit load of n , the aircraft reaches +PHA at aircraft speeds of V_A .
2. *Positive Intermediate Angle of Attack (+PIA)*. This occurs at a high-speed level flight when control is actuated to set the wing incidence at an angle of attack. The aircraft has a maximum operating speed limit of V_C when +PIA reaches the maximum limit load of n , in maneuver; it is now in transition.
3. *Positive Low Angle of Attack (+PLA)*. This occurs when an aircraft gains the maximum allowable speed, sometimes in a shallow dive (dive speed, V_D). Then, at a very small elevator pull (i.e., low angle of attack), the aircraft would hit the maximum limit load of n . Some high-powered military aircraft can reach V_D during level flight. The higher the speed, the lower is the angle of attack, α , to reach the limit load – at the highest speed, it would be +PLA.

Negative Loads

This is when an aircraft (and its occupants) experiences a force less than its weight. In an extreme maneuver in “bunt” (i.e., developing – negative g in a nose-down

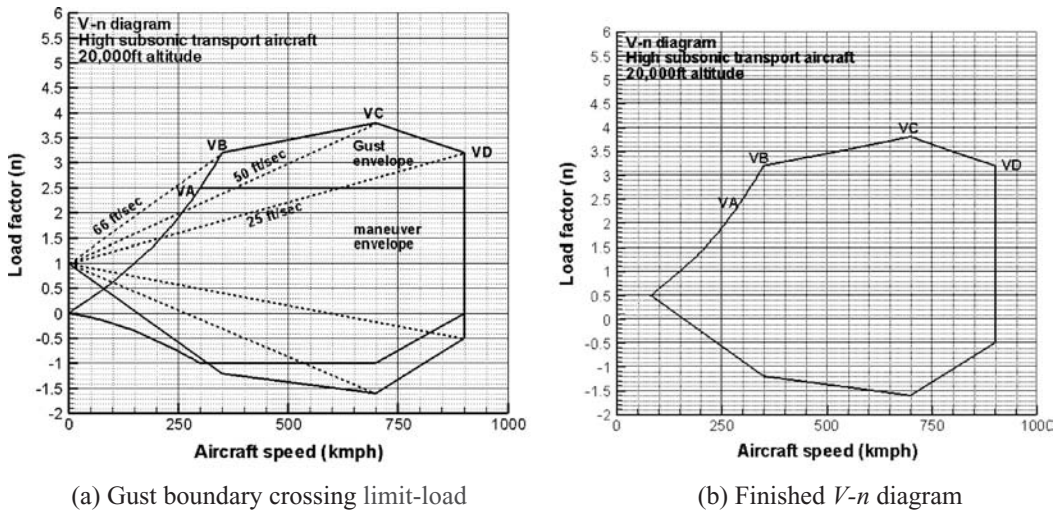


Figure 5.4. Example of a V - n diagram with a gust envelope (FAR/JAR 25)

curved trajectory), the centrifugal force pointing away from the center of the Earth can cancel the weight when the pilot feels weightless during the maneuver. The corner points follow the same logic of the positive load description except that the limit load of n is on the negative side, which is lower because it is not in the normal flight regime. It can occur in an aerobatic flight, in combat, or in an inadvertent situation caused by atmospheric gusts.

1. *Negative High Angle of Attack (-NHA)*. This is the inverted scenario of +PHA explained previously. With $-g$, the aircraft must be in a maneuver.
2. *Negative Intermediate Angle of Attack (-NIA)*. In +PLA, the possibility of $-$ α was mentioned when the elevator is pushed down, called the “bunting” maneuver. Negative α classically occurs at inverted flight at the highest design speed, V_C (coinciding with the PIA). When it reaches the maximum negative limit load of n , the aircraft takes the NIA.
3. *Negative Low Angle of Attack (-NLA)*. At V_D , an aircraft should not exceed zero g .

5.8 Gust Envelope

Encountering unpredictable atmospheric disturbance is unavoidable. Weather warnings are helpful but full avoidance is not possible. A gust can hit an aircraft from any angle and the gust envelope is shown in a separate set of diagrams. The most serious type is a vertical gust (see Figure 5.1), which affects load factor n . The vertical gust increases the angle of attack, α , developing ΔL . Regulatory agencies have specified vertical gust rates that must be superimposed on the V - n diagrams to describe the operation limits. It is common practice to combine the maneuver and gust envelope in one diagram, as shown in Figure 5.4. The FAR provides a detailed description of required gust loads. To stay within the ultimate load, the limits of vertical gust speeds are reduced with increases in aircraft speed. Pilots should fly at a lower speed if high turbulence is encountered. The gust envelope crosses the limit load and its boundary varies with increases in speed. Equation 5.5 shows that

Table 5.3. FAR-specified gust velocity

	Altitudes 20,000 ft and below	Altitudes 50,000 ft and above
V_B (rough air gust)	66 ft/s	38 ft/s
V_C (gust at max design speed)	50 ft/s	25 ft/s
V_D (gust at max dive speed)	25 ft/s	12.5 ft/s

aircraft with low wing-loading (W/S_w) and flying at high speed are affected more by gust load.

V_B is the design speed for maximum gust intensity. This definition assumes that the aircraft is in steady-level flight at speed V_B when it enters an idealized upward gust of air, which instantaneously increases the aircraft angle of attack and, hence, the load factor. The increase in the angle of attack must not stall the aircraft – that is, take it beyond the positive or negative stall boundaries.

From statistical observations, the regulatory agencies have established the maximum gust load at 66 ft/s. Except for extreme weather conditions, this gust limit is essentially all-weather flying. In a gust, the aircraft load may cross the limit load but it must not exceed the ultimate load, as shown in Figure 5.4. If an aircraft crossed the limit load, then an appropriate action through inspection is taken.

Table 5.3 outlines the construction of a V - n diagram superimposed with a gust load. Flight speed, V_B , is determined by the gust loads and can be summarized as shown in the table.

Linear interpolation is used to obtain appropriate velocities between 20,000 and 50,000 ft. The construction of V - n diagrams is relatively easy using aircraft specifications, in which the corner points of V - n diagrams are specified. Computations to superimpose gust lines are more complex, for which FAR has provided the semi-empirical relations.

Vertical-gust velocity, U_g , on forward velocity, V , would result in an increase of the angle of attack, $\Delta\alpha = U_g/V$, that would generate an increase in load factor $\Delta n = (C_{L\alpha} U_g/V)/(W/S)$. Airspeed V is varied to obtain Δn versus speed. DATCOM and ESDU provide the expressions needed to obtain $C_{L\alpha}$. A typical V - n diagram with gust speeds intersecting the lines is illustrated in Figures 5.2 and 5.4.

V_C is the design cruise speed. For transport aircraft, the V_C must not be less than $V_B + 43$ knots. The JARs contain more precise definitions as well as definitions for several other speeds.

In civil aviation, the maximum maneuver load factor is typically +2.5 for aircraft weighing less than 50,000 lbs. The appropriate expression to calculate the load factor is as follows:

$$n = 2.1 + 24,000/(W + 10,000) \text{ up to a maximum of } 3.8 \quad (5.6)$$

This is the required maneuver-load factor at all speeds up to V_C , unless the maximum achievable load factor is limited by a stall.

Within the limit load, the negative value of n is -1.0 at speeds up to V_C , decreasing linearly to 0 at V_D . The maximum elevator deflection at V_A and pitch rates from V_A to V_D also must be considered.

6 Configuring Aircraft

6.1 Overview

The coursework now starts with this chapter. It follows the mock market study in [Chapter 2](#), which generated customer-specified aircraft requirements. Civil and military aircraft configuration layouts are addressed separately because of the fundamental differences in their approach, especially in the layout of the fuselage. A civil aircraft has “hollow” fuselages to carry passengers. Conversely, a combat-aircraft fuselage is densely packed with fixed equipments and crew members.

Industry uses its considerable experience and imagination to propose several candidate configurations that would satisfy customer (i.e., operator) requirements and be superior to existing designs. Finally, a design is chosen (in consultation with the operators) that would ensure the best sale. In the coursework, after a quick review of possible configurations with the instructor’s guidance, it is suggested that only one design be selected for classwork that would be promising in facing market competition. This chapter describes how an aircraft is conceived, first to a preliminary configuration; that is, it presents a methodology for generating a preliminary aircraft shape, size, and weight. Finalizing the preliminary configuration is described in [Chapter 11](#).

The market specification itself demands improvements, primarily in economic gains but also in performance. A 10 to 15% all-around gain over existing designs, delivered when required by the operators, would provide market leadership for the manufacturers. Historically, aircraft designers played a more dominant role in establishing a product line; gradually, however, input by operators began to influence new designs. Major operators have engineers who are aware of the latest trends, and they competently generate realistic requirements for future operations in discussion with manufacturers. To encompass diverse demands by various operators, the manufacturers offer a family of variants to maximize the market share.

The product has to be right the first time and a considerable amount of background work is needed. This chapter describes how to arrive at an aircraft preliminary configuration that will be best suited to market specifications and could be feasibly manufactured. Finalizing the design comes later through an involved iterative process using aircraft sizing and engine matching (see [Chapter 11](#)). In the

coursework, one iteration is sufficient. An experienced chief designer could start with a preliminary configuration that is close to the final arrangement.

There is no mathematics in this chapter; rather, past designs and their reasoning are important in configuring a new aircraft. Readers need to review Sections 4.11, 12.8, 12.9, and 13.7 on design considerations and discussion to gain insight from experience. Statistics is a powerful tool that should be used discriminately. Researchers and academics have worked on statistics to a great extent; however, in many cases, current market demands have stabilized statistics (Section 6.4).

6.1.1 What Is to Be Learned?

This chapter covers the following topics:

- Section 6.2: Introduction to configuring aircraft geometry: shaping and layout
- Section 6.3: Shaping and layout of civil aircraft
- Section 6.4: Civil aircraft fuselage shaping and layout with example
- Section 6.5: Configuration of civil aircraft wing design with example
- Section 6.6: Configuration of civil aircraft empennage design with example
- Section 6.7: Configuration of civil aircraft nacelle design with example
- Section 6.8: Undercarriage design considerations
- Section 6.9: Finalizing civil aircraft configuration
- Section 6.10: Miscellaneous considerations for civil aircraft
- Section 6.11: Shaping and layout of military aircraft
- Section 6.12: Configuration of military advanced jet trainer with example
- Section 6.13: Configuration of military aircraft CAS version with example

6.1.2 Coursework Content

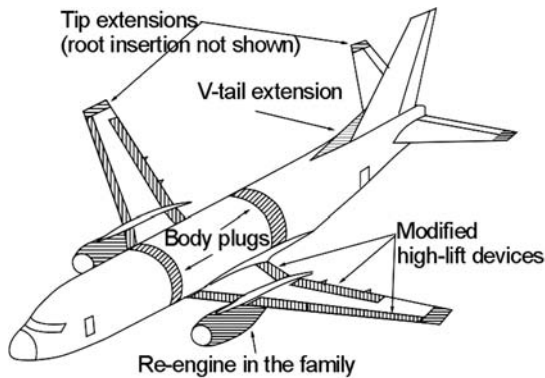
Intensive classroom work starts with this chapter, one of the most important in the book. Readers begin with the layout of aircraft geometry derived from customer specifications. The information in Chapters 3 and 4 is used extensively to configure the aircraft.

6.2 Introduction

Section 2.6 stressed that the survival of the industry depends on finding a new and profitable product line with a competitive edge. A market study is the tool to establish a product by addressing the fundamental questions of why, what, and how. It is like “crystal-ball gazing” to ascertain the feasibility of a (ad)venture, to assess whether the manufacturer is capable of producing such a product line.

Ideally, if cost were not an issue, an optimum design for each customer might be desirable, but that is not commercially viable. Readers can begin to appreciate the drivers of commercial aircraft designs: primarily, economic viability.

The product line should be offered in a family of variants to encompass a wide market area, at lower unit cost, by maintaining component commonalities. The first few baseline aircraft are seen as preproduction aircraft, which are flight-tested and subsequently sold to operators.



Typical modifications for derivative in the family

Possible changes (shaded area) in civil aircraft family derivatives (B737)

Figure 6.1. Variants in the Boeing 737 family

The final configuration is a “satisfying” design, which implies that the family of variants is best suited to satisfy as many customers as possible. Figure 6.1 shows how variants of the Boeing 737 family have evolved. Here, many of the fuselage, wing, and empennage components are retained for both the variants.

However, military aircraft designs are dictated by national requirements when superiority, safety, and survivability are dominant, of course, but without ignoring economic constraints. Today’s military aircraft designs start with technology demonstrators to prove the advanced concepts, which are considered prototype aircraft. Production versions could be larger, incorporating the lessons learned from the demonstrator aircraft.

Finalizing the aircraft configuration as a marketable product follows a formal methodology, as outlined in Chart 6.1; it is an iterative process.

Chapter 2 presents several aircraft specifications and performance requirements of civil and military aircraft classes. From these examples, the Learjet 45 class and RAF Hawk class – one each in the civil and the military categories, respectively – are worked out as coursework examples. These examples of civil aircraft family derivatives are shown in Figure 6.8; the baseline aircraft is in the middle of the figure and shown in Figure 6.2.

Initially, the conceptual study proposes several candidate aircraft configurations to search for the best choice. Comparative studies are carried out to confirm which choice provides the best economic gains. Although in practice there are potentially several candidate configurations for a specification, only one is addressed. Figure 6.3 shows four possible configurations (i.e., author-generated for coursework only). Comparative studies must follow in order to select one. The first configuration offers the best market potential (Figure 6.2).

Today, the industry uses CAD-generated aircraft configurations as an integral part of the conceptual design process, which must be implemented in classwork as soon in the process as possible. Most universities have introduced CAD training early enough so that students become proficient. If the use of CAD is not feasible, then accurate manual drawings are required; it is imperative that practitioners maintain accuracy and control of manual drawings. CAD enables changes in drawings to be made easily and quickly; in manual drawings, the new shape may necessitate a total redraw.

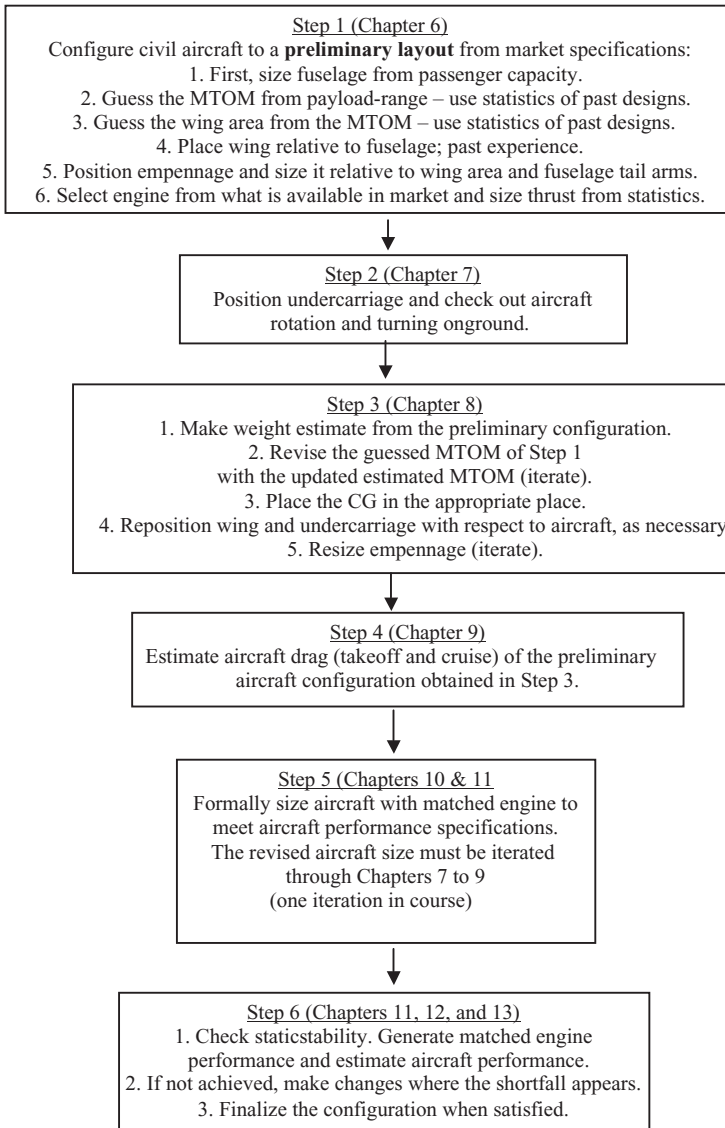


Chart 6.1. Phase I, conceptual study: methodology for finalizing civil aircraft configurations

A three-view diagram should show the conceptualized aircraft configuration. A preliminary configuration will change when it is sized; for experienced engineers, the change is relatively minor. Having CAD 3D parametric modeling allows changes to be easily, quickly, and accurately incorporated. Making 2D drawings (i.e., three-view) from 3D models is simple with a few keystrokes.

6.3 Shaping and Layout of a Civil Aircraft Configuration

The objective is to generate aircraft components, piece by piece in building-block fashion, and mate them as shown in the middle diagram of Figure 2.3. Section 4.11 summarizes civil aircraft design methodology.

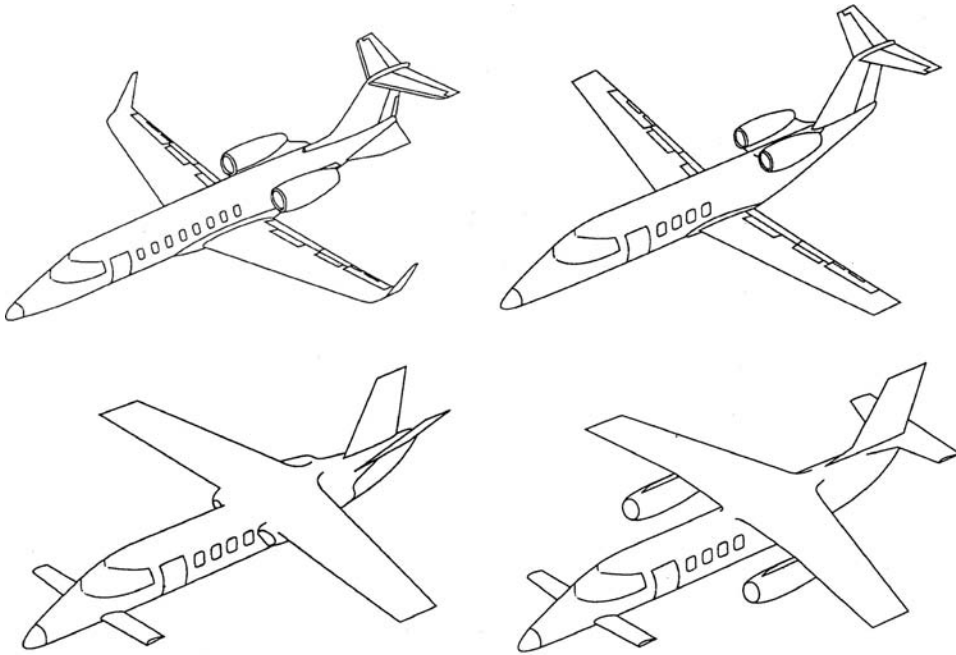


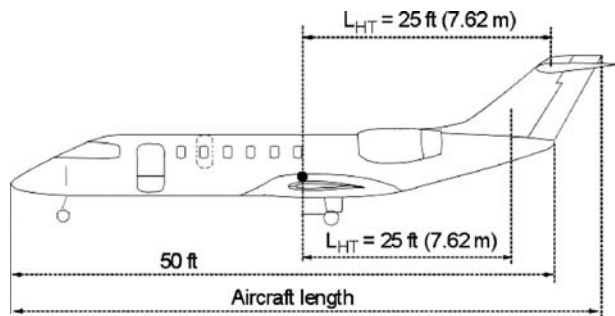
Figure 6.2. Four candidate aircraft configurations

Subsequently, in the next level, a more detailed breakdown (see first diagram in Figure 2.3) of the aircraft components in subassembly groups provides a better understanding of the preliminary layout of the internal structures and facilitates preliminary cost estimates. DFM/A consideration for subassembly components design is important in reducing production cost because the aircraft cost contributes significantly to the DOC (see Chapter 16).

The general methodology is to start with the fuselage layout, which is determined from the payload requirement (i.e., passenger capacity, number of seats abreast, and number of rows). The aerodynamic consideration is primarily deciding the front and aft closure shape for civil aircraft designs. The following section describes seating-layout schemes for 2- to 10-abreast arrangements encompassing passenger capacity from 4 to more than 600.

The next step is choosing a wing planform and an aerofoil section suitable for the desired aircraft performance characteristics. Initially, the wing reference area is estimated from statistics and is sized later in the process. The next step is to

Figure 6.3. The baseline version of the family concept of the classwork example



configure the empennage based on the current wing area. It will be resized (i.e., iteration) when the wing area is more accurately sized. Initially, the location of the wing relative to the fuselage and empennage is based on past experience and fine-tuned iteratively after establishing the aircraft CG and wing geometry. Finally, a matched engine is selected from what is available in the market. Engine matching is worked out simultaneously with wing sizing (see Chapter 11).

6.3.1 Considerations in Configuring the Fuselage

Following are general considerations important for the fuselage layout. Section 3.23 provides definitions of associated fuselage geometries.

<i>Geometry</i>	<i>Aerodynamics</i>
(1) diameter (e.g., comfort level, appeal)	(1) front-end closure
(2) abreast seating	(2) aft-end closure
(3) length, fineness ratio	(3) surface roughness
(4) upsweep for rotation angle and rear door, if any	(4) wing-body fairing
(5) cross-section to suit under floorboards and headroom volume and space	(5) wing and tail position
	(6) drag
<i>Structure</i> (affecting weight and external geometry)	<i>Systems</i>
(1) doors and windows	(1) flight deck design
(2) wing and undercarriage attachments	(2) passenger facilities
(3) weight	(3) all other systems

Section 6.4 describes typical fuselage layouts from two-abreast seating to the current widest seating of ten abreast.

The important considerations for civil aircraft fuselage layout are as follow:

1. The current ICAO limit on fuselage length is 80 m. This is an artificial limit based on current airport infrastructure size and handling limitations.
2. The fuselage fineness ratio must be from 7 to 14 (see Table 4.3). Section 4.7.3 lists front- and aft-fuselage closure shapes. Section 6.3.1.2 describes how to make the fuselage closure. There is aft luggage space in front of the pressure bulkhead, especially in smaller aircraft.
3. Seat and aisle dimensions are obtained from Table 4.5.
4. For a fuselage with four-abreast seating or more, the cross-section could use space below the floorboards. If the bottom half is elongated (i.e., oval), then the space can be maximized. Full standing headroom is easily achievable for a fuselage with four-abreast seating or more. Cargo container sizes are described in Section 4.7.8.
5. Two aisles are provided for a fuselage with seven-abreast seating and more (the current maximum is ten). In the future, if a wider cabin is designed (e.g., with a BWB), then more than two aisles will be necessary.

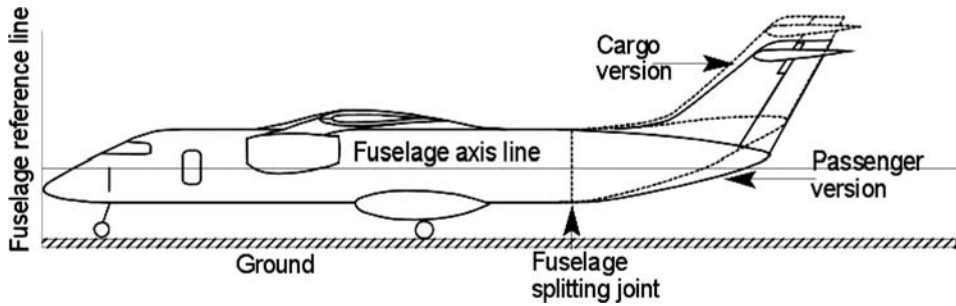


Figure 6.4. Fuselage upswEEP angle

6. The minimum number of cabin crew depends on the maximum passenger capacity that the airframe can accommodate. Although not required for up to 19 passengers, a cabin crew is provided by some operators.
7. A pressurized fuselage is invariably circular or near circular to minimize weight. Unpressurized cabins for aircraft operating below 4,300 m (14,000 ft) need not be circular in the cross-section. Smaller utility aircraft demonstrate the benefits of a rectangular cross-section. A box-like rectangular cross-section (see Figure 4.14) would not only offer more leg space but also is considerably less costly to manufacture (e.g., the Short SD360).
8. The FAA and CAA have mandatory requirements on the minimum number of passenger doors, their types, and corresponding sizes dependent on the maximum passenger capacity for which the fuselage is intended to accommodate. This requirement ensures passenger safety: certification authorities stipulate a time limit (e.g., 90 s for big jets) within which all passengers must egress if an unlikely event occurs (e.g., fire). The larger the passenger capacity, the more doors are to be installed. Not all doors are the same size – emergency doors are smaller. Passenger doors have several categories and are described in Section 15.7. All doors are kept locked while airborne.
9. The fuselage provision typically includes a toilet, a galley, and cabin crew seating – the extent depends on the number of passengers and the duration of flight. Chapter 4 describes toilet and galley details. For smaller aircraft with a shorter duration of flight, it is desirable that at least a toilet be provided. To reduce cost, smaller aircraft with a low mission range do not have a toilet, but these aircraft can therefore be uncomfortable.

Closure of the Fuselage

When the seating arrangement is determined in the midfuselage section, it must be closed at the front and aft ends for a streamlined shape, maintaining a fineness ratio from 7 to 14 (see Table 4.3). Typical front- and aft-fuselage closure ratios are in Table 4.4.

The fuselage upswEEP angle of the aft-end closure depends on the type of aircraft. If it has a rear-loading ramp as in a cargo version, then the upswEEP angle is higher, as shown in Figure 6.4. The fuselage clearance angle, θ , depends on the main-wheel position of the undercarriage relative to the aircraft CG position (see

Chapter 7). The typical angle for θ is between 12 and 16 deg to approach C_{Lmax} at aircraft rotation.

The next step is to construct a fuselage axis and set the zero reference plane normal to the fuselage axis, as explained in Section 3.23. In Figure 6.4, the fuselage axis is shown passing through the tip of the nose cone, where the zero reference plane starts. In this book, the zero reference plane is at the nose of the aircraft (it could be ahead of the nose cone tip). The zero reference plane and the fuselage axis are data for measuring relative distances of various aircraft components and for aerodynamic geometries for use in calculations.

The fuselage axis is an arbitrary line but it must be in the plane of aircraft symmetry. In general, for aircraft with a constant fuselage section, the fuselage axis is placed conveniently in the middle of the aircraft. The fuselage axis line could be the fuselage centerline. It is easier to assess if the reference lines are vertical and horizontal. If the aircraft's normal position on the ground does not render the aircraft centerline horizontal, then the ground is tilted to show it with the associated angle. For simplification, this book keeps the centerline and ground horizontal, as shown in Figure 6.4. For military and smaller civil aircraft, there is no constant fuselage section, and the aircraft centerline must be conveniently chosen; it is the designer's choice as long as the reference lines are clearly defined and adhered to for the entire life cycle of an aircraft that could encounter design modifications in its service life. The other possible choice is the fuselage axis as the principal inertia axis.

An interesting concept is to make variants of a modular fuselage – that is, with two types of aft ends easily interchangeable (see Figure 6.4). One type is for the conventional passenger version with a pointed aft-end closure, the other is for the cargo version with an increased upsweep to accommodate a rear-loading ramp. It can even be a “quick-change” version, swapping the type of fuselage needed for the mission; the changeover joint is located behind the main undercarriage.

Attaching the wing to the fuselage could have a local effect on the fuselage external shape. Following are the basic types of attachments:

1. *Carry-through wing box.* For larger aircraft, this is separately constructed and attached to the fuselage recess. Subsequently, wings are mated at each side in accurate assembly jigs. For smaller aircraft, it could be integral to the wing and then attached to the fuselage recess. In that case, the wing box is built into the wing, either in two halves or as a tip-to-tip assembly. A fairing at the junction reduces the interference drag. These wing boxes are primarily suited to civil aircraft designs. A central wing box is a part of the wing structure that integrates with the fuselage and is positioned high, low, or at a convenient mid-location (see Section 3.16).
2. *Central beam and root attachments.* These have a simpler construction and therefore are less costly, suited to smaller aircraft.
3. *Wing roots (with multispar) joined to a series of fuselage frames.* These are mostly suited to military aircraft designs. They are heavier and can be tailored to varying fuselage contours. The wing root is then secured to the fuselage structure, sometimes outside the shell, with attachments.
4. *Strut/braced wing support.* This is suited to smaller, low-speed, high-wing aircraft. Some low-wing agricultural aircraft have braced wings. Struts add to drag

but for a low-speed operation, the increment can be tolerated when it is less costly to build and lighter in construction.

5. *Swing wing*. Attachment of a swing wing is conveniently outside the fuselage such that the pivots have space around them to allow wing rotation.

For smaller aircraft, the wing must not pass through the fuselage interior, which would obstruct passenger movement. If the wing is placed outside the fuselage (i.e., top or bottom), then a large streamlined fairing on the fuselage would accommodate the wing box. The example of the Cessna Excel shows a low-wing design; the DO328 includes a fairing for the high-wing design. The Dornier 328 (see Figure 3.33) conceals the fairing that merges with the fuselage mould lines. The extra volume could be beneficial; however, to arrive at such a configuration, a proper DOC analysis must demonstrate its merits. High-wing aircraft must house the undercarriage in a fuselage fairing, although some turboprop aircraft have the undercarriage tucked inside the engine nacelles positioned below the wing (see Figure 10.19).

6.3.2 Considerations in Configuring the Wing

Following are general considerations important for designing the wing:

<i>Geometry</i>	<i>Aerodynamics</i>
(1) wing reference area, S_W	(1) drag
(2) span and aspect ratio	(2) lift and moment
(3) aerofoil section, t/c ratio	(3) stall, critical Mach
(4) sweep, twist, dihedral, taper	(4) high-lift devices
(5) position (for the CG)	(5) control surfaces
(6) glove/yehudi, if any	(6) wing/tail position
<i>Structure</i> (affecting weight and external geometry)	<i>Systems</i>
(1) spar and rib positions	(1) control linkage
(2) stiffness, aeroelasticity, and torsion stability	(2) fuel system
(3) fuel volume	(3) electrical
(4) undercarriage and nacelle, if any	(4) anti-icing
(5) weight	

The first task for wing design is to select a suitable aerofoil. This book does not undertake aerofoil design; rather, it uses established 2D aerofoil data from the public domain (the aerofoil data in Appendix C are sufficient for this book). Industry takes an arduous route to extract as much benefit from its in-house research that is kept commercial in confidence. It is an established technology in which there is a diminishing return on investment. However, the differences between the best designs and those in the public domain are enough to encourage industrial competition. The next task is to configure a wing planform with a reference area typically for the class of aircraft. It is not determined by the passenger number as in the fuselage; the initial wing size is determined from statistics. Subsequently, the preliminary wing reference area must be sized using the methodology described in [Chapter 11](#).

Positioning of the wing relative to the fuselage is an important part of configuring an aircraft. It requires knowledge of the CG position and its range of movement with weight variation (i.e., fuel and payload). Because the aircraft weight distribution is not yet established, it is initially estimated based on experience and past statistics in the aircraft class. If nothing is known, then a designer may position the wing just behind the middle of the fuselage for rear-mounted engines or at the middle of the fuselage for wing-mounted engines. Subsequently, the wing position must be iterated after the aircraft component weights are known and the wing is sized. This may not be easy because moving the wing will alter the CG position – an inexperienced engineer could encounter what is called “wing chasing”; however, this is not a major concern. Here, the “zero reference plane” (typically at the nose of the fuselage) assists in tracking the aircraft-component positions.

A generous wing root fairing is used to reduce interference drag as well as vortex intensity at the aft-fuselage flow. A large aircraft BWB is an extreme example that eliminates wing root fairing problems. There is no analytical expression to specify the fairing curvature – a designer should judge the geometry from past experience and CFD analysis, considering the internal structural layout and the associated weight growth. In principle, a trade-off study between weight growth and drag reduction is needed to establish the fairing curvature. At this stage, visual approximation from past experience is sufficient: Observe the current designs and make decisions.

6.3.3 Considerations in Configuring the Empennage

Following are general considerations important for configuring the empennage (see also Section 6.6):

<i>Geometry</i>	<i>Aerodynamics</i>
(1) H-tail and V-tail reference area, S_H and S_V	(1) drag, lift, moment
(2) span and aspect ratio	(2) tail volume coefficient
(3) aerofoil section, t/c ratio	(3) stall and yaw recovery
(4) sweep, twist, or dihedral, whichever is applicable	(4) control and trim surfaces
(5) position relative to wing (tail arm)	(5) spin recovery
(6) position H-tail to avoid shielding of V-tail	(6) balancing
(7) H-tail position (high α clearance, T-tail)	(7) engine-out cases
<i>Structure</i> (affecting weight and external geometry)	<i>Systems</i>
(1) spar and rib positions	(1) control linkage
(2) stiffness, aeroelasticity, and torsion stability	(2) control actuation
(3) fuel volume (if any)	(3) electrical (if any)
(4) weight	

The descriptions and definitions of the empennage are in Sections 3.22 and 4.9. The dominant civil aircraft empennage consists of the H-tail and V-tail placed symmetrically about the fuselage axis. The H-tail could be positioned anywhere (see Figure 4.24), going through the aft fuselage to the tip of the V-tail forming a T-tail. Some aircraft have twin booms, where the empennage has the same function; the V-tail is split over two booms.

It is important that the V-tail remains effective for the full flight envelope. Shielding of the V-tail, especially the control areas, may prove to be dangerous. A designer must ensure that the V-tail keeps at least 50% of the rudder unshielded (see Figure 4.26) at a high angle of attack. (The canard configuration is not worked out in this book). Also, at a high angle of attack, the H-tail should not remain within the wing wake; otherwise, it must be enlarged to be effective.

If a FBW control system is incorporated, the empennage sizes can be reduced because the aircraft would be able to fly safely under relaxed stabilities. However, this book is not concerned with control laws as design input in an introductory course. The FBW concept is introduced in [Chapter 12](#) but not analyzed. It will not be long until tailless aircraft such as the B2 bomber appear in civil aircraft designs, especially for BWB aircraft.

6.3.4 Considerations in Configuring the Nacelle

Following are general considerations important for configuring the nacelle (see also [Section 6.7](#)):

Geometry

- (1) diameter (comfort level, appeal)
- (2) length, fineness ratio
- (3) wing and fuselage position and pylon geometry
- (4) ground clearance
- (5) cross-section to house accessories
- (6) intake geometry and lip section

Structure (affecting weight and external geometry)

- (1) engine burst considerations
- (2) foreign-object ingestion problems
- (3) fuel volume
- (4) weight
- (5) nose gear collapse
- (6) access

Aerodynamics

- (1) drag
- (2) interference
- (3) surface roughness
- (4) noise/emission
- (5) vibration
- (6) thrust and bypass ratio (BPR) level

Systems

- (1) control linkage
- (2) fuel system
- (3) electrical
- (4) thrust reverser
- (5) fire prevention
- (6) anti-icing

Civil aircraft designs are invariably externally pod-mounted on either the wing or the aft fuselage (smaller low-wing turbofan engines). The demonstration of high engine reliability enables an ETOPS clearance by the FAA for a two-engine

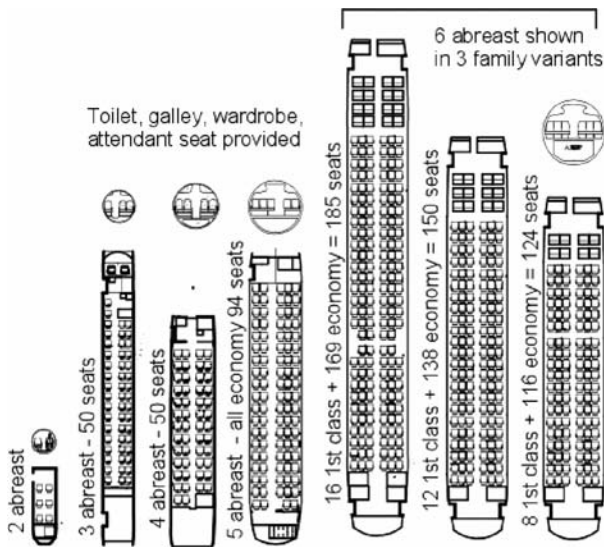


Figure 6.5. Narrow-body, single-aisle fuselage layout (not to scale)

configuration. Three-engine designs (e.g., B727, DC10, and Lockheed Tristar) are no longer pursued except for a few designs. An underwing-mounted nacelle should remain clear of the ground in the event of a nose-wheel collapse. A minimum of 30 deg of separation (see [Chapter 9](#)) is necessary to avoid wheel-spray ingestion.

Nacelles should have their thrust lines positioned close to the aircraft CG to minimize associated pitching moments. In general, the nacelle aft end is slightly inclined (i.e., 1 to 1.5 deg) downward, which also assists in takeoff. Because of the lack of ground clearance for smaller aircraft, engines are mounted on the fuselage aft end, forcing the H-tail to be placed higher. Aft-mounted engines are less desirable than wing-mounted engines. Therefore, when aircraft size and wing position allows, engines take the natural position mounted on the wing, generally slung underneath. It is for this reason that the designers of smaller aircraft are currently considering mounting the engine over the wing, as in the Honda small-jet-aircraft design.

6.4 Civil Aircraft Fuselage: Typical Shaping and Layout

Passenger-capacity and seating-arrangement requirements dictate the layout, which is generally limited to the constant cross-section midpart of the fuselage. Options for various types of fuselage cross-sections are described in Section 4.7.1. Typical geometric and interior details for aircraft with 2- to 10-abreast seating accommodating from 4 to 600 passengers with possible cabin width, fuselage length, and seating arrangement are described in this subsection and shown in [Figures 6.5](#) and [6.6](#). The figures are from the stabilized statistics of market demand, which varies slightly among cases. The public domain has many statistics for seating and aisle dimensions relative to passenger number, cabin volume, and so forth. The diagrams in this section reflect current trends. [Figures 6.5](#) and [6.6](#) show the spaces for toilets, galleys, wardrobes, attendant seating, and so forth but are not indicated as such. There are considerable internal dimensional adjustments required for the

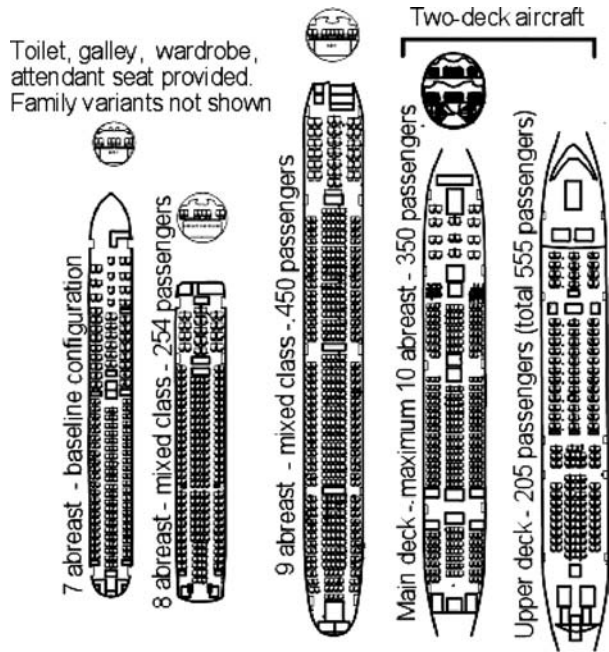


Figure 6.6. Wide-body, double-aisle fuselage layout (not to scale)

compromise between comfort and cost. The fuselage fineness ratio is kept from 7 to 14 (in the family of variants; the baseline design can start at around 10). Table 4.2 lists the typical relationship between the number of passengers and the number of abreast seating.

The first task is to determine the abreast seating for passenger capacity. The standard practice for seat dimensions is to cater to the 95th percentile of European men. Section 4.7.6 describes typical seat and aisle dimensions. Elbowroom is needed on both sides of a seat; in the middle seats, it is shared. Typical elbowroom is from 1.5 to 2 inches for economy class and double that for first class. In addition, there is a small space between the window elbowrest and the fuselage wall, larger for more curved, smaller aircraft – typically, about an inch (see Figure 3.50). A wider cabin provides more space for passenger comfort at an additional cost and drag. A longer seat pitch and wider seats offer better comfort, especially for oversized people. Aircraft with a seating capacity of 150 to 200 passengers and as many as 6 abreast with a single aisle is known as a narrow body. With more than six abreast, a two-aisle arrangement is the general practice. Fuselage width is the result of adding the thickness of the fuselage structural shell and soft wall furnishings to the cabin width (see Figure 3.50). During Phase 2 (i.e., the project-definition stage), when sufficient structural details emerge, the interior-cabin geometric dimensions are defined with better resolution; the external geometry remains unaffected. The number of abreast seating and total passenger capacity determine the number of rows. Table 4.5 lists typical dimensions of seat pitch and width.

When the interior arrangement is determined, the constant cross-section mid-fuselage needs to be closed at the front and aft ends. The midsection fuselage could exhibit closure trends at both the front and aft ends, with diminishing interior arrangements at the extremities. The front-end fuselage mould lines have a favorable pressure gradient and therefore are blunter with large curvatures for rapid

Table 6.1. *Fuselage seating dimensions – narrow body (in inches)*

	2-Abreast (1–1)	3-Abreast (1–2)	4-Abreast (2–2)	5-Abreast (2–3)	6-Abreast (3–3)
Seat width, B (LHS)	19	19	2 × 18	2 × 18	3 × 18
Aisle width, A	17	18	19	20	21
Seat width, B (RHS)	19	2 × 19	2 × 18	3 × 18	3 × 18
Total elbowroom	4 × 1.5	5 × 1.5	6 × 1.5	7 × 2	8 × 2
Gap between wall & seat, G	2 × 1.5	2 × 1	2 × 1	2 × 0.5	2 × 0.5
Total cabin width, W_{cabin}	64	85	102	126	141
Total wall thickness, T	2 × 2.5	2 × 4	2 × 4.5	2 × 5	2 × 5.5
Total fuselage width, W_{fuselage}	69	93	111	136	151
Cabin height, H_{cabin}	60	72*	75	82	84
Typical fuselage height, H_{fus}	70	85	114	136	151

* Recessed floor.

front-end closure. Basically, a designer must consider the space for the flight crew at the front end and ensure that the pilot's view polar is adequate. Conversely, the aft end is immersed in an adverse pressure gradient with low energy and a thick boundary layer – therefore, a gradual closure is required to minimize airflow separation (i.e., minimize pressure drag). The aft end also contains the rear pressure-bulkhead structure (see Section 4.7.3 and Figure 4.16 for closure shapes). The longer aft-end space could be used for payload (i.e., cargo) and has the scope to introduce artistic aesthetics without incurring cost and performance penalties.

An important current trend is a higher level of passenger comfort (with the exception of low-cost airlines). Specifications vary among customers. Designers should conduct trade-off studies on cost versus performance in consultation with customers (i.e., operators) to satisfy as many potential buyers as possible and to maximize sales. This is implied at every stage of aircraft component sizing, especially for the fuselage.

Dimensions listed in Tables 6.1 and 6.2 are estimates. The figures of seat pitch, seat width, and aisle width are provided as examples of what exists in the market.

Table 6.2. *Fuselage seating dimensions: wide body (in inches)*

	7-Abreast (2–3–2)	8-Abreast (2–4–2)	9-Abreast (2–5–2)	10-Abreast (3–4–3)
Seat width, B (LHS)	2 × 19	2 × 19	2 × 19	3 × 19
Aisle width, A	22	22	22	22
Seat width, B (Center)	3 × 19	4 × 19	5 × 19	4 × 19
Aisle width, A (RHS)	22	22	22	22
Seat width, B (RHS)	2 × 19	2 × 19	2 × 18	3 × 19
Total elbowroom	9 × 1.5	10 × 1.5	11 × 1.5	12 × 1.5
Gap between wall and seat, G	2 × 0.5	2 × 0.5	2 × 0.5	2 × 0.5
Total cabin width, W_{cabin}	192	212	232	253
Total wall thickness, T	2 × 6	2 × 6.5	2 × 7	2 × 7.5
Total fuselage width, W_{fuselage}	204	225	246	268
Cabin height, H_{cabin}	84	84	84 to 86	84 to 86
Typical fuselage height, H_{fus}	204	225	246	268

The dimensions in the tables can vary to a small extent, depending on customer requirements. The seat arrangement is shown by numbers in clusters of seats, as a total for the full row with a dash for the aisle. For example, “3–4–3” indicates that the row has a total of 10 seats, in a cluster of 3 at the 2 window sides of the fuselage and a cluster of 4 in the middle flanked by 2 aisles.

Variants in the family of aircraft are configured by using a constant cross-section fuselage plug in units of one row of pitch. The changes in passenger numbers are discreet increases in the total number of passengers in a row (an example of six-abreast seating is shown in [Figure 6.5](#)). An increase in capacity results from adding plugs as required. If more than one, they are distributed in front and aft of the wing. When in odd numbers, their distribution is dictated by the aircraft CG position. In most cases, the front of the wing has the extra row. Conversely, a decrease in passenger numbers is accomplished by removing the fuselage plug using the same logic. For example, a 50-passenger increase of 10-abreast seating has 2 plugs distributed as 3 rows in a subassembly in front of the wing and a subassembly of 2 rows aft of the wing. Conversely, a 50-passenger decrease is accomplished by removing 3 rows from the rear and 2 from the front. For smaller aircraft with smaller reductions, unplugging may have to be entirely from the front of the wing.

Readers are required to work out dimensions using the information provided in the following subsections – intensive coursework begins now. However, readers should be aware that the worked-out examples demonstrate only the proposed methodology. Designers are free to configure aircraft with their own choices, which are likely to be within the ranges defined herein.

6.4.1 Narrow-Body, Single-Aisle Aircraft

[Figure 6.5](#) shows a typical seating arrangement for single-aisle, narrow-body aircraft carrying up to about 220 passengers (all economy class). [Section 6.3.1](#) lists the general considerations regarding doors, fineness ratio, closure angles, seat and aisle dimensions, internal facilities, and so forth for each type.

[Table 6.1](#) provides typical dimensions for establishing narrow-body fuselage widths. All dimensions are in inches. [Figure 3.50](#) defines the symbols used. Additional fuselage interior details follow. [Figure 6.5](#) shows examples of seating arrangements from two to six passengers abreast.

Two abreast (4 to 24 passengers). Two-abreast seating is the lowest arrangement. The passenger comfort level demands relatively large variations in fuselage width. The typical passenger capacity extends from 4 to 19 (e.g., Beech 1900D) and could expand to 24 passengers in an extreme derivative version.

A circular cross-section is ideal to obtain the minimum weight for a pressurized cabin; however, a circular cross-section may not always prove to be best. The aircraft fuselage diameter for two-abreast seating does not provide enough space for passengers to straighten their legs when seated; therefore, a widening of the bottom half could provide more comfort, as shown in [Figure 6.7](#). The fuselage top is semi-circular, making headroom clearance a fallout of the design. Cabin height is on the order of 60 inches and most passengers would have to bend down during boarding. A toilet facility is preferred.

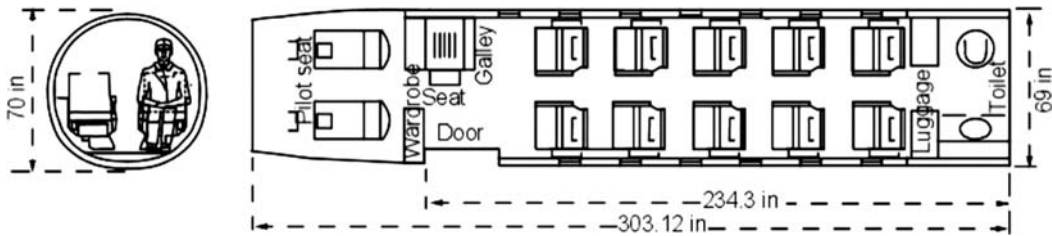


Figure 6.7. Example of configuring the fuselage for the medium comfort level (in inches)

Current regulations do not require a cabin crew for up to 19 passengers, but some operators prefer to have one crew member, who uses a folding seat secured in a suitable location. An expanded variant of 2-abreast seating can exceed 19 passengers, but a new high-capacity design should move into 3-abreast seating, described next. The baggage area is at the rear, which is the preferred location in smaller aircraft.

Summary. A typical two-abreast fuselage would have the following features:

- Cabin Width:** This consists of one seat on each side of the center aisle. To avoid tightness of space in a smaller aircraft, seats could be slightly wider, sacrificing aisle width where there is little traffic. Typically, cabin width is between 64 and 70 inches.
- Cross-Section:** The fuselage cross-section is typically circular or near circular (i.e., the overall width is greater than the height). Designers must compromise their choices to maximize the sales. The bottom half could be opened up for better legroom. There is no payload space below the floorboards but it could be used for aircraft equipment and fuel storage. Luggage space is located in the aft fuselage.

Front/Aft Closure: See Table 4.4 for the range of dimensions.

Fuselage Length: This depends on the number of passengers and facilities provided (see Figure 6.5). Add front and aft closures to the fuselage midsection.

Family Variants: Addition or subtraction of fuselage plugs, to a maximum of four rows, conveniently distributed on each side of the wing, is possible. The worked-out example baseline version starts with ten passengers (see Figure 6.7).

Three abreast (24 to 50 passengers). A typical 3-abreast seating arrangement accommodates 24 to 45 passengers, but variant designs change that from 20 to 50 passengers (e.g., ERJ145). Full standing headroom is possible; for smaller designs, a floorboard recess may be required (see Figure 4.12). A floorboard recess could trip passengers when they are getting to their seat. Space below the floorboards is still not adequate for accommodating any type of payload. Generally, space for luggage in the fuselage is located in a separate compartment at the rear but in front of the aft pressure bulkhead (the luggage-compartment door is sealed).

At least 1 cabin crew member is required for up to 30 passengers. With more passengers, 2 crew members are required for up to 50 passengers. A new design with potential for growth to more than 50 passengers should start with 4-abreast seating, described next.

Summary. A typical three-abreast fuselage would have the following features:

Cabin Width: This consists of two seats in a cluster and one seat on each side of the aisle. The aisle width could be increased to ease cabin-crew access. Cabin width is from 82 to 88 inches, depending on the customer's demand for the comfort level.

Cross-Section: The fuselage cross-section is typically circular but follows the cabin-section contour with added wall thickness. There is no payload space below the floorboards, but it can be used for aircraft equipment and fuel storage.

Front/Aft Closure: See Table 4.4 for the range of dimensions.

Fuselage Length: This depends on the number of passengers and facilities provided (see Figure 6.5). Add front and aft closures to the fuselage midsection.

Family Variants: Addition or subtraction of fuselage plugs, to a maximum of five rows, conveniently distributed on each side of wing, is possible. The baseline version could start with 36 passengers and range from 24 to 50 passengers (Figure 6.5 shows the largest in the family).

Four abreast (44 to 80 passengers). A typical 4-abreast seating arrangement accommodates 44 to 80 passengers, but variant designs could change that number from 40 to 96 passengers (e.g., the Bombardier CRJ1000; the Canadair CL-600 is an executive version that accommodates 19 passengers – another example of a derivative). The cabin crew increases to at least three for higher passenger loads. The increase in the fuselage diameter can provide space below the floorboards for payload, but it is still somewhat limited. To maximize the below-floorboard space, the fuselage height could be slightly oval, with the upper-half semicircular and the bottom half elongated to suit smaller container sizes. Figure 4.12 shows a four-abreast seating arrangement; note the facilities and luggage-compartment arrangement. As the fuselage radius increases, the gap between the elbowrest and the fuselage wall can be reduced to 1 inch (2.54 cm) on each side, increasing the seat width.

Summary. A typical four-abreast fuselage would have the following features:

Cabin Width: A four-abreast arrangement is two seats in a cluster on both sides of a center aisle. Cabin width is from 100 to 106 inches depending on the customer's demand for the comfort level. The aisle width could be increased to ease cabin-crew access and passenger traffic.

Cross-Section: The fuselage cross-section is typically circular but can be elongated. It follows the cabin-section contour with added wall thickness (see Table 6.1). Full standing headroom is easily achievable. There is aft-fuselage luggage space.

Front/Aft Closure: See Table 4.4 for the range of dimensions.

Fuselage Length: This depends on the number of passengers and facilities provided. Add front and aft closures to the fuselage midsection.

Family Variants: Addition or subtraction of fuselage plugs, to a maximum of seven rows, conveniently distributed on each side of the wing, is possible. The baseline version could start with 60 passengers and range from 40 to 96 passengers.

Five abreast (80 to 150 passengers). A typical 5-abreast seating arrangement can accommodate 85 to 130 passengers, but variant designs could extend that number somewhat on both sides. The number of cabin crew increases with passenger capacity. There are not many aircraft with five-abreast seating because the increase from four abreast to six abreast better suited market demand. A prominent five-abreast design is the MD-9 series (now the Boeing 717).

The fuselage diameter widens to provide more generous space. Space below the floorboards is conspicuous to accommodate standard containers (see Section 4.7.8).

The fuselage aft closure could affect seating – that is, the last row could be reduced to four abreast. To ease cabin access, the aisle width widens to at least 20 inches plus the armrest at each side. To maximize the below-floor space, the fuselage could be slightly elongated, with the bottom half stretched to accommodate container sizes. A separate cargo space exists at the rear fuselage in the closure area.

Summary. A typical five-abreast fuselage would have the following features:

Cabin Width: Five-abreast is seating arranged as three in a cluster on one side of the single aisle and two in a cluster on the other side. Very little gap is required between the armrest and the cabin wall because the fuselage radius is adequate. Cabin width is from 122 to 130 inches depending on the customer's demand for the comfort level. The aisle width could be increased to facilitate passenger and crew traffic.

Cross-Section: The fuselage cross-section is typically circular but can be elongated. It follows the cabin-section contour with added wall thickness (see Table 6.1). Full standing headroom is easily achievable. There is potential for aft-fuselage luggage space.

Front/Aft Closure: See Table 4.4 for the range of dimensions.

Fuselage Length: This depends on the number of passengers and facilities. Add front and aft closures to the fuselage midsection.

Family Variants: Addition or subtraction of fuselage plugs, to a maximum of eight rows, conveniently distributed on each side of the wing, is possible. The baseline version could start with 100 passengers and range from 85 to 150 passengers.

Six abreast (120 to 230 passengers). This class of passenger capacity has the most commercial transport aircraft in operation (more than 8,000), including the Airbus 320 family and the Boeing 737 and 757 families. The Boeing 757–300 has the largest passenger capacity of 230 and the highest fineness ratio of 14.7. There is considerable flexibility in the seating arrangement to accommodate a wide range of customer demands.

Figure 6.5 shows an aircraft family of variant designs to accommodate three different passenger-loading capacities in mixed classes. A typical 6-abreast seating arrangement accommodates 120 to 200 passengers, but variant designs could change that number from 100 to 230 passengers. The number of cabin crew increases accordingly. The fuselage diameter is wider to provide generous space. Space below the floorboards can accommodate standard containers (see Section 4.7.8). To maximize the below-floor space, the fuselage height could be slightly elongated, with the bottom half suitable for container sizes. A separate cargo space is located at the rear fuselage.

Summary. A typical six-abreast fuselage would have the following features:

- Cabin Width:** Six-abreast seating is arranged as three in a cluster on both sides of the single center aisle. Very little gap is required between the armrest and the cabin wall because the fuselage radius is adequate. Cabin width is from 138 to 145 inches, depending on the customer's demand for the comfort level. The aisle width is increased to facilitate passenger and crew traffic.
- Cross-Section:** The fuselage cross-section is typically circular but can be elongated. It follows the cabin-section contour with added wall thickness (see Table 6.1). Full standing headroom is adequate. There is potential for aft-fuselage luggage space.

Front/Aft Closure: See Table 4.4 for the range of dimensions.

- Fuselage Length:** This depends on the number of passengers and facilities. Add front and aft closures to the fuselage midsection.
- Family Variants:** Addition or subtraction of fuselage plugs, to a maximum of ten rows, conveniently distributed on each side of the wing, is possible. The baseline version could start with 150 passengers and range from 85 to 210 passengers. The Boeing 757 baseline starts with a higher passenger load, enabling the variant to reach 230 passengers.

6.4.2 Wide-Body, Double-Aisle Aircraft

Seven-abreast seating and more would require more than one aisle to facilitate passenger and crew traffic in the cabin. These aircraft are also known as wide-bodied aircraft. Figure 6.6 shows a typical seating arrangement for a double-aisle, wide-body aircraft carrying up to 555 passengers; however, high-density seating of all economy-class passengers can exceed 800 (e.g., A380). These large passenger numbers require special attention to manage comfort, amenities, and movement.

Section 6.3.1 discusses general considerations for each type of aircraft seating (e.g., doors, fineness ratio, closure angles, seat and aisle dimensions, and internal facilities). A typical cross-section is circular but can be elongated, as shown in Figure 4.12. A double-deck aircraft has an elongated cross-section.

Table 6.2 provides typical dimensions to establish a wide-body fuselage width. All dimensions are in inches, and decimals are rounded up. Refer to Figure 3.50 for the symbols used. More fuselage-interior details are given in Table 6.2. Designers are free to adjust the dimensions – the values in the table are typical.

Seven abreast (160 to 260 passengers). The Boeing 767 appears to be the only aircraft with seven-abreast seating and it can reconfigure to eight-abreast seating. Typical 7-abreast seating accommodates 170 to 250 passengers, but variant designs could change that number on either side. The number of cabin crew increases accordingly. The fuselage diameter is wider to provide generous space. Space below the floorboards can accommodate cargo containers (see Section 4.7.8). To maximize the below-floorboard space, the fuselage height could be slightly elongated, with the bottom half suitable for container sizes. A separate cargo space is located at the rear fuselage.

Summary. A typical seven-abreast fuselage (with better comfort) would have the following features:

Cabin Width: Seven-abreast seating is arranged as 2–3–2 in a cluster of two at the window sides and a cluster of three at the center between the two aisles. Very little gap is required between the armrest and the cabin wall because the fuselage radius is adequate. The cabin width is from 190 to 196 inches, depending on the customer's demand for the comfort level. The aisle width could be increased to facilitate cabin-crew access and passenger movement.

Cross-Section: The fuselage cross-section is typically circular but can be oval. It follows the cabin-section contour with added wall thickness (see Table 6.2). Full standing headroom is no longer an issue. There is potential for aft-fuselage luggage space.

Front/Aft Closure: See Table 4.4 for the range of dimensions.

Fuselage Length: This depends on the number of passengers and facilities. Add front and aft closures to the fuselage midsection.

Family Variants: Addition or subtraction of fuselage plugs, to a maximum of ten rows, conveniently distributed on each side of the wing, is possible. The baseline version could start with 200 passengers and range from 160 to 260 passengers.

Eight abreast (250 to 380 passengers, wide-body aircraft). The Airbus 300/310/330/340 series has been configured for eight-abreast seating. Figure 6.6 shows an example of an 8-abreast seating arrangement for a total of 254 passengers (in mixed classes; for all economy-class, 380 passengers in a variant design is possible). Space below the floorboards can accommodate larger containers. Seat width, pitch, and layout with two aisles results in considerable flexibility to cater to a wide range of

customer demands. The cross-section is typically circular, but to maximize below-floor board space, it could be slightly elongated, with the bottom half suitable for cargo container sizes. There is potential for a separate cargo space at the rear fuselage.

Summary. A typical eight-abreast fuselage would have the following features:

Cabin Width: Eight-abreast seating is arranged as 2–4–2 in a cluster of two at the window sides and a cluster of four in the center between the two aisles. Very little gap is required between the armrest and the cabin wall because the fuselage radius is adequate. The cabin width is from 210 to 216 inches, depending on the customer’s demand for the comfort level. The aisle width is nearly the same as for a wide-bodied layout to facilitate cabin-crew and passenger movement.

Cross-Section: The fuselage cross-section is typically circular but can be oval. It follows the cabin-section contour with added wall thickness (see [Table 6.2](#)). Full standing headroom is adequate. There is potential for aft-fuselage luggage space.

Front/Aft Closure: See [Table 4.4](#) for the range of dimensions.

Fuselage Length: This depends on the number of passengers and facilities. Add front and aft closures to the fuselage midsection.

Family Variants: Addition or subtraction of fuselage plugs, to a maximum of eleven rows, conveniently distributed on each side of the wing, is possible. The baseline version could start with 300 passengers and range from 250 to 380 passengers.

Nine to Ten Abreast (350 to 480 passengers, wide-body aircraft). The current ICAO restriction for fuselage length is 80 m. The associated passenger capacity for a single-deck aircraft is possibly the longest currently in production. It appears that only the Boeing 777 has been configured to nine- or ten-abreast seating in a single deck.

[Figure 6.6](#) is an example of a 9-abreast seating layout for a total of 450 passengers. Seat width, pitch, and a layout with two aisles has a similar approach to the earlier seven-abreast seating designs, which embeds considerable flexibility for catering to a wide range of customer demands. Cabin-crew numbers can be as many as twelve. Space below the floorboards can carry larger containers (i.e., LD3). The cross-section is typically circular, but to maximize below-floorboard space, it could be slightly elongated, with the bottom half suitable for container sizes. There is potential for a separate cargo space at the rear fuselage.

Summary. A typical nine- or ten-abreast fuselage seating arrangement would have the following features:

Cabin Width: Nine-abreast seating is arranged as 2–5–2 in a cluster of two at the window sides and a cluster of five in the center between the two aisles. A 3–3–3 arrangement is also possible but not shown. Very little gap is required between the armrest and the cabin

wall because the fuselage radius is adequate. The cabin width is from 230 to 236 inches, depending on the customer's demand for the comfort level. The aisle width is nearly the same as for the wide-bodied layout to facilitate cabin-crew access and passenger movement.

Cross-Section: The fuselage cross-section is typically circular but can be oval. It follows the cabin-section contour with added wall thickness (see [Table 6.2](#)). Full standing headroom is no longer an issue. There is potential for an aft-fuselage luggage space.

Front/Aft Closure: See [Table 4.4](#) for the range of dimensions.

Fuselage Length: This depends on the number of passengers and facilities. Add front and aft closures to the fuselage midsection.

Family Variants: Addition or subtraction of fuselage plugs, to a maximum of eleven rows, conveniently distributed on each side of the wing, is possible. The baseline version could start with 400 passengers and range from 300 to 480 passengers.

Ten abreast and more (more than 400 to almost 800 passenger capacity, wide-body and double-decked). A more than 450-passenger capacity provides the largest class of aircraft with variants exceeding an 800-passenger capacity. This would invariably become a double-decked configuration to keep fuselage length below the current ICAO restriction of 80 m. Double-decking could be partial (e.g., Boeing 747) or full (e.g., Airbus 380), depending on the passenger capacity; currently, there are only two double-decked aircraft in production.

With a double-decked arrangement, there is significant departure from the routine adopted for a single-decked arrangement. Passenger numbers of such large capacity would raise many issues (e.g., emergency escape compliances servicing and terminal handling), which could prove inadequate compared to current practice. Reference [4] may be consulted for double-decked aircraft design. The double-decked arrangement produces a vertically elongated cross-section. Possible and futuristic double-decked arrangements are shown in [Figure 4.12](#). The number of cabin crew increases accordingly. The space below the floorboards is sufficient to accommodate larger containers (i.e., LD3).

Summary. A typical ten-abreast fuselage would have the following features:

Cabin Width: The lower deck of a double-decked aircraft has at most 10 abreast, arranged as 3–4–3 in a cluster of 3 at the window sides and a cluster of 4 in the center between the 2 aisles. Very little gap is required between the armrest and the cabin wall because the fuselage radius is adequate. The cabin width is from 250 to 260 inches, depending on the customer's demand for the comfort level. The aisle width is nearly the same as for a wide-bodied layout to facilitate cabin-crew and passenger movement.

Cross-Section: A double-decked fuselage cross-section is elongated at this design stage. It follows the cabin-section contour with added wall thickness (see Table 6.2). Full standing headroom is no longer an issue. There is potential for aft-fuselage luggage space.

Front/Aft Closure: See Table 4.4 for the range of dimensions.

Fuselage Length: This depends on the number of passengers and facilities. Add front and aft closures to the fuselage midsection.

Family Variants: Addition or subtraction of fuselage plugs, to a maximum of 10 rows, conveniently distributed on each side of the wing, is possible. Fuselage length is less than 80 m.

6.4.3 Worked-Out Example: Civil Aircraft Fuselage Layout

The purpose of the worked-out example is only to substantiate the methodology outlined. Readers can decide their own dimensions of the class of aircraft on which they are working. The available range of dimensions offers several choices; it is unlikely that fuselage sizing would fall outside of the given ranges – if at all, a marginal deviation is possible in an extreme design. Readers need not be confined to this classwork example and may explore freely; simplicity can be an asset.

Example 2 in Section 2.6 is used here to provide an example of configuring a civil aircraft: a Learjet45 class Bizjet that offers variants in a family of designs. Following are the important specifications for the aircraft:

Baseline Version (8 to 10 passengers)

Payload: 1,100 kg
 High Comfort Level: $8 \times 100 + 300 = 1,100$ kg
 Low Comfort Level: 10×90 (averaged) + 200 = 1,100 kg
 Range: 2,000 miles + reserve

Longer Variant (12 to 14 Passengers)

Payload: 1,500 kg
 High Comfort Level: $12 \times 100 + 300 = 1,500$ kg
 Low Comfort Level: 14×90 (averaged) + 240 = 1,500 kg
 Range: 2,000 miles + reserve

Shorter Variant (4 to 6 passengers)

Payload: 600 kg
 High Comfort Level: $4 \times 100 + 200 = 600$ kg
 Low Comfort Level: 6×90 (averaged) + 60 = 600 kg
 Range: 2,000 miles + reserve

The fuselage size is determined from the required passenger load. Following the considerations listed in Section 6.3.1, a stepwise approach is suggested.

Step 1: Configure the mid-fuselage width, which mostly consists of the constant cross-section.

Decide the number of abreast seating using Table 4.2 and the comfort level (aisle and seat width are made more comfortable at the

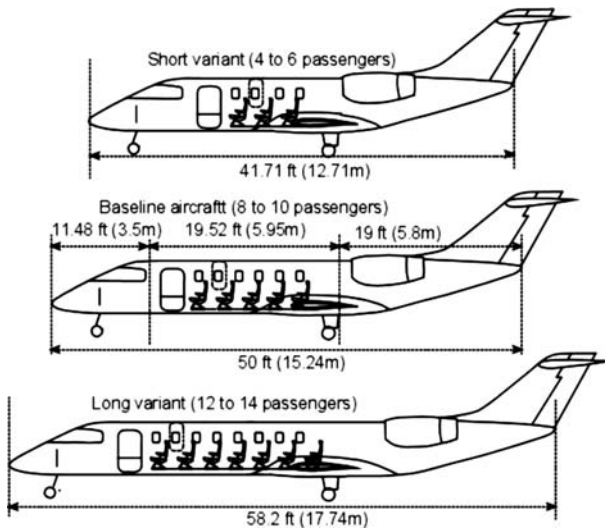


Figure 6.8. Fuselage lengths of the three variants

expense of cost). In this case, it is two-abreast seating. This gives the cabin width and, adding the fuselage thickness, the result is the fuselage width. For a pressurized cabin, keeping the cross-section as close as possible to a circular shape is preferred; for an unpressurized cabin, it can approach a rectangular shape.

Step 2: Configure the mid-fuselage length, which consists mostly of the constant cross-section.

Determine the number of seat rows by dividing the total passenger capacity by the number of abreast seating. If it is not divisible, then the extreme rows will have seating with fewer abreast. Decide the passenger facilities (e.g., toilets, galleys, closets, and cabin-crew seating) and add those dimensions. The extremities of the fuselage midsection can be tapered to begin the fuselage closure. With Step 1, this provides the fuselage midsection size.

Step 3: Configure the front and aft closures.

Section 4.7.3 suggests various fuselage closures; there are many to choose from as observed from past designs in the aircraft class. Although there are benefits from past experience, designers should develop their own configuration based on pilot vision, drag considerations, space for storage, rotation for takeoff, and so forth. Following is a worked-out example to configure a baseline aircraft with a midsection fuselage.

The baseline aircraft cabin with medium comfort and a 10 seat layout is shown in Figure 6.8.

As discussed previously, two-abreast seating in the cross-section results in a widening of the bottom half for legroom, shown here in the inclined position for a man in the 95-percentile size. The fuselage width is 173 cm (68.11 inches) and the fuselage height is 178 cm (70 inches). To simplify the computation, an equivalent approximation uses an average circular diameter of the cross-section of 175.5 cm (69.1 inches) (e.g., for estimation of the fuselage wetted area). Standing height

inside the cabin is 152 cm (59.85 inches). The total fuselage shell thickness is 14 cm (5.5 inches), which makes the cabin width 159 cm (62.6 inches). The two-abreast seating arrangement is in accordance with Section 6.4.1, with detailed dimensions adding up to $4.5 + 53S + 44A + 53S + 4.5 = 159$ cm (or $1.78 + 21S + 17A + 21S + 1.78 = 62.6$ inches), fitting the cabin width exactly.

The medium-comfort seat pitch is 32 inches (81.28 cm). With the toilet facility 1 m (39.65 inches) long, the entry door of 76.2 cm (30 inches), and the interior space of 12.4 cm, the fuselage midsection (i.e., cabin) length totals $(5 \times 81.28) + 100 + 76.2 + 12.4 = 595$ cm (234.3 inches). With the flight-crew cockpit space (1.85 m in length), the total is 7.8 m (303.12 inches), as shown in Figure 6.7. It is suggested that readers compare this with competition aircraft – this design has more room than is typical of the class.

For the longer variant with a higher density, a 14-passenger seat pitch is 30 inches (76.2 cm). The variant cabin dimension is now $(7 \times 76.2) + 100 + 76.2 + 12.4 = 722$ cm (284.25 inches). Adding the cockpit length, the length becomes $(7.22 + 1.85) = 9.07$ m.

The shorter 6-passenger variant has the scope to retain a seat pitch of 32 inches (81.28 cm). The cabin midsection length becomes $(3 \times 81.28) + 100 + 76.2 + 12.4 = 432.44$ cm (170.25 inches). With the length of the flight-crew cockpit space added in (1.85 m), it totals 6.37 m (250.8 inches).

The overall fuselage length is reached after adding front and aft closures, as given in Table 4.4. The windscreen shape and size must comply with FAR regulations, as shown in Figure 4.17. This is an opportunity to streamline the fuselage, incorporating aesthetics without incurring additional cost and performance degradation. After streamlining, the various ratios are checked out to be within the acceptable range. Choosing a suitable ratio, the following dimensions are estimated:

- The front-fuselage closure length is 11.48 ft (3.5 m), of which 1.85 m is the cockpit length.
- The front-fuselage closure ratio becomes $L_f = 350/175.5 = 1.994$ (see Section 4.7.3).
- The aft-fuselage closure length works out to be 18.54 ft (5.65 m), with the upsweep angle to be checked out later.
- The aft-fuselage closure ratio becomes $L_a = 565/175.5 = 3.22$, within the range. Therefore, the baseline version fuselage length, $L = L_f + L_m + L_a = 3.5 + 5.95 + 5.65 = 15.1$ m (49.54 ft).
- Fineness ratio = $1,510/175.5 = 8.6$.
- Use the same closure lengths for the variants. The longer variant has a fineness ratio = $(722 + 350 + 565)/175.5 = 9.33$, well within the prescribed range. Here, one fuselage plug of 64 inches in the front and 40 inches in the aft of the wing are added (see Figure 6.2).
- The shorter variant has a fineness ratio = $(432.44 + 350 + 565)/175.5 = 7.68$, within the prescribed range. Here, one fuselage plug of 64 inches in the front and 30 inches in the aft of the wing are subtracted (see Figure 6.2).

The three variants of the family are shown in Figures 6.2 and 6.8 along with the wing positioned nearly at the middle of the fuselage. The rotation clearance is to be checked out after the undercarriage is positioned. This is not a problem because the

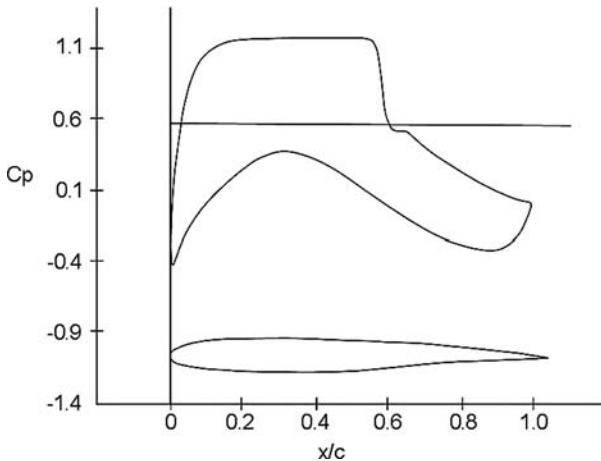


Figure 6.9. A CAST 7 (Germany) aerofoil and its characteristics

main undercarriage length can be tailored in conjunction with the longest fuselage; this is the iterative process.

6.5 Configuring a Civil Aircraft Wing: Positioning and Layout

The first task for designing the wing is to select a suitable aerofoil. Aerofoil design is a protracted and complex process that is beyond the scope of this book. After an aerofoil is selected (it could vary spanwise), the next task is to configure a wing planform with reference area. It is not like the fuselage sizing determined by the passenger number; initially, it is from statistics for the aircraft class. At the conceptual stage of the project study, typical values of wing twist and other refinements are taken from the past experience of a designer. The values must be substantiated and, if required, modified through CFD analysis and wind-tunnel testing to a point when the flight test may require final local refinements (e.g., flap and aileron rigging). Initially, an isolated wing is analyzed to quickly arrive at a suitable geometry and then studied with the fuselage integrated. Subsequently, the wing is sized formally (see [Chapter 11](#)).

6.5.1 Aerofoil Selection

Section 3.7 outlines the strategy to search for an aerofoil that would provide a high C_{Lmax} as well as a high lift-curve slope ($dC_L/d\alpha$), a high L/D ratio for the prescribed cruise speed, a low pitching moment, and gentle stalling characteristics. While retaining these characteristics, consultation with structural designers should decide an aerofoil t/c ratio that would permit good structural integrity to increase the aspect ratio. This is an area in which designers should gain over the competition with a better aerofoil and material. Finally, for high-subsonic cruise speed, the aerofoil shape should minimize compressibility effects (i.e., wave drag). Typically, a supercritical aerofoil with a relatively flat upper-surface profile (i.e., Whitcomb) reduces the transonic effects. [Figure 6.9](#) shows a typical flat upper-surface pressure distribution at cruise (i.e., supercritical aerofoil). Good aerofoil sections are proprietary information and mostly are not available in the public domain.

To minimize repeating work that is similar in nature, the chosen aerofoil section for worked-out examples is kept the same for both civil and military aircraft designs. For a relatively low cruise Mach number of 0.65 at the LRC and 0.74 at the HSC, the NACA 65–410 is chosen for both designs. It is not exactly a supercritical aerofoil but serves the learning process because it is a known aerofoil successfully applied to many aircraft (Appendix C gives the details of NACA 65–410 aerofoil).

6.5.2 Wing Design

When the aerofoil section has been selected, the next task is to obtain the following information, which would be iterated to the final size through various design phases, as shown in Chart 2.1. Initially, all geometric details are taken from past experience (i.e., the statistical data of the aircraft class), followed by formal sizing, fine-tuned through CFD analyses and wind-tunnel testing, and finally substantiated through flight-testing (modifications are made, if required).

1. Determine the wing planform shape and its reference area. It should maximize the aspect ratio and optimize the taper ratio. In addition, the wing ensures adequate fuel volume. At this stage, it is considered that the wing structural layout can accommodate fuel capacity and movable control and lifting surfaces.
2. Determine the wing sweep, which is dependent on maximum cruise speed (see Section 3.16).
3. Determine the wing twist; a typical statistical value is 1 to 2 deg, mostly as washout (see Section 3.14).
4. Determine the wing dihedral/anedral angle; initially, this is from the statistical data (see Section 3.14).
5. Determine high-lift devices and control areas. At first, the type is selected to satisfy the requirements at low cost. The values of its aerodynamic properties initially are taken from statistical data (see Section 3.10).

Section 6.3.2 discusses general considerations for wing design. Given here are suggestions to establish these parameters (see also Section 3.16).

Planform Shape

A civil aircraft designer would seek the maximum possible aspect ratio that a structure would allow. This minimizes induced drag (see Equation 3.13). The V - n diagram (see Section 5.7) determines the strength requirement in pitching maneuvers creating maximum stress from the bending moment at the wing root. Civil aircraft do not have high roll rates (unless it is a small aerobatic aircraft). Choice of material and aerofoil t/c ratio contributes to structural integrity. For civil aircraft, a trapezoidal wing planform (with or without extensions; see Section 3.14) would be the dominant choice. The least expensive to manufacture is a rectangular planform, but there is no cost benefit for highly utilized commercial aircraft to offset drag reduction (i.e., fuel-saving). Rectangular planforms are used in smaller club and sports aircraft with a low level of utilization.

Wing Reference Area

The wing reference area is obtained from the sizing of wing-loading W/S . At this stage, without knowing the aircraft weight, an initial estimate is derived from statistical values reflecting successful past designs. Subsequently, the wing will be sized to the requirement (see [Chapter 1](#)). Some iteration is required because component weights are revised at the stages of the study. In coursework activity, one iteration is sufficient.

Wing Sweep

Wing sweep, Λ , is a function of aircraft speed to delay transonic effects. For aircraft flying at less than Mach 0.6, a wing sweep is not required. A tapered wing with a zero quarter-chord sweep has some LE sweep; the trailing-edge sweep depends on the taper ratio.

Wing Twist

It is an essential geometrical adjustment to ensure that wing-tip effects do not create adverse conditions. A major requirement is to make the wing root stall earlier to retain aileron effectiveness at a high angle of attack (low speed) – especially during landings. A wing twist with washout would favor such behavior (and is the prevailing practice).

Wing Dihedral/Anhedral

To ensure roll stability (see Section 12.3.3), wing dihedral and anhedral angles are used. Generally, the dihedral is associated with low-wing design and the anhedral with high-wing design; however, there are designs that are the reverse: a high wing can accommodate a dihedral. The type and extent are settled through stability analysis, which is not discussed in this book. All civil aircraft have some dihedral or anhedral angle between 1 and 5 deg. If a high wing and/or a high-wing sweep increases lateral stability more than what is required, the anhedral angle is required to reduce it to the desired level. Some low-wing Russian bombers have a high-wing sweep that necessitates an anhedral angle, when the undercarriage struts must be longer to provide the desired ground clearance.

6.5.3 Wing-Mounted Control-Surface Layout

Chapter 3 introduces a host of wing-mounted control surfaces (e.g., aileron, flap, slat, spoilers, and trim tabs), none of which are sized in this book; however, geometry from current designs is extracted and their placement should be earmarked. Control surface sizing is accomplished after the wing is sized and is addressed in subsequent design phases.

Flaps and slats are wing components that are selected for field-performance demands to generate high lift. In general, the more demanding aircraft-performance requirements, the more sophisticated are the high-lift devices, which are progressively more complex and therefore more expensive (see Section 3.12). Associated incremental lift gains by each type are shown in Figure 3.21. In general, a single- or double-slotted Fowler action flap suffices for the majority of civil transport aircraft. The simpler types are less costly to manufacture and are used in low-speed, low-cost smaller aircraft, usually compensated by the relatively larger wing area.

The aileron span is about a third of the wing span at the extremities. Ailerons and flaps are hinged aft of the rear spar for up and down movements; provision for them should be made during the conceptual design phase. On some designs, flap tracks are used to support the flaps traveling outward to increase lift. A *flaperon* serves as both a flap and an aileron.

Flaps are positioned behind the wing rear spar (about 60 to 66% of the chord) and typically run straight or piecewise. Flaps take up about two thirds of the inner wing span. It is apparent that designers must have a good knowledge of the internal structural layout to configure an aircraft. [Chapter 15](#) provides information on aircraft structure pertaining to the aircraft-configuration study.

Not all aircraft have wing spoilers; however, aircraft with speed over Mach 0.6 generally have spoilers. These are installed close to the aircraft CG line to minimize pitch change. Spoilers also act as air brakes. The differential use of spoilers is for lateral control and they are referred to as *spoilerons*. This book does not size spoilerons or air brakes but schematically earmarks their position on the wing.

6.5.4 Positioning of the Wing Relative to the Fuselage

Positioning of the wing relative to the fuselage is an iterative process dictated by the location of the aircraft CG at a desired position, expressed in terms of percentage of the wing MAC. The aircraft CG is kept close to the quarter-chord position of the wing MAC. Unfortunately, at this stage of design, the aircraft weight and CG are not accurately known.

A designer's expertise is the way to estimate the wing position relative to the fuselage as a starting point. Experienced designers minimize the number of iterations that could occur with "wing-chasing," explained in [Section 4.11](#). The CG position varies with aircraft loading, fuel status, and military aircraft armament carried. Positioning of the wing should be such that the aircraft stability margin is not jeopardized by extremes of the operational CG position.

For newcomers to aircraft design, this offers an interesting exercise: Very quickly, a "feel" for locating the wing can be developed. A starting position for wing placement relative to the fuselage is approximately at the middle of the fuselage (somewhat farther behind for aft-mounted engines).

6.5.5 Worked-Out Example: Configuring the Wing in Civil Aircraft

Continuing with the fuselage-design example outlined in [Section 6.4](#), following are specifications required for wing design:

Maximum Cruise Speed:	Mach 0.74 (HSC)
Initial Cruise Altitude:	Above 40,000 ft (ceiling more than 50,000 ft)
Takeoff Field Length:	1,000 m at sea level (balanced field length)
Landing Distance from 50 ft:	1,000 m at maximum landing weight, as high as 0.95 MTOM at sea level
Initial Rate of Climb:	16 m/s

Unlike the fuselage, the approach to wing design starts with past statistics and is properly sized in [Chapter 11](#). Following the considerations listed in [Sections 6.3.2](#) and [6.5.2](#), a wing design could progress in a stepwise approach as suggested herein.

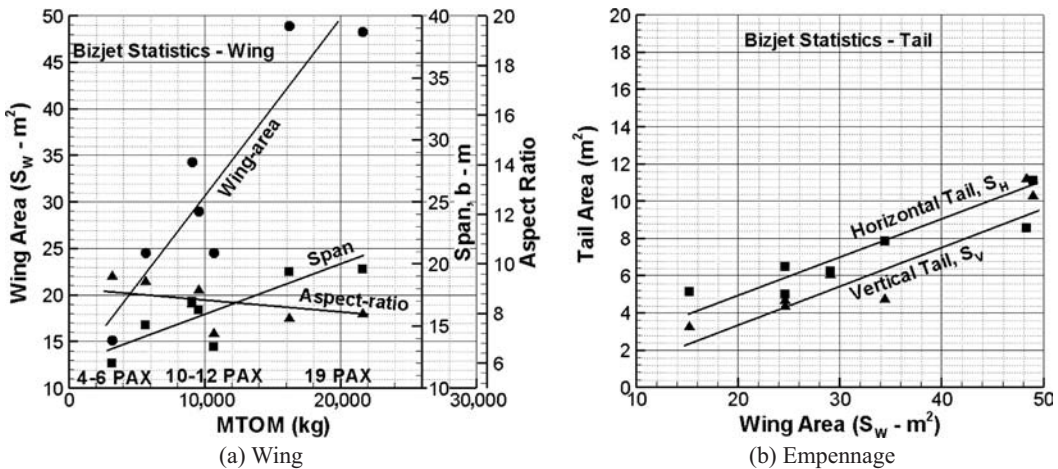


Figure 6.10. Statistics for the Bizjet class of aircraft

A worked-out example follows. Figure 6.10 is specifically for the aircraft class under consideration. Aircraft in the graphs are the Century, Cessna CJ2, Cessna Excel, Cessna 650, Lear 60, Cessna 750, and Challenger.

Step 1: Decide the aerofoil section.

This is one of the most important aspects of aircraft design. Aircraft performance depends considerably on the type of aerofoil adopted. Today, most designers in the major aircraft industry design their own aerofoil and keep the profile “commercial in confidence.” There are also many industries that use the established NACA-type aerofoil. This book uses the established aerofoil section available in the public domain. Aerodynamicists prefer the aerofoil to be as thin as possible, whereas structural engineers prefer it to be as thick as possible. A compromise is reached based on the aircraft design Mach number and the chosen wing sweep.

Step 2: Establish the wing reference area.

Initially, the wing reference area must be estimated from previous statistics. First, estimate the aircraft MTOW from the payload-range capability (see Figure 4.5). Next, estimate the wing reference area, S_w , from the MTOW (see Figure 6.10a); this gives the wing-loading. Both the S_w and the MTOW are accurately sized in Chapter 11. Position the wing relative to the fuselage, considering the aerodynamic and structural features.

Step 3: Establish the aspect ratio, wing sweep, taper ratio, dihedral, and twist (see Section 3.16).

The wing planform is generally of but not restricted to a trapezoidal shape – it can be modified with a glove and/or a yehudi. The choices for the wing-aspect ratio, wing sweep, and taper ratio are interlinked to keep the compressibility drag increase within twenty drag counts at the high-speed design specification (see Section 3.18). The aspect ratio should be the highest that the structural integrity will permit for the aerofoil t/c ratio and the wing root chord based on the taper

ratio. At this stage, wing twist is empirically determined to improve stalling effects. The wing dihedral is decided from stability considerations. All these parameters are eventually fine tuned through CFD analysis and wind-tunnel testing, with the hope that flight-test results will not require further tweaking.

- Step 4: Establish the control surfaces (e.g., aileron and spoilers). Initially, these are approximated by reference to statistics and semi-empirical data; the sizing could be postponed until more details are available. In this book, the control surfaces are not sized.
- Step 5: Establish the high-lift devices (e.g., flap and slats). The first task is to decide the type of high-lift device required to meet the maximum C_L to satisfy the specified field performance requirements (i.e., takeoff and landing). Once established, the area and other geometrical parameters are initially approximated by reference to the statistics and semi-empirical data. The sizing can be postponed until more details are available. In this book, the high-lift devices are not sized.

To maintain component commonality, the wing should be the same for all three variants; obviously, it would be slightly larger for the smaller variant and slightly smaller for the larger variant. How this is determined satisfactorily is addressed in [Chapter 11](#).

Maintaining the established design trends, the planform shape of the example is taken as trapezoidal and assembled as a low wing to the aircraft. The aerofoil for the aircraft is a NACA 65–410 (i.e., 10% t/c ratio; see [Appendix C](#)).

At this stage, the wing reference area and aircraft weight are not known. This is when the statistics of previous designs prove useful to initiate the starting point. Unfortunately, [Figure 4.8](#) is very coarse; however, [Figure 6.10](#) provides similar information in finer detail confined to the aircraft class. The author recommends that readers produce similar graphs in better resolution for the aircraft class under consideration.

[Figure 6.10a](#) indicates a MTOM of approximately 9,000 to 10,000 kg, corresponding to 10 passengers. An average value of 9,500 kg (21,000 lb) is used for the example. The corresponding wing area is $\approx 30 \text{ m}^2$ (322.9 ft^2) of trapezoidal wing planform, which gives a wing-loading of 316.67 kg/m^2 (65 lb/ft^2). These are preliminary values and are formally sized in [Chapter 11](#). However, the aspect ratio is reduced to 7.5 to keep the OEW light (it will be iterated). A taper ratio of 0.4 is used, which reduces the wing span. With a relatively low LRC Mach of 0.65, the compressibility effect is low and a quarter-chord sweep angle of 14 deg (see [Figure 3.36](#)) would keep the wave drag to zero.

The wing span is worked out as $b = \sqrt{AR \times S_W} = \sqrt{225} = 15 \text{ m}$ (49.2 ft). The wing root and tip chord (C_R and C_T) can now be worked out from the taper ratio of 0.4:

$$C_T/C_R = 0.4 \quad \text{and} \quad S_W = 30 = b \times (C_T + C_R)/2, \quad \text{solving the equations}$$

$$C_R = 2.86 \text{ m} (9.38 \text{ ft}) \quad \text{and} \quad C_T = 1.143 \text{ m} (3.75 \text{ ft}).$$

Using [Equation 3.21](#), the wing MAC = $\frac{2}{3} \times [2.87 + 1.148 - (2.87 \times 1.148)/(2.87 + 1.148)] = 2.132 \text{ m}$ (7 ft). [Figure 6.11](#) gives the wing plan form geometry.

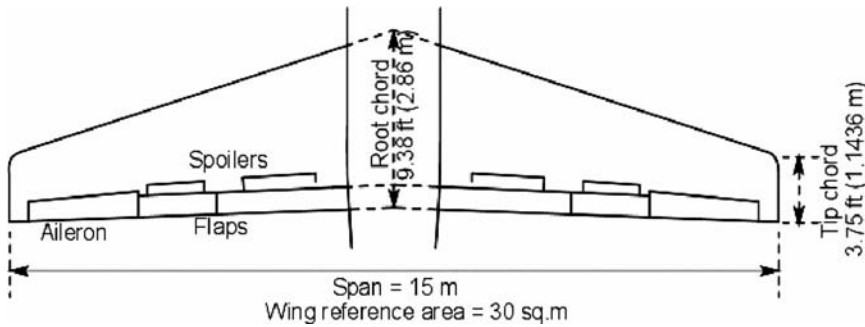


Figure 6.11. Example of wing design

It is interesting that most typical values of taper, twist, and dihedral are derived from statistics and are about the same for the aircraft class. From the statistics, a twist of -2 deg (i.e., washout) and a dihedral of 3 deg are typical for the class. Eventually, CFD and wind-tunnel testing will fine-tune the values. A wing-loading of 316.67 kg/m^2 ($3,106.5 \text{ N/m}^2$) is a moderate value that would provide good field performances. A single-slotted Fowler flap without a LE slat would be sufficient, saving considerably on costs.

Control areas are provisional and are sized in Phase 2. Initially, a company's statistical data of previous experience serve as a good guideline. Aileron, flaps, and spoilers are placed behind the wing rear spar, which typically runs straight (or piecewise straight) at about 60 to 66% of the chord. With a simple trapezoidal wing planform, the rear spar runs straight, which keeps manufacturing costs low and the operation simpler; therefore, it has a lower maintenance cost. With a third of the wing span exposed, the aileron area per side is about 1 m^2 (10.764 ft^2). Similarly, the flap area is 2.2 m^2 (23.68 ft^2) per side. Subsequent performance analysis would ascertain whether these assumptions satisfy field-performance specifications. If not, further iterations with improved flap design are carried out.

From the test data, the following maximum lift coefficients are given:

Flap deflection – deg	0	8	20	40
C_{Lmax}	1.5	1.7	1.9	2.1

For a small aircraft with limited ground clearance, the engines would be mounted on the rear fuselage. At this stage, the wing is placed just behind the middle of the fuselage. The wing location is subsequently fine-tuned when the CG and undercarriage positions are known. A smaller aircraft wing could be manufactured in one piece and placed under the fuselage floorboards, minimizing a “pregnant-looking” fairing (Figure 3.35 shows a generous fairing to smooth the hump; however, the example in this book has more streamlined fairing).

6.6 Configuring a Civil Aircraft Empennage: Positioning and Layout

The function of the empennage is to provide a force/moment for stability and control. The fuselage length, wing reference area (S_W), and tail arms L_{HT} and L_{VT} are the main parameters governing the empennage size. Semi-empirical relations given in the definition of tail volume coefficient (see Section 12.5) provide the statistical empennage size required (see Figure 12.11).

The H-tail is placed as a T-tail on a swept-back V-tail that would provide an increased tail arm, L_{HT} and L_{VT} , which would save weight by not having a longer fuselage. Smaller aircraft would benefit from a T-tail; however, to support the T-tail load, the V-tail must be made stronger with a small increase in its weight. Care must be taken to ensure that the T-tail does not enter the wing wake at a high angle of attack. This can be achieved by positioning it high above the wing wake at near stall or having a larger H-tail and/or an all-moving H-tail acting as an elevator. (Earlier aircraft encountered these problems; in a deep stall, there was insufficient elevator power in the low-energy wing wake for the aircraft to recover in the pitch plane before crashing.)

Selection of the empennage aerofoil and planform follows the same logic as for the wing design. V-tail designs have symmetrical aerofoil sections. The H-tail camber is influenced by the aircraft's CG position. In general, negative camber is used to counter a nose-down moment of the wing. H-tail and V-tail designs are discussed separately in the following subsections. The current design tendency indicates a little higher tail volume coefficient as compared to the historical design trend (see Figure 12.11).

6.6.1 Horizontal Tail

Typically, for civil aircraft, the H-tail planform area is from one fifth to one fourth of the wing planform size. Figure 12.11 shows a cluster of H-tail designs with a tail volume coefficient of 0.7. As in wing design, the H-tail can have a sweep and a dihedral (a twist is not required). Sweeping of the H-tail would effectively increase the tail arm L_{HT} , which is an important consideration when sizing the H-tail. For a T-tail configuration, the tail arm further increases.

6.6.2 Vertical Tail

Typically, for civil aircraft, the V-tail planform area is about 12 to 20% of the wing reference area. For propeller-driven aircraft, the V-tail could be kept slightly skewed (less than 1 deg) to offset a swirled-slipstream effect and gyroscopic torque of rotating engines and propellers. The V-tail design is critical to takeoff – especially in tackling yawed ground speed resulting from a crosswind and/or asymmetric power of a multiengine aircraft. A large V-tail can cause snaking of the flight path at low speed, which can be resolved easily by introducing a “yaw-damper” (a matter of aircraft control analysis). At cruise, a relatively large V-tail is not a major concern.

From the statistics given in Figure 12.11, it can be seen that there is a cluster of V-tail designs with a tail volume coefficient of 0.07. For the T-tail configuration, the tail volume coefficient could be reduced to 0.06 because the T-tail acts as an endplate at the tip of the V-tail. As in wing design, the V-tail can have a sweep, but the dihedral and anhedral angles and the twist are meaningless because the V-tail needs to be symmetric about the fuselage centerline. Sweeping of the V-tail would effectively increase the tail arm L_{VT} , an important dimension in sizing the V-tail. It is important to ensure that the V-tail, especially the rudder, is not shielded by the H-tail to retain effectiveness, especially during spin recovery. With a T-tail, there is no shielding.

The empennage design has considerable similarity to the wing design. Section 4.9 describes various types of empennage; here, only the conventional design with an H-tail and a V-tail are considered. Following is a stepwise approach to empennage design:

Step 1: Decide the aerofoil section.

In general, the V-tail aerofoil section is symmetrical but the H-tail has an inverted section with some (negative) camber. The t/c ratio of the empennage is close to the wing-aerofoil considerations. A compromise is selected based on the aircraft design Mach number and the wing sweep chosen.

Step 2: Establish the H-tail and V-tail reference areas.

Initially, during the conceptual study, the H-tail and V-tail reference areas are established from the statistical data of the tail volume coefficients (see Section 12.5). The positions of the H-tail and V-tail relative to the fuselage and the wing are decided by considering the aerodynamic, stability, control, and structural considerations.

Step 3: Establish the empennage aspect ratio, sweep, taper ratio, and dihedral. The empennage planform is generally but not restricted to a trapezoidal shape. A strake-like surface could be extended to serve the same aerodynamic gains as for the wing. The choices for the empennage aspect ratio, wing sweep, and taper ratio are interlinked and follow the same approach as for the wing design. The empennage aspect ratio is considerably lower than that of the wing. All these parameters are decided from stability considerations and eventually fine-tuned through CFD analysis and wind-tunnel testing, with the hope that flight-test results will not require further tweaking.

Step 4: Establish the control surfaces.

Initially, the control areas and dimensions of the elevator and the fin are earmarked from statistics and semi-empirical data. At this stage of study, the control surfaces can be postponed until more details are available to accurately size the control areas. In this book, the control surfaces are not sized. Subsequently, in the next design phase, when the finalized aircraft geometry is available, the empennage dimensions are established by formal stability analysis. A worked-out example follows in the next section.

6.6.3 Worked-Out Example: Configuring the Empennage in Civil Aircraft

Continuing with the fuselage and wing design example carried out in the previous sections, this section presents a worked-out example of empennage design. The aircraft specification used so far to configure the fuselage and wing is sufficient for empennage design. Figure 6.10b provides empennage statistics of the current Bizjet aircraft class. The empennage area size depends on tail arm length, which is not compared in the graphs. A coursework example would have a slightly smaller tail area than shown in Figure 6.10b for having a relatively larger tail arm (the high sweep of the V-tail is added to the tail arm – shown is an example of a designer's choice for weight reduction). It is the tail volume coefficients that decide the tail areas.

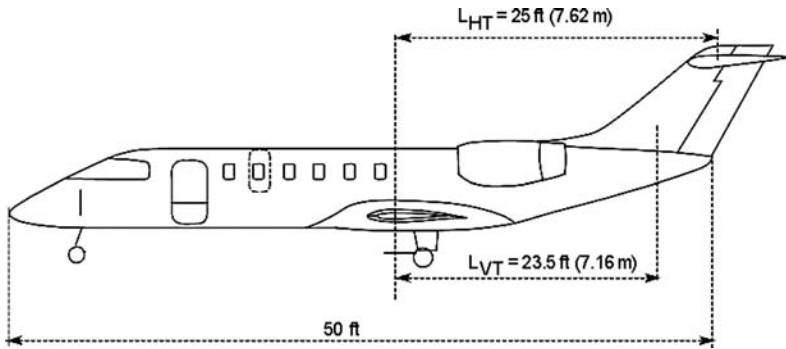


Figure 6.12. Civil aircraft example of empennage sizing

To maintain component commonality, the empennage is the same for all three variants. The baseline-designed empennage area is made sufficient for smaller aircraft; larger aircraft have a longer tail arm to enhance the empennage effectiveness.

So far, the civil aircraft design exercise provided the following data:

- Estimated aircraft weight = 9,500 kg (at this stage, not required for empennage sizing)
- Wing reference area = 30 m² (low-wing design is popular and therefore chosen)
- Wing MAC = 2.2 m (computed from Equation 3.21)
- Fuselage length = 50 ft (aircraft length is different – see Figure 6.3)

To minimize the fuselage length, a T-tail configuration is chosen. The V-tail design arrangement is determined first to accommodate the position of the T-tail on top. Figure 6.12 illustrates the tail-arm lengths used to compute empennage areas.

Section 12.5 provides statistics for the V-tail volume coefficient, C_{VT} , within the range $0.05 < C_{VT} < 0.12$. In the example, $C_{VT} = 0.07$ is appropriate for the smaller aircraft variant. The V-tail quarter-chord sweepback is 15 deg in line with the wing sweep, to increase the tail arm $L_{VT} = 7.16$ m (23.5 ft) measured from the aircraft CG to the V-tail MAC. In general, $S_{VT}/S_W \approx 0.12$ to 0.2. The symmetrical aerofoil section is the NACA64-010. The V-tail height (semispan) = 7 ft (2.14 m) and the taper ratio = 0.6 to bear the load of a T-tail.

Equation 3.31 gives the V-tail reference area $S_{VT} = (C_{VT})(S_W \times \text{wing span})/L_{VT}$.

The V-tail is positioned on the fuselage end in consultation with structural engineers. Then, $S_{VT} = (0.07 \times 30 \times 15)/7.16 = 4.4$ m² (47.34 ft²). This would result in sensible geometric details of the V-tail, as follows:

- Note: Area, $S_V = \frac{1}{2} (C_R + C_T) \times b$ or $4.4 = 0.5 \times 1.6 C_R \times 2.14$
- Root Chord = 8.43 ft (2.57 m)
- Tip Chord = 5.05 ft (1.54 m)
- Aspect Ratio = 2.08
- MAC = $(\frac{2}{3} \times [(8.43 + 5.05) - (8.43 \times 5.05)/(8.43 + 5.05)]) = 6.8$ ft (2.07 m)
- The V-tail area must be shared by the rudder and the fin. Typically, the rudder encompasses 15 to 20% of the V-tail area – in this case, it is 17%. This gives a rudder area of 0.75 m² (8 ft²).

To check the C_{VT} for the smaller variant, it should be more than 0.06. With one seat pitch plug removed from the aft fuselage, $L_{VT_short} = 7.16 - 0.813 = 6.347$ m

(20.823 ft). This gives $C_{VT_short} = (4.4 \times 6.347)/(30 \times 15) = 0.062$ (sufficient for the shorter variant).

Section 12.5 provides the statistics of the H-tail volume coefficient, C_{HT} , within the range $0.5 < C_{HT} < 1.2$. In this example, $C_{HT} = 0.7$ is appropriate for the smaller aircraft variant. The H-tail is placed as a T-tail (dominant for smaller aircraft to increase the tail arm). The H-tail sweepback is 15 deg, in line with the wing sweep, and slightly more to increase the tail arm $L_{VT} = 7.62$ m (25 ft) measured from the aircraft CG to the H-tail MAC. In general, $S_{HT}/S_W \approx 0.2$ to 0.25. The aerofoil section is the NACA64–210 and the installation is inverted. The H-tail span equals 16.7 ft (5.1 m) and the taper ratio equals 0.5. Equation 3.30 gives the H-tail reference area, $S_{HT} = (C_{HT})(S_W \times MAC)/L_{HT}$.

The H-tail is positioned to give $S_{HT} = (0.7 \times 30 \times 2.132)/7.62 = 5.88$ m² (63.3 ft²), which is about 20% of the wing area. This area must be shared by the elevator and the stabilizer. Typically, the elevator uses 18 to 25% of the H-tail area; in this case, it is 20%, which results in an elevator area of 1.21 m² (13 ft²).

This would result in sensible geometric details of the H-tail, as follows:

- Note: Area, $S_H = \frac{1}{2} (C_R + C_T) \times b$ or $5.88 = 0.5 \times 1.5 C_R \times 5.1$
- Root Chord = 5.04 ft (1.54 m)
- Tip Chord = 2.52 ft (0.77 m)
- Aspect Ratio = 4.42
- MAC = $(\frac{2}{3}) \times [(5.04 + 2.52) - (5.04 \times 2.52)/(5.04 + 2.52)] = 3.9$ ft (1.19 m)

To check the C_{HT} for the smaller variant, it should be more than 0.6. With one seat pitch plug removed from the aft fuselage, $L_{HT_short} = 7.62 - 0.813 = 6.807$ m (22.33 ft). This gives $C_{HT_short} = (6.063 \times 6.807)/(30 \times 2.2) = 0.625$ (sufficient for the shorter variant).

6.7 Configuring a Civil Aircraft Nacelle: Positioning and Layout of an Engine

The nacelle pod size depends on the choice of engine. At this design stage, a statistical value of uninstalled T_{SLs} per engine is considered to determine the size of an engine. A formal engine sizing and matching is accomplished in [Chapter 11](#). For better fuel economy, a large bypass ratio is desired. Dialogue with engine manufacturers (that can offer the class of engines) continues with “rubberized” engines (i.e., engines scalable and finely tuned to match the aircraft performance requirements for all variants). There are not many engine manufacturers from which to choose.

Numerous engine accessories (see [Chapter 10](#)) are part of the engine power plant. They are located externally around the casing of the engine (i.e., turbofan or turboprop). In general, these accessories are located below the engine; some are distributed at the sides (if the engine is underwing-mounted with less ground clearance). Therefore, the nacelle pods are not purely axi-symmetric and show faired bulges where the accessories are located.

Long-duct nacelles, chosen for the example, appear to be producing a higher thrust to offset the weight increase of the nacelle, while also addressing environmental issues of substantial noise reduction. Also, long-duct designs could prove more suitable to certain types of thrust reverser designs. This book only considers

long-duct design but it does not restrict the choice of short-duct nacelles.

For this example, the maximum nacelle diameter $\approx <1.5 \times$ engine-face diameter (6.6)

In general, the intake length in front of the engine face $\approx <1.0 \times$ engine-face diameter, and the exhaust jet-pipe length aft of the last stage turbine disc $\approx <1.5 \times$ engine-face diameter.

The total nacelle length \approx (engine length) + ($k \times$ engine-face diameter) (6.7)

where $1.5 < k < 2.5$. For smaller engines, the value of k is lower.

For long-duct nacelles, the fineness ratio (i.e., length/maximum diameter) is between 2 and 3.

Pylons are the supporting structures (i.e., cross-section streamlined to the aerofoil shape) of the nacelle attaching to the aircraft and carrying all the linkages for engine operation. Aft-fuselage-mounted pylons are generally horizontal but can be inclined if the nacelle inlet must be raised. For wing-mounted nacelles, the pylon is invariably vertical. The depth of the pylon is about half of the engine-face diameter; the pylon length depends on the engine position. For an aft-fuselage-mounted installation, the pylon is nearly as long as the nacelle. For a wing-mounted installation, the nacelle is positioned ahead of the wing LE to minimize wing interference. In general, the t/c ratio of the pylon is between 8 and 10%.

The nacelle size is determined from the matched-engine dimensions. Using the considerations listed in Section 6.3.4, the following stepwise approach is suggested. The engine-thrust level indicates engine size (Figure 6.13). It is best to obtain the engine size from the manufacturer as a bought-out item.

Step 1: Configure the podded nacelle size.

The maximum engine diameter determines the maximum nacelle diameter. The ratio of the maximum nacelle diameter to the maximum engine diameter is given statistically in Chapter 10. Similarly, the length of the nacelle is established from the engine length. The keel cut is typically thicker than the crown cut to house accessories. In this book, the nacelle is symmetrical to the vertical plane but it is not a requirement.

Step 2: Position the nacelle relative to the fuselage.

The nacelle position depends on the aircraft size, wing position, and stability considerations (see Section 4.10). Subsequently, CFD analysis and wind-tunnel testing will fine-tune the nacelle size, shape, and position.

Step 3: Use pylons to attach the nacelle to the aircraft.

A worked-out example follows in the next section.

6.7.1 Worked-Out Example: Configuring and Positioning the Engine and Nacelle in Civil Aircraft

This section provides an example for configuring the nacelle based on an engine bought from an engine manufacturer. (Figure 4.9 gives the relationship between MTOM and engine thrust. Chapter 10 gives more details of engine dimensions).

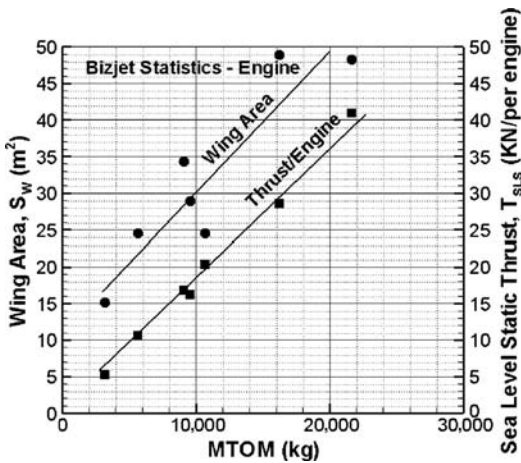


Figure 6.13. Statistics in the aircraft class: the uninstalled thrust of a turbofan

Unfortunately, Figure 4.8 is very coarse; however, Figure 6.13 provides similar information in finer detail confined to the aircraft class. The author recommends that readers produce graphs in higher resolution for the aircraft class under consideration. Unlike aircraft in general, the external dimensions of variant engines in a family do not change – the thrust variation is accomplished through internal changes of the engine (see Chapter 10). The same nacelle geometry can be used in all variants. For major variations, the engine size changes slightly, with minimal changes affecting the nacelle mould lines.

From the statistics in Figure 6.13, for a MTOM of 9,500 kg, a typical uninstalled engine thrust for this aircraft class indicates that $T_{SLs}/\text{engine} = 3,800 \text{ lb} \pm 25\%$ for the derivative variants for the aircraft family to be offered. This may be considered a smaller engine. For better fuel economy, a larger BPR is desirable. Not many engines are available in this class. It is important that a proven, reliable engine from a reputable manufacturer be chosen; of interest are the following:

Honeywell (originally Garrett) TFE731 turbofan-series class.

Pratt and Whitney (Canada) PW 530 series class (not many variants available)

(In the small engine class, Williams is coming up but is still below the required size.)

The Rolls Royce Viper and the Turbomeca Larzac have a low BPR and are suited to a military application. This leaves the Honeywell TFE731–20 turbofan class as practically the only choice. It has a fan diameter of 0.716 m (28.2 inches), a bare engine length of 1.547 m (60.9 inches), and a dry weight of 379 kg (836 lb). At this stage, a generic long-duct nacelle pod to house is used (see Figure 6.13).

Using the relationship given in Equation 6.6, the maximum nacelle diameter = $1.5 \times 0.716 = 1.074 \text{ m}$ (5.52 ft).

Using the relation given in Equation 6.7, the nacelle length = $1.5 \times 0.716 + 1.547 = 2.62 \text{ m}$ (8.6 ft).

The nacelle fineness ratio = $2.62/1.074 = 2.44$.

Being a small aircraft, the engines are aft-fuselage-mounted, one at each side. At this stage, a horizontal plate may represent the pylons that support the nacelles. The pylon length = 2.44 m (8 ft) with a thickness of 25 cm (9.8 in) and having a symmetrical cross-section aerofoil-like structure for ease of manufacture. Inlet and exhaust areas are established in Chapter 10.

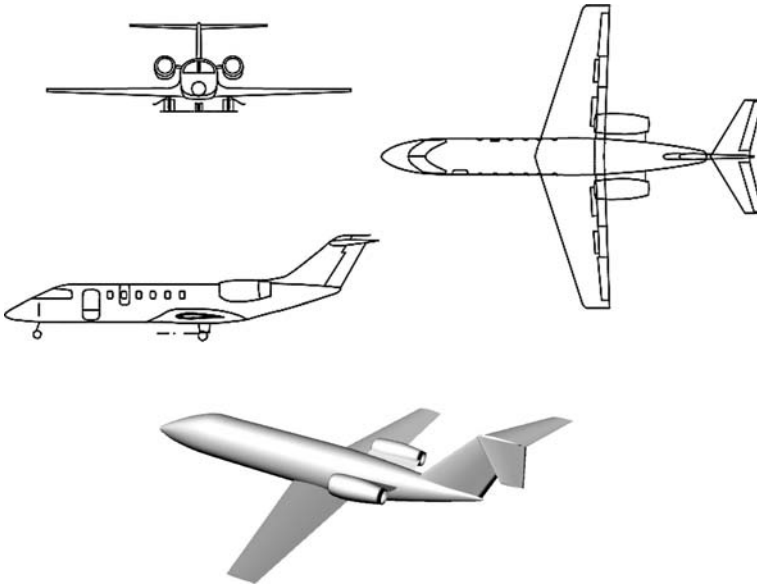


Figure 6.14. Three-view diagram and a CAD drawing of the preliminary aircraft configuration

6.8 Undercarriage Positioning

Chapter 7 provides details of the undercarriage (i.e., landing gear) design. There is little difference between civil and military aircraft design layouts in undercarriage positioning.

Undercarriage positioning is CG-dependent. At this design stage, the CG position is not established because aircraft component weights are not known. It is now evident that an iterative process is necessary. From experience, the undercarriage may be positioned after estimating the CG position and rotational tail clearances. Ensure that the aircraft does not tip in any direction for all possible weight distributions. (Tipping occurs in some homebuilt designs – especially the canards – when the pilot steps out of the aircraft.) This book addresses only the tricycle type – that is, a forward nose wheel followed by two main wheels behind the aftmost CG. The undercarriage position shown in Figure 6.13 is approximately 60% of the MAC. Readers should use the three views.

6.9 Worked-Out Example: Finalizing the Preliminary Civil Aircraft Configuration

It is interesting to observe how the aircraft is gradually taking shape – it is still based on a designer’s past experience but soon will be formally sized to a satisfying rational configuration to offer the best characteristics for the design.

A preliminary three-view diagram of the civil aircraft can now be drawn (Figure 6.14). It will be revised after the remaining aircraft components are positioned and a revised CG location is established. The next iteration is after aircraft sizing in Chapter 11.

At this stage, all aircraft components are ready to be assembled using the building-block concept to generate a preliminary aircraft configuration, as shown in Figure 6.14. The three variants (see Figure 6.8) maintain the same wing, empennage,

and nacelle (some internal structures are lightened or reinforced without affecting manufacturing jigs and tools).

The configuration is similar to the Learjet 45 but it is not the same; there are considerable differences in configuration, component weights, and performance. Readers may compare the two using the *Jane's All the World's Aircraft Manual*.

Chapter 11 sizes the aircraft to its final dimensions and finalizes the configuration based on the aircraft and component mass worked out in Chapter 8. Following is a summary of the worked-out civil aircraft preliminary details (from statistics):

Market Specifications

Payload: 10 Passengers + Baggage: 1,100 lb	Range: 2,000 nm
HSC Mach: 0.74	LRC Mach: 0.65
Initial Climb Rate: 16 miles/s	Initial Cruise Altitude: >40,000 ft
Takeoff Field Length: 1,000 m	Landing Distance From 50 ft: 1,000 m

Baseline Aircraft Mass (from statistics)

MTOM: 9,500 kg (\approx 21,000 lb)	OEM: 5,900 kg (\approx 13,000 lb)
Fuel Mass: 1,200 kg (\approx 2,650 lb)	

Baseline External Dimensions

Fuselage (determined from passenger capacity)	
Length: 15.24 m (50 ft)	Upsweep: 10 deg
Overall Width: 173 cm (68.11 in)	Overall Height (Depth): 178 cm (70 in)
Average Diameter: 175.5 cm (70 in)	Fineness Ratio: 8.6

Wing (aerofoil 65–410)

Planform (Reference) Area: 30 m ²	Span: 15 m, Aspect Ratio: 7.5
Root Chord, C_R : 2.87 m (9.4 ft)	Tip Chord, C_T : 1.143 m (3.75 ft)
MAC: 2.132 (7 ft)	Taper Ratio, λ : 0.4 $\Lambda_{\frac{1}{4}}$ 14 deg
Dihedral: 3 deg, Twist: 1 deg (washout)	t/c: 10%

V-Tail (Aerofoil 64–010)

Planform (Reference) Area: 4.4 m ² (47.34 ft ²)	Height: 2.13 m (7 ft) AR = 2.08
Root Chord, C_R : 2.57 m (8.43 ft)	Tip Chord, C_T : 1.54 m (5.05 ft)
MAC: 2.16 (7.1 ft) t/c: 10%	Taper Ratio, λ : 0.6 $\Lambda_{\frac{1}{4}}$ = 40 deg
Rudder: 0.75 m ² (8 ft ²)	t/c: 10%

H-Tail (T-tail, aerofoil 64–210 – installed with negative camber)

Planform (Reference) Area: 5.88 m ² (63.3 ft ²)	Span: 5 m (16.4 ft) AR = 4.42
Root Chord, C_R : 1.54 m (5.04 ft)	Tip Chord, C_T : 0.77 m (2.52 ft)
MAC: 1.19 m (3.9 ft)	Taper Ratio, λ : 0.5 $\Lambda_{\frac{1}{4}}$ = 15 deg
Dihedral: 5 deg	Elevator: 1.21 m ² (13 ft ²) t/c: 10%

Nacelle

Length: 2.62 m (8.6 ft)	Maximum Diameter: 1.074 m (3.52 ft)
-------------------------	-------------------------------------

Bare Engine (each)

Takeoff Static Thrust at ISA Sea Level: 3,800 lb (17,235 N) per engine with BPR = 5

Engine Dry Weight: 379 kg (836 lb)

Fan Diameter: 0.716 m (28.2 in)

Length: 1.547 m (60.9 in)

Short Variant (all component dimensions except the fuselage length are invariant)

Fuselage: Length: 13.47 m (44.2 ft) (see Figure 6.8).

Long Variant (all component dimensions except the fuselage are invariant)

Fuselage: Length: 16.37 m (53.7 ft) (see Figure 6.8).

6.10 Miscellaneous Considerations in Civil Aircraft

Following are additional considerations that could enhance aircraft performance but are not addressed here. At this design stage, none of the additional surfaces described needs to be considered except the dorsal fin. All add to aircraft weight.

1. *Winglets*. It took some time to establish the merits of having winglets that can reduce or induce drag – some manufacturers claim a reduction as high as 5% of induced drag (i.e., approximately 1.5% in total drag reduction), which is substantial. Currently, almost all large-aircraft designs incorporate winglets. Learjet has been using them for some time and they have become a symbol of its design.
2. *Dorsal Fin*. A dorsal fin ahead of the V-tail could work like strakes on a wing, and they are incorporated in many aircraft – at least to a small degree. They prevent the loss of directional stability.
3. *Ventral Fin*. This is sometimes installed at the tail end as an additional surface to the V-tail. The ventral fin also serves as a skidding structure to protect the fuselage from damage at excessive early rotation, which causes tail-dragging.
4. *Delta Fins*. These fins come in pairs at the aft end of the lower fuselage. Not all designs have delta fins; they are used if an aircraft shows poor stability and/or control problems. Aircraft with a flat, rear-loading, raised fuselage upsweep demonstrate these problems and delta fins are deployed to resolve them. A good design should avoid incorporating delta fins; however, on some designs, drag reduction can be achieved with their installation.

Several external-surface perturbations on aircraft add to parasitic drag, including antennas, inspection-hatch covers, vent pipes, and lightning dischargers. Engine and system intake and exhaust ducts and vents also increase drag.

It is suggested that readers determine whether there are any innovative requirements that should be incorporated in the conceptual design. Trends should be investigated continually for ideas to improve on aircraft design.

6.11 Configuring Military Aircraft – Shaping and Laying Out

This extended section of the book can be found on the Web at www.cambridge.org/Kundu and gives a brief overview of today's military aircraft shapes and their layout arrangements, as shown in the following charts and figures.

Figure 6.15. Falcon F16 fuselage cross-section and layout

Figure 6.16. Flight deck (cockpit) layout – military aircraft

Figure 6.17. USAF F18 details showing internal structural layout and armament load

Chart 6.2. Phase I, conceptual study: methodology to freezing military aircraft configuration

6.12 Worked-Out Example – Configuring Military Advanced Jet Trainer

This extended section of the book can be found on the Web at www.cambridge.org/Kundu and presents details of worked-out examples of the Advanced Jet

Trainer (AJT). The section is divided into subsections, with a step-by-step discussion of workflow. Associated figures and table are listed.

6.12.1 Use of Statistics in the Class of Military Trainer Aircraft

This extended subsection, on the Web at www.cambridge.org/Kundu, includes the following figures.

Figure 6.18. Military trainer aircraft – MTOM

Figure 6.19. Military trainer aircraft wing area and engine size

6.12.2 Worked-Out Example – Advanced Jet Trainer Aircraft (AJT) – Fuselage

This extended subsection, on the Web at www.cambridge.org/Kundu, includes the following figures and table.

Figure 6.20. AJT fuselage layout

Figure 6.21. AJT and its CAS variant

Table 6.3. Flap setting versus C_{Lmax}

6.12.3 Miscellaneous Considerations – Military Design

This subsection, on the Web at www.cambridge.org/Kundu, describes intake, exhaust, and CG position of the AJT.

6.13 Variant CAS Design

This extended section of the book can be found on the Web at www.cambridge.org/Kundu and develops presents details of a worked-out example of a VAS variant of the Advanced Jet Trainer. The section is divided into subsections, each with a step-by-step discussion of workflow, as shown below by their titles. Associated figures are listed.

6.13.1 Summary of the Worked-Out Military Aircraft Preliminary Details

This subsection, on the Web at www.cambridge.org/Kundu, summarizes in tabulated form the AJT and the CAS variant configurations and some resulting geometric and weights details.

7 Undercarriage

7.1 Overview

Chapter 6 illustrates how to arrive at a preliminary aircraft configuration of a new project starting from scratch, with the expectancy of satisfying the market specification. To progress further, the next task is to lay out the undercarriage (also known as the landing gear) position relative to the aircraft CG, which is accurately established in Chapter 8. This chapter addresses the undercarriage quite extensively but not the detailed design; rather, it focuses on those aspects related to undercarriage layout and sizing during the conceptual study phase. More details on undercarriage design are in the cited references.

This chapter first introduces the undercarriage to serve vehicle ground handling, followed by basic definitions, terminologies, and information used in the design process and integration with an aircraft. Finally, methodologies for layout of the undercarriage and tire sizing are presented to complete the aircraft configuration generated thus far. Considerable attention is required to lay out the undercarriage position and to determine tire size and geometric details to avoid hazards during operation. This book limits the topic to the fundamentals to the extent of the requirements for positioning the undercarriage and sizing the wheels and tires. These fundamentals are shown schematically in the three-view aircraft drawings. Relevant information on wheel tires is also presented in this chapter.

The undercarriage is a complex and heavy item and, therefore, expensive to manufacture. It should be made right the first time. Aircraft designers should know the operational basics, leaving the details to those who specialize in the undercarriage as a system that is integrated with an aircraft as a subsystem. Aircraft designers consult with undercarriage specialists during the conceptual stage.

The location of the aircraft CG is important in laying out the undercarriage. Initially, the CG position is guessed from statistics and past experience. Once the basics of the undercarriage are explained, Chapter 8 addresses aircraft weight estimation and CG location. An iterative assessment follows to revise the undercarriage positioning due to the differences, between the guessed and estimated CG location. The final iteration occurs after the aircraft is sized in Chapter 11.

The undercarriage, as a major component, creates a considerable amount of drag in its extended position during flight. Therefore, its retraction within the aircraft mould lines is necessary to minimize drag. Evolution shows that early designs of a tail-dragging type of undercarriage virtually disappeared and have been replaced by the nose-wheel tricycle type. It is interesting that the first nose wheel-design undercarriage appeared in 1908 on a Curtiss aircraft. The blowout of tires during takeoff and landing is dangerous; the Concorde crash due to a tire bursting is extremely rare but designers must learn from that situation.

In the past, aircraft manufacturers handled the undercarriage design in a vertically integrated factory setup. Today, its complexity has created specialized organizations (e.g., Messier of France and Dowty of the United Kingdom) that are dedicated to undercarriage design, thereby making its management and integration more efficient and resulting in better designs. However, for smaller aircraft in the class of club and private use, manufacturers can make their own undercarriages, and most of them are of the fixed type.

7.1.1 What Is to Be Learned?

This chapter covers the following topics:

- Section 7.2: Introduction to the undercarriage as a system and its functions
- Section 7.3: Types of undercarriage
- Section 7.4: Undercarriage layout relative to the CG, nomenclature, and definitions
- Section 7.5: Undercarriage retraction and stowage issues
- Section 7.6: Undercarriage design drivers and considerations
- Section 7.7: Undercarriage performance on the ground – turning of an aircraft
- Section 7.8: Types of wheel arrangements
- Section 7.9: Load on wheels, shock absorber, and deflection
- Section 7.10: Runway pavement types
- Section 7.11: Tire nomenclature, designation, and types
- Section 7.12: Tire friction with ground, rolling, and braking coefficients
- Section 7.13: Undercarriage layout methodologies
- Section 7.14: Worked-out examples
- Section 7.15: Miscellaneous considerations
- Section 7.16: Undercarriage and tire data

7.1.2 Coursework Content

Readers will make a comprehensive layout of the nose wheel-type tricycle undercarriage and position it to fit the aircraft configured in Chapter 6. The first task is to ensure that the layout is safe and satisfies all of its functionality. The wheel and tire are then sized to complete the layout. This section requires computational work when the aircraft CG position is still unknown. The author recommends that readers prepare spreadsheets for repeated calculations because iterations will ensue after the CG is established and the aircraft is sized.



Figure 7.1. Antonov 225 (Mriya) main undercarriage

7.2 Introduction

The undercarriage, also known as the landing gear, is an essential aircraft component for the following functions: (1) support the aircraft when in place or towed, (2) taxi and steer on the ground using an aircraft's own power, (3) the takeoff run, and (4) landing and braking on the runway. For these reasons, the author prefers the term *undercarriage* rather than *landing gear* because the functions encompass more than mere landings. Once an aircraft is airborne, the undercarriage becomes redundant – an appendage that causes drag that can be minimized through retraction.

The undercarriage is seen as a subsystem consisting of a strong support spindle (i.e., strut) with a heavy-duty shock absorber to tackle heavy landings due to a rapid descent, whether inadvertently or on the short runway length of an aircraft-carrier ship. The undercarriage has a steering mechanism with *shimmy control* (i.e., control of dynamic instability; wheel oscillation about the support shaft and strut axis). The wheels have heavy-duty brakes that cause the temperature to reach high levels, resulting in a potential fire hazard. Heavy braking requires heavy-duty tires, which wear out quickly and are frequently replaced with new ones. Most undercarriages are designed to retract; the longer ones have articulated folding kinematics at retraction. The undercarriage retraction mechanism has hydraulic actuation; smaller aircraft may get by with an electrical motor drive.

The undercarriage is a complex system – the main undercarriage of the world's largest aircraft (i.e., Antonov 225) is shown in [Figure 7.1](#) (note the relative size of the people in the photograph). It is a bogey system (see [Section 7.3](#)) carrying 7 struts (i.e., support shafts with shock absorbers) per side, each carrying 2 wheels for a total of 32 wheels when the 4 nose wheels are added ($2 \times 2 \times 7 + 4 = 32$).

The undercarriage stowage bay within the aircraft is compactly sized to the extent that articulation allows. The stowage bay is located in the wing and/or the fuselage, or sometimes in the wing-mounted nacelles, depending on the realistic details of the design considered by aircraft designers at the conceptual stage. It is a challenging task for structural designers to establish a satisfactory design that integrates all the relationships and functionality of the undercarriage with the airframe. The author recommends keeping the undercarriage layout design as simple as possible for better reliability and maintainability without using too much of the articulation and/or stowage space in an aircraft. [Reference 7.4](#) provides more details.

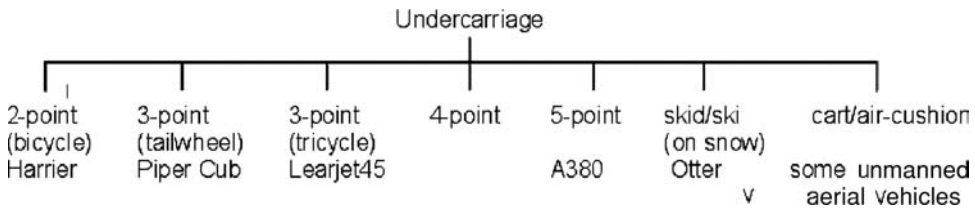


Chart 7.1. Undercarriage types (land-based)

A large aircraft is heavy enough to damage a metal runway; therefore, its weight is distributed over many wheels on a bogey system, which itself has articulation for retraction. The undercarriage mass can encompass as much as 7% (typically 4 to 5%) of the MTOM for large aircraft, it can weigh up to 3 tons with a corresponding cost of up to 5% of the aircraft total price, and the drag can be 10 to 20% of the total aircraft drag, depending on the size – smaller aircraft have a higher percentage of drag. For small, low-speed aircraft with a low-cost fixed undercarriage without a streamlined shroud, the drag could be as high as nearly a third of the total aircraft drag.

The undercarriage design should be based on the most critical configuration in the family of derivative aircraft offered. Generally, it is the longest one and therefore the heaviest, requiring the longest strut to clear the aft fuselage at maximum rotation. For the smaller version of the family, minor modifications assist in weight savings, yet retain a considerable amount of component commonality that reduces cost. In general, tires are the same size for all variants.

Other special types of undercarriages are not addressed herein. Today, all “flying boats” are amphibians with a retractable undercarriage. Undercarriage types are classified in the next section. [Section 7.15](#) provides statistics. The Harrier VTOL/STOL and B52 aircraft have a bicycle-type undercarriage. These are difficult decisions for designers because there are no easier options other than the bicycle type, which requires an outrigger support wheel to prevent the wing from tipping at the sides. Aircraft with skids are intended for application on snow (the skids are mounted on or replace the wheels) or for gliders operating on grass fields. Some “tail-draggers” get by with using a skid instead of a tail wheel. Special designs use takeoff carts to get airborne; however, landing is another matter.

7.3 Types of Undercarriage

The undercarriage has an attachment point to the aircraft and can have more than one strut (i.e., support point). [Chart 7.1](#) classifies various types in an elementary way, as if each support point has one strut with one wheel, with designations similar to a common bicycle. For example, the Airbus 380 aircraft has five support points (i.e., one nose wheel, two fuselage-mounted wheels, and two wing-mounted wheels) (see [Figure 7.11](#)) and many wheels and struts.

A nose wheel-type tricycle undercarriage is, by far, the dominant type, which is the type addressed in this book. The tail wheel type (i.e., fixed undercarriage) causes less drag, which can increase aircraft speed by 2 to 3%. However, on the ground, the raised nose impairs forward visibility and is more prone to “ground looping”

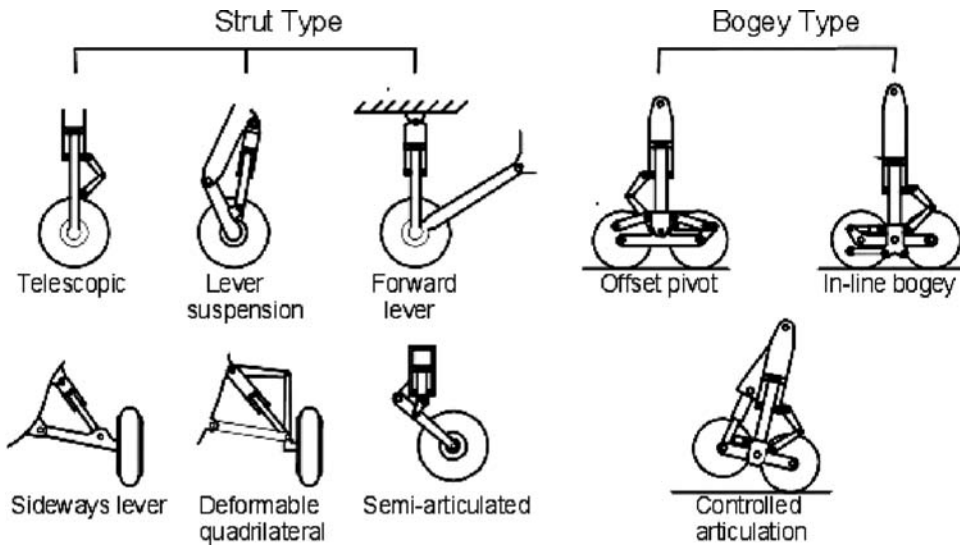


Figure 7.2. Undercarriage strut and bogey types

(described in Section 7.7). Currently, tail wheels are adapted for some lighter aircraft.

The simplest form of undercarriage was the earliest rigid axle type not in use any longer. Some form of shock absorber is favored nowadays. Struts with shock absorbers also are designed in many variations, as shown in Figure 7.2. When one strut has more than one wheel, it is seen as a bogey, as shown in the figure. There is a range of bogey designs not included in the figure.

7.4 Undercarriage Layout, Nomenclature, and Definitions

The position of the aircraft CG is a most important consideration when laying out wheel locations relative to an aircraft. Basically, the undercarriage consists of wheels on struts attached to aircraft points. The geometric parameters in placing wheels relative to the aircraft CG position are shown in Figure 7.3, along with the basic nomenclature of related parameters. The geometric definitions are as follows:

Wheel Base: The distance between the front and rear wheel axles in the vertical plane of symmetry

Wheel Tread or Wheel Track: The distance between the main wheels in the lateral plane of the aircraft

The wheel base and wheel track determine the aircraft turning radius (see Section 7.7) on the ground. The forwardmost aircraft CG position relative to the wheel base and wheel track determines the aircraft over-turn characteristics. The *over-turn angle*, θ , is the maximum angle for a tilted aircraft with the CG on top of a main wheel; beyond that, the aircraft would turn over on its side. Determination of the angle θ is shown in Figure 7.3. Over-turn tipping is not exactly around the X-axis (i.e., sideways) when a low-wing aircraft could have a wing tip touching the ground before θ is reached. The tipping occurs about the axis joining the nose-wheel and main-wheel ground contact point, when the wing LE is likely to hit the ground.

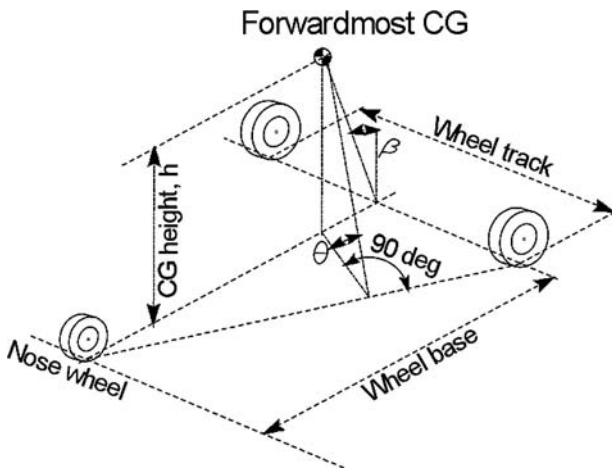


Figure 7.3. Aircraft CG position relative to the undercarriage layout

It is better to maintain a lower angle θ to avoid an aircraft turning over; the value depends on the airfield surface, and the tendency increases with higher sideways ground friction. For simplification yet still representative, typical values used in this book follow (see the references for more details). For a paved runway, keep the angle θ less than 60 deg; for an unprepared field, it should be less than 50 deg. There are aircraft with $\theta = 35$. Most of the aircraft have a θ between 40 and 50 deg.

An aircraft also can tip backwards if its rearmost CG goes behind the main wheel of a tricycle-type undercarriage; it can tip forward if its CG is in front of the main wheels of a tail-wheeled aircraft (Figure 7.4).

Definitions of the related parameters concerning wheel and strut provided in Figure 7.5 are more pertinent to the nose wheel ahead of the aircraft CG. These are not critical items at the conceptual design phase and can be omitted from the coursework. In the industry, these parameters are considered at an early stage.

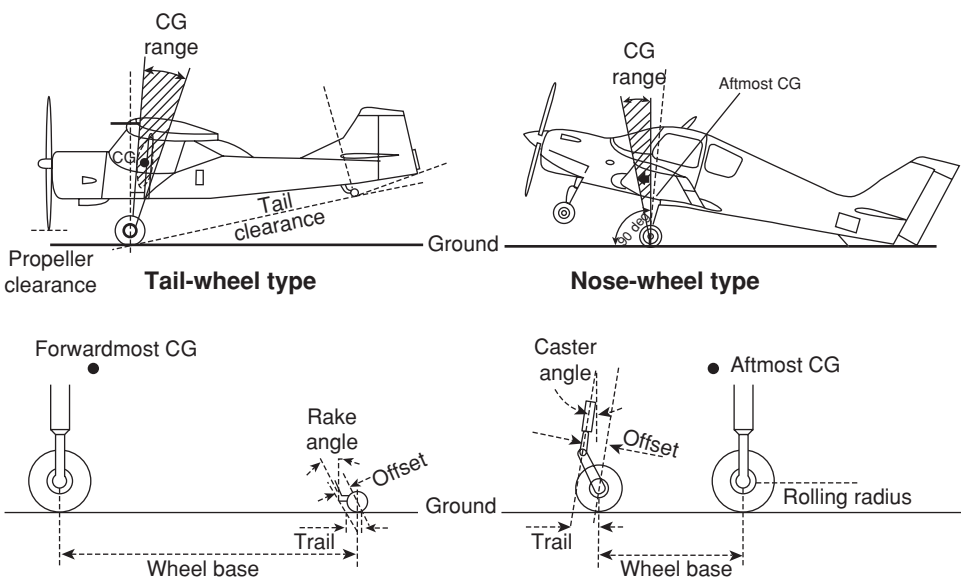


Figure 7.4. Undercarriage layout and nomenclature

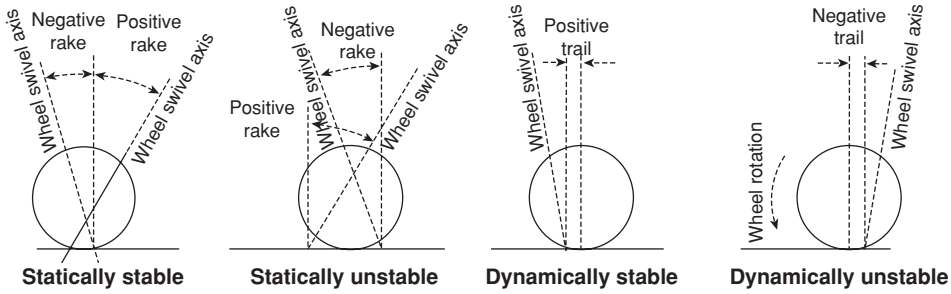


Figure 7.5. Signs for rake angle and trail angle

1. *Caster or Rake Angle*. Angle between the spindle axis and the vertical line from the ground contact point of the swivel axis.
2. *Caster Length*. Perpendicular distance from wheel contact point to ground and spindle axis.
3. *Trail*. Distance from wheel contact point to ground and spindle-axis contact point to ground.
4. *Offset*. Perpendicular distance from wheel axis and spindle axis.
5. *Loaded Radius*. Distance from wheel axis to ground contact point under static loading.
6. *Rolling Radius*. Distance from wheel axis to ground contact point under dynamic loading.

Wheel alignment and wheel camber (i.e., the tilt from being vertical) are important issues for wheel positioning, which can be omitted from the coursework preliminary aircraft layout.

7.5 Undercarriage Retraction and Stowage

Retraction is required for aircraft operating at more than 150 to 200 knots. A rapid increase in drag starts building up for speeds of more than 150 knots. There are basically three situations, as shown in Figure 7.6:

1. *No Retraction*. The fixed undercarriage is primarily for smaller aircraft or larger aircraft that have a high wing and are operating at low speed (e.g., the Twin Otter and the Shorts 330).
2. *Partial Retraction (Kneeling Position)*. A large wheel bogey with restricted stowage space would have to sacrifice full retraction; however, partial retraction helps considerably to reduce drag.
3. *Full Retraction*. Stowage space must be provided for a wheel bogey (i.e., for higher-speed aircraft).

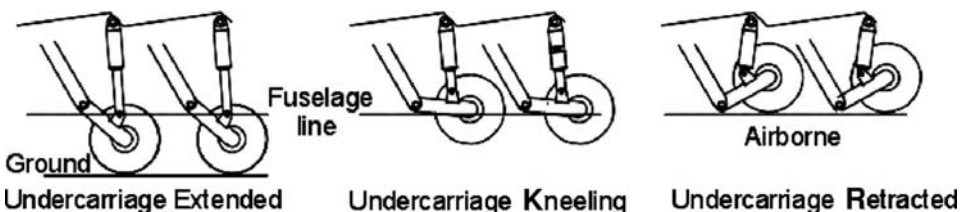


Figure 7.6. Types of undercarriage retraction

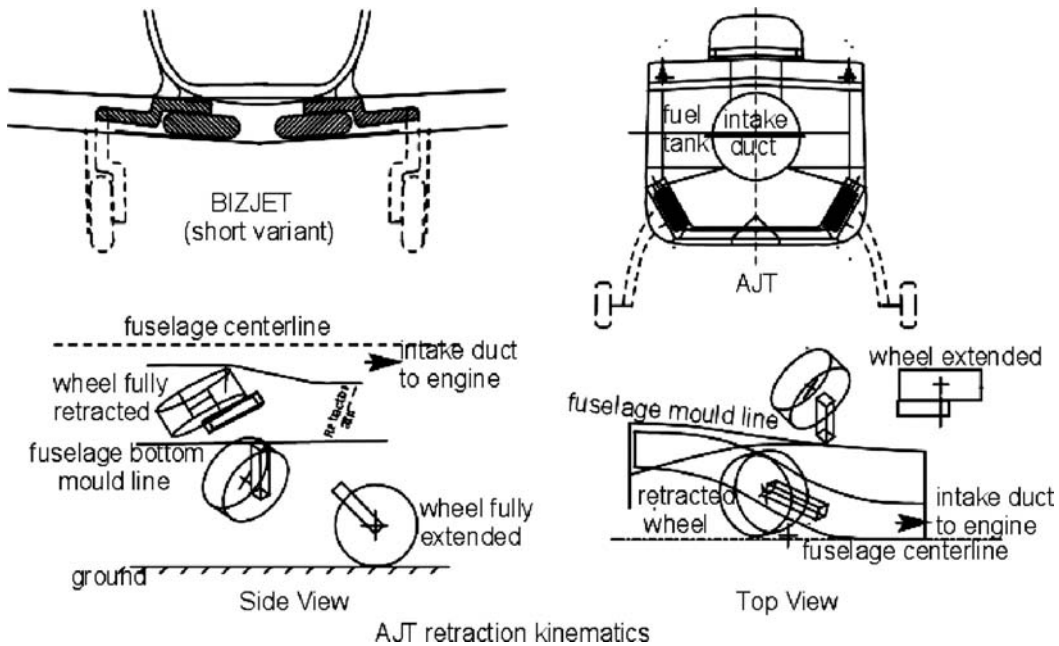


Figure 7.7. Undercarriage stowage space and retraction

Provision for stowage must be made early in the conceptual design phase. Only the space provision, after consultation with structural and undercarriage designers, is sufficient at this early stage of the project. Typical extended and retracted positions of civil and military type aircraft are shown in Figure 7.7. Following are areas where the undercarriage can be stowed:

1. *In the Wing.* If wing thickness is sufficient, then a maximum of twin wheels can be retracted. Provision for the wing recess is made as early as possible in the design phase. For a thinner wing, if the strut is mounted on the wing, it can go through the wing recess and the wheel to reach the fuselage stowage space (e.g., Learjet 45; although it has a single wheel, the wing thickness does not have sufficient space).
2. *In the Fuselage.* This is the dominant pattern for a large undercarriage because the fuselage underbelly could provide generous stowage space. If not, then it can be kept outside encased by a fairing that appears as a bulge (e.g., Antonov 225). For fighter aircraft with a very thin wing, the entire undercarriage is mounted on and retracted within the fuselage (e.g., the F104). The coursework example is a high-wing aircraft (see Figure 7.7) and the undercarriage is stowed in the fuselage.
3. *In an under-the-Wing Nacelle.* High-wing turboprop aircraft have a long strut; therefore, stowing the undercarriage in the nacelle (see Figure 10.19) slung under the wing reduces the strut length (e.g., the Fokker27 and Saab340).

Once the gear is extended, it must be locked to avoid an inadvertent collapse. A schematic retraction path of an AJT also is shown in Figure 7.7. Retraction kinematics is not addressed in this book. It is assumed that during the conceptual design phase, designers have succeeded in retraction within the stowage space provided by

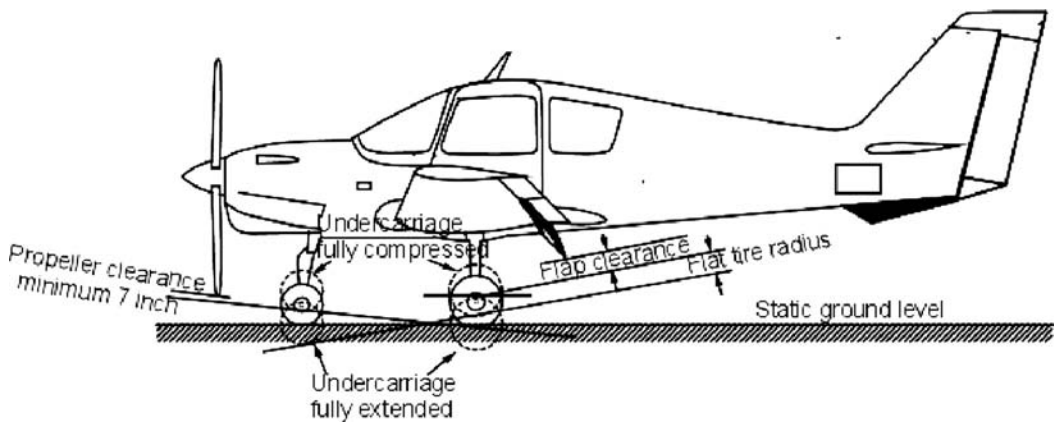


Figure 7.8. Three possible wheel positions

the aircraft engineers. See the references for more details on undercarriage retraction kinematics.

7.5.1 Stowage Space Clearances

A tire expands as the fabric stretches during service. It also expands on account of heat generated during ground operations. It keeps spinning (further enlargement occurs due to centrifugal force of spinning) within the stowage space immediately after retraction. Stowage space within an aircraft should be of the minimum volume occupied by the retracted undercarriage with some clearance to avoid any interference that may occur. Enough cavity space should be inside the aircraft structure to accommodate tire expansions. Stowage space is dictated by the articulated mechanism for retraction from its unloaded free position. Semi-empirical relations govern the clearance gap to accommodate retraction. As mentioned previously, this book assumes that aircraft designers are in a position to offer proper stowage space with adequate clearances. This book does not discuss stowage-space computation. For thin-wing combat aircraft, stowage must be within the tightly packed fuselage, where space is limited.

Unless there is a breakthrough innovation (typically associated with unconventional new designs beyond the scope of this book) on retraction kinematics, the state-of-the-art undercarriage design has been established to maximize compactness. This book addresses articulation in its simplest form. The author recommends using CAD animation to check retraction kinematics and storage space during the second-term coursework.

7.6 Undercarriage Design Drivers and Considerations

There are three wheel positions, as shown in [Figure 7.8](#). The application logic for the various types of aircraft is the same. The three positions are as follows:

1. *Normal Position*. This is when the aircraft is on the ground and the undercarriage carries the aircraft weight with tires deflected and the spring compressed.

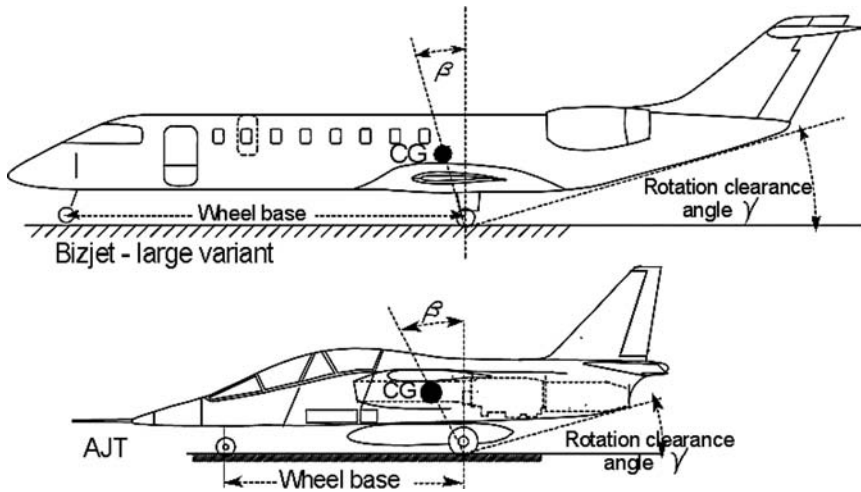


Figure 7.9. Positioning of main wheels and strut length

2. *Free Position.* When an aircraft is airborne, the undercarriage spring is then relieved of aircraft weight and extends to its free position at its maximum length. Stowage space is based on the undercarriage in a free but articulated position.
3. *Failed/Collapsed Position.* This is the abnormal case when the spring/oleo collapsed as a result of structural failure, as well as tires deflated with loss of air pressure. This is the minimum undercarriage length.

The failed position of the aircraft on the ground is the most critical design driver in determining the normal length of the undercarriage strut. Following are design considerations for the failed positions:

1. *Nose Wheel Failed.* The nose will drop down and the length of the collapsed nose wheel should still prevent the propeller from hitting the ground with adequate clearance.
2. *Main Wheel Failed.* There are two scenarios:
 - (a) When one side fails, the wing tilts to one side and it must not touch the ground.
 - (b) If both sides collapse (the most critical situation is when the aircraft rotates for liftoff at the end of the takeoff ground run), it must be ensured that the fully extended flap trailing edges have adequate ground clearance.

Figure 7.9 depicts an important design consideration for fuselage clearance angle γ , at aircraft rotation for liftoff, when the CG should not go behind the wheel contact point. Both civil and military aircraft types are shown in the figure. The angle β is the angle between the vertical and the line joining the wheel contact point with the ground and the aircraft CG. Ensure that β is greater than γ ; otherwise, the CG position will go behind the wheel contact point. Keep β greater than or equal to 15 deg. The fuselage clearance angle, γ , must be between 12 and 16 deg to reach C_{Lmax} at aircraft rotation. The fuselage upswEEP angle for clearance is discussed in Section 4.7.3 and it is revised here after the undercarriage layout is completed. Figure 7.9 corresponds to the worked-out examples.

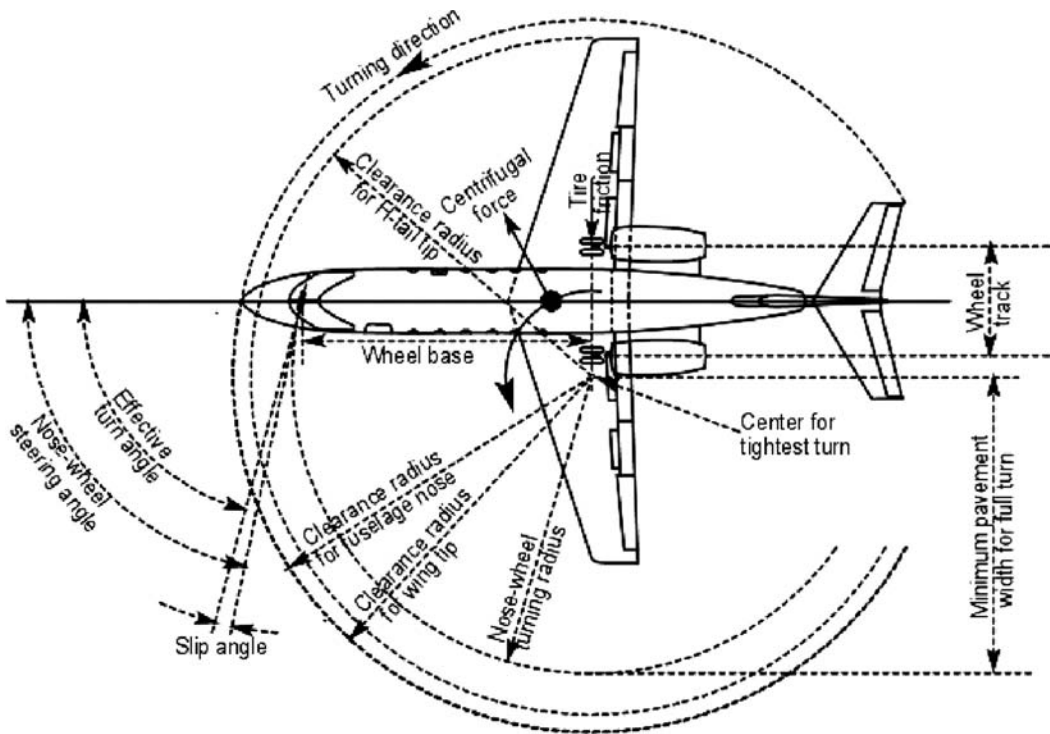


Figure 7.10. Aircraft turn

7.7 Turning of an Aircraft

Aircraft designers must ensure that an aircraft can turn in the specified radius within the runway width (Figure 7.10). Turning is achieved by steering the nose wheel (i.e., the maximum nose wheel turn is ≈ 78 deg) activated by the pilot's foot pedal. There is a slip angle and the effective turn would be approximately 75 deg. Pressing the left pedal would steer the nose wheel to the left and vice versa. The tightest turn is achieved when asymmetric braking and thrust (for a multiengine aircraft) are applied. The braked wheel remains nearly stationary. The center of the turn is slightly away from the braked wheel (see Figure 7.10) and the steered nose wheel guides the turn. The radius of the turn is the distance between the nose wheel and the center of the turn. Checks must be made to verify that the aircraft nose, outer wing tip, and outer H-tail tip are cleared from any obstruction. If the inner wheel were not braked, the turning radius would be higher. Turning is associated with the centrifugal force at the CG and side force at the turning wheels.

A tail wheel aircraft turning poses a special problem for “ground looping,” particularly when the aircraft is still at speed after landing. If the tail of the aircraft swings out more than necessary in an attempt to keep the aircraft straight using pedal-induced turns, then the centrifugal force of the turn could throw the aircraft rear end outward to the point where the forward-momentum component could move outside the wheel track. This results in instability with an uncontrolled ground loop, which can tilt the aircraft to the point of tipping if the over-turn angle θ is breached.

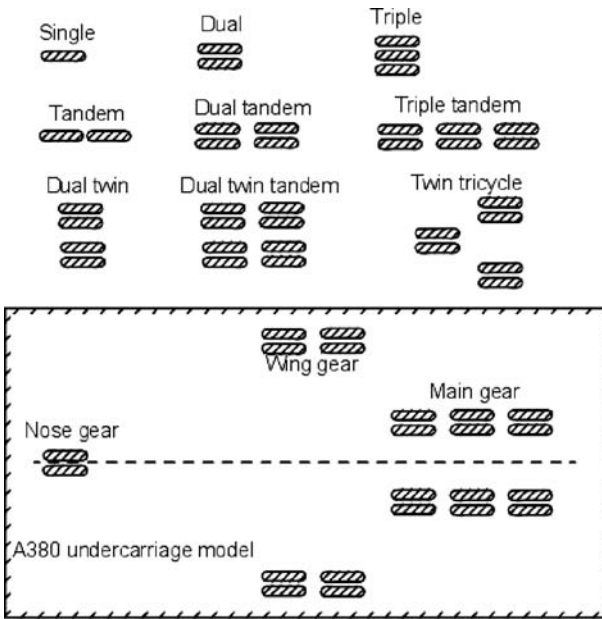


Figure 7.11. Wheel arrangements

7.8 Wheels

As an aircraft weight increases, the runway must bear the reaction and retain integrity to keep the vehicle's field performance safe. Heavy commercial transport aircraft are intended to operate from a prepared runway (i.e., Types 2 and 3; see [Section 7.10](#)) to stay within the pavement strength; the load per wheel is restricted by distributing the total over several wheels. Various arrangements for more than one wheel per strut style are shown in [Figure 7.11](#). Aircraft and undercarriage designers must plan for the number of struts, number of wheels per strut, and tire spacing and pressure (which determine the size) to distribute the load. As the aircraft MTOM increases, so does the number of wheels required, as well as considerations for stowing and articulation for retraction.

The fundamental wheel arrangements are single, twin, triple, and quadruple on a bogey. Wheel arrangements higher than a quadruple are not seen. The next level is their placement in a dual row as a single tandem, twin tandem (i.e., four wheels), triple tandem (i.e., six wheels), and so forth. The A380 wheel-arrangement model is shown in [Figure 7.11](#). [Figure 7.1](#) shows the wheel bogey of the world's largest aircraft (i.e., the Antonov 225) with twin wheels per strut, for a total of seven struts.

7.9 Loads on Wheels and Shock Absorbers

In its elementary representation, the undercarriage system acts as a *spring-mass* system, shown in [Figure 7.12](#). Shock absorption is accomplished by its main spring and, to a smaller extent, by the tire pneumatics. Both spring and tire deflect under load. The oleo system acts as a damper; that is, it dissipates kinetic energy of vertical velocity. The strut can act as a spring for the lateral load of the ground friction.

The length of the strut is influenced by the extent that its shock absorber is compressed to the maximum. The minimum strut length is when both tire and shock

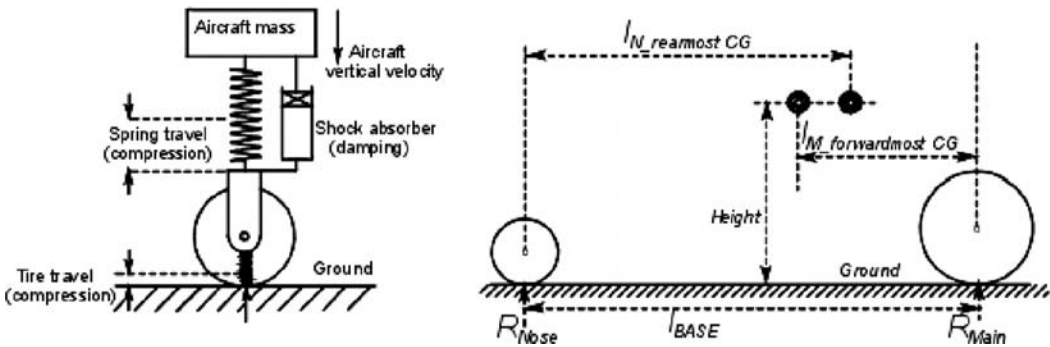


Figure 7.12. Undercarriage as a spring-mass system

absorber collapse simultaneously, yet provide sufficient ground clearance for flaps fully extended (see Figure 7.8). The most critical situation for flap clearance is when the main wheel has collapsed and the nose wheel is at the fully extended position. (In a practical situation, the nose wheel tire would also remain deflected under load, but the margin of the fully extended position is safer.) The flap trailing edge is at its lowest at aircraft rotation for liftoff. A simultaneous failure of the tire and shock absorber after decision speed V_1 (see Chapter 13) would force the pilot to continue with the aircraft rotation and liftoff.

During landing, as lift is depleting with speed reduction, more aircraft weight is reacting at the ground contact, which increases the spring load of the strut. The energy is stored in the spring. On brake application, the kinetic energy of the aircraft is absorbed by the brake pads, increasing temperature. If the limits are crossed with rapid deceleration, a fire hazard exists.

7.9.1 Load on Wheels

The load on the wheels determine the tire size. *Wheel load* is the aircraft weight distributed over the number of wheels. The aircraft CG position could vary depending on the extent of payload and fuel-load distribution; therefore, both the forwardmost and aftmost CG positions must be considered. (Table 7.4 provides an idea of the A380 load.)

As soon as the preliminary undercarriage information is known from the methodology described in this chapter, aircraft weights and the CG can be estimated through the formal procedure described Chapter 8.

Estimating the aftmost CG with the angle $\beta \approx 15$ coinciding with 40% of the MAC gives a preliminary idea of the main-wheel position relative to the wing. The wing position relative to the fuselage could change when the formal weight and CG estimations are determined after the wing is sized. In that case, the wheel-load calculation must be revised. For transport aircraft design, at this stage, the forwardmost CG is 20 to 25% of the MAC ahead of the aftmost CG. For the nontransport category, including combat aircraft design, at this stage the forwardmost CG is 15% of the MAC ahead of the aftmost CG. The MTOW rather than the MTOM is used in the computation because the load is a force. (A simplified approach is to divide the main- and nose-wheel loads as 90 and 10% distribution, which has a

reasonable result, but the author recommends making the formal estimation at the beginning.)

Linear distance is represented by l with associated subscripts; R represents reaction forces. For more than one wheel, the load would then be divided accordingly. The force balance gives:

$$MTOW = 2 \times R_{MAIN} + R_{NOSE} \quad (7.1)$$

To compute the maximum main-wheel load at the aftmost CG position, take the moment about the nose wheel. The moment equilibrium equation becomes:

$$\begin{aligned} l_{BASE} \times R_{MAIN} &= l_{N_REAR_CG} \times MTOW \\ \text{or } R_{MAIN} &= (l_{N_REAR_CG} \times MTOW) / l_{BASE} \end{aligned} \quad (7.2)$$

The load per strut on the main wheel is:

$$L_M = R_{MAIN} / \text{number of struts} \quad (7.3)$$

To compute the maximum nose-wheel load at the forwardmost CG position, take the moment about the main wheel. The moment equilibrium equation becomes:

$$\begin{aligned} l_{BASE} \times R_{NOSE} &= l_{M_FORWARD_CG} \times MTOW \\ \text{or } R_{NOSE} &= (l_{M_FORWARD_CG} \times MTOW) / l_{BASE} \end{aligned} \quad (7.4)$$

The nose wheel typically has one strut.

Ensure that the load at the nose gear is not too high (i.e., no more than 20% of the MTOW) to avoid a high elevator load to rotate the aircraft for liftoff at takeoff. Also, it must not be too low – that is, not less than 8% of the MTOW; otherwise, there could be steering problems.

For more than one wheel per strut, the load per tire is calculated based on what each tire would produce on the same runway pavement stress at the same tire pressure as a single wheel. This is the equivalent single wheel load (ESWL) because loads are not shared equally when arranged side by side, unlike tandem arrangements. Wheel arrangements determine the ESWL as given here based on statistical means. Readers may consult the references for more details on other types of wheel arrangements.

The tandem twin wheel is:

$$ESWL = \text{load per strut} / 2 \quad (7.5)$$

The side-by-side twin wheel is:

$$ESWL = \text{load per strut} / (1.5 \text{ to } 1.33) \text{ (this book uses } 1.5) \quad (7.6)$$

The tandem triple wheel is:

$$ESWL = \text{load per strut} / 3 \quad (7.7)$$

The side-by-side triple wheel is:

$$ESWL = \text{load per strut} / (1.5 \text{ to } 1.33) \text{ (this book uses } 1.5) \quad (7.8)$$

Table 7.1. *Vertical speed*

$V_{Vert.} = < 12$ fps – FAR 23 (semi-empirical formula for exact rate, $n_l = 3$)
$V_{Vert.} = < 12$ fps – FAR 25 ($n_l = 2$)
$V_{Vert.} = < 10$ fps – Military transport ($n_l = 2$)
$V_{Vert.} = < 13$ fps – Military trainer ($n_l = \text{maximum } 5$)
$V_{Vert.} = < 17$ fps – Military land-based combat aircraft ($n_l = \text{maximum } 6$)
$V_{Vert.} = < 22$ fps – Military naval (aircraft-carrier)-based combat aircraft ($n_l = 8$)

The twin tandem is

$$\text{ESWL} = \text{load per strut}/(3 \text{ to } 2.67) \quad (7.9)$$

The main-wheel loads are calculated based on the aftmost CG position and the nose-wheel loads are based on the forwardmost CG position. The dynamic load on the wheel is 50% higher than the static load.

7.9.2 Energy Absorbed

Both the tire and the shock absorber absorb the energy to cushion the impact of an aircraft's vertical descent rate at landing in order to maintain structural integrity and avoid the tire bottoming out. FAA safety requirements limit the vertical descent velocity, $V_{Vert.}$, for civil aircraft applications; military specifications limit military applications. Table 7.1 lists limits for various types of aircraft. In turn, $V_{Vert.}$ produces g -load at the sudden termination of $V_{Vert.}$ at landing – it can be expressed as load factor n (see Section 5.5). Equation 5.4 gives $n = (1 + a/g)$; it is loosely termed as the number of the g -load; for an undercarriage design, it is designated n_l (see Table 7.1). During landing, n_l takes a positive value; that is, it would experience heavier weight. For example,

$$n_l = x \text{ (a number) means that the weight has changed by } x \text{ times.} \quad (7.10)$$

These are extreme values for safety; in practice, 4 fps is a hard landing in a civil aircraft operation. The maximum landing aircraft mass M_L is taken as 0.95 MTOM for aircraft with a high wing-loading.

The vertical velocity kinetic energy to be absorbed is

$$E_{ab} = \frac{1}{2} M_L \times V_{Vert.}^2 \quad (7.11)$$

This is the energy to be absorbed by all the main wheels (m wheels) and struts (n struts) at touchdown during landing. The nose wheel touches the ground much later, after the main wheels have already absorbed the impact of landing.

$$E_{ab} = E_{ab_strut} + E_{ab_tire} \quad (7.12)$$

ENERGY ABSORPTION BY STRUT (Let n be the number of struts.)

Assume that a landing is even and all struts have equal deflection of δ_{strut} .

Then, energy absorbed by all the struts is

$$E_{ab_strut} = n \times n_l \times g M_L \times k_{strut} \times \delta_{strut}, \quad (7.13)$$

where k_{strut} is an efficiency factor representing the stiffness of the spring and has values between 0.5 and 0.8, depending on the type of shock absorber used.

In this book, 0.7 is used for modern aircraft and 0.5 is used for small club and homebuilt categories.

ENERGY ABSORPTION BY TIRE (Let m be the number of tires.)

Assume that a landing is even and all tires have equal deflection of δ_{tire} .

Then, energy absorbed by all the tires is

$$E_{ab_tire} = m \times n_l \times g M_L \times k_{\text{tire}} \times \delta_{\text{tire}} \quad (7.14)$$

where $k_{\text{tire}} = 0.47$ is an efficiency factor representing the stiffness of all types of tires.

The following can be written by equating Equation 7.11 with Equation 7.12 and then substituting Equations 7.13 and 7.14 in Equation 7.12 and replacing n_l by Equation 7.10. Here, the load factor n_l is replaced by x :

$$E_{ab} = \frac{1}{2} M_L \times V_{\text{vert}}^2 = n \times x \times g M_L \times k_{\text{strut}} \times \delta_{\text{strut}} + m \times x \times g M_L \times k_{\text{tire}} \times \delta_{\text{tire}}$$

Simplifying as follows:

$$\left(\frac{1}{2} \times V_{\text{vert}}^2\right)/g = x \times (n \times k_{\text{strut}} \times \delta_{\text{strut}} + m \times k_{\text{tire}} \times \delta_{\text{tire}}) \quad (7.15)$$

7.9.3 Deflection under Load

The total vertical deflection of the strut and tire during landing can be computed by using Equation 7.15. Other types of lateral strut deflection during turning and other maneuvers are not addressed in this book.

Total deflection is

$$\delta = \delta_{\text{strut}} + \delta_{\text{tire}} \quad (7.16)$$

It is recommended that a cushion be kept in the strut deflection (compression) so that ends do not hit each other. In general, 1 inch (2.54 cm) is the margin.

7.10 Runway Pavement Classification

The undercarriage design depends on how the wheels interact with the airfield surface. An airport runway surface must be designed to withstand an aircraft's weight not only at the static condition but also at dynamic loading (e.g., for a heavy landing). Runway pavement loading is known as *flotation*. Among airports, the runway pavement strength varies. There are three main types of surfaces, as follows:

1. *Type 1: Unprepared Surface.* A grass field or a gravel field, for example, is designated as a Type 1 surface. These are soft runways that are prone to depressions under a heavy load. Low-pressure tires with a maximum 45 to 60 lb per square inch (psi) and a total ESWL load less than 10,000 lb are the limits of operation on a soft runway. The ground friction is the highest and these airfields are not necessarily long. This type of runway is the least expensive to prepare and they serve remote areas, as an additional airfield close to a business center, or as a private airfield. Small utility aircraft can operate from Type 1 airfields.

Table 7.2. Load classification group

LCN range	LCG	LCN range	LCG	LCN range	LGG
101 to 120	I	31 to 50	IV	11 to 15	VI
76 to 100	II	16 to 30	V	10 and below	VII
51 to 75	III				

2. *Type 2: Prepared Macadam Surface.* These are asphalt- or tar-topped runways with strength built in by the thick macadam filler; these are designated as a Type 2 surface. These surfaces are less expensive to prepare by using a heavily rolled macadam filler. However, local depressions can cause the surface to undulate, and it requires frequent maintenance with longer downtime. This type of runway can accommodate heavy aircraft such as the B747.
3. *Type 3: Prepared Concrete Surface.* This is a rigid concrete runway designated as a Type 3 surface. These runways are built with pavement-quality concrete (i.e., about a half-meter thick) and are covered by asphalt (e.g., 150 mm thick). All major international airports have Type 3 runways, which can take a load similar to a Type 2 surface and do not have to be as thick. This type is expensive to prepare and maintenance downtime is minimal. Cracks are the typical type of failure that occurs. A Type 3 surface can accommodate heavy aircraft such as the B747 and the A380.

Aircraft designers must design aircraft to be compatible with existing airfields in order to operate. If the market demand necessitates larger and heavier aircraft, then designers must make the aircraft comply with the pavement strength of existing airfields or the airfield must be reinforced to accept the heavy aircraft. Runway reinforcement depends on new designs; therefore, airport authorities communicate with aircraft manufacturers to remain current with market demand. When the B747 began operating, almost all international airfields needed reinforcement to accept them – some were not operational for several years.

7.10.1 Load Classification Number Method

The ICAO, as an international agency, established ground rules to match aircraft and runway performance requirements. The ICAO developed the strength classifications of Type 2 and Type 3 runways by designating a load classification number (LCN) that represents the extent of load that a runway can accommodate based on construction characteristics. All Type 2 and Type 3 runways must have a LCN and the aircraft undercarriage design must comply with it. The LCN range of the airfield's type is grouped under the load classification group (LCG). For example, an aircraft with the LCN 62 can operate on any airfield with an LCG of I to III. [Table 7.2](#) provides the LCN range for the types of runways.

The relationship among the LCN, tire pressure, and ESWL is presented in [Figure 7.13](#). The procedure is to first obtain the LCN of the airfield in question. Then, compute the ESWL of the undercarriage (see [Section 7.9](#)). Finally, find the tire pressure required using [Table 7.6](#) (see [Section 7.11](#)); this provides a guideline to choose tire size. [Section 7.13](#) outlines the methodology followed by worked-out

Table 7.3. Aircraft weight to comply with LCN and corresponding tire pressure

Aircraft	MTOM (lb)	Tire pressure (psi)	LCN
Fokker F27	45,000	80	19
McDonnell DC-9	65,000	129	39
B737-200	110,000	162	49
B757	210,000	157	50
B707	300,000	180	80

examples (see the references for more details on other types). Typical examples of aircraft complying with the LCN and the corresponding MTOM and tire pressures are given in Table 7.3.

The B757, which is twice as heavy as the B737, maintains nearly the same LCN by having more wheels to distribute load per tire.

7.10.2 Aircraft Classification Number and Pavement Classification Number Method

The LCN is airfield-specific and aircraft must comply with it. Subsequently, ICAO introduced a new classification system, known as the aircraft classification number (ACN), which represents the tire-loading limit, and another system that represents the airfield pavement-strength limit, known as the pavement classification number (PCN). Both numbers must be the same to operate at an airport without any restrictions. However, the LCN method is still in use and conversion is needed to use the ACN/PCN method. This book uses Figure 7.13 to obtain the LCN.

The ACN/PCN method is described in [9]. According to the design manual, the ACN/PCN method is intended only for publication of pavement-strength data in the Aeronautical Information Publication (AIP). It is not intended for design or

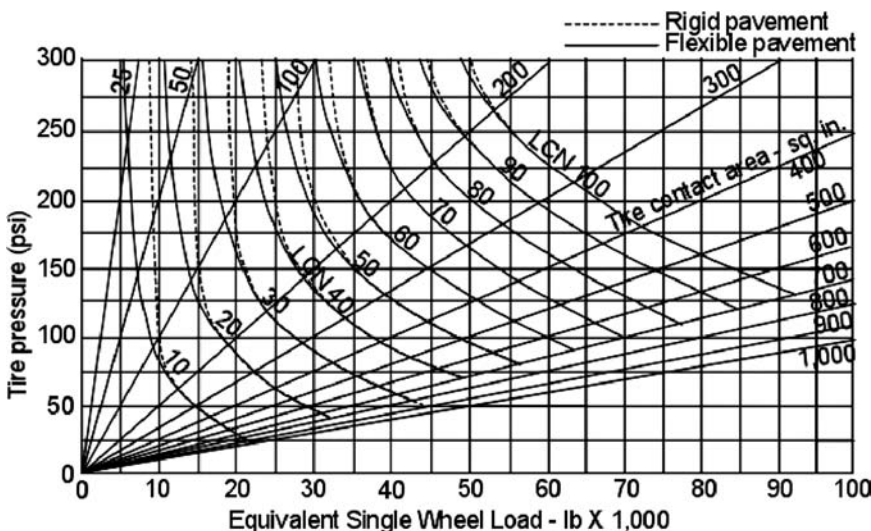


Figure 7.13. Equivalent single-wheel load versus LCN

Table 7.4. A380 Data

Maximum Ramp Weight = 592,000 kg (1,305,125 lb)

Maximum Landing Weight = 427,000 kg (941,365 lb)

Zero Fuel Weight = 402,000 kg (886,250 lb)

Tire size and pressure	Maximum load per strut*	CG position
Nose-gear tire size = 1,400 × 530R23 40PR	77,100 kg (169,975 lb)	Forwardmost
Nose-gear tire pressure = 11.8 bar (171 psi)	(at 10 ft/s ² braking)	(at 36% MAC)
Wing-gear tire size = 56 × 22R24 40PR	112,500 kg (242,025 lb)	Aftmost
Wing-gear tire pressure = 13.6 bar (197 psi)		(at 42.8% MAC)
Body-gear tire size = 56 × 22R24 40PR	168,750 kg (372,025 lb)	Aftmost
Body-gear tire pressure = 13.6 bar (197 psi)		(at 42.9% MAC)

Note:

* Maximum load is at maximum ramp weight and at the limiting CG positions.

evaluation of pavements, nor does it contemplate the use of a specific method by the airport authority for either the design or evaluation of pavements. The ACN/PCN method is more elaborate and involved. Parameters like the California Bearing Ratio (CBR) for subgrade-strength soil tests are required to determine tire pressure. The LCN method is still in use and can be converted to the ACN and PCN. According to the AIP, “The ACN of an aircraft is numerically defined as two times the derived wheel load, where the derived single wheel load is expressed in thousands of kilograms.”

The author was able to locate the Airbus publication for the largest passenger-carrying aircraft, the A380–800F model; pertinent data are listed in Table 7.4. The weight per wheel is distributed relative to the wheel arrangement (see Figure 7.11). The braking deceleration is 10 ft/s². The horizontal ground load is calculated at a brake coefficient of 0.8. The main landing gears can take as much as 95.5% of the weight.

7.11 Tires

The pavement-loading (i.e., flotation) limit is one of the drivers for tire design. This section presents relevant information for preliminary tire sizing to establish the section width (W_G), height (H), and diameter (D), as shown in Figure 7.14. The rim diameter of the hub is designated d . Under load, the lower half deflects with the radius, R_{load} . The number of wheels and tire size is related to its load-bearing capacity for inflation pressure and the airfield LCN for an unrestricted operation. For heavy aircraft, the load is distributed over the number of wheel and tires. The FAA regulates tire standards.

Table 7.5. Tire types (tire aspect ratio H/W_G and tire lift ratio, D/d)

Size	11.00–12	6.50–10	22 × 5.5	22 × 7.7–12
Type	III	III	VII	VIII
Lift ratio	2.67	2.17	1.81	1.83
Aspect ratio	0.90	0.91	0.89	0.67

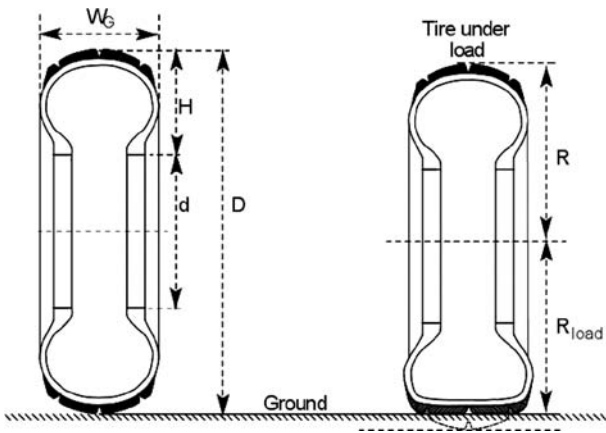


Figure 7.14. Tire designations

Tires are rated based on (1) unloaded inflation pressure, (2) ply ratings for holding shape under pressure, (3) maximum static load for the MTOW (i.e., flotation consideration), and (4) maximum aircraft speed on the ground. Basically, there are mainly three types of tires from nine categories, as described herein. (See the Michelin and Goodyear data sourcebooks listed in the references.)

Types I and II: These types are becoming obsolete and are no longer produced.

Type I is intended for a fixed undercarriage.

Type III: This type includes *low-pressure tires* that provide a larger footprint or flotation effect. They have a relatively small rim diameter (d) compared to overall tire diameter. Speed is limited to less than 160 mph. The tire designation is expressed by its section width, W_G , and rim diameter, d (Figure 7.14). All dimensions are in inches. For example, a typical small-aircraft tire designation of 6.00–6 means that it has a width of 6.00 inches (in hundredths) and a rim diameter hub of 6 inches.

Types IV, V, and VI: These types no longer exist.

Type VII: These are high-pressure tires that are relatively narrower than other types. They are widely used in aircraft with pressure levels from 100 to more than 250 psi that operate on Type 2 and Type 3 airfields. Military-aircraft tire pressure can reach as high as 400 psi. Tire designation is expressed by the overall section diameter (D) and the nominal section width, W_G , with the multiplication sign (\times) in between. All dimensions are in inches. For example, 22×5.5 has an overall section diameter of 22 inches and a section width of 5.5 inches.

New Design Tire (three-part nomenclature): Except for Type III tires, all newly designed tires are in this classification. A Type VIII tire also has this designation. This type uses a three-part designation shown as (outside diameter, D) \times (section width, W_G) – (rim diameter, d). These are also known as biased tires, which are intended for high-speed aircraft with high tire-inflation pressures. Dimensions in FPS are in inches and dimensions in SI are in millimeters but the rim diameter is always in inches. For example, a B747 tire has the designation, $49 \times 19.0-20$, meaning that it has an outside diameter of 49 inches, a section width of 19 inches, and a rim diameter of 20 inches. New

Table 7.6. *Tire pressure*

Weight in lb (kg)	Pressure in psi (kg/cm ²)*	Typical tire size (main wheel)**
<3,000 (1,360)	≈50 (3.52)	500–5, 600–6
≈5,000 (2,268)	≈25 to 50 (1.76 to 3.52)	600–6, 700–7, H22 × 8.25–10
≈10,000 (4,990)	≈25 to 90 (1.76 to 6.33)	750–6, 850–6, 900–6, 22 × 5
≈20,000 (9,072)	≈45 to 240 (3.16 to 16.87)	850–10, 24 × 7.7, 22 × 6.6
≈50,000 (22,680)	≈60 to 240 (4.22 to 16.87)	26 × 6.6, 30 × 7.7, 32 × 7.7, 34 × 9.9
≈100,000 (49,900)	≈75 to 240 (5.27 to 16.87)	34 × 11, 40 × 12, 15.50 × 20
≈200,000 (90,720)	≈100 to 240 (7.03 to 16.87)	44 × 16, 17.00 × 20, 50 × 20
≈300,000 (136,080)	≈110 to 240 (7.73 to 16.87)	50 × 20, 20.00 × 20
>500,000 (226,800)	≈150 to 250	

Notes:

* Depends on number of wheels.

** See Appendix E for more options. Also consult *Jane's* manual.

tires also have radial types; the three-part designation has an “R” instead of a hyphen. An example of a radial tire in SI is 1400 × 530 R 23. There is a special designation that precedes the three-part nomenclature tires with a B, C, or H. The description of these construction details is beyond the scope of this book.

There are small tires not approved by the FAA that are used in the homebuilt aircraft category. This book addresses only Types III and VII and the New Design Tire.

Several tire manufacturers are available from which to choose, as in the case of the automobile industry. Tire manufacturers (e.g., Goodyear, Goodrich, Dunlop, and Michelin) publish tire catalogs, which provide important tire data (e.g., dimensions and characteristics) in extensive detail. Appendix E lists data from the manufacturers' catalogs needed for the coursework in this book. Aircraft designers have the full range of tire catalogs and contact tire manufacturers to stay informed and benefit mutually from new tire designs.

Under load, a tire deflects and creates a footprint on the ground. Therefore:

$$\text{load on tire} = (\text{footprint} \times \text{tire pressure}) \quad (7.17)$$

For tire static deflection:

$$\begin{aligned} \delta_{\text{tire}} &= (\text{maximum radius at no load}) - (\text{minimum radius under static load}) \\ &= D/2 - R_{\text{load}}, \end{aligned} \quad (7.18)$$

where R_{load} equals the radius of the depressed tire under load. It can be expressed as a percentage of the maximum radius.

Table 7.6 lists the typical tire pressures for the range of aircraft weights.

Under a typical static load, tire deflection is kept at a maximum of a third of the maximum height (H). As aircraft speed increases, the load also increases on tires as dynamic loading. During landing impact, the deflection would be higher and would recover sooner, with the tire acting as a shock absorber. Bottom-out occurs at maximum deflection (i.e., three times the load); therefore, shock absorbers take the

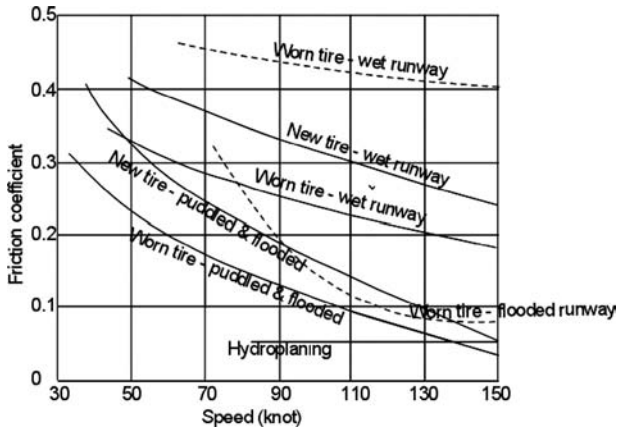


Figure 7.15. Ground friction coefficient

impact deflection to prevent a tire from bottoming-out. Section 7.9 discusses tire-deflection calculations; corresponding typical tire pressures for the sizes are given in Table 7.6.

Tire sizing is a complex process and depends on the static and dynamic loads it must sustain. This book addresses tire sizing for Type 2 and Type 3 runways. One of the largest tires used by the B747–200F has a main and nose gear tire size of $49 \times 19-20$ with an unloaded inflation pressure of 195 psi. Sizes used by existing designs of a class are a good guideline for selecting tire size.

Use of an unprepared runway (i.e., Type 1) demands a low-pressure tire; higher pressure tires are for a metal runway (i.e., Types 2 and 3). The higher the pressure, the smaller is the tire size. Civil aircraft examples in this book use a Type 3 airfield; military aircraft examples use Types 2 and 3 airfields. Small aircraft use a Type 1 airfield for club usage.

7.12 Tire Friction with Ground: Rolling and Braking Friction Coefficient

Ground movement would experience friction between the tire and the ground. During the takeoff run, this friction is considered drag that consumes engine power. Figure 7.15 is a representation of the ground-rolling friction coefficient, μ , versus aircraft speed for various types of runways. Conceptual studies use the value for the friction coefficient, μ .

- A Type 3 runway (concrete pavement) = 0.02 to 0.025 (0.025 is recommended for coursework)
- A Type 2 runway = 0.025 to 0.04 (0.03 is recommended for coursework)
- A Type 1 runway = 0.04 to 0.3, depending on the surface type, as follows:
 - hard turf = 0.04
 - grass field = 0.04 to 0.1 (0.05 is recommended for a maintained airfield)
 - soft ground = 0.1 to 0.3 (not addressed in this book)

The braking friction coefficient, μ_b , would be much higher depending on the runway surface condition (e.g., dry, wet, slush, or snow- or ice-covered) (Table 7.7). A typical value is $\mu_b \approx 0.5$. Locked wheels skid that wear out a tire to the point of a possible blowout. Most high-performance aircraft that touch down above 80 knots

Table 7.7. Average braking coefficient, μ_b

Aircraft speed (mph)	20	40	60	80	100
Dry concrete runway, μ_b	0.85	0.77	0.67	0.57	0.46
Wet concrete runway, μ_b	0.56	0.44	0.35	0.28	0.23
Iced runway	0.1 to 0.2	0.1 to 0.2	0.1 to 0.2	0.1 to 0.2	0.1 to 0.2

have an antiskid device when the μ_b value could be as high as 0.7. Slipping wheels are not considered during the conceptual study phase. Tire-tread selection should be compatible with the runway surface condition (e.g., to avoid hydroplaning). The braking friction coefficient, $\mu_b = 0.45$ to 0.5, is the average value used in this book. The tire load is based on a brake coefficient of 0.8.

7.13 Undercarriage Layout Methodology

After obtaining the necessary information available on the undercarriage as a system, the next step is to systematically lay down the methodology to configure the undercarriage arrangement in order to integrate it with the aircraft conceived in Chapter 6. All aircraft designers benefit from existing designs by having guidelines – this is what is meant by “experience”: past designs provide a good databank.

First, the undercarriage commonality for variant designs is considered. In general, in civil aircraft design, the baseline aircraft is the middle of the three main sizes (other variants are possible). Therefore, the largest version is more critical to the undercarriage layout for carrying the heaviest load. The methodology described herein should be applied to the largest of the variants and then all other variants should be checked for commonality. At the conceptual design stage, all versions have an identical undercarriage layout except for the wheel base and wheel track. A production version has the scope to shave off metal, making it lighter for smaller variants; this requires only minor changes in the manufacturing setup. Following is the stepwise approach for the undercarriage layout geometry, load estimation, and tire sizing:

1. Determine the type of undercarriage: nose wheel or tail wheel. For the reason explained in Section 7.3, it is a nose wheel type. Low-speed smaller aircraft sensitive to weight and drag could have a tail wheel type.
2. If the aircraft operating speed exceeds 150 knots, the undercarriage should be retractable.
3. Estimate from statistics and experience the CG position; it is suggested 20 to 40% of the wing MAC at about the fuselage centerline, depending on the wing position. Ensure that the CG angle β with the vertical is about 15 deg.
4. The main-wheel strut length should allow full rotation that clears the fuselage aft end, solves oleo-collapse problems, allows for full flap-deflection clearance, and makes a trade-off with the wheel track to prevent the aircraft from turning over. The fuselage clearance angle γ is between 12 and 16 deg, which should clear the fuselage aft end at the rotation when the oleo is fully extended at liftoff.

5. The nose wheel strut length should be relative to the main-wheel strut length in order to keep civil aircraft payload floorboards level (for a propeller-driven aircraft, ensure that there is propeller clearance at the nose-oleo collapse). Avoid making the strut length too long. The nose wheel attachment point ideally should be located ahead of the cockpit.
6. Determine that the wheel-track turn-over angle θ is less than the recommended value and satisfies the desired turn radius. A trade-off may be required but, in general, runway widths are wide enough. A wider wheel track is better but it should not be too wide, which would create turning and structural problems on the wing attachment.
7. Determine the stowage space; less articulation is simpler and requires less maintenance and lower cost. In general, civil aircraft articulation is simpler than the military aircraft type. Ensure that the storage space has adequate tire clearance. At this point, it is assumed that stowage space is available.
8. Compute the loads on each point of support and determine the number of wheels (see Section 7.9). Establish the operational airfield LCN. If an aircraft is to use a Type 1 airfield, it is better for the wheel load to be less than 10,000 lb; then, the LCN also will be low. Use Table 7.6 to determine tire pressure; there are options: the higher the pressure for the LCN, the smaller is the tire size.
9. Use tire manufacturers' catalogs to select a tire (see Appendix E and www.airmichelin.com and www.goodyearaviation.com).

Two worked-out examples follow. As discussed previously, the civil and military aircraft design methodologies are similar but differ considerably in their operational mission profile. There are various levels of options available to maintain component commonality, including the following:

1. *Low-Cost Option.* Maintain the same undercarriage for all variants even when there are performance penalties. In this situation, design the undercarriage for the biggest aircraft and then use it for other variants. The biggest aircraft may have tighter design criteria to sacrifice some margin in order to benefit smaller designs.
2. *Medium-Cost Option.* In this situation, design the undercarriage for the biggest aircraft and then make minor modifications to suit the smaller variants and to retrieve some of the performance loss associated with the low-cost option. These modifications maintain the external geometry but shave off metal to lighten the structure, to the extent possible. The smallest aircraft may require a shortening of the strut length without affecting the shock-absorber geometry, which may require a spring change. Wheel, brake, and tire size are kept the same. The smallest variant is nearly half the weight of the largest but may be unchanged; it may be possible to change a dual wheel to a single wheel.
3. *High-Cost Option.* Make major modifications to the undercarriage. In this situation, design three strut lengths for each variant, maintaining the maximum manufacturing-process commonality – this would reduce costs when NC machines are used. Maintain the other items with the maximum component commonality. The spring of the smallest variant may change without affecting the external geometry. Performance gain could be maximized by this option.

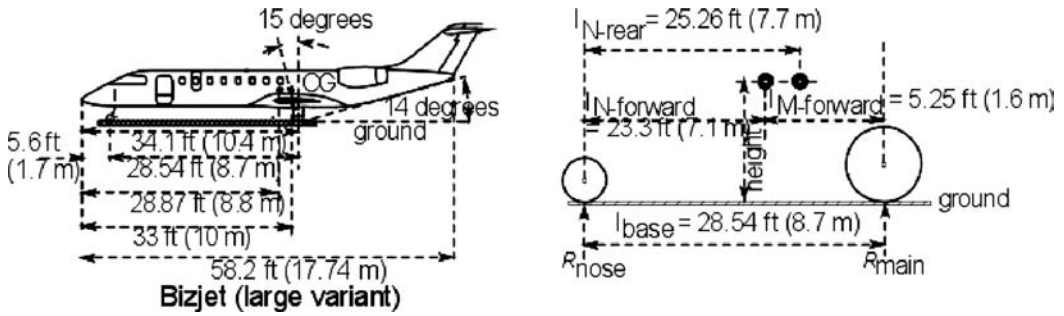


Figure 7.16. Bizjet undercarriage positions

In all cases, the nose wheel attachment point remains unchanged but the wheel base and wheel track change with new attachment points for the main wheels on the wing or elsewhere.

The industry conducts a trade-off study to examine which options offer the maximum cost benefit to operators. This book uses the second option – that is, start with the biggest variant shown in Figure 7.9. Iteration is likely to occur after accurate sizing (see Chapter 11).

7.14 Worked-Out Examples

The worked-out example continues with the aircraft configuration developed in Chapter 6 (both civil and military). The heaviest and the longest in the family is the most critical from the undercarriage design perspective (see Figures 7.17 and 7.18 for undercarriage positioning).

7.14.1 Civil Aircraft: Bizjet

The largest 14/16 passenger variant design is the most critical to maintain for undercarriage commonality. For the largest variant, the wheel base is 28.54 ft (8.66 m), $\beta = 15$, and $\gamma = 14$ deg. The undercarriage and tire sizing for the family of civil aircraft variants are more involved procedures than combat aircraft because the fuselage length and weight changes are relatively high, affecting both the wheel base and the strut load.

The undercarriage is the tricycle type and retractable. The aftmost CG position is considered first, placed at 35% (40% is a limiting situation) of the wing MAC. It will be revised when the CG is determined from actual weight computation. The nose wheel load is based on the forwardmost CG position.

The growth version of the MTOM = 11,000 kg (24,250 lb) (at this time, it is estimated from the baseline MTOM of 9,500 kg [21,000 lb]). It will be subsequently sized to a more accurate mass. The wing and empennage sizes are the same as for the baseline aircraft. The main-wheel attachment point is at a reinforced location on the rear-wing spar and is articulated with the ability to fold inward for retraction. It is assumed that there is no problem for stowage space in the fuselage with adequate wheel clearance. The following dimensions are of interest; the large growth variant is shown in Figure 7.16. At this time, the CG position is estimated and is refined in Chapter 8 when the undercarriage position is iterated.

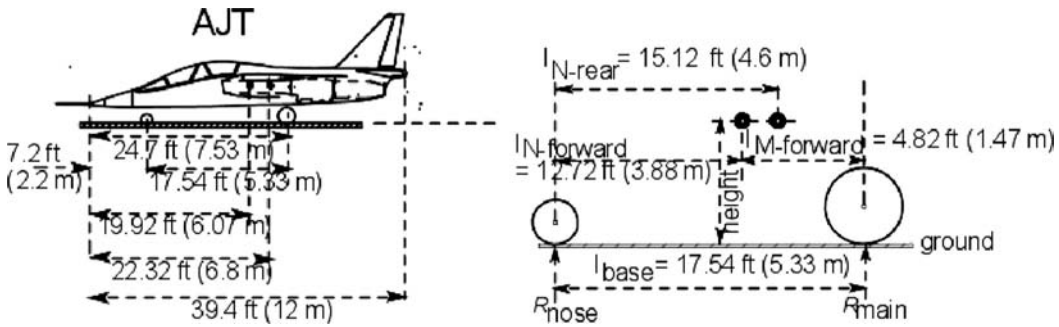


Figure 7.17. AJT undercarriage positions

1. Fuselage length = 17.74 m (58.2 ft). The wing is positioned as shown in Figure 7.17.
2. The aftmost CG position is estimated at 10 m (33 ft) from the zero reference plane and 1.83 m (6 ft) above the ground, just below the centerline.
3. The forwardmost CG position is estimated at 8.8 m (28.87 ft) from the zero reference plane.
4. Place the main wheel at 55% of the wing MAC and check that the fuselage clearance angles, $\gamma = 14$ deg and $\beta = 15$ deg, are sufficient for rotation. This measures 10.4 m (34.1 ft) from the zero reference plane with a height of 1 m from the wing attachment point to the ground in a normal loading condition. The ground clearance from the bottom of the fuselage is 0.914 m (3 ft). The main wheel extends 1 ft in a free unloaded situation (i.e., it clears the fuselage aft end at rotation).
5. The nose wheel is kept at the front bulkhead at 1.7 m (5.6 ft) from the zero reference plane. It folds forward into the nose-cone bay and extends 22.86 cm (9 in) in the free unloaded situation.
6. The wheel base is computed as $l_{BASE} = 10.4 - 1.7 = 8.7$ m (28.6 ft).
7. The wheel track = 2.9 m (9.5 ft). Use Figure 7.3 to compute the turn-over angle θ . It results in a low angle of 40 deg in a very stable aircraft.
8. The CG angle β can be worked out as $\tan^{-1}[(10.4-9.4)/1.83]$. This results in $\beta = 28.6$ deg, a safe angle well over 15 deg.

Wheel-loading, LCN, and tire sizing (use Figure 7.17 to compute wheel-loading):

- The main-wheel load is computed at the aftmost CG, which gives $l_{REAR} = 9.4 - 1.7 = 7.7$ m (25.26 ft).
- Equation 7.2 gives $R_{MAIN} = (l_{REAR} \times MTOW) / l_{BASE} = (7.7 \times 11,000) / 8.7 = 9,736$ kg (21,463 lb).
- The load per strut is 4,868 kg (10,732 lb). It is better to keep the wheel load below 10,000 lb in order to have a smaller wheel and tire.
- Then, make the twin-wheel arrangement. For this arrangement, Equation 7.5 gives the $ESWL = 4,868 / 1.5 = 3,245$ kg (7,155 lb).

A typical airfield LCN for this aircraft class is low, anywhere from 10 to 20. Table 7.6 provides several options. From the tire catalogs (see Appendix E), a suitable match is the New Tire Type (i.e., Type VII, with inch code) with a designation of $22 \times 6.6-10$ (18-ply), an inflation pressure of 260 psi, and a maximum wheel load of 10,700 lb. The maximum speed capability is 200 knots (this aircraft class does not exceed 130 knots during an approach). Although this is about the smallest size for wheel-loading, it has some redundancy with a twin wheel.

Nose-wheel and tire sizing are based on the forwardmost CG position; therefore, the aft CG nose-wheel load is not computed. The nose-wheel load at the forward CG at 8.8 m (28.87 ft) from the zero reference plane gives $l_{FORWARD} = 10.4 - 8.8 = 1.6$ m (5.25 ft).

Equation 7.3 gives $R_{NOSE} = (l_{FORWARD} \times MTOW) / l_{BASE} = (1.6 \times 11,000) / 8.7 = 2,203$ kg (4, 460 lb).

To maintain a smaller nose wheel, a twin-wheel tire arrangement is chosen. For the twin-wheel arrangement, the $ESWL = 2,203 / 1.5 = 1,469$ kg (3,238 lb).

From the tire catalogs, a suitable match is Type VII, with the designation of 18×4.4 (10-ply) and an inflation pressure of 185 psi that can take 3,550 lb (1,610 kg). The maximum speed capability is 210 mph, the same as for the main wheel.

Landing is most critical for deflection. Typically, the maximum landing weight is 95% of the MTOM. To calculate deflection on landing (in Table 7.1, FAR25 $V_{Vert} = 12$ fps), the energy to be absorbed is given in Equation 7.10 (it is computed in correlate with FPS to FAR data) as:

$$E_{ab} = \frac{1}{2} M_L \times V_{Vert}^2 = 0.5 \times 0.95 \times 21,463 \times 12^2 = 1,468,070 \text{ lb ft}^2$$

In Equation 7.14, total deflection by tire and strut is:

$$(1/2 \times V_{Vert}^2) / g = x \times (n \times k_{strut} \times \delta_{strut} + m \times k_{tire} \times \delta_{tire})$$

In Equation 7.18:

$$\delta_{tire} = D/2 - R_{load} = 22/2 - 9.6 = 1.4 \text{ in} = 0.1167 \text{ ft}$$

This can be expressed as a percentage of the maximum radius. Tire and inflation pressures result in the tire footprint (see Equation 7.17) from which the tire deflection can be computed. Use the following values:

$$x = 2(\text{maximum civil aircraft } g\text{-load at landing})$$

$$m = 4(\text{number of tires}), n = 2(\text{number of struts})$$

$$k_{strut} = 0.7 \quad k_{tire} = 0.47 \quad \delta_{tire} = 0.1167 \text{ ft}$$

Then, Equation 7.14 becomes:

$$(1/2 \times 12^2) / 32.2 = 2 \times (2 \times 0.7 \times \delta_{strut} + 4 \times 0.47 \times 0.1167)$$

$$\text{or } 1.12 = 1.4 \times \delta_{strut} + 0.22$$

$$\delta_{strut} = 0.643 \text{ ft plus } 0.077 \text{ as the margin, totaling } 0.72 \text{ ft (220 mm)}$$

The total deflection is $\delta_{\text{tire}} + \delta_{\text{strut}} = 0.1167 + 0.72 = 0.837 \text{ ft} = 10 \text{ in}$ (25.4 cm).

Baseline Aircraft with 10 Passengers at a 33-Inch Pitch

To maintain component commonality, the same undercarriage and tire size are used. The tire-ply rating can be reduced to 10 to make it less expensive. It is left to readers to repeat the calculation as given previously, using the following data:

- Baseline aircraft MTOM = 9,500 kg (\approx 21,000 lb) (refined in Chapter 8)
- Fuselage length = 15.24 m (50 ft): The CG from the zero reference plane = 8.75 m (28.7 ft)
- Fuselage clearance angle $\gamma = 15 \text{ deg}$, sufficient for rotation, and $\beta = 15 \text{ deg}$
- Distance of the main wheel from the nose wheel reference = 9.2 m (30.2 ft) (at about 55% of the wing MAC)
- Wheel base = 7.925 m (26 ft)
- Wheel track = 2.9 m (9.5 ft) (no change)

To size the main tire, the aftmost CG position is considered:

$$l_{\text{REAR}} = 8.75 - 1.8 = 6.95 \text{ m (22.8 ft)}$$

$$R_{\text{MAIN}} = (6.95 \times 9,500)/7.925 = 8,331 \text{ kg (18,367 lb)}. \text{ The load per strut} \\ = 4,166 \text{ kg (9,184 lb)}.$$

It will require a twin-wheel arrangement. From Equation 7.5, the ESWL = $4,166/1.5 = 2,777 \text{ kg (6,123 lb)}$.

From the tire catalogs, a lower-width tire designation of $22 \times 5.75 - 12$ (12-ply) with a speed rating of 230 mph and a tire inflation pressure of 220 psi can be used.

A nose wheel tire is sized based on the forwardmost CG position at 8.14 m (26.7 ft) from the zero reference plane. This gives $l_{\text{REAR}} = 8.14 - 1.8 = 6.34 \text{ m (20.8 ft)}$.

$R_{\text{NOSE}} = (6.34 \times 9,500)/7.925 = 7,600 \text{ kg (16,755 lb)}$, giving a nose wheel load $R_{\text{NOSE}} = 1,900 \text{ kg (4,400 lb)}$. The ESWL = $1,900/1.5 = 1,267 \text{ kg (2,792 lb)}$.

To maintain commonality, the same tire designation of 18×4.4 (10-ply) that takes 3,550 lb is used.

Readers can proceed in the same way with deflection calculations. The deflection will be lower than the previous case and the spring could change without changing the geometric size.

Shrunk Aircraft (Smallest in the Family Variant) with 6 Passengers at a 33-Inch Pitch

The last task is to check the smallest aircraft size to maintain as much component commonality of the undercarriage and tire size as possible (which may not be easy to do).

- Small variant aircraft MTOM = 7,000 kg (15,400 lb) (refined in Chapter 8)
- Fuselage length = 13.56 m (44.5 ft)

- The CG from the zero reference plane = 7.7 m (25.26 ft), which gives $l_{REAR} = 7.7 - 1.8 = 5.9$ m (19.35 ft)
- Fuselage clearance angle $\gamma = 16$ deg, sufficient for rotation, and $\beta = 16$ deg
- Distance of main wheel from nose wheel reference = 8.29 m (27.2 ft) (at about 55% of the wing MAC)
- Wheel base = 7.1 m (23 ft)
- Wheel track = 2.9 m (9.5 ft)
- $R_{MAIN} = (5.9 \times 7,000)/7.1 = 5,817$ kg (12,824 lb). Load per strut = 6,412 lb.

In this case, one wheel with the same tire designation of $22 \times 5.75 - 12$ (12-ply) would suffice (see [Figure 7.8](#)). The nose wheel tire also could remain the same.

It would be beneficial to shave off metal from the strut shank, if possible, and to reduce the height for both the nose and main wheels. Readers can proceed with the remaining calculations in the same manner; the spreadsheet method is helpful.

7.14.2 Military Aircraft: AJT

The worked-out example of an AJT aircraft, as developed in [Chapter 6](#) (see [Figure 6.14](#)), continues with sizing of the undercarriage and tires. The combat aircraft tire sizing for the variant designs is considerably simpler because the affecting geometries are not altered, only the weight changes. This military aircraft example has only two variants, the AJT and CAS versions. The CAS role of the variant aircraft has the same geometric size but is heavier.

Because the affecting geometries (i.e., the wheel base and wheel track) do not change, the cost option logic is less stringent for maintaining undercarriage and tire component commonality – especially for the worked-out example. In this case, it is designed for the heaviest variant with shaved-off metal for the baseline trainer version. Therefore, only the CAS version design is discussed; it is assumed that the AJT baseline will have lighter struts but the same undercarriage and tires.

The reference lines are constructed using [Figure 7.17](#). The aircraft centerline is taken conveniently through the center of the engine exhaust duct. Although at this stage, when the exact CG is not known and placement of the undercarriage is based on a designer's experience, the example of the AJT given here has been sized to avoid repetition. The exercise for readers is to start with their own layout and then iterate to size.

Even as a tandem seat arrangement, the aircraft CG travel in this aircraft class would be less than that of the civil aircraft example – for example, from 20 to 35% (aftmost) of the wing MAC. The CAS version of the CG variation is from 25 to 38% (fully loaded).

The nose wheel load is based on the forwardmost CG position. An armament payload is placed around the aircraft CG, and the CAS aircraft CG movement is insignificant between a clean configuration and a loaded configuration. Following is the relevant information for the two variants. Only the heaviest aircraft needs to be considered in this case, as explained previously.

The most critical situation for both the main wheel and the nose wheel and the tire is the CAS version with a fully loaded MTOM equal to 9,000 kg. The aftmost CG position from the reference plane is 6.8 m (22.32 ft). The AJT has an MTOM equal to 6,500 kg.

The following information is used to determine wheel loading, LCN, and tire sizing (use Figure 7.17 to compute wheel loading):

- Place the main-wheel ground contact point at 45% of the MAC. The aftmost CG position is considered first, placed at 35% (40% is a limiting situation) of the wing MAC. It will be revised when the CG is known by actual computation.
- The fuselage clearance angle, $\gamma > 15$ deg, is adequate for both variants.
- Then, the most critical CG angle $\beta = \tan^{-1}(0.874/1.9)$; i.e., $\beta = 24.7$ deg.
- The main-wheel load is computed at the aftmost CG, which gives $l_{REAR} = 6.8 - 2.2 = 4.6$ m (15.1 ft).
- Equation 7.2 gives $R_{MAIN} = (l_{REAR} \times MTOW)/l_{BASE}$
- Or $R_{MAIN} = (4.6 \times 9,000)/5.33 = 7,767$ kg (17,127 lb).

The load per strut is 3,883.5 kg (8,563 lb). It is better to keep the wheel load below 10,000 lb in order to have a smaller wheel and tire. Appendix E provides the tire data from which to choose; there are many options.

The typical airfield LCN for this class of CAS aircraft is low. From Figure 7.13, the LCN is below 15 for the CAS variant and the AJT is still lower. This means there is good flotation and the aircraft can operate from semiprepared airfields. Several options are listed in Table 7.6. From the tire catalogs (see Appendix E), a suitable match is the New Tire Type (Type VII; although the equivalent inch code is available, the metric code is used to familiarize readers) with a designation of $450 \times 190 - 5$ (22-ply) and an inflation pressure of 15.5 bar (225 psi) that takes 4,030 kg (8,886 lb). The maximum speed capability is 190 mph (165 knots), which is a sufficient margin because this aircraft class does not exceed 130 knots during an approach. The AJT is much lighter with a MTOM of 6,500 kg and, therefore, the same tire at a reduced pressure can be used (or a suitable smaller tire can be used, if changing the hub is required).

Nose wheel and tire sizing are based on the forwardmost CG position; therefore, the aft CG nose-wheel load is not computed. The nose-wheel load at the forward CG at 6.07 m (19.92 ft) from the zero reference plane gives $l_{FORWARD} = 7.53 - 6.07 = 1.46$ m (4.8 ft).

Equation 7.3 gives $R_{NOSE} = (l_{FORWARD} \times MTOW)/l_{BASE}$, or $R_{NOSE} = (1.46 \times 9,000)/5.33 = 2,465.3$ kg (5,436 lb). A single nose wheel of a smaller size is chosen.

From the tire catalogs (see Appendix E), a suitable match is the New Tire Type (Type VII, inch code) with a designation of $17.5 \times 4.4 - 8$ (14-ply) and an inflation pressure of 220 psi (14.47 bar) that takes 6,000 lb (2,721 lb). The maximum speed capability is 210 mph (182 knots). The AJT is much lighter with the MTOM of 6,500 kg; therefore, the same tire with a reduced pressure can be used.

Deflection is estimated as in the civil aircraft case and therefore is not shown here. The high-wing configuration also shows sufficient clearance. The author suggests that readers undertake the computation.

Table 7.8. *Undercarriage and main wheel tire data*

Airplane	MTOM (lb)	Wheel (per/strut)	Type	Tire size	Tire pressure (psi)	Turn radius (ft)
Cessna 152	2,500	1	S	6.00–6		
Beech 58	5,500	1	S	6.50–8	56	
Beech 200	12,600	2	T	18 × 5.5	105	
Learjet45	22,000	2	T	22 × 5.75–8	200	
ATR42	41,000	2	T	32 × 8.8R16	126	57
CL600	48,300	2	T	H27 × 8.5–14	175	40
CR200	53,000	2	T	H29 × 9.0–15	162	75
BD700	95,000	2	T	H38 × 12.0–19	200	68
B737–700	140,000	2	T	H40 × 14.5–19	200	68
Airbus 320	170,000	2	T	49 × 19–20		75
B727–200	173,000	2	TT	49 × 17	168	
B707–720	336,000	4	TT	46 × 16	180	
DC8–63	358,000	4	TT	44 × 16	200	
L1011	409,000	4	TT	50 × 20	175	
B747B	775,000	4	DTT	46 × 16	210	159
C130A	124,000	2	ST	56 × 20	65	85
C17	586,000	3	TTT	50 × 21–20	138	90
Hawk	20,000	1	S	650–10	143	
F14	74,300	1	S	37 × 11	245	

Notes:

Abbreviations: S – Single, T– tandem, ST – single tandem, TT – twin tandem, DTT – double twin, TTT – triple twin tandem

7.15 Miscellaneous Considerations

This chapter discussing undercarriage design is a relatively large, complex, and standalone chapter without which an aircraft design cannot be completed. Only the preliminary information – what is needed by aircraft designers to conduct a conceptual study – is presented here. Details of the undercarriage design are implemented by specialists after the go-ahead on a project is obtained. Aircraft designers and undercarriage designers maintain communication to integrate the undercarriage with the aircraft, doing it right the first time.

There is a tendency to minimize undercarriage design work in coursework exercises, possibly because of time constraints. As now understood, this is an involved procedure; if time is a constraint, then the undercarriage should be addressed in a second term, using CAD and including work on retraction kinematics. A good spreadsheet must be prepared for the calculations because they are required for subsequent iterations.

In summary, the chosen undercarriage should be the tricycle type with retraction. The runway LCN and ESWL decide tire pressure (the higher level of inflation pressure may be necessary), which in turn decides the number of wheels and struts required. Tire manufacturers' catalogs list the correct sizes of the tires.

The methodologies for civil and military aircraft undercarriages and tire sizing are nearly the same. The differences are in operational requirements. In general, civil aircraft design poses more difficulty in maintaining component commonality

within the variants. The cost options for component commonality for variant designs must be decided early during the conceptual design phase. Trade-off studies on cost versus weight must be conducted.

7.16 Undercarriage and Tire Data

Table 7.8 gives some production aircraft undercarriage and tire data.

8 Aircraft Weight and Center of Gravity Estimation

8.1 Overview

An aircraft must ascend to heights by defying gravity and sustain the tiring task of cruise – naturally, it is weight-sensitive. Anyone who has climbed a hill knows about this experience, especially if one has to carry baggage. An inanimate aircraft is no exception; its performance suffers by carrying unnecessary mass (i.e., weight). At the conceptual design stage, aircraft designers have a daunting task of creating a structure not only at a low weight but also at a low cost, without sacrificing safety. Engineers also must be accurate in weight estimation, well ahead of manufacture. This chapter presents a formal method to predict an aircraft and its component mass (i.e., weight), which results in locating the CG during the conceptual design phase. The aircraft inertia estimation is not within the scope of this book.

In the past, aircraft weight was expressed in FPS units in pound (lb) weight in the United Kingdom and the United States. With the use of kg as mass in SI, the unit for weight is a *Newton*, which is calculated as the mass multiplied by gravitational acceleration (9.81 m/s^2). This book uses both the FPS and SI systems; this chapter addresses mass in SI and weight in FPS, sometimes interchangeably.

Material strength contributes to structural integrity. As stated previously, aircraft conceptual designers must have broad-based knowledge in all aspects of technology; in this case, they must have a sound knowledge in material properties (e.g., strength-to-weight and strength-to-cost ratios). Higher strength-to-weight and strength-to-cost ratios are the desired qualities, but they act in opposition. Higher strength-to-weight–ratio material is more expensive, and designers must stay current about materials technology to choose the best compromises.

In the early days, designers had no choice but to use the best quality wood for aircraft construction material. Today, it is not a viable option for the type of load encountered and it also poses an environmental issue. Fortunately, the advent of *duralumin* (i.e., an aluminum alloy) in the 1930s resolved the problem, providing a considerably higher strength-to-weight ratio than wood. Having a mass-produced aluminum alloy also offers a lower material cost-to-strength ratio. Wood is easier to work with, having a low manufacturing infrastructure suitable for homebuilt aircraft, but other civil and military aircraft use predominantly metal alloys and

composites. The last two decades have seen a growing use of composite material, and more exotic metal alloys offer still better strength-to-weight ratios.

Composites are basically fabric and resin bonded together, generally formed to shape in moulds. The manufacturing process associated with composites is yet to achieve the quality and consistency of metal; hence, at this point, the certifying authorities are compelled to apply reduced values of stress levels to allow for damage tolerance and environmental issues, as well as to keep the factor of safety at 1.5 (see Section 5.6). The manufacturing process also plays a role in deciding the allowable stress level. These considerations can erode the benefits of weight savings. Research on new material, whether metal alloys (e.g., lithium–aluminum and beryllium alloy) or composites (e.g., fabric and resin) or their hybrid is an area where there is potential to reduce aircraft weight and cost. New materials are still relatively expensive, and they are steadily improving in both strength and lower costs.

8.1.1 What Is to Be Learned?

This chapter covers the following topics:

- Section 8.2: Aircraft mass, component mass, and CG position
- Section 8.3: Parameters that act as drivers for aircraft mass
- Section 8.4: Aircraft mass breakdown sequence
- Section 8.5: Desirable CG location relative to aircraft
- Section 8.6: Aircraft mass decomposed into component groups
- Section 8.7: Aircraft component mass estimation methods
- Section 8.8: Civil aircraft rapid mass estimation method
- Section 8.9: Civil aircraft graphical mass estimation method
- Section 8.10: Civil aircraft semi-empirical mass estimation method
- Section 8.11: Bizjet example
- Section 8.12: Methodology to establish aircraft CG with Bizjet example
- Section 8.13: Military aircraft rapid mass estimation method
- Section 8.14: Military aircraft graphical method for mass estimation
- Section 8.15: Military aircraft semi-empirical mass estimation method
- Section 8.16: AJT and CAS examples (military aircraft)
- Section 8.17: Methodology to locate aircraft CG with AJT and CAS examples

8.1.2 Coursework Content

The coursework task continues linearly with the examples worked out thus far. Readers must now estimate aircraft-component mass, which gives the aircraft mass and its CG location. This is an important aspect of aircraft design because it determines aircraft performance, stability, and control behavior.

Experience in the industry has shown that weight can only grow. Aircraft performance is extremely sensitive to weight because it must defy gravity. Aerodynamicists want the least weight, whereas stress engineers want the component to be strong so that it will not fail and have the tendency to beef up a structure. The structure must go through ground tests when revisions may be required. It is easy to omit an item (there are thousands) in weights estimation. Most aeronautical companies

have a special division to manage weights – weights-control engineers – a difficult task to perform.

8.2 Introduction

Because aircraft performance and stability depends on aircraft weight and the CG location, the aircraft weight and its CG position are paramount in configuring an aircraft. The success of a new aircraft design depends considerably on how accurately its weight (mass) is estimated. A pessimistic prediction masks product superiority and an optimistic estimation compromises structural integrity.

Once an aircraft is manufactured, the component weights can be easily determined by actual weighing. The aircraft CG then can be accurately determined. However, the problem in predicting weight and the CG is at the conceptual design stage, before the aircraft is built. When the first prototype is built, the weights engineers have the opportunity to verify the predictions – typically, a 4-year wait! Many of the discrepancies result from design changes; therefore, weights engineers must be kept informed in order to revise their estimations. It is a continuous process as long as the product is well supported after the design is completed.

Mass is the product of the solid volume and average density. For an aircraft component (e.g., wing assembled from a multitude of parts and fasteners), it is a laborious process to compute volumes of all those odd-shaped parts. In fact, the difficulty is that the mass prediction of complex components is not easily amenable to theoretical derivations. The typical approach to estimate weights at the conceptual design stage is to use semi-empirical relationships based on theory and statistical data of previously manufactured component masses. (A 3-D CAD model of parts provide the volume but may not be available in the early stages of conceptual design.)

The mass of each component depends on its load-bearing characteristics, which in turn depend on the operational envelope (i.e., the V - n diagram). Each manufacturer has a methodology developed over time from the statistics of past products combined with the physical laws regarding mass required for the geometry to sustain the load in question. These semi-empirical relations are proprietary information and are not available in the public domain. All manufacturers have developed mass-prediction relationships yielding satisfactory results (e.g., an accuracy of less than $\pm 3\%$ for the type of technology used). The semi-empirical relations of various origins indicate similarity in the physical laws but differ in associated coefficients and indices to suit their application domain (e.g., military or civil, metal or nonmetal, and level of desired accuracy). Nowadays, computers are used to predict weight through solid modeling – this is already in conjunction with semi-empirical relations. The industry uses more complex forms with involved and intricate manipulations that are not easy to work with in a classroom.

The fact is that no matter how complex academia may propose semi-empirical relations to improve accuracy in predicting component mass, it may fall short in supplanting the relationship available in the industry based on actual data. Of necessity, the industry must keep its findings “commercial in confidence.” At best, the industry may interact with academia for mutual benefit. An early publication by Torenbeek [3] with his semi-empirical relations is still widely used in academic circles. Roskam [4] presented three methods (i.e., Torenbeek, Cessna, and U.S. Datcom)

that clearly demonstrate the difficulty in predicting mass. Roskam's book presents updated semi-empirical relations, corroborated with civil aircraft data showing satisfactory agreement (this may be useful to homebuilt aircraft designers). The equations are not complex – complexity does not serve the purpose of coursework. Readers will have to use industrial formulae when they join a company. This chapter explains the reasons associated with formulating the relationships to ensure that readers understand the semi-empirical relations used in the industry.

The author recommends the Society of Allied Weights Engineers (SAWE) (U.S.) as a good source for obtaining semi-empirical relations in the public domain. Some of the relations presented herein are taken from SAWE, Torenbeek, Sechler, Roskam, Niu, and Jenkinson ([2] through [7]). Some of the equations are modified by the author. It is recommended that readers collect as much component weights data as possible from various manufacturers (both civil and military) to check and modify the correlation and to improvise if necessary.

Revision of mass (i.e., weight) data is a continuous process. In each project phase, the weight-estimation method is refined for better accuracy. During the conceptual design phase, semi-empirical relations based on statistical data are used; in subsequent phases, more detailed analytical and statistical methods are used. CAD solid models offer accurate geometric representations to improve volume prediction. Actual mass is known when components are manufactured, providing an opportunity to assess the mass-prediction methodology. The unavoidable tendency is that aircraft weight grows over time primarily due to modifications (e.g., reinforcements and additions of new components per user requirements). Although strength-testing of major aircraft components is a mandatory regulatory requirement before the first flight, structural-fatigue testing continues after many aircraft are already in operation. By the time results are known, it may not prove cost-effective to lighten an overdesigned structural member until a major retrofit upgrading is implemented at a later date.

The importance of the Six Sigma approach to make a design right the first time is significant to weights engineers. Many projects have suffered because of prototypes that were heavier than prediction or even experienced component failure in operation resulting in weight growth. The importance of weight prediction should not be underestimated due to not having an analytical approach involving high-level mathematical complexity, as in the case of aerodynamics. Correct weight estimation and its control are vital to aircraft design. One cannot fault stress engineers for their conservatism in ensuring structural integrity – lives depend on it. Weight-control engineers check for discrepancies throughout project development.

Mass prediction methodology starts with component weight estimation categorized into established groups, as described in Section 8.6. The methodology culminates in overall aircraft weight and locating the CG and its range of variation that can occur in operation. Estimations of aircraft inertia are required to assess dynamic behavior in response to control input but then are not needed until completion of the conceptual design study – hence, inertia is not addressed in this book. Iteration of the aircraft configuration is required after the CG is located because it is unlikely to coincide with the position guesstimated from statistics in [Chapters 6 and 7](#). A spreadsheet is recommended for calculations.

8.3 The Weight Drivers

The factors that drive aircraft weight are listed herein. References [4] through [6] discuss more detail on aircraft material, stress, and structures. Aircraft material properties given herein are typical for comparing relative merits. Material elasticity, E , and density, ρ , provide the strength-to-weight ratio. In the alloys and material categories, there is variation.

1. Weight is proportionate to size, indicated by geometry (i.e., length, area, and volume).
2. Weight depends on internal structural-member density – that is, the denser, the heavier.
3. Weight depends on a specified limit-load factor n (see [Chapter 5](#)) for structural integrity.
4. Fuselage weight depends on pressurization, engine and undercarriage mounts, doors, and so forth.
5. Lifting-surface weight depends on the loading, fuel carried, engine and undercarriage mounts, and so forth.
6. Weight depends on the choice of material. There are seven primary types used in aircraft, as follows:
 - (a) Aluminum alloy (a wide variety is available – in general, the least expensive)

$$\text{typical } E = 11 \times 10^6 \text{ lb/in}^2; \text{ typical density} = 0.1 \text{ lb/in}^3$$

- (b) Aluminum–lithium alloy (fewer types available – relatively more expensive)

$$\text{typical } E = 12 \times 10^6 \text{ lb/in}^2; \text{ typical density} = 0.09 \text{ lb/in}^3$$

- (c) Stainless-steel alloy (hot components around engine – relatively inexpensive)

$$\text{typical } E = 30 \times 10^6 \text{ lb/in}^2; \text{ typical density} = 0.29 \text{ lb/in}^3$$

- (d) Titanium alloy (hot components around engine – medium-priced but lighter)

$$\text{typical } E = 16 \times 10^6 \text{ lb/in}^2; \text{ typical density} = 0.16 \text{ lb/in}^3$$

- (e) Composite type varies (e.g., fiberglass, carbon fiber, and Kevlar); therefore, there is a wide variety in elasticity and density (price relatively inexpensive to expensive). (For details, refer to [5] and [6].)
 - (f) Hybrid (metal and composite “sandwich” – very expensive; e.g., Glare).
 - (g) Wood (rarely used except for homebuilt aircraft; is not discussed in this book – price increasing).

In this book, the primary load-bearing structures are constructed of metal; secondary structures (e.g., floorboard and flaps) could be made from composites. On the conservative side, it generally is assumed that composites and/or new alloys

comprise about 10 to 15% of the MEM for civil aircraft and about 15 to 25% of the MEM for military aircraft. The use of composites is increasing, as evidenced in current designs. Although composites are used in higher percentages, this book remains conservative in approach. All-composite aircraft have been manufactured, although only few in number (except small aircraft). The metal-composite sandwich is used in the Airbus 380 and Russia has used aluminum–lithium alloys. In this book, the consequences of using newer material is addressed by applying factors.

8.4 Aircraft Mass (Weight) Breakdown

Definitions of various types of aircraft mass (i.e., weight) (see Section 4.5) are repeated here for the convenience of readers.

$$\text{MEM (manufacturer's empty mass)} \quad (8.1)$$

is the mass of an aircraft as it rolls out of the factory before it is taken to a flight hangar for the first flight.

$$\text{OEM (operator's empty mass)} = \text{MEM} + \text{Crew} + \text{Consumable} \quad (8.2)$$

The aircraft is now ready for operation (residual fuel from the previous flight remains).

$$\text{MTOM (maximum takeoff mass)} = \text{OEM} + \text{Payload} + \text{Fuel} \quad (8.3)$$

The MTOM is the reference mass loaded to the rated maximum. This is also known as the brake release mass (BRM) ready for takeoff.

Aircraft are allowed to carry a measured amount of additional fuel for taxiing to the end of the runway, ready for takeoff at the BRM (MTOM). This additional fuel mass would result in the aircraft exceeding the MTOM to the maximum ramp mass (MRM). Taxiing fuel for midsized aircraft would be approximately 100 kg, and it must be consumed before the takeoff roll is initiated – the extra fuel for taxiing is not available for the range calculation. On busy runways, the waiting period in line for takeoff could extend to more than an hour in extreme situations.

$$\begin{aligned} \text{MRM (maximum ramp mass)} &\approx 1.0005 \times \text{MTOM (very large aircraft) to} \\ &1.001 \times \text{MTOM} = \text{MTOM} + \text{fuel to taxi to end of runway for takeoff} \end{aligned} \quad (8.4)$$

This is also known as the maximum taxi mass (MTM) and it is heavier than the MTOM.

$$\text{ZFM (zero fuel mass)} = \text{MTOM minus all fuel (nonusable residual fuel remains)} \quad (8.5)$$

8.5 Desirable CG Position

Proper distribution of mass (i.e., weight) over the aircraft geometry is key to establishing the CG. It is important for locating the wing, undercarriage, engine, and empennage for aircraft stability and control. The convenient method is to first estimate each component weight separately and then position them to satisfy the CG

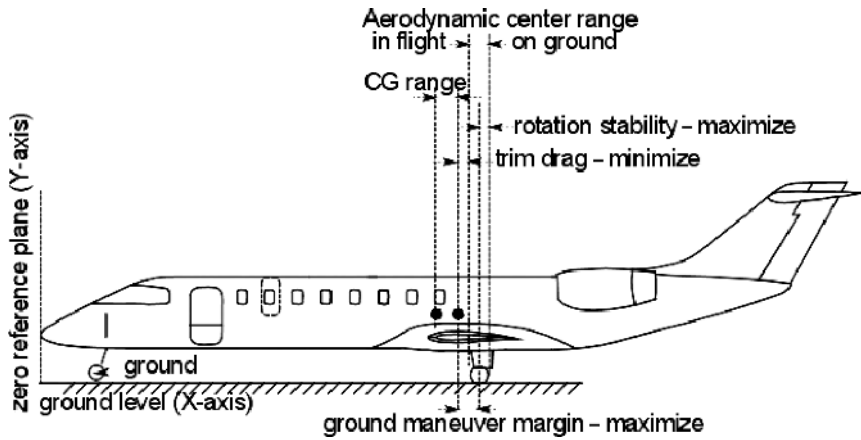


Figure 8.1. Aircraft CG position showing stability margin

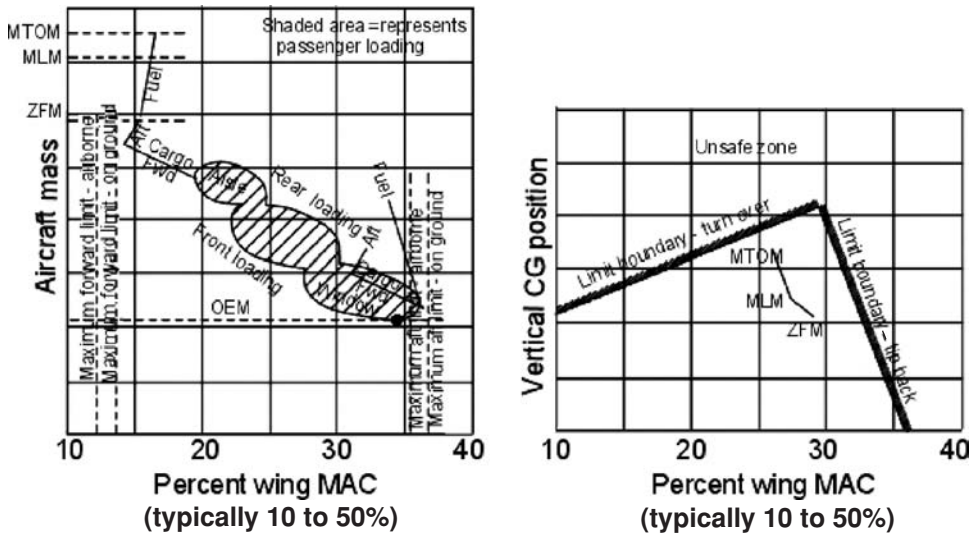
location relative to overall geometry. A typical aircraft CG margin that affects aircraft operation is shown in [Figure 8.1](#).

The aircraft aerodynamic center moves backward on the ground due to the flow field being affected by ground constraints. There is also movement of the CG location depending on the loading (i.e., fuel and/or passengers). It must be ensured that the preflight aftmost CG location is still forward of the in-flight aerodynamic center by a convenient margin, which should be as low as possible to minimize trim. Where the main-wheel contact point (and strut line) is aft of the aftmost CG, the subtending angle, β , should be greater than the fuselage-rotation angle, α , as described in Section 7.6. The main wheel is positioned to ease rotation as well as to assist in good ground handling.

Advanced military combat aircraft can have relaxed static stability to provide quicker responses. That is, the margin between the aftmost CG and the in-flight aerodynamic center is reduced (it may be even slightly negative), but the other design considerations relative to the undercarriage position are the same.

Initially, locations of some of the components (e.g., the wing) were arbitrarily chosen based on designers' past experience, which works well (see [Chapter 6](#)). Iterations are required that, in turn, may force any or all of the components to be repositioned. There is flexibility to fine-tune the CG position by moving heavy units (e.g., batteries and fuel-storage positions). It is desirable to position the payload around the CG so that any variation will have the least effect on CG movement. Fuel storage should be distributed to ensure the least CG movement; if this is not possible, then an in-flight fuel transfer is necessary to shift weight to maintain the desired CG position (as in the Supersonic Concorde).

Fuel loads and payloads are variable quantities; hence, the CG position varies. Each combination of fuel and payload results in a CG position. [Figure 8.2](#) shows variations in CG positions for the full range of combinations. Because it resembles the shape of a potato, the CG variation for all loading conditions is sometimes called the "potato curve." Designers must ensure that at no time during loading up to the MTOM does the CG position exceed the loading limits endangering the aircraft to tip over on any side. Loading must be accomplished under supervision. Whereas



(a) Range of CG variations – horizontal limits

(b) Range of CG variations – vertical limits

Figure 8.2 Aircraft CG limits

passengers have free choice in seating, cargo and fuel-loading are done in prescribed sequences, with options.

It has been observed that passengers first choose window seats and then, depending on the number of abreast seating, the second choice is made. Figure 8.2 shows the window seating first and the aisle seating last; note the boundaries of front and aft limits. Cargo- and fuel-loading is accomplished on a schedule with the locus of CG travel in lines. In the figure, the CG of the OEM is at the rear, indicating that the aircraft has aft-mounted engines. For wing-mounted engines, the CG at the OEM moves forward, making the potato curve more erect.

For static-stability reasons, it must be ensured that the aircraft has a static margin at all loading conditions. With the maximum number of passengers, the CG is not necessarily at the aftmost position. Typically, the CG should be approximately 18% of the MAC when fully loaded and approximately 22% when empty. The CG is always forward of the neutral point (i.e., the aircraft's aerodynamic center, established through CFD and wind-tunnel tests). The aerodynamic center is assumed to be 50% of the MAC and must be iterated until the final configuration is reached.

Figure 8.2 represents a typical civil aircraft loading map, which indicates the CG travel to ensure that the aircraft remains in balance within horizontal and vertical limits. Loading starts at the OEM point; if the passengers boarding first opt to sit in the aft end, then the CG can move beyond the airborne aft limit, but it must remain within the ground limit. Therefore, initial forward cargo-loading should precede passenger boarding; an early filling of the forward tank fuel is also desirable.

8.6 Aircraft Component Groups

The recognized groups of aircraft components are listed in exhaustive detail in the ATA's publication. This section presents consolidated, generalized groups (for both civil and military aircraft) suitable for studies in the conceptual design phase. Both aircraft classes have similar nomenclature; the difference in military aircraft is

described in Section 8.6.2. Each group includes subgroups of the system at the next level. Care must be taken that items are not duplicated – accurate bookkeeping is essential. For example, although the passenger seats are installed in the fuselage, for bookkeeping purposes, the fuselage shell and seats are counted separately.

8.6.1 Civil Aircraft

$$\text{Structure group } (M_{STR} = M_{FU} + M_W + M_{HT} + M_{VT}M_N + M_{PY} + M_{UC} + M_{MISC}) \quad (8.6)$$

- Fuselage group (M_{FU})
- Wing group (M_W): includes all structural items (e.g., flaps and winglets)
- H-tail group (M_{HT})
- V-tail group (M_{VT})
- Nacelle group (M_N and M_{PY}) (nacelle and pylon)
- Undercarriage group (M_{UC})
- Miscellaneous (M_{MISC}) (e.g., delta wing)

The basic structure of the aircraft – the fuselage shell (seats are listed separately under the Furnishing group) is as follows:

$$\text{Power plant group } (M_{PP} = M_E + M_{TR} + M_{EC} + M_{FS} + M_{OI}) \quad (8.7)$$

- Dry-equipped engine (M_E)
- Thrust reverser (M_{TR})
- Engine control system (M_{EC})
- Fuel system (M_{FS})
- Engine oil system (M_{OI})

The power plant group comes as a package, with all items dedicated to the power plant installation. These are mostly bought-out items supplied by specialists:

$$\text{Systems group } (M_{SYS} = M_{ECS} + M_{FC} + M_{HP} + M_{ELEC} + M_{INS} + M_{AV}) \quad (8.8)$$

- Environmental control system (M_{ECS})
- Flight-control system (M_{FC})
- Hydraulic and pneumatic system (M_{HP}) (sometimes grouped with other systems)
- Electrical system (M_{ELEC})
- Instrument system (M_{INS})
- Avionics system (M_{AV})

The systems group includes a variety of equipment, all vendor-supplied, bought-out items:

$$\text{Furnishing group } (M_{FUR} = M_{SEAT} + M_{OX} + M_{PN}) \quad (8.9)$$

- Seat, galleys, and other furnishings (M_{SEAT})
- Oxygen system (M_{OX})
- Paint (M_{PN})

Most of the weight is in the fuselage, yet the furnishings are itemized under different headings. Paint can be quite heavy. A well-painted B737 with airline livery can use as much as 75 kg of paint:

Contingencies (M_{CONT})

- This is a margin to allow unspecific weight growth (M_{CONT}).

The MEM is the total of the previous twenty-two items. This is the weight of the complete aircraft as it comes off the production line to be come airborne for the first time.

Add the following items to the MEM to obtain the OEM:

- Crew: flight and cabin crews (M_{CREW})
- Consumables: food, water, and so forth (M_{CON})

The OEM is when the aircraft is ready for operation.

Add the payload and requisite fuel to obtain the MRM. At the takeoff point at the edge of the runway, the MRM becomes the MTOM = (MRM – taxi fuel):

- Payload (M_{PL}) (passengers at 90 kg per passenger, including baggage)
- Fuel (M_{FUEL}) (for the design range, which may not fill all tanks)

MTOM: The aircraft at the end of the runway is ready for takeoff. The civil-aircraft MTOM is the total weight of all component groups, as shown in Equation 8.10.

The MTOM = $\int M(x) dx = \sum M_i$, where the subscript i stands for each component group listed previously.

For civil aircraft, the MTOM is equal to

$$\begin{aligned}
 & (M_{FU}) + (M_W) + (M_{HT}) + (M_{VT}) + (M_N) + (M_{PY}) + (M_{UC}) + (M_{MISC}) \\
 & + (M_E) + (M_{TR}) + (M_{EC}) + (M_{FS}) + (M_{OI}) + (M_{ECS}) + (M_{FC}) + (M_{HP}) \\
 & + (M_{ELEC}) + (M_{INS}) + (M_{AV}) + (M_{SEAT}) + (M_{OX}) + (M_{PN}) + (M_{CONT}) \\
 & + (M_{CREW}) + (M_{CONS}) + M_{PL} + M_{FUEL} \qquad (8.10)
 \end{aligned}$$

8.6.2 Military Aircraft (Combat Category)

This extended section of the book can be found on the Web site www.cambridge.org/Kundu and lists generic military aircraft-component mass as required in the conceptual design stage. The list covers aircraft components in the following groups.

Structure Group
 Power Plant Group
 Systems Group
 Furnishing
 Manufacture's Empty Mass
 Operators Empty Mass
 Maximum Takeoff Mass
 Maximum Ramp Mass

8.7 Aircraft Component Mass Estimation

Mass estimation at the conceptual design stage must be predicted well in advance of detailed drawings of the parts being prepared. Statistical fitment of data from the past designs is the means to predict component mass at the conceptual design phase. The new designs strive for improvement; therefore, statistical estimation is the starting point. During the conceptual design stage, iterations are necessary when the configuration changes.

Typically, there are three ways to make mass (i.e., weight) estimations at the conceptual design stage:

1. *Rapid Method.* This method relies on the statistical average of mass one level below major aircraft components (i.e., in more detail). The mass is expressed in terms of percentage (alternatively, as a fraction) of the MTOM. All items should total 100% of the MTOM; this also can be expressed in terms of mass per wing area (i.e., component wing-loading). This rapid method is accomplished at the price of considerable approximation.
2. *Graphical Method.* This method consists of plotting component weights of various aircraft already manufactured to fit into a regression curve. Graphs are generated from analytical considerations (see [3]), superimposed by actual data. The graphical method does not provide fine resolution but it is the fastest method without the next level of mass estimation, as explained previously. It is difficult to capture the technology level (and types of material) used because there is considerable dispersion. Obtaining details of component mass for statistical analysis from various industries is difficult.
3. *Semi-Empirical Method.* This method is a considerable improvement, in that it uses semi-empirical relations derived from a theoretical foundation and backed by actual data that have been correlated statistically. The indices and factors in the semi-empirical method can be refined to incorporate the technology level and types of material used. The expressions can be represented graphically, with separate graphs for each class. When grouped together in a generalized manner, they are the graphs in the graphical method described previously.

The first two methods of component mass estimation provide a starting point for the design progression.

The state-of-the-art in weight prediction has room for improvement. The advent of solid modeling (i.e., CAD) of components improved the accuracy of the mass-prediction methodology; with CAD, weight change due to a change in material can be easily captured. As soon as the component drawing is completed, the results are instantaneous and carry on through subassembly to final assembly. CAD modeling of parts occurs after the conceptual design phase has been completed.

The design drivers for civil aircraft have always been safety and economy. Civil-aircraft design developed in the wake of military aircraft evolution. Competition within these constraints kept civil aircraft designs similar to one another. Following are general comments relative to civil aircraft mass estimation:

1. For a single-engine, propeller-driven aircraft, the fuselage starts aft of the engine bulkhead because the engine nacelle is accounted for separately. These are mostly small aircraft; this is not the case for wing-mounted nacelles.

2. The fixed-undercarriage mass fraction is lower than the retractable type. The extent depends on the retraction type (typically 10% higher).
3. Neither three-engine aircraft nor fuselage-mounted, turboprop-powered aircraft are discussed in this book. Not many of these types of aircraft are manufactured. Sufficient information has been provided herein for readers to adjust mass accordingly for these aircraft classes.

The three methods are addressed in more detail in the following sections.

8.8 Rapid Mass Estimation Method: Civil Aircraft

A rapid mass estimation method is used to quickly determine the component weight of an aircraft by relating it in terms of a fraction given in the percentage of maximum takeoff mass ($M_i/MTOM$), where the subscript i represents the i th component. With a range of variation among aircraft, the tables in this section are not accurate and serve only as an estimate for a starting point of the initial configuration described in Chapter 6. Roskam [4] provides an exhaustive breakdown of weights for aircraft of relatively older designs. A newer designs show improvements, especially because of the newer materials used.

Because mass and weight are interchangeable, differing by the factor g , wing-loading can be expressed in either kg/m^2 or N/m^2 ; this chapter uses the former to be consistent with mass estimation. To obtain the component mass per unit wing area (M_i/S_w , kg/m^2), the $M_i/MTOM$ is multiplied by the wing-loading; that is, $M_i/S_w = (M_i/MTOM) \times (MTOM/S_w)$. Initially, the wing-loading is estimated (multiply 0.204816 to convert kg/m^2 to lb/ft^2).

Tables 8.1 and 8.2 summarize the component mass fractions, given in a percentage of the MTOM for quick results. The OEM fraction of the MTOM fits well with the graphs (see Figures 4.7 and 4.8). This rapid method is not accurate and only provides an estimate of the component mass involved at an early stage of the project. A variance of $\pm 10\%$ is allowed to accommodate the wide range of data.

It is better to use more accurate semi-empirical relations (see Section 8.10) to obtain the component mass at the conceptual design phase. The tables are useful for estimating fuel mass and engine mass, for example, which are required as a starting point for semi-empirical relations.

8.9 Graphical Method for Predicting Aircraft Component Weight: Civil Aircraft

The graphical method is based on regression analyses of an existing design. To put all the variables affecting weight in graphical form is difficult and may prove impractical because there will be separate trends based on choice of material, maneuver loads, fuselage layout (e.g., single or double aisle; single or double deck), type of engine integrated, wing shape, control architecture (e.g., FBW is lighter), and so forth. In principle, a graphical representation of these parameters can be accomplished at the expense of simplicity, thereby defeating the initial purpose. The simplest form, as presented in this section, obtains a preliminary estimate of component and aircraft weight. At the conceptual design stage – when only the technology level to be adopted and the three-view drawing are available to predict weights – the

Table 8.1. *Smaller aircraft mass fraction (fewer than or 19 passengers – 2 abreast seating)*

Rapid mass estimation method: Summary of mass fraction of MTOM for smaller aircraft. A range of applicability is shown; add another $\pm 10\%$ for extreme designs.

Group		Small-piston aircraft		Agriculture aircraft	Small aircraft 2-engine (Bizjet, utility)	
		1-Engine	2-Engine	(1-Piston)	(Turboprop)	(Turbofan)
Fuselage	$F_{fu} = M_{FU}/MTOM$	12 to 15	6 to 10	6 to 8	10 to 11	9 to 11
Wing	$F_w = M_W/MTOM$	10 to 14	9 to 11	14 to 16	10 to 12	9 to 12
H-tail	$F_{ht} = M_{HT}/MTOM$	1.5 to 2.5	1.8 to 2.2	1.5 to 2	1.5 to 2	1.4 to 1.8
V-tail	$F_{vt} = M_{VT}/MTOM$	1 to 1.5	1.4 to 1.6	1 to 1.4	1 to 1.5	0.8 to 1
Nacelle	$F_n = M_N/MTOM$	1 to 1.5	1.5 to 2	1.2 to 1.5	1.5 to 1.8	1.4 to 1.8
Pylon	$F_{py} = M_{PY}/MTOM$	0	0	0	0.4 to 0.5	0.5 to 0.8
Undercarriage	$F_{uc} = M_E/MTOM$	4 to 6	4 to 6	4 to 5	4 to 6	3 to 5
Engine	$F_{uc} = M_{UC}/MTOM$	11 to 16	18 to 20	12 to 15	7 to 10	7 to 9
Thrust rev.	$F_{tr} = M_{TR}/MTOM$	0	0	0	0	0
Engine control	$F_{ec} = M_{EC}/MTOM$	1.5 to 2.5	2 to 3	1 to 2	1.5 to 2	1.7 to 2
Fuel system	$F_{fs} = M_{FS}/MTOM$	0.7 to 1.2	1.4 to 1.8	1 to 1.4	1 to 1.2	1.2 to 1.5
Oil system	$F_{os} = M_{OS}/MTOM$	0.1 to 0.3	0.25 to 0.4	0.1 to 0.3	0.3 to 0.5	0.3 to 0.5
APU		0	0	0	0	0
Flight con. sys.	$F_{fc} = M_{FC}/MTOM$	1.5 to 2	1.4 to 1.6	1 to 1.5	1.5 to 2	1.5 to 2
Hydr./pneu. sys.	$F_{hp} = M_{HP}/MTOM$	0 to 0.3	0.3 to 0.6	0 to 0.3	0.5 to 1.5	0.7 to 1
Electrical	$F_{elc} = M_{ELEC}/MTOM$	1.5 to 2.5	2 to 3	1.5 to 2	2 to 4	2 to 4
Instrument	$F_{ins} = M_{INS}/MTOM$	0.5 to 1	0.5 to 1	0.5 to 1	0.5 to 1	0.8 to 1.5
Avionics	$F_{av} = M_{AV}/MTOM$	0.2 to 0.5	0.4 to 0.6	0.2 to 0.4	0.3 to 0.5	0.4 to 0.6
ECS	$F_{ecs} = M_{ECS}/MTOM$	0 to 0.3	0.4 to 0.8	0 to 0.2	2 to 3	2 to 3
Oxygen	$F_{ox} = M_{OX}/MTOM$	0 to 0.2	0 to 0.4	0	0.3 to 0.5	0.3 to 0.5
Furnishing	$F_{fur} = M_{FUR}/MTOM$	2 to 6	4 to 6	1 to 2	6 to 8	5 to 8
Miscellaneous	$F_{msc} = M_{MSC}/MTOM$	0 to 0.5	0 to 0.5	0 to 0.5	0 to 0.5	0 to 0.5
Paint	$F_{pn} = M_{PN}/MTOM$	0.01	0.01	0 to 0.01	0.01	0.01
Contingency	$F_{con} = M_{CON}/MTOM$	1 to 2	1 to 2	0 to 1	1 to 2	1 to 2
MEW (%)		57 to 67	60 to 65	58 to 62	58 to 63	55 to 60
Crew		6 to 12	6 to 8	4 to 6	1 to 3	1 to 3
Consumable		0 to 1	0 to 1	0	1 to 2	1 to 2
OEM (%)		65 to 75	65 to 70	62 to 66	60 to 66	58 to 64
Payload and fuel are traded						
Payload		12 to 25	12 to 20	20 to 30	15 to 25	15 to 20
Fuel		8 to 14	10 to 15	8 to 10	10 to 20	18 to 28
MTOM (%)		100	100	100	100	100

Notes: Lighter/smaller aircraft would show a higher mass fraction.

A fuselage-mounted undercarriage is shorter and lighter for the same MTOM.

Turbofan aircraft with a higher speed would have a longer range as compared to turboprop aircraft and, therefore, would have a higher fuel fraction (typically, 2,000-nm range will have around 0.26).

prediction is approximate. However, with rigorous analyses using semi-empirical prediction, better accuracy can be achieved that captures the influence of various parameters, as listed previously.

Not much literature in the public domain entails graphical representation. An earlier work (1942; in FPS units) in [3] presents analytical and semi-empirical treatment that culminates in a graphical representation. It was published in the United States before the gas-turbine age, when high-speed aircraft were nonexistent; those graphs served the purpose at the time but are now no longer current. Given herein

Table 8.2. Larger aircraft mass fraction (more than 19 passengers – abreast and above seating). Rapid Mass Estimation Method: Summary of mass fraction of MTOM for larger aircraft. A range of applicability is shown; add another $\pm 10\%$ for extreme designs.

Group		RJ/Midsized aircraft 2 engines		Large aircraft turbofan	
		Turboprop	Turbofan	2-engine	4-engine
Fuselage	$F_{fu} = M_{FU}/MTOM$	9 to 11	10 to 12	10 to 12	9 to 11
Wing	$F_w = M_W/MTOM$	7 to 9	9 to 11	12 to 14	11 to 12
H-tail	$F_{ht} = M_{HT}/MTOM$	1.2 to 1.5	1.8 to 2.2	1 to 1.2	1 to 1.2
V-tail	$F_{vt} = M_{VT}/MTOM$	0.6 to 0.8	0.8 to 1.2	0.6 to 0.8	0.7 to 0.9
Nacelle	$F_n = M_N/MTOM$	2.5 to 3.5	1.5 to 2	0.7 to 0.9	0.8 to 0.9
Pylon	$F_{py} = M_{PY}/MTOM$	0 to 0.5	0.5 to 0.7	0.3 to 0.4	0.4 to 0.5
Undercarriage	$F_{uc} = M_{UC}/MTOM$	4 to 5	3.4 to 4.5	4 to 6	4 to 5
Engine	$F_{eng} = M_{ENG}/MTOM$	8 to 10	6 to 8	5.5 to 6	5.6 to 6
Thrust rev.	$F_{tr} = M_{TR}/MTOM$	0	0.4 to 0.6	0.7 to 0.9	0.8 to 1
Engine con.	$F_{ec} = M_{EC}/MTOM$	1.5 to 2	0.8 to 1	0.2 to 0.3	0.2 to 0.3
Fuel system	$F_{fs} = M_{FS}/MTOM$	0.8 to 1	0.7 to 0.9	0.5 to 0.8	0.6 to 0.8
Oil system	$F_{os} = M_{OS}/MTOM$	0.2 to 0.3	0.2 to 0.3	0.3 to 0.4	0.3 to 0.4
APU		0 to 0.1	0 to 0.1	0.1	0.1
Flight con. sys.	$F_{fc} = M_{FC}/MTOM$	1 to 1.2	1.4 to 2	1 to 2	1 to 2
Hydr./pneu. sys.	$F_{hp} = M_{HP}/MTOM$	0.4 to 0.6	0.6 to 0.8	0.6 to 1	0.5 to 1
Electrical	$F_{elc} = M_{ELEC}/MTOM$	2 to 4	2 to 3	0.8 to 1.2	0.7 to 1
Instrument	$F_{ins} = M_{INS}/MTOM$	1.5 to 2	1.4 to 1.8	0.3 to 0.4	0.3 to 0.4
Avionics	$F_{av} = M_{AV}/MTOM$	0.8 to 1	0.9 to 1.1	0.2 to 0.3	0.2 to 0.3
ECS	$F_{ecs} = M_{ECS}/MTOM$	1.2 to 2.4	1 to 2	0.6 to 0.8	0.5 to 0.8
Oxygen	$F_{ox} = M_{OX}/MTOM$	0.3 to 0.5	0.3 to 0.5	0.2 to 0.3	0.2 to 0.3
Furnishing	$F_{fur} = M_{FUR}/MTOM$	4 to 6	6 to 8	4.5 to 5.5	4.5 to 5.5
Miscellaneous	$F_{msc} = M_{MSC}/MTOM$	0 to 0.1	0 to 0.1	0 to 0.5	0 to 0.5
Paint	$F_{pn} = M_{PN}/MTOM$	0.01	0.01	0.01	0.01
Contingency	$F_{con} = M_{CON}/MTOM$	0.5 to 1	0.5 to 1	0.5 to 1	0.5 to 1
MEW (%)		53 to 55	52 to 55	50 to 54	48 to 50
Crew		0.3 to 0.5	0.3 to 0.5	0.4 to 0.6	0.4 to 0.6
Consumable		1.5 to 2	1.5 to 2	1 to 1.5	1 to 1.5
OEW (%)		54 to 56	53 to 56	52 to 55	50 to 52
Payload and fuel are traded					
Payload		15 to 18	12 to 20	18 to 22	18 to 20
Fuel		20 to 28	22 to 30	20 to 25	25 to 32
MTOM (%)		100	100	100	100

Notes: Lighter aircraft would show higher mass fraction.

A fuselage-mounted undercarriage is shorter and lighter for the same MTOM.

Turbofan aircraft with a higher speed would have a longer range as compared to turboprop aircraft and, therefore, would have a higher fuel fraction.

Large turbofan aircraft have wing-mounted engines: 4-engine configurations are bigger.

are updated graphs based on the data in Table 8.3; they are surprisingly representative with values that are sufficient to start the sizing analysis in Chapter 11. Most of the weight data in the table are from Roskam [4] with additions by the author notated with an asterisk (these data are not from the manufacturers). The best data is obtained directly from manufacturers.

In all of the graphs, the MTOW is the independent variable. Aircraft-component weight depends on the MTOW; the heavier the MTOW, the heavier

Table 8.3. Aircraft component weights data

Aircraft	MTOW	Weight (lb)				Eng	U/C	n
		Fuse	Wing	Emp	Nacelle			
Piston-engined aircraft								
1. Cessna182	2,650	400	238	62	34	417	132	5.70
2. Cessna310A	4,830	319	453	118	129	852	263	5.70
3. Beech65	7,368	601	570	153	285	1,008	444	6.60
4. Cessna404	8,400	610	860	181	284	1,000	316	3.75
5. Herald	37,500	2,986	4,365	987	830		1,625	3.75
6. Convair240	43,500	4,227	3,943	922	1,213		1,530	3.75
Gas-turbine-powered aircraft								
7. Lear25	15,000	1,575	1,467	361	241	792	584	3.75
8. Lear45 class	20,000	2,300	2,056	385	459	1,672	779	3.75
9. Jet Star	30,680	3,491	2,827	879	792	1,750	1,061	3.75
10. Fokker27-100	37,500	4,122	4,408	977	628	2,427	1,840	3.75
11. CRJ200 class	51,000	6,844	5,369	1,001			1,794	5.75
12. F28-1000	65,000	7,043	7,330	1,632	834	4,495	2,759	3.75
13. Gulf GII (J)	64,800	5,944	6,372	1,965	1,239	6,570	2,011	3.75
14. MD-9-30	108,000	16,150	11,400	2,780	1,430	6,410	4,170	3.75
15. B737-200	115,500	12,108	10,613	2,718	1,392	6,217	4,354	3.75
16. A320 class	162,000	17,584	17,368	2,855	2,580	12,300	6,421	3.75
17. B747-100	710,000	71,850	86,402	11,850	10,031	34,120	31,427	3.75
18. A380 class	1,190,497	115,205	170,135	24,104		55,200	52,593	3.75

are the component weights (see Chapter 4). Strictly speaking, wing weight could have been presented as a function of the wing reference area, which in turn depends on the sized wing-loading (i.e., the MTOW) (see Chapter 11).

To use the graph, the MTOW must first be guesstimated from statistics (see Chapters 4 and 6). After the MTOW is worked out in this chapter, iterations are necessary to revise the estimation.

Figure 8.3 illustrates civil aircraft component weights in FPS units. The first provides the fuselage, undercarriage, and nacelle weights. Piston-engine-powered aircraft are low-speed aircraft and the fuselage group weight shows their lightness. There are no large piston-engine aircraft in comparison to the gas-turbine type.

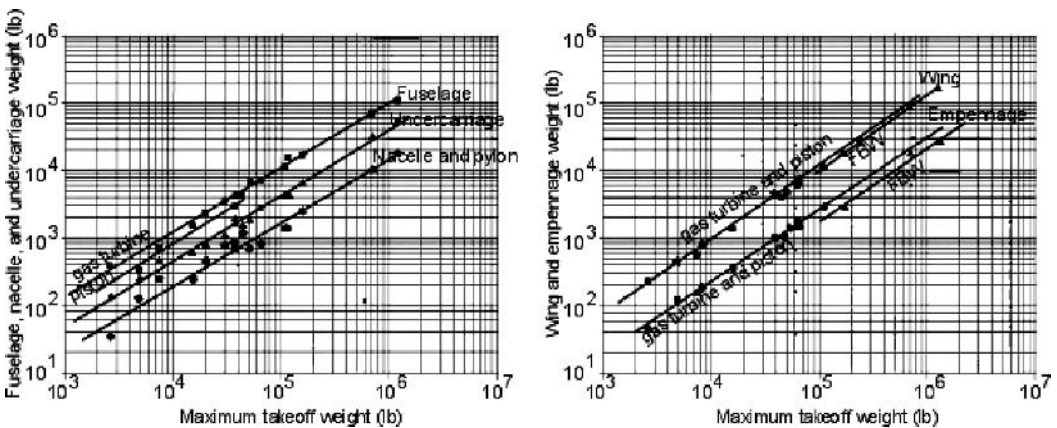


Figure 8.3 Aircraft component weights in pounds

The lower end of the graph represents piston engines; piston-engine nacelles can be slightly lighter in weight.

The second graph in [Figure 8.3](#) shows the wing and empennage group weights. The piston- and gas-turbine engine lines are not clearly separated. FBW-driven configurations have a smaller wing and empennage (see [Chapter 13](#)), as shown in separate lines with lighter weight (i.e., A320 and A380 class). The newer designs have composite structures that contribute to the light weight.

Figure 8.3 shows consistent trends but does not guarantee accuracy equal to semi-empirical relations, which are discussed in the next section.

8.10 Semi-empirical Equation Method (Statistical)

Semi-empirical relations are derived from theoretical formulation and then refined with statistical data to estimate aircraft component mass. It is an involved process to capture the myriad detailed parts. Mass estimation using semi-empirical relations can be inconsistent until a proper one is established. Several forms of semi-empirical weight-prediction formulae have been proposed by various analysts, all based on key drivers with refinements as perceived by the proponent. Although all of the propositions have similarity in the basic considerations, their results could differ by as much as 25%. In fact, in [5], Roskam describes three methods that yield different values, which is typical when using semi-empirical relations. One of the best ways is to have a known mass data in the aircraft class and then modify the semi-empirical relation for the match; that is, first fine-tune it and then use it for the new design. For a different aircraft class, different fine-tuning is required; the relations provided in this chapter are amenable to modifications (see [5] and [6]).

For coursework, the semi-empirical relations presented in this chapter are from [2] through [7]; some have been modified by the author and are satisfactory for conventional, all-metal (i.e., aluminum) aircraft. The accuracy depends on how closely aligned is the design. For nonmetal and/or exotic metal alloys, adjustments are made depending on the extent of usage.

To demonstrate the effect of the related drivers on mass, their influence is shown as mass increasing by (\uparrow) and decreasing by (\downarrow) as the magnitude of the driver is increased. For example, $L(\uparrow)$ means that the component weight increases when the length is increased. This is followed by semi-empirical relations to fit statistical data as well as possible. Initially, the MTOM must be guesstimated from statistics as in [Chapter 6](#). When the component masses are more accurately estimated, the MTOW is revised to the better accuracy.

8.10.1 Fuselage Group – Civil Aircraft

A fuselage is essentially a hollow shell designed to accommodate a payload. The drivers for the fuselage group mass are its length, $L(\uparrow)$; diameter, $D_{ave}(\uparrow)$; shell area and volume, (\uparrow); maximum permissible aircraft velocity, $V(\uparrow)$; pressurization, (\uparrow); aircraft load factor, $n(\uparrow)$; and mass increases with engine and undercarriage installation. The maximum permissible aircraft velocity is the dive speed explained in the V - n diagram in [Chapter 5](#). For a noncircular fuselage, it is the average diameter obtained by taking half the sum of the width and depth of the fuselage; for a

rectangular cross-section (invariably unpressurized), it is obtained using the same method. Length and diameter give the fuselage shell area: the larger the area, the greater is the weight. A higher velocity and limit load n require more material for structural integrity. The installation of engines and/or the undercarriage on the fuselage requires additional reinforcement mass. Pressurization of the cabin increases the fuselage-shell hoop stress that requires reinforcement, and a rear-mounting cargo door is also a large increase in mass. (The nonstructural items in the fuselage – e.g., the furnishings and systems – are computed separately.)

Following are several sets of semi-empirically derived relations by various authors for the transport aircraft category (nomenclature is rewritten according to the approach of this book). The equations are for all-metal (i.e., aluminum) aircraft.

By Niu [6] in FPS:

$$W_{Fcivil} = k_1 k_2 \left\{ 2,446.4 \left[\begin{array}{l} 0.5(W_{flight_gross_weight} + W_{landing_weight}) \times \left(1 + \frac{1.5\Delta P}{4} \right)^{0.5} \times \\ S_{net_fus_wetted_area} \times [0.5(W + D)]^{0.5} \times L^{0.6} \times 10^{-4} - 678 \end{array} \right] \right\} \quad (8.11)$$

where k_1 = 1.05 for a fuselage-mounted undercarriage

= 1.0 for a wing-mounted undercarriage

where k_2 = 1.1 for a fuselage-mounted engine

= 1.0 for a wing-mounted engine

$S_{net_fus_wetted_area}$ = fuselage-shell gross area less cutouts

Two of Roskam's suggestions are as follows [5]:

1. The General Dynamic method:

$$W_{Fcivil} = 10.43 (K_{inlet})^{1.42} (q_D/100)^{0.283} (MTOW/1,000)^{0.95} (L/D)^{0.71} \quad (8.12)$$

where $K_{inlet} = 1.25$ for inlets in or on the fuselage; otherwise, 1.0

q_D = dive dynamic pressure in psf

L = fuselage length

D = fuselage depth

2. The Torenbeek method:

$$W_{Fcivil} = 0.021 K_f \{ V_D L_{HT} / (W + D) \}^{0.5} (S_{fus_gross_area})^{1.2} \quad (8.13)$$

where $K_f = 1.08$ for a pressurized fuselage

= 1.07 for the main undercarriage attached to the fuselage

= 1.1 for a cargo aircraft with a rear door

V_D = design dive speed in knots equivalent air speed (KEAS)

L_{H_tail} = tail arm of the H-tail

$S_{fus_gross_area}$ = fuselage-shell gross area

By Jenkinson (from Howe) [7] in SI:

$$M_{Fcivil} = 0.039 \times (2 \times L \times D_{ave} \times V_D^{0.5})^{1.5} \quad (8.14)$$

The author does not compare the equations here. As mentioned previously, the best method depends on the type – weight equations show inconsistency. Torenbeek's equation has been used for a long time, and Equation 8.14 is the simplest one.

The author suggests using Equation 8.14 for coursework. The worked-out example appears to have yielded satisfactory results, capturing more details of the technology level.

$$M_{Fcivil} = c_{fus} \times k_e \times k_p \times k_{uc} \times k_{door} \times (MTOM \times n_{ult})^x \times (2 \times L \times D_{ave} \times V_D^{0.5})^y, \quad (8.15)$$

where c_{fus} is a generalized constant to fit the regression, as follows:

$$\begin{aligned} c_{fus} &= 0.038 \text{ for small unpressurized aircraft (leaving the engine bulkhead forward)} \\ &= 0.041 \text{ for a small transport aircraft } (\leq 19 \text{ passengers}) \\ &= 0.04 \text{ for 20 to 100 passengers} \\ &= 0.039 \text{ for a midsized aircraft} \\ &= 0.0385 \text{ for a large aircraft} \\ &= 0.04 \text{ for a double-decked fuselage} \\ &= 0.037 \text{ for an unpressurized, rectangular-section fuselage} \end{aligned}$$

All k -values are 1 unless otherwise specified for the configuration, as follows:

$$\begin{aligned} k_e &= \text{for fuselage-mounted engines} = 1.05 \text{ to } 1.07 \\ k_p &= \text{for pressurization} = 1.08 \text{ up to } 40,000\text{-ft operational altitude} \\ &= 1.09 \text{ above } 40,000\text{-ft operational altitude} \\ k_{uc} &= 1.04 \text{ for a fixed undercarriage on the fuselage} \\ &= 1.06 \text{ for wheels in the fuselage recess} \\ &= 1.08 \text{ for a fuselage-mounted undercarriage without a bulge} \\ &= 1.1 \text{ for a fuselage-mounted undercarriage with a bulge} \\ k_{VD} &= 1.0 \text{ for low-speed aircraft below Mach } 0.3 \\ &= 1.02 \text{ for aircraft speed } 0.3 < \text{Mach} < 0.6 \\ &= 1.03 \text{ to } 1.05 \text{ for all other high-subsonic aircraft} \\ k_{door} &= 1.1 \text{ for a rear-loading door} \end{aligned}$$

The value of index x depends on the aircraft size: 0 for aircraft with an ultimate load (n_{ult}) < 5 and between 0.001 and 0.002 for ultimate loads of (n_{ult}) > 5 (i.e., lower values for heavier aircraft). In general, $x = 0$ for civil aircraft; therefore, $(MTOM \times n_{ult})^x = 1$. The value of index y is very sensitive. Typically, y is 1.5, but it can be as low as 1.45. It is best to fine-tune with a known result in the aircraft class and then use it for the new design.

Then, for civil aircraft ($n_{ult} < 5$), Equation 8.15 can be simplified to:

$$M_{Fcivil} = c_{fus} \times k_e \times k_p \times k_{uc} \times k_{door} \times (2 \times L \times D_{ave} \times V_D^{0.5})^{1.5} \quad (8.16)$$

For the club-flying-type small aircraft, the fuselage weight with a fixed undercarriage can be written as:

$$M_{Fsmall/c} = 0.038 \times 1.07 \times k_{uc} \times (2 \times L \times D_{ave} \times V_D^{0.5})^{1.5} \quad (8.17)$$

If new materials are used, then the mass changes by the factor of usage. For example, $x\%$ mass is new material that is $y\%$ lighter; the component mass is as follows:

$$M_{Fcivil_new-material} = M_{Fcivil} - x/y \times M_{Fcivil} + x \times M_{Fcivil} \quad (8.18)$$

In a simpler form, if there is reduction in mass due to lighter material, then it is reduced by that factor. For example, if there is 10% mass saving, then:

$$M_{Fcivil} = 0.9 \times M_{Fcivil_all\ metal}$$

8.10.2 Wing Group – Civil Aircraft

The wing is a thin, flat, hollow structure. The hollow space is used for fuel storage in sealed wet tanks or in separate tanks fitted in; it also houses control mechanisms – accounted for separately. As an option, the engines can be mounted on the wing. Wing-mounted nacelles are desirable for wing-load relief; however, for small turbofan aircraft, they may not be possible due to the lack of ground clearances (unless the engine is mounted over the wing or it is a high-wing aircraft – few are manufactured).

The drivers for the wing group mass are its planform reference area, $S_W(\uparrow)$; aspect ratio, $AR(\uparrow)$; quarter-chord wing sweep, $\Lambda_{1/4}(\uparrow)$; wing-taper ratio, $\Lambda(\uparrow)$; mean-wing t/c ratio, (\downarrow) ; maximum permissible aircraft velocity, $V(\uparrow)$; aircraft limit load, $n(\uparrow)$; fuel carried, (\downarrow) ; and wing-mounted engines, (\downarrow) . The aspect ratio and wing area give the wing span, b . Because the quarter-chord wing sweep, $\Lambda_{1/4}$, is expressed in the cosine of the angle, it is placed in the denominator, as is the case with the t/c ratio because the increase in the t/c ratio decreases the wing weight by having better stiffness.

A well-established general analytical wing-weight equation published by SAWE [2] is as follows (others are not included):

$$M_W = K(M_{dg} N_Z)^{x1} S_W^{x2} AR^{x3} (t/c)^{x4} (1 + \lambda)^{x5} (\cos \Lambda_{1/4})^{x6} (B/C)_t^{x7} S_{CS}^{x8} \quad (8.19)$$

where C = wing-root chord, B = width of box beam at wing root, S_{CS} = wing-mounted control-surface reference area, and $M_{dg} = \text{MTOM}$.

The equation is modified for coursework. The term $(M_{dg} N_Z)^{x1}$ in this book's nomenclature is $(\text{MTOM} \times n_{ult})^{0.48}$. The term $(B/C)_t^{x7} S_{CS}^{x8}$ is replaced by the factor 1.005 and included in the factor K . The lift load is upward; therefore, mass carried by the wing (e.g., fuel and engines) would relieve the upward bending (like a bow), resulting in stress relief that saves wing weight. Fuel is a variable mass and when it is emptied, the wing does not get the benefit of weight relief; but if aircraft weight is reduced, the fixed mass of the engine offers relief. Rapid methods should be used to obtain engine mass for the first iteration.

Writing the modified equation in terms of this book's notation, Equation 8.19 is replaced by Equation 8.20 in SI (the MTOM is estimated; see Chapter 6):

$$M_W = c_w \times k_{uc} \times k_{sl} \times k_{sp} \times k_{wl} \times k_{re} \times (\text{MTOM} \times n_{ult})^{0.48} \times S_W^{0.78} \times A_R \times (1 + \lambda)^{0.4} \times (1 - W_{Fuel_mass_in_wing}/\text{MTOW})^{0.4} / [(\text{Cos} \Lambda) \times t/c^{0.4}] \quad (8.20)$$

where $c_w = 0.0215$ and flaps are a standard fitment to the wing.

$k_{uc} = 1.002$ for a wing-mounted undercarriage; otherwise, 1.0

$k_{sl} = 1.004$ for the use of a slat

$k_{sp} = 1.001$ for a spoiler

$k_{wl} = 1.002$ for a winglet (a generalized approach for a standard size)

$k_{re} = 1$ for no engine, 0.98 for two engines, and 0.95 for four engines (generalized)

If nonmetal is used, then mass changes by the factor of usage. For example, $x\%$ mass is nonmetal that is $y\%$ lighter, the component mass would be as follows:

$$M_{W_{civil_nonmetal}} = M_{W_{civil}} - x/y \times M_{W_{civil}} + x \times M_{W_{civil}} \quad (8.21)$$

In a simpler form, if there is reduction in mass due to lighter material, then mass is reduced by that factor. If there is a 10% mass saving, then:

$$M_{W_{civil_nonmetal}} = 0.9 \times M_{W_{civil_all\ metal}} \quad (8.22)$$

8.10.3 Empennage Group – Civil Aircraft

H- and V-tails also are lifting surfaces and use semi-empirical equations similar to those used for the wing. The empennage does not have an engine or undercarriage installation. It may carry fuel, but in this book, fuel is not stored in the empennage. The drivers are the same as those in the wing group mass.

Equation 8.20 is modified to suit the empennage mass estimation. Both the H-tail and V-tail plane mass estimations have a similar form but they differ in the values of constants used.

$$M_{EMP_{civil}} = 0.0213 \times (\text{MTOM} \times n_{ult})^{0.48} \times S_W^{0.78} \times AR \times (1 + \lambda)^{0.4} / (\text{Cos}\Lambda \times t/c^{0.4}) \quad (8.23)$$

If nonmetals are used, then mass changes by the factor of usage. For example, $x\%$ mass is nonmetal that is $y\%$ lighter, the component mass would be as follows:

$$M_{EMP_{civil_nonmetal}} = M_{EMP_{civil}} - x/y \times M_{EMP_{civil}} + x \times M_{EMP_{civil}} \quad (8.24)$$

In a simpler form, if there is reduction in mass due to lighter material, then the mass is reduced by that factor. If there is a 10% mass saving, then:

$$M_{EMP_{civil_nonmetal}} = 0.9 M_{EMP_{civil_all\ metal}} \quad (8.25)$$

Writing the modified equations in terms of this book's nomenclature, Equation 8.23 is changed to the empennage for an H-tail and a V-tail as follows. For all H-tail movement, use $k_{conf} = 1.05$; otherwise, 1.0.

$$M_{HT} = 0.02 \times k_{conf} \times (\text{MTOM} \times n_{ult})^{0.48} \times S_W^{0.78} \times AR \times (1 + \lambda)^{0.4} / (\text{Cos}\Lambda \times t/c^{0.4}) \quad (8.26)$$

For V-tail configurations, use $k_{conf} = 1.1$ for a T-tail, 1.05 for a midtail, and 1.0 for a low tail.

$$M_{VT} = 0.0215 \times k_{conf} \times (\text{MTOM} \times n_{ult})^{0.48} \times S_W^{0.78} \times AR \times (1 + \lambda)^{0.4} / (\text{Cos}\Lambda \times t/c^{0.4}) \quad (8.27)$$

8.10.4 Nacelle Group – Civil Aircraft

The nacelle group can be classified distinctly as a pod that is mounted and interfaced with pylons on the wing or fuselage, or it can be combined. The nacelle size depends on the engine size and type. The nacelle mass semi-empirical relations are as follow.

Jet Type (Includes Pylon Mass)

For a BPR greater than 4.0, $M_{NAC_jet} = 6.7 \times thrust (kN)$ per nacelle. (8.28)

For a BPR less than 4.0, $M_{NAC_jet} = 6.2 \times thrust (kN)$ per nacelle. (8.29)

Turboprop Type

Pods are slung under the wing or placed above the wing with little pylon, unless it is an aft-fuselage-mounted pusher type (e.g., Piaggio Avanti). For the same power, turboprop engines are nearly 20% heavier, requiring stronger nacelles; however, they have a small or no pylon.

For a wing-mounted turboprop nacelle:

$$M_{NAC_prop} = 6.5 \times SHP \text{ per nacelle} \quad (8.30)$$

For a turboprop nacelle housing an undercarriage:

$$M_{NAC_prop_uc} = 8 \times SHP \text{ per nacelle} \quad (8.31)$$

For a fuselage-mounted turboprop nacelle with a pylon:

$$M_{NAC_prop} = 7 \times 4 \times SHP \text{ per nacelle} \quad (8.32)$$

Piston-Engine Nacelle

For tractor types, the nacelle is forward of the engine bulkhead; for pusher types, it is aft of the engine bulkhead – both have an engine mount. This mass is not considered a fuselage mass, even when it is an extension of the fuselage mould line.

For a fuselage-mounted, piston-engine nacelle:

$$M_{nac_piston} = 0.4 \times HP \text{ per nacelle} \quad (8.33)$$

For a wing-mounted, piston-engine nacelle:

$$M_{nac_piston} = 0.5 \times HP \text{ per nacelle} \quad (8.34)$$

If a nonmetal is used, then mass changes by the factor of usage. For example, $x\%$ mass is nonmetal that is $y\%$ lighter, the component mass would be as follows:

$$M_{nac_civil_nonmetal} = M_{nac_civil} - x/y \times M_{nac_civil} + x \times M_{nac_civil} \quad (8.35)$$

8.10.5 Undercarriage Group – Civil Aircraft

Chapter 7 describes undercarriages and their types in detail. Undercarriage size depends on an aircraft's MTOM. Mass estimation is based on a generalized approach of the undercarriage classes that demonstrate strong statistical relations, as discussed herein.

Tricycle Type (Retractable) – Wing-Mounted (Nose and Main Gear Estimated Together)

For a low-wing-mounted undercarriage:

$$M_{UC_wing} = 0.04 \times MTOM \quad (8.36)$$

For a midwing-mounted undercarriage:

$$M_{UC_wing} = 0.042 \times MTOM \quad (8.37)$$

For a high-wing-mounted undercarriage:

$$M_{UC_wing} = 0.044 \times MTOM \quad (8.38)$$

Tricycle Type (Retractable) – Fuselage-Mounted (Nose and Main Gear Estimated Together)

These are typically high-wing aircraft. A fuselage-mounted undercarriage usually has shorter struts.

$$M_{UC_fus} = 0.04 \times MTOM \quad (8.39)$$

For a fixed undercarriage, the mass is 10 to 15% lighter; for a tail-dragger, it is 20 to 25% lighter.

8.10.6 Miscellaneous Group – Civil Aircraft

Carefully examine which structural parts are omitted (e.g., delta fin). Use mass per unit area for a comparable structure (i.e., a lifting surface or a body of revolution; see Section 8.4). If any item does not fit into the standard groups listed herein, then it is included in this group. Typically, this is expressed as:

$$M_{MISC} = 0 \text{ to } 1\% \text{ of the MTOM} \quad (8.40)$$

8.10.7 Power Plant Group – Civil Aircraft

The power plant group consists of the components listed in this section. At the conceptual design stage, they are grouped together to obtain the power plant group mass. It is better to use the engine manufacturer's weight data available in the public domain. However, given here are the semi-empirical relations to obtain the engine weight.

Turbofans

- (1) Equipped dry-engine mass (M_E)
- (2) Thrust-reverser mass (M_{TR}), if any – mostly installed on bigger engines
- (3) Engine control system mass (M_{EC})
- (4) Fuel system mass (M_{FS})
- (5) Engine oil system mass (M_{OI})

Turboprops

- (1) Equipped dry-engine mass (M_E) – includes reduction gear mass to drive propeller

- (2) Propeller (M_{PR})
- (3) Engine control system mass (M_{EC})
- (4) Fuel system mass (M_{FS})
- (5) Engine oil system mass (M_{OI})

Piston Engines

- (1) Equipped dry-engine mass (M_E) – includes reduction gear, if any
- (2) Propeller mass (M_{PR})
- (3) Engine control system mass (M_{EC})
- (4) Fuel system mass (M_{FS})
- (5) Engine oil system mass (M_{OI})

In addition, there could be a separate auxiliary power unit (APU) – generally in bigger aircraft – to supply electrical power driven by a gas turbine.

Engine manufacturers supply the equipped dry-engine mass (e.g., fuel pump and generator) and the engine thrust-to-weight ratio ($T/M_{dry.engine}$; thrust is measured in Newtons) as a measure of dry-engine weight in terms of rated thrust (T_{SLS}). Typically, $T/M_{dry.engine}$ varies between 4 and 8 (special-purpose engines can be more than 8). For turboprop engines, the mass is expressed as ($SHP/M_{dry.engine}$); for piston engines, it is ($HP/M_{dry.engine}$).

The remainder of the systems including the thrust reverser (for some turbofans), oil system, engine controls, and fuel system are listed here. The total power plant group mass can be expressed semi-empirically (because of the similarity in design, the relationship is fairly accurate). The power plant group mass depends on the size of the engine expressed by the following equations:

Turbofan

Civil aircraft power plant (with no thrust reverser):

$$M_{ENG_tf} = 1.4 \times M_{DRYENG} \text{ per engine} \quad (8.41)$$

Civil aircraft power plant (with thrust reverser):

$$M_{ENG_tf} = 1.5 \times M_{DRYENG} \text{ per engine} \quad (8.42)$$

Turboprop

Civil aircraft power plant:

$$M_{ENG_tp} = k_{tp} \times M_{DRYENG} \text{ per engine} \quad (8.43)$$

where $1.4 \leq k_{tp} \leq 1.5$.

Piston Engine

Civil aircraft power plant:

$$M_{ENG_ps} = k_p \times M_{DRYENG} \text{ per engine} \quad (8.44)$$

where $1.4 \leq k_p \leq 1.5$.

APU (if any)

$$M_{APU} = 0.001 \text{ to } 0.005 \times M_{DRYENG} \text{ of an engine} \quad (8.45)$$

8.10.8 Systems Group – Civil Aircraft

The systems group includes flight controls, hydraulics and pneumatics, electrical, instrumentation, avionics, and environmental controls (see [Section 8.6.1](#)). At the conceptual design stage, these are grouped together to obtain the power plant group.

$$M_{SYS} = 0.1 \text{ to } 0.11 \times \text{MTOW for large aircraft } > 100 \text{ passengers} \quad (8.46)$$

$$M_{SYS} = 0.11 \text{ to } 0.12 \times \text{MTOW for smaller transport aircraft of} \\ < 100 \text{ passengers} \quad (8.47)$$

$$M_{SYS} = 0.05 \text{ to } 0.07 \times \text{MTOW for unpressurized aircraft} \quad (8.48)$$

8.10.9 Furnishing Group – Civil Aircraft

This group includes the seats, galleys, furnishings, toilets, oxygen system, and paint (see [Section 8.6.1](#)). At the conceptual design stage, they are grouped together to obtain the furnishing group.

$$M_{FUR} = 0.07 \text{ to } 0.08 \times \text{MTOW for large aircraft } > 100 \text{ passengers} \quad (8.49)$$

$$M_{FUR} = 0.06 \text{ to } 0.07 \times \text{MTOW for smaller transport aircraft of} \\ < 100 \text{ passengers} \quad (8.50)$$

$$M_{FUR} = 0.02 \text{ to } 0.025 \times \text{MTOW for unpressurized aircraft} \quad (8.51)$$

8.10.10 Contingency and Miscellaneous – Civil Aircraft

A good designer plans for contingencies; that is:

$$M_{CONT} = (0.01 \text{ to } 0.025) \times \text{MTOW} \quad (8.52)$$

Miscellaneous items should also be provided for; that is:

$$M_{MSC} = 0 \text{ to } 1\% \text{ of MTOW} \quad (8.53)$$

8.10.11 Crew – Civil Aircraft

A civil aircraft crew consists of a flight crew and a cabin crew. Except for very small aircraft, the minimum flight crew is two, with an average of 90 kg per crew member. The minimum number of cabin crew depends on the number of passengers. Operators may employ more than the minimum number, which is listed in [Table 8.4](#).

8.10.12 Payload – Civil Aircraft

A civil aircraft payload is basically the number of passengers at 90 kg per person plus the cargo load. The specification for the total payload capacity is derived from the operator's requirements. The payload for cargo aircraft must be specified from market requirements.

Table 8.4. *Minimum cabin-crew number for passenger load*

Number of passengers	Minimum number of cabin crew	Number of passengers	Minimum number of cabin crew
≥ 19	1	200 to <250	7
19 to <30	2	250 to <300	8
21 to <50	3	300 to <350	9
50 to <100	4	350 to <400	10
100 to <150	5	400 to <450	11
150 to <200	6	450 to <500	12

8.10.13 Fuel – Civil Aircraft

The fuel load is mission-specific. For civil aircraft, required fuel is what is needed to meet the design range (i.e., market specification) plus mandatory reserve fuel. It can be determined by the proper performance estimation described in [Chapter 13](#). At this design stage, statistical data are the only means to estimate fuel load, which is then revised in [Chapter 13](#).

The payload and fuel mass are traded for off-design ranges; that is, a higher payload (if accommodated) for less range and vice versa.

8.11 Worked-Out Example – Civil Aircraft

The semi-empirical relations described in [Section 8.10](#) are now applied to obtain an example of the configuration worked out in [Chapters 6 and 7](#) in the preliminary configuration layout. This chapter more accurately estimates component and aircraft mass along with the CG locations (Figure 8.4). Therefore, the preliminary configuration needs to be refined through an iterative process with more accurate data. The iteration process may require the repositioning of aircraft components (see [Section 8.13](#)). The aircraft configuration is finalized in [Chapter 11](#). From [Chapter 6](#), the following specifications are obtained for the baseline-aircraft preliminary configuration. They are required to estimate aircraft component mass, as shown here:

MTOM = 9,500 kg (refined in this exercise)

Two turbofans (i.e., Honeywell TFE731), each having $T_{SLs} = 17,235$ N (3,800 lbs), BPR < 4 and dry weight of 379 kg (836 lbs)

The results from this section are compared with the graphical solutions in [Figure 8.3](#) and in [Table 8.5](#).

8.11.1 Fuselage Group Mass

Consider a 5% weight reduction due to composite usage in nonload-bearing structures (e.g., floorboards). Use [Equation 8.15](#):

$$L = 15.24 \text{ m}, D_{ave} = 1.75 \text{ m}, V_D = 380 \text{ KEAS} = 703.76 \text{ kmph} = 195.5 \text{ m/s} \text{ and } c_{fus} = 0.04, k_e = 1.04, k_p = 1.09, k_{uc} = 1.06, \text{ and } k_{mat} = (0.9 + 0.9 \times 0.1) = 0.99$$

Table 8.5. Bizjet mass (weight) summary

Component	Semi-empirical (kg)	Mass fraction %	Graphical solution – lb (kg)
1. Fuselage group	930	10	≈2,050 (932)
2. Wing group	864	9.2	≈2,100 (946)
3. H-tail group	124	1.32	H-Tail+V-Tail≈460 (209)
4. V-tail group	63	0.67	
5. Undercarriage group	380	4	≈900 (409)
6. Nacelle + pylon group	212	2.245	≈410 (186)
7. Miscellaneous			
Structures group total	2,591		27.56
8. Power plant group	1,060	11.28	
9. Systems group	1,045	11.12	
10. Furnishing group	618	6.57	
11. Contingencies	143	0.7	
MEM	5,457		58.05
12. Crew	180	1.92	
13. Consumables	≈ 119	1.73	
OEM	5,800		61.7
13. Payload (as positioned)	1,100	11.7	
14. Fuel (as positioned)	2,500	26.6	
MTOM	9,400		100
MRM	9,450		100.53

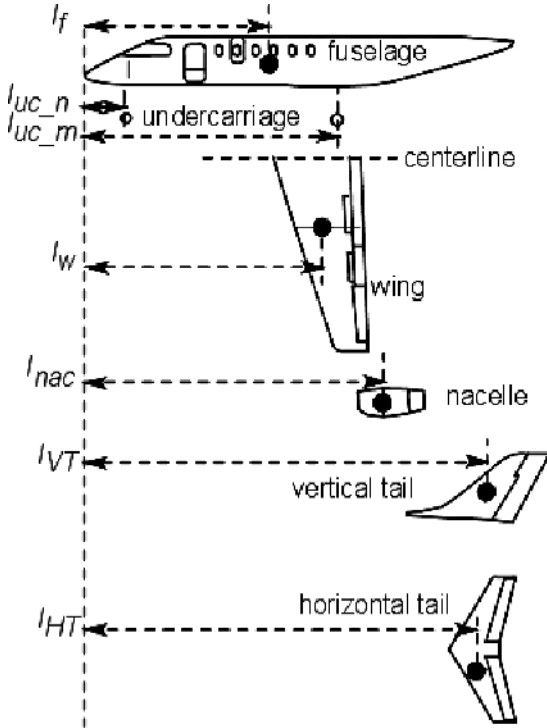


Figure 8.4 Aircraft component CG locations

Then:

$$M_{Fcivil} = c_{fus} \times k_e \times k_p \times k_{uc} \times k_{door} \times (\text{MTOM} \times n_{ult})^x \times (2 \times L \times D_{ave} \times V_D^{0.5})^y$$

For civil aircraft, $(\text{MTOM} \times n_{ult})^x = 1$; therefore:

$$\begin{aligned} M_{Fcivil} &= 0.04 \times 1.04 \times 1.09 \times 1.06 \times 1 \times 1 \times (2 \times 15.24 \times 1.75 \times 195.5^{0.5})^{1.5} \\ &= 0.048 \times (2 \times 15.24 \times 1.75 \times 195.5^{0.5})^{1.5} = 0.048 \times (53.35 \times 13.98)^{1.5} \\ &= 0.048 \times (745.95)^{1.5} = 0.048 \times 20,373.3 = 978 \text{ kg} \end{aligned}$$

There is a 5% reduction of mass due to the use of composites:

$$M_{Fcivil} = 0.95 M_{Fcivil_all\ metal} \approx 930 \text{ kg}$$

This is checked using Torenbeek's method (Equation 8.13); refer to Chapters 6 and 9 for dimensions:

$$\begin{aligned} W_{Fcivil} &= 0.021 K_f \{V_D L_{HT} / (W + D)\}^{0.5} (S_{fus_gross_area})^{1.2} \\ K_f &= 1.08, L = 50 \text{ ft}, W = 5.68 \text{ ft}, D = 5.83 \text{ ft}, L_{HT} = 25 \text{ ft}, V_D = 380 \text{ KEAS}, \\ S_{fus_gross_area} &= 687 \text{ ft}^2 \end{aligned}$$

Therefore,

$$\begin{aligned} W_{Fcivil} &= 0.021 \times 1.08 \times 1.07 \times \{380 \times 25 / (5.68 + 5.83)\}^{0.5} \times (687)^{1.2} \\ &= 0.0243 \times (825.4)^{0.5} \times 2,537.2 = 0.0243 \times 28.73 \times 2,537.2 = 1,770 \text{ lb} (805 \text{ kg}) \end{aligned}$$

The higher value of the two (i.e., 930 kg) is retained, which gives a safer approach initially.

8.11.2 Wing Group Mass

Consider a 10% composite secondary structure; that is:

$$k_{mat} = (0.9 + 0.9 \times 0.1) = 0.99$$

It has no slat, making $k_{sl} = 1$, and without a winglet, $k_{wl} = 1$. For the spoiler, $k_{sl} = 1.001$, and for a wing-mounted undercarriage, $k_{uc} = 1.002$.

$$\begin{aligned} S_W &= 30 \text{ m}^2, n_{ult} = 4.125, b = 15 \text{ m}, AR = 6.75, \lambda = 0.375, \text{ fuel in wing}, M_{WR} \\ &= 1,140 \text{ kg}, \Lambda = 14^\circ, t/c = 0.105, \text{ and } V_D = 380 \text{ knots} = 703.76 \text{ kmph} \\ &= 195.5 \text{ m/s}. \text{ The load factor } n = 3.8. \end{aligned}$$

Equation 8.21 becomes:

$$\begin{aligned} M_W &= 0.0215 \times 0.99 \times 1.002 \times 1.001 \times (9,500 \times 4.125)^{0.48} \times 29^{0.78} \\ &\quad \times 6.75 \times (1 + 0.375)^{0.4} \times (1 - 1,140/9,500)^{0.4} / (\text{Cos}14 \times 0.105^{0.4}) \\ M_W &= 0.0213 \times 1.003 \times 160.2 \times (13.8 \times 6.75 \times 1.136) \times 0.88^{0.4} / (0.97 \times 0.406) \\ M_W &= 3.42 \times 105.8 \times 0.95 / (0.3977) = 351.8 / 0.3977 = 864 \text{ kg} \end{aligned}$$

8.11.3 Empennage Group Mass

For a H-tail, a conventional split tail has a $k_{conf} = 1.0$. Consider a 20% composite secondary structure; that is:

$$k_{mat} = (0.8 + 0.9 \times 0.2) = 0.98$$

$$MTOM = 9,500 \text{ kg}, n_{ult} = 4.125, S_{HT} = 5.5 \text{ m}^2 \text{ (exposed)}, AR = 3.5, \lambda = 0.3,$$

$$\Lambda = 16^\circ, t/c = 0.105, \text{ and } V_D = 380 \text{ knots} = 703.76 \text{ kmph} = 195.5 \text{ m/s.}$$

$$M_{HT} = 0.02 \times 0.98 \times (9,500 \times 4.125)^{0.484} \times 5.5^{0.78} \times 3.5 \\ \times (1 + 0.3)^{0.4} / (\text{Cos}16 \times 0.105^{0.4})$$

$$= 0.0196 \times 167.1 \times 3.8 \times 3.5 \times 1.11 / (0.961 \times 0.406) = 47.7 / 0.39 = 124 \text{ kg}$$

For a V-tail (T-tail), $k_{conf} = 1.1$. Consider a 20% composite in a secondary structure; that is:

$$k_{mat} = (0.8 + 0.9 \times 0.2) = 0.98$$

$$MTOM = 9,200 \text{ kg}, n_{ult} = 4.125, S_{VT} = 3.5 \text{ m}^2 \text{ (exposed)}, AR = 2.0, \lambda = 0.5,$$

$$\Lambda = 20^\circ, t/c = 0.105, \text{ and } V_D = 380 \text{ knots} = 703.76 \text{ kmph} = 195.5 \text{ m/s}$$

$$M_{VT} = 0.0215 \times 0.98 \times 1.1 \times (9,500 \times 4.125)^{0.484} \times 3.5^{0.78} \times 2 \times (1 + 0.5)^{0.4} / \\ (\text{Cos}20 \times 0.105^{0.4})$$

$$= 0.02318 \times 167.1 \times 2.66 \times 2 \times 1.176 / (0.94 \times 0.406)$$

$$= 23.877 / 0.382 = 63 \text{ kg}$$

Figure 8.5 provides the graphical solution. It reads $\mu/Wf = 0.02$ (top line corresponding to span, $b = 49.2$ ft). Therefore, wing weight $\mu = 22,000 \times 3.8 \times 0.021 = 1,756 \text{ lb} = 800 \text{ kg}$, a difference of about 6%.

8.11.4 Nacelle Group Mass

Engine thrust = 17,230 N (3,800 lb) per engine with a BPR < 4.

$$M_{nac+pylon} = 6.2 \times \text{thrust (kN)} \text{ per nacelle} = 6.2 \times 17.23 = 106 \text{ kg per nacelle Two} \\ \text{nacelles} = 212 \text{ kg.}$$

8.11.5 Undercarriage Group Mass

$$MTOM = 9,500 \text{ kg low-wing mount; } M_{U/C_wing} = 0.04 \times 9,500 = 380 \text{ kg}$$

8.11.6 Miscellaneous Group Mass

Fortunately, there are no miscellaneous structures in the examples considered herein.

8.11.7 Power Plant Group Mass

This is determined from statistics until it is sized in [Chapter 10](#). A typical engine is of the class Allison TFE731–20 turbofan with thrust per engine = 15,570 N to 17,230 N (3,500 to 3,800 lbs).

If a manufacturer's dry weight is available, it is better to use it rather than semi-empirical relations. In this case, the manufacturer's dry weight is in the public domain. $M_{DRYENG} = 379$ kg per engine. This gives:

$$(T/W_{dry_engine}) = 17,230/(379 \times 9.81) = 4.63$$

The total power plant group mass can be expressed semi-empirically as

$$M_{ENG} \text{ per engine} = 1.5 \times M_{DRYENG} \text{ per engine} = 1.5 \times 379 = 568.5 \text{ kg.}$$

For two engines, $M_{ENG} = 1,137$ kg.

8.11.8 Systems Group Mass

$$\text{MTOW} = 9,500 \text{ kg (use Equation 8.47), } M_{SYS} = 0.11 \times 9,500 = 1,045 \text{ kg.}$$

8.11.9 Furnishing Group Mass

$$\text{MTOW} = 9,500 \text{ kg (use Equation 8.50), } M_{FUR} = 0.065 \times 9,500 = 618 \text{ kg}$$

8.11.10 Contingency Group Mass

$$\text{MTOW} = 9,500 \text{ kg (use Equation 8.52), } M_{CONT} = 0.015 \times 9,500 = 143 \text{ kg}$$

8.11.11 Crew Mass

There are two flight crew members and no cabin crew. Therefore, $M_{CREW} = 2 \times 90 = 180$ kg.

8.11.12 Payload Mass

There are ten passengers. Therefore, $M_{PL} = 10 \times 90 = 900$ kg.

8.11.13 Fuel Mass

The range requirement is 2,000 nm carrying ten passengers. From statistical data given in Table 8.1, take the highest value of 26% of MTOW, $M_{FUEL} = 0.26 \times 9,500 = 2,470 \approx 2,500$ kg.

8.11.14 Weight Summary

Table 8.5 is the weight summary obtained by using the coursework example worked out thus far. The last column provides the estimation as a result of the graphical solution (in bracket –kg).

This computation requires further iterations to be fine-tuned for better accuracy. The CG position is established in the next section, when further iterations will yield a better picture.

Variant Aircraft in the Family

For simplification, linear variations are considered, which should be worked out as a coursework exercise.

Table 8.6. Typical values of component CG locations: civil aircraft

Component	CG and typical % of component characteristic length
1. Fuselage group	45%
2. Wing group	No slat – 30% of MAC With slat – 25% MAC
3. H-tail group	30%
4. V-tail group	30%
5. Undercarriage group	At wheel center (nose and main wheels taken separately)
6. Nacelle + pylon group	35%
7. Miscellaneous	As positioned – use similarity
8. Power plant group	50%
9. Systems group	As positioned – use similarity (typically 40% of fuselage)
10. Furnishing group	As positioned – use similarity
11. Contingencies	As positioned – use similarity
MEM	(do not need to compute CG)
12. Crew	As positioned – use similarity
OEM	Compute
13. Payload	As positioned (distribute around CG)
14. Fuel	As positioned (distribute around CG)
MTOM	Compute
MRM	Compute

Longer Variant. Increase Δ Payload = 400 kg, Δ Fuselage = 300 kg, Δ Furnish = 200 kg, Δ Fuel = 300 kg, and Δ Others = 200 kg. Total increase = +1,400 kg; $MTOM_{Long} = 10,900$ kg (no structural changes).

Smaller Variant. Decrease Δ Payload = 500 kg, Δ Fuselage = 350 kg, Δ Furnish = 250 kg, Δ Fuel = 350 kg, and Δ Others = 250 kg (lightening of the structures). Total decrease = –1,700 kg; $MTOM_{Small} = 7,800$ kg.

8.12 Center of Gravity Determination

After obtaining the component masses (i.e., weights), it is now time to locate the aircraft CG. A reference-coordinate system is essential for locating the CG position relative to an aircraft. A suggested coordinate system is to use the X-axis along the ground level (or at another suitable level) and the Z-axis passing through the farthest point of the nose cone (i.e., tip), as shown in Figure 8.1. Typically, the fuselage axis is parallel or nearly parallel to the X-axis. In the example, it is parallel, with x measured from the aircraft nose and then converted to the MAC_w . Table 8.6 can be used to determine the CG location.

The first task is to estimate the CG position for each component group from the statistical data. Figure 8.4 provides generic information for locating the positions. During Phase 2, when more details of the components emerge, the CG positions are fine-tuned and the estimation is iterated. Typical ranges of the CG position relative to the component are given in Table 8.6. At this stage, the extreme forwardmost and rearmost CG positions (i.e., x coordinates) have not been determined and will be done later. In this book, it is demonstrated that the CG falls within the forward and aft CG limits, as shown in the worked-out example in Section 7.14. The CG

height from the ground is represented by the z coordinates. The CG should lie in the plane of symmetry (there are unsymmetrical aircraft).

It must be emphasized that the conceptual design phase relies on designers' experience that is available in statistical data. Typical aircraft-component CGs result in the CG locations; therefore, the components must be positioned accordingly. At the conceptual design phase (i.e., not yet manufactured), it is not possible to obtain accurate component weights and their CG locations are yet to evolve. Designers' experience is the way to minimize error. However, errors at this stage do not hinder the progress of the conceptual design, which is revised through iterations for better accuracy. The industry can then confidently predict the final accuracy level within ± 3 to $\pm 5\%$, which is sufficient to study the competition before the go-ahead is given.

The expressions for x , y , and z coordinates are as follows:

$$\bar{x} = \sum_i^n \frac{(\text{component weight} \times \text{distance from nose reference point})}{\text{aircraft weight}} \quad (8.54)$$

$$\bar{z} = \sum_i^n \frac{(\text{component weight} \times \text{distance from ground reference line})}{\text{aircraft weight}} \quad (8.55)$$

$$\bar{y} = 0 \text{ (CG is at the plane of symmetry)} \quad (8.56)$$

Section 8.14 presents the worked-out example to compute \bar{x} and \bar{z} .

Immediately after the go-ahead is obtained, significant budget funds are released for the project-definition phase (see [Chapter 2](#)). During this phase, major structural details are drawn in CAD to obtain more accurate component weights and the CG location. Bought-out items for the systems, undercarriage, and power plant also are identified, and the suppliers provide accurate weight and CG data. During the project-definition phase, very accurate predictions (i.e., $< \pm 2$ to $\pm 3\%$) can be obtained.

If the computations do not indicate the CG within the specified ranges, the wing and/or the engine(s) are moved to bring the CG near the desired percentages of the MAC until a satisfactory solution is reached. Moving the wing also moves the CG and the neutral point, which may require iteration (also known as wing-chasing problems). The fuel tankage can be slightly modified. Batteries are heavy and can be moved to fine-tune the CG location to the desired position (as well as any other heavy items that can be moved).

8.12.1 Bizjet Aircraft CG Location Example

[Table 8.7](#) and [Equations 8.54](#) and [8.55](#) are used to locate the CG. SI units are used.

Both the mass and the CG location are slightly different than the preliminary data. This results in the CG angle, $\beta = \tan^{-1} (8.4 - 7.44)/1.357 = \tan^{-1} 0.7 = 35$ deg. This is a satisfactory angle to cover the maximum fuselage-rotation angle at takeoff.

The CG is located almost at the middle of the baseline aircraft length, and the wing is positioned just behind it, which indicates that the CG is in the forward position. Proper CG positioning can be established after the aircraft neutral point is determined; the forward and aft CG limits can be ascertained by fine-tuning the

Table 8.7. *Determination of Bizjet CG location*

Item Group	Mass (kg)	X (m)	Moment	Z (m)	Moment
Fuselage	930	6.8	4,284	1.6	1,488
Wing	864	7.8	6,739.2	1	864
H-tail	124	14	1,736	8	992
V-tail	63	15	945	3	189
Undercarriage (nose)	110	1.2	132	0.4	44
Undercarriage (main)	270	8.4	2,268	0.5	135
Nacelle/pylon	212	10.2	2,346	2.1	460
Miscellaneous					
Power plant	1,060	11	11,660	1.9	2,014
Systems	1,045	6.5	6,792.5	1	1,045
Furnishing	618	6	3,708	2	1,236
Contingencies	143	3	429	1.2	171.6
MEM	5,457				
Crew	180	3	540	1.4	252
Consumable	119	4.25	505	1.5	152
OEM	5,800				
Payload	1,100	6	6,600	1.1	1,210
Fuel	2,500	8.5	21,250	1	2,500
Total moment at MTOM	9,400		69,934.7		12,752.6
		$\bar{x} = 7.44$ m		$\bar{z} = 1.357$ m	
MRM	9,450				

component positions. Determining the aircraft neutral point is not addressed in this book, but it is approximately 50 to 55% of the wing MAC. Therefore, in this case, only small changes may be required to fine-tune the aircraft CG limits. Changing the wing position may be problematic, but a small degree of engine repositioning can be effective. Relocating heavy onboard items is easy and effective for last-minute fine-tuning, especially during flight-testing.

8.12.2 First Iteration to Fine Tune CG Position Relative to Aircraft and Components

The preliminary aircraft configuration begins in [Chapter 6](#) with a guesstimated MTOM, engine size, and CG position. It is unlikely that the computed aircraft mass as worked out in this chapter will match the estimated mass. In fact, the example shows that it is lighter, with a more accurate CG position; therefore, this replaces the estimated values in [Chapter 6](#).

In principle, the aircraft configuration must be revised at this stage of progress as the first iteration. Final sizing is accomplished in [Chapter 11](#), when iteration is required. Coursework may require only one iteration cycle of computation.

8.13 Rapid Mass Estimation Method – Military Aircraft

This extended section presents the military aircraft rapid mass estimation method in terms of mass fraction (in percentage) of maximum take-off mass ($M_i/MTOM$),

where subscript ' i ' represents the i th component. The range of fractions are obtained from statistics given in tabular form in Table 8.8.

Table 8.8. *Military trainer aircraft mass fraction*

8.14 Graphical Method to Predict Aircraft Component Weight – Military Aircraft

This extended section presents statistical data on military aircraft component mass in graphical form, as illustrated in the following figures.

Figure 8.5. Military aircraft fuselage mass

Figure 8.6. Military aircraft wing mass

Figure 8.7. Military aircraft empennage mass

Figure 8.8. Military aircraft engine mass

Figure 8.9. Military aircraft undercarriage mass

Figure 8.10. Military aircraft system mass

8.15 Semi-empirical Equation Methods (Statistical) – Military Aircraft

This extended section presents military aircraft mass estimation semi-empirical relations derived from theoretical formulation and refined with statistical data. The section is divided into subsections, each with a step-by-step discussion of workflow, as shown below by their titles.

8.15.1 Military Aircraft Fuselage Group (SI System)

8.15.2 Military Aircraft Wing Mass (SI System)

8.15.3 Military Aircraft Empennage

8.15.4 Nacelle Mass Example – Military Aircraft

8.15.5 Power Plant Group Mass Example – Military Aircraft

8.15.6 Undercarriage Mass Example – Military Aircraft

8.15.7 System Mass – Military Aircraft

8.15.8 Aircraft Furnishing – Military Aircraft

8.15.9 Miscellaneous Group (M_{MISC}) – Military Aircraft

8.15.10 Contingency (M_{CONT}) – Military Aircraft

8.15.11 Crew Mass

8.15.12 Fuel (M_{FUEL})**8.15.13 Payload (M_{PL})****8.16 Classroom Example of Military AJT/CAS Aircraft Weight Estimation**

This extended section of the book presents details of a worked-out example of Advanced Jet Trainer (AJT). The section is divided into subsections, each with a step-by-step discussion of workflow as their titles (below) show. The associated table is listed.

8.16.1 AJT Fuselage Example (Based on CAS Variant)**8.16.2 AJT Wing Example (Based on CAS Variant)****8.16.3 AJT Empennage Example (Based on CAS Variant)****8.16.4 AJT Nacelle Mass Example (Based on CAS Variant)****8.16.5 AJT Power Plant Group Mass Example (Based on AJT Variant)****8.16.6 AJT Undercarriage Mass Example (Based on CAS Variant)****8.16.7 AJT Systems Group Mass Example (Based on AJT Variant)****8.16.8 AJT Furnishing Group Mass Example (Based on AJT Variant)****8.16.9 AJT Contingency Group Mass Example****8.16.10 AJT Crew Mass Example****8.16.11 Fuel (M_{FUEL})****8.16.12 Payload (M_{PL})****8.16.13 Weights Summary – Military Aircraft**

Table 8.9. *AJT component and weight summary*

8.17 CG Position Determination – Military Aircraft*

This extended section of the book presents the methodology adopted to determine aircraft CG. The section is divided into subsections, each with a step-by-step discussion of workflow, as their titles show. The associated tables are listed.

Table 8.10. *Typical values of component CG locations – military aircraft*

8.17.1 Classroom Worked-Out Military AJT CG Location Example

This subsection includes Table 8.11.

Table 8.11. *Typical values of component CG locations – AJT*

8.17.2 First Iteration to Fine Tune CG Position and Components Masses

9 Aircraft Drag

9.1 Overview

An important task in aircraft design is to make the best possible estimation of all the different types of drag associated with aircraft aerodynamics. Commercial aircraft design is sensitive to the DOC, which is aircraft-drag-dependent. Just one count of drag (i.e., $C_D = 0.0001$) could account for several million U.S. dollars in operating cost over the lifespan of a small fleet of mid-sized aircraft. This will become increasingly important with the increasing trend in fuel costs. Accurate estimation of the different types of drag remains a central theme. (Equally important are other ways to reduce DOC as described in Section 2.1; these are discussed in [Chapter 17](#).)

For a century, a massive effort has been made to understand and estimate drag, and the work is still continuing. Possibly some of the best work on aircraft drag in English is compiled by NACA/NASA, RAE, AGARD, ESDU, DATCOM, Royal Aeronautical Society (RAeS), AIAA, and others. These publications indicate that the drag phenomena are still not fully understood and that the way to estimate aircraft drag is by using semi-empirical relations. CFD (see [Chapter 14](#)) is gaining ground but it is still some way from supplanting the proven semi-empirical relations. In the case of work on excrescence drag, efforts are lagging.

The 2D-surface skin friction drag, elliptically loaded induced drag, and wave drag can be accurately estimated – together, they comprise most of the total aircraft drag. The problem arises when estimating drag generated by the 3D effects of the aircraft body, interference effects, and excrescence effects. In general, there is a tendency to underestimate aircraft drag.

Accurate assessments of aircraft mass, drag, and thrust are crucial in the aircraft performance estimation. They also contribute to aircraft stability and control analyses.

Sections 3.2, 3.3, 3.12, and 3.16 define the basic elements of drag. This chapter outlines the considerations and methodology to estimate aircraft drag using worked-out examples.

9.1.1 What Is to Be Learned?

This chapter covers the following topics:

- Section 9.2: Introduction to aircraft drag
- Section 9.3: Parasite drag
- Section 9.4: Aircraft drag breakdown structure
- Section 9.5: Theoretical background of aircraft drag
- Section 9.6: Subsonic aircraft drag estimation methodology
- Section 9.7: Methodology to estimate minimum parasite drag (C_{Dpmin})
- Section 9.8: Semi-empirical relations to estimate C_{Dpmin}
- Section 9.9: Excrescence drag
- Section 9.10: Summary of aircraft parasite drag (C_{Dpmin})
- Section 9.11: Methodology to estimate ΔC_{Dp}
- Section 9.12: Methodology to estimate subsonic wave drag
- Section 9.13: Summary of total aircraft drag
- Section 9.14: Low-speed aircraft drag at takeoff and landing
- Section 9.15: Drag of propeller-driven aircraft
- Section 9.16: Military aircraft drag
- Section 9.17: Empirical methodology for supersonic drag estimation
- Section 9.18: Bizjet example – civil aircraft
- Section 9.19: Military aircraft example

9.1.2 Coursework Content

The coursework task continues linearly. Readers will carry out aircraft component drag estimation and obtain the total aircraft drag.

9.2 Introduction

The drag of an aircraft depends on its shape and speed, which are design-dependent, as well as on the properties of air, which are nature-dependent. Drag is a complex phenomenon arising from several sources, such as the viscous effects that result in skin friction and pressure differences as well as the induced flow field of the lifting surfaces and compressibility effects (see Sections 3.12 and 3.16).

The aircraft drag estimate starts with the isolated aircraft components (e.g., wing and fuselage). Each component of the aircraft generates drag largely dictated by its shape. Total aircraft drag is obtained by summing the drag of all components plus their interference effects when the components are combined. The drag of two isolated bodies increases when they are brought together due to the interference of their flow fields.

The Re has a deciding role in determining the associated skin-friction coefficient, C_f , over the affected surface and the type, extent, and steadiness of the boundary layer (which affects parasite drag) on it. Boundary-layer separation increases drag and is undesirable; separation should be minimized.

A major difficulty arises in assessing drag of small items attached to an aircraft surface such as instruments (e.g., pitot and vanes), ducts (e.g., cooling), blisters,

and necessary gaps to accommodate moving surfaces. In addition, there are the unavoidable discrete surface roughness from mismatches (at assembly joints) and imperfections, perceived as defects, that result from limitations in the manufacturing processes. Together, from both manufacturing and nonmanufacturing origins, they are collectively termed *excrescence drag*.

The review in Section 2.6 makes clear that accurate total aircraft drag estimation is not possible using analytical or CFD methods. Schmidt of Dornier in the AGARD 256 is categorical about the inability of CFD, analytical methods, or even wind-tunnel model-testing to estimate drag. CFD is steadily improving and can predict wing-wave drag (C_{Dw}) accurately but not total aircraft drag – most of the errors are due to the smaller excrescence effects, interference effects, and other parasitic effects. Industrial practices employ semi-empirical relations (with CFD) validated against wind-tunnel and flight tests and are generally proprietary information. Most of the industrial drag data are not available in the public domain.

The methodology given in this chapter is a modified and somewhat simplified version of standard industrial practices ([1], [3], and [7]). The method is validated by comparing its results with the known drag of existing operational aircraft.

The design criterion for today's commercial high-subsonic jet transport aircraft is that the effects of separation and local shocks are minimized (i.e., compressibility drag almost equal to zero) at the LRC (before the onset of wave drag) condition. At HSC, a twenty-count drag increase is allowed, reaching M_{crit} , due to local shocks (i.e., transonic flow) covering small areas of the aircraft. Modern streamlined shapes maintain low separation at M_{crit} ; therefore, such effects are small at HSC. The difference in the Mach number at HSC and LRC for subsonic aircraft is small – on the order of Mach 0.05 to Mach 0.075. Typically, estimation of the drag coefficient at LRC is sufficient because it has a higher C_f , which gives conservative values at HSC when ΔC_{Dw} is added. The LRC condition is by far the longest segment in the mission profile; the industry standard practice at the conceptual study phase uses the LRC drag polar for all parts of the mission profile (e.g., climb and descent). The Re at the LRC provides a conservative estimate of drag at the climb and descent segments. At takeoff and landing, the undercarriage and high-lift device drags must be added. In the next phase of the project, more detailed drag estimation is carried out.

Supersonic aircraft operate over a wider speed range: The difference between maximum aircraft speed and M_{crit} is on the order of Mach 1.0 to Mach 1.2. Therefore, estimation of C_{Dpmin} is required at three speeds: (1) at a speed before the onset of wave drag, (2) at M_{crit} , and (3) at maximum speed (e.g., Mach 2.0).

It is difficult for the industry to absorb drag-prediction errors of more than 5% (the goal is to ensure errors of <3%) for civil aircraft; overestimating is better than underestimating. Practitioners are advised to be generous in allocating drag – it is easy to miss a few of the many sources of drag, as shown in the worked-out examples in this chapter. Underestimated drag causes considerable design and management problems; failure to meet customer specifications is expensive for any industry. Subsonic aircraft drag prediction has advanced to the extent that most aeronautical establishments are confident in predicting drag with adequate accuracy. Military aircraft shapes are more complex; therefore, it is possible that predictions will be less accurate.

9.3 Parasite Drag Definition

The components of drag due to viscosity do not contribute to lift. For this reason, it is considered “parasitic” in nature. For bookkeeping purposes, parasite drag is usually considered separately from other drag sources. The main components of parasite drag are as follows:

- drag due to skin friction
- drag due to the pressure difference between the front and the rear of an object
- drag due to the lift-dependent viscous effect and therefore seen as parasitic (to some extent resulting from the nonelliptical nature of lift distribution over the wing); this is a small but significant percentage of total aircraft drag (at LRC, it is $\approx 2\%$)

All of these components vary (to a small extent) with changes in aircraft incidence (i.e., as C_L changes). The minimum parasite drag, C_{Dpmin} , occurs when shock waves and boundary-layer separation are at a minimum, by design, around the LRC condition. Any change from the minimum condition (C_{Dpmin}) is expressed as ΔC_{Dp} . In summary:

$$\begin{aligned} \text{parasite drag } (C_{Dp}) &= (\text{drag due to skin friction [viscosity]} + \text{drag due to} \\ &\text{pressure difference [viscosity]}) = \text{minimum parasite drag } (C_{Dpmin}) \\ &+ \text{incremental parasite drag } (\Delta C_{Dp}) \end{aligned} \quad (9.1)$$

Oswald’s efficiency factor (see Section 3.12) is accounted for in the lift-dependent parasite drag. The nature of ΔC_{Dp} is specific to a particular aircraft. Numerically, it is small and difficult to estimate.

Parasite drag of a body depends on its form (i.e., shape) and is also known as *form drag*. The form drag of a wing profile is known as *profile drag*. In the past, parasite drag in the FPS system was sometimes expressed as the drag force in pound force (lb_f) at 100 ft/s speed, represented by D_{100} . This practice was useful in its day as a good way to compare drag at a specified speed, but it is not used today. These two terms are not used in this book.

The current industrial practice using semi-empirical methods to estimate C_{Dpmin} is a time-consuming process. (If computerized, then faster estimation is possible, but the author recommends relying more on the manual method at this stage.) Parasite drag constitutes one-half to two-thirds of subsonic aircraft drag. Using the standard semi-empirical methods, the parasite drag units of an aircraft and its components are generally expressed as the drag of the “equivalent flat-plate area” (or “flat-plate drag”), placed normal to airflow as shown in [Figure 9.1](#) (see Equation 9.7). These units are in square feet to correlate with literature in the public domain. This is not the same as air flowing parallel to the flat plate and encountering only the skin friction.

The inviscid idealization of flow is incapable of producing parasite drag because of the lack of skin friction and the presence of full pressure recovery.

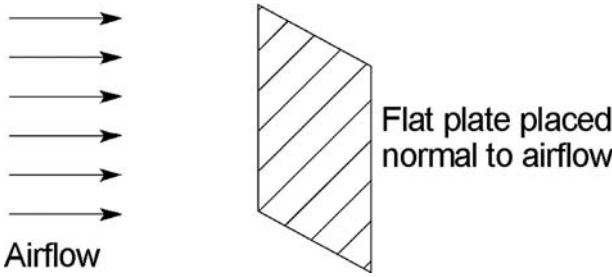


Figure 9.1. Flat plate equivalent of drag

9.4 Aircraft Drag Breakdown (Subsonic)

There are many variations and definitions of the bookkeeping methods for components of aircraft drag; this book uses the typical U.S. practice [2]. The standard breakdown of aircraft drag is as follows (see Equation 9.1):

$$\begin{aligned}
 \text{total aircraft drag} &= (\text{drag due to skin friction} + \text{drag due to pressure difference}) \\
 &\quad + \text{drag due to lift generation} + \text{drag due to compressibility} \\
 &= \text{parasite drag } (C_{Dp}) + \text{lift-dependent induced drag } (C_{Di}) \\
 &\quad + \text{wave drag } (C_{Dw}) \\
 &= (\text{minimum parasite drag } [C_{Dpmin}] \\
 &\quad + \text{incremental parasite drag } [\Delta C_{Dp}]) \\
 &\quad + \text{induced drag } (C_{Di}) + \text{wave drag } (C_{Dw})
 \end{aligned}$$

Therefore, the total aircraft drag coefficient is:

$$C_D = C_{Dpmin} + \Delta C_{Dp} + C_L^2 / \pi AR + C_{Dw} \tag{9.2}$$

The advantage of keeping pure induced drag separate is obvious because it is dependent only on the lifting-surface aspect ratio and is easy to compute. The total aircraft drag breakdown is shown in Chart 9.1.

It is apparent that the C_D varies with the C_L . When the C_D and the C_L relationship is shown in graphical form, it is known as a *drag polar*, shown in Figure 9.2 (all components of drag in Equation 9.2 are shown in the figure). The C_D versus the C_L^2 characteristics of Equation 9.2 are rectilinear, except at high and low C_L values (see

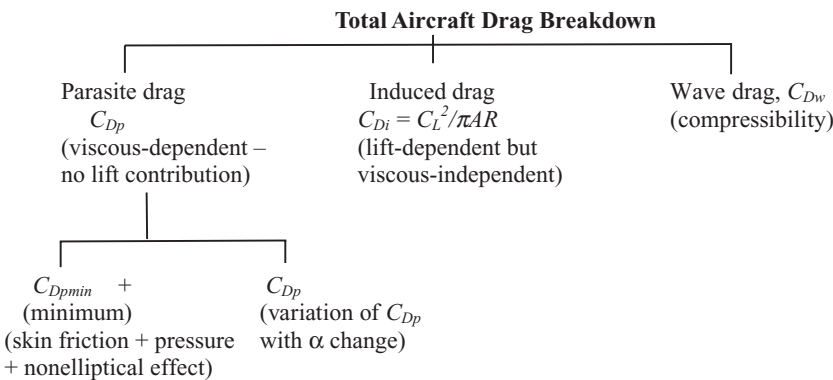


Chart 9.1. Total aircraft drag breakdown

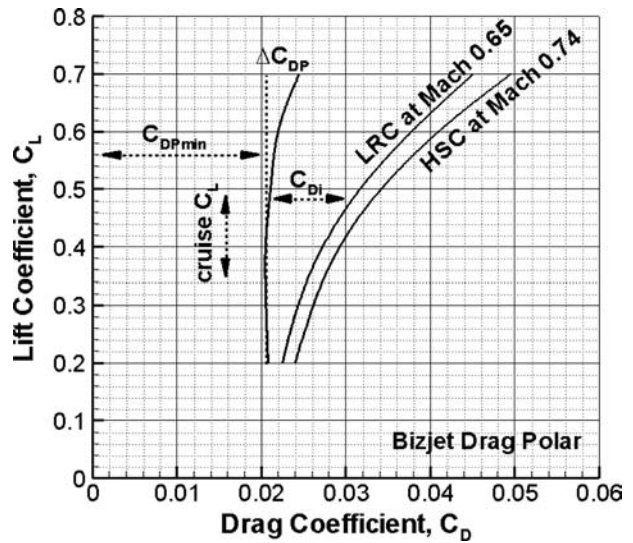


Figure 9.2. Aircraft drag polar

Figure 9.15), because at a high C_L (i.e., low speed, high angle of attack), there could be additional drag due to separation; at a very low C_L (i.e., high speed), there could be additional drag due to local shocks. Both effects are nonlinear in nature. Most of the errors in estimating drag result from computing ΔC_{Dp} , three-dimensional effects, interference effects, excrescence effects of the parasite drag, and nonlinear range of aircraft drag. Designers should keep $C_{Dw} = 0$ at LRC and aim to minimize to $\Delta C_{Dp} \approx 0$ (perceived as the design point).

An aircraft on a long-range mission typically has a weight change of more than 25% from the initial to the final cruise condition. As the aircraft becomes lighter, its induced drag decreases. Therefore, it is more economical to cruise at a higher altitude to take advantage of having less drag. In practical terms, this is achieved in the *step-climb* technique, or a gradual climb over the cruise range.

9.5 Aircraft Drag Formulation

A theoretical overview of drag is provided in this section to show that aircraft geometry is not amenable to the equation for an explicit solution. Even so, CFD is yet to achieve an acceptable result for the full aircraft.

Recall the expression in Equation 9.2 for the total aircraft drag, C_D , as:

$$C_D = C_{Dparasite} + C_{Di} + C_{Dw} = C_{Dpmin} + \Delta C_{Dp} + C_{Di} + C_{Dw}$$

where $C_{Dparasite} = C_{Dfriction} + C_{Dpressure} = C_{Dpmin} + \Delta C_{Dp}$

At LRC, when $C_{Dw} \approx 0$, the total aircraft drag coefficient is given by:

$$C_D = C_{Dpmin} + \Delta C_{Dp} + C_{Di} \tag{9.3}$$

The general theory of drag on a 2D body (Figure 9.3a) provides the closed-form Equation 9.4. A 2D body has infinite span. In the diagram, airflow is along the x direction and wake depth is shown in the y direction. The wake is formed due to viscous effects immediately behind the body, where integration occurs. The subscript ∞ denotes the free-stream condition. Consider an arbitrary CV large enough

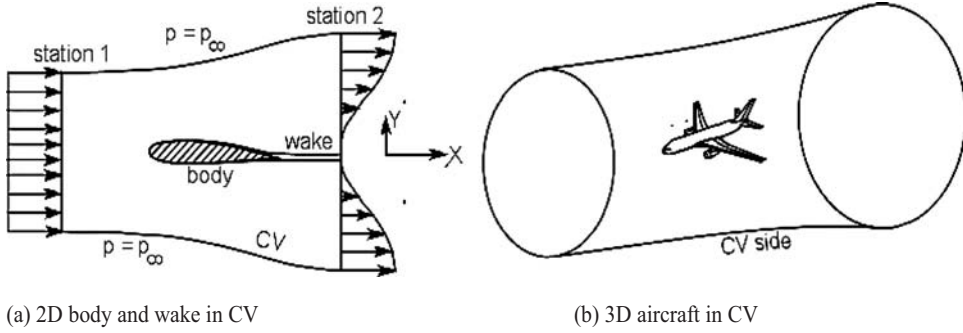


Figure 9.3. CV approach to formulate aircraft drag

in the y direction where static pressure is equal to free-stream static pressure (i.e., $p = p_\infty$). Wake behind a body is due to the viscous effect in which there is a loss of velocity (i.e., momentum) and pressure shown in the figure. Measurement and computation across the wake are performed close to the body; otherwise, the downstream viscous effect dissipates the wake profile. Integration over the y direction on both sides up to the free-stream value gives:

$$\begin{aligned}
 D &= D_{press} + D_{skin} = \int_{-\infty}^{\infty} (p_\infty - p) dy + \int_{-\infty}^{\infty} \rho u (U_\infty - u) dy \\
 &= \int_{-\infty}^{\infty} [(p_\infty - p) + \rho u (U_\infty - u)] dy \tag{9.4}
 \end{aligned}$$

An aircraft is a 3D object (Figure 9.3b) with the additional effect of a finite wing span that produces induced drag. In that case, the previous equation can be written as:

$$D = D_{skin} + D_{press} + D_i = \int_{-\infty}^{\infty} \int_{-b/2}^{b/2} [(p_\infty - p) + \rho u (U_\infty - u)] dx dy \tag{9.5}$$

where b is the span of the wing in the x direction (i.e., the axis system has changed).

The finite-wing effects on the pressure and velocity distributions result in induced drag D_i embedded in the expression on the right-hand side of Equation 9.5. Because the aircraft cruise condition (i.e., LRC) is chosen to operate below M_{crit} , the wave drag, D_w , is absent; otherwise, it must be added to the expression. Therefore, Equation 9.5 can be equated with the aircraft drag expression as given in Equation 9.3. Finally, Equation 9.5 can be expressed in nondimensional form, by dividing $\frac{1}{2} \rho_\infty U_\infty^2 S_W$. Therefore,

$$\begin{aligned}
 C_D &= \frac{1}{S_W} \int_{-\infty}^{\infty} \int_{-b/2}^{b/2} \left[-\frac{(p - p_\infty)}{\frac{1}{2} \rho_\infty U_\infty^2} + \frac{2\rho u}{\rho_\infty U_\infty} \left(1 - \frac{u}{U_\infty} \right) \right] dx dy \\
 &= \frac{1}{S_W} \int_{-\infty}^{\infty} \int_{-b/2}^{b/2} \left[-C_p + \frac{2\rho u}{\rho_\infty U_\infty} \left(1 - \frac{u}{U_\infty} \right) \right] dx dy \tag{9.6}
 \end{aligned}$$

Unfortunately, the complex 3D geometry of an entire aircraft in Equation 9.6 is not amenable to easy integration. CFD has discretized the flow field into small domains that are numerically integrated, resulting in some errors. Mathematicians have successfully managed the error level with sophisticated algorithms (see Chapter 14 for a discussion of CFD). The proven industrial-standard, semi-empirical methods are currently the prevailing practice and are backed up by theories and validated by flight tests. CFD assists in the search for improved aerodynamics.

9.6 Aircraft Drag Estimation Methodology (Subsonic)

The semi-empirical formulation of aircraft drag estimation used in this book is a credible method based on [1], [3], and [7]. It follows the findings from NACA/NASA, RAE, and other research-establishment documents. This chapter provides an outline of the method used. It is clear from Equation 9.2 that the following four components of aircraft drag are to be estimated:

1. *Minimum parasite drag*, C_{Dpmin} (see Section 9.7).

Parasite drag is composed of skin friction and pressure differences due to viscous effects that are dependent on the Re. To estimate the minimum parasite drag, C_{Dpmin} , the first task is to establish geometric parameters such as the characteristic lengths and wetted areas and the Res of the discrete aircraft components.

2. *Incremental parasite drag*, ΔC_{Dp} (see Section 9.10).

ΔC_{Dp} is characteristic of a particular aircraft design and includes the lift-dependent parasite drag variation, 3D effects, interference effects, and other spurious effects not easily accounted for. There is no theory to estimate ΔC_{Dp} ; it is best obtained from wind-tunnel tests or the ΔC_{Dp} of similarly designed aircraft wings and bodies. CFD results are helpful in generating the ΔC_{Dp} -versus- C_L variation.

3. *Induced drag*, C_{Di} (see Section 3.12).

The pure induced drag, C_{Di} , is computed from the expression $C_{Di} = C_L^2 / \pi AR$.

4. *Wave drag*, C_{Dw} (see Section 9.11).

The last component of subsonic aircraft drag is the wave drag, C_{Dw} , which accounts for compressibility effects. It depends on the thickness parameter of the body: for lifting surfaces, it is the t/c ratio, and for bodies, it is the diameter-to-length ratio. CFD can predict wave drag accurately but must be substantiated using wind-tunnel test data. Transport aircraft are designed so that HSC at M_{crit} (e.g., for the Airbus 320 type, ≈ 0.82 Mach) allows a twenty-count ($\Delta C_{Dw} = 0.002$) drag increase. At LRC, wave-drag formation is kept at zero. Compressibility drag at supersonic speed is caused by shock waves.

9.7 Minimum Parasite Drag Estimation Methodology

The practiced method to compute C_{Dpmin} is first to dissect (i.e., isolate) the aircraft into discrete identifiable components, such as the fuselage, wing, V-tail, H-tail, nacelle, and other smaller geometries (e.g., winglets and ventral fins). The wetted

area and the Re of each component establishes skin friction associated with each component. The 2D flat-plate basic mean skin-friction coefficient, $C_{F.basic}$, corresponding to the Re of the component, is determined from Figure 9.19b for the flight Mach number. Sections 3.5.1 and 9.7.1 explain the worked-out examples carried out in this book for fully turbulent flow, as shown in Figure 9.19.

The various ΔC_F arising from the 3D effects (e.g., superelevancy) and wrapping effects of the components are added to the basic flat-plate $C_{F.basic}$. Superelevancy effects result from the 3D nature (i.e., curvature) of aircraft-body geometry where, in the critical areas, the local velocity exceeds the free-stream velocity (hence, the term *superelevancy*). The axi-symmetric curvature of a body (e.g., fuselage) is perceived as a wrapping effect when the increased adverse pressure gradient increases the drag. The interference in the flow field is caused by the presence of two bodies in proximity (e.g., the fuselage and wing). The flow field of one body interferes with the flow field of the other body, causing more drag. Interference drag must be accounted for when considering the drag of adjacent bodies or components – it must not be duplicated while estimating the drag of the other body.

The design of an aircraft should be streamlined so that there is little separation over the entire body, thereby minimizing parasite drag obtained by taking the total C_F (by adding various ΔC_F , to $C_{F.basic}$). Hereafter, the total C_F will be known as the C_F . Parasite drag is converted to its flat-plate equivalent expressed in f square feet. Although it can be easily converted into the SI system, in this book, the FPS system is used for comparison with the significant existing data that uses the FPS system. The flat-plate equivalent f is defined as:

$$f_{component} = (A_w \times C_F)_{component} \quad (9.7)$$

where A_w is the wetted area (unit in ft^2).

The minimum parasite drag C_{Dpmin} of an aircraft is obtained by totaling the contributing f s of all aircraft components with other sundries. Therefore, the minimum parasite drag of the aircraft is obtained by:

$$(C_{Dpmin}) = \left(\sum f_{component} + \text{sundries} \right) / S_W = \left[\sum (A_w \times C_F)_{component} / S_W \right] \quad (9.8)$$

The stepwise approach to compute C_{Dpmin} is described in the following three subsections.

9.7.1 Geometric Parameters, Reynolds Number, and Basic C_F Determination

The Re has the deciding role in determining the skin-friction coefficient, C_F , of a component. First, the Re -per-unit-length speed and altitude is computed. Then, the characteristic lengths of each component [i.e., $Re = (\rho_\infty L_{comp} V_\infty) / \mu_\infty$] are determined. The characteristic length L of each component is as follows:

- Fuselage: axial length from the tip of the nose cone to the end of the tail cone (L_{fus})
- Wing: the wing MAC
- Empennage: the MACs of the V-tail and the H-tail
- Nacelle: axial length from the nacelle-highlight plane to the nozzle-exit plane (L_{nac})

Figure 9.19 shows the basic 2D flat-plate skin-friction coefficient, C_{F_basic} , of a fully turbulent flow for local and average values. For a partial laminar flow, the C_{F_basic} correction is made using factor f_l , given in Figure 9.20. It has been shown that the compressibility effect increases the boundary layer, thus reducing the local C_F . However, in LRC until the M_{crit} is reached, there is little sensitivity of the C_F change with Mach number variations; therefore, the incompressible C_F line (i.e., the Mach 0 line in Figure 9.19b) is used. At HSC at the M_{crit} and above, the appropriate Mach line is used to account for the compressibility effect.

The methodology presented herein considers fully turbulent flow from the LE of all components. Here, no credit is taken for drag reduction due to possible laminar flow over a portion of the body and lifting surface. This is because it may not always be possible to keep the aircraft surfaces clear of contamination that would trigger turbulent flow. The certifying agencies recommend this conservative approach.

The basic C_F changes with changes in the Re, which depends on speed and altitude of the aircraft. The chapter introduction in Section 9.2 explains that a subsonic aircraft C_{Dpmin} computed at LRC would cater to the full flight envelope during Phase 1 of a project.

9.7.2 Computation of Wetted Areas

Computation of the wetted area, A_w , of the aircraft component is shown herein. Skin friction is generated on that part of the surface over which air flows, the so-called wetted area.

Lifting Surfaces

These are approximate to the flat surfaces, with the wetted area slightly more than twice the reference area due to some thickness. Care is needed in removing the areas at intersections, such as the wing area buried in the fuselage. A factor k is used to obtain the wetted area of lifting surfaces, as follows:

$$A_w = k \times (\text{reference area, } S - \text{the area buried in the body}),$$

$$\begin{aligned} \text{where } k &= 2.02 \text{ for } t/c = 0.08\% \\ &= 2.04 \text{ for } t/c = 0.12\% \\ &= 2.06 \text{ for } t/c = 0.16\% \end{aligned}$$

The factor k may be interpolated linearly for other t/c ratios.

Fuselage

The fuselage is divided conveniently into sections – typically, for civil transport aircraft, into a constant cross-section mid-fuselage with varying cross-section front- and aft-fuselage closures. The constant cross-section mid-fuselage barrel has a wetted area of $A_{wf_mid} = \text{perimeter} \times \text{length}$.

The forward- and aft-closure cones could be sectioned more finely, treating each thin section as a constant section “slice.” A military aircraft is unlikely to have a constant cross-section barrel, and its wetted area must be computed in this way. The wetted areas must be excluded where the wing and empennage join the fuselage or for any other considerations.

Nacelle

Only the external surface of the nacelle is considered the wetted area and it is computed in the same way as the fuselage, taking note of the pylon cutout area. (Internal drag within the intake duct is accounted for as installation effects in engine performance as a loss of thrust.)

9.7.3 Stepwise Approach to Compute Minimum Parasite Drag

In this book, the following seven steps are carried out to estimate the minimum parasite drag, C_{Dpmin} :

- Step 1: Dissect and isolate aircraft components such as the wing, empennage, fuselage, and nacelle. Determine the geometric parameters of the aircraft components such as the characteristic length and wetted areas.
- Step 2: Compute the Re per foot at the LRC condition. Then, obtain the component Re by multiplying its characteristic length.
- Step 3: Determine the basic 2D average skin-friction coefficient $C_{F, basic}$, corresponding to the Re for each component (see Figure 9.19b).
- Step 4: Estimate the ΔC_F as the increment due to 3D effects on each component.
- Step 5: Estimate the interference drag of two adjacent components; avoid duplication of this effect.
- Step 6: Add the results obtained in Steps 3, 4, and 5 to obtain the minimum parasite drag of a component in terms of flat-plate equivalent area (ft^2 or m^2); that is, $C_F = C_{F, 2D} + \sum \Delta C_F$ for the component: $(f)_{comp} = (A_w)_{comp} C_F$, where $(C_{Dpmin})_{comp} = (f)_{comp} / S_w$.
- Step 7: Total all the component minimum parasite drags. Then, add other drags such as the trim and excrescence drags. Finally, add 3% drag due to surface-roughness effects. The aircraft minimum parasite drag is expressed in the coefficient form, C_{Dpmin} .

The semi-empirical formulation for each component is provided in the following subsections.

9.8 Semi-empirical Relations to Estimate Aircraft Component Parasite Drag

Isolated aircraft components are worked on to estimate component parasite drag. The semi-empirical relations given here embed the necessary corrections required for 3D effects. Associated coefficients and indices are derived from actual flight-test data. (Wind-tunnel tests are conducted at a lower Re and therefore require correction to represent flight-tested results.) The influence of the related drivers is shown as drag increasing by \uparrow and drag decreasing by \downarrow . For example, an increase of the Re reduces the skin-friction coefficient and is shown as Re (\downarrow).

9.8.1 Fuselage

The fuselage characteristic length, L_{fus} , is the length from the tip of the nose cone to the end of the tail cone. The wetted area, A_{wf} (\uparrow), and fineness ratio (length/diameter) (\downarrow) of the fuselage are computed. Ensure that cutouts at the wing and

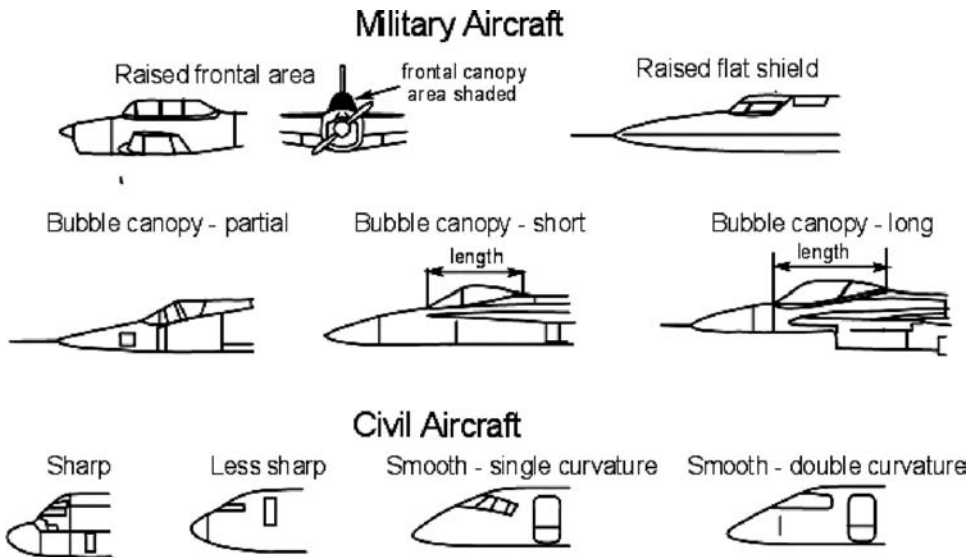


Figure 9.4. Canopy types for drag estimation

empennage junctions are subtracted. Obtain the $Re_f (\downarrow)$. The corresponding basic C_{Ff} for the fuselage using Figures 9.19 and 9.20 is intended for the flat plate at the flight Mach number. Figure 9.19 is accurate and validated over time.

The semi-empirical formulation is required to correct the 2D skin friction drag for the 3D effects and other influencing parameters, as listed herein. These are incremental values shown by the symbol Δ . There are many incremental effects and it is easy to miss some of them.

1. 3D effects [1] are due to surface curvature resulting in a change in the local flow speed and associated pressure gradients, as follows:

- (a) Wrapping:

$$\Delta C_{Ff} = C_{Ff} \times [k \times (\text{length}/\text{diameter}) \times Re^{-0.2}] \quad (9.9)$$

where k is between 0.022 and 0.025 (use the higher value)
and Re = the Re of the fuselage

- (b) Supervelocity:

$$\Delta C_{Ff} = C_{Ff} \times (\text{diameter}/\text{length})^{1.5} \quad (9.10)$$

- (c) Pressure:

$$\Delta C_{Ff} = C_{Ff} \times 7 \times (\text{diameter}/\text{length})^3 \quad (9.11)$$

2. Other effects on the fuselage (increments are given in a percentage of 2D C_{Ff}) are listed herein. The industry has more accurate values of these incremental ΔC_{Ff} . Readers in the industry should not use the values given here – they are intended only for coursework using estimates extracted from industrial data. (See Section 3.21 for an explanation of the terminology used in this section.)

- (a) *Canopy drag*. There are two types of canopy (Figure 9.4), as follows:

- (i) *Raised or bubble-type canopy or its variants*. These canopies are mostly associated with military aircraft and smaller aircraft. The canopy drag

coefficient $C_{D\pi}$ is based on the frontal cross-sectional area shown in the military type aircraft in Figure 9.4 (the front view of the raised canopy is shaded). The extent of the raised frontal area contributes to the extent of drag increment and the $C_{D\pi}$ accounts for the effects of canopy rise. $C_{D\pi}$ is then converted to $\Delta C_{E_{f,canopy}} = (A_{\pi} \times C_{D\pi}) / A_{wf}$, where A_{wf} is the fuselage wetted area. The dominant types of a raised or bubble-type canopy and their associated $C_{D\pi}$ are summarized in Table 9.1.

- (ii) *Windshield-type canopy for larger aircraft.* These canopies are typically associated with payload-carrying commercial aircraft from a small Bizjet and larger. Flat panes lower the manufacturing cost but result in a kink at the double-curvature nose cone of the fuselage. A curved and smooth transparent windshield avoids the kink that would reduce drag at an additional cost. Smoother types have curved panes with a single or double curvature. Single-curvature panes come in smaller pieces, with a straight side and a curved side. Double-curvature panes are the most expensive and considerable attention is required during manufacturing to avoid distortion of vision. The values in square feet in Table 9.2 are used to obtain a sharp-edged windshield-type canopy drag.
- (b) Body pressurization – fuselage surface waviness (use 5.5%), 5 to 6%
- (c) Nonoptimum fuselage shape (interpolate the in-between values)
 - (i) Nose fineness ratio, F_{cf} (see Figure 4.17 and Table 4.5)
 - For $F_{cf} \leq 1.5$: 8%
 - For $1.5 \leq F_{cf} \leq 1.75$: 6%
 - For $F_{cf} \geq 1.75$: 4%
 - For military aircraft type with high nose fineness: 3%
 - (ii) Fuselage closure – above Mach 0.6 (see Table 4.5)
 - Less than 10 deg: 0
 - 11 to 12 deg closure: 1%
 - 13 to 14 deg: 4%
 - (iii) Upsweep closure (see Section 3.21) use in conjunction with (iv)
 - No upsweep: 0
 - 4 deg of upsweep: 2%
 - 10 deg of upsweep: 8%
 - 15 deg of upsweep: 15%
 - (interpolate in-between values)
 - (iv) Aft-end cross-sectional shape
 - Circular: 0
 - Shallow keel: 0 to 1%
 - Deep keel: 1 to 2%
 - (v) Rear-mounted door (with fuselage upsweep): 5 to 10%
- (d) Cabin-pressurization leakage (if unknown, use higher value): 3 to 5%
- (e) Excrescence (nonmanufacturing types such as windows)
 - (i) Windows and doors (use higher values for larger aircraft): 2 to 4%
 - (ii) Miscellaneous: 1%
- (f) Wing fuselage belly fairing, if any: 1 to 5%
(use higher value if houses undercarriage)

Table 9.1. Typical $C_{D\pi}$ associated with raised- or bubble-type canopies

Raised frontal area (older boxy design, sharp edges)	$C_{D\pi} = 0.2$
Raised flat shield (fewer sharp edges)	$C_{D\pi} = 0.15$
Bubble canopy (partial)	$C_{D\pi} = 0.12$
Bubble canopy (short)	$C_{D\pi} = 0.08$
Bubble canopy (long)	$C_{D\pi} = 0.06$

(g) Undercarriage fairing – typically for high-wing aircraft (if any fairing): 2 to 6%
 (based on fairing protrusion height from fuselage)

- The interference drag increment with the wing and empennage is included in the calculation of lifting-surface drag and therefore is not duplicated when computing the fuselage parasite drag. Totaling the C_{Ff} and ΔC_{Ff} from the wetted area A_{wF} of the isolated fuselage, the flat-plate equivalent drag, f_f (see Step 6 in Section 9.7.3), is estimated in square feet.
- Surface roughness is 2 to 3%. These effects are from the manufacturing origin, discussed in Section 9.8.4. Because surface-roughness drag is the same percentage for all components, it is convenient to total them after evaluating all components. In that case, the term $\Delta C_{Ffrough}$ is dropped from Equation 9.13 and it is accounted for as shown in Equation 9.27.

Total all the components of parasite drag to obtain C_{Dpmin} , as follows. It should include the excrescence-drag increment. Converted into the fuselage contribution to $[C_{Dpmin}]_f$ in terms of aircraft wing area, it becomes:

$$C_{Ff} = 1.03 \times \left(\text{Basic } C_{Ff} + \sum \Delta C_{Ff} \right) \tag{9.12}$$

$$f_f = (C_{Ff} + \Delta C_{Ffwrap} + \Delta C_{Ffsupervel} + \Delta C_{Ffpress} + \Delta C_{Ffother} + \Delta C_{Ffrough}) \times A_{wf} \tag{9.13}$$

$$[C_{Dpmin}]_f = f_f / S_W \tag{9.14}$$

See the worked-out examples.

9.8.2 Wing, Empennage, Pylons, and Winglets

The wing, empennage, pylon, and winglets are treated as lifting surfaces and use identical methodology to estimate their minimum parasite drag. It is similar to the fuselage methodology except that it does not have the wrapping effect. Here, the

Table 9.2. Typical $C_{D\pi}$ associated with sharp windshield type canopies

2-abreast-seating aircraft	0.1 sq.ft.	8-abreast-seating aircraft	0.4 sq.ft.
4-abreast-seating aircraft	0.2 sq.ft.	10-abreast or more	0.5 sq.ft.
6-abreast-seating aircraft	0.3 sq.ft.		
Adjust the values for the following variations:			
Kinked windshield (less sharp)		Reduce the value by 10%	
Smoothed (single-curvature) windshield		Reduce the value by 20 to 30%	
Smoothed (double-curvature) windshield		Reduce the value by 30 to 50%	

interference drag with the joining body (e.g., for the wing, it is the fuselage) is taken into account because it is not included in the fuselage f_f .

The methodology for the wing (denoted by the subscript w) is discussed in this section. The Re_w is calculated first using the wing MAC as the characteristic length. Next, the exposed wing area is computed by subtracting the portion buried in the fuselage and then the wetted area, A_{Ww} , using the k factors for the t/c as in Section 9.7.2. Using the Re_w , the basic C_{Fw_BASIC} is obtained from the graph in Figure 9.19b for the flight Mach number. The incremental parasite drag formulae are as follows:

1. 3D effects [1].

(a) Supercritical:

$$\Delta C_{Fw} = C_{Fw} \times K_1 \times (\text{aerofoil t/c ratio})_{ave} \quad (9.15)$$

where $K_1 = 1.2$ to 1.5 for the supercritical aerofoil and $K_1 = 1.6$ to 2 for the conventional aerofoil

(b) Pressure:

$$\Delta C_{Fw} = C_{Fw} \times 60 \times (\text{aerofoil t/c ratio})_{ave}^4 \times \left(\frac{6}{AR} \right)^{0.125} \quad (9.16)$$

where the aspect ratio, $AR \geq 2$ (modified from [1]). The last term of this expression includes the effect of nonelliptical lift distribution.

2. Interference.

$$\Delta C_{Fw} = C_B^2 \times K_2 \times \left\{ \frac{0.75 \times (t/c)_{root}^3 - 0.0003}{A_w} \right\} \quad (9.17)$$

where $K_2 = 0.6$ for high- and low-wing designs and C_B is the root chord at the fuselage intersection. For the midwing, $K_2 = 1.2$. This is valid for a t/c ratio up to 0.07. For a t/c ratio below 0.07, use the interference drag:

$$\Delta C_{Fw} = 3 \text{ to } 5\% \text{ of } C_{Fw} \quad (9.18)$$

The same relationships apply for the V-tail and H-tail. For pylon interference, use 10 to 12%. Interference drag is not included in the fuselage drag; rather, it is accounted for in the wing drag. (Pylon interference is both at aircraft side and with the nacelle.)

3. Other effects. (9.19)

Excrescence (i.e., nonmanufacturing such as control-surface gaps):

Flap gaps: 4 to 5%

Slat gaps: 4 to 5%

Others: 4 to 5%

4. Surface roughness (to be added later).

The flat-plate equivalent of the wing-drag contribution is as follows (the subscripts are self-explanatory):

$$f_w = (C_{Fw} + \Delta C_{Fw_supercrit} + \Delta C_{Fw_press} + \Delta C_{Fw_inter} + \Delta C_{Fw_other} + \Delta C_{Fw_rough}) \times A_{ww}, \quad (9.20)$$

which can be converted to C_{Dpmin} in terms of the aircraft wing area; that is:

$$[C_{Dpmin}]_w = f_w/S_w \quad (9.21)$$

(Note: Omit the term $\Delta C_{F_{wrough}}$ in Equation 9.20 if it is accounted for after computing f_s for all components, as shown in Equation 9.27).

The same procedure is used to compute the parasite drag of the empennage, pylons, and so forth, which are considered to be wing-like lifting surfaces.

$$f_{lifting_surface} = [(C_F + \Delta C_{F_supervel} + \Delta C_{F_press} + \Delta C_{F_inter} + \Delta C_{F_other} + \Delta C_{F_rough}), \times A_w]_{lift_sur} \quad (9.22)$$

which can be converted to:

$$[C_{Dpmin}]_{lifting_surface} = f_{lifting_surface}/S_w \quad (9.23)$$

9.8.3 Nacelle Drag

The nacelle requires different treatment, with the special consideration of throttle-dependent air flowing through as well as over it, like the fuselage. This section provides the definitions and other considerations needed to estimate nacelle parasite drag (see [2], [9], and [21]). The nacelle is described in Section 10.8.

The throttle-dependent variable of the internal flow passing through the turbofan engine affects the external flow over the nacelle. The dominant changes in the flow field due to throttle dependency are around the nacelle at the lip and aft end. When the flow field around the nacelle is known, the parasite drag estimation method for the nacelle is the same as for the other components but must also consider the throttle-dependent effects.

Civil aircraft nacelles are typically pod-mounted. In this book, only the long duct is considered. Military aircraft engines are generally buried in the aircraft shell (i.e., fuselage). A podded nacelle may be thought of as a wrapped-around wing in an axi-symmetric shape like that of a fuselage. The nacelle section shows aerofoil-like sections in Figure 9.5; the important sources of nacelle drag are listed here (a short duct nacelle [see Figure 10.16] is similar except for the fan exhaust coming out at high speed over the exposed outer surface of the core nozzle, for which its skin friction must be considered):

Throttle-independent drag (external surface)

- skin friction
- wrapping effects of axi-symmetric body
- excrescence effects (includes nonmanufacturing types such as cooling ducts)

Throttle-dependent drag

- inlet drag (front end of the diffuser)
- nacelle base drag (zero for an engine operating at cruise settings and higher)
- boat-tail drag (curvature of the nozzle at the aft end of the nacelle)

Definitions and typical considerations for drag estimation associated with the flow field around an isolated long-duct podded nacelle (approximated to circular

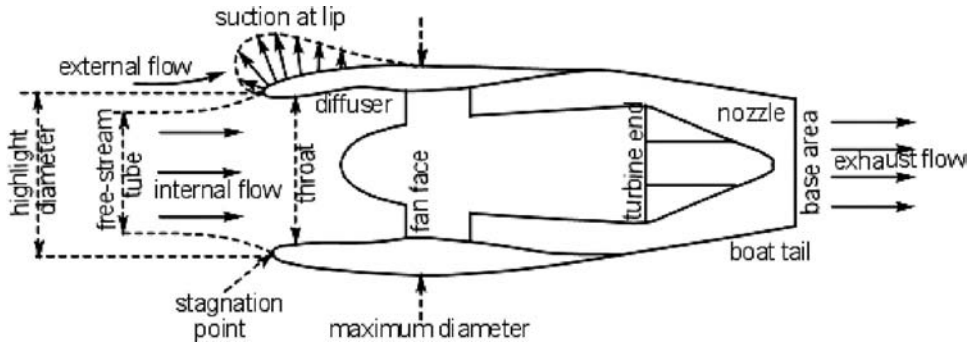


Figure 9.5. Aerodynamic considerations for an isolated long-duct nacelle drag

cross-section) are shown in [Figure 9.5](#). Although there is internal flow through the nacelle, the external geometry of the nacelle may be treated as a fuselage, except that there is a lip section similar to the LE of an aerofoil. The prevailing engine-throttle setting is maintained at a rating for LRC or HSC for the mission profile. The *intake drag* and the *base drag/boat-tail drag* are explained next.

Intake Drag

The intake stream tube at cruise operates in a subcritical condition (see [Section 10.8](#)), which is complex and makes the intake-drag estimation difficult. There is spillage during the subcritical operation due to the stream tube being smaller than the cross-sectional area at the nacelle highlight diameter, where external flow turns around the lip creating suction (i.e., thrust). This can be considered precompression, ahead of the intake, when the intake velocity is slower compared to the free-stream velocity expressed in the fraction (V_{intake}/V_{∞}). At $(V_{intake}/V_{\infty}) < 0.8$, the excess air flow spills over the nacelle lip. The intake lip acts as the LE of a circular aerofoil. The subcritical air-flow diffusion ahead of the inlet results in preentry drag called *additive drag*. The net effect results in *spillage drag*, as described herein. The spillage drag added to the friction drag at the lip results in the *intake drag*, which is a form of parasite drag. (For the military aircraft intake, see [Section 9.17](#) and [Chapter 10](#).)

- spillage drag = additive drag + lip suction (thrust sign changes to -ve)
- intake drag = spillage drag + friction drag at the lip (supervelocity effect)

[Figure 9.6](#) shows intake-drag variations with the mass flow rate for both subsonic and supersonic (i.e., sharp LE) intake.

Base Drag

The design criteria for the nozzle-exit area sizing is such that at LRC, the exit-plane static pressure P_e equals the ambient pressure P_{∞} (a perfectly expanded nozzle, $P_e = P_{\infty}$) to eliminate any base drag. At higher throttle settings, when $P_e > P_{\infty}$, there still is no base drag. At lower settings – for example, idle rating – there is some base drag as a result of the nozzle-exit area being larger than required.

Boat-Tail Drag

The long-duct contour for closure (i.e., “boat-tail” shape) at the aft end is shallow enough to avoid separation, especially with the assistance of entrainment effects of

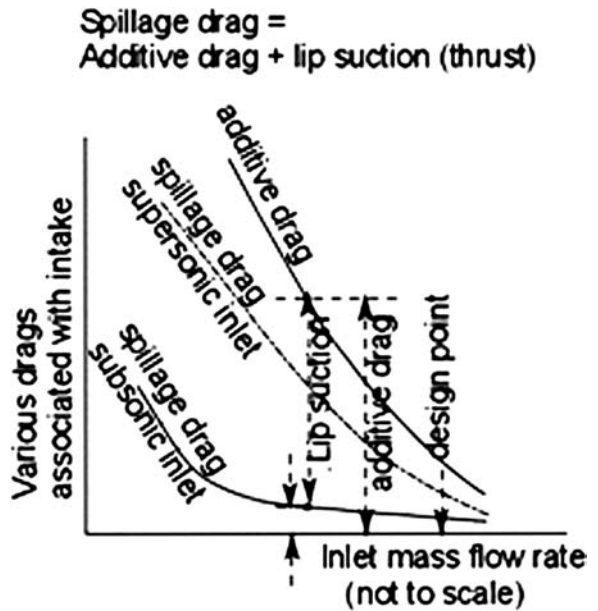


Figure 9.6. Throttle-dependent spillage drag

the exhaust plume. Hence, the boat-tail drag is kept low. At the idle throttle setting, considerable flow separation can occur and the magnitude of boat-tail drag would be higher, but it is still small compared to the nacelle drag.

For bookkeeping purposes and to avoid conflict with aircraft manufacturers, engine manufacturers generally include internal drag (e.g., ram, diffuser, and exhaust-pipe drag) in computing the net thrust of an engine. Therefore, this book only needs to estimate the parasite drag (i.e., external drag) of the nacelle. Intake-duct loss is considered engine-installation losses expressed as intake-recovery loss. Intake- and exhaust-duct losses are approximately 1 to 3% in engine thrust at LRC (throttle- and altitude-dependent). The net thrust of the turbofan, incorporating installation losses, is computed using the engine-manufacturer-supplied program and data. These manufacturers work in close liaison to develop the internal contour of the nacelle and intake. External nacelle-contour design and airframe integration remain the responsibility of the aircraft manufacturer.

The long-duct nacelle characteristic length, L_{nac} , is the length measured from the intake-highlight plane to the exit-area plane. The wetted area A_{Wn} , Re_n , and basic C_{Fn} are estimated as for other components. The incremental parasite drag formulae for the nacelle are provided herein. The supersonic effect around the nacelle-lip section is included in the intake-drag estimation; hence, it is not computed separately. Similarly, the pressure effect is included in the base/boat-tail drag estimation. These two items are addressed this way because of the special consideration of throttle dependency. Following are the relationships used to compute the nacelle drag coefficient ΔC_{Dn} :

1. ΔC_{Dn} effects (same as the fuselage being axi-symmetric).

Wrapping:

$$\Delta C_{Fn} = 0.025 \times (\text{diameter}/\text{length})^{-1} \times Re^{-0.2} \tag{9.24}$$

Table 9.3. *Nacelle interference drag (per nacelle)*

Wing-mounted (Figure 9.7)	Interference drag	Fuselage-mounted (Figure 9.7)	Interference drag
High (long) overhang	0	Raised	5% of C_{Fn}
Medium overhang	4% of C_{Fn}	Medium	5% of C_{Fn}
Low (short) overhang	7% of C_{Fn}	Low	5% of C_{Fn}
		S-duct	6.5% of C_{Fn}
		Straight duct (center)	5.8% of C_{Fn}

2. Other incremental effects. Drag contributions made by the following effects are given in percentage of C_{Fn} . These are typical of the generic nacelle design:
 - (a) Intake drag at LRC – includes supersonic effects ≈ 40 to 60% (higher BPR with higher percentage)
 - (b) Boat-tail/base drag (throttle-dependent) – includes pressure effects ≈ 10 to 12% (higher value for smaller aircraft)
 - (c) Excrescence (nonmanufacturing type such as cooling-air intakes) ≈ 20 to 25% (higher value for smaller aircraft)
3. Interference drag. A podded nacelle near the wing or body would have interference drag as follows (per nacelle). For a wing-mounted nacelle, the higher the overhang forward of the wing, the less would be the interference drag. Typical values of the interference drag by each pylon interacting with the wing or the body) are listed in Table 9.3.
4. Surface roughness (add later, $\approx 3\%$.) A long overhang in front of the wing keeps the nacelle free from any interference effects. A short overhang has the highest interference. However, there is little variation of interference drag of a nacelle mounted on a different position at the aft fuselage. Much depends on the proximity of other bodies, such as the wing and empennage. If the nacelle is within one diameter, then interference drag may be increased by another 0.5%. The center engine is close to the fuselage and with the V-tail, they have increased interference.

By totaling all the components, the flat-plate equivalent of the nacelle drag contribution is given by the following equation (omit the term ΔC_{Fn_rough} in Equation 9.25 if it is accounted for at the end, as shown in Equation 9.27):

$$f_n = (C_{Fn} + \Delta C_{Fn_wrap} + \Delta C_{Fn_intake} + \Delta C_{Fn_boat\ tail} + \Delta C_{Fn_excres} + \Delta C_{Fn_rough}) \times A_{wn} \quad (9.25)$$

Converting the nacelle contribution to C_{Dpmin} in terms of the aircraft wing area, it becomes:

$$[C_{Dpmin}]_n = f_n/S_w \quad (9.26)$$

In the last three decades, the nacelle drag has been reduced by approximately twice as much as what has been achieved in other aircraft components. This demonstrates the complexity of and unknowns associated with the flow field around nacelles. CFD is important in nacelle design and its integration with aircraft.

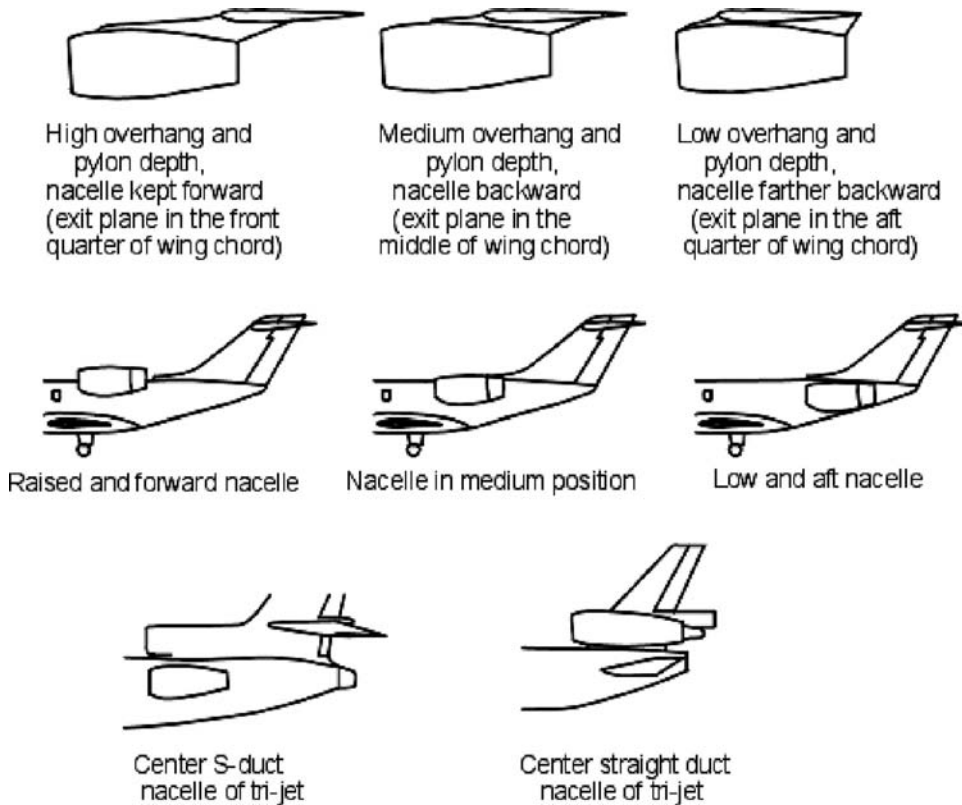


Figure 9.7. Wing- and fuselage-mounted nacelles

In this book, nacelle geometry is simplified to the axi-symmetric shape without loss of methodology.

9.8.4 Excrescence Drag

An aircraft body is not smooth; located all over the body are probes, blisters, bumps, protrusions, surface-protection mats for steps, small ducts (e.g., for cooling), and exhausts (e.g., environmental control and cooling air) – these are unavoidable features. In addition, there are mismatches at subassembly joints – for example, steps, gaps, and waviness originating during manufacture and treated as discreet roughness. Pressurization also causes the fuselage-skin waviness (i.e., areas ballooning up).

In this book, excrescence drag is addressed separately as two types:

1. *Manufacturing origin.* This includes aerodynamic mismatches as discreet roughness resulting from tolerance allocation. Aerodynamicists must specify surface-smoothness requirements to minimize excrescence drag resulting from the discrete roughness, within the manufacturing-tolerance allocation.
2. *Nonmanufacturing origin.* This includes airdals, flap tracks and gaps, cooling ducts and exhausts, bumps, blisters, and protrusions.

Tablet 9.4. *Air-conditioning drag*

No. of passengers	Drag – $f \text{ ft}^2$	Thrust – $f \text{ ft}^2$	Net drag – $f \text{ ft}^2$
50	0.1	–0.04	0.06
100	0.2	–0.10	0.10
200	0.5	–0.20	0.40
300	0.8	–0.30	0.50
600	1.6	–0.60	1.00

Excrescence drag due to surface-roughness drag is accounted for by using 2 to 3% of component parasite drag as roughness drag ([1] and [7]). As indicated in discussion after Equation 9.13, it is factored using 3% after computing all component parasite drag, as follows:

$$f_{comp\ total} = 1.03(f_f + f_w + f_n + f_p + f_{other\ comp}) \quad (9.27)$$

The difficulty in understanding the physics of excrescence drag was summarized by Haines ([10]) in his review by stating “...one realises that the analysis of some of these early data seems somewhat confused, because three major factors controlling the level of drag were not immediately recognised as being separate effects.” These factors are as follows:

- how skin friction is affected by the position of the boundary-layer transition
- how surface roughness affects skin friction in a fully turbulent flow
- how geometric shape (nonplanar) affects skin friction

Haines’s study showed that a small but significant amount of excrescence drag results from manufacturing origin and was difficult to understand.

9.8.5 Miscellaneous Parasite Drags

In addition to excrescence drag, there are other drag increments such as ECS drag (e.g., air-conditioning), which is drag at a fixed value depending on the number of passengers); and aerals and trim drag, which are included to obtain the minimum parasite drag of the aircraft.

Air-Conditioning Drag

Air-conditioning air is inhaled from the atmosphere through flush intakes that incur drag. It is mixed with hot air bled from a midstage of the engine compressor and then purified. Loss of thrust due to engine bleed is accounted for in the engine-thrust computation, but the higher pressure of the expunged cabin air causes a small amount of thrust. Table 9.4 shows the air-conditioning drag based on the number of passengers (interpolation is used for the between sizes).

Trim Drag

Due to weight changes during cruise, the CG could shift, thereby requiring the aircraft to be trimmed in order to relieve the control forces. Change in the trim-surface angle causes a drag increment. The average trim drag during cruise is approximated

Table 9.5. Trim drag (approximate)

Wing reference area – ft ²	Trim drag – f ft ²	Wing reference area – ft ²	Trim drag – f ft ²
200	0.12	2,000	0.3
500	0.15	3,000	0.5
1,000	0.20	4,000	0.8

as shown in Table 9.5, based on the wing reference area (interpolation is used for the between sizes).

Aerials

Navigational and communication systems require aerials that extend from an aircraft body, generating parasite drag on the order 0.06 to 0.1 ft², depending on the size and number of aerials installed. For midsized transport aircraft, 0.075 ft² is typically used. Therefore:

$$f_{aircraft_parasite} = f_{comp_total} + f_{aerial} + f_{air\ cond} + f_{trim} \quad (9.28)$$

9.9 Notes on Excrescence Drag Resulting from Surface Imperfections

This section may be omitted because there is no coursework exercise involved. Semi-empirical relations discussed in Sections 9.8.4 and 9.8.5 are sufficient for the purpose. Excrescence drag due to surface imperfections is difficult to estimate; therefore, this section provides background on the nature of the difficulty encountered. Capturing all the excrescence effects over the full aircraft in CFD is yet to be accomplished with guaranteed accuracy.

A major difficulty arises in assessing the drag of small items attached to the aircraft surface, such as instruments (e.g., pitot and vanes), ducts (e.g., cooling), and necessary gaps to accommodate moving surfaces. In addition, there is the unavoidable discrete surface roughness from mismatches and imperfections – *aerodynamic defects* – resulting from limitations in the manufacturing processes. Together, all of these drags, from both manufacturing and nonmanufacturing origins, are collectively termed *excrescence drag*, which is parasitic in nature. Of particular interest is the excrescence drag resulting from the discrete roughness, within the manufacturing tolerance allocation, in compliance with the surface-smoothness requirements specified by aerodynamicists to minimize drag.

Mismatches at the assembly joints are seen as discrete roughness (i.e., aerodynamic defects) – for example, steps, gaps, fastener flushness, and contour deviation – placed normal, parallel, or at any angle to the free-stream air flow. These defects generate excrescence drag. In consultation with production engineers, aerodynamicists specify tolerances to minimize the excrescence drag – on the order of 1 to 3% of the $C_{D_{pmin}}$.

The “defects” are neither at the maximum limits throughout nor uniformly distributed. The excrescence dimension is on the order of less than 0.1 inch; for comparison, the physical dimension of a fuselage is nearly 5,000 to 10,000 times larger. It poses a special problem for estimating excrescence drag; that is, capturing the resulting complex problem in the boundary layer downstream of the mismatch.

The methodology involves first computing excrescence drag on a 2D flat surface without any pressure gradient. On a 3D curved surface with a pressure gradient, the excrescence drag is magnified. The location of a joint of a subassembly on the 3D body is important for determining the magnification factor that will be applied on the 2D flat-plate excrescence drag obtained by semi-empirical methods. The body is divided into two zones (see Figure 16.5): Zone 1 (the front side) is in an adverse pressure gradient, and Zone 2 is in a favorable pressure gradient. Excrescences in Zone 1 are more critical to magnification than in Zone 2. At a LRC flight speed (i.e., below M_{crit} for civil aircraft), shocks are local, and subassembly joints should not be placed in this area (Zone 1).

Estimation of aircraft drag uses an average skin-friction coefficient C_F (see Figure 9.19b), whereas excrescence-drag estimation uses the local skin-friction coefficient C_f (see Figure 9.19a), appropriate to the location of the mismatch. These fundamental differences in drag estimation methods make the estimation of aircraft drag and excrescence drag quite different.

After World War II, efforts continued for the next two decades – especially at the RAE by Gaudet, Winters, Johnson, Pallister, and Tillman et al. – using wind-tunnel tests to understand and estimate excrescence drag. Their experiments led to semi-empirical methods subsequently compiled by ESDU as the most authoritative information on the subject. Aircraft and excrescence drag estimation methods still remain state of the art, and efforts to understand the drag phenomena continue.

Surface imperfections inside the nacelle – that is, at the inlet diffuser surface and at the exhaust nozzle – could affect engine performance as loss of thrust. Care must be taken so that the “defects” do not perturb the engine flow field. The internal nacelle drag is accounted for as an engine-installation effect.

9.10 Minimum Parasite Drag

The aircraft C_{Dpmin} can now be obtained from $f_{aircraft}$. The minimum parasite drag of the entire aircraft is $C_{Dpmin} = (1/S_w)\sum f_i$, where $\sum f_i$ is the sum of the total f_s of the entire aircraft:

$$C_{Dpmin} = f_{aircraft}/S_w \quad (9.29)$$

9.11 ΔC_{Dp} Estimation

Equation 9.2 shows that ΔC_{Dp} is not easy to estimate. ΔC_{Dp} contains the lift-dependent variation of parasite drags due to a change in the pressure distribution with changes in the angle of attack. Although it is a small percentage of the total aircraft drag (it varies from 0 to 10%, depending on the aircraft C_L), it is the most difficult to estimate. There is no proper method available to estimate the ΔC_{Dp} -versus- C_L relationship; it is design-specific and depends on wing geometry (i.e., planform, sweep, taper ratio, aspect ratio, and wing-body incidence) and aerofoil characteristics (i.e., camber and t/c). The values are obtained through wind-tunnel tests and, currently, by CFD.

During cruise, the lift coefficient varies with changes in aircraft weight and/or flight speed. The design-lift coefficient, C_{LD} , is around the mid-cruise weight of the

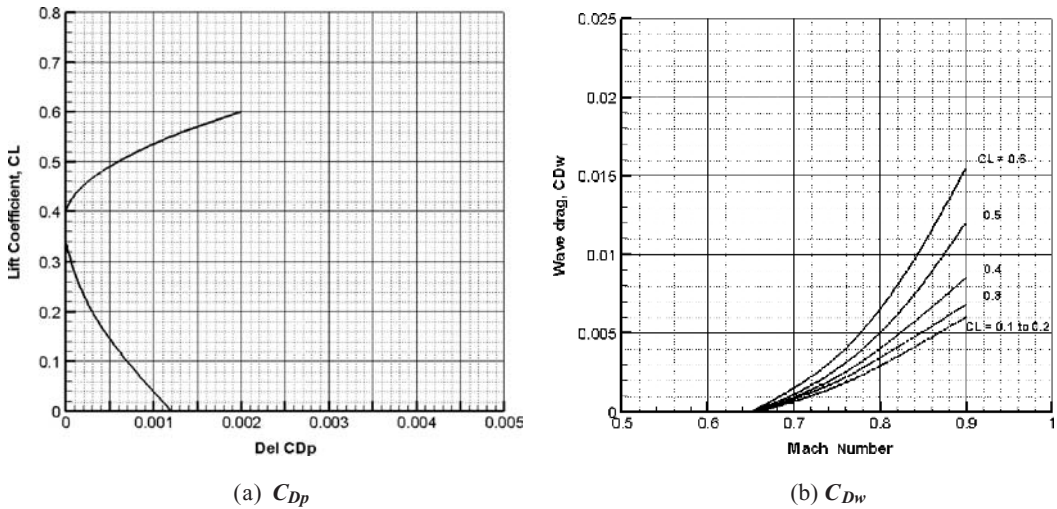


Figure 9.8. Typical ΔC_{Dp} and C_{Dw}

LRC. Let C_{LP} be the lift coefficient when $\Delta C_{Dp} = 0$. The wing should offer C_{LP} at the three-fourths value of the designed C_{LD} . This would permit an aircraft to operate at HSC (at M_{crit} ; i.e., at the lower C_L) with almost zero ΔC_{Dp} . Figure 9.8a shows a typical ΔC_{Dp} -versus- C_L variation. This graph can be used only for coursework in Sections 9.18 and 9.19.

For any other type of aircraft, a separate graph must be generated from wind-tunnel tests and/or CFD analysis. The industry has a large databank to generate such graphs during the conceptual design phase. In general, the semi-empirical method takes a tested wing (with sufficiently close geometrical similarity) ΔC_{Dp} -versus- C_L relationship and then corrects it for the differences in wing sweep (\downarrow), aspect ratio (\downarrow), t/c ratio (\uparrow), camber, and any other specific geometrical differences (Figure 9.8a).

9.12 Subsonic Wave Drag

Wave drag is caused by compressibility effects of air as an aircraft approaches high subsonic speed because local shock (i.e., supersonic) appears on a curved surface as aircraft speed increases. This is in a transonic-flow regime, in which a small part of the flow over the body is supersonic while the remainder is subsonic. In some cases, a shock interacting with the boundary layer can cause premature flow separation, thus increasing pressure drag. Initially, it is gradual and then shows a rapid rise as it approaches the speed of sound. The industry practice is to tolerate a twenty-count (i.e., $\Delta C_D = 0.002$) increase due to compressibility at a speed identified as M_{crit} (Figure 9.8b). At higher speeds, higher wave-drag penalties are incurred.

A typical wave drag (C_{Dw}) graph is shown in Figure 9.8b, which can be used for coursework (civil aircraft) described in Section 9.19. Wave-drag characteristics are design-specific; each aircraft has its own C_{Dw} , which depends on wing geometry (i.e., planform shape, quarter-chord sweep, taper ratio, and aspect ratio) and aerofoil characteristics (i.e., camber and t/c). Wind-tunnel testing and CFD can predict wave drag accurately but must be verified by flight tests. The industry has a large

databank to generate semi-empirically the C_{Dw} graph during the conceptual design phase. Today, CFD can generate wave drag accurately and is an indispensable tool (see Chapter 14), replacing the empirical/semi-empirical approach. CFD analysis is beyond the scope of this book. It is suggested that practitioners use data from tests or from CFD analysis in conjunction with an empirical approach.

9.13 Total Aircraft Drag

Total aircraft drag is the sum of all drags estimated in Sections 9.8 through 9.12, as follows for LRC and HSC:

At LRC,

$$C_D = C_{Dpmin} + \Delta C_{Dp} + \frac{C_L^2}{\pi AR} \quad (9.30)$$

At HSC,

$$(M_{crit})C_D = C_{Dpmin} + \Delta C_{Dp} + \frac{C_L^2}{\pi AR} + C_{Dw} \quad (9.31)$$

At takeoff and landing, additional drag exists, as explained in the next section.

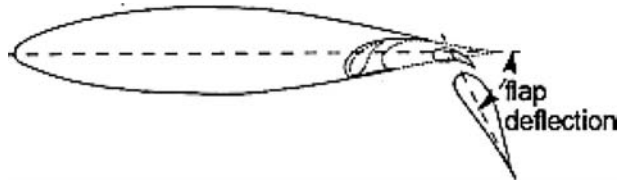
9.14 Low-Speed Aircraft Drag at Takeoff and Landing

For safety in operation and aircraft structural integrity, aircraft speed at takeoff and landing must be kept as low as possible. At ground proximity, lower speed would provide longer reaction time for the pilot, easing the task of controlling an aircraft at a precise speed. Keeping an aircraft aloft at low speed is achieved by increasing lift through increasing wing camber and area using high-lift devices such as a flap and/or a slat. Deployment of a flap and slat increases drag; the extent depends on the type and degree of deflection. Of course, in this scenario, the undercarriage remains extended, which also would incur a substantial drag increase. At approach to landing, especially for military aircraft, it may require “washing out” of speed to slow down by using fuselage-mounted speed brakes (in the case of civil aircraft, this is accomplished by wing-mounted spoilers). Extension of all these items is known as a *dirty configuration* of the aircraft, as opposed to a *clean configuration* at cruise. Deployment of these devices is speed-limited in order to maintain structural integrity; that is, a certain speed for each type of device extension should not be exceeded.

After takeoff, at a safe altitude of 200 ft, pilots typically retract the undercarriage, resulting in noticeable acceleration and gain in speed. At about an 800-ft altitude with appropriate speed gain, the pilot retracts the high-lift devices. The aircraft is then in the clean configuration, ready for an enroute climb to cruise altitude; therefore, this is sometimes known as *enroute configuration* or *cruise configuration*.

9.14.1 High-Lift Device Drag

High-lift devices are typically flaps and slats, which can be deployed independently of each other. Some aircraft have flaps but no slats. Flaps and slats conform to the

Figure 9.9. NACA 63₂-118 aerofoil

aerofoil shape in the retracted position (see Section 3.10). The function of a high-lift device is to increase the aerofoil camber when it is deflected relative to the baseline aerofoil. If it extends beyond the wing LE and trailing edge, then the wing area is increased. A camber increase causes an increase in lift for the same angle of attack at the expense of drag increase. Slats are nearly full span, but flaps can be anywhere from part to full span (i.e., flaperon). Typically, flaps are sized up to about two thirds from the wing root. The flap-chord-to-aerofoil-chord (c_c/c) ratio is in the order of 0.2 to 0.3. The main contribution to drag from high-lift devices is proportional to their projected area normal to free-stream air. The associated parameters affecting drag contributions are as follows:

- type of flap or slat (see Section 3.10)
- extent of flap or slat chord to aerofoil chord (typically, flap has 20 to 30% of wing chord)
- extent of deflection (flap at takeoff is from 7 to 15 deg; at landing, it is from 25 to 60 deg)
- gaps between the wing and flap or slat (depends on the construction)
- extent of flap or slat span
- fuselage width fraction of wing span
- wing sweep, t/c , twist, and AR

The myriad variables make formulation of semi-empirical relations difficult. References [1], [4], and [5] offer different methodologies. It is recommended that practitioners use CFD and test data. Reference [14] gives detailed test results of a double-slotted flap (0.309c) NACA 63₂-118 aerofoil (Figure 9.9). Both elements of a double-slotted flap move together, and the deflection of the last element is the overall deflection. For wing application, this requires an aspect-ratio correction, as described in Section 3.13.

Figure 9.10 is generated from various sources giving averaged typical values of ΔC_L and $\Delta C_{D_{flap}}$ versus flap deflection. It does not represent any particular aerofoil and is intended only for coursework to be familiar with the order of magnitude involved without loss of overall accuracy. The methodology is approximate; practicing engineers should use data generated by tests and CFD.

The simple semi-empirical relation for flap drag given in Equation 9.32 is generated from flap-drag data shown in Figure 9.10. The methodology starts by working on a straight wing (Λ_0) with an aspect ratio of 8, flap-span-to-wing-span ratio (b_f/b) of two-thirds, and a fuselage-width-to-wing-span ratio of less than one-fourth. Total flap drag on a straight wing (Λ_0) is seen as composed of two-dimensional parasite drag of the flap ($C_{Dp_flap_2D}$), change in induced drag due to flap deployment (ΔC_{Di_flap}), and interference generated on deflection ($\Delta C_{D_{int_flap}}$). Equation 9.33 is

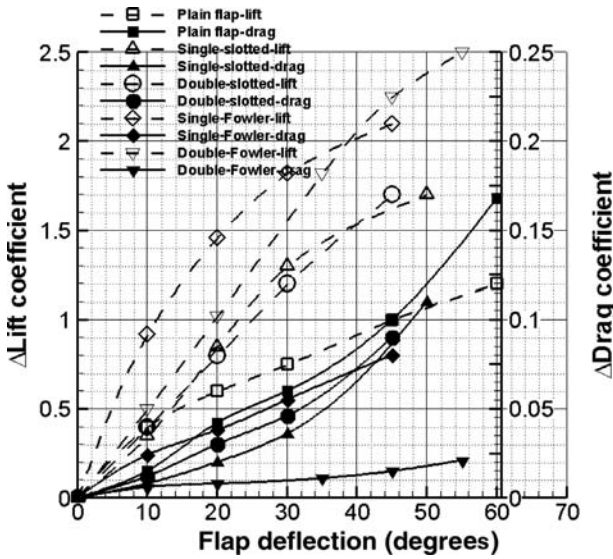


Figure 9.10. Flap drag

intended for a swept wing. The basic expressions are corrected for other geometries, as given in Equations 9.34 and 9.35.

Straight wing:

$$C_{D_flap_A0} = \Delta C_{D_flap_2D} + \Delta C_{Di_flap} + \Delta C_{Dint_flap} \tag{9.32}$$

Swept wing:

$$C_{D_flap_A1/4} = C_{D_flap_A0} \times \cos \Lambda_{1/4} \tag{9.33}$$

The empirical form of the second term of Equation 9.32 is given by:

$$\Delta C_{Di_flap} = 0.025 \times (8/AR)^{0.3} \times [(2b)/(3b_f)]^{0.5} \times (\Delta C_L)^2 \tag{9.34}$$

where AR is the wing-aspect ratio and (b_f/b) is the flap-to-wing-span ratio.

The empirical form of the third term of Equation 9.32 is given by:

$$\Delta C_{Dint_flap} = k \times C_{D_flap_2D} \tag{9.35}$$

where k is 0.1 for a single-slotted flap, 0.2 for a double-slotted flap, 0.25 to 0.3 for a single-Fowler flap, and 0.3 to 0.4 for a double-Fowler flap. Lower values may be used at lower settings.

Figure 9.10 shows the $C_{D_flap_2D}$ for various flap types at various deflection angles with the corresponding maximum ΔC_L gain given in Table 9.1. Aircraft fly well below C_{Lmax} , keeping a safe margin. Increase ΔC_{Di_flap} by 0.002 if the slats are deployed.

WORKED-OUT EXAMPLE. An aircraft has an aspect ratio, $AR = 7.5$, $\Lambda_{1/4} = 20$ deg, $(b_f/b) = 2/3$, and fuselage-to-wing-span ratio less than $1/4$. The flap type is a single-slotted Fowler flap and there is a slat. The aircraft has $C_{Dpmin} = 0.019$. Construct its drag polar.

At 20 deg deflection:

It is typical for takeoff with $C_L = 2.2$ (approximate) but can be used at landing.

From Figure 9.10:

$$\Delta C_{D_flap_2D} = 0.045 \quad \text{and} \quad \Delta C_L = 1.46.$$

From Equation 9.34:

$$\begin{aligned} \Delta C_{D_{i_flap}} &= 0.025 \times (8/7.5)^{0.3} \times [(2/3)/(3/2)]^{0.5} \times (1.46)^2 \\ &= 0.025 \times 1.02 \times 2.13 = 0.054 \end{aligned}$$

From Equation 9.35:

$$\begin{aligned} \Delta C_{D_{int_flap}} &= 0.25 \times 0.045 = 0.01125; \\ C_{D_flap_A0} &= 0.045 + 0.054 + 0.01125 = 0.11, \quad \text{with slat on } C_{D_highlift} = 0.112 \end{aligned}$$

For the aircraft wing:

$$C_{D_flap_A1/4} = C_{D_flap_A0} \times \cos \Lambda_0 = 0.112 \times \cos 20 = 0.105$$

Induced drag:

$$C_{D_i} = (C_L^2)/(\pi AR) = (2.2)^2/(3.14 \times 7.5) = 4.48/23.55 = 0.21$$

Total aircraft drag:

$$C_D = 0.019 + 0.105 + 0.21 = 0.334$$

At 45 deg deflection:

It is typical for landing with $C_L = 2.7$ (approximate).

From Figure 9.10:

$$\Delta C_{D_flap_2D} = 0.08 \quad \text{and} \quad \Delta C_L = 2.1$$

From Equation 9.34:

$$\begin{aligned} \Delta C_{D_{i_flap}} &= 0.025 \times (8/7.5)^{0.3} \times [(2/3)/(3/2)]^{0.5} \times (2.1)^2 \\ &= 0.025 \times 1.02 \times 4.41 = 0.112 \end{aligned}$$

From Equation 9.34:

$$\begin{aligned} \Delta C_{D_{int_flap}} &= 0.3 \times 0.08 = 0.024 \\ C_{Dp_flap_A0} &= 0.08 + 0.112 + 0.024 = 0.216 \end{aligned}$$

With slat on:

$$C_{Dp_highlift} = 0.218$$

For the aircraft wing:

$$C_{D_flap_A1/4} = C_{D_flap_A0} \times \cos \Lambda_0 = 0.218 \times \cos 20 = 0.201 \times 0.94 = 0.205$$

Induced drag:

$$C_{D_i} = (C_L^2)/(\pi AR) = (2.7)^2/(3.14 \times 7.5) = 7.29/23.55 = 0.31$$

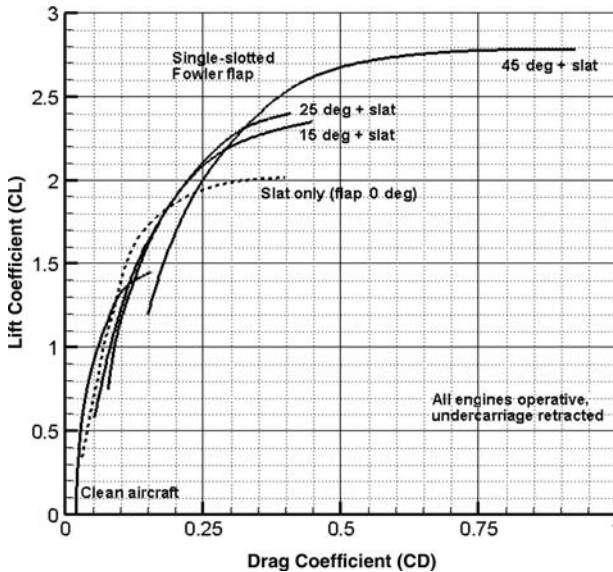


Figure 9.11. Typical drag polar with high-lift devices

Total aircraft drag:

$$C_D = 0.019 + 0.205 + 0.31 = 0.534$$

Drag polar with a high-lift device extended is plotted as shown in [Figure 9.11](#) (after [Figure 9.1](#)) at various deflections. It is cautioned that this graph is intended only for coursework; practicing industry-based engineers must use data generated by tests and CFD.

A typical value of C_L/C_D for high-subsonic commercial transport aircraft at takeoff with flaps deployed is on the order of 10 to 12; at landing, it is reduced to 6 to 8.

A more convenient method is shown in [Figure 9.12](#), and it is used for the coursework example (civil aircraft) worked out in [Section 9.19](#).

9.14.2 Dive Brakes and Spoilers Drag

To decrease aircraft speed, whether in combat action or at landing, flat plates – which are attached to the fuselage and shaped to its geometric contour when retracted – are used. They could be placed symmetrically on both sides of the wing or on the upper fuselage (i.e., for military aircraft). The flat plates are deployed during subsonic flight. Use $C_{Dn,brake} = 1.2$ to 2.0 (average 1.6) based on the projected frontal area of the brake to air stream. The force level encountered is high and controlled by the level of deflection. The best position for the dive brake is where the aircraft moment change is the least (i.e., close to the aircraft CG line).

9.14.3 Undercarriage Drag

Undercarriages, fixed or extended (i.e., retractable type), cause considerable drag on smaller, low-speed aircraft. A fixed undercarriage (not streamlined) can cause

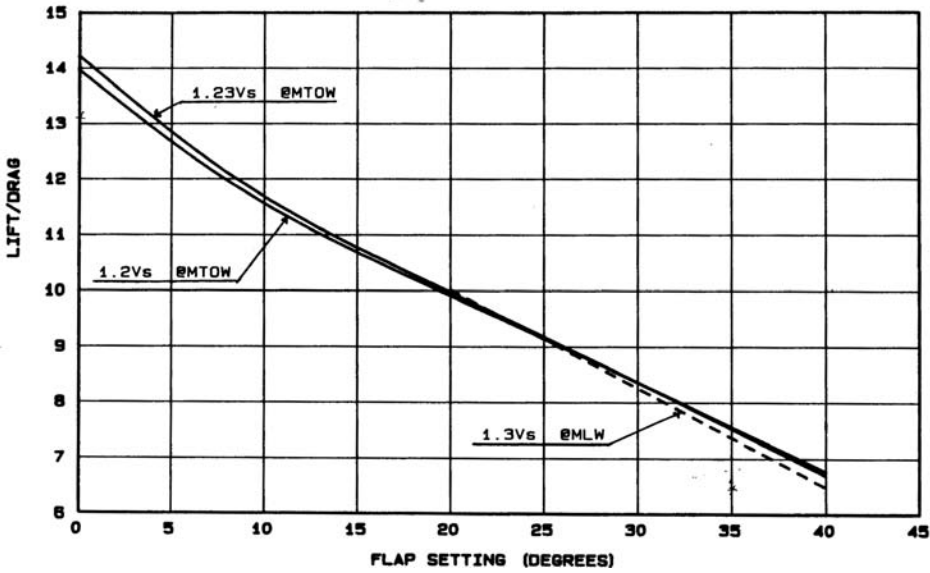


Figure 9.12. Drag polar with single-slotted Fowler flap extended (undercarriage retracted)

up to about a third of aircraft parasite drag. When the undercarriage is covered by a streamlined wheel fairing, the drag level can be halved. It is essential for high-speed aircraft to retract the undercarriage as soon as it is safe to do so (like birds). Below a 200-ft altitude from takeoff and landing, an aircraft undercarriage is kept extended. Again, it is cautioned that the data in this book are intended for coursework so readers have some sense of the order of magnitude involved.

The drag of an undercarriage wheel is computed based on its frontal area: A_{π_wheel} product of wheel diameter and width (see Figure 7.15). For twin side-by-side wheels, the gap between them is ignored and the wheel drag is increased by 50% from a single-wheel drag. For the bogey type, the drag also would increase – it is assumed by 10% for each bogey, gradually decreasing to a total maximum 50% increase for a large bogey. Finally, interference effects (e.g., due to doors and tubing) would double the total of wheel drag. The drag of struts is computed separately. The bare single-wheel C_{D_wheel} based on the frontal area is in Table 9.6 (wheel aspect ratio = D/W_b).

For the smooth side, reduce by half. In terms of an aircraft:

$$C_{Dp_wheel} = (C_{D\pi_wheel} \times A_{\pi_wheel}) / S_W$$

A circular strut has nearly twice the amount of drag compared to a streamlined strut in a fixed undercarriage. For example, the drag coefficient of a circular strut based on its cross-sectional area per unit length is $C_{D\pi_strut} = 1.0$ because it

Table 9.6. Bare single-wheel drag with side ridge (Figure 7.15)

Wheel aspect ratio	3	4	5	6
$C_{D\pi_wheel}$	0.15	0.25	0.28	0.30

operates at a low Re during takeoff and landing. For streamlined struts with fairings, it decreases to 0.5 to 0.6, depending on the type.

Torenbeek [10] suggests using an empirical formula if details of undercarriage sizes are not known at an early conceptual design phase. This formula is given in the FPS system as follows:

$$C_{D_UC} = 0.00403 \times (MTOW^{0.785})/S_W \quad (9.36)$$

Understandably, it could result in a slightly higher value (see the following example).

WORKED-OUT EXAMPLE. Continue with the previous example using the largest in the design (i.e., MTOM = 24,200 lb and $S_W = 323 \text{ ft}^2$) for the undercarriage size. It has a twin-wheel, single-strut length of 2 ft (i.e., diameter of 6 inches, $A_{\pi_strut} \approx 0.2 \text{ ft}^2$) and a main wheel size with a 22-inch diameter and a 6.6-inch width (i.e., wheel aspect ratio = 3.33, $A_{\pi_wheel} \approx 1 \text{ ft}^2$). From Table 9.6, a typical value of $C_{D\pi_wheel} = 0.18$, based on the frontal area and increased by 50% for the twin-wheel (i.e., $C_{D0} = 0.27$). Including the nose wheel (although it is smaller and a single wheel, it is better to be liberal in drag estimation), the total frontal area is about 3 ft^2 :

$$\begin{aligned} f_{_wheel} &= 0.27 \times 3 = 0.81 \text{ ft}^2 \\ f_{_strut} &= 1.0 \times 3 \times 2 \times 0.2 = 1.2 \text{ ft}^2 \end{aligned}$$

Total $f_{UC} = 2 \times (0.81 + 1.2) = 4.02 \text{ ft}^2$ (100% increase due to interference, doors, tubing, and so on) in terms of $C_{Dpmin_UC} = 4.02/323 = 0.0124$. Checking the empirical relation in Equation 9.36, $C_{D_UC} = 0.00403 \times (24,200^{0.785})/323 = 0.034$, a higher value that is acceptable when details are not known.

9.14.4 One-Engine Inoperative Drag

Mandatory requirements by certifying agencies (e.g., FAA and CAA) specify that multiengine commercial aircraft must be able to climb at a minimum specified gradient with one engine inoperative at “dirty” configuration. This immediately safeguards an aircraft in the rare event of an engine failure; and, in certain cases, after liftoff. Certifying agencies require backup for mission-critical failures to provide safety regardless of the probability of an event occurring.

Asymmetric drag produced by the loss of an engine would make an aircraft yaw, requiring a rudder to fly straight by compensating for the yawing moment caused by the inoperative engine. Both the failed engine and rudder deflection substantially increase drag, expressed by $\Delta C_{D_engine\ out+ruddert}$. Typical values for coursework are in Table 9.7.

9.15 Propeller-Driven Aircraft Drag

Drag estimation of propeller-driven aircraft involves additional considerations. The slipstream of a tractor propeller blows over the nacelle, which blocks the resisting flow. Also, the faster flowing slipstream causes a higher level of skin friction over the downstream bodies. This is accounted for as a loss of thrust, thereby keeping

Table 9.7. *One-engine inoperative drag*

	$\Delta C_{D_{one\ engine\ out+rudder}}$
Fuselage-mounted engine	0.0035
Wing-mounted twin-engine	0.0045
Wing-mounted four-engine (outboard failure)	0.0050

the drag polar unchanged. The following two factors arrest the propeller effects with piston engines (see [Chapter 10](#) for calculating propeller thrust):

1. Blockage factor, f_b , for tractor-type propeller: 0.96 to 0.98 applied to thrust (for the pusher type, there is no blockage; therefore, this factor is not required – i.e., $f_b = 1.0$)
2. A factor, f_h , as an additional profile drag of a nacelle: 0.96 to 0.98 applied to thrust (this is the slipstream effect applicable to both types of propellers)

Turboprop nacelles have a slightly higher value of f_b than piston-engine types because of a more streamlined shape. However, the slipstream from a turboprop is higher and therefore has a lower value of f_h .

9.16 Military Aircraft Drag

Although military aircraft topics are not discussed here, and instead are found in the Web at www.cambridge.org/Kundu, this important topic of military aircraft drag estimation is kept here.

Military aircraft drag estimation requires additional considerations to account for the weapon system because few are carried inside the aircraft mould lines (e.g., guns, ammunition, and bombs inside the fuselage bomb bay, if any); most are external stores (e.g., missiles, bombs, drop-tanks, and flares and chaff launchers). Without external carriages, military aircraft are considered at typical configuration (the pylons are not removed – part of a typical configuration). Internal guns without their consumables is considered a typical configuration; with armaments, the aircraft is considered to be in a loaded configuration. In addition, most combat aircraft have a supersonic-speed capability, which requires additional supersonic-wave drag.

Rather than drag due to passenger doors and windows as in a civil aircraft, military aircraft have additional excrescence drag (e.g., gun ports, extra blisters and antennas, and pylons) that requires a drag increment. To account for these additional excrescences, [3] suggests an increment of the clean flat-plate equivalent drag, f , by 28.4%.

Streamlined external-store drag is shown in Table 9.8 based on the frontal maximum cross-sectional area.

Table 9.8. *External-store drag*

External store	$C_{D\pi}$ (Based on frontal area)
Drop tanks	0.10 to 0.20
Bombs (length/diameter < 6)	0.10 to 0.25
Bombs/missiles (length/diameter > 6)	0.25 to 0.35

Bombs and missiles flush with the aircraft contour line have minor interference drag and may be ignored at this stage. Pylons and bomb racks create interference, and Equation 9.17 is used to estimate interference on both sides (i.e., the aircraft and the store). These values are highly simplified at the expense of unspecified inaccuracy; readers should be aware that these simplified values are not far from reality (see [1], [4], and [5] for more details).

Military aircraft engines are buried into the fuselage and do not have nacelles and associated pylons. Intake represents the air-inhalation duct. Skin friction drag and other associated 3D effects are integral to fuselage drag, but their intakes must accommodate large variations of intake air-mass flow. Military aircraft intakes operate supersonically; their power plants are very low bypass turbofans (i.e., on the order of less than 3.0 – earlier designs did not have any bypass). For speed capabilities higher than Mach 1.9, most intakes and exhaust nozzles have an adjustable mechanism to match the flow demand in order to extract the best results. In general, the adjustment aims to keep the V_{intake}/V_{∞} ratio more than 0.8 over operational flight conditions, thereby practically eliminating spillage drag (see Figure 9.7). Supersonic flight is associated with shock-wave drag.

9.17 Supersonic Drag

A well-substantiated reference for industrial use is [3], which was prepared by Lockheed as a NASA contract for the National Information Service, published in 1978. A comprehensive method for estimating supersonic drag that is suitable for coursework is derived from this exercise. The empirical methodology (called the Delta Method) is based on regression analyses of eighteen subsonic and supersonic military aircraft (i.e., the T-2B, T37B, KA-3B, A-4F, TA-4F, RA-5C, A-6A, A-7A, F4E, F5A, F8C, F-11F, F100, F101, F104G, F105B, F106A, and XB70) and fifteen advanced (i.e., supercritical) aerofoils. The empirical approach includes the effects of the following:

- wing geometry (AR, Λ , t/c , and aerofoil section)
- cross-sectional area distribution
- C_D variation with C_L and Mach number

The methodology presented herein follows [3], modified to simplify ΔC_{Dp} estimation resulting in minor discrepancies. The method is limited and may not be suitable to analyze more exotic aircraft configurations. However, this method is a learning tool for understanding the parameters that affect supersonic aircraft drag buildup. Results can be improved when more information is available.

The introduction to this chapter highlights that aircraft with supersonic capabilities require estimation of C_{Dpmin} at three speeds: (1) at a speed before the onset of wave drag, (2) at M_{crit} , and (3) at maximum speed. The first two speeds follow the same procedure as for the high-subsonic aircraft discussed in Sections 9.7 through 9.14. In the subsonic drag estimation method, the viscous-dependent ΔC_{Dp} varying with the C_L is separated from the wave drag, C_{Dw} (i.e., transonic effects), which also varies with the C_L but independent of viscosity.

For bookkeeping purposes in supersonic flight, such a division between the ΔC_{Dp} and the C_{Dw} is not clear with the C_L variation. In supersonic speed, there is little complex transonic flow over the body even when the C_L is varied. It is not

clear how shock waves affect the induced drag with a change in the angle of attack. For simplicity, however, in the empirical approach presented here, it is assumed that supersonic drag estimation can use the same approach as the subsonic drag estimation by keeping ΔC_{Dp} and C_{Dw} separate. The ΔC_{Dp} values for the worked-out example are listed in Table 9.13. Here, drag due to shock waves is computed at $C_L = 0$, and C_{Dw} is the additional shock-wave drag due to compressibility varying with $C_L > 0$. The total supersonic aircraft drag coefficient can then be expressed as follows:

$$C_D = C_{Dpmin} + \Delta C_{Dp} + C_L^2/\pi AR + (C_{D_shock@CL = 0}) + C_{Dw} \quad (9.37)$$

It is recommended that in current practice, CFD analysis should be used to obtain the variation of ΔC_{Dp} and ΔC_{Dw} with C_L . Reference [3] was published in 1978 using aircraft data before the advent of CFD. Readers are referred to [1], [4], and [5] for other methods. The industry has advanced methodologies, which are naturally more involved.

The aircraft cross-section area distribution should be as smooth as possible, as discussed in Section 3.13 (see Figure 3.23). It may not always be possible to use narrowing of the fuselage when appropriate distribution of areas may be carried out.

The stepwise empirical approach to estimate supersonic drag is as follows:

- Step 1: Progress in the same manner as for subsonic aircraft to obtain the aircraft-component Re for the cruise flight condition and the incompressible $C_{Fcomponent}$.
- Step 2: Increase drag in Step 1 by 28.4% as the military aircraft excrescence effect.
- Step 3: Compute C_{Dpmin} at the three speeds discussed previously.
- Step 4: Compute induced drag using $C_{Di} = C_L^2/\pi AR$.
- Step 5: Obtain ΔC_{Dp} from the CFD and tests or from empirical relations.
- Step 6: Plot the fuselage cross-section area versus the length and obtain the maximum area, S_n , and base area, S_b (see example in Figure 9.17).
- Step 7: Compute the supersonic wave drag at zero lift for the fuselage and the empennage using graphs; use the parameters obtained in Step 6.
- Step 8: Obtain the design C_L and the design Mach number using graphs (see example in Figure 9.19).
- Step 9: Obtain the wave drag, C_{Dw} , for the wing using graphs.
- Step 10: Obtain the wing-fuselage interference drag at supersonic flight using graphs.
- Step 11: Total all the drags to obtain the total aircraft drag and plot as C_D versus C_L .

The worked-out example for the North American RA-5C Vigilante aircraft is a worthwhile coursework exercise. Details of the Vigilante aircraft drag are in [3]. The subsonic drag estimation methodology described in this book differs with what is presented in [3] yet is in agreement with it. The supersonic drag estimation follows the methodology described in [3]. A typical combat aircraft of today is not too different than the Vigilante in configuration details, and similar logic can be applied. Exotic shapes (e.g., the F117 Nighthawk) should depend more on information generated from CFD and tests along with the empirical relations. For this reason, the

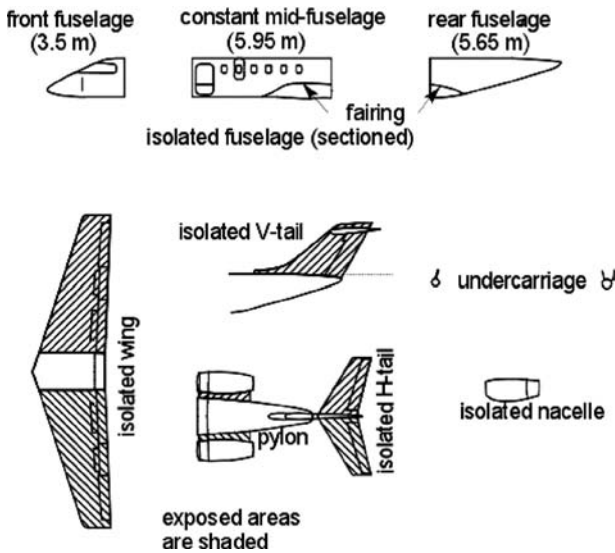


Figure 9.13. Dissected aircraft components

author does not recommend undertaking coursework on exotic-aircraft configurations unless the results can be substantiated. Learning with a familiar design that can be substantiated gives confidence to practitioners. Those in the industry are fortunate to have access to more accurate in-house data.

9.18 Coursework Example: Civil Bizjet Aircraft

The discussion on subsonic aircraft continues linearly from previous chapters.

9.18.1 Geometric and Performance Data

The geometric and performance parameters discussed herein were used in previous chapters. Figure 9.13 illustrates the dissected anatomy of the coursework baseline aircraft.

Aircraft cruise performance for the basic drag polar is computed as follows:

- cruise altitude = 40,000 ft
- LRC Mach = 0.65 (630 ft/s)
- ambient pressure = 391.68 lb/ft²
- ambient temperature = 390 K
- ambient density = 0.00058 sl/ft³
- ambient viscosity = $2.96909847 \times 10^{-7}$ lbs/ft²
- $Re/ft = 1.2415272 \times 10^6$ (use the incompressible zero Mach line, as explained in Section 9.7.1)
- C_L at LRC (Mach 0.65) = 0.5
- C_L at HSC (Mach 0.7) = 0.43

Fuselage (see Figure 9.13)

- fuselage length, $L_f = 15.24$ m (50 ft)
- average diameter at the constant cross-section barrel, $D_f = 1.75$ m (5.74 ft)

- $L_f/D_f = 8.71$
- fuselage upsweep angle = 10 deg
- fuselage closure angle = 10 deg

Wing (see Figure 9.13)

- planform reference area, $S_W = 30 \text{ m}^2$ (323 ft²)
- span = 15 m (49.2 ft)
- aspect ratio = 7.5
- wing MAC = 2.132 m (7 ft)
- root chord at centerline = 2.86 m (9.38 ft)
- tip chord = 1.143 m (3.75 ft)
- quarter-chord wing sweep = 14 deg
- aerofoil: NACA 65-410 with 10% t/c ratio for design $C_L = 0.4$

Empennage (see Figure 9.13)

- V-tail: $S_V = 4.4 \text{ m}^2$ (47.34 ft²)
- span = m (ft)
- MAC = (7 ft)
- H-tail: $S_H = 6.063 \text{ m}^2$ (65.3 ft²)
- span = 5 m (ft)
- MAC = (4.2 ft)

Nacelle (see Figure 9.13)

- nacelle length = 2.62 m (8.6 ft)
- nacelle diameter = 1.074 m (3.52 ft)
- nacelle fineness ratio = $2.62/1.074 = 2.44$

9.18.2 Computation of Wetted Areas, Re, and Basic C_F

An aircraft is first dissected into isolated components, as shown in Figure 9.15. The Re, wetted area, and basic 2D flat-plate C_{F_basic} of each component are worked out herein.

Fuselage

The fuselage is conveniently sectioned into three parts:

1. Front fuselage length, $L_{Ff} = 3.5 \text{ m}$ with a uniformly varying cross-section
2. Mid-fuselage length $L_{Fm} = 5.95 \text{ m}$ with an average constant cross-section diameter = 1.75 m
3. Aft-fuselage length $L_{Fa} = 5.79 \text{ m}$, with a uniformly varying cross-section
 - Wetted area
 - front fuselage, A_{wFf} (no cutout) = 110 ft²
 - Mid-fuselage, A_{wFm} (with two sides of wing cutouts) = $352 - 2 \times 6 = 340 \text{ ft}^2$
 - Aft fuselage, A_{wFs} (with empennage cutouts) = $180 - 10 = 170 \text{ ft}^2$
 - Include additional wetted area for the wing-body fairing housing the undercarriage $\approx 50 \text{ ft}^2$

- total wetted area, $A_{wf} = 110 + 340 + 170 + 50 = 670 \text{ ft}^2$
- fuselage $Re = 50 \times 1.2415272 \times 10^6 = 6.2 \times 10^7$
- from **Figure 9.19b** (fully turbulent) at LRC, the incompressible basic $C_{Ff} = 0.0022$

Wing

- wing exposed reference area = $323 - 50$ (area buried in the fuselage) = 273 ft^2
- MAC = 2.132 m (7 ft), AR = 7.5
- For $t/c = 10\%$ of the wing wetted area, $A_{ww} = 2.024 \times 273 = 552.3 \text{ ft}^2$
- root chord, $C_R = 2.86 \text{ m}$ (9.38 ft)
- tip chord, $C_T = 1.143 \text{ m}$ (3.75 ft)
- wing $Re = 7 \times 1.2415272 \times 10^6 = 8.7 \times 10^6$
- from **Figure 9.19b** at LRC, the incompressible basic $C_{Fw} = 0.003$

Empennage (same procedure as for the wing)

- V-tail
 - reference area, $S_V = 4.4 \text{ m}^2$ (47.34 ft^2)
 - exposed reference area = $47.34 - 7.34$ (area buried in the fuselage) = 40 ft^2
 - for $t/c = 10\%$ the V-tail wetted area, $A_{wVT} = 2.024 \times 40 = 81 \text{ ft}^2$
 - taper ratio = 0.6
 - MAC = 2.132 m (7 ft)
- V-tail
 - $Re = 7 \times 1.2415272 \times 10^6 = 8.7 \times 10^6$
 - from **Figure 9.19b** (fully turbulent) at LRC, the incompressible basic $C_{F_{V-tail}} = 0.003$
- H-tail
 - reference area, $S_H = 6.063 \text{ m}^2$ (65.3 ft^2); it is a T-tail and it is fully exposed
 - for $t/c = 10\%$, the H-tail wetted area, $A_{wHT} = 2.024 \times 65.3 = 132.2 \text{ ft}^2$
 - taper ratio = 0.5
 - MAC = 1.28 m (4.22 ft)
 - H-tail $Re = 4.22 \times 1.2415272 \times 10^6 = 5.24 \times 10^6$

From **Figure 9.19b** (fully turbulent) at LRC, the incompressible basic $C_{F_{H-tail}} = 0.003185$.

Nacelle

- length = 2.62 m (8.6 ft)
- maximum diameter = 1.074 m (3.52 ft)
- fineness ratio = 2.45
- nacelle $Re = 8.6 \times 1.2415272 \times 10^6 = 1.07 \times 10^7$
- two-nacelle wetted area, $A_{wn} = 2 \times 3.14 \times 3.1(D_{ave}) \times 8.6 - 2 \times 5$ (two pylon cutouts) = 158 ft^2
- from **Figure 9.19b** (fully turbulent) at LRC, the incompressible basic $C_{Fnac} = 0.0029$

Pylon

- each pylon exposed reference area = 14 ft^2
- length = 2.28 m (7.5 ft)

Table 9.9. Summary of Bizjet component Reynolds number and 2-D basic skin friction (C_{Fbasic})

Parameter	Reference area ft ²	Wetted area ft ²	Characteristic length ft	Reynolds number	2-D C_{F_basic}
Fuselage	n/a	670.0	50	6.2×10^7	0.00220
Wing	323	552.3	7 (MAC_w)	8.7×10^6	0.00300
V-tail	47.34	81.0	7 (MAC_{VT})	8.7×10^6	0.00300
H-tail	65.30	132.2	4.22 (MAC_{HT})	5.24×10^6	0.00320
2 × nacelle	n/a	152.0	8.6	1.07×10^7	0.00290
2 × pylon	2 × 12	48.6	7.5	9.3×10^6	0.00295

- $t/c = 10\%$
- two-ptylon wetted area $A_{wp} = 2 \times 2.024 \times 14 = 56.7 \text{ ft}^2$
- pylon $Re = 7.5 \times 1.2415272 \times 10^6 = 9.3 \times 10^6$
- from Figure 9.19b (fully turbulent) at LRC, the incompressible basic $C_{Fpylon} = 0.00295$

Table 9.9 gives the summary of Bizjet components Re and 2D C_{F_basic} .

9.18.3 Computation of 3D and Other Effects to Estimate Component C_{Dpmin}

A component-by-component example of estimating C_{Dpmin} is provided in this section. The corrected C_F for each component at LRC (i.e., Mach 0.6) is computed in the previous section.

Fuselage

The basic $C_{Ff} = 0.0022$.

- 3D effects (Equations 9.9, 9.10, and 9.11)
 - Wrapping

$$\begin{aligned}\Delta C_{Ff} &= C_{Ff} \times 0.025 \times (\text{length/diameter}) \times R_e^{-0.2} \\ &= 0.0022 \times 0.025 \times (8.71) \times (6.2 \times 10^7)^{-0.2} \\ &= 0.00048 \times 0.0276 = 0.0000132 \text{ (0.6\% of basic } C_{Ff}\text{)}\end{aligned}$$

- Supercriticality

$$\begin{aligned}\Delta C_{Ff} &= C_{Ff} \times (\text{diameter/length})^{1.5} = 0.0022 \times (1/8.71)^{1.5} \\ &= 0.0022 \times (0.1148)^{1.5} = 0.0000856 \text{ (3.9\% of basic } C_{Ff}\text{)}\end{aligned}$$

- Pressure

$$\begin{aligned}\Delta C_{Ff} &= C_{Ff} \times 7 \times (\text{diameter/length})^3 = 0.0022 \times 7 \times (0.1148)^3 \\ &= 0.0154 \times 0.00151 = 0.0000233 \text{ (1.06\% of basic } C_{Ff}\text{)}\end{aligned}$$

- Other effects on fuselage (see Section 9.8.1)
 - body pressurization – fuselage surface waviness: 5%
 - nonoptimum fuselage shape
 - (a) nose fineness – for $1.5 \leq F_{cf} \leq 1.75$: 6%
 - (b) fuselage closure – above Mach 0.6, less than 10 deg: 0%
 - (c) upsweep closure – 10-deg upsweep: 8%

Table 9.10. Bizjet fuselage ΔC_{Ff} correction (3D and other shape effects)

Item	ΔC_{Ff}	% of $C_{Ff\text{basic}}$
Wrapping	0.0000132	0.60
Supervelocity	0.0000856	3.90
Pressure	0.0000233	1.06
Body pressurization		5
Fuselage upsweep of 10 deg		8
Fuselage closure angle of 9 deg	0	0
Nose fineness ratio 1.7		6
Aft-end cross-section – circular		
Cabin pressurization/leakage		5
Excrescence (e.g., windows and doors)		3
Belly fairing		5
ECS exhaust		3.60
Total ΔC_{Ff}	0.0009060	41.16

- (d) aft-end cross-sectional shape – circular: 6
- cabin pressurization leakage (if unknown, use higher value): 5%
- excrescence (nonmanufacturing types; e.g., windows)
 - (a) windows and doors (higher values for larger aircraft): 2%
 - (b) miscellaneous: 1%
- wing–fuselage–belly fairing, if any (higher value if it houses undercarriage): 5%
- ECS (see Section 9.8) gives 0.06 ft²: 3.6%
- Total ΔC_{Ff} increment: 41.8%

Table 9.10 gives the Bizjet fuselage ΔC_{Ff} components.

Add the canopy drag for two-abreast seating $f = 0.1 \text{ ft}^2$ (see Section 9.8.1). Therefore, the equivalent flat-plate area, f , becomes = $C_{Ff} \times A_{wF} + \text{canopy drag}$.

$$f_f = 1.416 \times 0.0022 \times 670 + 0.1 = 2.087 + 0.1 = 2.187 \text{ ft}^2$$

Surface roughness (to be added later): 3%

Wing

The basic $C_{Fw} = 0.003$.

- 3D effects (Equations 9.14, 9.15, and 9.16)
- Supervelocity

$$\begin{aligned} \Delta C_{Fw} &= C_{Fw} \times 1.4 \times (\text{aerofoil } t/c \text{ ratio}) \\ &= 0.003 \times 1.4 \times 0.1 = 0.00042 \text{ (14\% of basic } C_{Fw}) \end{aligned}$$

- Pressure

$$\begin{aligned} \Delta C_{Fw} &= C_{Fw} \times 60 \times (\text{aerofoil } t/c \text{ ratio})^4 \times \left(\frac{6}{AR}\right)^{0.125} \\ &= (0.003 \times 60) \times (0.1)^4 \times (6/7.5)^{0.125} \\ &= 0.18 \times 0.0001 \times 0.973 = 0.0000175 \text{ (0.58\% of basic } C_{Fw}) \end{aligned}$$

Table 9.11. *Bizjet wing ΔC_{Fw} correction (3-D and other shape effects)*

Item	ΔC_{Fw}	% of $C_{Fwbasic}$
Supervelocity	0.0004200	14
Pressure	0.0000175	0.58
Interference (wing-body)	0.0000430	1.43
Flaps gap		5
Excrescence (others)		5
Total ΔC_{Fw}		26

- Interference

$$\begin{aligned} \Delta C_{Fw} &= C_B^2 \times 0.6 \times \left\{ \frac{0.75 \times (t/c)_{root}^3 - 0.0003}{A_w} \right\} \\ &= 9.38^2 \times 0.6 \times \{ [0.75 \times (0.1)^3 - 0.0003] / 552.3 \} \\ &= 87.985 \times 0.6 \times (0.00075 - 0.0003) / 552.3 \\ &= 0.02375 / 552.3 = 0.000043 \text{ (1.43\% of basic } C_{Fw}) \end{aligned}$$

- Other effects. For excrescence (nonmanufacturing; e.g., control-surface gaps):
 - flap gaps: 5%
 - others: 5%
 - total ΔC_{Fw} increment: 25%

Table 9.11 gives the Bizjet wing ΔC_{Fw} components.

Therefore, the equivalent flat-plate area, f , becomes $= C_{Fw} \times A_{ww}$.

$$f_f = 1.26 \times 0.003 \times 552.3 = 2.09 \text{ ft}^2$$

- surface roughness (to be added later): 3%

Empennage

Because the procedure is the same as for the wing, it is not repeated. The same percentage increment as the wing is used for the coursework exercise. In the industry, engineers must compute systematically as shown for the wing.

- V-tail
 - wetted area, $A_{wVT} = 81 \text{ ft}^2$
 - basic $C_{F_{H-tail}} = 0.003$

It is a T-tail configuration with interference from the T-tail (add 1.2%).

- $f_{VT} = 1.262 \times 0.003 \times 81 = 0.307 \text{ ft}^2$
- H-tail
 - wetted area, $A_{wHT} = 132.2 \text{ ft}^2$
 - basic $C_{F_{V-tail}} = 0.0032$
 - $f_{HT} = 1.25 \times 0.0032 \times 132.2 = 0.529 \text{ ft}^2$
 - surface roughness (to be added later): 3%

Table 9.12. Bizjet nacelle ΔC_{Fn} correction (3D and other shape effects)

Item (One Nacelle)	ΔC_{Fn}	% of $C_{Fnbasic}$
Wrapping (3D effect)	0.0000072	0.25
Excrescence (nonmanufacture)		22
Boat tail (aft end)		11
Base drag (at cruise)	0	0
Intake drag (BPR 4)		50
Total ΔC_{Fn}		83.25

Nacelle

- fineness ratio = 2.45
- nacelle $Re = 1.07 \times 10^7$
- wetted area of two nacelles, $A_{wn} = 158 \text{ ft}^2$
- basic $C_{Fnac} = 0.0029$
- 3D effects (Equations 9.14, 9.15, and 9.16)
 - Wrapping (Equation 9.9):

$$\begin{aligned}\Delta C_{Fn} &= C_{Fn} \times 0.025 \times (\text{length/diameter}) \times R_e^{-0.2} \\ &= 0.025 \times 0.003 \times 2.45 \times (1.07 \times 10^7)^{-0.2} \\ &= 0.000184 \times 0.0393 = 0.0000072 \text{ (0.25\% of basic } C_{Ff}\text{)}\end{aligned}$$

- Other increments are shown in Table 9.4 for one nacelle. For two nacelles (shown in wetted area):

$$f_n = 1.8325 \times 0.0029 \times 158 = 0.84 \text{ ft}^2$$

- surface roughness (to be added later): 3%

Pylon

Because the pylon has the same procedure as the wing, it is not repeated. The same percentage increment as for the wing is used in the coursework exercise. There is interference on both sides of the pylon.

- each pylon exposed reference area = 14 ft^2
- length = 2.28 m (7.5 ft)
- $t/c = 10\%$
- two-pylon wetted area $A_{wp} = 56.7 \text{ ft}^2$
- pylon $Re = 7.5 \times 1.2415272 \times 10^6 = 9.3 \times 10^6$
- basic $C_{Fpylon} = 0.00295$
- for two pylons (shown in wetted area):

$$f_{py} = 1.26 \times 0.00295 \times 56.7 = 0.21 \text{ ft}^2$$

- surface roughness (to be added later): 3%

Table 9.13. Bizjet parasite drag buildup summary and C_{Dpmin} estimation

	Wetted area, A_w ft ²	Basic C_F	ΔC_F	Total C_F	f -ft ²	C_{Dpmin}
Fuselage + U/C fairing	670	0.00220	0.000906	0.003106	2.080	0.006440
Canopy					0.100	0.000310
Wing	552.3	0.00300	0.000780	0.003784	2.090	0.006470
V-tail	81	0.00300	0.000786	0.003786	0.302	0.000950
H-tail	132.2	0.00320	0.000800	0.004000	0.529	0.001640
2 × nacelle	2 × 79	0.00290	0.002414	0.005314	0.840	0.002600
2 × pylon	2 × 28.35	0.00295	0.000767	0.003720	0.210	0.000650
Rough (3%)	Eq. 9.27				0.182	0.000560
Air-conditioning					0.100	0.000310
Aerial, lights					0.050	0.000155
Trim drag					0.130	0.000400
Total					6.610	0.020500

9.18.4 Summary of Parasite Drag

Table 9.13 provides an aircraft parasite drag buildup summary in tabular format. The surface roughness effect of the 3% increase (see Equation 9.27) in f is added in the table for all surfaces. The wing reference area $S_w = 323$ ft²; the $C_{Dpmin} = f/S_w$; ISA day; 40,000-ft altitude; and Mach 0.65.

9.18.5 ΔC_{Dp} Estimation

Table 9.14 gives the Bizjet ΔC_{Dp} taken from Figure 9.8.

9.18.6 Induced Drag

The formula used for induced drag is $C_{Di} = C_L^2 / (3.14 \times 7.5) = C_L^2 / 23.55$.

The Bizjet induced drag is given in Table 9.15.

9.18.7 Total Aircraft Drag at LRC

The drag polar at LRC is summarized in Table 9.16. The drag polar at HSC (Mach 0.74) requires the addition of wave drag from Figure 9.8b. (As discussed in Section 9.7.1, the C_{Dpmin} at only LRC is sufficient.) This drag polar is plotted in Figure 9.2. The C_L^2 versus the C_D is plotted in Figure 9.14; the nonlinearity at low and high C_L is of interest.

9.19 Coursework Example: Subsonic Military Aircraft

The coursework example of military aircraft was conducted for the subsonic AJT/CAS-type aircraft of the class BAe Hawk, which uses the same procedure as

Table 9.14. Bizjet ΔC_{Dp} estimation

C_L	0.1	0.2	0.3	0.4	0.5	0.6	0.7
ΔC_{Dp}	0.00070	0.00030	0.00006	0	0.00060	0.00200	0.00400

Table 9.15. *Bizjet-induced drag*

	0.2	0.3	0.4	0.5	0.6	0.7	0.8
C_L	0.2	0.3	0.4	0.5	0.6	0.7	0.8
C_{Di}	0.00170	0.00382	0.00680	0.01060	0.01530	0.02060	0.02720

in the civil aircraft drag estimation method. To avoid repetition, only the drag polar and other drag details of the AJT are shown in Figure 9.15. The drag polar at Mach 0.7 and at Mach 0.8 is tabulated in Table 9.17 and plotted in Figure 9.16.

To demonstrate the proper supersonic drag estimation method, a North American RA-C5 Vigilante aircraft, shown in Figure 9.16, is used as an example here. Reference [3] provides the Vigilante drag polar for comparison. The subsonic drag estimation of a Vigilante aircraft follows the same procedure as in the civil aircraft example. Therefore, the results of drag at Mach 0.6 (i.e., no compressibility) and at Mach 0.9 (i.e., at M_{crit}) are worked out briefly and tabulated. The supersonic drag estimation is worked out in detail using the empirical methodology described in [3].

9.19.1 Geometric and Performance Data of a Vigilante RA-C5 Aircraft

A three-view diagram of an RA-C5 Vigilante aircraft is shown in Figure 9.16. The following pertinent geometric and performance parameters are from [3]: two crew; engine: 2 x turbo-jet GE J-79-8(N), 75.6 kN; wingspan: 16.2 m; length: 22.3 m; height: 5.9 m; wing area: 65.0 m²; start mass: 27,300 kg; max speed: Mach 2+; ceiling: 18,300 m; range: 3,700 km; armament: nuclear bombs and missiles (only a clean configuration is evaluated).

Fuselage

- fuselage length = 73.25 ft
- average diameter at the maximum cross-section = 7.785 ft
- fuselage length/diameter = 9.66 (fineness ratio)
- fuselage upsweep angle = 0 deg
- fuselage closure angle \approx 0 deg

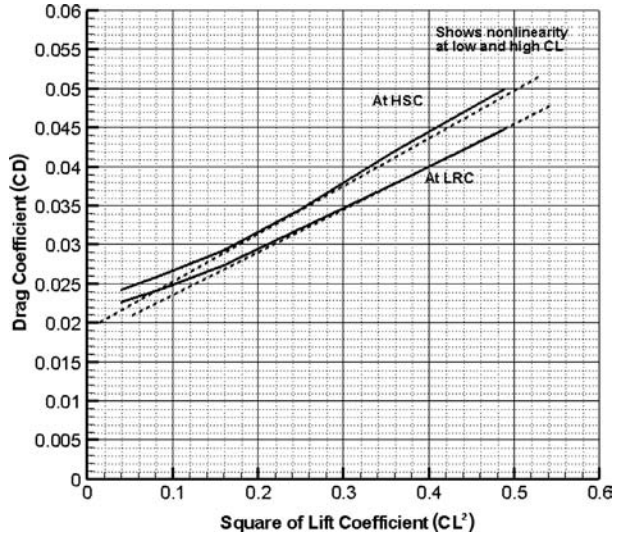
Wing

- planform reference area, $S_W = 65.03 \text{ m}^2$ (700 ft²)
- span = 16.2 m (53.14 ft)
- aspect ratio = 3.73 deg
- t/c = 5%

Table 9.16. *Bizjet total aircraft drag coefficient, C_D*

	0.2	0.3	0.4	0.5	0.6	0.7
C_L						
$C_{D_{pmin}}$				0.0205 (Table 9.5)		
ΔC_{Dp} (Table 9.6)	0.0003	0.00006	0	0.0006	0.0020	0.0040
C_{Di} (Table 9.7)	0.0017	0.00382	0.0068	0.0106	0.0153	0.0206
Total aircraft C_D @ LRC	0.0225	0.02438	0.0273	0.0317	0.0378	0.0451
Wave drag, C_{D_w} (Figure 9.9)	0.0014	0.00170	0.0020	0.0025	0.0032	0.0045
Total aircraft C_D @ HSC	0.0240	0.02618	0.0293	0.0342	0.0410	0.0496

Figure 9.14. Drag polar of Figure 9.1 plotted C_L^2 versus C_D



- taper ratio, $\lambda = 0.19$
- camber = 0
- wing MAC = 4.63 m (15.19 ft)
- $\Lambda_{\frac{1}{4}} = 37.5$ deg
- $\Lambda_{LE} = 43$ deg
- root chord at centerline = 6.1 m (20 ft)
- tip chord = 1.05 m (3.46 ft)

Empennage

- V-tail
- $S_V = 4.4 \text{ m}^2$ (47.34 ft^2)
- span = 3.6 m (11.92 ft)
- MAC = (8.35 ft)
- t/c 4%

Figure 9.15. AJT drag polar

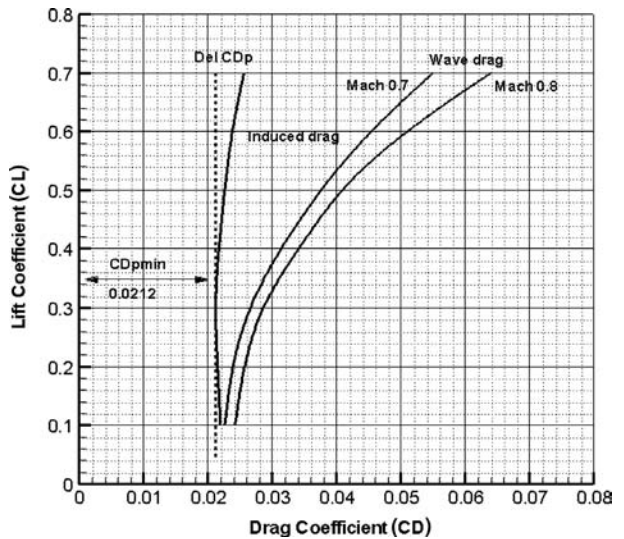


Table 9.17. *AJT total aircraft drag coefficient, C_D*

C_L	0.1	0.2	0.3	0.4	0.5	0.6
C_{Dpmin}						0.02120
ΔC_{Dp}	0.0007	0.0003	0	0.00050	0.0014	0.0026
$C_{Di} = C_L^2 / (3.14 \times 5.3)$	0.0006	0.0024	0.0054	0.00961	0.0150	0.0216
Total aircraft C_D @ 0.7 M	0.0226	0.0239	0.0266	0.03140	0.0376	0.0454
Wave drag, C_{Dw}	0.0016	0.0018	0.0020	0.00271	0.0033	0.0056
Total aircraft C_D @ 0.8 M	0.0242	0.0257	0.0286	0.03411	0.0409	0.0510

- H-tail
- $S_H = 6.063 \text{ m}^2$ (65.3 ft²)
- span = 9.85 m (32.3 ft)
- MAC = (9.73 ft)
- t/c = 4%

Nacelle/pylon (the engine is buried in the fuselage – no nacelle pylon)

- aircraft cruise performance, where the basic drag polar must be computed
- drag estimated at cruise altitude = 36,152 ft
- Mach number = 0.6 (has compressibility drag)
- ambient pressure = 391.68 lb/ft²
- $Re/ft = 1.381 \times 10^6$
- design $C_L = 0.365$
- design Mach number = 0.896 (M_{crit} is at 0.9)
- maximum Mach number = 2.0

9.19.2 Computation of Wetted Areas, Re, and Basic C_F

The aircraft is first dissected into isolated components to obtain the Re, wetted area, and basic 2D flat-plate C_F of each component, as listed herein. There is no correction factor for C_F at Mach 0.6 (i.e., no compressibility drag). The C_F compressibility correction factor (computed from Figure 9.19b) at Mach 0.9 and at Mach 2.0 is applied at a later stage.

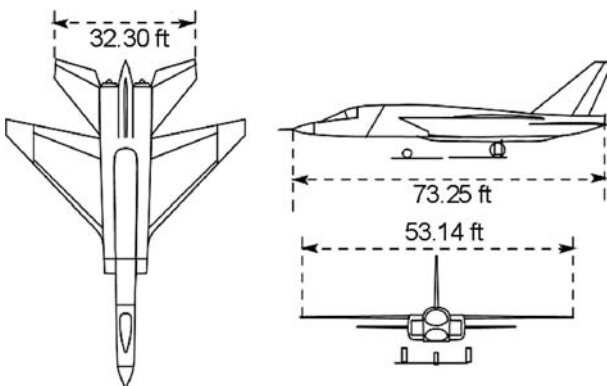


Figure 9.16. North American RA-C5 Vigilante aircraft (no pylon shown)

Fuselage

- fuselage wetted area = $A_{wf} = 1,474 \text{ ft}^2$
- fuselage $Re = 69 \times 1.381 \times 10^6 = 9.53 \times 10^7$ (length trimmed to what is pertinent for Re)
- use Figure 9.19b to obtain basic $C_{Ff} = 0.0021$

Wing

- wing wetted area = $A_{ww} = 1,144.08 \text{ ft}^2$
- wing $Re = 15.19 \times 1.381 \times 10^6 = 2.1 \times 10^7$
- use Figure 9.19b to obtain basic $C_{Fw} = 0.00257$

Empennage (same procedure as for the wing)

- V-tail wetted area = $A_{wVT} = 235.33 \text{ ft}^2$
- V-tail $Re = 8.35 \times 1.381 \times 10^6 = 1.2 \times 10^7$
- use Figure 9.19b to obtain basic $C_{F,V-tail} = 0.00277$
- H-tail wetted area = $A_{wHT} = 388.72 \text{ ft}^2$
- H-tail $Re = 9.73 \times 1.381 \times 10^6 = 1.344 \times 10^7$
- use Figure 9.19b to obtain basic $C_{F,H-tail} = 0.002705$

9.19.3 Computation of 3D and Other Effects to Estimate Component $C_{D_{pmin}}$

A component-by-component example follows.

Fuselage

From the previous section, at Mach 0.6, the basic $C_{Ff} = 0.0021$.

- 3D effects (Equations 9.9, 9.10, and 9.11):
 - Wrapping:

$$\begin{aligned}\Delta C_{Ff} &= C_{Ff} \times 0.025 \times (\text{length/diameter}) \times R_e^{-0.2} \\ &= 0.025 \times 0.0021 \times (9.66) \times (9.53 \times 10^7)^{-0.2} \\ &= 0.000507 \times 0.0254 \\ &= 0.0000129 \text{ (0.6\% of basic } C_{Ff}\text{)}\end{aligned}$$

- Supercriticality:

$$\begin{aligned}\Delta C_{Ff} &= C_{Ff} \times (\text{diameter/length})^{1.5} = 0.0021 \times (1/9.66)^{1.5} \\ &= 0.0021 \times 0.033 = 0.0000693 \text{ (3.3\% of basic } C_{Ff}\text{)}\end{aligned}$$

- Pressure:

$$\begin{aligned}\Delta C_{Ff} &= C_{Ff} \times 7 \times (\text{diameter/length})^3 = 0.0021 \times 7 \times (0.1035)^3 \\ &= 0.0147 \times 0.00111 = 0.0000163 \text{ (0.8\% of basic } C_{Ff}\text{)}\end{aligned}$$

- Other effects on the fuselage (intake included – see Section 9.18):

Reference [3] suggests applying a factor of 1.284 to include most other effects except intake. Therefore, unlike the civil aircraft example, it is simplified to only the following:

- Intake (little spillage – remainder taken in 3D effects): 2%

Table 9.18. *Vigilante fuselage ΔC_{Ff} correction (3-D and other shape effects)*

Item	ΔC_{Ff}	% of $C_{Ff\text{basic}}$
Wrapping	0.000015	0.6
Supervelocity	0.000100	3.3
Pressure	0.0000274	0.8
Intake (little spillage)		2.0
Total ΔC_{Ff}	0.001050	6.7

The total ΔC_{Ff} increment is provided in Table 9.11. Table 9.18 lists the components of the Vigilante fuselage ΔC_{Ff} .

Therefore, in terms of the equivalent flat-plate area, f , it becomes $= C_{Ff} \times A_{wF}$:

$$f = 1.067 \times 0.0021 \times 1,474 = 3.3 \text{ ft}^2$$

Add the canopy drag, $C_{Dn} = 0.08$ (approximated from Figure 9.4).

Therefore, $c_{anopy} = 0.08 \times 4.5 = 0.4 \text{ ft}^2$; $f_f = 3.3 + 0.36 = 3.66 \text{ ft}^2$

Wing

From the previous section, at Mach 0.06, the basic $C_F = 0.00257$.

- 3D effects (Equations 9.14, 9.15, and 9.16):
 - Supervelocity:

$$\begin{aligned} \Delta C_{Fw} &= C_{Fw} \times 1.4 \times (\text{aerofoil } t/c \text{ ratio}) \\ &= 0.00257 \times 1.4 \times 0.05 = 0.00018 \text{ (7\% of basic } C_{Fw}) \end{aligned}$$

Table 9.18 gives the components of the Vigilante fuselage ΔC_{Ff} .

- Pressure:

$$\begin{aligned} \Delta C_{Fw} &= C_{Fw} \times 60 \times (\text{aerofoil } t/c \text{ ratio})^4 \times \left(\frac{6}{AR}\right)^{0.125} \\ &= 0.00257 \times 60 \times (0.05)^4 \times (6/3.73)^{0.125} \\ &= 0.1542 \times 0.00000625 \times 1.06 = 0.00000102 \text{ (0.04 \% of basic } C_{Fw}) \end{aligned}$$

- Interference: ΔC_{Fw} for a thin high wing, use 3% of C_{Fw}
- Other effects:
 - Excrescence (nonmanufacturing; e.g., control surface gaps):
 - flap and slat gaps: 2%
 - others (increased later): 0%
 - total ΔC_{Fw} increment: 12.04%

Table 9.19 lists the components of the Vigilante wing ΔC_{Fw} .

Therefore, in terms of the equivalent flat-plate area, f , it becomes $= C_{Fw} \times A_{ww}$:

$$f_w = 1.12 \times 0.00257 \times 1,144.08 = 3.3 \text{ ft}^2$$

Table 9.19. *Vigilante wing ΔC_{Fw} correction (3-D and other shape effects)*

Item	ΔC_{Fw}	% of $C_{Fwbasic}$
Supervelocity	0.0003850	7.00
Pressure	0.0000136	0.04
Interference (wing-body)	0.0000328	3.00
Flap/Slat Gap		2.00
Total ΔC_{Fw}		12.04

Empennage

Because it is the same procedure as for the wing, it is not repeated. The same percentage increment as for the wing is used for the coursework exercise. In the industry, engineers must compute systematically as shown for the wing.

- V-tail:
 - wetted area, $A_{wVT} = 235.33 \text{ ft}^2$
 - basic $C_{F_V-tail} = 0.00277$
 - $f_{VT} = 1.12 \times 0.00277 \times 235.33 = 0.73 \text{ ft}^2$
- H-tail:
 - wetted area, $A_{wHT} = 388.72 \text{ ft}^2$
 - basic $C_{F_H-tail} = 0.002705$
 - $f_{HT} = 1.12 \times 0.002705 \times 388.72 = 1.18 \text{ ft}^2$

9.19.4 Summary of Parasite Drag

The wing reference area $S_w = 700 \text{ ft}^2$, $C_{Dpmin} = f/S_w$. Table 9.20 summarizes the Vigilante parasite drag. As indicated in Section 9.16, [3] provides a correlated factor of 1.284 to include all the so-called other effects. Therefore, the final flat-plate equivalent drag is $f_{aircraft} = 1.284 \times 8.87 = 11.39 \text{ ft}^2$, 28.4% = 11.62 ft^2 , to include military aircraft excrescence. This gives C_{Dpmin} at Mach 0.6 = $11.39/700 = 0.01627$ ([3] uses 0.1645). This is the C_{Dpmin} at the flight Mach number before compressibility effects begin to appear; that is, it is seen as the C_{Dpmin} at incompressible flow. At higher speeds, there is a C_F shift to a lower value. The C_{Dpmin} estimation must be repeated with a lower C_F at Mach 0.9 and Mach 2.0. To avoid repetition in accounting for compressibility, a factor of 0.97 is used (i.e., a ratio of values at Mach 0.9 and Mach 0 in Figure 9.20b – a reduction of 3%) is taken at 0.9 Mach. A factor of 0.8 (i.e., a reduction of 20%) is taken at Mach 2.0, as shown in Table 9.16. At

Table 9.20. *Vigilante parasite drag summary*

Fuselage	3.66 ft^2
Wing	3.30 ft^2
V-Tail	0.73 ft^2
H-Tail	1.18 ft^2
Total	8.87 ft^2

Table 9.21. *Vigilante* ΔC_{Dp} estimation

C_L	0	0.10	0.16	0.20	0.30	0.40	0.50	0.60
ΔC_{Dp}	0.00080	0.00015	0	0.00010	0.00080	0.00195	0.00360	0.00600

the compressible flow, the wave drag is added. At supersonic speed, shock waves contribute to it.

To correlate with the methodology presented herein, the following values of ΔC_{Dp} were extracted from [3].

9.19.5 ΔC_{Dp} Estimation

The data for ΔC_{Dp} given in Table 9.21 were extracted from [3] and are approximate.

9.19.6 Induced Drag

The formula for induced drag used is:

$$C_{Di} = C_L^2 / (3.14 \times 3.73) = C_L^2 / 11.71 \text{ (Table 9.22)}$$

9.19.7 Supersonic Drag Estimation

Supersonic flight would have a bow shock wave that is a form of compressibility drag, which is evaluated at zero C_L . Drag increases with a change of the angle of attack. The difficulty arises in understanding the physics involved with an increase in the C_L . Clearly, the increase – although lift-dependent – has little to do with viscosity unless the shock interacts with the boundary layer to increase pressure drag. Because the very purpose of design is to avoid such interaction up to a certain C_L , this book addresses the compressibility drag at a supersonic speed composed of compressibility drag at a zero C_L (i.e., $C_{D_{shock}}$) plus compressibility drag at a higher C_L (i.e., ΔC_{Dw}).

To compute compressibility drag at a zero C_L , the following empirical procedure is adopted from [3]. The compressibility drag of an object depends on its thickness parameter; for the fuselage, it is the fineness ratio and for the wing it is the t/c ratio. The fuselage (including the empennage) and wing compressibility drags are computed separately and then added in with the interference effects. Graphs are used extensively for the empirical methodology (Figures 9.19 through 9.26). Compressibility drag at both Mach 0.9 and Mach 2.0 is estimated.

Drag estimation at Mach 0.9 follows the same method as worked out in the civil aircraft example and is tabulated in Section 9.19.8. For the fuselage compressibility drag (including the empennage contribution) at Mach 2.0, the thickness parameter is the fuselage fineness ratio.

Table 9.22. *Vigilante* induced drag

C_L	0.2	0.3	0.4	0.5	0.6	0.7
C_{Di}	0.00342	0.00768	0.01370	0.02140	0.03070	0.04180

Table 9.23. *Vigilante supersonic drag summary*

	C_{Dw} at Mach 2.0
Fuselage and empennage contribution	0.01271
Wing contribution	0.00458
Wing–fuselage interference (supersonic only)	0.00075
Total	0.01804

- Step 1: Plot the fuselage cross-section along the fuselage length as shown in Figure 9.17 and obtain the maximum cross-section $S_\pi = 45.25 \text{ ft}^2$ and the fuselage base $S_b = 12 \text{ ft}^2$. Find the ratios $(1 + S_b/S_\pi) = 1 + 12/45.25 = 1.27$ and $S_\pi/S_w = 45.25/700 = 0.065$.
- Step 2: Obtain the fuselage fineness ratio $l/d = 73.3/7.788 = 9.66$ (d is minus the intake width). Obtain $(l/d)^2 = (9.66)^2 = 93.3$.
- Step 3: Use Figure 9.21 to obtain $C_{D\pi}(l/d)^2 = 18.25$ at $M_\infty = 2.0$ for $(1 + S_D/S_\pi) = 1.27$. This gives $C_{D\pi} = 18.25/93.3 = 0.1956$. Convert it to the fuselage contribution of compressibility drag expressed in terms of the wing reference area: $C_{Dwf} = C_{D\pi} \times (S_\pi/S_w) = 0.1956 \times 0.065 = 0.01271$.

For the wing compressibility drag at Mach 2.0, use the following steps:

- Step 1: Obtain the design C_{L_DES} from Figure 9.22 for the supersonic aerofoil for the $AR \times (t/c)^{1/3} = 3.73 \times (0.05)^{1/3} = 1.374$. This gives $C_{L_DES} = 0.352$. Test data of C_{L_DES} from [3] gives 0.365, which is close enough and used here.
- Step 2: Obtain from Figure 9.23 the two-dimensional design Mach number, $M_{DES,2D} = 0.784$. Using Figure 9.24, obtain $\Delta M_{AR} = 0.038$ for $1/AR = 0.268$. Using Figure 9.24, obtain $\Delta M_{D\Lambda_{\frac{1}{4}}} = 0.067$ for $\Lambda_{\frac{1}{4}} = 37.5 \text{ deg}$.

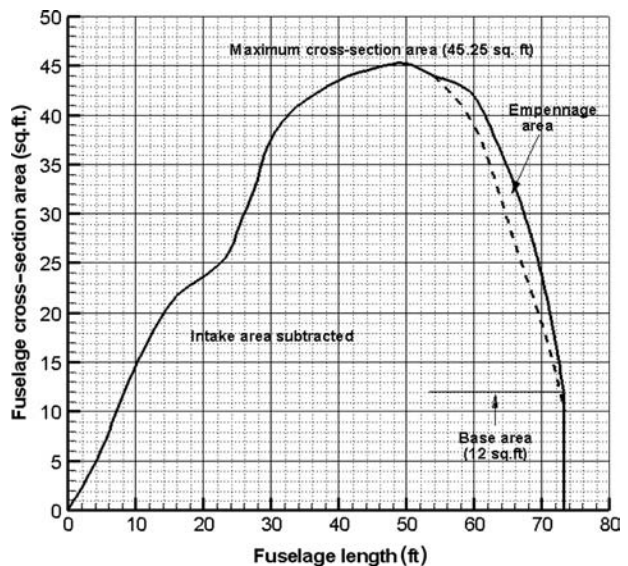


Figure 9.17. Vigilante RA-C5 fuselage cross-section area distribution

Table 9.24. Vigilante total aircraft drag coefficient, C_D

At Mach 0.6							
C_L	0.0	0.1	0.2	0.3	0.4	0.5	0.6
$C_{D_{pmin}}$				0.01627			
ΔC_{Dp}	0.00080	0.000150	0.00010	0.0008	0.00195	0.00360	0.0060
C_{Di}	0	0.000854	0.00342	0.00768	0.01370	0.02140	0.0307
Aircraft C_D @ Mach 0.6	0.01707	0.017270	0.01980	0.02475	0.03192	0.04127	0.0523
At Mach 0.9							
C_L	0.0	0.1	0.2	0.3	0.4	0.5	0.6
$C_{D_{pmin}}$		$0.97 \times 0.01627 = 0.01582$ (Ref. [3] gives 0.01575)					
ΔC_{Dp}	0.00080	0.000150	0.00010	0.00080	0.00195	0.00360	0.0060
C_{Di}	0	0.000854	0.00342	0.00768	0.01370	0.02140	0.0307
Wave drag, C_{Dw}	0.000300	0.00100	0.00200	0.00320	0.00550	0.01000	0.0200
Aircraft C_D @ Mach 0.9	0.01737	0.01827	0.02180	0.02795	0.03742	0.05127	0.0723
C_{Dw} versus C_L is from CFD/test data. Here, it is reduced from Ref. [3].							
At Mach 2.0							
C_L	0	0.1	0.2	0.3	0.4	0.5	0.6
$C_{D_{pmin}}$		$0.8 \times 0.01627 = 0.01300$ (Ref. [3] gives 0.01302)					
ΔC_{Dp}	0.0008	0.000150	0.00010	0.00080	0.00195	0.0036	0.0060
C_{Di}	0	0.000854	0.00342	0.00768	0.01370	0.0214	0.0307
Shock drag		0.01804 at zero C_L ($C_{D_{shock}}$)					
Wave drag, ΔC_{Dw}	0	0.003000	0.01100	0.02300	0.04100		
Aircraft C_D @ Mach 2.0	0.0318	0.035000	0.04550	0.06250	0.08700		

ΔC_{Dw} versus C_L is to be taken from CFD/test data.

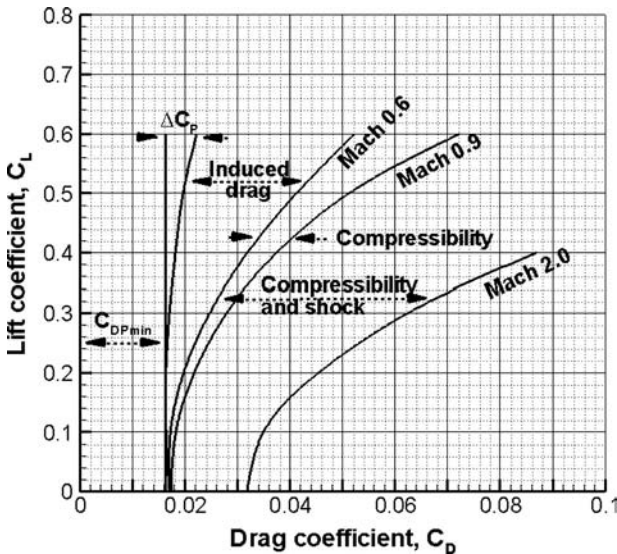
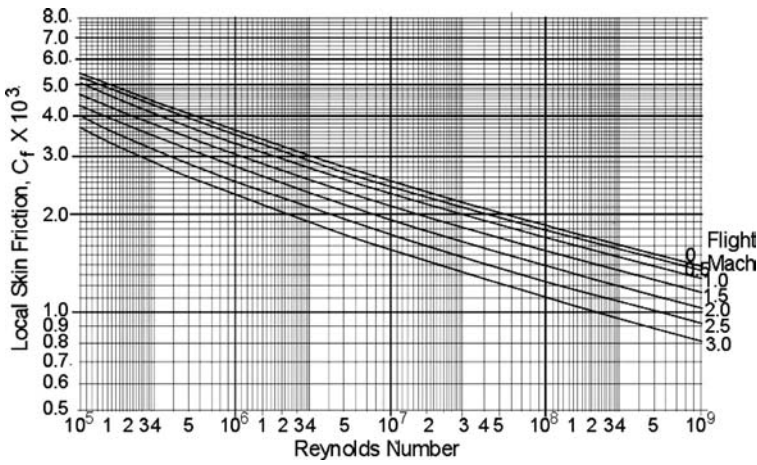
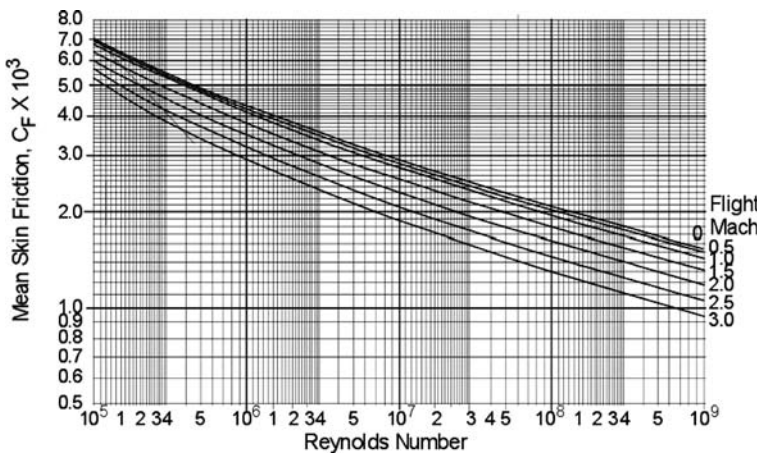


Figure 9.18. Vigilante RA-C5 drag polar



(a) Local skin friction



(b) Mean skin friction

Figure 9.19. Flat-plate skin friction coefficient C_F variation

Step 3: Make the correction to obtain in the design Mach as $M_{DES} = M_{DES_2D} + \Delta M_{AR} + \Delta M_{D\Delta 1/4}$ or $M_{DES} = 0.784 + 0.038 + 0.067 = 0.889$. Then, $\Delta M = M_\infty - M_{DES} = 2.0 - 0.889 = 1.111$.

Step 4: Compute $(t/c)^{5/3} \times [1 + (h/c)/10] = (0.05)^{5/3} \times [1 + (0)/10] = 0.00679$.

Step 5: Compute $AR \tan \Lambda_{LE} = 3.73 \times \tan 43 = 3.73 \times 0.9325 = 3.48$.

Step 6: Use Figure 9.25 and the values in Step 5 to obtain $[\Delta C_{DC_WING} / \{(t/c)^{5/3} \times [1 + (h/c)/10]\}] = 0.675$. Compute $\Delta C_{DC_WING} = 0.675 \times 0.00679 = 0.00458$.

Finally, the interference drag at supersonic speed must be added to the fuselage and wing compressibility drag. Following is the procedure for estimating the wing-fuselage interference drag:

Step 1: Compute (fuselage diameter at maximum area/wing span) = $7.785/53.14 = 0.1465$.

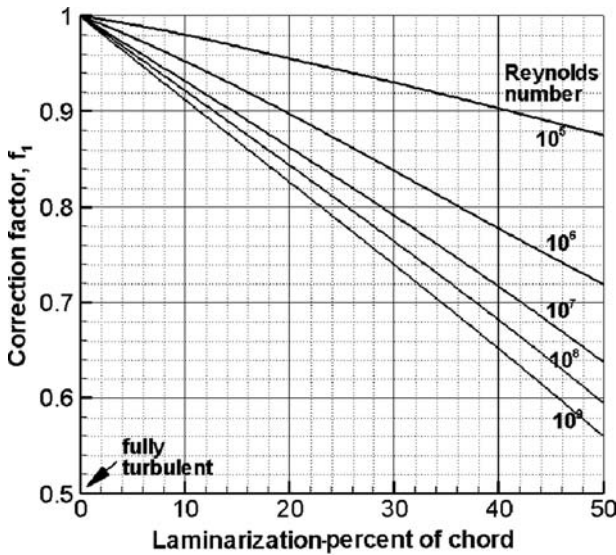


Figure 9.20. Corrections for laminarization

Step 2: With the taper ratio, $\lambda = 0.19$, compute $(1 - \lambda) \cos \Lambda_{1/4} = (1 - 0.19) \cos 37.5 = 0.643$.

Step 3: Using Figure 9.26, obtain $\Delta C_{D_INT} \times [(1 - \lambda) \cos \Lambda_{1/4}] = 0.00048$. Compute $\Delta C_{D_INT} = 0.00048 / 0.643 = 0.00075$.

The compressibility drag of the Vigilante aircraft at zero lift is summarized in Table 9.23.

The compressibility drag at Mach 0.9 is computed as for the civil aircraft example and is given in Table 9.24 along with the drag at both Mach 0.6 and Mach 2.0.

9.19.8 Total Aircraft Drag

The total Vigilante drag at the three Mach numbers is tabulated in Table 9.24. Figure 9.18 shows the Vigilante drag polar at the three aircraft speeds. Figures 9.20 through 9.26 are replotted at the end of this chapter from [3].

9.20 Concluding Remarks

Unlike other chapters, this important chapter warrants some concluding remarks. Drag estimation is state of the art and encompasses a large territory, as described herein. The tendency to underestimate drag is primarily due to failing to note some of the myriad items that must be considered in the process of estimation. The objectives of this chapter are to make readers aware of the sources of drag and to provide a methodology in line with typical industrial practices (without CFD results).

Some of the empirical relations are estimates based on industrial data available to the author that are not available in the public domain. The formulation could not possibly cover all aspects of drag estimation methodologies and therefore must be simplified for coursework. For example, the drag for high-lift devices is only approximate to give some idea.

Figure 9.21. Supersonic fuselage compressibility drag

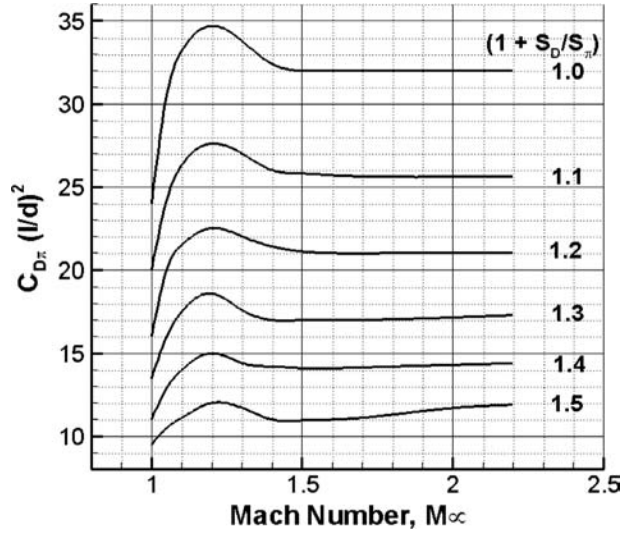


Figure 9.22. Design lift coefficient

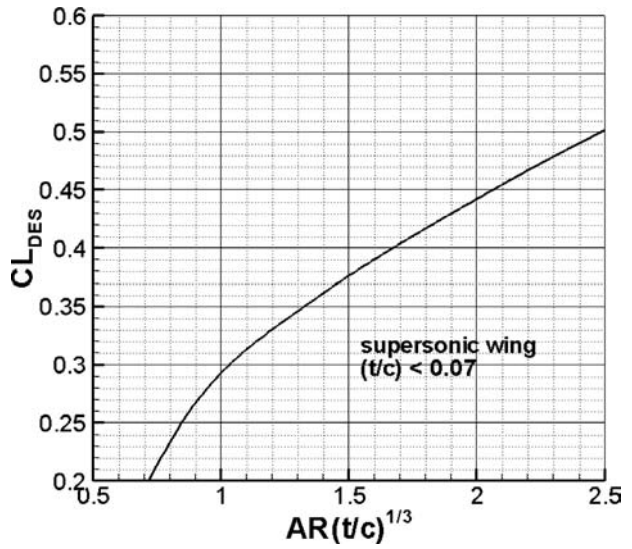
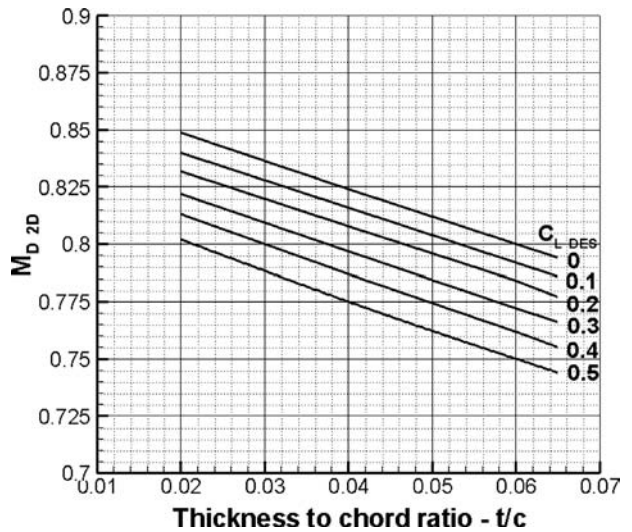


Figure 9.23. 2D drag divergence Mach number for supersonic aerofoil



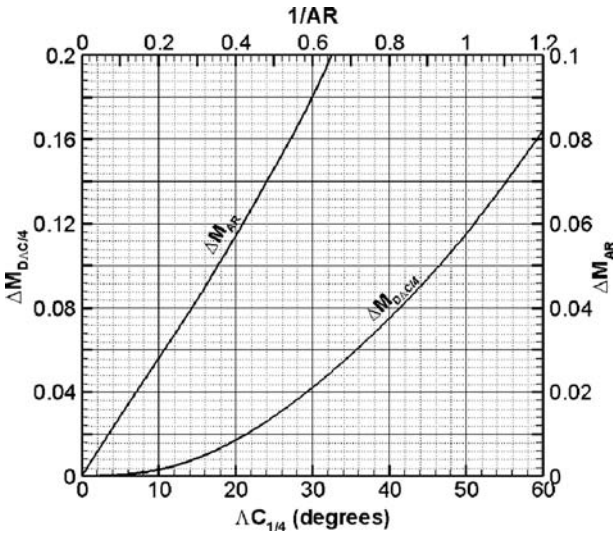


Figure 9.24. Design Mach number

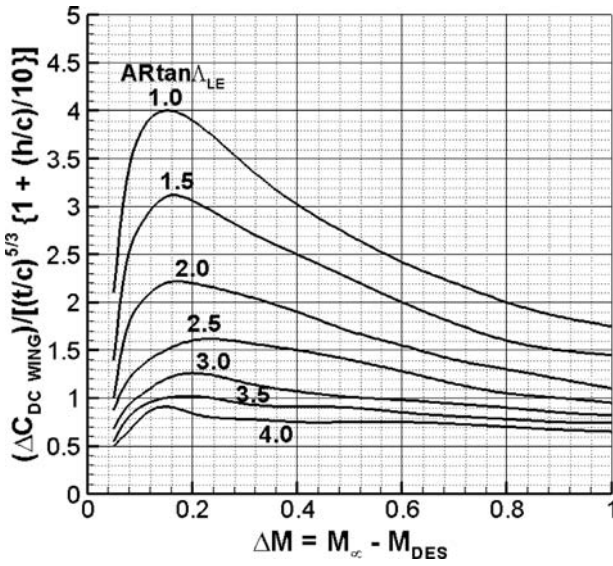


Figure 9.25. Supersonic wing compressibility drag

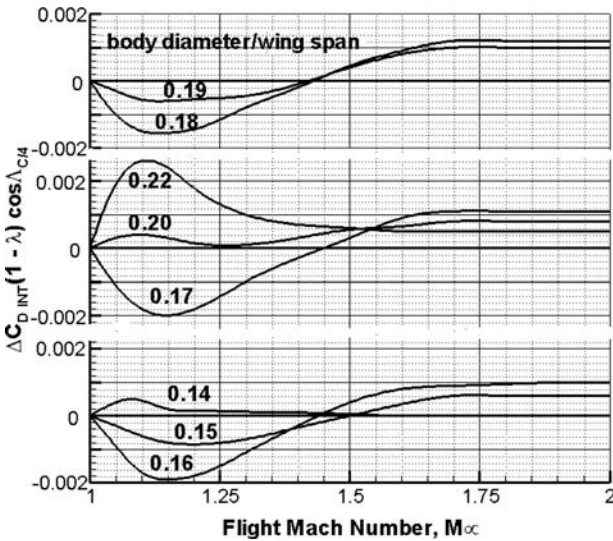


Figure 9.26. Wing-body zero-lift interference drag

Readers are advised to rely on industrial data or to generate their own databank through CFD and tests. The author would gratefully receive data and/or substantiated formulations that would improve the accuracy of future editions of this book (with acknowledgment).

Figures 9.19 through 9.26 are replotted from the NASA report in [3].

10 Aircraft Power Plant and Integration

10.1 Overview

The engine may be considered the heart of any powered-aircraft system. This book is not concerned with engine design, but it covers the information needed by aircraft designers to find a matched engine, install it on an aircraft, and evaluate its performance. The chapter begins with an introduction to the evolution of an engine followed by the classification of engine types available and their domain of application. This chapter primarily discusses gas turbines (both jet- and propeller-driven) and – to a lesser extent – piston engines, which are used only in smaller general-aviation aircraft. Therefore, a discussion of propeller performance is also included in the chapter. The derivation of thrust equations precedes propeller theory.

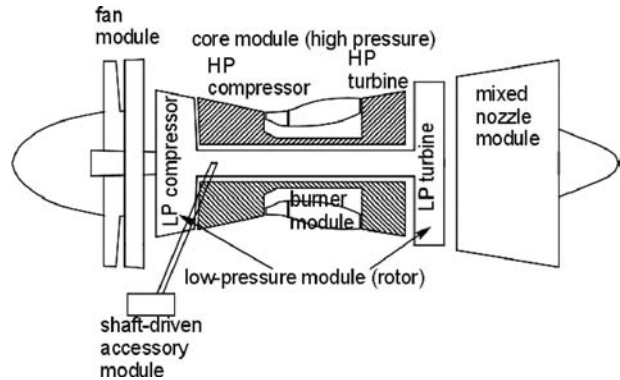
It is difficult to obtain industry-standard engine-performance data for coursework because the information is proprietary. The performance of some types of engines in nondimensional form is described in [Section 10.11](#). Readers must be careful when applying engine data – an error could degrade or upgrade the aircraft performance and corrupt the design. Verification and substantiation of aircraft design are accomplished through performance flight tests. It is difficult to locate the source of any discrepancy between predicted and tested performance, whether the discrepancy stems from the aircraft, the engine, or both. The author suggests that appropriate engine data may be obtained beyond what is provided in the scope of this book. As mentioned previously, the U.S. contribution to aeronautics is indispensable and its data are generated using the FPS system. Much of the data and worked-out examples in this book are in the FPS system. An extensive list of conversion factors is in Appendix A.

10.1.1 What Is to Be Learned?

This chapter covers the following topics:

- Section 10.2: Background on and classification of aircraft engines
- Section 10.3: Definitions
- Section 10.4: Introduction to air-breathing aircraft engine types
- Section 10.5: Engine cycles
- Section 10.6: Theories involved in engine-performance analysis

Figure 10.1. Modular concept of gas turbine design



- Section 10.7: Considerations for engine installation
- Section 10.8: Intake and nozzle design
- Section 10.9: Nozzle and thrust reversers
- Section 10.10: Propeller
- Section 10.11: Engine-performance data

10.1.2 Coursework Content

This chapter creates engine-performance graphs that are used in Chapter 11 for aircraft-performance analysis. In this chapter, readers generate thrust and fuel-flow levels for matched engines at various power settings, speeds, and altitudes, all in a standard atmosphere.

10.2 Background

Gliders were flying long before the Wright brothers first flew, but an engine could not be installed even when automobile piston engines became available – they were too heavy for gliders. The Wright brothers made their own lightweight gasoline engine with the help of Glenn H. Curtiss. Until World War II, aircraft were designed around available engines. Aircraft sizing was a problem – it was not optimized for the mission role but rather based on the number and/or the size of the engine installed.

During the late 1930s, Frank Whittle in the United Kingdom (who died in England in 1996) and Hans von Ohain in Germany (who died in the United States in 1998) were working independently and simultaneously on reaction-type engines using vane-blade-type precompression before combustion. Their efforts resulted in today's gas turbine engines; however, at the time, it was difficult for Whittle to convince his peers. By the end of World War II, gas-turbine-powered jet aircraft were in operation.

Post-World War II research led to the rapid advancement of gas turbine development such that from a core gas-generator module, a family of engines can be designed using a modular concept (Figure 10.1); this allowed engine designers to offer engines as specified by aircraft designers. Similar laws in thermodynamic-design parameters permitted power plants to be scaled (i.e., rubberized) to the requisite size around the core gas-generator module to meet the demands of the

mission requirements. The size and characteristics of an engine are determined by matching them with the aircraft mission. It is now possible for both the aircraft and the engine to be sized to the mission role, thereby improving operational economics. Modular engine design also favors low downtime for maintenance.

The potential energy locked in fuel is released through combustion. In gas-turbine technology, the high energy of the combustion product can be used in two ways: (1) converted to an increase in the kinetic energy of the exhaust to produce the reactionary thrust (i.e., turbojet and turbofan); or (2) further extracted through an additional turbine to drive a propeller (i.e., turboprop) to generate thrust.

Initially, reactionary-type engines were simple straight-through airflow turbojets (see [Figure 10.4](#)). Subsequently, turbojet development improved with the addition of a fan (i.e., long compressor blades that are visible from the outside) in front of the compressor; this is called a *turbofan*. The intake air mass flow is split into two streams (see [Figure 10.5](#)): the core air mass flow passes through the engine as primary flow and is made to burn; the secondary flow through the fan is bypassed (hence, also called the bypass engine) around the engine and remains as cold flow. For this reason, the primary flow is known as *hot flow* and the secondary bypassed flow is known as *cold flow*.

Significant general progress has been made in the aircraft power plant design. Engine technology is substantially more complex than aircraft technology. A gas-turbine operating environment demands more aerodynamic considerations than an aircraft. Stringent design considerations must accommodate very high stress levels on an engine at elevated temperatures, yet it must be as lightweight as possible. The manufacture of gas turbine parts is also a difficult task – a tough material must be machined in a complex 3D shape to a tight tolerance level. These considerations make gas turbine design a complex technology and requires an involved microprocessor-based management.

Gas turbine engines have a wide range of applications, from land-based, large prime movers for power generation and ships (both civil and military) to weight-critical airborne applications. The theory behind all the types has a common base; however, the hardware design differs, driven by the application requirements and technology level adopted. For example, land-based engines are not weight-critical and do not need to stand alone; therefore, they are less constrained in design. Surface-based gas turbines must run economically for days and/or months, generating significant power compared to standalone, lightweight aircraft engines that run for hours on varying power, altitude, *g*-load, and airflow demands. Even the largest aircraft gas turbine engines are small compared to land-based engines.

The success of a new gas turbine design is achieved by fully understanding and appreciating previous designs. Progress is made in increments by incorporating proven, newer technologies that emerge in the interim. Gas turbine development has a long gestation period compared to aircraft and it depends on previous designs. Typically, a technology demonstrator leads the way in introducing a new design.

Gas turbine designs have advanced to incorporate sophisticated microprocessor-based control systems with automation, which are called full authority digital electronic control (FADEC) and work in conjunction with the FBW control of aircraft. CAD, CAM, CFD, and FEM are now the standard tools for engine design.

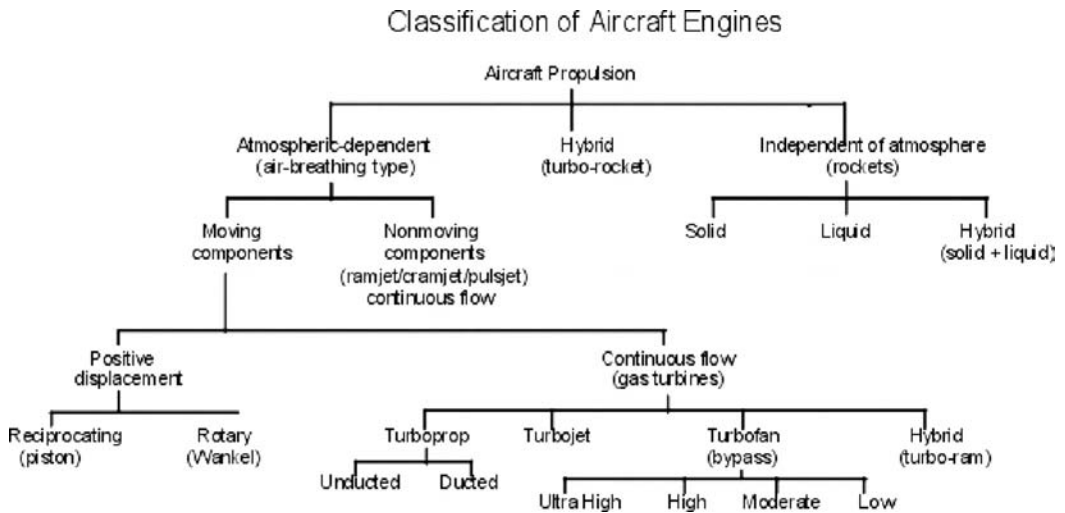


Chart 10.1. Classification of current aircraft engine types

Liquid-cooled aircraft piston engines of more than 3,000 HP have been built. However, except for a few types, they are no longer in production because they are too heavy for the power they generate; in their place, gas turbines predominate. Gas turbine engines have a better thrust-to-weight ratio. Two successful pistons were the World War II types: the Rolls Royce (RR) Merlin and the Griffon, which produced 1,000 to 1,500 HP and weighed approximately 1,500 lb dry. Also, AVGAS is considerably more expensive than aviation turbine fuel (i.e., kerosene) (AVTUR). Today, the biggest piston engine in production is approximately 500 HP. Recently, diesel-fuel piston engines (i.e., less than 250 HP) have entered the general-aviation market. In the homebuilt market, motor gasoline (MOGAS)–powered engines have been used and are approved by the certifying agencies.

Chart 10.1 classifies all types of aircraft engines in current use; this book is concerned only with the air-breathing types.

The application domains of the types addressed in this book are shown in Figure 10.2. High BPR turbofans are intended for high-subsonic speeds. At supersonic speeds, the BPR is less than 3. Typically, turboprop-powered aircraft speeds are at and below Mach 0.5. Piston-engine–powered aircraft are at the lowest end of the speed range.

Typical levels of *specific thrust* (F/\dot{m}_a , lb/lb/s) and *specific fuel consumption* (*sfc*, lb/hr/lb) of various types of gas turbine engines are shown in Figure 10.3.

Table 10.1 lists various efficiencies of the different classes of aircraft engines. Table 10.2 shows the progress made in the last half-century, indicating the advances made in engine-weight savings. Since the 1970s, compliance regarding engine-noise levels has been a requirement of the certifying agencies. Pollution levels due to noise and emissions are steadily decreasing (see Chapter 14).

If required (or preferred), the internal contours of the intake and exhaust of a civil aircraft nacelle pod are designed by engine designers in consultation with airframe designers. Shaping of the nacelle’s external contour is the responsibility of aircraft designers. Military aircraft intakes and exhausts have higher degrees of

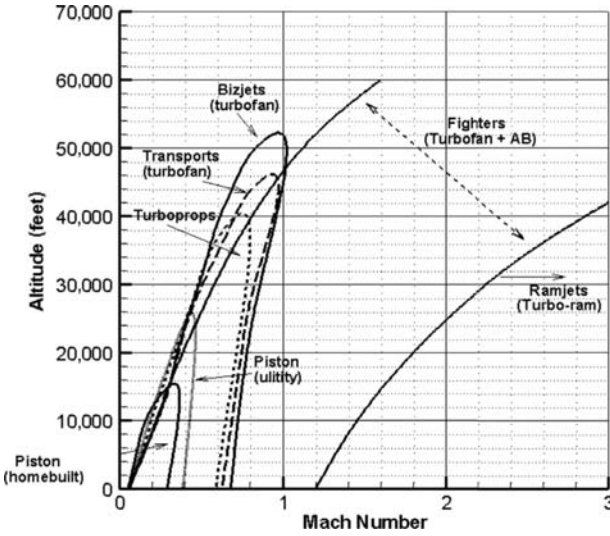
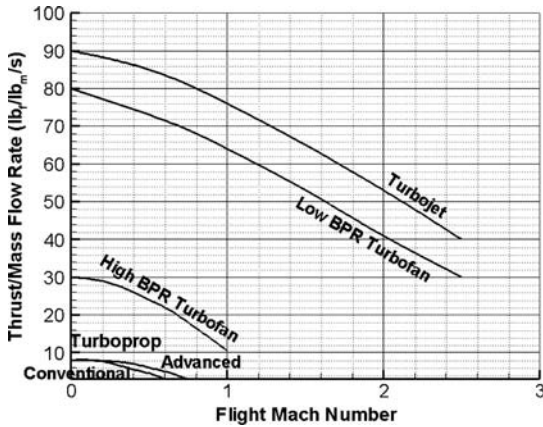
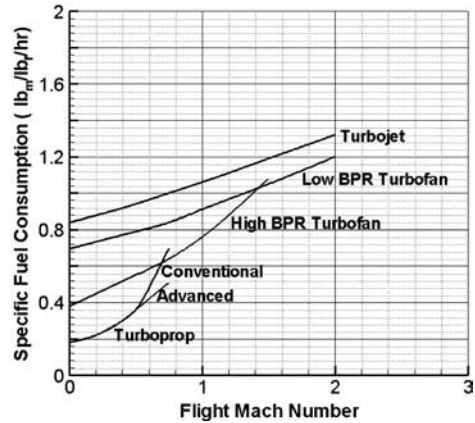


Figure 10.2. Application domains of various types of air-breathing aircraft engines



(a) Specific Thrust



(b) Specific Fuel Consumption

Figure 10.3. Typical performance levels of various gas turbine engines

Table 10.1. Efficiencies of engine types

	Thermal efficiency	Propulsive efficiency	Overall efficiency
Current types	0.60–0.65	0.75–0.85	0.50–0.55
Propfan	0.52–0.55	0.80–0.85	0.54–0.55
Propfan (ad)*	0.52–0.55	0.70–0.76	0.46–0.50
High BPR	0.48–0.55	0.62–0.68	0.40–0.42
Low BPR	0.40–0.50	0.55–0.60	0.35–0.38
Turbojet	0.40–0.45	0.45–0.52	0.28–3.20

Notes:

* Advanced propfan

BPR = bypass ratio

Table 10.2. *Progress in jet engines*

	Thrust/weight ratio
1950s (J69 class)	2.8–3.2
1960s (JT8D, JT3D class)	3.2–3.6
1970s (J79 class)	4.5–5.0
1980s (TF34 class)	6.0–6.5
1990s (F100, F404 class)	0.5–8.0
Current	8.0–9.0

complexity and are design-specific. Military aircraft intake and exhaust ducts are developed by aircraft designers in consultation with engine designers.

10.3 Definitions

This section defines various terms used in jet-engine performance analysis. References [3] through [6] may be consulted for derivations of the expressions.

SFC: The fuel-flow rate required to produce one unit of thrust, or shaft horsepower (SHP):

$$\text{SFC} = (\text{fuel flow rate})/(\text{thrust or power}) \quad (10.1)$$

Units of SFC are in lb/hr per pound of thrust produced (in SI units, gm/s/N) – the lower the better. More precisely, reaction-type engines use TSFC and propeller-driven engines use PSFC, where T and P denote thrust and power, respectively.

For turbofan engines (see Section 10.4.2):

$$\text{BPR} = \frac{\text{secondary airmass flow over the core engine}}{\text{primary airmass flow through the core (combustion)}} = \dot{m}_s/\dot{m}_p \quad (10.2)$$

Following are the definitions of various types of jet engine efficiencies. The subscripts indicate the gas turbine component station numbers, as shown in Figure 10.4 (in the figure, 5 represents e).

$$\begin{aligned} \text{thermal efficiency, } \eta_t &= \frac{\text{mechanical energy produced by the engine}}{\text{heat energy of (air + fuel)}} = \frac{W_E}{Q} \\ &= \frac{V_e^2 - V_\infty^2}{2C_p(T_3 - T_2)} = \left(1 - PR^{\frac{1-\gamma}{\gamma}}\right) \end{aligned} \quad (10.3)$$

For a particular aircraft speed, V_∞ , the higher the exhaust velocity V_e , the better is the η_t of the engine. Heat addition at the combustion chamber, $q_{2-3} = C_p(T_3 - T_2) \approx C_p(T_{t3} - T_{t1})$.

$$\begin{aligned} \text{propulsive efficiency, } \eta_p &= \frac{\text{useful work done on airplane}}{\text{mechanical energy produced by the engine}} \\ &= \frac{W_A}{W_E} = \frac{2V_\infty}{V_e + V_\infty} \end{aligned} \quad (10.4)$$

For subsonic aircraft, $V_e \gg V_\infty$. Clearly, for a given engine exhaust velocity, V_e , the higher the aircraft speed, the better is the propulsion efficiency, η_p . A jet aircraft

flying below Mach 0.5 is not preferred – it is better to use a propeller-driven aircraft flying at or below Mach 0.5.

$$\begin{aligned} \text{overall efficiency, } \eta_o &= \frac{\text{useful work done on airplane}}{\text{heat energy of (air + fuel)}} = \frac{W_A}{Q} = \eta_t \times \eta_p \\ &= \frac{(V_e - V_\infty)V_\infty}{q_{2-3}} \end{aligned} \quad (10.5)$$

It can be shown (see [2] through [4]) that, ideally, for nonafterburning engines, the best overall efficiency, η_o , is when the engine-exhaust velocity, V_e , is twice the aircraft velocity, V_∞ . Bypassed turbofans provide this efficiency at high-subsonic aircraft speeds.

10.4 Introduction: Air-Breathing Aircraft Engine Types

This section describes various types of gas turbines and introduces piston engines. Aircraft propulsion depends on the extent of thrust produced by the engine. Section 10.11 presents the thrust and power available from various types of engines. Statistics for various types of aircraft engines are previous at the end of this chapter. Gas turbine sizes are progressing in making engines both larger and smaller than current sizes – that is, expanding the application envelope.

10.4.1 Simple Straight-Through Turbojet

The most elementary form of a gas turbine engine is a simple straight-through turbojet, shown schematically in Figure 10.4. In this case, the intake airflow goes straight through the entire length of the engine and exits at a higher velocity and temperature after the processes of compression, combustion, and expansion. This type of engine burns like a stove in a pressurized environment. Readers may note the “waisting” of the airflow passage as a result of the compressor reducing the volume as the turbine expands. Typically, at the LRC condition, the free-stream tube located far upstream is narrower in diameter than at the compressor face. As a result, airflow ahead of the intake plane slows down during the precompression phase.

Components associated with the thermodynamic processes within the engine have assigned station numbers, as listed in Table 10.3. (A bare engine does not have an intake and exhaust nozzle.)

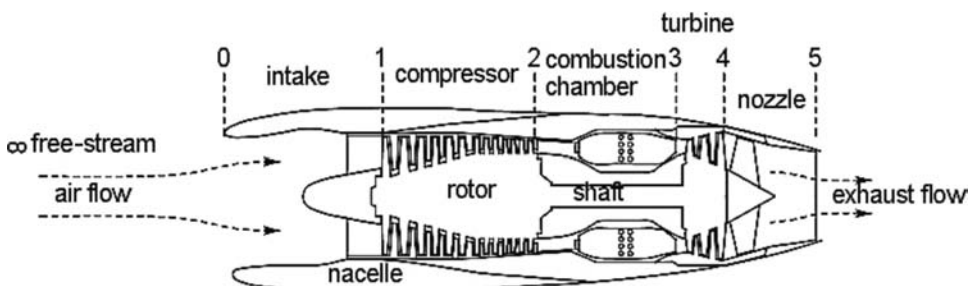


Figure 10.4. A simple straight-through turbojet (pod-mounted)

Table 10.3. *Gas turbine station number*

Number	Station	Description
∞	Free Stream	Far upstream (if precompression is ignored, then it is the same as 0)
0–1	Intake	A short divergent duct as a diffuser to compress inhaled air mass
1–2	Compressor	Active compression to increase pressure; temperature rises
2–3	Burner*	Fuel is burned to release the heat energy
3–4	Turbine	Extracts the power from heat energy to drive the compressor
4–5	Nozzle*	Generally convergent to increase flow velocity
e		(Station 5 is also known as e , representing the exit plane)

Note:

* The burner is also known as the combustion chamber (CC) and the nozzle as the exhaust duct.

Overall engine efficiency improves if the higher energy of the exhaust gas of a straight-through turbojet is extracted through an additional turbine, which can drive a fan in front of a compressor (i.e., for a turbofan engine) or a propeller (i.e., for a turboprop engine).

10.4.2 Turbofan: Bypass Engine

The energy extraction through the additional turbine lowers the rejected energy at the exhaust, resulting in a lower exhaust velocity, pressure, and temperature. The additional turbine drives a fan in front of the compressor. The large amount of air mass flowing through the fan provides thrust. Part of the intake air mass flow through the fan is diverted (i.e., bypassed as the cold secondary flow) around the engine core and does not burn. The primary flow flows through the combustion chamber and is known also as the core flow or hot flow. [Figure 10.5](#) is a schematic diagram of a turbofan engine (the top of the figure is a bare PW 4000). The lower exhaust velocity reduces engine noise. At the design point (i.e., LRC), the lower exhaust pressure permits the nozzle exit area to be sized to make the exit pressure equal to the ambient pressure (i.e., in a perfectly expanded nozzle). This is unlike simple turbojets, which can have a higher exit pressure.

Readers should note that the component-station-numbering system follows the same pattern as for the simple straight-through turbojet. The combustion chamber in the middle maintains the same numbers (i.e., 2–3). The only difference is the fan exit, which has the subscript f . The intermediate stages of the compressor and the turbine are primed.

Typically, the BPR (see [Equation 10.2](#)) for commercial jet-aircraft turbofans (i.e., high-subsonic flight speeds of less than Mach 0.98) is around 4 to 7. Recently, turbofans for the newer Boeing 787, Airbus 350 and Bombardier Cseries have reached BPR of 8 to 12. For military aircraft applications (i.e., supersonic flight speeds of up to Mach 2.5), the BPR is around 1 to 3. A lower BPR keeps the fan diameter smaller and, hence, lowers the frontal drag. Multispool drive shafts offer better efficiency and response characteristics, mostly with two concentric shafts. The shaft driving the low-pressure (LP) section runs inside the hollow shaft of the high-pressure (HP) section (see [Figure 10.5](#)). Three shaft turbofans have been designed, but most of the current designs use a twin spool. The recent advent of a geared turbofan is indicative of better fuel efficiencies.

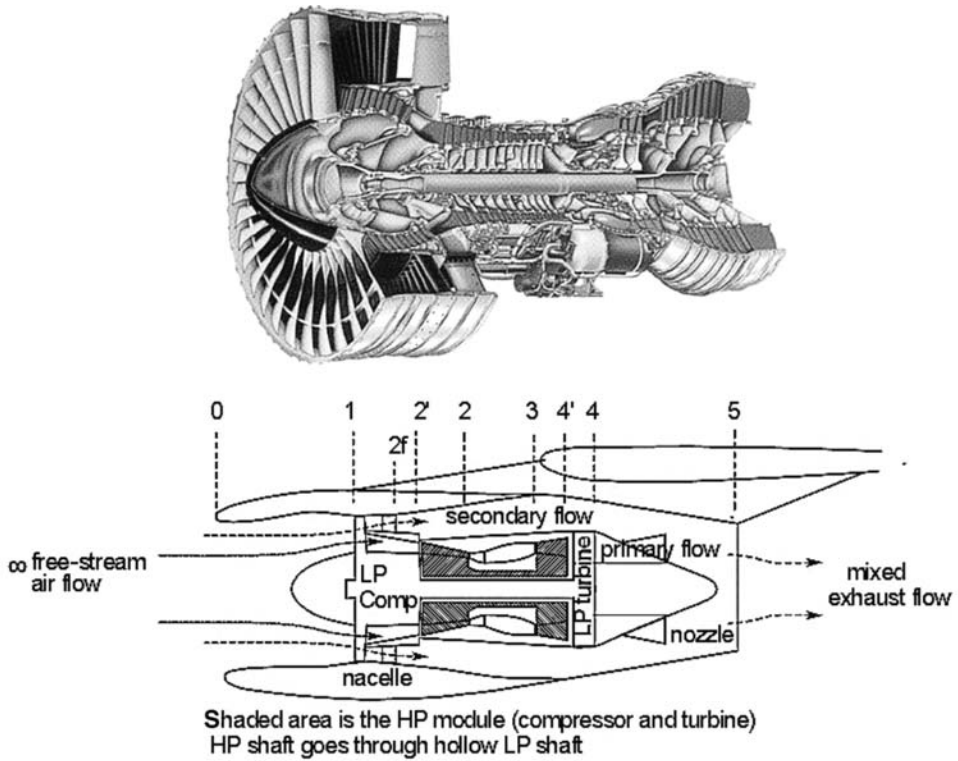


Figure 10.5. Schematic diagram of a pod-mounted, long-duct, two-shaft turbofan engine

A lower fan diameter compared to the propeller permits higher rotational speed and provides the scope for a thinner aerofoil section to extract better aerodynamic benefits. The higher the BPR, the better is the fuel economy. A higher BPR demands a larger fan diameter when reduction gears may be required to keep the revolutions per minute (rpm) at a desired level. Ultra-high BPR (UHBPR) turbofans approach the class of a ducted-fan, ducted-propeller, or propfan engine. This type of engine has been built, but its cost versus performance has prevented it from breaking into the market.

10.4.3 Afterburner Engine

Afterburning (AB) is another way of thrust augmentation intended exclusively for the supersonic combat aircraft category (the Concorde is the only civil aircraft that used AB). Figure 10.6 is a cutaway diagram of a modern AB engine intended for combat aircraft.

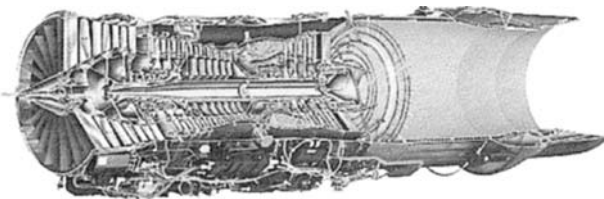
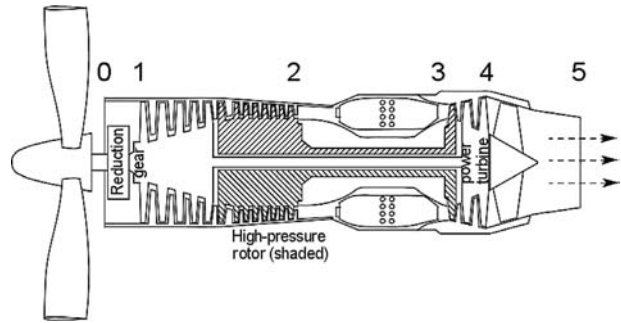


Figure 10.6. Afterburning engine

Figure 10.7. Schematic diagram of a turboprop engine



The simple straight-through turbojets have a relatively small frontal area resulting in low drag and excess air in the exhaust flow. If additional fuel can be burned in the exhaust nozzle beyond the turbine exit plane, additional thrust can be generated to propel an aircraft at a considerably higher speed and acceleration, thereby also possibly improving propulsive efficiency. However, the reason for using AB arises from the mission demand, such as at takeoff with a high payload and acceleration to engage or disengage during combat and evasion maneuvers. Mission demand overrides the fact that there is a high level of energy rejection in the high exhaust velocity. Fuel economy degrades with AB – it takes 80 to 120% more fuel burn to gain a 30 to 50% increase in thrust. Currently, most supersonic aircraft engines have some BPR when AB is done in the cooler mixed flow past the turbine section of the primary flow.

10.4.4 Turboprop Engine

Lower-speed aircraft can use propellers for thrust generation. Therefore, instead of driving a smaller enclosed fan (i.e., turbofan), a large propeller (i.e., *turboprop*) can be driven by a gas turbine engine to improve efficiency because the exhaust energy can be further extracted to a very low exhaust velocity (i.e., nearly zero nozzle thrust). Some residual jet thrust is left at the nozzle exit plane when it needs to be added to the propeller thrust. The nozzle thrust is converted to HP and, together with the SHP generated, it becomes the equivalent SHP (ESHP).

However, a large propeller diameter limits rotational speed due to both aerodynamic (i.e., transonic blade tips) and structural (i.e., centrifugal force) considerations. Heavy reduction gears are required to reduce the propeller rpm to a desirable level. Propeller efficiency decreases when aircraft are operating at flight speeds above Mach 0.5. For shorter-range flights, a turboprop's slower speed does not become time-critical to the users, yet it offers better fuel economy. Figure 10.7 is a schematic diagram of a typical turboprop engine. Modern turboprops have up to eight blades (see Figure 10.31), which allow a reduction of the diameter size and operate at a relatively higher rpm and aircraft speed.

10.4.5 Piston Engine

Most aircraft piston engines are the reciprocating type (i.e., positive displacement, intermittent combustion): The smaller ones have an air-cooled, two-stroke cycle; the

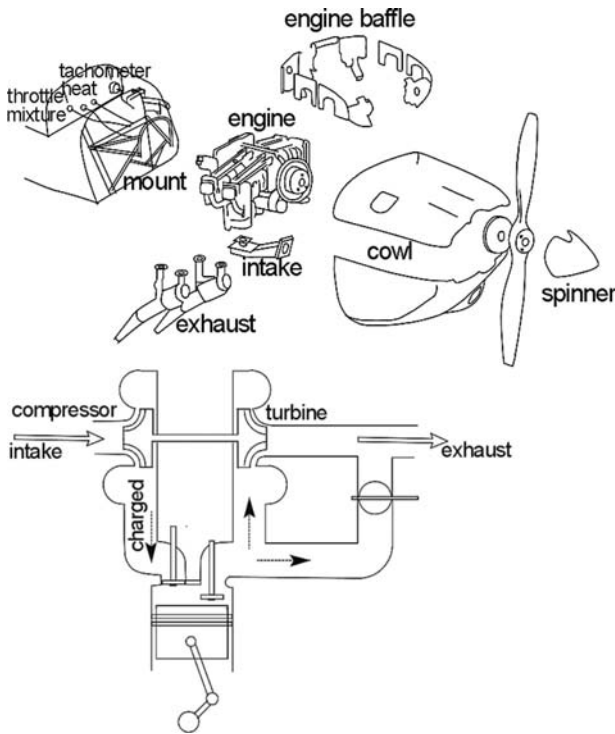


Figure 10.8. Aircraft piston engine with installation components

larger ones (typically, more than 200 HP) have a liquid-cooled, four-stroke cycle. There are a few rotary-type positive-displacement engines (e.g., Wankel) – attractive in principle but they have sealing problems. Cost-wise, rotary-type positive-displacement engines are not yet popular; cost will decrease with increased production. Figure 10.8 shows an aircraft piston engine with installation components.

To improve high-altitude performance (with low air density), supercharging is used. Figure 10.8 shows a vane-supercharging type for precompression. Also, AVGAS differs slightly from MOGAS. Recently, some engines for the homebuilt category have been allowed to use MOGAS. Recently for small aircraft application, diesel fuel-powered piston engines have appeared in the market.

Piston engines are the oldest type used for powering aircraft. Over the life cycle of an aircraft, gas turbines are more cost effective for engine sizes of more than 500 HP. Currently, general-aviation aircraft are the main users of piston engines. Small recreational aircraft invariably are powered by piston engines.

10.5 Simplified Representation of the Gas Turbine Cycle

Figure 10.9a depicts a standard schematic diagram representing a simple straight-through turbojet engine, as shown in Figure 10.4, with appropriate station numbers. The thermodynamic cycle associated with gas turbines is known as the *Joule cycle* (also known as the *Brayton cycle*). Figure 10.9b is the corresponding temperature–entropy diagram of an ideal Joule cycle in which compression and expansion take place isentropically.

Real engine processes are not isentropic and losses are involved associated with increased entropy. Figure 10.10 is a comparison of real and ideal cycles.

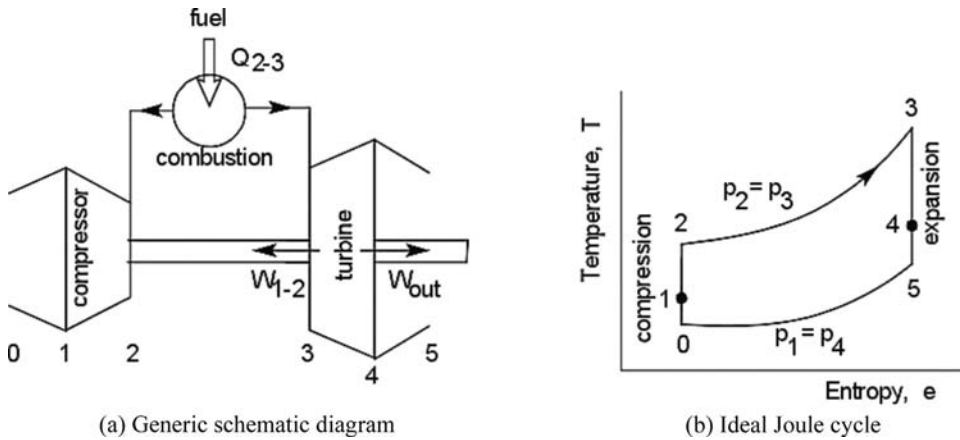


Figure 10.9. Simple straight-through jet

10.6 Formulation and Theory: Isentropic Case

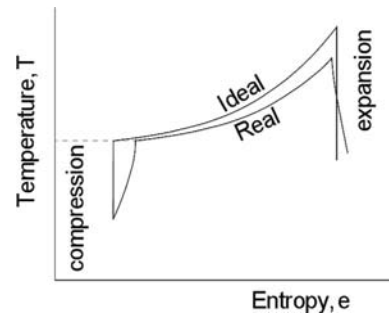
Gas turbine equations relevant to this book are provided in this section and are valid for all types of processes. For more details, see [2] through [6].

10.6.1 Simple Straight-Through Turbojet Engine: Formulation

In Figure 10.11, consider a CV (dashed line; note the waist-like shape of the simple turbojet) representing a straight-through, axi-symmetric turbojet engine. The CV and the component station numbers are as shown in the drawing and conventions in Figure 10.5; the gas turbine intake starts with the subscript 0, or ∞ , and ends at the nozzle exit plane with subscript 5, or e . The free-stream air mass flow rate, \dot{m}_a , is inhaled into the CV at the front face perpendicular to the flow, the fuel-mass flow rate \dot{m}_f (from the onboard tank) is added at the combustion chamber, and the product flow rate $(\dot{m}_a + \dot{m}_f)$ is exhausted from the nozzle plane perpendicular to flow. It is assumed that the inlet-face static pressure is p_∞ , which is fairly accurate. Precompression exists but, for the ideal consideration, it has no loss.

Flow does not cross the other two lateral boundaries of the CV because it is aligned with the walls of the engine. Force experienced by this CV is the thrust produced by the engine. Consider a cruise condition with an aircraft velocity of V_∞ . At cruise, the demand for air inhalation is considerably lower than at takeoff.

Figure 10.10. Real and ideal Joule (Brayton) cycle comparison of a straight-through jet



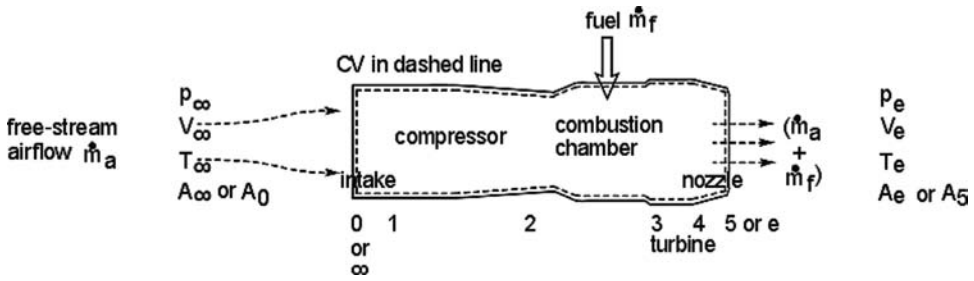


Figure 10.11. Control volume representation of a straight-through turbojet

The intake area is sized between the two demands. At cruise, the intake-stream-tube cross-sectional area is smaller than the intake-face area – it is closer to that of the exit-plane area, A (the gas exits at a very high velocity). Because in an ideal condition there is no precompression loss, Station 0 may be considered to have free-stream properties with the subscript ∞ .

From Newton’s second law, applied force $F =$ rate of change of momentum + net pressure force (the momentum rate is given by the mass flow rate), where the inlet momentum rate $= \dot{m}_a V_\infty$ and the exit momentum rate $= (\dot{m}_a + \dot{m}_f) V_e$.

Therefore:

$$\text{the rate of change of momentum} = (\dot{m}_a + \dot{m}_f)V_e - \dot{m}_a V_\infty \quad (10.6)$$

The net pressure force between the intake and exit planes $= p_e A_e - p_\infty A_\infty$ (i.e., the axi-symmetric side pressure at the CV walls cancels out). Typically, at cruise, a sufficiently upstream $A_e \approx A_\infty$. Therefore:

$$F = (\dot{m}_a + \dot{m}_f)V_e - \dot{m}_a V_\infty + A_e(p_e - p_\infty) = \text{net thrust} \quad (10.7)$$

Then:

$$(\dot{m}_a + \dot{m}_f)V_e + A_e(p_e - p_\infty) = \text{gross thrust}$$

and $\dot{m}_a V_\infty =$ ram drag (with $-ve$ sign, it must be drag). It is the loss of energy seen as drag due to the slowing down of the incoming air as the ram effect. This gives:

$$\text{net thrust} = \text{gross thrust} - \text{ram drag}; A_e(p_e - p_\infty) = \text{pressure thrust}$$

In general, subsonic commercial transport turbofans have a convergent nozzle, and the exit area is sized such that during cruise, $p_e \approx p_\infty$ (known as a perfectly expanded nozzle). This is different for military aircraft engines, especially with AB, when $p_e > p_\infty$ requires a convergent–divergent nozzle.

For a perfectly expanded nozzle, net thrust:

$$F = (\dot{m}_a + \dot{m}_f)V_e - \dot{m}_a V_\infty \quad (10.8)$$

Further simplification is possible by ignoring the effect of fuel flow, \dot{m}_f , because $\dot{m}_a \gg \dot{m}_f$.

Then, the thrust for a perfectly expanded nozzle is:

$$F = \dot{m}_a V_e - \dot{m}_a V_\infty = \dot{m}_a (V_e - V_\infty) \quad (10.9)$$

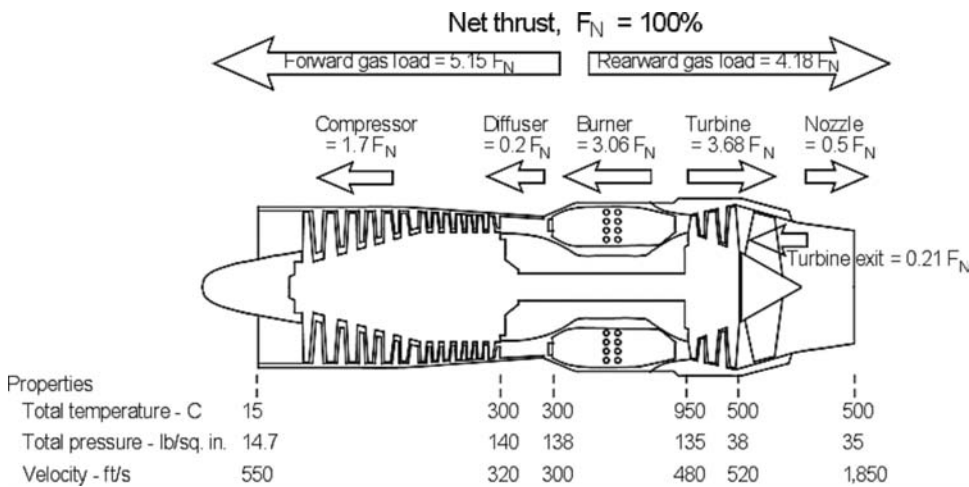


Figure 10.12. Where does the thrust act?

At sea-level, static-takeoff thrust (T_{SLs}) ratings $V_\infty = 0$, which gives:

$$F = \dot{m}_a V_e + A_e(p_e - p_\infty) \tag{10.10}$$

Equation 10.10 indicates that the thrust increase can be achieved by increasing the intake airmass flow rate and/or increasing the exit velocity.

Equation 10.4 gives the propulsive efficiency:

$$\eta_p = \frac{2V_\infty}{V_e + V_\infty} \tag{10.11}$$

Clearly, jet-propelled aircraft with low flight speeds have poor propulsive efficiency, η_p . Jet propulsion is favored for aircraft flight speeds above Mach 0.6.

The next question is: Where does the thrust act? Figure 10.12 shows a typical gas turbine engine in which the thrust is acting over the entire engine; the aircraft senses the net thrust transmitted through the engine-mounted bolts.

Figure 10.12 shows a typical straight-through turbojet pressure, velocity, and temperature variation along the length as airmass flows through. Readers may note the scale; within each component, the velocity change is negligible.

10.6.2 Bypass Turbofan Engine: Formulation

Typically, in this book, a long-duct nacelle is preferred to obtain better thrust and fuel economy and to offset the weight gain as compared to short-duct nacelles (see Figure 10.21). The pressure increase across the fan (i.e., secondary cold flow) is substantially lower than the pressure increase of the primary airflow. The secondary airflow does not have the addition of heat as in the primary flow. The cooler and lower exit pressure of the fan exit – when mixed with the primary hot flow within the long duct – reduces the final pressure to lower than the critical pressure, favoring a perfectly expanded exit nozzle ($p_e = p_\infty$). Through mixing, there is a reduction in the jet velocity, which provides a vital benefit in noise reduction (see Chapter 15) to meet airworthiness requirements. The long-duct nacelle exit plane can be sized to expand perfectly.

Primary flow has a subscript designation of p and secondary flow has a subscript designation of s . Therefore, F_p and V_{ep} denote primary flow thrust and exit velocity, respectively, and F_s and V_{sp} denote bypass flow thrust and its exit velocity, respectively. Thrust (F) equations of perfectly expanded turbofans are computed separately for primary and secondary flows and then added to obtain the net thrust, F , of the engine (i.e., a perfectly expanded nozzle):

$$F = F_p + F_s = [(\dot{m}_p + \dot{m}_f) \times V_{ep} - \dot{m}_p \times V_\infty] + [\dot{m}_s \times (V_{es} - V_\infty)]$$

Specific thrust in terms of primary flow becomes (f = fuel-to-air ratio), or:

$$F/\dot{m}_p = [(1 + f) \times V_{ep} + \text{BPR} \times V_{es} - V_\infty \times (1 + \text{BPR})] \quad (10.12)$$

If the fuel flow is ignored, then:

$$F/\dot{m}_p = [V_{ep} - V_\infty] + \text{BPR} \times (V_{es} - V_\infty) \quad (10.13)$$

For kinetic energy (KE):

$$\begin{aligned} KE &= \dot{m}_p [1/2(V_{ep}^2 - V_i^2)] + \dot{m}_s [1/2(V_{sp}^2 - V_\infty^2)] \\ \text{or} & \\ KE/\dot{m}_p &= [1/2(V_{ep}^2 - V_i^2)] + \text{BPR} \times [1/2(V_{sp}^2 - V_\infty^2)] \end{aligned} \quad (10.14)$$

At a given design point (i.e., flight speed V_∞), BPR, fuel consumption, and \dot{m}_p are held constant. Then, the best specific thrust and KE are found by varying the fan exit velocity for a given V_{ep} , setting the differentiation relative to V_{es} equal to zero. (This may be considered as trend analysis for ideal turbofan engines; real engine analysis is more complex.)

Then, by differentiating Equation 10.13:

$$d(F/\dot{m}_p)/d(V_{es}) = 0 = d(V_{ep})/d(V_{es}) + \text{BPR} \quad (10.15)$$

Equation 10.14 becomes:

$$d(KE/\dot{m}_p)/d(V_{es}) = 0 = V_{ep}d(V_{ep})/d(V_{es}) + \text{BPR} \times V_{sp} \quad (10.16)$$

Combining Equations 10.15 and 10.16:

$$-\text{BPR} \times V_{ep} + \text{BPR} \times V_{sp} = 0$$

Because $\text{BPR} \neq 0$, the optimum is when:

$$V_{ep} = V_{sp} \quad (10.17)$$

That is, the best specific thrust is when the primary (i.e., hot core) exit-flow velocity equals the secondary (i.e., cold fan) exit-flow velocity.

Equation 10.4 gives the turbojet propulsive efficiency, $\eta_p = \frac{2V_\infty}{V_e + V_\infty}$, for a simple turbojet engine; however, for the turbofan, there are two exit-plane velocities – for the hot-core primary flow (V_{ep}) and for the cold-fan secondary flow (V_{es}). Therefore, an equivalent mixed turbofan exit velocity (V_{eq}) can substitute for V_e in the previous equation. Fuel-flow rates are minor and can be ignored. The equivalent turbofan exit velocity (V_{eq}) is obtained by equating the total thrust (i.e., a perfectly expanded nozzle) as if it were a turbojet engine with total air mass flow ($\dot{m}_p + \dot{m}_s$).

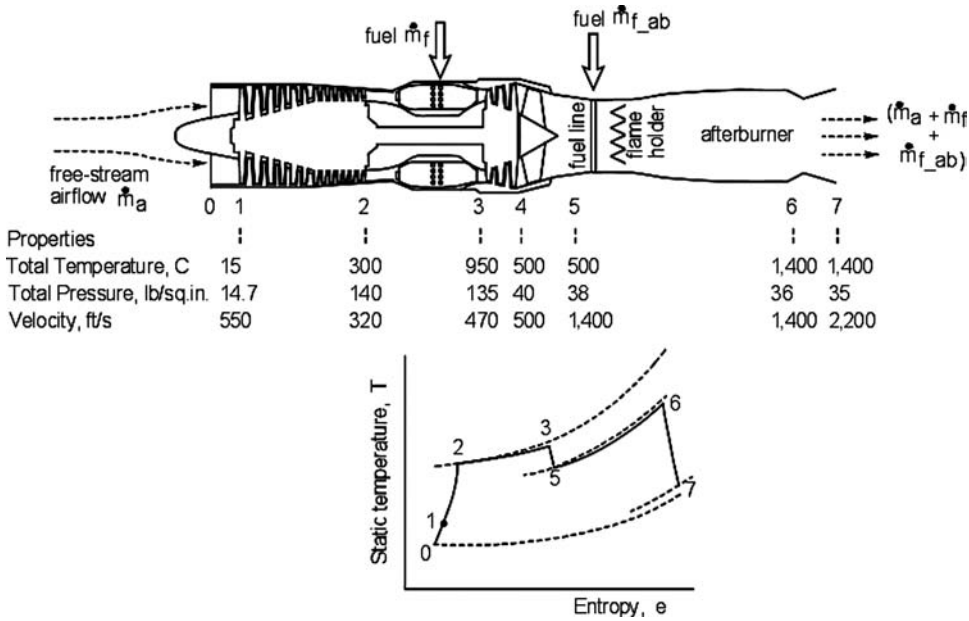


Figure 10.13. Afterburning turbojet and T-s diagram (real cycle)

Thus:

$$\begin{aligned}
 (\dot{m}_p + \dot{m}_s) \times (V_{eq} - V_\infty) &= \dot{m}_p \times (V_{ep} - V_\infty) + \dot{m}_s \times (V_{es} - V_\infty) \\
 \text{or } (1 + \text{BPR}) \times (V_{eq} - V_\infty) &= (V_{ep} - V_\infty) + \text{BPR} \times (V_{es} - V_\infty) \\
 \text{or } (1 + \text{BPR}) \times V_{eq} &= (V_{ep} - V_\infty) + \text{BPR} \times (V_{es} - V_\infty) + V_\infty \times (1 + \text{BPR}) \\
 &= V_{ep} + \text{BPR} \times V_{es} \\
 \text{or } V_{eq} &= [V_{ep} + \text{BPR} \times V_{es}] / (1 + \text{BPR}) \tag{10.18}
 \end{aligned}$$

Then, turbofan propulsive efficiency:

$$\eta_{pf} = \frac{2V_\infty}{V_{eq} + V_\infty} \tag{10.19}$$

Large engines could benefit from weight savings by installing short-duct turbofans; some smaller aircraft also use short-duct nacelles.

10.6.3 Afterburner Engine: Formulation

Figure 10.13 is a schematic diagram showing the station numbers for an AB jet engine. To keep numbers consistent with the turbojet numbering system, there is no difference between Stations 4 and 5, which represent the turbine exit condition. Station 5 is the start and Station 6 is the end of AB. Station 7 is the final exit plane. Figure 10.13 also shows the isentropic AB cycle in a T-s diagram.

AB is deployed only in military aircraft (except in the civil supersonic Concorde) as a temporary thrust-augmentation device to meet the mission demand at takeoff and/or fast acceleration and maneuvers to engage or disengage in combat. AB is applied at full throttle by activating a fuel switch. The pilot can feel the deployment by the sudden increase in the g-level in the flight direction. A ground observer

notices a sudden increase in the noise level, which can exceed the physical threshold. An AB glow is visible at the exit nozzle; in the dark, it appears as a spectacular plume with supersonic expansion “diamonds.” In the absence of any downstream rotating machines, the AB temperature limit can be increased from 2,000 to 2,200 deg K, at the expense of a significant increase in the fuel flow (i.e., a richer fuel-to-air ratio than in the core combustion).

An AB exit nozzle invariably runs choked and requires a convergent–divergent nozzle for the supersonic expansion to increase the gain in momentum for the thrust augmentation. Typically, to gain a 50% thrust increase, fuel consumption increases from 100 to 120%; that is why it is used only for a short period, not necessarily in one burst. It is interesting that AB in bypass engines is an attractive proposition because the AB inlet temperature is lower. In fact, all modern combat-category engines use a low bypass of 1 to 3.

Losses in an AB exit nozzle are high – the flameholders and so forth act as obstructions. It is preferable to diffuse the flow speed at the AB from higher speed to Mach 0.2 to 0.3, which results in a small bulge in the jet-pipe diameter around that area. A combat aircraft fuselage must be able to house this bulge.

10.6.4 Turboprop Engine: Formulation

Turbo props are described in Section 10.4.4. They are very similar to turbojets and turbofans except that the high energy of the exhaust jet is utilized to drive a propeller by incorporating additional low-pressure turbine stages, as shown in Figure 10.7. Thrust developed by the propellers is the propulsive force for the aircraft. A small amount of residual thrust could be left at the nozzle exit plane, which should be added to the propeller thrust. The relationship between the thrust power (TP) and the gas turbine SHP is related to propeller efficiency, η_{prop} , as:

$$\text{TP} = \text{SHP} \times \eta_{\text{prop}} + F \times V_{\infty} \quad (10.20)$$

ESHP is a convenient way to define the combination of shaft and jet power, as follows:

$$\text{ESHP} = \text{TP}/\eta_{\text{prop}} = \text{SHP} + (F \times V_{\infty})/\eta_{\text{prop}} \quad (10.21)$$

Aircraft at a static condition have an $\text{ESHP} = \text{SHP}$ because the small thrust at the exit nozzle is not utilized. As speed increases, $\text{ESHP} > \text{SHP}$, as there is some thrust at the nozzle. SFC and specific power are expressed in terms of ESHP.

Summary

The formulae provide good reasoning for the gas turbine domain of application, as shown in Figure 10.2. Turboprops provide the best economy for a design flight speed at and below Mach 0.5 and are well suited for shorter ranges of operation. At higher speeds, up to Mach 0.98, turbofans with a high BPR provide better efficiencies (see the comments following Equation 10.5). At supersonic speeds, the BPR is reduced and, in most cases, uses an AB. Smaller aircraft have piston engines up to a certain size (i.e., $\approx \leq 500$ HP). Above 500 HP, turboprops prove better than piston engines.

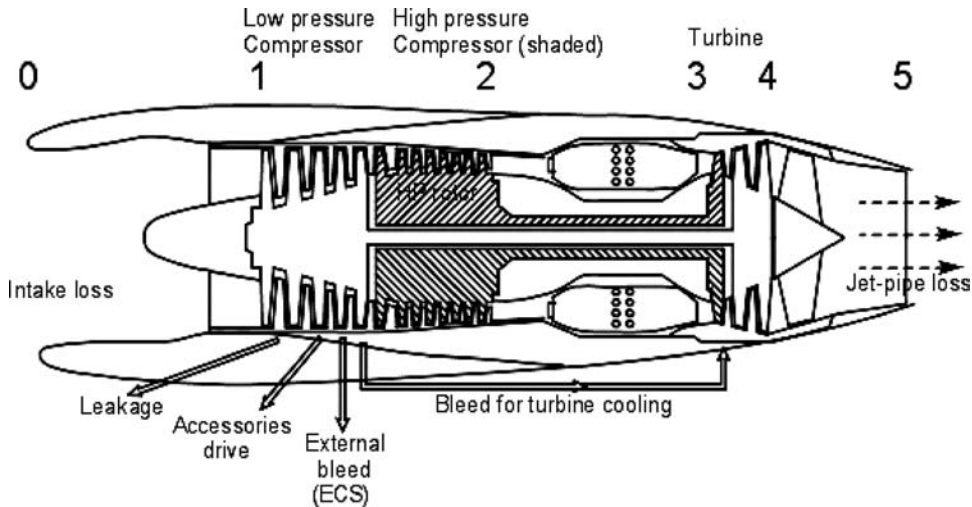


Figure 10.14. Installation effects

10.7 Engine Integration with an Aircraft: Installation Effects

Engine manufacturers typically supply bare engines to aircraft manufacturers, which install them to integrate with an aircraft. The same type of engines can be used by different aircraft manufacturers; each has its own integration requirements. Installing an engine in an aircraft is a specialized technology with which aircraft designers must be knowledgeable. Engine integration is accomplished by aircraft manufacturers in consultation with engine manufacturers.

A bare engine at the test stand performs differently than an installed engine on an aircraft. The installation effects of an engine result from having a nacelle – that is, the losses of intake and exhaust plus off-takes of power (e.g., driving motors and generators) and air-bleeds (e.g., anti-icing and environmental control). The total loss of thrust at takeoff could be as high as 8 to 10% of what is generated by a bare engine at the test bed; at cruise, the loss can be reduced to less than 5%. Figure 10.14 shows typical off-takes that are required due to various installation effects. Designers conduct analytical and empirical studies to establish key parameters in order to arrive at a design that produces satisfactory thrust to meet aircraft-performance requirements.

A nacelle is the housing for the engine and it interfaces with an aircraft; typically, it is pod/pylon-mounted in civil aircraft designs. A nacelle on an aircraft with more than one engine is pod/pylon-mounted on the wing and/or the fuselage. Propeller-driven engine nacelles are also similar to podded nacelles, modified by the presence of a propeller (see Section 10.7.2). An aircraft with one engine is aligned in the plane of the aircraft symmetry; engines with propellers can have a small lateral inclination of 1 or 2 deg about the aircraft centerline to counter the slipstream and gyroscopic effects from a rotating propeller. As discussed previously, wing-mounted nacelles are best for relieving wing-bending in the flight load. The engines on military aircraft are buried in the fuselage and therefore do not have a nacelle unless the designer chooses to have pods (e.g., some older designs). Military-aircraft designers must consider intake design as described in Section 10.8.2. The

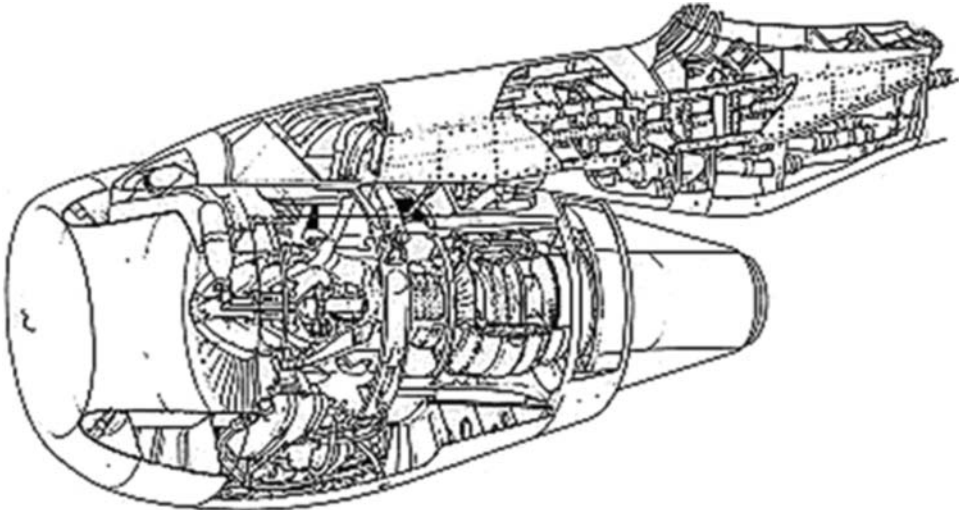


Figure 10.15. Installed turbofan housed in a nacelle pod under slung below aircraft wing (Courtesy of Bombardier-Aerospace Shorts)

position of the nacelle relating to the aircraft and the shaping to reduce drag are important considerations (see Section 9.8).

10.7.1 Subsonic Civil Aircraft Nacelle and Engine Installation

Nacelle design and engine integration typically are the responsibility of aircraft designers. A nacelle is a multifunctional system consisting of (1) an inlet; (2) an exhaust nozzle; (3) a thrust reverser, if required; and (4) a noise-suppression system. The goal of nacelle design is to minimize associated drag and noise and to provide a smooth airflow to the engine in all flight conditions. Therefore, the aerodynamic shaping – streamline as much as possible – is very important for aerodynamicists. Typical nacelle positions in current practice are shown in Figures 4.31 through 4.33.

Except for the Concorde, all civil aircraft currently are subsonic with a maximum speed of less than Mach 0.98. All subsonic aircraft use some form of a pod-mounted nacelle such that the design has become generic. Readers should note that designs with the engine buried in the wing (e.g., the Comet) are no longer practiced. Recently, with the advent of very small turbofans competing with propeller-driven engines, in some smaller jet aircraft the engine can be integrated with the fuselage instead of using pod mounts. The approach of this book continues with the dominant pod-mounted nacelles. Figure 10.15 shows a turbofan installed in a civil aircraft nacelle pod. An over-wing nacelle like that of the VFW614 is a possibility that has yet to be explored properly (Honda has reintroduced a jet aircraft). An under-wing nacelle is the current best practice; however, for smaller aircraft, ground-clearance issues force the nacelle to be fuselage-mounted.

There are two types of podded nacelles. Figure 10.16a shows a long-duct nacelle in which both the primary and secondary flows mix within the nacelle. The mixing increases the thrust and reduces the noise level compared to a short-duct nacelle, possibly compensating the weight gain through fuel- and cost-savings. Figure 10.16b shows a short-duct nacelle in which the bypassed cold flow does not

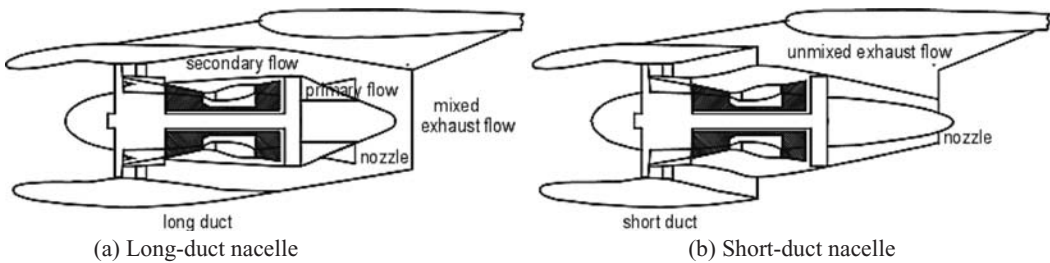


Figure 10.16. Podded nacelle types

mix with the hot-core flow. Advantages include weight, interference drag, and cost reduction by decreasing the length of the outside nacelle casing. The length of a short-duct nacelle can vary. The length depends on a designer's assessment; the shortest is about half of the nacelle length. Although larger nacelles can benefit from having short ducts, designers may decide on a smaller nacelle with a short duct if the engine-noise level is low.

Three typical positions of the nacelle relative to the wing are shown in Figure 10.17 (see [3] for details). The top wing represents a B747, the middle wing represents an A300, and the bottom wing represents a DC10. All nacelles are hung over well ahead of the wing to keep interference drag low, almost at zero. There is no quick answer for the degree of incidence, which is design-specific and varies for the type of installation. It depends on aerodynamic consideration, the engine position relative to the wing (e.g., how much inboard on the wing and the flexure of the wing during flight). Post-conceptual design studies using CFD and wind-tunnel and flight tests fine-tune the nacelle geometry and its positional geometry to the production standard. Readers should note the typical gap between the nacelle and the wing.

Aircraft designers must make their best compromises in positioning the engine on the wing. In the coursework, Table 10.4 may be used to position wing-mounted nacelles. The most-inboard engine should be kept at least 30 deg from the nose-wheel spray angle, as shown in Figure 10.18 (the B747 is somewhat widely spaced).

Fuselage-mounted nacelle contours are similar in design but the positioning relative to the fuselage requires special consideration. A gap of at least one half of the nacelle diameter can be left between the fuselage and the nacelle. The vertical position can be close to the fuselage centerline or high up on the fuselage (see Figures 4.31 and 4.33). For the coursework exercise, consider the following points for positioning the nacelle on the fuselage:

- Stay clear of the wing wake.
- Keep the exhaust flow from interfering with the empennage.

Figure 10.17. Typical position of the nacelle relative to the wing

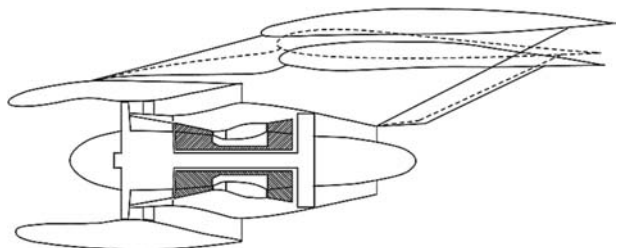


Table 10.4. *Wing-mounted nacelle position*

2-engine	0.3 to 0.32 of semiwing span from the aircraft centerline
3-engine	Same as 2-engine; the third engine is at the aircraft centerline
4-engine	Inboard at 0.29 to 0.32 and outboard at 0.62 to 0.66 of the semi-wing span

- Keep the thrust line close to the aircraft CG to comply with the first two points.
- Keep the engine sufficiently forward to satisfy the CG position relative to the aircraft.

In the past, both the internal and external contours of a nacelle were designed by the aircraft manufacturer. Although there was no strict requirement, it gradually became convenient to develop the internal contour in consultation with or even entirely by the engine manufacturer. The external contour of a nacelle is developed by aircraft designers who match it with the lines of the internal contour. The contour of the nacelle cross-section is like that of an aerofoil except that it is not uniform all around – it may be perceived as a wrapped wing around the engine. The crown-cut section is thinner than the keel-cut section, as shown in Figure 10.16. The keel-cut section is thicker in order to house accessories and its fuller lip contour helps avoid separation at a high angle of attack. In principle, it is preferable to have circular cross-sectional areas for the intake throat area, but it may not always be possible – for example, for ground clearance. The Boeing 737 has a flat keel line in order to gain some ground clearance. In this book, the intake areas are considered to be circular.

In principle, the external contour lines of a good nacelle design are not necessarily symmetrical to the vertical plane. However, to keep costs down by maintaining commonality, many nacelles are designed to be symmetrical with the vertical plane. This allows manufacturing jigs to produce interchangeable nacelles between the port and starboard sides and to be able to minimize the essential difference at the finishing end. Efforts for the nacelle aerodynamic design (i.e., external mould-line shaping and internal contouring) have progressed to a point of diminishing returns and are approaching a generic shape.

Engine designers provide aircraft designers with the engine performance – currently, using a computer program amenable to input of the various off-takes. Aircraft designers must substantiate for the certifying agencies that the thrust available

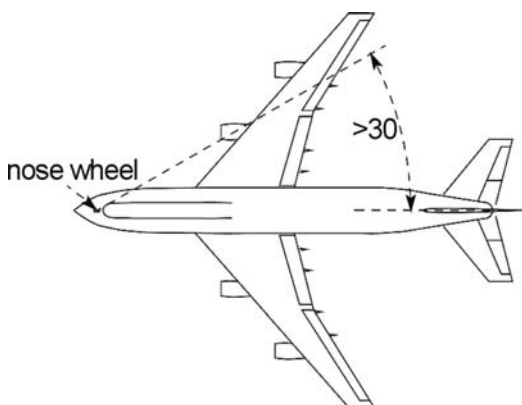


Figure 10.18. Inboard nacelle position

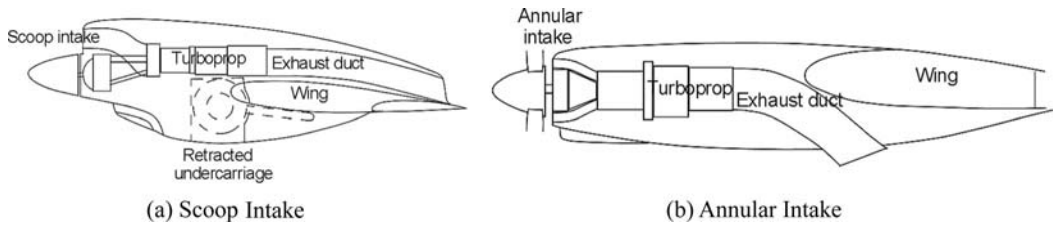


Figure 10.19. Typical wing-mounted turboprop installation

from the engine after deducting the losses is sufficient for the full flight envelope as specified. In hot and high-altitude conditions, it becomes critical at takeoff if the runway is not sufficiently long and/or there is an obstruction to clear. In that case, an aircraft may take off with lighter weight. Airworthiness requirements require that an aircraft maintain a minimum gradient (see [Chapter 11](#)) at takeoff with its critical engine inoperative (customer requirements may demand more than the minimum).

Following are the obligations of designers when installing an engine and integrating it with an aircraft:

- Generate the external and internal contours of the nacelle. Multiengines are either wing-mounted (i.e., larger aircraft) or fuselage-mounted (i.e., smaller aircraft).
- Compute the compressor air-bleed for the ECS (e.g., cabin air-conditioning and pressurization, de-icing and anti-icing, and other purposes).
- Compute power off-takes from the engine shaft to drive the electric generator, accessories, and so forth.
- Substantiate for the certifying agencies that the thrust available from the installed engine is sufficient for the full flight envelope.

Current developments involve laminar flow control over the external surface of the intake duct and technologies for noise and emission reduction.

10.7.2 Turboprop Integration to Aircraft

This section is a basic description of the subject and is intended only for coursework. The discussion highlights the technical challenges but exacting details are beyond the scope of this book. Turboprop nacelle design is subjected to the same considerations as the turbofan design. A turboprop nacelle is also a multifunctional system consisting of (1) an inlet, (2) an exhaust nozzle, and (3) a noise-suppression system. Thrust-reversing can be achieved by sufficiently changing the propeller pitch angle. There are two primary types of turboprop nacelles, as shown in [Figure 10.19](#). The scoop intake can be above or below (as a chin) the propeller spinner. It is interesting that several turboprop nacelles have integrated the undercarriage mount with storage space in the same nacelle housing, as shown in [Figure 10.19a](#). The other type has an annular intake, as shown in [Figure 10.19b](#). Installation losses are on the same order as those discussed for a turbofan installation.

A turboprop's nacelle position is dictated by the propeller diameter. The key geometric parameters for a wing-mounted turboprop installation are shown in [Figure 10.20](#).

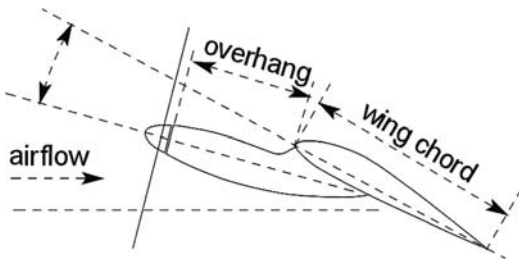


Figure 10.20. Typical parameters for a wing-mounted turboprop installation

Typically, there can be one fourth of the propeller-diameter gap between the fuselage and the propeller tip and between other propeller tips if there are four engines. The overhang should be as far forward as the design can accommodate (like the turbofan overhang) to reduce interference drag – at least a quarter to nearly one wing-chord length is sufficient. For a high-wing aircraft, the turboprop nacelle is generally underslung, especially if it also houses the undercarriage (e.g., the Bombardier Q400). For a low-wing aircraft, the nacelle is generally over the wing to give the propeller ground clearance. The propeller slipstream assists lift and has a strong effect on static stability; flap deployment aggravates the stability changes. Depending on the extent of wing incidence relative to the fuselage, there is some angle between the wing-chord line and the thrust line – typically, from 2 to 5 deg.

A fuselage-mounted, propeller-driven system is shown in Figure 10.21. The angle between the thrust line and the wing-chord line is the same as a wing-mounted, propeller-driven nacelle. Sometimes the propeller axis has about a 1-deg downward inclination relative to the fuselage axis. These parameters assist longitudinal stability. An inclination of 1 or 2 deg in the yaw direction can counter the propeller slipstream. Otherwise, the V-tail can be inclined to counter the effect.

A piston engine nacelle on the wing follows the same logic. Older designs had a more closely coupled installation.

10.7.3 Combat Aircraft Engine Installation

Combat aircraft have engines that are integral to the fuselage, mostly buried inside; however, in cases with two engines, they can bulge out to the sides. Therefore, pods are not featured unless having more than two engines on a large aircraft is required.

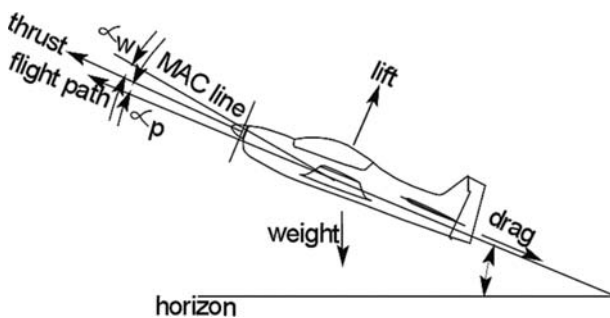


Figure 10.21. Typical flight parameters for a fuselage-mounted turboprop installation

Figure 10.22. Engine installed in a combat aircraft

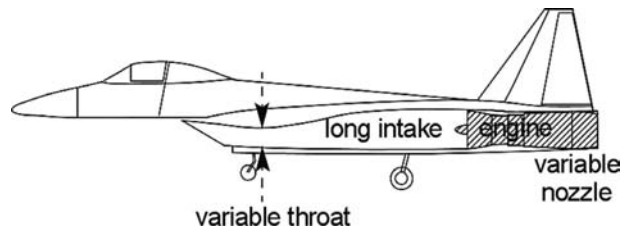


Figure 10.22 shows a turbofan installed on a supersonic combat aircraft. In this case, it is buried inside the fuselage with a long intake duct. The external contour of the engine housing is integral to the fuselage mould lines. The internal contours of the intake and exit nozzle are the responsibility of aircraft designers in consultation with engine manufacturers.

Early designs had the intake at the front of the aircraft: the pitot type for subsonic fighters (e.g., the Sabrejet F86) and with a movable center body (i.e., bullet translates forward and backward) for supersonic fighters (e.g., the MIG 21). The long intake duct snaking inside the fuselage below the pilot's seat incurs high losses. The side-intake superseded the nose-intake designs. Possible choices for side intakes are described in Section 4.19 – primarily, they are either side-mounted or chin-mounted. The intake is placed on a plate above the fuselage boundary layer. A center body is required for aircraft-speed capability above Mach 1.8; otherwise, it can be a pitot intake, and boundary layer plates can act as the center body.

Web Figure 10.25 shows the various flow regimes associated with supersonic intake. To install and integrate an engine in a military aircraft, designers are faced with the same considerations as for a civil aircraft design, but the technology is more complex. Designers must make justifiable choices based on the following:

- Design the engine intake and its internal contour and compute the intake losses plus those from supersonic shock waves. Multiengines are side by side.
- Design the engine exit nozzle and its internal contour and compute the nozzle losses. Military aircraft nozzle design is complex and addressed in [Section 10.10.4](#).
- Suppression of exhaust temperature for a stealth aircraft incurs additional losses at the intake and the nozzle.
- Compute the compressor air-bleed for the ECS (i.e., cabin air-conditioning and pressurization, de-icing and anti-icing, and other purposes). The extent of the air-bleed is less than in a civil aircraft because there is no large cabin environment to control.
- Compute the power off-takes from the engine shaft to drive the electric generator and accessories (e.g., pumps).
- Substantiate to the certifying agencies that the thrust available from the engine – after deducting the off-take losses – is sufficient for the full flight envelope.

Military aircraft have excess thrust (with or without AB) to accommodate hot and high-altitude conditions and to operate from short airfields; they can climb at a steeper angle than civil aircraft.

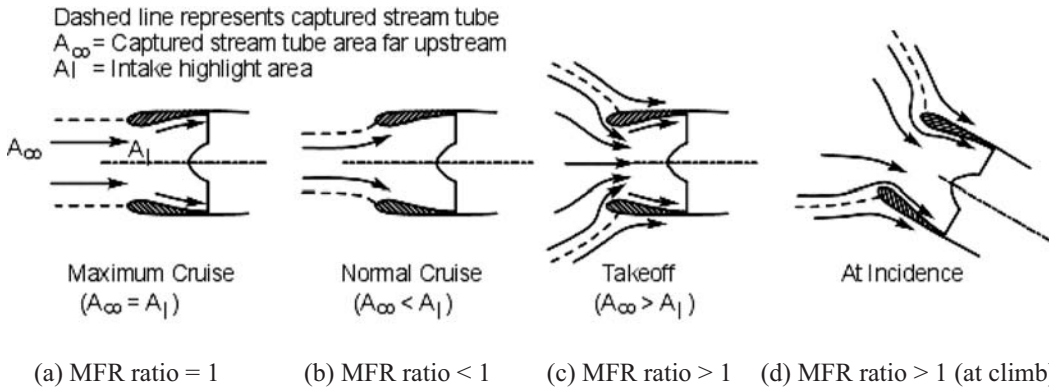


Figure 10.23. Airflow demand at various conditions (civil and military aircraft intakes)

10.8 Intake and Nozzle Design

Engine mass-flow demand varies significantly, as shown in Figure 10.23. To size the intake area, the reference cross-section of the incoming airmass-stream tube is taken at the maximum cruise condition, as shown in Figure 10.23a, when it has a cross-sectional area almost equal to that of the highlighted area (i.e., $A_\infty = A_1$; see Section 10.8.1 for nomenclature). The ratio of mass flow rates (MFR) relative to the reference condition (i.e., airmass flow at maximum cruise) is a measure of the spread the intake would encounter. At the maximum cruise condition, $MFR = 1$ as a result of $A_\infty = A_1$. At the typical cruise condition, the intake-airmass demand is lower ($MFR < 1$, as shown in Figure 10.23b). At the maximum takeoff rating ($MFR > 1$), the intake airmass-flow demand is high; the streamlined patterns are shown in Figure 10.23c. Variations in the intake airmass-flow demand are significant.

If the takeoff airmass flow demand is high enough, then a blow-in door – which closes automatically when demand drops off – can be provided. Figure 10.23d shows a typical flow pattern at incidence at high demand, when an automatic blow-in door may be necessary. At idle, the engine continues running with little thrust generation ($MFR \ll 1$). At an inoperative condition, the rotor continues windmilling to minimize drag. If a rotor seizes due to mechanical failure, there is a considerable drag increase.

Currently, the engine (i.e., fan) face should not exceed Mach 0.5 to avoid degradation due to compressibility effects. At a fan-face Mach number above 0.5, the relative velocity at the fan-tip region approaches sonic speed due to the high blade-rotational speed.

The purpose of the intake is to provide engine airmass-flow demand as smoothly as possible – there should be no flow distortion at the compressor face due to separation and/or flow asymmetry. The nacelle intake-lip cross-section is designed using logic similar to the aerofoil LE cross-section – that is, the flow should not separate within the flight envelope.

10.8.1 Civil Aircraft Intake Design: Inlet Sizing

This section describes an empirical approach for developing the intake contour of a podded nacelle that is sufficient for the conceptual design stage. This would

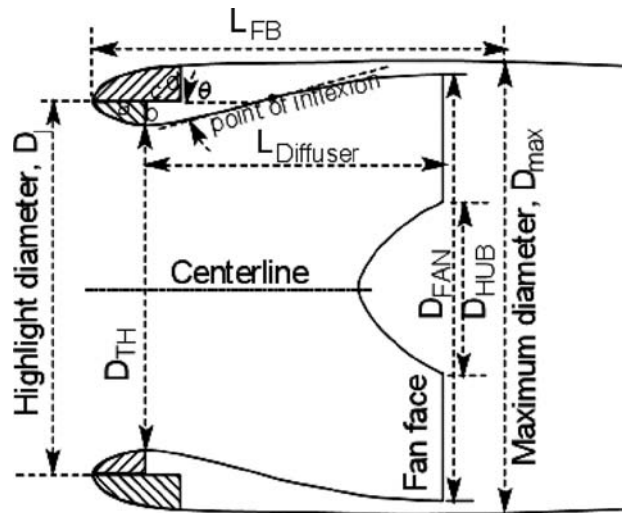


Figure 10.24. Schematic diagram of nacelle forebody section (crown cut)

generally be followed by proper refinement using extensive CFD analysis and wind-tunnel testing for substantiation. The nacelle external contour is influenced by interaction with the aircraft flow field. The simplified procedure is suitable for this coursework.

Figure 10.24 provides definitions of the design parameters required for the design of a pod-mounted subsonic civil aircraft intake. The nacelle section is similar to the aerofoil shape. The throat area is the minimum area of the intake duct and acts as a diffuser. The associated nomenclature follows (for the radius, replace D with R and the subscripts remain unchanged):

- D_I = highlight diameter; the forwardmost point of the nacelle. If the keel cut is not in the vertical plane with the crown cut, then its projection at the vertical line can be used.
- D_{TH} = throat diameter; the minimum cross-sectional area of the intake geometry
- D_{Tip} = D_{fan} = the tip of the fan (supplied by the engine manufacturer)
- D_{Hub} = rotor-hub diameter (supplied by the engine manufacturer)
- D_{MAX} = maximum external nacelle diameter
- L_{diff} = diffuser length, from throat to fan face
- L_{FB} = nacelle forebody length; the distance from the highlight to the maximum diameter, D_{MAX}
- a = semi-major axis of the internal lip
- b = semi-minor axis of the internal lip
- c = semi-major axis of the external lip
- d = semi-minor axis of the external lip
- θ = internal contour wall angle (below 10 deg; better at 6 deg)

Associated areas are as follows (radius R is half of diameter D in the nomenclature):

$$A_I = \text{highlighted area} = \pi(R_I)^2$$

$$A_{TH} = \text{throat area} = \pi(R_{TH})^2$$

$$A_\infty = \text{free-stream cross-sectional area}$$

To size the intake, the first parameter considered is establishing the throat area. The proper method is to obtain the maximum air-mass-flow demand at takeoff and the maximum-cruise demand. If the takeoff demand requires a much larger size, then blow-in doors (which close automatically when demand drops – mostly applicable to military designs) are provided. Using \dot{m}_a as the intake air-mass at the maximum cruise gives:

$$A_t = \dot{m}_a / (\rho_\infty V_\infty)$$

The throat area is sized from the lip contraction ratio (LCR) = A_1/A_{TH} (typically, from 1.05 to 1.20). LCR = 1.0 represents a sharp lip and 1.2 represents a well-rounded lip.

The highlighted diameter D_l is typically 0.9 to 0.95 times the fan-face diameter. Keep the $L_{diffuser} = 0.6$ at 1 time D_{fan} and $L_{FB} = 1$ to 2 times D_{fan} (it must conform with the lip contour).

The next task is to establish the lip contour before developing a suitable aerofoil section for the intake cowl. As for the wing aerofoil, NACA developed nacelle forebody aerofoil contours. NACA 1 is a good design guideline for the external contour (i.e., the upper lip is nearly elliptical). In general, the lower lip (i.e., elliptical) contour is developed by the engine manufacturer and matches the upper lip.

In Figure 10.24, the nacelle lip is in the shape of a quarter-ellipse with semi-major axis a and semiminor axis b . The parameters that define the inlet-lip internal-contour geometry are (1) the LCR R_1/R_{TH} (i.e., A_1/A_{TH}), and (2) the fineness ratio (a/b).

At the crown cut:

internal-lip fineness ratio, (a/b) = from 2 to 5 (typically 1.5 to 3.0)

external-lip fineness ratio, (c/d) = from 3 to 6 (typically 3 to 5)

At the crown cut, the lip-thickness ratio of $(b + d)/L_{diff}$ is around 15 to 20% (the lip-thickness ratio is not like the aerofoil t/c ratio because the cowl length extends beyond the fan face when the ratio decreases substantially). Typically, b is 1.5 to 2 times d .

At the keel cut, if it houses accessories, the thickness ratio is $(b + d)/L_{diffuser}$ by about 20 to 30%.

The side cuts of the nacelle result from the merging of the crown cut and the keel cut. If ground clearance is a problem, the accessories are distributed around the keel and the contours are merged accordingly. This book keeps the design simple by using crown-cut geometry all around, with the understanding of actual problems.

The throat Mach number and the air-mass-flow demand at maximum cruise determine the D_{TH} . The throat Mach number must be maximized to the point to maintain the fan-face Mach number below 0.5 at the maximum cruise condition. At $A_\infty < A_1$, there is precompression when associated spillage generates additive drag (see Figure 9.7). Then, long $L_{diffusion}$ is not required for internal diffusion because external diffusion has partially achieved it. At $A_\infty = A_1$, there is no additive drag, but it would need longer $L_{diffusion}$ for internal diffusion. Figure 9.6 indicates that additive drag decreases as the MFR increases. At cruise (i.e., MFR above Mach 0.6), additive drag is minor.

At the throat, if the Mach number is high (e.g., reaches the local sonic speed), there is more loss and a longer diffuser is needed to decrease air velocity to around Mach 0.5 at the fan face. It is best to keep the average Mach number at the throat just below 1.0. Care must be taken that at yaw and/or high angles of attack, the fan-face flow distortion is minimized.

Finally, to make a proper divergent part of the subsonic intake acting as the diffuser, the internal contour shows an inflection point (at around 0.5 to 0.75 L_{diff}). At that point, to avoid separation, the maximum wall angle θ should not exceed 8 or 9 deg.

Typically, the nacelle length, L_N , is 1.5 to 1.8 times the bare engine length, L_E . The maximum diameter is positioned around 0.25 to 0.40 of the nacelle length (L_{FB}) from the front end. The nacelle external cross-section is not purely circular but rather has a “pregnant-belly” shape at the keel cut to house engine accessories. Use the maximum radius at the crown cut as 1.1 to 1.4 times the engine fan-face radius and at the keel cut as 1.2 to 1.6 times the engine fan-face radius. The side cuts are faired between the two.

For the worked-out Bizjet example, use the following values (see [Section 10.10.3](#)):

Given fan-face diameter, $D_{fan} = 0.716$ m (2.35 ft)

$R_1 = 0.9 \times R_{fan}$

At maximum cruise, MFR = 1 ($A_\infty = A_H$)

At cruise, MFR = 0.7 ($A_\infty < A_H$)

LCR = 1.12

$D_{MAX} = 1.5 \times 0.716 = 1.074$ m (3.52 ft)

Lower-lip fineness ratio (a/b) = 3

Upper-lip fineness ratio (c/d) = 5

$L_{diff} = 0.65 D_{fan}$

$(b + d)/L_{diff} = 0.18$

$L_{FB} = 1.4$ times D_{fan}

Engine manufacturers supply the data for bare engines. A bare engine may come with an exhaust duct as a nozzle that fits within the nacelle exhaust.

10.8.2 Military Aircraft Intake Design

This extended section of the book can be found on the Web site www.cambridge.org/Kundu and discusses the important consideration for typical military aircraft intake design involving supersonic intakes. The associated figure is Figure 10.25.

Figure 10.25. Types of ideal supersonic intake demand conditions [21]

10.9 Exhaust Nozzle and Thrust Reverser

The thrust reverser (TR) is part of an exhaust nozzle and both are addressed in this section; an empirical sizing method for a nozzle is discussed but not the size and

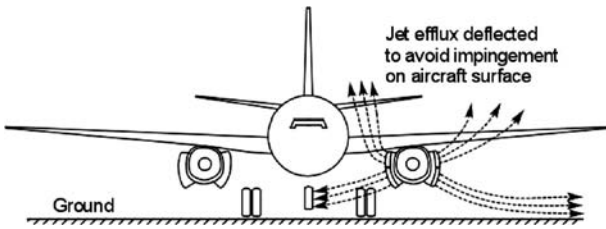


Figure 10.26. TR efflux pattern

design of the TR, which is a separate technology. Before explaining exhaust nozzles, it is helpful to understand TRs.

The role of a TR is to retard aircraft speed by applying thrust in the forward direction (i.e., in a reversed application). The rapid retardation by the TR application reduces the landing-field length. In a civil aircraft application, the TR is applied only on the ground. Because of its severity, certification rules require to either design for deployment in flight (e.g., Concorde) or prevent in-flight deployment. However, the latter is the more common approach. A TR reduces the wheel-brake load so there is less wear and fewer heat hazards. A TR is effective on slippery runways (e.g., ice and water) when braking is less effective. A typical benefit of having sufficient stopping distance at landing on an icy runway with TR application is that it reduces the field length by less than half. A midsized jet-transport aircraft stops at about 4,000 ft with a TR or at about 12,000 ft without it. Without a TR, the energy that was depleted to stop the aircraft is absorbed by the wheel brake and aerodynamic drag. Application of the TR also provides additional intake momentum drag (at full throttle), contributing to energy depletion. A TR is useful for an aircraft to go in reverse (e.g., a C17) on the ground for parking, alignments, and so forth – most aircraft with a TR do not use reverse but rather a specialized vehicle that pushes it.

A TR is integrated on the nacelle and it is the responsibility of an aircraft manufacturer to design it or it may be subcontracted to specialist organizations devoted to TR design. The next section introduces the TR in detail so that coursework can proceed on the nacelle without undertaking the detailed design.

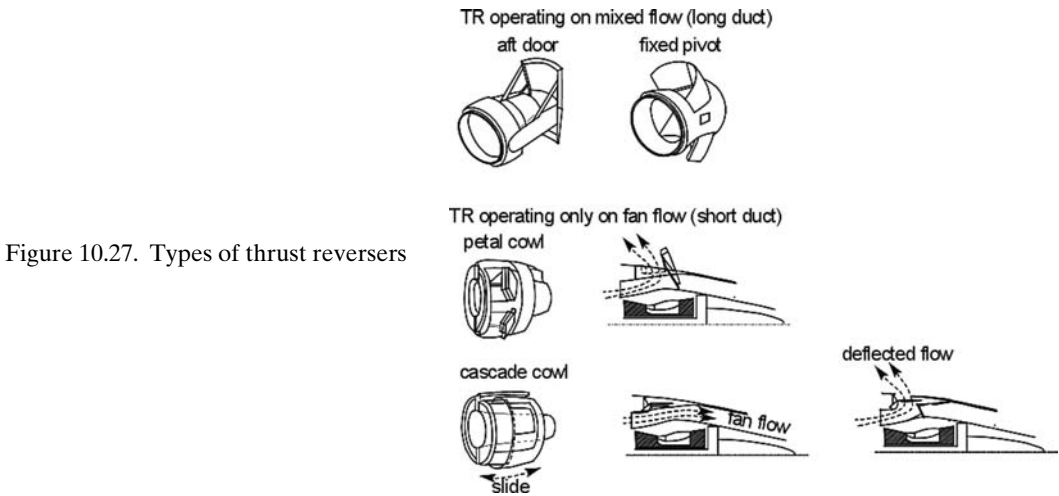
10.9.1 Civil Aircraft Thrust Reverser Application

TRs are not required by the regulatory authorities (i.e., FAA and CAA). The components are expensive, heavy, and only applied on the ground, yet their impact on an aircraft's operation is significant due to additional safety through better control and reduced time for stopping, especially during aborted takeoffs and other related emergencies. Most airlines want their aircraft to have TRs even with the increased DOC.

Aircraft designers must ensure that TR efflux is well controlled – there should be no adverse impingement of on aircraft surface or reingestion in the engine. [Figure 10.26](#) shows a typical satisfactory TR efflux pattern.

In general, there are two types of TRs: (1) operating on both the fan and core flow, and (2) operating on the fan flow only. The choice depends on the BPR, nacelle location, and customer specifications.

The first type, which operates on the total flow (i.e., both fan and core), is shown at the top of [Figure 10.27](#). There are two types: (1) the sliding-port aft-door type, in



which the doors slide to the aft end as they open up to deflect the exhaust flow; and (2) the fixed-pivot type, in which the doors rotate to a position that deflects the exhaust flow.

The second type of TR operates on the fan flow only. There are two types: (1) the petal-cowl type, shown in the middle of Figure 10.27; and (2) the cascade-cowl type, shown at the bottom of Figure 10.27. There are two cascade types: the conventional type and the natural-blockage type. The Bombardier CRJ700/900 aircraft uses a petal cowl TR of the natural-blockage type. The external cowls translate back, blocking the fan flow when it escapes through the fixed cascades that reverse the flow. This design is attractive with a low parts count, scalability, easier maintenance, and a relatively higher retarding energy. The petal-cowl type operating on the fan flow is suitable for short-duct nacelles, as shown in the figure. The petal doors open on a hinge to block the secondary flow of the fan when it deflects to develop reverse thrust.

TRs are applied below 150 kts and are retracted at around 50 kts (to avoid re-ingestion of engine efflux), when the wheel brakes become effective. The choice of the TR type depends on a designer's compromise with the available technology.

10.9.2 Civil Aircraft Exhaust Nozzles

Civil aircraft nozzles are conical in shape, on which the TR is integrated. Small turbofan aircraft may not need a TR but regional jet (RJ) aircraft and larger use a TR. Inclusion of a TR may slightly elongate the nozzle, but this is not discussed in this book.

In general, the nozzle exit area is sized as a perfectly expanded nozzle ($p_e = p_\infty$) at LRC condition; at higher engine ratings, it is $p_e > p_\infty$. The exit nozzle of a long-duct turbofan does not run choked at cruise ratings. At takeoff ratings, the back pressure is high at a lower altitude; therefore, a long-duct turbofan does not need to run choked (i.e., the low-pressure secondary flow mixes in the exhaust duct). An exhaust nozzle runs in a favorable pressure gradient; therefore, its shaping results

in a relatively simpler establishment of geometrical dimensions. However, it is not simple engineering at elevated temperatures and for suppressing noise levels.

The nozzle exit plane is at the end of the engine. Its length from the turbine exit plane is 0.8 to 1.5 times the fan-face diameter. The nozzle-exit-area diameter is roughly half to three fourths of the intake-throat diameter in this study.

10.9.3 Coursework Example of Civil Aircraft Nacelle Design

For coursework on the Bizjet, the following factors are taken from the turbofan class and type:

- Uninstalled $T_{SLs} = 15.6$ kn (3,500 lb)
- Bare engine length = 1.547 m (5.07 ft)
- Maximum diameter = 1.074 m (3.52 ft)
- Engine airmass flow at takeoff = 66.2 kg/s (146 lb/s)
- Engine airmass flow at maximum cruise rating ≈ 20 kg/s (44 lb/s)
- BPR = 4
- Fan-face diameter = 0.716 m (2.35 ft)

This results in the following nacelle dimensions (factors are from industrial experience).

Intake Geometry (see Section 10.8.1)

- Highlight diameter = 0.9×0.716 m = 0.644 m (2.11 ft)
- Throat diameter (use the contraction ratio 1.12) = 0.575 m (1.89 ft), $A_{TH} = 0.26$ m² (2.8 ft²)
- Check air velocity at the throat for the maximum cruise condition at Mach 0.74 (716 ft/s) and at 41,000-ft altitude ($p_{\infty} = 17,874$ N/m², $T_{\infty} = 216.65$ K, and $\rho_{\infty} = 0.284$ kg/m³)
- Therefore, $V_{TH} = 20 / (0.284 \times 0.26) = 270$ m/s (689 ft/s); i.e., Mach 0.922 is a preferred number
- This could result in low diffuser length: $L_{diff} = 0.65 \times D_{fan} = 0.65 \times 0.716 = 0.465$ m (1.5 ft)

Lip Section (Crown Cut)

- Use $(b + d) = 0.18 \times L_{diff} = 0.18 \times 0.465 = 0.0837$ m (0.275 ft)
- Use $b = 1.4 \times d$; this results in $b = 0.05$ m (0.164 ft) and $d = 0.0337$ m (0.11 ft)
- Use a lower-lip fineness ratio of $a/b = 2$; this gives $a = 0.1$ m (0.328 ft)
- Use an upper-lip fineness ratio of $c/d = 4$; this gives $c = 0.134$ m (0.44 ft)
- The intake length from the highlight (low-speed aircraft) = $0.465 + 0.1 = 0.565$ m (1.85 ft)
- The L_{FB} is about 1 m from the highlight, which is 1.4 times $D_{fan} = 1.4 \times 0.716 = 1$ m (3.28 ft)
- The crown-cut radius at L_{FB} is 1.15 times $R_{fan} = 1.1 \times 0.716/2 = 0.41$ m (1.34 ft)

Lip Section (Keel Cut)

This book keeps the internal contour of the intake circular to fit with the rotating circular fan face; even the constrained Boeing 737 with a flat keel section must be circular at the fan face. Therefore, the internal contour of the keel cut is the mirror

image of the crown cut about the centerline. However, the keel-cut radius at L_{FB} is 1.4 times $R_{fan} = 1.4 \times 0.716/2 = 0.5 \text{ m}$ (1.64 ft).

The intake internal contour can be finalized by taking the inflexion point at about mid L_{diff} , maintaining maximum θ within the range (i.e., 8 to 9 deg).

The average diameter at the maximum circumference $= 0.41 + (0.5 - 0.41)/2 = 0.91 \text{ m}$ (3 ft).

Nozzle Geometry

Use a nozzle length $= 0.75 \times \text{fan-face diameter} = 0.75 \times 0.716 \text{ m} = 0.537 \text{ m}$ (1.76 ft). Once the control points for the geometry are established, the contour can be generated in CAD using splined curves (i.e., smooth fairing when drawn manually).

The total nacelle length $= \text{intake length} + \text{engine length} + \text{nozzle length} = 0.565 + 1.547 + 0.537 = 2.65 \text{ m}$ ($\approx 8.7 \text{ ft}$), which is close to what was established in Chapter 6 from the statistical data.

The nacelle fineness ratio $= 2.62/1.074 = 2.44$ (i.e., within the range).

The author cautions that the empirical method presented from his industrial experience is coarse but nevertheless provides a representative geometry for the coursework exercise. This physical model serves as a starting point for further aerodynamic refinement to a more streamline shape through CFD and testing. To obtain the factors used in the example, significant nacelle geometric data are required for better substantiation. (Readers must study many designs to get a sense of the factors used here.) Each industry has its own approach based on past designs (which form the basis of statistical data) to generate a nacelle geometry. In the industry, nacelle design is an involved process that includes the points addressed herein.

10.9.4 Military Aircraft Thrust Reverser Application and Exhaust Nozzles

This extended section of the book can be found on the Web site www.cambridge.org/Kundu and discusses important considerations involving typical military aircraft thrust reversers (TR) and exhaust nozzles. Associated figures include the following.

Figure 10.28. Military aircraft nozzle adjustment scheme (from [19])

(a) Mechanism for nozzle adjustment

(b) Individual petal movement

Figure 10.29. Supersonic nozzle area adjustment and thrust vectoring

10.10 Propeller

Aircraft flying at speeds less than Mach 0.5 are propeller-driven, larger aircraft are powered by gas turbines, and smaller aircraft are powered by piston engines. More advanced turboprops have pushed the flight speed to more than Mach 0.7 (e.g., the Airbus A400). This book discusses conventional types of propellers that operate at a flight speed of less than or equal to Mach 0.5. After introducing the basics of propeller theory, this section concentrates on the engineering aspects of what is required by aircraft designers. References [16], [18], and [22] may be consulted

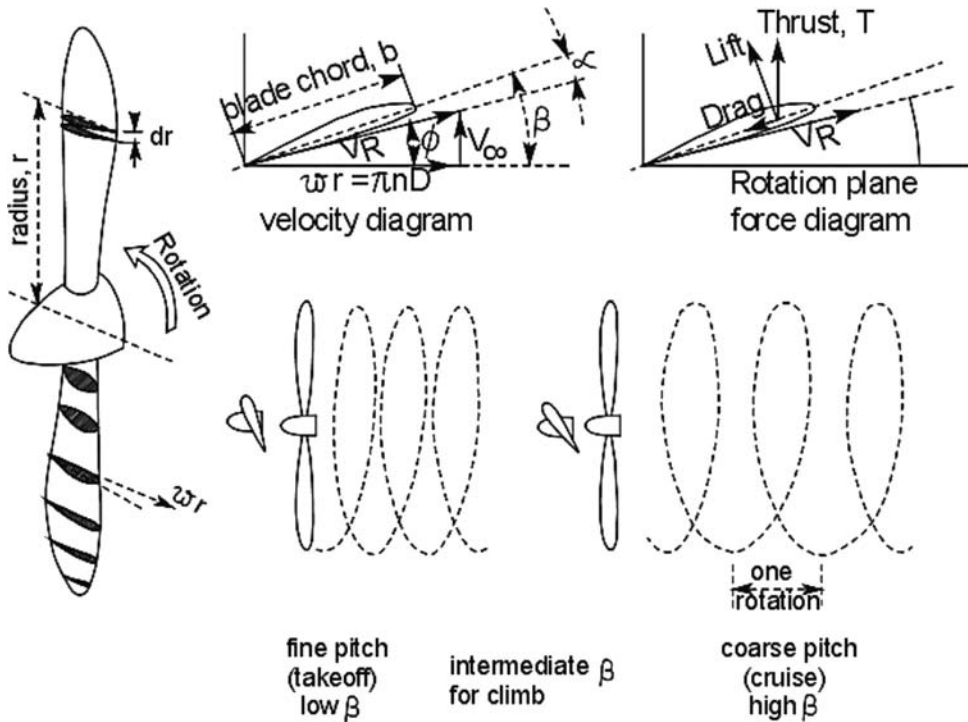


Figure 10.30. Aircraft propeller

for more details. It is recommended that certified propellers manufactured by well-known companies are used.

Propellers are twisted, wing-like blades that rotate in a plane normal to the aircraft (i.e., the flight path). The thrust generated by the propeller is the lift component produced by the propeller blades in the flight direction. It acts as a propulsive force and is not meant to lift weight unless the thrust line is vectored. It has aerofoil sections that vary from being thickest at the root to thinnest at the tip chord (Figure 10.30). In rotation, the tip experiences the highest tangential velocity.

A propeller can have from two blades to as many as seven or eight blades. Smaller aircraft have two or three blades, whereas larger aircraft can have from four to seven or eight blades. Propeller types are shown in Figure 10.31 with associated geometries and symbols used in analysis (see Section 10.10.1). The three important angles are the blade pitch angle, β ; the angle subtended by the relative velocity, φ ; and the angle of attack, $\alpha = (\beta - \varphi)$. Also shown in the figure is the effect of both coarse and fine propeller pitch, p . When a propeller is placed in front of an aircraft, it is called a *tractor* (Figure 10.21a); when it is placed aft, it is called a *pusher* (see Figure 3.47). The majority of propellers are the tractor type.

Blade pitch should match the aircraft speed, V , to keep the blade angle of attack α producing the best lift. To cope with aircraft speed changes, it is beneficial for the blade to rotate (i.e., varying the pitch) about its axis through the hub to maintain a favorable α at all speeds. This is called a *variable-pitch propeller*. For pitch variation, the propeller typically is kept at a constant rpm with the assistance of a *governor*, which is then called a *constant-speed propeller*. Almost all aircraft flying at higher speeds have a constant-speed, variable-pitch propeller (when

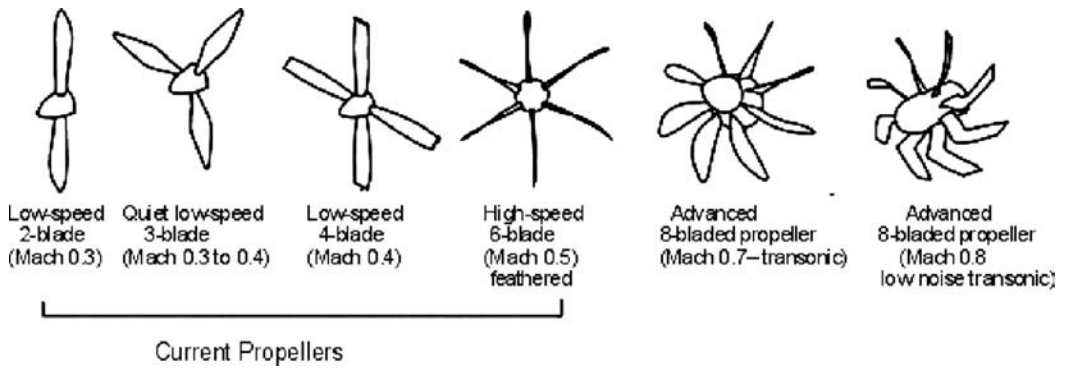


Figure 10.31. Multibladed aircraft propellers

operated manually, it is β -controlled). Smaller, low-speed aircraft have a fixed pitch, which runs best at one combination of aircraft speed and propeller rpm. If the fixed pitch is intended for cruise, then at takeoff (i.e., low aircraft speed and high propeller revolution), the propeller is less efficient. Typically, aircraft designers prefer a fixed-pitch propeller matched to the climb – a condition between cruise and takeoff – to minimize the difference between the two extremes. Obviously, for high-speed performance, the propeller should match the high-speed cruise condition. Figure 10.32 shows the benefits of a constant-speed, variable-pitch propeller over the speed range.

The β -control can extend to the reversing of propeller pitch. A full reverse thrust acts as all the benefits of a TR described in Section 10.9. The pitch can be controlled to a fine pitch to produce zero thrust when an aircraft is static. This could assist an aircraft to the *washout* speed, especially on approach to landing.

When an engine fails (i.e., the system senses insufficient power), the pilot or the automatic sensing device elects to *feather* the propeller (see Figure 10.30). *Feathering* is changing β to 75 to 85 deg (maximum course) when the propeller slows down to zero rpm – producing a net drag and thrust (i.e., part of the propeller has thrust and the remainder has drag) of zero.

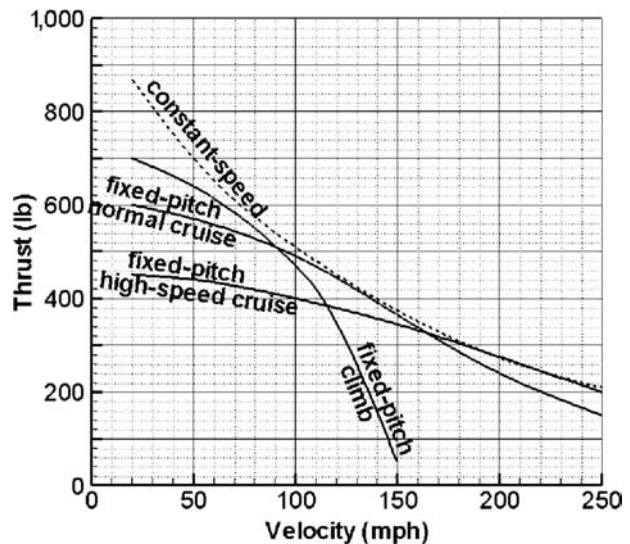


Figure 10.32. Comparison of a fixed-pitch and a constant-speed, variable-pitch propeller

Windmilling of the propeller is when the engine has no power and is free to rotate, driven by the relative air speed of the propeller when the aircraft is in flight. The β angle is in a fine position.

10.10.1 Propeller-Related Definitions

The industry uses propeller charts that incorporate special terminology. The necessary terminology and parameters are defined in this section. Figure 10.30 shows a two-bladed propeller with a blade-element section, dr , at radius r . The propeller has a diameter, D . If ω is the angular velocity, then the blade-element linear velocity at radius r is $\omega r = 2\pi nr = \pi nD$, where n is the number of revolutions per unit time. An aircraft with a true air speed of V and a propeller angular velocity of ω has the blade element moving in a helical path. At any radius, the relative velocity, V_R , has an angle $\varphi = \tan^{-1}(V/2\pi nr)$. At the tip, $\varphi_{tip} = \tan^{-1}(V/\pi nD)$.

D = propeller diameter = $2 \times r$

n = revolutions per second (rps)

ω = angular velocity

N = number of blades

b = propeller-blade width (varies with radius, r)

P = propeller power

C_p = power coefficient (not to be confused with the pressure coefficient) = $P/(\rho n^3 D^5)$

T = propeller thrust

C_{Li} = integrated design lift coefficient (C_{Ld} = sectional lift coefficient)

C_T = propeller thrust coefficient = $T/(\rho n^2 D^4)$

β = blade pitch angle subtended by the blade chord and its rotating plane

p = propeller pitch = no slip distance covered in one rotation = $2\pi r \tan \beta$ (explained previously)

V_R = velocity relative to the blade element = $\sqrt{(V^2 + \omega^2 r^2)}$ (blade Mach number = V_R/a)

φ = angle subtended by the relative velocity = $\tan^{-1}(V/2\pi nr)$ or $\tan \varphi = V/\pi nD$ (This is the pitch angle of the propeller in flight and is not the same as the blade pitch, which is independent of aircraft speed.)

α = angle of attack = $(\beta - \varphi)$

J = advance ratio = $V/(nD) = \pi \tan \varphi$ (a nondimensional quantity – analogues to α)

AF = activity factor = $(10^5/16) \int_0^{1.0} (r/R)^3 (b/D) d(r/R)$

TAF = total activity factor = $N \times AF$ (it indicates the power absorbed)

However, irrespective of aircraft speed, the inclination of the blade angle from the rotating plane can be seen as a solid-body, screw-thread inclination and is known as the *pitch angle*, β . The solid-body, screw-like linear advancement through one rotation is called *pitch*, p . The pitch definition is problematic because unlike mechanical screws, the choice of the inclination plane is not standardized. It can be the zero-lift line (which is aerodynamically convenient) or the chord line (which is easy to locate) or the bottom surface – each plane has a different pitch. All of these planes

are interrelated by fixed angles. This book uses the chord line for the pitch reference line as shown by the pitch angle, β , in Figure 10.30; this gives pitch, $p = 2\pi r \tan\beta$.

Because the blade linear velocity ωr varies with the radius, the pitch angle needs to be varied as well to make the best use of the blade-element aerofoil characteristics. When β is varied such that the pitch is not changed along the radius, then the blade has *constant pitch*. This means that β decreases with increases in r (the variation in β is about 40 deg from root to tip). The blade angle of attack is:

$$\alpha = (\beta - \varphi) = \tan^{-1}(p/2\pi r) - \tan^{-1}(V/2\pi nr) \quad (10.22)$$

This results in an analog nondimensional parameter, $J = \text{advance ratio} = V/(nD) = \pi \tan\varphi$.

10.10.2 Propeller Theory

The fundamentals of propeller performance start with the idealized consideration of momentum theory. Its practical application in the industry is based on the subsequent “blade-element” theory. Both are presented in this section, followed by engineering considerations appropriate to aircraft designers. Industrial practices still use a propeller that is supplied by the manufacturer and wind-tunnel-tested generic charts and tables to evaluate its performance. Of the various forms of propeller charts, two are predominant: the NACA method and the Hamilton Standard (i.e., propeller manufacturer) method. This book prefers the Hamilton Standard method used in the industry ([16]). For designing advanced propellers and propfans to operate at speeds greater than Mach 0.6, CFD is important for arriving at the best compromise, substantiated by wind-tunnel tests. CFD employs more advanced theories (e.g., vortex theory).

Momentum Theory: Actuator Disc

The classical incompressible inviscid momentum theory provides the basis for propeller performance ([21]). In this theory, the propeller is represented by a thin *actuator disc* of area, A , placed normal to the free-stream velocity, V_0 . This captures a stream tube within a CV that has a front surface sufficiently upstream represented by subscript “0” and sufficiently downstream represented by subscript “3” (Figure 10.33). It is assumed that thrust is uniformly distributed over the disc and the tip effects are ignored. Whether or not the disc is rotating is irrelevant because flow through it is taken without any rotation. The station numbers just in front and aft of the disc are designated as 1 and 2.

The impulse given by the disc (i.e., propeller) increases the velocity from the free-stream value of V_0 , smoothly accelerates to V_2 behind the disc, and continues to accelerate to V_3 (i.e., Station 3) until the static pressure equals the ambient pressure, p_0 . The pressure and velocity distribution along the stream tube is shown in Figure 10.33. There is a jump in static pressure across the disc (from p_1 to p_2), but there is no jump in velocity change.

Newton’s law states that the rate of change of momentum is the applied force; in this case, it is the thrust, T . Consider Station 2 of the stream tube immediately behind the disc that produces the thrust. It has a mass flow rate, $\dot{m} = \rho A_{disc} V_2$, and

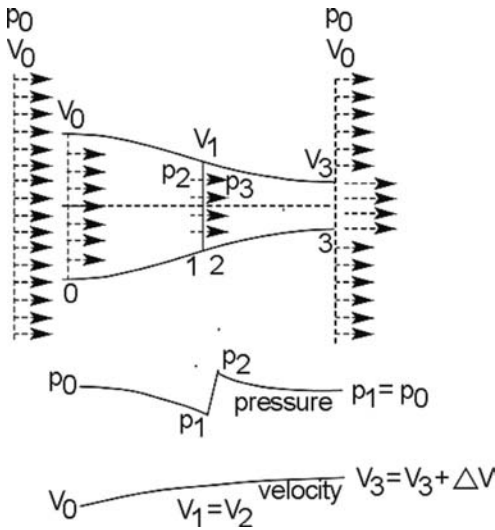


Figure 10.33. Control volume showing the stream tube of the actuator disc

the change of velocity is $\Delta V = (V_3 - V_0)$. This is the reactionary thrust experienced at the disc through the pressure difference multiplied by its area, A .

$$\begin{aligned}
 \text{Thrust produced by the disc } T &= \text{the rate of the change of momentum} = \dot{m} \Delta V \\
 &= \rho A_{disc} \times (V_3 - V_0) \times V_2 \\
 &= \text{pressure across the disc} \times A_{disc} \\
 &= A_{disc} \times (p_2 - p_1)
 \end{aligned} \tag{10.23}$$

Equation 10.23 now can be rewritten as:

$$\rho (V_3 - V_0) \times V_2 = (p_2 - p_1) \tag{10.24}$$

The incompressible flow in Bernoulli's equation cannot be applied through the disc imparting the energy. Instead, two equations are set up: one for conditions ahead of and the other aft of the disc. Ambient pressure, p_0 , is the same everywhere.

Ahead of the disc:

$$p_0 + \frac{1}{2}\rho V_0^2 = p_1 + \frac{1}{2}\rho V_1^2 \tag{10.25}$$

Aft of the disc:

$$p_0 + \frac{1}{2}\rho V_3^2 = p_2 + \frac{1}{2}\rho V_2^2 \tag{10.26}$$

Subtracting the front relation from the aft relation:

$$\frac{1}{2}\rho (V_3^2 - V_0^2) = (p_2 - p_1) \times \frac{1}{2}\rho (V_2^2 - V_1^2) \tag{10.27}$$

Because there is no jump in velocity across the disc, the last term is omitted.

Next, substitute the value of $(p_2 - p_1)$ from Equation 10.24 in Equation 10.25:

$$\begin{aligned}
 \frac{1}{2}(V_3^2 - V_0^2) &= (V_3 - V_0) \times V_2 \\
 \text{or} \quad (V_3 + V_0) &= 2V_2
 \end{aligned} \tag{10.28}$$

Note that $(V_3 - V_0) = \Delta V$, when added to Equation 10.26, gives $2V_3 = 2V_2 + \Delta V$, or:

$$V_3 = V_2 + \Delta V/2, \quad \text{which implies that } V_1 = V_0 + \Delta V/2 \tag{10.29}$$

Using conservation of mass, $A_3V_3 = AV_1$, Equation 10.23 becomes:

$$T = \rho A_{disc} V_1 \times (V_3 - V_0) = A_{disc}(p_2 - p_1)$$

or

$$(p_2 - p_1) = \rho V_1 \times (V_3 - V_0) \quad (10.30)$$

This means that half of the added velocity, $\Delta V/2$, is ahead of the disc and the remainder, $\Delta V/2$, is added aft of the disc.

Using Equations 10.29 and 10.30, thrust Equation 10.23 can be rewritten as:

$$T = A_{disc}\rho V_1 \times (V_3 - V_0) = A_{disc}\rho(V_0 + \Delta V/2) \times \Delta V \quad (10.31)$$

Applying this to an aircraft, V_0 may be seen as the aircraft velocity, V , by dropping the subscript “0”. Then, the useful work rate (power, P) on the aircraft is:

$$P = TV \quad (10.32)$$

For the ideal flow without the tip effects, the mechanical work produced in the system is the power, P_{ideal} , generated to drive the propeller force (thrust, T) times velocity, V_1 , at the disc.

$$P_{ideal} = T(V + \Delta V/2) \text{ (the maximum possible value in an ideal situation)} \quad (10.33)$$

Therefore, ideal efficiency:

$$\eta_i = P/P_{ideal} = (TV)/[T(V + \Delta V/2)] = 1/[1 + (\Delta V/2V)] \quad (10.34)$$

The real effects have viscous, propeller tip effects and other installation effects. In other words, to produce the same thrust, the system must provide more power (for a piston engine, it is seen as the BHP, and for a turboprop, the ESHP), where ESHP is the equivalent SHP that converts the residual thrust at the exhaust nozzle to HP, dividing by an empirical factor of 2.5. The propulsive efficiency as given in Equation 10.4 can be written as:

$$\eta_p = (TV)/[\text{BHP or ESHP}] \quad (10.35)$$

This gives:

$$\begin{aligned} \eta_p/\eta_i &= \{(TV)/[\text{BHP or SHP}]\}/\{1/[1 + (\Delta V/2V)]\} \\ &= \{(TV)[1 + (\Delta V/2V)]/[\text{BHP or SHP}]\} = 85 \text{ to } 86\% \text{ (typically)} \end{aligned} \quad (10.36)$$

Blade-Element Theory

The practical application of propellers is obtained through blade-element theory, as described herein. A propeller-blade cross-sectional profile has the same functions as that of a wing aerofoil – that is, to operate at the best L/D.

Figure 10.30 shows that a blade-element section, dr , at radius r , is valid for any number of blades at any radius, r . Because blades are rotating elements, their properties vary along the radius.

Figure 10.30 is a velocity diagram showing that an aircraft with a flight speed of V with the propeller rotating at n rps makes the blade element advance in a helical manner. V_R is the relative velocity to the blade with an angle of attack α . Here, β is the propeller pitch angle, as defined previously. Strictly speaking, each blade rotates in the wake (i.e., downwash) of the previous blade, but the current treatment ignores this effect and uses propeller charts without appreciable error.

Figure 10.30 is the force diagram of the blade element in terms of lift, L , and drag, D , that is normal and parallel, respectively, to V_R . Then, the thrust, ΔT , and force, ΔF (producing torque), on the blade element can be obtained easily by decomposing lift and drag in the direction of flight and in the plane of the propeller rotation, respectively. Integrating this over the entire blade length (i.e., nondimensionalized as r/R – an advantage applicable to different sizes) gives the thrust, T , and torque-producing force, F , of the blade. The root of the hub (with or without spinner) does not produce thrust, and integration is typically carried out from 0.2 to the tip, 1.0, in terms of r/R . When multiplied by the number of blades, N , this gives the propeller performance.

Therefore, propeller thrust:

$$T = N \times \int_{0.2}^{1.0} \Delta T d(r/R) \quad (10.37)$$

and force that produces torque:

$$F = N \times \int_{0.2}^{1.0} \Delta F d(r/R) \quad (10.38)$$

By definition, advance ratio: $J = V/(nD)$

It has been found that from $0.7r$ (i.e., tapered propeller) to $0.75r$ (i.e., square propeller), the blades provide the aerodynamic average value that can be applied uniformly over the entire radius to obtain the propeller performance.

It also can be shown that the thrust-to-power ratio is best when the blade element works at the highest lift-to-drag ratio (L/D_{max}). It is clear that a fixed-pitch blade works best at a particular aircraft speed for the given power rating (i.e., rpm) – typically, the climb condition is matched for the compromise. For this reason, constant-speed, variable-pitch propellers have better performance over a wider speed range. It is convenient to express thrust and torque in nondimensional form, as follows. From the dimensional analysis (note that the denominator omits the $1/2$):

Nondimensional thrust,

$$T_C = \text{Thrust}/(\rho V^2 D^2)$$

Thrust coefficient,

$$C_T = T_C \times J = \text{Thrust} \times [V/(nD)]^2 / (\rho V^2 D^2) = \text{Thrust}/(\rho n^2 D^4) \quad (10.39)$$

In FPS system:

$$C_T = 0.1518 \times \left[\frac{(T/1,000)}{\sigma \times (N/1,000)^2 \times (D/10)^4} \right] \quad (10.40)$$

where σ = ambient density ratio for altitude performance

Nondimensional force (for torque), $T_F = F/(\rho V^2 D^2)$

Force coefficient:

$$C_F = T_F \times J = F \times [V/(nD)]^2 / (\rho V^2 D^2) = F/(\rho n^2 D^4) \quad (10.41)$$

Therefore, torque:

$$Q = \text{force} \times \text{distance} = Fr = C_F \times (\rho n^2 D^4) \times D/2$$

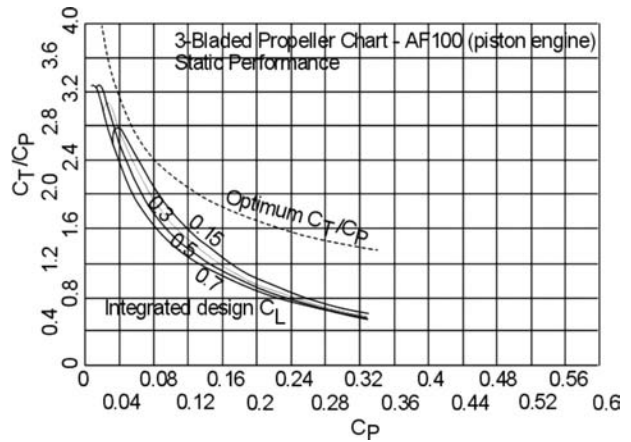


Figure 10.34. Static performance: three bladed propeller performance chart – AF100 (for a piston engine)

or torque coefficient:

$$C_Q = Q/(\rho n^2 D^5) = C_F/2 \tag{10.42}$$

power consumed,

$$P = 2\pi n \times Q$$

power coefficient:

$$C_P = P/(\rho n^3 D^5) = 2\pi C_Q = \pi C_F \tag{10.43}$$

In the FPS system:

$$\begin{aligned} C_P &= 0.5 \times \left[\frac{(\text{BHP}/1,000)}{\sigma \times (N/1,000)^3 \times (D/10)^5} \right] \\ &= \left[\frac{(237.8 \times \text{SHP})}{2,000 \times (6/100)^3 \rho n^3 D^5} \right] = \left[\frac{(550 \times \text{SHP})}{\rho n^3 D^5} \right] \end{aligned} \tag{10.44}$$

The wider the blade, the higher the power absorbed to a point when any further increase would offer diminishing returns in increasing thrust. A nondimensional number, defined as the total activity factor (TAF) = $N \times (10^5/16) \int_0^{1.0} (r/R)^3 (b/D) d(r/R)$, expresses the integrated capacity of the blade element to absorb power. This indicates that an increase in the outward blade width is more effective than at the hub direction.

A piston engine or a gas turbine drives the propeller. Propulsive efficiency η_p can be computed by using Equations 10.35, 10.39, and 10.44.

Propulsive efficiency,

$$\begin{aligned} \eta_p &= (TV)/[\text{BHP or ESHP}] \\ &= [C_T \times (\rho n^2 D^4) \times V]/[C_P \times (\rho n^3 D^5)] \\ &= (C_T/C_P) \times [V/(nD)] = (C_T/C_P) \times J \end{aligned} \tag{10.45}$$

The theory determines that geometrically similar propellers can be represented in a single nondimensional chart (i.e., propeller graph) combining the nondimensional parameters, as shown in Figures 10.34 and 10.35 (for three-bladed propellers) and Figures 10.36 and 10.37 (for four-bladed propellers). Considerable amount of

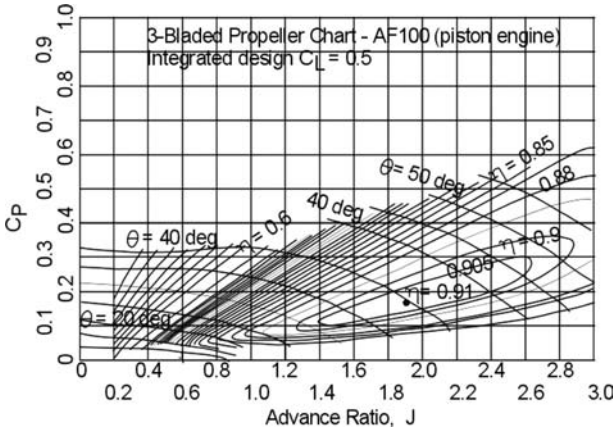


Figure 10.35. Three-bladed propeller performance chart – AF100 (for a piston engine)

coursework can be conducted using these graphs. These graphs and the procedures to estimate propeller performances are from [16], a courtesy of Hamilton Standard. These graphs are replotted retaining maximum fidelity. The reference provides the full range of graphs for other types of propellers and charts for propellers with a higher activity factor (AF).

Static computation is problematic when V is zero; then $\eta_p = 0$. Different sets of graphs are required to obtain the values of (C_T/C_P) to compute the takeoff thrust, as shown in Figures 10.34 and 10.36. Finally, Figure 10.38 is intended for selecting the design C_L for the propeller to avoid compressibility loss. Thrust for takeoff performance can be obtained from the following equations in FPS:

In flight, thrust:

$$T = (550 \times \text{BHP} \times \eta_p) / V, \quad \text{where } V \text{ is in ft/s}$$

$$= (375 \times \text{BHP} \times \eta_p) / V, \quad \text{where } V \text{ is in mph} \tag{10.46}$$

For static performance (takeoff):

$$T_{TO} = [(C_T/C_P) \times (550 \times \text{BHP})] / (nD) \tag{10.47}$$

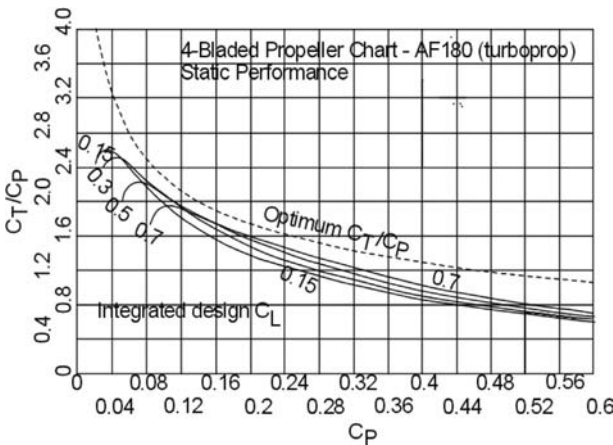
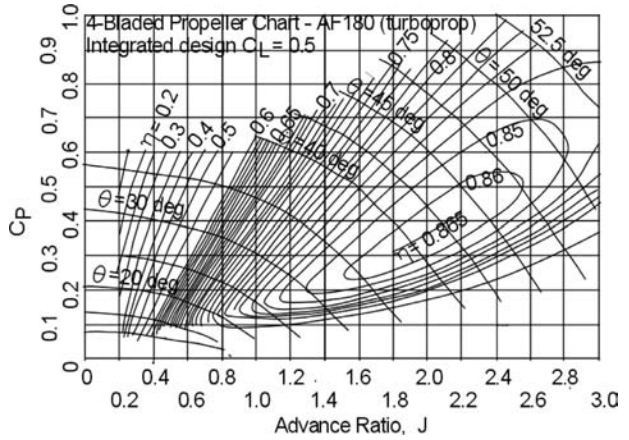


Figure 10.36. Four-bladed propeller performance chart – AF180 (for a high-performance turboprop)

Figure 10.37. Four-bladed propeller-performance chart – AF180 (for a high-performance turboprop)



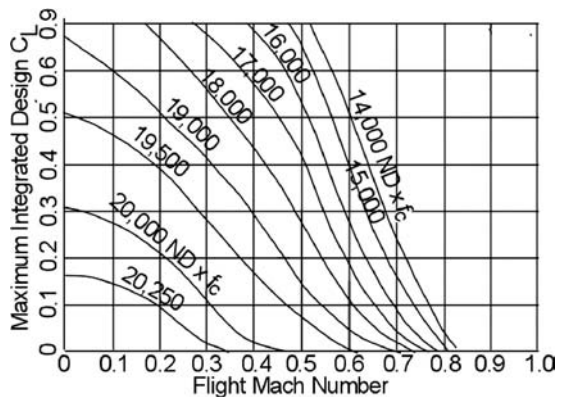
10.10.3 Propeller Performance: Practical Engineering Applications

This book does not discuss propeller design. Aircraft designers select propellers offered by the manufacturer, mostly off-the-shelf types, unless they are specially designed in consultation with aircraft designers, such as the rubberized turboprop. This section describes considerations that are necessary and appropriate to aircraft designers in selecting an appropriate propeller to match the sized engine in order to produce thrust for the full flight envelope.

Readers may note that the propeller charts for the number of blades use only three variables: C_p , β , and η (the subscript p is omitted); they do not specify the propeller diameter and rpm. Therefore, similar propellers with the same AF and C_{Li} can use the same chart. Aircraft designers must choose AF or C_{Li} based on the critical phase of operation. The propeller selection requires compromises because optimized performance for the full flight envelope is not possible, especially for fixed-pitch propellers.

Recently, certification requirements for noise have affected the issues of compromise, especially for high-performance propeller designs. A high-tip Mach number is detrimental to noise; to reduce it η is compromised by reducing the rpm and/or the diameter, thereby increasing J and/or the number of blades. Increasing the number of blades also increases the cost and weight of an aircraft. Propeller curvature is suitable for transonic operation and helps reduce noise.

Figure 10.38. Design C_L to avoid compressibility loss



Equation 10.22 gives the aerodynamic incidence – that is, the blade angle of attack, $\alpha = (\beta - \varphi)$, where φ is determined from the aircraft speed and propeller rpm (i.e., function of $J = V/nD$). It is best to keep α constant along the blade radius to obtain the best C_{Li} (i.e., α is maintained at 6 to 8 deg). The value of $0.7r$ or $0.75r$ is used as the reference point – the propeller charts list the reference radius.

The combination of the designed propeller rpm is matched to its diameter to prevent the operation from experiencing a compressibility effect at the maximum speed and specific altitude. A suitable reduction-gear ratio decreases the engine rpm to the preferred propeller rpm. Figure 10.36 is used to obtain the integrated design C_L for the propeller rpm and diameter combination. The factor $ND \times$ (ratio of speed of sound at standard day, sea level to the altitude) establishes the integrated design C_L . A spinner at the propeller root is recommended to reduce loss.

The following stepwise observations and information are important to progress the propeller-performance estimation by using the charts in Figures 10.34 through 10.38 (in the figure $f_c = a_{alt}/a_{SL}$, where a = speed of sound):

1. Establish the integrated design C_{Li} using Figure 10.38.
2. A typical blade AF is of the following order:
 - Low power absorption, 2- to 3-bladed, propellers for homebuilt flying = $80 < AF < 90$.
 - Medium power absorption, 3- to 4-bladed propellers for piston engines (utility) = $100 < AF < 120$.
 - High power absorption, 4-bladed and more propellers for turboprops = $140 < AF < 200$.
3. Keep the tip Mach number around 0.85 at cruise and ensure that at takeoff, the rpm does not exceed the value at the second segment climb speed.
4. Typically, for a constant-speed, variable-pitch propeller, β is kept low for take-off, gradually increasing at climb speed, reaching an intermediate value at cruise and a high value at the maximum speed. Figure 10.32 shows the benefit of β -control compared to fixed-pitch propellers. Although the figure demonstrates the merit of a constant-speed propeller, its constraints render the governor design and β -control as complex engineering, which requires two modes of operation (not addressed in this book). Design of an automatic blade-control mechanism is specialized engineering.
5. The propeller diameter in inches can be roughly determined by the following empirical relation:

$$D = K(P)^{0.25},$$

where $K = 22$ for a 2-blade propeller, 20 for a 3-blade propeller, and 18 for a 4-blade propeller. Power P is the installed power, which is less than the bare engine rating supplied by the engine manufacturer. Figure 10.39 provides the statistics of a typical relationship between engine power and propeller diameter. It is a useful graph for making empirically the initial size of the propeller. If n and J are known in advance, the propeller diameter can be determined using $D = 1,056V/(NJ)$ in the FPS system.

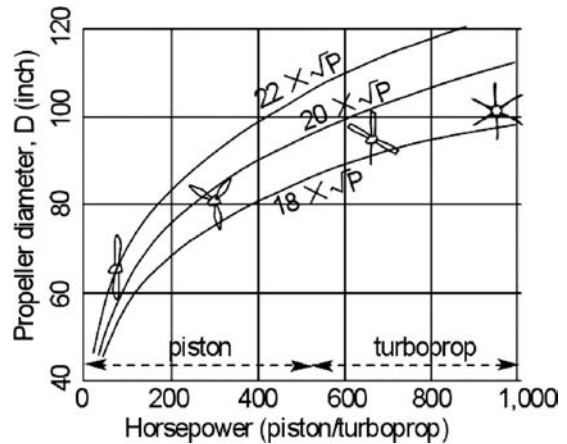


Figure 10.39. Engine power versus propeller diameter

6. Keep at least a 0.5 m (1.6 ft) propeller-tip clearance from the ground; in an extreme demand, this can be reduced slightly. This should prevent the nose-wheel tire from bursting and an oleo collapse.
7. At maximum takeoff static power, the thrust developed by the propellers is about four times the power.

Continue separately (in FPS) with propeller performance for static takeoff and in-flight cruise.

Static Performance (see Figures 10.34 and 10.36)

1. Compute the power coefficient, $C_P = (550 \times \text{SHP}) / (\rho n^3 D^5)$, where n is in rps.
2. From the propeller chart, find C_T / C_P .
3. Compute the static thrust, $T_S = (C_T / C_P)(33,000 \times \text{SHP}) / ND$, where N is in rpm.

In-Flight Performance (see Figures 10.35 and 10.37)

1. Compute the advance ratio, $J = V / (nD)$.
2. Compute the power coefficient, $C_P = (550 \times \text{SHP}) / (\rho n^3 D^5)$, where n is in rps.
3. From the propeller chart, find efficiency, η_P .
4. Compute thrust, T from $\eta_P = (TV) / (550 \times \text{SHP})$, where V is in ft/s.

If necessary, off-the-shelf propeller blade tips could be slightly shortened to meet geometrical constraints. Typical penalties are a 1% reduction of diameter affecting 0.65% reduction in thrust; for small changes, linear interpolation may be made.

10.10.4 Propeller Performance: Blade Numbers $3 \leq N \leq 4$

Using the graphs, a linear extrapolation can be made for two- and five-bladed propellers with a similar AF. Reference [18] discusses the subject in detail with propeller charts for other AF.

10.10.5 Propeller Performance at STD Day: Worked-Out Example

In a stepwise manner, thrust from a propeller is worked out as a coursework exercise. The method uses the Hamilton Standard charts intended for constant-speed propellers. These charts also can be used for fixed-pitch propellers when the pitch of the propeller should match the best performance at a specific speed: either cruise speed or climb speed. Two forms are shown: (1) from the given thrust, compute the HP (in turboprop case SHP) required; and (2) from the given HP (or SHP), compute the thrust. The starting point is the C_p . Typically, at sea-level takeoff rating at static condition, one SHP produces about 4 pounds on STD day. At the first guesstimate, a factor of 4 is used to obtain SHP to compute the C_p . One iteration may prove sufficient to refine the SHP.

Problem description. Consider a single, 4-bladed, turboprop military trainer aircraft of the class RAF Tucano operating with a constant speed propeller at $N = 2,400$ rpm giving installed $T_{SLS} = 4,000$ lbs. The specified aircraft speed is 320 mph at a 20,000-ft altitude (i.e., Mach 0.421). For the aircraft speed, the blade AF is taken as 180. Establish its rated SHP at sea-level static condition and thrusts at various speeds and altitudes. All computations are in STD day.

Case I: Takeoff performance (HP from thrust). This is used to compute the SHP at sea-level takeoff. Guesstimate installed SHP = $4,000/4 = 1,000$ SHP.

From Figure 10.39, for a four-bladed propeller, the diameter is taken to be 96 inches, or 8 ft. Figure 10.38 establishes the integrated design C_{Li} ; the ratio of the speed of sound at STD day sea level to the altitude, $f_c = 1.0$.

The factor $ND \times f_c = 2,400 \times 8 \times 1.0 = 19,200$. Corresponding to aircraft speed of Mach 0 and the factor $ND \times f_c = 19,200$; Figure 10.38 gives the integrated design $C_{Li} \approx 0.5$.

Equation 10.44 gives:

$$C_p = (550 \times SHP) / (\rho n^3 D^5)$$

$$\text{or } C_p = (550 \times 1,000) / (0.00238 \times 40^3 \times 8^5) = 5,50,000 / 49,91,222 = 0.11$$

Figure 10.36 (4-blade, AF = 180, $C_L = 0.5$) gives $C_T/C_P = 2.4$ corresponding to integrated design $C_{Li} = 0.5$ and $C_p = 0.11$.

Therefore, installed static thrust, $T_{SLS} = (C_T/C_P)(33,000 \times SHP)/ND = (2.4 \times 550 \times 1,000)/(40 \times 8) = 1,320,000/320 = 4,125$ lb.

The installed SHP is revised to 970 giving installed thrust $T_{SLS} = 4,000$ lb. It is close enough to avoid any further iteration.

Taking into account a 7% installation loss at takeoff, the uninstalled $T_{SLS} = 4,000/0.93 = 4,300$ lb, giving the uninstalled SHP = 1,043. It may now be summarized that to obtain 4,000 lb installed thrust, the uninstalled rated power is 1,043 SHP.

Aircraft configuration must ensure ground clearance at a collapsed nose-wheel tire and oleo. A higher number of blades (i.e., higher solidity) could reduce the diameter, at the expense of higher cost. For this aircraft class, it is best to retain the largest propeller diameter permissible, keeping the number of blades to four or five.

If ground clearance is required, then a 1.5-inch radius can be cut off from the tip (i.e., a 3% reduction to a 93-inch diameter), which requires slightly higher

Table 10.5. Propeller installed thrust results

	20 mph*	50 mph	80 mph	120 mph	160 mph
$J = 0.00463 \times \text{mph}$	0.092	0.23	0.37	0.55	0.74
C_p	0.11	0.11	0.11	0.11	0.11
Installed SHP	1000	1000	1000	1000	1000
From Figure 10.37, η_{prop}	0.19	0.4	0.56	0.7	0.77
Installed thrust, T lb	3820	3225	2820	2350	1940

* Too low velocity for Figure 10.37. It is close to static condition and agrees.

uninstalled power to $\approx 1,043/0.97 = 1,075$ SHP to obtain 4,000 lb installed thrust corresponding to installed 1,000 SHP.

Check the diameter with the empirical relation, $D = K(P)^{0.25} = 18 \times (1,050)^{0.25} = 102.5$ inch. The empirical relation is close to the cropped 93-inch diameter computed previously. The smaller diameter is retained for better ground clearance.

Case II: Thrust from HP (worked out with 1,000 SHP installed as maximum takeoff rating at sea-level static condition on STD day). Once the installed SHP_{SLS} is known, the thrust for the takeoff rating can be computed. The turboprop fuel control maintains a constant SHP at takeoff rating, keeping it almost invariant. This section computes the thrust available at speeds up to 160 mph to cover liftoff and enter the enroute climb phase. Available thrust is computed at 20, 50, 80, 120, and 160 mph, as shown in Table 10.5.

Compute:

$$J = V/nD = (1.467 \times V)/(40 \times 8) = 0.00458 \times V, \text{ where } V \text{ is in mph}$$

Power coefficient:

$$C_p = (550 \times \text{SHP})/(\rho n^3 D^5) = (550 \times 1,000)/(0.00238 \times 40^3 \times 8^5) = 0.11$$

For an integrated design, $C_{L_i} = 0.5$ and $C_p = 0.11$. The propeller η_{prop} corresponding to J and C_p is obtained from Figure 10.37 (4-blade, $AF = 180$, $C_L = 0.5$), as shown in Table 10.5.

Compute thrust: $T = (550 \eta_{\text{prop}} \times 1,000)/V = 550,000 \times \eta_{\text{prop}}/V$, where V is in mph (see Table 10.5). Use Equation 10.46 for the FPS system.

Figure 10.40 plots thrust versus speed at the takeoff rating (see Section 10.11). In a similar manner, thrust at any speed, altitude, and engine rating can be determined from the relevant graphs (Figures 10.41 through 10.44). Section 13.3.4 works out the installed turboprop thrust.

Refer to Section 10.11.2 to obtain the SHP at various engine ratings. For example, an engine throttles back from the takeoff rating to the maximum climb rating for an enroute climb. Up to about 4,000-ft altitude, it is kept at around 85% of the maximum power and goes down with altitude.

10.11 Engine-Performance Data

This section describes typical engine outputs. The data are presented in nondimensional form. All power plants have prescribed power settings, as discussed herein. Power settings are decided by the engine rpm and/or by the exhaust-pressure ratio

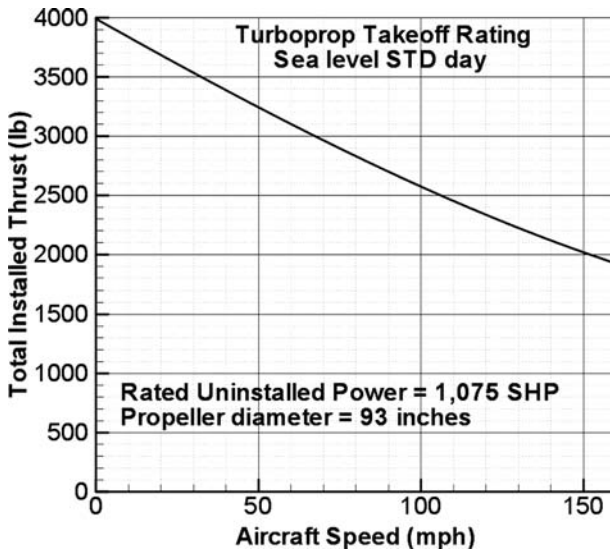


Figure 10.40. Takeoff thrust for a turboprop engine

(EPR) at the jet pipe temperature (JPT), which should remain lower than prescribed levels. An engine is identified at its sea-level STD day at takeoff in static conditions. For turbofans, it is denoted as T_{SLS} . Typical power settings (i.e., ratings) of engines are given in the following subsections.

Takeoff Rating

This is the highest rating that produces the maximum power and is rated at 100% (i.e., at static run of turbofans, it is T_{SLS}). At this rating, the engine runs the hottest and therefore has a time limit to ensure a longer life and less maintenance. For civil-aircraft engines, the limit is about 10 minutes; for military aircraft engines, it could extend somewhat longer. A situation may arise in which one engine is inoperative and the operative engine must supply more power at the augmented power rating (APR). Not all engines have an APR, which exceeds 100% power by $\approx 5\%$ for a short duration (e.g., ≈ 5 minutes).

Maximum Continuous Rating

This is the highest engine rating that can operate continuously at approximately 90 to 95% of the maximum power. It is more than what is required for climbing at a good fuel economy. Operational demand in this rating arises from specific situations – for example, a very fast climb to altitude (mainly in military use). Typically, a climb is accomplished at around 85% power to reduce stress on the engine and to achieve better fuel economy. For this reason, the maximum continuous rating is not included with some engines and rather is merged with the maximum climb rating.

Maximum Climb Rating

The climb schedule is accomplished at approximately 85 to 90% of the maximum power. A typical climbing time for a civil aircraft is less than 30 to 40 minutes, but it can run continuously.

Maximum Cruise Rating

This rating is approximately 80 to 85% of the maximum power matched to the maximum cruise-speed capability. Unless there is a need for higher speed, typical cruise is performed at a 70 to 75% power rating, called the *cruise rating*. This gives the best fuel economy for the LRC. In a holding pattern in an airport vicinity, engines run at still lower power, barely maintaining altitude while waiting for clearance to proceed. The rating depends on the weight of an aircraft; at the end of cruise (lightweight), an approximate 65% rating is sufficient.

Idle Rating

This rating is at approximately 40 to 50% of maximum power and is intended for an engine to run without flameout but also produces practically no thrust. This situation arises at descent, at approach, or on the ground. During a descent, it has been found that better economy can be achieved by descending at partial throttle, at about a 60% power rating. This results in a shallower glide slope to cover more distance and consume less fuel.

Representative engine performances of various types at takeoff, maximum climb, and maximum cruise ratings are given in this section for an ISA day. Engine manufacturers also supply performance data for non-ISA days, which is more critical for hot and high-altitude conditions when engines produce considerably less power. To protect engines from heat stress, a fuel-control system is tuned to cut off power generation to a *flat-rated value* (at an ISA-day engine rating) up to a hot day that can be 20°C above the ISA day. This book does not address non-ISA-day performances; in the industry, they are supplied.

10.11.1 Piston Engine

There are several ways to present piston engine performances. [Figure 10.41](#) shows a Lycoming IO-360 series 180-HP piston engine. Readers may obtain the appropriate engine chart from manufacturers of other engines, or this graph may be scaled for coursework.

Readers should note that the power ratings are given in rpm. A Lycoming IO-360 series takeoff is conducted at a maximum 2,700 rpm, whereas a climb is conducted at 2,500 to 2,600 rpm and cruise at 2,100 to 2,400 rpm. A partial throttle descent can be accomplished at 1,800 to 2,000 rpm. Idle is below 1,800 rpm (i.e., around 1,200 to 1,400 rpm; not shown). A fuel-flow graph is shown separately in [Figure 10.42](#).

Piston engine power depends on the amount of air mass inhaled, which is indicated by the rpm and manifold pressure, $p_{manifold}$, at a particular ambient condition. A throttle valve controls air mass aspiration; when it is closed, there is no power (i.e., $p_{manifold} = 0$). When it is fully open and the engine is running at full aspiration, suction is created and the $p_{manifold}$ reads the highest suction values. If there is less propeller load at the same rpm, less power is generated and the valve could be partially closed to inhale less air mass in order to run at equilibrium. At a low rpm, the aspiration level is low and there is a limiting $p_{manifold}$ line. Therefore, the variables affecting engine power are rpm, $p_{manifold}$, altitude, and atmospheric temperature (nonstandard days). If an engine is supercharged, then the graphs indicate the

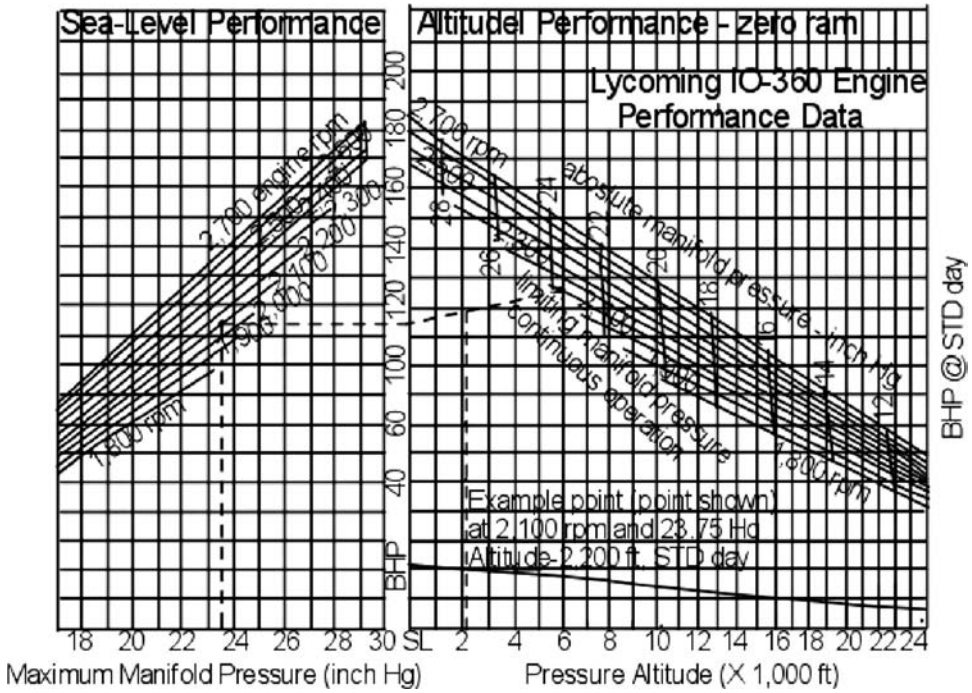


Figure 10.41. Lycoming IO-360 series 180-HP piston engine. (Courtesy of Lycoming Engine – re-traced maintaining high fidelity)

effect. Figure 10.41 shows the parameters in graphical form; how to use the graphs is explained herein.

Figure 10.41 shows two graphs that must be used together. The left-hand graph provides the starting point for reading conditions at sea level, and the ISA day

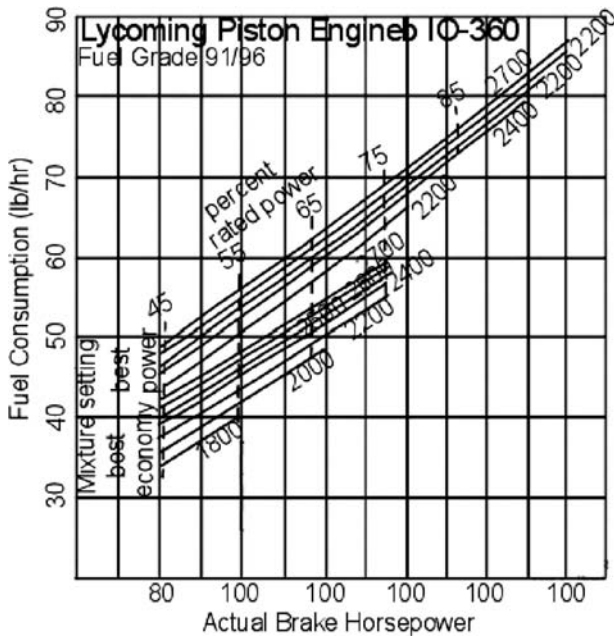


Figure 10.42. Lycoming IO-360 series-fuel flow graph

that must be converted to the operating condition at any altitude and atmospheric temperature are shown in the right-hand graph. The given engine condition must be known to obtain the HP at the ambient condition. In the example, the task is to find the HP that the engine is producing at 2,100 rpm, at a 23.75-inch *Hg* manifold pressure operating at a 2,100-ft altitude with an ambient temperature of 19°F (the ISA day is 511.2 R). The stepwise approach is as follows:

1. In the left-hand graph, locate the point corresponding to 2,100 rpm and at 23.75-inch *Hg* manifold pressure. Next, the HP at the Y-axis is found to be 114.
2. Transfer the 114-HP point to the Y-axis of the right-hand graph. Then, join that point to the point corresponding to 2,100 rpm and at 23.75-inch *Hg* manifold pressure in the same graph.
3. From the 2,100-ft altitude at the X-axis, draw a vertical line to the line drawn in Step 2. This gives 119 HP on a standard day.
5. For a nonstandard day, use the expression $[BHP_{act}/BHP_{std}] = \sqrt{(T_{std}/T_{act})}$.
6. Figure 10.42 provides information about fuel flow and has two settings – one for best power and one for best economy – which are adjusted by a mixture-ratio lever. For higher power and rpm, the mixture setting is at best power; for cruise, it is at best economy. It is evident that 2,100 rpm results in best economy. For the worked-out example, it is 50 lbs per hour at a power rating of approximately 68%.

10.11.2 Turboprop Engine (Up to 100 Passengers Class)

Engine performance characteristics vary from type to type. It is cautioned that real engine data are not easy to obtain. The graphs in this section are generic in nature, representing typical current turboprop engines in the class. The graphs include the small amount of jet thrust available at a 70% rating and higher. The jet power is converted to SHP and the total ESHP is labeled only “SHP” in the graph. Therefore, in the absence of industry data, readers can continue working with these graphs. In industry, engine manufacturers supply performance data incorporating exact installation losses for accurate computation.

The sizing exercise provides the required thrust at the specified aircraft-performance requirements. Using the propeller performance given in Section 10.10.5, the SHP at the sea-level static condition can be worked. From this information, engine performance at other ratings can be established for the full flight envelope. Takeoff rating maintains constant power but the thrust changes with speed. Figures 10.43 and 10.44 give the typical turboprop thrust and fuel flow (in terms of *psfc*) at maximum climb and maximum cruise ratings in a nondimensional form.

Typically, the higher the SHP, the lesser is the specific SHP (SHP/\dot{m}_a -SHP/lb/s). There is a similar trend for the specific dry-engine weight ($SHP_{SLS}/\text{dry engine weight-lb/lb}$). Table 10.6 may be used for these computations.

Takeoff Rating

Section 10.10.5 worked out for Tucano class trainer aircraft the uninstalled $SHP_{SLS} = 1,075$ to obtain 4,000 lb installed thrust. Once the SHP at sea-level static condition is established from the sizing exercise, the thrust requirement of an installed four-bladed propeller can be computed.

Table 10.6. *Turboprop-specific horsepower for sizes*

	SHP/ \dot{m}_a –SHP/lb/s	SHP _{SLs} /dry engine weight–SHP/lb
Smaller turboprops ≤ 1,000 SHP	≈ 0.012 (at TO)	≈ 2.2 to 2.75*
Larger turboprops > 1,000 SHP	≈ 0.010 (at TO)	≈ 2.5 to 3.00*

Notes:

- * Lower factor for lower SHP.
- SHP = shaft horsepower
- TO = takeoff

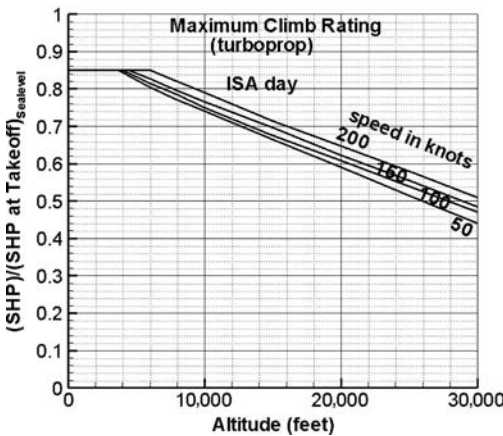
The psfc of turboprops at takeoff is from 0.475 to 0.6 lb/hr/shp. For an SHP of less than 1,000, use a psfc of 0.6 lb/hr/shp; for more than 1,000, use a psfc of approximately 0.48 lb/hr/shp.

Therefore, fuel flow at SHP_{SLs} is $0.5 \times 1,075 = 537.5$ lb/hr. From Table 10.6, the intake airmass flow at SHP_{SLs} is $0.011 \times 1,075 = 11.83$ lb/s. The dry-engine weight = $1,075/2.75 = 390$ lb.

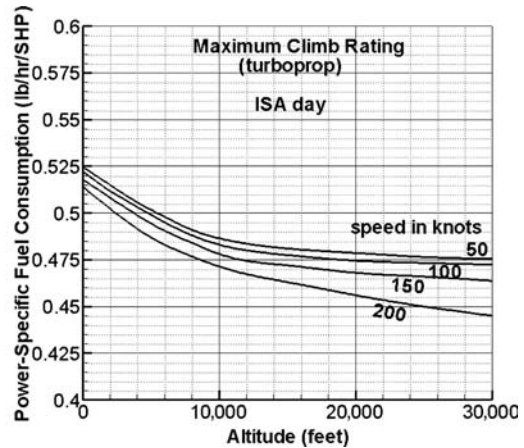
Maximum Climb Rating

Figure 10.43 shows the maximum climb SHP and fuel flow (sfc) in nondimensional form for the standard day up to a 30,000-ft altitude for four true air speeds from 50 to 200 kts. Intermediate values may be linearly interpolated. The break in SHP generation up to a 6,000-ft altitude is due to fuel control to keep the EGT low.

Equation 11.15 (see Chapter 11; the turboprop case is not worked out) requires a factor k_2 (varies with speed and altitude) to be applied to the SHP. From Figure 10.43a, a value of 0.85 may be used to obtain the initial climb SHP. Initial climb is at an 800-ft altitude. In the example, the uninstalled initial climb power is then $0.85 \times 1,075 = 914$ SHP. The integrated propeller performance after deducting the installation losses gives the available thrust. Typically, the initial climb starts at a constant EAS of approximately 200 kts, which is approximately Mach 0.3. At a constant EAS climb, the Mach number increases with altitude; when it reaches 0.4, it



(a) Shaft Horsepower



(b) Specific Fuel Consumption

Figure 10.43. Uninstalled maximum climb rating (turboprop)

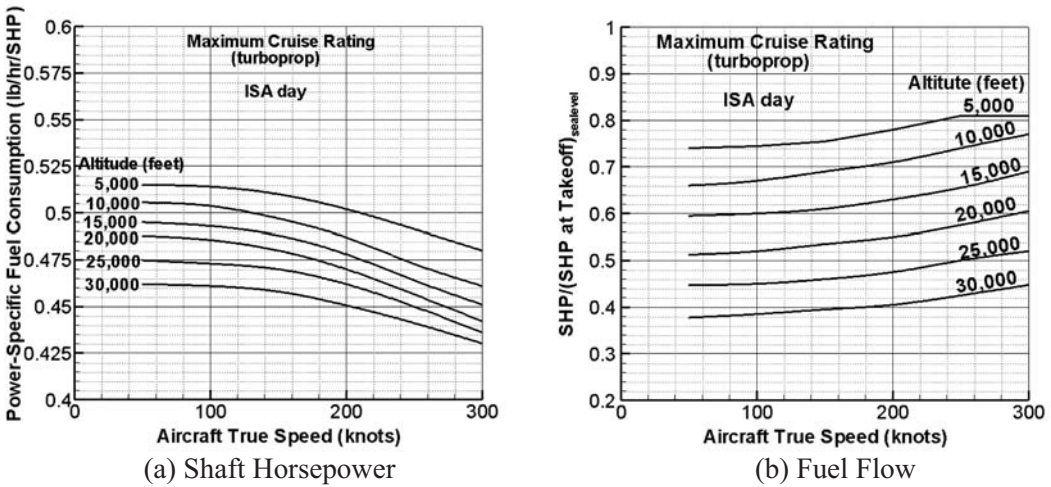


Figure 10.44. Uninstalled maximum cruise rating (turboprop)

is held constant. Fuel flow at the initial climb is obtained from Figure 10.43b. The example gives $0.522 \times 914 = 477$ lb/hr. With varying values of altitude, climb calculations are performed in small increments of altitude, within which the variation is taken as the mean and is kept constant for the increment.

Maximum Cruise Rating

Figure 10.44 shows the maximum cruise SHP and fuel flow in nondimensional form for the standard day from a 5,000- to 30,000-ft altitude for true air speed from 50 to 300 kts. Intermediate values may be linearly interpolated. The graph takes into account the factor k_1 (varies with speed and altitude) as indicated in Section 11.3.3, Equation 11.19.

In the example, the design initial maximum cruise speed is given as 300 kts at a 25,000-ft altitude. From Figure 10.44a, the uninstalled power available is $0.525 \times 1,075 = 564$ SHP. In Figure 10.44b, the corresponding fuel flow is $0.436 \times 564 = 246$ lb/hr. The integrated propeller performance after deducting the installation losses gives the available installed propeller performance.

10.11.3 Turbofan Engine: Civil Aircraft

All thrusts discussed in this section are uninstalled thrust. There is loss of power when an engine is installed in an aircraft, as discussed in Section 10.10, from 7 to 10% at the takeoff rating depending on how the ECS is managed. At cruise, the loss decreases to 3 to 5%. For simplicity, both military and civil aircraft installation losses are kept at a similar percentage, although the off-take demands are significantly different.

Figures 10.45 through 10.51 show the turbofan power at the three ratings in a nondimensional form for civil aircraft engines with low and high BPRs. Civil-aircraft turbofan performance is also divided into two categories: one for a lower BPR on the order of 4 and the other at 5 and above. The most recent engines (i.e., engines for the newer Boeing787, Airbus350, and Bombardier Cseries) have

Table 10.7. *Turbofan parameters, BPR, and specific thrust*

BPR	F/\dot{m}_a – lb/s/lb	T_{SLS} /dry engine weight
Around 4	35 to 40	0.21 to 0.23
Around 5	32 to 34	0.18 to 0.20
Around 6	30 to 32	0.16 to 0.18

reached a BPR of 8 to 12; however, the author could not obtain realistic data for this class of turbofans.

The higher the BPR, the less is the specific thrust (T_{SLS}/\dot{m}_a , lb/lb/s). There is a similar trend for the specific dry-engine weight (T_{SLS} /dry-engine weight, nondimensional). Table 10.7 may be used for the computations.

Turbofans with a BPR Around 4 (Smaller Engines; e.g., Bizjets)

Turbofan performance. An engine-matching and aircraft-sizing exercise that gives the T_{SLS} is conducted in Chapter 11. Chapters 11 and 13 work out the installed thrust and fuel flow for the matched engines of the sized aircraft under study.

Takeoff Rating. Figure 10.45 shows the takeoff thrust in nondimensional form for the standard day for turbofans with a BPR of 4 or less. The fuel-flow rate remains nearly invariant for the envelope shown in the graph. Therefore, the sfc at the takeoff rating is the value at the T_{SLS} of 0.498 lb/lb/hr per engine.

Maximum Climb Rating. Figure 10.46 gives the maximum climb thrust and fuel flow in nondimensional form for the standard day up to a 50,000-ft altitude for three Mach numbers. Intermediate values may be linearly interpolated. There is a break in thrust generation at an approximate 6,000- to 10,000-ft altitude, depending on the Mach number, due to fuel control to keep the EGT low.

Equation 11.14 (see Chapter 11) requires a factor k_2 to be applied to the T_{SLS} to obtain the initial climb thrust. In the example, the initial climb starts at an 800-ft altitude at 250 V_{EAS} (Mach 0.38), which gives $T/T_{SLS} = 0.67$ – that is, the factor $k_2 = T_{SLS}/T = 1.5$. At a constant EAS, the Mach number increases with altitude; in

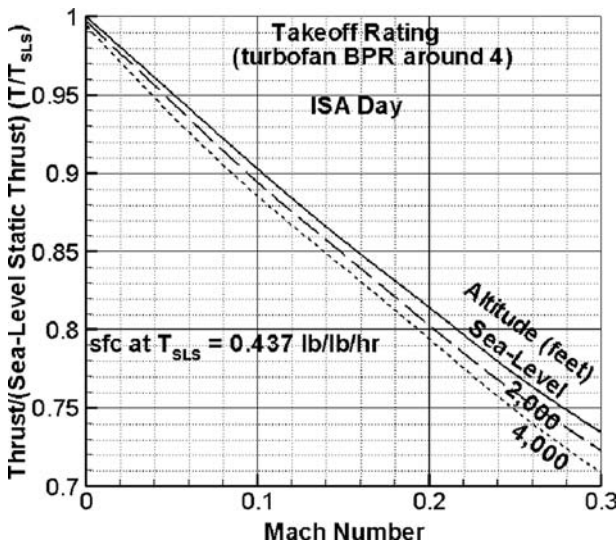
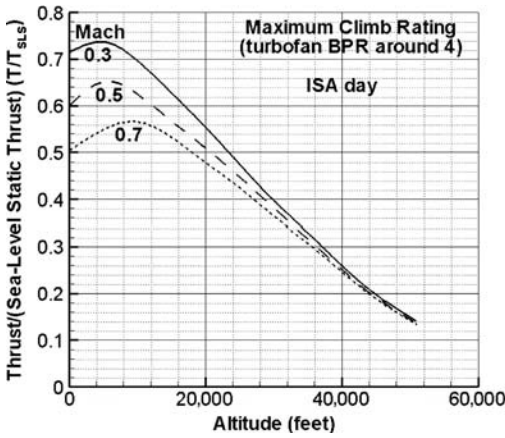
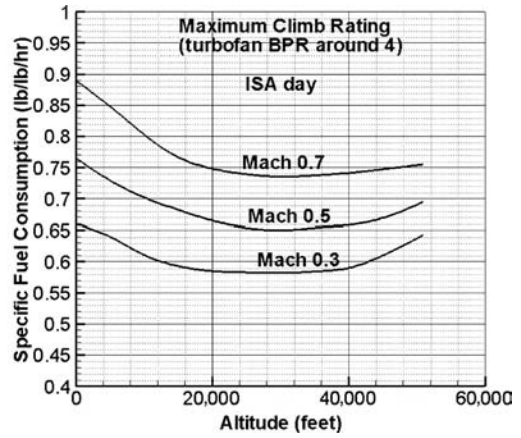


Figure 10.45. Uninstalled takeoff performance (\approx BPR 4)



(a) Nondimensional Thrust



(b) Specific Fuel Consumption

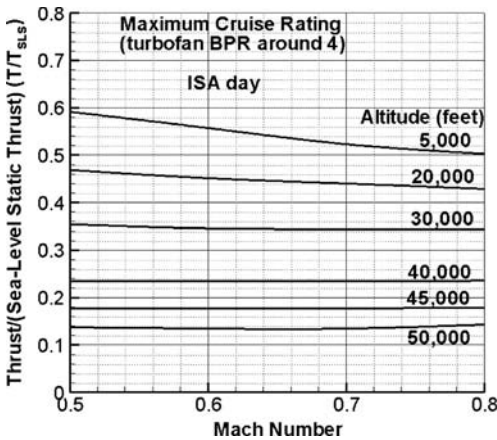
Figure 10.46. Uninstalled maximum climb rating ($\approx <BPR 4$)

the example, when it reaches 0.7 (depending on the aircraft type), the Mach number is held constant. Fuel flow at the initial climb is obtained from Figure 10.46b.

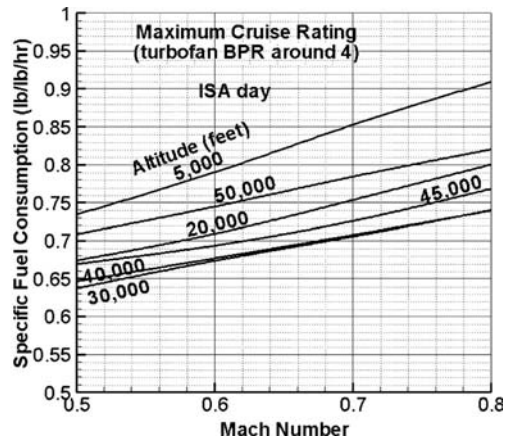
With varying values of altitude, climb calculations are performed in small increments of altitude within which the variation is taken as the mean and is kept constant for the increment.

Maximum Cruise Rating. Figure 10.47 shows the maximum cruise thrust and fuel flow in nondimensional form for the standard day from a 5,000- to 50,000-ft altitude for Mach numbers varying from 0.5 to 0.8, which is sufficient for this class of engine–aircraft combinations. Intermediate values may be linearly interpolated.

The coursework example of the design initial maximum cruise speed is Mach 0.7 at 41,000 ft. From the graph, that point is $T/T_{SLs} = 0.222$, which has $T_{SLs}/T = 4.5$ (i.e., k_2 in Chapter 11). Chapter 11 verifies whether the thrust is adequate for attaining the maximum cruise speed. Fuel flow per engine can be computed from Figure 10.47b.



(a) Nondimensional Thrust



(b) Specific Fuel Consumption

Figure 10.47. Uninstalled maximum cruise rating ($\approx <BPR 4$)

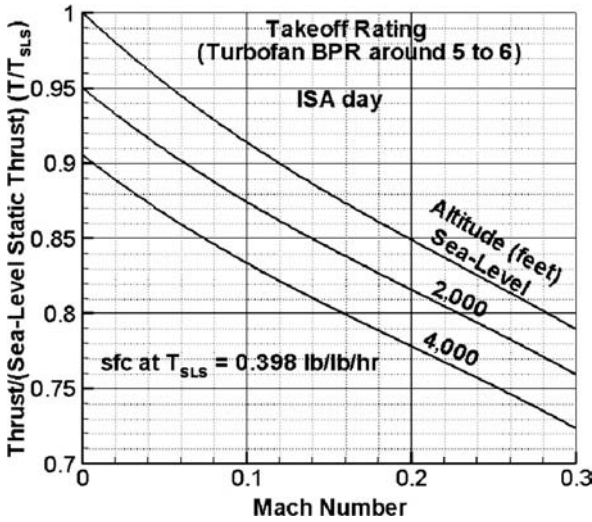
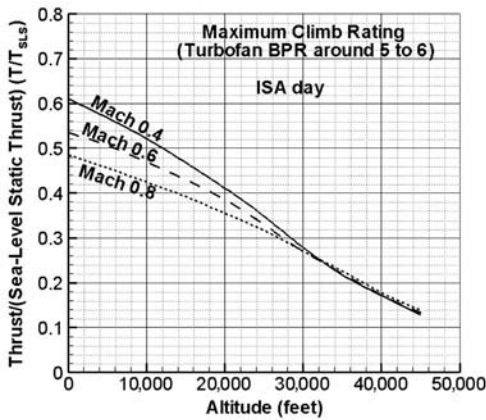
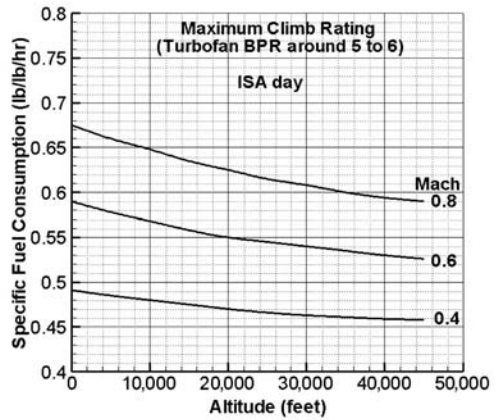


Figure 10.48. Uninstalled takeoff performance (\approx >BPR 5)

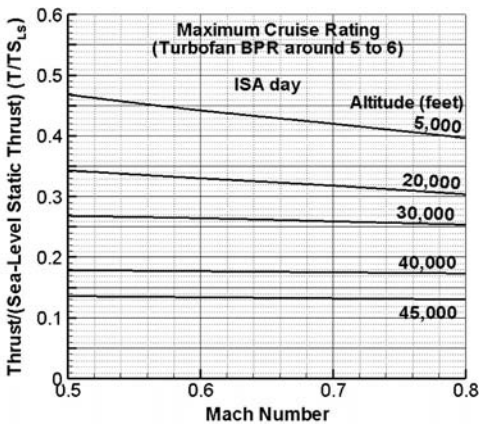


(a) Nondimensional Thrust

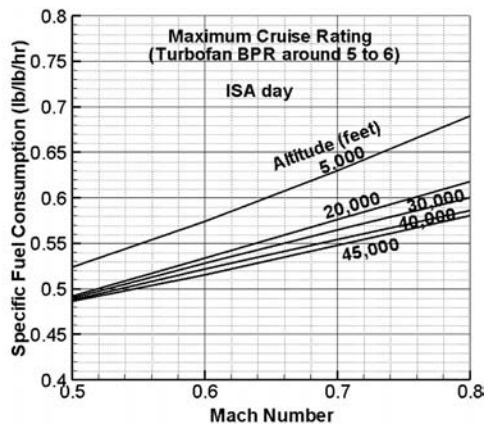


(b) Specific Fuel Consumption

Figure 10.49. Uninstalled maximum climb rating (\approx >BPR 5)



(a) Nondimensional Thrust



(b) Specific Fuel Consumption

Figure 10.50. Uninstalled maximum cruise rating (\approx >BPR 5)

Table 10.8. *Civil aircraft engine data: standard day*

Model	Takeoff						Cruise		
	Thrust lb	Fan dia (inches)	BPR	OPR	Airflow lb/s	Altitude 1,000 ft	Mach	Thrust lb	TSFC lb/lb/hr
CF6-50-C2	52,500	134.1	4.31	30.4	1,476	35	0.80	11,555	0.630
CF6-80-C2	52,500	86.4	4.31	27.4	1,450	35	0.80	12,000	0.576
GE90-B4	87,400	134	8.40	39.3	3,037	35	0.80	17,500	–
JT8D-15A	15,500	49.2	1.04	16.6	327	30	0.80	4,920	0.779
JT9D-59A	53,000	97	4.90	24.5	1,639	35	0.85	11,950	0.666
PW2040	41,700	84.8	6.00	27.6	1,210	35	0.85	6,500	0.582
PW4052	52,000	97	5.00	27.5	1,700	–	–	–	–
PW4084	87,500	118.5	6.41	34.4	2,550	35	0.83	–	–
CFM56-3	23,500	60	5.00	22.6	655	35	0.85	4,890	0.667
CFM56-5C	31,200	72.3	6.60	31.5	1,027	35	0.80	6,600	0.545
RB211-524B	50,000	85.8	4.50	28.4	1,513	35	0.85	11,000	0.643
RB211-535E	40,100	73.9	4.30	25.8	1,151	35	0.80	8,495	0.607
RB211-882	84,700	–	6.01	39.0	2,640	35	0.83	16,200	0.557
V2528-D5	28,000	63.3	4.70	30.5	825	35	0.80	5,773	0.574
ALF502R	6,970	41.7	5.70	12.2	–	35	0.70	2,250	0.720
TFE731-20	3,500	28.2	3.34	14.4	140	40	0.80	986	0.771
PW300	4,750	38.2	4.50	23.0	180	40	0.80	1,113	0.675
FJ44	1,900	20.9	3.24	12.8	63.3	30	0.70	600	0.750
Olympus593	38,000	–	–	11.30	410	53	2.00	10,030	1.150

Turbofans with a BPR around 5 or 7 (Larger Engines; e.g., RJs and Larger)

Turbofan performance. Larger engines have a higher BPR. The currently operational larger turbofans are at a 5 to 7 BPR, which has nondimensional engine performance characteristics slightly different than smaller engines, as shown by comparing Figures 10.48 through 10.50.

The engine-matching and aircraft-sizing exercise in Chapter 11 gives the T_{SLS} . Estimation of fuel flow is shown in the graph. Coursework follows the same routine as given herein.

Takeoff Rating. Figure 10.48 shows the takeoff thrust in nondimensional form for the standard day. The fuel flow rate remains nearly invariant for the envelope shown in the graph.

Table 10.9. *Military aircraft engine sea-level static data at takeoff – standard day*

Model	BPR	Weight lb	OPR	Airflow lb/s	Without afterburner		With afterburner	
					Thrust-lb	TSFC lb/lb/hr	Thrust-lb	TSFC lb/lb/hr
P&W F119	0.45	3,526	35.0	–	23,600	–	35,400	–
P&W F100	0.36	3,740	32.0	254.5	17,800	0.74	29,090	1.94
GE F110	0.77	3,950	30.7	270.0	17,020	–	29,000	–
GE F404	0.27	2,320	26.0	146.0	12,000	0.84	17,760	1.74
GE F414	0.40	2,645	30.0	170.0	12,600	–	22,000	–
Snecma-M88	0.30	1,980	24.0	143.0	11,240	0.78	16,900	1.8

Table 10.10. *Turboprop data – standard day model*

	SHP _{SLS}	Dry weight lb
RR-250-B17	450	195
PT6-A	850	328
TPE-331-12	1,100	400
GE-CT7	1,940	805
AE2100D	4,590	1,548

Maximum Climb Rating. Figure 10.49 shows the maximum climb thrust and fuel flow in nondimensional form for the standard day up to a 50,000-ft altitude for three Mach numbers. Intermediate values may be linearly interpolated.

Maximum Cruise Rating. Figure 10.50 shows the maximum cruise thrust and fuel flow in nondimensional form for the standard day from a 5,000- to 50,000-ft altitude for Mach numbers varying from 0.5 to 0.8, which is sufficient for this class of engine–aircraft combinations. Intermediate values may be linearly interpolated.

10.11.4 Turbofan Engine – Military Aircraft

This extended section of the book can be found on the Web at www.cambridge.org/Kundu and presents a typical military turbofan-engine performance in nondimensional form (with and without reheat) at maximum rating suited to the classroom example of an AJT and a derivative in a *CAS* role. Figure 10.51 gives the thrust ratios from sea level to 36,000 ft altitude in an ISA day. *Sfc* is worked out.

Figure 10.51. Military turbofan engine with and without reheat (BPR = 0.75)

11 Aircraft Sizing, Engine Matching, and Variant Derivative

11.1 Overview

Chapter 6 proposes a methodology with worked-out examples to conceive a “first-cut” (i.e., preliminary) aircraft configuration, derived primarily from statistical information except for the fuselage, which is deterministic. A designer’s past experience is vital in making the preliminary configuration. Weight estimation is conducted in Chapter 8 for the proposed first-cut aircraft configuration, revising the MTOM taken from statistics. Chapter 9 establishes the aircraft drag (i.e., drag polar), and Chapter 10 develops engine performance. From these building blocks, finally, the aircraft size can be fine-tuned to a “satisfactory” (see Section 4.1) configuration offering a family of variant designs. None may be the optimum but together they offer the best fit to satisfy many customers (i.e., operators) and to encompass a wide range of payload-range requirements, resulting in increased sales and profitability.

The two classic important sizing parameters – wing-loading (W/S) and thrust-loading (T_{SLS}/W) are instrumental in the methodology for aircraft sizing and engine matching. This chapter presents a formal methodology to obtain the sized W/S and T_{SLS}/W for a baseline aircraft. These two loadings alone provide sufficient information to conceive of aircraft configuration in a preferred size. Empennage size is governed by wing size and location on the fuselage. This study is possibly the most important aspect in the development of an aircraft, finalizing the external geometry for management review in order to obtain a go-ahead decision for the project.

Because the preliminary configuration is based on past experience and statistics, an iterative procedure ensues to fine-tune the aircraft for the correct size of the wing reference area for a family of variant aircraft designs and matched engines selected after discussion with engine manufacturers. Reference [1] provides an excellent presentation on the subject.

11.1.1 What Is to Be Learned?

This chapter covers the following topics:

- Section 11.2: Introduction to the concept of aircraft sizing and engine matching
- Section 11.3: Theoretical considerations

- Section 11.4: Coursework exercises for civil aircraft
- Section 11.5: Coursework exercises for military aircraft
- Section 11.6: Sizing analysis and variant designs of civil aircraft
- Section 11.7: Sizing analysis and variant designs of military aircraft
- Section 11.8: Sensitivity analysis
- Section 11.9: Future growth potential

11.1.2 Coursework Content

This chapter is important for continuing the coursework linearly. Readers compute the parameters that establish the criteria for aircraft sizing and engine matching. The final size is unlikely to be identical to the preliminary configuration; the use of spreadsheets facilitates the iterations.

11.2 Introduction

In a systematic manner, the conception of a new aircraft progresses from generating market specifications followed by the preliminary candidate configurations that rely on statistical data of past designs in order to arrive at a baseline design. In this chapter, the baseline design of an aircraft is formally sized with a matched engine (or engines) along with the family of variants to finalize the configuration (i.e., external geometry). An example from each class of civil (i.e., Bizjet) and military (i.e., AJT) aircraft is used to substantiate the methodology.

As of the circa 2000 fuel prices, the aircraft cost contributes to the DOC three to four times the contribution made by the fuel cost. (Fuel price fluctuates considerably. Of late, fuel price has shot up, making its contribution to DOC substantially higher. In this book, circa 2000 price level is maintained. That level of price held for a long time and large number of literature use this approximate value.) It is not cost-effective for aircraft manufacturers to offer custom-made new designs to each operator with varying payload-range requirements. As discussed previously, aircraft manufacturers offer aircraft in a family of variant designs. This approach maintains maximum component commonality within the family to reduce development costs and is reflected in aircraft unit-cost savings. In turn, it eases the amortization of non-recurring development costs, particularly as sales increase. It is therefore important for the aircraft-sizing exercise to ensure that the variant designs are least penalized to maintain commonality of components. This is what the introductory comments in Section 4.1 referred to in producing satisfying robust designs; these are not necessarily the optimum designs.

Multidisciplinary optimization is not easily amenable to this type of industrial use; it is currently explored more as research work. The industry uses a more simplistic parametric search for satisfying robust designs.

To generate a family of variant civil aircraft designs, the tendency is to retain the wing and empennage almost unchanged while plugging and unplugging the constant fuselage to cope with varying payload capacities (see Figure 11.4). Typically, the baseline aircraft remains as the middle design. The smaller aircraft results in a wing that is larger than necessary, providing better field performances (i.e., takeoff and landing); however, cruise performance is slightly penalized. Conversely, larger aircraft have smaller wings that improve the cruise performance; the shortfall in

takeoff is overcome by providing a higher thrust-to-weight ratio (T_{SLS}/W) and possibly with better high-lift devices, both of which incur additional costs. The baseline-aircraft approach speed, V_{app} , initially is kept low enough so that the growth of V_{app} for the larger aircraft is kept within the specifications. Of late, high investment with advanced composite wing-manufacturing method is in a position to produce separate wing sizes for each variant (large aircraft), offering improved economics in the long run. However, for some time to come, metal wing construction will continue with minimum change in wing size to maximize component commonality.

Matched engines are also in a family to meet the variation of thrust (or power) requirements for the aircraft variants (see Chapter 10). The sized engines are bought-out items supplied by engine manufacturers. Aircraft designers stay in constant communication with engine designers in order to arrive at the type of family of engines required. A variation of up to $\pm 30\%$ from the baseline engine is typically sufficient for larger and smaller aircraft variants from the baseline. Engine designers can produce scalable variants from a proven core gas-generator module of the engine – these scalable projected engines are known loosely as rubberized engines. The thrust variation of a rubberized engine does not affect the external dimensions of an engine (typically, the bare engine length and diameter change only around $\pm 2\%$). This book uses an unchanged nacelle external dimension for the family variants, although there is some difference in weight for the different engine thrusts. The generic methodology presented in this chapter is the basis for the sizing and matching practice.

11.3 Theory

The parameters required for aircraft sizing and engine matching derive from market studies that reflect user requirements. In general, both civil and military aircraft use similar specification parameters, as discussed herein, as the basic input for aircraft sizing. All performance requirements in this chapter are at ISA day and all field performances are at sea level. The parameters are as follows:

1. Payload and range (fuel load): These determine the MTOW. This is not a sizing exercise but needs to be substantiated (see Chapter 13).
2. Takeoff field length (TOFL): This determines the engine-power ratings and wing size.
3. Landing field length (LFL): This determines wing size (balked landing included).
4. Initial maximum cruise speed and altitude capabilities determine wing and engine sizes.
5. Initial rate of climb establishes wing and engine sizes.

These five requirements must be satisfied simultaneously. The governing parameters to satisfy TOFL, initial climb, initial cruise, and landing are wing-loading (W/S) and thrust-loading (T_{SLS}/W).

Additional parameters for military aircraft sizing are as follows:

- turn performance g -load
- maneuver g -load
- roll rate g -load

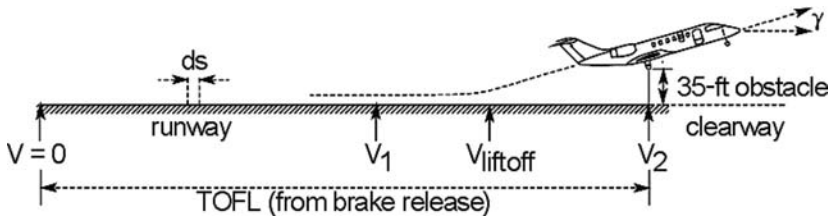


Figure 11.1. Sizing for takeoff

These three parameters are primarily dependent on control-surface sizing (as well as engine sizing, to an extent), which is not addressed in this book. It is assumed that engine size for fast initial climb rates are sufficient and that enough control surface is available to perform the g requirements. A lower aspect ratio for the wing is considered for higher roll rates to reduce the wing-root bending moments.

As mentioned previously, an aircraft must simultaneously satisfy the takeoff field length, initial climb rate, initial maximum cruise speed–altitude capabilities, and LFL. Low wing-loading (i.e., a larger wing area) is required to sustain low speed at liftoff and touchdown (for a pilot's ease), whereas high wing-loading (i.e., a low wing area) is suitable at cruise because high speeds generate the required lift on a smaller wing area. The large wing area for takeoff and landing results in excess wing for high-speed cruise. To obtain the minimum wing area and satisfy all requirements, a compromise for sizing of the wing area must be found; this may require suitable high-lift devices to keep the wing area smaller. The wing area is sized in conjunction with a matched engine for takeoff, climb, cruise, and landing; landing is performed at the idle-engine rating.

In general, W/S varies with time as fuel is consumed and T/W is throttle-dependent. Therefore, a reference design condition of the MTOW and T_{SLS} at ISA + SL are used for sizing considerations. This means that the MTOW, T_{SLS} , and S_W are the only parameters considered for aircraft sizing and engine matching. In general, wing-size variations are associated with changes in all other affecting parameters (e.g., AR , λ , and wing sweep). However, at this stage, they are kept invariant – that is, the variation in wing size only scales the wing span and chord, leaving the general planform unaffected (like zoom in/zoom out).

At this point in the discussion, readers require knowledge of aircraft performance, and the important derivations of the equations used are provided in [Chapter 13](#). References [2] through [6] are textbook sources for the detailed derivation of the performance equations. Other proven semi-empirical relations are in [4]. Although the methodology described herein is the same, the industry practice is more detailed and involved in order to maintain a high degree of accuracy.

Worked-out examples continue with the Learjet 45 Bizjet class for civil aircraft and the BAe Hawk class for military aircraft. Throughout this chapter, *wing-loading* (W/S) in the SI system is in N/m^2 to align with the thrust (in Newtons) in *thrust loading* (T_{SLS}/W) as a nondimensional parameter.

11.3.1 Sizing for Takeoff Field Length

TOFL is the field length (i.e., runway plus clearway; [Figure 11.1](#)) required to clear a 35-ft (10-m) obstacle in the clearway while maintaining a specified minimum climb

gradient, γ , with one engine inoperative and flaps and undercarriage extended. The FAR requirement for a two-engine aircraft minimum climb gradient is 1.2 (see Table 13.3 for aircraft with more than two engines).

For sizing, field-length calculations are at the sea-level standard day (no wind) and at a zero airfield gradient of paved runway. For further simplification, drag changes are ignored during the transition phase of liftoff to clear the obstacle (flaring after liftoff takes less than 3 s); in other words, the equations applied to $V_{lift-off}$ are extended to $V_2 = 1.2V_{stall}$. This gives $V_2^2 = [2 \times 1.44 \times (W/S)]/(\rho C_{Lstall})$. An aircraft stalls at C_{Lmax} . Chapter 13 addresses takeoff performance in detail.

A simplified expression for all engines is:

$$\text{TOFL} = \int dS = \int V dt = \int V(dV/dV)dt = \int_0^{V_2} (V/a)dV \quad (11.1)$$

where $dV/dt = a$ and V and a are instantaneous velocity and acceleration of the aircraft on the ground encountering friction (coefficient $\mu = 0.025$ for a paved, metalled runway). Average acceleration, \bar{a} , is taken at $0.7V_2$. By replacing V_2 in terms of C_{Lstall} , Equation 11.1 reduces to:

$$\text{TOFL} = (1/\bar{a}) \int_0^{V_2} V dV = (V_2^2/2\bar{a}) = \frac{1.44W/S}{\rho C_{Lstall}\bar{a}} \quad (11.2)$$

In terms of wing-loading, Equation 11.2 can be written as:

$$(W/S) = (\text{TOFL} \times \rho \times \bar{a} \times C_{Lstall})/1.44 \quad (11.3)$$

where average acceleration, $\bar{a} = F/m$ and applied force $F = (T - D) - \mu(W - L)$.

Until liftoff is achieved, $W > L$ and F is the average value at $0.7V_2$. Therefore:

$$\bar{a} = [(T - D) - \mu(W - L)]g/W = g(T/W)[1 - D/T - \mu W/T + \mu L/T] \quad (11.4)$$

Substituting Equation 11.3, it becomes:

$$(W/S) = (\text{TOFL} \times \rho \times [g(T/W)(1 - D/T - \mu W/T + \mu L/T)] \times C_{Lstall})/1.44 \quad (11.5)$$

In the FPS system, it can be written as $\rho = 0.00238$ slugs and $g = 32.2$ ft/s². Therefore:

$$(W/S) = (\text{TOFL} \times (T/W)(1 - D/T - \mu W/T + \mu L/T)] \times C_{Lstall})/18.85 \quad (11.6a)$$

In the SI system, it becomes $\rho = 1.225$ kg/m³ and $g = 9.81$ m/s². Therefore,

$$(W/S) = 8.345 \times (\text{TOFL} \times (T/W)(1 - D/T - \mu W/T + \mu L/T)] \times C_{Lstall} \quad (11.6b)$$

where W/S is in Newton/m² to remain in alignment with the units of thrust in Newtons.

Checking of the second-segment climb gradient occurs after aircraft drag estimation, which is explained in Sections 13.5.1 and 13.5.3. If it falls short, then the T_{SLS} must be increased. In general, TOFL requirements are not generous; therefore, satisfying the TOFL is also likely to satisfy the second-segment climb gradient.

Civil Aircraft Design: Takeoff

The contribution of the last three terms ($-D/T - \mu W/T + \mu L/T$) in Equation 11.4 is minimal and can be omitted at this stage for the sizing calculation. In addition, for the one-engine inoperative condition after the decision speed (V_1 ; see Section 13.4), the acceleration slows down, making the TOFL longer than the all-engines-operative case. Therefore, in the sizing computations to produce the specified TOFL, further simplification is possible by applying a semi-empirical correction factor primarily to compensate for loss of an engine. The correction factors are as follows (see [4]); all sizing calculations are performed at the MTOW and with T_{SLS} :

For two engines, use a factor of 0.5 (loss of thrust by a half). Then, Equation 11.6 in the FPS system reduces to:

$$(W/S) = (\text{TOFL} \times (T/W) \times C_{Lstall})/3.75 \quad (11.7a)$$

For the SI system:

$$(W/S) = 4.173 \times \text{TOFL} \times (T/W) \times C_{Lstall} \quad (11.7b)$$

For three engines, use a factor of 0.66 (loss of thrust by a third). Then, Equation 11.6 in the FPS system reduces to:

$$(W/S) = (\text{TOFL} \times (T/W) \times C_{Lstall})/28.5 \quad (11.8a)$$

For the SI system:

$$(W/S) = 5.5 \times \text{TOFL} \times (T/W) \times C_{Lstall} \quad (11.8b)$$

For four engines, use a factor of 0.75 (loss of thrust by a fourth). Then, Equation 11.6 in the FPS system reduces to:

$$(W/S) = (\text{TOFL} \times (T/W) \times C_{Lstall})/25.1 \quad (11.9a)$$

For the SI system:

$$(W/S) = 6.25 \times \text{TOFL} \times (T/W) \times C_{Lstall} \quad (11.9b)$$

Military Aircraft Design: Takeoff

Because military aircraft mostly have a single engine, there is no requirement for one engine being inoperative; ejection is the best solution if the aircraft cannot be landed safely. Therefore, Equation 11.6 can be directly applied (for a multiengine design, the one-engine inoperative case generally uses measures similar to the civil-aircraft case).

In the FPS system, this can be written as:

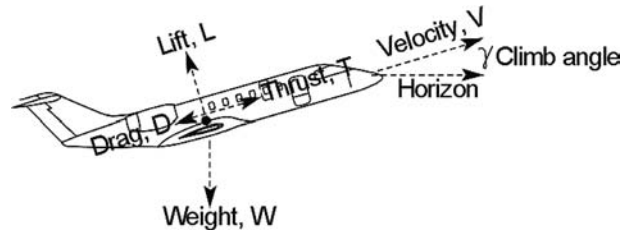
$$(W/S) = (\text{TOFL} \times (T/W)(1 - D/T - \mu W/T + \mu L/T)] \times C_{Lstall}/18.85 \quad (11.10a)$$

In the SI system, it becomes:

$$(W/S) = 8.345 \times (\text{TOFL} \times (T/W)(1 - D/T - \mu W/T + \mu L/T)] \times C_{Lstall} \quad (11.10b)$$

Military aircraft have a thrust, T_{SLS}/W , that is substantially higher than civil aircraft, which makes $(D/T - \mu W/T + \mu L/T)$ even smaller. Therefore, for a single-engine

Figure 11.2. Aircraft climb trajectory



aircraft, no correction is needed and the simplified equations are as follows:

In the FPS system, this can be written as:

$$(W/S) = [\text{TOFL} \times (T/W) \times C_{L\text{stall}}]/18.85 \quad (11.11a)$$

In the SI system, this becomes:

$$(W/S) = 8.345 \times (\text{TOFL} \times (T/W) \times C_{L\text{stall}}) \quad (11.11b)$$

11.3.2 Sizing for the Initial Rate of Climb

The initial rate of climb is a user specification and not a FAR requirement. In general, the FAR requirement for the one-engine inoperative, second-segment climb gradient provides sufficient margin to give a satisfactory all-engine initial climb rate. However, from the operational perspective, higher rates of climb are in demand when it is sized accordingly. Military aircraft (some with a single engine) requirements stipulate faster climb rates and sizing for the initial climb rate is important. The methodology for aircraft sized to the initial climb rate is described in this section. Figure 11.2 shows a typical climb trajectory.

For a steady-state climb, the expression for rate of climb, $RC = V \times \sin \gamma$. Steady-state force equilibrium gives $T = D + W \times \sin \gamma$ or $\sin \gamma = (T - D)/W$. This gives:

$$RC = [(T - D) \times V]/W = (T/W - D/W) \times V \quad (11.12)$$

Equation 11.12 is written as:

$$\begin{aligned} T/W &= RC/V + (D/W) \\ \text{or } T/W &= RC/V + [(C_D \times 0.5 \times \rho \times V^2 \times S_W)/W] \end{aligned} \quad (11.13)$$

Equation 11.13 is based on a climb-thrust rating that is lower than the T_{SLS} ; it must be written in terms of T_{SLS} . The T_{SLS}/T ratio (factor k_2 ; see Section 10.11.3 and Figure 10.46) varies depending on the engine BPR.

$$[T_{SLS}/W]/k_2 = RC/V + [(C_D \times 0.5 \times \rho \times V^2)S_W/W] \quad (11.14)$$

$$[T_{SLS}/W] = k_2 \times RC/V + k_2 \times [(C_D \times 0.5 \times \rho \times V^2)S_W/W] \quad (11.15)$$

The drag polar is now required to compute the relationships given in Equation 11.15.

11.3.3 Sizing to Meet Initial Cruise

There are no FAR or MILSPECS regulations to meet the initial cruise speed; initial cruise capability is a user requirement. Therefore, both civil and military aircraft sizing for initial cruise use the same equations. At a steady-state level flight, thrust required (airplane drag, D) = thrust available (T_a); that is:

$$D = T_a = 0.5\rho V^2 C_D \times S_W \quad (11.16)$$

Dividing both sides of the equation by the initial cruise weight, $W_{incr} = k \times \text{MTOW}$ due to fuel burned to climb to the initial cruise altitude. The factor k lies between 0.95 and 0.98, depending on the operating altitude for the class of aircraft, and it can be fine-tuned through iteration – in the coursework exercise, one round of iterations is sufficient. The factor cancels out in the following equation but is required later. Henceforth, in this part of cruise sizing, W represents the MTOW, in line with the takeoff sizing:

$$0.5\rho V^2 C_D \times S_W / W = T_a / W \quad (11.17)$$

The drag polar is now required to compute the relationships given in Equation 11.17. Use the C_D value to correspond to the initial cruise C_L (because they are nondimensional, both the FPS and SI systems provide the same values). Initial cruise:

$$C_L = k \times \text{MTOW} / (0.5 \times \rho \times V^2 \times S_W) \quad (11.18)$$

The thrust-to-weight ratio sizing for initial cruise capability is expressed in terms of T_{SLS} . Equation 11.18 is based on the maximum-cruise thrust rating, which is lower than the T_{SLS} . Equation 11.18 must be written in terms of T_{SLS} . The T_{SLS}/T_a ratio (factor k_I ; see Section 10.11.3 and Figure 10.47) varies depending on the engine BPR. The factor k_I is computed from the engine data supplied. Then, Equation 11.18 can be rewritten as:

$$T_{SLS}/W = k_I \times 0.5\rho V^2 \times C_D / (W/S_W) \quad (11.19)$$

Variation in wing size affects aircraft weight and drag. The question now is: How does the C_D change with changes in W and S_W ? (T_a changes do not affect the drag because it is assumed that the physical size of an engine is not affected by small changes in thrust.) The solution method is to work with the wing only – first by scaling the wing for each case and then by estimating the changes in weight and drag and iterating – which is an involved process.

This book simplifies the method by using the same drag polar for all wing-loadings (W/S) with little loss of accuracy. As the wing size is scaled up or down (the AR invariant), it changes the parasite drag. The induced drag changes as the aircraft weight increases or decreases. However, to obtain the C_D value, the drag is divided by a larger wing, which keeps the C_D change minimal.

11.3.4 Sizing for Landing Distance

The most critical case is when an aircraft must land at its maximum landing weight of 0.95 MTOW. In an emergency, an aircraft lands at the same airport for an aborted takeoff, assuming a 5% weight loss due to fuel burn in order to make the return

Table 11.1. *Bizjet takeoff sizing*

Computing and listing in tabular form:					
W/S (FPS – lb/ft ²)	40	50	60	70	80
W/S (SI – N/m ²)	1,915.9	2,395.6	2,874.3	3,353.7	3,832.77
T/W (nondimensional)	0.180	0.225	0.270	0.315	0.360

circuit. Pilots prefer to approach as slow as possible for ease of handling at landing. For this class of aircraft, the approach velocity, V_{app} (FAR requirement at $1.3 V_{stall}$) is less than 125 kts to ensure that it is not constrained by the minimum control speed, V_c . Wing C_{Lstall} is at the landing flap and slat setting.

For sizing purposes, an engine is set to the idle rating to produce zero thrust.

At approach:

$$V_{stall} = \sqrt{[(0.95W/S_W)/(0.5 \times \rho \times C_{Lstall})]} \quad (11.20)$$

At landing:

$$V_{app} = 1.3 V_{stall}$$

Therefore:

$$\begin{aligned} V_{app} &= 1.3 \times \sqrt{[(0.95W/S_W)/(0.5 \times \rho \times C_{Lstall})]} \\ &= 1.793 \times \sqrt{[(W/S_W)/(\rho \times C_{Lstall})]} \end{aligned} \quad (11.21)$$

$$\text{or } (V_{app})^2 \times C_{Lstall} = 3.211 \times (W/S_W)/\rho$$

$$\text{or } (W/S_W) = 0.311 \times \rho \times (V_{app})^2 \times C_{Lstall} \quad (11.22)$$

11.4 Coursework Exercises: Civil Aircraft Design (Bizjet)

Both the FPS and the SI units are worked out in the examples. Sizing calculations require the generic engine data in order to obtain the factors used (see Section 10.11.3). The Bizjet drag polar is provided in Figure 9.2.

11.4.1 Takeoff

Requirements: TOFL 4,400 ft (1,341 m) to clear a 35-ft height at ISA + sea level. The maximum lift coefficient at takeoff (i.e., flaps down, to 20 deg, and no slat) is $C_{Lstall(TO)} = 1.9$ (obtained from testing and CFD analysis). The result is computed in Table 11.1. Using Equation 11.7a, the expression reduces to:

$$W/S = 4,400 \times 1.9 \times (T/W)/37.5 = 222.9 \times (T/W)$$

Using Equation 11.7b, it becomes:

$$W/S = 4.173 \times 1,341 \times 1.9 \times (T/W) = 10,633.55 \times (T/W)$$

The industry must also examine other takeoff requirements (e.g., an unprepared runway) and hot and high ambient conditions.

Table 11.2. *Bizjet climb sizing*

Computing and listing in tabular form (use Figure 9.1 for the drag polar):					
W/S (lb/ft ²)	40	50	60	70	80
W/S (N/m ²)	1,915.9	2,395.6	2,874.3	3,353.7	3,832.77
C_{Lclimb}	0.190	0.236	0.283	0.331	0.378
C_D (from drag polar)	0.0240	0.0246	0.0256	0.0266	0.0282
T_{SLS}/W	0.340	0.310	0.286	0.272	0.265

11.4.2 Initial Climb

From the market requirements, an initial climb starts at an 800-ft altitude at a speed $V_{EAS} = 250$ knots (Mach 0.38) = $250 \times 1.68781 = 422$ ft/s (128.6 m/s) and the required rate of climb, $RC = 2,600$ ft/min (792.5 m/min) = 43.33 ft/s (13.2 m/s). From the TFE731 class engine data, T_{SLS}/T ratio = 1.5 (factor k_2 from Section 10.11.3, Figure 10.46). The undercarriage and high-lift devices are in a retracted position. Lift coefficient:

$$C_{Lclimb} = W / (0.5 \times 0.002378 \times 422^2 S_W) = 0.004723 \times W / S_W$$

Using Equation 11.14:

$$[T_{SLS}/W] / 1.5 = 43.33 / 422 + (C_D \times 0.5 \times 0.00232 \times 422^2 S_W) / W$$

$$T_{SLS}/W = 0.154 + 310 \times C_D \times (S_W/W)$$

11.4.3 Cruise

Requirements: Initial cruise speed must meet the high-speed cruise (HSC) at Mach 0.74 and at 41,000 ft (flying higher than bigger jets in less congested traffic corridors) using $k = 0.972$ in Equation 11.14.

In FPS at 41,000 ft:

$$\rho = 0.00056 \text{ slug/ft}^3 \quad \text{and} \quad V^2 = (0.74 \times 968.076)^2 = 716.38^2 = 513,195 \text{ ft}^2/\text{s}^2$$

In SI at 12,192 m:

$$\rho = 0.289 \text{ kg/m}^3 \quad \text{and} \quad V^2 = (0.74 \times 295.07)^2 = 218.35^2 \times 47,677.5 \text{ m}^2/\text{s}^2$$

Equation 11.18 gives the initial cruise:

$$\begin{aligned} C_L &= 0.972 \text{ MTOW} / (0.5 \times 0.289 \times 47,677.5 \times S_W) \\ &= 0.0001414 (W/S_W) \end{aligned}$$

where W/S_W is in N/m².

Equation 11.19 gives:

$$T_{SLS}/W = k_1 \times 0.5 \rho V^2 \times C_D / (W/S_W)$$

(Use factor $k_1 = T_{SLS}/T_a = 4.5$ from Figure 10.47.)

In FPS:

$$T_{SLS}/W = 4.5 \times 0.5 \times 0.00056 \times 459,208.2 \times C_D / (W/S_W) = 565.73 \times C_D / (W/S_W)$$

Table 11.3. *Bizjet cruise sizing*

Computing and listing in tabular form (use Figure 9.1 for the drag polar):					
W/S (lb/ft ²)	40	50	60	70	80
W/S (N/m ²)	1,915.9	2,395.6	2,874.3	3,353.7	3,832.77
C_L (from Equation 10.14)	0.2710	0.3390	0.4064	0.4740	0.5420
C_D (from drag polar)	0.0255	0.0269	0.0295	0.033	0.0368
T_{SLS}/W at 41,000 feet	0.360	0.305	0.278	0.267	0.260

In SI:

$$T_{SLS}/W = 4.5 \times 0.5 \times 0.289 \times 42,662.5 \times C_D/(W/S_W) = 27,741.3 \times C_D/(W/S_W)$$

11.4.4 Landing

From the market requirements, $V_{app} = 120$ knots = $120 \times 1.68781 = 202.5$ ft/s (61.72 m/s). Landing $C_{Lmax} = 2.1$ at a 40-deg flap setting (from testing and CFD analysis). For sizing purposes, the engine is set to the idle rating, producing zero thrust using Equation 11.22.

In the FPS system, $W/S_W = 0.311 \times 0.002378 \times 2.1 \times (202.5)^2 = 63.8$ lb/ft². In the SI system, $W/S_W = 0.311 \times 1.225 \times 2.1 \times (61.72)^2 = 3,052$ N/m². Because the thrust is zero (i.e., idle rating) at landing, the W/S_W remains constant.

Performance. Chapter 13 verifies whether the design meets the aircraft performance specifications.

11.5 Coursework Exercises: Military Aircraft Design (AJT)

This extended section of the book on coursework exercises – military aircraft design (AJT) is found on the Web at www.cambridge.org/Kundu and includes the following subsections.

11.5.1 Takeoff – Military Aircraft

Table 11.4. *AJT takeoff sizing*

11.5.2 Initial Climb – Military Aircraft

Table 11.5. *AJT climb sizing*

11.5.3 Cruise – Military Aircraft

Table 11.6. *AJT cruise sizing*

11.5.4 Landing – Military Aircraft

11.6 Sizing Analysis: Civil Aircraft (Bizjet)

The four sizing relationships (Sections 11.3.1 through 11.3.4) for wing-loading, W/S_W , and thrust-loading, $T_{SLS_INSTALLED}/W$, meet (1) takeoff, (2) approach speed

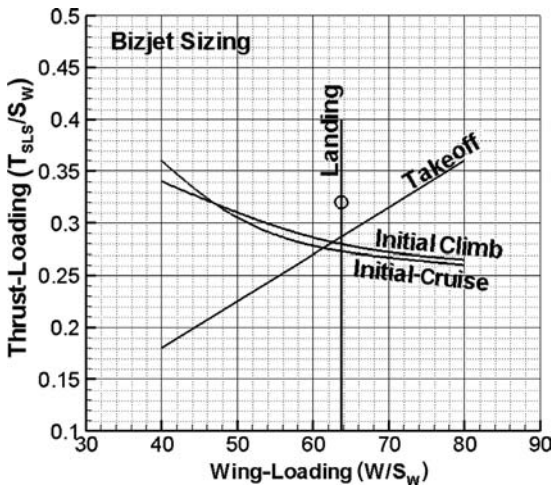


Figure 11.3. Aircraft sizing: civil aircraft

for landing, (3) initial cruise speed, and (4) initial climb rate. These are plotted in Figure 11.3.

The circled point in Figure 11.3 is the most suitable for satisfying all four requirements simultaneously. To ensure performance, there is a tendency to use a slightly higher thrust-loading $T_{SLS_INSTALLED}/W$; in this case, the choice becomes $T_{SLS_INSTALLED}/W = 0.32$ at a wing-loading of $W/S_W = 63.75 \text{ lb/ft}^2$ ($2,885 \text{ N/m}^2$).

Now is the time for the iterations for the preliminary configuration generated in Chapter 6 from statistics, in which only the fuselage was deterministic. At 20,720 lb (9,400 kg) MTOM, the wing planform area is 325 ft², close to the original area of 323 ft²; hence, no iteration is required. Otherwise, it is necessary to revisit the empennage sizing and revise the weight estimates. The $T_{SLS_INSTALLED}$ per engine then becomes $0.32 \times 20,720/2 = 3,315$ lbs. At a 7% installation loss at takeoff, this gives uninstalled $T_{SLS} = 3,315/0.93 = 3,560$ lb/engine ($T_{SLS}/W = 3,560 \times 2/20,720 = 0.344$). This is very close to the TFE731–20 class of engine; therefore, the engine size and weight remain the same. For this reason, iteration is avoided; otherwise, it must be carried out to fine-tune the mass estimation.

The entire sizing exercise could have been conducted well in advance, even before a configuration was settled – if the chief designer’s past experience could “guesstimate” a close drag polar and mass. Statistical data of past designs are useful in guesstimating aircraft close to an existing design. Mass fractions as provided in Section 8.8 offer a rapid mass estimation method. Generating a drag polar requires some experience with extraction from statistical data.

In the industry, more considerations are addressed at this stage – for example, what type of variant design in the basic size can satisfy at least one larger and one smaller capacity (i.e., payload) size. Each design may have to be further varied for more refined variant designs.

11.6.1 Variants in the Family of Aircraft Design

The family concept of aircraft design is discussed in previous chapters and highlighted again at the beginning of this chapter. Maintaining large component commonality (genes) in a family is a definite way to reduce design and manufacturing costs – in other words, “design one and get two or more almost free.” This

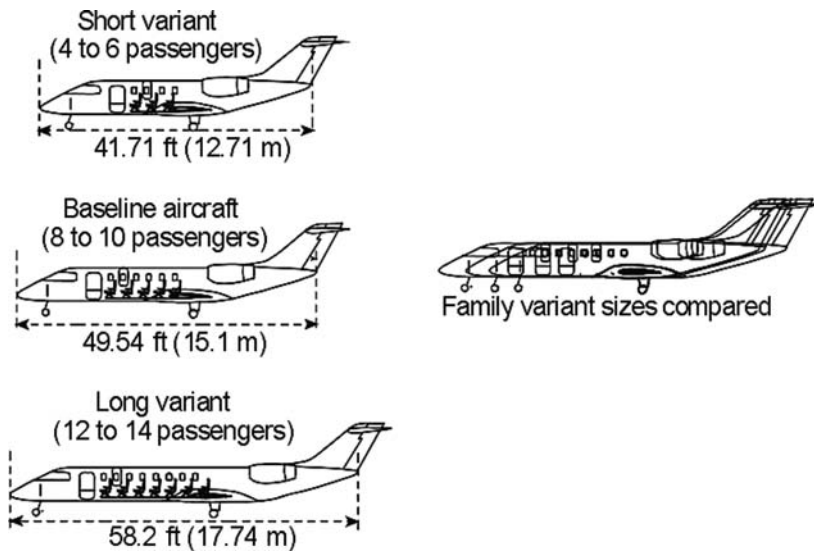


Figure 11.4 Variant designs in the family of civil aircraft

encompasses a much larger market area and, hence, increased sales to generate resources for the manufacturer and nation. The amortization is distributed over larger numbers, thereby reducing aircraft costs.

Today, all manufacturers produce a family of derivative variants. The Airbus 320 series has 4 variants and more than 3,000 have been sold. The Boeing 737 family has 6 variants, offered for nearly 4 decades, and nearly 6,000 have been sold. It is obvious that in three decades, aircraft manufacturers have continuously updated later designs with newer technologies. The latest version of the Boeing 737–900 has vastly improved technology compared to the late 1960s 737–100 model. The latest design has a different wing; the resources generated by large sales volumes encourage investing in upgrades – in this case, a significant investment was made in a new wing, advanced cockpit/systems, and better avionics, which has resulted in continuing strong sales in a fiercely competitive market.

The variant concept is market and role driven, keeping pace with technology advancements. Of course, derivatives in the family are not the optimum size (more so in civil aircraft design), but they are a satisfactory size that meets the demands. The unit-cost reduction, as a result of component commonalities, must compromise with the nonoptimum situation of a slight increase in fuel burn. Readers are referred to Figure 16.6, which highlights the aircraft unit-cost contribution to DOC as more than three to four times the cost of fuel, depending on payload-range capability.

The worked-out examples in the next section offer an idea of three variants in the family of aircraft.

11.6.2 Example: Civil Aircraft

Figure 11.4 shows the final configuration of the family of variants; the baseline aircraft is in the middle (see Figure 6.1 for the plug sizes).

Section 6.10 proposes one smaller (i.e., four to six passengers) and one larger (i.e., fourteen to sixteen passengers) variant from the baseline design that carries ten to twelve passengers by subtracting and adding fuselage plugs from the front and aft

of the wing box. The baseline and variant details are worked out in Chapter 6 as the preliminary configuration, followed by the undercarriage design in Chapter 7. Aircraft mass is calculated in Chapter 8. After obtaining the aircraft drag, this chapter finalizes the size of the baseline along with the two variants.

The final sized aircraft came very close to the preliminary baseline aircraft configuration suggested in Section 6.10. Therefore, iterations to fine-tune the aircraft mass, drag, and so forth have been avoided. It is unlikely for a coursework exercise to be that fortunate. It is highly recommended that any exercise should make at least one iteration in order to get a sense of the task. Setting up a spreadsheet is part of the learning process; all equations in this book are provided to set up the required spreadsheet.

11.7 Sizing Analysis: Military Aircraft

This extended section of the book on military aircraft sizing analysis can be found on the Web at www.cambridge.org/Kundu and includes the following:

Figure 11.5. Aircraft sizing – military aircraft

11.7.1 Single-Seat Variant in the Family of Aircraft Design

Figure 11.6. Variant designs in the family of military aircraft

11.8 Sensitivity Study

The sizing exercise offers an opportunity to conduct a sensitivity study of the physical geometries so that designers and users have better insight in making finer choices. An example of an AJT wing-geometry sensitivity study is in Table 11.7 showing what happens with small changes in the wing reference area, S_W ; aspect

Table 11.7. AJT sensitivity study

		<u>Perturbed Geometry</u>
(2.71 kts) <u>Sized Geometry</u> $S_W = 17 \text{ m}^2$ $AR = 5.0$ $t/c = 10\%$ $\Lambda_{1/4} = 20 \text{ degrees}$	→	$\Delta S_W = \pm 1.0 \text{ m}^2$ $\Delta Mach = \pm 0.004$ $\Delta V = \pm 4.35 \text{ mph (3.78 kts)}$ $\Delta V_{touch_down} = \pm 3.12 \text{ mph}$ $\Delta M = \pm 65 \text{ kg (143.3 lb)}$
	→	$\Delta AR = \pm 0.5$ $\Delta M = \pm 40 \text{ kg (88.2 lb)}$ $\Delta n \text{ (acceleration)} = \pm 0.18$
	→	$\Delta t/c = \pm 2\%$ $\Delta Mach = \pm 0.023$ $\Delta V = \pm 15.6 \text{ mph (13.6 kts)}$ $\Delta M = \pm 45 \text{ kg (99.2 lb)}$
	→	$\Delta \Lambda_{1/4} = \pm 10 \text{ degrees}$ $\Delta Mach = \pm 0.01$ $\Delta V = \pm 6.25 \text{ mph (5.43 kts)}$

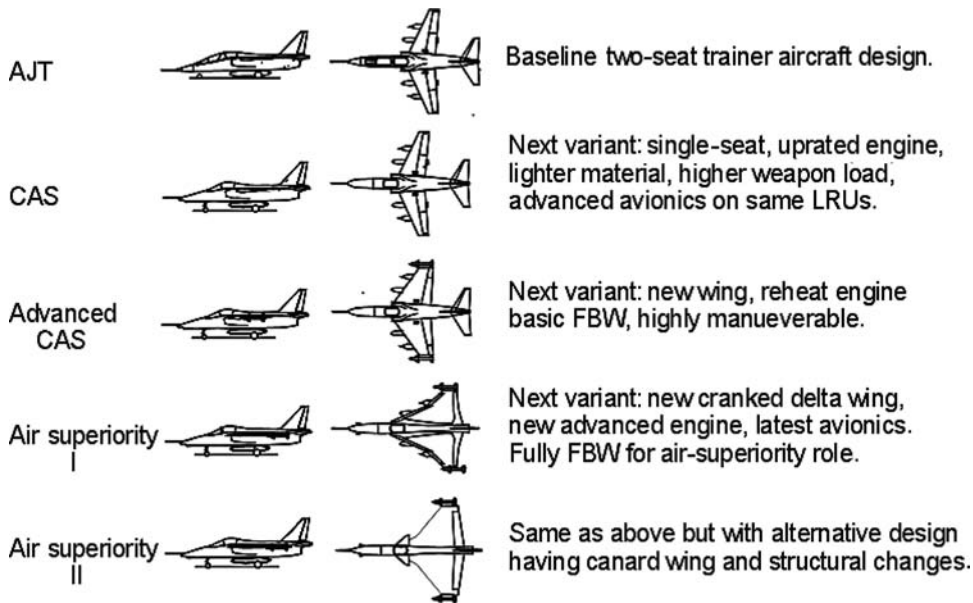


Figure 11.7. Further growth of the military AJT/CAS design

ratio, AR ; aerofoil t/c ratio, t/c ; and wing quarter-chord sweep, $\Lambda_{1/4}$. (A Bizjet aircraft sensitivity study is not provided in this book.)

A more refined analysis could be made with a detailed sensitivity study on various design parameters, such as other geometrical details, materials, and structural layout, to address cost-versus-performance issues in order to arrive at a satisfying design. This may require local optimization with full awareness that global optimization is not sacrificed. Although a broad-based MDO is the ultimate goal, dealing with a large number of parameters in a sophisticated algorithm may not be easy. It is still researched intensively within academic circles, but the industry tends to use MDO conservatively, if required in a parametric search, by addressing one variable at a time. The industry cannot afford to take risks with an unproven algorithm simply because it bears promise. The industry takes a more holistic approach to minimize costs without sacrificing safety, but it may compromise performance if it pays off.

11.9 Future Growth Potential

Previous military aircraft designs laid the foundation for future designs. Even a radically new design extracts information and, if possible, salvageable component commonalities from older designs. Figure 11.7 is a conceptual example showing how far newer designs can benefit from older designs through their systematic exploitation. The figure summarizes designs from the AJT to the light air superiority aircraft. It could be debated about how effective the last two designs could be (without the stealth consideration); however, at this stage, it only reflects a scheme.

The designs of the AJT and CAS are sized in detail. The advanced CAS (ACAS) is an AB version of the CAS with a new wing for high-subsonic flight. Missions for these aircraft are more suited to the counterinsurgency-type role, where the 1960s and 1970s designs are still creating havoc. The 6,900-lb thrust can reach

10,000 lb with AB that should enable the ACAS to carry a high weapon load ($\approx 5,000$ lb) (this design has not been properly checked).

The ultimate extension can be toward the air superiority role (two possibilities are shown in [Figure 11.7](#)). In this case, it is unlikely that the baseline engine can be further extended; therefore, re-engine work with a more powerful turbofan (i.e., an AB producing around 18,000 lb) and a totally new wing (i.e., $S_w \approx 22$ m²) are required. A clean aircraft weight would reach approximately 5,700 kg, pushing the supersonic speed to approximately Mach 1.8, but with a very tight turning capability at subsonic speed. However, such a design may be controversial because its viability in combat would be questioned. A new combat aircraft design should have a stealth factor, which is not discussed herein due to having few backup data. However, there may be substantial commonalities in the forward fuselage and the systems design.

12 Stability Considerations Affecting Aircraft Configuration

12.1 Overview

Chapter 11 completed the aircraft configuration in the conceptual study phase of an aircraft project by finalizing the external dimensions through the formal-sizing and engine-matching procedures. The design now awaits substantiation of aircraft performance to ensure that the requirements are met (see [Chapter 13](#)). Substantiation of aircraft performance alone is not sufficient if the aircraft-stability characteristics do not provide satisfactory handling qualities and safety, which are *flying qualities* that have been codified by NASA. Many good designs required considerable tailoring of the control surfaces, which sometimes affected changes to and/or repositioning of the wing and incorporated additional surfaces (e.g., dorsal fin and ventral fins).

Preliminary stability analyses, using semi-empirical methods (e.g., DATCOM and RAE data sheets [now ESDU]), are conducted during the conceptual study as soon as the three-view aircraft configuration is available. The analyses include the CG location (see [Chapter 8](#)) and preliminary stability results from geometric parameters (e.g., surface areas, wing dihedral, sweep, and twist), which are determined from past experience and statistics. Aircraft dynamic-stability analysis requires accurate stability derivatives obtained from extensive wind-tunnel and flight testing. These are cost-intensive exercises and require more budget appropriation after the project go-ahead is obtained in the next phase (i.e., Project Definition, Phase 2). Manufacturing philosophy is firmed up during Phase 2 after aircraft geometry is finalized, when the jig and tool designs can begin. Phase 2 activities are beyond the scope of this book.

New-generation aircraft incorporate artificial stability such as the use of FBW technology, which is *control-configured vehicles (CCV)*. This is a good example of a systems approach (see [Figure 2.1](#)) to aircraft design. Phase 1 activities of commercial transport aircraft design with FBW can begin with available statistics of similar designs and then proceed to developing the aircraft-control laws. Advanced combat aircraft design requires the control laws to establish the initial FBW architecture at an early stage, which is not addressed in this book. For this reason, the author suggests that coursework on complex designs be postponed until the basics are learned. This book is limited to conventional aircraft design, a generalized procedure that also can be applied to CCV designs.

Aeroelasticity affects control but, in general, during the conceptual phase of the study, the aircraft is seen as a rigid body. The next phase takes into account the aeroelastic effects using an integral approach to fine-tune the control-surfaces design.

This chapter is not a definitive study of aircraft stability and control (see [1] through [4] for more details on the subject), but it qualitatively examines and provides an understanding of the geometrical arrangement of aircraft components that affect aircraft stability. The reason for discussing stability here is to provide experience through the use of statistics in shaping aircraft as early as possible so that, if necessary, fewer changes are required in subsequent design phases. This chapter presents a rationale for a designer's experience and provides an opportunity to examine whether the final aircraft configuration reflects all other considerations at this stage of the design process. There are no changes in the worked-out examples.

Only the equations governing static stability are given to explain design features. A classic example of how stability affects aircraft configuration is the departure of what the Wright brothers accomplished with the "tail" in the front (see Section 1.2) by later designers to put the tail where it should be, at the back. The Wright brothers used a warping wing for lateral control; later designers introduced ailerons. A tail-in-front canard later returned to aircraft design with far better application than what the Wright brothers had contemplated.

12.1.1 What Is to Be Learned?

This chapter covers the following topics:

- Section 12.2: Introduction to stability considerations affecting aircraft design
- Section 12.3: Basic information on static and dynamic stability
- Section 12.4: Elementary theory examining uncoupled pitch and coupled directional and lateral stability to determine empennage size
- Section 12.5: Current statistical trends in empennage-sizing parameters
- Section 12.6: Inherent aircraft motions as characteristics of design
- Section 12.7: Aircraft spinning
- Section 12.8: Design considerations for stability
- Section 12.9: Military aircraft stability: nonlinear effects
- Section 12.10: Active control technology

12.1.2 Coursework Content

Readers may examine the final configuration to review its merits. There is little coursework in this chapter. (The aircraft configuration is unlikely to change unless performance falls short of the requirements; see [Chapter 13](#).)

12.2 Introduction

Inherent aircraft stability is a result of the CG location, the wing and empennage sizing and shaping, the fuselage and nacelle sizing and shaping, and their relative locations. Because the initial control-surface positioning and sizing are accomplished

empirically from statistical data, the important aspect of whether the aircraft has safe-handling characteristics is not examined. This chapter highlights some of the lessons learned on how to arrange aircraft components relative to one another.

The pitching motion of an aircraft is in the plane of aircraft symmetry (about the Y-axis, elevator-actuated) and is uncoupled with any other type of motion. Directional (about the Z-axis, rudder-actuated) and lateral (about the X-axis, aileron-actuated) motions are not in the plane of symmetry. Activating any of the controls (e.g., rudder or ailerons) causes a coupled aircraft motion in both the directional and lateral planes.

Finally, at the end of a project, flight tests reveal whether the aircraft satisfies the flying qualities and safety considerations. Almost all projects require some type of minor tailoring and/or rigging of control surfaces to improve the flying qualities as a consequence of flight tests – in hindsight, possibly making it better than what was initially envisaged. For civil aircraft designs, this is a routine procedure and is neither expensive nor a major hurdle to program milestones. Military aircraft design projects are preceded by technology demonstrators, which results in obtaining vital information for the final design that may incorporate configuration changes from the lessons learned. The design still must undergo fine-tuning as a result of flight tests. This is a relatively more expensive and time-consuming process, but it saves funds by minimizing errors during the design of military aircraft, which often incorporates cutting-edge advanced technologies that are yet to be operationally proven.

Designers should be aware of the preferred flying qualities so that the aircraft is configured intelligently to minimize changes in the final stages; this is the main objective of this chapter.

12.3 Static and Dynamic Stability

It is pertinent here to briefly review the terms *static* and *dynamic stability*. Stability analyses examine what happens to an aircraft when it is subjected to forces and moments applied by a pilot and/or induced by external atmospheric disturbances. There are two types of stability, as follows:

1. *Static Stability*. This is concerned with the instantaneous tendency of an aircraft when disturbed during equilibrium flight. The aircraft is statically stable if it has restoring moments when disturbed; that is, it shows a tendency to return to the original equilibrium state. However, this does not cover what happens in the due course of time. The recovery motion can overshoot into oscillation, which may not return to the original equilibrium flight.
2. *Dynamic Stability*. This is the time history of an aircraft response after it has been disturbed, which is a more complete picture of aircraft behavior. A statically stable aircraft may not be dynamically stable, as explained in subsequent discussions. However, it is clear that a statically unstable aircraft also is dynamically unstable. Establishing static stability before dynamic stability is for procedural convenience.

The aircraft motion in 3D space is represented in the three planes of the Cartesian coordinate system (see Section 3.4). Aircraft have six degrees of freedom of motion

in 3D space. They are decomposed into the three planes; each exhibits its own stability characteristics, as listed herein. The sign conventions associated with the pitch, yaw, and roll stabilities need to be learned (they follow the right-handed rule). The brief discussion of the topic herein is only for what is necessary in this chapter. The early stages of stability analyses are confined to small perturbations – that is, small changes in all flight parameters.

1. *Longitudinal Stability in the Pitch Plane.* The pitch plane is the XZ plane of aircraft symmetry. The linear velocities are u along the X-axis and w along the Z-axis. Angular velocity about the Y-axis is q , known as *pitching* (+ve nose up). Pilot-induced activation of the elevator changes the aircraft pitch. In the plane of symmetry, the aircraft motion is uncoupled; that is, motion is limited only to the pitch plane.
2. *Directional Stability in the Yaw Plane.* The yaw plane is the XY plane and is not in the aircraft plane of symmetry. Directional stability is also known as *weathercock stability* because of the parallel to a weathercock. The linear velocities are u along the X-axis and v along the Y-axis. Angular velocity about the Z-axis is r , known as *yawing* (+ve nose to the left). Yaw can be initiated by the rudder; however, pure yaw by the rudder alone is not possible because yaw is not in the plane of symmetry. Aircraft motion is coupled with motion in the other plane, the YZ plane.
3. *Lateral Stability in the Roll Plane.* The roll plane is the YZ plane and also is not in the aircraft plane of symmetry. The linear velocities are v along the Y-axis and w along the Z-axis. Angular velocity about the X-axis is p , known as *rolling* (+ve when right wing drops). Rolling can be initiated by the aileron but a pure roll by the aileron alone is not possible because roll is associated with yaw. To have a pure rolling motion in the plane, the pilot must activate both the yaw and roll controls.

It is convenient now to explain the static and dynamic stability in the pitch plane using diagrams. The pitching motion of an aircraft is in the plane of symmetry and is uncoupled; that is, motion is limited only to the pitch plane. The static and dynamic behavior in the other two planes has similar characteristics, but it is difficult to depict the coupled motion of yaw and roll. These are discussed separately in Sections 12.3.2 and 12.3.4.

Pitch-plane stability may be compared to a spring-mass system, as shown in Figure 12.1a. The oscillating characteristics are represented by the spring-mass system, with the resistance to the rate of oscillation as the damping force (i.e., proportional to pitch rate, q) and the spring compression proportional to pitch angle θ . Figure 12.1b shows the various possibilities of the vibration modes. Stiffness is represented by the stability margin, which is the distance between the CG and the neutral point (NP). The higher the force required for deforming, the more is the stiffness. Damping results from the rate of change and is a measure of resistance (i.e., how fast the oscillation fades out); the higher the H-tail area, the more is the damping effect. An aircraft only requires adequate stability; making it more stable than what is required poses other difficulties in the overall design.

Figure 12.2 depicts the stability characteristics of an aircraft in the pitch plane, which provide the time history of aircraft motion after it is disturbed from an initial

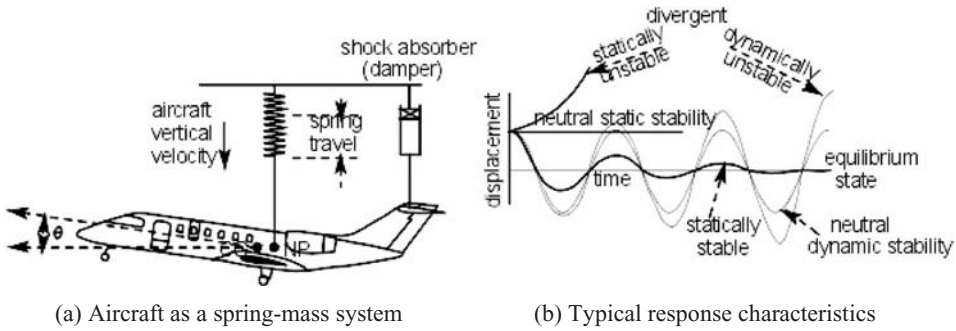


Figure 12.1. Aircraft stability compared to a spring-mass system

equilibrium. It shows that aircraft motion is in an equilibrium level flight – here, motion is invariant with time. Readers may examine what occurs when forces and moments are applied.

A statically and dynamically stable aircraft tends to return to its original state even when it oscillates about the original state. An aircraft becomes statically and dynamically unstable if the pitching motion diverges outward – it neither oscillates nor returns to the original state. The third diagram of Figure 12.2 provides an example of neutral static stability – in this case, the aircraft does not have a restoring

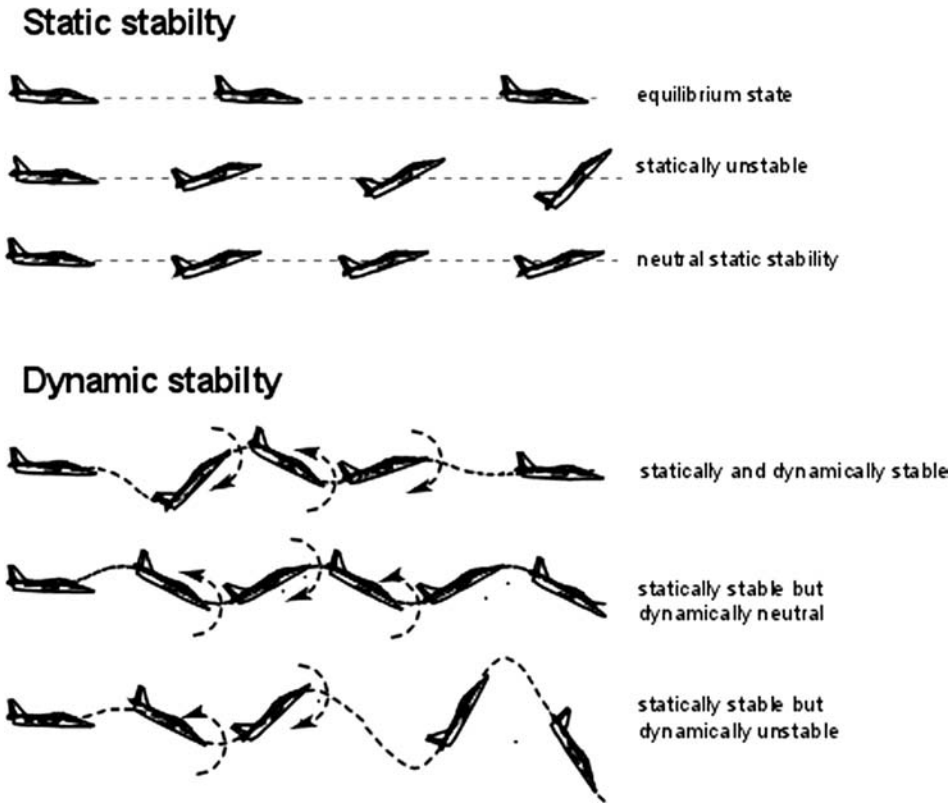


Figure 12.2. Stability in the pitch plane

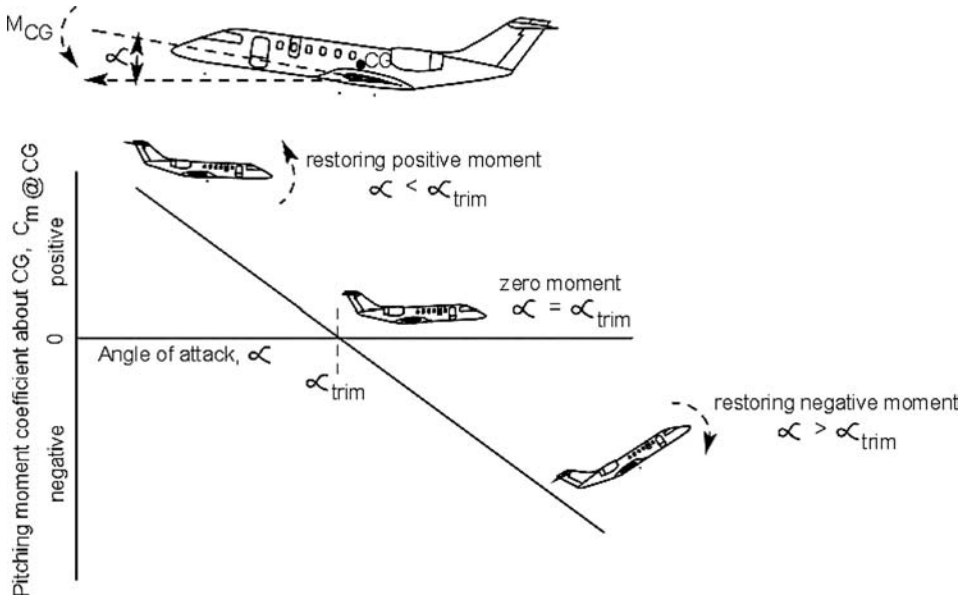


Figure 12.3. Longitudinal static stability

moment. It remains where it was after the disturbance and requires an applied pilot effort to force it to return to the original state. The tendency of an aircraft to return to the original state is a good indication of what could happen in time: Static stability makes it possible but does not guarantee that an aircraft will return to the equilibrium state.

As an example of dynamic stability, Figure 12.2 also shows the time history for when an aircraft returns to its original state after a few oscillations. The time taken to return to its original state is a measure of the aircraft's damping characteristics – the higher the damping, the faster the oscillations fade out. A statically stable aircraft showing a tendency to return to its original state can be dynamically unstable if the oscillation amplitude continues to increase, as shown in the last diagram of Figure 12.2. When the oscillations remain invariant to time, the aircraft is statically stable but dynamically neutral – it requires an application of force to return to the original state.

12.3.1 Longitudinal Stability: Pitch Plane (Pitch Moment, M)

Figure 12.3 depicts the conditions for aircraft longitudinal static stability. In the pitch plane, by definition, the angle of attack, α , is positive when an aircraft nose is above the direction of free-stream velocity. A nose-up pitching moment is considered a positive. Static-stability criteria require that the pitching-moment curve exhibit a negative slope, so that an increase in the angle of attack, α , causes a restoring negative (i.e., nose-down) pitching moment. At equilibrium, the pitching moment is equal to zero ($C_m = 0$) when it is in trimmed condition (α_{trim}). The higher the static margin (see Figure 12.11), the greater is the slope of the curve (i.e., the greater is the restoring moment). Using the spring analogy, the stiffness is higher for the response.

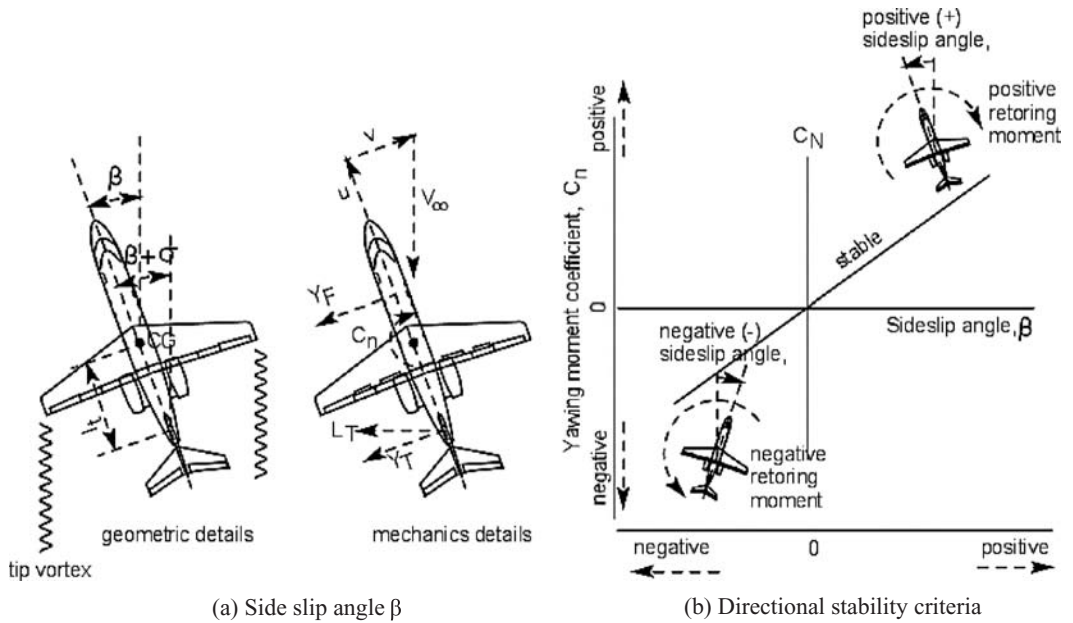


Figure 12.4. Direction stability

The other requirement for static stability is that at a zero angle of attack, there should be a positive nose-up moment, providing an opportunity for equilibrium at a positive angle of attack ($+\alpha_{trim}$), typical in any normal flight segment.

12.3.2 Directional Stability: Yaw Plane (Yaw Moment, N)

Directional stability can be compared to longitudinal stability but it occurs in the yaw plane (i.e., the XY plane about the Z-axis), as shown in Figure 12.4. By definition, the angle of sideslip, β , is positive when the free-stream velocity vector, V , relative to aircraft is from the right (i.e., the aircraft nose is to the left of the velocity). V has component aircraft velocities u along the X-axis and v along the Y-axis, subtending the sideslip angle $\beta = \tan^{-1}(v/u)$.

The V-tail is subjected to an angle of incidence ($\beta + \sigma$), where σ is the sidewash angle generated by the wing vortices (like the downwash angle in longitudinal stability). Static stability criteria require that an increase in the sideslip angle, β , should generate a restoring moment, C_n , that is positive when turning the nose to the right. The moment curve slope of C_n is positive for stability. At zero β , there is no yawing moment (i.e., $C_n = 0$).

Yaw motion invariably couples with roll motion because neither is in the plane of symmetry. In yaw, the windward wing works more to create a lift increase while the lift decreases on the other wing, thereby generating a rolling moment. Therefore, a pure yaw motion is achieved by the use of compensating, opposite ailerons. The use of an aileron is discussed in the next section.

12.3.3 Lateral Stability: Roll Plane (Roll Moment, L)

Roll stability is more difficult to analyze compared to longitudinal and lateral stabilities. A banked aircraft attitude through a pure roll keeps the aircraft motion in

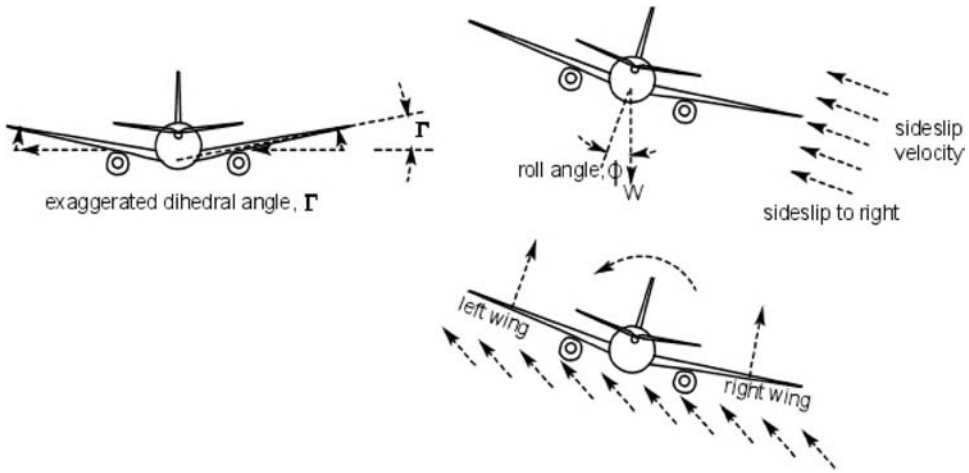


Figure 12.5. Lateral stability

the plane of symmetry and does not provide any restoring moment. However, roll is always coupled with a yawed motion, as explained previously. As a roll is initiated, the sideslip velocity, v , is triggered by the weight component toward the down-wing side, as shown in Figure 12.5. Then (see the previous section), the sideslip angle is $\beta = \tan^{-1}(v/u)$. The positive angle of roll, Φ , is when the right wing drops as shown in the figure (the aircraft is seen from the rear showing the V-tail but no windscreen). A positive roll angle Φ generates a positive sideslip angle, β . The angle of attack increases the sideslip.

Recovery from a roll is possible as a result of the accompanying yaw (i.e., coupled motion) with the restoring moment contributed by increasing the lift acting on the wing that has dropped. Roll static-stability criteria require that an increase in the roll angle, Φ , creates a restoring moment coefficient, C_l (not to be confused with the sectional aerofoil-lift coefficient). The restoring moment has a negative sign.

Having a coupled motion with the sideslip, Figure 12.6 shows that C_l is plotted against the sideslip angle β , not against the roll angle Φ because it is β that generates the roll stability. The sign convention for restoring the rolling moment with respect

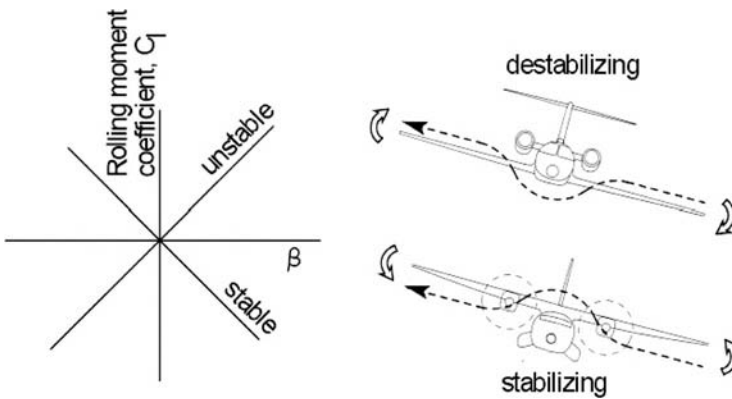


Figure 12.6. Lateral stability: fuselage contributions

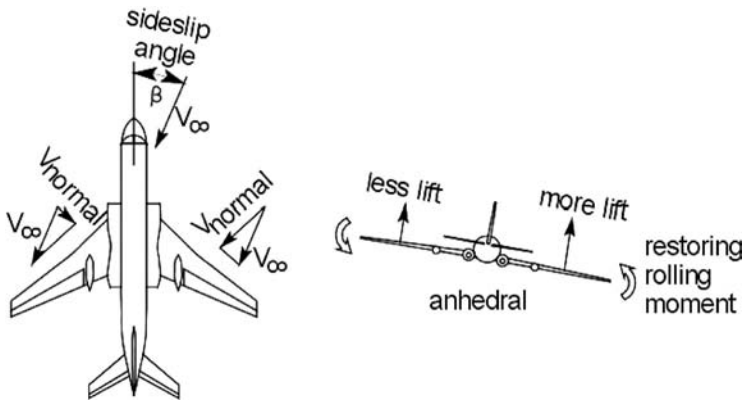


Figure 12.7. Effect of wing sweep on roll stability

to β must have $C_{l\beta}$ negative; that is, with an increase of roll angle Φ , the sideslip angle β increases to provide the restoring moment. An increase in β generates a restoring roll moment due to the dihedral. At zero Φ , there is no β ; hence, the zero rolling moment ($C_l = 0$).

The wing dihedral angle, Γ , is one way to increase roll stability, as shown in Figure 12.5. The dropped wing has an airflow component from below the wing generating lift, while at the other side, the airflow component is from the upper side of the wing that reduces the angle of attack (i.e., the lift reduction creates a restoring moment).

The position of the wing relative to the aircraft fuselage has a role in lateral stability, as shown in Figure 12.6. At yaw, the relative airflow about the low wing has a component that reduces the angle of attack; that is, the reduction of lift and the other side act in opposite ways: a destabilizing effect that must be compensated for by the dihedral, as explained previously. Conversely, a high-wing aircraft has an inherent roll stability that acts opposite to a low-wing design. If it has too much stability, then the anhedral (-ve dihedral) is required to compensate it. Many high-wing aircraft have an anhedral (e.g., the Harrier and the BAE RJ series).

An interesting situation occurs with a wing sweepback on a high-speed aircraft, as explained in Figure 12.8. At sideslip, the windward wing has an effectively reduced sweep; that is, the normal component of air velocity increases, creating a lift increment, whereas the leeward wing has an effectively increased sweep with a slower normal velocity component, thereby losing lift. This effect generates a rolling moment, which can be quite powerful for high-swept wings; even for low-wing aircraft, it may require some anhedral to reduce the excessive roll stability (i.e., stiffness) – especially for military aircraft, which require a quick response in a roll. Tu-104 in Figure 12.7 is a good example of a low-wing military aircraft with a high sweep coupled with an anhedral.

The side force by the fuselage and V-tail contributes to the rolling moment, as shown in Figure 12.8. If the V-tail area is large and the fuselage has a relatively smaller side projection, then the aircraft CG is likely to be below the resultant side force, thus increasing the stability. Conversely, if the CG is above the side force, then there is a destabilizing effect.

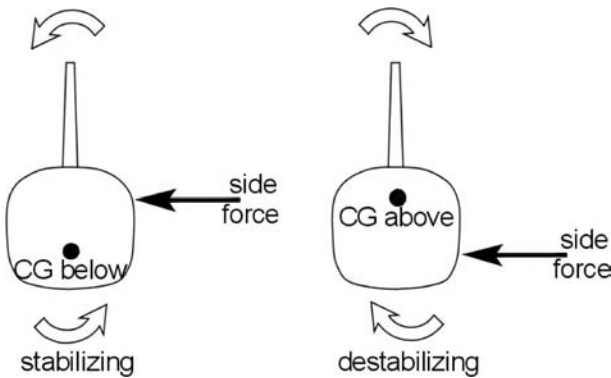


Figure 12.8. V-tail contribution to roll

12.3.4 Summary of Forces, Moments, and Their Sign Conventions

Given below is the summary of sign convention in the three planes.

	Longitudinal Static Stability	Directional Stability	Lateral Stability
Angles	Pitch angle α	Sideslip angle β	Roll angle, Φ
Positive Angle	Nose up	Nose to left	Right wing down
Moment Coefficient	C_m	C_n	C_l
Positive Moment	Nose up	Nose left	Right wing down

12.4 Theory

Forces and moments affect aircraft motion. In a steady level flight (in equilibrium), the summation of all forces is zero; the same applies to the summation of moments. When not in equilibrium, the resultant forces and moments cause the aircraft to maneuver. The following sections provide the related equations for each of the three aircraft planes. A sense of these equations helps in configuring aircraft in the conceptual design phase.

12.4.1 Pitch Plane

In equilibrium, $\sum \text{force} = 0$, when drag = thrust and lift = weight (see Figure 3.9). An imbalance in drag and thrust changes the aircraft speed until equilibrium is reached. Drag and thrust act nearly collinearly; if they did not, pitch trim would be required to balance out the small amount of pitching moment it can develop. The same is true with the wing lift and weight, which are rarely collinear and generate a pitching moment. This scenario also must be trimmed, with the resultant lift and weight acting collinearly.

Together in equilibrium, $\sum \text{moment} = 0$. Any imbalance results in an aircraft rotating about the Y-axis. Figure 12.9 shows the generalized forces and moments (including the canard) that act in the pitch plane. The forces are shown normal and parallel to the aircraft reference lines (i.e., body axes) and abnormal to aircraft velocity. Lift and drag are obtained by resolving the forces of Figure 12.9 into

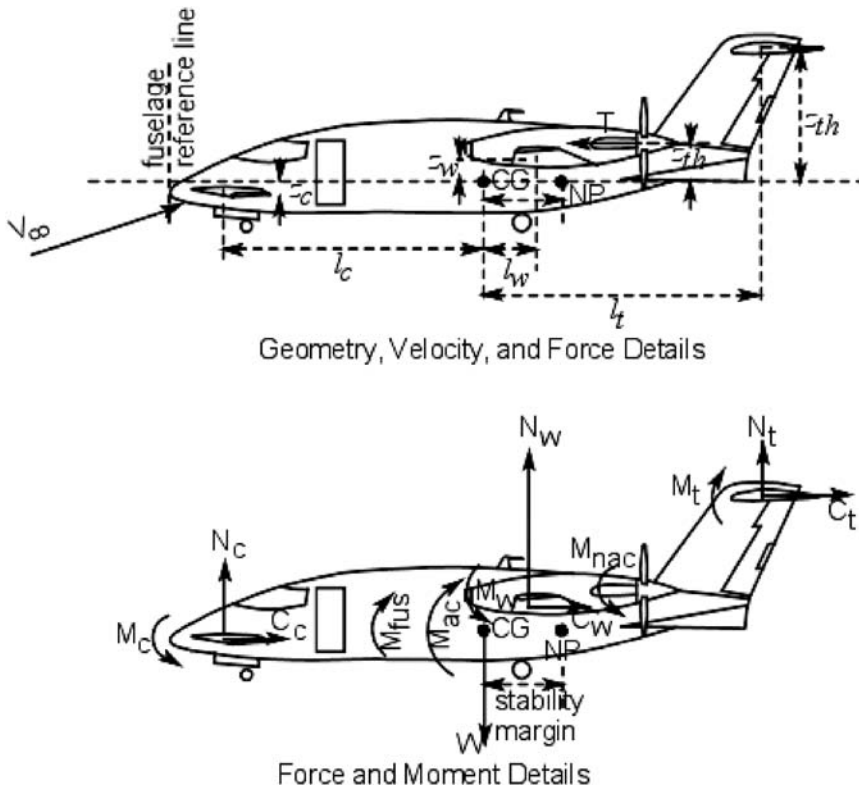


Figure 12.9. Generalized force and moment in the pitch plane

perpendicular and parallel directions to the free-stream velocity vector (i.e., aircraft velocity). The forces can be expressed as lift and drag coefficients, dividing by qS_w , where q is the dynamic head and S_w is the wing reference area. Subscripts identify the contribution made by the respective components. The arrowhead directions of component moments are arbitrary – they must be assessed properly for the components. With its analysis, [Figure 12.9](#) gives a good idea of where to place aircraft components relative to the aircraft CG and NP. The static margin is the distance between the NP and the CG.

The generalized expression for the moment equation can be written as in [Equation 12.1](#), which sums up all the moments about the aircraft CG. In the trimmed condition, the aircraft moment about the aircraft CG must be zero ($M_{ac_cg} = 0$):

$$\begin{aligned}
 M_{ac_cg} = & (N_c \times l_c + C_c \times z_c + M_c)_{canard} + (N_w \times l_w + C_w \times z_w + M_w)_{wing} \\
 & + (N_t \times l_t + C_t \times z_t + M_t)_{tail} \\
 & + M_{fus} + M_{nac} + (\text{thrust} \times z_{th} + nac_drag \times z_{th}) + \text{any other item} \quad (12.1)
 \end{aligned}$$

In the conceptual design stage, the forces and moments of each component are estimated semi-empirically (i.e., US DATCOM and RAE data sheets [now ESDU]) from the drawings. When assembled together as an aircraft, each component is influenced by the flow field of the others (e.g., the flow over the H-tail is affected by the wing flow). Therefore, a correction factor, η , is applied. This is shown in [Equation 12.2](#) written in coefficient form, dividing by $qS_w c$, where q is the dynamic head,

c is the wing MAC, and S_w is the wing reference area. Subscripts identify the contribution of the respective components. The moment coefficients of the components are computed initially as isolated bodies and then converted to the reference wing area:

$$\begin{aligned}
 C_{mcg} = & [C_{Nc}(S_c/S_w)(l_c/c) + C_{Cc}(S_c/S_w)(z_c/c) + C_{mc}(S_c/S_w)]_{\text{for canard}} \\
 & + [C_{Nw}(l_a/c)\eta_w + C_{Cw}(z_a/c)\eta_w + C_{mw}\eta_w]_{\text{for wing}} \\
 & + [C_{Nt}(S_t/S_w)(l_t/c)\eta_t + C_{Ct}(S_t/S_w)(z_t/c)\eta_t + C_{mt}(S_t/S_w)\eta_t]_{\text{for tail}} \\
 & + C_{mfus} + C_{nac} + (\text{thrust} \times z_{th} + nac_drag \times z_{th})/qS_w c \quad (12.2)
 \end{aligned}$$

where:

1. $\eta (= q_i/q_\infty)$ represents the wake effect of lifting surfaces behind another lifting surface producing downwash, q_i is the incident dynamic head, and q_∞ is the free-stream dynamic head.
2. The vertical distances (z) of each component can be above or below the CG, depending on the configuration, described as follows:
 - (a) For fuselage-mounted engines, z_{th} is likely to be above the aircraft CG and its thrust generates a nose-down moment. In underslung wings, engines have the z_{th} below the CG, generating a nose-up moment. For most military aircraft, the thrust line is very close to the CG; therefore, for a preliminary analysis, the z_{th} term can be ignored (i.e., no moment is generated with thrust unless it is vectored).
 - (b) The drag of a low wing below the CG (z_a) has a nose-down moment and vice versa for a high wing. For midwing positions, which side of the CG must be noted; the (z_a) may be small enough to be ignored in the preliminary analysis.
 - (c) The position of the H-tail shows the same effect as for the wing but is invariably above the CG. For a low H-tail, z_t can be ignored. In general, the drag generated by the H-tail is small and can be ignored; this is also true for a T-tail design.
 - (d) For the same reason, the contribution of the canard vertical distance, z_c , also can be ignored.

In summary, Equation 12.2 can be further simplified by comparing the order of magnitude of the contributions of the various terms. Initially, the following simplifications are suggested:

1. The vertical z distance of the canard and the wing from the CG is small. Therefore, the terms with z_c and z_a can be omitted.
2. The canard and H-tail reference areas are much smaller than the wing reference area and their C (\approx drag) component force is less than a tenth of their lifting forces. Therefore, the terms with $C_{Cc}(S_c/S_w)$ and $C_{Ct}(S_t/S_w)$ can be omitted – even for a T-tail, but it is best to check its overall contribution.
3. A high or low wing has z_a with opposite signs. For a midwing, z_a may be small enough to be ignored.

Equation 12.2 can be simplified as follows:

$$C_{mcg} = [C_{Nc}(S_c/S_w)(l_c/c) + C_{mc}(S_c/S_w)] + [C_{Nw}(l_a/c)\eta_w + C_{mw}\eta_w] \\ + [C_{Nt}(S_t/S_w)(l_t/c)\eta_t + C_{mt}(S_t/S_w)\eta_t] \\ + C_{mfus} + C_{nac} + (\text{thrust} \times z_{th} + nac_drag \times z_{th})/qS_wc \quad (12.3)$$

A conventional aircraft does not have a canard. Then, Equation 12.3 can be further simplified to Equation 12.4. The conventional aircraft CG is possibly ahead of the wing MAC. In this case, the H-tail must have negative lift to trim the moment generated by the wing and the body:

$$C_{mcg} = [C_{Nw}(l_a/c) + C_{mw}] + [C_{Nt}(S_t/S_w)(l_t/c)\eta_t + C_{mt}(S_t/S_w)\eta_t] \\ + C_{mfus} + C_{nac} + (\text{thrust} \times z_{th} + nac_drag \times z_{th})/qS_wc \quad (12.4)$$

Normal forces now can be resolved in terms of lift and drag; for small angles of α , the cosine of the angle is 1. The drag components of all the C_N are very small and can be neglected.

Then, the first term:

$$C_{Nw}(l_a/c) + C_{mw} \approx C_{Lw}(l_a/c) + C_{mw}$$

and the second term:

$$C_{Nt}(S_t/S_w)(l_t/c)\eta_t + C_{mt}(S_t/S_w)\eta_t \approx C_{Lt}(S_t/S_w)(l_t/c)\eta_t + C_{mt}(S_t/S_w)\eta_t$$

where

$$C_{mt}(S_t/S_w)\eta_t \ll C_{Lt}(S_t/S_w)(l_t/c)\eta_t$$

Hence, the moment contribution by the H-tail is represented as $C_{m-HT} = C_{Lt}(S_H/S_w)(l_t/c)\eta_{HT}$.

Then, Equation 12.4 is rewritten (note the sign) as:

$$C_{mcg} = [C_{Lw}(l_a/c) + C_{mw}] + C_{m-HT} + C_{mfus} + C_{nac} \\ + (\text{thrust} \times z_{th} + nac_drag \times z_{th})/qS_wc \quad (12.5)$$

where

$$C_{m-HT} = -C_{LHT} \times [(l_t/S_{HT})/(S_wc)]\eta_{HT} = -V_H \eta_{HT} C_{LHT} \quad (12.6)$$

For conventional aircraft, C_{LHT} has a downward direction to keep the nose up; therefore, it has a negative sign. Here,

$$V_H = \text{H-tail volume coefficient} = (l_t/S_{HT})/(S_wc) \quad (12.7)$$

(introduced in Section 3.20, derived here).

Then, Equation 12.5 without engines becomes:

$$C_{mcg} = [C_{Lw}(l_a/c) + C_{mw}] - C_{m-HT} + C_{mfus} \quad (12.8)$$

A convenient method is to analyze the effects on aircraft pitching moments of isolated aircraft components. Next, the airplane less the empennage is estimated, thereby determining the appropriate H-tail moment required to balance the moments at the cruise condition. Figure 12.10 shows the pitching moment contribution by components of a conventional aircraft (considered mass-less to examine only

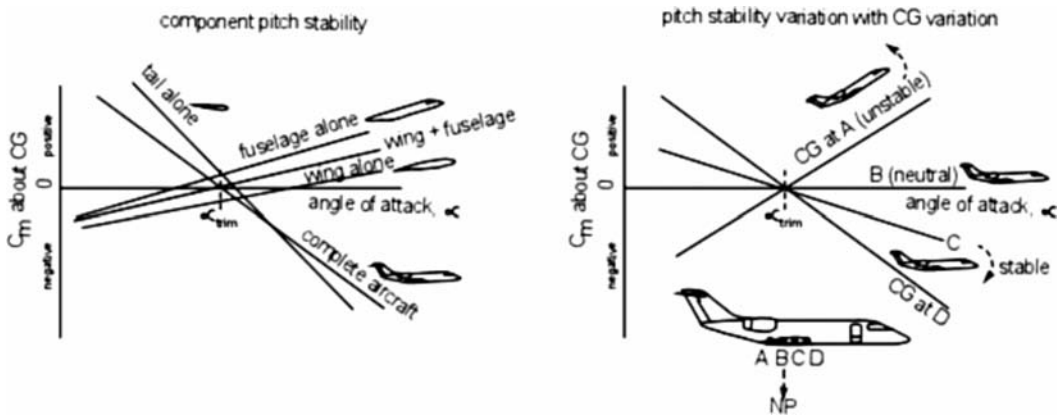


Figure 12.10. Pitch stability

the aerodynamic characteristics). The wing and fuselage have destabilizing moments (i.e., nose up), which must be compensated for by the tail to counter the wing and fuselage moments; hence, Equation 12.6 has negative sign.

The second diagram in Figure 12.10 shows the stability effects of different CG positions on a conventional aircraft. The stability margin is the distance between the aircraft CG and the NP (i.e., a point through which the resultant force of the aircraft passes). When the CG is forward of the NP, then the static margin has a positive sign and the aircraft is statically stable. The stability increases as the CG moves farther ahead of the NP.

There is a convenient range from the CG margin in which the aircraft design exhibits the most favorable situation. In Figure 12.10, the position B is where the CG coincides with the NP and shows neutral stability (i.e., at a zero stability margin) – the aircraft can still be flown with the pilot's efforts controlling the aircraft attitude. In fact, an aircraft with relaxed stability can have a small negative margin that requires little force to make rapid maneuvers – these aircraft invariably have a FBW control architecture (see Section 12.10) in which the aircraft is flown continuously controlled by a computer.

Engine thrust has a powerful effect on stability. If it is placed above and behind the CG such as in an aft-fuselage-mounted nacelle, it causes an aircraft nose-down pitching moment with thrust application. For an underslung wing nacelle ahead of the CG, the pitching moment is with the aircraft nose up. It is advisable for the thrust line to be as close as possible to the aircraft CG (i.e., a small z_e to keep the moment small). High-lift devices also affect aircraft pitching moments and it is better that these devices be a small arm's-length from the CG.

In summary, designers must carefully consider where to place components to minimize the pitching-moment contribution, which must be balanced by the tail at the expense of some drag – this is unavoidable but can be minimized.

12.4.2 Yaw Plane

The equation of motion in the yaw plane can be set up similarly to the pitch plane. The weathercock stability of the V-tail contributes to the restoring moment.

Figure 12.4 depicts moments in the yaw plane. In the diagram, the aircraft is yawing to the left with a positive yaw angle β . This generates a destabilizing moment by the fuselage with the moment ($N_F = Y_F \times l_f$), where Y_F is the resultant side force by the fuselage and l_f is the distance of L_f from the CG. Contributions by the wing, H-tail, and nacelle are small (i.e., small projected areas and/or shielded by the fuselage projected area). The restoring moment is positive when it tends to turn the nose to the right to realign with the airflow. The weathercock stability of the V-tail causes the restoring moment ($N_{VT} = Y_T \times l_t$), where Y_T is the resultant side force on the V-tail (for small angles of $(\beta + \sigma)$, it can be approximated as the lift generated by the V-tail, L_{VT}) and l_t is the distance of L_T from the CG. Therefore, the total aircraft yaw moment, N (for conventional aircraft), is the summation of N_F and N_{VT} , as given in Equation 12.9:

$$N_{ac_cg} = N_F + N_{VT} \quad (12.9)$$

At equilibrium flight:

$$N_{ac_cg} = 0; \quad \text{i.e., } N_{VT} = -N_F \quad (12.10)$$

In coefficient form, the fuselage contribution can be written as:

$$C_{nf} = -k_n k_{RI} N_F [(S_f l_f)/(S_w b)] \beta \quad (12.11)$$

where k_n = empirical wing-body interference factor

k_{RI} = empirical correction factor

S_f = projected side area of the fuselage

l_f = fuselage length

b = wing span

In coefficient form, the V-tail contribution can be written as in Equation 12.11 (L_{VT} is in the coefficient form C_{LVT}):

$$C_{nVT} = [(l_t/S_{VT})/(S_w c)] \eta_{VT} C_{LVT} = L_{VT} V_V \eta_{VT} C_{LVT} \quad (12.12)$$

where

$$V_V = \text{V-tail volume coefficient} = (l_t/S_{VT})/(S_w c) \quad (12.13)$$

(introduced in Section 3.20, derived here).

Equation 12.9 in coefficient form becomes:

$$C_{n_cg} = -k_n k_{RI} N_F [(S_f l_f)/(S_w b)] \beta + L_{VT} V_V \eta_{VT} C_{LVT} \quad (12.14)$$

12.4.3 Roll Plane

As explained previously, roll stability derives primarily from the following three aircraft features:

1. *Wing Dihedral* Γ (see Figure 12.5). Sideslip angle β increases the angle of attack, α , on the windward wing, $\Delta\alpha = (V \sin \Gamma)/u$ generating ΔLift . For small dihedrals and perturbations, $\beta = v/u$, which approximates $\Delta\alpha = \beta \Gamma$. The restoring moment is the result of ΔLift generated by $\Delta\alpha$. It is quite powerful – for a

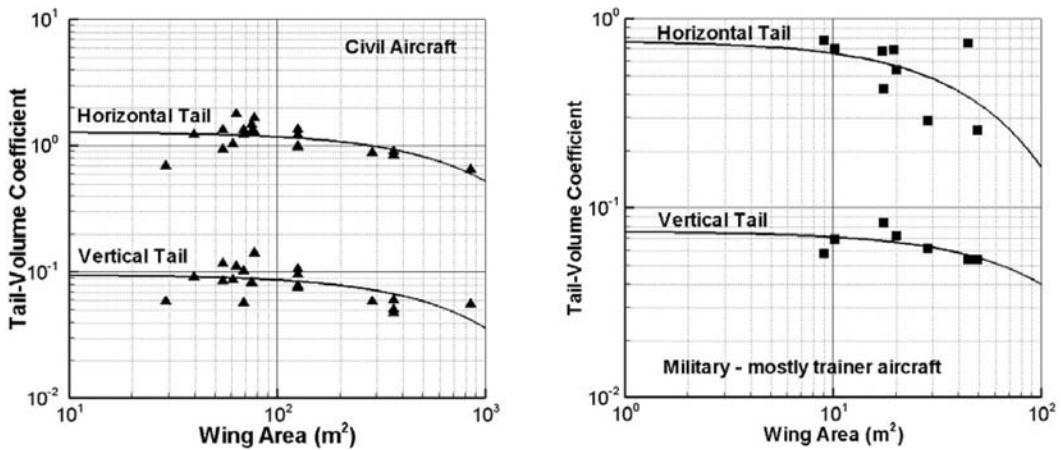


Figure 12.11. Statistics of current tail-volume coefficients

low-wing Γ , it is typically between 1 and 3 deg, depending on the wing sweep. For a straight-wing aircraft, the maximum dihedral rarely exceeds 5 deg. For a high-wing sweep, it may require an anhedral, as discussed herein.

2. *Wing Position Relative to the Fuselage* (see Figure 12.7). Section 12.3.3 explains the contribution to the rolling moment caused by different wing positions relative to the fuselage. Semi-empirical methods are used to determine the extent of the rolling-moment contribution.
3. *Wing Sweep at Quarter-Chord*, $\Lambda_{1/4}$ (see Figure 12.8). The lift produced by a swept wing is a function of the component of velocity, V_n , normal to the $c_{1/4}$ line; that is, in steady rectilinear flight:

$$V_n = V \cos \Lambda$$

When an aircraft sideslips with angle β , the component of velocity normal to the $c_{1/4}$ line becomes (small β):

$$V'_n = V \cos(\Lambda_{1/4} - \beta) = V(\cos \Lambda_{1/4} + \beta \sin \Lambda_{1/4})$$

For the leeward wing:

$$V'_{n\downarrow w} = V \cos(\Lambda_{1/4} + \beta) = V(\cos \Lambda_{1/4} - \beta \sin \Lambda_{1/4})$$

The windward wing has $V'_n > V_n$ and vice versa; therefore, it provides $\Delta Lift$ as the restoring moment in conjunction with the lift decrease on the leeward wing. As $\Lambda_{1/4}$ increases, the restoring moment becomes powerful enough that it must be compensated for by the use of the wing anhedral.

12.5 Current Statistical Trends for H- and V-Tail Coefficients

During Phase 1 (conceptual design) of an aircraft design project, the initial empennage is sized using statistical data. Section 3.20 provides preliminary statistics of the empennage tail-volume coefficients. Figure 12.11 provides additional statistics for current aircraft (twenty-one civil and nine military aircraft types), plotted

separately for the H-tail and the V-tail. Statistics for aircraft using FBW are included in the figure. It is advised that readers create separate plots to generate their own aircraft statistics for the particular aircraft class in which they are interested to obtain an appropriate average value.

For civil aircraft designs, the typical H-tail area is about a quarter of the wing reference area. The V-tail area varies from 12% of the wing reference area, S_w , for large, long aircraft to 20% for smaller, short aircraft. There may be minor changes in empennage sizing when more detailed analyses are carried out in Phase 2 of the design.

Military aircraft require more control authority for greater maneuverability and they have shorter tail arms that require larger tail areas. The H-tail area is typically about 30 to 40% of the wing reference area. The V-tail area varies from 20 to 25% of the wing reference area. Supersonic aircraft have a movable tail for control. If a V-tail is too large, then it is divided in two halves.

Modern aircraft with FBW technology can operate with more relaxed stability margins, especially for military aircraft designs; therefore, they require smaller empennage areas compared to older conventional designs (see [Figure 12.18](#)).

In this book, trim surfaces are earmarked and not sized. Designers must ensure that there is adequate trim authority (i.e., the trim should not run out) in any condition. This is typically accomplished in Phase 2 after the configuration is finalized.

12.6 Inherent Aircraft Motions as Characteristics of Design

Once an aircraft is built, its flying qualities are the result of the effects of its mass (i.e., inertia), CG location, static margin, wing geometry, empennage areas, and control areas. Flying qualities are based on a pilot's assessment of how an aircraft behaves under applied forces and moments. The level of ease or difficulty in controlling an aircraft is a subjective assessment by a pilot. In a marginal situation, recorded test data may satisfy airworthiness regulations yet may not prove satisfactory to the pilot. Typically, several pilots evaluate aircraft flying qualities to resolve any debatable points.

It is important that the design maintain flying qualities within preferred levels by shaping the aircraft appropriately. Whereas theoretical analyses help to minimize discrepancies, flying qualities can be determined only by actual flight tests. Like any other system analysis, control characteristics are rarely amenable to the precise theory due to a lack of exact information about the system. Therefore, accurate design information is required to make predictions with minimal error. It is cost-intensive to generate accurate design information, such as the related design coefficients and derivatives required to make theoretical analyses, which are conducted more intensively during Phase 2 of a project. Practically all modern aircraft incorporate active control technology (ACT) to improve flying qualities. This is a routine design exercise and provides considerable advantage in overcoming any undesirable behavior, which is automatically and continuously corrected.

Described herein are six important flight dynamics of particular design interest. They are based on fixed responses associated with small disturbances, making

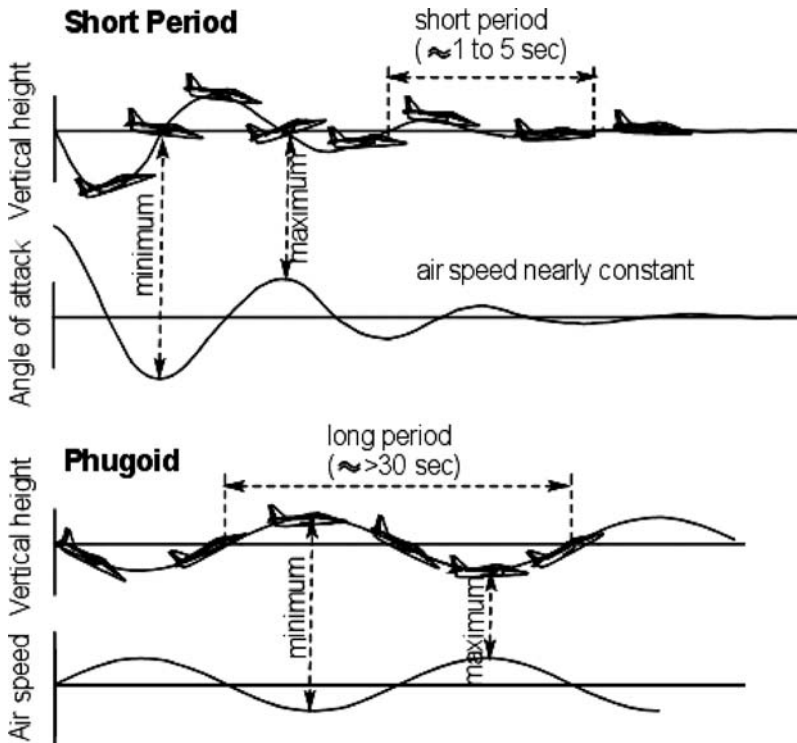


Figure 12.12. Short-period oscillations and phugoid motion

the rigid-body aircraft motion linearized. Military aircraft have additional considerations as a result of nonlinear, hard maneuvers, which are discussed in [Section 12.9](#). The six flight dynamics are as follows:

- short-period oscillation
- phugoid motion (long-period oscillation)
- Dutch roll
- slow spiral
- roll subsidence
- spin

12.6.1 Short-Period Oscillation and Phugoid Motion

The diagrams in [Figure 12.12](#) show an exaggerated aircraft flight path (i.e., altitude changes in the pitch plane). In the pitch plane, there are two different types of aircraft dynamics that result from the damping experienced when an aircraft has a small perturbation. The two longitudinal modes of motion are as follows:

1. *Short-period oscillation* (SPO) is associated with pitch change (α change) in which the H-tail plane acts as a powerful damper (see [Figure 12.1](#)). If a disturbance (e.g., a sharp flick of the elevator and return) causes the aircraft to enter this mode, then recovery is also quick for a stable aircraft. The H-tail acts

like an aerodynamic spring that naturally returns to equilibrium. The restoring moment comes from the force imbalance generated by the angle of attack, α , created by the disturbance. Damping (i.e., resistance to change) comes as a force generated by the tail plane, and the stiffness (i.e., force required) comes from the stability margin. The heavy damping of the H-tail resists changes to make a quick recovery.

The bottom diagram of a short period in Figure 12.12 plots the variation of the angle of attack, α , with time. All aircraft have a short-period mode and it is not problematic for pilots. A well-designed aircraft oscillatory motion is almost unnoticeable because it damps out in about one cycle. Although aircraft velocity is only slightly affected, the angle of attack, α , and the vertical height are related. Minimum α occurs at maximum vertical displacement and maximum α occurs at about the original equilibrium height. The damping action offered by the H-tail quickly smooths out the oscillation; that is, one oscillation takes a few seconds (typically, 1 to 5 s). The exact magnitude of the period depends on the size of the aircraft and its static margin. If the H-tail plane area is small, then damping is minimal and the aircraft requires more oscillations to recover.

2. *Phugoid motion* is the slow oscillatory aircraft motion in the pitch plane, as shown in the bottom diagram in Figure 12.12. It is known as the *long-period oscillation* (LPO) – the period can last from 30 s to more than 1 min. Typically, a pilot causes the LPO by a slow up and down movement of the elevator. In this case, the angle of attack, α , remains almost unchanged while in the oscillatory motion. The aircraft exchanges altitude gain (i.e., increases in potential energy [PE]) for decreases in velocity (i.e., decreases in kinetic energy [KE]). The phugoid motion has a long period, during which time the KE and PE exchange. Because there is practically no change in the angle of attack, α , the H-tail is insignificant in the spring-mass system. Here, another set of spring-mass is activated but is not shown in schematic form (it results from the aircraft configuration and inertia distribution – typically, it has low damping characteristics). These oscillations can continue for a considerable time and fade out comparatively slowly.

The frequency of a phugoid oscillation is inversely proportional to an aircraft's speed. Its damping also is inversely proportional to the aircraft L/D ratio. A high L/D ratio is a measure of aircraft performance efficiency. Reducing the L/D ratio to increase damping is not preferred; modern designs with a high L/D ratio incorporate automatic active control (e.g., FBW) dampers to minimize a pilot's workload. Conventional designs may have a dedicated automatic damper at a low cost. Automatic active control dampers are essential if the phugoid motion has undamped characteristics.

All aircraft have an inherent phugoid motion. In general, the slow motion does not bother a pilot – it is easily controlled by attending to it early. The initial onset, because it is in slow motion, sometimes can escape a pilot's attention (particularly when instrument-flying), which requires corrective action and contributes to pilot fatigue.

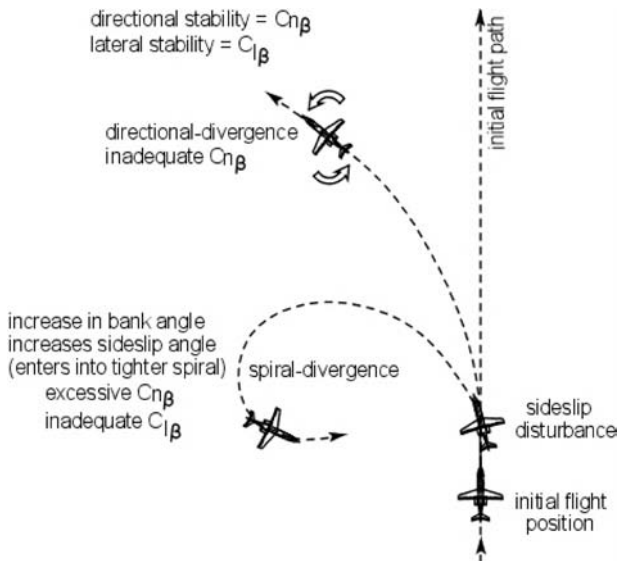


Figure 12.13. Spiral mode of motion showing divergence

12.6.2 Directional and Lateral Modes of Motion

Aircraft motion in the directional (i.e., yaw) and the lateral (i.e., roll) planes is coupled with sideslip and roll; therefore, it is convenient to address the lateral and directional stability together. These modes of motion are relatively complex in nature. FAR 23, Sections 23–143 to 23.181, address airworthiness aspects of these modes of motion. Spinning is perceived as a post-stall phenomenon and is discussed separately in [Section 12.7](#).

The four typical modes of motion are (1) directional divergence, (2) spiral, (3) Dutch roll, and (4) roll subsidence. The limiting situation of directional and lateral stability produces two types of motion. When yaw stability is less than roll stability, the aircraft can enter directional divergence. When roll stability is less than yaw stability, the aircraft can enter spiral divergence. [Figure 12.13](#) shows the two extremes of directional and spiral divergence. The Dutch roll occurs along the straight initial path, as shown in [Figure 12.14](#).

The wing acts as a strong damper to the roll motion; its extent depends on the wing aspect ratio. A large V-tail is a strong damper to the yaw motion. It is important to understand the role of damping in stability. When configuring an aircraft, designers need to optimize the relationship between the wing and V-tail geometries. The four modes of motion are as follows:

1. *Directional Divergence.* This results from directional (i.e., yaw) instability. The fuselage is a destabilizing body, and if an aircraft does not have a sufficiently large V-tail to provide stability, then sideslip increases accompanied by some roll, with the extent depending on the roll stability. The condition can continue until the aircraft is broadside to the relative wind, as shown in [Figure 12.13](#).
2. *Spiral.* However, if the aircraft has a large V-tail with a high degree of directional (i.e., yaw) stability but is not very stable laterally (i.e., roll) (e.g., a low-wing aircraft with no dihedral or sweep), then the aircraft banks as a result of rolling while sideslipping.

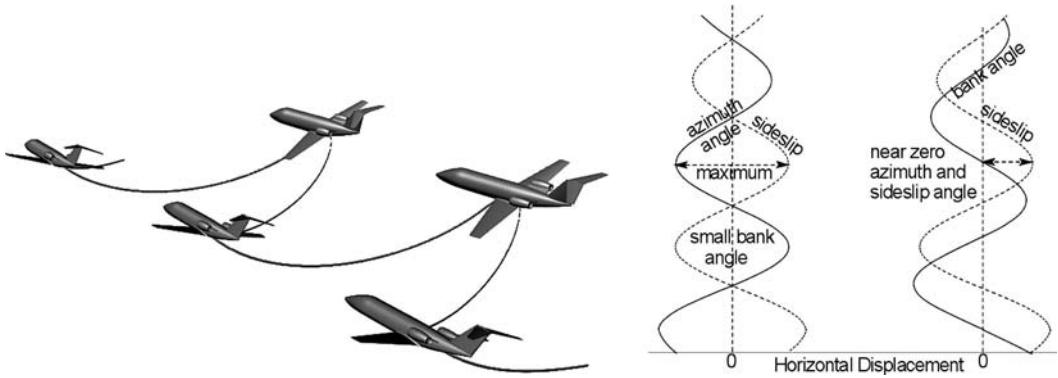


Figure 12.14. Dutch roll motion

This is a nonoscillatory motion with characteristics that are determined by the balance of directional and lateral stability. In this case, when an aircraft is in a bank and sideslipping, the side force tends to turn the plane into the relative wind. However, the outer wing is traveling faster, generating more lift, and the aircraft rolls to a still higher bank angle. If poor lateral stability is available to negate the roll, the bank angle increases and the aircraft continues to turn into the sideslip in an ever-increasing (i.e., tighter) steeper spiral, which is *spiral divergence* (see Figure 12.13). In other words, spiral divergence is strongly affected by C_{lr} .

The initiation of a spiral is typically very slow and is known as a *slow spiral*. The time taken to double the amplitude from the initial state is long – 20 s or more. The slow buildup of a spiral-mode motion can cause high bank angles before a pilot notices an increase in the g -force. If a pilot does not notice the change in horizon, this motion may become dangerous. Night-flying without proper experience in instrument-flying has cost many lives due to spiral divergence. Trained pilots should not experience the spiral mode as dangerous – they would have adequate time to initiate recovery actions. A 747 has a nonoscillatory spiral mode that damps to half amplitude in 95 s under typical conditions; many other aircraft have unstable spiral modes that require occasional pilot input to maintain a proper heading.

3. **Dutch Roll.** A dutch roll is a combination of yawing and rolling motions, as shown in Figure 12.14. It can happen at any speed, developing from the use of the stick (i.e., aileron) and rudder, which generate a rolling action when in yaw. If a sideslip disturbance occurs, the aircraft yaws in one direction and, with strong roll stability, then rolls away in a counter motion. The aircraft “wags its tail” from side to side, so to speak. The term *Dutch roll* derives from the rhythmic motion of Dutch iceskaters swinging their arms and bodies from side to side as they skate over wide frozen areas.

When an aircraft is disturbed in yaw, the V-tail performs a role analogous to the H-tail in SPO; that is, it generates both a restoring moment proportional to the yaw angle and a resisting, damping moment proportional to the rate of yaw. Thus, one component of the Dutch roll is a damped oscillation in yaw. However, lateral stability responds to the yaw angle and the yaw rate by rolling the wings of the aircraft. Hence, the second component of a Dutch roll is an

oscillation in a roll. The Dutch-roll period is short – on the order of a few seconds.

In other words, the main contributors to the Dutch roll are two forms of static stability: the directional stability provided by the V-tail and the lateral stability provided by the effective dihedral and sweep of the wings – both forms offer damping. In response to an initial disturbance in a roll or yaw, the motion consists of a combined lateral–directional oscillation. The rolling and yawing frequencies are equal but slightly out of phase, with the roll motion leading the yawing motion.

Snaking is a pilot term for a Dutch roll, used particularly at approach and landing when a pilot has difficulty aligning with the runway using the rudder and ailerons. Automatic control using yaw dampers is useful in avoiding the snaking/Dutch roll. Today, all modern transport aircraft have some form of yaw damper. The FBW control architecture serves the purpose well.

All aircraft experience the Dutch-roll mode when the ratio of static directional stability and dihedral effect (i.e., roll stability) lies between the limiting conditions for spiral and directional divergences. A Dutch roll is acceptable as long as the damping is high; otherwise, it becomes undesirable. The characteristics of a Dutch roll and the slow spiral are both determined by the effects of directional and lateral stability; a compromise is usually required. Because the slow-spiral mode can be controlled relatively easily, slow-spiral stability is typically sacrificed to obtain satisfactory Dutch-roll characteristics.

High directional stability ($C_{n\beta}$) tends to stabilize the Dutch-roll mode but reduces the stability of the slow-spiral mode. Conversely, a large, effective dihedral (rolling moment due to sideslip, $C_{l\beta}$) stabilizes the spiral mode but destabilizes the Dutch-roll motion. Because sweep produces an effective dihedral and because low-wing aircraft often have excessive dihedral to improve ground clearance, Dutch-roll motions often are poorly damped on swept-wing aircraft.

4. *Roll Subsidence.* The fourth lateral mode is also nonoscillatory. A pilot commands the roll rate by application of the aileron. Deflection of the ailerons generates a rolling moment, but the aircraft has a roll inertia and the roll rate builds up. Very quickly, a steady roll rate is achieved when the rolling moment generated by the ailerons is balanced by an equal and opposite moment proportional to the roll rate. When a pilot has achieved the desired bank angle, the ailerons are neutralized and the resisting rolling moment very rapidly damps out the roll rate. The damping effect of the wings is called *roll subsidence*.

12.7 Spinning

Spinning of an aircraft is a post-stall phenomenon (see [5]). An aircraft stall occurs in the longitudinal plane. Unavoidable manufacturing asymmetry in geometry and/or asymmetric load application makes one wing stall before the other. This creates a rolling moment and causes an aircraft to spin around the vertical axis, following a helical trajectory while losing height – even though the elevator has maintained in an up position. The vertical velocity is relatively high (i.e., descent speed on the order of 30 to 60 m/sec), which maintains adequate rudder authority, whereas the wings have stalled, losing aileron authority. Therefore, recovery from a spin is by

the use of the rudder, provided it is not shielded by the H-tail (see Section 4.9). After straightening the aircraft with the rudder, the elevator authority is required to bring the aircraft nose down in order to gain speed and exit the stall.

Spinning is different than spiraling; it occurs in a helical path and not in a spiral. In a spiral motion, there is a large bank angle; in spinning, there is only a small bank angle. In a spiral, the aircraft velocity is sufficiently high and recovery is primarily achieved by using opposite ailerons. Spin recovery is achieved using the rudder and then the elevator.

There are two types of spin: a steep and a flat-pitch attitude of an aircraft. The type of spin depends on the aircraft inertia distribution. Most general-aviation aircraft have a steep spin with the aircraft nose pointing down at a higher speed, making recovery easy – in fact, the best aircraft recover on their own when the controls are released (i.e., hands off). Conversely, the rudder authority in a flat spin may be low. A military aircraft with a wider inertia distribution can enter into a flat spin from which recovery is difficult and, in some cases, impossible. A flat spin for transport aircraft is unacceptable. Records show that the loss of aircraft in a flat spin is primarily from not having sufficient empennage authority in the post-stall wake of the wing.

The prediction of aircraft-spinning characteristics is still not accurate. Although theories can establish the governing equations, theoretical calculations are not necessarily reliable because too many variables are involved that require accurate values not easily obtainable. Spin tunnels are used to predict spin characteristics, but the proper modeling on a small scale raises questions about its accuracy. In particular, the initiation of the spin (i.e., the throwing technique of the model into the tunnel) is a questionable art subjected to different techniques. On many occasions, spin-tunnel predictions did not agree with flight tests; there are only a few spin tunnels in the world.

The best method to evaluate aircraft spinning is in the flight test. This is a relatively dangerous task for which adequate safety measures are required. One safe method is to drop a large “dummy” model from a flying “mother” aircraft. The model has onboard, real-time instrumentation with remote-control activation. This is an expensive method. Another method is to use a drag chute as a safety measure during the flight test of the piloted aircraft. Spin tests are initiated at a high altitude; if a test pilot finds it difficult to recover, the drag chute is deployed to pull the aircraft out of a spin. The parachute is then jettisoned to resume flying. If a test pilot is under a high g -strain, the drag chute can be deployed by ground command, where the ground crew maintains real-time monitoring of the aircraft during the test. Some types of military aircraft may not recover from a spin once it has been established. If a pilot does not take corrective measures in the incipient stage, then ejection is the routine procedure. FBW technology avoids entering spins because air data recognize the incipient stage and automatic-recovery measures take place.

12.8 Design Considerations for Stability: Civil Aircraft

From the discussion on aircraft behavior in a small disturbance, it is clear that both aircraft geometry and mass distribution are important in the design of an aircraft with satisfactory flying qualities. The position of the CG is obtained by arranging the

aircraft components relative to one another to suit good in-flight static stability and on-ground stability for all operational envelopes. The full aircraft and its component moments are estimated semi-empirically (e.g., DATCOM and RAE data sheets) as soon as drawings are available and followed through during the next phase; the prediction is improved through wind-tunnel tests and CFD analyses. In the conceptual design stage, the control area on the wing and empennage (i.e., flap, aileron, rudder, and elevator) are sized empirically from past experience (and DATCOM and RAE data sheets). However, the CG position relative to the aircraft NP is tuned afterwards.

Chapter 6 describes the aerodynamic design of major aircraft components. Chapter 11 considers the sizing of the wing and empennage and also establishes the matched-engine size. Whereas statistics of past designs proved vital for configuring the empennage, the placement of components relative to one another is based on a designer's experience, which forms a starting point for the conceptual design phase.

The important points affecting aircraft configuration are reviewed as follows:

1. *Fuselage*. The fuselage has a destabilizing effect – the fuselage lift (although minimal) and moment add to instability – and its minimization is preferred. In addition to keeping costs down, the fuselage may be kept straight (with the least camber). Mass distribution should keep inertia close to the fuselage centerline. A BWB requires special considerations.

The fuselage length and width are determined from the payload specifications. The length-to-average-diameter ratio for the baseline aircraft version may be around 10. The closure angles are important, especially the gradual closure of the aft end, which should not have an upsweep of more than what is necessary – even for a rear-loading door arrangement that must have an upsweep. The front closure is blunter and must provide adequate vision polar without excessive upper-profile curvature.

For a pressurized cabin, the cross-section should be maintained close to the circular shape. Vertical elongation of the cross-section should be at a minimum to accommodate the below-floorspace requirements. For small aircraft, fuselage-depth elongation may be due to placement of the wing box; for larger aircraft, it may be due to the container size. Care must be taken so that the wing box does not interfere with the interior cabin space. Generous fairing at the wing–body junction and for the fuselage-mounted undercarriage bulge is recommended. An unpressurized fuselage may have straight sides (i.e., a rectangular cross-section) to reduce the production costs. In general, a rectangular fuselage cross-section is used in conjunction with a high wing. The undercarriage for a high-wing aircraft has a fuselage bulge.

2. *Wing*. Typically, an isolated wing has a destabilizing effect unless it has a reflex at the trailing edge (i.e., the tail is integrated into the wing such as all-wing aircraft like the delta wing and BWB). The larger the wing camber, the more significant is the destabilizing effect. Optimizing an aerofoil with a high L/D ratio and with the least C_{m_wing} is a difficult task not discussed herein. Wind-tunnel tests and CFD analyses are the ways to compromise. It is assumed that aerodynamicists have found a suitable aerofoil with the least destabilizing moment for

the best L/D ratio. The coursework worked-out example uses an aerofoil from the proven NACA series.

Sizing of an aircraft, as described in [Chapter 11](#), determines the wing reference area. The structures philosophy settles the aspect ratio; that is, maximizing the wing aspect ratio is the aim but at the conceptual design stage, it starts with improving on past statistics on which a designer can be confident of its structural integrity under load. The wing sweep is obtained from the design maximum cruise speed. It has been found that, in general, a wing-taper ratio from 0.4 to 0.5 is satisfactory. The twist and dihedral in the conceptual design stage are based on past experience and data sheets.

Positioning of the wing relative to the fuselage depends on the mission role, but it is sometimes influenced by a customer's preference. A high- or low-wing position affects stability in opposite ways (see [Figure 12.6](#)). The wing dihedral is established in conjunction with the sweep and position relative to the fuselage. Typically, a high-wing aircraft has an anhedral and a low-wing aircraft has a dihedral, which also assist in ground clearance of the wing tips. In extreme design situations, a low-wing aircraft can have an anhedral (see [Figure 12.7](#)) and a high-wing aircraft can have a dihedral. There are case-based “gull-wing” designs, which are typically for “flying boats.” Passenger-carrying aircraft are predominantly low-winged but there is no reason why they should not have high wings; a few successful designs exist. Wing-mounted, propeller-driven aircraft favor a high wing for ground clearance, but there are low-wing, propeller-driven aircraft with longer undercarriage struts. Military transport aircraft invariably have a high wing to facilitate the rear-loading of bulky items.

3. *Nacelle*. The stability effects of a nacelle are similar to those of a fuselage. An isolated nacelle is destabilizing but, when integrated to the aircraft, its position relative to the aircraft CG determines its effect on the aircraft. That is, an aft-mounted nacelle increases stability and a forward-mounted nacelle on a wing decreases stability. The stability contribution of a nacelle also may be throttle-dependent (i.e., engine-power effects).

The position of the nacelle on an aircraft is dictated by the aircraft size. The best position is on the wing, thereby providing bending relief during flight. The large forward overhang of a nacelle decreases air-flow interference with the wing. For smaller aircraft, ground clearance mitigates against wing-mounting; for these aircraft, nacelles are mounted on the aft fuselage. An over-wing nacelle mount for smaller aircraft is feasible – a practice yet to gain credence. Even a fuselage-mounted nacelle must adjust its position relative to how close the vertical height is from the aircraft CG without jet efflux interfering with the empennage in proximity.

4. *Fuselage, Wing, and Nacelle*. It is good practice to assemble these three components without the empennage in order to verify the total moment in all three planes of reference. The CG position is established with the empennage installed; then it is removed for a stability assessment. This helps to design the empennage as discussed herein. [Figure 12.10](#) shows the typical trends of pitching moments of the isolated components; together, they will have a destabilizing effect (i.e., positive slope). The aim is to minimize the slope – that is, the least destabilizing moment.

Equation 12.2 provides insight to the pitching-moment contribution from the geometrical arrangement. It shows that minimizing the vertical distance of the components from the aircraft CG also minimizes their pitching-moment contributions.

5. *Empennage*. The empennage configuration is of primary importance in an aircraft design. The reference sizes are established by using statistical values of tail-volume coefficients, but the positioning and shaping of the empennage require considerable study. This is another opportunity to check whether the statistical values are adequate. The sweeping of the empennage increases the tail arm and may also enhance the appearance; even low-speed, smaller aircraft incorporate sweep. Chart 4.2 and Figures 4.24 and 4.25 show several possible empennage configurations.

A conventional aircraft H-tail has a negative camber, the extent depending on the moment produced by an aircraft's tail-less configuration, as described previously. For larger, wing-mounted turbofan aircraft, the best position is a low H-tail mounted on the fuselage, the robust structure of which can accommodate the tail load. A T-tail on a swept V-tail increases the tail arm but should be avoided unless it is essential, such as when dictated by an aft-fuselage-mounted engine. T-tail drag is destabilizing and requires a larger area if it is in the wing wake at nearly stalled attitudes. The V-tail requires a heavier structure to support the T-tail load. Smaller turbofan aircraft are constrained with aft-fuselage-mounted engines, which force the H-tail to be raised up from the middle to the top of the V-tail. The canard configuration affords more choices for the aircraft CG location. In general, if an aircraft has all three surfaces (i.e., canard, wing, and H-tail), then they can provide lift with a positive camber of their sectional characteristics. It is feasible that future civil aircraft designs of all sizes may feature a canard.

Typically, a V-tail has a symmetric aerofoil but for propeller-driven airplanes, it may be offset by 1 or 2 deg to counter the skewed flow around the fuselage (as well as gyroscopic torque).

The discussion is the basis for the design of any other type of empennage configuration, as outlined in Table 4.2. If a designer chooses a twin-boom fuselage, the empennage design must address the structural considerations of twin booms. (Tail-less aircraft are less maneuverable.)

An H-tail also can be dihedral or adhedral, not necessarily for stability reasons but rather to facilitate positional clearances, such as to avoid jet efflux.

6. *Undercarriage*. A retracted undercarriage does not contribute to the aerodynamic load but when it is extended, it generates substantial drag, creating a nose-down moment. To address this situation, there should be sufficient elevator nose-up authority at a near-stall, touch-down attitude, which is most critical at the forwardmost CG position. Designers must ensure that there is adequate trim authority (i.e., the trim should not run out) in this condition.
7. *Use of Any Other Surface*. It is clear how stability considerations affect aircraft configurations. Despite careful design, an aircraft prototype may show unsatisfactory flying qualities when it is flight-tested. Then, additional surfaces (e.g., ventral fin and delta fin) may be added to alleviate the problem. Figure 12.15 shows two examples of these modifications. It is preferable to avoid the need for additional surfaces, which add penalties in both weight and drag.

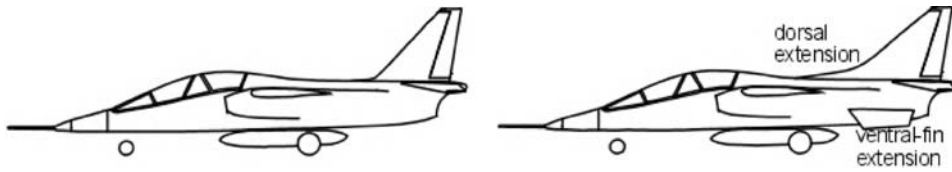


Figure 12.15. Aircraft configurations with modifications of additional surfaces

12.9 Military Aircraft: Nonlinear Effects

A discussion on military aircraft nonlinear effects is found at the Cambridge University Web site.

Figure 12.16. Typical modern fighter aircraft

12.10 Active Control Technology: Fly-by-Wire

It is clear that stability considerations are important in aircraft-design configurations. Although the related geometrical parameters are from statistical data of past designs and subsequently sized, this chapter provides a rationale for their role in the conceptual design stage. It also has been shown that to control inherent aircraft motions, feedback-control systems such as a *stability augmentation system* (SAS) (e.g., a yaw damper) and a *control augmentation system* (CAS) have been routinely deployed for some time. In this final section, the rationale continues with a discussion on how the feedback-control system has advanced to the latest technologies, such as FBW and fly-by-light (FBL), known collectively as ACT. Today, almost all types of larger aircraft incorporate some form of ACT.

The advantages of FBW are discussed in various sections of this book; the concept is not new. FBW is basically a feedback-control system based on the use of digital data. Figure 12.17 shows the control of one axis, which can be used for all three axes. Earlier SAS and CAS had mechanical linkage from the pilot to the controls; FBW does not have the direct linkage (hence, the name). It permits the transmission of several digital signal sources through one communications system, known as *multiplexing*. A microprocessor is in the loop that continuously processes air data (i.e., flight parameters) to keep an aircraft in a preferred motion with or without pilot commands. Aircraft-control laws – algorithms relating a pilot’s

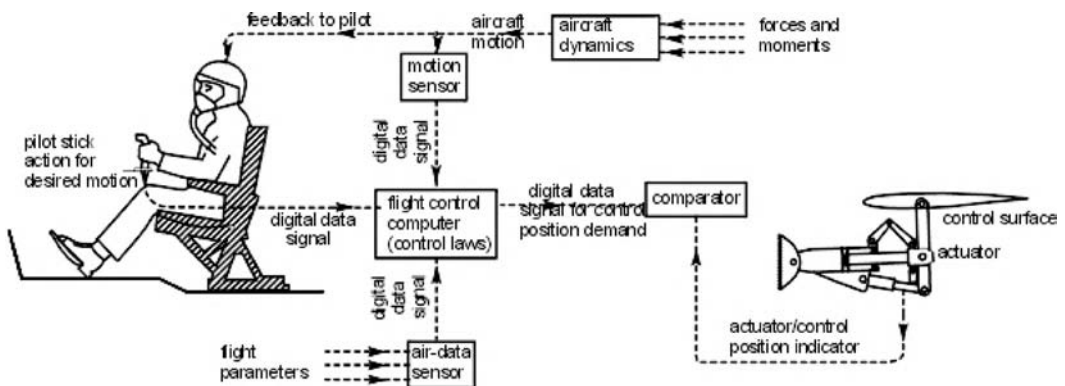


Figure 12.17. A schematic diagram of FBW

command to the control-surface demand and aircraft motion, height, and speed, which involve equations of motion, aircraft coefficients, and stability parameters – are embedded in the computer to keep the aircraft within the permissible flight envelope. Under the command of a human pilot, the computer acts as a subservient flier. The computer continuously monitors aircraft behavior and acts accordingly, ensuring a level of safety that a human pilot cannot match.

Figure 12.17 is a schematic diagram of the FBW feedback arrangement for pitch control. The flight-control computer takes the pilot's steering commands, which are compared to the commands necessary for aircraft stability to ensure safety and that control surfaces are activated accordingly. Air data are continually fed to the computers (i.e., speed, altitude, and attitude). Built into the computer are an aircraft's limitations, which enables it to calculate the optimum control-surface movements. Steering commands are no longer linked mechanically from the cockpit to the control surface but rather via electrical wiring. FBW flight-control systems seem to be the ideal technology to ensure safety and reduce a pilot's workload.

Because analog point-to-point wire bundles are an inefficient and cumbersome means of interconnecting sensors, computers, actuators, indicators, and other equipment onboard a modern military aircraft, a serial digital multiplex data bus was developed. MIL-STD-1553 (in use since 1983) defines all aspects of the bus (i.e., a subsystem of electrical lines for communication, named after electrical bus bars); therefore, many groups working with the military have adopted it. The MIL-STD-1553 multiplex data bus provides an integrated, centralized system control and a standard interface for all equipment connected to the bus. The bus concept provides a means by which all traffic is available and can be accessed using a single connection for testing and interfacing with the system.

FBW reacts considerably faster than a conventional control system and does not encounter fatigue problems. A strong driver for incorporating FBW in military-aircraft design is the ability to operate at relaxed stability (even extending to a slightly unstable condition) used for rapid maneuver (increased agility) as a result of minimal stiffness in the system. It is difficult for a typical pilot to control an unstable aircraft without assistance; a computer is needed and a regulator supplies the necessary stability. This system does not generate the natural stability of a conventional aircraft but automatically trims the aircraft to the preferred flight conditions. Progress in FBW systems depends to a great extent on the progress of onboard computer power.

An aircraft flying under relaxed stability using FBW does not have the same requirement for geometrical features to provide low stiffness and damping. Hence, stability and control-surface sizing are different than in a conventional design: They are smaller and, hence, lighter with less drag. This is what is meant by a CCV.

Stable designs already have a down-pitching force because of the position of the NP aft of the CG. Any balancing force must be generated by a larger downward lift of the H-tail. Again, this decreases the maximum possible lift and increases the trim drag. In an unstable layout (e.g., the CG moving aft), the elevator's lift is directed upward to counterbalance the moment. In this way, the aircraft's total lift is increased; the aircraft wing therefore can be designed to be smaller and lighter and still provide the same performance. There is another benefit from the use of an unstable design: In addition to the aircraft's increased agility, there is a reduction in drag and weight.

Table 12.1. *Conventional and CCV comparison*

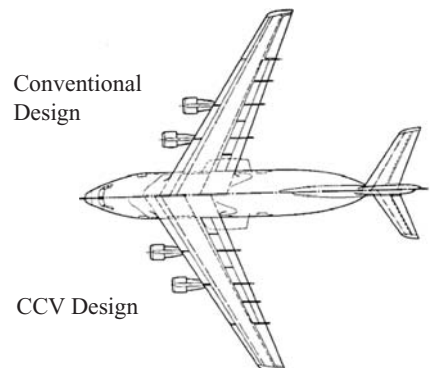
	Conventional	CCV
MTOM (kg)	38,000	38,000
OEM (kg)	27,490	26,764
S_w (m ²)	130	130
S_H (m ²)	26	15.8
Payload (kg)	5,000	5,730
CG range (-%MAC)	15–35	32–53

The difference between a conventional and a CCV design is shown in Table 12.1 and Figure 12.18 (see [13]) for longitudinal stability. The wing area and MTOM of both designs were unchanged; the CCV design yielded a smaller H-tail area with a larger CG range. The directional stability exhibits similar gains with a smaller V-tail area, thereby further reducing the OEM and permitting a bigger payload.

In summary, FBW provides considerable advantages, as follows:

- a simple and flexible system architecture although its design is complex
- consistent handling
- automatic stabilization
- safe maneuvering to the envelope limits
- ability to integrate with a wide range of designs (e.g., slats and swing-wing)
- ability to integrate with engine control through FADEC and the thrust vector
- use of side stick controller – provides free space in the cockpit layout and weight-saving
- incorporates relaxed stability for rapid maneuver, yet uses smaller control surfaces
- permits complex configurations for stealth aircraft, which may not be favorable for aerodynamic considerations leading to unstable aircraft (e.g., the F117 Nighthawk)
- digital data-handling allows multiplexing, which saves weight
- overall weight reduction
- allows standardization
- failure detection
- fault isolation
- built-in tests and monitoring

Figure 12.18. Comparison between a conventional and a CCV design



FBW has been in use for nearly a half-century but the obvious advantages were kept secret for a long time for military reasons. Early development in the pioneering stages progressed slowly with some mishaps. Nearly two decades later, civil aviation took bold steps and Aircraft Radio Inc. (ARINC) standards emerged to control FBW designs. The Airbus was the first aircraft to incorporate full FBW in a major project. The mid-sized A320 twin-jet aircraft is the first commercial transport aircraft to incorporate full FBW without manual override. The Habsheim (June 26, 1988) and the Bangalore (February 14, 1990, near the author's residence) disasters posed many questions; however, practically all mid-sized and larger transport aircraft currently incorporate some form of FBW technology.

The FBW system architecture has built-in redundancies. During the 1980s, such systems had quadruple-redundant architecture in which each system works independently. Nowadays, with improved reliability, a triplex system (with voting and consolidation) dominates design. FBW can be applied to one, two, or all three axes of control; modern systems incorporate all three. MIL-STD-1553 specifies that all devices in the system must be connected to a redundant pair of buses, which provides a second path for bus traffic if one bus is damaged. Signals are allowed to appear only on one of the two buses at a time. If a message cannot be completed on one bus, the bus controller may switch to the other bus. In some applications, more than one bus may be implemented on a given aircraft.

To avoid electromagnetic interference, the use of fiber optics for signaling using light was developed recently. Aptly, it is called FBL and is guided by MIL-STD-1773.

In summary, FBW and FBL designs offer weight reduction with a smaller wing and empennage, fewer control surfaces, less cabling, and the elimination of mechanical linkages. As a consequence, drag is reduced. In addition, FBW and FBL designs provide enhanced safety and reliability as well as improved failure detection.

13 Aircraft Performance

13.1 Overview

This chapter assesses whether the aircraft being configured, thus far, meets the FAR and customer requirements given in the form of specifications. Coursework follows linearly from the mock market survey (see [Chapter 2](#)). Specification requirements addressed in this chapter include aircraft performance to meet the (1) TOFL, (2) LFL, (3) initial rate of climb, (4) maximum speed at initial cruise (especially for civil aircraft design), and (5) payload range. [Chapter 16](#) computes the aircraft DOC, which should follow the aircraft performance estimation.

Aircraft performance is a subject that aeronautical schools offer as a separate course. Therefore, to substantiate the FAR and customer requirements, this chapter addresses only what is required – that is, the related governing equations and computational examples associated with the five substantiation parameters listed previously. Substantiation of the payload range requires integrated performances of climb and descent that show fuel consumed, distance covered, and time taken for the flight segments. Integrated climb and descent performances are not specification requirements at this stage; therefore, their detailed computational examples are not provided. Instead, the final results in graphical form carry out the payload-range estimation. It is suggested that readers refer to appropriate textbooks for details on this topic. The turboprop example is not worked out but there is sufficient information to compute it similarly.

The remainder of the book after this chapter (except [Chapter 16](#)) presents information that aircraft designers should know and apply to their configurations. These topics may comprise the coursework of a second term following the finalized conceptual study in the first term. The discussion in [Section 13.7](#) is useful to readers.

13.1.1 What Is to Be Learned?

This chapter covers the following topics:

- Section 13.2: Preliminary information on aircraft performance
- Section 13.3: Engine performance graphs
- Section 13.4: Pertinent aircraft performance equations

- Section 13.5: Performance equations to substantiate Bizjet aircraft capabilities
- Section 13.6: Performance equations to substantiate AJT aircraft capabilities
- Section 13.7: Discussion in summary form

13.1.2 Coursework Content

Readers perform the following steps for their design projects:

- Step 1: Generate the appropriate engine performance graphs from the non-dimensional graphs provided in [Chapter 10](#).
- Step 2: Using the engine thrust thus obtained, compute the aircraft performances of the sized Bizjet and AJT as coursework exercises. (The instructor's assistance may be required to compute integrated climb, descent, and specific-range performances.)
- Step 3: If aircraft performance requirements are not met, then iterate the aircraft-configuration, sizing, and engine-matching exercises until they are. The spreadsheet method is helpful for the iterations.

13.2 Introduction

The final outcome of any design is to substantiate the performance it is intended to do. In the conceptual design phase, aircraft performance substantiation must be conducted mainly for those critical areas specified by the FAR and customer requirements; a full aircraft performance estimation is conducted subsequently (it is beyond the scope of this book). All worked-out aircraft performance estimations (i.e., Bizjet and AJT) use the standard day. Non-ISA-day performance computations are calculated in the same way using non-ISA-day data.

The sizing exercises in [Chapter 11](#) demonstrate a rapid-performance method to generate relationships between wing-loading (W/S_W) and thrust-loading (T_{SLS}/W) to obtain the sizing point that simultaneously satisfies the requirements of the TOFL and LFL, initial rate of climb capability, and maximum speed at initial cruise. The aircraft-sizing point gives the installed, maximum sea-level takeoff static thrust, $T_{SLS\,INSTALLED}$, of the matched engines. [Chapter 10](#) presents the generic, uninstalled-engine performances of rubberized engines in nondimensional form, from which the installed-engine performances are obtained.

This chapter develops available engine performance in terms of installed thrust and fuel-flow rates at various speeds and altitudes at the power settings of takeoff, maximum climb, and maximum cruise ratings at standard day, matched for the sized aircraft under study. Applying the installed-engine data, the chapter continues with more accurate computations of aircraft performance to substantiate requirements of the TOFL and LFL, initial rate of climb, maximum speed at initial cruise, and payload range. At this point, it may be necessary to revise the aircraft configuration if performance capabilities are not met. If the aircraft performance indicates a shortfall (or an excess) in meeting the requirements, the design is iterated for improvement. In coursework, normally one iteration is sufficient.

Finally, at the end of the design stage, the aircraft should be flight-tested over the full flight envelope, including various safety issues, to demonstrate compliance.

13.2.1 Aircraft Speed

Aircraft speed is a vital parameter in computing performance. It is measured using the difference between the total pressure, p_t , and the static pressure, p_s , expressed as $(p_t - p_s)$. Static pressure is the ambient pressure in which an aircraft is flying. The value of $(p_t - p_s)$ gives the dynamic head, which depends on the ambient air density, ρ . Unlike the ground speed of an automobile that is measured directly, an aircraft ground speed must be computed from $(p_t - p_s)$; a pilot reads the gauge that is converted from $(p_t - p_s)$. Following are various forms of aircraft air speed that engineers and pilots use. As shown, some computations are required – currently, onboard computers perform all computations:

V_i : The gauge reading as a pilot sees it in the flight deck; this is flight speed, which is not the same as ground speed. The instrument includes standard adiabatic compressible-flow corrections for high-subsonic flights at the sea-level standard day; however, it still requires other corrections.

V_I : This is the indicated air speed (IAS). Manufactured instruments have some built-in instrumental errors, ΔV_i (typically minor but important considerations when an aircraft is close to stall speed). Manufacturers supply the error chart for each instrument. The instrument is calibrated to read the correct ground speed at the sea-level standard day with compressibility corrections. When corrected, the instrument reads the IAS as

$$V_I = \text{IAS} = V_i + \Delta V_i$$

V_C : This is the calibrated air speed (CAS). Instrument manufacturers calibrate an uninstalled, bare instrument for sea-level conditions. Once it is installed on an aircraft and depending on where it is installed, the aircraft flow field distorts the instrument readings. Therefore, it requires position-error (ΔV_p) corrections by the aircraft manufacturers:

$$V_C = \text{CAS} = V_I + \Delta V_p = V_i + \Delta V_i + \Delta V_p$$

V_{EAS} : This is the equivalent air speed (EAS). Air density ρ changes with altitude – it decreases because atmospheric pressure decreases with a gain in altitude. Therefore, at the same ground speed (also known as true air speed [TAS]), the IAS reads lower values at higher altitudes. The mathematical relationship between the TAS and the EAS, reflecting the density changes with altitude, can be derived as $\text{TAS} = \text{EAS}/\sqrt{\sigma}$, where σ is the density ratio (ρ/ρ_0) in terms of the sea-level value, ρ_0 . The constant EAS has a dynamic head invariant. For high-subsonic flights, it requires adiabatic compressibility corrections (ΔV_c) for the altitude changes:

$$V_{\text{EAS}} = \text{EAS} = V_C + \Delta V_c = V_i + \Delta V_i + \Delta V_p + \Delta V_c = \text{TAS}\sqrt{\sigma}$$

T_{EAS} : TAS is the aircraft ground speed. Compressibility corrections for position errors are available; however, at this stage of design, the details can

Table 13.1. Summary of installed thrust and fuel-flow data per engine at three ratings

Rating	Altitude		Loss %	Scaling factor	T/T_{SLS}	sfc lb/lb/hr	Available uninstalled	Thrust (lb) installed	Fuel flow (lb/hr)
	ft	Mach							
Takeoff	0	0	7	3,315	1	0.498	3,560	3,315	1,772
Maximum Climb	1,000	0.38	6	3,346	0.670	0.700	2,373	2,231	1,661
Maximum Cruise	41,000	0.74	4	3,418	0.222	0.730	790	758	578

Note: All computations are based on $T_{SLS.UNINSTALLED} = 3,560$ lb per engine.

be omitted without any loss of conceptual design work undertaken in this book. Supersonic flight requires further adjustments.

13.3 Establish Engine Performance Data

The discussion in this section generates the available installed thrust and fuel-flow graphs matched for the worked-out, sized-aircraft examples (see Chapter 11): a Bizjet and an AJT. In addition, the performance data for a 1,140-shp turboprop engine are provided for readers to work out the associated aircraft performance.

Because the given sfc graphs are based on uninstalled thrust, the fuel-flow rates are computed using uninstalled thrust. Installation loss at cruise is approximately half the percentage loss at takeoff.

13.3.1 Turbofan Engine (BPR < 4)

Figures 10.45 through 10.47 provide the typical uninstalled turbofan thrust in nondimensional form in terms of T_{SLS} , along with the corresponding sfc for the Bizjet aircraft class. Section 11.6 establishes the requirement of an uninstalled matched $T_{SLS.UNINSTALLED} = 3,560$ lb per engine. Worked out herein and summarized in Table 13.1 are examples of installed thrust and fuel flows for the three engine ratings. The data are sufficient for the example used in this book; intermediate values may be interpolated linearly.

Takeoff Rating (Bizjet): Standard Day

Depending on how the ECS is managed, installation loss typically varies from 6 to 8% of the uninstalled, sea-level static thrust. If required, the air-conditioning can be turned off for a brief period until the undercarriage is retracted. Using a 7% installation loss at takeoff, Section 11.6 works out the matched installed $T_{SLS.INSTALLED} = 0.93 \times 3,560 = 3,315$ lbs per engine for the sized Bizjet. Figure 13.1 shows the installed engine thrust at the takeoff rating.

The fuel-flow rate is computed from the sfc of 0.498 lb/hr/lb at the sea-level, static condition (see Section 10.11.3). Using the uninstalled $T_{SLS} = 3,560$ lbs per engine, the fuel-flow rate is $3,560 \times 0.498 = 1,772$ lbs per hour per engine. Fuel flow is kept nearly constant at takeoff up to the enroute climb segment, when the engine is throttled down to the maximum climb rating (computed in the following section).

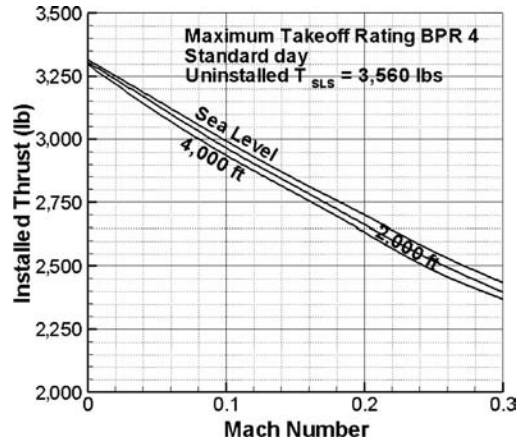


Figure 13.1. Installed takeoff performance per engine (\approx BPR 3 to 4)

Maximum Climb Rating (Bizjet): Standard Day

Figure 10.46 shows the uninstalled maximum climb thrust in nondimensional form in terms of T_{SLS} and fuel consumption (sfc) up to a 50,000-ft altitude for three Mach numbers. The installation loss during a climb is 6% of the uninstalled thrust. Using these graphs, the installed thrust and fuel-flow rates are plotted in Figure 13.2. This turbofan has a break in the fuel flow at a 5,000- to 10,000-ft altitude, depending on the flight Mach number, to keep the EGT within the limits, which results in a corresponding break in thrust generation (see Figure 13.2).

Equation 11.15 in Chapter 11 requires a factor k_2 to be applied to the T_{SLS} to obtain the initial climb thrust. In the example, k_2 is 1.5. Continuing with the coursework exercise, the uninstalled, initial climb thrust is $3,560/1.5 = 2,373$ lbs per engine and the installed thrust becomes $T_{SLS.INSTALLED} = 0.94 \times 2,373 = 2,231$ lbs per engine. Fuel flow at the initial climb is obtained from the sfc graph in Figure 10.46b. For the initial climb, the sfc is 0.7 pound per hour per pound, which results in a fuel flow of $0.7 \times 2,373 = 1,661$ lbs/hr per engine. Equations for the climb performance are derived in Section 13.4.3 and the coursework example is verified in Section 13.5.2. Estimation of the payload range requires the full aircraft climb performance up to the cruise altitude.

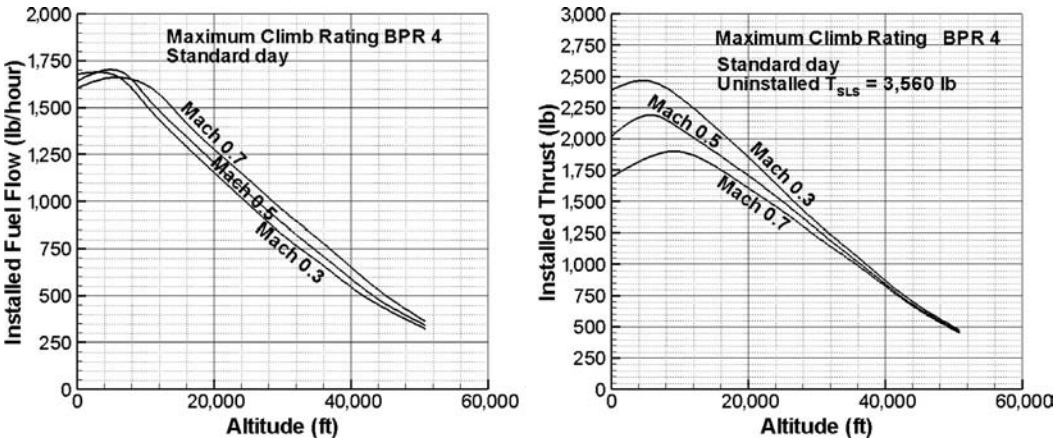


Figure 13.2. Installed maximum climb performance per engine (\approx BPR 4)

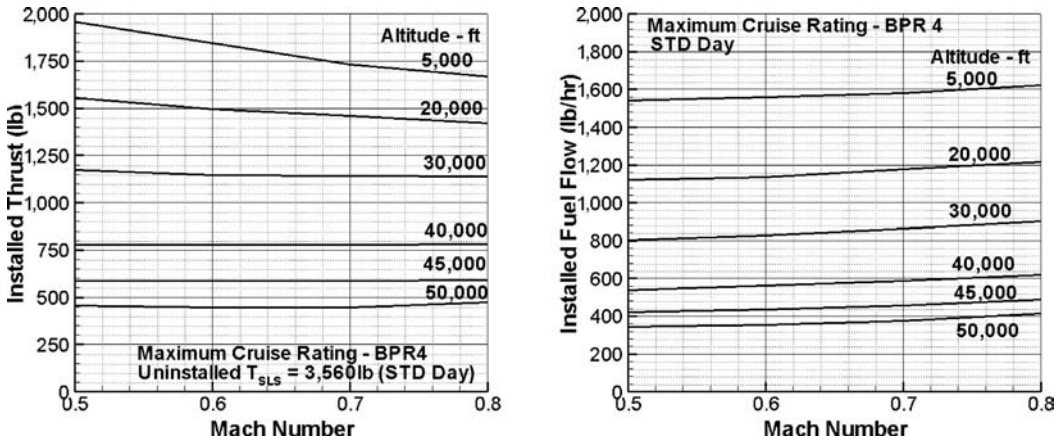


Figure 13.3. Installed maximum cruise performance per engine (\approx BPR 4)

Maximum Cruise Rating (Bizjet): Standard Day

Figure 10.47 shows the uninstalled maximum cruise thrust in nondimensional form and fuel consumption (sfc) from a 5,000- to 50,000-ft altitude for Mach numbers varying from 0.5 to 0.8. Figure 13.3 shows the installed-engine thrust at the maximum cruise rating for the sized Bizjet.

The coursework example specified an initial maximum cruise speed (i.e., HSC) of Mach 0.74 at 41,000 ft. From Figure 10.47, that point gives the uninstalled ratio $T/T_{SLS} = 0.222$ ($T_{SLS}/T = 4.5$). This is the k_I in Section 11.3.3 that results in an uninstalled thrust of $3,560 \times 0.222 = 790$ lbs per engine. Considering a 4% installation loss at cruise, the installed thrust of $T = 0.96 \times 790 = 758$ lbs per engine. Section 13.5.3 verifies whether the thrust is adequate for an aircraft to reach the maximum cruise speed. The fuel in Figure 13.4 (see Web at www.cambridge.org/Kundu) is $0.73 \times 790 = 577$ lb/hr per engine.

13.3.2 Turbofan Engine (BPR > 4)

Larger engines have a higher BPR. Current large operational turbofans have a BPR around 5 or 6 (new-generation turbofans have achieved a BPR > 8). These engines have performance characteristics slightly different than smaller engines – specifically, the maximum climb rating has no break in thrust with altitude gain. Using Figures 10.48 through 10.50, the installed thrust and fuel-flow rates can be worked out as in previous sections.

13.3.3 Military Turbofan (Advanced Jet Trainer/CAS Role – Very Low BPR) – STD Day

This extended section of the book can be found on the Web at www.cambridge.org/Kundu and presents a typical military turbofan-engine installed performance (with and without reheat) at maximum rating suited to the classroom example of an AJT and a derivative in a CAS role. The installed performance is computed from the graph given in Subsection 10.11.4.

Table 13.2. 30,000-ft altitude ($\rho = 0.00088$ slug/ft³, $\sigma = 0.37$) maximum climb

True air speed in knots	50	100	150	200
V in mph	57.54	115.08	172.62	230.16
$\text{SHP}_{\text{uninstall}}$ from Figure 10.43a $\times 1,075$	462	505	516	548
$J = 0.0046 \times \text{knots}$	0.264	0.528	0.792	1.055
$C_p = 0.000116 \times \text{SHP}$	0.138	0.150	0.154	0.163
η_{prop} (from Figure 10.35)	0.380	0.630	0.782	0.83
Uninstalled thrust, T (lb)	1,145	1,037	876	741
Installed thrust (lb)	1,098	996	842	712
Sfc (lb/hr/SHP) (Figure 10.43b)	0.475	0.472	0.465	0.445
Fuel-flow rate (lb/hr)	220	238	240	244

13.3.4 Turboprop Engine Performance

This type of turboprop engine is used in both civil and military aircraft design. The power settings are as in civil aircraft applications. Sizing of the Tucano class turboprop trainer aircraft requires a matched, installed engine $T_{\text{SLS}} = 4,000$ lbs. Section 10.11.2 presents the generic, uninstalled, turboprop engine performance in nondimensional form. Section 10.11.4 works out the propeller thrust from the turboprop engine and establishes that the rated engine power of $\text{SHP}_{\text{SLS}} = 1,075$ SHP (uninstalled) would develop as installed $T_{\text{SLS}} = 4,000$ lbs.

Thrust computations from the turboprop SHP is repetitious work, as shown in Section 10.11.4. In this section, one computation each at the maximum climb rating and the maximum cruise rating, both at a 30,000-ft altitude for four speeds, are given in Tables 13.2 and 13.3, respectively.

Takeoff Rating (Turboprop): Standard Day

The installed takeoff thrust of a turboprop is plotted in Figure 10.40. It is repeated in this section as Figure 13.5 to keep all available thrust graphs in one section. At the takeoff rating, engine power is kept nearly constant at a speed when the en-route climb can start at a reduced power setting of the maximum climb rating. The psfc of the turboprop at takeoff is 0.5 lb/hr/shp, based on uninstalled power. Therefore, at SHP_{SLS} , the fuel-flow rate is $0.5 \times 1,075 = 537.5$ lb/hr. The intake air mass

Table 13.3. 30,000-ft altitude ($\rho = 0.00088$ slug/ft³, $\sigma = 0.37$) maximum cruise

True air speed in knots	100	200	250	300
V in mph	115.08	230.16	287.70	345.24
$\text{SHP}_{\text{uninstall}} = \text{Figure 10.43a} \times 1,075$	413	440	462	484
$J = 0.00533 \times \text{knots}$	0.528	1.055	1.320	1.583
$C_p = 0.000116 \times \text{SHP}$	0.123	0.131	0.138	0.144
η_{prop} (from Figure 10.35)	0.66	0.81	0.82	0.81
Uninstalled thrust, T (lb)	888	582	494	426
Installed thrust (lb)	852	558	474	409
Sfc (lb/hr/SHP) (Figure 10.44b)	0.46	0.45	0.44	0.43
Fuel flow rate (lb/hr)	190	198	204	208

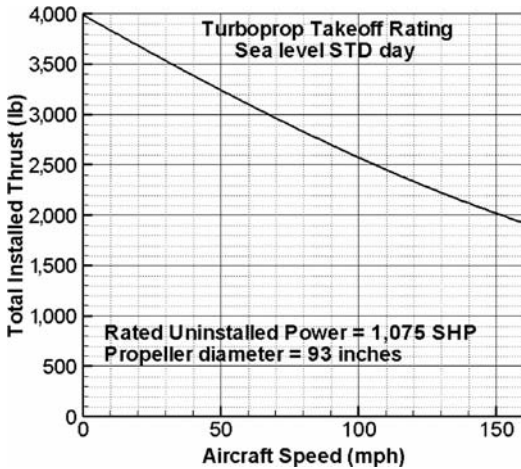


Figure 13.5. Available turboprop thrust at take-off rating from a 1,100-SHP engine

flow at SHP_{SLS} is $0.011 \times 1,075 = 11.83$ lb/s (the specific power of 0.11 lb/s/SHP is provided in Section 10.2.2).

Maximum Climb Rating (Turboprop): Standard Day

Figure 10.43a shows the uninstalled maximum climb SHP in nondimensional form and fuel consumption (sfc) up to a 30,000-ft altitude for four TAS from 50 to 200 kts. Following the same procedure as described in Section 10.11.4, the available installed thrust and fuel-flow rates at the maximum climb rating are worked out using a 4% loss of thrust due to installation effects. A sample computational table at a 30,000-ft altitude is in Table 13.2.

Figure 13.6 plots the available installed thrust and fuel flow at the maximum climb rating from sea level to a 30,000-ft altitude. The specified requirement of the initial climb rate for the example in this book is 4,500 ft/min.

Maximum Cruise Rating (Turboprop): Standard Day

Figure 10.44 shows the maximum cruise SHP in nondimensional form and fuel consumption (sfc) for speeds from the TAS of 50 to 300 kts and an altitude up to

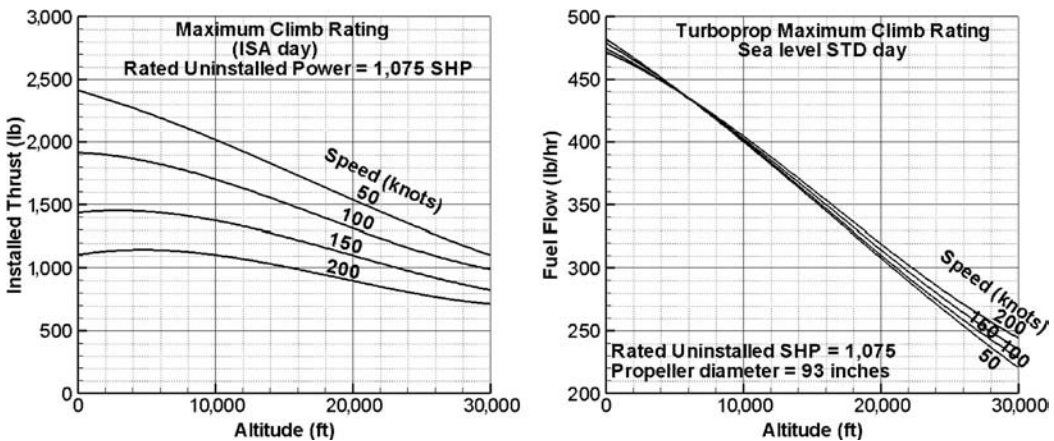


Figure 13.6. Thrust and fuel flow at maximum climb rating

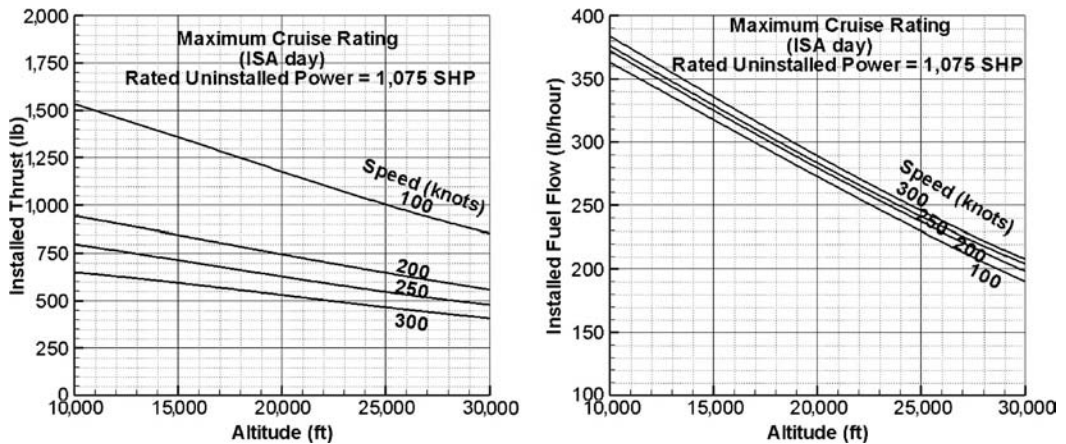


Figure 13.7. Thrust and fuel flow at maximum cruise rating

30,000 ft. Progressing as in the climb performance, the maximum cruise thrust and fuel-flow rate can be computed. A sample computation at a 30,000-ft altitude is in Table 13.3 using a 4% loss of thrust due to installation effects.

Figure 13.7 plots the available installed thrust and fuel flow at the maximum cruise rating. The initial maximum cruise speed in the example is 320 mph (270 kts) at a 25,000-ft altitude.

13.4 Derivation of Pertinent Aircraft Performance Equations

This section derives the relevant performance equations used in this book. For more details, readers may consult references [2] through [6].

Using the engine and aircraft data developed thus far during the conceptual design phase, the next section verifies whether the configured aircraft satisfies the airworthiness (i.e., FAR) and customer requirements in the takeoff/landing, the initial climb rates, and the maximum initial cruise speed, as well as the payload-range capability (i.e., civil aircraft). Certifying agencies have mandatory requirements to ensure safety at takeoff and landing. Airworthiness regulations differ among countries. For further details, readers may refer to the respective regulation – most of which appear in the official Web sites.

13.4.1 Takeoff

During a takeoff ground run, an aircraft under maximum thrust accelerates, gaining speed until a suitable safe speed is reached. The pilot then initiates rotation of the aircraft by gently pulling back the control stick or wheel (i.e., the elevator is going up) for a liftoff.

Designers must know the sequence of the takeoff speed schedules stipulated by the certifying agencies. To ensure safety, the agencies demand mandatory requirements for taking off with one engine inoperative to clear a 35-ft height that represents an obstacle. A one-engine inoperative TOFL is computed by considering the balanced field length (BFL) when the stopping distance after an engine failure at

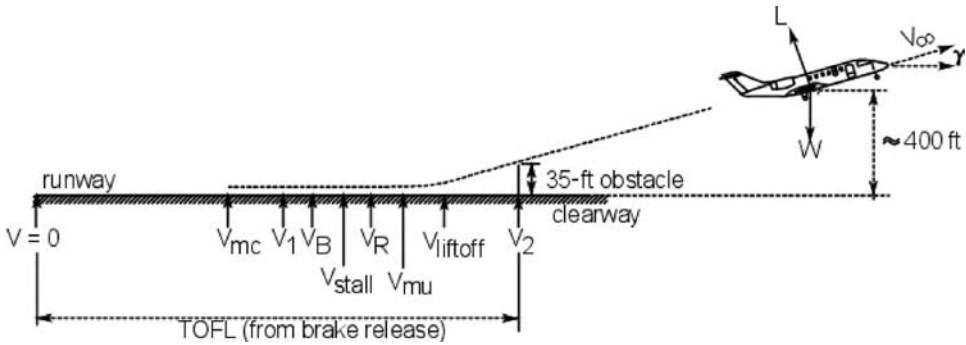


Figure 13.8. Takeoff, first- and second-segment climb

the decision speed, V_1 , is the same as the distance taken to clear the obstacle at the MTOM (Figure 13.8). Figure 13.8 gives the various speed schedules during a takeoff run, which are explained as follows:

- V_1 : This is the decision speed. An engine failure below this speed would result in an aircraft not being able to satisfy takeoff within the specified field length but able to stop. If an engine fails above the V_1 speed, the aircraft should continue the takeoff operation.
- V_{mc} : This is the minimum control speed at which the rudder is effective to control the asymmetry created by a one-engine failure. It should be lower than V_1 ; otherwise, at the loss of one engine at V_1 , an aircraft cannot be controlled if it continues the takeoff operation.
- V_R : This is the speed at which a pilot initiates the action to rotate an aircraft for liftoff; it should be $\geq 1.05 V_{mc}$. Once this is accomplished, reaching V_{LO} and V_2 occurs as an outcome of the action. V_R should be more than V_{stall} .
- V_{mu} : There is a minimum “unstick” speed, above which an aircraft can be made to lift off. The speed should be slightly above V_R . In fact, V_{mu} determines V_R . If a pilot makes an early rotation, then V_{mu} may not be sufficient for liftoff and the aircraft tail drags until it gains sufficient speed for liftoff.
- V_{LO} : This is the speed at which the aircraft lifts off the ground; it is closely associated with V_R . If one engine is inoperative, it should have a $V_{LO} \geq 1.05 V_{mu}$.
- V_2 : This is the takeoff climb speed at a 35-ft height, also known as the first-segment climb speed; it is also closely associated with V_R . FAR require that $V_2 = 1.2 V_{stall}$ (at a minimum; it can be higher).
- V_B : This is the brake-application speed with a one-engine failure ($V_B > V_1$).

The first-segment speed schedules are interrelated and expressed in terms of the ratios of V_{stall} , as given in Table 13.4. The velocity ratios in Table 13.4 comprise a typical range and can deviate a little as long as there is compliance with the FAR stipulation (marked with an asterisk in the table). Table 13.5 provides details of the climb segments.

Table 13.4. *Civil aircraft takeoff-speed schedule*

	Two-engine	Three-engine	Four-engine
Percent loss at an engine failure	50	33.3	25
Minimum climb gradient at 1st segment*	0%	0.3%	0.5%
Minimum climb gradient at 2nd segment*	2.4%	2.7%	3%
V_{LO}/V_{stall} (approximate)	1.12 to 1.14	1.15 to 1.16	1.17 to 1.18
V_{stall}/V_R (approximate)	1.10 to 1.18	1.14 to 1.18	1.16 to 1.18
V_{mu}/V_R (approximate)	1.02 to 1.04	1.02 to 1.04	1.02 to 1.04
V_1/V_R (approximate)	0.96 to 0.98	0.93 to 0.95	0.90 to 0.92
V_{mc}/V_1 (approximate)	0.94 to 0.98	0.94 to 0.98	0.94 to 0.98
V_2/V_{stall}	≥ 1.2	≥ 1.2	≥ 1.2

* FAR requirements

Some engines at the takeoff rating have an APR that could generate a 5% higher thrust than the maximum takeoff thrust for a short period. These types of engines are not considered in this book.

The higher the thrust loading (T/W), the higher is the aircraft acceleration. For smaller changes, V_R/V_{stall} and V_{LO}/V_{stall} may be linearly decreased with an increase in T/W. The decision speed V_1 is established through iterations, as described in Section 13.5.1. In a family of derivative aircraft, the smaller variant can have a V_1 close to the V_R .

Table 13.5 lists the aircraft configurations and power settings for the climb segments. The first- and second-segment climb schedule has FAR requirements; however, the initial enroute climb capability is a customer requirement, not a FAR requirement.

Military aircraft requirements (i.e., MIL-C5011A) are slightly different than civil aircraft requirements; the first-segment clearing height is 50 ft rather than 35 ft. Many military aircraft have a single engine in which the concept of BFL is not applicable. Military aircraft must satisfy the critical field length (CFL) as described in Section 13.6.1. The second-segment rate of climb must meet a minimum of 500 ft/minute for a multiengine aircraft.

Balanced Field Length: Civil Aircraft

The rated TOFL at the MTOM is determined by the BFL in the event of an engine failure. The BFL must comply with FAR requirements. A normal takeoff with all engines operating needs a considerably shorter field length than the rated TOFL. Designers must provide the decision speed V_1 for pilots that below which the takeoff must be aborted for safety reasons if an engine fails. Figure 13.9 shows the segments involved in computing the BFL.

Table 13.5. *Civil aircraft first- and second-segment climb configuration*

Climb schedule	Altitude	Undercarriage	Flaps/Slats	Throttle setting (rating)
First-segment climb (FAR)	Clear 35 ft	Extended	Extended	Maximum takeoff
Second-segment climb (FAR)	At \approx 400 ft	Retracted	Extended	Maximum takeoff
Enroute climb	At \approx 1,000 ft	Retracted	Retracted	Maximum climb

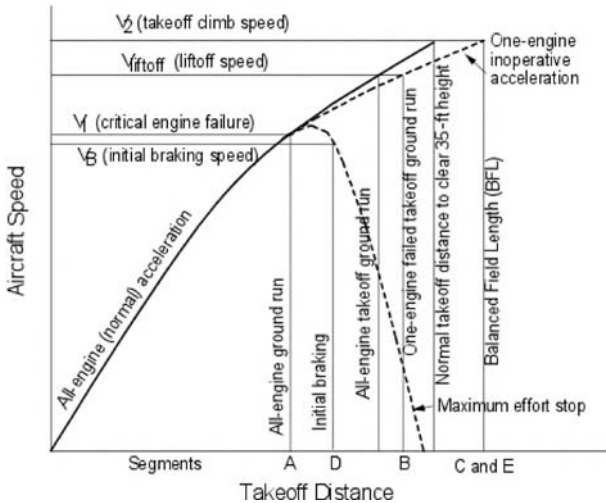


Figure 13.9. Balanced field length consideration

The figure shows that taking off with one engine inoperative (i.e., failed) has three segments to clear a 35-ft height, as follows:

- Segment A: Distance covered by all-engine operating ground run until one engine fails at the decision speed V_1 .
- Segment B: Distance covered by one-engine inoperative acceleration from V_1 to V_{LO} .
- Segment C: Continue with the flare distance from liftoff speed V_{LO} to clear a 35-ft obstacle height reaching aircraft speed V_2 .

For stopping at the decision speed V_1 , there are two segments (which replace segments B and C), as follows:

- Segment D: Distance covered during the reaction time for a pilot to take braking action. (Typically, 3 s is used as the pilot recognition time and braking to act, spoiler deployment, and so on. At engine failure, the thrust decay is gradual; within this reaction time before brake application, there is a minor speed gain, shown in Figure 13.9.)
- Segment E: Distance to stop from V_B to V_0 (maximum brake effort).

The BFL is established when Segments (B + C) = Segments (D + E).

Takeoff Equations

During takeoff, the aircraft accelerates. At the conceptual design phase, the average values of speed, acceleration, and thrust are taken as 0.7 of the velocity of the ground run segments. In later stages of a project, the computation is figured more accurately in smaller steps of speed increments within which average values of the variables are considered constant. C_L also varies with speed changes; typical values of C_L and C_D/C_L are given in Section 13.5.1.

Section 11.3.1 derives the associated governing equations to compute the TOFL. Equations 11.2 and 11.4 give:

$$\text{TOFL} = (1/\bar{a}) \int_0^{V_2} V dV = (V_2^2/2\bar{a}) \quad (13.1)$$

where average acceleration:

$$\begin{aligned} \bar{a} &= [(T - D) - \mu(W - L)]g/W \\ &= g(T/W)[1 - D/T - \mu W/T + \mu L/T] = g[(T/W - \mu) - (L/W)(D/L - \mu)] \end{aligned}$$

Values of the parameters are at 0.7 of the velocity of the segment.

Equation 13.1 now can be written separately for each segment and then equated for the BFL. The average acceleration \bar{a} is of the following segment:

$$\begin{aligned} \text{BFL} &= (1/\bar{a}) \int_0^{V_1} V dV + (1/\bar{a}) \int_{V_1}^{V_{10}} V dV + (1/\bar{a}) \int_{V_{LO}}^{V_2} V dV \quad (\text{continuing takeoff}) \\ &= (1/\bar{a}) \int_0^{V_1} V dV + (1/\bar{a}) \int_{V_1}^{V_B} V dV + (1/\bar{a}) \int_{V_B}^0 V dV \quad (\text{braked to stop}) \end{aligned} \quad (13.2)$$

The average acceleration is at 0.7 of the velocity interval and can be written in coefficient form as follows (in SI units, g is omitted):

$$\bar{a} = g[(T/W - \mu) - (C_L S_q/W)(C_D/C_L - \mu)] \quad (13.3)$$

The value of the friction coefficient μ on the hard runway surface is taken as $\mu = 0.03$ and at braking as $\mu_B = 0.3$ to 0.5 (for a Bizjet, it is 0.4). Thrust-loading (T/W) is obtained from the sizing exercise.

Let V_{ave} be the average velocity between the initial velocity V_i and the final velocity V_f . Then, the ground distance covered:

$$S_G = V_{ave} \times (V_f - V_i)/\bar{a} \quad (13.4)$$

The aircraft speed gain continues during the rotational (V_R) and flares out to V_2 . BLF is established at V_2 with one engine inoperative. Therefore, only a proper choice of the decision speed V_1 gives the BFL. A number of iterations may be required to arrive at the proper V_1 , as shown in the coursework example in Section 13.5.

13.4.2 Landing Performance

Computation of the LFL uses similar equations as for computing the TOFL; the difference is that a landing encounters deceleration (i.e., negative acceleration). Values of the friction coefficient, μ , vary when the main wheels followed by the nose wheel touch down. The brakes are applied after the nose wheel touches down (typically 2 s after touchdown). Considerable heat is generated at full braking and may pose a fire hazard. If the brake parachutes are deployed, the drag of the parachute is accounted for in the deceleration. With a thrust reverser, the negative thrust must be considered a decelerating force. With full flaps extended and spoilers activated, aircraft drag is substantially higher than at takeoff.

Table 13.6. FAA second-segment climb gradient at missed approach

Number of engines	2	3	4
Second-segment climb gradient	2.1%	2.4%	2.7%

The landing configuration is with full flaps extended and the aircraft at landing weight. The approach segment at landing is from a 50-ft altitude to touch down. At approach, the FAR requires that an aircraft must have a minimum speed $V_{app} = 1.3V_{stall@land}$. At touchdown, aircraft speed is $V_{TD} = 1.15V_{stall@land}$. Brakes are applied 2 s after all wheels touch down. A typical civil aircraft descent rate at touchdown is between 12 and 22 ft/s. The landing runway length should be 1.667 times the computed landing distance. Generally, this works out to be slightly less than the BFL at the MTOM (but not necessarily).

For a balked landing or missed approach at landing weight, the FAR requirements are given in Table 13.6. An aircraft is configured with full flaps, undercarriage extended, and engine in full takeoff rating. In general, this is not a problem because all engines are operational and the aircraft is lighter at the end of the mission. Military aircraft requirements are slightly different: $V_{app} = 1.2V_{stall@land}$ and $V_{TD} = 1.1V_{stall@land}$.

The approach has two segments, as follows:

- a steady, straight glide path from a 50-ft height
- flaring in a nearly circular arc to level out for touchdown, which incurs a higher g

The distances covered in these two segments depend on how steep is the glide path and how rapid is the flaring action. This book does not address these details of analysis; instead, a simplified approach is taken by computing the distance covered during the time from a 50-ft height to touchdown before the brakes are applied; it is assumed to be 6 s herein.

13.4.3 Climb and Descent Performance

Climb is possible when the available engine thrust is more than the aircraft drag; the excess thrust (i.e., thrust minus aircraft drag, $(T - D)$) is converted into the potential energy of height gain. The total energy of an aircraft is the sum of its PE and KE, expressed as follows:

Total energy:

$$E = mgh + (mgV^2/2g) = mg(h + V^2/2g)$$

Excess power:

$$EP = V(T - D) \quad (13.5)$$

Therefore, total specific energy (or specific energy):

$$E/mg = (h + V^2/2g) = h_e \text{ (energy height)} \quad (13.6)$$

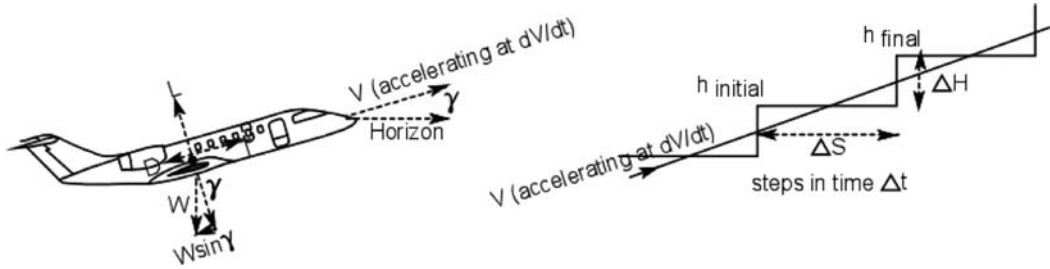


Figure 13.10. Climb performance

The term for the rate of change of specific energy is *specific excess power* (SEP):

$$\text{SEP} = dh/dt + V/g(dV/dt) = V(T - D)/(mg) = dh_e/dt \quad (13.7)$$

Equation 13.7 shows that $h_e > h$ by the term $V^2/2g$ in Equation 13.6. In other words, an aircraft can continue to climb by converting KE to PE until the speed is decreased to the point where the aircraft is unable to sustain the climb.

An enroute climb is performed in an accelerated climb. The equation for an accelerated climb is derived as follows (Figure 13.10). For simplicity, the subscript ∞ to represent aircraft velocity is omitted. From Figure 13.10, the force equilibrium gives:

$$(T - D) = mg \sin \gamma + (m)dV/dt$$

This gives the gradient:

$$\sin \gamma = [T - D - (W/g)dV/dt]/W = [(T - D)/W] - [(1/g) \times dV/dt] \quad (13.8)$$

Write:

$$dV/dt = (dV/dh) \times (dh/dt)$$

Then, rate of climb:

$$R/C_{accl} = dh/dt = V \sin \gamma = V(T - D)/W - (V/g) \times (dV/dh) \times (dh/dt) \quad (13.9)$$

By transposing and collecting dh/dt :

$$R/C_{accl} = dh/dt = \frac{V[(T - D)/W]}{1 + (V/g)(dV/dh)} \quad (13.10)$$

Combining Equations 13.7 and 13.9, the rate of climb is written as:

$$dh_e/dt = V(T - D)/W - (V/g)(dV/dt) + V/g(dV/dt) = V(T - D)/W \quad (13.11)$$

The rate of climb is a point performance and is valid at any altitude. The term $\frac{V}{g} \left(\frac{dV}{dh} \right)$ is dimensionless. It penalizes the unaccelerated rate (i.e., the numerator in Equation 13.10) of climb depending on how fast an aircraft is accelerating during the climb. Part of the propulsive energy is consumed for speed gain rather than altitude gain. Military aircraft make an accelerated climb in the operational arena when the $\frac{V}{g} \left(\frac{dV}{dh} \right)$ term reduces the rate of climb depending on how fast the aircraft is accelerating. Conversely, civil aircraft has no demand for a high-accelerated climb; rather, it makes an enroute climb to cruise altitude at a quasi-steady-state climb by holding

Table 13.7. $\frac{V}{g} \left(\frac{dV}{dh} \right)$ value (dimensionless quantity)

	Below tropopause	Above tropopause
At constant EAS	0.566 m ²	0.7 m ²
At constant Mach number	-0.133 m ²	0 (Mach held constant)

the climb speed at a constant EAS or Mach number. A constant-EAS climb causes the TAS to increase with altitude gain. A constant speed indication eases a pilot's workload. During a quasi-steady-state climb at a constant EAS, the contribution by the $\frac{V}{g} \left(\frac{dV}{dh} \right)$ term is minimal. The magnitude of the acceleration term decreases with altitude gain and becomes close to zero at the ceiling (i.e., defined as when $R/C_{accl} = 100$ ft/min). (Remember that $V = V_{EAS}/\sqrt{\sigma}$ and $V_{EAS} = Ma\sqrt{\sigma}$.)

Constant EAS Climb Below Tropopause ($\gamma = 1.4$, $R = 287$ J/kgK, $g = 9.81$ m/s²)

The term $\frac{V}{g} \left(\frac{dV}{dh} \right)$ can be worked out in terms of a constant EAS as follows:

$$\frac{V}{g} \left(\frac{dV}{dh} \right) = \frac{V_{EAS} V_{EAS}}{g\sqrt{\sigma}} \left(\frac{d(1/\sigma)}{dh} \right) = -\frac{V_{EAS}^2}{2g\sigma^2} \left(\frac{d\sigma}{dh} \right) = -\frac{M^2 a^2}{2g\sigma} \left(\frac{d\sigma}{dh} \right)$$

In SI, Equation 3.1 gives a troposphere $T = (288.16 - 0.0065h)$, and $\rho = 1.225 \times (T/288.16)^{(g/0.0065R)-1} = 1.225 \times (T/288.16)^{(9.81/0.0065 \times 287)-1} = 1.225 \times (T/288.16)^{4.255}$ derives the density ratio (up to the tropopause) by replacing T in terms of its lapse rate and h :

$$\sigma = \rho/\rho_0 = (288.16 - 0.0065h/288.16)^{4.255} = (1 - 2.2558 \times 10^{-5} \times h)^{4.255}$$

This gives $(d\sigma/dh) = -9.6 \times 10^{-5} \times (1 - 2.2558 \times 10^{-5} \times h)^{3.255}$

Therefore:

$$\begin{aligned} \frac{V}{g} \left(\frac{dV}{dh} \right) &= \frac{M^2 a^2}{2g\sigma} \times [9.6 \times 10^{-5} \times (1.2558 \times 10^{-5} \times h)^{3.255}] \\ &= \frac{M^2 \times 1.4 \times 287 \times (288.16 - 0.0065h)}{2 \times 9.81} \\ &\quad \times [9.6 \times 10^{-5}]/(1 - 2.2558 \times 10^{-5} \times h) \\ &= \frac{M^2 \times 1.4 \times 287 \times 288.16}{2 \times 9.81} \times (9.6 \times 10^{-5}) = 0.566 M^2 \quad (13.12) \end{aligned}$$

These equations are summarized in Table 13.7.

Constant Mach Climb Below Tropopause

($\gamma = 1.4$, $R = 287$ J/kgK, $g = 9.81$ m/s²)

The term $\frac{V}{g} \left(\frac{dV}{dh} \right)$ can be worked out in terms of a constant Mach-number climb as follows:

$$\frac{V}{g} \left(\frac{dV}{dh} \right) = \frac{MaM}{g} \left(\frac{da}{dh} \right) = \frac{aM^2 \sqrt{\gamma R}}{g} \left(\frac{d\sqrt{T}}{dh} \right)$$

From Equation 3.1, the atmospheric temperature, T , can be expressed in terms of altitude, h , as follows:

$$T = (288 - 0.0065h)$$

where h is in meters. Substituting the values of γ , R , and g , the following is obtained:

$$\frac{V}{g} \left(\frac{dV}{dh} \right) = \frac{aM^2 \sqrt{\gamma R}}{g} \left(\frac{d\sqrt{T}}{dh} \right) = - \frac{0.00664aM^2}{\sqrt{(288 - 0.0065h)}} \quad (13.13)$$

When evaluated for altitudes, the equation gives the value as shown in Table 13.7.

In a similar manner, the relationships above tropopause can be obtained. Up to 25 km above tropopause, the atmospheric temperature remains constant at 216.65 K; therefore, the speed of sound remains invariant.

With the loss of one engine at the second-segment climb, an accelerated climb penalizes the rate of climb. Therefore, a second-segment climb with one engine inoperative is achieved at an unaccelerated climb speed, at a speed a little above V_2 due to the undercarriage retraction. The unaccelerated climb equation is obtained by omitting the acceleration term in Equation 13.10, yielding the following equations:

$$T - D = W \sin \gamma \quad \text{becomes} \quad \sin \gamma = (T - D)/W$$

The unaccelerated rate of climb:

$$R/C = dh/dt = V \sin \gamma = V \times (T - D)/W \quad (13.14)$$

The climb performance parameters vary with altitude. An enroute climb performance up to cruise altitude is typically computed in discreet steps of altitude (i.e., 5,000 ft; see Figure 13.10), within which all parameters are considered invariant and taken as an average value within the altitude steps. The engineering approach is to compute the integrated distance covered, the time taken, and the fuel consumed to reach the cruise altitude in small increments and then totaled. The procedure is explained herein. The infinitesimal time to climb is expressed as $dt = dh/(R/C_{acc})$. The integrated performance within the small altitude steps is written as:

$$\Delta t = t_{final} - t_{initial} = (h_{final} - h_{initial})/(R/C_{acc})_{ave} \quad (13.15)$$

and

$$\Delta H = (h_{final} - h_{initial}) \quad (13.16)$$

Using Equation 13.8, the distance covered during a climb is expressed as:

$$\Delta s = \Delta t \times V_{ave} = \Delta t \times V \cos \gamma \quad (13.17)$$

where V = the average aircraft speed within the altitude step.

Fuel consumed during a climb can be expressed as:

$$\Delta fuel = \text{average fuel flow rate} \times \Delta t \quad (13.18)$$

Summary

The time used to climb, $time_{climb} = \sum \Delta t$, is obtained by summing the values obtained in the small steps of altitude gain. The distance covered during a climb,

$R_{climb} = \sum \Delta s$, is obtained by summing the values obtained in the small steps of altitude gain. The fuel consumed for a climb, $Fuel_{climb} = \sum \Delta fuel$, is obtained by summing the values obtained in the small steps of altitude gain.

Descent

A descent uses the same equations as for a climb except that the thrust is less than the drag; that is, the rate of descent (R/D_{accl}) is the opposite of the rate of climb. The rate of descent is expressed as follows:

$$R/D_{accl} = dh/dt = \frac{V[(D - T)/W]}{1 + (V/g)(dV/dh)} \quad (13.19)$$

Unlike in a climb, gravity assists a descent; therefore, it can be performed without any thrust (i.e., the engine is kept at an idle rating, producing zero thrust). However, passenger comfort and structural considerations require a controlled descent with the maximum rate limited to a certain value depending on the aircraft design. A controlled descent is carried out at a partial-throttle setting. To obtain the maximum range, an aircraft should ideally make its descent at the desired minimum rate. These adjustments entail varying the speed at each altitude. To ease the pilot's workload, a descent is made at a constant Mach number; when the V_{EAS} limit is reached, the aircraft adapts to a constant V_{EAS} descent, similar to a climb. Special situations may occur, as follows:

1. For an unaccelerated descent, Equation 13.19 becomes:

$$R/D_{unaccl} = dh/dt = \frac{V[(D - T)]}{W} \quad (13.20)$$

At a higher altitude, the prescribed speed schedule for a descent is at a constant Mach number; therefore, the previous tropopause V_{TAS} is constant and the descent is maintained in an unaccelerated flight.

2. At zero thrust, Equation 13.29 becomes:

$$R/D_{unaccl} = dh/dt = \frac{VD}{W} \approx \frac{VD}{L} \quad (13.21)$$

This indicates that at a constant $V(L/D)$, the $R/C_{descent}$ is the same for all weights.

As in a climb, the other parameters of interest during a descent are range covered ($R_{descent}$), fuel consumed ($Fuel_{descent}$), and time taken ($time_{descent}$). There are no FAR requirements for the descent schedule. The descent rate is limited by the cabin-pressurization schedule for passenger comfort. FAR requirements are enforced during an approach and a landing. At high altitude, the inside cabin pressure is maintained as an approximate 8,000-ft altitude. Depending on the structure design, the differential pressure between the inside and the outside is maintained at approximately 8.9 lb/in².

Integrated performances for a climb to cruise altitude and a descent to sea level are computed, and the values for distance covered, time taken, and fuel consumed are estimated to obtain the aircraft payload range. Textbooks may be consulted for details of climb and descent performances.

13.4.4 Initial Maximum Cruise Speed

Civil aircraft maximum speed is executed in HSC in a steady, level flight when the available thrust equals the aircraft drag. The first task is to compute drag at the maximum cruise speed and then check whether the available thrust (at the maximum cruise rating) is sufficient to achieve the required speed. Sometimes, the available maximum cruise thrust is more than what is required; in that case, the engine is adjusted to a slightly lower level. The LRC schedule is meant to maximize range and is operated at a lower speed to avoid the compressibility drag rise. [Section 13.5.6](#) explains the worked-out example.

13.4.5 Payload Range Capability

Finally, a civil aircraft must be able to meet the payload range capability as specified by the market (i.e., customer) requirements. The mission range and fuel consumed during the mission are given by the following two equations:

$$\text{mission range} = R_{climb} + R_{cruise} + R_{descent} \quad (13.22)$$

$$\text{mission fuel} = Fuel_{climb} + Fuel_{cruise} + Fuel_{descent} \quad (13.23)$$

$$\text{mission time} = Time_{climb} + Time_{cruise} + Time_{descent}$$

The method to compute fuel consumption, distance covered, and time taken during a climb and a descent is discussed in [Section 13.4.3](#). In this section, the governing equations for cruise range (R_{cruise}), cruise fuel ($Fuel_{cruise}$), and time taken during cruise are derived.

Let W_i = aircraft initial cruise weight (at the end of a climb) and W_f = aircraft final cruise weight (at the end of a cruise). Then:

$$\text{fuel burned during cruise} = Fuel_{cruise} = W_i - W_f \quad (13.24)$$

At any instant, rate of aircraft weight change, dW = rate of fuel burned (consumed). In an infinitesimal time dt , the infinitesimal weight change, $dW = sfc \times \text{thrust} (T) \times dt$, or:

$$dt = dW / (sfc \times T) \quad (13.25)$$

Integrating [Equation 13.25](#) gives the time taken for the R_{cruise} . At cruise, $T = D$ and $L = W$.

In [Equation 13.25](#), multiply both the numerator and the denominator by weight, W , and then equate $T = D$ and $W = L$.

Equation 13.25 reduces to:

$$dt = \frac{1}{sfc} \left(\frac{W}{T} \right) \left(\frac{dW}{W} \right) = \frac{1}{sfc} \left(\frac{L}{D} \right) \left(\frac{dW}{W} \right) \quad (13.26)$$

The elemental range:

$$ds = V \times dt = \frac{V}{sfc} \left(\frac{L}{D} \right) \left(\frac{dW}{W} \right) \quad (13.27)$$

Therefore, the range covered during cruise (R_{cruise}) is the integration of Equation 13.27 from the initial to the final cruise weight. At cruise, V and sfc remain nearly constant. Using the midcruise L/D , the change in L/D can be ignored and taken out of the integral sign:

$$R_{cruise} = \int ds = \int_{W_f}^{W_i} \frac{V}{sfc} \left(\frac{L}{D} \right) \left(\frac{dW}{W} \right) = \frac{V}{sfc} \left(\frac{L}{D} \right) \ln \left(\frac{W_i}{W_f} \right) \quad (13.28)$$

The value of $\ln(W_i/W_f) = k_{1_range}$ varies from 0.2 to 0.5; the longer the range, the higher is the value.

In Equation 13.28, the terms W_i and W_f are concerned with fuel consumed during cruise and the term sfc stems from the matched-engine characteristics. The other terms (VL/D) are concerned with aircraft aerodynamics. Aircraft designers aim to increase the VL/D as best as it is possible to maximize the range capability. The aim is not just to maximize the L/D but also to maximize the VL/D . Expressing this in terms of the Mach number, it becomes ML/D . To obtain the best of engine–aircraft gain, it is to maximize $(ML)/(sfcD)$.

Specific range (Sp.Rn) is defined as range covered per unit weight (or mass) of fuel burned. Using Equation 13.28:

$$Sp.Rn = R_{cruise}/\text{cruise fuel} = [k_{1_range} \times (VL)/(sfcD)]/(W_i - W_f) \quad (13.29)$$

The cruise fuel weight ($W_i - W_f$) can be expressed in terms of the MTOW and varies from 15 to 40% of the MTOW; the longer the range, the higher is the value. Let $k_{2_range} = k_{1_range}/(0.15 \text{ to } 0.4)$. Then, Equation 13.29 reduces to:

$$Sp.Rn = [k_{2_range} \times (VL)/(sfcD)]/\text{MTOW} \quad (13.30)$$

Equation 13.30 provides insight to what can maximize the range; that is, a good design to stay ahead of the competition:

1. Design an aircraft to be as light as possible without sacrificing safety. Material selection and structural efficiency are key; integrate with lighter bought-out equipment.
2. Use superior aerodynamics to lower drag.
3. Choose a better aerofoil for good lift, keeping the moment low.
4. Design an aircraft to cruise as fast as possible within the M_{crit} .
5. Match the best available engine with the lowest sfc .

However, these points do not address cost implications. In the end, the DOC dictates the market appeal and designers must compromise performance with cost. These points comprise the essence of good civil aircraft design, which is easily said but not so easy to achieve, as must be experienced by readers.

Equation 13.25 can be further developed. From the definition of the lift coefficient, C_L , the aircraft velocity, V , can be expressed as follows:

$$V = \sqrt{\frac{2W}{\rho S W C_L}}$$

Substituting in Equation 13.25, the cruise range, R_{cruise} , can be written as:

$$R_{cruise} = \int_{W_f}^{W_i} \frac{1}{sfc} \sqrt{\frac{2W}{\rho S_W C_L}} \left(\frac{L}{D}\right) \left(\frac{dW}{W}\right) = \sqrt{\frac{2}{\rho S_W}} \int_{W_f}^{W_i} \frac{1}{sfc} \left(\frac{\sqrt{C_L}}{C_D}\right) \left(\frac{dW}{\sqrt{W}}\right) \quad (13.31)$$

As mentioned previously, over the cruise range, changes in the sfc and L/D typically are minor. If the midcruise values are taken as an average, then they may be treated as constant and are taken outside the integral sign. Then, Equation 13.31 becomes:

$$R_{cruise} = \sqrt{\frac{2C_L}{\rho S_W}} \left(\frac{1}{sfc \times C_D}\right) \int_{W_f}^{W_i} \left(\frac{dW}{\sqrt{W}}\right) = 2\sqrt{\frac{2C_L}{\rho S_W}} \left(\frac{\sqrt{W_i} - \sqrt{W_f}}{sfc \times C_D}\right) \quad (13.32)$$

This equation is known as the *Breguet range formula*, originally derived for propeller-driven aircraft that had embedded propeller parameters (jet propulsion was not yet invented).

The LRC is carried out at the best sfc and at the maximum value of $\sqrt{C_L/C_D}$ (i.e., L/D) to maximize range. Typically, the best L/D occurs at the midcruise condition. For a very high LRC (i.e., 2,500 nm or more), the aircraft weight difference from initial to final cruise is significant. It is beneficial if cruise is carried out at a higher altitude when the aircraft becomes lighter, which can be done either in a stepped altitude or by making a gradual, shallow climb that matches the gradual lightening of the aircraft. Sometimes a mission may demand HSC to save time, in which case Equation 13.29 is still valid but not operating for the best range.

13.5 Aircraft Performance Substantiation: Worked-Out Examples (Bizjet)

This section computes aircraft performance to substantiate capabilities as required by the FAR and the operators. Table 13.4 gives the speed schedules appropriate to an aircraft takeoff; aircraft drag polar is given in Figure 9.1. The wing area, $S_W = 30 \text{ m}^2$ (323 ft²) and the MTOM = 9,400 kg (20,723 lb). Assuming that 20 kg of fuel is consumed during the taxi, the MTOM for the takeoff estimation = 9,380 kg (20,680 lb), and wing-loading, $W/S_W = 64 \text{ lb/ft}^2$. The known stalling speed is computed by using the following:

$$V_{stall} = \sqrt{\frac{2 \times MTOM}{\rho S_W C_L}} = \sqrt{\frac{2 \times 20,680}{0.002378 \times 323 \times C_L}} = \sqrt{\frac{53,847.6}{C_L}}$$

Table 13.8 provides the Bizjet aircraft data generated thus far. To make the best use of the available data, all computations are in the FPS system. The results subsequently can be converted to the SI system.

13.5.1 Takeoff Field Length (Bizjet)

Three decision speeds are worked out to establish the V_I for the BFL computation. Equation 13.2 gives average acceleration as:

$$\bar{a} = g[(T/W - \mu) - (C_L S q / W)(C_D / C_L - \mu)]$$

Table 13.8. Bizjet performance parameters (takeoff and landing)

Flap setting (deg)	0	8*	20*	Landing*
C_{Dpmin}	0.0205	0.0205	0.0205	0.0205
C_{Lmax}	1.55	1.67	1.90	2.20
ΔC_{Dflap}	0	0.013	0.032	0.060
$\Delta C_{D,U/C}$	0.0222	0.0220	0.0212	0.0212
$\Delta C_{D_one_eng}$ (fuselage-mounted)	0.003	0.003	0.003	0.003
$\Delta C_{D_one_eng}$ (wing-mounted)	0.004	0.004	0.004	0.004
Rolling-friction coefficient, μ	0.03	0.03	0.03	0.03
Braking-friction coefficient, μ_B	0.45	0.45	0.45	0.45
V_{stall} @ 20,680 lb (ft/s)	186.5	179.6	168.4	–
V_R (kt) (multiply 1.688 to obtain ft/s)		112 (189)	104 (175.5)	–
V_2 (kt) (1.688 ft/s)		128.2 (216.5)	124.8 (210.7)	–
T/W (all-engine)		0.32	0.32	–
T/W (single-engine)		0.16	0.16	–
C_D/C_L at ground run (all engine)		0.1	0.1	–
C_D/C_L at ground run (one engine out)		0.102	0.102	–

* Takeoff at 8- and 20-deg flaps. Landing at 35- to 40-deg flap, engines at idle, and V_{stall} at aircraft landing weight of 15,800 lb.

The average acceleration \bar{a} is at $0.7V$ of the segment of operation. For each segment of the BFL, \bar{a} is computed.

The lift coefficient during the ground run is changing with speed gain and is not easy to determine. During the ground run, the angle of attack is low, even when the aircraft reaches the stall speed, V_{stall} . Up to the decision speed V_I , only a fraction of the aircraft weight is taken up by the wing as a result of lift generation. Liftoff is not achieved until a pilot rotates the aircraft just above the V_{stall} . There is a rapid gain in lift generation because the angle of attack increases rapidly with rotation. Table 13.9 lists typical C_L and C_D/C_L values.

Segment A: All Engines Operating up to the Decision Speed V_I

Using Equation 13.2 and data from Table 13.6, the average acceleration becomes:

$$\bar{a} = 32.2 \times [(0.34 - 0.03) - (C_{Lq}/64)(0.1 - 0.03)] = 32.2 \times (0.31 - C_{Lq}/914.3)$$

At a representative speed of $0.7V_I$, the average $q = 0.5 \times 0.002378 \times 0.49V_I^2 = 0.0006 \times V_I^2$. At this segment, the average $C_L = 0.5$ (yet to reach the full value). Then:

$$\begin{aligned} \bar{a} &= 32.2 \times (0.31 - C_{Lq}/914.3) \\ &= 32.2 \times (0.31 - 0.0003 \times V_I^2/914.3) \text{ ft/s}^2 \end{aligned}$$

Table 13.9. Bizjet takeoff aerodynamic coefficients (from experiments and statistics)

	Average C_L	Average C_D
From V_0 to V_I	0.4	8-deg flap 0.031
*From V_I to V_{LO}	0.4	0.035
*From V_{LO} to V_2 (20-deg flap)	1.9	not used (see example)

* One engine inoperative

Table 13.10. *Segment A: Bizjet all-engine 0 to V_I (8-deg flap)*

Guess V_I (kt) (1.688 ft/s)	90 (151.92)	100 (168.8)	110 (185.7)
$0.7V_I$ (ft/s) (Mach)	101.34 (0.095)	118.16 (0.106)	130 (0.116)
T/W (from Figure 13.1)	0.296	0.290	0.286
q (dynamic head at $0.7V_I$)	13.45	16.6	20.09
\bar{a} (ft/s ²)	8.44	8.21	8.05
Ground distance, $S_{G_{V_I}}$ (ft)	1,367	1,735	2,142

Equation 13.3 gives the ground distance covered as:

$$S_G = V_{ave} \times (V_f - V_i) / \bar{a}$$

Table 13.10 computes the ground distance covered for all engines operating up to V_I .

Segment B: One-Engine Inoperative Acceleration from V_I to Liftoff Speed, V_{LO}

Because one engine is inoperative, there is a loss of power by half ($T/W = 0.17$) plus an asymmetric drag rise ($C_D/C_L = 0.102$). As the speed increases, the average C_L increases to 0.8, making the weight on the wheels lighter; therefore, the ground friction, μ , is reduced to 0.025. The acceleration Equation 13.2 is rewritten as follows:

$$\begin{aligned} \bar{a} &= 32.2 \times [(0.17 - 0.025) - (C_L q / 64)(0.102 - 0.025)] = 32.2 \\ &\times (0.145 - 0.8 \times q / 831.2) \end{aligned}$$

The velocity that would give the average acceleration is:

$$V_{0.7} = 0.7 \times (V_{LO} - V_I) + V_I$$

$$\bar{a} = 32.2 \times (0.145 - 0.000951 \times V_{0.7} / 831.2) = 32.2 \times (0.145 - 0.00000114 \times V_{0.7}^2)$$

Equation 13.3 gives the ground distance covered as:

$$S_G = V_{ave} \times (V_f - V_i) / \bar{a}$$

Table 13.11 computes the ground distance covered from V_I to V_{LO} for the two flap settings.

Table 13.11. *Segment B: Bizjet one-engine ground distance V_I to V_{LO} (8-deg flap)*

Guess V_I (kt) (1.688 ft/s)	90 (151.92)	100 (168.8)	110 (185.7)
V_{stall} at 20,600 lb (ft/s)	177.6	177.6	177.6
V_{LO} at 1.12 V_{stall}	199	199	199
$V_{0.7} = 0.7 \times (V_{LO} - V_I) + V_I$ (ft/s)	185 (0.166M)	191 (0.171M)	196 (0.176M)
T/W (from Figure 13.1)	0.138	0.136	0.134
q (dynamic head at $0.7V_I$)	41.09	43.37	45.7
\bar{a} (ft/s ²)	3.21	3.11	3.08
Ground distance, $S_{G_{V_{LO}}}$ (ft)	2,664	1,881	951

Table 13.12. Segment C: Bizjet one-engine ground distance V_{LO} to V_2 (8-deg flap)

Guess V_1 (kt) (1.688 ft/s)	90 (151.92)	100 (168.8)	110 (185.7)
Flap (deg)	8	8	8
V_{stall} (kt) (ft/s)	179.6	179.6	179.6
V_{LO} at 1.12 V_{stall}	200.5	200.5	200.5
V_2 at 1.2 V_{stall}	215.52	215.52	215.52
V_{ave} (ft/s) $[(V_{LO} + V_2)/2 + V_{LO}]$	208	208	208
Flaring distance in 3 s, S_{G-V_2} (ft)	624	624	624
Segments (B + C)	3,288	2,505	1,575
TOFL ($S_{G-V_1} + S_{G-VLO} + S_{G-V_2}$)	4,655	4,240	3,717

Segment C: Flaring Distance with One Engine Inoperative from V_{LO} to V_2

The flaring distance reaches V_2 from V_{LO} ; from statistics, the time to flaring is 3 s. Table 13.12 computes the ground distance covered from V_{LO} to V_2 with one engine inoperative for the two flap settings. In this segment, an aircraft is airborne; hence, there is no ground friction. Taking the average velocity between V_2 and V_{LO} gives the distance covered during flare.

The next step is to compute the stopping distance with the maximum application of brakes.

Segment D: Distance Covered in 1 s as Pilot-Recognition Time and 2 s for Brakes to Act from V_I to V_B (Flap Settings Are of Minor Consequence)

Table 13.13 computes the ground distance covered from V_I to V_B .

Segment E: Braking Distance from V_B to Zero Velocity (Flap Settings Are of Minor Consequence)

The reaction time to apply the brakes, after the decision speed, V_I , is 3 s. The aircraft continues to accelerate during the 3 s.

For an aircraft in full braking with $\mu_B = 0.4$, all engines shut down, and the average $C_L = 0.5$, Equation 13.2 for average acceleration, based on $0.7V_B (\approx 0.7V_I)$, reduces to:

$$\begin{aligned} \bar{a} &= 32.2 \times [(-0.4) - (C_{Lq}/64)/(0.1 - 04)] = 32.2 \times [-0.4 + (0.15q/64)] \\ &= 32.2 \times [-0.4 + q/426.7] = 0.075q - 12.88 \end{aligned}$$

Table 13.14 computes the ground distance covered from V_B to stopping.

The TOFL (see Table 13.12, Segments A + B + C) and the stopping distance (see Table 13.14, Segments A + D + E) are plotted in Figure 13.11 to obtain the BFL for a flap setting of 8 deg and summarized in Table 13.16. It satisfies the specified TOFL requirement of 4,400 ft.

Table 13.13. Segment D: Bizjet failure-recognition distance

Estimate V_1 (kt) (1.688 ft/s)	90 (151.92)	100 (168.80)	110 (185.70)
Distance in 3 sec at V_1 , S_{G-B} (ft)	456	506	557

Table 13.14. Segment E: Bizjet stopping distance

Estimate V_B (kt) (1.688 ft/s)	90 (151.92)	100 (168.80)	110 (185.70)
V_{ave} (ft/s) ($V_1/2$)	75.96	84.40	92.85
ΔV (ft/s)	151.92	168.80	185.70
q (dynamic head at $0.7V_1$ from Table 13.5)	13.85	17.10	20.69
\bar{a} (ft/s ²) (minus sign for retardation)	-11.84	-11.60	-11.33
Ground distance, $S_{G,0}$ (Equation 13.3) (ft)	954	1,228	1,522
Segments (D + E)	1,410	1,732	2,079
Stop distance ($S_{G,V_1} + S_{G,B} + S_{G,0}$)	2,595	3,104	3,871

Discussion of the Takeoff Analysis

Increasing the flap setting improves the BFL capability at the expense of a loss in climb gradient. The next section verifies the gradient requirements. With one engine inoperative, the loss of thrust percentage for a two-engine aircraft is the highest (i.e., 50%). With one engine failed, the aircraft acceleration suffers severely and the ground run from V_I to liftoff is high.

Table 13.16 summarizes the takeoff performance and associated speed schedules for the two flap settings and provides an example of the procedure. The ratio of speed schedules can be varied for pilot ease, as long as it satisfies FAR requirements.

At a lower flap setting of 8 deg, the decision speed V_I is close to the rotation speed $V_I = 0.93V_R$. The situation improves with a higher flap setting of 20 deg when $V_I = 0.9V_R$.

Higher flap settings provide more time between the decision speed V_I and the rotation speed V_R . However, it is not problematic if V_I is close to V_R . If one engine fails close to the decision speed, then the rotation speed V_R is reached very quickly; that is, even if a pilot's reaction is slow, the aircraft will still take off if there is sufficient runway length available (the BFL can be considerably lower than the available airfield length). Also, V_{mu} is close to V_R ; hence, tail dragging is not likely. If an engine fails early enough, then a pilot has sufficient time to recognize the failure and abort the takeoff.

With more than two engines, the decision speed V_I is farther from the rotation speed V_R . A pilot must remain alert as the aircraft speed approaches the decision speed V_I and must react quickly if an engine fails.

Figure 13.11. Balanced field length

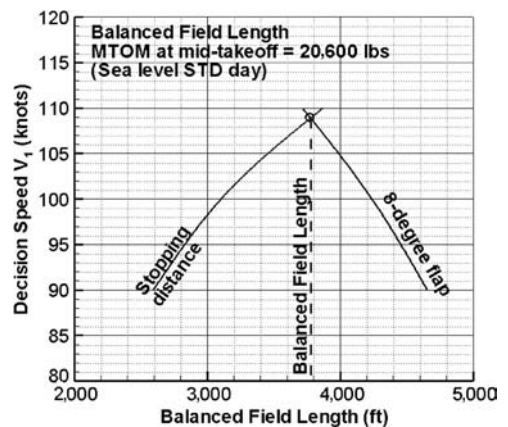


Table 13.15. *Bizjet decision speed*

Flap (deg)	8
Distance (ft) at (B + C) = (D + E)	2,100
TOFL at BFL (ft)	3,780 ($\approx 3,800$)
Decision speed, V_1 (kts)	109
V_1/V_R	0.93

13.5.2 Landing Field Length (Bizjet)

The landing weight of a Bizjet is 15,800 lb (wing-loading = 48.92 lb/ft²) and with full flap extended, it is $C_{Lmax} = 2.2$. Therefore:

$$V_{stall@land} = \sqrt{\frac{2 \times 15,800}{0.002378 \times 323 \times C_L}} = \sqrt{\frac{41,141}{2.2}} = 137 \text{ ft/s}$$

$$V_{appr} = 1.3V_{stall@land} = 178 \text{ ft/s}$$

$$V_{TD} = 1.15V_{stall@land} = 158 \text{ ft/s}$$

The average velocity from a 50-ft height to touchdown = 168 ft/s. The distance covered before brake application after 6 s (may differ) from a 50-ft height:

$$S_{G.TD} = 6 \times 168 = 1,008 \text{ ft}$$

An aircraft in full braking with $\mu_B = 0.4$, all engines shut down, and the average $C_L = 0.5$, $C_D/C_L = 0.1$. Equation 13.2 for average acceleration is based on $0.7V_{TD} = 110.6$ ft/s; then:

$$q = 0.5 \times 0.002378 \times 110.6^2 = 14.54$$

For deceleration:

$$\begin{aligned} \bar{a} &= 32.2 \times [(-0.4) - (C_L q / 48.92)(0.1 - 0.4)] \\ &= 32.2 \times [-0.4 + (0.15 \times 14.54 / 48.92)] \\ &= 32.2 \times [-0.4 + 0.0445] = -11.45 \end{aligned}$$

The distance covered during braking, $S_{G.0Land} = (158 \times 79) / 11.45 = 1,090$ ft. The landing distance $S_{G.Land} = 1,008 + 1,090 = 2,098$ ft.

Table 13.16. *Bizjet takeoff field length with 8-deg flap setting*

	knot	ft/s
V_{stall} @ 20,600 lb	106.4	179.6
V_1 decision speed	109	183.8
$V_2 = 1.2V_{stall}$ at 35-ft height*	128.2	216.5
V_{LO} at $1.12V_{stall}^{**}$	119.17	201.15
V_R at $1.1V_{stall}^{**}$	117	197.6
V_{mu} at $1.01 V_R$ (lower than V_{LO})	118.2	199.5
V_{mc} at $0.94V_1$	102	172.2
BFL (ft) (TOFL requirement 4,400 ft)	3,800	

V_1 is too close to V_{stall} but is acceptable. If required it can be raised by a few knots.

* If required, V_2 can be higher than $1.2V_{stall}$.

** If required, V_R and V_{LO} can be at higher speeds.

Table 13.17. First- and second-segment climb performance

	1st Segment Climb		2nd Segment Climb	
	35- to 400-ft altitude		400- to 1,000-ft altitude	
	$\rho_{ave} = 0.00235 \text{ lb/ft}^3$		$\rho_{ave} = 0.00232 \text{ lb/ft}^3$	
	$0.5\rho S_W = 0.3795$		$0.5\rho S_W = 0.3747$	
Flap (deg)	8	20	8	20
MTOM (kg)	20,680	20,680	20,680	20,680
V_{stall} (ft/s) (knot)	179.6 (106.4)	168.4 (99.8)	179.6 (106.4)	168.4 (99.8)
$V_2 =$ (ft/s) (Mach)	216.50 (0.194)	202.08 (0.181)	216.50 (0.194)	202.08 (0.181)
qS_W	17,788	15,497.4	17,563	15,301.4
C_L	1.16	1.33	1.177	1.35
$C_{D_{clean}}$ (see Figure 9.2)	0.075	0.100	0.076	0.101
$\Delta C_{D_{one_eng}}$	0.003	0.003	0.003	0.003
$\Delta C_{D_{flap}}$	0.013	0.032	0.013	0.032
$\Delta C_{D_{u/c}}$	0.022	0.022	–	–
C_{D1st_seg}	0.113	0.157	0.092	0.135
Drag (lb)	2,010	2,433	1,616	2,081
Thrust Available (lb)	2,740	2,750	2,740	2,750
Gradient (%)	+ve	+ve	5.4	3.24
FAR	Meets	Meets	Meets	Meets

Note: Aircraft flap and undercarriage extended, engine at takeoff rating (one engine inoperative). (Use drag polar Figures 9.2 and 9.12 to obtain drag.)

Multiplying by 1.667, the rated LFL = $1.667 \times 1,548 = 3,597$ ft, within the requirement of 4,400 ft. As expected, this is less than the BFL at an 8-deg flap. This is not always the case because at a 20-deg flap setting, LFL > BFL.

13.5.3 Climb Performance Requirements (Bizjet)

The three requirements for substantiation of the climb performance are given as follows for a two-engine aircraft (the first two are FAR requirements; Table 13.5 provides an aircraft configuration and FAR requirements for the first- and second-segment climb):

1. Verify that the FAR first-segment climb requirement of a positive gradient is maintained.
2. Verify that the FAR second-segment climb gradient requirement exceeds 2.4%.
3. Verify that the market requirement of the initial enroute rate of climb equals or exceeds 2,600 ft/min. The cabin-pressurization system should handle the rate of climb. (This is a customer requirement, not a FAR requirement.)

The second segment starts at a 400-ft altitude with flaps extended and the undercarriage retracted (i.e., one engine inoperative). From a 400- to 1,000-ft altitude, the undercarriage is retracted in the second-segment climb. An aircraft is maintained at the V_2 speed for the best gradient – a 50% loss of thrust does not favor an accelerated climb, which will be low in this case. The engine is at the takeoff rating. The available one-engine-installed thrust is from Figure 13.1. The thrust is kept invariant at the takeoff rating through the first- and second-segment climb. Table 13.17 summarizes the first- and second-segment climbs for both 8-deg and 20-deg flap settings. At one engine failed, the aircraft must return to the base immediately.

When verifying initial enroute rate of climb, the specification requirement is 2,600 ft/min. When the initial enroute climb starts at a 1,000-ft altitude ($\rho = 0.0023$ slug/ft³, $\sigma = 0.9672$) and all engines are throttled back to maximum climb rating, an aircraft has a clean configuration. An aircraft makes an accelerated climb from V_2 to reach 250 KEAS, which is kept constant in a quasi-steady-state climb until it reaches Mach 0.7 at about a 32,000-ft altitude. From there, the Mach number is held constant in the continued quasi-steady-state climb until it reaches the cruise altitude. Fuel consumed during the second-segment climb is small and assumed empirically (from statistics) to be 120 lb (see Table 13.17). Therefore, the aircraft weight at the beginning of the enroute climb is $M = 20,600$ lb. At 250 kts (422 ft/s, Mach 0.35), the aircraft lift coefficient $C_L = M/qS_W = 20,600/(0.5 \times 0.0023 \times 422^2 \times 33) = 20,600/66,150 = 0.311$.

The clean aircraft drag coefficient from Figure 9.2 at $C_L = 0.311$ gives $C_{D_{clean}} = 0.0242$. The clean aircraft drag, $D = 0.0242 \times (0.5 \times 0.0023 \times 422^2 \times 323) = 0.0242 \times 66,150 = 1,600$ lb. The available all-engine-installed thrust at the maximum climb rating from Figure 13.2 at Mach 0.378 is $T = 2 \times 2,260 = 4,520$ lb. From Equation 13.10, the quasi-steady-state rate of climb is given by:

$$R/C_{accl} = \frac{V_\infty[(T - D)/W]}{1 + (V/g)(dV/dh)}$$

At the quasi-steady-state climb, Table 13.5 gives $\frac{V}{g} \left(\frac{dV}{dh}\right) = 0.56 \text{ m}^2 = 0.56 \times 0.35^2 = 0.0686$. Hence:

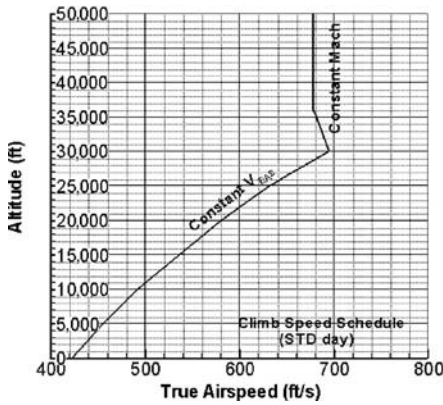
$$\begin{aligned} R/C_{accl} &= \{[422 \times (4,520 - 1,600)]/20,680\}/[1 + 0.0686] = 55.8 \text{ ft/s} \\ &= 3,345 \text{ ft/min}(17 \text{ m/s}) \end{aligned}$$

This capability satisfies the market requirement of 2,600 ft/min (13.2 m/s). (The civil aircraft rate of climb is limited by the cabin-pressurization schedule. An aircraft is limited to 2,600 ft/min at an altitude where the cabin pressurization rate reaches its maximum capability. Naturally, at the low altitude of 1,000 ft, this limit is not applicable.)

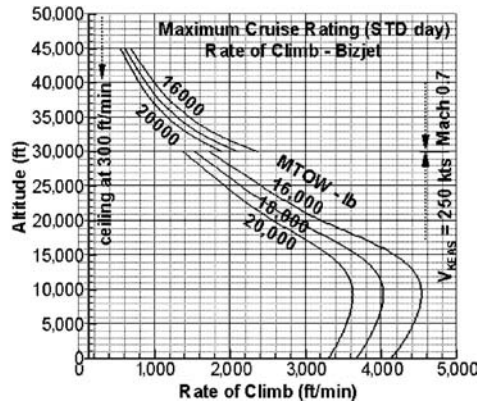
13.5.4 Integrated Climb Performance (Bizjet)

Integrated climb performance is not a requirement for substantiation – it is used to obtain the aircraft payload-range capability, which is a requirement for substantiation. Section 13.1 explains why only results of the integrated climb performances in graphical form are given as shown in Figures 13.12 and 13.13. Section 13.4.3 describes the theory for deriving the climb equations. Instructors may assist with the computational work to obtain similar performance graphs for the coursework projects. Readers redoing the graphs as given here may have minor differences in their results, which is understandable.

It is convenient to establish first the climb velocity schedule (Figure 13.12a) and the point performances of the rate of climb (Figure 13.12b) up to the ceiling altitudes and for at least three weights for interpolation. A Bizjet carries out the quasi-steady-state climb at a constant $V_{EAS} = 250$ knots until it reaches Mach 0.7; thereafter, it continues at a constant Mach number until it reaches the ceiling (i.e., rate of climb = 100 ft/min).



(a) Climb Speed Schedule



(b) Rate of Climb

Figure 13.12. Climb point performances

The next step is to perform the computations for the integrated climb performance in increments of approximately 5,000-ft altitudes (as convenient; at higher altitudes, smaller steps are appropriate) in which the variables are kept invariant using their mean values (see Figure 13.10). Equations 13.15 through 13.18 are used to compute the integrated performances. Figure 13.13 shows the integrated

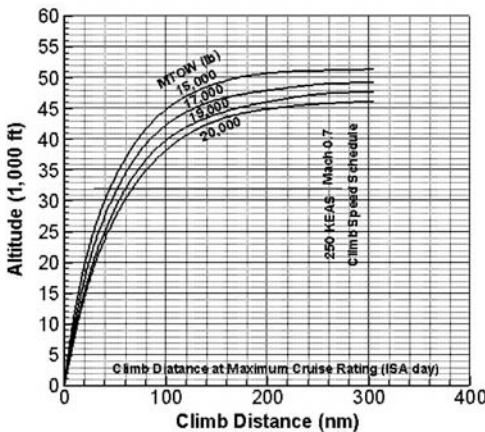
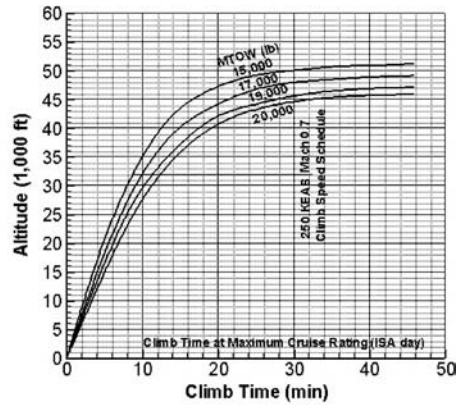
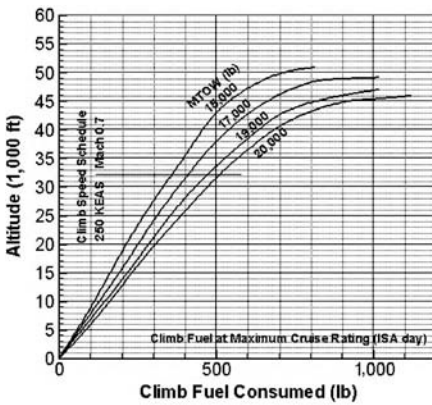


Figure 13.13. Integrated climb performances for a Bizjet

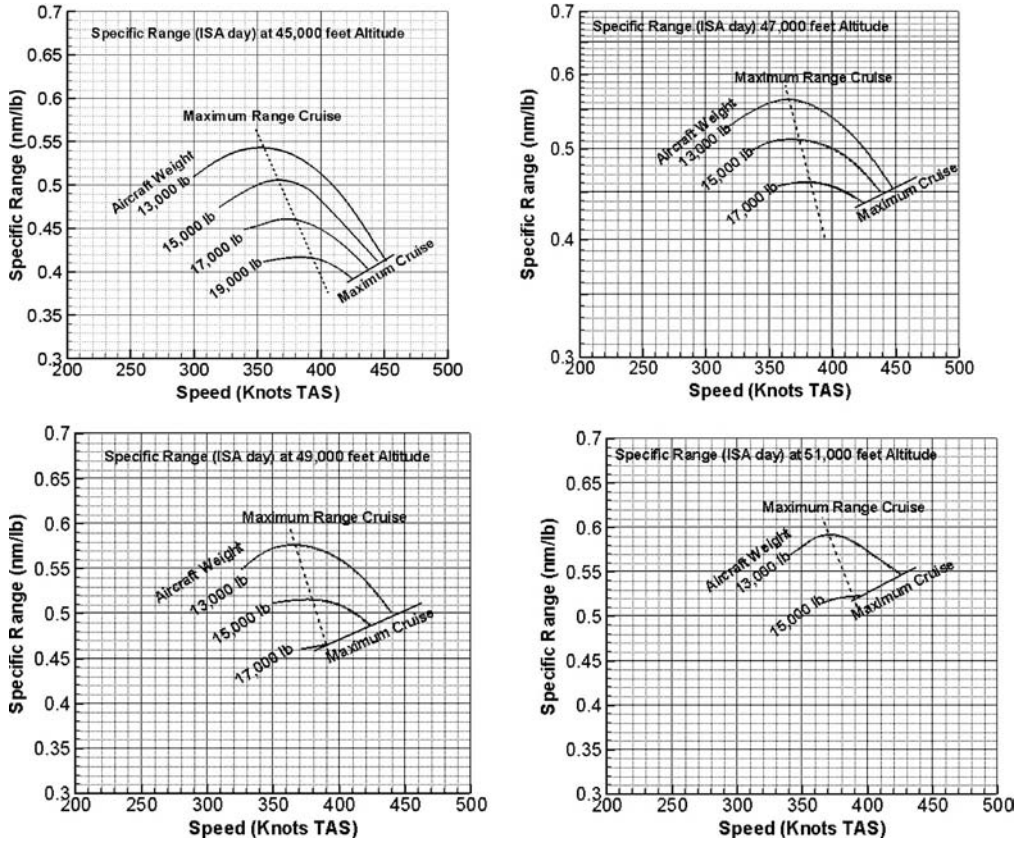


Figure 13.14. Specific range of a Bizjet

performances of fuel consumed, distance covered, and time taken to climb at the desired altitude.

13.5.5 Initial High-Speed Cruise (Bizjet)

An aircraft at the initial HSC is at Mach 0.74 (i.e., 716.4 ft/s) at a 41,000-ft altitude ($\rho = 0.00055 \text{ slug/ft}^3$). The fuel burned to climb is computed (but not shown) as 700 lb. The aircraft weight at initial cruise is 20,000 lb. At Mach 0.74, the aircraft lift coefficient $C_L = MTOM/qS_W = 20,000 / (0.5 \times 0.00055 \times 716.4^2 \times 323) = 20,000 / 45,627 = 0.438$.

The clean aircraft drag coefficient from Figure 9.2 at $C_L = 0.438$ gives $C_{D_{clean}} = 0.0324$. The clean aircraft drag, $D = 0.0324 \times (0.5 \times 0.00055 \times 716.4^2 \times 323) = 0.0324 \times 45,627 = 1,478 \text{ lb}$.

The available all-engines-installed thrust at maximum cruise rating at the speed and altitude from Figure 13.3 at Mach 0.74 is $T = 2 \times 790 = 1,580 \text{ lb}$ (adequate). The capability satisfies the market requirement of Mach 0.74 at HSC.

13.5.6 Specific Range (Bizjet)

Specific range is a convenient way to present cruise performance. Using Equation 13.27, the Sp.Rn is computed. The details of the specific range are not a direct

substantiation requirement; it is needed to compute the cruise-segment performances (i.e., fuel burned, distance covered, and time taken). Figure 13.14 shows the specific range for the Bizjet (i.e., the worked-out example). When readers redo the specific-range computations, there may be minor differences in the results. From the Sp. Rn values, the fuel burned and distance covered is worked out, which in turn gives the time taken for the distance.

13.5.7 Descent Performance (Bizjet)

It is also explained in Section 13.1 that only results of the integrated descent performance in graphical form are provided, as shown in Figures 13.16 through 13.18. It is convenient to establish first the descent velocity schedule (Figure 13.16) and the point performances of the rate of descent (Figure 13.17) down to sea level (this is valid for all weights; the difference between the weights is ignored). When readers redo the calculations, there may be minor differences in the results.

The related governing equations are explained in Section 13.4.3, which also mentions that the descent rate is restricted by the rate of the cabin-pressurization schedule to ensure passenger comfort. Two difficulties in computing the descent performance are the partial-throttle engine performance and the ECS pressurization capabilities, which dictate the rate of descent that, in turn, stipulates the descent velocity schedule (these are not provided in this book). Instructors may assist in establishing these two graphs, which – in the absence of any information – may be used. The following simplifications are useful.

The first simplification is in obtaining the partial-throttle engine performance, as follows:

1. The zero thrust at idle rpm is at about 40% of the maximum rated power/thrust.
2. The maximum cruise rating is taken at 85% of the maximum rated power/thrust.
3. The descent is carried out from 40 to 60% of the maximum cruise rating.

The second simplification is provision of the descent velocity schedule for the ECS capability.

In the industry, the exact installed-engine performance at each partial-throttle condition is computed from the engine deck supplied by the manufacturer. Also, the ECS manufacturer supplies the cabin-pressurization capability, from which aircraft designers work out the velocity schedule.

The inside cabin pressurization is restricted to the equivalent rate of 300 ft/min at sea level to ensure passenger comfort. An aircraft's rate of descent is then limited to the pneumatic capability of the ECS. A Bizjet is restricted to a maximum of 1,800 ft/min at any time (for a higher performance at lower altitudes, it can be increased to 2,500 ft/min). The descent speed schedule continues at Mach 0.6 from the cruise altitude until it reaches the approach height, when it then changes to a constant $V_{EAS} = 250$ knots until the end (for a higher performance, it can be increased to Mach 0.7 and $V_{EAS} = 300$ knots). The longest ranges can be achieved at the minimum rate of descent; this requires a throttle-dependent descent to stay within the various limits.

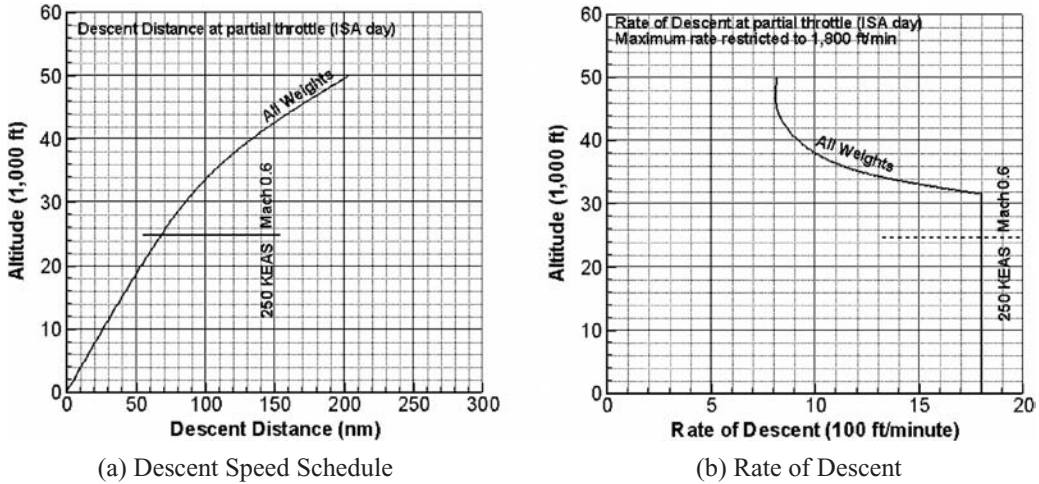


Figure 13.15. Descent point performance

It is convenient to establish first the point performances of the velocity schedule (Figure 13.15a) and the rate of descent (Figure 13.15b is for all weights; the variation is minor). The descent is performed within the limits of the passenger comfort level. However, in an emergency, a rapid descent is necessary to compensate for the loss of pressure and for oxygen recovery.

An integrated descent performance is computed in the same way as the climb performance; that is, it is computed in steps of approximate 5,000-ft altitudes (or as convenient) in which the variables are kept invariant. (Computation work is not shown herein.)

Figure 13.16 plots fuel consumed, time taken, and distance covered during the descent from the ceiling altitude to sea level. When readers redo the integrated descent performances, there may be minor differences in the results.

13.5.8 Payload Range Capability

A typical transport aircraft mission profile is shown in Figure 13.17. Equations 13.14 through 13.18 give the mission range and fuel consumption expressions as follows:

$$\begin{aligned} \text{mission range} = & \text{climb distance}(R_{climb}) + \text{cruise distance}(R_{cruise}) \\ & + \text{landing distance}(R_{descent}) \end{aligned}$$

where $R_{climb} = \Sigma \Delta s_{climb}$ and $R_{descent} = \Sigma \Delta s_{descent}$ are computed from the altitude increments.

$$\begin{aligned} \text{mission fuel} = & \text{climb fuel}(Fuel_{climb}) + \text{cruise fuel}(Fuel_{cruise}) \\ & + \text{descent fuel}(Fuel_{descent}) \end{aligned}$$

where $Fuel_{climb} = \Sigma \Delta fuel_{climb}$ and $Fuel_{descent} = \Sigma \Delta fuel_{descent}$ are computed from the altitude increments.

The minimum reserve fuel is computed for an aircraft maintaining a 5,000-ft altitude from Mach 0.35 to Mach 0.4 at about 60% of the maximum rating for

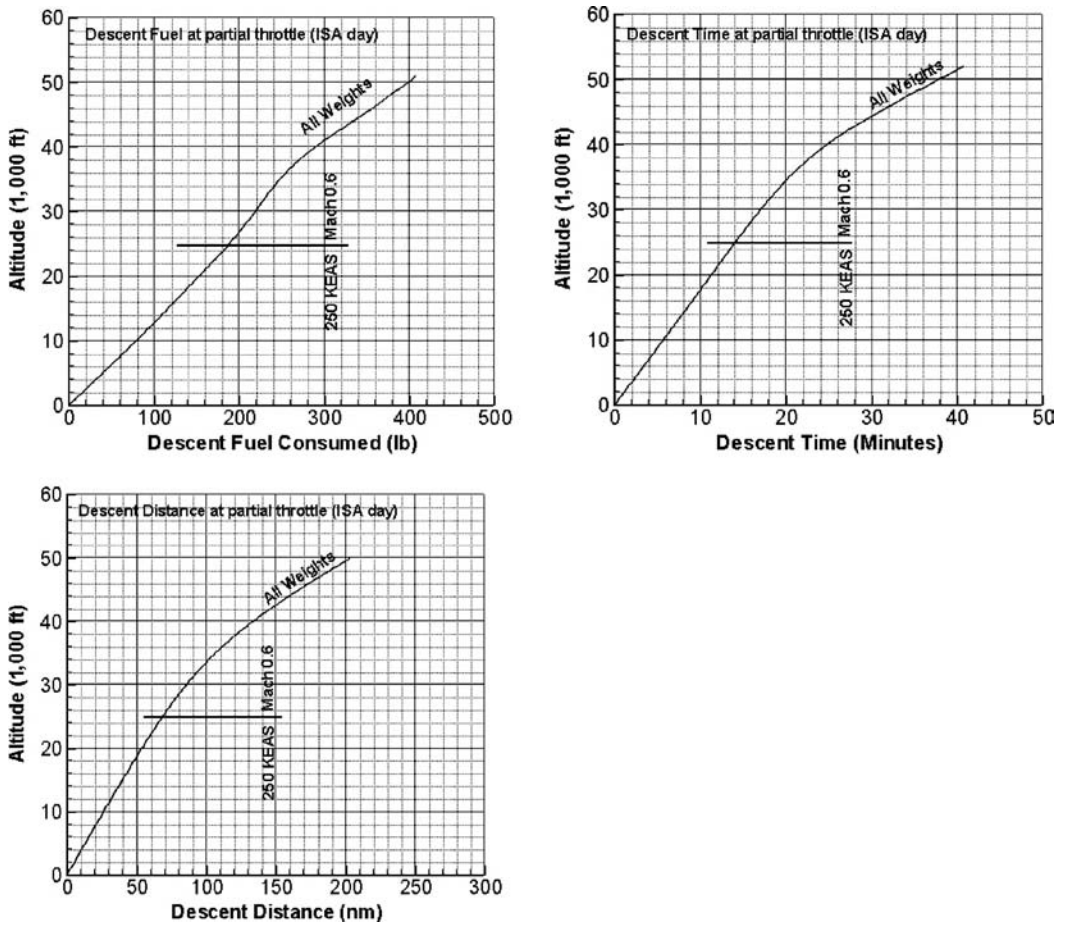


Figure 13.16. Integrated descent performance for a Bizjet

45 minutes or a 100 nm diversion cruising at Mach 0.5 and at a 25,000-ft altitude plus 20 minutes. The amount of reserve fuel must be decided by the operator and be suitable for the region of operation. The worked-out example uses the first option.

Fuel is consumed during taxiing, takeoff, and landing without any range contribution; this fuel is added to the mission fuel and the total is known as *block fuel*. The time taken from the start and stop of the engine at the beginning and the end of the mission is known as *block time*, in which a small part of time is not contributing to the gain in range. The additional fuel burn and time consumed without contributing

Figure 13.17. Transport-aircraft mission profile

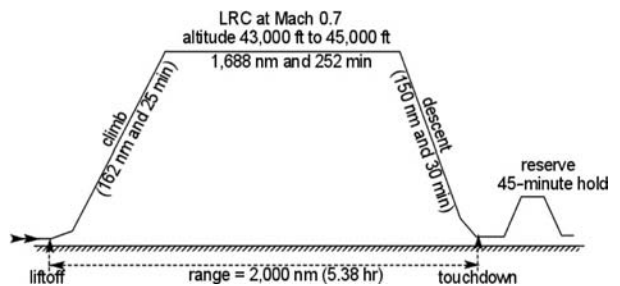


Table 13.18. *Bizjet range*

	Aircraft weight (lb)	Distance (nm)	Fuel (lb)	Time (min)
Start and taxi out	20,723	0	100*	3*
Takeoff to 1,500 ft	20,623	0	123*	5*
Climb to 43,000 ft	20,500	162	800	25
Initial cruise at 43,000 ft	19,700			
End cruise at 45,000 ft	16,240	1,688	3,460	252
Descent to 1,500 ft	15,900	150	340	30
Approach and land	15,800	0	100*	5*
Taxi in (from reserve)		0	20*	3*
Stage Total		2,000	4,923	323 (5.38 hrs)

* From operational statistics.

to range are shown in Table 13.17, taken from operational statistics. The descent fuel is estimated at 300 lb and the end cruise weight is computed as $W_{end.cruise} = 12,760 + 2,420 + 650 + 300 = 16,280$ lb. This is then iterated to correct the descent fuel in the final form, as shown in Table 13.17.

The cruise altitude of a Bizjet starts at 43,000 ft and ends at 45,000 ft (the design range is long in order to make an incremental cruise). The average value of cruising at 44,000 ft ($\rho = 0.00048$ slug/ft³) is used. The methods to compute R_{climb} and $R_{descent}$ are discussed in Section 13.4.3. Using Figures 13.11 through 13.13, the required values are given as $R_{climb} = 162$ nm, $Fuel_{climb} = 800$ lb, and $Time_{climb} = 25$ min, and $R_{descent} = 150$ nm, $Fuel_{descent} = 340$ lbs, and $Time_{descent} = 30$ min (in a partial-throttle, gliding descent). Table 13.18 displays the aircraft weight at each segment of the mission profile. The aircraft is at the LRC schedule operating at Mach 0.7 (OEW = 12,760 lb and payload = 2,420 lb).

For reserve fuel, at a 5,000-ft altitude ($\rho = 0.00204$ lb/ft³) and Mach 0.35 (384 ft/s) gives $C_L = 0.323$, resulting in $C_D = 0.025$ (see Figure 9.2). Equating thrust to drag, T/engine = 610 lb with sfc = 0.7 lb/hr/lb. For 45 minutes of holding, fuel consumed = $2 \times 0.75 \times 0.7 \times 610 = 640$ lbs. For safety, 800 lbs is used (operators can opt for higher reserves than the minimum requirement).

An aircraft must carry a reserve fuel for 45 minutes of holding and/or diversion around a landing airfield, which amounts to 600 lb. The range performance can be improved with a gradual climb from 43,000 to 47,000 ft as the aircraft becomes lighter with fuel consumed. From Table 13.18, the midcruise weight is $(19,700 + 16,240)/2 = 17,970$ lbs.

The LRC is at Mach 0.7 (677.7 ft/s). The engine-power setting is below the maximum cruise rating. The aircraft lift coefficient, $C_L = 17,970/(0.5 \times 0.00046 \times 677.7^2 \times 323) = 17,970/34,120 = 0.527$. From Figure 9.2, the clean aircraft drag coefficient, $C_D = 0.033$. The aircraft drag, $D = 0.033 \times (0.5 \times 0.00046 \times 677.7^2 \times 323) = 0.033 \times 34,120 = 1,126$ lb.

Therefore, the thrust required per engine is $1,126/2 = 563$ lbs. Figure 13.3 shows the available thrust of 620 lb per engine at the maximum cruise rating meant for HSC; that is, it allows throttling back for the LRC speed. The sfc is not much affected by the throttling back to the cruise rating. From Figure 10.6, the sfc at the

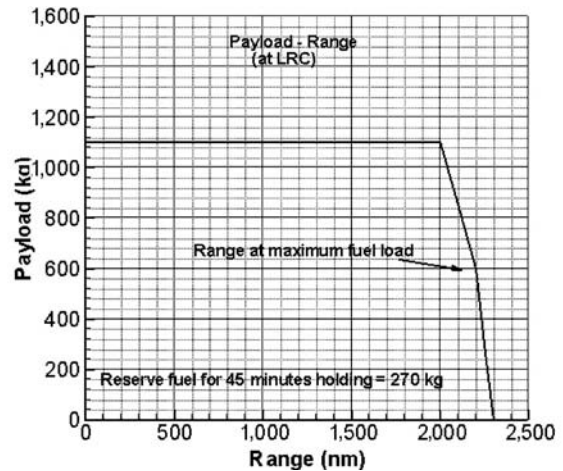


Figure 13.18. Bizjet payload-range capability

speed and altitude is 0.73 lb/hr/lb. The fuel flow per engine = $0.73 \times 563 = 411$ lb/hr; for two engines, it is 822 lb/hr.

From the initial and final cruise weight, the fuel burned during cruise is 3,460 lb. This results in a cruise time of $3,460 / (2 \times 411) = 4.21$ hr (252.5 min) of cruise time in which the distance covered is 4.21×0.68182 (the conversion factor from feet to miles) $\times 677.7 = 4.21 \times 462 = 1,945$ miles = 1,688 nm.

This mission range just satisfies the requirement of 2,000 nm. The block time for the mission is 5.38 hours and the block fuel consumed is 4,923 lb (2,233 kg). On landing, the return taxi-in fuel of 20 lb is taken from the reserve fuel of 600 lb. The total onboard fuel carried is therefore $4,923 + 600 = 5,523$ lb.

The payload-range graph is shown in Figure 13.18. A summarized discussion of the Bizjet design is in Section 13.7.

The fuel tank has a larger capacity than what is required for the design payload range. The payload can be traded to increase the range until the tanks fill up. Further reductions of payload make the aircraft lighter, thereby increasing the range.

13.6 Aircraft Performance Substantiation: Military Aircraft (AJT)

Military aircraft certification standards are different from civil aircraft standards. There is only one customer (MOD) requirement and the design standards vary among countries based on defense requirements. The safety issues are similar in reasoning but differ in the required specifications. It is suggested that readers obtain the regulatory MILSPECS from their respective Ministry or Department of Defense – they are generally available in the public domain. In this book, the procedure to substantiate performance capabilities is the same as for civil aircraft, covered in detail in the previous section.

13.6.1 Mission Profile

The fuel load and management depends on the type of mission. Military aircraft mission profiles are varied. Figure 13.19 shows a typical, normal training profile used to gain airmanship and navigational skills in an advanced aircraft.

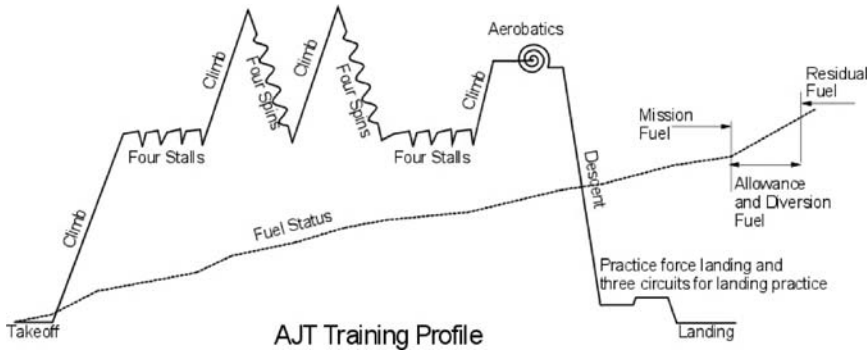


Figure 13.19. Normal training sortie profile (60 minutes)

Combat missions depend on the target range and expected adversary’s defense capability. Two typical missions are shown in Figure 13.20. Air defense requires continuous intelligence information feedback. Armament training practice closely follows a combat mission profile.

The study of combat missions requires complex analyses by specialists. Defense organizations conduct these studies and, understandably, they are confidential in nature. Game theory, twin-dome combat simulations, and so forth are some of the tools for such analyses. Actual combat may prove to be quite different because everything is not known about an adversary’s tactics and capabilities. A detailed study is beyond the scope of this book, as well as of most academies.

13.6.2 Takeoff Field Length (AJT)

With a single engine, there is no question about the BFL. The military aircraft TOFL must satisfy the CFL. The CFL also can have a decision speed V_I that is determined by whether a pilot can stop within the distance available; otherwise, the pilot ejects.

To obtain the CFL for a single-engine aircraft, the decision speed is at the critical time just before a pilot initiates rotation at V_R . Then, the decision speed V_I is worked out from the V_R by allowing 1 s for the recognition time. An engine failure occurring before this V_I leads a pilot to stop the aircraft by applying full brakes and deploying any other retarding facilities available (e.g., brake-parachute). There should be sufficient runway available for a pilot to stop the aircraft from this V_I .

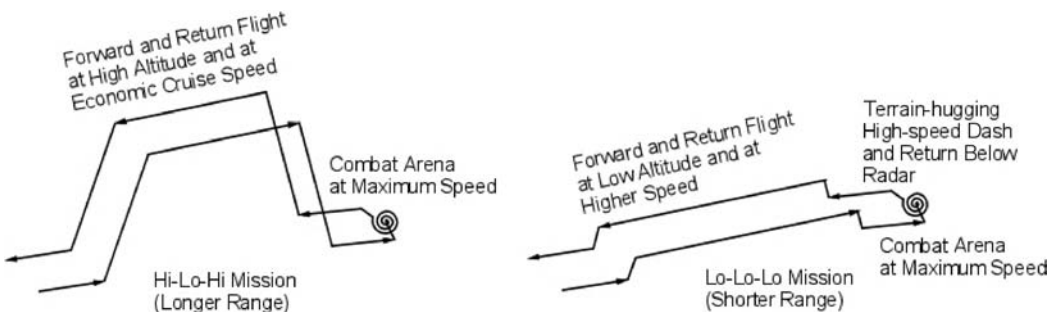


Figure 13.20. Typical combat profile

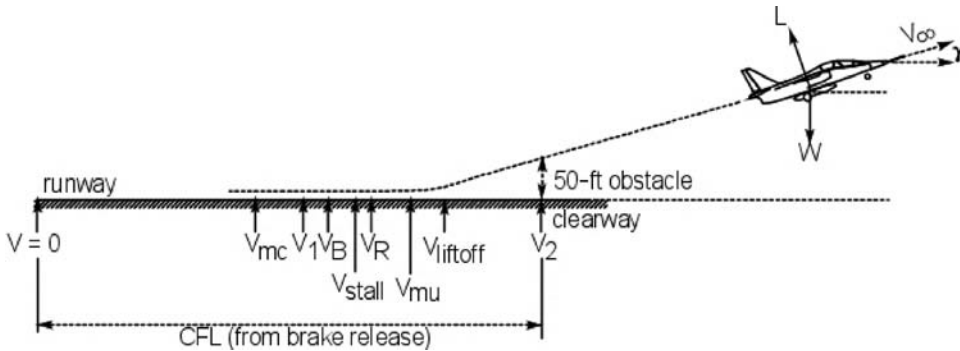


Figure 13.21. AJT takeoff

Engine failure occurring after the V_I means that a pilot will have no option other than to eject (i.e., if there is not enough clearway available to stop). For a multi-engine aircraft, determining the CFL follows the same procedure as in the civil-aircraft computation but it complies with MILSPECS.

Figure 13.21 shows the takeoff speed schedule of a single-engine military type aircraft.

In this book, the following three requirements for the AJT are worked out:

1. Meet the takeoff distance of 3,600 ft (1,100 m) to clear 15 m.
2. Meet the initial rate of climb (unaccelerated) of 10,000 ft/min (50 m/s).
3. Meet the maximum cruise speed of Mach 0.85 at a 30,000-ft altitude.

MIL-C501A requires a rolling coefficient, $\mu = 0.025$, and a minimum braking coefficient, $\mu_B = 0.3$. Training aircraft have a good yearly utilization operated by relatively inexperienced pilots (with about 200 hours of flying experience) carrying out numerous takeoffs and landings on relatively shorter runways. The AJT brakes are generally more robust in design, resulting in a brake coefficient, $\mu_B = 0.45$, which is much higher than the minimum MILSPEC requirement.

The Bizjet and the AJT have the same class of aerofoil and types of high-lift devices. Therefore, there is a strong similarity in the wing aerodynamic characteristics. Table 13.19 lists the AJT data pertinent to takeoff performance.

Equation 13.2 gives the average acceleration as:

$$\bar{a} = g[(T/W - \mu) - (S_L S_q / W)(C_D / C_L - \mu)]$$

Using the values given in Table 13.15:

$$\begin{aligned} \bar{a} &= 32.2 \times [(0.55 - 0.025) - (C_{Lq}/58)(0.1 - 0.025)] \\ &= 32.2 \times [0.525 - (C_{Lq}/773.33)] \end{aligned}$$

Refer to Figure 13.21, which shows the AJT takeoff profile with an 8-deg flap.

Distance Covered from Zero to the Decision Speed V_I

The decision speed V_I is established as the speed at 1 s before the rotation speed V_R . The acceleration of 16 ft/s^2 (which can be computed first and then iterated without estimating) is estimated as follows:

Table 13.19. *AJT takeoff distance, $S_W = 17 \text{ m}^2$ (183 ft^2)*

Flap setting (deg)	0	8*	20*	Landing*
$C_{D_{pmin}}$	0.0212	0.0212	0.0212	0.0212
$C_{L_{max}}$	1.50	1.65	1.85	2.20
$\Delta C_{D_{flap}}$	0	0.012	0.030	0.300
$\Delta C_{D_{U/C}}$	0.0222	0.0220	0.0212	0.0210
Rolling-friction coefficient, μ	0.025	0.025	0.025	0.025
Braking-friction coefficient, μ_B	0.3	0.3	0.3	0.3
V_{stall} @ 10,582 lb (ft/s)	180	171.7	162.1	—
V_R (kt) (1.688 ft/s) @ 1.11 V_{stall}		112.9 (190.6)	106.6 (180.0)	—
V_{LO} (kt) (1.688 ft/s) @ 1.12 V_{stall}		114 (192.5)	107.6 (181.6)	—
V_2 (kt) (1.688 ft/s)		122 (206.0)	115.2 (194.5)	—
T/W	0.55	0.55	0.55	—
W/S_W (lb/ ft^2)	58	58	58	—
C_D/C_L at ground run		0.1	0.1	—

* Takeoff at 8- and 20-deg flaps. Landing at 35- to 40-deg flaps, engines at idle, and V_{stall} at aircraft landing weight of 8,466 lb.

$V_I = 190.6 - 16 = 174.6$ ft/s. Aircraft velocity at 0.7 $V_I = 122.22$ ft/s. $q =$ (at 0.7 V_I) = $0.5 \times 0.002378 \times 0.49V_I^2 = 0.000583 \times V_I^2 = 8.7$. Up to V_I , the average $C_L = 0.5$ (still at low incidence). Then:

$$\begin{aligned}\bar{a} &= 32.2 \times (0.525 - C_L q / 773.33) = 32.2 \times (0.525 - 4.35 / 773.33) \\ &= 32.2 \times 0.519 = 16.72 \text{ ft/s}^2\end{aligned}$$

Using Equation 13.3, the distance covered until the liftoff speed is reached:

$$S_{G-1} = V_{ave} \times (V_1 - V_0) / \bar{a} \text{ ft} = 87.3 \times (174.6 - 0) / 16.72 = 912 \text{ ft}$$

However, provision must be made for engine failure at the decision speed, V_I , when braking must be applied to stop the aircraft. Designers must ensure that the operating runway length is adequate to stop the aircraft.

If the engine is operating, then an AJT continues with the takeoff procedure when liftoff occurs after rotation is executed at V_R .

Distance Covered from Zero to Liftoff Speed V_{LO}

Using the same equation for distance covered up to the decision speed V_I with the change to liftoff speed, $V_{LO} = 192.5$ ft/s. Aircraft velocity at 0.7 $V_{LO} = 134.75$ ft/s, $q =$ (at 0.7 V_I) = $0.5 \times 0.002378 \times 0.49V_{LO}^2 = 10.586$. Up to V_{LO} , the average $C_L = 0.5$ (still at low incidence). Then:

$$\begin{aligned}\bar{a} &= 32.2 \times (0.525 - C_L q / 773.33) = 32.2 \times (0.525 - 4.35 / 773.33) \\ &= 32.2 \times 0.519 = 16.72 \text{ ft/s}^2\end{aligned}$$

Using Equation 13.3, the distance covered until the liftoff speed is reached:

$$S_{G-LO} = V_{ave} \times (V_1 - V_0) / \bar{a} \text{ ft} = 96.25 \times (192.5 - 0) / 16.42 = 1,128 \text{ ft}$$

Distance Covered from V_{LO} to V_2

The flaring distance is required to reach V_2 , clearing a 50-ft obstacle height from V_{LO} . From statistics, the time to flare is 3 s with an 8-deg flap and at $V_2 = 206$ ft/s. In 3 s, the aircraft covers $S_{G,LO,V_2} = 3 \times 206 = 618$ ft.

Total Takeoff Distance

The takeoff length is thus $S_{G,LO} + S_{G,LO,V_2} = (1,128 + 618) = 1,746$ ft, much less than the required TOFL of 3,500 ft for the full weight of 6,800 kg ($\approx 15,000$ lb) for armament training. In this case, a higher flap setting of 20 deg may be required. At a higher flap setting, an aircraft has a shorter CFL for the same weight.

Stopping Distance and the CFL

- distance covered from zero to the decision speed V_I , $S_{G,I}$; it was previously computed as 912 ft
- distance covered from V_I to braking speed V_B , $S_{G,I,B}$
- braking distance from V_B ($\approx V_I$) to zero velocity, $S_{G,B,0}$

The next step is to verify what is required to stop the aircraft if an engine fails at V_I . The stopping distance has the following three segments. (The CFL is normally longer than the TDFL.)

Distance Covered from V_I to Braking Speed V_B

At engine failure, 3 s is assumed for a pilot's recognition and taking action. Therefore, the distance covered from V_I to V_B is $S_{G,I,B} = 3 \times 174.6 = 524$ ft.

Braking Distance from V_B ($\approx V_I$) to Zero Velocity (Flap Settings Are of Minor Consequence)

The most critical moment of brake failure is at the decision speed V_I , when the aircraft is still on the ground. With the full brake coefficient, $\mu = 0.45$, and the average $C_L = 0.5$, $V_I = 174.6$ ft/s. With aircraft velocity at 0.7, $V_1 = 122.22$ ft/s, $q = (\text{at } 0.7V_1) = 0.5 \times 0.002378 \times 0.49V_1^2 = 0.000583 \times V_1^2 = 8.7$.

Equation 13.2 for average acceleration reduces to:

$$\begin{aligned}\bar{a} &= 32.2 \times [(-0.45) - (0.5 \times 8.7)/58](0.1 - 0.45)] \\ &= 32.2 \times [-0.45 + (1.52/58)] \\ &= 32.2 \times (-0.45 + 0.026) = -13.65\end{aligned}$$

Using Equation 13.3, the distance covered with the liftoff speed is reached:

$$S_{G-0} = V_{ave} \times (V_1 - V_0)/\bar{a} \text{ ft} = 87.3 \times (174.6 - 0)/13.65 = 1,119 \text{ ft}$$

Therefore, the minimum runway length (CFL) for takeoff should be $= S_{G,I} + S_{G,I,B} + S_{G,0}$. The TOFL = $912 + 524 + 1,119 = 2,555$ ft, which is still within the specified requirement of 3,600 ft.

The takeoff length is thus 1,746 ft, much less than the CFL of 2,555 ft computed previously. The required TOFL is 3,500 ft (computation not shown) for the full weight of 6,800 kg ($\approx 15,000$ lb) for armament training. In this case, a higher flap setting of 20 deg may be required. At a higher flap setting, an aircraft has a shorter CFL for the same weight.

The length of the runway available dictates the decision speed V_I . If the airfield length is much longer, then a pilot may have a chance to land the aircraft if an engine failure occurs immediately after liftoff; it may be possible to stop within the available airfield length, which must have some clearway past the runway end.

This is compared with the minimum MILSPEC requirement of $\mu = 0.3$.

Equation 13.2 for average acceleration reduces to:

$$\begin{aligned}\bar{a} &= 32.2 \times [(-0.3) - (0.5 \times 8.7)/58](0.1 - 0.3) = 32.2 \times [-0.3 + (0.87/58)] \\ &= 32.2 \times (-0.3 + 0.015) = -9.18\end{aligned}$$

Using Equation 13.3, the distance covered from V_B to zero:

$$S_{G-0} = V_{ave} \times (V_I - V_0)/\bar{a} \text{ ft} = 87.3 \times (174.6 - 0)/9.18 = 1,660 \text{ ft}$$

This value is on the high side. The minimum runway length for takeoff should be $= S_{G-I} + S_{G-I-B} + S_{G-0}$.

The CRL = $912 + 524 + 1,660 = 3,096$ ft is on the high side but within the specification of 3,600 ft. Therefore, the higher brake coefficient of 0.4 is used. This is not problematic because wheels with good brakes currently have a much higher friction coefficient μ .

A reduction of the decision speed to 140 ft/s (83 kts) reduces the $S_{G-0} = 1,068$ ft, decreasing the CRL to 2,504 ft.

Verifying the Climb Gradient at an 8-Deg Flap

Using AJT $V_2 = 206$ ft/s (see Table 13.15) and $W = 10,580$ lb (4,800 kg) gives $C_L = (2 \times 10,580)/(0.5 \times 0.002378 \times 183 \times 206^2) = 21,160/22,680 = 0.932$.

The clean aircraft drag coefficient from Figure 9.16 gives $C_{D_{clean}} = 0.1$. Add $\Delta C_{D_{flap}} = 0.012$ and $\Delta C_{D_{U/C}} = 0.022$, giving $C_D = 0.1 + 0.012 + 0.022 = 0.134$. Therefore, drag, $D = 0.134 \times (0.5 \times 0.002378 \times 206^2 \times 183) = 0.134 \times 22,680 = 3,040$ lb. The available thrust is 5,000 lb (see Figure 13.4).

From Equation 13.5, the quasi-steady-state rate of climb is shown by:

$$R/C_{accl} = \frac{V[(T - D)/W]}{1 + (V/g)(dV/dh)}$$

At the quasi-steady-state climb, Table 13.5 shows $\frac{V}{g} \left(\frac{dV}{dh}\right) = 0.566 \text{ m}^2 = 0.56 \times 0.2^2 = 0.0224$. Hence, $R/C_{accl} = \{[206 \times (5,000 - 3,040) \times 60]/10,580\} / [1 + 0.0224] = (206 \times 1,960 \times 60)/(10,817) = 2,240$ ft/min. This capability satisfies the military requirement of 500 ft/min (2.54 m/s). Readers may verify the 20-deg flap setting.

13.6.3 Landing Field Length (AJT)

Keeping a reserve fuel of 440 lb (200 kg), the landing weight of an AJT is 8,466 lb (wing-loading = 42.26 lb/ft²) and at full flap extended, $C_{L_{max}} = 2.2$. Therefore:

$$\begin{aligned}V_{stall@land} \sqrt{\frac{2 \times 8,466}{0.002378 \times 183 \times C_L}} &= \sqrt{\frac{38,908}{2.2}} = 133 \text{ ft/s} \\ V_{appr} &= 1.2V_{stall@land} = 160 \text{ ft/s} \\ V_{TD} &= 1.1V_{stall@land} = 146 \text{ ft/s}\end{aligned}$$

The average velocity from a 50-ft altitude to touchdown = 153 ft/s. The distance covered before brake application after 6 s from a 50-ft altitude:

$$S_{G-TD} = 6 \times 153 = 918 \text{ ft}$$

For an aircraft in full braking with $\mu_B = 0.45$, all engines shut down, and average $C_L = 0.5$, $C_D/C_L = 0.1$.

Equation 13.2 for average acceleration is based on $0.7 V_{TD} = 107.1 \text{ ft/s}$. Then:

$$q = 0.5 \times 0.002378 \times 107.1^2 = 13.64$$

Deceleration, $\bar{a} = 32.2 \times [(-0.45) - (C_L q / 42.26)(0.1 - 0.45)] = 32.2 \times [-0.45 + (0.15 \times 13.64 / 42.26)] = 32.2 \times [-0.45 + 0.0484] = -12.93 \text{ ft/s}^2$.

The distance covered during braking, $S_{G-Land} = (146 \times 73) / 12.93 = 824 \text{ ft}$. The landing distance $S_{G-Land} = 918 + 824 = 1,742 \text{ ft}$. Multiplying by 1.667, the rated LFL = $1.667 \times 1,742 = 2,904 \text{ ft}$ and is expected to be less than the TOFL at an 8-deg flap setting (but not always). This is within the specification of 3,600 ft.

13.6.4 Climb Performance Requirements (AJT)

Military trainers should climb at a much higher rate of climb than civil aircraft. The requirement of 50 m/s (10,000 ft/min) at normal training configuration (NTC) is for an unaccelerated climb for comparison with accelerated climb. Unaccelerated rate of climb varies depending on the constant speed (i.e., EAS) climb, making a comparison difficult. This section presents calculations for both rates of climb.

This section checks only the enroute climb with a clean configuration. The unaccelerated climb Equation 13.7 is used. The MTOM at the NTC is 4,800 kg (10,582 lb). The wing area $S_W = 17 \text{ m}^2$ (183 ft²).

During an enroute climb, the aircraft has a clean configuration. Under maximum takeoff power, it makes an accelerated climb to 800 ft ($\rho = 0.00232 \text{ slug/ft}^3$, $\sigma = 0.9756$) from the second-segment velocity of V_2 to reach a 350-KEAS speed schedule to start the enroute climb. During enroute climb, the engine throttle is retarded to the maximum climb rating. The quasi-steady-state climb schedule maintains 350 KEAS and the aircraft accelerates with an altitude gain at a rate of dV/dh until it reaches Mach 0.8 at around 25,000 ft. From there, the Mach number is held constant until it reaches the cruise altitude. We assume that 100 kg of fuel is consumed to taxi and climb to an 800-ft altitude, where the aircraft mass is 4,700 kg (10,362 lb). At 350 kts (590.8 ft/s, Mach 0.49), the aircraft lift coefficient is:

$$\begin{aligned} C_L &= \text{MTOM} / q S_W = 10,362 / (0.5 \times 0.00232 \times 590.8^2 \times 183) \\ &= 10,582 / 74,905 = 0.138 \end{aligned}$$

The clean aircraft drag coefficient from (see Figure 9.19) at $C_L = 0.141$ gives $C_{Dclean} = 0.023$. The clean aircraft drag, $D = 0.023 \times (0.5 \times 0.002378 \times 590.8^2 \times 183) = 0.023 \times 74,905 = 1,723 \text{ lb}$. The available engine-installed thrust at a maximum continuous rating (95% of maximum thrust, as given in Figure 13.4) at Mach 0.49 (459.8 ft/s) is $T = 0.95 \times 5,000 = 4,750 \text{ lb}$. From Equation 13.10, the accelerated rate of climb is as follows:

$$R/C_{aacl} = \frac{V[(T - D)/W]}{1 + (V/g)(dV/dh)}$$

At a quasi-steady-state-climb, Table 13.5 gives:

$$\frac{V}{g} \left(\frac{dV}{dh} \right) = 0.56 \text{ m}^2 = 0.56 \times 0.49^2 = 0.1345$$

From Equation 13.5, the rate of climb is:

$$\begin{aligned} R/C_{accl} &= \{[590.8 \times (4,750 - 1,723) \times 60]/10,362\}/[1 + 0.1345] = 10,355/1.1345 \\ &= 9,127 \text{ ft/min} \end{aligned}$$

Therefore, the unaccelerated rate of climb, $R/C = 10,355 \text{ ft/min}$. The aircraft specification is based on an unaccelerated climb of $10,000 \text{ ft/min}$, which is just met. (Here, the cabin area is small and the pressurization limit is high.)

13.6.5 Maximum Speed Requirements (AJT)

An aircraft at HSC is at Mach 0.85 (845.5 ft/s) at a 30,000-ft altitude ($\rho = 0.00088 \text{ slug/ft}^3$). The fuel burned to climb is computed (but not shown) as 582 lb. The aircraft weight at the altitude is 10,000 lb.

At Mach 0.85, the aircraft lift coefficient $C_L = \text{MTOM}/qS_W = 10,000/(0.5 \times 0.00088 \times 845.5^2 \times 183) = 10,000/57,561.4 = 0.174$.

The clean aircraft drag coefficient (see Figure 9.16) at $C_L = 0.174$ gives $C_{D_{clean}} = 0.025$ (high speed). The clean aircraft drag, $D = 0.025 \times (0.5 \times 0.00088 \times 858.5^2 \times 183) = 0.025 \times 5,7561.4 = 1,440 \text{ lb}$.

The available engine-installed thrust at the maximum cruise rating (i.e., 85% of the maximum rating) is from Figure 13.4 at Mach 0.85, and at a 30,000-ft altitude is $T = 0.85 \times 2,000 = 1,700 \text{ lb}$. (In the industry, the thrust is computed.)

Therefore, the AJT satisfies the customer requirement of Mach 0.85 at HSC.

13.6.6 Fuel Requirements (AJT)

Other than a ferry flight, military aircraft are not dictated only by the cruise sector, unlike in a civil aircraft mission. A short combat time at the maximum engine rating, mostly at low altitudes, is responsible for a suitable part of the fuel consumed. However, the range to the target area dictates the fuel required. A long-distance ferry flight and combat arena require additional fuel to be carried by drop tanks. Immediately before combat, the drop tanks (they are empty) by then can be jettisoned to gain aircraft performance capability. The CAS variant has this type of mission profile.

A training mission has a varied engine demand and it returns to its own base covering no range, as shown in Figure 13.19. Mission fuel is computed sector by sector of fuel burn, as shown as follows for the coursework example. To compute the fuel requirement, climb and specific-range graphs for the AJT at NTC are required (Figures 13.22 and 13.23). To compute the varied engine demand of a training-mission profile, Figure 13.4 is used to establish the fuel-flow rate for the throttle settings. The graph is valid for 75% rpm to 100% ratings. Typically, it has the approximate following values:

- at idle (50% rpm) $\approx 8 \text{ kg/min}$
- at 75% rpm $\approx 11 \text{ kg/min}$
- at 95% rpm $\approx 16.5 \text{ kg/min}$

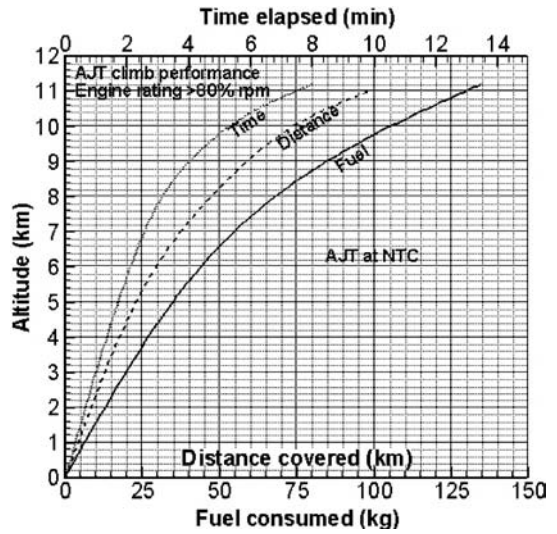


Figure 13.22. AJT climb performance

Fuel and time consumed for the NTC of the AJT is shown in Table 13.20.

13.7 Summary

This chapter is the culmination of progress on the configuring, sizing, and substantiating of the coursework examples. It is time to review whether the Bizjet and the AJT designs need any revision. With commonality in design considerations, the turboprop aircraft is not addressed herein. The remaining chapters contain information on topics in which designers must be knowledgeable.

The sizing exercise (see Chapter 11) provides a simultaneous solution to satisfy airworthiness and market requirements. Wing-loading (W/S_w) and thrust-loading (T/W) are the dictating parameters and they appear in the equations for takeoff, second-segment climb, enroute climb, and maximum speed capability; the first two are FAR requirements, the last two are customer requirements. Detailed information on engine performance is not required during the sizing exercise. Substantiation

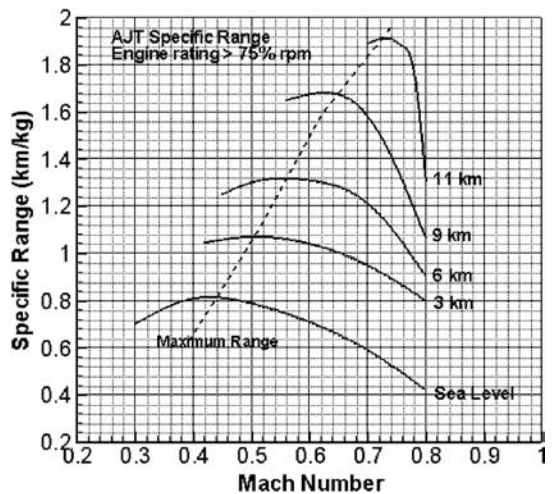


Figure 13.23. AJT specific range

Table 13.20. *AJT mission fuel and time consumed*

	Fuel burned kg	Time min	Engine rating = % rpm
Taxi and takeoff	60	6	60% (idle)
Takeoff and climb to 6-km altitude	125	5	Takeoff @ 100%, then @ 95%
Four turns	50	4	1 min @ 95% + 3 min @ 60%
Four stalls	60	5	1 min @ 95% + 4 min @ 60%
Climb from 5- to 8-km altitude	50	3	95%
Four turn spins	25	3	60%
Climb from 5- to 8-km altitude	50	3	95%
Four turn spins	25	3	60%
Climb from 5- to 6-km altitude	15	1	95%
Aerobatics practice	70	6	95%
Descent and practice force landing	95	8	2 min @ 95% + 6 min @ 60%
Three circuits for landing practice	110	10	Average 80%
Approach, land, return taxi	40	4	60%
Trainee pilot allowance	30	2	95%
Total mission fuel	805	59 (\approx 60)	
Diversion	200		
Residual fuel	105		
Total onboard fuel	1,110 (conservative estimate)		
	(Internal fuel capacity = 1,400 kg)		

of the payload-range estimation, as a customer requirement, is not possible during the sizing exercise because it requires detailed engine performance data. Subsequently, with detailed engine performance data, relevant aircraft performance analyses are conducted more accurately to guarantee airworthiness and market requirements.

A more detailed aircraft performance is estimated during the Detailed Definition Phase, which is beyond the scope of this book. The full aircraft performance does not affect aircraft configuration and mass unless the design review results in new demands for changes. These are management issues that are reviewed with potential customers to decide whether to give a go-ahead. Once a go-ahead is obtained, a full-blown detailed definition study ensues as Phase 2 activities, with significant financial commitments.

Figure 11.3 (Bizjet) and Figure 11.5 (AJT) show the lines of constraints for the various sizing requirements. The sizing point to satisfy all requirements shows a different level of margins for each capability. Typically, the initial enroute climb rate is the most critical to sizing. Therefore, the takeoff and maximum speed capabilities have a considerable margin, which is desirable because the aircraft can do better than what is required.

From statistics, experience shows that aircraft mass grows with time. This occurs primarily due to modifications resulting from mostly minor design changes and changing requirements – at times, even before the first delivery is made. If new requirements demand several changes, then a civil aircraft design may appear as a new variant. However, military aircraft design holds a little longer before a new variant emerges. It is therefore prudent for designers to maintain some margin,

especially reserve thrust capability – that is, keep the thrust-loading (T/W) slightly higher. Re-engining with an updated version is costly.

It can be seen that field performance requires a larger wing planform area (S_W) than at cruise. It is advisable to keep the wing area as small as possible (i.e., high wing-loading) by incorporating a superior high-lift capability, which is not only heavy but also expensive. Designers must seek a compromise to minimize operating costs (see Chapter 16). Iterations were not needed for the designs worked out in this book.

13.7.1 The Bizjet

The sizing point in Figure 11.3 shows a wing-loading, $W/S_W = 64 \text{ lb/ft}^2$, and a thrust-loading, $T/W = 0.32$; there is little margin given for the landing requirement. The maximum landing mass for this design is at 95% of the MTOM. If for any reason the aircraft OEW increases, then it is better if the sizing point for the W/S_W is somewhat lower than 64 lb/ft^2 – for example, 62 lb/ft^2 and/or increase T/W to 0.35. A quick iteration resolves the problem; however, this choice is not exercised to keep the wing area as small as possible. Instead, an aircraft is allowed to approach landing at a slightly higher speed because the LFL is generally shorter than the TOFL. This is easily achievable because the commonality of the undercarriage for all variants starts with the design of the heaviest (i.e., for the growth variant), and then the bulky components are reduced for lighter weights. The middle variant is used as the baseline version; its undercarriage can be made to accept the MTOM growth as a result of the OEW growth instead of making the wing larger.

Civil aircraft are recommended to come in a family of variants in order to cover wider market demands to maximize sales. However, none of the three variants is optimized, although the baseline is carefully sized in the middle to accept one larger and one smaller variant. Even when development costs are front-loaded, the variant aircraft cost is low by sharing the component commonality. The low cost is then translated to a lowering of the aircraft price, which absorbs the operating costs of the slightly nonoptimized designs.

It is interesting to examine the design philosophy of the Boeing 737 and the Airbus 320 families of aircraft variants in the same market arena. Together, more than 8,000 aircraft have been sold in the world market, which is no small achievement in engineering. The cost of these aircraft is about \$50 million each (in 2005). For airlines with deregulated fare structures, making a profit involves complex dynamics of design and operation. The cost and operational scenario changes from time to time (e.g., increases in fuel cost and terrorist threats).

As early as the 1960s, Boeing recognized the potential for keeping component commonality in offering new designs. The B707 was one of the earliest commercial-transport jet aircraft to carry passengers. It was followed by a shorter version, the B720. Strictly speaking, the B707 fuselage relied on the KC135 tanker design of the 1950s. From the four-engine B707 came the three-engine B727 and then the two-engine B737, both of which retained considerable fuselage commonality. This was one of the earliest attempts to utilize the benefits of maintaining component commonality. Subsequently, the B737 started to emerge in different sizes of variants, maximizing the component commonality. The original B737–100 was the baseline

design; all other variants that came later, up to the B737–900, are larger aircraft. This posed certain constraints, especially on the undercarriage length. Conversely, the A320 (serving as the baseline design) was in the middle of the family; its growth variant is the A321 and its smaller variants are the A319 and A318. Figure 4.7 illustrates how the OEW is affected by the two examples of family variants. A baseline aircraft starting in the middle of a family is better optimized; therefore, in principle, it provides a better opportunity to lower production costs of the variants.

The simultaneous failure of two engines is extremely rare. If it happens after the decision speed is reached and there is not enough clearway available, then it is a catastrophic situation. If the climb gradient is not in conflict with the terrain of operation, it is better to take off with higher flap settings. If a longer runway is available, then a lower flap setting can be used. Takeoff-speed schedules can slightly exceed FAR requirements, which stipulate the minimum values. There have been cases of all-engine failures occurring at cruise due to volcanic ash in the atmosphere, as well as in the rare event of fuel starvation. Fortunately, the engines were restarted just before the aircraft would have hit the surface. An all-engine failure due to a bird strike occurred in 2009 – miraculously, all survived after the pilot ditched the aircraft in the Hudson River in New York.

13.7.2 The AJT

Military aircraft serve only one customer, the Ministry or Department of Defense of the nation that designed the aircraft. Frontline combat aircraft incorporate the newest technologies at the cutting edge to stay ahead of potential adversaries. Development costs are high and only a few countries can afford to produce advanced designs. International political scenarios indicate a strong demand for combat aircraft, even for developing nations that must purchase them from abroad. Therefore, military aircraft design philosophy is different than civil aircraft design. Here, designers and scientists have a strong voice, unlike in civil design in which the users dictate the requirements. Selling combat aircraft to restricted foreign countries is one way to recover investment costs.

Once a combat aircraft performance is well understood over years of operation, consequent modifications follow capability improvements. Subsequently, a new design replaces an older design – there is a generation gap between the designs. Military modifications for the derivative design are substantial. Derivative designs primarily result from revised combat capabilities with newer types of armament, along with all around performance gains. There is also a need for modifications – perceived as variants rather than derivatives – to sell to foreign customers. These variants are substantially different than civil aircraft variants.

AJT designs have variants that serve as combat aircraft in CAS. AJTs are less critical in design philosophy compared with frontline combat aircraft, but they bear some similarity. Typically, an AJT has one variant in the CAS role produced simultaneously. There is less restriction to export these types of aircraft.

The military infrastructure layout influences aircraft design; here, the LCC is the primary economic consideration. For military trainer aircraft designs, it is best to have a training base located near the armament practice arena to save time. A dedicated training base may not have a runway as long as a major civil runway. This

is reflected in the user specifications necessary for beginning a conceptual study. The training mission includes aerobatics and flying with onboard instruments for navigation; therefore, the training base should be located far from the civil airline corridors.

The AJT sizing point in Figure 11.5 shows a wing-loading, $W/S_w = 58 \text{ lb/ft}^2$, and a thrust-loading, $T/W = 0.55$, which is a significant margin, especially for the landing requirements. The AJT can achieve a maximum level speed over Mach 0.88, but this is not demanded as a requirement. Mission weight for the AJT varies substantially; the NTC is at 4,800 kg and, for armament practice, it is loaded to 6,600 kg. The margin in the sizing graph encompasses an increase in loadings (the specification used in this book is for the NTC only). There is a major demand for higher power for the CAS variant. The choice of an uprated engine or an AB depends on the engine and the mission profile.

Competition for military aircraft sales is not as critical compared to the civil-aviation sector. The national demand supports the production of a tailor-made design with manageable economics. However, the trainer-aircraft market has competition – unfortunately, it is sometimes influenced by other factors that may fail to result in a national product, even if the nation has the capability. For example, the Brazilian design Tucano was re-engined and underwent massive modifications by Short Brothers of Belfast for the United Kingdom, RAF, and the BAe Hawk (UK) underwent major modifications in the United States for domestic use.

14 Computational Fluid Dynamics

14.1 Overview

Computational fluid dynamics (CFD) is a numerical tool for solving equations of fluid mechanics. CFD is a relatively recent development that has become an indispensable tool in the last two decades. It was developed originally for aeronautical uses but now pervades all disciplines involving flow phenomena, such as medical, natural sciences, and engineering applications. The built-in codes of the CFD software are algorithms of numerical solutions for the fluid-mechanics equations. Flow fields that were previously difficult to solve by analytical means – and, in some situations, impossible – are now accessible by means of CFD.

Today, the aircraft industry uses CFD during the conceptual study phase. There are limitations in obtaining accurate results, but research continues in academic and industrial circles to improve prediction. This chapter aims to familiarize newly initiated readers with the scope of CFD in configuring aircraft geometry (those already exposed to the subject may skip this chapter). This is not a book about CFD; therefore, this chapter does not present a rigorous mathematical approach but rather an overview.

CFD is a subject that requires considerable knowledge in fluid mechanics and mathematics. CFD is introduced late in undergraduate studies, when students have mastered the prerequisites. Commercial CFD tools are menu-driven and it is possible to quickly become proficient, but interpreting the results thus obtained requires considerable experience in the subject.

An accurate 3D model of an aircraft in CAD significantly reduces preprocessing time. The CAD software format must be compatible with CFD to transfer the drawing models. Together, CAD and CFD provide a CAE approach to paperless, electronic design methods.

Several good commercial CAD and CFD packages are available in the marketplace. Nowadays, all engineering schools have CAD and CFD application software.

14.1.1 What Is to Be Learned?

This chapter covers the following topics:

- Section 14.2: Introduction to the concept of CFD
- Section 14.3: Introduction to the current status of CFD
- Section 14.4: An approach to and considerations for CFD analysis
- Section 14.5: Case studies
- Section 14.6: Hierarchy of CFD simulation methods
- Section 14.7: Summary

14.1.2 Coursework Content

There is no coursework on CFD in the first term. However, it is recommended that CFD studies be undertaken in the second term after readers are formally introduced to the subject. Appropriate supervision is required to initiate the task and analyze the results. Any CFD coursework is separated from the scope of this book. The purpose of this chapter is to give newly initiated readers an introduction to aircraft-design work.

14.2 Introduction

Throughout this book, it is shown that the aerodynamic parameters of lift, drag, and moment associated with aircraft moving through the air are of vital importance. An accurate assessment of these parameters is the goal of aircraft designers.

Mathematically, lift, drag, and moment of an aircraft body can be obtained by integrating the pressure field around the aircraft computed from the governing conservation equations (i.e., differential or integral forms) of mass, momentum, and energy with the equation of state for air. Until the 1970s, wind-tunnel tests were the only way to obtain the best results of these parameters in the various aircraft attitudes representing what can be encountered within the full flight envelope. Semi-empirical formulae generated from vast amounts of test results, backed up by theory, provided a good starting point for any conceptual study.

Numerical methods for solving differential equations prevailed for some time. The Navier–Stokes equations provided an accurate representation of the flow field around the aircraft body under study. However, solving the equation for 3D shapes in compressible flow was difficult, if not sometimes impossible. Mathematicians devised methods to discretize differential equations into algebraic form that are solvable even for the difficult nonlinear, partial-differential equations. During the early 1970s, CFD results of simple 2D bodies in inviscid flow were demonstrated as comparable to wind-tunnel test results and analytical solutions.

The industry recognized the potential and progressed with in-house research; in some cases, complex flow phenomena hitherto unknown were understood. Subsequently, CFD proliferated in academies and there was rapid advancement in achieving solution techniques. Over time, the methodologies continued to improve. The latest technique discretizes the flow field into finite volumes in various sizes (i.e., smaller when the fluid properties have steeper variations) matching the wetted surface of the object, which also needs to be divided into cells/grids. The cells/grids do not overlap the adjoining volumes but rather mesh seamlessly. The mathematical

formulation of the small volumes now can be treated algebraically to compute the flux of conserved properties between neighboring cells. Discrete steps of algebraic equations are not the calculus of limiting values at a point; therefore, errors creep into the numerical solution. Mathematicians are aware of the problem and struggle with better techniques to minimize errors in the algorithms. This numerical method of solving fluid-dynamic problems became computation-intensive, requiring computers to tackle numerous cells; the numbers could run into the millions. The solution technique thus became known as computational fluid dynamics, abbreviated as CFD.

Another problem in the 1970s was the inadequacy of the computing power to deal with the domain consisting of the numerous cells and to handle the error functions. As computer power increased along with superior algorithms, the CFD capability gradually became applicable to the industry. Today, CFD is a proven method that is well supported by advanced computing power. CFD started in the industry and has become an indispensable tool for the industry as well as research organizations.

A difficult area of CFD simulation lies in turbulence modeling. Recently, computations of 3D Reynolds-average Navier–Stokes (RANS) equations for complete aircraft configurations have gained credence as a solution technique. Reference [13] summarizes the latest trends in turbulence modeling. Numerous credible software applications have emerged in the market, some catering to special-purpose applications.

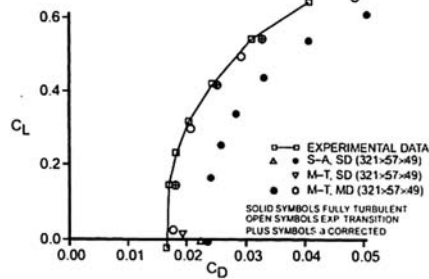
CFD still has limitations: Drag is a viscous-dependent phenomenon; inclusion of viscous terms makes the governing equations very complex, requiring intensive computational time. Capturing all of the elements contributing to the drag of a full aircraft is a daunting task – the full representation is yet to achieve credibility in industrial uses. It is not yet possible to obtain an accurate drag prediction using CFD without manipulating input data based on a designer’s experience. However, once it is set up for the solution, the incremental magnitudes of aerodynamic parameters of a perturbed geometry are well represented in CFD. It is a useful tool for obtaining accurate incremental values of a perturbed geometry from a baseline aircraft configuration with known aerodynamic parameters. CFD provides a capability for parametric optimization, to a degree (discussed in the next section).

14.3 Current Status

In his classic review, Chapman [1] (1979) advocated the indispensability of CFD, as computers began showing the promise of overtaking experiments as a principal source of detailed design information. His view is now regarded as an overly optimistic estimate. CFD capabilities complement experiments. Chapman listed the following three reasons for his conclusion:

- Experiments cannot represent the real flight envelope (e.g., Re and temperature) and are limited by flow nonuniformity, wall effects, and transient-dependent separation.
- There are very high energy costs associated with large wind tunnels.
- CFD is faster and less costly than experiments for obtaining valuable insight at an initial stage.

Figure 14.1. CFD simulation of wing-body drag polar [7]



Drag polar for M100 Wing-Body Combination; Experimental Data and Simulations Using Code TLNS3D. S-A = Spalart-Allmaras turbulence model, M-T = Menter blended $k-\omega/k-\epsilon$ model. SD = scalar artificial numerical dissipation, MD = matrix dissipation (from Figure 19 of Melnik et al. 1995).

Chapman showed the chronology of progress as four stages, starting in the late 1960s by solving linear potential flow equations and then reaching a stage where the nonlinear Navier–Stokes equations could be solved.

In a later paper, Chapman [2] reviewed the rapid progress achieved in the 1990s. With a better understanding of turbulence and advances in computer technology in both hardware and software development, researchers successfully generated aerodynamic results that had been impossible to obtain until then.

A more recent review by Roache [3] demonstrated that considerable progress has been achieved in CFD, but the promise is still far from being fulfilled in estimating complete aircraft drag. The AGARD AR256 report [4] is a technical status review of drag prediction and analysis from the CFD perspective. In the report, Schmidt [5] categorically stated that “consistent and accurate prediction of absolute drag for aircraft configuration is currently beyond CFD reach. . . .” Ashill [6] was of the same opinion, stating that the CFD flow modeling was found to be lacking in “certain respects.” Both agreed that the current state of the art in CFD is a useful tool at the conceptual design stages for comparison of shapes and diagnostic purposes.

An essential route to establish the robustness of CFD is through the success of the conceptual model code verification and validation. Roache [3] used the semantics of “verification” as solving the equations correctly and “validation” as solving the correct equations. The process of *benchmarking* (i.e., code-to-code comparison) results in the selection of software with the best economic value, although not necessarily the best software on the market.

Experimental results are used to validate and calibrate CFD codes. Various degrees of success have been achieved in the case studies. Melnik [5] showed that the CFD status in aircraft drag prediction of a subsonic-jet, transport-type aircraft wing on a simple circular cross-section fuselage had mixed success, as shown in Figure 14.1. Some correlation was achieved after considerable “tweaking” of the results. The results using these methods are not certifiable because of considerable “gray” areas.

Currently, the industry uses CFD as a tool for flow-field analysis wherever it is possible to estimate drag in inviscid flow (e.g., induced drag and wave drag), but it is not used for complete aircraft drag estimation. In the industry, CFD is a general-purpose tool to simulate flow around objects for qualitative studies and diagnostic purposes.

It is difficult to capture the numerous “manufacturing defects” (e.g., steps, gaps, and waviness that result from surface-smoothness requirements) over an entire aircraft. CFD flow-field analysis of simple geometries for benchmark work has been conducted (e.g., on large backward-facing steps). An example is Thangam [6] et al., who described a detailed study of flow past backward steps to understand turbulence modeling (κ - ε). This type of work neither represents the problems associated with the small geometries of excrescence effects nor guarantees accuracy. Another example is Berman’s [9] work on a large rearward-facing step, but it is not representative of the excrescence dimensions.

Assessment of excrescence drag using CFD requires a better understanding of the boundary-layer structure in turbulent flow. Although there is a voluminous literature on CFD code generation and qualitative assessment of the pressure field, no work has been cited in estimating parasitic drag of excrescences. As modern CFD software becomes more capable, it may be possible to predict excrescence drag by simulating real cases of double curvature in compressible flow, with or without shocks or separation.

Reference [11] is a verification of excrescence drag on a flat plate in the absence of a pressure gradient to estimate the excrescence drag on a 2D aerofoil in the pressure gradient. The study of an aerofoil [11] may be seen as a precursor to examining the scope of CFD estimates of excrescence drag in the generic 3D aerofoil configuration.

14.4 Approach to CFD Analyses

CFD analysis requires preprocessing of the geometric model before computation can begin. It consists of creating an acceptable geometry (i.e., 2D or 3D) amenable to analysis (e.g., no hole through which fluid leaks). A preprocessing package comes with its own CAD program to create geometry, specifically suited for a seamless entry to the solver for computation. However, considerable labor can be saved if the aircraft geometry already created in CAD can be used in CFD. This is possible if care has been taken in creating a geometry that is transferable to a CFD preprocessing environment.

The next task is to lay a grid on the geometry in order for CFD to work on small grids/cells until the entire domain is achieved. The surface grids should be laid intelligently to capture details where there are major local geometric variations, typically at the junction of two components and where there is steep curvature. The next task is to generate cells in the application domain that can encompass a large flow-field space around the aircraft body. At the far-field, variation in the flow field between the cells is small and therefore can be made larger. The preprocessor is menu-driven, providing options for various types of grid generation from which to select. Grids must meet the boundary conditions as the physics dictates. [Figure 14.2](#) is a good example of aircraft geometry (simplified by excluding the empennage and the nacelle) with structured grids and a section of the environment to be analyzed. Because it is symmetrical on the vertical plane, only half of the aircraft needs to be analyzed – the other half is the mirror image.

[Figure 14.3](#) is another example of 3D meshing on a complete aircraft with the nacelle included. After grid generation in the preprocessor, the model is then

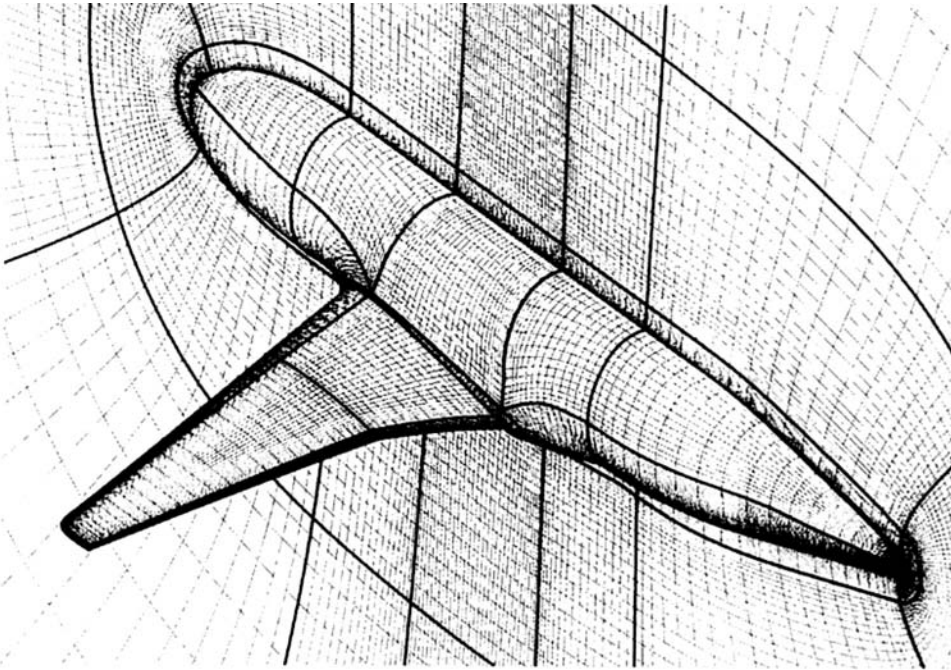


Figure 14.2. Wing-fuselage geometry with meshing on the surface and in the space [12]

introduced into the flow solver, which is also menu-driven. The options in the solver are specific and a user must know which to apply. The solver then computes the results: The runtime depends on the geometry, type of grid, and solver options, as well as the computing power.

The results can be examined in many different ways in a postprocessor; the most important on an aircraft body include the C_p distribution, temperature distribution, streamlines, and velocity vectors. The C_p and temperature distributions are shown in grades of color representing bands of ranges. Figure 14.4a is a gray-scale

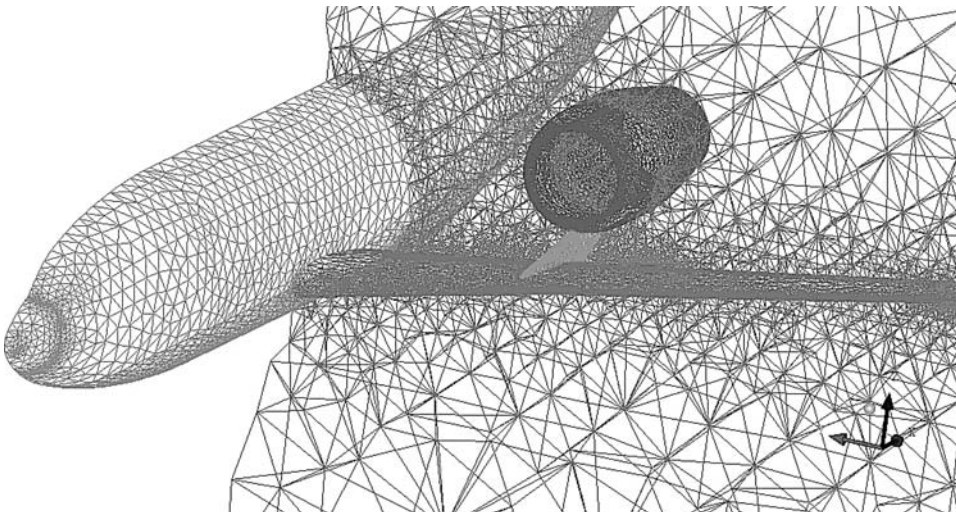


Figure 14.3. Grid mesh in 3D [14]

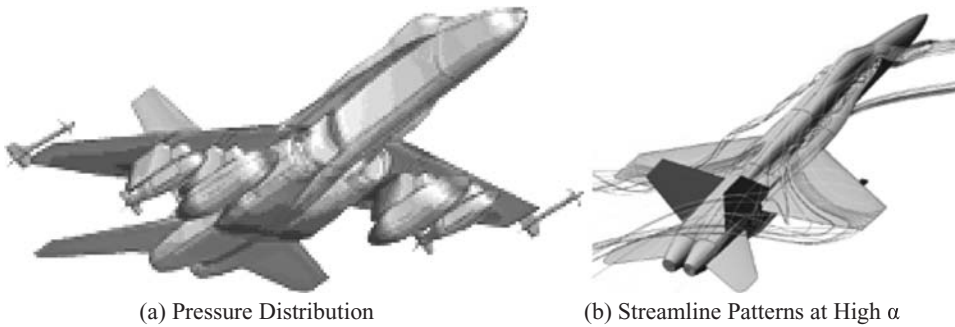


Figure 14.4. CFD postprocessor visualization [14 and 15]

version of the color distribution and [Figure 14.4b](#) depicts the flow-field streamlines. The results also can be obtained numerically in tabular form. It is now understood that readers must have the background information and be familiar with the CFD software package. For newly initiated readers, this instruction should be conducted with supervision.

Following is a summary of the approach to CFD.

14.4.1 In the Preprocessor (Menu-Driven)

- Step 1: Create the 3D geometry of an aircraft.
- Step 2: Generate the grid on the body surface and in the application domain; match it to the boundary conditions.

14.4.2 In the Flow Solver (Menu-Driven)

- Step 3: Bring the preprocessed geometry into the solver; set the boundary and initial conditions; make appropriate choices for the solver; run the solver; check results and refine (i.e., iterate) if necessary (including the grid pattern).

14.4.3 In the Postprocessor (Menu-Driven)

- Step 4: The result thus obtained from the solver can now be viewed in the solver; select a display format.
- Step 5: Analyze the results.
- Step 6: For a new setup, verify and validate the results.

The results can be presented in many ways, such as C_p distribution, pressure contours, streamlines, velocity patterns, C_L , C_D , L/D , or parameters defined by a user. CFD can depict shock patterns, location, and separation similar to flow visualization with wind tunnels. These results provide insight for aerodynamic designers to improve the design for the best L/D , aerodynamic moments, and compromise shapes to facilitate production, for example.

The results may need adjustments for the iteration that is necessary beginning with Step 2 and/or Step 3.

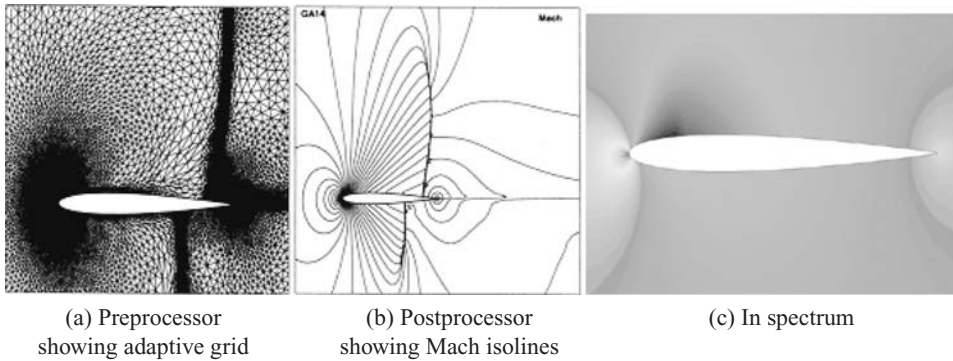


Figure 14.5. CFD analysis of a 2D aerofoil

14.5 Case Studies

This section includes elementary examples of case studies beginning with 2D cases, as shown in Figure 14.5. The first diagram represents an aerofoil showing the grid layout.

The domain of analysis is large with the anisotropic adaptive grid (Figure 14.5a), which is more dense the closer it is to the LE and trailing edge matching the surface grids and where shocks are present. When the solver has been run, the results can be seen in the postprocessor showing the Mach number isolines (Figure 14.5b). In another run with a different setup, the results are shown in a color spectrum (i.e., the gray-scale version in Figure 14.5c).

The next example is a simple, isolated 3D wing, as shown in Figure 14.6a. Half is shown with a simple grid and the other half is shown in shaded geometry. The drag polar from the CFD analysis is compared with results in Figure 14.6b.

CFD analysis of an isolated fuselage should be easy but internal and external flow through the nacelle (Figure 14.7) can prove to be difficult.

Whereas CFD studies on aerofoils exist, flow-field analysis on nacelles is rare. Chen [17] et al. presented a flow-field analysis over a symmetric isolated nacelle

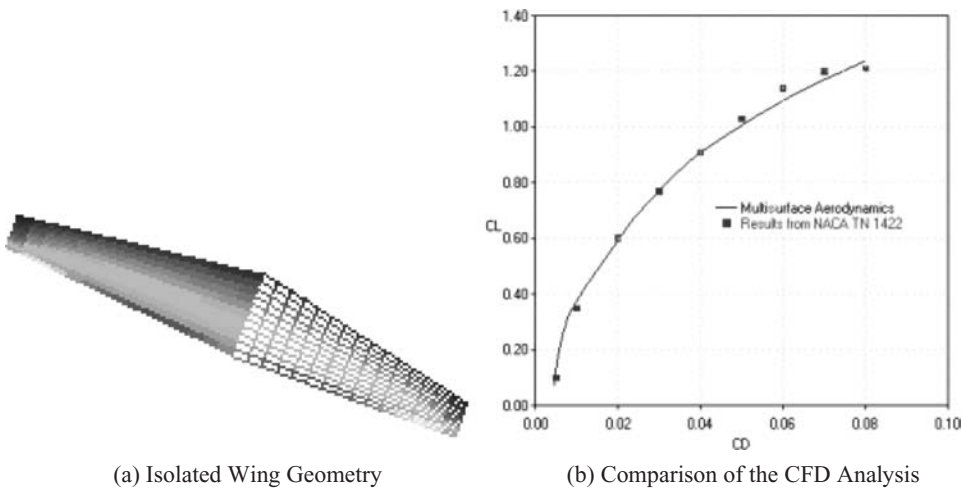


Figure 14.6. CFD analysis of a wing ([13] – Henley innovations)

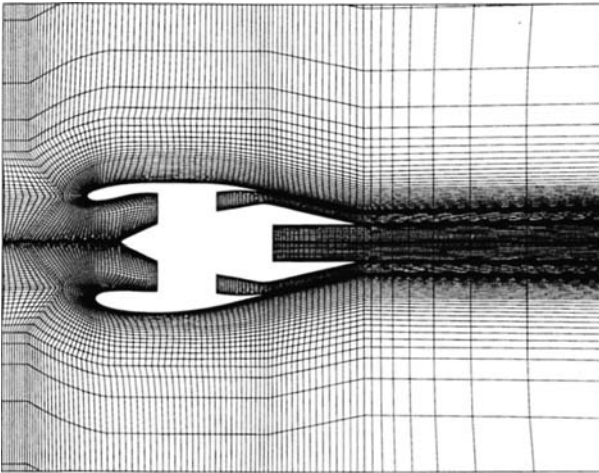


Figure 14.7. Nacelle grids for internal and external flow analysis

using a Euler solver (Figure 14.8). Subsequent studies by Uanishi [8] et al. showed confirmation of the velocity field obtained by Chen. No work has been found for velocity fields over the nacelle using Navier–Stokes solvers.

In a more recent analysis [12], it is stated that “... the observed scatter in the absolute CFD-based drag estimates is still larger than the desired single drag count error margin that is defined for drag prediction work. Yet, the majority of activities conducted during an aircraft development program are incremental in nature, i.e., testing/computing a number of options and looking for the best relative performance.”

14.6 Hierarchy of CFD Simulation Methods

A hierarchy of CFD simulation methods exists in which they are classified according to the physics they are capable of modeling. At the top of the hierarchy are direct

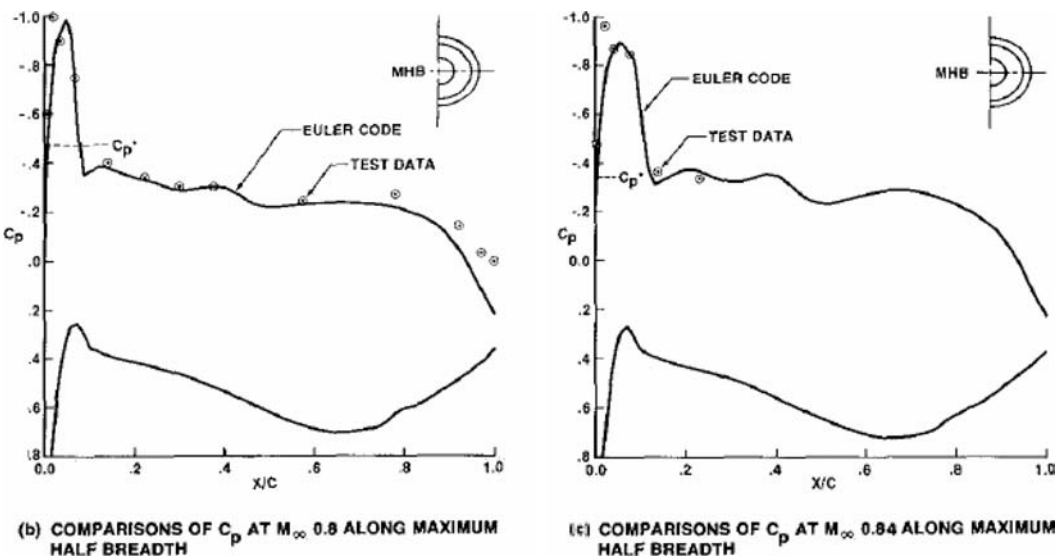


Figure 14.8. CFD results on a nacelle by Chen

numerical simulation (DNS) techniques; at the bottom are panel methods. A rough guide to the members of the hierarchy and their respective abilities is provided in the following subsections.

14.6.1 DNS Simulation Technique

DNS is capable of simulating time-dependent turbulent flows, capturing the dynamics of the entire spectrum of eddy sizes. This requires grids and time steps that are finer than the length and time scales at which turbulent energy is dissipated. Low-diffusion numerical schemes are necessary. DNS is useful for supplementing experimental data and aiding the development of turbulence models, but it is prohibitively expensive at the flight Re numbers. It is not used in the design process. Currently, DNS is the most sophisticated method.

14.6.2 Large Eddy Simulation (LES) Technique

LES takes advantage of the fact that the smallest dissipative eddies are isotropic and can be efficiently modeled using simple subgrid scale models. Meanwhile, the dynamics of larger eddies, which are anisotropic, is simulated using a grid and time step sufficiently fine to resolve them accurately. The method, therefore, is applicable to flows at relatively high Re numbers but is still expensive for use as an engineering design tool.

14.6.3 Detached Eddy Simulation (DES) Technique

DES is considered halfway between the LES and the Reynolds Averaged Navier–Stokes (RANS) techniques. The method employs a RANS turbulence model for near-wall regions of the flow and a LES-like model away from the wall. The method was first proposed by Spalart et al. in 1997 and is still the subject of research. It may become a standard engineering tool, but it is currently unlikely to be an element of the conceptual and preliminary design toolkits.

14.6.4 RANS Equation Technique

The time-dependence of turbulent fluctuations is averaged to form the RANS equations. This results in the appearance of the so-called Reynolds stresses in the equations, and the modeling of these equations (i.e., turbulence modeling) becomes problematic. There are many turbulence models but each falls prey to the fact that turbulence is flow-dependent; consequently, no turbulence model can be generally applicable, and a CFD practitioner must be cognizant of the strengths and failings of the models employed. Nonetheless, RANS allows relatively inexpensive modeling of complex flows; when allied to a suitable optimization method, it can be a powerful tool for design synthesis.

14.6.5 Euler Method Technique

Euler equations are obtained when the viscous terms are omitted from Navier–Stokes equations, allowing faster predictions of pressure distributions. They can be

usefully employed at the preliminary design stage. Viscous effects can be included by integrating boundary-layer methods and by displacing the surface of the aerofoil, wing, or aircraft by an amount equal to the local boundary-layer displacement thickness.

14.6.6 Full-Potential Flow Equations

The full-potential flow equations assume that the flow is irrotational. Compressible flows can be modeled but the “shocks” that are predicted are isentropic. The method is now quite dated but it can provide rapid information about pressure distributions and – like the Euler method – it can be integrated with a boundary-layer method.

14.6.7 Panel Method

This is simplest of all numerical methods for predicting flow around an aircraft. The surface of an aircraft is covered with panels, each one a source of sink, and some (e.g., those on lifting surfaces) are assigned a bound vortex (with its associated trailing vortex system). The strengths of the sources and bound vortices are initially unknown but can be determined through application of the boundary conditions (e.g., flow tangency at solid surfaces).

Descending through the hierarchy, the methods provide less physical fidelity but also require less computational effort. It is conceivable that the panel method, full-potential flow equations, Euler equations, and RANS method can be used in an undergraduate aircraft-design project (as a separate task), although not at the conceptual design stage. These methods provide a qualitative pressure-distribution pattern to help shape the geometrical details. Whichever method is used, the issue of grid generation must be addressed: More time is spent on the generation of a suitable mesh than on the prediction of flow.

A 3D model created in CAD is useful at this stage. The planning to prepare the 3D model in CAD should be done in such a way that Boolean operations can build it from isolated components, while still retaining the isolated components for a separate analysis. The wing-fuselage analysis provides the tail-less pitching moment data, which are useful in designing the aircraft H-tail and its setting relative to the fuselage to minimize trim drag.

CFD results can be compared with results obtained through use of the semi-empirical relationship (e.g., drag) (see [Chapter 9](#)). Generally, semi-empirical drag results are considered to provide good accuracy, validated on many aircraft consistent over a long period of use.

Figure 9.8 presents the wave drag, C_{Dw} , for the Mach number. CFD provides an opportunity to generate a more accurate viscous-independent wave drag versus the Mach number. When the CFD results are available, the data in Figure 9.9 may be replaced, thereby obtaining a further iteration on the drag polar of the aircraft. CFD is also a good place to generate ΔC_{Dp} values to be used for comparison. In general, CFD-generated ΔC_{Dp} values should provide good values if the CFD is set up properly.

If the CFD results are within 10% of the results obtained using semi-empirical relations, then they may be considered good. Some adjusting of the CFD runs should

improve the results – this is an area where experience is beneficial. Once the CFD is set up to yield good results, it is useful to improve and/or modify an aircraft configuration through extensive sensitivity studies. The spectrum plots in color show the hot spots that contribute to drag (e.g., local shocks and separation). These details cannot be seen as easily by any other means. Designers can follow through by repairing the hot spots to reduce drag. These opportunities are unique to CFD, making it an indispensable tool for optimizing a configuration for minimum drag. Any significant difference between the CFD and semi-empirical results should be investigated properly.

14.7 Summary

CFD simulation is a digital–numerical approach to design incorporated in the virtual-design process using computers. The current status is adequate for comparative analyses at low cost and time; therefore, it must be applied early in the conceptual design phase as soon as a CAD 3D model drawing is available. The development of CFD is not necessarily driven solely by aerodynamic considerations but rather by the requirement to have a tool to design a better product at a low cost and in less time.

CFD continues to develop with greater computing power at lower cost and in less time along with advances made in the algorithms for resolving solutions, providing considerable ease and automation to benefit users. Although researchers have achieved a degree of accuracy in drag prediction for a clean aircraft configuration, the generalized application by engineers is yet to achieve consistency in results. Verification and validation of results from CFD analysis are essential for substantiation, and the state of the art is still being scrutinized and continuing to develop. Verification of new CFD software comes before validation; together, they involve a protracted process in which research continues.

As a conservative user, the industry must ensure fidelity in a design. However, CFD is capable of comparison to recognize the better designs, even if the absolute values remain under scrutiny. This capability produces the best compromise in an early phase of the project at low cost and in less time, thereby avoiding subsequent costly modifications of an aircraft configuration – that is, it provides the opportunity to make the design right the first time. The design is subsequently tested in a wind tunnel for substantiation. Today, this approach requires few changes to the design after the final flight-test results.

The industrial effort in CFD is extensive and is not suitable for an undergraduate course. However, coursework can follow the industrial approach by solving smaller problems, such as those described in this chapter.

15 Miscellaneous Design Considerations

15.1 Overview

Although the main tasks of the aircraft configuration are now completed, there are other topics of interest that require understanding of design. This chapter is an overview of the impact made by technological advances that must be considered at the conceptual stages to arrive at a “satisfying” design. It offers an understanding of specialized topics, some of which may appear out of context during the conceptual phase, but they do contribute to aircraft design. The aircraft external geometry is not affected by these considerations (unless a radical approach is taken); however, there could be weight and cost changes. The semi-empirical weight equations in [Chapter 8](#) are sufficient and can be modified with improved data. In the industry, a more accurate weight estimation is required to reflect the changes affected by the topics discussed in this chapter.

A detailed study is beyond the scope of this book. Most academic institutions offer separate courses on some of the topics, such as aircraft structure, associated materials, and aircraft systems. Some of these topics sometimes escape attention because the undergraduate curriculum is already full with the main aeronautical subjects. Conceptual aircraft design is not only producing a geometry capable of meeting performance specifications; it also involves early thinking about environmental issues, safety issues, materials and structures, human interface with the flight deck, systems considerations, and military survivability issues that affect aircraft weight and cost. Therefore, whereas there is nothing to be altered on the finalized and substantiated configuration thus far obtained, it is beneficial for readers to appreciate the role of these varied topics. Some of the emerging scenarios are new and have yet to be implemented. It is important that newly initiated readers have a sense for what is required by these topics, which may be developed during a second term of coursework.

Environmental and safety issues must comply with standards specified by the FAA (United States), the EASA (Europe), and the ICAO (international). The differences among the agencies are minor. Military aircraft requirements are governed by MILSPECS/DEF standards. Aircraft doors (including emergency types) and environment standards, regulated by the FAA and the ICAO, also are described in this chapter.

The topics concerning military aircraft design are complex issues and must be studied separately (refer to specialized textbooks). Previous chapters clearly indicate the complexity of military aircraft design, which makes advanced military-aircraft design more difficult for undergraduate students.

Future designs indicate changes in aircraft configurations that are currently undergoing research and development (e.g., the BWB; see [Figure 15.10](#)). The basics of the current type of aircraft design must be understood before advanced designs can be undertaken.

15.1.1 What Is to Be Learned?

This chapter covers the following topics:

- Section 15.2: Introduction to the topics discussed
- Section 15.3: How noise emissions affect design
- Section 15.4: Engine exhaust emissions
- Section 15.5: Aircraft material selection
- Section 15.6: Laying out internal structural arrangements
- Section 15.7: Civil aircraft doors and emergency egress
- Section 15.8: Aircraft flight deck (i.e., cockpit) layout
- Section 15.9: Aircraft systems
- Section 15.10: Military aircraft survivability and stealth issues
- Section 15.11: Emerging scenarios

15.1.2 Coursework Content

The coursework exercises pertain only to [Section 15.7](#) in which readers verify the Bizjet emergency-door compliance with regulatory requirements. Also, the coursework discusses the choice of materials in [Section 15.5](#). Otherwise, there is no other coursework unless a second term explores these topics. Readers may obtain equipment sales brochures supplied by various manufacturers in which dimensions and weights are listed; the Internet is also a good source of information.

15.2 Introduction

The following topics are chosen deliberately to broaden the design perspective of readers. Some are of relatively recent origin, gradually evolving since the 1970s:

- environmental issues (i.e., noise and engine emissions and end-of-life recycling)
- materials and structures (i.e., the advent of new materials impacting design)
- safety issues (e.g., emergency exits and chutes)
- human interface (i.e., flight-deck description and displays)
- system-architecture issues (e.g., avionics, electrical, and mechanical systems)
- military aircraft survivability issues (e.g., stealth and ejection)
- emerging scenarios (e.g., terrorism and health protection)

15.2.1 Environmental Issues

Since the advent of large commercial jets in the 1960s (e.g., the B707, DC8, Convair 990, and VC10), the noise profile has become an issue for residents living in an airport vicinity. Litigation cases began to increase as a result of damages to property and health. First, the FAA and then the ICAO became involved in order to limit noise levels in a prescribed manner. Aircraft and engine designers strove to reduce or suppress noise during takeoffs and landings. Research is developing ways to reduce noise resulting from supersonic shock waves, also known as booms. Currently, there are no civil aircraft operating at supersonic speed – the Concorde was removed from service after a long operational period – partly on account of economic reasons. Supersonic aircraft are not addressed in this book; nevertheless, they fly subsonic during takeoffs and landings. References [1] through [3] may be consulted for more details on supersonic aircraft.

In the 1980s, concerns were raised on climate change to which engine emissions contribute. Again, regulatory agencies intervened to set achievable standards in order to limit pollution caused by engine exhaust gases.

The disposal of life-expired, grounded aircraft must be considered in an early design phase.

15.2.2 Materials and Structures

The choice of materials and the internal structural arrangement affect aircraft weight and cost. Materials used in the B787 made the aircraft lighter – it was a success with numerous sales even before its first flight. This demonstrates the importance of selecting appropriate materials during the conceptual design phase. The IPPD environment is a good forum in which to make choices.

15.2.3 Safety Issues

With increased passenger capacity, a quick egress is required by the regulatory agencies to ensure safety in the rare event of a fire hazard on the ground or a postcrash evacuation. The regulatory requirements stipulate a minimum number of exit doors (i.e., both main and emergency) and slides and chutes that ensure egress within a specified time. For military aircraft, the extreme measure of ejection is incorporated into design.

15.2.4 Human Interface

With an increased demand in a pilot's workload, it is important to understand the aircraft flight deck (i.e., cockpit) and the arrangement of systems. Readers must be aware of the nature of design features for the human-interface aspect, which can affect the aircraft weight, cost, and shape of the forward-fuselage–canopy area.

15.2.5 Systems Architecture

Aircraft subsystems consist of avionic, electrical, mechanical, hydraulic, and pneumatic systems. The extent of an aircraft's weight and cost depends on the subsystem

design philosophy. Automation and microprocessor-based data management have advanced to a wider operational capability without a corresponding increase in a pilot's workload. In this way, readers can see an aircraft as a system and sub-systems.

15.2.6 Military Aircraft Survivability Issues

Military aircraft design for combat survivability has been considered for some time, primarily as a consequence of potential damage occurring in combat. Crew-ejection capability is an integral part of survivability. In the last two decades, stealth technology – as a good survival measure – has advanced by minimizing an aircraft's signature. Electronic defense and countermeasures are other ways to thwart retaliation and increase survivability.

15.2.7 Emerging Scenarios

New topics are gaining importance and must be considered by the next generation of engineers. The emerging scenarios affecting civil aviation result from acts of terrorism in recent years. Aircraft design must include damage limitation from an explosion in the cargo compartments and containment of terrorist activities within the cabin. Also, damage incurred from runway debris demands a new perspective on an old problem (i.e., the Concorde crash case). With greatly increased numbers of passengers crossing international boundaries, general health care and contagious infections are becoming important issues.

15.3 Noise Emissions

Noise is produced by pressure pulses in air generated from any vibrating source. The pulsating energy is transmitted through the air and is heard within the audible frequency range (i.e., 20 to 20,000 Hz). The intensity and frequency of pulsation determine the physical limits of human tolerance. In certain conditions, acoustic (i.e., noise) vibrations can affect an aircraft structure. Noise is perceived as environmental pollution.

The intensity of sound energy can be measured by the sound pressure level (SPL); the threshold of hearing value is $20\mu\text{Pa}$. The response of human hearing can be approximated by a logarithmic scale. The advantage of using a logarithmic scale for noise measurement is to compress the SPL range extending to well over a million times. The unit of noise measurement is a *decibel*, abbreviated to *dB*, and is based on a logarithmic scale. One "Bel" is a tenfold increase in the SPL; that is, $1 \text{ Bel} = \log_{10}10$, $2 \text{ Bel} = \log_{10}100$, and so on. A reading of 0.1 Bel is a dB, which is $\text{antilog}_{10}0.1 = 1.258$ times the increase in the SPL (i.e., intensity). A twofold increase in the SPL is $\log_{10}2 = 0.301$ Bel, or 3.01 dB.

Technology required a meaningful scale suitable to human hearing. The units of noise continued to progress in line with technology demands. First was the "A-weighted" scale, expressed in dB(A), that could be read directly from calibrated instruments (i.e., sound meters). Noise is more a matter of human reaction to hearing than just a mechanical measurement of a physical property. Therefore, it was believed that human annoyance is a better measure than mere loudness. This

dB(A) CHART

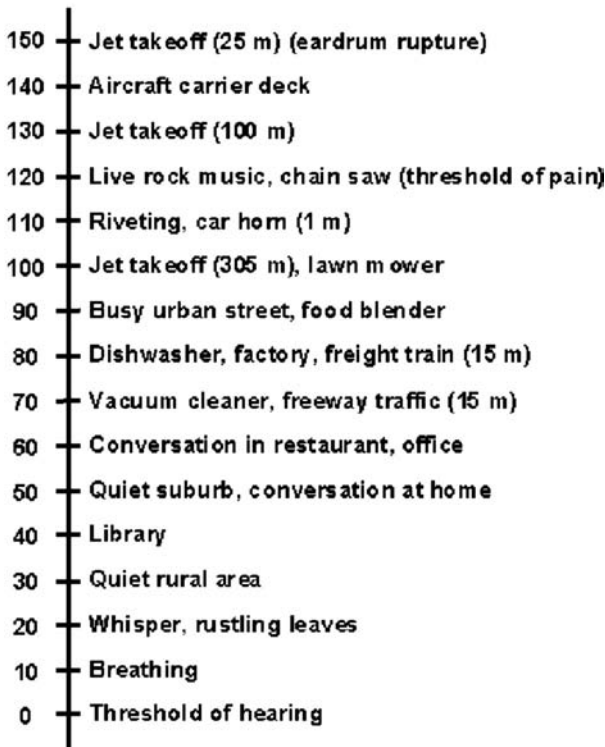


Figure 15.1. Perceived noise level (PNL) expressed in PNdB

resulted in the “perceived-noise” scale expressed in PNdB, which was labeled as the associated “perceived noise level (PNL),” shown in [Figure 15.1](#) from various origins.

Aircraft in motion presented a special situation with the duration of noise emanating from an approaching aircraft passing overhead and continuing to radiate rearward after passing. Therefore, for aircraft applications, it was necessary to introduce a time-averaged noise – that is, the effective perceived noise level (EPNL), expressed in EPNdB.

In the 1960s, litigation from damages caused by aircraft noise caused the government regulatory agencies to reduce noise and impose EPNdB limits for various aircraft classes. Many airports have a nighttime curfew for noise abatement and control, with additional fees being charged for using the airfield at night. Through research and engineering, significant noise reduction has been achieved despite the increase in engine sizes that produces several times more thrust.

The United States was first to impose noise certification standards for aircraft operating within that country. The U.S. airworthiness requirements on noise are governed by FAR Part 36. An aircraft MTOM of more than 12,500 lb must comply with FAR Part 36. The procedure was immediately followed by the international agency governed by ICAO (see Annexure 16, Volume I). The differences between the two standards are minor, and there has been an attempt to combine the two into one uniform standard. Readers may refer to FAR Part 35 and ICAO Annexure 16 for further details.

Because existing larger aircraft caused the noise problem, the FAA introduced regulations for its abatement in stages; older aircraft required modifications within

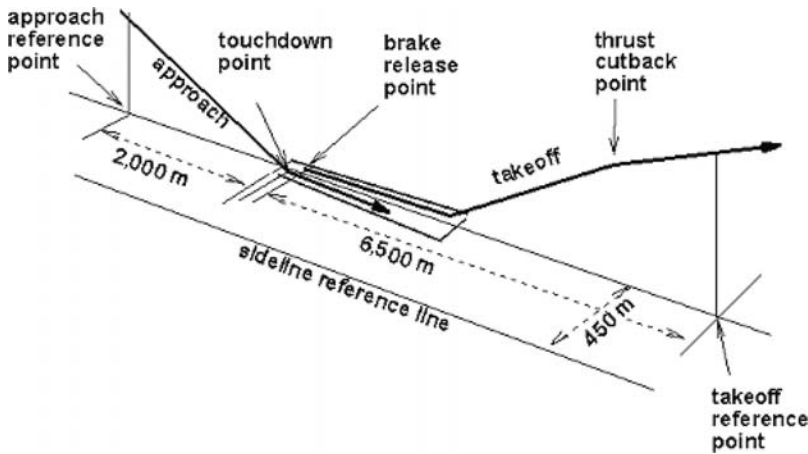


Figure 15.2. Noise measurement points at takeoff and landing

a specified period to remain in operation. In 1977, the FAA introduced noise-level standards in three tiers, as follows:

- Stage I: Intended for older aircraft already flying and soon to be phased out (e.g., the B707 and DC8). These are the noisiest aircraft but least penalized because they are soon to be grounded.
- Stage II: Intended for recently manufactured aircraft that have a longer life-span (e.g., the B737 and DC9). These aircraft are noisy but must be modified to a quieter standard than Stage I. If they are to continue operating, then further modifications are necessary to bring the noise level to the Stage III standard.
- Stage III: Intended for new designs with the quietest standards.
- Stage IV: Further increased stringency was applied for new aircraft certification during 2006.

ICAO standards are in Annexure 16, Volume I, in [Chapters 2](#) through [10](#), with each chapter addressing different aircraft classes. This book is concerned with [Chapters 3](#) and [10](#), which are basically intended for new aircraft (i.e., first flight of a jet aircraft after October 6, 1977, and a propeller-driven aircraft after November 17, 1988).

To certify an aircraft's airworthiness, there are three measuring points in an airport vicinity to ensure that the neighborhood is within the specified noise limits. [Figure 15.2](#) shows the distances involved in locating the measuring points, which are as follows:

1. Takeoff reference point: 6,500 m (3.5 nm) from the brake release (i.e., starting) point and at an altitude given in [Table 15.1](#).
2. Approach reference point: 2,000 m (1.08 nm) before the touchdown point, which should be within 300 m of the runway threshold line and maintained at least at a 3-deg glide slope with an aircraft at least at a 120-m altitude.
3. Sideline reference point: 450 m (0.25 nm) from the runway centerline. At the sideline, several measuring points are located along the runway. It is measured on both sides of the runway.

Table 15.1. *EPNdB limits*

No. of engines	Two engines		Three engines		Four engines	
MTOM (kg)	≤48,100	≥385,000	≤28,600	≥385,000	≤20,200	≥385,000
EPNdB limit	89	101	89	104	89	106
*Cutback altitude (m)	300		260		210	

Note:

* In certain airports, engine throttle cutback (i.e., a lower power setting) is required to reduce the noise level after reaching the altitude shown. At cutback, an aircraft should maintain at least a 4% climb gradient. In the event of an engine failure, it should be able to maintain altitude.

Make linear interpolations for in-between aircraft masses. For takeoff, make linear interpolations for in-between mass.

The arithmetic sum of noise levels at the three noise measuring position is referred to as the “cumulative noise level”; and the difference between this level and the arithmetic sum of the noise limits allowed at each measuring point is referred to as the “cumulative noise level margin.”

The maximum noise requirements in EPNdB from ICAO, Annexure 16, Volume I, Chapter 3, are listed in Table 15.1 and plotted in Figure 15.3.

Approach

This is for any number of engines (use linear interpolations for in-between masses).

MTOM (kg)	≤35,000	≥280,000
EPNdB limit	98	105

Sideline

This is for any number of engines (use linear interpolations for in-between masses).

MTOM (kg)	≤35,000	≥400,000
EPNdB limit	94	103

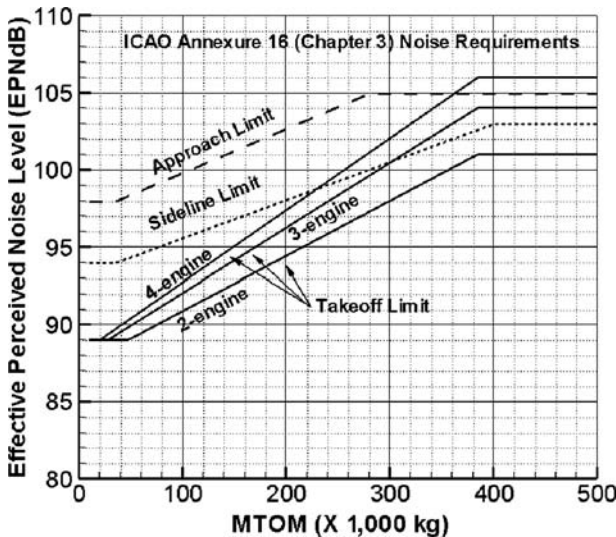


Figure 15.3. ICAO Annexure 16 (Chapter 3) noise requirements

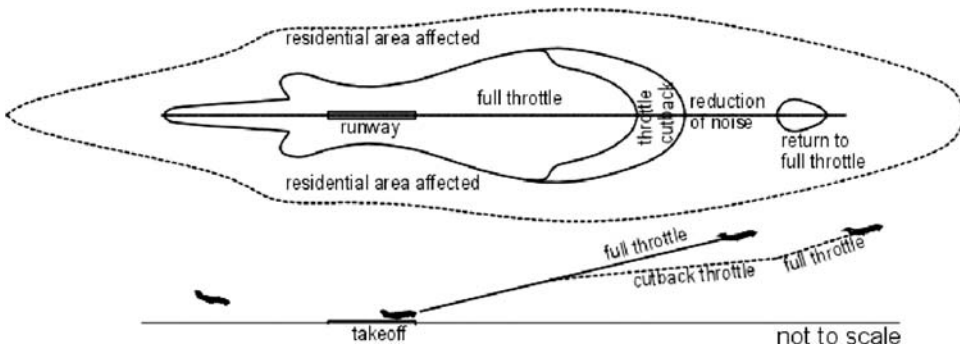


Figure 15.4. Typical noise footprint (≈ 10 km long) of aircraft showing engine cutback profile

A typical footprint of the noise profile around a runway is shown in [Figure 15.4](#). The engine cutback area is shown with the reestablished rated thrust for an enroute climb. Residential developments should avoid the noise-footprint areas.

Stage IV requirements for new type designs from January 1, 2006 are as follows:

- a cumulative margin of 10 EPNDB relative to Stage 3
- a minimum sum of 2 EPNDB at any 2 conditions
- no trades allowed

The airframe also produces a significant amount of noise, especially when an aircraft is in a “dirty” configuration (e.g., flaps, slats, and undercarriage deployed). [Figure 15.5](#) shows the sources of noise emanating from the airframe. The entire wetted surface of an aircraft – more so by the flow interference at the junction of two bodies (e.g., at the wing–body junction) – produces some degree of noise based on the structure of the turbulent flow causing pressure pulses that are audible to the human ear. The noise is aggravated when the undercarriage, flaps, and slats are deployed, creating a considerable vortex flow and unsteady aerodynamics; the fluctuation frequencies appear as noise. In the conceptual design phase, care must be taken to minimize gaps, provide fillets at the two-body junction, make streamlined struts, and so forth. Noise increases as speed increases. Care must be taken to eliminate acoustic fatigue in structures and to design them to be damage-tolerant; material selection is important.

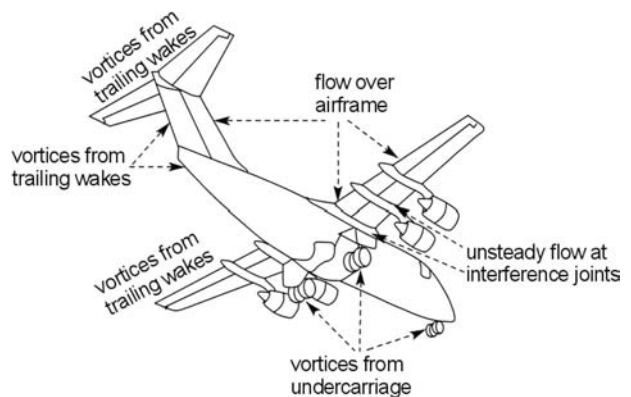


Figure 15.5. Typical sources of noise emanating from an airframe

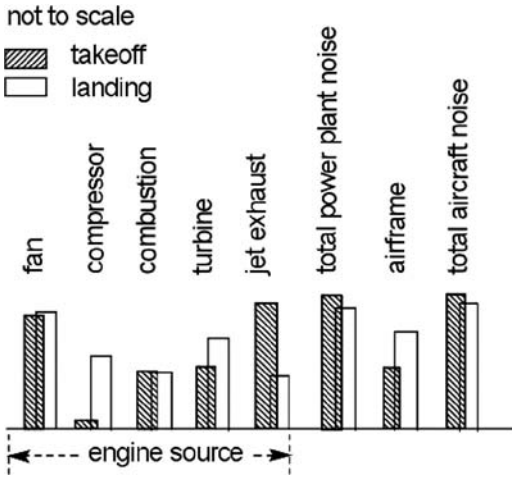


Figure 15.6. Relative noise distributions from various aircraft and engine sources

Typical noise levels from various sources are shown in [Figure 15.6](#) at both take-off and landing. Aircraft engines contribute the most noise, which is reduced at landing when the engine power is set low and the jet efflux noise is reduced substantially. There is more noise emanating from the airframe at landing due to higher flap and slat settings, and the aircraft altitude is lower at the measuring point than at the take-off measuring point. Because the addition of noise level is in a logarithmic scale, the total noise contribution during takeoff and landing is almost at the same level.

The power plant constitutes the nacelle and is the main sources of noise at take-off when an aircraft is running at maximum power. All of the gas turbine components generate noise: fan blades, compressor blades, combustion chamber walls, and turbine blades. With an increase in the BPR, the noise level decreases because a low exhaust velocity reduces the shearing action with ambient air. The difference in noise between an AB turbojet and a high-BPR turbofan can be as high as 30 to 40 EPNdB. [Figure 15.7](#) shows that in subsonic-flight speed, noise radiation moves ahead of an aircraft.

To reduce noise levels, engine and nacelle designers must address the sources of noise, as shown in [Table 15.2](#). The goal is to minimize radiated and vibrational noise. Candidate areas in engine design are the fan, compressor, and turbine-blade; gaps in rotating components; and, to an extent, the combustion chamber. Engines are bought-out items for aircraft manufacturers, which must make compromises between engine cost and engine performance in selecting what is available on the market. Aircraft and engine designers communicate constantly to make the best choice without compromising safety.

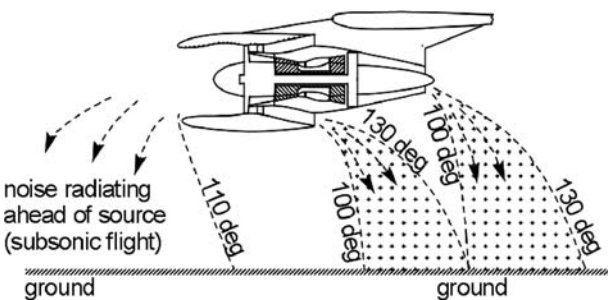


Figure 15.7. In-flight turbofan noise-radiation profile

Table 15.2. *Nacelle and turbofan technological challenges to reduce noise*

Nacelle	Fan/compressor and turbine	Burner
Internal liner – intake <ul style="list-style-type: none"> • absorbs fan noise 	<ul style="list-style-type: none"> • improved blade design • blade number optimized 	<ul style="list-style-type: none"> • efficient burning • low vibration
Internal liner – casing/fan duct <ul style="list-style-type: none"> • insulates compressor noise • absorbs burner noise 	<ul style="list-style-type: none"> • optimize gap around blades • minimize support strut vibration 	
Internal liner – jet pipe <ul style="list-style-type: none"> • absorbs turbine noise • absorbs burner noise • mixes hot and cold flows • improves exhaust-flow mixing 		

Figure 15.8 shows the positions of noise-suppression liners placed in various areas and the jet-pipe-flow mixing arrangements for noise abatement. Exhaust-noise suppression also is achieved by using a fluted duct (which increases the mixing area) at the exit plane. Many types of liners are available on the market and there is room for improvement in liner technology. Primarily, there are two types of liners: reactive and resistive. The reactive liners have different sizes of perforations to react with matched frequency range of noise and absorb. The resistive type of liner is a noise insulator in layers with screens. The most common type of acoustic liner comprises a combination of both types. It has resistive facing sheet covering a honeycomb structure between the insulator screens with cell sizes matched to the frequency range where noise attenuation is required. Nacelle certification is the responsibility of the aircraft manufacturer, even when it is subcontracted to a third party, because it is covered by FAR Part 25 requirements, rather than FAR Part 33, which are for the engine.

Propeller-driven aircraft must consider noise emanating (i.e., radiation and reflection) from the propellers. Here, the noise-reflection pattern depends on the direction of propeller rotation, as shown in Figure 15.9. The spread of reflected noise also depends on the propeller position relative to the wing and the fuselage.

Inside the aircraft cabin, noise comes from the ECS and must be maintained at the minimum level. These problems are addressed by specialists. Cabin-interior design considerations are addressed in Phase 2 of a project.

15.3.1 Summary

At this stage of study, design considerations for noise reduction do not substantially affect the aircraft external configuration other than using proper filleting at

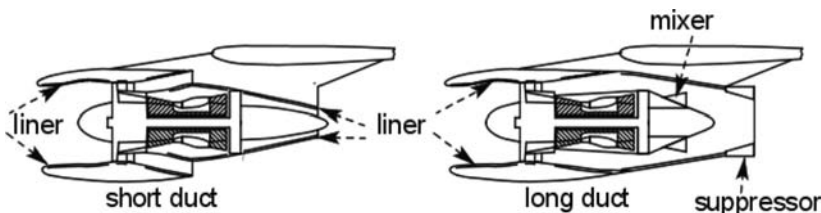


Figure 15.8. Positions of noise liners and suppression/mixing arrangements

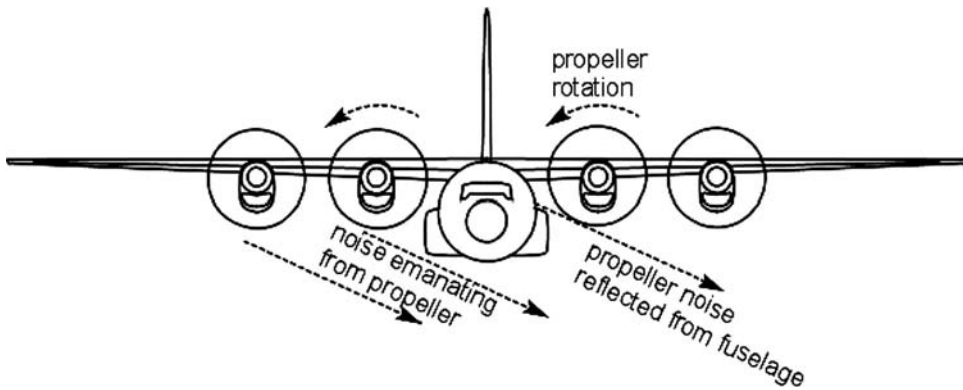


Figure 15.9. Noise considerations for propeller-driven aircraft

two-body junctions, streamlining the projected structure, minimizing gaps, and so forth. The finalized aircraft configuration – as obtained in [Chapter 6](#) and sized in [Chapter 11](#) – remains unaffected because the aircraft external geometry is assumed to have accounted for these considerations. The choice of materials (e.g., nacelle liners, cabin insulators, and fatigue-resistant material) can affect aircraft mass. Engine-noise abatement is generally the responsibility of engine designers.

The advancement of CFD capabilities in predicting noise has resulted in good judgments for improving design. Substantiation of the CFD results requires testing.

In the near future (i.e., gradually evolving in about two decades), remarkable improvement in noise abatement may be achieved using a multidisciplinary design approach, taking the benefits from various engineering considerations leading to a BWB shape. Cambridge University and the Massachusetts Institute of Technology have undertaken feasibility studies that show a concept configuration in [Figure 15.10](#) for an Airbus 320 class of subsonic-jet commercial transport aircraft. The engineers predict that the aircraft will be 25 dBs quieter than current designs – so quiet as to name it “silent aircraft.” The shaping of the aircraft is not based solely on noise reduction; it is also driven by general aerodynamic considerations (e.g., drag reduction and handling qualities). Noise reduction results from the aircraft body shielding the intake noise, minimizing two-body junctions by blending the wing and the fuselage, and eliminating the empennage. Of course, reduction in the engine noise is a significant part of the exercise. However, to bring the research to a marketable product will take time, but the author believes it will come in many sizes; heavy-lift cargo aircraft are good candidates.



Figure 15.10. Concept design of a futuristic “silent aircraft”

15.4 Engine Exhaust Emissions

Currently, the civil aviation sector burns about 12% of the fossil fuels consumed by the worldwide transportation industry. It is responsible for an approximate 3% annual addition to greenhouse gases and pollutant oxide gases. The environmental debate has become intense on issues such as climate change and depletion of the ozone layer, leading to the debate on long-term effects of global pollution. Smog consists of nitrogen oxide, which affects the pulmonary and respiratory health of humans. The success of the automobile industry in controlling engine emissions is evident by dramatic improvements achieved in many cities.

The U.S. Environment Protection Agency (EPA) recognized these problems decades ago. In the 1980s, the need for government agencies to tackle the engine emissions issue was emphasized. The early 1990s brought a formal declaration (i.e., the Kyoto agreement) to limit pollution (specifically around airports). Currently, there are no regulations for an aircraft's cruise segment. In the United States, FAR Part 35, and internationally, the ICAO (i.e., Annexure 16, Volume II), outline the emissions requirements. EPA has worked closely with both the FAA and the ICAO to standardize the requirements. Although military aircraft emissions standards are exempt, they are increasingly being scrutinized for MILSPECS standards. Emissions are measured by an emission index (EI).

Combustion of air (i.e., oxygen plus nitrogen) and fuel (i.e., hydrocarbon plus a small amount of sulphur) ideally produces carbon dioxide (i.e., CO_2), water (i.e., H_2O), residual oxygen (i.e., O_2), and traces of sulphur particles. In practice, the combustion product consists of all of these plus an undesirable amount of pollutants, such as carbon monoxide (i.e., CO , which is toxic), unburned hydrocarbons (UHC), carbon soot (i.e., smoke, which affects visibility), oxide of sulphur, and various oxides of nitrogen (i.e., NO_x , which affects the ozone concentration). The regulations aim to reduce the level of undesirable pollutants by improving combustion technology. The sustainability of air travel and growth of the industry depend on how technology keeps up with the demands for human-health preservation.

Lower and slower flying reduces the EI; however, this conflicts with the market demand for flying higher and faster. Designers must make compromises. Reduction of the EI is the obligation of the engine manufacturer; therefore, details of the airworthiness EI requirements are not provided herein (refer to the respective FAA and ICAO publications). Aircraft designers must depend on engine designers to supply certified engines that comply with regulatory standards.

15.5 Aircraft Materials

Aircraft that defy gravity necessarily must be weight-efficient, thereby forcing designers to choose lighter materials or – more precisely – those materials that give a better strength-to-weight ratio. Also implied are the questions of cost of raw materials, cost of fabrication, and stability during use. This section helps readers understand that choosing the appropriate materials is an involved topic and therefore is an integral part of the study during the conceptual design phase. Aircraft weight and cost are affected by the choice of materials and, therefore, aircraft performance and economy. The success or failure of a new aircraft design depends largely on the

choice of appropriate materials, especially when the number of those available is increasing.

In the early days of aviation, the only choice was to use an all-wood construction or a fabric cover to wrap around a wooden airframe to serve as an aerodynamic surface. Being anisotropic and without enough resistance to impact, wood properties have limitation. At that time, the available metals were heavy and the lighter ones were soft and corrosive. Today, wood is no longer used except in the homebuilt-aircraft category, primarily because wood is the easiest material with which to work. Moreover, the ethical question of forest conservation discourages the use of wood.

In the 1920s, the combination of progress in engines and in aerodynamic technologies allowed aircraft speed to exceed 200 mph, which required better materials. Technology changed in the 1930s when Durener Metallwerke of Germany introduced duralumin, an alloy of aluminum, with a higher strength-to-weight ratio, improved anticorrosion properties, and isotropic properties. The company followed with a variety of alloys for specific manufacturability, damage tolerance, crack propagation, and anticorrosive properties in the form of clad-sheets, rolled bars, ingots, and so forth. The introduction of metal also resulted in a new dimension to manufacturing philosophy. Progress in structures, aerodynamics, and engines paved the way for substantial gains in speed, altitude, and maneuverability performance. These improvements were seen primarily in the World War II designs, such as the Supermarine Spitfire, the North American P-51, the Focke Wolfe 190, and the Mitsubishi Jeero-Sen.

The last three decades have seen the appearance and increasing use of non-metals, such as fiberglass/epoxy, kevlar/epoxy, and graphite/epoxy, which are composite materials constructed in layers of fabric and resin. Composites have better strength-to-weight ratios compared to aluminum alloys, but they also have anisotropic properties. Because they are shaped in moulds during the fabrication of parts, difficult curvy 3D shapes can be produced relatively easily. The near future will see more variety of composite materials embedded with metal to obtain the best of both. The Bombardier C Series, Airbus 380, Boeing 787, and Airbus 350 are examples of how extensively composite materials are used. The technology of composite materials is evolving at a fast rate and there will be more variety in composite materials with better properties and capabilities at a lower cost.

Typically, composites may be used in secondary and tertiary structures in which loads are low and any failure does not result in catastrophe. [Figure 15.11](#) shows the composite materials in a Boeing 767 aircraft. As the technology progresses, more composites will appear in aircraft moving into primary load-bearing structures.

[Table 15.3](#) compares the extent of increase in composites from an older B747 (1960s) to the relatively newer design of the B777 (1990s). The latest B787 and A350 have considerably higher percentages of composites.

Composite materials are incorporated increasingly in percentage by weight. A few smaller aircraft are made of all composite materials but the FAR Part 23/25 certification procedure is more cumbersome than for metal construction. It was difficult to obtain airworthiness certification for early all-composite aircraft because there were insufficient data to substantiate the claims. Military certification standards for aircraft structures are different.

Table 15.3. Percentage mass of types of material used in the aircraft structure

Material	Boeing 747	Boeing 777
Aluminum alloys	81	70
Steel alloys	13	11
Titanium alloys	4	7
Composites (various types)	1	11
Other	1	1

The newer military aircraft designs use expensive, exotic materials (e.g., aluminum–lithium alloy and boron alloy) that have yet to prove their cost-effectiveness in commercial aircraft. More than half of the Eurofighter’s structural mass is constructed of various types of composite materials; a fifth is made of the aluminum–lithium alloy.

15.5.1 Material Properties

Under load (i.e., stress), all materials deform (i.e., strain) – some more than others – but they can recover their original shape when the load is removed, provided that the application is within a specific limit. Beyond this load level, materials do not recover to their original shape. See [4], [5], and [6] for details on stress and strain.

Stress is the applied force per unit area of a material. It is termed as *tensile* or *compressive stress* when the force is acting normal to an area and *shear stress* when it is acting tangentially. The associated deformation per unit length or area is the normal or shear strain, respectively. How a material is prepared affects the

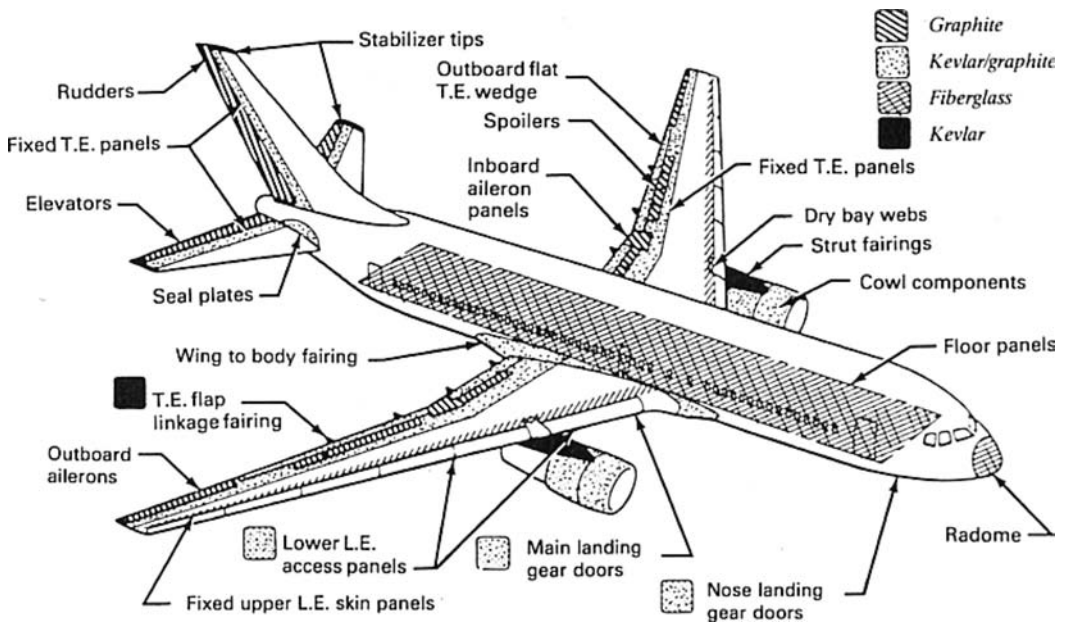


Figure 15.11. Composite materials in a Boeing 767

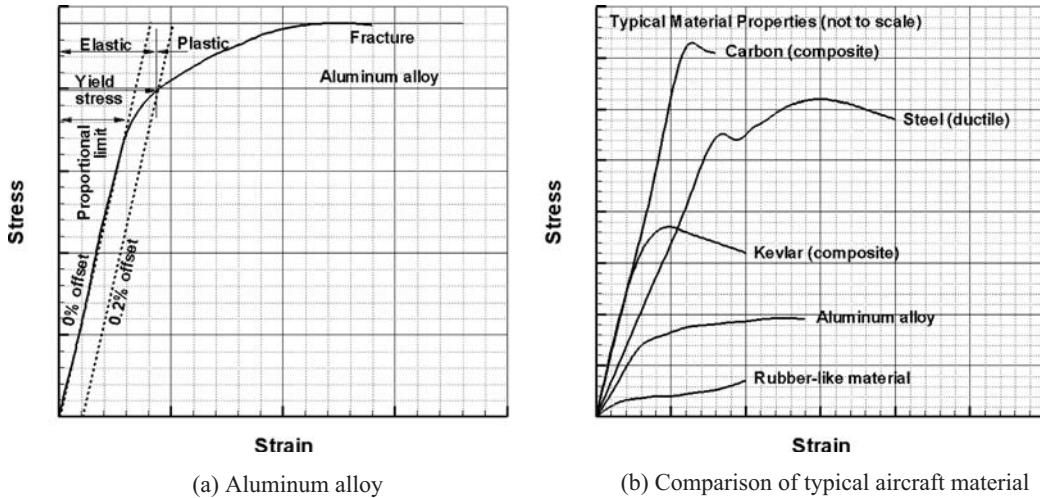


Figure 15.12. Material stress–strain relationship

characteristics of the stress–strain relationship. The nature of alloys, crystal formation, heat treatment, and cooling affects a materials characteristics.

A typical stress–strain characteristic of an aluminum alloy is shown in Figure 15.12. The figure shows that initially, the stress–strain relationship behaves linearly according to Hooke’s Law, which represents the elastic property of a material. Within the elastic limit, the material strength (i.e., how much stress it can bear) and stiffness (i.e., how much deformation occurs) are the two main properties considered by designers in choosing materials; of course, the cost, weight, and other properties are also factors to consider. The maximum point within which linearity holds is the *yield point*. Past the yield point, permanent deformation occurs: The material behaves like plastic and the slope is no longer linear. The highest point in the stress–strain graph is known as the *ultimate strength*, beyond which the component continues to deform and results in a rupture that is a catastrophic failure. The linear portion gives the following:

$$\text{stress/strain} = \text{constant} = \text{Young's Modulus (the slope of the graph)}$$

Sometimes raw material is supplied with a small amount of prestretching (i.e., strain hardening) and a permanent deformation set in which the yield point is higher. Typically, some aluminum sheet metals are supplied with 0.2% built-in prestretched strain (see Figure 15.12a). However, with prestretching, the ultimate strength is unchanged. Figure 15.12b compares various types of typical aircraft materials. A steeper slope indicates higher stiffness, which often has a higher elastic limit. Brittle materials rupture abruptly with minimal strain buildup; ductile materials exhibit significant strain buildup before rupturing, thereby warning of an imminent failure. Rubber-like materials do not have a linear stress–strain relationship. The pertinent properties associated with materials follow (some are shown in Figure 15.12):

- brittleness: when a sudden rupture occurs under stress application (e.g., glass)
- ductility: the opposite of brittleness (e.g., aluminum)

- hardness: a measure of strength
- resilience: a measure of energy stored in an elastic manner; that is, the strain is restored when the stress is relieved
- toughness (fracture toughness): a measure of resistance to crack propagation
- creep resistance: a slow deformation with time under load; strain can increase without applying much stress
- wearability: a measure of surface degradation mainly under exposure (e.g., corrosion)
- fatigue quality: set up with alternate cycling of applied load; a good material dissipates vibration energy for a number of cycles
- ability to hold strength at elevated temperature

The limit load, ultimate load, and factor of safety (FS) associated with material are described in Section 5.5.2. Limit load is up to the point where there is no permanent deformation under load. Certifying agencies stipulate strict control on aircraft structural integrity. For unpredictability (e.g., under a gust load or material defect), an FS is incorporated to accept an ultimate load when some deformation is allowed but is still below the ultimate strength. For metals, the $FS = 1.5$; that is, a 50% increase from the limit load is allowed. The properties of composite materials have reduced values of the stress level to allow for damage tolerance and environmental issues and to maintain an FS of 1.5 (see Section 5.6). The manufacturing process also determines the allowable stress level. These considerations can penalize part of the weight-saving associated with using lighter materials.

The strength and other properties vary among materials. [Table 15.4](#) lists important materials used in the aircraft industry (only typical values are given). Wood has many variations and is not used much anymore.

With an increase in temperature, material properties degrade. Special alloys of steel and titanium retain better strength at elevated temperatures. Components experiencing a hot temperature have titanium and stainless-steel alloys that are available in many variations. In the quest to find still-better materials, nickel, beryllium, magnesium, and lithium alloys have been produced. The more exotic the nature of an alloy, the more costly it is. Typically, an aluminum–lithium alloy is three to four times more expensive than duralumin (in 2005). Aluminum alloys are still the dominant material used in the aircraft industry. The variety of aluminum alloys indicates a wide range available for specific uses. Various types of aluminum alloys are designated (i.e., classified) with a numbering system, as shown in [Table 15.5](#).

15.5.2 Material Selection

Material selection for any engineering product depends on its function, shape, manufacturability (i.e., process), and cost. For aircraft applications, there is the additional consideration of weight. Within the material classes, there are subclasses of alloys: composites that offer appropriate properties to suit a product – a large variety is available with ever-increasing newer types. In the conceptual design phase, engineers must screen and rank the types of materials that suit the requirements, listing the limitations and constraints involved and whether a change to another type is

Table 15.4. *Properties of various types of material for comparison (typical values)*

Material	Density ρ —lb/in ³	Elasticity, Young's Modulus E—10 ⁶ lb/in ²	Ultimate tensile E/ ρ	Specific strength	Relative cost
<i>Aluminum alloys</i>					
2014-T6 Alclad sheet	0.101	10.7	68	106	base price
2024-T4 extrusion	0.100	10.7	57	107	slightly less
7076-T6	0.101	10.3	78	102	slightly more
7076-T6 extrusion	0.101	10.4	78	103	slightly more
<i>Steel alloys</i>					
Stainless steel	0.276	29	177	103	more
Maraging steel	0.283	29	252	94	more
H-11	0.281	30	280	107	more
<i>Titanium alloy</i>					
Lithium–aluminum alloy					
Nickel alloy	0.300	31	155	103	much more
Magnesium alloy	0.064	6.5	40	102	expensive
Beryllium alloy–rolled	0.067	42.5	65	634	expensive
<i>Composite nonmetals</i>					
Fiberglass/epoxy	0.065	5	80	77	relatively inexpensive
Kevlar/epoxy	0.050	12	160	240	more expensive
Carbon/epoxy	0.056	22	170	393	more expensive

required. Military aircraft designers can use case-specific materials that have never been tried.

To select an appropriate material for a component, the following factors must be considered:

<i>Property</i>	<i>Production</i>	<i>Operation</i>
strength	availability	erosion, wear, and abrasion quality
stiffness	fabrication ease	thermal and electrical characteristics
toughness	manufacturability	plating/galvanic/paint compatibility
crack propagation	handling	compatibility with contact material
aging and corrosion		
tolerance to environment		

Table 15.5. *Aluminum alloys (other types do not have numerical designations)*

Series starting with 1xxx:	pure aluminum
Series starting with 2xxx:	aluminum + copper (e.g., 2014-T6 Alclad sheet,* 2024-T4 extrusion)
Series starting with 3xxx:	aluminum + manganese
Series starting with 4xxx:	aluminum + silicon
Series starting with 5xxx:	aluminum + magnesium
Series starting with 6xxx:	aluminum + magnesium + silicon
Series starting with 7xxx:	aluminum + zinc – high strength, heat treatable, prone to fatigue (e.g., 7076-T6, 7076-T6 extrusion)

Note:

* Both surfaces of the aluminum-alloy sheet are clad with copper. These have high electrical and thermal conductivity, corrosion resistance, good formability, and are not heat treatable.

Table 15.6. *Typical composite material usage in various aircraft classes*

Aircraft type	Typical percentage of composite by weight	Typical components
Small aircraft*	20% to 40%	Control surfaces, floorboards, some skins (e.g., cowling, fillet)
Regional jets/turboprops	15% to 30%	As above, furnishing
Medium jets**	15% to 25%	As above
Large jets	15% to 20%	As above
Military trainers	20% to 30%	As above
Combat	30% to 50% or more	As above + some primary structures

Notes:

* Some smaller aircraft, including the Bizjet, are constructed of all-composite structures.

** B787 has over 50% composite material by weight.

Several options are available for appropriate materials to make the best compromise. Thus, aircraft-weight estimation is more complex, and engineers must identify and compute numerous parts to estimate component weights before an aircraft is built; CAD 3D modeling helps.

Choice of material affects aircraft weight and cost. The semi-empirical relation for weight estimation in [Chapter 8](#) considers all-metal construction and describes how to adjust the prediction if some parts are made of a lighter material. For a rapid method, the OEW may be factored accordingly – only the structural weight is affected; the remainder is unchanged. Composites may be used in secondary and tertiary structures, where loads are low and failure does not result in catastrophe.

In general, for the same Young's Modulus, metals have higher density. However, when the strength-to-weight ratio (i.e., specific strength) is considered, then composites overtake metals; that is, engineers can obtain the same strength with lighter components even when the higher FS erodes the weight savings. Metals demonstrate a better Young's Modulus for the same strength. Metals also show better fracture toughness for the same Young's Modulus. Another important comparison is the relative cost per unit volume versus the Young's Modulus when metal alloys are less costly.

15.5.3 Coursework Overview

Aluminum alloys continue to be the most prevalent material in aircraft structure. [Table 15.6](#) is a conservative presentation of typical percentages of composite use for the coursework project. The table reflects the typical current practice, although there are some newer designs that perform better than what is listed.

The introductory coursework exercise may use the following strategy. The weight equations provided in [Chapter 8](#) are valid.

Civil Aircraft Design

For civil aircraft, the design is all-metal construction. If nonmetals (i.e., composites) are introduced, they may be limited to secondary and tertiary structures up to only approximately 25% of the OEW. Typical nonmetal structures include the floorboards, control surfaces, complex fairings, and empennage.

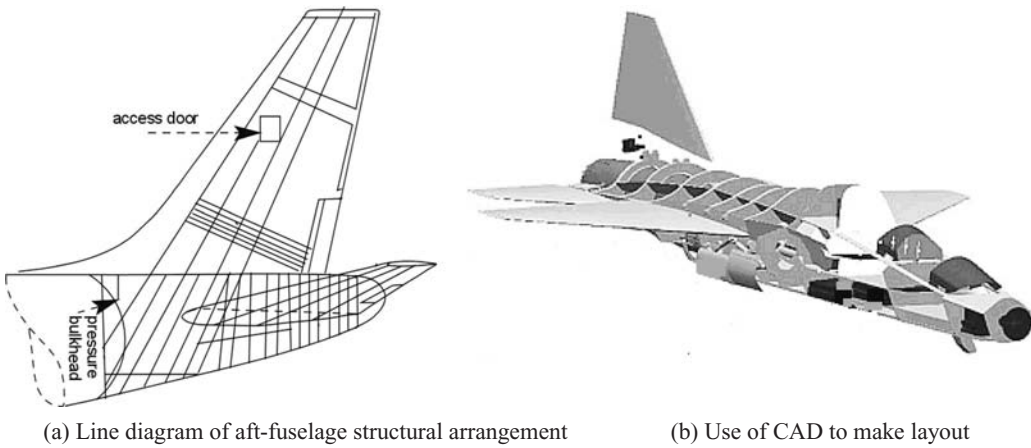


Figure 15.13. Typical scheme of aircraft structural layout

Military Aircraft Design

For military aircraft design, the same philosophy about nonmetal (i.e., composites) components is maintained, with weights increased to 40% of the OEW. Typical non-metal structures include the floorboards, control surfaces, complex fairings (e.g., intake ducting and wing-body junction), and empennage.

15.6 Aircraft Structural Considerations

Creating just the aircraft shell, satisfying only aerodynamic needs, has consequences during manufacture. It is simple to create the drawings but not as easy to produce the hardware. During the conceptual study phase, it is routine procedure in the industry to obtain the valued opinion of production engineers in an IPPD environment. Compromises may be made in shaping an aircraft if doing so facilitates manufacturability, which in turn saves cost – more so in the commercial aircraft business, where operational economic gains are more important than in pure aerodynamics.

Manufacturing philosophy is associated with the choice of materials, machining routine, forming, fabrication, and assembly-tool (i.e., jigs and fixtures) concepts (see [Chapter 17](#)). Typically, the aim is to shape components as simply as possible with fewer parts and faster assembly time. Attention is given to minimizing complex 3D curvatures; applying more circular shapes than complex, convoluted curves; maintaining commonality of geometry; and providing accessibility for maintenance.

Therefore, it is suggested that a second-term project be assigned to introduce the structural philosophy in harmony with the manufacturing philosophy, beginning with internal structural arrangements in simple line diagrams, as shown for an aft-fuselage in [Figure 15.13a](#). Similar line drawings for the wing and empennage are not shown herein. The advantages of using CAD are discussed in previous chapters of this book, which are apparent, as shown for a typical military aircraft fuselage in [Figure 15.13b](#). If a basic aircraft configuration is created in CAD, then the external aircraft contour lines guide the shape of the internal arrangement, with the added benefit of being able to examine accessibility and production complexity to establish manufacturing philosophy.

Table 15.7. Aircraft door types

	Position	Minimum height (inches)	Minimum width (inches)	Maximum corner radii (inches)	Number of passengers**
Type A	Floor level	72	42	7	110
Type B	Floor level	72	32	6	75
Type C	Floor level	48	30	10	55
Type I	Floor level	48	24	8	45
Type II*	Floor level	44	20	7	40
Type III	Over wing	36	20	7	35
Type IV	Over wing	26	19	6.3	9

Notes:

* If Type II is located over the wing, it can have an inside step up of 10 inches and an outside step down of 17 inches.

** The types of doors are related to the minimum number of passengers carried. The higher the number of passengers, the larger is the door size.

The strategy is to lay out the main internal structural arrangements, such as the position of the ribs, spars, longerons, bulkheads, wing box–fuselage, flap–empennage attachment, engine attachment, and fuel tank. At this stage, it is not detailed component design. In the next phase (i.e., Phase 2, project definition), line diagrams are developed into shapes after stressing to consolidate the manufacturing philosophy and, if necessary, to prepare for the bidding process to subcontract work. During Phase 3 (i.e., detailed design), the parts are developed into detailed production drawings ready for manufacture. The use of CAD avoids duplication in generating components and the subassemblies outline. CAD is capable of making the procedures paperless. Reference [5] provides a good description and analyses of aircraft structural design.

15.7 Doors: Emergency Egress

Emergency situations (e.g., fire hazard and ditching on water or land) require a fast exit from the aircraft cabin to safety. The FAA initially imposed a 120-s egress time but, in 1967, changed it to a maximum of 90 s. This was feasible through advances made in slide and chute technology. To obtain an airworthiness certification, an aircraft manufacturer must demonstrate that complete egress is possible within 90 s by conducting simulated tests. The EASA has similar requirements.

FAR Part 25, Sections 25.783 and 25.807, give requirements for the main cabin doors and emergency exit doors, respectively. Several types of emergency exit doors are listed in Table 15.7 (in inches); all are rectangular in shape with a corner radius. The sizes are a minimum size and designers can make them larger. Oversized doors need not be rectangular as long as the minimum rectangular size is inscribed.

All doors except Type III (i.e., an inside step up of 20 inches and an outside step down of 27 inches) and Type IV (i.e., an inside step up of 29 inches and an outside step down of 36 inches) are from the floor level. If a Type II door is located over the wing, it can have an inside step up of 10 inches and an outside step down

Table 15.8. *Aircraft emergency-door types*

Number of passengers	Minimum size emergency-door type	Minimum number of emergency doors
1 to 9	Type IV	One in each side of the fuselage
10 to 19	Type III	One in each side of the fuselage*
20 to 40	Type II	Two in each side of the fuselage*
41 to 110	Type I	Two in each side of the fuselage
>110		

Note:

*One door could be one size smaller.

of 17 inches. Emergency doors are placed at both sides of the aircraft and do not need to be diametrically opposite; however, they should be uniformly distributed (i.e., no more than 60 ft apart) and easily accessible for evenly distributing loading passengers when required. The safety drill by the cabin crew is an important aspect in saving lives, and all passengers should listen to the demonstration regardless of how frequently one flies. There are differences among door types.

An aircraft should have at least one easily accessible external main door. The combination of main and emergency doors is at the discretion of the manufacturer, which must demonstrate a simulated evacuation within the stipulated time. The fuselage length also determines the number of emergency doors because they should not be spaced more than 60 ft apart. Table 15.8 lists the minimum number of emergency doors; it is recommended that more than the minimum be provided. Types A, B, and C also can be used and they are deployed in larger aircraft.

There may be other types of doors such as a door at the tail cone and ventral doors, the dimensions of which are listed in Table 15.9. Flight-crew emergency-exit doors are provided separately in the flight deck.

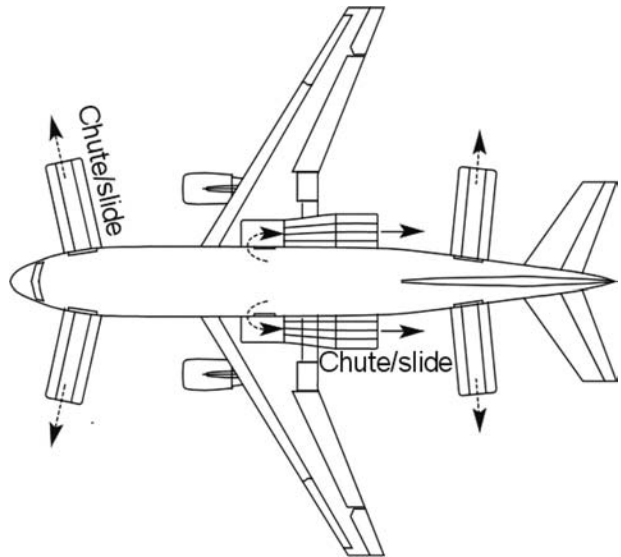
When the door level is high above the ground, inflatable escape slides and chutes are provided, as shown in Figure 15.14. In an emergency situation in which stairs may not be available (or there may not be time to wait for them to arrive), inflatable chutes are used for passenger evacuation within the specified time. The slides and chutes also serve as rafts with floating attachments.

As aircraft size increases, the technological demand to facilitate quick egress becomes a more challenging task. In March 2006, the Airbus 380 demonstrated that 850 passengers could be evacuated in 80 sec (although with minor injuries). However, a typical Airbus 380 passenger load is fewer than 650 passengers with a mixed-class arrangement. The Airbus has sixteen exits but was successful in the evacuation using only eight doors (i.e., half remained closed).

Table 15.9. *Door dimensions*

	Step height inside (outside) (inches)	Minimum height (inches)	Minimum width (inches)	Maximum corner radii (inches)
Ventral	–	≥48	≥24	8
Tail cone	24 (27)	42	72	7

Figure 15.14. Inflatable escape chute and slide



Coursework Exercise

There is a coursework exercise in this chapter. The configuration developed in Chapter 6 is to be reverified. The Bizjet must have the following features:

Version	Number of Passengers	Emergency-Door Type
Baseline	10	1 Type III and 1 Type IV
Long	14	1 Type III and 1 Type IV
Short	6	1 Type IV

It is best for all doors to have Type III standards for component commonality, which reduces production costs.

15.8 Aircraft Flight Deck (Cockpit) Layout

The *aircraft flight deck* is a better term than the older usage of the word *cockpit*, which originated in ship design in the sixteenth century; it was similar to men working in a confined area under stress, like cocks that were forced to fight in a pit for sport. *Crew station* is another term meaning the same as a workplace for operators of any type of vehicle. To standardize terminology, this book uses *flight deck*, intended specifically for aircraft. The flight deck serves as a human–machine interface by providing (1) an outside reference of topography through the cabin windows, (2) onboard instruments to measure flight parameters, (3) control facilities to operate an aircraft safely for the mission role, and (4) management of aircraft systems (e.g., the internal environment). Future designs with advanced displays could result in a visually closed flight deck (i.e., a TV replacing the windows). The front-fuselage shape can be influenced by the flight-deck design. Transport aircraft have two pilots sitting next to one another at a pitch of about 1.2 meters in smaller aircraft to 1.4 meters in larger aircraft. Understanding the flight-deck arrangements also provides a sense of the equipment requirements that result in a measure of the associated weights involved. The space and adequacy of vision polar, which establishes the window-size requirements, also can be better understood.

Both civil and military aircraft pilots have the following common functions:

- mission management (planning, checks, takeoff, climb cruise, descent, and landing)
- flight-path control
- systems management
- communication*
- navigation*
- routine postflight debriefing
- emergency action when required (drills differ between civil and military aircraft)*

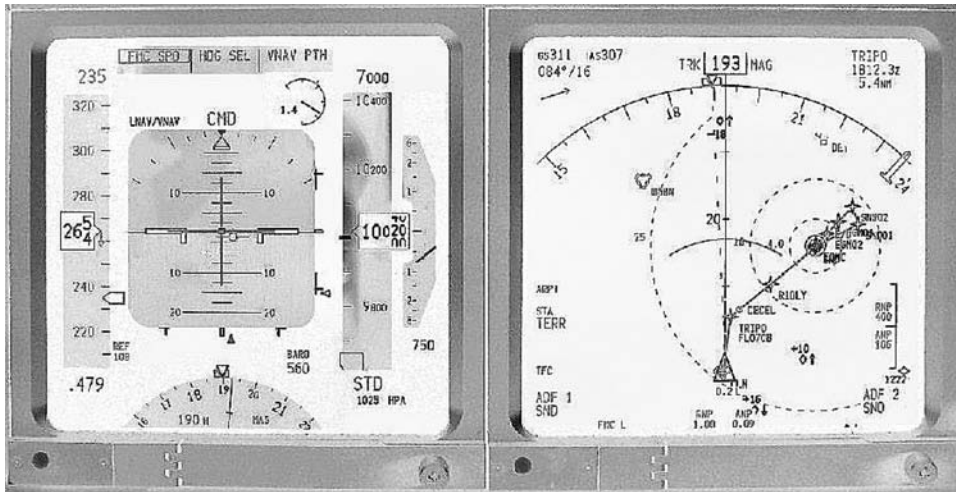
*Civil aircraft pilots are assisted by ground control (i.e., communication and navigation), whereas in a critical situation, combat pilots must manage the aircraft themselves – which is a significant difference. Both situations may require taking emergency actions, but for a combat pilot, this could be drastic in nature (i.e., ejection; see [Section 15.10](#)). In addition, military aircraft pilots have an intense workload, as follows:

- mission planning (e.g., Lo/High combination; see [Chapter 13](#)); this is required for mission management (preflight briefing may change if the situation demands)
- target acquisition
- weapons management and delivery
- defensive measures and maneuvers
- counterthreats; use of tactics
- management of situation when hit
- in-flight refueling, where applicable
- detailed postflight briefing in special situations

The military aircraft flight deck is under more stringent design requirements. The civil aircraft flight-deck design is in the wake of military standards and the provision of space is less constrained. This is why the military aircraft flight deck is discussed first (see [Figure 15.16](#)). An aircraft flight-deck design has changed dramatically since the early analog-dial displays (i.e., four-engine aircraft gauges now fill the front panel; see [Figure 15.17](#)) to modern microprocessor-based data management in an integrated, all-glass, multifunctional display (MFD), which is also known as an electronic flight information system (EFIS).

15.8.1 Multifunctional Display and Electronic Flight Information System

MFD started as a display on a cathode ray tube (CRT) but has advanced to a liquid crystal display (LCD), which is a lighter and clearer technology. All relevant data for pilot use (e.g., air, engine, and navigational data) are displayed simultaneously on the screen. To reduce clutter, the displays are divided into primary and secondary displays. Separate-system displays are accommodated in one or two



(a) Air-Data Systems Display

(b) Navigational Display

Figure 15.15. Multifunctional display

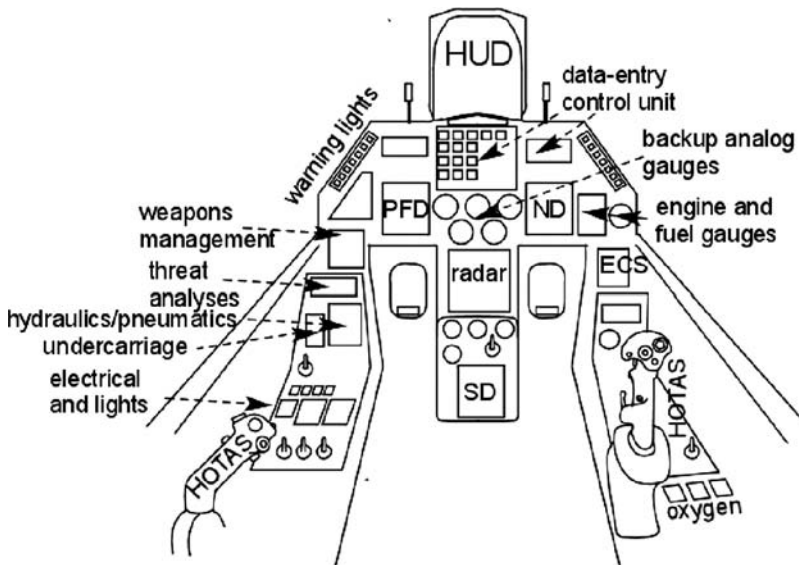
EFISs: the primary air-data system display (SD), and the navigational display (ND); each type of system has several pages and each display screen can be changed for specific information. Figure 15.15 shows typical EFIS displays. EFIS/MFD/ND/SD have many pages that can be flipped to as desired, including pages for the engine, cruise, flight-control, fuel, electrical, avionics, oxygen, air-bleed, air-conditioning, cabin-pressurization, hydraulics, undercarriage, doors, and the APU (military aircraft have weapons-management pages).

The primary flight display (PFD) consists of air-data systems, including aircraft speed, altitude, attitude, aircraft reference, and ambient conditions. The secondary system consists of the ND, which provides directional bearings (i.e., GPS and inertial system), flight plan, route information, weather information, airport information, and so forth. For pilot facility, each type has some duplication. In a separate panel, the SD shows the engine data and all other system data, including those required for the ECS. EFISs have removed the clutter of analog dials, one for each type of data. In some designs, the engine display (ED) is shown separately. Forward-looking weather radar can have the ND or a separate display unit.

Initially, flight decks also had basic analog gauges showing air data as redundancies in case the EFIS failed. Currently, with vastly improved reliability in the EFIS, older analog gauges are gradually being removed.

15.8.2 Combat Aircraft Flight Deck

Figure 15.16 shows a typical modern flight deck for military aircraft. Backup analog gauges are provided as well as the MFD-type EFIS. The left-hand side is the throttle and the right-hand side is the side-stick controller known as the hands-on throttle and stick (HOTAS) (see Section 15.8.6). The figure indicates which type of data and control a pilot requires. A single pilot's workload is exceptionally high when computer assistance is required.



Flight data EFIS at the left and navigational data EFIS at the right

Figure 15.16. Schematic fighter-aircraft flight deck

15.8.3 Civil Aircraft Flight Deck

An old-type panel with analog dial gauges is shown in Figure 15.17. With two pilots, some of the displays are duplicated, which are deliberate redundancies.

The latest Airbus 380 flight-deck panel replaces myriad gauges by EFISs, which are MFD units. The minimum generic layout of a modern flight-deck panel is shown in Figure 15.18. Numerous redundancies are built into the display with independent circuits. PFDs, NDs, and SDs have several pages that display significant data.

15.8.4 Head-Up Display

The flight-deck displays shown in Figures 15.16 through 15.18 are on the instrument panel in front of the pilot, who must look down for flight information – more frequently in critical situations. When flying close to the ground or chasing a target, however, pilots should keep their head up, looking for external references. This inflicts severe strain on pilots who must frequently alternate the head-up and head-down positions. Engineers have solved the problem to a great extent by projecting the most important flight information (both primary and navigational data) in bright green light on transparent glass mounted in front of the windscreen. With a head-up display (HUD), pilots can see all necessary information without moving their head and, at the same time, they can see through the HUD for external references. Figures 15.17 and 15.18 show a modern HUD.

Initially, a HUD was installed in combat aircraft but the technology recently has trickled into civil aviation as well. HUDs are being installed on most new medium- and large-sized commercial transport aircraft if requested by operators.

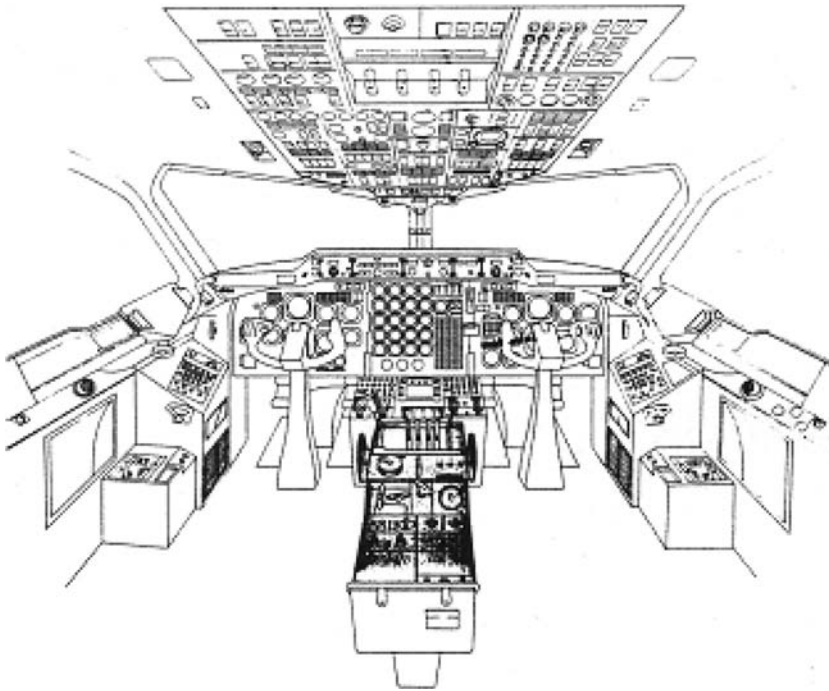


Figure 15.17. Old-type (BAe146) flight deck with analog head-down display

15.8.5 Helmet-Mounted Display

Although the HUD has relieved pilots from frequently looking down, the head-up observation is restricted to forward vision only. Military aircraft pilots needed to ease the workload while making a peripheral visual search when the HUD is no longer in the line of sight. Engineers designed a novel device that projects flight information on a helmet-mounted visor. Now pilots can turn their head with all the relevant information still visible on the transparent visor, through which external references can be taken.

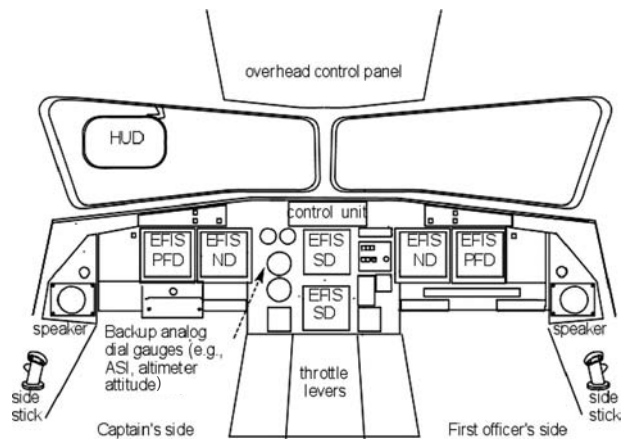


Figure 15.18. Typical civil aircraft flight deck

Outline of a generic modern flight-deck panel with HUD

Table 15.10. *HOTAS control buttons*

On the throttle (left side)		On the stick (right side)	
Target	Weapons	Trigger	Weapon release
Communications	Antenna	Missile	Sensor select
Radar	In-flight start	Trim	Flight control
Flaps	Dive brakes		

15.8.6 Hands-On Throttle and Stick

Other examples of easing a pilot's workload include the essentials of weapons management and other requirements being incorporated on two controls so that combat pilots can keep their hands on the engine throttle control and the flight control stick. This arrangement of control buttons on the engine throttle and stick is known as HOTAS (see Figure 15.16). The essential control buttons are ergonomically located (Table 15.10). Most modern aircraft have buttons on the flight-control stick for communication, trimming, and so forth.

15.8.7 Voice-Operated Control

Voice-operated control (VOC) through voice recognition – still in the development stage – has been installed in advanced combat aircraft. All voice commands also are visually displayed and are very effective for a pilot operating under severe stress, especially if incapacitated by injury.

All of these advancements help a pilot but the systems still require the pilot's familiarity. Pilots undergo extensive training and practice to gain familiarity with a mass of information in a rather claustrophobic presentation. A pilot's workload is nearly an inhuman task. They are a special breed of personnel, rigorously trained for years to face the unknown in a life-or-death situation. It is the moral duty of any combat aircraft designer to enhance pilot survivability as best as possible in an integrated manner, embracing all types of technologies.

15.9 Aircraft Systems

Figure 2.1 shows the aircraft-design process in a systems approach. The definition of *system* is provided in Section 2.2. In that regard, an aircraft can be seen as a system composed of many subsystems. Chart 15.1 illustrates a typical top-level subsystem architecture of aircraft as a system. The subsystems can be designed in separate modules and then integrated with an aircraft.

Together, the system and subsystem mass is 10 to 12% of an aircraft's MTOM. Typically, this amounts to nearly a quarter of the OEM. Practically all of the items in aircraft subsystems are bought-out. A better understanding of the subsystems improves weight and cost predictions. It is important for good information about subsystem items at the conceptual design stage for better weight and cost estimation. Designers are continually assessing cost versus performance of the subsystems to obtain the best value for the expense.

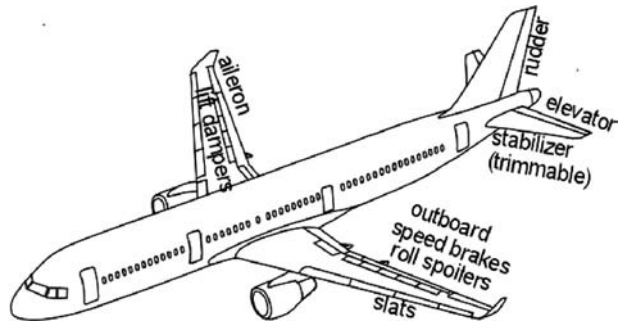
moments of the deflecting control surfaces, which reduces a pilot's workload. Some operational types are as follows:

1. **Wire-Pulley Type.** This is the basic type. Two wires per axis act as tension cables, moving over low-friction pulleys to pull the control surfaces in each direction. Although there are many well-designed aircraft using this type of mechanism, it requires frequent maintenance to check the tension level and the possible fraying of wire strands. If the pulley has improper tension, the wires can jump out, making the system inoperable. Other associated problems include dirt in the mechanism, the rare occasion of jamming, and the elastic deformation of support structures leading to a loss of tension. [Figure 15.19](#) shows the wire-pulley (i.e., rudder and aileron) and push-pull rod (i.e., H-tail) types of control linkages.
2. **Push-Pull-Rod Type.** The problems of the wire-pulley type are largely overcome by the use of push-pull rods to move the control surfaces. Designers must ensure that the rods do not buckle under a compressive load. In general, this mechanism is slightly heavier and somewhat more expensive, but it is worth installing for the ease of maintenance. Many aircraft use a combination of push-pull-rod and wire-pulley arrangement (see [Figure 15.19](#)).
3. **Mechanical Control Linkage Boosted by a Power Control Unit (PCU).** As an aircraft size increases, the forces required to move the control surfaces increase to a point where a pilot's workload exceeds the specified limit. Power assistance by a PCU resolves this problem. However, a problem of using a PCU is that the natural feedback "feel" of control forces is obscured. Therefore, an artificial feel is incorporated for finer adjustment, leading to smoother flights. PCUs are either hydraulic or electric motors driven by linear or rotary actuators (there are several types). [Figure 12.16](#) is supported by a PCU.
4. **Electromechanical Control System.** In larger aircraft, considerable weight can be saved by replacing mechanical linkages with electrical signals to drive the actuators. Aircraft with FBW use this type of control system (see [Figure 12.16](#)). Currently, many aircraft routinely use secondary controls (e.g., high-lift devices, spoilers, and trim tabs) driven by electrically signalled actuators.
5. **Optically Signaled Control System.** This latest innovation uses an optically signaled actuator. Advanced aircraft already have fiber-optic lines to communicate with the control system.

Modern aircraft, especially the combat aircraft control system, have become very sophisticated. A FBW architecture is essential to these complex systems so that aircraft can fly under relaxed stability margins. Enhanced performance requirements and safety issues have increased the design complexities by incorporating various types of additional control surfaces. [Figure 15.20](#) shows the typical subsonic-transport aircraft-control surfaces.

[Figure 15.21](#) shows the various control surfaces and areas as well as the system retractions required for a three-surface configuration. As shown in the figure, there is more control than what most modern civil aircraft have. Military aircraft control requirements are at a higher level due to the demand for difficult maneuvers and a possible negative stability margin. The F117 is incapable of flying without FBW. Additional controls are the canard, intake-scheduling, and thrust-vectoring devices.

Figure 15.20. Civil aircraft control surfaces



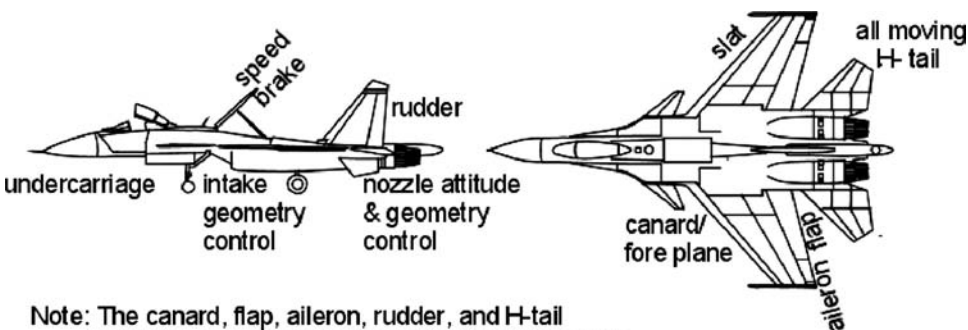
Fighter aircraft may use stabilators (e.g., the F15) in which the elevators can move differentially to improve roll capability. Stabilators are used collectively for pitch and differentially for roll control. Also, the aileron and rudder can be interconnecting. There also can be automatic control that parallels the basic system.

15.9.2 Engine and Fuel Control Subsystems

In this section, the engine and fuel control subsystems are addressed together. The engine and fuel/oil control subsystems must have a fire-extinguishing capability. A better understanding of the engine and fuel/oil control subsystems improves weight- and cost-prediction accuracy. The dry-engine weight supplied by an engine manufacturer is accounted for separately. The earliest aircraft were piston-engine-powered. Piston engines use petrol (i.e., AVGAS). Diesel-powered engines were introduced recently. Figure 15.22 shows a basic fuel system for a small piston-engine-powered aircraft.

Piston Engine Fuel Control System (The total system weight is approximately 1 to 1.5% of the MTOW)

- ignition and starting system
- throttle to control fuel flow
- fuel storage (tank) and flow management: This must incorporate fuel refueling and defueling and venting arrangements. High-wing, smaller aircraft may have



Note: The canard, flap, aileron, rudder, and H-tail can have collective and/or differential movements. Air-data sensors are distributed at various convenient locations.

Figure 15.21. Military aircraft control surfaces

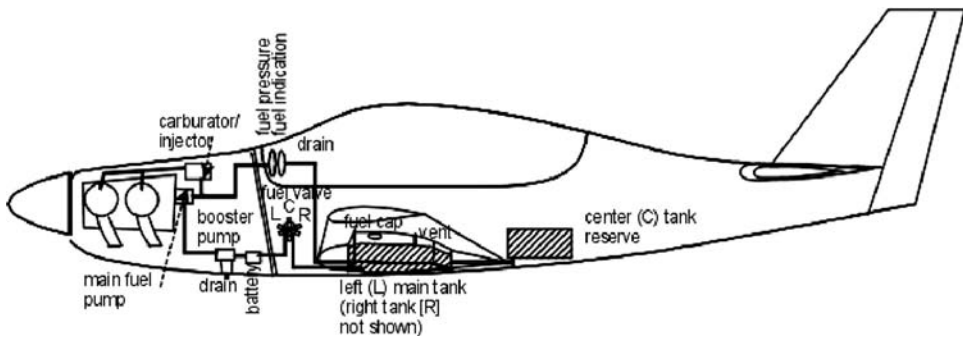


Figure 15.22. Piston engine fuel system

a gravity-fed fuel supply to the engine, but most aircraft use fuel pumps. Aerobatic aircraft should be capable of flying in an inverted position for at least a minute

- mixture control to adjust air-density changes when the altitude changes
- propeller-pitch control (see [Chapter 12](#)); smaller aircraft may have a fixed pitch
- engine-cooling system
- engine anti-icing system
- oil system
- fire protection system
- instrumentation and sensor devices

Smaller aircraft can store fuel in the wing. Although a few aircraft store fuel in the fuselage, it is not recommended. Fuel in the fuselage can affect a larger CG shift and, in the case of a crash, the occupants may get doused by leftover fuel. Fuselage fuel tanks are an optional installation in order to increase range.

Gas turbine engine control at the pilot interface is simpler in that it does not require mixture control by a pilot. For turboprops, there are no propellers; hence, there is no pitch control by a pilot. The turboprop engine/fuel control system is described as follows and shown in [Figure 15.23](#).

Turboprop Engine Fuel Control System (The total system weight is approximately 1.5 to 2% of the MTOW)

- ignition and starting system
- throttle to control fuel flow (thrust adjustment); larger jets have thrust reversers
- fuel storage (tank) and flow management: This must incorporate fuel refueling and defueling and venting arrangements. Some combat aircraft need mid-air refueling. In an emergency, aircraft should be able to dump (i.e., jettison) fuel (this is an environmental hazard and is discouraged)
- engine-cooling system
- engine anti-icing system
- oil system
- fire-sensing and protection system
- built-in tests for the fault-detection system; there should be flight and ground crew interface
- instrumentation and sensor devices

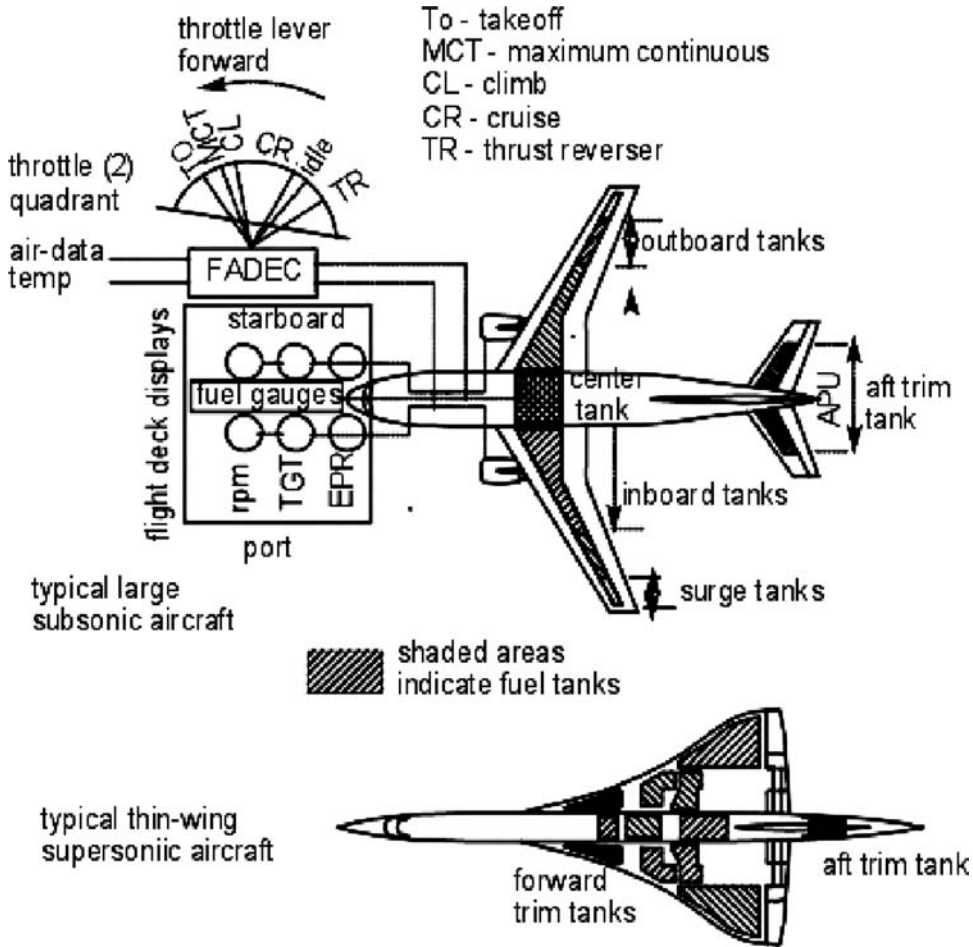


Figure 15.23. Turbofan engine fuel control system

Modern military aircraft and commercial aircraft engine control is microprocessor-based and known as FADEC. It is linked with FBW using air data to respond correctly as demanded by a pilot. A typical turbofan and fuel/oil control system (see Figure 15.23) is discussed in more detail in the following paragraphs.

Fuel Storage and Flow Management

The fuel supply to an engine must be made smoothly and accurately. There must be adequate fuel-storage capacity to meet the mission profile with mandatory excess as a reserve. These requirements are an important part of the study during the conceptual design phase. Fuel management is complex: Fuel weight is a significant percentage of an aircraft MTOW and consumption from full to empty has the potential for major movement of the CG, affecting the aircraft’s stability. It is important for fuel consumption to be managed for the least shift in the CG. In a demanding situation, this is achieved by an in-flight fuel transfer.

A typical commercial aircraft tank arrangement is shown in Figure 15.23. Storage of fuel is located primarily in the cavity of the wing box that extends from the

wing root to close to the wing tip (a tapered wing tip has a lower volumetric capacity). Fuel storage in the wing is advantageous because it is close to the aircraft's CG, which lowers the range of the CG shift. If the volume available in the wing is not adequate, especially for thin-winged combat aircraft, then the fuselage space can be used for storage. Typically, fuel storage in the fuselage can be above or below the floorboards and forward, rearward, and/or at the center of the wing. When there are several tanks, it is convenient to collect fuel at a central location before delivering it to the engines. Fuel from tanks at various locations is pumped into a centrally located collector tank following a transfer schedule that minimizes the CG shift. A symmetrical fuel level in the wings also is important. Note the compartmentalization of the wing tank; surge tanks are provided at the wing tips and internal baffles restrict fuel-sloshing. Some long-range aircraft have volume available in the stabilizer to balance the CG shift through an in-flight fuel transfer.

The fuel-tank arrangement for a thin-winged aircraft (i.e., the supersonic type) is complex because there is insufficient volume available for the mission. Therefore, fuel is provisioned in the fuselage wherever space is available. The Concorde example, shown in [Figure 15.23](#), carries a substantial amount of fuel and the CG shift is minimized by in-flight balancing through a fuel transfer from the forward and aft trim tanks. The military aircraft fuel-tank arrangement is similar to the Concorde. There can be as many as sixteen tanks, all interconnected to meet the fuel requirements of the mission.

Fuel tanks can be either rigid, made of metal or composite material, or flexible, made of a rubber-neoprene-like material. Tanks are installed during component assembly. Flexible-tank maintenance requires a change of tanks, which can be a laborious task. Most modern aircraft have wet tanks, in which the skin at the joints is treated with a sealant. A wet-tank system is lighter and more volume-efficient; however, leakage is problematic and these aircraft require strict inspection, especially older aircraft. Sealant technology has improved and wet tanks are favored.

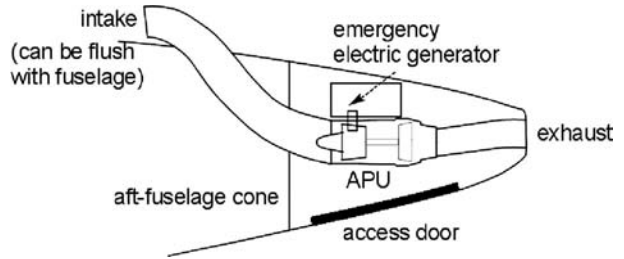
Heat generated in stagnant regions of an aircraft flying faster than Mach 2.4 can be cooled by recirculating cold fuel around the hot zones before being fed to the engine. The preheating of fuel also helps in the combustion process.

15.9.3 Emergency Power Supply

Most midsize and larger aircraft install an APU, which performs many functions. An APU is a small power plant, invariably a turboshaft engine that uses the same fuel (i.e., AVTUR). When ground facilities are not available, the APU can provide an emergency electrical supply and air-conditioning, and it can start the main aircraft gas turbines. It is interesting that an APU exhaust can reduce aircraft drag, regardless of how small. A typical example of an aft-mounted APU is shown in [Figure 15.24](#) (i.e., a schematic layout). The APU and its installation weight range from 100 to 300 kg depending on the size. The size of an APU in a military aircraft depends on user requirements. An APU can be started using onboard batteries.

A ram air turbine (RAT) is another way to supply emergency power. This is a propeller-driven device mounted on an aircraft surface (at the fuselage underbelly) that operates when an aircraft is in motion. A RAT is retractable. [Figure 15.25](#) shows the schematic layout.

Figure 15.24. Auxiliary power unit



15.9.4 Avionics Subsystems

A host of avionics “black boxes” support the flight deck and beyond. The black boxes serve navigation, communication, aircraft-control, and environment-control systems; and record and process important data to analyze and monitor malfunctions and so forth.

With increasing features, the electrical cable length is long and relatively heavy. Multiplexing of data transmission significantly reduces cable weight. Recently, fiber optics have been used for data transmission; when used with a FBW system, it is appropriately termed FBL (see Chapter 12). This section introduces readers to design features (i.e., hardware) that assist in a more accurate prediction of weight and cost.

Most avionics black boxes have microprocessors, which help to standardize connections for data flow. The connection of wires is called a *bus*. Following are the prevailing standards for a bus architecture.

Military Aircraft Application

MIL-STD-1553B: U.S. military aircraft were the first to use the data-bus architecture, especially to handle the large amount of data for FBW and combat operations. In the United Kingdom, it is covered by DEF STAN 00-18. MIL-STD-1773 is the fiber-optics version of MIL-STD-1553B and STANAG 3838 is the NATO standard for bus architecture.

Figure 15.25. Ram air turbine

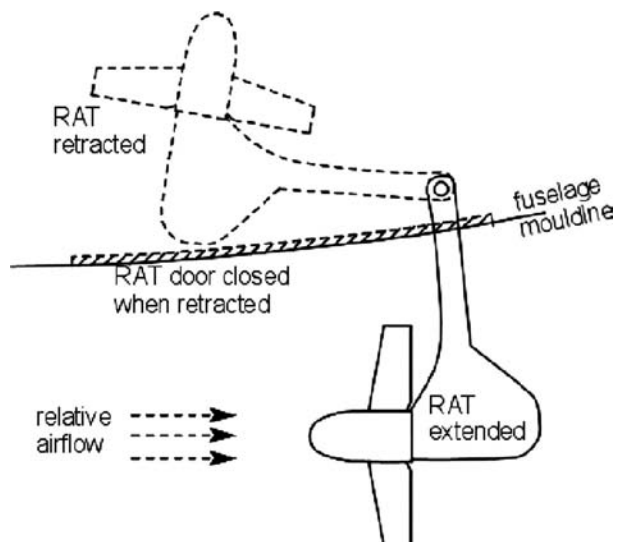


Table 15.11. *Aircraft avionics items*

EFIS/MFDs	Computers	Communication	Navigation
System display	Air data	ATC	DME
Analog gauges	FBW	VHF	GPS
Radar	FADEC	Television	DME
	Autopilot		VHF

Civil Aircraft Application

ARINC 429 (originated in the 1970s): The success of the military standard was followed by civil standards, which began in a simplified manner. The Airbus 320 was the first large transport aircraft to use a full FBW system. ARINC 629 is the updated version that replaces ARINC 429.

Line replacement units (LRUs) are a convenient hardware design to facilitate installation and maintenance of electrical and avionics transmissions and connections following the bus standards. LRUs are constructed in the modular concept as a subassembly and then installed on an aircraft. LRUs are also standardized to comply with the bus architecture.

Aircraft communication and navigation equipment is part of an avionics package. The components of a typical civil aircraft avionics package are listed in Table 15.11.

Typical antenna locations for aircraft communication and navigation are shown in Figure 15.26. Antennas are installed in the symmetrical plane of an aircraft. Surveillance aircraft have a specific large housing for special-purpose avionics.

15.9.5 Electrical Subsystem

All aircraft must have some form of electrical supply to power the aircraft subsystems. The supply of electricity is executed by a combination of generators and batteries. Most modern aircraft require both AC and DC supplies. The typical AC voltage is 115 volts at 400 Hz, but there are higher-voltage AC supplies. Typically, the DC voltage supply is 28 volts. The electrical-supply control must ensure safety and comply with mandatory requirements.

The following systems are associated with electrical power:

- engine starting and operation; management of the fuel system
- lighting – both internal and external (Figure 15.27 shows external requirements)
- flight deck instrumentation
- communication and navigation

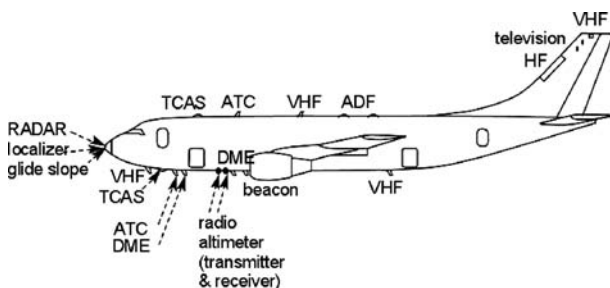
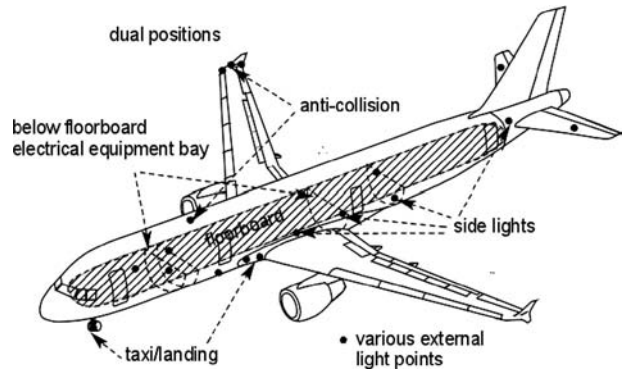


Figure 15.26. Antenna locations

Figure 15.27. Aircraft lighting requirements



- avionics system
- flight-control system using the PCU
- passenger services for civil aircraft
- APU: emergency electrical power generation and supply
- armament management, electronic defensive and countermeasures for military aircraft

Typically, the electrical supply is generated at the primary and secondary levels. Engine-driven generators supply the primary power. The secondary supply serves before an engine starts and is a standby in an emergency situation. The secondary supply is generated from batteries, the APU, or an auxiliary system such as RAT.

The below-floorboard equipment bay houses items such as batteries, chargers, power controllers, transformers, and inverters (see [Figure 15.27](#)).

The weight of an electrical system depends on the load requirements. The cable weight is significant. An avionics system can be 0.4 to 4% for civil aircraft and 0.5 to 5% for military aircraft.

15.9.6 Hydraulic Subsystem

All larger aircraft have a hydraulic system, which includes a fluid reservoir, electricity-driven pumps, hydraulic lines, valves, and pilot interface at the flight deck. Hydraulic-driven actuators are incorporated at a higher force level to activate the following uses:

- aircraft control system (e.g., elevator, rudder, aileron, and high-lift devices)
- engine thrust reversers
- undercarriage deployment and retraction
- brake application

For modern civil aircraft, hydraulic pressure is from 2,000 psia (older designs) to 3,000 psia (current designs); military aircraft hydraulic oil pressure has reached 8,000 psia. A higher pressure lowers the system weight but requires stringent design considerations.

[Figure 15.28](#) shows the hydraulics system scheme of a four-engine aircraft. To ensure safety and reliability, at least two independent, continuously operating hydraulic systems are positioned in separate locations. The port side is identified as

Table 15.12. *Hydraulics-driven subsystems (BAe RJ family)*

Separately in both systems	Yellow system	Green system
Wheel brake and parking brake	Flap brake	Lift spoilers (center and outboard)
Power transfer unit (PTU)	Roll spoilers	Air brake
1 Flap mode	Lift spoilers (inboard)	Undercarriage (landing gear)
Oil reservoir	Undercarriage emergency lock	Nose-gear steering
Accumulator	1 Rudder control	Wheel brake only
	Standby fuel pumps	Standby AC/DC generator drive
	Internal stair	Engine-driven pump (EDP)

the yellow system and the starboard side is the green system. (Airbus introduced a third independent line – the blue line.) Each line has its own reservoir and functionality. Table 15.12 lists the subsystems activated by the hydraulics system. All systems include gauges, switches, valves, tubing, and connectors.

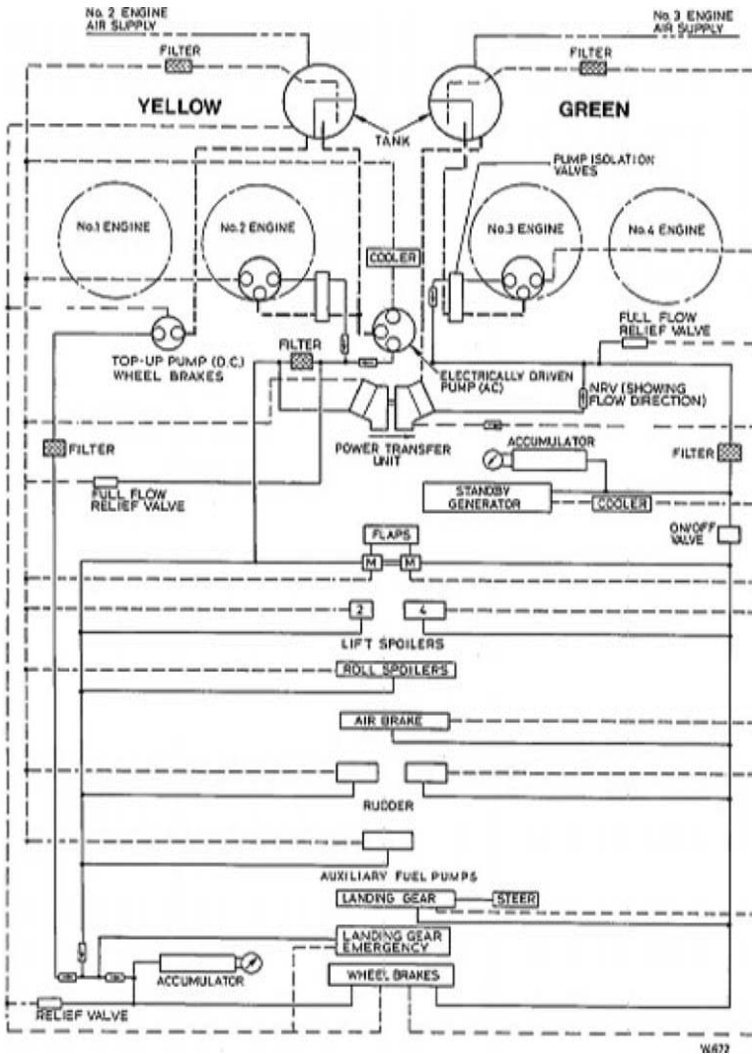


Figure 15.28. Aircraft hydraulics system

The weight of the hydraulics system depends on the load requirements. Together with the pneumatic system, the hydropneumatic system can be 0.4 to 1% for civil aircraft and 0.5 to 2% for military aircraft.

15.9.7 Pneumatic System

The pneumatic system consists of the use of a high-pressure air-bleed from the engine (gas turbines) serving the (1) ECS, which consists of cabin pressurization and air-conditioning; (2) anti-icing; (3) defogging system; and (4) engine starting. The APU is linked to the pneumatic system. An aircraft's oxygen needs are supplied by a separate pneumatic system that is fitted with a pressure-reducing shutoff valve (PRSOV) and a cross-flow shutoff valve (SOV) to control and isolate airflow according to the scheduled demand.

Other uses for pneumatics include pressurizing the hydraulic reservoir, fuel system, and water tank; driving the accessories; and as a medium for rain repellent. Some thrust reversers are actuated by the pneumatic system.

ECS: Cabin Pressurization and Air-Conditioning

At cruise altitude, the atmospheric temperature drops to -50°C and below, and the pressure and density reduce to less than one fifth and one fourth of sea-level values, respectively. Above a 14,000-ft altitude, the aircraft interior environment must be controlled for crew and passenger comfort as well as equipment protection. The cabin ECS consists of cabin pressurization and air-conditioning. Smaller, unpressurized aircraft flying below a 14,000-ft altitude suffice with air-conditioning only; the simplest form uses engine heat mixing with ambient cold air supplied under controlled conditions.

The cabin-interior pressure maintained at sea-level conditions is ideal but expensive. Cabin pressurization is like inflating a balloon – the fuselage skin bulges. The major differential between the outside and the inside pressure requires structural reinforcement, which makes an aircraft heavier and more expensive. For this reason, the aircraft cabin pressure is maintained no higher than 8,000 ft, and a maximum differential pressure is maintained at 8.9 psi. During ascent, the cabin is pressurized gradually; during descent, cabin depressurization is also gradual in a prescribed schedule acceptable to the average passenger. Passengers feel it in their ears as they adjust to the change in pressure.

Cabin air-conditioning is an integral part of the ECS along with cabin pressurization. Supplying a large passenger load at a uniform pressure and temperature is a specialized design obligation. The engine compressor, which is bled at an intermediate stage with sufficient pressure and temperature, becomes contaminated and must be cleaned with moisture removed to an acceptable level. Maintaining a proper humidity level is also part of the ECS. The bled-air is then mixed with cool ambient air. In addition, there is a facility for refrigeration. The internal system turbine and compressor are driven by the system pressure. The heat exchanger, water extractor, condenser, valves, and sensors comprise a complex subsystem, as shown in [Figure 15.29](#).

[Figure 15.30](#) depicts the BAe RJ family anti-icing system. A generic pattern for the supply of air-conditioning in the passenger cabin is shown in [Figure 15.31](#).

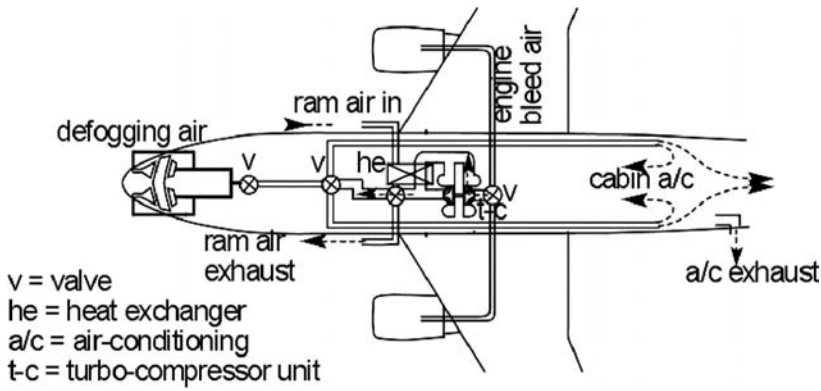
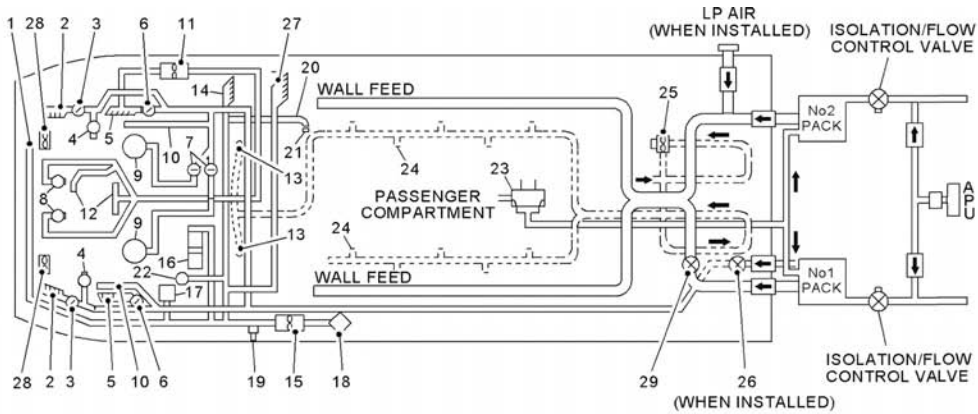


Figure 15.29. Schematic of a civil aircraft ECS



- | | |
|--|---|
| 1 PILOTS INSTRUMENT PANEL COOLING | 17 PRINTED CIRCUIT BOARD BOX COOLING |
| 2 FORWARD FLOOR VENTS | 18 SMOKE DETECTOR |
| 3 FORWARD FLOOR AIR SELECTOR VALVE | 19 PRESSURE SWITCH |
| 4 SIDE CONSOLE ADJUSTABLE OUTLET | 20 CABIN TEMPERATURE SENSOR (CONTROL) |
| 5 AFT FLOOR VENTS | 21 CABIN TEMPERATURE SENSOR (INDICATOR) |
| 6 F/DECK AIR SELECTOR FLAP VALVE | 22 F/DECK TEMPERATURE SENSOR (CONTROL) |
| 7 F/DECK ROOF FLOOD OUTLET SHUTOFF VALVE | 23 RECIRCULATION VALVE |
| 8 ADJUSTABLE ROOF OUTLET | 24 PASSENGER ADJUSTABLE OUTLETS |
| 9 ROOF FLOOD OUTLET | 25 CABIN FAN |
| 10 WINDSHIELD PANEL C DE-MIST | 26 RAM AIR ISOLATION VALVE |
| 11 FLIGHT DECK FAN | 27 2R GALLEY VENTILATION (WHEN 2R GALLEY INSTALLED) |
| 12 ROOF INSTRUMENT PANEL COOLING | 28 EFIS COOLING FANS (MOD.00950D) |
| 13 TOILET AND GALLEY AIR OUTLETS | 29 FLIGHT DECK COOLING VALVE (MOD.50084A, MOD.50084B OR MOD.50084C) |
| 14 1R GALLEY VENTILATION | |
| 15 ELECTRICAL EQUIPMENT BAY COOLING FAN | |
| 16 AVIONIC EQUIPMENT RACK COOLING | |

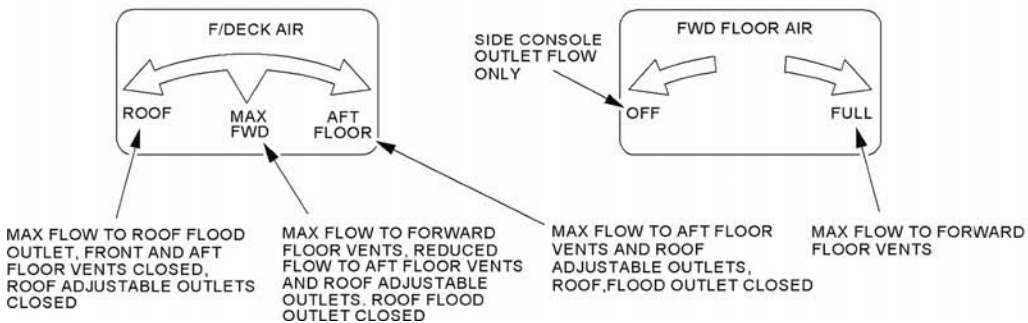
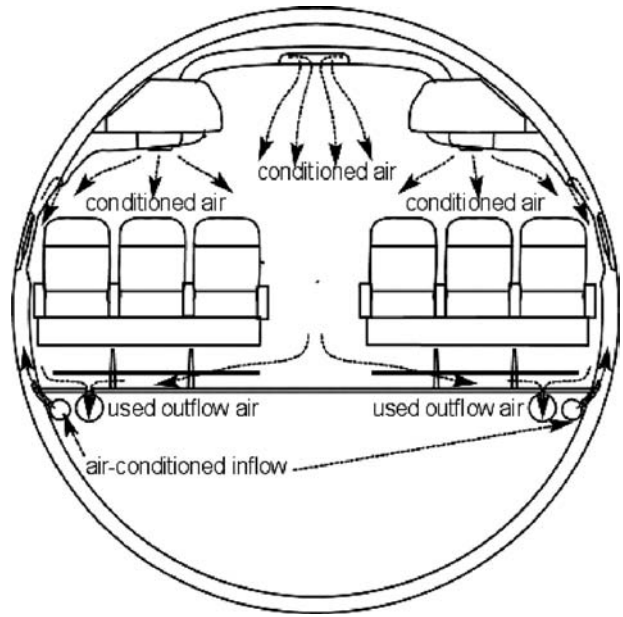


Figure 15.30. BAe RJ family air-conditioning system

Figure 15.31. Cabin airflow ECS



The avionics black boxes heat up and must be maintained at a level that keeps equipment functioning. The equipment bay is below the floorboards, as shown in [Figure 15.27](#). Typically, a separate cooling system is employed to keep the equipment cool. Ram-air cooling is a convenient and less expensive way to achieve the cooling. Scooping ram air increases the aircraft drag. The cargo compartment also requires some heating.

An advanced military aircraft ECS differs significantly ([Figure 15.32](#)), using a boot-strap refrigeration system, which has recently also been deployed in civil aircraft applications.

Oxygen Supply

If there is a drop in cabin pressure while an aircraft is still at altitude, the oxygen supply for breathing becomes a critical issue. The aircraft system supplies oxygen to each passenger by dropping masks from the overhead panel. Military aircraft have fewer crew members and the oxygen supply is directly integrated in a pilot's mask, as shown in [Figure 15.33](#).

Anti-icing, De-icing, Defogging, and Rain-Removal Systems

Icing is a natural phenomenon that occurs anywhere in the world depending on weather conditions, operating altitude, and atmospheric humidity. Ice accumulation

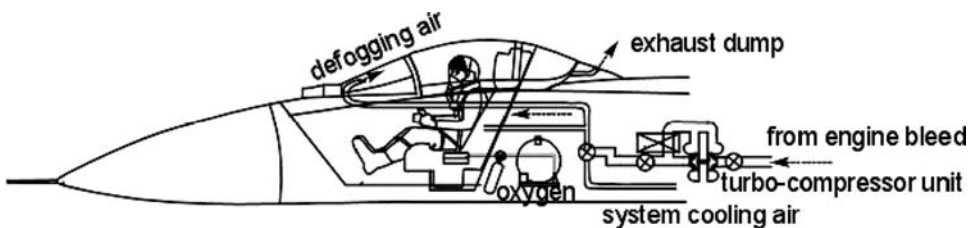


Figure 15.32. Military aircraft ECS

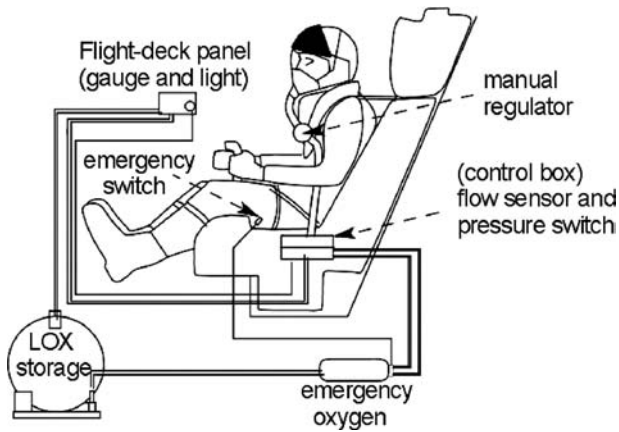


Figure 15.33. Military aircraft oxygen system

on the wing, empennage, and/or engine intake can have disastrous consequences. Icing increases the drag and weight, decreases the lift and thrust, and even degrades control effectiveness. On the wing and empennage, icing alters the profile geometry, leading to loss of lift. Ice accumulation at the intake degrades engine performance and can damage the engine if large chunks are ingested. It is a mandatory requirement to keep an aircraft free from icing degradation. This can be achieved by either anti-icing, which never allows ice to form on critical areas, or by de-icing, which allows ice buildup to a point and then sheds it before it becomes harmful. De-icing results in blowing away chunks of ice, which could hit or be ingested into an engine. Figure 15.34 shows the typical anti-icing envelopes.

There are several methods for anti-icing and de-icing. Not all anti-icing, de-icing, defogging, and rain-removal systems use pneumatics; some have an electrical system. Following are the methods currently in practice:

1. *Hot Air Blown Through Ducts*. This pneumatic system is the dominant one used for larger civil aircraft. Both anti-icing and de-icing can use a pneumatic system, which is achieved by routing high-pressure hot air bled from the midcompressor stage of a gas turbine and blown around the critical areas through perforated ducts (i.e., *Piccolo tubes*). Typical pressure and temperature in the duct is about 25 psi (regulated between 25 psi and 40 psi) and 200°C (military aircraft reaching 500°C). Designers must ensure that damage does not occur due

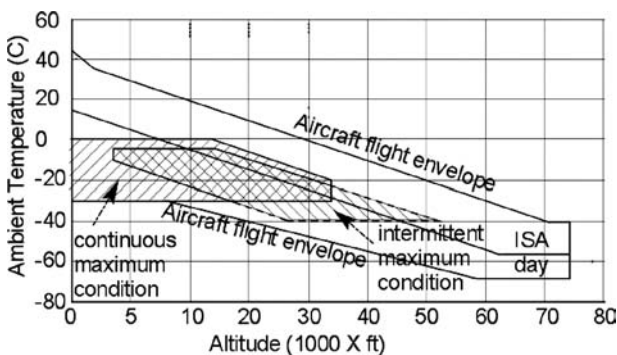
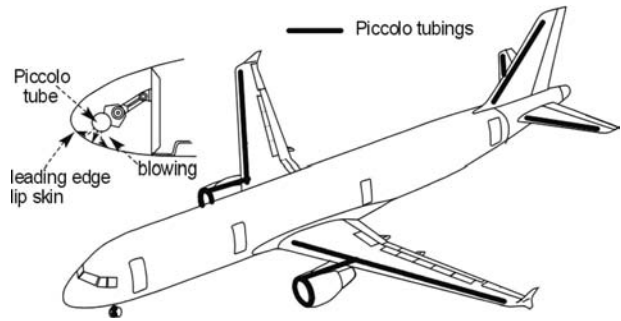


Figure 15.34. Typical anti-icing envelopes

Figure 15.35. Generic civil aircraft anti-icing subsystem (Piccolo tubes)



to overheating. Figure 15.35 shows a typical system. Figure 15.36 depicts the BAe RJ family anti-icing system.

2. *Boots.* Both anti-icing and de-icing can use a boot specially designed with an integrated electrical heater or passages for hot airflow. Rubber boots are wrapped (i.e., capped) around the critical areas (e.g., LEs of lifting surfaces, propeller LEs, and intake lips) and are heated by either electrical elements or passing hot air, as in the pneumatic system. Electrically heated boots are lighter but can be relatively more expensive. The boot-type method is used in smaller aircraft. Figure 15.37 shows a typical boot system.
3. *Electric Impulse.* This is a not common but quite effective de-icing system. Ice is allowed to accumulate to a point when vibrations generated by electrical impulses break the ice layer, which is then blown away. This method has low power consumption but can be a heavy and expensive system.
4. *Chemicals.* This also is not a common system and is used primarily for anti-icing. Glycol-based antifreeze is allowed to “sweat” through small holes in critical areas where the chemical is stored. This process is limited to the amount of antifreeze carried onboard.

The piston engine carburetor and critical instruments must be heated to keep them functioning.

Defogging and Rain-Removal Systems

The defogging and rain-removal systems are like an automobile using windshield wipers with embedded electrical wire in the windscreen. Rain-repellent chemicals assist in rain removal. Figure 15.38 shows a defogging and rain-removal system. Figure 15.38a is a generic layout with wipers, and Figure 15.38b shows the RJ family rain-repellent system in better detail.

15.9.8 Utility Subsystem

Utility systems are composed of water and waste systems, as shown in Figure 15.39. Passengers need water and restroom facilities. As the number of passengers and the duration of flights increase, the demand for drinking water and waste-disposal management also increases. The entire system is self-contained.

Typically, a third of a U.S. gallon of water per passenger (i.e., 100 U.S. gallons for 300 passengers) is the quantity carried onboard. Both hot and cold water is supplied. Typically, 1 lavatory per 10 to 15 passengers is provided. Chemicals are used

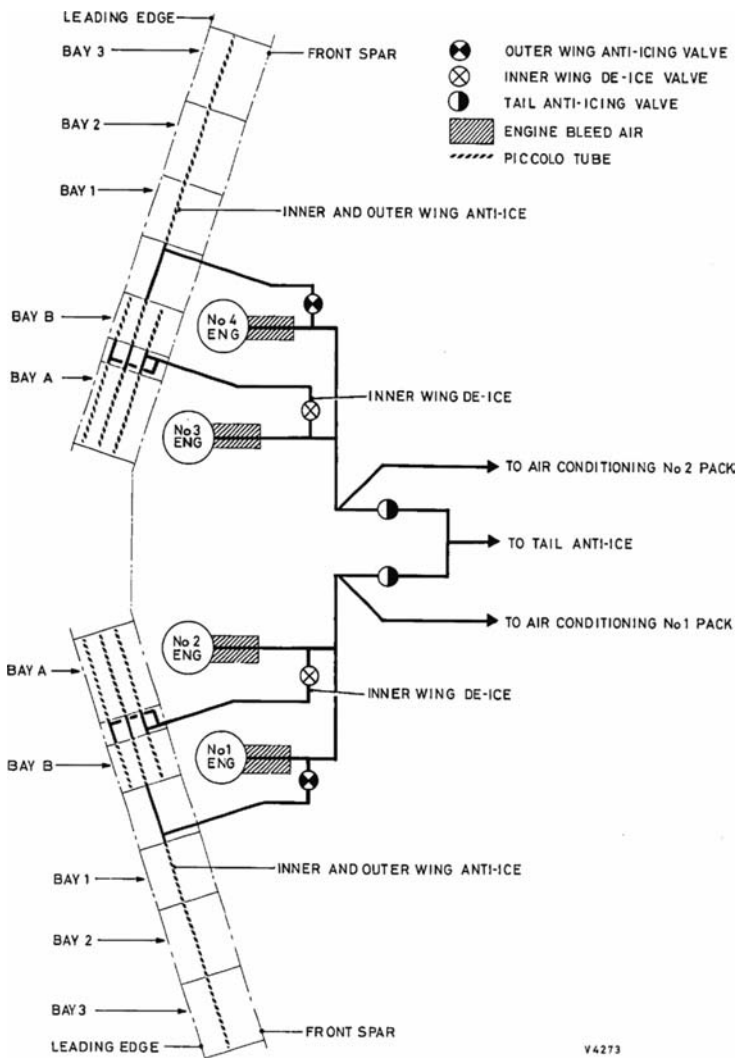


Figure 15.36. The BAe RJ family anti-icing system

with water to flush the commodes. Waste must be contained inside until the aircraft lands, whereupon the systems are cleaned and refilled with fresh supplies for the next sortie. Figure 15.40 shows the RJ family wastewater-management system in detail.

Aircraft must be prepared for passenger services and utility use. Specific locations are designated for preparing aircraft such that they do not interfere with and delay one another. Figure 15.41 shows the typical utility-service points. Access to servicing should not interfere with other activities in and around aircraft. Freezing of water is prevented by heating the critical areas.

15.9.9 End-of-Life Disposal

In general, the operational life of a civil aircraft ranges from twenty to thirty years depending on operational demand and profitability. A few World War II C47s

Figure 15.37. Anti-icing subsystem using boots

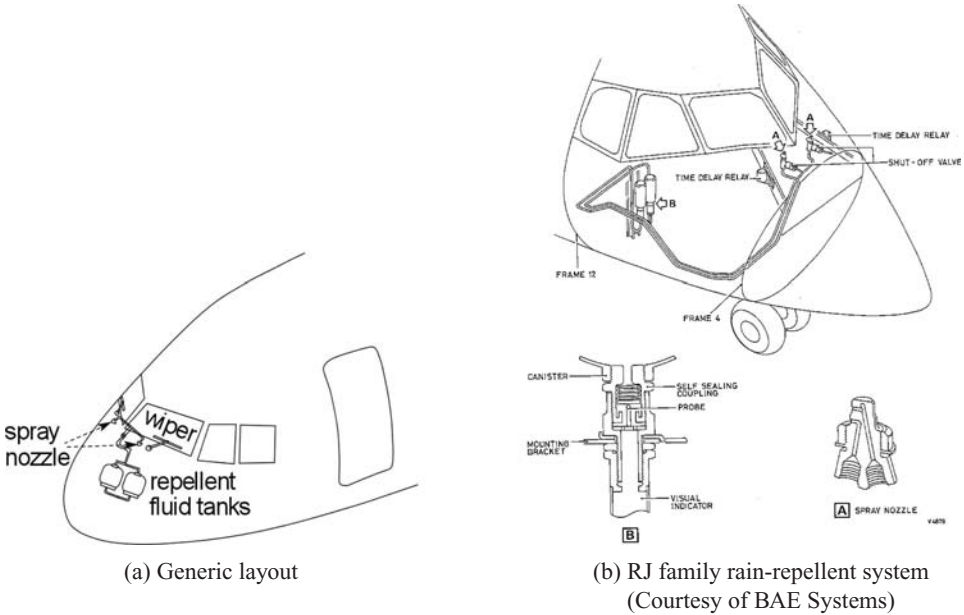
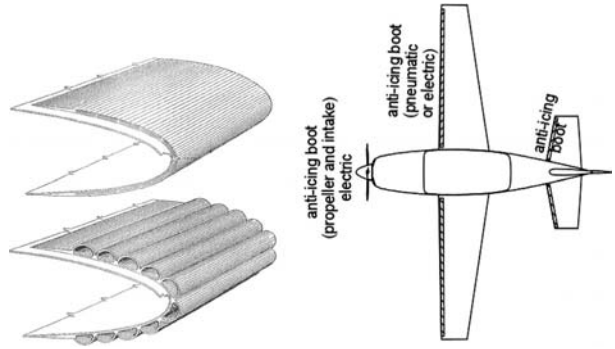


Figure 15.38. Civil aircraft rain-repellent system

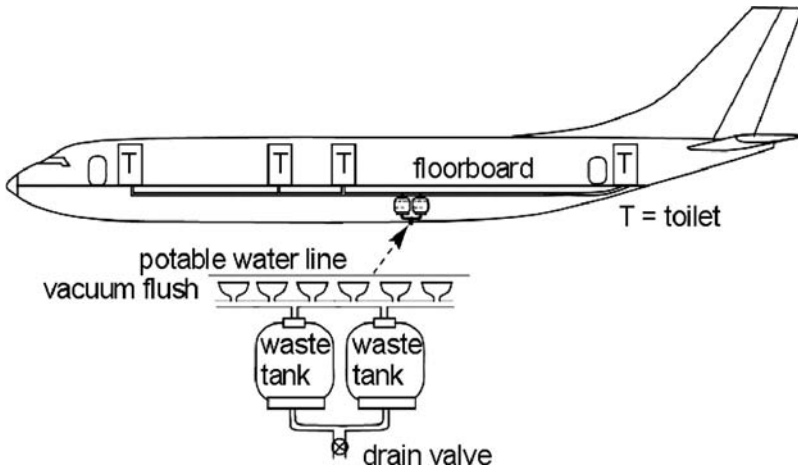


Figure 15.39. Water and waste systems

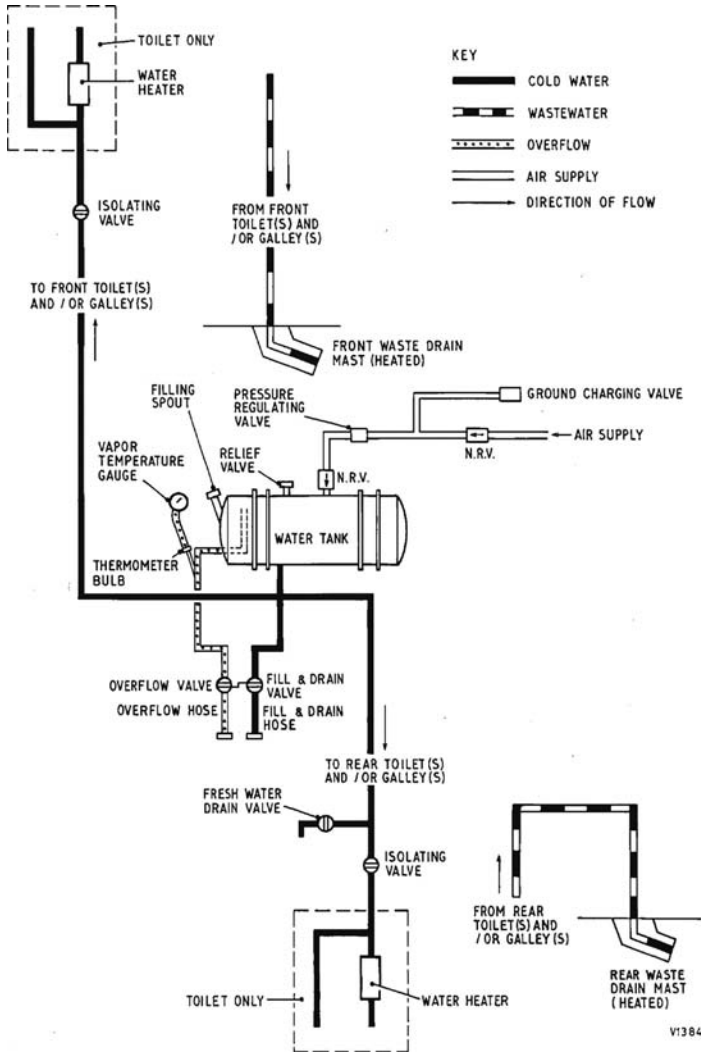


Figure 15.40. The RJ family wastewater system

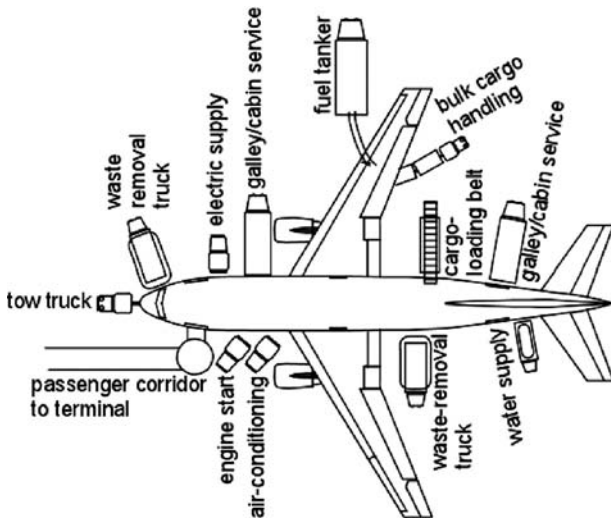


Figure 15.41. Civil aircraft turnaround servicing locations

(Dakota) are still flying. Thousands of aircraft already have been grounded and thousands more will be grounded forever in the immediate future. Their storage occupies much land and aircraft disposal is not the same as for automobiles. The disposal of older aircraft is a serious problem.

Metal sold as scrap can be recycled but increasing amounts of composite material are accumulating. Disposal of composite materials is difficult because they serve no useful purpose as scrap – attempts are being made to make them recyclable. Avionics black boxes and microprocessors contain toxic materials; the fluids in display units also are toxic. It is expensive to rid the environment of toxic materials. Incineration plants are specifically designed to keep the efflux clean.

More research is continuing to find suitable materials that are less toxic and also can cost effectively be disposed of. This is a concern of material scientists; however, aircraft designers must stay current with materials technology and make proper selections.

15.10 Military Aircraft Survivability

This extended section of the book can be found on the Web site www.cambridge.org/Kundu and presents a typical military turboprop survivability consideration in the following subsections.

15.10.1 Military Emergency Escape

The subsection introduces a typical ejection seat and ejection sequences as a survivability issue with the following figures.

Figure 15.42. Typical military aircraft ejection seat

Figure 15.43. Typical ejection sequence

Figure 15.44. Typical ejection sequence showing separation of seat and parachute deployment

15.10.2 Military Aircraft Stealth Consideration

The subsection introduces various military aircraft stealth considerations and strategies as survivability issues. It covers system integration of operational needs before, during, and after combat (e.g., audio-visual detection, radar signature, heat signature, on-board passive system, use of defensive aids, secure communication, on-board stand-alone navigational system, and returning to home base).

15.10.3 Low Observable (LO) Aircraft Configuration

The subsection deals with military aircraft typical stealth considerations issues such as heat and radar signature suppression as survivability issues. Following are the figures in this subsection.

Figure 15.45. Typical comparisons of radar signatures (sphere versus stealth aircraft)

Figure 15.46. Three stealth aircraft configurations

15.11 Emerging Scenarios

There have been four emerging topics: two concerning terrorist activities, one concerning health issues, and one ongoing problem related to aircraft debris on the runway. This section familiarizes future designers with the types of problems they may face related to these topics.

Counterterrorism Design Implementation

Much thought is now applied to ways to counter onboard terrorism. These topical considerations have yet to be determined for implementation. There is concern about the increased weight and cost of an aircraft. Some design-change ideas are as follows:

1. Install a bulletproof flight-deck barrier at the cockpit door. Compartmentalize the cabin to isolate trouble. Whether these measures are effective must be debated, but aircraft designers must use foresight rather than hindsight.
2. Improve the structural integrity of the cargo compartment/bay against in-flight explosions. The space below the floorboards must be compartmentalized and have a shock-absorbing, impact-resisting shell structure to retain integrity in the event of an explosion.
3. The aircraft flight system must have an automated-recovery ability, homing to the nearest landing field (military aircraft already have this type of system).

Health Issues

The steady annual increase in the number of passengers crossing international boundaries results in health issues that must be addressed. Space must be allotted to treat and isolate patients (like on cruise ships). Until recently, this measure was on an ad-hoc basis; however, manufacturers can increase market appeal by providing health-care facilities, especially for larger aircraft with long flight durations. Cardiovascular conditions, pregnancies, infections, and other emergency-health scenarios are increasing during international flights.

Damage from Runway Debris

The catastrophic crash of the Concorde was a result of runway debris hitting the fuel tank, which then burst into flames. Vulnerable areas must be protected with stronger impact-resistant materials. This is a relatively simple task but designers must examine the point in new designs, which does incur additional weight and cost considerations.

16 Aircraft Cost Considerations

16.1 Overview

An aircraft design, construction, and operation is an expensive endeavor, and not all nations can afford it. Countries that can must be cost-conscious, whether in a totalitarian or a free-market-economy society – the ground rules for accounting may differ but all strive for the least expensive endeavor for the task envisaged. The success or failure of an aircraft project depends on its cost-effectiveness. Cost-consciousness starts in the conceptual design phase to ensure competitive success. In fact, cost estimation should start before the conceptual design phase in a topdown analysis. If funds cannot be managed through the end of the project, then starting it is not viable.

Visibility on costing forces long-range planning and provides a better understanding of the design's system architecture for trade-off studies to explore alternate designs and the scope for sustainability and eco-friendliness of the product line. The product passes through well-defined stages during its lifetime: conception, design, manufacture, certification, operation, maintenance and modification, and finally disposal at the end of the life cycle. Cost information for previous products should be sufficiently comprehensive and available during the conceptual stages of a new project. The differential evaluation of product cost and technology – offering reliability and maintainability – as well as risk analysis are important considerations in cost management. Cost details also assist preliminary planning for procurement and partnership sourcing through an efficient bidding process. The final outcome ensures acquisition of an aircraft and its components with the objective of balancing the trade-off between cost and performance, which eventually leads to ensuring affordability and sustainability for operators over a product's life cycle. Cost analysis stresses the importance of a more rigorous role, as an integrated tool embedded in the multidisciplinary systems architecture of an aircraft design that arrives at a "best value," specifically for manufacturing and operational needs.

During the last two decades, the aerospace industry has increasingly addressed factors such as cost, performance, delivery schedule, and quality to satisfy the "customer-driven" requirements of affordability by reducing the aircraft acquisition costs. The steps to address these factors include synchronizing and integrating design with the manufacturing and process planning as a business strategy; this

lowers production costs while it ensures reliability and maintainability to lower operational costs. Therefore, more rigorous cost assessment at each design stage is needed to meet the objective of a more effective, value-added, customer-driven product. At this time, data from the emerging geopolitical scenario, national economic infrastructure, increasing fuel prices, and emerging technological considerations (e.g., sustainable development, anti-terrorism design features, and passenger health issues) are scarce and fluctuating.

The civil aviation industry expects a return on investment with cash flowing back for self-sustaining growth, with or without government assistance. The sustainability and growth of civil aviation depend on profitability. In a free-market economy, the industry and operators face severe competition for survival, forcing them to operate under considerable pressure to manage efficiently the manufacture and operation of aircraft. Although substantial detail about civil aircraft cost is available in the public domain, the cost of manufactured parts is not readily available.

Conversely, the military aircraft industry is driven by defense requirements with the primary objective of meeting the national defense needs. The export potential is a byproduct, which is restricted to friendly nations with the risk of disclosure of technical confidentiality. There are differences between the ground rules for costing the manufacture and operation of military and civil aircraft. Because by its nature it must stay ahead of adversaries' capabilities, military aircraft designs must explore newer technologies, which are expensive and require laborious testing to ensure safety and effectiveness. Many military projects were abandoned even after prototypes had been flown (e.g., the TSR2 [U.K.] and the Northrop F20 [U.S.]); the reasons may be different but the common factor is always cost-effectiveness. A product must have the appeal for the best value. Readers are encouraged to review both types of aircraft project history. This chapter primarily addresses civil-aircraft cost considerations with a passing mention of military aircraft costing.

There are two types of costs to consider: (1) the research, development, design, and manufacturing costs (RDDMC), including testing and production launch costs; and (2) the operational cost (OC). An aircraft must be built before it can operate for a mission. OC depends on aircraft cost, which is known when it is purchased. For this reason, aircraft manufacturing costs are analyzed first in [Section 16.4](#), followed by OC analysis in [Section 16.5](#). Aircraft cost analysis, as discussed herein, is not possible without the instructor's help. The analysis depends on industrial data, which are not available due to confidentiality. An instructor must obtain these data or generate equivalent data – it is difficult to obtain realistic data that can be substantiated – in order to progress with establishing the appropriate indices. However, the DOC estimation can be carried out easily if the aircraft price is known. Other methods are available to estimate aircraft costs, but their accuracy is debatable without industrial input. Aircraft cost estimation is included in this section to show readers that otherwise relatively simple mathematics involved in cost analysis actually are complex. This discussion provides some exposure to cost analysis.

Research, design, development, and test (RDD&T) costs occur once and are termed nonrecurring cost (NRC); however, manufacturing costs continue into production and are termed recurring cost (RC). Typical RDDMC (i.e., the project cost) of a new civil aircraft project in the midrange class of high-subsonic aircraft can

be in billions of dollars with a 4-year wait until delivery, when the return on the investment begins to flow back. A new advanced combat aircraft costs several times more and taxpayers bear all costs. The cost of a large, high-subsonic-jet aircraft project (i.e., RDDMC) could approach \$20 billion.

Without industry participation, it will not prove realistic for academics/consultants to offer cost models; these will remain exploratory in nature. Industries depend on their own cost models, which are constantly reviewed for improvements. This chapter outlines various levels of aircraft cost considerations practiced in a free-market economy. Based on in-house data, each industry generates specific cost models (with or without external assistance) at different levels of accuracy suited to different departments at various phases of project activities. The estimation of project cost is a laborious task involving numerous parameters and a large database. Cost estimators and accountants devote considerable time to predicting project costs; they subsequently verify actual expenditures if their estimation is close to their prediction. Experience has taught costing teams to use company-generated factors to predict estimates; these are not available in the public domain. In a competitive market, cost details are sensitive information and are therefore kept in strict confidence.

Because access to actual cost data is not easy, a good method for the aircraft cost estimate is to first assess the manhours involved and then use the average manhour rates (they vary) at the time. Material and bought-out item costs can be obtained from suppliers. The scope of this book does not include accurate industrial-cost details; academic institutes must generate data as required. This chapter provides a generic, rapid methodology for predicting manufacturing costs, which is more suited to coursework, without ignoring what is considered in the industry. It is based on a parametric method, and a normal market situation without any unpredictable trends (i.e., global issues) is assumed.

The scope of a cost study allows those working with a highly complex system architecture of aircraft design to explore cost control beyond current practices and to understand through trade-off studies how a diverse range of systems works, allowing the transfer of best practices and risk-management experience throughout the operating life of ownership. This chapter stresses the need for cost analyses of different disciplines at an early stage in order to exploit the advantages of advanced digital design and manufacturing processes (see [Chapter 17](#)). Cost trade-off studies at the conceptual design stage lead to a “satisfying” robust design with the least expenditures. Strong multidisciplinary interaction is essential between various design departments to attain the overall, global goal of minimizing cost rather than individual (i.e., departmental) minimization. Initially, a proper cost optimization may not be easily amenable to industrial use.

Aircraft DOC is the most important parameter of concern to airline operators. The DOC depends on how many passengers the aircraft carries for what range; the unit is expressed in cents per seat nautical miles (seat-nm). There are standard rules (e.g., the Association of European Airlines [AEA] method; see [Section 16.4](#)) for comparison when each industry or airline has its own DOC ground rules, which results in different values as compared to those obtained from standard methods.

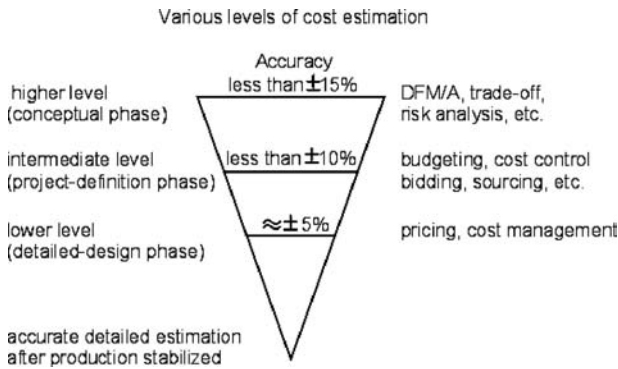


Figure 16.1. Levels of cost-prediction methodologies at various project phases

16.1.1 What Is to Be Learned?

This chapter covers the following topics:

- Section 16.2: Important aspects of costing
- Section 16.3: Aircraft and operational costs
- Section 16.4: A rapid-cost method for manufacture (see [1])
- Section 16.5: DOC details and computation methods

16.1.2 Coursework Content

Readers are to estimate the Bizjet DOC. All relevant information to estimate the aircraft's DOC is provided. However, the estimation of aircraft costs can be omitted if it has been covered in another course by specialists. In this book, cost studies do not alter the finalized and substantiated configuration obtained thus far through the worked-out examples. It is beneficial to be aware of the cost implications in aircraft design and operation.

16.2 Introduction

Typically, at the conceptual design phase of a new aircraft program, insufficient information about design details is available to estimate costs. In-house previous experience on cost becomes crucial in the trade-off studies of cost versus performance of various design parameters. A preliminary and fast but realistic cost-estimating methodology (e.g., an accuracy of less than $\pm 15\%$, set at a high-level data structure) (Figure 16.1) is needed to help designers investigate and adopt new proven technologies in order to advance a product to a competitive edge.

The post-conceptual design study phase leads to the project-definition phase, followed by the detailed-design phase when manufacturing activities produce a finished aircraft. At later stages of a project, when more accurate cost data are available, the use of an *analytical cost method* at a lower level of data structure fine-tunes the cost estimates obtained in the earlier conceptual stages. Figure 16.1 shows the levels of cost-model architecture to serve various groups at different stages of the program milestones. The deeper the breakdown of a parametric method, the more it converges to an analytical method. The proposed rapid-cost model based on parametric method is quite different from the analytical-cost method. The latter

procedure is time-consuming and may omit some of the myriad details involved. The parametric method is generally intended for designers, whereas the analytical method is intended for corporate use to establish aircraft pricing and gain a better understanding of a customer's cost goals, constraints, and competitive market requirements; it also is useful at the bidding stage and for other budgetary purposes. The state of the art of cost modeling predictions is close to the actual cost after production has been stabilized.

Less accurate cost considerations at the conceptual design stage, specifically intended for designers, are no less meaningful than what accountants and estimators provide to management for assessing profitability and running a lean organization. Extending the frontiers of cost-saving through IPPD rather than merely running lean on manpower adds a new dimension to harnessing human resources by organizations investing in people, which is where it counts. In fact, the preliminary cost estimates at higher levels of architecture flow to the lower level when more data are generated as a project advances through the milestones. Cost estimations made by different methods should converge within close tolerance, benefiting from in-house experience. Other cost-estimation models are not pertinent to the scope of this book.

The success or failure of cost estimation using a parametric method depends on identifying correct cost drivers and then establishing a good cost relationship with available in-house data to embed accuracy. Ensuring quality while making the product converge on cost (i.e., design for cost) rather than allowing cost to make the product (i.e., design to cost) is the essence of cost control. The core of cost modeling is to identify and define the cost drivers and functions of a product and to generate information, which are tools for DFM/A (see [Chapter 17](#)) in an IPPD environment. The DFM/A studies lead to design to cost and are part of the Six Sigma concept (see [Chapter 17](#)) to make a product right the first time, which reduces costs. Based on an awareness of the customer's affordability and requirements, the designing and manufacturing target costs are established.

The industry needs to recover its investment with the sale of approximately 400 aircraft, preferably fewer. About 4 to 6% of the aircraft selling price is intended to recover the project cost (i.e., RDDMC), known as amortization of the investment made. For this reason, offering aircraft in a family concept covers a wider market at a considerably lower investment when the cost of amortization is closer to 2 to 4%. Smaller aircraft break even at approximately 200 sales. In current practice, civil aircraft manufacturers sell preproduction aircraft used for flight testing to recover costs. Military aircraft manufacturers incorporate new, unproven technologies and invest in technology-demonstrator aircraft (on a reduced scale) to prove the concept and subsequently substantiate the design by flight-testing on preproduction aircraft, some which could be retained for future testing.

The general definition of an aircraft price includes amortization of the RDDMC but not spare parts and support costs:

$$\text{aircraft price} = \text{aircraft manufacturing cost} + \text{profit} = \text{aircraft acquisition cost}$$

In this book, the aircraft price and cost are synonymous; the aircraft price is also known as the aircraft acquisition cost. The profit margin is a variable quantity and depends on what the market can bear. This book does not address the aircraft

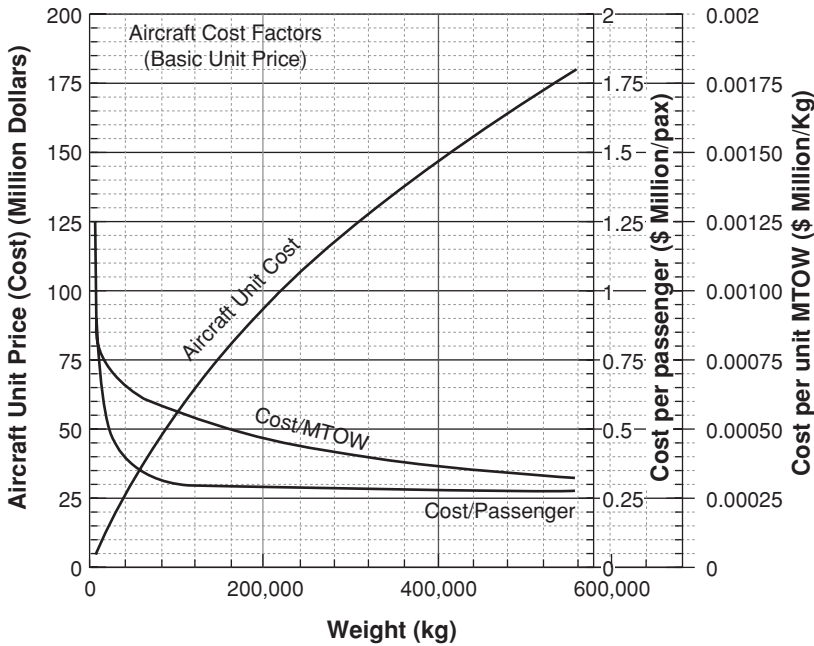


Figure 16.2. Aircraft cost factors

pricing method. In general, the profit from a new aircraft sale is rather low. Most of the profits are from sales of spare parts and maintenance support. Operators depend on the manufacturer as long as an aircraft is in operation – that is, two to three decades. Manufacturers are in a healthy financial position for several decades if their products sell in large numbers.

16.3 Aircraft Cost and Operational Cost

Figure 16.2 shows a typical high-subsonic civil aircraft cost at the 2000 price level in millions of dollars, reflecting the basic (i.e., lowest) aircraft cost. This graph is generated from a few accurate industrial data that are kept commercial in confidence.

In general, exact aircraft cost data are not readily available and the overall accuracy of the graph is not substantiated. The aircraft price varies for each sale depending on the terms, conditions, and support involved. The values in the figure are crude but offer a sense for newly initiated readers of the expected cost of the aircraft class. Figure 4.5 can be used to obtain the relationship between the MTOW and the number of passengers. The basic price of a midrange, 150-passenger class, high-subsonic turbofan aircraft is \$47 million (2000 price level).

The aircraft MTOW reflects the range capability, which varies among types. Therefore, strictly speaking, cost factors should be based on the MEW. Readers should be able to compute the MEW from the data provided in Chapter 8. In general, larger aircraft have a longer range (see Figure 4.4b). The exception is when an aircraft with a low passenger load has a long-range mission (e.g., the Bombardier Global Express).

Typical cost fractions (related to aircraft cost) of various groups of civil aircraft components are listed in Table 16.1, providing preliminary information for

Table 16.1. *Typical cost fractions of mid-size civil aircraft (two engines) at the shop-floor level*

		Cost fraction	Cost fraction
1.	Aircraft empty-shell structures*		
	Wing-shell structure	10 to 12%	
	Fuselage-shell structure	6 to 8%	
	Empennage-shell structure	1 to 2%	
	Two-nacelle shell structure**	2 to 3%	
	Miscellaneous structures	0 to 1%	
	Subtotal		20 to 25%
2.	Bought-out vendor items		
	Two turbofan dry, bare engines**	18 to 22%	
	Avionics and electrical system	8 to 10%	
	Mechanical systems***	6 to 10%	
	Miscellaneous****	4 to 6%	
	Subtotal		40 to 50%
3.	Final assembly to finish (labor-intensive)	25 to 30%	25 to 30%
	(component subassembling, final assembling, equipping/installing, wiring, plumbing, furnishing, finishing, testing)		

* Individual component subassembly cost fraction.

** Smaller aircraft engine cost fraction is higher (up to 25%).

*** Includes control linkages, servos, and undercarriage.

**** Cables, tubing, furnishing, and so on.

two-engine aircraft (four-engine aircraft are slightly higher). It is best to obtain actual data from the industry whenever possible.

Combat-aircraft cost fractions are different: The empty-shell structure is smaller but it houses sophisticated avionics black boxes for the complex task of combat and survivability. Typical cost fractions of various groups of combat aircraft components are listed in Table 16.2, in which the avionics cost fraction is separate. The table provides preliminary information for two-engine aircraft; it is best to obtain actual data from the industry whenever possible.

In the United States, military aircraft costing uses AMPR weight, also known as Defense Contractor's Planning Report (DCPR) weight, for the manufacturer to bid. The AMPR weight represents the weight of an empty aircraft shell structure without any bought-out vendor items (e.g., engines, undercarriages, or avionics packages).

Operating Cost

Other costs arise during operation after an aircraft is sold – this is the operating cost (OC) and is the concern of airline operators. Military OC uses a different bookkeeping method. Revenue earned from passenger airfare covers the full expenditure of airline operators, which covers the aircraft price and support costs. The DOC is the measure of cost involved with an aircraft mission. Standards for DOC ground rules exist – in the United States, they are proposed by the ATA (1967) and in Europe by the AEA (1989) (medium range; see [1]); both standards are comparable. Aircraft designers must be aware of operational needs to ensure that their design meets the expectations of the operators. In fact, the manufacturers and operators are in constant communication to ensure that current and future products are fine-tuned to the best profitability for all. Major airline operators have permanent representatives

Table 16.2. Typical cost fractions of combat aircraft (two engines) at the shop-floor level

	Cost fraction	Cost fraction
1. Aircraft empty-shell structures*		
Wing-shell structure	6 to 7%	
Fuselage-shell structure	4 to 6%	
Empennage-shell structure	≈1%	
Two-nacelle-shell structure**	part of the fuselage	
Miscellaneous structures	0 to 1%	
Subtotal		12 to 15%
2. Bought-out vendor items		
Two turbofan dry, bare engines**	25 to 30%	
Mechanical systems***	5 to 8%	
Miscellaneous****	1 to 2%	
Subtotal		30 to 40%
3. Avionics and electrical system	30 to 35%	30 to 35%
4. Final assembly to finish (labor-intensive)	12 to 15%	12 to 15%
(component subassembling, final assembling, equipping/installing, wiring, plumbing, furnishing, finishing, testing)		

* Individual component subassembly costs fraction.

** Single engine at lower cost fraction.

*** Includes control linkages, servos, and undercarriage.

**** Cables, tubing, furnishing.

onsite at the manufacturing plant to provide general support and dialogue for all aspects of the product line. Civil aircraft OC includes two types, as follows:

1. DOC: These are the operational costs directly involved with a mission flown. Each operator has its own ground rules depending on criteria such as the country, pay scales, management policies, and fuel prices. Standard ground rules are used for comparison of a similar class of product manufactured by different companies. In Europe, the AEA ground rules are accepted as the basis for comparison and provide a good indication of aircraft capability. A less expensive aircraft may not prove profitable in the long run if its OC is high.
2. IOC: The IOC breakdown in the United States is slightly different from European standards. Airline operators have “other costs” that involve training, evaluation, logistics support, special equipment, and ground-based resource management, which are not directly related to the aircraft design and mission-sector operation; they are independent of the aircraft type. These are the total costs of the operator, termed *life cycle cost* (LCC). Unlike the DOC, there is no standard for the LCC proposed by any established commercial-aircraft associations; each organization has its own ground rules to compute the LCC. Together with the DOC, they result in the total operating cost (TOC). Unlike military aircraft, the impact of other costs on the LCC in a commercial aircraft design application may be considered separately and then totaled to LCC – the DOC covers most of the design dependent costs. This book is concerned only with the DOC. The breakdown of LCC components is listed in Table 16.3. Most commercial aircraft operate beyond the design life span; hence disposal cost is considered as applicable.

Table 16.3. *Life-cycle cost (civil aircraft)*

Aircraft-related elements	Passenger-related elements	Cargo-related elements
Property Depreciation*	Handling and Insurance	Handling and Insurance
Property Amortization*	Baggage Handling	Administration/Office
Property Maintenance*	Emergencies	Sales and Support
Ground Support	Administration/Office	Fees and Commissions
Administrative Cost	Sales and Support	Publicity
Ground Handling/Control	Publicity	
Training	Fees and Commissions	

Note:

* Ground property (e.g., hangar and equipment).

The military uses the LCC rather than the DOC for the ownership of an aircraft in service. In general terms, it is the costs involved for the entire fleet from “cradle to grave,” including disposal. Military operations have no cash flowing back – there are no paying customers such as passengers and cargo handlers. Taxpayers bear the full costs of military design and operations. There was a need for LCC of military operations, which differ significantly from civil operations. Military aircraft OC ground rules are based on total support by the manufacturer for the entire operating lifespan, which can be extended by renewed contracts. A design to life-cycle cost (DTLCC) concept has been suggested but not yet standardized, which poses problems in providing a credible LCC comparison. Therefore, military aircraft operations deal with the LCC, although it has various levels of cost breakdowns, including aircraft- and sortie-related costs. Table 16.4 is an outline that categorizes the elements that affect the military aircraft LCC model.

Recently, the customer-driven civil aircraft market prefers the LCC estimation. Academics and researchers have suggested various types of LCC models, the principles of which are directed to cost management and cost control, providing advice on assigning responsibilities, effectiveness, and other administrative measures at the conceptual design stages in an IPPD environment.

16.4 Aircraft Costing Methodology: Rapid-Cost Model

This section presents a rapid-cost modeling methodology [2] specifically aimed to the coursework needs of DFM/A considerations during the conceptual design phase of commercial transport aircraft. This is why [Chapter 15](#) suggests the layout of the structural concept and the use of CAD. The basic structural philosophy is to address

Table 16.4. *Life cycle cost (military aircraft)*

RDDMC	Production	In-service	Disposal
Engineering	Parts manufacture	Operation	(See Section 15.9.9)
Ground testing	Assembly	Maintenance	
Technology demonstrator	Tooling	Ground support	
Prototype flight test	Deliveries	Training	
Technical support		Post-design services	
Publication		Administration	

Table 16.5. Turbofan engine and nacelle data

	A (Baseline: existing design)	B (New Design: to estimate)
T_{SLS} lb	9,220	14,000
Engine dry weight (lb)	1,625	2,470
Engine-face diameter (inches)	49	50.6
Nacelle weight (lb)	536	860
Nacelle maximum diameter (inches)	56	60
Nose-cowl length (inches)	35	29

DFM/A considerations as early as possible to provide a sense of manufacturing cost reductions through trade-off studies. Many publications suggest empirical relations to predict aircraft cost based on various types of aircraft weights, performance capabilities, and other details. Empirical relations use coefficients and indices with some degree of success; however, without the actual industrial-cost details, it is difficult to fine-tune the DFM/A gains. A methodology must have input based on real data in order for gains to be obtained through the application of the fundamentals of modern manufacturing philosophy.

The rapid-cost model is based on parametric methods in which cost drivers are identified. In the nacelle example, eleven drivers are involved. From a known baseline cost, the rapid-cost model demonstrates a fast and relatively accurate prediction and identifies areas that contribute to cost. A normal market situation without any unpredictable trends (i.e., global issues) is assumed for the methodology. The methodology is based on a generic turbofan nacelle, which typically represents the investigative areas associated with other aircraft components and makes use of industrial data. Figure 16.3 shows the generic nacelle components: (1) nose cowl, (2) fan cowl, (3) core cowl with thrust reverser, and (4) aft cowl. The method does not reflect practices by any organization and does not guarantee accuracy; it is intended only to provide exposure to the complexities involved in costing.

The example of the rapid-cost methodology concentrates cost modeling of the nose cowl structural elements of two generic nacelles – Nacelle A and Nacelle B – in the same aircraft and engine family. The methodology uses indices and factors, which is why two nacelles are used. Nacelle A is an existing product and is used for the baseline design. All cost data for Nacelle A are known, from which the indices are generated. Nacelle B has a higher standard of specification and a new design, in which the indices are adjusted and then used to predict cost. The two nacelles are compared in Table 16.5. All figures are in FPS, as obtained from the industry.

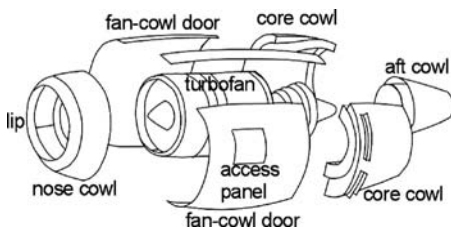


Figure 16.3. Nacelle components

Table 16.6. *Manufacturing cost components*

Cost of materials (raw and finished product)
Cost of parts manufacture
Cost of parts assembly to finish the product
Cost of support (e.g., rework/concessions/quality)
Amortization of nonrecurring costs
Miscellaneous costs (other direct costs, contingencies)

For dissimilar components, a similar methodology can still be applied with extensive data analyses to establish the appropriate indices.

Although the aerodynamic mould lines of both nacelles are similar, their structural design philosophy – hence, the subassembly (i.e., tooling concept) – differs. With commonality in the design family, the study presents a focused comparative study of the two geometrically similar nose cowls in a complex multidisciplinary interaction that affects cost. The total manufacturing cost of the finished product is the sum of the items listed in Table 16.6; the cost of manufacture is not the selling price.

Generic nacelles typically represent the investigative areas associated with the design and manufacture of other aircraft components (e.g., the wing and fuselage). The rapid-cost-model methodology presented herein can be applied to all other aircraft components, with their appropriate cost drivers, to establish the cost of a complete aircraft. Industrial shop-floor data are required to estimate the cost in dollars. All data are normalized to keep proprietary information commercial in confidence.

16.4.1 Nacelle Cost Drivers

Given herein are the eleven specific parameters, in two groups, identified as the design- and manufacture-sensitive cost drivers for generic nacelles. These cost drivers are applicable to all four nacelle subassembly components shown in Figure 16.3. Group 1 consists of eight cost drivers, which relate to in-house data within an organization. Group 2 cost drivers are not concerned with in-house capability issues; therefore, they are not within the scope of this discussion. Indices and coefficients obtained during the DFM/A study are used.

Group 1

1. *Size*: Nacelle size is the main parameter in establishing the base cost. Size and weight are correlated. The nacelle cowl size depends on the engine size – that is, primarily the fan diameter (D_F) of the engine – which in turn depends on the thrust (T_{SLS}) ratings as a function of BPR and the thermodynamic cycle. The relationship between the T_{SLS} and the D_{fan} can be expressed as follows:

$$(T_{SLS}) = (KD_{fan}^2) \quad (16.1)$$

where K = constant of proportionality.

The variants in the family of turbofans are the result of tweaking the baseline design, keeping the core gas generator nearly unchanged. This improves cost effectiveness by maintaining component commonality. Hence, the variant fan diameter is marginally affected, with the growth variant having a better

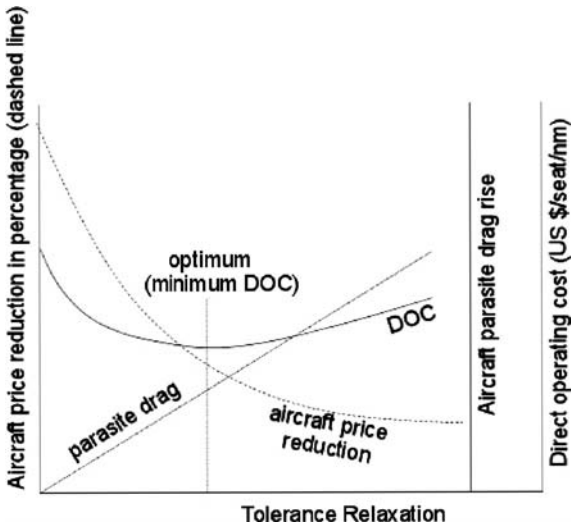


Figure 16.4. Cost versus tolerance

thrust-to-dry-weight ratio (T/W) and vice versa. As a consequence, the nacelle maximum diameter (D_{max}) and length (L) change minimally. The size factor for the nacelle, K_{size} , that affects cost is given in semi-empirical form, as follows:

$$K_{size} = \left(\frac{(D_{fan} \times D_{max})_{derivative}}{(D_{fan} \times D_{max})_{baseline}} \right) \times \left(\frac{L_{derivative}}{L_{baseline}} \right) \times \left(\frac{T_{SLS_derivative}}{T_{SLS_baseline}} \right)^{0.35} \quad (16.2)$$

The effect of size on parts-fabrication and assembly costs is less pronounced than material cost unless a large size calls for drastically different fabrication and assembly philosophies.

2. *Materials*: Parts weight data provide a more accurate material cost than applying the size factor; K_{size} may be used when weight details are not available. Two types of material are considered based on industrial terminology: raw and finished; the latter consists of the subcontracted items.
3. *Geometry*: The double curvature at the nacelle surface requires stretch-formed sheet metal or a complex mould for composites in shaping the mould lines. Both nacelles are symmetrical to the vertical plane. The nacelle-lip cross-section is necessarily of the aerofoil section with the crown cut, thinner than the keel cut, where engine accessories are housed (Figure 16.4). This does not make the outer and inner surfaces concentric. Straight longitudinal and circumferential joints facilitate the auto-riveting. In brief, there are four “Cs” associated with geometric cost drivers: circularity, concentricity, cylindricity, and commonality. Nacelles A and B are geometrically similar and therefore do not show any difference made by the four C considerations. A geometric cost-driver index of 1 is used for both nacelles as a result of their similarity.
4. *Technical Specifications*: These standards form the finishing and maintainability of the nacelle including the surface-smoothness requirements (i.e., manufacturing tolerance at the surface), safety issues (e.g., fire detection), interchangeability criteria, and pollution standards. Figure 16.4 shows the cost-versus-tolerance relationship from [2].

At the wetted surface, Zone 1 (Figure 16.5) is in an adverse pressure gradient that requires tighter tolerances compared to Zone 2 in a favorable pressure

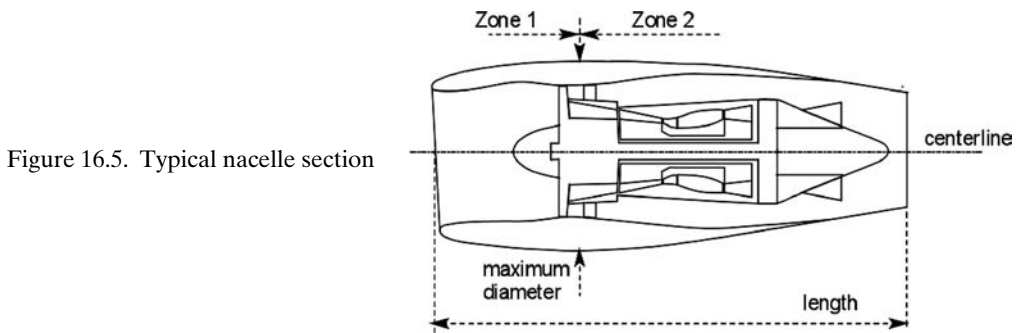


Figure 16.5. Typical nacelle section

gradient. The tighter the tolerance at the wetted surface, the higher is the cost of production due to the increased reworking and concessions involved. Because the technical specifications are similar, both have an index of 1.

5. *Structural Design Concept*: Component-design concepts contribute to the cost drivers and is a NRC amortized over the production run (typically, four hundred units). The aim is to have a structure with a low parts count involving low production manhours. Compared to the baseline design of Nacelle A, an *index factor* is associated with the derivative new design. Nacelle B has a more involved design with an index greater than 1. Manufacturing considerations are integral to structural design as a part of the DFM/A requirements.
6. *Manufacturing Philosophy*: This is closely linked to the structural-design concept, as described previously. There are two components of the cost drivers: (1) the NRC of the tool and jig design, and (2) the recurring cost during production (i.e., parts manufacture and assembly). An expensive tool setup for the rapid-learning process and a faster assembly time with lower rejection rates (i.e., concessions and reworking) results in a front-loaded budgetary provision, but considerable savings can be realized. Nacelle B has a NRC index >1 and a RC index <1 . Nacelle B is an improvement compared to Nacelle A.
7. *Functionality*: This is concerned with the enhancements required compared to the baseline nacelle design, including anti-icing, thrust reversing, treatment of environmental pollution (e.g., noise and emissions), position of engine accessories, and bypass-duct type. A “complexity factor” is used to describe the level of sophistication incorporated in the functionality. Being in the same family, the nose cowl of both nacelles has the same functionality – hence, a factor of 1 – otherwise, it must be revised. Other nacelle components could differ in functionality.
8. *Manhour Rates and Overhead*: Manhour rates and overhead are constant for both nacelles; therefore, the scope of applicability is redundant in this study.

Group 2 (These do not relate to in-house issues; therefore, it is not considered in this book.)

9. *Role*: Basically, this describes the difference between military and civil aircraft design.
10. *Scope and Condition of Supply*: This is concerned with the packaging quality of a nacelle supplied to a customer; it is not a design or manufacturing issue.
11. *Program Schedule*: This is an external cost driver that is not discussed herein.

Table 16.7. *Nose cowl build–work breakdown*

	Nacelle A				Nacelle A			
	STR	MP	EBU	AGS	STR	MP	EBU	AGS
Forward-bulkhead assembly	4	3	33	482	4	4	1	0
Aft-bulkhead assembly	3	0	33	395	3	1	25	644
Primary assembly	1	6	0	393	1	1	10	970
First-stage assembly	11	0	105	939	6	0	19	708
Second-stage assembly	8	2	78	873	2	2	82	1,617
Third-stage assembly	0	5	7	1,480	0	0	15	95
Total	28	16	256	4,562	16	8	152	4,034

In summary, only four cost drivers in Group 1 – size, material, structural-design concept, and manufacturing philosophy – are required to establish the cost of component manufacture and assembly. The other four cost drivers in Group 1 can be evaluated similarly for nacelles that differ in geometry, technical specifications, functionality, and manhour rates.

16.4.2 Nose Cowl Parts and Subassemblies

The build–work breakdown of the two nacelles from start to finish is grouped in six stages, as shown in Table 16.7; however, the cost of their parts is different. Nacelle A is an existing design and its cost is known. Nacelle B is a later design with a lower parts count and assembly time, achieved by superior structural and manufacturing considerations through DFM/A studies. The nose cowl consists of pure structures (STRs), minor parts (MPs) (e.g., brackets and splices), engine-built units (EBUs) (e.g., anti-icing units and valves), and aircraft general supply (AGS) (e.g., fasteners, rivets, nuts, and bolts). EBU costs are studied separately and not herein.

The expensive components are the STR and the installation of EBU parts. Clearly, these costs are reduced to almost half, thereby saving the cost of the Nacelle B nose cowl even with a larger engine. Assembly hours are also reduced to nearly half. AGS is not expensive but there are numerous rivets, nuts, bolts, and so forth.

16.4.3 Methodology (Nose Cowl Only)

The author points out that this seemingly simple algebraic procedure with elementary mathematics becomes a complex workout. Newly initiated readers may find it difficult to follow. It will require the instructor’s help and industrial data to understand the coursework for their project.

The methodology generates the factors and indices from existing Nacelle A, the cost data for which are known. Based on the similar geometry, these factors and indices are then adjusted using the DFM/A considerations and applied to Nacelle B. The conceptual design phase outlines the basis of the manufacturing philosophy under the DFM/A, relying heavily on the Nacelle A experience. Table 16.8 lists the necessary factors and indices for the eight cost drivers (i.e., the data from the industry). The table is followed by expanding the eight cost drivers.

Table 16.8. Normalized indices for the eight cost drivers in Group 1

Cost drivers	Nacelle A		Remarks
	(Baseline: known)	Nacelle B (to predict)	
1. K_{size}	1.0	1.133	
2. Material (weight ratio)	1.0	1.135	
(a) Raw material	1.0	(See Tables 16.9 and 16.10)	Nacelle B better
(b) Finished material (subcontracted)	1.0	(See Table 16.9)	
3. Geometry	1.0	1	Similar
4. Technical specifications	1.0	1	Similar
5. Structural design*	1.0	1.1	NRC
6. Manufacturing philosophy*			
(a) Nonrecurring (tool and jig design)	1.0	1.2	NRC
(b) Recurring (manufacture and assembly)	1.0	0.95	Nacelle B better
7. Functionality	1.0	1	Similar
8. Manhour rates	1.0	1	Same

Note:

* Primary cost driver.

The shop-floor learning characteristics are an important factor in cost consideration. Initially, parts fabrication and their assembly take longer (actual manhours) than when it is a routine task with a stabilized time frame of standard manhours, which initially is the target time. If actual manhours do not reach standard manhours, the investigation is required to change the standard manhours. The faster people learn, the greater is the savings for taking fewer manhours to manufacture. The number of attempts required to reach the standard manhours varies, and the DFM/A study must consider this aspect. In this case, Nacelle B has a faster learning-curve factor, with fewer parts.

1. K_{size} : Geometric details of the nacelles and engine parameters are listed in Table 16.5 to estimate K_{size} .
2. *Material Cost*: Material is classified in two categories: (1) raw materials (e.g., sheet metal, bar stock, and forging), and (2) finished materials (e.g., lipskin, engine ring, and some welded and cast parts acquired as subcontracted items). The weight fractions of both nacelles are listed in Table 16.9. The unit cost for each type varies, depending on the procurement policy (see notes in the table). The next part of the table lists details of the raw-material weight fractions. The last column provides various material costs per unit weight, normalized relative to the aluminum sheet-metal cost. The AGS consists of various types of fasteners including blind rivets (more expensive) and solid rivets; they are classified as raw materials because it is impractical to cost each type separately.
3. *Cost of Manufacture*: The core of the manufacturing cost buildup considers the cost drivers of geometry, technical specifications, manufacturing philosophy, functionality, and manhour rates. For this study, only the evaluation of the manufacturing philosophy is required, as discussed in the next two subsections.

Table 16.9. *Material weight fraction*

	Nacelle A		Nacelle B		Cost of material per unit weight	
	<i>weight</i>	<i>weight</i>	<i>weight</i>	Nacelle A	Nacelle B	
	(W_A/W_{AT})	(W_B/W_{AT})	(W_B/W_{BT})			
<i>Material weight fraction</i>						
All material	1.0	1.135	1.0			
Raw material	0.7136	0.8744	0.77	see below		
Finished material	0.2864	0.2607	0.23	1.0	0.92	
<i>Raw material weight fraction (finished material not included)</i>						
Total weight fraction	1.0000	1.2253	1.0			
Aluminum alloy sheet	0.2288	0.4778	0.39	1.0	1.0	
Aluminum alloy forging	0.1213	0	0	4.19	4.19	
Aluminum alloy honeycomb	0.3104	0.38687	0.3157	2.25	2.25	
Titanium alloy	0.2752	0.34254	0.2795	3.50	3.5	
Composite	0.0175	0	0	3.62	2.9*	
Mechanical fasteners (e.g., nuts)	0.0366	0.0050	0.0041	18.44	18.44	
Solid rivets	0.0101	0.0139	0.0113	0.63	0.63	

Notes:

* There is no composite in the nose cowl of Nacelle B, but it is used in the core cowls of both nacelles. The subscript "T" stands for total weight of nose cowl; A and B stand for each nacelle.

Cost of Parts Fabrication

Table 16.10 lists the cost of parts fabrication in a nondimensional form from the manhours involved. Actual manhours needed to manufacture parts for each of the six Nacelle A stages can be obtained from the shop-floor engineering process sheets. Factored indices for Nacelle B can be established through DFM/A studies at the conceptual design stage.

At each stage of parts manufacture, manhours are given in fractions of the total manhours for all parts; manhour rates are invariant. The Nacelle B learning-curve factor for parts fabrication is about the same as for Nacelle A but not for the assembly. Nacelle B has fewer parts, thereby saving on costs.

$$\begin{aligned} \text{manufacturing cost} &= \text{rates} \times \text{manhours} \times \text{learning-curve factor} \\ &\times \text{size factor} \times \text{manufacturing philosophy} \end{aligned} \quad (16.3)$$

Table 16.10. *Manhours fraction required to fabricate parts*

	Nacelle A	Nacelle B
Total manhours cost for all parts	1.000	1.0878
Learning-curve factor	1.000	1.022
Parts in the forward-bulkhead assembly – Stage 1 (start):	0.056	0.120
Parts in primary assembly – Stage 2:	0.038	0.003
Parts in aft-bulkhead assembly – Stage 3:	0.111	0.130
Parts in first subassembly – Stage 4:	0.623	0.355
Parts in second subassembly – Stage 5:	0.073	0.294
Parts in third subassembly – Stage 6 (final):	0.099	0.098

Table 16.11. *Manhour fractions required to assemble*

	Nacelle A	Nacelle B
Total manhours required to assemble	1.0	0.7587
Learning-curve factor	1.0	0.735
Stage 1 (start): Forward-bulkhead assembly	0.1	0.032
Stage 2: Primary assembly	0.116	0.191
Stage 3: Aft-bulkhead assembly	0.056	0.141
Stage 4: First subassembly	0.27	0.241
Stage 5: Second subassembly	0.211	0.267
Stage 6: Third subassembly (final)	0.247	0.128

The rate and factor for Nacelle A are 1; details for Nacelle B are in [Table 16.7](#).

Subassemblies

[Table 16.7](#) lists details for the Nacelles A and B nose cowl subassembly in six stages of processing. [Table 16.10](#) lists subassembly costs in a nondimensional form in fractions of the total assembly manhours for all stages. Costs of the pure structure of the nacelle mould lines are separated from those of all other nonstructural components (e.g., anti-icing ducting, linkages, cables, and accessories) that are part of the complete EBU fitment for a nacelle that is ready for a turbofan engine. The costs of installing EBUs in the assembly process are considered but not the actual EBU cost. The assembly cost is expressed as follows:

$$\begin{aligned} \text{assembly cost} = & \text{rates} \times \text{manhours} \times \text{learning-curve factor} \\ & \times \text{size factor} \times \text{manufacturing philosophy} \end{aligned} \quad (16.4)$$

The rate and factor for Nacelle A are 1; details for Nacelle B are shown in [Table 16.11](#). Savings are realized through the DFM/A study.

4. *Cost of Support:* Certain additional costs are incurred when a product fails to adhere to the desired quality during inspection. In that case, reworking and/or design concessions are required to salvage the product from rejection as scrap. These are the support costs – generally minor but difficult to determine. A flat-rate of 5% of the cost of material plus parts manufacture plus assembly is added as the support cost. DFM/A studies attempt to ensure design and manufacturing considerations that minimize support costs by making the product right the first time (i.e., the Six Sigma concept).

Cost of Amortization of the NRCs

[Table 16.12](#) shows the two types of NRCs in nondimensional form. Amortization is performed for more than 200 aircraft – that is, distributed over 400 nacelle units.

Table 16.12. *Nonrecurring costs*

	Nacelle A	Nacelle B
Product design cost	1.0	1.1
Methods/tool design cost	1.0	1.1

5. *Miscellaneous Costs*: These are unavoidable (e.g., insurance and packaging) and unforeseen costs of contingencies involved in the supply chain and necessarily charged as a manufacturing cost. Normally, these costs are minimal; in this study, 3 to 5% of the costs of material plus parts manufacture plus assembly is used. In the industry, the exact costs are available.

16.4.4 Cost Formulas and Results

This section provides the semi-empirical cost formulas for establishing Nacelle B costs, as well as for any aircraft component. The input required is relatively simple: (1) geometry with dimensions; (2) materials used; (3) weight breakdown; and (4) the array of manhours required to design, fabricate, and assemble an aircraft to completion. The factors and indices involved in the design and manufacture are listed in Tables 16.8 through 16.12 and obtained through DFM/A studies. The total manufacturing cost of a nacelle is the sum of individual costs of each of the four components, as follows:

$$\text{nacelle cost: } C_N = \sum_i^5 C_i = C_{NC} + C_{FC} + C_{TR} + C_{TC} + C_{EBU} \quad (16.5)$$

where C_{NC} = cost of nose cowl
 C_{FC} = cost of fan cowl
 C_{TR} = cost of thrust reverser
 C_{TC} = cost of tail-cone assembly
 C_{EBU} = cost of EBU (e.g., anti-icing)

The nose cowl is the only component studied herein; methodologies for the other components follow the same procedure. The cost of each nacelle component is individually estimated for the six headings in Table 16.7. The nose-cowl cost, C_{NoseCowl} , is the sum of the following six items:

$$C_{\text{NoseCowl}} = \sum_i^5 C'_i = C'_{\text{Mat}} + C'_{\text{Fab}} + C'_{\text{Asm}} + C'_{\text{Sup}} + C'_{\text{Amr}} + C'_{\text{Misc}} \quad (16.6)$$

where C'_{Mat} = cost of material
 C'_{Fab} = cost of fabrication
 C'_{Asm} = cost of assembly
 C'_{Sup} = cost of support
 C'_{Amr} = cost of amortization
 C'_{Misc} = miscellaneous cost

1. *Nose-Cowl Material Cost, C'_{Mat}* .

$$C'_{\text{Mat}} = \text{cost of material} = \sum_i^n C'_{i_raw} + \sum_i^n C'_{i_finish} \quad (16.7)$$

where n is the number of different types of materials.

In general,

$$C'_{i_raw} = W_i \times u_i \times P_i$$

where W_i = weight of the material

u_i = standard cost of raw material per unit weight

P_i = procurement factor (for nose cowl = 1)

Table 16.9 lists seven types of raw materials. The parts weight captures the effects of size; therefore, the size factor need not be applied here.

$\sum_i^n C'_{i_finish}$ is the actual cost and is obtained from the bill for subcontracted materials. Therefore, the cost of material C'_{Mat} for the nose cowl in this study is as follows (subscripts “al” and “ti” stand for aluminum and titanium alloys, respectively):

$$\begin{aligned} C'_{Mat} &= \sum_i^n C'_{i_raw} + \sum_i^n C'_{i_finish} \\ &= (W_{al} \times u_{al} \times P_{al})_{sheet} + (W_{al} \times u_{al} \times P_{al})_{forge} + (W_{al} \times u_{al} \times P_{al})_{honeycomb} \\ &\quad + W_{ti} \times u_{ti} \times P_{ti} + W_{comp} \times u_{comp} \times P_{comp} + (W_{AGS} \times u_{AGS} \times P_{AGS})_{fastener} \\ &\quad + (W_{AGS} \times u_{AGS} \times P_{AGS})_{rivet} + C'_{i_finish} \end{aligned} \quad (16.8)$$

Using Table 16.9, the following relationship can be worked out:

$$\begin{aligned} &\left(\frac{\text{Nacelle B cost of raw material}}{\text{Nacelle A cost of raw material}} \right) \\ &= [(0.4778 \times 1)_{sheet} + (0.3868 \times 2.25)_{honeycomb} + (0.34254 \times 3.5)_{ti} \\ &\quad + (0.005 \times 18.44)_{fasteners} + (0.0139 \times 0.63)_{rivet}]_{nacelle_B} / [(0.2288 \times 1)_{sheet} \\ &\quad + (0.1213 \times 4.19)_{forge} + (0.3104 \times 2.25)_{honeycomb} + (0.2752 \times 3.5)_{ti} \\ &\quad + (0.175 \times 3.62)_{comp} + (0.0366 \times 18.44)_{fasteners} + (0.0101 \times 0.63)_{rivet}]_{nacelle_A} \\ &= 2.6/3.14 = 0.828 \end{aligned}$$

The finished materials comprise a variety of items that go straight to the assembly line without in-house work involved. Their acquisition policies vary during each negotiation (see Table 16.6).

$$\left(\frac{\text{Nacelle B cost of finished material}}{\text{Nacelle A cost of finished material}} \right) = 0.92 \times 0.2607/0.2864 = 0.837$$

Table 16.9 lists 0.77 of Nacelle B as composed of raw materials and 0.23 of finished materials. Using these proportions:

$$\left(\frac{\text{Nacelle B cost of material}}{\text{Nacelle A cost of material}} \right) = 0.77 \times 0.828 + 0.23 \times 0.837 = 0.8302$$

2. *Nose Cowl Part Fabrication Cost, C'_{Fab} .* Table 16.7 lists the number of parts fabricated in each of the six stages of both nacelles. The manhours required to fabricate each part are a combination of operations (e.g., machining, forming, and fitting). The nose-cowl part fabrication cost is expressed as follows:

$$\begin{aligned} \text{manufacturing cost } (C'_{Fab}) &= \text{rates} \times \text{manhours} \\ &\quad \times \text{learning-curve factor} \\ &\quad \times \text{size factor} \times \text{manufacturing philosophy} \end{aligned} \quad (16.9)$$

$$\text{or } C'_{Fab} = (K_{size})^{0.5} \sum_i^m \left[\sum_i^n F_1 F_2 \dots F_n \right]_m \times (\text{manhour} \times \text{rates} \times \text{learning-curve factor})$$

Table 16.7 shows that both nacelles have six stages ($m = 6$). Each stage has four classes of parts: structure, minor parts, AGS, and EBU. The EBU is separated from the other classes, which are classified as one ($n = 1$).

Although geometrically similar, in the DFM/A study, Nacelle B has fewer parts to reduce the assembly time. Although there are few parts for Nacelle B, the parts fabrication needs about the same amount of time for both nacelles. Therefore, the various factors are as follows:

- size factor $K_{size} = 1.133$ from Equation 16.1
- geometry factor $F_1 = 1$ (geometrically similar)
- complexity factor, $F_2 = 1$ (functionality issues, same for both nacelles)
- parts-manufacturing philosophy factor (methods factor), $F_3 = 1.0$
- learning-curve factor = 1.022 (slightly higher)

Engineering process sheets provide all the information for Nacelle A to compute cost; for nondimensionalizing, all the factors use 1 as the baseline value.

Therefore, using Equation 16.7, the parts-manufacturing cost of

$$\text{Nacelle B} = (1.133)^{0.5} \times 1.022 = 1.0878 \times \text{Nacelle A}$$

3. *Nose-Cowl Assembly Cost, C'_{Asm} .* The manhours required for assembly at each stage are listed in Table 16.10 in nondimensional form. The nose-cowl assembly is expressed as:

$$\text{assembly cost } (C'_{Fab}) = \text{rates} \times \text{manhours} \times \text{learning-curve factor} \times \text{size factor} \\ \times \text{manufacturing philosophy} \quad (16.10)$$

The rate and factor for Nacelle A are 1; Table 16.2 lists them for Nacelle B:

$$C'_{Fab} = (K_{size})^{0.25} \sum_i^m \left[\sum_i^n F_i \right] \times (\text{manhours} \times \text{rates} \times \text{learning-curve factor}) \quad (16.11)$$

In this case, $m = 6$ stages and $n =$ consists of the following cost-driver factors:

- $F_1' = 0.735$ for the tooling concept (assembly methods – Nacelle B takes less time)
- $F_2' = 1.0$, the complexity factor (functionality – same for both nacelles)
- $F_3' = 1.0$, aerodynamic smoothness requirements (surface tolerance is the same)

Then, Equation 16.7 reduces to:

$$C'_{Fab} = (K_{size})^{0.25} \sum_i^6 \left[\sum_i^3 F_i \right] \times (\text{manhours} \times \text{rates} \times \text{learning-curve factor})$$

To simplify, all stages are combined to obtain the Nacelle B cost. Using 1 as the baseline Nacelle A factors and indices, the Nacelle B assembly cost is expressed as follows:

$$\text{assembly cost of Nacelle B} = (1.133)^{0.25} \times 0.735 = 0.759 \times \text{Nacelle A}$$

It is interesting that considerable assembly costs can be reduced at the expense of a slightly increased parts-fabrication cost and, of course, with some increase in

the tooling cost (i.e., NRC). Establishing these factors is the main purpose of the DFM/A trade-off studies. Basically, they summarize the manhours required compared to the baseline manhours.

4. *Nose-Cowl Support Cost, C'_{Sup}* . Separate support costs are taken as a percentage of material, fabrication, and assembly costs. Support costs arise from reworking and concessions when the build quality is not met (e.g., tolerances). In this book, the support cost is flat-rated as follows:

$$C'_{Sup} = 0.05 \times (\text{material cost} + \text{parts-fabrication cost} + \text{assembly cost}) \quad (16.12)$$

5. *Nose-Cowl Amortization Cost, C'_{Amr}* . Cost is amortized for 400 finished products. It is a variant design and therefore has low amortization costs; it can be included in the manhour rates at all stages or separately at the end. In this book, the cost is accounted for in the manhour rates and is not computed separately. Typically, because it is produced in twice more in number, the amortization cost is taken as 2% of material costs plus parts-fabrication costs plus assembly cost:

$$C'_{Amr} = \text{cost of amortization} = (\text{design} + \text{methods} + \text{tool}) \text{ cost}/N \quad (16.13)$$

where $N = 400$, or

$$C'_{Amr} = 0.02 \times (\text{material costs} + \text{parts-fabrication costs} + \text{assembly costs})$$

6. *Nose-Cowl Miscellaneous Costs, C'_{Misc}* . Miscellaneous costs are unavoidable, as follows (taken as 3%):

$$C'_{Misc} = 0.03 \times (\text{material costs} + \text{parts-fabrication costs} + \text{assembly costs}) \quad (16.14)$$

Total Costs of the Nacelle B Nose Cowl. The final costs of the Nacelle B nose cowl can now be computed, in nondimensional form – that is, relative to the Nacelle A costs. Using Equation 16.4, the following is estimated (i.e., costs of amortization embedded in manhour rates and costs of support and miscellaneous cost estimated as 10% of other costs):

$$C_{NoseCowl} = \sum_i^5 C'_i = C'_{Mat} + C'_{Fab} + C'_{Asm} + C'_{Sup} + C'_{Misc}$$

$$\text{where } (C'_{Sup} + C'_{Misc}) = 0.1 \times (C'_{Mat} + C'_{Fab} + C'_{Asm}) \quad (16.15)$$

Nacelle B nose-cowl cost:

$$C_{NoseCowl_B} = 0.8302 C'_{Mat_NacA} + 1.0878 C'_{Fab_NacA} + 0.759 C'_{Asm_NacA}$$

$$+ 0.1 \times (0.8302 C'_{Mat_NacA} + 1.0878 C'_{Fab_NacA} + 0.759 C'_{Asm_NacA})$$

$$= 0.9132 C'_{Mat_NacA} + 1.1966 C'_{Fab_NacA} + 0.8349 C'_{Asm_NacA}$$

From company records, the Nacelle A cost fractions are as follows:

$$C'_{Mat_NacA} / C_{NoseCowl_A} = 0.408$$

$$C'_{Fab_NacA} / C_{NoseCowl_A} = 0.349$$

$$C'_{Asm_NacA} / C_{NoseCowl_A} = 0.149$$

Table 16.13. *DOC components*

Fixed-cost elements	Trip-cost elements
1. Ownership cost	3. Fuel charges
(a) Depreciation	4. Maintenance (airframe and engine)
(b) Interest on loan	5. Navigational and landing charges
(c) Insurance premium	
2. Crew salary and cost	

Dividing Equation 16.15 by $C_{NoseCowl_A}$, the relative cost of Nacelle B is as follows:

$$C_{NoseCowl_B}/C_{NoseCowl_A} = 0.9132 \times 0.408 + 1.1966 \times 0.349 + 0.8349 \times 0.149 = 0.9146$$

The results show that although the two nacelles are geometrically similar, Nacelle B – with a 13.5% higher-thrust engine – could be produced at an 8.5% lower cost through DFM considerations in an IPPD environment. Changes in material, structural, tooling, procurement, and subcontracting policies contribute to cost reduction. A preliminary weight of a new design and the procurement policy for the raw materials can be established at the conceptual design stage (i.e., DFM/A studies). Accuracy improves as a project progresses. In the absence of the actual weight, approximations can be made from the geometry. If it had been costed with prevailing empirical relations using weight, size, performance, and manufacturing considerations, the cost of Nacelle B would be higher than Nacelle A. The prevailing equations do not capture the subtlety of DFM/A considerations. Chapter 17 describes the myriad changes that have occurred in the manufacturing technology; these benefits must be reflected in a new approach to formulation.

16.5 Aircraft Direct Operating Cost

Each airline generates its own in-house DOC computations, with variances in man-hour rates and schedules. Although the ground rules for DOC vary among companies, the AEA standardization (1989; short–medium range) has been accepted as the basis for comparison. ATA rules are used in the United States.

The NASA report [4] provides American Airlines–generated economics. The NASA document proposed in 1978 is an analytical model associated with advanced technologies in aircraft design; however, it has yet to be accepted as a standard method for comparison. The AEA and ATA ground rules appear to have considered all pertinent points and have become the benchmarking and comparison standard for the operational and manufacturing industries. This book deals with AEAL ground rules.

Table 16.13 lists the breakdown of DOC components under two basic headings. The ownership cost elements depend on the aircraft acquisition cost.

The NRCs (i.e., design and development) of a project and the costs of aircraft manufacture contribute to the ownership-cost elements, whereas the cost of fuel, landing fees, and maintenance contribute to trip-cost elements. Once the aircraft has been purchased, ownership costs are incurred even when crews have been

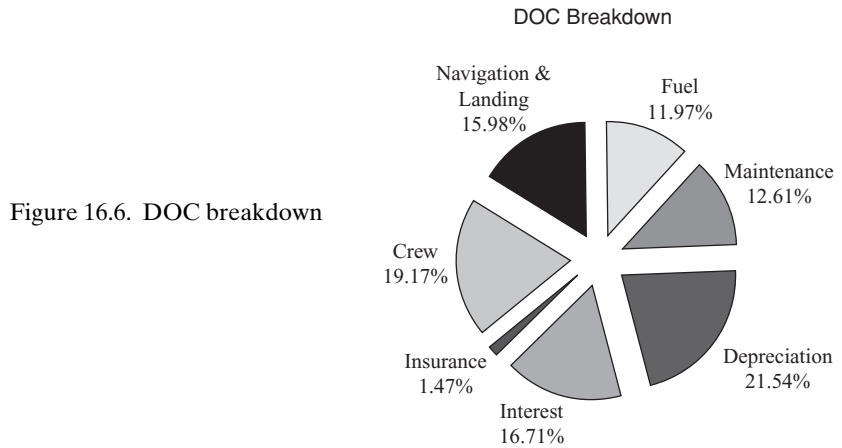


Figure 16.6. DOC breakdown

hired but flight operations are not carried out. The crew cost added to the ownership cost results in the fixed-cost elements. The crew cost added to the trip cost is the running cost of the trip (i.e., mission sortie). Aircraft-price-dependent DOC contributions include depreciation, interest, insurance, and maintenance (airframe plus engine), with a total nearly three to four times higher than the fuel cost (year 2000 level); with increased fuel cost (year 2008 level) it has come to about two to three times. Crew salary and cost and navigational and landing charges are aircraft-weight-dependent, which is second-order aircraft-price dependent, but is based on manhour rates herein.

For the reason of high ownership cost contribution to DOC, the industry was driven to reduce manufacturing costs and the demand was as high as a 25% cost reduction. Clearly, the design philosophy is significant in facilitating manufacturing cost reductions. One consideration was to relax certain quality issues (see [2] and [Chapter 17](#)), sacrificing aerodynamic and structural considerations without sacrificing safety. However, when the price of fuel rises, consideration for such a driver would be affected. Fuel price already increased significantly in 2008; any further increase would require drastic measures because the return from pure aerodynamic cleanliness at a high investment level may not be sufficient. These are important considerations during the conceptual design stage. RD&D efforts sometimes seem to look to the future through a crystal ball. There are diminishing returns on investment for aerodynamic gains. Fuel prices fluctuate severely and efforts to invest in reduced drag could move slowly until the situation stabilizes. A parallel effort to use less expensive alternative biofuels is underway, and the demand for a turboprop operation is a reality.

[Figure 16.6](#) shows the DOC components of a midsize-class aircraft. For an average midrange sector, the midsize aircraft cost contribution to the aircraft DOC is three to four times higher than the contribution of the cost of fuel (2000 prices).

The passenger load factor (LF) is defined as the ratio of occupied seats to the total number of seats available. Typically, an airline prefers the sector DOC to break even at approximately one third full (i.e., a LF of 0.33, or 33%); due to recent fuel price increases, the figure has increased to about half full. Revenue earned from passengers carried above the break-even LF is profit. Although some flights can operate at 100% LF, the yearly average for a high-demand route may be much lower. Passenger accommodations can be either in different classes with fare-structure tiers or

in one class, decided by the airline. Even in the same class, airfare can vary depending on different promotions. Among airlines, the break-even LF varies: with deregulated airfares, ticket prices can vary by the hour depending on passenger demand. The standard fare is the ceiling fare of the class and it offers better privileges.

16.5.1 Formulation to Estimate DOC

The DOC formulation is presented in this section, based on the AEA ground rules [1]. The formulae compute the component DOC per block hour. To obtain a trip cost, the DOC per block hour is multiplied by the block time. Aircraft performance calculates the block hour and block time for the mission range (see Section 13.5.6). The next section works out the DOC values, continuing with the Bizjet example used thus far.

Normally, the DOC is computed for a fleet of aircraft. The AEA suggests a ten-aircraft fleet with a 14-year lifespan and a residual value of 10% of the total investment; these values can be changed, as shown in the next section. Fuel prices, insurance rates, salaries, and manhour rates vary with time. Engine-maintenance costs depend on the type of engine; here, only the turbofan type is discussed. For other types of power plants, readers may refer to [1].

Aircraft Price

$$\text{Total Investment} = (\text{aircraft} + \text{engine price}) \times (1 + \text{spares allowance fraction})$$

Readers must be sure to obtain the Standard Study Price from the manufacturer. The AEA uses the total investment, which includes the aircraft delivery price, cost of spares, any changes in the order, and other contractual financial obligations. In the example, the aircraft and engine price are taken as the total investment per aircraft.

$$\text{Outstanding Capital} = \text{total capital cost} \times (1 - \text{purchase down-payment fraction})$$

Utilization (per block hour per annum in hours/year)

$$\text{Utilization, } U = \left(\frac{3,750}{t + 0.5} \right) \times t$$

where t = block time for the mission.

Fixed-Cost Elements

- Depreciation = $\frac{0.9 \times \text{total investment}}{14 \times \text{utilization}}$
- Loan interest repayment = $\frac{0.053 \times \text{total capital cost}}{\text{utilization}}$
- Insurance premium = $0.005 \times \left[\frac{\text{aircraft cost}}{\text{utilization}} \right]$
- Crew salary and cost

For the flight crew, the AEA uses \$493 per block hour for a two-crew operation. For the cabin crew, the AEA uses \$81 per block hour for each crew member.

Trip-Cost Elements

- Landing fees = $\left(\frac{7.8 \times \text{MTOW in tons}}{t} \right)$
where t = block time for the mission

- Navigational charges = $\left(\frac{0.5 \times \text{range in km}}{t}\right) \times \sqrt{\frac{\text{MTOW in tons}}{50}}$
where t = block time for the mission
- Ground-handling charges = $\left(\frac{100 \times \text{payload in tons}}{t}\right)$
where t = block time for the mission

The landing and navigational charges are MTOW-dependent and the ground-handling charges are payload-dependent. In practice, the crew salary is also MTOW-dependent but the AEA has kept it invariant.

- Airframe maintenance, material, and labor
(a) airframe labor

$$\left(0.09 \times W_{\text{airframe}} + 6.7 - \frac{350}{(W_{\text{airframe}} + 75)}\right) \times \left(\frac{0.8 + 0.68 \times (t - 0.25)}{t}\right) \times R$$

where W_{airframe} = the MEW less engine weight in tons

R = labor manhour rate of \$63 per hour at the 1989 level

t = block time for the mission

- (b) airframe material cost

$$\left(\frac{4.2 + 2.2 \times (t - 0.25)}{t}\right) \times C_{\text{airframe}}$$

where C_{airframe} = price of aircraft less engine price in millions of dollars

- Engine maintenance, material, and labor
(a) engine labor

$$0.21 \times R \times C_1 \times C_3 \times (1 + T)^{0.4}$$

where R = labor manhour rate of \$63 per hour at the 1989 level

T = sea-level static thrust in tons

$C_1 = 1.27 - 0.2 \times \text{BPR}^{0.2}$

where BPR = bypass ratio

$C_3 = 0.032 \times n_c + K$

where n_c = number of compressor stages

$K = 0.50$ for one shaft

$= 0.57$ for two shafts

$= 0.64$ for three shafts

- (b) engine material cost

$$2.56 \times (1 + T)^{0.8} \times C_1 \times (C_2 \times C_3)$$

where T = sea-level static thrust in tons

$$C_2 = 0.4 \times (\text{OAPR}/20)^{1.3} + 0.4$$

where OAPR is the overall pressure ratio; C_1 and C_3 are the same as before.

- (c) direct engine maintenance cost (labor + material)

$$N_e \times (\text{engine labor cost} + \text{material cost}) \frac{(t + 1.3)}{(t - 0.25)}$$

where N_e = number of engines

- Fuel charges = $\frac{\text{block fuel} \times \text{fuel cost}}{\text{block time}}$

Table 16.14. Bizjet data for DOC estimation

Aircraft details	Turbofan details (two engines)	Conversion factors
MTOW – 9,400 kg	T _{SLS} /Engine – 17.23 kN	1 nm = 1.852 km
OEW – 5,800 kg	Dry Weight – 379 kg	U.S. gallon = 6.78 lb
MEW – 5,519 kg	Bypass Ratio – 3.2	1 lb = 0.4535 kg
Payload – 1,100 kg*	No. of Compressor Stages – 10**	1 ft = 0.3048 m
Range – 2,000 nm	Overall Compressor Ratio – 14	1 kg fuel = 0.3245 gallon
Block Time – 5.38 hr	No. of Shafts = 2	
Block Fuel – 2,233 kg	Fuel Cost = \$0.75 per U.S. gallon	

Notes:

* 10 passengers

** It has one high-pressure compressor, four-stage low-pressure compressor, and one fan.

Aircraft price = \$7 million

Engine price = \$1 million

Total aircraft acquisition cost = \$8 million (total investment per aircraft; price includes spares)

Then, DOC per hour = (fixed charges + trip charges)_{per hour} and DOC per trip = $t \times (\text{DOC})_{\text{per hour}}$ and DOC per aircraft mile = $\frac{\text{DOC} \times 100 \times \text{block time}}{\text{range}}$ and DOC per passenger mile per nautical mile = $\frac{\text{DOC} \times 100 \times \text{block time}}{\text{range} \times \text{number of passengers}}$.

16.5.2 Worked-Out Example of DOC: Bizjet

Based on the previous formulations, this section works out the DOC of the Bizjet example. Rather than working on an entire fleet, only one aircraft is worked out herein. Input for the DOC calculation of the Bizjet is provided herein; manhour rates are in [3]. All cost figures are in U.S. dollars and are rounded up to the next higher figure. Table 16.14 provides aircraft and engine details.

The DOC is computed for a single aircraft to obtain the *trip cost* rather than the per-hour cost. A lifespan of 14 years is used with a residual value of 10% of the total investment.

Aircraft Price

- Total investment = \$8 million
Utilization (per block hour per annum in hours/year)
- Utilization, $U = \left(\frac{3,750}{5.38+0.5}\right) \times 5.38 = 637.75 \times 5.38 = 3,431$ hours per year
where t = block time for the mission = 5.38 hours

Fixed-Cost Elements

- Depreciation = $\frac{0.9 \times 8 \times 10^6}{14 \times 3,431} \times 5.38 = \807 per trip
- Loan interest repayment = $\frac{0.053 \times 8 \times 10^6}{3,431} \times 5.38 = \665 per trip
- Insurance premium = $0.005 \times \left[\frac{8 \times 10^6}{3,431} \times 5.38\right] = \63 per trip
- Crew salary and cost

(a) Flight crew

$$493 \times 5.38 = \$2,652 \text{ per trip for two crew}$$

(b) Cabin crew = 0 because there is no cabin crew

Trip-Cost Elements

- Landing fees = $\left(\frac{7.8 \times 9.4}{5.38}\right) \times 5.38 = \74 per trip

- Navigational charges = $\left(\frac{0.5 \times 2,000 \times 1.852}{5.38}\right) \times \sqrt{\frac{9.4}{50}} \times 5.38 = \803 per trip
- Ground-handling charges = $\left(\frac{100 \times 1.1}{5.38}\right) \times 5.38 = \110 per trip
- Airframe maintenance, material, and labor
 - (a) airframe labor

$$= (0.09 \times 5.52 \times 1.02 + 6.7 - \frac{350}{(5.52 \times 1.02 + 75)}) \times \left(\frac{0.8 + 0.68 \times (5.38 - 0.25)}{5.38}\right) \times 63 = (1.853) \times 1.448 \times 63 = \$169 \text{ per trip}$$

$$(b) \text{ airframe material cost} = \left(\frac{4.2 + 2.2 \times (5.38 - 0.25)}{5.38}\right) \times 7 \times 5.38 = \$109 \text{ per trip}$$

where $C_{\text{airframe}} = \$7$ million

Total airframe maintenance (material + labor) = 169 + 109 = \$278 per trip

- Engine maintenance, material, and labor

$$(a) \text{ engine labor} = 0.21 \times 63 \times 1.018 \times 0.89 \times (1 + 1.72)^{0.4} = \$17.88 \text{ per hour}$$

where $T = 17.23 \text{ KN} = 1.72 \text{ tons}$

$$C_1 = 1.27 - 0.2 \times 3.2^{0.2} = 1.018$$

$$C_3 = 0.032 \times 10 + 0.57 = 0.89$$

$$(b) \text{ engine material cost} = 2.56 \times (1 + 1.72)^{0.8} \times 1.018 \times (0.652 + 0.89) = 5.7 \times 1.542 = \$8.79 \text{ per hour}$$

$$\text{where } C_2 = 0.4 \times (14/20)^{1.3} + 0.4 = 0.652$$

C_1 and C_3 are the same as before.

- (c) direct engine maintenance cost (labor + material)

$$= 2 \times (17.88 + 8.79) \times \frac{(5.38 + 1.3)}{(5.38 - 0.25)} = \$308 \text{ per trip}$$

- Fuel charges = $2,233 \times 0.3245 \times 0.75 = \544 per trip

The baseline Bizjet DOC is summarized in Table 16.15. Then, DOC per hour = $7,045/5.38 = \$1,309.50$ per hour.

$$\text{DOC per aircraft nm} = \frac{7,045}{2,000} = \$3.52 \text{ per nm per trip}$$

$$\text{DOC per passenger mile per nm} = \frac{7,045}{2,000 \times 10} = \$0.352 \text{ per nm per passenger}$$

DOC details of a midsize, high-subsonic transport aircraft are in Appendix C.

OC of the Variants in the Family

Large Variant: MTOM = 10,800 kg and 14 passengers

Aircraft Price = \$9 million

Ownership Cost Element = \$1,727

Crew Cost = \$3,047

Fuel Cost = \$625

Maintenance/Operational Charges = \$2,650

Total Operational Cost = \$8,049

Then, DOC per hour = $\$8,049/5.38 = \$1,496.40$ per hour

The DOC per aircraft nm = $\frac{8,049}{2,000} = \$4.025$ per nm per trip

Table 16.15. *Bizjet summary of DOC per trip (in U.S. dollars)*

Fixed cost elements	
Depreciation	807
Interest on Loan	665
Insurance Premium	63
Total Ownership Cost	1,535
Flight Crew	2,652
Cabin Crew	0
Total Fixed Cost Elements	4,187
Trip Cost Elements	
Fuel Charges	544
Navigational Charges	803
Landing Charges	74
Ground-handling Charges	110
Maintenance (Airframe)	1,019
Maintenance (Engine)	308
Total Trip Cost Elements	2,858
Total DOC	\$7,045 per trip

The DOC per passenger mile per nm = $\frac{8,049}{2,000 \times 14} = \0.2875 per nm per passenger.

Smaller Variant: MTOM = 7,900 kg and six passengers

Aircraft Price = \$6.2 million

Ownership Cost Element = \$1,228

Crew Cost = \$2,201

Fuel Cost = \$451

Maintenance/Operational Charges = \$1,916

Total Operational Cost = \$5,796

Then, DOC per hour = $\$5,796/5.38 = \$1,077.30$ per hour.

The DOC per aircraft nm = $\frac{5,796}{2,000} = \$2.898$ per nm per trip.

The DOC per passenger mile per nm = $\frac{5,796}{2,000 \times 6} = \0.483 per nm per passenger.

17 Aircraft Manufacturing Considerations

17.1 Overview

Cost analysis and manufacturing technology are subjects that require specialized instruction in academies, and they are not the main topics of this book. They are included to make readers aware that the classical aeronautical subjects of aerodynamics, structures, and propulsion are not sufficient for a successful aircraft design. Cost analysis and manufacturing technology must be considered during the conceptual design study and integrated with classical aeronautical subjects. The following terms are used extensively in this chapter; some were referred to previously:

Design Built Team (DBT): This is a team of hand-picked, experienced engineers and specialists drawn from various related disciplines, who synthesize design for DFM/A considerations in multidisciplinary interactions with the classical subjects.

Design for Manufacture and Assembly (DFM/A): This is an engineering approach with the object of minimizing costs of production without sacrificing design integrity.

Integrated Product and Process Development (IPPD) (also known as Concurrent Engineering): This offers an environment in which DBT uses IPPD to synthesize the trade-off studies in a multidisciplinary study to arrive at the best value for the product as a global optimum, rather than optimizing to a particular design study. DFM/A is part of IPPD.

Design for Six Sigma (DFSS): This is an integrated approach to design with the key issue of reducing the scope of mistakes and inefficiencies – that is, making a product right the first time to prevent the waste of company resources. It is a management-driven task to extract more from employees in order to find new ways to improve on routine approaches. In this way, the product is of the highest quality and lowest cost, satisfying all of a customer's requirements.

Lean and Agile Manufacturing (LAM): This is a management tool to minimize costs by effective personnel management for improvements in the areas of assembly, system profitability, and the working environment.

Product Life-Cycle Management (PLM): This is a business strategy that helps companies share product data, apply common processes, and leverage corporate knowledge to develop products from conception to retirement, across the extended enterprise.

Manufacturing Process Management (MPM): This is a management strategy that provides a common environment for manufacturing, preplanning, and cost estimation, as well as detailed production planning, reconciliation analysis (i.e., estimate versus actual), and shop-floor work-instruction authoring.

Product, Process, and Resource (PPR): This is the hub environment, which provides a direct use of CAD-based data as a basis for work instructions. Emphasis is on use of single data set feeding all user systems.

Commercial aircraft design strategy is steadily evolving. It was initially driven by the classical aeronautical subjects, but recently it is customer-driven design strategies that consider DFM/A problems with the object of minimizing production costs without sacrificing design integrity and specifications. Manufacturing methodologies, jigless assembly, and “flyaway” tooling concepts facilitate DFM/A. Designing for ease of assembly can be improved in the areas of assembly effectiveness and product quality.

Chapter 16 stresses the importance of rigorous costing as an integrated tool embedded in the multidisciplinary systems architecture of aircraft design to arrive at a best value. Cost estimation is used to trade-off studies between the classical aeronautical subjects and DFM/A methodology, with its guiding principles of parts count and manhour reduction, standardization of parts, and emphasis on designing for ease of assembly, which has wider implications for engineers and managers in the manufacturing industry. Whereas specialist groups concentrate on design for their task obligations – whether technology- or manufacture-driven or any other demand – the IPPD environment must synthesize the trade-off studies for the best value of a product as a global optimum rather than optimizing to a particular design study.

The paradigm of “better, faster [time], and cheaper to market” has replaced the old mantra of “higher, faster [speed], and farther” [6]. Aircraft manufacturers are meeting the challenges of this new paradigm by assessing how things are done, discarding old methods and working practices for newer, right-the-first-time alternatives. An increase in product value is achieved through improved performance (better), lower cost (cheaper), and in less time (faster). The paradigm shift from classical aeronautical studies led to new considerations for various types of *design for...* terms, more so in the academic circle (see Section 17.7). This chapter takes a holistic approach to aircraft design by consolidating various *design for...* considerations. The author suggests the introduction of an index of “Design for Customer” as a measure for establishing a product value.

The digital design and manufacturing process (see Section 17.9) leads to paperless offices. The advent of the digital-manufacturing process greatly facilitated the DFM/A concept by addressing the role of MPM in the industry. MPM provides a common environment for manufacturing, preplanning, and cost estimation, as well as detailed production planning, reconciliation analysis (i.e., estimate versus actual), and shop-floor work-instruction authoring. It provides a means to integrate across the full product life cycle, ranging from concept to field maintenance to retirement

(i.e., “cradle to grave”). Shop-floor execution systems are fed directly from the PPR-hub environment, providing a direct reuse of CAD-based data as a basis for work instructions. As-built data are captured and available for use within the PPR hub for follow-on planning and validation as the product evolves throughout its life cycle.

In some ways, automobile-manufacturing technology is ahead of the aerospace industry by successfully implementing digital-manufacturing technology and advancing to futuristic visions. A successful automobile design can sell a million per year and last for a decade with minor modifications; whereas, in peacetime, fewer than 500 per year of a successful high-subsonic commercial transport aircraft are produced and none has yet reached the 10,000 mark in terms of total aircraft sales. The automobile industry can invest large sums in modern production methods yet keep amortization costs per car low.

17.1.1 What Is to Be Learned?

This chapter covers the following topics:

- Section 17.2: Manufacturing considerations
- Section 17.3: DFM/A
- Section 17.4: Manufacturing practices
- Section 17.5: DFSS concept
- Section 17.6: Tolerance relaxation
- Section 17.7: Reliability and maintainability
- Section 17.8: Designs for consideration: a holistic approach
- Section 17.9: Index of design for customer
- Section 17.10: Digital manufacturing

17.1.2 Coursework Content

Readers may compute the index of the design for customer. However, it is neither essential nor important because the industry is not adopting this system at this stage; more study is needed. However, the DFM/A considerations can be addressed in a second term. Such studies need not alter the finalized and substantiated configuration obtained thus far through the worked-out examples (in the industry, DFM/A is carried out in parallel during the conceptual design stage). It is beneficial to have an idea of DFM/A implications in aircraft design and operation. However, if it is a second-term topic, it may not be practical without specialist instructors using realistic data. This chapter provides only a glimpse of the scope of DFM/A during the conceptual study phase.

17.2 Introduction

Today, it is not the operators who are the only customer. The future trends suggest the entire society as a customer of the high-tech aerospace engineering, which could “make or break” any society depending on how the technology is used. This also is true for other types of technology, including nuclear and bioengineering.

In the past, trade-off studies were limited to the interaction among aerodynamics, structures, and propulsion, as discussed through [Chapter 13](#) of this book.

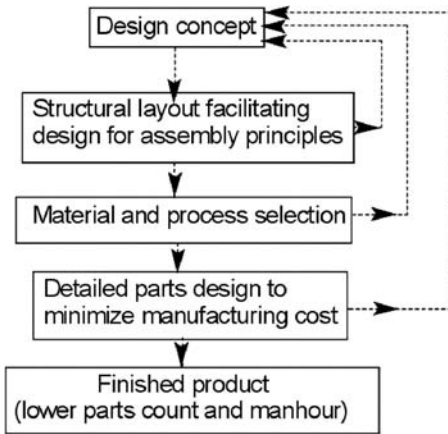


Chart 17.1. DFM/A steps

Subsequently, during the 1990s, the need for DFM/A considerations in an IPPD environment gained credence. The IPPD process continues to evolve for the customer-driven design trends in order to minimize ownership costs without sacrificing integrity, performance, quality, reliability, safety, and maintainability. The recent economic downturn demands general and significant cost-cutting measures, severely affecting the commercial aircraft industry. In this economic climate, the roles of reliability, maintainability, recyclability, and so forth are design- and manufacturing-process-dependent. This chapter introduces an index of design for customer and incorporates value engineering.

The eventual affordability for operators as the “best buy” (i.e., product value), in turn, will allow manufacturers to thrive. Design considerations should not impose difficulties in their manufacturability. The associated aerodynamic-shape and structural-design concepts facilitate parts fabrication, their assembly, enhanced interchangeability, and so forth. Bought-out items should be selected for efficient and cost-effective system integration that leads to better reliability and maintainability during the aircraft lifespan. Recent events have resulted in the additional constraints of cost-effectiveness and environmental issues, requiring increased attention. The issues of global sustainable-development and anti-terrorism require additional design considerations. The choice of materials from a recycling (i.e., disposal) perspective is an additional issue when the use of composites gains ground over metals.

17.3 Design for Manufacture and Assembly

The public domain proliferates with acronyms, such as DFM and DFA. These do not comprise a standalone concept; there is a relationship between design for manufacturing (DFM) and design for assembly (DFA) to meet the objective of lower production costs. In this book, *fabrication* and *assembly* are two components of the manufacturing process and are combined as DFM/A. [Chart 17.1](#) shows the typical steps in DFM/A application.

DFM/A is concerned with the design synthesis of parts fabrication and assembly as an integral part of manufacturability. DFM/A analyses involve competition and risk – that is, balancing the trade-off between cost and performance. This eventually

ensures affordability for operators as the best buy. This multidisciplinary study searches for aerodynamic mould lines with surface-smoothness requirements (i.e., tolerance specification) to minimize performance penalties without imposing difficulties in manufacturability. The associated structural-design concepts facilitate parts fabrication and assembly (i.e., low manhours and low parts count, as well as enhanced interchangeability). Bought-out items are selected for efficient and cost-effective system integration leading to better reliability and maintainability during the aircraft's operational lifespan. Based on an awareness of customer affordability and requirements, designing and manufacturing target costs are established, which measure the objectives of lower production costs, improved quality, and reduced manufacturing cycle times, while increasing the product value without sacrificing design integrity, safety, and established specifications.

As a complex product, an aircraft is constructed of myriad parts. Assembleability, as a measure of the relative ease of product assembly, plays a prominent role for produceability. Following are the main goals of DFM/A considerations, which reduce parts count and assembly time:

- improvement of the efficiency of individual parts fabrication
- improvement of the efficiency of assembly
- improvement of product quality
- improvement of the assembly-system profitability
- improvement of the working environment within the assembly system
- product's usefulness in satisfying customer's needs
- relative importance of the needs being satisfied
- availability of the product relative to when it is needed
- best cost of ownership to the customer

17.4 Manufacturing Practices

Depending on the manufacturing philosophy, jigs and fixtures need to be designed for the type of tooling envisaged for parts fabrication and assembly. Jigs and fixtures are special holding devices for making fast the workpiece for accurate fabrication and assembly of parts. Naturally, jig and fixture design starts early during Phase 2 of a project, along with planning for the facility and process layout. This can be expensive, requiring additional production-launch costs; however, there is a payback in saving labor costs when production starts. Investment in the aerospace industry is front-loaded.

Accurate dimensioning during fabrication and assembly is important for reducing manufacture and maintenance costs. The following are used to maintain dimensional accuracy (these are not precise definitions but make sense in context):

Tools: This equipment cuts and shapes material in the parts fabrication process. They can be handheld or fixed in place. Examples include drills, lathes, hammers, riveters, and welders. Tools, jigs, and fixtures work in conjunction with one another.

Gauges: These are measuring devices for accurately locating tools relative to the fixture in which a workpiece is held.

Fixtures: These are special working and clamping devices that facilitate processing, fabrication, and assembly. Fixtures are fixed frames designed to hold one or several workpieces in the correct position relative to one another. A gauge may be required initially to position a tool for cutting. Fixtures can be large, depending on the size of the workpiece. They should be solid and heavy structures to withstand any vibrations.

Jigs: These have a similar function as fixtures but they also incorporate guides for the tool. Jigs also are fixed items. Jigs typically are used for drilling, reaming, and welding.

Given herein are seven of many best-practices techniques that contribute to DFM/A practices. The basic idea of the seven techniques uses a modern manufacturing and tooling philosophy, moving away from the older, manual procedures to digital processing (see [Section 17.10](#)), where most tasks are performed. Modern methods make extensive use of CAD, CAM, and computer-aided process planning (CAPP) to ensure a high standard of accuracy and productivity. Numerically controlled (NC) machines are part of CAM.

1. *Jigless Assembly:* Designing for ease of assembly should not be restricted exclusively to the task of concept-design engineers. Tooling engineers contribute to the reduction of costs through a jigless assembly approach to manufacturing. Jigless assembly is an approach toward reducing the costs and increasing the flexibility of tooling systems for manufacture through minimization of product-specific jigs, fixtures, and tooling. During the development phase, tooling costs are high; consequently, savings in this aspect of aircraft manufacture are significant and they impact the time from concept to market as well. Jigless assembly does not mean toolless assembly; rather, it means the eradication or at least the reduction of jigs. Simple fixtures still may be needed to hold the parts during specific operations, but other methods are being found to correctly locate parts relative to one another. Assembly techniques are simplified by using precision-positioned holes in panels and other parts of the structure to “self-locate” the panels; here, parts serve as jigs. This process, known as *determinant assembly*, uses part-to-part indexing rather than the conventional part-to-tool systems used in the past.
2. *Flyaway Tooling:* Within the airframe-manufacturing industry, it is generally accepted that approximately 10% of overall manufacturing costs for each airframe can be attributed to the manufacture and maintenance of assembly jigs and fixtures. The traditional “hard-tooling” philosophy requires that the desired quality of the finished structure be built into the tooling. The tooling therefore must be regularly calibrated to ensure build quality. An alternative philosophy, “flyaway tooling,” was conceived to reduce tooling costs and improve build quality. This approach envisions future airframe components designed with integral location features with incorporated positional data that transfer to the assembly. This enables in-process measurement and aids in-service repairs. It also may be possible to design an aerospace structure with sufficient inherent stiffness, allowing the assembly tooling to be reduced to a simple, reusable, and reconfigurable support structure.

3. *Gaugeless Tooling*: This is achieved using a theodolite system linked through a central processor. Coordinated geometry, obtained directly from CAD, is used to establish the “hard points” to meet the build, interface, and interchangeability requirements. Gaugeless tooling is required for the manufacture and periodic inspection of the assembly process.
4. *Inline Assembly*: This provides a progressive and balanced assembly build sequence, utilizing the maximum number of subassemblies in a cellular-type environment, which improves interchangeability.
5. *Automatic Riveting*: The assembly is first slave-riveted on the fixture and then moved to the automatic machine. This improves productivity and accuracy; hence, the quality impacts from human error are minimized. The manpower engaged is also reduced.
6. *Tolerance Relaxation at the Wetted Surface [2]*: Aircraft surface-smoothness requirements are aerodynamically driven with a stricter manufacturing tolerance to minimize drag – that is, the tighter the tolerance, the higher is the assembly cost. Trade-off studies between surface tolerance and aerodynamic drag rise can reduce manufacturing costs (see [Section 17.6](#)).
7. *Six Sigma and Supporting Methodologies*: An important framework in which DFM/A techniques should be conducted is that of concurrent engineering (i.e., IPPD) focusing on improvement of the product-development process by concentrating on the design stage for the entire life cycle of a product. Management strategies such as DFSS and LAM as well as effective personnel management also must be considered if improvements are to be made in assembly-system profitability. DFM/A should strengthen the team activity in all phases of the design process, thereby ensuring that the technical expertise of the participants is successfully utilized; this is a management tool.

Decisions made during product design have a major impact on cost, defects, and cycle time. In fact, about 70% of production cost is locked in during the design process. DFM/A helps reduce product complexity through minimization of parts and fastener counts, assembly and manufacturing time, and material costs. Additionally, DFM/A application reduces the potential for defects. Robust design, statistical tolerancing, and geometric dimensioning and tolerancing actually help reduce defects. A better understanding of DFM/A in reducing the cost of production requires detailed studies in material selection and different process capabilities, which are beyond the scope of this book. The DFM/A concept assists the Six Sigma management strategy.

17.5 Six Sigma Concept

The objective of robust design is to achieve product designs with few defects during manufacture and very few latent defects after a product is delivered to a customer. It focuses on identifying the characteristics of the product that are critical to meeting the product requirements and then seeking the DFSS process capability.

The DFSS is an integrated approach to design with the key issue of reducing the scope for mistakes and inefficiencies – that is, make a product right the first time to prevent the waste of company resources [2]. DFSS is a collection of product tools

Table 17.1. *Sigma distribution of defects*

Sigma distribution process capability	Defects per million
2	308,537
3	66,807
4	6,210
5	233
6	3.4

and topics used to assist the design of products for manufacture by processes operating at the Six Sigma capability. It is a management-driven task to facilitate the improvement of labor efficiencies from employees and find new ways to improve on any routine approach so that the product can be manufactured at the highest quality and lowest cost, thereby satisfying all of a customer's requirements. Six Sigma helps expose the "hidden factory" of waste that robs organizations of profits by using a routine approach to issues with the product and manufacturing process. The vision of Six Sigma is as follows:

- reduce costs and improve margins in a context of declining prices
- surpass customer expectations by a margin few competitors can match
- improve at a faster rate than the competition
- grow a new generation of leaders

Six Sigma is a systematic methodology for eliminating defects in products, services, and processes while also yielding cost and cycle-time reductions. By significantly improving process capability, it can achieve operational excellence in delivering almost defect-free products and services, at the lowest possible cost, and on time.

For manufactured products, the Six Sigma methodology makes use of a variety of managerial, technological, and statistical techniques to change the manufacturing processes, the product, or both in order to achieve the Six Sigma process capability. DFSS is the collection of tools and topics used during the design phase to achieve a Six Sigma product.

One measure of process capability is in the sigma, σ , a statistical measure. For example, when a process is operating at Six Sigma capability, the long-term yield is 99.99966%, corresponding to 3.4 defects per million opportunities. The demand for Six Sigma is high, thereby guaranteeing a robust design. Table 17.1 lists the sigma distribution in a statistical histogram of defect levels relative to process capability.

To gain a competitive advantage through customers' satisfaction, their needs must be understood. One way to capture customer requirements is by using selected *quality function deployment* (QFD), which consists of a series of interlocking matrixes that are used to translate customer requirements into product functional requirements and process characteristics.

However, development and implementation of DFSS is difficult. It requires employee behavior characteristics such as leadership, commitment, professionalism, and perseverance to overcome the attitudes heard in phrases such as "no time," "not invented here," "doesn't apply to us," "we've been doing it for years," "I prefer

design rules,” and “I refuse to use the tools.” DFSS demands a culture change – not easy to achieve but possible.

17.6 Tolerance Relaxation at the Wetted Surface

Section 17.3 mentions that a best practice to reduce production costs is tolerance relaxation at the wetted aerodynamic surfaces, which contribute to an increase in parasitic drag. This section describes the important DFM/A consideration of tolerance relaxation, which is a concern of aerodynamicists and structural designers.

Tolerance relaxation during component manufacture could incur problems of the tolerance-chain buildup at the assembly joint. All aspects of tolerance are beyond the scope of this book; only the tolerance allocation at the surface as the aerodynamic smoothness specification is discussed [5].

In current manufacturing philosophy, the main features contributing to excrescence drag are as follows:

- manufacturing mismatches seen as aerodynamic defects (i.e., discrete roughness; e.g., steps, gaps, and waviness)
- surface contamination with fine particles and dirt adhering to it
- damage, wear, and tear during the life cycle
- fatigue deformation
- attachments of small items on the surface (e.g., blisters, antenna, pitot tubes, gaps/holes, and cooling air intakes/exhausts)

The first and last items are the consequences of design considerations; the remainder happens during operational usage. This chapter addresses only the first item, which gives rise to excrescence drag (i.e., parasitic drag). The nonmanufacturing origin of excrescence drag arising from the last item is treated separately for the $C_{D_{pmin}}$ estimation. To keep excrescence drag within limits, aerodynamicists specify aircraft smoothness requirements, which then are translated into tolerance allocations at the subassembly joints on the wetted surfaces. If the finish exceeds the tolerance limits, it must be reworked to bring it within the limits and/or obtain concessions to pass the product to the final line. Tolerance specifications affect aircraft manufacturing costs.

Aircraft wetted surfaces are primarily manufactured from sheet metals and composites. At the subassembly joints, there are some mismatches (e.g., steps, gaps, and waviness) that must be kept under strict control by specifying surface-smoothness requirements. Mismatches result in parasitic drag as an excrescence effect. Aerodynamicists specify aircraft surface-smoothness requirements to keep the drag increase within limits. The stricter is the tolerance, the more is the cost of production on account of rework or rejection. Any tolerance relaxation at the wetted surface reduces manufacturing costs at the expense of an aircraft parasitic drag increase, perceived as a “loss of quality function.” It is assumed that the sheet metal and composites at the surface accommodate a certain degree of tolerance relaxation. In addition, cosmetic appeal is perceived as a customer preference. Loss of some cosmetic quality can save on costs without unduly penalizing the parasitic drag. However, with increases in fuel price, aerodynamicists must be careful in specifying surface-smoothness tolerances.

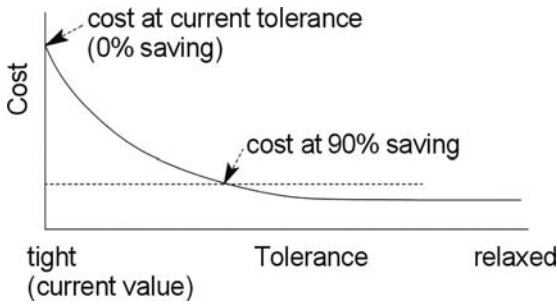


Figure 17.1. Cost-versus-tolerance relationship. Manufacturing cost reduces as tolerance is relaxed. Savings = amount reduced from the existing level to a lower level due to tolerance relaxation

17.6.1 Sources of Aircraft Surface Degeneration

In aircraft application, degeneration of the wetted surface area results from surface deviations from the specified level. It has many origins; the important ones are as follows:

1. Lifting Surface (e.g., wing, flaps, and empennage)
 - control of LE profile and surface-panel profiles (i.e., aerofoil contour)
 - rivet and fastener flushness for skin joints
 - component geometry and subassembly joint mismatches
 - fitment of access panels on the surface
2. Bodies of Revolution (e.g., fuselage and nacelle)
 - control of nose profile and profile of the rest of the body joined in sections
 - rivet/fastener flushness for skin joints
 - component geometry and subassembly joint mismatches
 - fitment of doors, windows, and access panels on the surface

17.6.2 Cost-versus-Tolerance Relationship

The relationship for establishing the manufacturing cost, C , at the assembly is derived by summing all costs involved, as shown:

$$\begin{aligned}
 \text{manufacturing cost, } C = & (\text{basic work time} + \text{rework time}) \times \text{manhour cost} \\
 & + \text{number of concessions} \times \text{cost of concessions} \\
 & + \text{nonrecurring costs} + \text{cost of support/} \\
 & \text{redeployment/management} \qquad (17.1)
 \end{aligned}$$

Changes in tolerance affect the rework time, number of concessions, and the cost of support. Tolerance relaxation reduces manufacturing costs because more components and their assemblies are made right the first time. Tolerance relaxation reaches a limit when any further relaxation has no significant benefit because all components and their assemblies require no rework and/or concessions for acceptance – it is done right the first time. At the limit of relaxation, the cost of manufacturing levels out to what is required for the “basic” work time and the NRC. [Figure 17.1](#) illustrates the nature of the cost-versus-tolerance relationship, a trend that is common to all features.

The X-axis represents the tolerance variation, from the existing level to the level where any further tolerance relaxation has no further benefit in cost reduction.

The Y-axis represents the cost of manufacture, from the existing tolerance level, with current manufacturing costs representing zero savings. Tolerance relaxation results in cost reductions up to the maximum possible level (100%).

Summing tolerance relaxation over an entire aircraft can reduce the manufacturing cost by a small percentage while incurring an increase in excrescence (parasitic) drag. The aircraft DOC reflects the change in cost reduction and drag increase when a trade-off study is conducted. Figure 16.4 shows trends in the trade-off between cost and tolerance. If the initial tolerance is too strict, the relaxation shows a reduction up to a point at which thereafter the DOC increases as a result of the additional fuel burn due to the drag rise, whereas the aircraft price reduction has leveled out.

Reference [1] is a study of the trade-offs, describing how a midsized jet aircraft can average about 33% tolerance relaxation with a corresponding net savings in DOC of 0.42%. The conservative estimation given herein is a typical aircraft cost reduction through DFM/A studies (a fuel price of \$0.75/U.S. gallon is used):

- an approximate 1.28% DOC savings due to 2% aircraft costs saving through DFM/A studies involving no drag increase
- an approximately 0.42% DOC savings due to 1% aircraft costs saving through tolerance relaxation involving drag increase

This study demonstrates a total of 1.7% DOC savings, which translates into a savings of \$530 per sortie for a 150-passenger/3,000-nm range aircraft class. With an annual utilization of 500 sorties, the total is \$26,500 per aircraft. For a fleet of 10 aircraft, the savings total \$26.5 million in 10 years. For smaller aircraft, the percentage savings is even higher.

This is a good example of how aerodynamic, structure, and manufacturing considerations are needed to conceive designs that result in reduced DOC. Manufacturing cost reductions can be achieved through many other efforts, which is the aim of the DFSS concept. During the trade-off studies of various design parameters, the benefit of cost-estimating activities helps designers investigate and adopt new technologies to advance a product to a competitive edge and generate specification requirements (e.g., tolerance allocations). Designers also analyze the risks involved, balancing the trade-off between cost and performance that eventually leads to affordability for operators as the best buy (i.e., product value), which in turn enables manufacturers to thrive.

17.7 Reliability and Maintainability

Poor reliability is unacceptable. An aircraft as a system must achieve a user's confidence that it will work as and when required. This entails a multidisciplinary study for an efficient and cost-effective system integration leading to better reliability and maintainability (R&M) during the operational lifespan. In the current economic climate, the role of reliability, maintainability, and recyclability must be scrutinized for cost control – not only the in-house product line but also the supply chain of bought-out items. Even those systems that are perceived as reliable are only reliable due to the significant redundancy built into the system or the vast amount of corrective maintenance that keeps a system running. Despite immense efforts to predict and

improve the components used in the systems, their R&M often remain at the same levels.

The design must guarantee integrity with significant time between failures that repairs can be made in a specific downtime period. An aircraft must have more TBO than the competition, which is linked to the system reliability as a function of the operational environment and length of operational time. Although the avionic and engine suites come with a well-studied R&M status, many other aircraft components (i.e., mainly structures with many built-in redundancies) have yet to evolve to address maintenance issues at the conceptual design stage. Almost all bought-out items and subsystems have reliability figures obtained from rigorous testing. An aircraft as a system maintains a systematic log, recording failures and defects so they can be followed up with modifications to make designs more robust, for those already built and those that are yet to be built.

17.8 Design Considerations

In the chapter overview (see [Section 17.1](#)), it is pointed out that the public-domain literature is replete with *Design for . . .* considerations, including Design for Manufacture, Design for Assembly, Design for Quality, Design for R&M, DFSS, Design for Recycling, Design for Antipollution, Design for Life Cycle, and Design for Cost, all heading toward a generic Design for X. These considerations led to the appearance of new considerations (sixteen listed in this section), with more from the academic circle. The fresh insights of academia may shed new light but may not be amenable to industrial implementation. Only recently have the drive for Design for R&M and DFSS become part of industrial practices and they are still evolving. The industry has yet to address decisively the other costs of LCC (e.g., training and evaluation, logistic supports, and special equipment) at the conceptual design stages of civil aircraft design in order to reduce the ownership costs of operators. Of the various *Design for . . .* considerations, only a third are applicable to DFM/A considerations. A robust cost model would support trade-off studies to arrive at the best value.

The new challenge for the industry is to examine all aspects of ownership costs at the conceptual design stages of a project. Performance evaluations based on setting individual goals of cost minimization at each design consideration may not result in the global minimum when strong interaction within the multidisciplines exists. In an IPPD design environment, the combined effort of various disciplines provides a better approach to make a product right the first time at a lower cost. The holistic approach suggests the role of cost modeling as a tool to address all considerations simultaneously; this facilitates performance-versus-cost trade-off studies in order to arrive at the most satisfying product line with the widest customer coverage. With this approach, the author introduces the term *design for customer* as a measuring index for “value for the money” defined in [Section 17.9](#).

The sixteen design considerations appearing as *Design for . . .* terms are broadly classified in four categories with brief descriptions. They must provide designers with complete product information in the conceptual design stages based on their expertise and technology level. The purpose of this strategy is to make a product

yield the specific benefits of the lowest LCC (or in civil aviation applications DOC) in a unified manner, leading to the Design for Customer.

17.8.1 Category I: Technology-Driven Design Considerations

Design for Performance: Classical aircraft design entails aerodynamics, structures, propulsion, and systems to minimize fuel consumption. Aeronautical engineers strive to make an aircraft light, with low drag and matched engine, low sfc, and bought-out items (e.g., engine, avionics, and actuators) that offer the best value for the money. It is a proven technology for generic, subsonic, commercial aircraft design, with diminishing returns on investment to incorporate advancements.

Design for Safety: Crashworthiness, emergency exits, and so forth are also proven considerations.

Design for Component Commonality: The family concept of derivative aircraft design offers considerable benefits of cost reduction by maintaining several component commonalities within the variants. Derivative designs cover a wider market at a much lower unit cost because amortization of NRC is distributed over larger numbers of units sold. Some of the variant aircraft designs may not be sized for the least fuel burned, but the lower unit cost offsets to a lower DOC. This consideration at the conceptual design stage is crucial to the success of the product range.

Design for Reliability and Maintenance: Currently, significant maintenance resources are planned after the design and then acquired to fit the requirements. This is due to the difficulty of translating statistical feedback from the operational arena, which can be quite abstract. Design attributes – which can make maintenance difficult by demanding additional time and training for highly skilled technicians – must have more detailed considerations to reduce maintenance costs. Cost trade-off studies with the attributes of reliability, repairability, and fault detection and isolation must be investigated more stringently at the conceptual design stage. Reliability issues are most important for improving the support environment – in generic terminology, this is a *robust design*.

Design for Ecology: Since the 1970s, environmental issues (e.g., antipollution) have been enforced through government legislation on noise and emissions at additional cost. The use of alternative fuels for sustainability is also an issue. The growing stringency of existing requirements as well as additional issues only increase the product cost. This is approaching a matured technology with diminishing returns on investment for improvement.

Design for Recycling: Aerospace technology cannot ignore the emphasis on recyclability, a concern that is gaining strength, as evidenced by the topical agenda of “sustainable development” in recent United Nations summit meetings. The design for stripping is an integral part of the Design for Recycling to minimize the costs of disassembly. New materials (i.e., composites and metals) result in additional disposal considerations. Cost trade-off studies on

LCC versus material selection for recycling may infringe on marginal gains in weight reduction or fabrication costs.

Design for Anti-terrorism: In the offing is a newer demand for Design for Anti-terrorism. In-flight safety features for protection against terrorist activities include an explosion-absorbing airframe and compartmentalization of the cabin for isolation, which incur additional cost.

17.8.2 Category II: Manufacture-Driven Design Considerations

Design for Manufacture: The trade-off study is concerned with the appropriate process required for parts fabrication, including cost-versus-material selection, process selection, the use of NC machines, parts commonality, and modularity considerations to facilitate assembly. A key issue in the conceptual design stage is a low parts count to reduce assembly time. The lowest parts count may not be the least expensive method – compromise may be necessary.

Design for Assembly: This is concerned with the fewest manhours required to assemble parts. Traditional practices in aircraft assembly include numerous components and a complex organizational structure in the engineering, logistics, and management disciplines. This results in an inefficient use of factory floorspace, and quality is compromised due to the unnecessary operations and fasteners required to join mating parts. DFA minimizes manufacturing costs by optimizing engineering methods using innovative best-practice techniques of jigs and tool design, whether a manual or computerized assembly method. Product configuration and the detailed design of parts are important in the assembly process.

Design for Quality: Adherence to the specification requirements is the essence of quality control. One example is meeting the aerodynamic surface-smoothness requirements through surface-tolerance specifications at the component final assembly. Currently, many quality issues are addressed in the post-conceptual design stage; they should be advanced to the conceptual design stage.

17.8.3 Category III: Management-Driven Design Considerations

Design for Six Sigma: This is an integrated approach to design with the key issue of reducing the scope for mistakes and inefficiencies – that is, make a product right the first time to prevent the waste of company resources (see [Section 17.5](#)). A measure of its success is reflected in the final cost of a product; therefore, an estimation method indicates at what cost (i.e., at what efficiency) the Six Sigma approach is working.

Design for Cost/Design to Cost: This is the classical question of Design to Cost (DTC) or Design for Cost (DFC) or a combination of both. The tendency of management to emphasize DTC through a “lean” organizational setup may be counterproductive if it is carried to the extreme application.

17.8.4 Category IV: Operator-Driven Design Considerations

Design for Training and Evaluation: This is an area that currently is not under strong consideration at the conceptual design stage. Aircraft DOC estimation does not include the cost of T&E. Design considerations including commonality and modular concepts could reduce T&E costs and, therefore, must be addressed in an early stage.

Design for Logistic Support: This is an operational aspect with second-order consideration for civil aircraft design. The existing support system addresses most of the logistic details without infringing on any major changes required in aircraft design, unless a special situation arises. Early input from operators for any design consideration helps control costs.

Design for Ground-Based Resources: This also may be deemed a lower-order consideration for civil aircraft design at the conceptual design stage, unless special-purpose equipment is required. In general, ground-based support resources are becoming standardized and can be shared by a large fleet, thereby distributing the operation costs at a lower priority in the conceptual design stage.

Design for Special Equipment: This is more meaningful in military aircraft applications. If any special-purpose equipment must be introduced for ground-based serviceability, then a cost trade-off study at the conceptual design stage is beneficial.

Separate minimization of individual costs through the separate design considerations listed previously may prove counterproductive by preventing the overall minimization of ownership cost. In a holistic overview, this chapter introduces the term *Design for Customer* to unify the individual considerations in the early stages of design evolution in order to offer the best value of the product by satisfying requirements, specifications, and integrity to lower the LCC (or DOC). It is a front-loaded investment for eventual savings in LCC (or DOC).

17.9 “Design for Customer”

Nicolai [8] introduced a meaningful term, *Design for Mankind*, which should be the goal for all designs, not exclusive to the aerospace industry. This book focuses on specific issues of engineering design and operation by suggesting the Design for Customer, as explained in this section.

Using a holistic approach as a tool to address simultaneously the sixteen “*Design for...*” considerations in trade-off studies, the author suggests a Design for Customer index to measure the merits of a product [3]. This applies to pricing of the variants in a family of derivatives but also can include the pricing structure of competition aircraft. The expression of Design for Customer is not substantiated by a large database; it may require fine-tuning for better accuracy. However, it conveys the idea that there is a need for such an index to compare the merits of any aircraft within a class. It suggests a pricing policy to arrive at the most satisfying product line that offers the best value with the widest sales coverage.

Using an empirical formula, a set of standard parameters can be established for the baseline aircraft in the class (i.e., payload range). To remain within the linear range of variation, the family-variant parameters and competition aircraft should not differ by more than about $\pm 15\%$. The baseline standard parameters of interest are denoted by an asterisk as in the DOC^* in U.S. dollars per seat per nautical mile, the Unit Cost* in millions of U.S. dollars, and the delivery time t^* in years (from the placement of an order). To evaluate variant designs, they must be compared to the baseline design. DOC levels out well before it reaches the design range.

A baseline aircraft is designed to have the best L/D ratio at midcruise weight (i.e., the LRC condition). Normally, the L/D characteristic is relatively flat and the family derivative designs have an L/D ratio close to the maximum design value of the baseline aircraft. The Breguet range equation indicates that the range is proportional to the square root of the W/S . A shortened variant with a lower payload and range has a lower W/S with a derated engine. This aircraft has more wing than what is required and has a better takeoff performance but a slightly degraded range performance. Conversely, the extended version has more payload; weight control may have to be traded with range capability. The takeoff mass invariably increases, requiring uprated engines, especially to make up the takeoff performance due to a higher W/S (i.e., undersized wing).

This formulation is inline for comparison, satisfying the customer's operational requirements for the product usefulness in terms of unit cost, operational cost, and timing to meet the demand. From this definition, an increase in the product value is achieved through improved performance (better), lower cost (cheaper), and less time (faster delivery). The DFM/A methodology contributes directly to lower cost, improves quality, and reduces manufacturing cycle time, thereby increasing the product value.

The higher the value, the better it is for a customer to use a product family incorporating a wide range of design considerations to satisfy operational requirements at the optimal ownership cost and purpose. In the absence of standard LCC data, the DOC is used. In this context, the following section introduces a design for customer index to compare the values of other aircraft in the class.

17.9.1 Index for "Design for Customer"

The definition of *design for customer* relates to the merit of the design by establishing a value index. The suggested definition is as follows:

$$\text{design for customer, } K_n = \frac{(DOC^*/DOC) \times (Unit\ Cost^*/Unit\ Cost)}{(t/10t^* + 0.9)}$$

K_n is inversely proportional to the DOC and aircraft unit cost; that is, a lower DOC gives a higher K_n ; a value of more than 1 is better. The unit cost includes the engine and aircraft size and the DOC includes the design merits, passenger number, and range capability. Typically, an aircraft with more passengers has a lower DOC, driving the value to more than 1, but it is evaluated with respect to price and delivery time.

17.9.2 Worked-Out Example

From the worked-out example of the Bizjet, the following values are obtained. Because derivative aircraft values are obtained through simplified assumptions, they must be worked out in better detail. The linear relationship is used to work out the following example to provide a general idea.

Standard Parameters of the Baseline Aircraft

Unit cost* in millions of U.S. dollars = \$8 million; MTOM = 9,400 kg.

DOC* in U.S. dollars per seat/nm = \$0.352 per nautical mile per passenger (ten passengers).

Delivery time t^* in years (from the placement of order) = 1 year.

Baseline aircraft = \$0.8 million/passenger and \$0.000851/kg MTOW.

Parameters of the Extended Variant Aircraft

Unit cost in millions of U.S. dollars = \$9 million; MTOM = 10,800 kg.

DOC in U.S. dollars per seat/nm = \$0.2875 per nautical mile per passenger (fourteen passengers).

Delivery time t in years (from the placement of order) = 1 year.

Large variant aircraft = \$0.6428 million/passenger and \$0.000833/kg MTOW.

$$K_{n_larger} = \frac{(DOC^*/DOC)}{(UnitCost/UnitCost^*) \times (t/10t^* + 0.9)} = \frac{(0.352/0.2875)}{(9/8) \times (1/10 + 0.9)}$$

$$= 1.224/(1.125 \times 1) = 1.088 \text{ (a better value)}$$

Parameters of the Shortened Variant Aircraft

Unit cost in millions of U.S. dollars = \$6 million; MTOM = 7,600 kg.

DOC in U.S. dollars per seat/nm = \$0.482 per nautical mile per passenger (six passengers).

Delivery time t in years (from the placement of order) = 1 year.

Small variant aircraft = \$1 million/passenger and \$0.00079 kg MTOW.

$$K_{n_smaller} = \frac{(DOC^*/DOC)}{(UnitCost/UnitCost^*) \times (t/10t^* + 0.9)} = \frac{(0.352/0.482)}{(6/8) \times (1/10 + 0.9)}$$

$$= 0.7303/(0.75 \times 1) = 0.974 \text{ (a lower value)}$$

In general, a smaller derivative aircraft is penalized because it is heavier than it would be if it were a baseline design. The wing area is larger than what is required. The smaller variant is competitive aircraft, and there are aircraft in this class with similar DOC. Several new all-composite, four-passenger lighter jet aircraft have appeared recently and are selling at less than \$5 million with better DOC. These new aircraft are yet to be proven in operational usage, and it will be some time before all-composite aircraft overtake conventional construction. The example of a six-passenger, smaller variant is a robust, all-metal aircraft with a larger cabin volume and high-end amenities suited to corporate demand. In a mixed fleet of three sizes, the total package offers benefits that are difficult to match. When an airline operates a mixed fleet of variants along with its baseline aircraft, the spare-parts

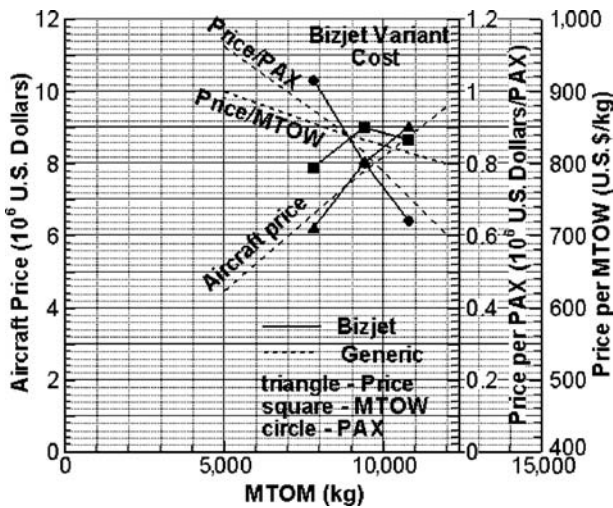


Figure 17.2. Aircraft cost factors of the worked-out Bizjet example

stock, training, and maintenance costs can be shared. Private ownership in this class is increasing and there is room for both types.

However, modifications to the smaller variant can improve the index $K_{n_smaller}$. If re-engined with a smaller turbofan (i.e., the Williams type) and re-engineered with lighter and less expensive equipment, the aircraft price could be decreased to about \$5 million, making it even more attractive; however, it loses some component commonality and incurs additional development costs. If the wing tips can be shortened at practically no extra cost, then the weight can be decreased to less than 7,000 kg, and the index can reach a value of more than 1.

Design for customer can help manufacturers establish the aircraft price for a family of variants, giving each type a comparative value for the customer. Typically, the smaller variant should be priced lower with a smaller profit; other aircraft prices are adjusted, with the baseline aircraft price unchanged. That is, the price of the larger aircraft can be increased to compensate the family price structure. The goal of the baseline size is maximum sales. In the example, the price of the smaller variant is \$6 million, resulting in a small profit. The baseline aircraft aims for the most sales to maximize profit.

In general, route traffic load continues to increase; consequently, sales of the larger variant also increase and also the associated profits for the manufacturer, making up for the relatively smaller profit from the smaller variants. When a new market emerges for a larger traffic load, manufacturers seize the opportunity for a new baseline design.

The aircraft price per passenger and unit mass are explained herein. There is a sharp increase in per-passenger price with a smaller payload, as shown in Figure 17.2. In the figure, the dashed lines represent generic data; it is a magnified version of Figure 16.2. The solid lines represent the Bizjet family. The smaller aircraft price is slightly depressed to suit the market.

17.10 Digital Manufacturing Process Management

The digital manufacturing process management is a newer concept and is still evolving; it is software-driven. Although the industry has already deployed digital

manufacturing in some areas, the full scope of application is yet to stabilize. This section describes a model briefly studied at the QUB [7]. It outlines the nature of changes taking place. These types of studies are conducted in many places, proposing many different models. The core fact is that digital manufacture is here to stay, grow, and replace or merge with traditional manufacturing philosophies.

Today, the microprocessor-driven digital manufacturing process is rapidly overtaking older methods. In fact, all modern production plants are already using it to the extent that it can be advanced. The advantage of microprocessor-based tools is that they are digitally controlled and driven by software. These tools deliver the desired “quantum leap” in manufacturing assembly techniques for future aircraft. This section outlines the role of MPM and identifies the benefits of PLM through the reconciliation perspective (i.e., estimation versus actual) between design and manufacturing engineering disciplines. PLM is a business strategy and part of MPM as a management strategy. (*Life cycle* is used in a generic sense, meaning all aspects of a product, from concept to retirement.)

Digital-manufacturing solutions enable the continuous creation and validation of the manufacturing processes throughout a product’s life cycle. It allows manufacturers to digitally plan, create, monitor, and control production and maintenance processes, providing complete coverage of the manufacturing processes. With the advent of new processes and techniques, there has been a greater use of software in the design and engineering of aircraft. CAD, CAM, CAE, and CAPP tools are now used to determine electronically how an aircraft system must be built. NC machines are linked with CAM.

The new frontier with software suites focuses on PLM, emphasizing the manufacturing processes. PLM is a business strategy that allows companies to share product data, apply common processes, and leverage corporate knowledge to develop products from conception to retirement across the extended enterprise. By including all participants in this process (i.e., company departments, business partners, suppliers, and operators and customers), PLM enables the entire network to operate as a single entity to conceptualize, design, build, and support products.

MPM is segmented into process detailing and validation, resource modeling, and process planning simulation. Within each segment are several modules, discussed as follows.

Process Detailing and Validation

This software suite provides engineers with the tools to bring the process planning solutions into the application-specific disciplines of manufacturing. It assists engineers in verifying process methodologies with actual product geometry and defining processes within a 3D environment. The human module offers tools that allow users to manipulate accurate, standard, digital, human mannequins, referred to as “workers,” and to simulate task activities in the process-simulation environment. Thus, worker processes can be analyzed early in the manufacturing and assembly life cycle. The assembly process simulation module sets a new paradigm for developing manufacturing and maintenance processes. It offers manufacturing engineers and assembly process planners an end-to-end solution by incorporating a single, unified interface for preplanning, detailed planning, process verification, and shop-floor instructions.

Resource Modeling and Simulation

This software suite provides engineers with the tools to develop, create, and implement resource, mechanical programming, and application routines that are integral to the process planning and the process detailing and validation solutions. Within this set of solutions, resources such as robots, tooling, fixtures, machinery, automation, and ergonomics are defined for completing a manufacturing solution. Digital manufacturing also offers flexible, object-based, discrete event-simulation tools for efficient modeling, experimenting, and analyzing of a facility layout and process flow. Both 2D schematic and 3D physical models are quickly created (i.e., rapid prototyping) through pushbutton interfaces, dialog boxes, and extensive libraries. Real-time interaction enables modification of model variables and viewing parameters during runs.

Process Planning and Simulation

The process planning software suite provides an effective process and resource-planning support environment. It improves methodically structured planning, early recognition of process risks, reuse of proven processes, traceable changes and decisions, and the use of scattered-process knowledge. The module is often used during the conceptual design phase, with the process-design and alternative-manufacturing concepts maturing through all the stages to production. The treatment of the relationships among product, process, and manufacturing resource data, including the plant layout, helps to avoid planning mistakes and to obtain a precise overview of the needed investment costs, production space, and manpower at an early stage.

17.10.1 Product, Process, and Resource Hub

Digital manufacturing allows manufacturing engineers and process planners to define, validate, manage, and deliver to the shop floor the content needed to manufacture an aircraft. The combination of this PPR hub environment is uniquely able to provide savings to an enterprise in the following ways by reducing risk, time to market, and overall costs of manufacturing:

- Concurrent engineering design and manufacturing planning and process validation occur before release is final, in the midst of ongoing change.
- Manufacturing producibility analysis directly influences design, thus providing a true DFM/A environment.
- The enterprise is able to formally capture and reuse manufacturing best practices.
- Manufacturing plans are prevalidated in a 3D environment to avoid unexpected problems on the shop floor.
- Unbuildable conditions are found early in the design cycle when the cost of change is minimal.
- Quality targets are met sooner due to reduction (or elimination) of reworking and engineering change orders generated on the shop floor.

Through a combination of methodologies, significant reductions can be achieved in time to market, overall cost, and effective risk for an aircraft program. A key enabler for reducing the time to market is the ability to support concurrent engineering

design and manufacturing planning before a release is final. When this is possible, manufacturing producibility analysis directly influences design, thus providing a true DFM/A environment. In this scenario, the total costs of the engineering changes that occur during the program are dramatically less because they are identified and resolved much earlier in the life cycle. The total effective cost of the changes is dramatically less because they are mostly identified and resolved before tooling is procured and production starts.

The key technology enabler for the digital manufacturing solution, product/process design, and validation is the PPR hub and business transformation. This database environment – supporting complex configuration and affectivity rules that are required in the aerospace world – provides the infrastructure to allow process and resource planning to occur in the context of the engineering data and continuously changing environment. In contrast to traditional systems, the PPR hub provides the means to explicitly manage PPR objects and the relationships among them. Because such relationships are explicitly defined and managed within the database, it is possible to see directly the impact of changes of one object class on any other (e.g., “If a part is changed, which manufacturing plans are affected?”).

17.10.2 Integration of CAD/CAM, Manufacturing, Operations, and In-Service Domains

One of the major areas for improvement within an aerospace enterprise is in the integration among engineering, manufacturing, and operations organizations. The drivers for such integration are to allow the maximum reuse and appropriate consolidation of data and business systems throughout the program life cycle. The degree to which this is achieved typically has a major influence on overall costs, both recurring and nonrecurring. Traditionally, the engineering and manufacturing (i.e., CAD and CAM) domains operate in a self-contained operating unit. As a result, it is difficult – if not impossible – to actually leverage engineering data downstream in the shop-floor operations area where typically bills of material (BOMs) are defined, along with related procurement data and shop-floor work instructions. One major problem with this traditional scenario is that effectively managing engineering changes and reconciling the parallel worlds of CAD and CAM and shop-floor operations is extremely difficult and expensive to do accurately. Digital manufacturing provides a means to integrate these two domains (i.e., CAD/CAM and operations), as well as the in-service domain, through several core technologies and application layers.

An additional benefit of this type of integration is the ability to reduce the number of redundant business systems between the CAD/CAM and operations organizations. This reduces recurring and overhead costs. Specifically, the following classes of business systems can be consolidated into the PPR-hub-based solution suite:

- parts list and tool list
- BOM definition
- bill of resources
- routings
- process sheets/work instructions

- reconciliation analysis: estimate versus actual (e.g., in preparing BOM)
- simulation-based validation
- cost estimating
- production-flow analysis
- human resources

17.10.3 Shop-Floor Interface

A key area where this integrated environment provides value is in the ability to define, evaluate, and document various manufacturing alternatives, such as alternate routings and resource utilization, based on evolving conditions in operations. The PPR-hub-based manufacturing database can be used to drive discrete event simulations of the alternatives to determine the impact on material flow, throughput, and utilization under various scheduling and product-mix conditions. The process plans, resource allocations, and precedence requirements in the PPR hub can be further analyzed to balance the work across the manufacturing facility and to provide proper utilization of workers. It provides an interface to feed the shop floor directly from the PPR hub database, ensuring optimal reuse of data created in the CAD/CAM and manufacturing and planning environments. One of the most significant ways to leverage a PPR-based database is to reuse the data directly as the basis for 3D work instructions on the shop floor. The immediate benefits of this approach are as follows:

- Eliminate the possibility for a mismatch between shop-floor instructions and engineering data because the instructions are derived directly from the PPR hub database, including the related CAD geometry and attributes.
- CAD-based work instructions provide a means to eliminate paper drawings on the shop floor because all required data, tolerance, notes, and related specifications can be embedded within the 3D dataset that also provides all required manufacturing information.
- Intuitive 3D (i.e., CAD-based) work instructions, combined with authoritative engineering data and attributes, empower machinists to perform their job faster and with fewer mistakes. In such cases, the reduction in overall manufacturing flow time and cost can be dramatic.
- Provide a data-feedback loop from the shop floor to the manufacturing planning environment to provide visibility on shop-floor-based changes representing as-built product buildup and processing.
- Leverage this data-feedback loop and related PPR-hub infrastructure to reconcile and evaluate the differences among the as-designed, as-planned, and as-built datasets.

Finally, with respect to the in-service phase of the products' life cycle, this architecture provides a means to also capture and manage the evolving (i.e., complex) configuration of the related BOMs and collection of processes performed during ongoing maintenance operations. As appropriate, PPR-hub data defined in one phase of the life cycle can be reused for other phases, thus providing potentially significant savings.

17.10.4 Design for Maintainability and 3D-Based Technical Publication Generation

During the evolution of a product design and manufacturing process planning, the same PPR dataset can be used to validate the maintainability of a product, as well as to develop technical-publication documents containing text, images, and movies derived directly from the 3D-based process plans. The core PPR technology supports any number of views of process-planning data related to product and resource, thereby providing a way to associatively develop maintenance plans concurrent with manufacturing planning. This ability to concurrently validate the design as well as the maintenance operations for a product is one more example of the significant leverage provided by the PPR data model. This allows the idea of leveraging the results of 3D process planning and analysis directly into Web-based technical publications for maintenance operations (e.g., analysis of 3D process plans for producibility and Web-based technical publications for maintenance). 3D enables a new business paradigm, as follows:

- 3D is now leveraged not only for design but also for manufacturing planning, simulation-based validation, work-instruction authoring, and delivery to the shop-floor workforce, enabling a true paperless manufacturing process. This is easily extended for 3D maintenance and repair instructions.
- Operational and maintenance scenarios can be simulated using ergonomic analysis early in the design cycle to provide efficiencies later in the life cycle of a product. With a systematic methodology, a true design for customer business process can be supported.
- The virtual production mock-up eliminates the requirement for prototype parts to prove out mock-ups of production tooling and fixtures, reducing cost and time.
- Tooling orders can be placed much later in the development plan with the latest design revisions incorporated because they will work the first time, eliminating costly change orders to tools and parts designs.
- Designs can be modified early in the design cycle to accommodate manual assembly and maintenance tasks; therefore, the requirement for special tools can be eliminated.

In the near future, the conceptual design stage of a new aircraft project must assess in detail and then incorporate the benefits that can be derived from the digital manufacturing process management.

APPENDIX A

Conversion

<i>Linear</i>		<i>Linear</i>	
1 inch	= 2.54 cm	1 cm	= 0.3937 in
1 foot	= 30.48 cm	1 cm	= 0.0328 ft
1 yd	= 0.9144 m	1 m	= 1.0936 yd
1 mile	= 1.6093 km	1 km	= 0.6214 mile
1 mile	= 5,280 ft	1 ft	= 0.000189 mile
1 nm	= 1.852 km	1 km	= 0.54 nm
1 nm	= 1.1508 mile	1 mile	= 0.869 nm
<i>Area</i>		<i>Area</i>	
1 in ²	= 6.5416 cm ²	1 cm ²	= 0.155 in ²
1 ft ²	= 929.03 cm ²	1 cm ²	= 0.00108 ft ²
1 ft ²	= 0.092903 m ²	1 m ²	= 10.764 ft ²
1 yd ²	= 0.8361 m ²	1 m ²	= 1.196 yd ²
1 mile ²	= 2.59 km ²	1 km ²	= 0.3861 mile ²
<i>Volume</i>		<i>Volume</i>	
1 in ³	= 16.387 cm ³	1 cm ³	= 0.061 in ³
1 ft ³	= 28,316.85 cm ³	1 cm ³	= 0.0000353 ft ³
1 yd ³	= 0.764555 m ³	1 m ³	= 1.308 yd ³
1 ft ³	= 28.317 L	1 L	= 0.0353 ft ³
1 U.S. gallon	= 3.7854 L	1 L	= 0.2642 U.S. gallon
1 U.K. gallon	= 4.546 L	1 L	= 0.22 U.K. gallon
1 U.S. pint	= 0.0004732 m ³	1 m ³	= 2,113.376 U.S. pint
1 U.K. pint	= 0.0005683 m ³	1 m ³	= 1,759.754 U.K. pint
1 quart	= 946.353 cm ³	1 cm ³	= 0.001057 quart
<i>Density</i>		<i>Density</i>	
1 lb/ft ³	= 16.1273 g/m ³	1 kg/m ³	= 0.06242796 lb/ft ³
1 lb/ft ³	= 16.0185 kg/m ³	1 kg/m ³	= 0.06243 lb/ft ³
<i>Speed</i>		<i>Speed</i>	
1 ft/s	= 1.0973 km/hr	1 km/hr	= 0.9113 ft/s
1 ft/min	= 0.00508 m/s	1 m/s	= 196.85 ft/min
1 mph	= 0.447 m/s	1 m/s	= 2.237 mph
1 mph	= 0.869 knots	1 knot	= 1.151 mph
1 knot	= 0.51444 m/s	1 m/s	= 1.944 knot
1 knot	= 1.853 km/hr		
<i>Angle</i>		<i>Angle</i>	
1 deg	= 0.01716 radian	1 radian	= 57.296 deg

<i>Density</i>		<i>Density</i>	
1 lb/in ³	= 27.68 g/cm ³	1 g/cm ³	= 0.03613 lb/in ³
1 lb/ft ³	= 16.0185 kg/m ³	1 kg/m ³	= 0.06243 lb/ft ³
<i>Mass</i>		<i>Mass</i>	
1 lb	= 0.454 kg	1 kg	= 2.2046 lb
<i>Force</i>		<i>Force</i>	
1 lb	= 4.4482 N	1 N	= 0.2248 lb
1 lb	= 0.454 kg	1 kg	= 2.2046 lb
1 oz	= 28.35 gm	1 gm	= 0.3527 oz
1 oz	= 0.278 N	1 N	= 3.397 oz
<i>Pressure</i>		<i>Pressure</i>	
1 lb/in ²	= 6,894.76 pascal	1 pascal	= 0.000145 lb/in
1 lb/ft ²	= 44.88 pascal	1 pascal	= 0.02089 lb/ft ²
1 lb/in ²	= 703.07 kg/m ²	1 kg/m ²	= 0.0001422 lb/in ²
1 lb/ft ²	= 4.8824 kg/m ²	1 kg/m ²	= 0.020482 lb/ft ²
1 atm	= 1,013.25 milibar	1 milibar	= 0.000987 atm
1 bar	= 14.5 lb/in ²	1 atm	= 14.7 lb/in ²
<i>Energy</i>		<i>Energy</i>	
1 lb/ft	= 1.356 joule	1 joule	= 0.7376 lb/ft
1 watt-hr	= 3,600 joule	1 joule	= 0.000278 watt-hr
1 lb/ft	= 1.356 joule	1 joule	= 0.7376 lb/ft
1 watt-hr	= 0.00134 hp-hr	1 hp-hr	= 745.7 watt-hr
<i>Power</i>		<i>Power</i>	
1 hp (550 ft lbf)	= 0.7457 kw	1 kw	= 1.341022 hp
<i>Fuel properties</i>			
AVGAS			
1 U.S. gallon	= 5.75 lb		
1 ft ³	= 43 lb		
AVTUR			
1 U.S. gallon (JP4)	= 6.56 lb		
1 ft ³	= 48.6 lb		
AVTUR			
1 U.S. gallon (JP5)	= 7.1 lb		
1 ft ³	= 53 lb		

APPENDIX B

International Standard Atmosphere (Table below from hydrostatic equations)

Altitude ft	Pressure lb/ft ²	Temperature R	Density lb/ft ³	Viscosity 10 ⁻⁷ lbsec/ft ²	Sound speed ft/s	C _{f,turbulent}
0	2116.22	518.67	0.00237	3.7372	1116.5	0.01449
1000	2040.85	515.1	0.0023	3.7172	1112.6	0.01459
2000	1967.68	511.54	0.00224	3.6971	1108.75	0.0147
3000	1896.64	507.97	0.00217	3.677	1104.88	0.0148
4000	1827.69	504.41	0.00211	3.657	1100.99	0.01491
5000	1760.79	500.84	0.00204	3.637	1097.09	0.1502
6000	1695.89	497.27	0.00198	3.616	1093.178	0.01513
7000	1632.93	493.71	0.00192	3.596	1089.25	0.01525
8000	1571.88	490.14	0.00186	3.575	1085.31	0.01536
9000	1512.7	486.57	0.00181	3.555	1081.35	0.01548
10000	1455.33	483.01	0.00175	3.534	1077.38	0.0156
11000	1399.73	479.44	0.0017	3.513	1073.4	0.01572
12000	1345.87	475.88	0.00164	3.4927	1069.4	0.01585
13000	1293.7	472.31	0.00159	3.4719	1065.39	0.01597
14000	1243.18	468.74	0.00154	3.451	1061.36	0.0161
15000	1194.27	465.18	0.00149	3.43	1057.31	0.01623
16000	1146.92	461.11	0.00144	3.4089	1053.25	0.01637
17000	1101.11	458.05	0.0014	3.388	1049.17	0.0165
18000	1056.8	454.48	0.00135	3.3666	1045.08	0.01664
19000	1013.93	450.91	0.0013	3.3453	1040.97	0.01678
20000	1036.85	447.35	0.00126	3.324	1036.95	0.01693
21000	932.433	443.78	0.00122	3.3025	1032.71	0.01707
22000	893.72	440.21	0.00118	3.281	1028.55	0.01722
23000	856.32	436.65	0.00114	3.26	1024.38	0.01738
24000	820.19	433.08	0.0011	3.238	1020.18	0.01753
25000	785.31	429.52	0.00106	3.216	1015.98	0.01769
26000	751.64	425.95	0.00102	3.1941	1011.75	0.01785
27000	719.15	422.38	0.00099	3.1722	1007.5	0.01802
28000	687.81	418.82	0.00095	3.1502	1003.24	0.01819
29000	657.58	415.25	0.00092	3.128	998.96	0.01836
30000	628.43	411.69	0.00088	3.1059	994.66	0.01854
31000	600.35	408.12	0.00085	3.0837	990.35	0.01872
32000	573.28	404.55	0.00082	3.0614	986.01	0.0189
33000	547.21	400.97	0.00079	3.0389	981.65	0.01909
34000	522.12	397.42	0.00076	3.0164	977.28	0.0193
35000	497.96	393.85	0.00073	2.9938	972.88	0.01948
36089	472.68	389.97	0.0007	2.969	968.08	0.0197
37000	452.43	389.97	0.00067	2.969	968.08	0.01999
38000	431.2	389.97	0.00064	2.969	968.08	0.02032
39000	410.97	389.97	0.00061	2.969	968.08	0.02065
40000	391.68	389.97	0.00058	2.969	968.08	0.02099

41000	373.3	389.97	0.00055	2.969	968.08	0.02134
42000	355.78	389.97	0.00053	2.969	968.08	0.02169
43000	339.09	389.97	0.0005	2.969	968.08	0.02205
44000	323.08	389.97	0.00048	2.969	968.08	0.02243
45000	308.01	389.97	0.00046	2.969	968.08	0.02281
46000	299.56	389.97	0.00043	2.969	968.08	0.0232
47000	279.78	389.97	0.00041	2.969	968.08	0.02359
48000	266.65	389.97	0.00039	2.969	968.08	0.024
49000	254.14	389.97	0.00037	2.969	968.08	0.02442
50000	242.21	389.97	0.00036	2.969	968.08	0.02485
55000	190.47	389.97	0.00028	2.969	968.08	0.02716
60000	149.78	389.97	0.00022	2.969	968.08	0.02977
65000	117.79	389.97	0.00017	2.969	968.08	0.03275
70000	92.684	392.37	0.00013	2.984	971.06	0.03632
75000	73.053	395.12	0.00010	3.002	974.44	0.04045
80000	57.675	397.86	0.00008	3.019	977.82	0.04523

Altitude m	Pressure N/m ²	Temperature K	Density kg/m ³	Viscosity Nsec/m ²	Sound speed m/s	C _{f,turbulent}
0	101327	288.15	1.225	0.00001789	340.3	0.00263
500	95463	284.9	1.16727	0.00001773	338.37	0.00264
1000	89876.7	281.65	1.11164	0.00001757	336.44	0.00266
1500	84558	278.4	1.05807	0.00001741	334.49	0.00267
2000	79497.2	275.15	1.00649	0.00001725	332.53	0.00269
2500	74684.4	271.9	0.95686	0.00001709	330.56	0.00271
3000	70110.4	268.65	0.90912	0.0001693	328.58	0.00273
3500	65765.8	265.4	0.86323	0.00001677	326.59	0.00274
4000	61641.9	262.15	0.81913	0.00001661	324.58	0.00276
4500	57729.9	258.9	0.77678	0.00001644	322.56	0.00278
5000	54021.5	255.65	0.73612	0.00001628	320.53	0.0028
5500	50508.3	252.4	0.69711	0.00001611	318.49	0.00282
6000	47182.5	249.15	0.6597	0.00001594	316.43	0.00284
6500	44036.2	245.9	0.62385	0.00001577	314.36	0.00286
7000	41062.1	242.65	0.5895	0.0000156	312.28	0.00288
7500	38252.7	239.4	0.55663	0.00001543	310.18	0.0029
8000	35601	236.15	0.52517	0.00001526	308.07	0.00292
8500	33100.2	232.9	0.49509	0.00001509	305.94	0.00294
9000	30743.6	229.65	0.46635	0.00001492	303.8	0.00297
9500	28524.7	226.4	0.4389	0.00001474	301.64	0.00299
10000	26437.3	223.15	0.41271	0.00001457	299.47	0.00301
10500	24475.3	219.9	0.38773	0.00001439	297.28	0.00304
11000	22633	216.65	0.36392	0.00001421	295.07	0.00306
11500	20916.8	216.65	0.33633	0.00001421	295.07	0.0031
12000	19331	216.65	0.31983	0.00001421	295.07	0.00314
12500	17865	216.65	0.28726	0.00001421	295.07	0.00318
13000	16511	216.65	0.26548	0.00001421	295.07	0.00323
13500	15259.2	216.65	0.24536	0.00001421	295.07	0.00327
14000	14102.3	216.65	0.22675	0.00001421	295.07	0.00331
14500	13033.2	216.65	0.20956	0.00001421	295.07	0.00336
15000	12045.1	216.65	0.19367	0.00001421	295.07	0.0034
16000	10287.9	216.65	0.16542	0.00001421	295.07	0.00366
17000	8787.12	216.65	0.14129	0.00001421	295.07	0.00387
18000	7505.24	216.65	0.12068	0.00001421	295.07	0.00398
19000	6410.36	216.65	0.10307	0.00001421	295.07	0.00409
20000	5475.21	216.65	0.08803	0.00001421	295.07	0.00421
25000	2511.18	221.65	0.03946	0.00001448	298.46	0.00492

APPENDIX C*

Aerofoils

* Appendix C on aerofoils is found on the Web at www.cambridge.org/Kundu

APPENDIX D

Case Studies

Midrange Aircraft (Airbus 320 class)

All computations carried out herein follow the book instructions. The results are not from the Airbus industry. Airbus is not responsible for the figures given here. They are used only to substantiate the book methodology with industry values to gain confidence. The industry drag data are not available but, at the end, it will be checked if the payload-range matches the published data.

Given: LRC Speed and Altitude: Mach 0.75 at 36,089 ft.

Dimensions (to scale the drawing for detailed dimensions)

Fuselage length = 123.16 ft (scaled measurement differs slightly from the drawings)

Fuselage width = 13.1 ft, Fuselage depth = 13 ft.

Wing reference area (trapezoidal part only) = 1,202.5 ft²; add yehudi area = 118.8 ft²

Span = 11.85 ft; MAC_{wing} = 11.64 ft; AR = 9.37; Δ¼ = 25 deg; C_R = 16.5 ft, λ = 0.3

H-tail reference area = 330.5 ft²; MAC_{H-tail} = 8.63 ft

V-tail reference area = 235.6 ft²; MAC_{V-tail} = 13.02 ft

Nacelle length = 17.28 ft; Maximum diameter = 6.95 ft

Pylon = measure from the drawing

Reynolds number per ft is given by:

$$\begin{aligned} Re_{per\ foot} &= (V\rho)/\mu = (aM\rho)/\pi = [(0.75 \times 968.08)(0.00071)]/ \\ &\quad (0.7950 \times 373.718 \times 10^{-9}) \\ &= 1.734 \times 10^6 \text{ per foot} \end{aligned}$$

Drag Computation

Fuselage

Table D1 gives the basic average 2D flat plate for the fuselage, $C_{Ff\text{basic}} = 0.00186$. Table D2 summarizes the 3D and other shape-effect corrections, ΔC_{Ff} , needed to estimate the total fuselage C_{Ff} .

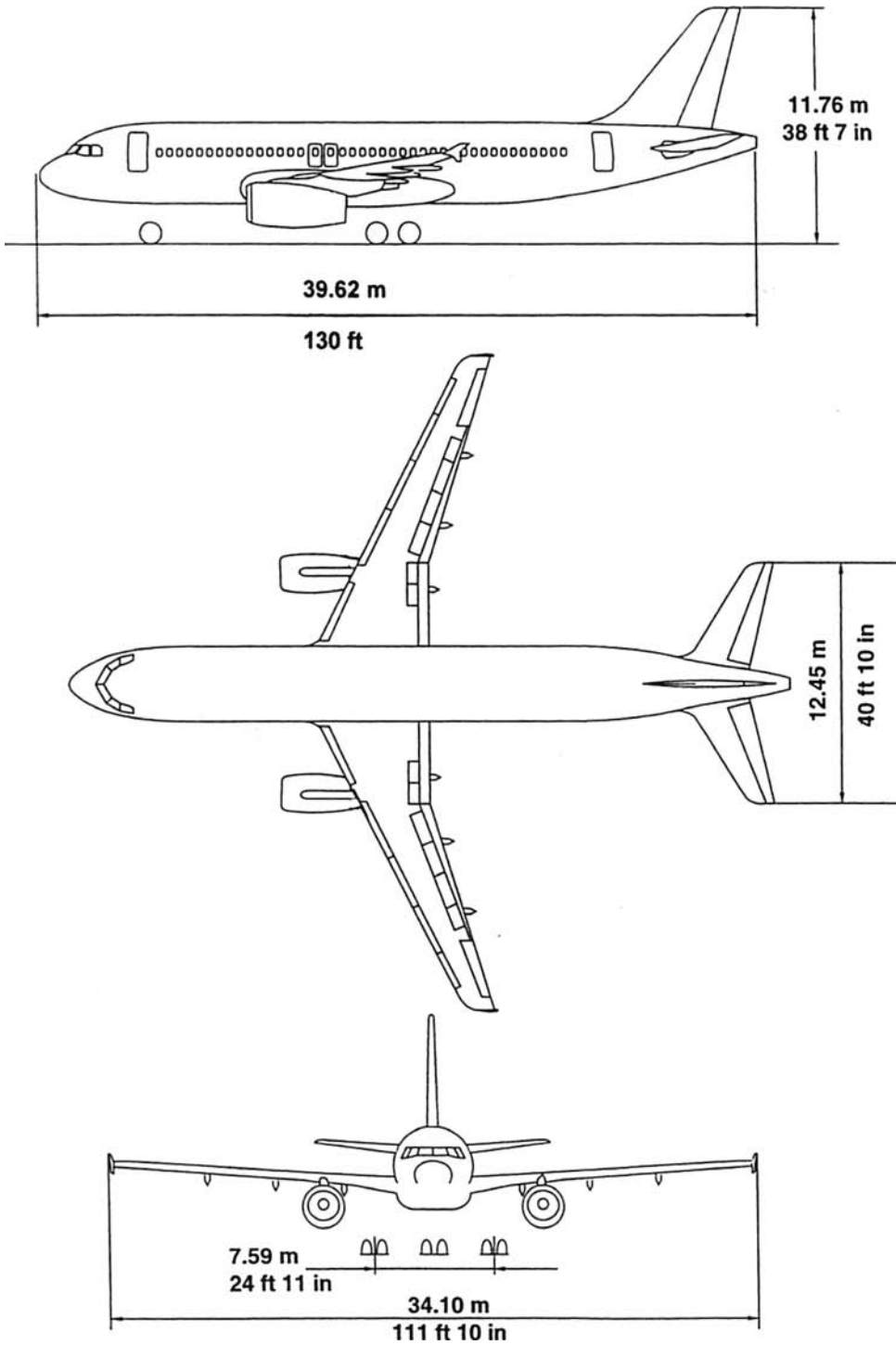


Figure D1. Airbus 320 three-view with major dimensions (Courtesy of Airbus)

Table D1. Reynolds number and 2D basic skin friction C_{Fbasic}

Parameter	Reference area (ft ²)	Wetted area (ft ²)	Characteristic length (ft)	Reynolds number	2D C_{Fbasic}
Fuselage	n/a	4,333	123.16	2.136×10^8	0.00186
Wing	1,202.5	2,130.94	11.64 (MAC_w)	2.02×10^7	0.00255
V-tail	235	477.05	13.02 (MAC_{VT})	2.26×10^7	0.00251
H-tail	330.5	510.34	8.63 (MAC_{HT})	1.5×10^7	0.00269
2 × nacelle	n/a	2 × 300	17.28	3×10^7	0.00238
2 × pylon	n/a	2 × 58.18	12 (MAC_p)	2.08×10^7	0.00254

Table D2. Fuselage ΔC_{Ff} correction (3D and other shape effects)

Item	ΔC_{Ff}	% of $C_{Ffbasic}$
Wrapping	0.00000922	0.496
Supervelocity	0.0001	5.36
Pressure	0.0000168	0.9
Fuselage-upsweep of 6 deg	0.000127	6.8
Fuselage-closure angle of 9 deg	0	0
Nose-fineness ratio	0.000163	8.7
Fuselage nonoptimum shape	0.0000465	2.5
Cabin pressurization/leakage	0.000093	5
Passenger windows/doors	0.0001116	6
Belly fairing	0.000039	2.1
Environmental Control System Exhaust	-0.0000186	-1
Total ΔC_{Ff}	0.0006875	36.9

Therefore, the total fuselage $C_{Ff} = C_{Ffbasic} + \Delta C_{Ff} = 0.00186 + 0.0006875 = 0.002547$.

Flat-plate equivalent f_f (see Equation 9.8) = $C_{Ff} \times A_{wf} = 0.002547 \times 4333 = 11.03 \text{ ft}^2$.

Add the canopy drag $f_c = 0.3 \text{ ft}^2$.

Therefore, the total fuselage parasite drag in terms of $f_{f+c} = 11.33 \text{ ft}^2$.

Wing

Table D1 gives the basic the average 2D flat plate for the wing, $C_{Fwbasic} = 0.00257$, based on the MAC_w .

The important geometric parameters include the wing reference area (trapezoidal planform) = 1,202.5 ft² and the gross wing planform area (including Yehudi) = 1,320.8 ft². Table D3 summarizes the 3D and other shape-effect corrections needed to estimate the total wing C_{Fw} .

Table D3. Wing ΔC_{Fw} correction (3D and other shape effects)

Item	ΔC_{Fw}	% of $C_{Fwbasic}$
Supervelocity	0.000493	19.2
Pressure	0.000032	1.25
Interference (wing-body)	0.000104	4.08
Excrescence (flaps and slats)	0.000257	10
Total ΔC_{Fw}	0.000887	34.53

Therefore, the total wing: $C_{Fw} = C_{Fwbasic} + \Delta C_{Fw} = 0.00257 + 0.000889 = 0.00345$.

Flat-plate equivalent: f_w (Equation 9.8) = $C_{Fw} \times A_{ww} = 0.00345 \times 2,130.94 = 7.35\text{ft}^2$.

Vertical Tail

Table D1 gives the basic average 2D flat plate for the V-tail:

$C_{FVTbasic} = 0.00251$ based on the MAC_{VT} ; V-tail reference area = 235ft^2

Table D4 summarizes the 3D and other shape-effect corrections (ΔC_{FVT}) needed to estimate the V-tail C_{FVT} .

Table D4. V-tail ΔC_{FVT} correction (3D and other shape effects)

Item	ΔC_{FVT}	% of $C_{FVTbasic}$
Supervelocity	0.000377	15
Pressure	0.000015	0.6
Interference (V-tail – body)	0.0002	8
Excrescence (rudder gap)	0.0001255	5
Total ΔC_{FVT}	0.000718	28.6

Therefore, the V-tail: $C_{FVT} = C_{FVTbasic} + \Delta C_{FVT} = 0.00251 + 0.000718 = 0.003228$
 Flat-plate equivalent f_{VT} (see Equation 9.8) = $C_{FVT} \times A_{wVT} = 0.003228 \times 477.05 = 1.54\text{ft}^2$.

Horizotal Tail

Table D1 gives the basic average 2D flat plate for the H-tail:

$C_{FHTbasic} = 0.00269$, based on the MAC_{HT} ; the H-tail reference area $S_{HT} = 330.5\text{ft}^2$

Table D5 summarizes the 3D and other shape-effect corrections (ΔC_{FHT}) needed to estimate the H-tail C_{FHT} .

Table D5. H-tail ΔC_{FHT} correction (3D and other shape effects)

Item	ΔC_{FHT}	% of $C_{FHTbasic}$
Supervelocity	0.0004035	15
Pressure	0.0000101	0.3
Interference (H-tail – body)	0.0000567	2.1
Excrescence (elevator gap)	0.0001345	5
Total ΔC_{FHT}	0.000605	22.4

Therefore, the H-tail: $C_{FHT} = C_{FHTbasic} + \Delta C_{FHT} = 0.00269 + 0.000605 = 0.003295$

Flat-plate equivalent f_{HT} (see Equation 9.8) = $C_{FHT} \times A_{wHT} = 0.003295 \times 510.34 = 1.68\text{ft}^2$.

Nacelle, C_{Fn}

Because the nacelle is a fuselage-like axisymmetric body, the procedure follows the method used for fuselage evaluation but needs special attention due to the throttle-dependent considerations.

Important geometric parameters include:

Nacelle length = 17.28 ft

Maximum nacelle diameter = 6.95 ft

Average diameter = 5.5 ft
 Nozzle exit-plane diameter = 3.6 ft
 Maximum frontal area = 37.92 ft²
 Wetted area per nacelle $A_{wn} = 300$ ft²

Table D1 gives the basic average 2D flat plate for the nacelle:

$C_{Fnbasic} = 0.00238$, based on the nacelle length

Table D6 summarizes the 3D and other shape-effect corrections, ΔC_{Fn} , needed to estimate the total nacelle C_{Fn} for one nacelle.

For nacelles, a separate supervelocity effect is not considered because it is accounted for in the throttle-dependent intake drag; pressure drag also is accounted for in the throttle-dependent base drag.

Table D6. *Nacelle ΔC_{Fn} correction (3D and other shape effects)*

Item	ΔC_{Fn}	% of $C_{Fnbasic}$
Wrapping (3D effect)	0.0000073	0.31
Excrescence (nonmanufacture)	0.0005	20.7
Boat tail (aft end)	0.00027	11.7
Base drag (aft end)	0	0
Intake drag	0.001	41.9
Total ΔC_{Fn}	0.001777	74.11

Thrust Reverser Drag

The excrescence drag of the thrust reverser is included in Table D6 because it does not result from manufacturing tolerances. The nacelle is placed well ahead of the wing; hence, the nacelle–wing interference drag is minimized and assumed to be zero.

Therefore the nacelle: $C_{Fn} = C_{Fnbasic} + \Delta C_{Fn} = 0.00238 + 0.001777 = 0.00416$
 Flat plate equivalent f_n (Equation 9.8) = $C_{Fn} \times A_{wn} = 0.00416 \times 300 = 1.25$ ft² per nacelle.

Pylon

The pylon is a wing-like lifting surface and the procedure is identical to the wing parasite-drag estimation. Table D1 gives the basic average 2D flat plate for the pylon;

$C_{Fpbasic} = 0.0025$ based on the MAC_p .

The pylon reference area = 28.8 ft² per pylon. Table D7 summarizes the 3D and other shape-effect corrections (ΔC_{Fp}) needed to estimate C_{Fp} (one pylon).

Table D7. *Pylon ΔC_{Fp} correction (3D and other shape effects)*

Item	ΔC_{Fp}	% of $C_{Fpbasic}$
Supervelocity	0.000274	10.78
Pressure	0.00001	0.395
Interference (pylon–wing)	0.0003	12
Excrescence	0	0
Total ΔC_{Fp}	0.000584	23

Therefore, the pylon $C_{Fp} = C_{Fpbasic} + \Delta C_{Fp} = 0.0025 + 0.00058 = 0.00312$
 Flat-plate equivalent: f_p (see Equation 9.8) = $C_{Fp} \times A_{wp} = 0.182$ ft² per pylon.

Roughness Effect

The current production standard tolerance allocation provides some excrescence drag. The industry standard uses 3% of the total component parasite drag, which includes the effect of surface degradation in use. The value is $f_{roughness} = 0.744 \text{ ft}^2$, given in [Table D8](#).

Trim Drag

Conventional aircraft produce trim drag during cruise and it varies slightly with fuel consumption. For a well-designed aircraft of this class, the trim drag of $f_{trim} = 0.1 \text{ ft}^2$ may be used.

Aerial and Other Protrusions

For this class of aircraft, $f_{aerial} = 0.005 \text{ ft}^2$.

Air-Conditioning

This is accounted for in the fuselage drag as ECS exhaust. It could provide a small amount of thrust.

Aircraft Parasite Drag Buildup Summary and C_{Dpmin}

[Table D8](#) provides the aircraft parasite drag buildup summary in tabular form.

Table D8. *Aircraft parasite drag buildup summary and C_{Dpmin} estimation*

	Wetted area A_w ft^2	Basic C_F	ΔC_F	Total C_F	f (ft^2)	C_{Dpmin}
Fuselage + undercarriage fairing	4,333	0.00186	0.00069	0.00255	11.03	0.00918
Canopy					0.3	0.00025
Wing	2,130.94	0.00255	0.00089	0.00346	7.35	0.00615
V-tail	477.05	0.00251	0.00072	0.00323	1.54	0.00128
H-tail	510.34	0.00269	0.00061	0.0033	1.68	0.0014
2 × Nacelle	2 × 300	0.00238	0.00178	0.00415	2.5	0.00208
2 × Pylon	2 × 58.18	0.00254	0.000584	0.00312	0.362	0.0003
Rough (3%)					0.744	0.00062
Aerial					0.005	0.000004
Trim drag					0.1	0.00008
	TOTAL				25.611	0.0213

Notes:

$C_{Dpmin} = 0.0213$.

Wing reference area $S_w = 1,202 \text{ ft}^2$; $C_{Dpmin} = f/S_w$ ISA day; 36,089-ft altitude; and Mach 0.75.

ΔC_{Dp} Estimation

The ΔC_{Dp} is constructed, corresponding to the C_L values, as given in [Table D9](#).

Table D9. *ΔC_{Dp} estimation*

C_L	0.2	0.3	0.4	0.5	0.6
ΔC_{Dp}	0.00044	0	0.0004	0.0011	0.0019

Induced Drag, C_{Di}

The wing aspect ratio:

$$AR = \frac{\text{span}^2}{\text{gross wing area}} = (111.2)^2 / 1,320 = 9.37$$

induced drag, $C_{Di} = \frac{C_L^2}{\pi AR} = 0.034C_L^2$

Table D10 gives the C_{Di} corresponding to each C_L .

Table D10. Induced drag

C_L	0.2	0.3	0.4	0.5	0.6	0.7	0.8
C_{Di}	0.00136	0.00306	0.00544	0.0085	0.01224	0.0167	0.0218

Total Aircraft Drag

Aircraft drag is given as:

$$CD = C_{Dpmin} + \Delta C_{Dp} + C_{Di} + [C_{Dw} = 0]$$

The total aircraft drag is obtained by adding all the drag components in Table D11.

Note that the low and high values of C_L are beyond the flight envelope.

Table D11. Total aircraft drag coefficient, C_D

C_L	0.2	0.3	0.4	0.5	0.6
C_{Dpmin}	0.0213 from Table 7.9				
ΔC_{Dp}	0.00038	0	0.0004	0.0011	0.0019
C_{Di}	0.00136	0.00306	0.00544	0.0085	0.01224
Total aircraft C_D	0.0231	0.02436	0.02714	0.0309	0.03544

Table D11 is drawn in Figure D2 to show that the PIANO software aircraft drag checks out well with what is manually estimated in this book; hence, the PIANO value is unchanged.

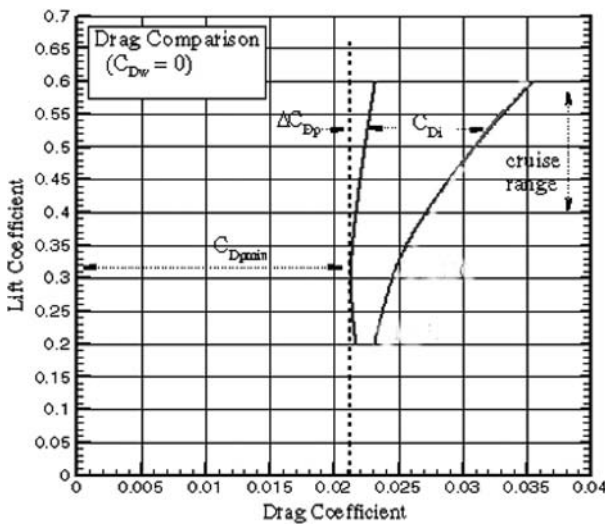


Figure D2. Aircraft drag polar at LRC

Engine Rating

Uninstalled sea-level static thrust = 25,000 lb per engine.

Installed sea-level static thrust = 23,500 lb per engine.

Weight Breakdown (with variations)

Design cruise speed, $V_C = 350$ KEAS

Design dive speed, $V_D = 403$ KEAS

Design dive Mach number, $M_D = 0.88$

Limit load factor = 2.6

Ultimate load factor = 3.9

Cabin differential pressure limit = 7.88 psi

Component	Weight (lb)	Percentage of MTOW
Wing	14,120	
Flaps + slats	2,435	
Spoilers	380	
Aileron	170	
Winglet	265	
Wing group total	17,370	(above subcomponent weights from [10])
Fuselage group	17,600	(Torenbeek's method)
H-tail group	1,845	
V-tail	1,010	
Undercarriage group	6,425	
Total structure weight	44,250	
Power plant group (two)	15,220	
Control systems group	2,280	
Fuel systems group	630	
Hydraulics group	1,215	
Electrical systems group	1,945	
Avionics systems group	1,250	
APU	945	
ECS group	1,450	
Furnishing	10,650	
Miscellaneous	4,055	
MEW	83,890	
Crew	1,520	
Operational items	5,660	
OEW	91,070	
Payload (150 × 200)	30,000	
Fuel (see range calculation)	41,240	
MTOW	162,310	

This gives:

Wing-loading = $162,310/1,202.5 = 135 \text{ lb/ft}^2$

Thrust-loading = $50,000/162,310 = 0.308$

The aircraft is sized to this with better high-lift devices.

Payload Range (150 Passengers)

MTOM – 162,000 lb

Onboard fuel mass: 40,900 lb

Payload – $200 \times 150 = 30,000 \text{ lb}$

LRC: Mach 0.75, 36,086 feet (constant condition)

Initial cruise thrust per engine: 4,500 lb

Final cruise thrust per engine: 3,800 lb

Average specific range: 0.09 nm/lb fuel

Climb at 250 KEAS reaching to Mach 0.7

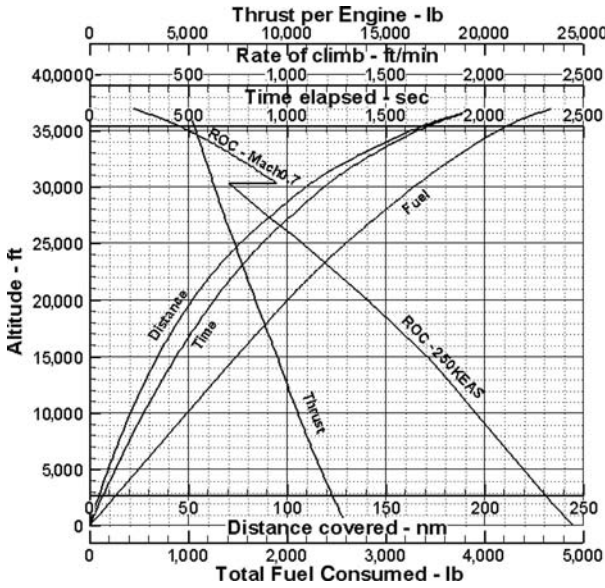


Figure D3. Aircraft performance

Summary of the Mission Sector

Sector	Fuel consumed (lb)	Distance covered (nm)	Time elapsed (min)
Taxi out	200	0	8
Takeoff	300	0	1
Climb	4,355	177	30
Cruise	28,400	2,560	357
Descent	370	105	20
Approach/land	380	0	3
Taxi in	135	0	5
Total	34,140	2,842	424

Diversion-fuel calculation:

diversion distance = 2,000 nm, cruising at Mach 0.675 and at 30,000-ft altitude
 Diversion fuel = 2,800 lb; contingency fuel (5% of mission fuel) = 1,700 lb

Holding-fuel calculation:

Holding time = 30 min at Mach 0.35 and at a 5,000-ft altitude
 Holding fuel = 2,600 lb

Total reserve fuel carried = 2,800 + 1,700 + 2,600 = 7,100 lb.

Total onboard fuel carried = 7,100 + 34,140 = 41,240 lb.

Cost Calculations (U.S. \$ - Year 2000)

Number of passengers	150
Yearly utilization	497 trips per year
Mission (trip) block time	7.05 hrs
Mission (trip) block distance	2,842 nm
Mission (trip) block fuel	34,140 lb (6.68 lbs/U.S. gallons)

Fuel cost = 0.6 U.S.\$ per U.S. gallon

Airframe price = \$38 million

Two engines price = \$9 million

Aircraft price = \$47 million

Operating costs per trip – AEA 89 ground rules for medium jet-transport aircraft:

Depreciation	\$6,923
Interest	\$5,370
Insurance	\$473
Flight crew	\$3,482
Cabin crew	\$2,854
Navigation	\$3,194
Landing fees	\$573
Ground handling	\$1,365
Airframe maintenance	\$2,848
Engine maintenance	\$1,208
Fuel cost	\$3,066 (5,110.8 U.S. gallons)
Total DOC	\$31,356
DOC/block hour	\$4,449
DOC/seat	\$209
DOC/seat/nm	0.0735 U.S.\$/seat/nm

Readers may compare this with data available in the public domain.

APPENDIX E*

Tire Data (Courtesy of Goodyear Tire Co.)

* Appendix E on tire data is found on the Web at www.cambridge.org/Kundu

References

ROAD MAP OF THE BOOK

- [1] Wood, K. D. *Aircraft Design*. Johnson Publishing Co.; Boulder, CO; 1966.
- [2] Corning, Gerald. *Supersonic and Subsonic Airplane Design*. Published by the author (1960).
- [3] Nicolai, L. M. *Fundamentals of Aircraft Design*. METS, Inc.; San Jose, CA; 1975.
- [4] Torenbeek, E. *Synthesis of Subsonic Airplane Design*. Delft University Press; Amsterdam, The Netherlands; 1982.
- [5] Roskam, J. *Aircraft Design*. Published by the author as an eight-volume set; 2007.
- [6] Stinton, D. *The Design of the Airplane*. van Nostrand Reinhold; New York; 1983.
- [7] Raymer, D. *Aircraft Design: A Conceptual Approach*, 4th edition. AIAA; Reston, VA; 2006.
- [8] Thurston, D. *Design for Flying*, 2nd edition. Tab Books; 1995.
- [9] Fielding, J. *Introduction to Aircraft Design*. Cambridge University Press; Cambridge, UK; 1999.
- [10] Jenkinson, L. R., Simpson, P., and Rhodes, D. *Civil Jet Aircraft Design*. Arnold Publishers; London, UK; 1999.
- [11] Jenkinson, L. R., and Marchman, James F. *Aircraft Design Project Studies*. Butterworth; 2003.
- [12] Howe, D. *Aircraft Conceptual Design Synthesis*. Professional Engineering Ltd.; London; 2000.
- [13] Whitford, Ray. *Fundamentals of Fighter Design*. Airlife; England; 2000.
- [14] Schaufele, Roger D. *The Elements of Aircraft Preliminary Design*. ARIES Publications; Santa Ana, CA; 2000.
- [15] Huenecke, Klaus. *Modern Combat Aircraft Design*. Airlife; England, 1987.
- [16] Schmitt, Dieter. *Flugzeugentwurf Umdruck zur Vorlesung (Aircraft Design Handout)*; Technische Universität München; 2000.
- [17] Talay, Theodore A. *Introduction to the Aerodynamics of Flight*. NASA SP-367; 1975.
- [18] Mason, W. H. *Aircraft Design Information Sources by VPI*. An excellent annotated bibliography on many aspects of aircraft design; available on the Web.
- [19] Yechout, Thomas R. (Lt. Col. USAF). “*Degrees of Expertise: A Survey of Aerospace Engineering Programs*.” Aerospace America; April 1992.
- [20] Walker, B. K., Jeng, S. M., Orkwis, G. L., Slater, G. L., Khosla, P. K., et al. *Educating Aerospace Engineers for the Twenty-First Century: Results of Survey*. ASEE Conference Proceedings; 1995.
- [21] Williams, James C. and Young, Robert L. “*Making the Grade with ABET*.” Aerospace America; April 1992.

- [22] McMasters, John H. *Paradigms Lost, Paradigms Regained: Paradigms Shift in Engineering Education*. SAE Technical Paper Series No. 911179; 1991.
- [23] Moulton, A. E., et al. *Engineering Design Education*. Design Council; UK; April 1976.
- [24] *Engineering Design: The Fielding Report*. Council of Scientific and Industrial Research; HMSO; UK; 1963.
- [25] Nicolai, Leland M. *Designing a Better Engineer*. Aerospace America; April 1992.
- [26] *Jane's All the World's Aircraft Manual*. Jane's Information Group; Surrey, UK, and Alexandria, VA; published annually. Author's name in 1983–1984 and 1984–1985 editions.
- [27] *Aerospace America*. AIAA publication for competition; July 2003.

CHAPTER 1. INTRODUCTION

- [1] Anderson, John D. *The Airplane: A History of Its Technology*. AIAA; Reston, VA; 2002.
- [2] Taylor, Michael J. H. *Milestones of Flight*. Chancellor Press; 1983.
- [3] Anderson, John D. *History of Aerodynamics*. Cambridge University Press; 1998.
- [4] Von Braun, W., and Ordway, F. *History of Rocketry and Space Travel*; Thomas Y. Crowell Co.; New York; 1969.
- [5] Kundu, A. K., Watterson, J., et al. "Parametric Optimization of Manufacturing Tolerances at the Aircraft Surface." *Journal of Aircraft*; Vol. 39, No. 2; AIAA; Reston, VA; 2002.
- [6] Murman, E., Walton, M., and Rebentisch, E. "Challenges in the Better, Faster, Cheaper Era of Aeronautical Design, Engineering, and Manufacturing." *The Aeronautical Journal*; October 2000.
- [7] McMasters, John, and Cummings, Russell. "Rethinking the Airplane Design Process: An Early 21st Century Perspective." 42nd Aerospace Science Meeting; January 5–8, 2004.
- [8] *Flight International*; July 1–7, 2003.
- [9] Nicolai, Leland M. "Designing a Better Engineer." *Aerospace America*; April 1992.
- [10] Kundu, A. K., et al. "A Proposition in Design Education with a Potential in Commercial Venture in Small Aircraft Manufacture." *Journal of Aircraft Design*; Vol. 3, No. 4; pp. 261–273; Elsevier Science Ltd.; 2000.
- [11] Kundu, A., Curran, R., Crosby, S., et al. "Rapid Cost Modeling at the Conceptual Stage of Aircraft Design." AIAA Aircraft Technology, Integration, and Operations Forum; Los Angeles, CA; 2002.

CHAPTER 2. METHODOLOGY TO AIRCRAFT DESIGN, MARKET SURVEY, AND AIRWORTHINESS

- [1] *Jane's All the World's Aircraft Manual*. Jane's Information Group; Surrey, UK, and Alexandria, VA; published annually.
- [2] *Flight International*. Reed Elsevier, UK; published weekly.
- [3] *Aviation Week and Space Technology (AW&ST) Journal*. McGraw-Hill; published weekly.
- [4] *Interavia*. UK; published weekly.
- [5] Jackson, Scott. *Systems Engineering for Commercial Aircraft*. ISBN: 0-291-39846-4; 1997.
- [6] Aircraft Transport Association of America (ATA). *Specifications for Manufacturers' Technical Data*. Specification 100; 1989.
- [7] Kundu, A. K., Watterson, J., et al. "Parametric Optimization of Manufacturing Tolerances at the Aircraft Surface." *Journal of Aircraft*; Vol. 39, No. 2.; AIAA; Reston, VA; 2002.

- [8] *Aerospace America*. AIAA; Reston, VA; July 2003.
- [9] Federal Aviation Regulations.
- [10] Niu, Michael. *Airframe Structural Design*. Commlit Press Ltd.; Hong Kong; 1999.

CHAPTER 3. AERODYNAMIC CONSIDERATIONS

- [1] Kuethe and Chow. *Foundations of Aerodynamics*. John Wiley; 1986.
- [2] International Standard Atmosphere.
- [3] Schlichting, H., and Gersten, H. *Boundary Layer Theory*. 8th edition; Springer Berlin; Heidelberg; 2003.
- [4] Abbott, I. R., and von Doenhoff, A. E. *Theory of Wing Sections, Including a Summary of Airfoil Data*. McGraw Hill; New York; 1949.
- [5] Torenbeek, Egbert. *Synthesis of Subsonic Airplane Design*. Delft University Press; Amsterdam, The Netherlands; 1982.
- [6] Roskam, Jan. *Aircraft Design*. DARcorporation; Lawrence, KS; 2007.
- [7] Talay, Theodore A. NASA SP-367, *Introduction to the Aerodynamics of Flight*. 1975.
- [8] Perkins, C. D., and Hage, R. E. *Aircraft Performance Stability and Control*. Wiley; 1949.
- [9] Hanne, P. A. *Applied Computational Aerodynamics*. Progress in Astronautics and Aeronautics Series; Vol. 125; AIAA; Reston, VA; 1990.

CHAPTER 4. AIRCRAFT CLASSIFICATION, STATISTICS, AND CHOICES FOR CONFIGURATION

- [1] McCanny, Ronan. *Statistics and Trends in Commercial Transport Aircraft*. Final-year project with the author as supervisor; May 2005.
- [2] *Jane's All the World's Aircraft Manual*. Jane's Information Group; Surrey, UK, and Alexandria, VA; published annually.
- [3] Torenbeek, E.. *Synthesis of Subsonic Airplane Design*. Delft University Press; Amsterdam, The Netherlands; 1982.
- [4] NASA SP-367. *Introduction to the Aerodynamics of Flight*, by Theodore A. Talay; 1975.
- [5] Fielding, J. *Introduction to Aircraft Design*. Cambridge University Press; Cambridge, UK; 1999.
- [6] Adair, K., and McAneney, C. "Parametric Sensitivity Study of Fuselage Parasite Drag." Undergraduate project at the Queen's University Belfast. Belfast, UK; May 2007.
- [7] McMasters, John H. Boeing Commercial Aircraft General Engineering Division, Summer Intern Training Program; 1994.
- [8] Web sites:

richard.ferriere.free.fr/3vues
www.globemaster.de
fighterjets.milavia.net
www.aerosite.net/caravelle.htm
www.aerospace.web.org
www.aviastar.org
www.commonswikimedia.org
[www.daviesturner.com/logistics/interactive/
resources.aircargo.unitload.asp](http://www.daviesturner.com/logistics/interactive/resources.aircargo.unitload.asp)
www.aircargolive.com/inf/ul/DESIGNS.htm
www.unitedcargo.com/shipping/RRcont.jsp
www.tradeway.com.au/aircspecs.cfm#1
[www.soton.ac.uk/~jps7/AircraftDesignResources/
LloydJenkinson%20data](http://www.soton.ac.uk/~jps7/AircraftDesignResources/LloydJenkinson%20data)

CHAPTER 5. AIRCRAFT LOAD

- [1] Niu, Michael. *Airframe Structural Design*. Commlit Press Ltd.; Hong Kong; 1999.

CHAPTER 6. CONFIGURING AIRCRAFT

- [1] *Jane's All the World's Aircraft Manual*. Jane's Information Group; Surrey, UK, and Alexandria, VA; published annually.
- [2] Niu, Michael. *Airframe Structural Design*. Commlit Press Ltd.; Hong Kong; 1999.
- [3] NASA SP-367. *Introduction to the Aerodynamics of Flight*, by Theodore A. Talay; 1975.
- [4] Torenbeek, E. *Synthesis of Subsonic Airplane Design*. Delft University Press; Amsterdam, The Netherlands; 1982.
- [5] Yan-Yee, Andy Ko. *The Role of Constraints and Vehicle Concepts in Transport Design: A Comparison of Cantilever and Strut-Braced Wing Airplane Concepts*. Masters Thesis. Virginia Polytechnic Institute and State University; April 2000.

CHAPTER 7. UNDERCARRIAGE

- [1] Pazmany, Ladislao. *Landing Gear Design for Light Aircraft*. Pazmany Aircraft Corp.; May 1986.
- [2] Tanner, John. *Aircraft Landing Gear Systems*. SAE; 1997.
- [3] Roskam, Jan. *Airplane Design, Part IV*. DARcorporation; Lawrence, KS; 2007.
- [4] Niu, Michael. *Airframe Structural Design*. Commlit Press Ltd.; Hong Kong; 1999.
- [5] Currey, N.D. *Aircraft Landing Gear Design: Principle and Practice*. AIAA; Reston, VA; 1988.
- [6] Torenbeek, E. *Synthesis of Subsonic Airplane Design*. Delft University Press; Amsterdam, The Netherlands; 1982.
- [7] Conway, H. G. *Landing Gear Design*. Chapman and Hall; London, UK; 1958.
- [8] *Aerodrome Design Manual, Part 3; Pavements*. Second Edition. International Civil Aviation Organization; 1983.
- [9] *Tire and Rim Association Yearbook*. Copley, OH.
- [10] *Jane's All the World's Aircraft Manual*. Jane's Information Group; Surrey, UK, and Alexandria, VA; published annually.
- [11] Goodyear Tire Catalogue, available at www.goodyearaviation.com/img/pdf/datatires.pdf.
- [12] MIL-PRF-5041J.

CHAPTER 8. AIRCRAFT WEIGHT AND CENTER OF GRAVITY ESTIMATION

- [1] Society of Allied Weight Engineers. *Introduction to Aircraft Weight Engineering*. Los Angeles, CA; 1996.
- [2] Society of Allied Weight Engineers. *Weight Engineer's Handbook*. Los Angeles, CA; 2002.
- [3] Sechler, E. E., and Dunn, L. G. *Airplane Structural Analysis and Design*. Dover Publications; Mineola, NY; 1963.
- [4] Torenbeek, E. *Synthesis of Subsonic Aircraft Design*. Delft University Press; Amsterdam, The Netherlands; 1982.
- [5] Roskam, J. *Aircraft Design*, Vol. 1 to 8. DARcorporation; Lawrence, KS; 2007.
- [6] Niu, Michael. *Airframe Structural Design*. Commlit Press Ltd.; Hong Kong; 1999.
- [7] Jenkinson, L. R., Simpson, P., and Rhodes, D. *Civil Jet Aircraft Design*. Arnold Publishers; 1999.

- [8] Howe, D. *Aircraft Conceptual Design Synthesis*. Professional Engineering Ltd.; London; 2000.
- [9] Raymer, D. *Aircraft Design: A Conceptual Approach*, 4th edition. AIAA; Reston, VA; 2006.
- [10] Kundu, A. K. *A Multidisciplinary Study of Aerodynamic Smoothness Requirements Based on V2500 Turbofan Nacelle Data to Reduce Operating Cost*. Ph.D. Thesis; October 1999.

CHAPTER 9. AIRCRAFT DRAG

- [1] Hoerner, S. F. *Fluid Dynamic Drag*. DARcorporation; Lawrence, KS; 1965.
- [2] AGARD LS 67: *Prediction Method for Aircraft Aerodynamic Characteristics*; May 1974.
- [3] Feagan, R. C., and Morrison, W. D. "Delta Method: An Empirical Drag Build-up Technique." Lockheed California Company; NASA Contractor Report 151971; 1978.
- [4] USAF DATCOM.
- [5] ESDU.
- [6] Roskam, J. *Airplane Design*. DARcorporation; Lawrence, KS; 2007.
- [7] Kundu, A. K. *Subsonic Aircraft Drag Estimation*. Shorts Document No. AR/0001 (not in public domain); October 1995.
- [8] AGARD AR 256. *Technical Status Review on Drag Prediction and Analysis from Computational Fluid Dynamics: State of the Art*. June 1989.
- [9] Torenbeek, E. *Synthesis of Subsonic Airplane Design*. Delft University Press; Amsterdam, the Netherlands; 1982.
- [10] Haines, A. B. "Subsonic Aircraft Drag: An Appreciation of Present Standards." *Aeronautical Journal*; Vol. 72, No. 687; March 1968.
- [11] *Aircraft Drag Estimation*, Cranfield University Notes; 1983.
- [11] Young, A. D., and Paterson, J. H. AGARD AG 264. *Aircraft Excrescence Drag*; 1981.
- [12] Kundu, A. K., Watterson, J., et al. "Parametric Optimization of Manufacturing Tolerances at the Aircraft Surface." *Journal of Aircraft*, Vol. 39, No. 2; AIAA; Reston, VA; 2002.
- [13] AGARD CP 124. April 1973.
- [14] Abbott, I. R., and Von Doenhoff, A. E. *Theory of Wing Sections*. Dover Publications; Mineola, NY; 1949.

CHAPTER 10. AIRCRAFT POWER PLANT AND INTEGRATION

- [1] Kundu, A. K. Class Lecture Notes at Queen's University Belfast. Belfast, UK.
- [2] *The Jet Engine*. Rolls-Royce plc, 5th Edition; 1996.
- [3] Cohen H., Rogers, G. F. C., and Saravanamutto, H. I. H. *Gas Turbine Theory*. Prentice Hall; 2008.
- [4] Mattingly, Jack D. *Elements of Gas Turbine Propulsion*. McGraw-Hill; 1996.
- [5] Flack, Ronald D. *Fundamentals of Jet Propulsion with Application*. Cambridge University Press; 2005.
- [6] Hill, P. G., and Peterson, C. R. *Mechanics and Thermodynamics of Propulsion*. Prentice Hall; 1992.
- [7] Oates, Gordon. *Aerothermodynamics of Gas Turbines and Rocket Propulsion*. AIAA; Reston, VA; 1984.
- [8] Swavelly, C. E. *Propulsion System Overview*. Pratt and Whitney short course; 1985.
- [9] Farokhi, Saeed, et al. *Propulsion System Integration*. Short course. University of Kansas; Lawrence, KS; 1991.
- [10] Riordan, David. Lecture notes to Queen's University Belfast. Belfast, UK; 2003.

- [11] Whitford, Ray. *Design for Combat Aircraft*. Jane's Information Group; Surrey, UK, and Alexandria, VA; 1987.
- [12] *Jane's All the World's Aircraft Manual* (later editions). Jane's Information Group; Surrey, UK, and Alexandria, VA.
- [13] McCormick, Barnes W. *Aerodynamics, Aeronautics, and Flight Mechanics*. Wiley; 1985.
- [14] Dommasch, Daniel O., et al. *Airplane Aerodynamics*. Pitman; New York; 1967.
- [15] Perkins, C. D., and Hage, R. E. *Aircraft Performance Stability and Control*. Wiley; 1949.
- [16] *Propeller Performance Manual*. Hamilton Standard, PD6101A; 1963.
- [17] *SBAC Standard Method of Performance Estimation*. London, UK.
- [18] Lan, C. T. E., and Roskam, J. *Aeroplane Aerodynamics and Performance*; University of Kansas; Lawrence, KS; 1980.
- [19] Gunston, Bill. *The Development of Jet and Turbine Aero Engines*. 4th edition; Hayes North America; Newbury Park, CA; 2006.
- [20] Stinton, Darrol. *The Design of the Airplane*. AIAA; Reston, VA; 2001.
- [21] Seddon, J., and Goldsmith, E. *Practical Intake Aerodynamic Design*. AIAA; Reston, VA; 1965.
- [22] Glauert, H. *Elements of Aerofoil and Airscrew Theory*. 2nd edition; Cambridge University Press; 1983.
- [23] Available at www.bh.com/companions/034074152X/appendices; compiled by Lloyd Jenkinson, et al.

CHAPTER 11. AIRCRAFT SIZING, ENGINE MATCHING, AND VARIANT DERIVATIVE

- [1] Wallace, Richard E. *Parametric and Optimization Techniques for Airplane Design Synthesis*. AGARD-LS-56; 1972.
- [2] Miele, Angelo. *Flight Mechanics, Vol. I: Theory of Flight Paths*. Addison-Wesley; Reading, MA; 1962.
- [3] Perkins, C. D., and Hage, R. E. *Airplane Performance, Stability and Control*. Wiley; 1949.
- [4] Loftin, E.A. NASA TM 1998-207644.

CHAPTER 12. STABILITY CONSIDERATIONS AFFECTING AIRCRAFT CONFIGURATION

- [1] Perkins, C. D., and Hage, R. E. *Airplane Performance, Stability and Control*. Wiley; 1949.
- [2] Bernard Etkin. *Dynamics of Atmospheric Flight*. Dover Publications; 2005.
- [3] Nelson, Robert C. *Flight Stability and Automatic Control*. McGraw-Hill; 1998.
- [4] Phillip, Warren F. *Mechanics of Flight*. Wiley; 2004.
- [5] Talay, Theodore A. *Introduction to the Aerodynamics of Flight*. NASA SP-367; 1975.
- [6] Watterson, John. Class Lecture Notes at the Queen's University Belfast. Belfast, UK.
- [7] Munroe, Amy. "Statistics and Trends for Vertical and Horizontal Tails of Commercial Transport and Military Aircraft." Undergraduate project, with author as a supervisor; May 2006.
- [8] Murphy, Steven. "Statistics and Trends for Vertical and Horizontal Tails of Commercial Transport and Military Aircraft." Undergraduate project, with author as a supervisor; May 2006.
- [9] Miele, Angelo. *Flight Mechanics, Vol. I: Theory of Flight Paths*. Addison-Wesley; Reading, MA; 1962.
- [10] Collinson, R. P. G. *Introduction to Avionics Systems*. Kluwer; Boston; 2006.
- [11] US DATCOM.

- [12] Available at www.centennialofflight.gov/essay/Theories_of_Flight/Stability_II/TH27G6.htm.
- [13] Klug, Heinz G. *Messerschmitt Bolkow-Blohm GmbH*. Hamburg, Germany; 1988.
- [14] Roskam, J. *Aircraft Design*. DARcorporation; Lawrence, KS; 2007.

CHAPTER 13. AIRCRAFT PERFORMANCE

- [1] Perkins, C. D., and Hage, R. E. *Airplane Performance, Stability and Control*. Wiley; 1949.
- [2] Miele, Angelo. *Flight Mechanics, Vol. I: Theory of Flight Paths*. Addison-Wesley; Reading, MA; 1962.
- [3] Roskam, J. *Airplane Design*, DARcorporation; Lawrence, KS; 2007.
- [4] Phillip, Warren F. *Mechanics of Flight*. Wiley; 2004.
- [5] Talay, Theodore A. *Introduction to the Aerodynamics of Flight*. NASA SP-367; 1975.
- [6] Watterson, John. Class Lecture Notes at the Queen's University Belfast. Belfast, UK.
- [7] Bernard, R. H., and Philpot, D. R. *Aircraft Flight*. Prentice-Hall; 1996.
- [8] McCormick, Barnes W. *Aerodynamics, Aeronautics and Flight Mechanics*. Wiley; 1985.
- [9] Hale, F. J. *Aircraft Performance, Selection and Design*. Wiley; 1984.

CHAPTER 14. COMPUTATIONAL FLUID DYNAMICS

- [1] Chapman, D. "Computational Aerodynamics Development and Outlook," *AIAA Journal*; Reston, VA; December 1979.
- [2] Chapman, D. "A Perspective on Aerospace CFD." *Aerospace America*; January 1992.
- [3] Roache, Patrick J. *Verification and Validation in Computational Science and Engineering*. ISBN 0-913478-08-3; 1998.
- [4] ARARD AR256. *Technical Status Review on Drag Prediction and Analysis from Computational Fluid Dynamics: State of the Art*. June 1989.
- [5] Melnik, R. E., Siclari, M. J., Marconi, F., Barber, T., and Verhoff, A. "An Overview of a Recent Industry Effort at CFD Code Validation." AIAA Paper No. 95-2229. 26th AIAA Fluid Dynamic Conference; June 1995.
- [6] Thangam, S., and Speziale, C. G. "Turbulent Flow Past a Backward-Facing Step: A Critical Evaluation of Two-Equation Method." *AIAA Journal*, Vol. 30, No. 5; May 1992.
- [7] Chen, H. C., Yu, N. J., Rubbert, P. E., and Jameson, A. "Flow Simulation of General Nacelle Configurations Using Euler Equations." AIAA Conference Paper No. 83-0539; 1983.
- [8] Uanishi, K., Pearson, N. S., Lahnig, T. R., and Leon, R. M. "CFD-Based 3D Turbofan Nacelle Design System." AIAA Paper No. A91-16278.
- [9] Berman, H., Anderson, J. D., and Drummond, P. A. "Numerical Solution of the Supersonic Flow over a Rearward-Facing Step with Transverse, Nonreacting Hydrogen Injection." AIAA Paper No. 82-1002; 1982.
- [10] Kundu, A. K., Morris, W. H., and Raghunathan, S. "Effect of Manufacturing Tolerances on Aircraft Aerodynamics and Cost." WMC 97 Conference Paper No. 711-003; 1997.
- [11] Cook, T. A. "The Effects of Ridge Excrescences and Trailing Edge Control Gaps on Two-Dimensional Aerofoil Characteristics." ARC R&M No. 3698; 1971.
- [12] Laban, M. "Application of CFD to Drag Analysis and Validation with Wind-Tunnel Data." Nationaal Lucht-en Ruimtevaartlaboratorium, Von Karman Institute for Fluid Dynamics; Lecture Series; 2003.

- [13] Devine, Raymond, et al. "A Comparison of Conventional Pylon Design to a Compression Pylon Design using Computational Fluid Dynamics." CEIAT; The Queen's University Belfast. Belfast, UK.
- [14] Bell, Mark. "An Investigation into the Complex Aerodynamic Interaction of a Nacelle-Pylon-Wing in Over-Wing Nacelle Configuration." MEng Thesis. The Queen's University Belfast. Belfast, UK; May 2006.
- [15] Web sites
www.hanleyinnovations.com/multisurface/msaexperiment01.html
www.cfdrc.com/bizareas/aerospace/aeromechanics/aircraft_aerodynamics.html
www.esi-group.com/SimulationSoftware/CFD_Fastran/appl_aircraft_aero.html

CHAPTER 15. MISCELLANEOUS DESIGN CONSIDERATIONS

- [1] Smith, Michael J. T. *Aircraft Noise*. Cambridge University Press; 1983.
- [2] Ruijgrok, G. J. J. *Elements of Aviation Acoustics*. Eburon Academic Publishers; 2003.
- [3] ESDU 02020. *An Introduction to Aircraft Noise*.
- [4] Gunston, Bill. *The Development of Jet and Turbine Aero Engines*. Sparkland Somerset; Patrick Stephens; 2002.
- [5] Niu, Michael C. Y. *Airframe Structural Design*. Commlit Press, Ltd.; Hong Kong; 1999.
- [6] Ashby, Michael F. *Material Selection in Mechanical Design*. Butterworth and Hinemann; Burlington, MA; 1992.
- [7] Jukes Malcolm. *Aircraft Display Systems*. AIAA; Reston, VA; 2004.
- [8] Jarrett, D. N. *Cockpit Engineering*. Ashgate Publishing, Ltd.; 2005.
- [9] Moir, Ian, and Seabridge, Allen. *Aircraft Systems*. Wiley; 2006.
- [10] Roskam, Jan. *Airplane Design*, Vol. 3 and 4. DARcorporation; Lawrence, KS; 2007.
- [11] Bingelis, Tony. *Engines*. EAA; 2000.
- [12] *Jane's All the World's Aircraft Manual, 2001–2002*. Jane's Information Group; Surrey, UK, and Alexandria, VA.
- [13] Fielding, John P. *Introduction to Aircraft Design*. Cambridge University Press; 1999.
- [14] McMasters, John H. Boeing Commercial Aircraft, General Engineering Division, Summer Intern Training Program; 1994.
- [15] Moir, Ian, and Seabridge, Allen. *Civil Avionics Systems*. Wiley; Chichester; 2006.
- [16] Moir, Ian, and Seabridge, Allen. *Military Avionics Systems*. Wiley; 2006.
- [17] Dhenin, G. (ed.). *Aviation Medicine: Health and Clinical Aspects*. Tri-Med Books Limited; London; 1978.
- [18] Society of U.S. Air Force Flight Surgeons. *Flight Surgeons Handbook of Life Support Equipment*; October 1, 1987.
- [19] "Advanced Concept Ejection Seat ACES II." Report MDC J4576 Revision D; March 1, 1988.
- [20] Shannon, R. H. "Operational Aspects of Forces on Man During Escape in the U.S. Air Force, 1 January 1968 – 31 December 1970." In *AGARD Linear Acceleration of Impact Type*; June 1971.
- [21] Available at www.fas.org.

CHAPTER 16. AIRCRAFT COST CONSIDERATIONS

- [1] Association of European Airlines. "Short–Medium Range Aircraft: AEA Requirements." 1989.

- [2] Kundu, A., Curran, R., Crosby, S., and Raghunathan, S. "Rapid Cost Modeling at the Conceptual Stage of Aircraft Design." 2002 AIAA Aircraft Technology, Integration, and Operations Forum; Los Angeles, CA; October 1–3, 2002.
- [3] Kundu, A. K., Crosby, S., Curran, R., et al. "Aircraft Component Manufacture Case Studies and Operating Cost Reduction Benefit." AIAA Conference ATIO; Denver, CO; November 2003.
- [4] NASA CR 145190. *A New Method for Estimating Current and Future Transport Aircraft Operating Cost*; March 1978.
- [5] Apgar, H. "Design to Life Cycle Cost in Aerospace." IAA/AHS/ASEE Part G. *Journal of Aero. Engineering, Aerospace Design Conference*; February 16–19, 1993.

CHAPTER 17. AIRCRAFT MANUFACTURING CONSIDERATIONS

- [1] Kundu, A. K. "A Multidisciplinary Study of Aerodynamic Surface Smoothness Requirements of Aircraft Based on V2500 Turbofan Nacelle Data to Reduce Operating Cost." Doctoral Thesis. Queen's University Belfast; Belfast, UK; 1999.
- [2] Kundu, A., Curran, R., et al. "Cost Consideration in Commercial Aircraft Manufacture." Internet Aviation 2001 Conference. Available at www.rmr-aviation2001.com.
- [3] Kundu, A. K., and Curran, R. *Design for Customer*. ICAS Proceedings; Yokohama; November 2004.
- [4] Kundu, A., Raghunathan, S., and Curran, R. "Cost Modeling as a Holistic Tool in the Multidisciplinary Systems Architecture of Aircraft Design: The Next Step, Design for Customer." 41st AIAA Aerospace Sciences Meeting and Exhibit; Reno, NV; January 6–9, 2003.
- [5] Kundu, A. K., Crosby, S., Curran, R., et al. "Aircraft Component Manufacture Case Studies and Operating Cost Reduction Benefit." AIAA Conference ATIO; Denver, CO; November 2003.
- [6] Murman, E., Walton, M., and Rebentisch, E. "Challenges in the Better, Faster, Cheaper Era of Aeronautical Design, Engineering and Manufacturing." *The Aeronautical Journal*; October 2000.
- [7] Crosby, S. Unpublished document on digital manufacture. Queen's University Belfast; Belfast, UK; 2004.
- [8] Nicolai, L. M. *Fundamentals of Aircraft Design*. METS, Inc.; San Jose, CA; 1975.

Index

Note: Terms followed by asterisks are found on the Web at www.cambridge.org/Kundu

- A-weighted scale, 479
- acceleration
 - gravity, 46, 47
- active control technology, 403, 405, 413
- actuator disc, 349
- advanced tactical support*
- aerofoil, 58, 60, 61
 - camber, 60
 - characteristics, 65
 - chord, 60
 - comparison, 66
 - four-digit, 59
 - five-digit, 60
 - GAW, 61
 - mean line, 60, 94
 - section, * 60
 - selection, 60
 - thickness-to-chord, 58
 - thickness ratio, 81
 - supercritical, 69
 - Whitcomb, 61, 69
- after-burning gas turbine, 322
- aileron, 78, 82, 87, 88, 176, 389, 503
- airborne early warning*
- Airbus, 11, 115, 122, 170, 194, 496, 500
- aircraft (*see also* NACA)
 - civil mission, 104
 - classification, 101, 102
 - classification – military*
 - component, 113, 153, 193, 225, 226, 229, 265
 - component groups – mass, 236
 - design choices – civil, 133
 - evolution, 100
 - family variants, 114, 164, 462
 - force, 56, 57
 - load, 108, 138, 141, 225, 228
 - moment, 58, 62, 389, 392, 393
 - motion, 56, 389, 390, 393
 - sizing, 363, 369
 - specification, 35, 36, 39
 - speed, 148, 414
 - statistics – civil, 105
 - statistics – military*
 - system, 21, 502
 - turning, 195, 201
 - variant, 163, 183, 397, 399, 458
- aircraft cost, 372, 461, 522, 526, 528
- aircraft lighting, 510, 511
- aircraft performance,
 - balanced field length, 426, 427
 - climb, 426, 427, 431, 443, 444
 - constant speed climb, 432
 - descent, 430, 434, 447
 - landing, 282, 381, 425, 429, 481
 - military mission profile, 451
 - payload range, 435, 448
 - takeoff, 373, 375, 376, 379, 421, 425, 426, 433, 437
- aircraft price, 524, 529, 545, 546
- aircraft structural consideration, 494
- air defense, * 452
- air speed
 - calibrated, 419
 - equivalent, 419
 - indicated, 419
 - true, 419
- air superiority, * 101, 385
- air-to-air refueling*
- AJT (*see* worked-out examples),
- AJT undercarriage layout, 219
- AJT and growth potential, 385
- AJT performance, 452
- aluminum alloy, * 490, 491
- amortization, * 527, 539
- angle
 - downwash, 72, 393
 - effective, 72
 - incidence, 67, 72, 393
- anhedral, 79, 90, 128, 175, 176, 395
- antenna location, 510

- anti-icing, 506, 513, 515
- approach velocity, 379
- area rule, 68, 69, 70
- ARINC, 416, 510
- aspect ratio
 - correction, 73, 283
- aspiration design space, 19, 40
- AST, 35
- atmosphere, 46
- automatic riveting, 557
- avionics, 499, 509

- B2 (F), 10, 145
- balanced field length, 425, 427, 428, 441
- bel, 479
- Bernoulli's equation, 50
- beyond visual range (BVR), 101, 104
- Bizjet (*see* worked-out examples)
- blade element theory, 349, 351
- Blanchard, Jean-Pierre, 3
- blended wing body, 13, 88, 115, 122, 132, 486
- Bleriot, 5
- Boeing 737 variants, 151
- Boeing 787 (F), 10
- Boeing Sonic Cruiser (F), 10, 98
- BPR (*see* by-pass ratio)
- boundary layer, 50, 51, 52
- Brayton (Joule) cycle, 324
- Breguet range equation, 437
- buffet, 140
- BWB (*see* blended wing body)
- by-pass ratio (turbofan), 318

- Cabin
 - air flow, 515
 - crew, 121, 246
 - width, 113
- CAD, 16
- CAS,* 219, 419, 422, 458, 462
(*see* worked-out examples)
- canard, 90, 140, 396, 398
- candidate aircraft, 114, 151
- cargo container, 124, 168
 - sizes, 124, 169
- caster angle, 197
- caster length, 197
- Cayley, 3
- center
 - aerodynamic, 64, 91, 229
 - pressure, 64
- center of gravity (CG)
 - position, 228, 252
 - range, 196, 228, 230
- chord
 - mean aerodynamic, 79
 - root, 79, 178
 - tip, 77
- chronology – fighter aircraft*
- circulation, 64
- civil aircraft configuration, 152, 187
- climb, 426
 - first segment, 427
 - second segment, 427
 - gradient, 375, 427, 431, 441, 452, 456
 - initial climb, 377, 380
- close air support*
- cockpit layout (*see* flight deck)
- coefficient
 - drag, 61, 62, 260, 262
 - friction, 53
 - lift, 61, 62
 - moment, 62, 394, 396
 - pressure, 62, 63, 348
- comparison
 - civil versus military, 40
- component, aircraft, 113, 152
- compressibility effect, 80
- computational fluid dynamics, 464
 - case studies, 471
 - hierarchy of CFD, 472
 - postprocessor, 470
 - preprocessor, 470
- conceptual study, 24, 26, 152
- concrete surface, 207
- Congrave, William, 7
- conservation equations
 - energy, 49
 - mass, 49
 - momentum, 49
- container
 - cargo, 124
 - standard, 125
- control augmented system (CAS), 413
- control configured vehicle (CCV), 387
- control subsystem, 503
 - electromechanical, 504
 - mechanical control linkage, 504
 - optical signal, 504
 - push–pull rod type, 504
 - wire–pulley type, 504
- control surface layout, 176
- control volume (CV), 49, 326
- cost
 - fraction, 528
 - frame, 26
- cost methodology, 532
- Curtiss, 5, 192, 315
- customer, 34

- DBT, 15, 24, 551
- d'Arlandes, Francois Laurent, 3
- da Vinci, Leonardo, 2
- decibel, 475
- de-icing, 516
- deflection under load, 206
- de Rozier, Pilatre, 3
- design
 - driver, 34, 200, 233
 - process, 21, 191, 557

- design consideration
 - technology-driven, 563
 - manufacture-driven, 564
 - management-driven, 551, 564
 - operator-driven, 565
- design for customer, 565
 - index, 566
- design for manufacture/assembly, 551
 - DFM/A steps, 9, 527, 531, 554
- digital manufacturing process management (MPM), 568
- dihedral angle, 79, 395
- direct operating cost (DOC), 544
 - breakdown, 544
 - formulation, 546
 - fixed-cost element, 544, 545, 546
 - trip-cost element, 545, 548, 550
- directional divergence, 406
- dive brake, 98, 286
 - (*see* speed brake)
- doors
 - emergency egress, 495
 - types, 495
- downwash angle, 72, 393, 398
- drag
 - base, 274
 - boat tail, 274
 - breakdown, 262
 - canopy, 269
 - dive brake/spoiler, 286
 - excrescence, 277
 - flat-plate equivalent, 262, 266
 - form, 261
 - formulation, 263
 - high-lift device, 282
 - induced, 73, 262, 299, 306
 - intake, 274
 - low speed, 282
 - methodology, 265
 - minimum parasitic, 265, 268, 280
 - nacelle, 273
 - one-engine inoperative, 288
 - parasitic, 54, 261, 265, 268, 278, 299, 305
 - polar, 260, 262, 286, 302, 308, 378
 - profile, 54, 261, 289
 - propeller, 288
 - spillage, 274, 275
 - supersonic, 290
 - total, 262
 - undercarriage, 286
- Dumas, Santos, 5
- Duralumin, 6, 223, 488
- EASA, 6, 41, 476
- ECS, 499, 503, 513
- EFIS, 498
- effective noise level, 480
- efficiency
 - overall, 318, 320
 - propulsive, 318, 319
 - thermal, 318, 319
- ejection, * 479, 498, 521
- Ekranoplane, 14
- electrical subsystem, 510
- electronic warfare*
 - elevator, 90, 140, 182, 184
- emerging scenario, 478, 498, 521
- emergency power supply, 508
- empennage, 90, 112, 128, 158, 180
- end-of-life disposal, 518
- energy absorbed, 205
- engine and fuel control subsystem, 505
 - fuel storage and flow management, 505
 - piston engine, 505
 - turbofan system, 506
- engine performance, 359
 - military gas turbofan, 370
 - piston engine, 361
 - turbofan (civil), 365
 - turboprop, 363
- engine-performance data
 - turbofan (civil), 420
 - turbofan (military)*
 - turboprop, 423
- engine position, 131, 333
- engine ratings, 359
 - idle, 361
 - maximum continuous, 360, 420, 423, 488
 - maximum climb, 360, 420, 424
 - maximum cruise, 360, 420, 424
 - takeoff, 360, 420, 423, 424
- environmental control system (*see* ECS)
- equation of state, 50
- escape slide, 496
- Euler's equation, 49
- F22 Raptor (F),* 97
- F117 Nighthawk (F),* 7
- FAA, 6, 205, 288, 430, 476, 478, 481, 495
- FADEC, 316, 415, 507
- FAR, 144, 417, 418, 425, 480, 495
- factor of safety, 143, 425, 451
- family variants, 112, 114, 164, 218
- fence, 89
- fin, 32, 129, 189
- fixtures, 494, 551
- flap, 67, 176, 203, 272, 282
- flight deck, 497
 - layout (civil), 500
 - layout (military), 499
- flutter, 140
- flotation, 206, 210
- flyaway tooling, 552, 556
- fly by light, 413
- fly by wire, 413
- force
 - aircraft, 56, 396
- fps, 17, 31
- fuel fraction, 108

- fuel load, 108, 229, 247, 373
- fuselage, 93
 - aft-closure angle, 95
 - axis, 93, 156, 252, 336
 - closure, 94
 - configure, 165
 - cross-section, 94, 97, 116, 117, 161, 164
 - fineness ratio, 94
 - front-closure angle, 94
 - height, 95
 - layout (civil), 160
 - length, 94, 114, 117, 119, 154, 164
 - multiboom, 126
 - nose cone, 32, 94, 117, 118, 266, 268
 - reference line, 93, 156
 - twin boom, 129, 133, 159
 - upsweep angle, 94, 120
 - width, 95, 114
 - zero-reference plane, 90
- galley, 123, 124
- gas turbine station number, 319, 321, 325, 326, 331
- gauges, 499, 555
- gaugeless tooling, 557
- geopotential altitude, 48
- glove, 77, 80, 127, 157
- golf ball, 54
- grass turf, 194, 206, 212
- ground attack aircraft*
- ground-effect vehicle, 13
- ground loop, 194, 201
- gust envelope, 147

- hands on throttle and stick (HOTAS), 502
- hard turf, 212
- head-up display, 500
- helmet-mounted display, 501
- Henson, Samuel, 3
- high-lift device, 32, 67, 68, 88, 282, 286
- horizontal-tail, 90, 130, 181
- hydraulic subsystem, 511
- hydrostatic equations, 46, 47
- hypersonic aircraft, 12, 101

- INCOSE, 21
- induced drag, 71, 73, 83, 262, 299
- inline assembly, 557
- intake, 96, 338
 - design (civil), 338
 - design (military)*
 - diffuser, 339
 - highlight diameter, 339
 - position (nacelle), 98, 131
 - supersonic*
 - throat, 339
 - (*see also* nacelle)*
- installation (military), 348
- integration
 - engine, 331
 - turboprop, 335
- interdiction*
 - IPPD, 9, 22, 494, 527, 531, 544
- isentropic relations, 49, 325
- ISA, 46

- JAA, 6
- Jatho, Karl, 4
- jigs, 494, 555, 556
- jigless assembly, 552, 556
- joined wing aircraft, 13, 14
- Johnson, Clarence, 7
- Joule (Brayton), cycle, 325
- JUCAS,* 14

- laminar, 50, 52, 267, 331, 335
- Langley, Samuel P., 4
- LCN, 207, 208
- life cycle cost (LCC), 530
- lift, 57
 - curve slope, 74
 - dumper, 32, 88
- Lilienthal, Gustav and Otto, 3
- limit
 - load, 143
 - low speed, 146
 - high speed, 145
 - speed, 143
- lip contraction ratio, 340
- lip suction, 270
- load
 - factor, 142, 147, 205, 227, 238
 - factor, maximum limit, 154
 - limit, 144
 - negative, 146
 - positive, 146
 - ultimate, 143, 491
- load classification group, 207
- load classification number (*see* LCN)
- load on wheel, 203
- low observable*

- macadam surface, 207
- Mach
 - critical, 81, 381
 - number, 49, 50
- main wheel failed, 200
- maneuver
 - pitch, 144
 - roll, 141
 - yaw, 141
- manufacturer's empty mass, 106, 228
- manufacturing practices, 568
- maritime patrol*
- market, 33
 - military,* 39
 - survey, 33
- mass estimation, 233
- mass flow ratio, 349
- mass (weight) fraction (civil), 235, 237
- mass (weight) fraction (military)*

- material
 - aircraft, 478
 - composite, 489
 - properties, 489
 - selection, 491
 - stress–strain relationship, 490
- maximum takeoff mass (MTOM), 106, 220, 228
- MDA, 24, 29
- MDO, 17, 24, 385
- mean aerodynamic chord, 79
- military
 - aircraft component*
 - mission*
 - mission profile, 451
 - statistics*
 - transport aircraft*
- modular concept, 31, 156, 315, 510
- Montgolfier, Joseph and Etienne, 3
- motion, aircraft, 56, 503
- multifunctional display (MFD), 498, 510
- multirole fighter*
- NACA
 - four-digit aerofoil, 59
 - five-digit aerofoil, 60
 - six-digit aerofoil, 60
- nacelle/intake, 96
 - external diameter, 339
 - fuselage-mounted, 130
 - layout, 184
 - long-duct, 322, 327, 333
 - overwing, 130, 131, 332, 411
 - position, 128, 184, 332, 334
 - short-duct, 333, 337
 - underwing, 130, 332
 - wing tip, 132
- nacelle cost driver, 533
- Newton, Isaac, 3
- Night Hawk, F117, 11, 291, 415, 504
- noise, 479
 - propeller, 486
 - radiation, 484
 - source, 483
 - standards, 493
 - suppression, 335, 485
- nose wheel, 196, 201
- nose wheel failed, 200
- nozzle,* 273, 337, 338, 349, 343
- OEM fraction, 107, 234
- operating cost (OC), 529
- operational empty mass (OEM), 106, 228
- Oswald's efficiency factor, 72, 77, 261
- oxygen supply, 515
- pavement (*see* runway)
- payload range, 29, 104, 435, 448
- perceived noise level, 480
- phases of project, 23, 26
- phugoid, 404
- Piaggio, 92
- pilot seat dimension, 122
- pilot vision, 114
- piston engine, 101, 243, 289, 317, 323, 362, 505
- piston engine – supercharged, 324
- Pline, Joseph, 3
- pneumatic subsystem, 503, 513
- potato curve, 229
- power control unit, 504
- propeller, 345, 349, 355, 358
 - activity factor, 348, 353
 - advance ratio, 349
 - blade element theory, 351
 - blade-pitch angle, 346, 348
 - constant pitch, 347, 349
 - definition, 348
 - design C_L , 355
 - momentum theory, 349
 - performance, 355, 358
 - power, 348, 356
 - power coefficient, 348, 353
 - theory, 349
 - thrust, 330, 348, 352
 - thrust coefficient, 348
 - type, 346
 - variable pitch, 346
- radar cross-section*
- rain removal, 516, 517
- rake angle, 196, 197
- ram air turbine (RAT), 508
- Raptor F22*
- RD&D, 34
- reconnaissance*
- reliability and maintainability (R&M), 524, 561
- remotely piloted vehicles*
- return to base*
- Reynolds number, 51, 266
 - critical, 52
- RFP, 34
- RPM, 10
- rudder, 32, 90, 97, 389
- runway pavement classification, 206
- runway types, 206
- sea-level static thrust, 111, 420
- Sears–Haack body, 69
- seat
 - mile cost, 105
 - pitch, 123, 162
 - posture, 122
 - width, 123
- seating
 - two-abreast, 163
 - three-abreast, 164
 - four-abreast, 165
 - five-abreast, 166
 - six-abreast, 167
 - seven-abreast, 168
 - eight-abreast, 168

- seating (*cont.*)
 - nine/ten-abreast, 169
 - ten-abreast, 170
- separation, 52, 54, 55
- service
 - galley, 114, 123
 - trolley, 123
 - location, 520
- shock absorber, 202
- shop-floor interface, 572
- short period, 330, 404
- silent aircraft, 486
- simple straight-through
 - turbojet, 320, 325
- sizing theory, 373
 - initial cruise, 378
 - initial rate of climb, 377
 - landing, 378
 - takeoff, 374
- Six Sigma
 - concept, 558
 - distribution, 558
- skin friction coefficient, 52, 54, 261, 265, 295, 309
- slat, 32, 67, 88, 241, 282, 427
- sonic cruiser, 10
- sound pressure level, 479
- Space Ship One, 7, 13
- specific range, 432, 446, 459
- specific thrust, 317, 328, 366
- speed
 - brake application, 203, 426
 - decision, 426, 428
 - minimum control, 426
 - minimum unstuck, 426
 - rotation, 420
- speed brake (*see* dive brake)
- spinning, 408
- spiral, 408
- spoiler, 32, 88, 96, 97, 241, 286
- square-cube law, 84
- stabilator, 505
- stability
 - design considerations, 389, 413
 - directional, 189, 393
 - dynamic, 389, 391
 - lateral, 390, 393, 406
 - pitch plane, 140, 392, 396
 - static, 389, 391, 396, 409
 - theory, 412
- stability augmented system, 413
- stabilizer, 90, 184, 508
- STAGNAG 3838, 509
- stall, 55, 65, 82
 - type, 65
- stealth considerations
 - heat signature*
 - radar signature*
- stowage space, 199
- strategic bomber*
- stress-strain relationship, 490
- Stringfellow, John, 4
- subsystem, 503
- supersonic transport aircraft, 12
- survivability (military aircraft)
 - ejection seat*
 - emergency escape*
- system
 - aircraft, 21, 503
- T-s diagram, 325, 329
- tail
 - asymmetric, 128
 - canard, 140, 396, 412
 - circular, 129
 - H-tail, 90, 128, 181
 - T-tail (high tee), 33, 78, 90, 128, 181
 - high, 128
 - low, 128
 - mid, 128
 - twin boom, 129
 - multiboom, 128
 - position, 128
 - single boom, 128
 - statistics, 112, 402
 - V-tail, 90, 114, 128, 181, 189, 396, 402
 - Y-tail, 129
- tail volume coefficient, 399
- takeoff, 379, 425, 428
- thrust loading, 110, 111, 373, 381, 382
- thrust reverser,* 332, 341
 - effect on stopping distance, 429
 - efflux pattern, 342
 - military*
 - types, 343
- thrust vectoring*
- time frame, 27
- Tippu, Sultan, 7
- Tire, 209
 - braking friction, 212
 - data (*see* Appendix E*)
 - designation, 211
 - extra-high pressure, 210
 - friction with ground, 212
 - low pressure, 210
 - new design, 210
 - pressure, 210
 - rolling friction, 212
 - sizing, 213, 215
 - types, 210
- tolerance relaxation, 559
- tools, 555
- TQM, 15
- transonic,
 - effect, 68, 80, 281
- trim drag, 65, 278
- trolley, 124
- true air speed, 419
- turbofan engine, 321, 327, 365
- turbojet engine, 325
- turboprop engine, 323, 330, 360, 363, 423
- turbulent, 56, 62, 306
- turning of aircraft, 201

- UAV*
- undercarriage, 194
 - CG position, 195
 - data, 221
 - deflection, 199
 - energy absorbed, 202
 - layout, 213
 - layout methodology, 213
 - layout/nomenclature/definitions, 195
 - nose wheel type, 196
 - retraction, 197
 - stowage, 197
 - strut, 195
 - tail-dragging type, 196
 - turnover, 195
 - type, 195, 197
- unit load device (ULD), 125
- unprepared surface, 206
- utility system, 517

- V-n* diagram, 145
- verified design space, 19, 40
- vertical tail (*see* tail – V-tail)
- voice-operated control (VOC)*
- von Braun, W., 7
- von Ohain, Hans, 6
- vortex
 - generator, 89
 - lift, 87
- vortilon*

- water and waste system, 517, 519
- weight (*see also* mass)
 - data, 251
 - driver, 227
 - estimation graphical, 234
 - semi-empirical method, 238
- Weisskopf, Gustav, 4
- wetted area, 85
- wheel
 - arrangement, 202
 - load, 202
 - shock absorber, 202
- Whitcomb aerofoil, 61, 174
- White Knight, 13
- Whitte, Frank, 6
- wing
 - anhedral, 79
 - configuration, 78
 - dihedral, 79
 - generic*
 - group,* 114, 126
 - high, 79, 120, 131
 - layout, 174
 - loading, 84, 109, 113, 180, 373
 - low, 78, 120, 131
 - reference area, 76, 176, 279
 - root chord, 77, 79
 - shape, 128
 - stall, 82
 - sweep angle, 81, 82, 176
 - taper ratio, 77
 - three-surface*
 - tip chord, 77
 - twist, 78
 - two-surface*
 - wing design
 - planform shape, 86, 126
 - position, 133, 174
 - wing planform
 - area, 76
 - cranked, 127
 - elliptical, 127
 - generic, 136
 - rectangular, 127
 - tapered, 127
 - wing reference area, 76
 - winglet, 88
 - worked-out example
 - AJT
 - baseline, 294
 - (CAS), 207
 - CG location, 274
 - discussion, 475
 - drag evaluation, 314
 - fuselage layout, 204
 - growth potential, 385
 - performance, 452
 - sensitivity study, 401
 - sizing, 398
 - undercarriage layout, 219
 - variant (CAS), 399
 - wing, 204
 - Bizjet
 - baseline aircraft, 188
 - CG location, 254
 - design for customer, 567
 - discussion, 461
 - DOC estimation, 548
 - drag evaluation, 292
 - empennage layout, 182
 - finalized configuration, 383
 - fuselage layout, 171
 - nacelle design, 185
 - performance, 437
 - sizing analysis, 379, 384
 - undercarriage layout, 215
 - variants, 171, 379
 - weight and CG analysis, 226, 254
 - weight estimation, 260–263
 - wing layout, 178
 - costing of nacelle nose cowl, 536
 - design for customer, 565, 567
 - propeller performance, 358
 - supersonic drag evaluation, 299
 - turboprop performance, 636
- Wright brothers (Orville and Wilber), 2, 4

- Yeager, Chuck, 6
- Yehudi, 77
- yield point, 490
- Young's Modulus, 490